Inorganic and Inorganic–Organic Hybrid Polymers Containing BN Units in the Main Chain

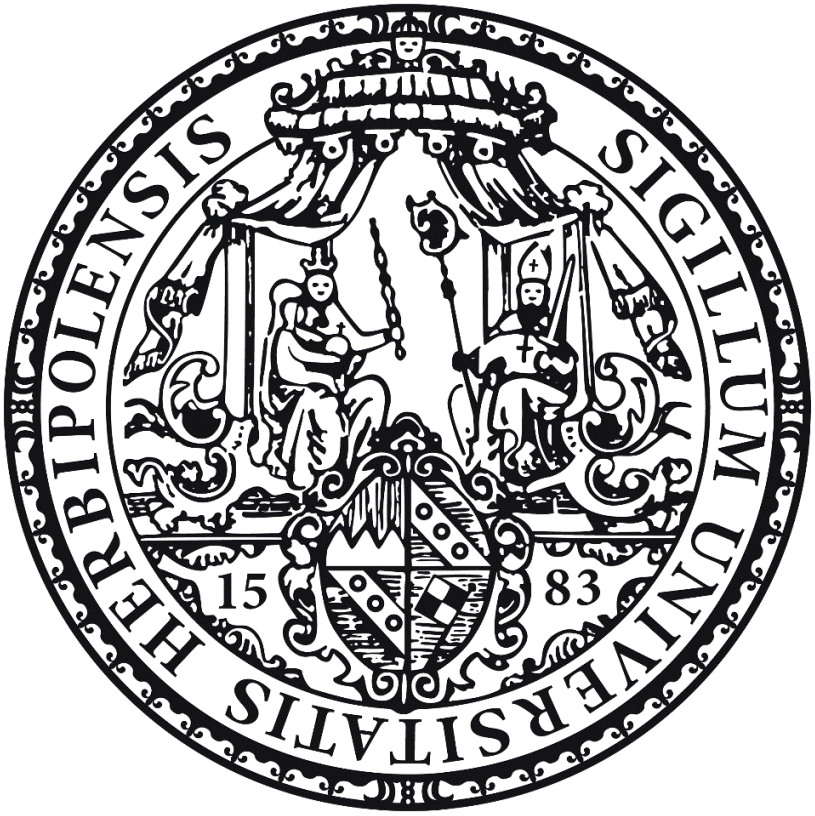

Dissertation zur Erlangung des naturwissenschaftlichen Doktorgrades der Julius-Maximilians-Universität Würzburg

vorgelegt von

Matthias Maier

aus Kempten im Allgäu

Würzburg 2024

Eingereicht bei der Fakultät für Chemie und Pharmazie am

17.01.2024

Gutachter der schriftlichen Arbeit

1. Gutachter:	Prof. Dr. Holger Helten
2. Gutachter:	Prof. Dr. Maik Finze

Prüfer des öffentlichen Promotionskolloquiums

1. Prüfer:	Prof. Dr. Holger Helten
2. Prüfer:	Prof. Dr. Maik Finze
3. Prüfer:	Prof. Dr. Lutz Nuhn

Datum des öffentlichen Promotionskolloquiums

23.02.2024

Doktorurkunde ausgehändigt am

meinen Eltern

gewidmet

Danksagung

Als Erstes möchte ich mich bei Prof. Dr. Holger Helten für die Möglichkeit bedanken meine Doktorarbeit in seinem Arbeitskreis zu absolvieren. Ich danke Dir für die erstklassigen Arbeitsbedingungen und dass deine Tür immer für Fragen geöffnet war. Ich möchte mich auch für die Gelegenheit bedanken, dass ich meine Forschung auf internationalen Konferenzen präsentieren durfte. Ich konnte während meiner Zeit in deinem Arbeitskreis nicht nur meine chemischen Kenntnisse ausweiten, sondern mich auch menschlich weiterentwickeln.

Ich möchte mich auch bei Prof. Dr. Maik Finze für die Übernahme des Zweitgutachten bedanken.

Den ganzen Mitgliedern des aktuellen und ehemaligen Arbeitskreis Helten möchte ich für die schöne Zeit danken. Der größte Dank gilt hier auf jeden Fall Dr. Nicolas Riensch, Dr. Lars Fritze und Dr. Merian Crumbach für die super Aufnahme in den damals noch recht kleinen Arbeitskreis. Ihr habt mir den Start in die Promotion enorm erleichtert, indem ihr mich schnell integriert und mir mit eurer Erfahrung auch chemisch weitergeholfen habt. Mit euch waren auch private Aktivitäten stets mit sehr viel Spaß verbunden. Bei Dr. Thomas Lorenz möchte ich mich für zahlreiche Tipps und Tricks zur BN-Chemie bedanken.

Ein großer Dank gilt auch Johannes Chorbacher. Du hast in meinem letzten Promotionsjahr nochmal frischen Wind in meinen Arbeitsalltag gebracht und mich mit deiner grenzenlosen Motivation angesteckt. Ohne dich wären einige Ergebnisse dieser Arbeit sicherlich gar nicht mehr entstanden.

Johannes Schneider, Maximilian Fest, Julian Glock, Jonas Bachmann und Julian Günther möchte ich für das Messen und Lösen von Kristallstrukturen danken. Lukas Swoboda und Christoph Mahler danke ich für zahlreiche Messungen am Massenspektrometer und bei Jonas Klopf möchte ich mich für die vielzähligen quantenchemischen Rechnungen bedanken. Für die Übernahme der Vielzahl von administrativen Aufgaben danke ich Mihaela Schneider. Des Weiteren möchte ich mich aber auch bei Dr. Alexandra Friedrich bedanken. Danke, dass Du mich zur Finalisierung meiner Doktorarbeit in deinem Büro aufgenommen hast.

Während meiner Promotion hatte ich auch das Vergnügen mit einer Vielzahl von Studenten zu arbeiten, die durch ihre synthetische Unterstützung zu dieser Arbeit beigetragen haben. Dafür möchte ich mich bei Julian Glock, Nadine Munker, Heiko Lackinger, Nils Rehmeier, Johannes Chorbacher und Anna Hellinger bedanken.

Ich danke auch allen Kooperationspartnern für ihre Unterstützung bei den gemeinsam vorbereiteten, eingereichten und akzeptierten Publikationen, die Teil dieser Arbeit sind.

Ohne die Festangestellten, die das Institut der Anorganische Chemie am Laufen halten, wäre der Laboralltag unter diesen einwandfreien Bedingungen nicht möglich gewesen. Dafür möchte ich mich bei Dr. Stephan Wagner, Cornelia Walter, Stephan Köper, Gertrud Wunderling, Dr. Rüdiger Bertermann, Liselotte Michels, Laura Wolz, Christoph Mahler, Bernhard Werner und Manfred Reinhart sowie den Ehemaligen Alfred Scherzer, Maria Kromm, Sabine Timmroth und Marie-Luise Schäfer bedanken.

Für das Korrekturlesen der Arbeit möchte ich mich bei Dr. Alexandra Friedrich, Johannes Chorbacher und Lukas Swoboda bedanken.

Abseits der Uni war es insbesondere mein privates Umfeld, dass für den perfekten Ausgleich zum meist stressigen Arbeitsalltag gesorgt hat. Dafür möchte ich mich insbesondere bei meinen Allgäuer Freunden sowie meinen Eishockey Teamkollegen danken.

Ein großer Dank geht auch an meine Familie. Ich kann mich glücklich schätzen, dass ich euch habe und Ihr immer hinter mir steht. Insbesondere meinen Eltern Vera und Ewald danke ich für die kontinuierliche Unterstützung während meines Werdegangs. Ihr habt immer an mich geglaubt, was mich immer motiviert hat weiterzumachen. Ein weiterer Dank gilt aber auch meinen Schwiegereltern *in spe*, Claudia und Hermann, Ihr habt mich direkt von Anfang an in eure Familie aufgenommen und in jeder erdenklichen Weise unterstützt. Vielen Dank!

Mein letzter Dank gilt meiner Freundin Svenja. Ich möchte mich bei Dir für deine unermüdliche Unterstützung und Liebe bedanken! Du hast in frustrierenden Zeiten immer Geduld bewiesen und mir gleichzeitig das Leben durch viele kleine Aufmerksamkeiten leichter gemacht. Ohne dich wäre diese Arbeit so niemals möglich gewesen. Ich liebe dich!

List of Publications

The publications listed below are partly reproduced in this dissertation with permission from The Royal Society of Chemistry [1] and John Wiley & Sons [2–4]. The table itemizes at which position in this work the paper has been reproduced.

Publication	Chapter
[1] M. Maier, J. Klopf, C. Glasmacher, F. Fantuzzi, J. Bachmann, O. Ayhan, A. Koner, B. Engels, H. Helten, *Chem. Commun.* **2022**, *58*, 4464-4467.	2.1
[2] M. Maier, V. Zeh, N. Munker, J. Glock, K. Oberdorf, O. Ayhan, C. Lichtenberg, H. Helten, *Eur. J. Inorg. Chem.* **2024**, *27*, e202300490.	2.5
[3] J. Chorbacher, M. Maier, J. Klopf, M. Fest, H. Helten, *Macromol. Rapid Commun.* **2023**, *44*, 2300278.	2.7
[4] M. Maier, J. Chorbacher, A. Hellinger, J. Klopf, J. Günther, H. Helten, *Chem. Eur. J.* **2023**, *29*, e202302767.	2.8

List of Abbreviations

Å	Ångström
abs	absorbance
$Ag[Al\{OC(CF_3)_3\}_4]$	silver tetrakis(perfluoro-*tert*-butoxy)aluminate
APCI	atmospheric pressure chemical ionization
Ar	aryl group
ASAP	atmospheric solid analysis probe
BN	boron-nitrogen
BNCT	boron neutron capture therapy
BN-PPV	poly(*p*-phenylene iminoborane)
BN-PTV	poly(thiophene iminoborane)
br	broad
BPA	boron doped polyacetylene
°C	degree celsius
calcd.	calculated
cat.	catalyst
cm	centimeter
CV	cyclic voltammetry
d	days (time information) or doublet
dd	doublet of doublet
Đ	dispersity
Da	Dalton
DCM	dichloromethane
DLS	dynamic light scattering
DMSO	dimethyl sulfoxide
DP_n	number average degree of polymerization
$E_{1/2}$	half wave potential
e.g.	exempli gratia
elem. anal.	elemental analysis
em	emission
equiv.	equivalents
et al.	and others
Et	ethyl group
eV	electron volt
Fc/Fc^+	ferrocene/ferrocenium cation
g	gram

GPC	gel permeation chromatography
h	hour
HCl	hydrochloric acid
HMBC	heteronuclear multiple bond correlation spectroscopy
HOMO	highest occupied molecular orbital
HRMS	high resolution mass spectrometry
HSQC	heteronuclear single quantum correlation spectroscopy
Hz	Hertz
*i*Pr	iso-propyl
J	coupling constant
K	Kelvin
kJ	kilojoule
LIFDI	liquid injection field desorption ionization
LED	light-emitting diode
LUMO	lowest unoccupied molecular orbital
M	molar, mol per liter
m	multiplet
max	maximum
mbar	millibar
Me	methyl
Mes	2,4,6-trimethylphenyl
mg	milligram
MHz	megahertz
mL	milliliter
mmol	millimole
M_n	number average molar mass
MS	mass spectrometry
mV	millivolt
mW	milliwatt
M_z	mass average molar mass
m/z	mass per charge
n-BuLi	*n*-butyllithium
[*n*-Bu_4N][PF_6]	tetra-*n*-butylammonium hexafluorophosphate
nm	nanometers
NMR	nuclear magnetic resonance
NOESY	nuclear Overhauser effect spectroscopy
norm.	normalized

ns	nanoseconds
o-	*ortho*-position
o-DCB	*ortho*-dichlorobenzene
o-DFB	*ortho*-difluorobenzene
OFET	organic field-effect transistor
OLED	organic light-emitting diode
OPV	organic photovoltaic
p-	*para*-position
PAB	poly(aminoborane)
PC-PPV	poly(*p*-phenylene phosphaalkene)
PDI	polydispersity index
Ph	phenyl group
PIB	poly(iminoborane)
PLED	polymer light-emitting diode
PMMA	poly(methyl methacrylate)
ppm	parts per million
PPV	poly(*p*-phenylene vinylene)
PSV	poly(selenylene vinylene)
PTV	poly(thiophene vinylene)
PTeV	poly(tellurophenylene vinylene)
R	organic substituent
RI	refractive index
ROESY	rotating frame nuclear Overhauser effect spectroscopy
r.t.	room temperature
s	singlet
sept	septet
T	temperature
TD-DFT	time-dependent density functional theory
TGA	thermogravimetric analysis
THF	tetrahydrofuran
Thi	thienyl group
Tip	2,4,6-triisopropylphenyl
TMEDA	tetramethylethylenediamine
TMS	trimethylsilyl
TMS-NTf_2	trimethylsilyl-bis(trifluoromethylsulfonyl)imide
UV	ultraviolet
vis	visible

vs	versus
VT	variable temperature
ε	extinction coefficient
λ	wavelength
Φ	quantum yield
δ	chemical shift

Table of Contents

1 Introduction

π-Conjugated organic polymers have attracted tremendous attention in the last decades.[1] The interest in these materials is mainly driven by their applicability in next-generation electronic and optoelectronic devices, such as organic/polymer light-emitting diodes (OLED/PLED),[2] organic field-effect transistors (OFET),[3] and organic photovoltaic cells (OPV).[3e,4] Furthermore, they have drawn increased attention in biomedical applications.[5] However, the partial or complete replacement of carbon atoms by main group elements in conjugated polymers can significantly change the characteristics and applications of these macromolecules.

1.1 Main Group Elements in Organic Conjugated Polymers

The selective replacement of carbon atoms by inorganic (heavier) main group elements in conjugated macromolecules allows for effective tuning of the electronic structure.[6] Thus, exciting characteristics and novel applications can be realized that cannot be achieved with purely organic compounds. It is worth mentioning that some main group elements are indispensable and well established in organic conjugated polymers and became a standard in organic chemistry. The chalcogens oxygen and sulfur are often incorporated, for example, in the five-membered heterocycles furan and thiophene, respectively. Especially the thiophene-based organic materials have been recognized as an emergent class of organic electronic materials.[7] Furan-based materials, on the other hand, have received less consideration in the past.[8] However, also nitrogen-based building blocks have become an essential part of organic conjugated polymers. Often, the nitrogen is incorporated in pyrrole-based cyclic structures with fused thiophene units or in cyclic structures with further hetero elements (e.g. thiadiazoles).[9] Apart from sulfur, oxygen, and nitrogen, the interest of other main group element-functionalized conjugated polymers increased in the last decades.

In general, main group elements (E) can be incorporated either in the main chain or in the side groups of the polymer (Figure 1.1.1). If the polymer backbone exclusively contains elements other than carbon (**I**), its referred to as an “inorganic polymer”, even though it may feature organic side groups (chapter 1.3). Polymers composed of both main group elements and organic building blocks are classified as “inorganic-organic hybrid polymers”. Structurally, the main group element can be embedded into the main chain (**II**) or appended in the side chain (**III**) of the conjugated polymers.

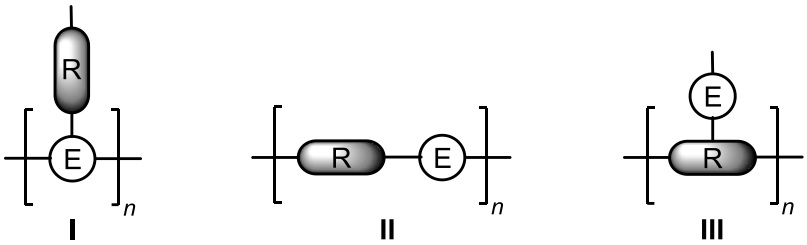

Figure 1.1.1. General structures of polymers containing main group elements (E) and organic moieties (R).

One of the most extensively studied class of organic conjugated polymers are poly(*p*-phenylene vinylene)s (PPV)[2c,10] and it is therefore not surprising that some researchers incorporated main group elements into the polymer backbone of PPVs or their respective oligomers.[11]

The selenium and tellurium analogs of thiophene, that are, selenophene and tellurophene, respectively, are of considerably growing interest in heterocyclic conjugated polymers.[6b,12] Replacing the phenylene units of PPV by these heterocycles was considered to be a viable strategy to gain PPV derivatives with modified optoelectronic properties.[13]

In 2011, Heeney and co-workers achieved the synthesis of the first poly(selenylene vinylene) (PSV) derivate by microwave-assisted Stille-type coupling polycondensation of 2,5-dibromoselenophene (**1**) and 1,2-bis(tributylstannyl)ethylene (**2**) in presence of a palladium catalyst (Scheme 1.1.1, top).[13b] To enhance the solubility of the polymer **3**, they introduced alkyl chains on the selenophene rings. In solution, **3** exhibit an absorbance maximum at 621 nm and in the solid state (thin film) a considerably broad, red-shifted absorbance with a maximum at 652 nm and a noticeable shoulder at 730 nm, which suggests enhanced structural ordering in the solid state.

Recently, Qin and co-worker reported the synthesis of PSV derivatives containing cross-conjugated side chains, which enabled to uncover a detailed structure-property relationship for the first time.[13e]

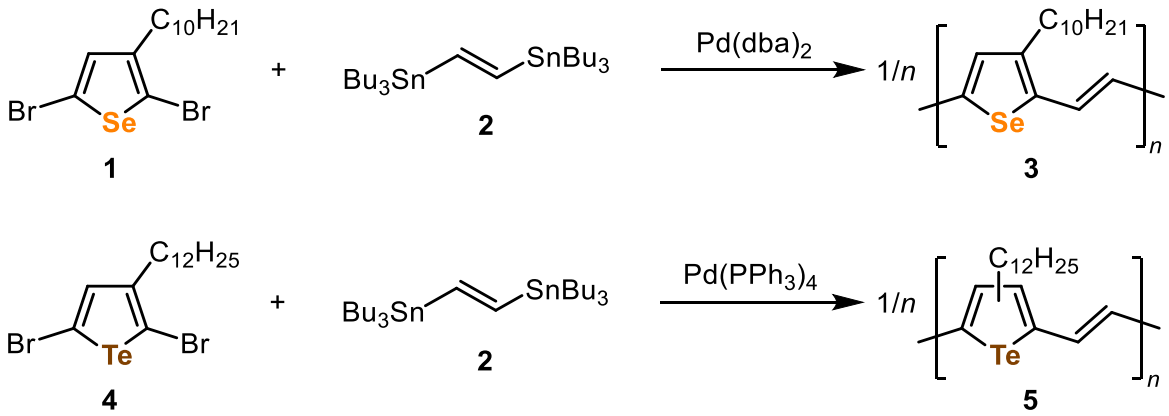

Scheme 1.1.1. Pd-catalyzed synthesis of poly(selenylene vinylene) **3** and poly(tellurophenylene vinylene) **5**.

The synthesis of the first soluble poly(tellurophenylene vinylene) (PTeV) derivative was performed by Heeney, Al-Hashimi and co-workers in 2016. They compared the optoelectronic properties to the thiophene and selenophene analogs, PTV and PSV.[13d] After the synthesis of the 2,5-dibromotellurophene monomer **4** and further polymerization with **2** in presence of palladium(0), they were able to isolate PTeV **5** (Scheme 1.1.1, bottom). Different to the microwave assisted reaction to PTV and PSV, **5** was synthesized by conventional heating in toluene. Attempted microwave polymerization to **5** resulted in insoluble materials which were assigned to high-molecular-weight polymers. PTeV was slightly soluble at room temperature in chlorinated solvents, but a decreasing solubility trend was observed between the polymers (PTV > PSV > PTeV). The absorption spectra of PTV, PSV and PTeV in solution and as thin films show that the absorbance maxima are red-shifted with increased size of the heteroatom. The estimation of optical band gaps from the onset absorption of the thin films revealed the lowest band gap for PTeV (1.4 eV).

In 2002, Gates and co-worker prepared and characterized the first π-conjugated polymer containing P=C bonds in the backbone.[11a] This PPV analog, poly(*p*-phenylene phosphaalkene) (PC-PPV), was prepared via the established Becker reaction for the formation of phosphaalkenes. The synthesis of PC-PPV was achieved by the reaction of a bifunctional silylphosphine with diacid chloride at elevated temperatures (Scheme 1.1.2, top). Unexpectedly, ^{31}P NMR revealed that the polymer **6a** was obtained with an approximately 1:1 ratio of *E*- and *Z*-configured P=C bonds. In a follow-up study, Gates and co-workers achieved the formation of various oligomers and polymer **6b** with purely *Z*-configured P=C bonds by increasing the steric demand around the phosphorus atom.[11d] The authors observed evidence for π-conjugation between the P=C and phenylene groups in PC-PPV from UV/vis spectroscopy and X-ray diffraction, which was supported by molecular oligomer data.

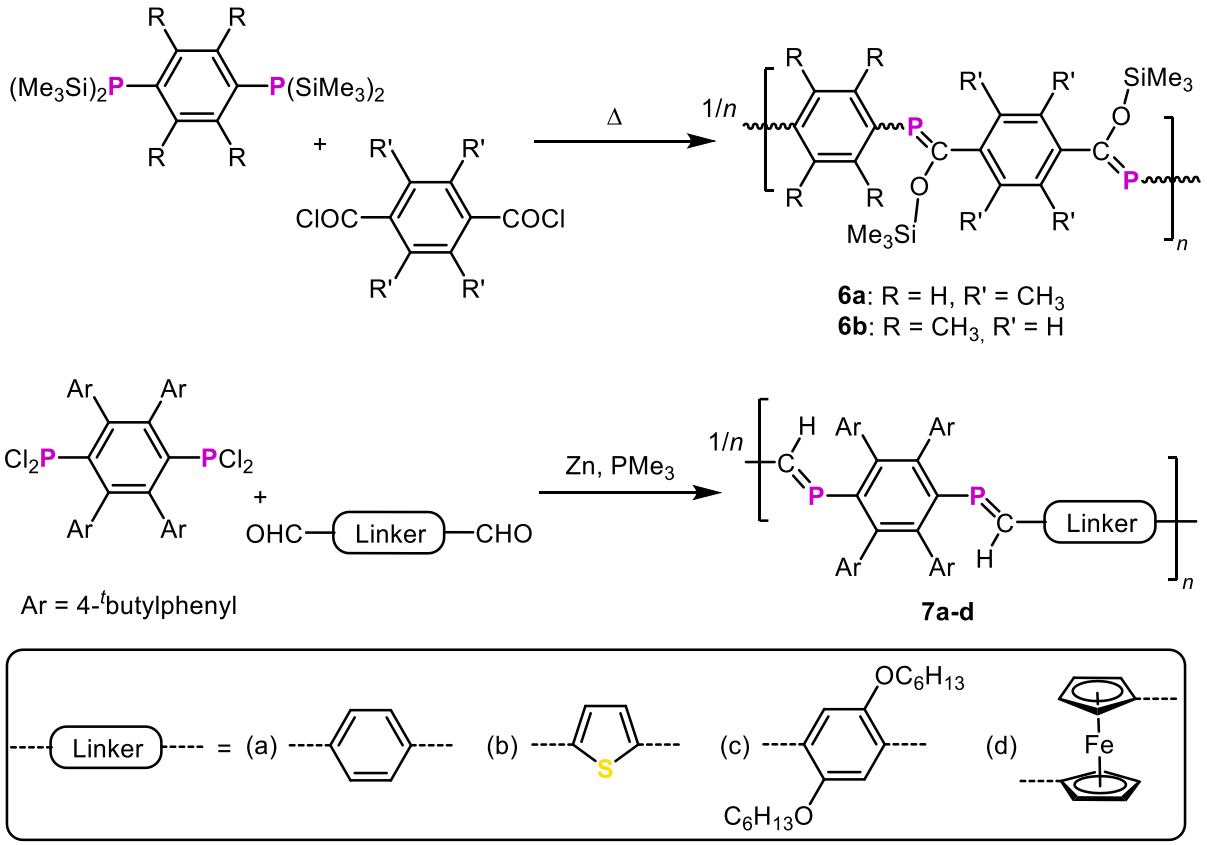

Scheme 1.1.2. Synthesis of poly(*p*-phenylene phosphaalkene)s **6** and **7**.

Protasiewicz and co-workers applied a different synthetic approach to PC-PPVs.[11b] After generation of the phospha-Wittig reagent by the reaction of a bis(dichlorophosphino)benzene derivative with PMe_3 in the presence of zinc, the further reaction with a dialdehyde yielded the predominantly *E*-configured PC-PPVs **7** (Scheme 1.1.2, bottom). They found that the polymers are weakly or non-emissive, what they attributed to fluorescence quenching by the phosphorus lone pair or the heavy atom effect.

One year later, Protasiewicz and co-worker used a similar strategy for the synthesis of diphosphene-PPVs (PP-PPV), which are the first polymers containing P=P bonds in the main chain.[11c] Either photolysis in solution or thermolysis of the neat intermediate at 250 °C were performed to obtain the respective PP-PPV **8** (Scheme 1.1.3). NMR end group analysis in conjugation with gel permeation chromatography (GPC) revealed a molecular weight of 5.9 kDa, which corresponds to a degree of polymerization (DP) of 6. No fluorescence was observed for **8**, but the absorption spectra feature a characteristic π-π* transition band at λ = 435 nm, that is, in the same range with related organic systems (λ = 426-459 nm). The presence of a second band was assigned to the n-π* transition involving the phosphorus lone pairs.

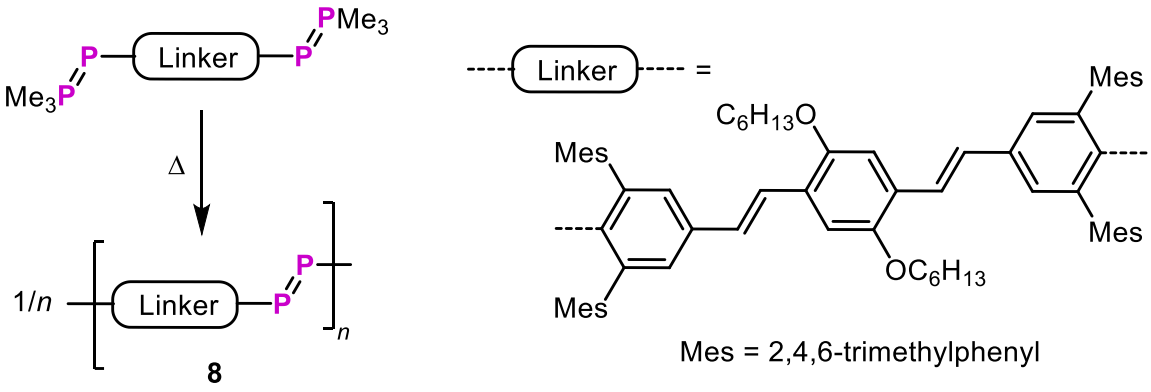

Scheme 1.1.3. Synthesis of the diphosphene-doped PPV **8**.

In 2015, Tamao, Matsuo and co-workers reported the synthesis of oligo(*p*-phenylene disilenylene)s (Si-OPV), which are Si=Si analogs of PPV.[11g] By introduction of a bulky protection group with solubilizing substituents they aimed to realize a coplanar Si-OPV. It is worth noting that small model compounds, with up to two Si=Si units and bulky silicon substituents, were already published by the group of Scheschkewitz[11e] and Tamao, Tsuji with co-workers.[11f] The Si-OPVs **9**-**12** were synthesized via one-pot reductive coupling reaction of a dibromosilane and a 1,4-bis(dibromosilyl)benzene (2:1 ratio) in the presence of lithium naphthalene (Scheme 1.1.4).

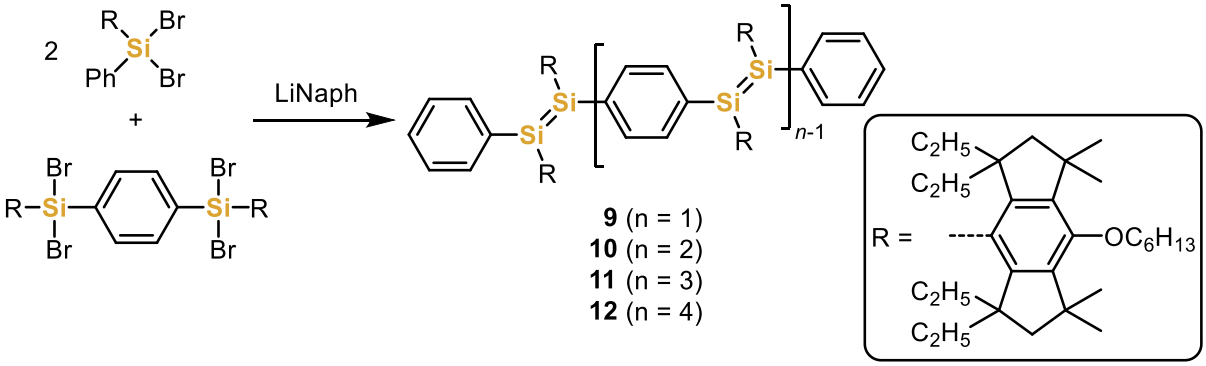

Scheme 1.1.4. Synthesis of oligo(*p*-phenylene disilenylene)s **9**-**12**.

The absorption maxima in THF solution (λ_{abs}) are bathochromic shifted with increasing chain length from **9** (465 nm) to **12** (610 nm) and were assigned to π-π^* transitions, which was also confirmed by theoretical studies. The colors of the oligomers in THF solution show a broad range from yellow to blue. The deep blue colored oligomer **12** shows a bright red fluorescence (λ_{em} = 668 nm) with a quantum yield of Φ = 48 %. Computational investigations revealed that the HOMOs are prominently located on the Si=Si bonds, while the LUMOs are delocalized over the entire Si-OPV backbone.[11g]

Recently, polymers containing heavier group 13 elements such as gallium were also studied.[14] After the first reported air stable gallium-containing polymer by Müller and co-workers in 2010,[14a] Chujo, Tanaka and co-workers reported the incorporation of gallium in the main chain of poly(*p*-phenylene) based polymers (Scheme 1.1.5).[14c] By introduction of the third aryl substituent 2,4-di-*tert*-butyl-6-[(dimethylamino)methyl]phenyl (Mamx), which internally coordinates to the gallium center, the authors were able to isolate the air stable monomer **13**. The subsequent polymerization via Yamamoto-type homocoupling led to polymer **14**, which showed good solubility in common organic solvents. UV-vis spectroscopy revealed some degree of electronic interaction through the tetracoordinate gallium centers due to the bathochromic shift of the absorption bands from **13** to **14**, which was supported by theoretical studies.

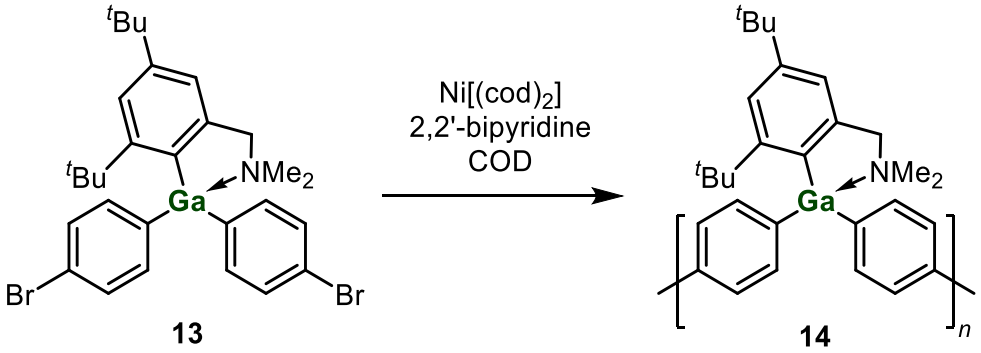

Scheme 1.1.5. Synthesis of poly(*p*-phenylene)-based polymer **14** with gallium in the main chain.

In a further study, Chujo, Tanaka and co-worker studied a series of gallafluorene-based[15] π-conjugated polymers.[14d] They demonstrated the incorporation of the gallafluorene building block **15** in a series of alternating co-polymers by palladium-catalyzed cross-coupling reactions with diverse co-monomers (Scheme 1.1.6).[14d] The air stable polymers **16** show high thermal stability with decomposition temperatures above 300 °C. GPC measurements of the co-polymers revealed number average molecular weights between 6.1 (**16f**) and 13.8 kDa (**16e**), corresponding to degrees of polymerization between 6 and 14. Depending on the respective organic co-monomer building block, the polymers showed colorful emissions over a wide range from blue to red. Except for the co-polymer **16g** with a benzothiadiazole unit, the luminescence lifetimes of the polymers were less than 1 ns, suggesting that all emissions are assigned to fluorescence processes. Electrochemical measurements revealed the presence of higher HOMO energy levels for the gallafluorene-containing polymers than analogous fluorene-based polymers, thus the authors suggested the gallafluorene unit could work as an electron-donating group in polymer backbones.

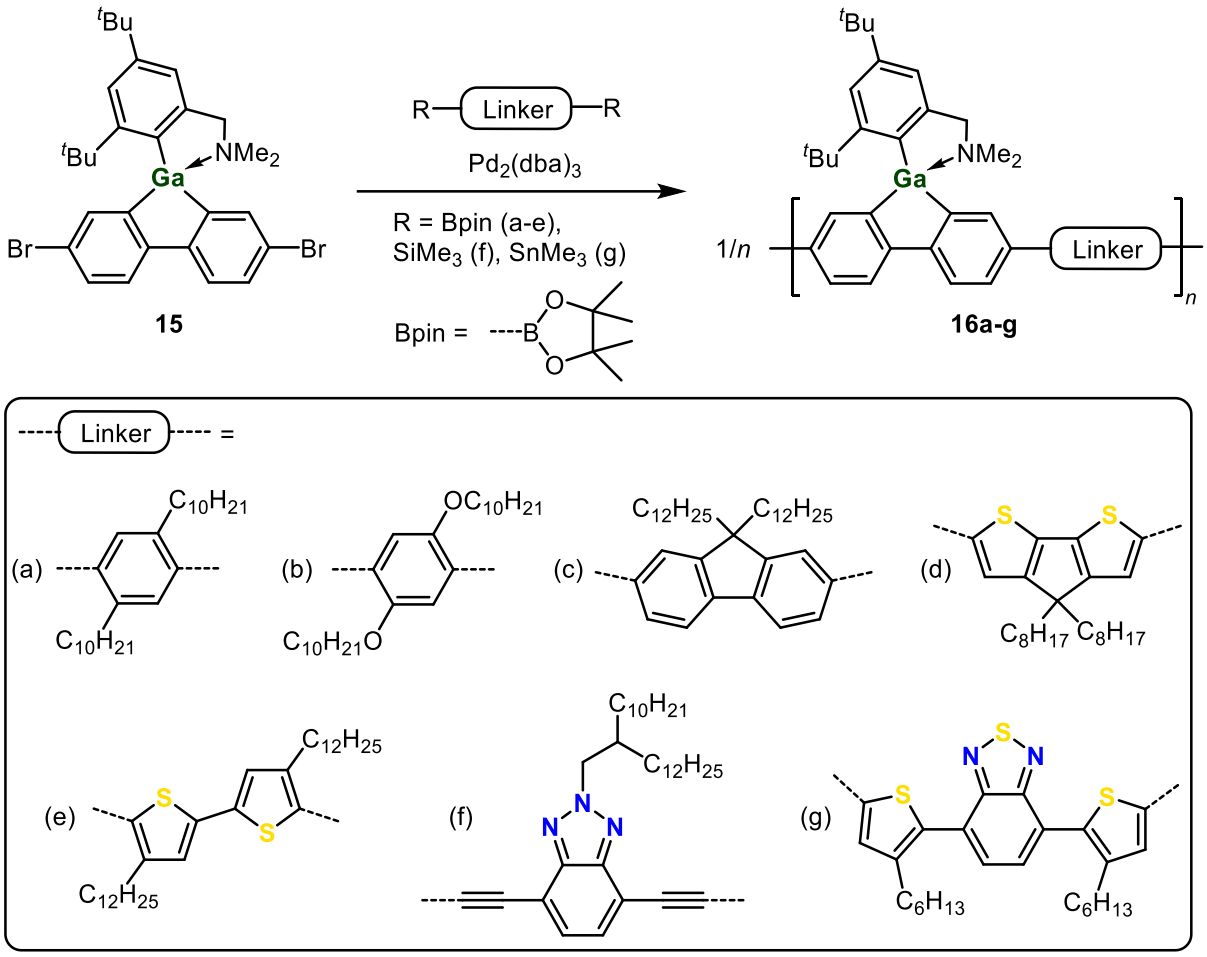

Scheme 1.1.6. Synthesis of co-polymers **16** comprising gallafluorene units by Pd-catalyzed cross coupling.

1.2 Conjugated Organoborane Polymers

The lightest group 13 element boron offers exciting opportunities, especially if it is embedded into the backbone of a π-conjugated polymer via the vacant p-orbital.[16] In the past, the applicability of tricoordinate boron was limited due to intrinsic susceptibility of the boron centers towards small nucleophiles such as oxygen and water. The nucleophilic attack would cause a tetrahedral geometry and loss of the π-conjugation, thus, three methods were developed to protect the vacant p-orbital of the boron centers (Figure 1.2.1). The boron center can be stabilized by sterically demanding substituents (kinetic stabilization, **I**),[17] embedding into a rigid, planar structure to prevent the formation of a tetrahedral structure (**II**),[17d,18] or attaching a π-donor substituent such as an amino group (**III**).[17d] The latter could result in a loss of π-conjugation between the organic π-systems and the boron center by partial double-bond formation.

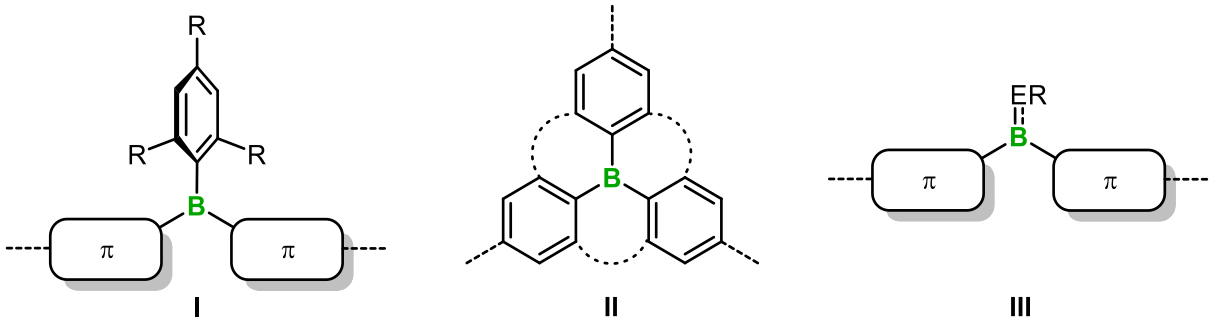

Figure 1.2.1. Stabilization types of tricoordinate boron.

In general, the synthesis of organoboron polymers follows one of three possible synthetic approaches: B–C coupling, C–C coupling, and B–E coupling (E denotes another hetero element such as nitrogen or oxygen). While the first two cases are briefly discussed in this part, the B–E coupling route was the main approach in this thesis and is mentioned in sections 1.4 and 1.5.

In the 1990s, Chujo and co-workers presented various conjugated organoborane polymers via B–C coupling reactions, which followed a polyaddition step-growth process (Scheme 1.2.1). In 1990, they reported the haloboration polymerization of tribromoborane and 1,7-octadiyne.[19] The resulting polymer **17** was poorly stable due to the remaining B–Br bonds. The stability of the polymers can be significantly increased when the diyne species is reacted with a diarylhaloborane in a haloboration-phenylboration polymerization to give **18**.[20] Due to the lower reactivity of the borane, these reactions only proceeded at elevated temperatures.

Chujo and co-workers also succeeded in the synthesis of poly(vinylene-arylene-vinylene borane)s using the regioselective hydroboration of diethynylarenes with mesitylborane ($MesBH_2$, Mes = 2,4,6-trimethylphenyl).[21] Some years later they managed to polymerize di-

ethynylarenes with the more sterically demanding $TipBH_2$ (Tip = 2,4,6-triisopropylphenyl) which further enhances the stability of the boron centers by kinetic stabilization.[22]

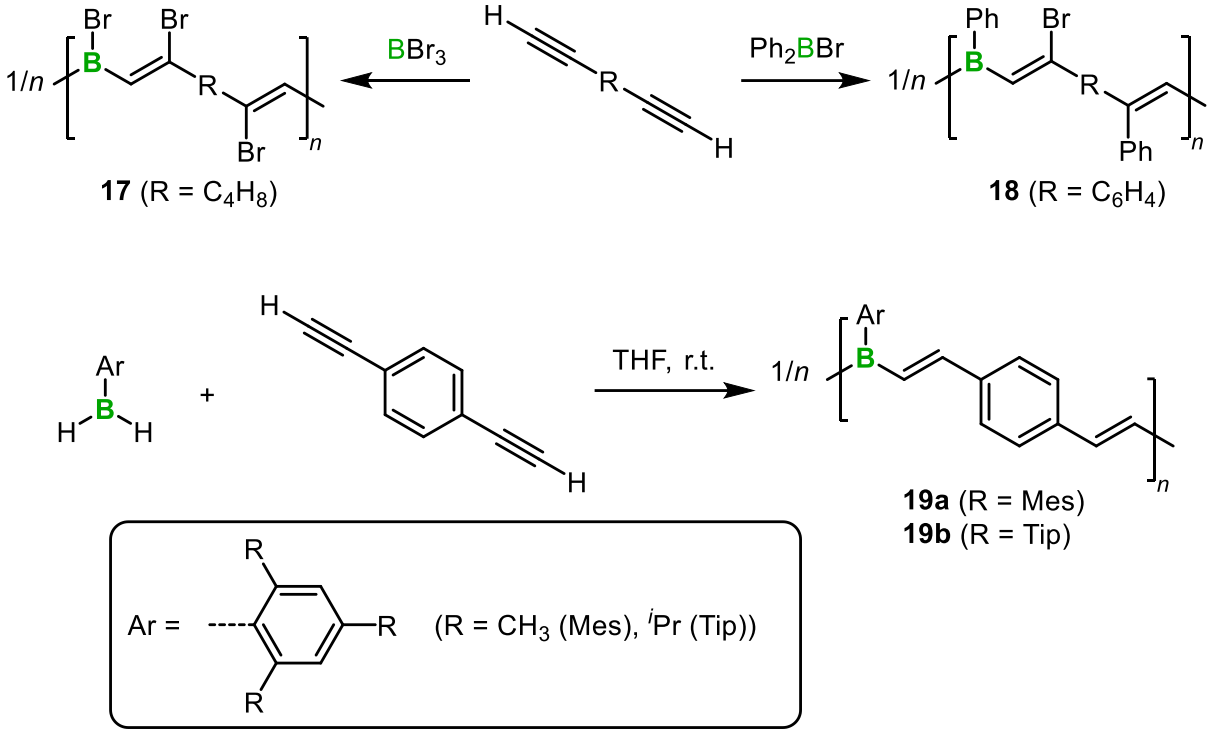

Scheme 1.2.1. Synthesis of organoboron polymers **17**-**19** by polyaddition of boranes and dialkynes.

The hydroboration polymerizations were performed in THF at ambient temperature and the polymers **19a** and **19b** showed good stability towards air and moisture and were readily soluble in common organic solvents.[21a,22] The photophysical characteristics of **19a** revealed a large bathochromic shift of the absorption band compared to a related molecular model compound, which indicates effective π-conjugation along the backbone.[21a] Polymer **19a**, furthermore, showed a strong blue fluorescence (λ_{em} = 441 nm) and replacement of the phenylene group by heteroarenes further red-shifted the emission maxima.[21b] Addition of electron-donating substituents at the phenylene unit of **19b** resulted in bathochromic shifts of the absorption and emission spectra.[22]

Recently, Qin and co-workers presented the first examples of main-chain boron containing conjugated polymers without aromatic moieties in the polymer backbone.[23] The boron doped polyacetylenes (BPA) **20** can be considered as polyacetylenes in which every fourth C=C double bond is replaced with a C–B single bond. The BPAs were synthesized according to the previously described procedure via hydroboration polymerization in THF at room temperature (Scheme 1.2.2).

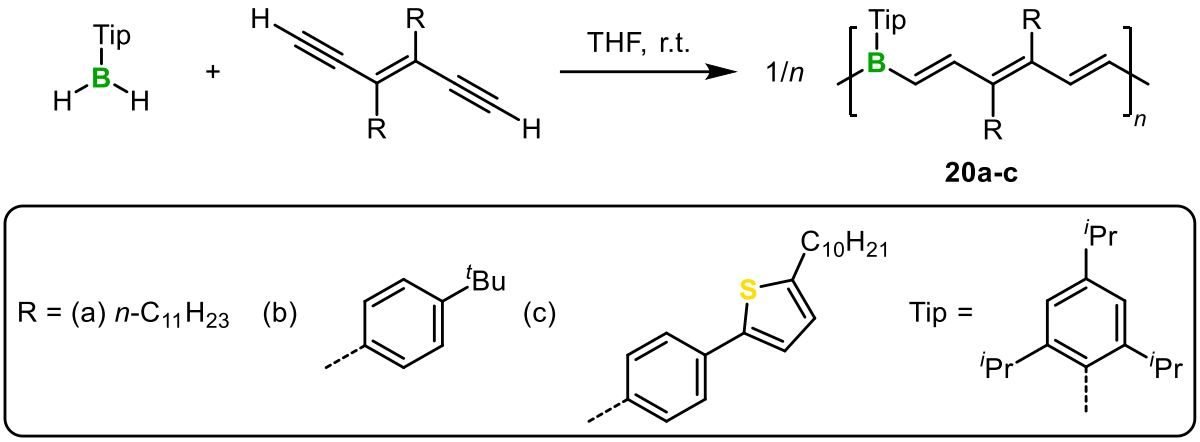

Scheme 1.2.2. Hydroboration polymerization to boron-doped polyacetylenes **20**.

The absorption maximum (λ_{abs}) of **20** in THF redshifts with increasing conjugation lengths of the side chain (442 (**20a**) < 452 (**20b**) < 464 nm (**20c**)). All polymers were fluorescent, but only **20a** showed a significant quantum yield of Φ = 25 %. During solvent dependent studies, Qin and co-workers also observed bathochromic shifts with increasing solvent polarity, which indicates better stabilized charge transfer excited states. While polymers **20** were stable in anhydrous solvents under inert atmosphere for 3 weeks, they gradually decomposed in wet THF in air.[23]

While hydroboration polymerizations seemed very promising for the synthesis of B-vinyl linked polymers, they are not suitable to access B-aryl or B-alkynyl linked polymers. A useful synthetic approach for latter two are polycondensation reactions either via B–C or C–C coupling, which can be divided into AA/BB type or AB type reactions. Chujo and co-workers reported on the successful synthesis of poly(phenylene borane)s[24] and poly(ethynylene-phenylene-ethynylene borane)s[25] by polycondensation reactions (B–C coupling) of aryldimethoxy-boranes with bifunctional Grignard reagents or bifunctional lithium acetylides, respectively. Jäkle and co-workers developed a particularly efficient approach to gain access to various organoborane macrocycles and polymers by making use of the Sn/B exchange condensation approach.[26] However, the pronounced toxicity of the organotin compounds involved resulted in the development of a new synthetic approach to avoid this issue.

Helten and co-workers used the less toxic organosilicon compounds for the controlled synthesis of π-conjugated organoborane compounds such as poly(thienylborane)s and poly(furylborane)s.[27] Compared to Sn/B exchange reactions, Si/B exchange reactions proceed significantly slower. While $ArSnMe_3$ species react readily with $ArBBr_2$ at room temperature to diarylhaloboranes, their related silyl congeners ($ArSiMe_3$) show no reaction with $PhBBr_2$ at this condition.[26e] In order to ensure the diarylation of the respective borane via the Si/B exchange reaction, they effectively catalyzed the reaction with the electrophilic silyl reagent Me_3SiNTf_2 (Scheme 1.2.3, Tf = SO_2CF_3).

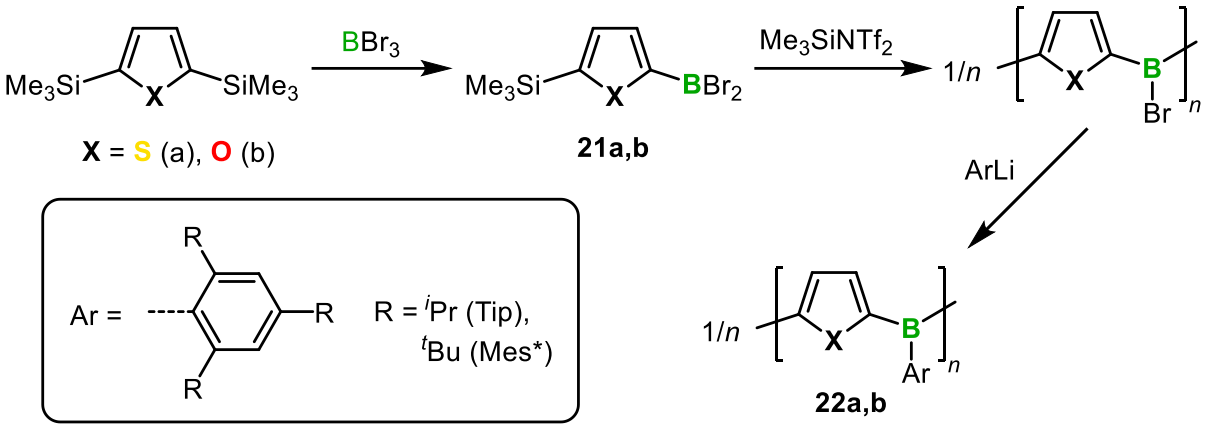

Scheme 1.2.3. Catalyzed Si/B exchange approach to polymers **22** (Tf = SO_2CF_3).

After complete polymerization they accomplished to postmodify the obtained polymers by introducing different sterically demanding substituents, to access air and moisture stable organoborane polymers **22**. The lower reactivity of the Si/B exchange reaction allowed the selective synthesis of AB type monomers **21**, which are very desirable for AB type polycondensations as they are not dependent on the exact stoichiometry of the monomers (Scheme 1.2.3). Helten and co-workers used the Si/B exchange approach for the synthesis of several mixed organoboranes and oligomers.[28]

The synthesis of organoboron polymers via C–C coupling polymerizations are generally performed by transition metal catalyzed cross-coupling protocols.[26i,29] Thus, reactants with a kinetically stabilized boron center, to endure the generally harsh reaction conditions, are required. Wagner, Jäkle and co-workers reported about air and water stable π-conjugated organoborane polymers containing both thiophene and 9,10-dihydro-9,10-diboraanthracene units.[29a] The donor-acceptor-type polymers **23** were prepared through Stille-type C–C coupling protocols, and the polymer features mesityl groups as bulky substituents on boron (Scheme 1.2.4). Due to infeasible separation of two positional isomers of the 9,10-diboraanthracene monomer, they did not obtain a defined polymer. However, **23** shows a dark orange fluorescence with a quantum yield of Φ = 47 % in benzene.

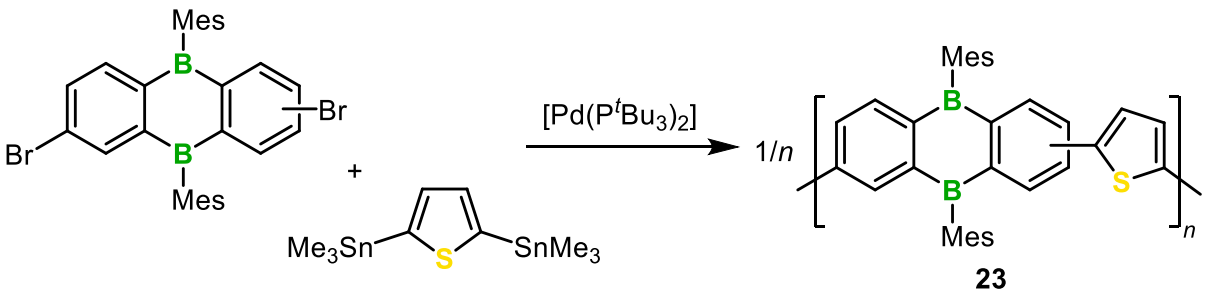

Scheme 1.2.4. Synthesis of polymer **23** by Stille cross-coupling (Mes = 2,4,6-trimethylphenyl).

In another study, Jäkle and co-workers presented a series of poly(oligothiopheneborane)s (**24a**-**28a**) featuring m = 1 to 5 thiophene units in their repeat unit.[26i] Recently, a series of poly(oligofuranborane)s (**24b**-**28b**) with 1 to 5 furan moieties in the repeat unit was published by Helten and co-workers.[29e] Both organoboron polymer classes were accessed via a microwave irradiation-assisted Stille-type catalytic cross-coupling polycondensation reaction in the presence of palladium(0) (Scheme 1.2.5). For m = 1, they applied their Sn/B exchange[26] (**24a**) or Si/B exchange[27,28a] (**24b**) polycondensation protocol, respectively. Both groups introduced a hexyl group on the central chalcogen ring for m = 5 for better solubility of the resulting polymer.

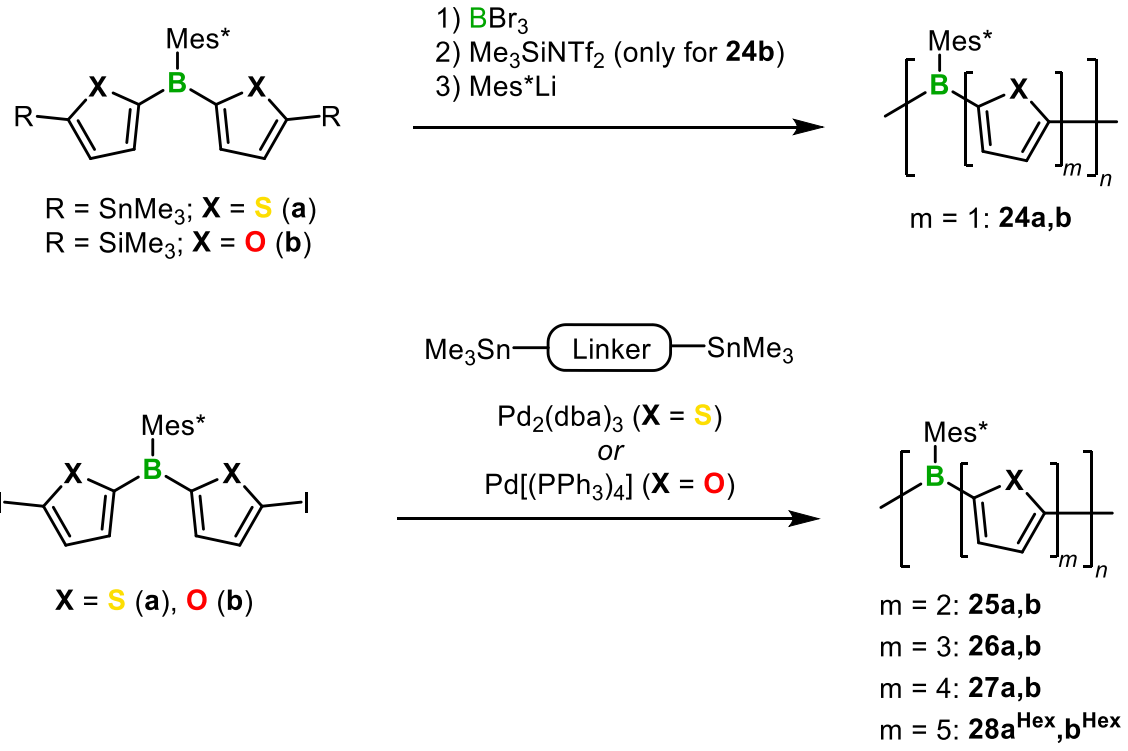

Scheme 1.2.5. Synthesis of poly(oligothiopheneborane)s **24a**-**28a** and poly(oligofuranborane)s **24b**-**28b** (hexyl groups of **28a**^{Hex} and **28b**^{Hex} are omitted for clarity).

Both, **24a**-**28a** and **24b**-**28b** showed long-term chemical stability to air and moisture and thermal stability up to around 300 °C. All polymers were isolated as light yellow (**24a**,**b**) to red solids (**28a**,**b**) and were soluble in common organic polar solvents such as THF and $CHCl_3$. All polymers show intense fluorescence in THF with quantum yields up to Φ = 38 % for the

dithiophene-bridged (**25a**, m = 2) and up to Φ = 87 % for the difuran-bridged polymers (**25b**, m = 2). They show bathochromic emissions from blue to deep orange by increasing the length of the π-conjugated oligothiophene and -furan linker between the boron atoms.

Very recently, Jäkle and co-workers also prepared aryl-bis(thienylborane)s where the 3-position of the thiophenes are attached to the boron atom.[29f] Polymers featuring three thiophene units in between the boron centers were synthesized via Stille-type polymerization. In THF solution the absorption and fluorescence maxima of the 3-thienylborane polymers were blue-shifted compared to the 2-thienylborane polymers, which is indicative of less effective extension of conjugation between the thiophene linkers and boron centers for the 3-thienylborane polymers.[29f]

1.3 Inorganic Polymers

Polymers with a backbone composed of exclusively main group elements are termed “inorganic polymers”, and they offer a variety of useful properties that complement those of organic materials.[6c,6f,30] The possibility to functionalize them with different (organic) side groups can lead to a broad range of expanded material properties and applications. Most reactions in inorganic chemistry are based on stoichiometric reactions, but initiated or catalytic procedures are of increasing interest, e.g. for the synthesis of inorganic polymers.[31] In the following part, the well-known examples polysiloxanes (**I**), polysilanes (**II**), poly(phosphazene)s (**III**), and poly(phosphinoborane)s (**IV**) will be briefly discussed.

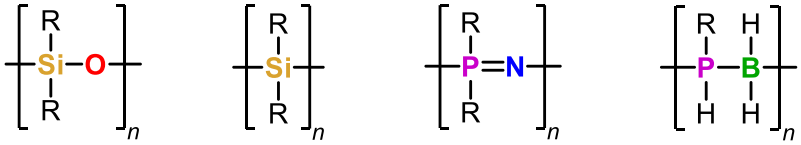

Figure 1.3.1. Inorganic polymers: polysiloxanes (**I**), polysilanes (**II**), poly(phosphazene)s (**III**), and poly-(phosphinoborane)s (**IV**).

The most prominent examples of inorganic polymers are polysiloxanes (Figure 1.3.1, **I**), also known as silicones, with a backbone of alternating silicon and oxygen atoms. Strong Si–O bonds and the flexible Si–O–Si linkages in the polymer chain feature low-temperature flexibility and high thermal stability.[32] Due to their inertness and chemical stability, polysiloxanes are often used in various medical applications such as implants, catheters and contact lenses.[33] In combination with organic electronic groups, polysiloxanes are also useful for optoelectronic applications.[34] Main methods for the synthesis of linear polysiloxanes are polycondensations of dichlorosilanes and ionic-initiated ring-opening polymerizations of cyclic siloxanes.[30a,33b,35] The $B(C_6F_5)_3$-catalyzed Piers–Rubinsztajn reaction has been used to significantly expand the range of polysiloxanes **29**, by coupling of alkoxysilanes and hydrosilanes (Scheme 1.3.1).[36] This reaction also enables the synthesis of alternating co-polymers,[36c,37] 3D architectures,[38] and silicone resins.[39] Recently, Shimada and Sato with co-workers reported the one-pot synthesis of oligosiloxanes by a highly selective and sequence-controlled iteration of a catalyzed hydrosilylation and the Piers–Rubinsztajn reaction.[40]

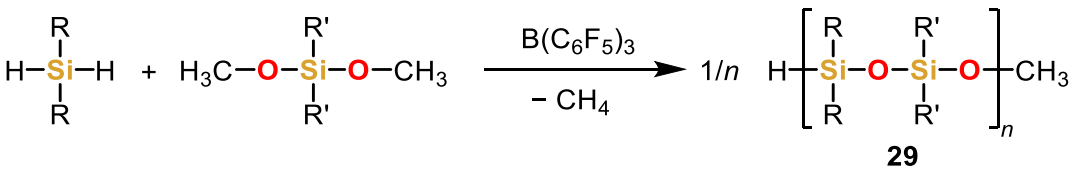

29

Scheme 1.3.1. General synthesis of polysiloxanes by the Piers-Rubinsztajn polymerization method.

Polysilanes are inorganic, homoatomic polymers featuring a backbone composed of exclusively silicon atoms (Figure 1.3.1, **II**). Research into this class started in the 1920s with the reports of Kipping about the reaction of dichlorodiphenylsilane with elemental sodium.[41] Over 50 years later, West and co-workers reported the Wurtz-coupling co-condensation of two dichloro(organo)silanes to yield the first solution-processible polysilanes, which become semiconducting upon contact with strong electron acceptors.[42] However, the harsh conditions of the Wurtz coupling route often lead to multimodal and broad molecular weight distributions and the formation of cyclic by-products.[43] Thus, research moved towards alternative routes to catenated silanes, such as catalytic dehydrocoupling[44] and anionically initiated routes.[6c,45] The first example of controlling the stereochemistry of polysilanes was reported by Sakurai and Sanji with co-workers.[46] By the *n*-BuLi-initiated anionic ring opening polymerization (ROP) of masked disilenes, highly ordered poly(aminosilane)s were obtained (Scheme 1.3.2). The reaction with acetyl chloride led to a chloride derivative **30**. This enables further reaction with nucleophiles to various polysilanes **31**, which are inaccessible otherwise.

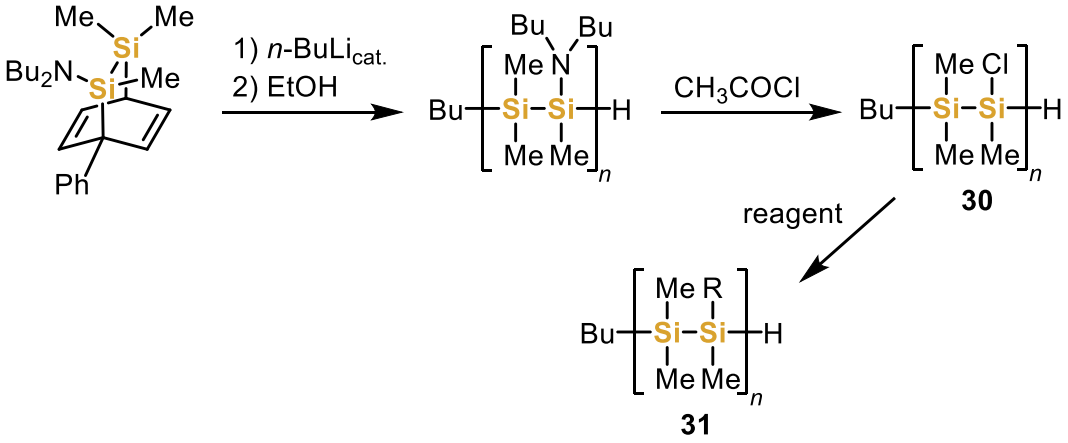

Scheme 1.3.2. Synthesis of polysilanes by anionic ROP of a masked disilene, followed by side chain functionalization with Grignard or lithium organyl reagents (R = alkyl, aryl).

Polysilanes show σ-conjugation along their Si-backbone, enabling their application in electronic applications.[47] Very recently, Klausen and co-workers reported Si-rich polymers, which show distinctive force-coupled extensional behavior in single polymer chains.[48] Thus, they proposed that incorporation of catenated Si-atoms into polymer backbones could also modify the mechanical properties of bulky polymer networks.

Polyphosphazenes, polymers with an inorganic backbone composed of alternating phosphorus and nitrogen atoms, are one of the best studied classes of inorganic polymers (Figure 1.3.1, **III**).[49] After the first report of "inorganic rubber" by Stokes in the 1890s, Allcock extensively explored this polymer class in the second half of the last century.[50] A traditional method to synthesize polyphosphazenes **35** is the thermal ROP of hexachloro-cyclotriphosphazenes **32** $(NPCl_2)_3$ (Scheme 1.3.3, top). After heating $(NPCl_2)_3$ under anhydrous conditions, linear, soluble, and high molecular weight polymers can be obtained. Organic substituents are typically introduced upon nucleophilic substitution of the chlorinated polymers **34**. It was proposed that Stokes' "inorganic rubber" material was a cross-linked polymer, due to hydrolysis of P–Cl bonds by followed condensation of resulting P–OH moieties.[49c] A modern method to synthesize polyphosphazenes is the PCl_5-initiated living cationic chain growth polycondensation of phosphoranimines (Scheme 1.3.3, bottom).[51] In the presence of traces of the initiator PCl_5, (trimethylsilyl)phosphoranimine **33** can be polymerized to the corresponding polyphosphazene **34**. Molecular weights can be controlled by varying the monomer to initiator ratio.

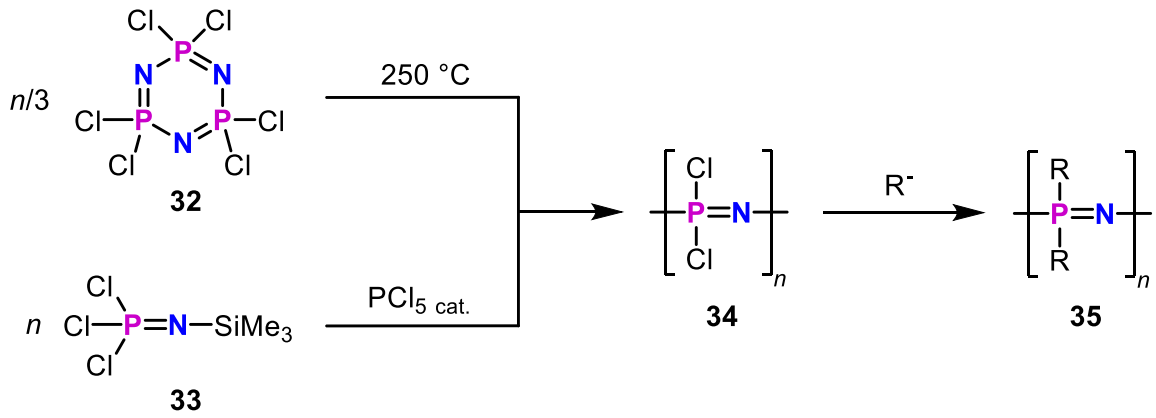

Scheme 1.3.3. Synthesis of polyphosphazenes **35** by thermal ROP of **32** and PCl_5-initiated cationic living polycondensation of phosphoranimines **33**.

Through the possibility to introduce various organic side groups to the phosphorus atoms, poly(organo)phosphazenes are suitable for a wide range of applications, such as biomedicals,[52] flame retardants,[53] and as components of solar cell and battery electrolyts.[54] Block co-polymers of polyphosphazenes are also of great interest in self-assembly studies.[55]

In 1999, the first well-definded poly(phosphinoborane)s (Figure 1.3.1, **IV**), comprising a backbone of exclusively boron and phosphorus atoms, were reported by Manners and co-workers.[56] Based on the work from others,[57] they obtained an air and moisture stable poly(phosphinoborane) **36** after dehydrocoupling of a primary phosphine-borane ($PhPH_2 \cdot BH_3$), in presence of a rhodium(I) catalyst at elevated temperatures (Scheme 1.3.4). A broad field of potential applications are reported for poly(phosphinoborane)s, such as lithography,[58] swellable gels,[59] flame-retardants,[60] and precursors for boron phosphides.[61] The use of aluminum,[62] iridium,[63] or iron[64] catalysts and metal-free routes[65] also proved to be suitable for poly(phosphinoborane) synthesis. An iron catalyst was described to provide linear and high polymers of significantly lower polydispersity.[66] In the same work, Manners and co-workers also demonstrated the post-functionalization of poly(phosphinoborane)s by Sonogashira coupling, which enables the development of more complex P–B based materials.[66] Very recently, Manners and Weller with co-workers reported the synthesis of poly-(phosphinoborane) block co-polymers, which show self-assembly to well-defined micellar structures in solution.[67]

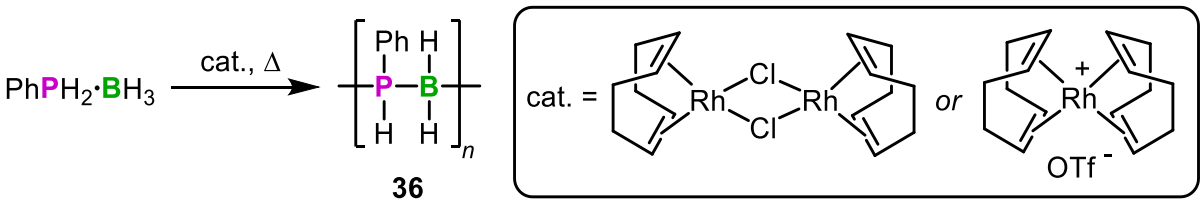

Scheme 1.3.4. Synthesis of poly(phosphinoborane) **36** by the Rh(I)-catalyzed dehydrogenation of phosphine-boranes (Tf = SO_2CF_3).[56]

1.4 Inorganic Polymers Comprising a Boron-Nitrogen Main Chain

Making use of their isoelectronic and isosteric relationship, the replacement of C=C units by B=N units is an emerging strategy to alter the electronic and optical properties while maintaining the basic structure of materials.[68] The B–N bond has a significant double bond character due to π-bond contributions of the filled nitrogen p_π-orbital into the empty p_π-orbital of boron. Due to the difference in electronegativity between boron and nitrogen, the σ-bond is polarized towards nitrogen which decreases the polarization induced by the π-contribution. The dipole moment results from these two opposing forces which lead to the addition of a negative-formal or positive-partial charge to boron and a positive-formal or negative-partial charge to nitrogen, respectively (Figure 1.4.1).

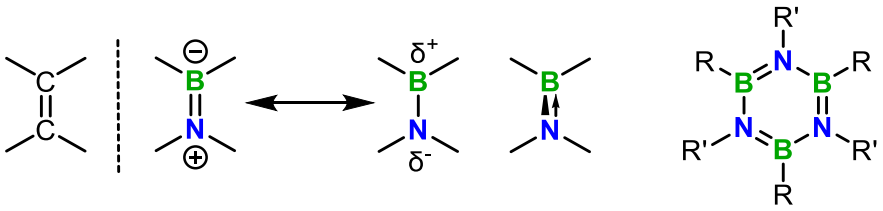

Figure 1.4.1. Isoelectronic relationship between C=C and B=N units and the BN/CC benzene analog borazine (in this work the formal charges are omitted for clarity).

The discovery of borazine by Stock and Pohland in 1926,[69] which is commonly referred to as "inorganic benzene", led to the concept of BN/CC isosterism. According to the current understanding, borazine has a significantly lower aromatic character than its organic all-carbon analog benzene (Figure 1.4.1).[70]

Polymers comprising a saturated backbone of only tetracoordinated boron and nitrogen atoms are known as poly(aminoborane)s (PAB).[71] Through their isoelectronic structure to polyolefins, PABs have become of general interest in the fields of BN containing materials and inorganic chemistry.[72] In the past the synthesis of PABs was often carried out via thermal methods,[73] the recently published approaches are usually metal-catalyzed dehydro-polymerizations.[71,74]

The first well-characterized PABs were presented by Manners and co-workers in 2008, synthesized by iridium-catalyzed dehydrocoupling of amine-borane adducts.[75] While they obtained a mixture of borazines and insoluble oligomeric materials with a rhodium catalyst, the use of iridium in catalytic amounts led to the formation of soluble and high polymers **37a**,**b** (Scheme 1.4.1). Wide-angle X-ray scattering and thermogravimetric analysis (TGA) measurements led them to interpret **37c** as a predominantly linear PAB. Significant progress has been made since the report of Manners and co-workers[75] with various transition metal (pre)catalysts for dehydrocoupling, based on rhodium,[76] iron,[77] titanium,[78] zirconium,[79] and cobalt.[80] Furthermore, also noncatalytic routes have been reported from multiple groups.[49a,81]

Manners and co-workers also reported catalytic depolymerizations of PABs.[82] Such processes have become increasingly important from an ecological point of view due to generation of million tons of plastic waste.[83]

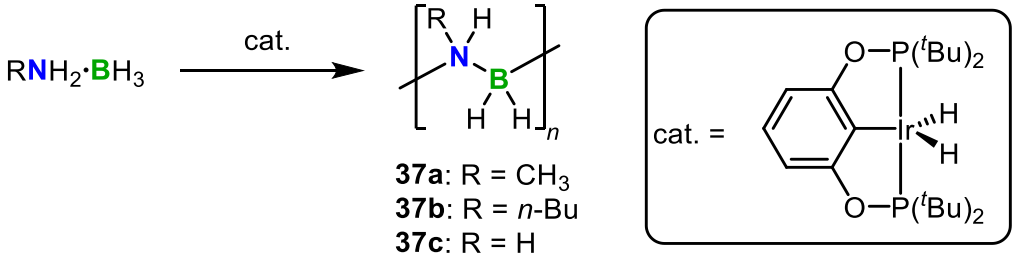

Scheme 1.4.1. Synthesis of the first well-characterized poly(aminoborane)s **37a**-**c** by Ir-catalyzed dehydrocoupling.

The first kinetically stable iminoborane (RN≡BR') was reported by Paetzold and co-workers in 1984.[84] Decades later, the formation of molecular iminoborane intermediates is still present in recent research.[85] However, upon their extensive research on generating iminoborane monomers in the 1980s, Paetzold and co-workers obtained in some cases insoluble waxy materials for which they proposed the constitution of linear poly(iminoborane)s (PIB), which are polyacetylene isosteres.[86] They made their assumption based on mass spectrometry, elemental analysis and transformation of one polymer into the corresponding borazine. In literature, the term "polyiminoborane" is often found in combination with the pyrolysis of ammonia-borane.[87] During the dehydrogenation process, an insoluble solid is formed as intermediate which has the approximate composition of $[HNBH]_n$. More recent studies have revealed that its constitution can be described as a poorly defined network of partially fused borazine rings and thus is probably better described as polyborazylene.[[87b,87d] However, the main obstacle in the synthesis of linear PIBs is the undesired formation of cyclic species, e.g. dimer or trimer, from monomeric iminoborane starting materials (Scheme 1.4.2).[88]

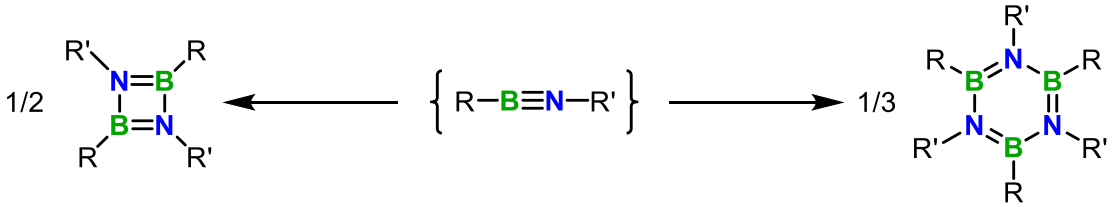

Scheme 1.4.2. Possible formation of dimer (left) and trimer (right) by cyclo-oligomerization of unstable iminoboranes.

Recently, Helten and co-workers achieved the first synthesis of well-characterized linear PIBs by preventing the formation of cyclic by-products such as borazine.[89] Therefore, they used the concept of linking adjacent nitrogen atoms by a hydrocarbon bridge, to obtain 1,3,2-diazaborolidine monomers.[90] The cyclolinear PIBs were synthesized by Si/B exchange poly-

condensation (B-E coupling) of 1,3-bis(trimethylsilyl)-1,3,2-diazaborolidines with various dichloroboranes under mild conditions (Scheme 1.4.3). In one of these studies, Helten and co-workers also reported on the synthesis of an AB-monomer which was polymerized in the presence of Brønsted acids to the corresponding PIB.[89b]

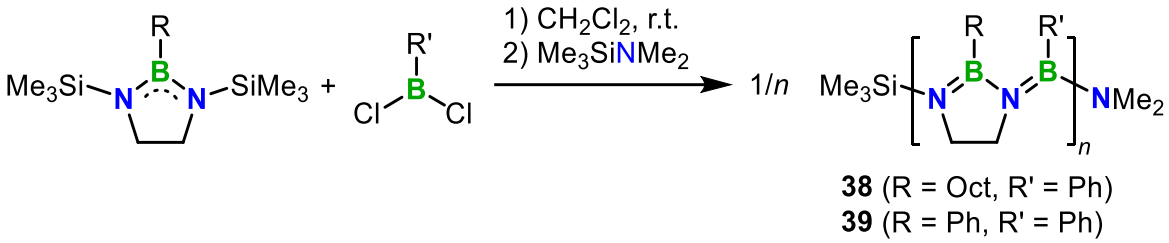

38 (R = Oct, R' = Ph)
39 (R = Ph, R' = Ph)

Scheme 1.4.3. Synthesis of cyclolinear poly(iminoborane)s **38** and **39** by Si/B exchange polycondensation.

The glass transition temperature of the PIBs systematically increased with the aryl group content. The residual mass after thermal gravimetric analysis (TGA) suggested that these PIBs are of possible interest as preceramic polymers, due to good agreement with theoretical values. Mass loss occurs in two steps: While in the first step the side chains are expulsed, in the second one the cleavage of ethylene bridges is observed, which demonstrates its stabilizing effect. The closest approach to PIBs is **38** with an average of 18 catenated BN units. In general, the incorporation of organic side groups resulted in good solubility in common organic solvents. Only the all-phenyl derivative **39** turned out to be insoluble in all used solvents, which points to a pronounced degree of crystallinity. So far, the knowledge of the microstructures of cyclolinear PIBs in the solid state is limited but some linear molecular compounds with limited number of concatenated B=N units are known.[91] However, in many cases the BN chains are embedded in fused polycyclic molecular frameworks.[92] Braunschweig and co-workers reported on linear BN chains with up to two B=N units in the coordination sphere of different metals such as ruthenium,[93] platinum[94] and tungsten.[95]

1.5 Boron-Nitrogen-Doped Conjugated Polymers

The incorporation of BN units in specific positions of polycyclic aromatic hydrocarbons (PAH) has evolved into a viable concept to modify the electronic and photophysical properties compared to the parent carbonaceous systems.[96] The application of this concept in conjugated polymers has been less extensively explored so far and is still in its infancy.[6e,16g,97] In 1962, Mulvaney and co-workers achieved the synthesis of the first π-conjugated polymers featuring B=N units in their main chain.[98] These polymers, featuring 1,3,2-benzodiazaboroline building blocks, were synthesized by the polycondensation of diboronic esters with 3,3'-diaminobenzidines above 200 °C. The macromolecular character was explored by viscosity measurements of their solutions, and some of the polymers were thermally stable up to 500 °C. Yamaguchi and co-workers reported related 1,3,2-benzodiazaboroline containing polymers, which were synthesized by Stille polycondensation under milder conditions (Scheme 1.5.1).[99]

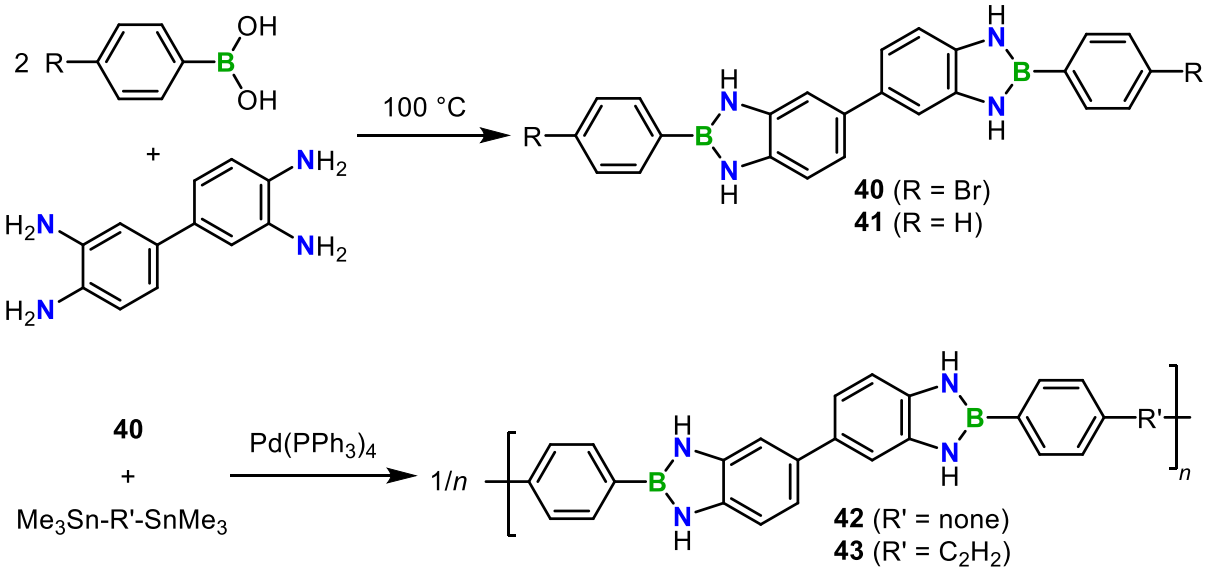

Scheme 1.5.1. Synthesis of 1,3,2-benzodiazaboroline-based oligomers **40** and **41** by thermal polycondensation and polymers **42** and **43** by Stille-coupling polycondensation.

The absorption maximum of the polymers **42** (349 nm) and **43** (358 nm) in solution shows a slight red-shift compared to that of model compound **41** (329 nm). This points to an extension of the conjugation path over the diazaboroline units along the polymer chain. In a thin film, the absorption maximum further shifted to longer wavelength (395 nm) for **42**, which was assigned to π-stacking of the polymer in the solid state.

Yamamoto and co-workers published the first incorporation of 1,3,2-benzodiazaboroline units into a polymer backbone across the 4,7-positions of the benzo core.[100] First, they synthesized a π-conjugated poly(*p*-phenylene) type main chain polymer **46** by the palladium(0) catalyzed polycondensation of a dibromo phenylenediamine species **44** and a diborylated fluorene **45**.

By further reaction with aromatic boronic acids, **46** was transformed to the benzodiazaboroline-based polymers **47**, by subsequent modification of the polymer backbone (Scheme 1.5.2).

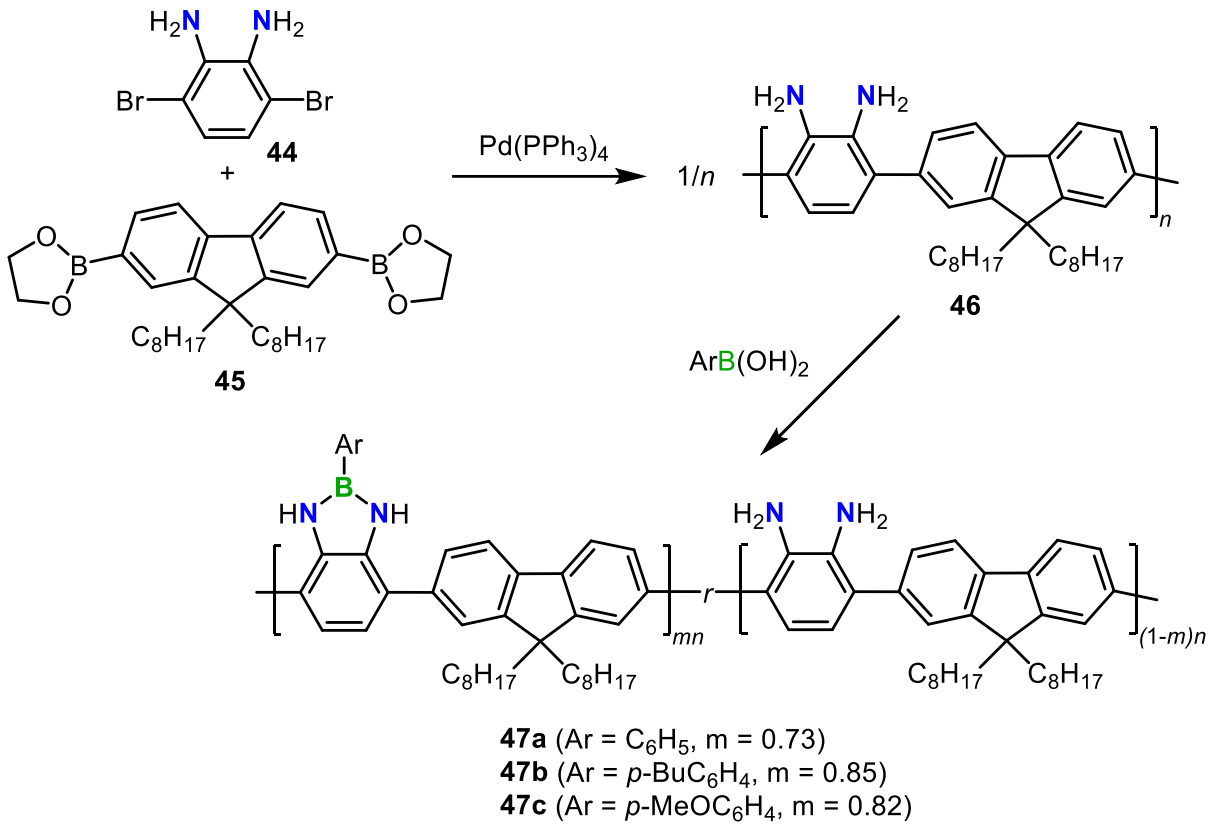

47a (Ar = C_6H_5, m = 0.73)
47b (Ar = *p*-BuC_6H_4, m = 0.85)
47c (Ar = *p*-$MeOC_6H_4$, m = 0.82)

Scheme 1.5.2. Synthesis of polymer **47** by Pd-catalyzed cross-coupling and subsequent modification of the backbone.

The degree of the diazaborole group formation was estimated to 73–85% by NMR spectroscopy. Polymerizations between a preformed benzodiazaboroline unit and **45** did not lead to the desired product due to diazaborole-ring cleavage under the basic reaction conditions. The thermal stability of **47** (395–428 °C) shows an improvement compared to **46** (372 °C). The comparison of the weight-average molecular weights obtained by GPC analysis (chloroform or THF) and static light scattering measurements (toluene) revealed the formation of larger aggregates in toluene solution. All polymers show a blue emission when irradiated with UV light and the introduction of the diazaborole side chain increases the quantum yield from Φ = 11 % (**46**) to Φ = 48 % (**47b**). A related donor-acceptor type 1,3,2-benzodiazaborole-based co-polymer was prepared by Hayashi and co-worker via electro-polymerization.[101]
Lee and co-workers were able to directly polymerize 1,3,2-benzodiazaboroline units across the 4,7-positions of the benzo core with a further co-monomer.[102] By introduction of sulfonate side chains they obtained a water-soluble polymer, which can operate as a selective turn-off fluorescence sensor for cyanide anions in water. However, related polymers linked via the

nitrogen atoms of 1,3,2-benzodiazaboroline building blocks along the main chain are still unknown.

Chujo and co-workers reported a series of polymers with linear NBN[103] or B=N[104] units in their main chain. Through alkoxyboration polymerization of aromatic diisocyanates with various borane reagents, poly(boronic carbamate)s such as air-stable **48** were prepared (Scheme 1.5.3).[103] Attempts to synthesize defined co-polymers in a one-pot reaction of diynes, diisocyanates and $PhBCl_2$ by utilizing the different phenylboration and haloboration reactivities were not successful and resulted in random co-polymers. In a stepwise procedure, **49** was obtained after twofold bromoboration of a diyne monomer under mild conditions. Subsequently, the reaction with a diisocyanate afforded the alternating co-polymers **50** with B=N units in the backbone (Scheme 1.5.3).[104] According to UV-vis data only a poorly extended conjugation was implied for **50**, which is presumably due to interruption of the effective conjugation by the presence of the amide moieties.

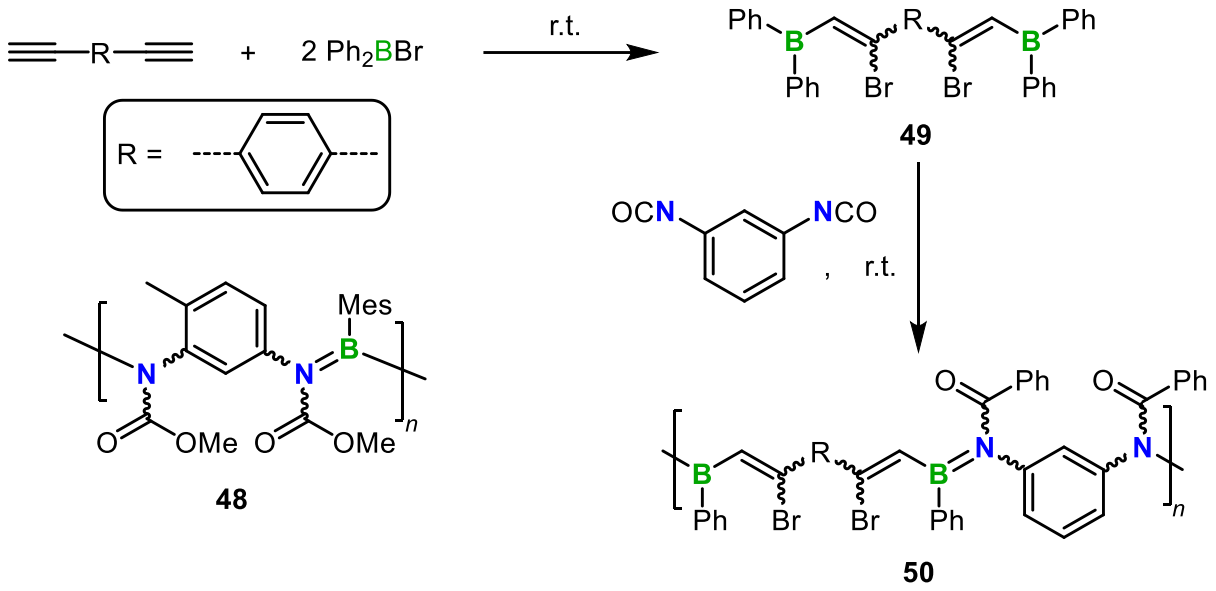

Scheme 1.5.3. Polymer **48** with linear NBN units and synthesis of **50** with linear BN units in the polymer main chain.

Jäkle and Liu with co-workers achieved the synthesis of the first conjugated 1,2-azaborinine polymers by Suzuki-Miyaura coupling methods (Scheme 1.5.4).[105] The crystallization of a related oligomer (dimer) enabled the structural characterization using X-ray diffraction. The structure revealed regioregular orientation of the B=N units with almost perfectly coplanar *syn* arrangement of the heterocycles, which is favored by N–H···π(Mes) interactions. After the synthesis of the AB monomer **51** and polymerization in presence of catalytic amounts of palladium, polymer **52** was obtained with a molecular weight of 2.3 kDa. However, photophysical and computational studies indicate that **52** has a closer similarity to

poly(cyclohexadiene) instead of the isoelectronic poly(*p*-phenylene) (PPP). This leads to the assumption that π-conjugation occurs mainly over the carbon chain.

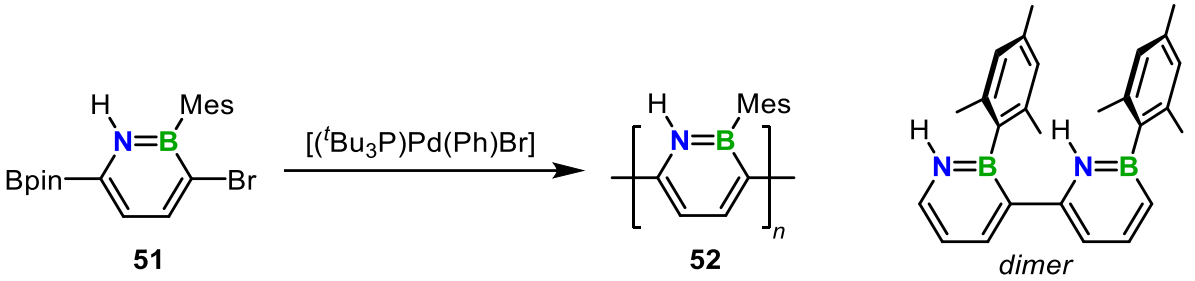

51 **52**

Scheme 1.5.4. Synthesis of the first conjugated 1,2-azadiborinine polymer **52** and the structure of the related dimer.

In the same year, Pei, Wang and co-workers presented the synthesis of poly(thiophene) derivatives containing polycyclic building blocks by Stille polycondensation.[106] In this case, the B=N unit is embedded in the thiophene-fused polycyclic azaborinine skeleton,[107] and the authors suggested that the B=N units are regio-randomly oriented in the polymers. The UV-vis absorption spectra of the polymers in solution and the solid state show a high-energy band for the BN-containing side group and a low-energy band for the conjugated poly(thiophene) backbone. The polymers exhibit relatively low HOMO levels, which is an important property to make them suitable for air stable OFETs.

Very recently, the groups of Duan and He published promising π-conjugated polymers for optoelectronic applications based on building blocks containing azaborinine moieties (Figure 1.5.1).[108] In 2018, He and co-workers published the synthesis of the 9,10-azaboraphenanthrene-containing polymers **53** by Suzuki-Miyaura or Stille cross-coupling polycondensations.[108a] Beside their good air and moisture stability, the polymers show bright fluorescence, and they can be used as highly selective colorimetric sensors for fluoride detection. The fluorescence color of the polymers appear blue with quantum yields of Φ = 57 % (**53a**) and Φ = 88 % (**53b**) and change to green after fluoride addition. In a follow-up study, He and co-workers reported the synthesis of dithienoazaborinine based polymers **55**-**57** by the same cross-coupling methods as mentioned above.[108b] Through AA/BB polymerization, **55** and **56** resulted in regio-irregular orientation, while polymer **57** shows a regio-regular structure due to the AB polymerization procedure. Compared to small model systems, **55** and **56** show strongly red-shifted absorption maxima indicating increased conjugation along the polymer chain. However, π-conjugation is forced over the B=N unit in the case of **55**, while for **56** and **57** conjugation can occur over the carbon scaffold. Polymers **56** and **57** exhibit lower LUMO energy levels and smaller band gaps than **55**, indicating weaker π-conjugation along the B=N bonds in the backbone of **55**.

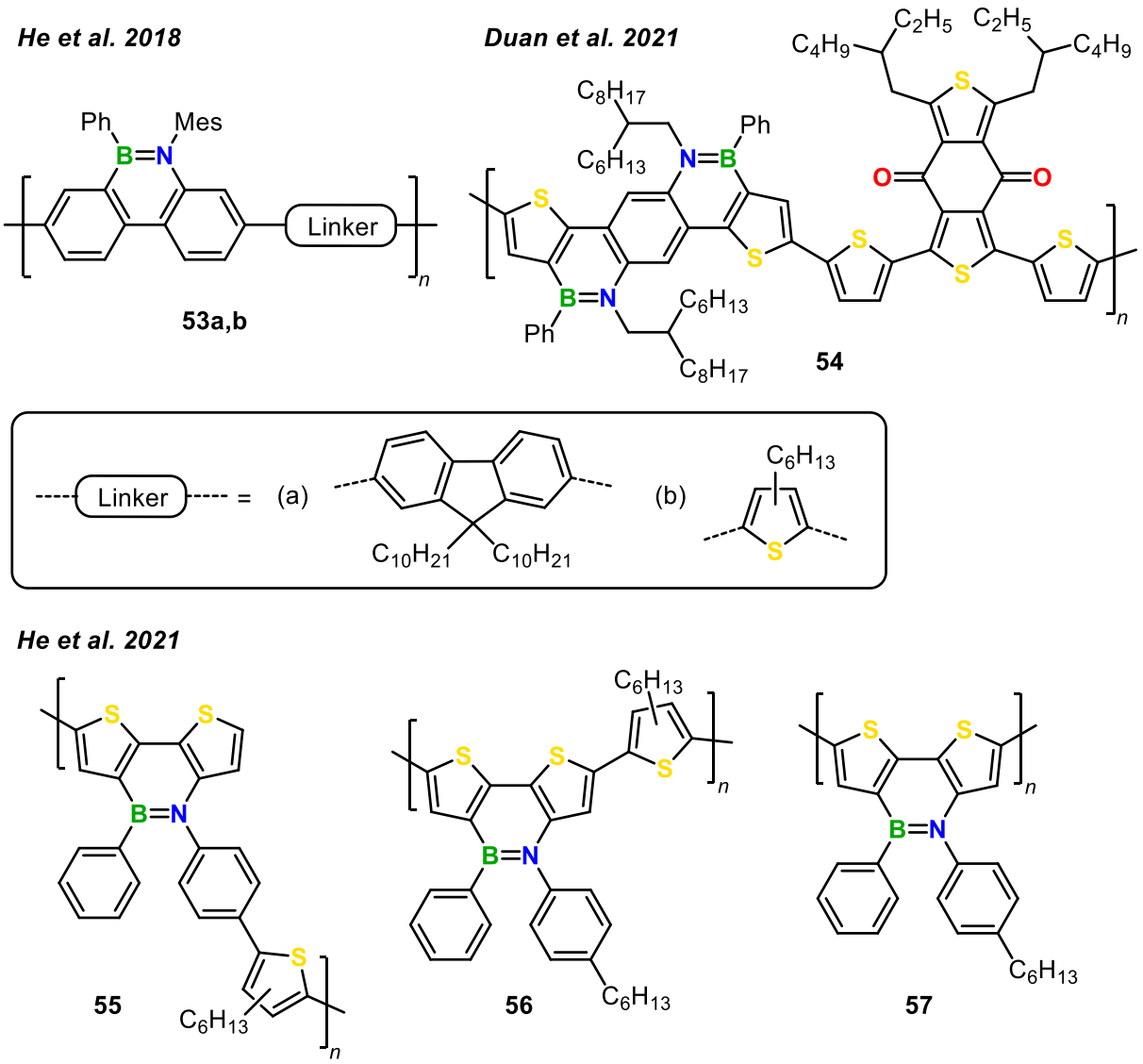

Figure 1.5.1. π-Conjugated azaborinine-based polymers **53**-**57**.

Duan and co-workers achieved the synthesis of **54** via Stille polycondensation.[108c] By using a more cost-effective B=N doped monomer, compared to the established benzodithiophene derivatives (BDT)[109] in donor-acceptor polymers for organic solar cells, they were able to obtain polymer **54** (Figure 1.5.1). Beside the complementary light absorption and energy levels with established acceptor systems, **54** requires less synthetic effort and exhibits lower crystallinity, which leads to increased device stability. After blending **54** with a non-fullerene acceptor, a power conversion efficiency of 16.1 % was achieved in an organic solar cell.

In 2016, Helten and co-workers reported the synthesis of the first π-conjugated inorganic–organic hybrid polymer containing linear NBN units that are not embedded in a cyclic structure.[110] Poly[*N*-(*p*-phenylene)diimidoborane] **59** was obtained after the reaction between **58** and dichloromesitylborane via Si/B exchange polycondensation (Scheme 1.5.5, top). Polymerizations following this B–E coupling method provide facile access to soluble materials under mild conditions. Photophysical data and theoretical calculations of oligomeric model

compounds and **59** revealed moderate extension of π-conjugation along the main chain with increased chain length. In addition, the authors used **59** as macromolecular ligand and demonstrated cross-linking reactions with zirconium to demonstrate a possible applicability of this new class.

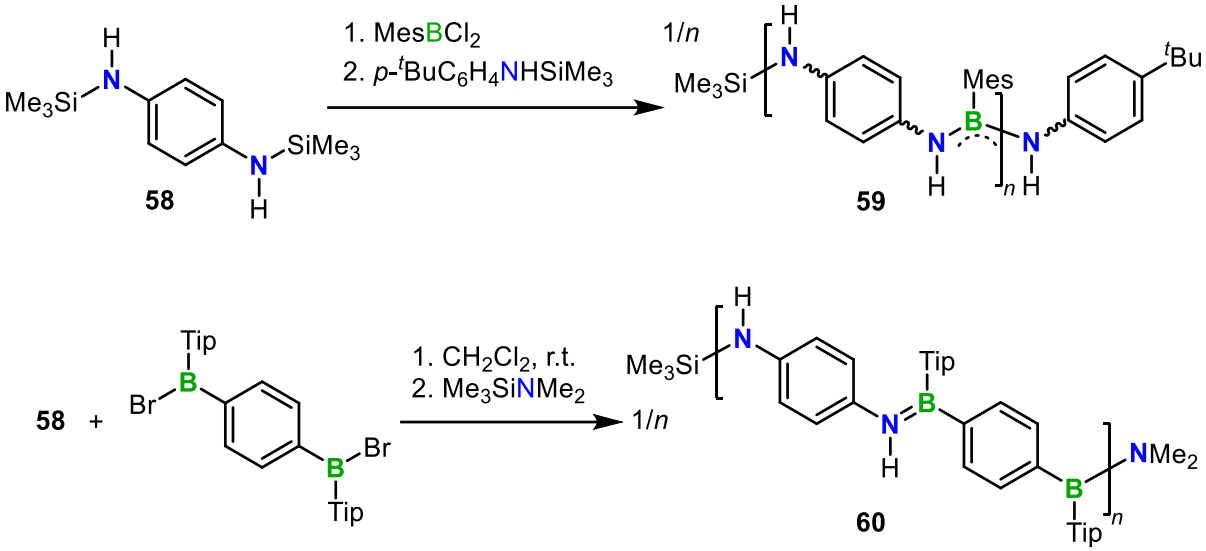

Scheme 1.5.5. Synthesis of π-conjugated linear NBN and BN linked polymers **59** and **60**, respectively.

Subsequently, Helten and co-workers achieved the synthesis of the first BN analog of PPV, namely poly(*p*-phenylene iminoborane) (BN-PPV).[11h] In addition to various molecular model compounds, BN-PPV **60** was obtained by the Si/B exchange polycondensation of **58** and a 1,4-diborylated phenylene species (Scheme 1.5.5, bottom). Solid state structures of molecular oligomers revealed *trans* configuration of the phenylene groups at each B=N unit and the B–N bond lengths are in the range between a single and a double bond, indicating some π-bond character. Comparison of the absorption maxima of molecular oligomers and **60** showed a systematic bathochromic shift with longer chain lengths and thus an increased extent in conjugation. Computational studies revealed that the respective HOMO-LUMO excitations can be classified as π-π* transitions.

Bolm, Helten and co-workers prepared an inorganic–organic hybrid polymer with a sulfoximine core unit in the backbone (Figure 1.5.2, left).[111] Sulfoximine species are relevant in medicinal chemistry, and their functionalization proved to be useful in drug design and bioactivity adjustment.[112] Polymer **61** was obtained by Si/B exchange polycondensation of a bisborane and a silylated dianiline-sulfoximine building block. Performing the reaction at elevated temperatures proved to be advantageous and led to molecular weights up to 9.8 kDa.

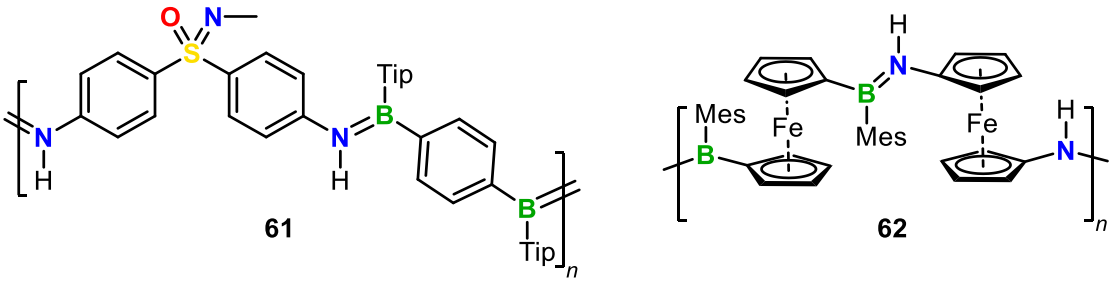

Figure 1.5.2. Inorganic–organic hybrid polymer with sulfoximine core unit **61** and poly(ferrocenylene iminoborane) **62** (Tip = 2,4,6-triisopropylphenyl; Mes = 2,4,6-trimethylphenyl).

Very recently, Helten and co-workers aimed at the synthesis of poly(*p*-phenylene iminoborane)s featuring pendent ferrocene substituents.[113] After they achieved the synthesis of respective oligomers, an unprecedented macrocycle was unexpectedly formed in a stoichiometric reaction. In a follow-up study, Helten and co-workers reported the synthesis of poly(ferrocenylene iminoborane) **62** by the Si/B exchange polycondensation of a bis-boryl ferrocene and a bis-(trimethylsilyl)amino ferrocene building block. Polymer **62** showed moderate electronic communication between the ferrocene moieties (Figure 1.5.2, right).[114]

1.6 References

[1] a) S. R. Forrest, *Nature* **2004**, *428*, 911–918; b) U. Scherf, A. Gutacker, N. Koenen, *Acc. Chem. Res.* **2008**, *41*, 1086–1097; c) A. Facchetti, *Chem. Mater.* **2011**, *23*, 733–758; d) K. Takimiya, I. Osaka, M. Nakano, *Chem. Mater.* **2014**, *26*, 587–593; e) L. Dou, Y. Liu, Z. Hong, G. Li, Y. Yang, *Chem. Rev.* **2015**, *115*, 12633–12665; f) T. M. Swager, *Macromolecules* **2017**, *50*, 4867–4886; g) T. Mikie, I. Osaka, *J. Mater. Chem. C* **2020**, *8*, 14262–14288; h) R. M. Pankow, B. C. Thompson, *Polymer* **2020**, *207*, 122874.

[2] a) A. Kraft, A. C. Grimsdale, A. B. Holmes, *Angew. Chem. Int. Ed.* **1998**, *37*, 402–428; b) U. Mitschke, P. Bäuerle, *J. Mater. Chem.* **2000**, *10*, 1471–1507; c) A. C. Grimsdale, K. L. Chan, R. E. Martin, P. G. Jokisz, A. B. Holmes, *Chem. Rev.* **2009**, *109*, 897–1091; d) J. Liang, L. Ying, F. Huang, Y. Cao, *J. Mater. Chem. C* **2016**, *4*, 10993–11006.

[3] a) S. Allard, M. Forster, B. Souharce, H. Thiem, U. Scherf, *Angew. Chem. Int. Ed.* **2008**, *47*, 4070–4098; b) C. Wang, H. Dong, W. Hu, Y. Liu, D. Zhu, *Chem. Rev.* **2012**, *112*, 2208–2267; c) J. Mei, Y. Diao, A. L. Appleton, L. Fang, Z. Bao, *J. Am. Chem. Soc.* **2013**, *135*, 6724–6746; d) H. Sirringhaus, *Adv. Mater.* **2014**, *26*, 1319–1335; e) M. Saito, I. Osaka, Y. Suda, H. Yoshida, K. Takimiya, *Adv. Mater.* **2016**, *28*, 6921–6925; f) S. Riera-Galindo, F. Leonardi, R. Pfattner, M. Mas-Torrent, *Adv. Mater. Technol.* **2019**, *4*, 1900104; g) R. Zhao, Y. Min, C. Dou, B. Lin, W. Ma, J. Liu, L. Wang, *ACS Appl. Polym. Mater.* **2020**, *2*, 19–25.

[4] a) C. Li, M. Liu, N. G. Pschirer, M. Baumgarten, K. Müllen, *Chem. Rev.* **2010**, *110*, 6817–6855; b) P.-L. T. Boudreault, A. Najari, M. Leclerc, *Chem. Mater.* **2011**, *23*, 456–469; c) H. Zhou, L. Yang, W. You, *Macromolecules* **2012**, *45*, 607–632; d) Y. Cai, L. Huo, Y. Sun, *Adv. Mater.* **2017**, *29*, 1605437; e) O. Inganäs, *Adv. Mater.* **2018**, *30*, e1800388; f) C. Yang, R. Yu, C. Liu, H. Li, S. Zhang, J. Hou, *ChemSusChem* **2021**, *14*, 3607–3613.

[5] a) C. Zhu, L. Liu, Q. Yang, F. Lv, S. Wang, *Chem. Rev.* **2012**, *112*, 4687–4735; b) T. Repenko, A. Rix, S. Ludwanowski, D. Go, F. Kiessling, W. Lederle, A. J. C. Kuehne, *Nat. Commun.* **2017**, *8*, 470; c) J. Wang, F. Lv, L. Liu, Y. Ma, S. Wang, *Coord. Chem. Rev.* **2018**, *354*, 135–154; d) Q. Xu, P. He, J. Wang, H. Chen, F. Lv, L. Liu, S. Wang, J. Yoon, *Dyes Pigm.* **2019**, *160*, 519–523; e) J. Li, K. Pu, *Chem. Soc. Rev.* **2019**, *48*, 38–71; f) H. Lin, H. Bai, Z. Yang, Q. Shen, M. Li, Y. Huang, F. Lv, S. Wang, *Chem. Commun.* **2022**, *58*, 7232–7244.

[6] a) X. He, T. Baumgartner, *RSC Adv.* **2013**, *3*, 11334–11350; b) E. I. Carrera, D. S. Seferos, *Macromolecules* **2015**, *48*, 297–308; c) A. M. Priegert, B. W. Rawe, S. C. Serin, D. P. Gates, *Chem. Soc. Rev.* **2016**, *45*, 922–953; d) S. M. Parke, M. P. Boone, E. Rivard, *Chem. Commun.* **2016**, *52*, 9485–9505; e) H. Helten, *Encyclopedia of Inorganic and Bioinorganic Chemistry (Ed.: R. A. Scott), Wiley, Chichester* **2017**; f) F. Vidal, F. Jäkle, *Angew. Chem. Int. Ed.* **2019**, *58*, 5846–5870; g) E. Rivard, *Chem. Rec.* **2020**, *20*, 640–648.

[7] a) T. Higashihara, H.-C. Wu, T. Mizobe, C. Lu, M. Ueda, W.-C. Chen, *Macromolecules* **2012**, *45*, 9046–9055; b) Q. Wang, X. Dong, M. He, M. Li, H. Tian, J. Liu, Y. Geng, *Polymer* **2018**, *140*, 89–95; c) F. A. Larik, M. Faisal, A. Saeed, Q. Abbas, M. A. Kazi, N. Abbas, A. A. Thebo, D. M. Khan, P. A. Channar, *J. Mater. Sci. Mater. Electron.* **2018**, *29*, 17975–18010; d) Q. Wang, Y. Qin, M. Li, L. Ye, Y. Geng, *Adv. Energy Mater.* **2020**, *10*, 2002572; e) P. Bi, J. Ren, S. Zhang, J. Wang, Z. Chen, M. Gao, Y. Cui, T. Zhang, J. Qin, Z. Zheng, L. Ye, X. Hao, J. Hou, *Nano Energy* **2022**, *100*, 107463; f) C. Yang, S. Zhang, J. Hou, *Aggregate* **2022**, *3*, e111; g) G. Zhang, F. R. Lin, F. Qi, T. Heumüller, A. Distler, H.-J. Egelhaaf, N. Li, P. C. Y. Chow, C. J. Brabec, A. K.-Y. Jen, H.-L. Yip, *Chem. Rev.* **2022**, *122*, 14180–14274; h) L. Ma, S. Zhang, J. Ren, G. Wang, J. Li, Z. Chen, H. Yao, J. Hou, *Angew. Chem. Int. Ed.* **2023**, *62*, e202214088.

[8] a) Y. Miyata, T. Nishinaga, K. Komatsu, *J. Org. Chem.* **2005**, *70*, 1147–1153; b) M. J. González-Tejera, E. S. de La Blanca, I. Carrillo, *Synth. Met.* **2008**, *158*, 165–189; c) X. Wang, Y. Sun, S. Chen, X. Guo, M. Zhang, X. Li, Y. Li, H. Wang, *Macromolecules* **2012**,

45, 1208–1216; d) O. Gidron, M. Bendikov, *Angew. Chem. Int. Ed.* **2014**, *53*, 2546–2555; e) H. Cao, P. A. Rupar, *Chem. Eur. J.* **2017**, *23*, 14670–14675.

[9] a) H. Q. Nguyen, E. A. Rainbolt, P. Sista, M. C. Stefan, *Macromol. Chem. Phys.* **2012**, *213*, 425–430; b) K. H. Hendriks, W. Li, M. M. Wienk, R. A. J. Janssen, *J. Am. Chem. Soc.* **2014**, *136*, 12130–12136; c) C. Bulumulla, R. Gunawardhana, P. L. Gamage, J. T. Miller, R. N. Kularatne, M. C. Biewer, M. C. Stefan, *ACS Appl. Mater. Interfaces* **2020**, *12*, 32209–32232; d) T. Zhang, C. An, P. Bi, Q. Lv, J. Qin, L. Hong, Y. Cui, S. Zhang, J. Hou, *Adv. Energy Mater.* **2021**, *11*, 2101705; e) H. Mori, Y. Asanuma, R. Hosogi, Y. Nishihara, *Polym. J.* **2023**, *55*, 405–415.

[10] a) J. H. Burroughes, D. D. C. Bradley, A. R. Brown, R. N. Marks, K. Mackay, R. H. Friend, P. L. Burns, A. B. Holmes, *Nature* **1990**, *347*, 539–541; b) C. Li, M. Liu, N. G. Pschirer, M. Baumgarten, K. Müllen, *Chem. Rev.* **2010**, *110*, 6817–6855; c) J. Banerjee, K. Dutta, *Chem. Pap.* **2021**, *75*, 5139–5151.

[11] a) V. A. Wright, D. P. Gates, *Angew. Chem. Int. Ed.* **2002**, *41*, 2389–2392; b) R. C. Smith, X. Chen, J. D. Protasiewicz, *Inorg. Chem.* **2003**, *42*, 5468–5470; c) R. C. Smith, J. D. Protasiewicz, *J. Am. Chem. Soc.* **2004**, *126*, 2268–2269; d) V. A. Wright, B. O. Patrick, C. Schneider, D. P. Gates, *J. Am. Chem. Soc.* **2006**, *128*, 8836–8844; e) I. Bejan, D. Scheschkewitz, *Angew. Chem. Int. Ed.* **2007**, *46*, 5783–5786; f) A. Fukazawa, Y. Li, S. Yamaguchi, H. Tsuji, K. Tamao, *J. Am. Chem. Soc.* **2007**, *129*, 14164–14165; g) L. Li, T. Matsuo, D. Hashizume, H. Fueno, K. Tanaka, K. Tamao, *J. Am. Chem. Soc.* **2015**, *137*, 15026–15035; h) T. Lorenz, M. Crumbach, T. Eckert, A. Lik, H. Helten, *Angew. Chem. Int. Ed.* **2017**, *56*, 2780–2784.

[12] a) A. Patra, M. Bendikov, *J. Mater. Chem.* **2010**, *20*, 422–433; b) M. Jeffries-EL, B. M. Kobilka, B. J. Hale, *Macromolecules* **2014**, *47*, 7253–7271; c) J. Razzell-Hollis, F. Fleischli, A. A. Jahnke, N. Stingelin, D. S. Seferos, J.-S. Kim, *J. Phys. Chem. C* **2017**, *121*, 2088–2098; d) S. Ye, V. Lotocki, H. Xu, D. S. Seferos, *Chem. Soc. Rev.* **2022**, *51*, 6442–6474; e) A. V. Marsh, M. Heeney, *Polym. J.* **2023**, *55*, 375–385.

[13] a) H. Saito, S. Ukai, S. Iwatsuki, T. Itoh, M. Kubo, *Macromolecules* **1995**, *28*, 8363–8367; b) M. Al-Hashimi, M. A. Baklar, F. Colleaux, S. E. Watkins, T. D. Anthopoulos, N. Stingelin, M. Heeney, *Macromolecules* **2011**, *44*, 5194–5199; c) Z. Zhang, Y. Qin, *ACS Macro Lett.* **2015**, *4*, 679–683; d) M. Al-Hashimi, Y. Han, J. Smith, H. S. Bazzi, S. Y. A. Alqaradawi, S. E. Watkins, T. D. Anthopoulos, M. Heeney, *Chem. Sci.* **2016**, *7*, 1093–1099; e) Z. Zhang, Y. Qin, *Polym. Chem.* **2019**, *10*, 1018–1025.

[14] a) B. Bagh, J. B. Gilroy, A. Staubitz, J. Müller, *J. Am. Chem. Soc.* **2010**, *132*, 1794–1795; b) M. L. Mejía, G. Reeske, B. J. Holliday, *Chem. Commun.* **2010**, *46*, 5355–5357; c) T. Matsumoto, Y. Onishi, K. Tanaka, H. Fueno, K. Tanaka, Y. Chujo, *Chem. Commun.* **2014**, *50*, 15740–15743; d) T. Matsumoto, K. Tanaka, Y. Chujo, *Macromolecules* **2015**, *48*, 1343–1351; e) S. Ito, A. Hirose, M. Yamaguchi, K. Tanaka, Y. Chujo, *Polymers* **2017**, *9*, 68–78.

[15] T. Matsumoto, K. Tanaka, K. Tanaka, Y. Chujo, *Dalton Trans.* **2015**, *44*, 8697–8707.

[16] a) N. Matsumi, Y. Chujo, *Polym. J.* **2008**, *40*, 77–89; b) F. Jäkle, *Chem. Rev.* **2010**, *110*, 3985–4022; c) F. Jäkle, *Top. Organomet. Chem.* **2015**, *49*, 297–325; d) Y. Ren, F. Jäkle, *Main Group Strategies towards Functional Hybrid Materials (Eds: T. Baumgartner, F. Jäkle), Wiley, Hoboken, NJ* **2017**, 79–110; e) H. Helten, *Chem. Asian J.* **2019**, *14*, 919–935; f) X. Yin, J. Liu, F. Jäkle, *Chem. Eur. J.* **2021**, *27*, 2973–2986; g) H. Helten, *Comprehensive Organometallic Chemistry IV (Eds: D. O'Hare, K. Meyer, G. Parkin), Elsevier, New York* **2022**, *14*, 71–134.

[17] a) C. Reus, S. Weidlich, M. Bolte, H.-W. Lerner, M. Wagner, *J. Am. Chem. Soc.* **2013**, *135*, 12892–12907; b) Z. Zhang, R. M. Edkins, J. Nitsch, K. Fucke, A. Steffen, L. E. Longobardi, D. W. Stephan, C. Lambert, T. B. Marder, *Chem. Sci.* **2015**, *6*, 308–321; c) S. Griesbeck, Z. Zhang, M. Gutmann, T. Lühmann, R. M. Edkins, G. Clermont, A. N. Lazar, M. Haehnel, K. Edkins, A. Eichhorn, M. Blanchard-Desce, L. Meinel, T. B. Marder, *Chem. Eur. J.* **2016**, *22*, 14701–14706; d) E. von Grotthuss, A. John, T. Kaese, M. Wagner, *Asian J. Org. Chem.* **2018**, *7*, 37–53.

[18] a) V. M. Hertz, N. Ando, M. Hirai, M. Bolte, H.-W. Lerner, S. Yamaguchi, M. Wagner, *Organometallics* **2017**, *36*, 2512–2519; b) H. Narita, H. Choi, M. Ito, N. Ando, S. Ogi,

S. Yamaguchi, *Chem. Sci.* **2022**, *13*, 1484–1491; c) M. Sakai, M. Mori, M. Hirai, N. Ando, S. Yamaguchi, *Chem. Eur. J.* **2022**, *28*, e202200728.
[19] Y. Chujo, I. Tomita, T. Saegusa, *Macromolecules* **1990**, *23*, 687–689.
[20] M. Miyata, N. Matsumi, Y. Chujo, *Polym. Bull.* **1999**, *42*, 505–510.
[21] a) N. Matsumi, K. Naka, Y. Chujo, *J. Am. Chem. Soc.* **1998**, *120*, 5112–5113; b) N. Matsumi, M. Miyata, Y. Chujo, *Macromolecules* **1999**, *32*, 4467–4469; c) Y. Chujo, Y. Sasaki, N. Kinomura, N. Matsumi, *Polymer* **2000**, *41*, 5047–5051.
[22] A. Nagai, T. Murakami, Y. Nagata, K. Kokado, Y. Chujo, *Macromolecules* **2009**, *42*, 7217–7220.
[23] K. Hu, Z. Zhang, J. Burke, Y. Qin, *J. Am. Chem. Soc.* **2017**, *139*, 11004–11007.
[24] N. Matsumi, K. Naka, Y. Chujo, *J. Am. Chem. Soc.* **1998**, *120*, 10776–10777.
[25] N. Matsumi, T. Umeyama, Y. Chujo, *Polym. Bull.* **2000**, *44*, 431–436.
[26] a) A. Sundararaman, M. Victor, R. Varughese, F. Jäkle, *J. Am. Chem. Soc.* **2005**, *127*, 13748–13749; b) H. Li, F. Jäkle, *Angew. Chem. Int. Ed.* **2009**, *48*, 2313–2316; c) H. Li, F. Jäkle, *Macromol. Rapid Commun.* **2010**, *31*, 915–920; d) P. Chen, F. Jäkle, *J. Am. Chem. Soc.* **2011**, *133*, 20142–20145; e) P. Chen, R. A. Lalancette, F. Jäkle, *J. Am. Chem. Soc.* **2011**, *133*, 8802–8805; f) P. Chen, R. A. Lalancette, F. Jäkle, *Angew. Chem. Int. Ed.* **2012**, *51*, 7994–7998; g) P. Chen, X. Yin, N. Baser-Kirazli, F. Jäkle, *Angew. Chem. Int. Ed.* **2015**, *54*, 10768–10772; h) P. Chen, A. S. Marshall, S.-H. Chi, X. Yin, J. W. Perry, F. Jäkle, *Chem. Eur. J.* **2015**, *21*, 18237–18247; i) X. Yin, F. Guo, R. A. Lalancette, F. Jäkle, *Macromolecules* **2016**, *49*, 537–546.
[27] A. Lik, L. Fritze, L. Müller, H. Helten, *J. Am. Chem. Soc.* **2017**, *139*, 5692–5695.
[28] a) A. Lik, S. Jenthra, L. Fritze, L. Müller, K.-N. Truong, H. Helten, *Chem. Eur. J.* **2018**, *24*, 11961–11972; b) L. Fritze, N. A. Riensch, H. Helten, *Synthesis* **2019**, *51*, 399–406; c) N. A. Riensch, M. Fest, L. Fritze, A. Helbig, I. Krummenacher, H. Braunschweig, H. Helten, *New J. Chem.* **2021**, *45*, 14920–14924.
[29] a) C. Reus, F. Guo, A. John, M. Winhold, H.-W. Lerner, F. Jäkle, M. Wagner, *Macromolecules* **2014**, *47*, 3727–3735; b) X. Yin, J. Chen, R. A. Lalancette, T. B. Marder, F. Jäkle, *Angew. Chem. Int. Ed.* **2014**, *53*, 9761–9765; c) Y. Adachi, Y. Ooyama, Y. Ren, X. Yin, F. Jäkle, J. Ohshita, *Polym. Chem.* **2018**, *9*, 291–299; d) B. Meng, Y. Ren, J. Liu, F. Jäkle, L. Wang, *Angew. Chem. Int. Ed.* **2018**, *130*, 2205–2209; e) L. Fritze, M. Fest, A. Helbig, T. Bischof, I. Krummenacher, H. Braunschweig, M. Finze, H. Helten, *Macromolecules* **2021**, *54*, 7653–7665; f) A. F. Alahmadi, X. Yin, R. A. Lalancette, F. Jäkle, *Angew. Chem. Int. Ed.* **2023**, *29*, e202203619.
[30] a) I. Manners, *Angew. Chem. Int. Ed.* **1996**, *35*, 1602–1621; b) W. Caseri, *Chem. Soc. Rev.* **2016**, *45*, 5187–5199.
[31] E. M. Leitao, T. Jurca, I. Manners, *Nat. Chem.* **2013**, *5*, 817–829.
[32] J. E. Mark, *Acc. Chem. Res.* **2004**, *37*, 946–953.
[33] a) K. J. Quinn, J. M. Courtney, *Brit. Poly. J.* **1988**, *20*, 25–32; b) J. A. González Calderón, D. Contreras López, E. Pérez, J. Vallejo Montesinos, *Polym. Bull.* **2020**, *77*, 2749–2817.
[34] Z. Ren, S. Yan, *Prog. Mater Sci.* **2016**, *83*, 383–416.
[35] a) G. J. J. Out, A. A. Turetskii, M. Möller, D. Oelfin, *Macromolecules* **1994**, *27*, 3310–3318; b) A. Colas, *Silicones: preparation, properties and performance, Dow Corning Corporation, Midland, MI,* **2005**.
[36] a) D. J. Parks, J. M. Blackwell, W. E. Piers, *J. Org. Chem.* **2000**, *65*, 3090–3098; b) J. Chojnowski, S. Rubinsztajn, J. A. Cella, W. Fortuniak, M. Cypryk, J. Kurjata, K. Kaźmierski, *Organometallics* **2005**, *24*, 6077–6084; c) M. A. Brook, *Chem. Eur. J.* **2018**, *24*, 8458–8469.
[37] S. Rubinsztajn, J. A. Cella, *Macromolecules* **2005**, *38*, 1061–1063.
[38] D. B. Thompson, M. A. Brook, *J. Am. Chem. Soc.* **2008**, *130*, 32–33.
[39] J. Chojnowski, S. Rubinsztajn, W. Fortuniak, J. Kurjata, *Macromolecules* **2008**, *41*, 7352–7358.
[40] K. Matsumoto, Y. Oba, Y. Nakajima, S. Shimada, K. Sato, *Angew. Chem. Int. Ed.* **2018**, *57*, 4637–4641.

[41] a) F. S. Kipping, J. E. Sands, *J. Chem. Soc., Trans.* **1921**, *119*, 830–847; b) F. S. Kipping, *J. Chem. Soc., Trans.* **1924**, *125*, 2291–2297.
[42] R. West, L. D. David, P. I. Djurovich, K. L. Stearley, K. S. V. Srinivasan, H. Yu, *J. Am. Chem. Soc.* **1981**, *103*, 7352–7354.
[43] R. West, *J. Organomet. Chem.* **1986**, *300*, 327–346.
[44] a) C. T. Aitken, J. F. Harrod, E. Samuel, *J. Am. Chem. Soc.* **1986**, *108*, 4059–4066; b) H.-G. Woo, T. D. Tilley, *J. Am. Chem. Soc.* **1989**, *111*, 8043–8044.
[45] a) K. Sakamoto, K. Obata, H. Hirata, M. Nakajima, H. Sakurai, *J. Am. Chem. Soc.* **1989**, *111*, 7641–7643; b) M. Cypryk, Y. Gupta, K. Matyjaszewski, *J. Am. Chem. Soc.* **1991**, *113*, 1046–1047.
[46] a) T. Sanji, S. Isozaki, M. Yoshida, K. Sakamoto, H. Sakurai, *J. Organomet. Chem.* **2003**, *685*, 65–69; b) H. Sakurai, R. Honbori, T. Sanji, *Organometallics* **2005**, *24*, 4119–4121.
[47] a) H. Suzuki, H. Meyer, J. Simmerer, J. Yang, D. Haarer, *Adv. Mater.* **1993**, *5*, 743–746; b) C.-H. Yuan, S. Hoshino, S. Toyoda, H. Suzuki, M. Fujiki, N. Matsumoto, *Appl. Phys. Lett.* **1997**, *71*, 3326–3328; c) Y. Xu, T. Fujino, H. Naito, K. Oka, T. Dohmaru, *Chem. Lett.* **1998**, *27*, 299–300.
[48] H. Wakefield, I. Kevlishvili, K. E. Wentz, Y. Yao, T. B. Kouznetsova, S. J. Melvin, E. G. Ambrosius, A. Herzog-Arbeitman, M. A. Siegler, J. A. Johnson, S. L. Craig, H. J. Kulik, R. S. Klausen, *J. Am. Chem. Soc.* **2023**, *145*, 10187–10196.
[49] a) O. J. Metters, A. M. Chapman, A. P. M. Robertson, C. H. Woodall, P. J. Gates, D. F. Wass, I. Manners, *Chem. Commun.* **2014**, *50*, 12146–12149; b) S. Rothemund, I. Teasdale, *Chem. Soc. Rev.* **2016**, *45*, 5200–5215; c) H. R. Allcock, C. Chen, *J. Org. Chem.* **2020**, *85*, 14286–14297; d) P. Ilayaperumal, P. Chelladurai, K. Vairan, P. Anilkumar, B. Balagurusamy, *Macromol. Mater. Eng.* **2023**, *308*, 2200553.
[50] H. R. Allcock, *Science* **1976**, *193*, 1214–1219.
[51] a) C. H. Honeyman, I. Manners, C. T. Morrissey, H. R. Allcock, *J. Am. Chem. Soc.* **1995**, *117*, 7035–7036; b) H. R. Allcock, S. D. Reeves, C. R. de Denus, C. A. Crane, *Macromolecules* **2001**, *34*, 748–754; c) V. Blackstone, A. Presa Soto, I. Manners, *Dalton Trans.* **2008**, 4363–4371; d) V. Blackstone, S. Pfirrmann, H. Helten, A. Staubitz, A. Presa Soto, G. R. Whittell, I. Manners, *J. Am. Chem. Soc.* **2012**, *134*, 15293–15296.
[52] W.-H. Hsu, N. Csaba, C. Alexander, M. Garcia-Fuentes, *J. Appl. Polym. Sci.* **2020**, *137*, 48688.
[53] X. Zhou, S. Qiu, X. Mu, M. Zhou, W. Cai, L. Song, W. Xing, Y. Hu, *Composites, Part B* **2020**, *202*, 108397.
[54] J. Bartels, A. Hess, H.-S. Shiau, H. R. Allcock, R. H. Colby, J. Runt, *Macromolecules* **2015**, *48*, 111–118.
[55] G. A. Carriedo, R. de La Campa, A. P. Soto, *Eur. J. Inorg. Chem.* **2018**, *2018*, 2484–2499.
[56] H. Dorn, R. A. Singh, J. A. Massey, A. J. Lough, I. Manners, *Angew. Chem. Int. Ed.* **1999**, *38*, 3321–3323.
[57] a) A. B. Burg, R. I. Wagner, *J. Am. Chem. Soc.* **1953**, *75*, 3872–3877; b) R. I. Wagner, F. F. Caserio, *J. Inorg. Nucl. Chem.* **1959**, *11*, 259; c) A. B. Burg, *J. Inorg. Nucl. Chem.* **1959**, *11*, 258; d) P. P. Power, *Angew. Chem. Int. Ed. Engl.* **1990**, *29*, 449–460.
[58] a) T. J. Clark, J. M. Rodezno, S. B. Clendenning, S. Aouba, P. M. Brodersen, A. J. Lough, H. E. Ruda, I. Manners, *Chem. Eur. J.* **2005**, *11*, 4526–4534; b) J. R. Turner, D. A. Resendiz-Lara, T. Jurca, A. Schäfer, J. R. Vance, L. Beckett, G. R. Whittell, R. A. Musgrave, H. A. Sparkes, I. Manners, *Macromol. Chem. Phys.* **2017**, *218*, 1700120.
[59] A. W. Knights, S. S. Chitnis, I. Manners, *Chem. Sci.* **2019**, *10*, 7281–7289.
[60] A. W. Knights, M. A. Nascimento, I. Manners, *Polymer* **2022**, *247*, 124795.
[61] a) S. Pandey, P. Lönnecke, E. Hey-Hawkins, *Eur. J. Inorg. Chem.* **2014**, 2456–2465; b) H. Cavaye, F. Clegg, P. J. Gould, M. K. Ladyman, T. Temple, E. Dossi, *Macromolecules* **2017**, *50*, 9239–9248.
[62] F. Schön, L. M. Sigmund, F. Schneider, D. Hartmann, M. A. Wiebe, I. Manners, L. Greb, *Angew. Chem. Int. Ed.* **2022**, *61*, e202202176.
[63] U. S. D. Paul, H. Braunschweig, U. Radius, *Chem. Commun.* **2016**, *52*, 8573–8576.

[64] a) A. Schäfer, T. Jurca, J. Turner, J. R. Vance, K. Lee, an van Du, M. F. Haddow, G. R. Whittell, I. Manners, *Angew. Chem. Int. Ed.* **2015**, *54*, 4836–4841; b) N. T. Coles, M. F. Mahon, R. L. Webster, *Organometallics* **2017**, *36*, 2262–2268.
[65] a) C. Marquardt, T. Jurca, K.-C. Schwan, A. Stauber, A. V. Virovets, G. R. Whittell, I. Manners, M. Scheer, *Angew. Chem. Int. Ed.* **2015**, *54*, 13782–13786; b) N. L. Oldroyd, S. S. Chitnis, V. T. Annibale, M. I. Arz, H. A. Sparkes, I. Manners, *Nat. Commun.* **2019**, *10*, 1370; c) M. A. Wiebe, S. Kundu, E. A. LaPierre, B. O. Patrick, I. Manners, *Chem. Eur. J.* **2023**, *29*, e202202897.
[66] M. I. Arz, A. W. Knights, I. Manners, *Macromol. Rapid Commun.* **2020**, *41*, 1900468.
[67] J. J. Race, A. Heyam, M. A. Wiebe, J. Diego-Garcia Hernandez, C. E. Ellis, S. Lei, I. Manners, A. S. Weller, *Angew. Chem. Int. Ed.* **2023**, *62*, e202216106.
[68] Z. Liu, T. B. Marder, *Angew. Chem. Int. Ed.* **2008**, *47*, 242–244.
[69] A. Stock, E. Pohland, *Ber. Dtsch. Chem. Ges.* **1926**, *59*, 2210–2215.
[70] a) R. Islas, E. Chamorro, J. Robles, T. Heine, J. C. Santos, G. Merino, *Struct Chem* **2007**, *18*, 833–839; b) W. Wu, X. Li, L. Meng, S. Zheng, Y. Zeng, *J. Phys. Chem. A* **2015**, *119*, 2091–2097.
[71] T. Beweries, H. Helten, *Encyclopedia of Inorganic and Bioinorganic Chemistry (Ed.: R. A. Scott), Wiley* **2020**, 1–25.
[72] a) C. W. Hamilton, R. T. Baker, A. Staubitz, I. Manners, *Chem. Soc. Rev.* **2009**, *38*, 279–293; b) V. A. Du, T. Jurca, G. R. Whittell, I. Manners, *Dalton Trans.* **2016**, *45*, 1055–1062; c) X. Wang, T. N. Hooper, A. Kumar, I. K. Priest, Y. Sheng, T. O. M. Samuels, S. Wang, A. W. Robertson, M. Pacios, H. Bhaskaran, A. S. Weller, J. H. Warner, *CrystEngComm* **2017**, *19*, 285–294.
[73] a) G. Schaeffer, L. J. Basile, *J. Am. Chem. Soc.* **1955**, *77*, 331–332; b) A. K. Holliday, N. R. Thompson, *J. Chem. Soc.* **1960**, 2695–2699; c) R. Komm, R. A. Geanangel, R. Liepins, *Inorg. Chem.* **1983**, *22*, 1684–1686; d) D.-P. Kim, K.-T. Moon, J.-G. Kho, J. Economy, C. Gervais, F. Babonneau, *Polym. Adv. Technol.* **1999**, *10*, 702–712.
[74] a) A. Rossin, M. Peruzzini, *Chem. Rev.* **2016**, *116*, 8848–8872; b) D. Han, F. Anke, M. Trose, T. Beweries, *Coord. Chem. Rev.* **2019**, *380*, 260–286; c) A. L. Colebatch, A. S. Weller, *Chem. Eur. J.* **2019**, *25*, 1379–1390.
[75] A. Staubitz, A. Presa Soto, I. Manners, *Angew. Chem. Int. Ed.* **2008**, *47*, 6212–6215.
[76] a) C. N. Brodie, T. M. Boyd, L. Sotorríos, D. E. Ryan, E. Magee, S. Huband, J. S. Town, G. C. Lloyd-Jones, D. M. Haddleton, S. A. Macgregor, A. S. Weller, *J. Am. Chem. Soc.* **2021**, *143*, 21010–21023; b) P. Hasche, J. Haak, F. Anke, C. Kubis, W. Baumann, H.-J. Drexler, H. Jiao, T. Beweries, *Catal. Sci. Technol.* **2021**, *11*, 3514–3526.
[77] a) A. Glüer, M. Förster, V. R. Celinski, J. Schmedt auf der Günne, M. C. Holthausen, S. Schneider, *ACS Catal.* **2015**, *5*, 7214–7217; b) F. Anke, S. Boye, A. Spannenberg, A. Lederer, D. Heller, T. Beweries, *Chem. Eur. J.* **2020**, *26*, 7889–7899.
[78] a) T. Jurca, T. Dellermann, N. E. Stubbs, D. A. Resendiz-Lara, G. R. Whittell, I. Manners, *Chem. Sci.* **2018**, *9*, 3360–3366; b) E. A. LaPierre, B. O. Patrick, I. Manners, *J. Am. Chem. Soc.* **2019**, *141*, 20009–20015.
[79] M. Trose, M. Reiß, F. Reiß, F. Anke, A. Spannenberg, S. Boye, A. Lederer, P. Arndt, T. Beweries, *Dalton Trans.* **2018**, *47*, 12858–12862.
[80] a) S. Todisco, L. Luconi, G. Giambastiani, A. Rossin, M. Peruzzini, I. E. Golub, O. A. Filippov, N. V. Belkova, E. S. Shubina, *Inorg. Chem.* **2017**, *56*, 4296–4307; b) T. M. Boyd, K. A. Andrea, K. Baston, A. Johnson, D. E. Ryan, A. S. Weller, *Chem. Commun.* **2020**, *56*, 482–485.
[81] a) C. A. de Albuquerque Pinheiro, C. Roiland, P. Jehan, G. Alcaraz, *Angew. Chem. Int. Ed.* **2018**, *57*, 1519–1522; b) M. Devillard, C. A. de Albuquerque Pinheiro, E. Caytan, C. Roiland, C. Dinoi, I. Del Rosal, G. Alcaraz, *Adv. Synth. Catal.* **2021**, *363*, 2417–2426.
[82] a) N. E. Stubbs, T. Jurca, E. M. Leitao, C. H. Woodall, I. Manners, *Chem. Commun.* **2013**, *49*, 9098–9100; b) N. L. Oldroyd, S. S. Chitnis, E. A. LaPierre, V. T. Annibale, H. T. G. Walsgrove, D. P. Gates, I. Manners, *J. Am. Chem. Soc.* **2022**, *144*, 23179–23190.
[83] a) X.-B. Lu, Y. Liu, H. Zhou, *Chem. Eur. J.* **2018**, *24*, 11255–11266; b) J.-B. Zhu, E. M. Watson, J. Tang, E. Y.-X. Chen, *Science* **2018**, *360*, 398–403; c) P. R. Christensen, A. M. Scheuermann, K. E. Loeffler, B. A. Helms, *Nat. Chem.* **2019**, *11*, 442–448.

[84] P. Paetzold, C. von Plotho, G. Schmid, R. Boese, B. Schrader, D. Bougeard, U. Pfeiffer, R. Gleiter, W. Schäfer, *Chem. Ber.* **1984**, *117*, 1089–1102.

[85] a) A. K. Swarnakar, C. Hering-Junghans, M. J. Ferguson, R. McDonald, E. Rivard, *Chem. Sci.* **2017**, *8*, 2337–2343; b) M. Nutz, B. Borthakur, R. D. Dewhurst, A. Deißenberger, T. Dellermann, M. Schäfer, I. Krummenacher, A. K. Phukan, H. Braunschweig, *Angew. Chem. Int. Ed.* **2017**, *56*, 7975–7979; c) B. L. Frenette, A. A. Omaña, M. J. Ferguson, Y. Zhou, E. Rivard, *Chem. Commun.* **2021**, *57*, 10895–10898; d) R. Guo, T. Li, R. Wei, X. Zhang, Q. Li, L. L. Liu, C.-H. Tung, L. Kong, *J. Am. Chem. Soc.* **2021**, *143*, 13483–13488; e) Y. Fan, J. Cui, L. Kong, *Eur. J. Org. Chem.* **2022**, e202201086; f) S. Qiu, X. Zhang, C. Hu, H. Chu, Q. Li, D. A. Ruiz, L. L. Liu, C.-H. Tung, L. Kong, *Angew. Chem. Int. Ed.* **2022**, *61*, e202205814; g) J. Wang, P. Jia, W. Sun, Y. Wei, Z. Lin, Q. Ye, *Inorg. Chem.* **2022**, *61*, 8879–8886; h) M. Bao, Y. Dai, C. Liu, Y. Su, *Inorg. Chem.* **2022**, *61*, 11137–11142.

[86] a) P. Paetzold, T. von Bennigsen-Mackiewicz, *Chem. Ber.* **1981**, *114*, 298–305; b) H.-U. Meier, P. Paetzold, E. Schröder, *Chem. Ber.* **1984**, *117*, 1954–1964.

[87] a) R. S. Chellappa, T. Autrey, M. Somayazulu, V. V. Struzhkin, R. J. Hemley, *ChemPhysChem* **2010**, *11*, 93–96; b) K. Shimoda, K. Doi, T. Nakagawa, Y. Zhang, H. Miyaoka, T. Ichikawa, M. Tansho, T. Shimizu, A. K. Burrell, Y. Kojima, *J. Phys. Chem. C* **2012**, *116*, 5957–5964; c) L. H. Jepsen, J. Skibsted, T. R. Jensen, *J. Alloys Compd.* **2013**, *580*, 287-291; d) T. Kobayashi, S. Gupta, M. A. Caporini, V. K. Pecharsky, M. Pruski, *J. Phys. Chem. C* **2014**, *118*, 19548–19555.

[88] a) K.-H. van Bonn, T. von Bennigsen-Mackiewicz, J. Kiesgen, C. von Plotho, P. Paetzold, *Z. Naturforsch. B* **1987**, *43*, 61–68; b) B. Anand, H. Nöth, H. Schwenk-Kircher, A. Troll, *Eur. J. Inorg. Chem.* **2008**, 3186–3199.

[89] a) O. Ayhan, T. Eckert, F. A. Plamper, H. Helten, *Angew. Chem. Int. Ed.* **2016**, *55*, 13321–13325; b) O. Ayhan, N. A. Riensch, C. Glasmacher, H. Helten, *Chem. Eur. J.* **2018**, *24*, 5883–5894.

[90] a) S. Y. Shaw, R. H. Neilson, *Inorg. Chem.* **1994**, *33*, 3239–3245; b) N. Retta, R. H. Neilson, *Bull. Chem. Soc. Ethiop.* **1999**, *13*, 51–55; c) N. Retta, R. H. Neilson, *Bull. Chem. Soc. Ethiop.* **1999**, *13*, 121–125.

[91] a) H. C. Johnson, A. P. M. Robertson, A. B. Chaplin, L. J. Sewell, A. L. Thompson, M. F. Haddow, I. Manners, A. S. Weller, *J. Am. Chem. Soc.* **2011**, *133*, 11076–11079; b) H. Helten, A. P. M. Robertson, A. Staubitz, J. R. Vance, M. F. Haddow, I. Manners, *Chem. Eur. J.* **2012**, *18*, 4665–4680; c) X. Chen, J. Gallucci, C. Campana, Z. Huang, H. K. Lingam, S. G. Shore, J.-C. Zhao, *Chem. Commun.* **2012**, *48*, 7943–7945; d) W. C. Ewing, P. J. Carroll, L. G. Sneddon, *Inorg. Chem.* **2013**, *52*, 10690–10697.

[92] a) K. Ota, R. Kinjo, *J. Am. Chem. Soc.* **2021**, *143*, 11152–11159; b) S. Zhou, Y. Liu, W. Jin, T. Qin, X. Liu, C. Zhao, Z. Liu, X. Yu, *Org. Lett.* **2023**, *25*, 1573–1577; c) S. Jeong, E. Park, J. Kim, S. B. Park, S. H. Kim, W. Choe, J. Kim, Y. S. Park, *Angew. Chem. Int. Ed.* **2023**, *62*, e202314148.

[93] H. Braunschweig, C. Kollann, K. W. Klinkhammer, *Eur. J. Inorg. Chem.* **1999**, 1523–1529.

[94] C. Brunecker, M. Arrowsmith, F. Fantuzzi, H. Braunschweig, *Angew. Chem. Int. Ed.* **2021**, *60*, 16864–16868.

[95] L. C. Haufe, L. Endres, M. Arrowsmith, R. Bertermann, M. Dietz, F. Fantuzzi, M. Finze, H. Braunschweig, *J. Am. Chem. Soc.* **2023**, *145*, 23986–23993.

[96] a) K. Liu, R. A. Lalancette, F. Jäkle, *J. Am. Chem. Soc.* **2017**, *139*, 18170–18173; b) J. Huang, X. Wang, Y. Xiang, L. Guo, G. Chen, *Adv. Energy Sustainability Res.* **2021**, *2*, 2100016; c) M. Crumbach, J. Bachmann, L. Fritze, A. Helbig, I. Krummenacher, H. Braunschweig, H. Helten, *Angew. Chem. Int. Ed.* **2021**, *60*, 9290–9295; d) J. Full, S. P. Panchal, J. Götz, A.-M. Krause, A. Nowak-Król, *Angew. Chem. Int. Ed.* **2021**, *60*, 4350–4357; e) X. Chen, D. Tan, D.-T. Yang, *J. Mater. Chem. C* **2022**, *10*, 13499–13532; f) M. Franceschini, M. Crosta, R. R. Ferreira, D. Poletto, N. Demitri, J. P. Zobel, L. González, D. Bonifazi, *J. Am. Chem. Soc.* **2022**, *144*, 21470–21484; g) W. Li, C.-Z. Du, X.-Y. Chen, L. Fu, R.-R. Gao, Z.-F. Yao, J.-Y. Wang, W. Hu, J. Pei, X.-Y. Wang, *Angew. Chem. Int. Ed.* **2022**, *61*, e202201464; h) J. Bachmann, A. Helbig, M. Crumbach, I.

Krummenacher, H. Braunschweig, H. Helten, *Chem. Eur. J.* **2022**, *28*, e202202455; i) D. Marchionni, S. Basak, A. N. Khodadadi, A. Marrocchi, L. Vaccaro, *Adv. Funct. Mater.* **2023**, *33*, 2303635; j) R. P. Nandi, N. K. Kalluvettukuzhy, S. Pagidi, P. Thilagar, *Inorg. Chem.* **2023**, *62*, 1122–1134; k) C. Chen, Y. Zhang, X.-Y. Wang, J.-Y. Wang, J. Pei, *Chem. Mater.* **2023**, *35*, 10277–10294.

[97] a) H. Helten, *Chem. Eur. J.* **2016**, *22*, 12972–12982; b) H. Helten, O. Ayhan, T. Lorenz, *Nachr. Chem.* **2017**, *65*, 535–541; c) D. Marinelli, F. Fasano, B. Najjari, N. Demitri, D. Bonifazi, *J. Am. Chem. Soc.* **2017**, *139*, 5503–5519; d) R. Zhao, J. Liu, L. Wang, *Acc. Chem. Res.* **2020**, *53*, 1557–1567; e) Y. Fu, H. Yang, Y. Gao, L. Huang, R. Berger, J. Liu, H. Lu, Z. Cheng, S. Du, H.-J. Gao, X. Feng, *Angew. Chem. Int. Ed.* **2020**, *59*, 8873–8879; f) Y. Chen, W. Chen, Y. Qiao, X. Lu, G. Zhou, *Angew. Chem. Int. Ed.* **2020**, *59*, 7122–7130; g) P. Lu, K.-Y. Chung, A. Stafford, M. Kiker, K. Kafle, Z. A. Page, *Polym. Chem.* **2021**, *12*, 327–348.

[98] J. E. Mulvaney, J. J. Bloomfield, C. S. Marvel, *J. Polym. Sci.* **1962**, *62*, 59–72.

[99] I. Yamaguchi, T. Tominaga, M. Sato, *Polym. Int.* **2009**, *58*, 17–21.

[100] I. Yamaguchi, B.-J. Choi, T. Koizumi, K. Kubota, T. Yamamoto, *Macromolecules* **2007**, *40*, 438–443.

[101] S. Hayashi, T. Koizumi, *Polym. Chem.* **2012**, *3*, 613–616.

[102] J. H. Son, G. Jang, T. S. Lee, *Polymer* **2013**, *54*, 3542–3547.

[103] N. Matsumi, Y. Chujo, *Macromolecules* **1998**, *31*, 3802–3806.

[104] a) N. Matsumi, K. Kotera, K. Naka, Y. Chujo, *Macromolecules* **1998**, *31*, 3155–3157; b) N. Matsumi, K. Kotera, Y. Chujo, *Macromolecules* **2000**, *33*, 2801–2806.

[105] A. W. Baggett, F. Guo, B. Li, S.-Y. Liu, F. Jäkle, *Angew. Chem. Int. Ed.* **2015**, *54*, 11191–11195.

[106] X.-Y. Wang, F.-D. Zhuang, J.-Y. Wang, J. Pei, *Chem. Commun.* **2015**, *51*, 17532–17535.

[107] a) X.-Y. Wang, H.-R. Lin, T. Lei, D.-C. Yang, F.-D. Zhuang, J.-Y. Wang, S.-C. Yuan, J. Pei, *Angew. Chem. Int. Ed.* **2013**, *52*, 3117–3120; b) X.-Y. Wang, F.-D. Zhuang, X. Zhou, D.-C. Yang, J.-Y. Wang, J. Pei, *J. Mater. Chem. C* **2014**, *2*, 8152–8161.

[108] a) W. Zhang, G. Li, L. Xu, Y. Zhuo, W. Wan, N. Yan, G. He, *Chem. Sci.* **2018**, *9*, 4444–4450; b) S. Zhang, X. Yang, X. Liu, L. Xu, B. Rao, N. Yan, G. He, *J. Mater. Chem. C* **2021**, *9*, 4053–4061; c) S. Pang, Z. Wang, X. Yuan, L. Pan, W. Deng, H. Tang, H. Wu, S. Chen, C. Duan, F. Huang, Y. Cao, *Angew. Chem. Int. Ed.* **2021**, *60*, 8813–8817.

[109] L. Ye, S. Zhang, L. Huo, M. Zhang, J. Hou, *Acc. Chem. Res.* **2014**, *47*, 1595–1603.

[110] T. Lorenz, A. Lik, F. A. Plamper, H. Helten, *Angew. Chem. Int. Ed.* **2016**, *55*, 7236–7241.

[111] F. Brosge, T. Lorenz, H. Helten, C. Bolm, *Chem. Eur. J.* **2019**, *25*, 12708–12711.

[112] a) U. Lücking, *Angew. Chem. Int. Ed.* **2013**, *52*, 9399–9408; b) K. M. Foote, J. W. M. Nissink, T. McGuire, P. Turner, S. Guichard, J. W. T. Yates, A. Lau, K. Blades, D. Heathcote, R. Odedra, G. Wilkinson, Z. Wilson, C. M. Wood, P. J. Jewsbury, *J. Med. Chem.* **2018**, *61*, 9889–9907; c) U. Lücking, *Org. Chem. Front.* **2019**, *6*, 1319–1324.

[113] J. S. Schneider, I. Krummenacher, H. Braunschweig, H. Helten, *Chem. Commun.* **2023**, *59*, 8408–8411.

[114] V. Zeh, J. S. Schneider, J. Bachmann, I. Krummenacher, H. Braunschweig, H. Helten, *Chem. Commun.* **2023**, *59*, 13723–13726.

2 Results and Discussion

2.1 Electrophilic activation of difunctional aminoboranes: B–N coupling versus intramolecular Cl/Me exchange

The following section is slightly modified and reproduced from published article[*] with permission from The Royal Society of Chemistry.

Abstract. Treatment of an *N*-silyl-*B*-chloro-aminoborane with substoichiometric quantities of Me_3SiOTf afforded B–N coupling, whereas activation with 5 mol% of $Ag[Al\{OC(CF_3)_3\}_4]$ led to Cl/Me exchange between the boron and the silicon center. Combined experimental and computational studies of the latter process support a chain reaction that is initiated by nucleation-limited chloride abstraction.

2.1.1 Introduction

Chemical transformations that are induced by substoichiometrically employed reagents, that is, catalyses or initiated chain reactions, respectively, belong to the standard toolbox of contemporary organic chemistry.[1] Inorganic main group chemistry, on the other hand, still mainly relies on stoichiometric reactions, although a few very successful catalytic or initiated procedures have been elaborated, especially in the field of inorganic polymer chemistry.[2] These include the $B(C_6F_5)_3$-catalyzed Piers-Rubinsztajn reaction for the synthesis of oligo- and polysiloxanes,[3] the PCl_5-initiated living cationic chain growth polycondensation of phosphoranimines leading to polyphosphazenes,[4] as well as catalytic dehydrocoupling routes[5] and anionically initiated procedures[6] towards polysilanes. Catalytic dehydrocoupling reactions of amine–boranes, RR'HN–BH_2R'', first demonstrated by Manners and co-workers,[7] leads to B–N catenated products of the form $[RR'N–BHR'']_{x/n}$, which are either ring systems, linear oligomers, or polymers (Scheme 2.1.1i).[2,7-9] Catalytic or initiated transformations of their unsaturated congeners, aminoboranes, RXN=BR'Y, have not been systematically explored thus far. Paetzold and co-workers extensively explored the generation of iminoboranes, RN≡BR', through thermolysis of suitable molecular precursors (including *N*-silyl-*B*-chloro-aminoboranes), and studied their follow-up chemistry (Scheme 2.1.1ii).[10] In the cases where the iminoboranes were unstable in the monomeric form, mostly cyclic oligomers formed. In some instances, insoluble waxy materials were obtained, for which the constitution of linear poly(iminoborane)s was proposed.[10c,d] Braunschweig and co-workers reported on the

* M. Maier, J. Klopf, C. Glasmacher, F. Fantuzzi, J. Bachmann, O. Ayhan, A. Koner, B. Engels, H. Helten, *Chem. Commun.* **2022**, *58*, 4464-4467. (M.M. and J.K. contributed equally to this work)

coupling of B=N units in the coordination sphere of ruthenium[11a] and platinum[11b] to give metal-coordinated linear $(BN)_2$ chains;[12] though this proceeded by stoichiometric reactions.

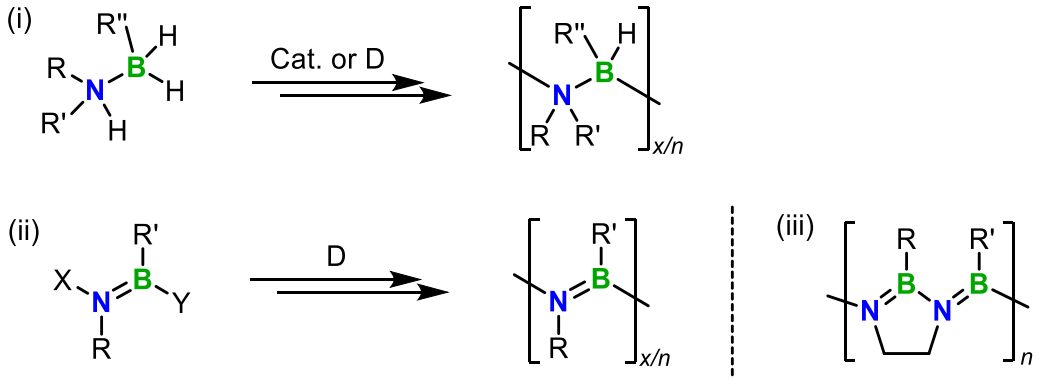

Scheme 2.1.1. Transformations with B–N coupling of amine–boranes (i) and aminoboranes (ii; leaving groups: X = electrofuge, Y = nucleofuge; R, R', R'' = organic substituents or H); and structure of cyclolinear poly(iminoborane)s (iii).

Our group has been engaged in the development of various novel B-[13] and B=N-doped[14] inorganic–organic hybrid polymers and oligomers. The former were synthesized via catalytic B–C or C–C coupling routes. The B–N coupling polycondensation processes applied to obtain the latter compounds, on the other hand, generally proceeded in a spontaneous manner. In this way, we accomplished the preparation of well-defined cyclolinear B=N catenated species (Scheme 2.1.1iii), which represent the closest approach to poly(iminoborane)s to date.[8e,15]
We now aimed at developing novel catalytic or initiated B–N coupling routes with a view to devise procedures towards the controlled formation of such kinds of macromolecular materials. To this end, we decided to investigate the activation of *N*-silyl-*B*-chloro-aminoboranes, as model substrates, using electrophilic reagents. Whereas Me_3SiOTf proved to efficiently initiate the transformation of **1a** to the expected borazine product, **2a**, Krossing's silver(I) salt $Ag[Al\{OC(CF_3)_3\}_4]$,[16] in substoichiometric quantities, initiated an intramolecular Cl/Me exchange process. Very recently, Chiu and co-workers observed such a Cl/Me exchange reaction at an *N*-silyl-*B*-chloro-aminoborane as well.[17-19] Herein, we demonstrate that 5 mol% of $Ag[Al\{OC(CF_3)_3\}_4]$ are sufficient to achieve full conversion of **1a,b** to **3a,b**, and we present in-depth experimental and theoretical studies shedding light on the mechanism of this unusual transformation.

2.1.2 Results and Discussion

We synthesized the difunctional aminoboranes **1a,b**, previously reported by us (**1a**)[15b] and Paetzold et al. (**1b**), respectively,[10b] via Si/B exchange condensation between heptamethyl-disilazane and $RBCl_2$ (R = Oct or Mes) (Scheme 2.1.2). Compounds **1a,b** were obtained as mixtures of (*E*/*Z*)-diastereomers, thus evidencing hindered rotation about their B=N double

bonds. Their ^{1}H and ^{13}C{^{1}H} NMR spectra showed two sets of resonances. For **1b**, we succeeded in assigning them to the respective *E*- and *Z*-isomer with the aid of 2D ^{1}H,^{1}H NOESY (Figure S5.1.9). The ^{11}B{^{1}H} NMR spectra of (*E*/*Z*)-**1a,b** each showed a single, broad peak at about 44 ((*E*/*Z*)-**1a**) and 42 ppm ((*E*/*Z*)-**1b**).

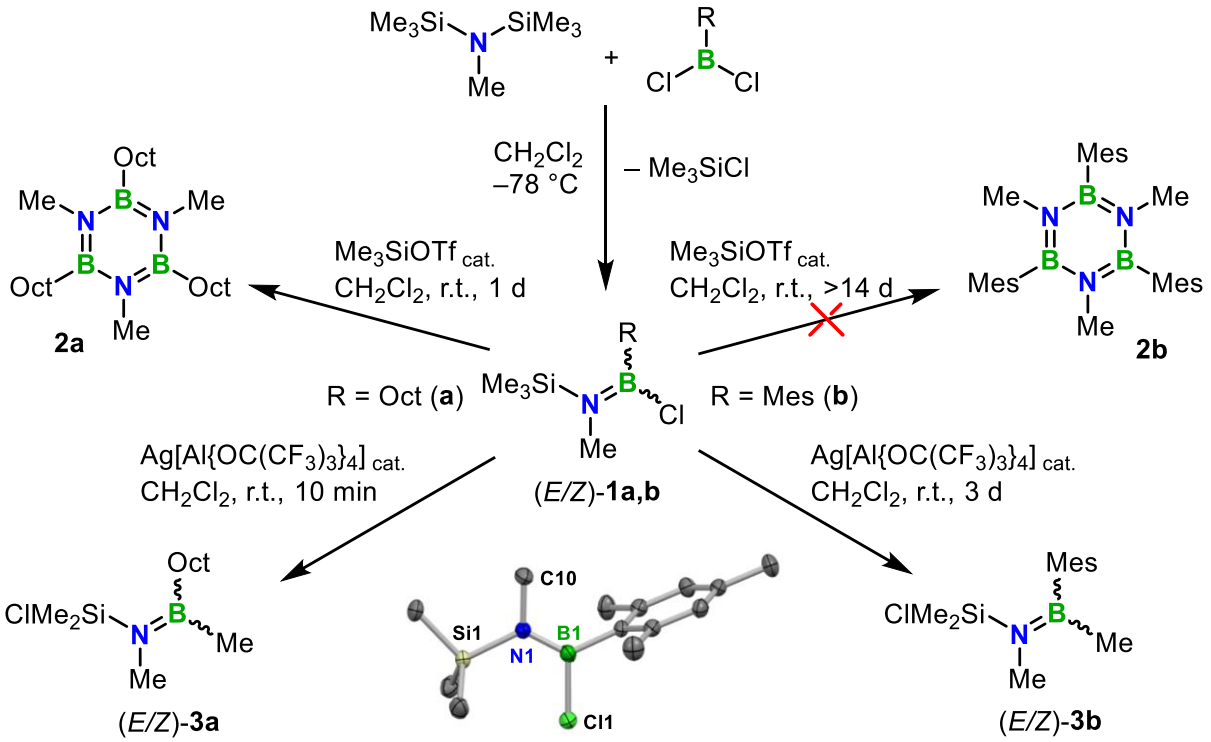

Scheme 2.1.2. Synthesis and transformations of difunctional aminoboranes (*E*/*Z*)-**1a,b**, and molecular structure of (*Z*)-**1b** in the solid state (H atoms omitted for clarity).

Upon slow crystallization from a concentrated solution of (*E*/*Z*)-**1b** in *n*-hexane we obtained single-crystals suitable for X-ray diffractometry of exclusively the *Z*-isomer (see inset in Scheme 2.1.2). Its molecular structure features trigonal-planar coordinated boron and nitrogen centers (Σ(BR_3) and Σ(NR_3) = 360.0°), connected by a relatively short B–N bond[20] (1.393(4) Å), in agreement with a pronounced double bond character. The mesityl group of (*Z*)-**1b** is orthogonal to the plane of the R_2BNR_2 moiety (∢87.2°); thus, π-conjugation between the aryl ring and the B=N bond is excluded. In order to investigate a potential temperature-dependent interconversion between the two diastereomers, we dissolved crystals of pure (*Z*)-**1b** at low temperature (−80 °C) in CD_2Cl_2 and gradually increased the temperature while monitoring the progress by ^{1}H NMR spectroscopy (Figure S5.1.26). No interconversion occurred below −30 °C. Upon further increase of the temperature, the equilibration process set in. It was complete within 16 h at 25 °C, resulting in a mixture of (*Z*)-**1b** and (*E*)-**1b** of approximately 1:1 ratio.

Compound (*E*/*Z*)-**1a** showed slow degradation when kept in CH_2Cl_2 solution at ambient temperature for an extended period. After 39 h, ^{11}B{^{1}H} NMR spectroscopy revealed the

emergence of an additional small signal at about 37 ppm, which could indicate the formation of borazine **2a**;[21a] however, the transformation was still far from complete after 6 d (Figure S5.1.22). When we treated an (*E*/*Z*)-**1a** solution under otherwise identical conditions with 5 mol% of Me_3SiOTf, we observed selective transformation of **1a** to borazine **2a** within 24 h (Figure S5.1.23). The constitution of **2a** was confirmed by comparison of its ^{1}H and $^{11}B\{^{1}H\}$ NMR data with literature data[21a] for that compound.

An attempt to apply the same procedure to the bulkier derivative (*E*/*Z*)-**1b** did not result in an accordingly clean transformation. Only traces of **2b**[21b] were detected by $^{11}B\{^{1}H\}$ NMR spectroscopic monitoring after 14 days (Figure S5.1.24). Therefore, we decided to probe the stronger electrophilic reagent $Ag[Al\{OC(CF_3)_3\}_4]$ as an initiator (5 mol%). After 23 h, the $^{11}B\{^{1}H\}$ NMR spectrum revealed the emergence of a single new signal at 53 ppm, which in the further course grew at the expense of that of **1b**. The transformation was complete within 3 days. The NMR data for the product was consistent with the formation of aminoborane **3b**, also as a mixture of (*E*/*Z*)-isomers. Hence, an exchange of the chlorine and the methyl group between the boron and the silicon center had occurred.[17-19] (*E*/*Z*)-**3b** was isolated after workup in 76 % yield. Its ^{1}H NMR spectrum displayed diagnostic signals for the B-CH_3 moiety at 0.68 ppm for (*Z*)-**3b** and at 0.75 ppm for (*E*)-**3b** (3 H each). In the $^{13}C\{^{1}H\}$ NMR spectrum these B-CH_3 groups give rise to significantly broadened resonances at 6.9 ppm ((*Z*)-**3b**) and 8.5 ppm ((*E*)-**3b**). Also in this case, a 2D $^{1}H,^{1}H$ NOESY measurement allowed for the assignment of the two isomers (Figures S5.1.19 and S5.1.20). Similar observations were made in the reaction of (*E*/*Z*)-**1a** in the presence of 5 mol% of $Ag[Al\{OC(CF_3)_3\}_4]$. In this case, full conversion to (*E*/*Z*)-**3a** was observed within 10 min (Figure S5.1.23).

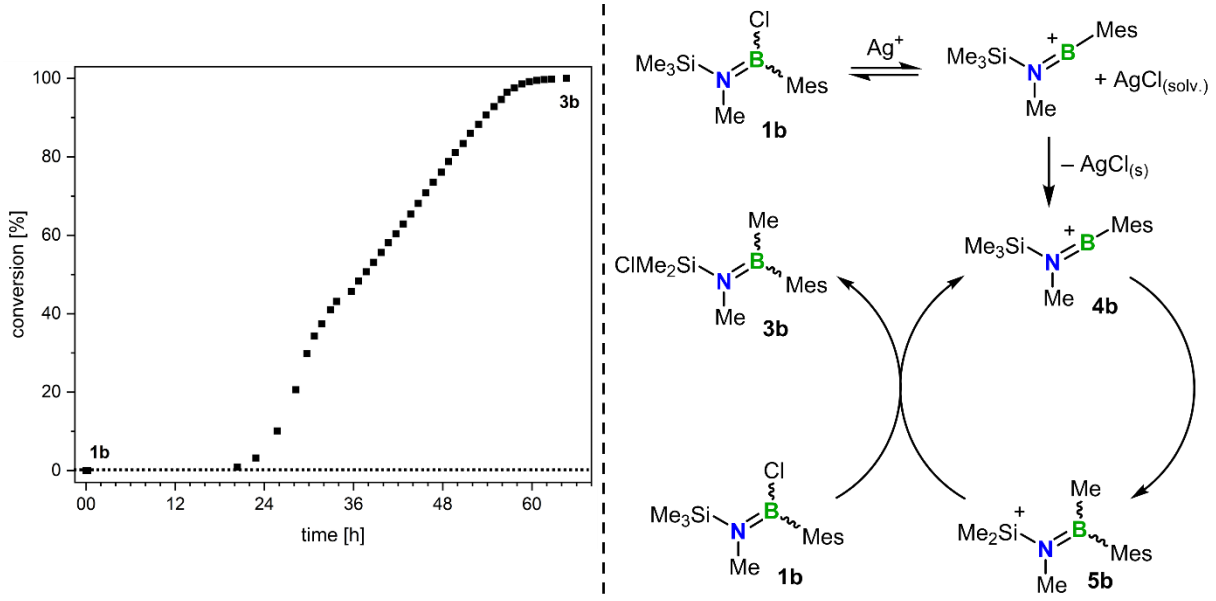

Figure. 2.1.1. Reaction progress of the rearrangement of (*E*/*Z*)-**1b** (0.15 M in CD_2Cl_2, in a sealed amber glass NMR tube, 5 mol% $Ag[Al\{OC(CF_3)_3\}_4]$, 25 °C) to (*E*/*Z*)-**3b** (conversion determined by ^{1}H NMR spectroscopy, left) and the proposed cycle for this chain reaction (right).

Next, we investigated the reaction of **1b** in the presence of Ag[Al{OC(CF$_3$)$_3$}$_4$] under various conditions and monitored its progress by ^{1}H and ^{11}B{^{1}H} NMR spectroscopy. The plot of the conversion of **1b** (0.15 M in CD_2Cl_2, 5 mol% Ag[Al{OC(CF$_3$)$_3$}$_4$], 25 °C) against time displayed a sigmoidal shape (Figure 2.1.1, left). Thus, the reaction started after an induction period of about 20 h, within which virtually no conversion was observed. Upon initiation, the rate gradually increased, before entering a phase (between ca. 36 and 56 h after mixing) with a largely linear course suggestive of zero-order kinetics. Towards the end of the reaction (56 – 64 h), saturation was observed, where the progress followed approximately first order in [**1b**].
In various trials conducted the length of the induction period differed in a seemingly random manner. We noticed that stirring apparently had a detrimental effect. When the reaction was performed in a vial and the mixture was stirred, while all other parameters were identical to the trial described above, the induction period was considerably longer (> 2 d, Figure S5.1.28). Interestingly, the overall concentration of the substrate (with the substrate:initiator ratio kept constant) had a negligible effect on the rate once initiation had occurred (Figures S5.1.28–S5.1.30). With an initiator loading of only 1 mol%, even after 12 d, no product formation was observed (Figure S5.1.25).
Based on these findings we propose the chain reaction depicted in Figure 2.1.1. It is initiated by chloride abstraction from **1b** through Ag[Al{OC(CF$_3$)$_3$}$_4$]. This step, however, is reversible at the molecular scale. Irreversible abstraction of chloride, however, is triggered by the formation of solid AgCl, the rate of which is limited by the slow kinetics of nucleation. This accounts for the observed induction phase. The apparently unpredictable nature of the reaction onset is thus a result of local effects on the nucleation process, which are difficult to control. Once initiated, rapid methyl migration occurs at a cationic intermediate (**4b**[22] → **5b**). The cycle is completed by transfer of the chloride from a further molecule of **1b** to **5b**. The lack of dependence of the rate on [**1b**] indicates that the latter step is not rate-limiting. Only towards the end, when the concentration of **1b** has significantly decreased, [**1b**] starts to show an impact.

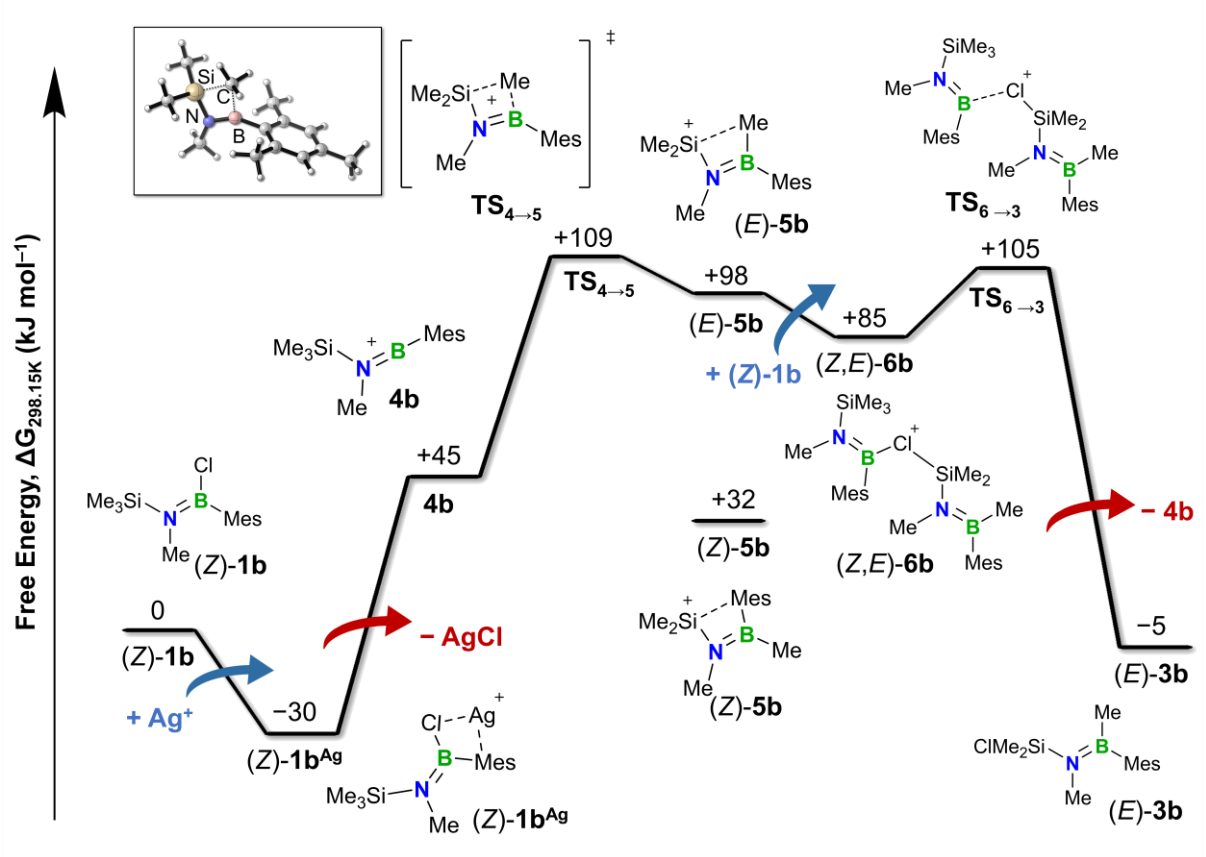

Figure 2.1.2. Free energy profile of the cycle depicted in Figure 2.1.1.

According to our DFT calculations, the abstraction of chloride from (*Z*)-**1b** by Ag^+ to give **4b** and AgCl (i.e., as an ion pair) in the first step is an endergonic reaction (Figure 2.1.2). Compound (*Z*)-**1b** may initially associate with the silver cation to form an ion–molecule complex, (*Z*)-$\mathbf{1b^{Ag}}$, accompanied by a free energy decrease of –30 kJ mol^{-1}. The free energy of reaction for (*Z*)-**1b** + Ag^+ → **4b** + AgCl is +45 kJ mol^{-1} with respect to separated (*Z*)-**1b** and Ag^+, which is naturally increased to +75 kJ mol^{-1} if one adds the energetic stabilization of the ion–molecule complex. We thus conclude that the thermodynamic driving force of this reaction step is the gain of lattice energy when solid AgCl forms. This explains the unusual behavior of the reaction progression, being in line with the observation of an induction phase.

The reaction from **4b** to (*E*)-**5b** proceeds over a computed barrier of +64 kJ mol^{-1}. Compound (*E*)-**5b** is energetically +53 kJ mol^{-1} above compound **4b**. Hence, the barrier of the reverse reaction corresponds to +11 kJ mol^{-1}. The reaction of (*E*)-**5b** with (*Z*)-**1b** to (*E*)-**3b** and **4b** represents a transfer of the chloride from the boron center of (*Z*)-**1b** to the silicon center of (*E*)-**5b**. The intermediate (*Z*,*E*)-**6b** describes an adduct between (*Z*)-**1b** and (*E*)-**5b**, in which the chlorine atom connects the two fragments in a bridging manner. In this complex, whose free energy is –13 kJ mol^{-1} lower than that of (*E*)-**5b**, the B–Cl bond is already lengthened by 0.163 Å with respect to (*Z*)-**1b**. If the B–Cl distance is increased further, and thus the

compounds (*E*)-**3b** and **4b** are generated, a barrier of +20 kJ mol^{-1} (**TS$_{6\rightarrow3}$**) is observed. This means that the last step of the cycle is nearly barrierless.

The free energy profile predicts that the cycle (Figure 2.1.1) starting with **4b** has a considerably lower barrier (+64 kJ mol^{-1} vs +109 kJ mol^{-1}) than that of the full reaction starting with **1b**. Furthermore, the cycle is exergonic by about −50 kJ mol^{-1} while the full reaction is nearly thermoneutral (ΔG = −5 kJ mol^{-1}). This higher exothermicity of the cycle presumably accelerates the reaction after some cycles since the excess energy facilitates the overcoming of the barrier between **4b** and (*E*)-**5b**.

Finally, we also computationally investigated whether the cycle runs exclusively via (*E*)-**5b** or if (*Z*)-**5b** is also involved. Indeed, (*Z*)-**5b** (Figure 2.1.3) resembles the cation in the salt obtained by Chiu and co-workers from the stoichiometric reaction of Ag[Al{OC(CF$_3$)$_3$}$_4$] with a different aminoborane substrate.[17] Our calculations, however, speak against the formation of (*Z*)-**5b** as an intermediate in the chain reaction. While **4b** may rearrange to (*E*)-**5b**, there is no pathway leading from **4b** directly to (*Z*)-**5b**. Conversion of (*E*)-**5b** to (*Z*)-**5b** by rotation about the B=N bond may proceed over a calculated barrier of about +87 kJ mol^{-1}. This reaction is thermodynamically favored by –66 kJ mol^{-1}. Therefore, it should irreversibly take place in the absence of further **1b**, consistent with the results obtained by Chiu.[17] However, if further **1b** is present, chloride transfer is much more facile, hence, this competitive reaction should be significantly faster. We therefore conclude that the (*E*/*Z*)-**3b** mixture results from the isomerization of the (*E*)-**3b** isomer, which is initially formed, to the (*Z*)-**3b** isomer; the calculated rotation barrier is +90 kJ mol^{-1}. It is plausible that, on the time scale of the overall rearrangement process (ca. 44 h), this isomerization proceeds in parallel.

2.1.3 Conclusion

In conclusion, we have demonstrated that *N*-silyl-*B*-chloro-aminoboranes can be activated by substoichiometric amounts of electrophilic reagents. Whereas Me$_3$SiOTf brought about clean B–N coupling of (*E*/*Z*)-**1a** to give **2a**, Ag[Al{OC(CF$_3$)$_3$}$_4$] initiated an intramolecular Cl/Me exchange, proceeding via a chain reaction that involves highly reactive cationic intermediates. We are currently elucidating the mechanism of the observed B–N coupling processes, which we will report in due course, and we are exploring further initiated or catalytic transformations of aminoboranes and related species with a focus on processes that are applicable to polymerizations.

2.1.4 Experimental Section

General procedures. Unless otherwise stated, all reagents were purchased from commercial suppliers and used without further purification. All reactions were performed under argon atmosphere using standard Schlenk techniques or an MBraun glovebox. Solvents (dichloromethane, *n*-pentane, *n*-hexane) were dried and degassed according to general purification methods. Solvents for NMR spectroscopy were dried and degassed prior to use. Heptamethyldisilazane, trimethylsilyl-trifluoromethanesulfonate Me_3SiOTf and silver tetrakis(perfluoro-*tert*-butoxy)aluminate $Ag[Al(OC(CF_3)_3)_4]$ were commercially purchased and used as received. Mesityllithium[23] and chloro(trimethylsilyl-(methyl)amino)-*n*-octylborane (**1a**)[15b] were prepared as described in literature. NMR spectra were recorded at 25 °C on a Bruker Avance III HD spectrometer operating at 300 MHz, on a Bruker Avance II-400 spectrometer, a Bruker Avance III HD spectrometer or on a Bruker Avance Neo 400 spectrometer operating at 400 MHz. Chemical shifts were referenced to residual protic impurities in the solvent (^1H) or the deuterated solvent itself (^{13}C) and reported relative to external $SiMe_4$ (^1H, ^{13}C, ^{29}Si) or $BF_3{\cdot}OEt_2$ (^{11}B) standards. Mass spectra were obtained with the use of a Thermo Scientific Exactive Plus Orbitrap MS system employing atmospheric sample analysis probe (ASAP). All MS spectra obtained showed excellent congruence with the calculated isotopic distribution patterns. Elemental analyses were performed on an Elementar vario MICRO cube elemental analyzer.

Spectra. All spectra and other result figures are shown in Appendix 5.1.

Synthesis of dichloro-(2,4,6-trimethylphenyl)borane.[24] To a suspension of mesityllithium (2.52 g, 20.0 mmol, 1 equiv.) in *n*-hexane (200 mL) was added a solution of BCl_3 (1M in *n*-hexane, 50 mmol, 2.5 equiv.) at −78°C. The mixture was warmed to room temperature overnight. The formed salt was removed by filtration with *n*-pentane (3 x 15 mL) and the solvent was removed *in vacuo*. After distillation, a colorless liquid was obtained (2.05 g, 10.2 mmol, 51 % yield). ^1H NMR (300 MHz, $CDCl_3$): δ = 6.85 (m, 2H, Ar-*H*), 2.35 (s, 6H, *o*-Mes-CH_3), 2.30 ppm (s, 3H, *p*-Mes-CH_3); $^{11}B\{^1H\}$ NMR (96 MHz, $CDCl_3$): δ = 60.9 (s) ppm.

Synthesis of 1b. To a solution of dichloro-(2,4,6-trimethylphenyl)borane (2.81 g, 13.99 mmol, 1 equiv.) in DCM (25 mL) was added heptamethyldisilazane (2.59 g, 14.76 mmol, 1.06 equiv.) dropwise at −78°C. After 30 min, the cooling bath was removed and the reaction was warmed to room temperature overnight. After removing the volatiles *in vacuo* and crystallization from *n*-hexane, colorless crystals were obtained (2.42 g, 9.04 mmol, 65 % yield). ^1H NMR (400 MHz, $CDCl_3$): (*Z*)-**1b**: δ = 6.86 (m, 2H, Mes-C*H*), 2.66 (s, 3H, N-CH_3), 2.32 (s, 3H, *p*-Mes-CH_3), 2.29 (s, 6H, *o*-Mes-CH_3), 0.43 ppm (s, 9H, Si-CH_3); (*E*)-**1b**: δ = 6.80 (m, 2H, Mes-C*H*),

3.04 (s, 3H, N-CH_3), 2.30 (s, 3H, *p*-Mes-CH_3), 2.29 (s, 6H, *o*-Mes-CH_3), −0.02 ppm (s, 9H, Si-CH_3); $^{11}B\{^1H\}$ NMR (128 MHz, $CDCl_3$): δ = 41.6 (s) ppm; $^{29}Si\{^1H\}$ NMR (60 MHz, $CDCl_3$): (*Z*)-**1b**: δ = 14.3 (s) ppm; (*E*)-**1b**: δ = 13.6 (s) ppm; $^{13}C\{^1H\}$ NMR (100 MHz, $CDCl_3$): (*Z*)-**1b**: δ = 137.6 (s, *o*-Mes-*C*), 137.7 (s, *p*-Mes-*C*), 127.3 (s, Mes-CH), 35.2 (s, N-*C*H_3), 21.4 (s, *o*-Mes-*C*H_3), 21.3 (s, *p*-Mes-*C*H_3), 1.5 ppm (s, Si-*C*H_3); (*E*)-**1b**: δ = 138.0 (s, *o*-Mes-*C*), 137.8 (s, *o*-Mes-*C*), 127.2 (s, Mes-*C*H), 34.2 (s, N-*C*H_3), 22.1 (s, *p*-Mes-*C*H_3), 21.3 (s, *o*-Mes-*C*H_3), 0.1 ppm (s, Si-*C*H_3); HRMS (ASAP): m/z calcd.: 267.1376 $[M]^+$, found: 267.1371; elem. anal. calcd. (%) for $C_{13}H_{23}BClNSi$: C 58.33, H 8.66, N 5.23; found: C 58.56, H 8.96, N 5.28.

Synthesis of 2a.[25] To Me_3SiOTf (3.7 mg, 17 µmol, 5 mol%) was added a cold solution (−30 °C) of **1a** in DCM (0.7 mL, 0.48 M). Subsequently, the reaction was monitored via $^{11}B\{^1H\}$ NMR in a sealed J. Young tube and showed full conversion to compound **2a** after 24 h. After removing all volatiles *in vacuo* a colorless oil was obtained quantitatively. ^1H NMR (300 MHz, CD_2Cl_2): δ = 2.94 (s, 9H, N-CH_3), 1.36-1.29 (m, 36H, CH_2), 1.07-1.04 (m, 6H, B-CH_2), 0.89 (t, 9H, CH_3); $^{11}B\{^1H\}$ NMR (96 MHz, CD_2Cl_2): δ = 36.7 (s) ppm.

Synthesis of 3a. To $Ag[Al(OC(CF_3)_3)_4]$ (17.6 mg, 16 µmol, 5 mol%) was added a cold solution (−30 °C) of **1a** in DCM (0.68 mL, 0.48 M). After 10 min, the $^{11}B\{^1H\}$ NMR revealed the formation of compound **3a**. $^{11}B\{^1H\}$ NMR (96 MHz, CH_2Cl_2): δ = 54.1 (s) ppm.

Synthesis of 3b. To a solution of **1b** (25 mg, 90 µmol, 1 equiv.) in CD_2Cl_2 (0.3 mL) was added a solution of $Ag[Al(OC(CF_3)_3)_4]$ (5 mg, 4.5 µmol, 5 mol%) in CD_2Cl_2 (0.3 mL). Subsequently, the reaction was stored in the dark for 3 days, after which NMR spectra revealed full conversion to compound **3b**. The solvent was removed in vacuo and the residue was washed with *n*-hexane. After removing *n*-hexane *in vacuo* a colorless oil was obtained (18.3 mg, 68 µmol, 76 % yield). ^1H NMR (400 MHz, CD_2Cl_2): (*Z*)-**3b**: δ = 6.75 (m, 2H, Mes-C*H*), 2.99 (s, 3H, N-CH_3), 2.26 (s, 3H, *p*-Mes-CH_3), 2.17 (s, 6H, *o*-Mes-CH_3), 0.68 (s, 3H, B-CH_3), 0.13 ppm (s, 6H, Si-(CH_3)$_2$Cl); (*E*)-**3b**: δ = 6.79 (m, 2H, Mes-C*H*), 2.64 (s, 3H, N-CH_3), 2.27 (s, 3H, *p*-Mes-CH_3), 2.15 (s, 6H, *o*-Mes-CH_3), 0.75 (s, 3H, B-CH_3), 0.72 ppm (s, 6H, Si-(CH_3)$_2$Cl); $^{11}B\{^1H\}$ NMR (128 MHz, CD_2Cl_2): δ = 52.7 (s) ppm; $^{29}Si\{^1H\}$ NMR (60 MHz, CD_2Cl_2): (*Z*)-**3b**: δ = 20.2 (s) ppm; (*E*)-**3b**: δ = 20.6 (s) ppm; $^{13}C\{^1H\}$ NMR (100 MHz, CD_2Cl_2): (*Z*)-**3b**: δ = 143.3 (s, *ipso*-Mes-*C*), 137.3 (s, *o*-Mes-*C*), 137.0 (s, *p*-Mes-*C*), 127.4 (s, Mes-*C*H), 33.6 (s, N-*C*H_3), 22.0 (s, *o*-Mes-*C*H_3), 21.3 (s, *p*-Mes-*C*H_3), 6.9 (br, B-*C*H_3), 3.4 ppm (s, Si-(*C*H_3)$_2$Cl); (*E*)-**3b**: δ = 143.3 (s, *ipso*-Mes-*C*), 136.6 (s, *p*-Mes-*C*), 136.6 (s, *o*-Mes-*C*), 127.4 (s, Mes-*C*H), 35.4 (s, N-*C*H_3), 21.3 (s, *p*-Mes-*C*H_3), 21.3 (s, *o*-Mes-*C*H_3), 8.5 (br, B-*C*H_3), 5.1 ppm (s, Si-(*C*H_3)$_2$Cl); HRMS (ASAP): m/z calcd.: 268.1454 $[M+H]^+$, found: 268.1449; elem. anal. calcd. (%) for $C_{13}H_{23}BClNSi$: C 58.33, H 8.66, N 5.23; found: C 58.48, H 8.79, N 5.08.

Crystallographic data

Crystals suitable for single-crystal X-ray diffraction were selected, coated in perfluoropolyether oil, and mounted on MiTeGen sample holders. Diffraction data were collected on Bruker X8 Apex II 4-circle diffractometers with CCD area detectors using Mo-Kα radiation. The crystals were cooled using an Oxford Cryostreams low-temperature device. Data were collected at 100 K. The images were processed and corrected for Lorentz-polarization effects and absorption as implemented in the Bruker software packages. The structures were solved using the intrinsic phasing method (SHELXT)[26] and Fourier expansion technique. All non-hydrogen atoms were refined in anisotropic approximation, with hydrogen atoms 'riding' in idealized positions, by full-matrix least squares against F^2 of all data, using SHELXL[27] software and the SHELXLE graphical user interface.[28] Other structural information was extracted using OLEX2 software.[29]

Table 2.1.1. Crystal structure and refinement data for (*Z*)-**1b**

No.	**(*Z*)-1b**
CCDC number	2130024
Size / mm	0.170 x 0.343 x 0.467
Empiric Formula	$C_{13}H_{23}BClNSi$
M / g mol^{-1}	267.67
Crystal system	monoclinic
Space group	P 1 21/c 1
a / Å	8.256(4)
b / Å	11.579(6)
c / Å	16.616(8)
α / °	90.00
β / °	103.076(15)
γ / °	90.00
V / Å^3	1547.3(13)
Z	4
μ / mm^{-1}	0.305
T / K	98.42
$\theta_{min,max}$	2.163, 26.431
Completeness	0.989
Reflections: total/independent	3160, 2693
R_{int}	0.0922
Final *R*1 and *wR*2	0.0705, 0.2042
Largest peak, hole / e Å^{-3}	0.699, −0.649
ρ_{calc} / g cm^{-3}	1.149

Computational information

DFT calculations were performed with the Gaussian 16, Revision C.01 program package[30] using the ωB97X-D[31] functional in combination with the 6-31+G(d,p)[32] basis sets for geometry optimizations in gas phase and the 6-311+G(d,p)[32a,32d,32h,33] basis sets for single-point energy calculations. The basis set SDD/ECP[34] was used for Ag atoms. Single-point energy calculations were performed with the PCM[35] solvation model mimicking dichloromethane ($\varepsilon = 8.93$) as solvent. To get a first insight, we investigated the geometrical structures and relative energies of possible intermediates. Their equilibrium geometries were determined by geometry optimization and proved by frequency computations. Scans along appropriate reaction coordinates were performed to compute possible reaction pathways between these minima. To compute the minimal energy path (MEP) all other coordinates have been optimized for each point. The connectivity between the obtained transition states and the corresponding intermediates was assessed by further geometry optimizations, visual inspection of the imaginary frequencies, and additional intrinsic reaction coordinate (IRC)[36] computations. Thermodynamic parameters were calculated at a temperature of 298.15 K and a pressure of 1.00 atm. A concentration correction of $\Delta G^{0\rightarrow *} = RT\cdot\ln(24.46) = 1.89$ kcal mol^{-1} (T = 298.15 K) was added to the free energies of all calculated species. This was done to change the 1.00 atm gas phase values to the condensed phase standard state concentration of 1.00 mol·L^{-1}, which leads to a proper description of associative/dissociative steps. This is necessary because pure gas estimations overestimate the entropy penalty for the formation of complexes.[37]

Table 2.1.2. Relative energies of calculated species.

Molecules	Relative Energies [kJ mol^{-1}]
[(*Z*)-**1b**][Ag$^+$][(*Z*)-**1b**]	0
[(*Z*)-**1b^{Ag}**][(*Z*)-**1b**]	−30
[**4b**][AgCl][(*Z*)-**1b**]	+45
[**TS$_{4\rightarrow5}$**][AgCl][(*Z*)-**1b**]	+109
[(*E*)-**5b**][AgCl][(*Z*)-**1b**]	+98
[(*Z*)-**5b**][AgCl][(*Z*)-**1b**]	+32
[(*Z*,*E*)-**6b**][AgCl]	+85
[**TS$_{6\rightarrow3}$**][AgCl]	+105
[(*E*)-**3b**][Ag$^+$][(*Z*)-**1b**]	−5
[**TS$_{Rot3}$**][Ag$^+$][(*Z*)-**1b**]	+86
[**TS$_{Rot5}$**][AgCl][(*Z*)-**1b**]	+185

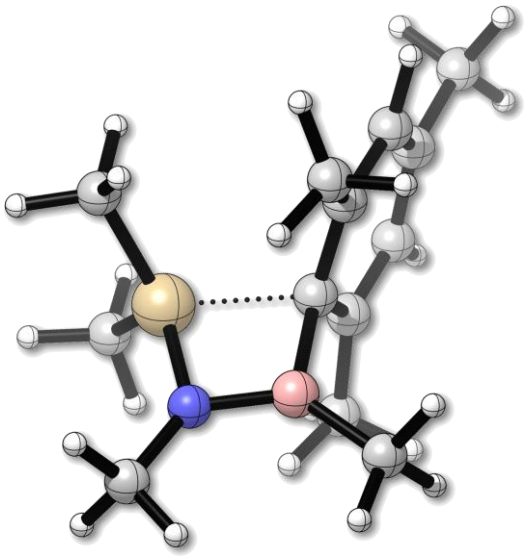

Figure 2.1.3. ωB97X-D/6-31+G(d,p)-optimized structure of (*Z*)-**5b**.

2.1.5 References

[1] (a) R. H. Grubbs, *Angew. Chem. Int. Ed.* **2006**, *45*, 3760; (b) B. List and J. W. Yang, *Science* **2006**, *313*, 1584.

[2] E. M. Leitao, T. Jurca and I. Manners, *Nat. Chem.* **2013**, *5*, 817.

[3] (a) D. J. Parks, J. M. Blackwell and W. E. Piers, *J. Org. Chem.* **2000**, *65*, 3090; (b) S. Rubinsztajn and J. Cella, *Polymer Prepr.* **2004**, *45*, 635; (c) M. A. Brook, *Chem. Eur. J.* **2018**, *24*, 8458.

[4] (a) C. H. Honeyman, I. Manners, C. T. Morrissey and H. R. All-cock, *J. Am. Chem. Soc.* **1995**, *117*, 7035; (b) V. Blackstone, S. Pfirrmann, H. Helten, A. Staubitz, A. Presa Soto, G. R. Whittell and I. Manners, *J. Am. Chem. Soc.* **2012**, *134*, 15293; (c) S. Rothemund and I. Teasdale, *Chem. Soc. Rev.* **2016**, *45*, 5200.

[5] (a) C. Aitken, J. F. Harrod and E. Samuel, *J. Am. Chem. Soc*. **1986**, *108*, 4059; (b) H.-G. Woo and T. D. Tilley, *J. Am. Chem. Soc.* **1989**, *111*, 8043.

[6] K. Sakamoto, K. Obata, H. Hirata, M. Nakajima and H. Sakurai, *J. Am. Chem. Soc*. **1989**, *111*, 7641.

[7] C. A. Jaska, K. Temple, A. J. Lough and I. Manners, *J. Am. Chem. Soc*. **2003**, *125*, 9424.

[8] Reviews: (a) A. Staubitz, A. P. M. Robertson, M. E. Sloan and I. Manners, *Chem. Rev*. **2010**, *110*, 4023; (b) N. E. Stubbs, A. P.M. Robertson, E. M. Leitao and I. Manners, J. *Organomet. Chem*. **2013**, *730*, 84; (c) H. C. Johnson, T. N. Hooper and A. S. Weller, *Top. Organomet. Chem*. **2015**, *49*, 153; (d) D. Han, F. Anke, M. Trose and T. Beweries, *Coord. Chem. Rev.* **2019**, *380*, 260; (e) T. Beweries and H. Helten, Poly(aminoborane)s and Poly(iminoborane)s. In Encyclopedia of Inorganic and Bioinorganic Chemistry; ed. R. A. Scott, Wiley, **2020**; DOI: 10.1002/9781119951438.eibc2717.

[9] (a) A. Staubitz, A. Presa Soto and I. Manners, *Angew. Chem. Int. Ed*. **2008**, *47*, 6212; (b) A. Staubitz, M. E. Sloan, A. P. M. Robertson, A. Friedrich, S. Schneider, P. J. Gates, J. Schmedt auf der Günne and I. Manners, *J. Am. Chem. Soc*. **2010**, *132*, 13332. (c) R. Dallanegra, A. P. M. Robertson, A. B. Chaplin, I. Manners and A. S. Weller, *Chem. Commun.* **2011**, *47*, 3763; (d) H. C. Johnson, A. P. M. Robertson, A. B. Chaplin, L. J. Sewell, A. L. Thompson, M. F. Haddow, I. Manners and A. S. Weller, *J. Am. Chem. Soc.* **2011**, *133*, 11076; (e) H. Helten, A. P. M. Robertson, A. Staubitz, J. R. Vance, M. F. Haddow and I. Manners, *Chem. Eur. J.* **2012**, *18*, 4665; (f) A. P. M. Robertson, E. M. Leitao, T. Jurca, M. F. Haddow, H. Helten, G. C. Lloyd-Jones and I. Manners, *J. Am. Chem. Soc.* **2013**, *135*, 12670; (g) A. N. Marziale, A. Friedrich, I. Klopsch, M. Drees, V. R. Celinski, J. Schmedt auf der Günne and S. Schneider, *J. Am. Chem. Soc.* **2013**,

135, 13342; (h) P. Cui, T. P. Spaniol, L. Maron and J. Okuda, *Chem. Eur. J.* **2013**, *19*, 13437; (i) H. C. Johnson, E. M. Leitao, G. R. Whittell, I. Manners, G. C. Lloyd-Jones and A. S. Weller, *J. Am. Chem. Soc.* **2014**, *136*, 9078; (j) A. Glüer, M. Förster, V. R. Celinski, J. Schmedt auf der Günne, M. C. Holthausen and S. Schneider, *ACS Catal.* **2015**, *5*, 7214; (k) C. Lichtenberg, M. Adelhardt, T. L. Gianetti, K. Meyer, B. de Bruin and H. Grützmacher, *ACS Catal.* **2015**, *5*, 6230; (l) N. T. Coles, M. F. Mahon and R. L. Webster, *Organometallics* **2017**, *36*, 2262; (m) M. Trose, M. Reiß, F. Reiß, F. Anke, A. Spannenberg, S. Boye, A. Lederer, P. Arndt and T. Beweries, *Dalton Trans*. **2018**, *47*, 12858; (n) G. M. Adams, A. L. Colebatch, J. T. Skornia, A. I. McKay, H. C. Johnson, G. C. Lloyd Jones, S. A. Macgregor, N. A. Beattie and A. S. Weller, *J. Am. Chem. Soc*. **2018**, *140*, 1481; (o) T. Jurca, T. Dellermann, N. E. Stubbs, D. A. Resendiz-Lara, G. R. Whittell and I. Manners, *Chem. Sci.* **2018**, *9*, 3360; (p) E. A. LaPierre, B. O. Patrick and I. Manners, *J. Am. Chem. Soc.* **2019**, *141*, 20009; (q) F. Anke, S. Boye, A. Spannenberg, A. Lederer, D. Heller and T. Beweries, *Chem. Eur. J.* **2020**, *26*, 7889.

[10] (a) P. I. Paetzold and W. M. Simson, *Angew. Chem. Int. Ed.* **1966**, *2*, 842; (b) P. Paetzold, A. Richter, T. Thijssen and S. Wür-tenberg, *Chem. Ber.* **1979**, *112*, 3811; (c) P. Paetzold and T. von Bennigsen-Mackiewicz, *Chem. Ber.* **1981**, *114*, 298; (d) H.-U. Meier, P. Paetzold and E. Schröder, *Chem. Ber.* **1984**, *117*, 1954; (e) J. Kiesgen, J. Münster and P. Paetzold, *Chem. Ber.* **1993**, *126*, 1559.

[11] (a) H. Braunschweig, C. Kollann and K. W. Klinkhammer, *Eur. J. Inorg. Chem.* **1999**, 1523; (b) C. Brunecker, M. Arrowsmith, F. Fantuzzi and H. Braunschweig, *Angew. Chem. Int. Ed.* **2021**, *60*, 16864.

[12] For fused $B_4C_4N_2$ ring systems comprising a $(BN)_4$ chain, see: K. Ota and R. Kinjo, *J. Am. Chem. Soc.* **2021**, *143*, 11152.

[13] (a) A. Lik, L. Fritze, L. Müller and H. Helten, *J. Am. Chem. Soc.* **2017**, *139*, 5692; (b) A. Lik, S. Jenthra, L. Fritze, L. Müller, K.-N. Truong and H. Helten, *Chem. Eur. J.* **2018**, *24*, 11961; (c) L. Fritze, N. A. Riensch and H. Helten, *Synthesis* **2019**, *51*, 399; (d) H. Helten, *Chem. Asian J.* **2019**, *14*, 919; (e) N. A. Riensch, M. Fest, L. Fritze, A. Helbig, I. Krummenacher, H. Braunschweig and H. Helten, *New J. Chem.* **2021**, *45*, 14920; (f) N. A. Riensch, L. Swoboda, A. Lik, I. Krummenacher, H. Braunschweig and H. Helten, *Z. Anorg. Allg. Chem.* **2021**, *647*, 421; (g) L. Fritze, M. Fest, A. Helbig, T. Bischof, I. Krummenacher, H. Braunschweig, M. Finze and H. Helten, *Macromolecules* **2021**, *54*, 7653.

[14] (a) T. Lorenz, A. Lik, F. A. Plamper and H. Helten, *Angew. Chem. Int. Ed.* **2016**, *55*, 7236; (b) H. Helten, *Chem. Eur. J.* **2016**, *22*, 12972; (c) T. Lorenz, M. Crumbach, T. Eckert, A. Lik and H. Helten, *Angew. Chem. Int. Ed.* **2017**, *56*, 2780; (d) N. A. Riensch, A. Deniz, S. Kühl, L. Müller, A. Adams, A. Pich and H. Helten, *Polym. Chem.* **2017**, *8*, 5264; (e) F. Brosge, T. Lorenz, H. Helten and C. Bolm, *Chem. Eur. J.* **2019**, *25*, 12708.

[15] (a) O. Ayhan, T. Eckert F. A. Plamper and H. Helten, *Angew. Chem. Int. Ed.* **2016**, *55*, 13321; (b) O. Ayhan, N. A. Riensch, C. Glasmacher and H. Helten, *Chem. Eur. J.* **2018**, *24*, 5883.

[16] I. Krossing, *Chem. Eur. J.* **2001**, *7*, 490.

[17] P.-H. Chen, C.-P. Hsu, H.-C. Tseng, Y.-H. Liu and C.-W. Chiu, *Chem. Commun.* **2021**, *57*, 13732.

[18] A related Br/Me rearrangement was observed upon heating 4-bromo-1-dibromoboryl-2-trimethylsilylbenzene in C_6D_6 at 120 °C; see: C. Reus, S. Weidlich, M. Bolte, H.-W. Lerner and M. Wagner, *J. Am. Chem. Soc.* **2013**, *135*, 12892.

[19] For related rearrangements at boryl-stannyl-ferrocenes; see: (a) F. Jäkle, A. J. Lough and I. Manners, *Chem. Commun.* **1999**, 453; (b) J. A. Gamboa, A. Sundararaman, L. Kakalis, A. J. Lough and F. Jäkle, *Organometallics* **2002**, *21*, 4169.

[20] Cf.: (a) G. J. Bullen and N. H. Clark, *J. Chem. Soc. A* **1970**, 992. (b) K. L. Bamford and D. W. Stephan, *Dalton Trans.* **2020**, *49*, 17571.

[21] (a) Y. Yamamoto, K. Miyamoto, J. Umeda, Y. Nakatani, T. Yamamoto and N. Miyaura, *J. Organomet. Chem.* **2006**, *691*, 4909; (b) K. Nagasawa, *Inorg. Chem.* **1966**, *5*, 442.

[22] For related cations, see refs. 17 and 20b.

[23] J. E. Borger, M. S. Bakker, A. W. Ehlers, M. Lutz, J. C. Slootweg and K. Lammertsma, *Chem. Commun.* **2016**, *52*, 3284.
[24] Further examples for the synthesis of dichloro-(2,4,6-trimethylphenyl)borane: (a) A. Sundararaman and F. Jäkle, *J. Organomet. Chem.* **2003**, *681*, 134; (b) W. Haubold, J. Herdtle, W. Gollinger and W. Einholz, *J. Organomet. Chem.* **1986**, *315*, 1; (c) W. Schacht and D. Kaufmann, *Chem. Ber.* **1987**, *120*, 1331; (d) K. Fujimoto, H. Yorimitsu and A. Osuka, *Chem. Eur. J.* **2015**, *21*, 11311.
[25] For further analytical data, see: Y. Yamamoto, K. Miyamoto, J. Umeda, Y. Nakatani, T. Yamamoto and N. Miyaura, *J. Organomet. Chem.* **2006**, *691*, 4909.
[26] G. M. Sheldrick, *Acta Crystallogr. A* **2015**, *71*, 3.
[27] Sheldrick, *Acta Crystallogr. A* **2008**, *64*, 112.
[28] C. B. Hübschle, G. M. Sheldrick and B. Dittrich, *J. Appl. Crystallogr*. **2011**, *44*, 1281.
[29] O. V. Dolomanov, L. J. Bourhis, R. J. Gildea, J. A. K. Howard and H. Puschmann, *J. Appl. Crystallogr.* **2009**, *42*, 339.
[30] Gaussian 16 Revision C.01, M. J. Frisch, G. W. Trucks, H. B. Schlegel, G. E. Scuseria, M. A. Robb, J. R. Cheeseman, G. Scalmani, V. Barone, G. A. Petersson, H. Nakatsuji, M. Caricato X. Li, A. V. Marenich, J. Bloino, B. G. Janesko, R. Gomperts, B. Mennucci, H. P. Hratchian, J. V. Ortiz, A. F. Izmaylov, J. L. Sonnenberg, D. Williams-Young, F. Lipparini F. Ding, J. Goings F. Egidi, B. Peng, A. Petrone, T. Henderson, D. Ranasinghe, V. G. Zakrzewski, J. Gao, N. Rega, G. Zheng, W. Liang, M. Hada, M. Ehara, K. Toyota, R. Fukuda, J. Hasegawa, M. Ishida, T. Nakajima, Y. Honda, O. Kitao, H. Nakai, T. Vreven, K. Throssell, Jr. J. A. Montgomery, J. E. Peralta, F. Ogliaro, M. J. Bearpark, J. J. Heyd, E. N. Brothers, K. N. Kudin, V. N. Staroverov, T. A. Keith, R. Kobayashi, J. Normand, K. Raghavachari, A. P. Rendell, J. C. Burant, S. S. Iyengar, J. Tomasi, M. Cossi, J. M. Millam, M. Klene, C. Adamo, R. Cammi, J. W. Ochterski, R. L. Martin, K. Morokuma, O. Farkas, J. B. Foresman and D. J. Fox, Gaussian, Inc., Wallingford CT, **2016**.
[31] J.-D. Chai and M. Head-Gordon, *Phys. Chem. Chem. Phys.* **2008**, *10*, 6615.
[32] (a) T. Clark, J. Chandrasekhar and G. W. Spitznagel, *J. Comput. Chem.* **1983**, *4*, 294; (b) J. D. Dill and J. A. Pople, *J. Chem. Phys.* **1975**, *62*, 2921; (c) R. Ditchfield, W. J. Hehre and J. A. Pople, *J. Chem. Phys.* **1971**, *54*, 724; (d) M. M. Francl, W. J. Pietro, W. J. Hehre, J. S. Binkley, M. S. Gordon, D. J. DeFrees and J. A. Pople, *J. Chem. Phys.* **1982**, *77*, 3654; (e) M. S. Gordon, J. S. Binkley, J. A. Pople, W. J. Pietro and W. J. Hehre, *J. Am. Chem. Soc.* **1982**, *104*, 2797; (f) P. C. Hariharan and J. A. Pople, *Theor. Chim. Acta* **1973**, *28*, 213; (g) W. J. Hehre, R. Ditchfield and J. A. Pople, *J. Chem. Phys.* **1972**, *56*, 2257; (h) G. W. Spitznagel, T. Clark, P. v. R. Schleyer and W. J. Hehre, *J. Comput. Chem.* **1987**, *8*, 1109.
[33] (a) R. Krishnan, J. S. Binkley, R. Seeger and J. A. Pople, *J. Chem. Phys.* **1980**, *72*, 650; (b) A. D. McLean and G. S. Chandler, *J. Chem. Phys.* **1980**, *72*, 5639.
[34] (a) D. Andrae, U. Häußermann, M. Dolg, H. Stoll and H. Preuß, *Theor. Chim. Acta* **1990**, *77*, 123; (b) J. M. L. Martin and A. Sundermann, *J. Chem. Phys.* **2001**, *114*, 3408.
[35] G. Scalmani and M. J. Frisch, *J. Chem. Phys.* **2010**, 114110.
[36] K. Ishida, K. Morokuma and A. Komornicki, *J. Chem. Phys.* **1977**, *66*, 2153.
[37] M. Sparta, C. Riplinger and F. Neese, *J. Chem. Theory Comput.* **2014**, *10*, 1099.

2.2 Poly(iminoborane)s with Aromatic Side Groups: Insights into the Microstructure from Monodisperse Model Oligomers

The following section is slightly modified and reproduced from a submitted manuscript[#].

Abstract. While certain inorganic main-group polymers such as silicones (polysiloxanes) are ubiquitous in our everyday life, poly(iminoborane)s have been elusive for a long time. Incorporation of heterocyclic building blocks into their backbone has recently enabled access to the first derivatives of this inorganic-polymer class, as this approach effectively prevents undesired side-reactions to borazines. Information about the microstructure of these cyclolinear macromolecules, however, has been scarce. Herein, we present the synthesis of a series of monodisperse oligomers with up to 7 boron and 8 nitrogen atoms, representing the longest well-defined molecular $[>B=N<]_x$ chain to date. We accomplished to characterize six of them structurally in the solid state by single-crystal X-ray diffraction, thus providing valuable insight into the microstructure of poly(iminoborane)s. In addition, we report on the synthesis of new poly(iminoborane) derivatives featuring aryl side groups, with an increased content of unsubstituted phenyl groups. The *p*-(*n*-butyl)phenyl-substituted species **13** represents the highest-molecular-weight sample of this class of inorganic polymers to date.

2.2.1 Introduction

Inorganic polymers composed of main group elements in the backbone are ubiquitous in our daily life. The commonly best-known examples of inorganic polymers are certainly the silicones (polysiloxanes), exhibiting a backbone of alternating silicon and oxygen atoms (Figure 2.2.1, **I**).[1] Further notable representatives of this class of materials are polyphosphazenes[2] and polysilanes.[3] Through incorporation of different side groups, their mechanical and thermal properties can be varied over a wide range.

The incorporation of boron in macromolecular frameworks has recently come into the focus of very active research.[4,5] For instance, tricoordinate boron can be embedded in the π-system of a conjugated polymer via its vacant p-orbital, resulting in novel materials with intriguing properties and functions.[4a-f] Boronic acid-containing polymers are of particular interest for medical applications.[5] Boron-rich polymers have been used in boron neutron capture therapy (BNCT) of cancer.[6] Furthermore, the introduction of pairs of boron and nitrogen atoms at specific positions of organic compounds has recently attracted considerable attention. As BN and CC units are isoelectronic and isosteric, this partial BN for CC substitution produces new

[#] M. Maier, A. Friedrich, J. S. Schneider, J. A. P. Sprenger, J. Klopf, L. Fritze, M. Finze, H. Helten, **2023**, *manuscript submitted*.

materials with structural similarities to their organic parents but with significantly modified properties.[7] Our group has reported several BN-doped inorganic–organic hybrid polymers and oligomers with B=N bonds embedded in the polymer backbone.[8-10]

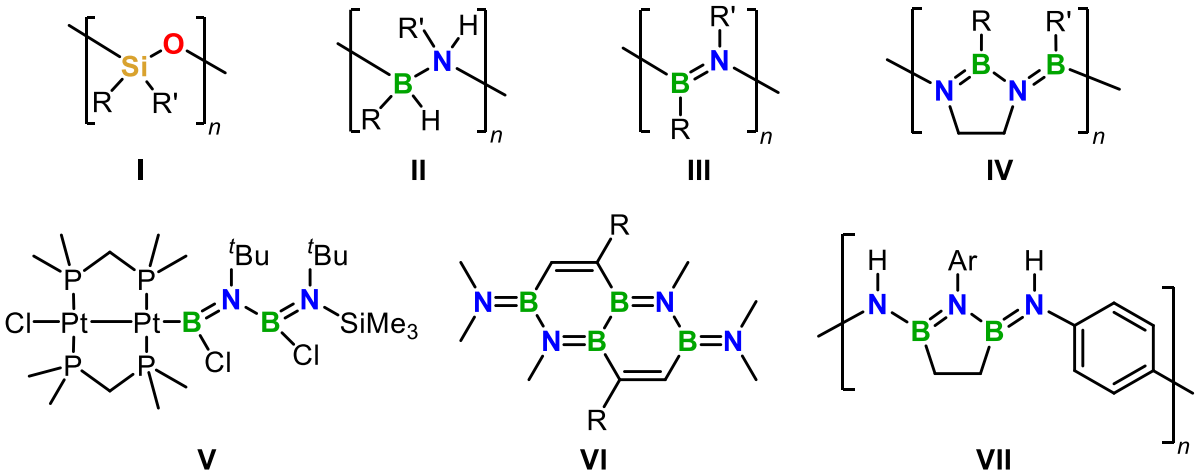

Figure 2.2.1. Structures of polysiloxanes (**I**), poly(aminoborane)s (**II**), poly(iminoborane)s (**III**), cyclolinear poly(iminoborane)s (**IV**), a transition metal coordinated $(BN)_2$ chain (**V**), an embedded BN chain (**VI**), and an azadiborolane-based inorganic–organic hybrid polymer (**VII**) (R, R' = different organic substituents; Ar = *p*-BrC_6H_4).

Poly(aminoborane)s (**II**), which are truly inorganic boron-containing polymers comprising a chain of alternating tetracoordinate B- and N-atoms, became accessible through seminal work by Manners and co-workers in 2008.[11,12] These species are formally main group analogs of polyolefins and can be used as polymeric precursors to shaped boron nitride.[13,14]

The unsaturated poly(iminoborane)s (PIBs, **III**/**IV**), featuring tricoordinate boron and nitrogen, are formally polyacetylene analogs, though with a considerably larger predicted electronic band gap.[15] In fact, these species had been effectively unknown prior to our first report on cyclolinear derivatives **IV** of this polymer class.[16] In several previous papers the term "polyiminoborane" or the formula $[BHNH]_n$ was associated with an intermediate of the thermal dehydrogenation of ammonia–borane ($NH_3{\cdot}BH_3$) at elevated temperature,[17] however, as we pointed out,[16] solid-state NMR studies had demonstrated that the material formed in such processes has rather the constitution of a polyborazylene (PBz),[18] which is in this case a poorly defined network of partially fused borazine rings.[14,19] Further studies reported on the putative formation of substituted poly(iminoborane)s, but the products obtained could not be unambiguously characterized as macromolecular species, due to either the lack of appropriate analytic tools at that time or the insolubility of the materials formed.[20,21]

Braunschweig and co-workers recently reported on transition metal-templated coupling of B=N units, thus affording coordinated $(BN)_2$ chains (**V**).[22,23] Worth mentioning in this context are furthermore a number of linear[24] and polycyclic[25] molecular compounds that feature a limited number of concatenated B=N units, for example, the rigid bicyclic $(BN)_4$ tetraene scaffold **VI**

by Kinjo and co-workers,[25c] besides borazine-based materials.[14] Very recently, we reported the 1,2,5-azadiborolane-based polymer **VII**, which represents the inorganic–organic hybrid polymer that comprises the longest inorganic BN chain part to date.[8i]

Previous observations and polymerization attempts suggested that the intended synthesis of linear poly(iminoborane)s (PIBs) from rational monomers is primarily hampered by the facile formation of small cyclic species, in particular borazines. Therefore, we decided to link the adjacent nitrogen centers of the main chain through incorporating them into a cyclic structure[26] of 1,3,2-diazaborolidine rings (**IV**). This geometrical constraint was effective in suppressing the undesired alternative pathways. Thereby, we obtained well-defined cyclolinear species of the form **IV** of moderate molecular weights, classifying them as the first examples of low poly(iminoborane)s or high oligo(iminoborane)s, respectively.[16]

So far, we have limited information on the microstructure of cyclolinear PIBs **IV** only from their analysis in solution and from computational studies. Therefore, we decided to aim at the synthesis of crystalline model oligomers of defined chain lengths, with a view to study their molecular structures in the solid state. We chose to target phenyl-substituted derivatives, as our previous investigations had suggested that aromatic side groups impart significantly enhanced crystallinity.[16b] In these studies, which are reported herein, we achieved to obtain a series of monodisperse oligomers with up to 7 boron and 8 nitrogen atoms. Furthermore, we synthesized a series of poly(iminoborane)s with a higher content of unsubstituted phenyl side groups. In this study, we also obtained the highest-molecular-weight PIB to date (M_n = 4.0 kDa, DP_n = 23).

2.2.2 Results and Discussion

For the synthesis of the targeted monodisperse oligo(iminoborane)s, we first prepared 2-phenyl-1,3,2-diazaborolidine (**1**),[16b] 1-mono- (**2**) and 1,3-disilylated (**3**)[16b] derivatives thereof, as well as the diborylated derivative **4**, to use them as modular building blocks in the following steps (Scheme 2.2.1). Compounds **2** and **3** were synthesized by reactions of **1** with one or two equiv. of chlorotrimethylsilane, respectively, in the presence of triethylamine as auxiliary base. We accomplished to isolate the new compound **2** in 75 % yield. By the addition of **3** to an excess of dichlorophenylborane, compound **4** was obtained as an off-white solid in 67 % yield. The constitution of oligo(iminoborane) **4** was unambiguously ascertained by multinuclear NMR spectroscopy and high-resolution mass spectrometry (HRMS); additionally, we accomplished to determine its molecular structure in the solid state by single-crystal X-ray diffraction analysis (see below, Figure 2.2.2 and 2.2.4). The ^{1}H NMR spectrum of **4** showed beside the aromatic signals, a single resonance at 4.04 ppm for the protons of the symmetric N-C_2H_4-N bridge. In the $^{11}B\{^{1}H\}$ NMR spectrum two resonances appeared at 40.5 and 45.2 ppm for the inner one and the outer two boron atoms, respectively.

After lithiation of **2** with *n*-BuLi at −78 °C and addition of $PhB(NMe_2)Cl$, we obtained **5** in nearly quantitative yield (98 %). The ^{1}H NMR spectrum of **5** showed two triplets for the $N\text{-}C_2H_4\text{-}N$ moiety due to the lack of symmetry along the chain. The $N\text{-}CH_3$ groups appeared as two singlets at 2.38 and 2.11 ppm. The $^{11}B\{^{1}H\}$ NMR spectrum showed two resonances at 36.3 and 34.7 ppm for the two different boron centers. In the $^{29}Si\{^{1}H\}$ NMR spectrum the resonance for the $SiMe_3$ group was observed at 4.5 ppm.

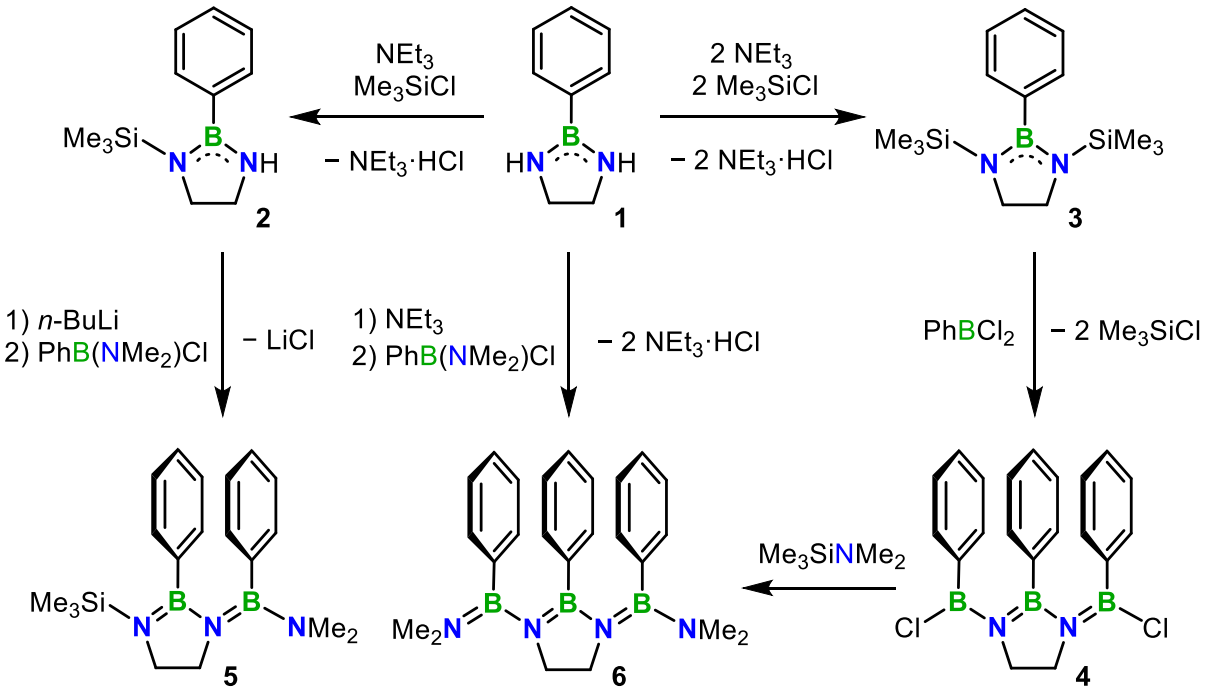

Scheme 2.2.1. Synthesis of modular building blocks **2**, **3**, and **4** and monodisperse oligo(iminoborane)s **5** and **6**.

We accomplished to prepare the longer oligo(iminoborane) **6** in two different ways. Reaction of **1** with $PhB(NMe_2)Cl$, using triethylamine as auxiliary base, gave compound **6** in 70 % yield. Alternatively, we achieved the synthesis of **6** by the reaction of **4** with Me_3SiNMe_2 in 75 % yield. The ^{1}H NMR spectrum of **6** showed a singlet at around 3.1 ppm for the $N\text{-}C_2H_4\text{-}N$ bridge and two singlets at about 2.5 and 2.1 ppm for the $N\text{-}CH_3$ moieties, due to hindered rotation about the outer B–N bond, indicating partial double bond character (as in **5**). The $^{11}B\{^{1}H\}$ NMR spectrum showed only one peak at around 35 ppm, as the boron atoms are in a very similar (NBN) environment in this case. We obtained single crystals suitable for X-ray diffraction analysis of **6** from a saturated solution in DCM and of **5** upon removal of the solvent from the reaction mixture (Figures 2.2.2, 2.2.5 and 2.2.6).

Aiming at oligo(iminoborane) species with even further extended BN chains, we synthesized compounds **7** and **8** in the next step (Scheme 2.2.2). Lithiation of **2** with *n*-BuLi to generate **Li[2–H]** *in situ* and addition of dichlorophenylborane at −78 °C gave **7**, which we isolated in

58 % yield. The ^{1}H NMR spectrum of **7** showed a single resonance for the $SiMe_3$ groups at −0.13 ppm and the N-C_2H_4-N bridges appeared as two triplets at 3.10 and 2.78 ppm.

For the synthesis of **8**, we added *in situ* generated **Li[2–H]** to a suspension of **4** in toluene at low temperature (−78 °C). After work-up, we obtained **8** in 54 % yield as an off-white solid. The ^{1}H NMR spectrum showed a single resonance at −0.23 ppm for the $SiMe_3$ groups. In fact, this signal appears on a small but systematic upfield shift with increasing BN chain length from **5** (−0.03 ppm) to **7** (−0.13 ppm) to **8**. The N-C_2H_4-N signals of **8** appeared as two triplets at 3.25 and 2.83 ppm, and one singlet at 2.38 ppm. In the ^{11}B{^{1}H} NMR spectrum a single peak at about 37 ppm and in the ^{29}Si{^{1}H} NMR spectrum one at 4.7 ppm was observed for both **7** and **8**. Upon slow crystallization of **7** from *n*-pentane and **8** from a mixture of THF and *n*-pentane, we obtained single crystals suitable for X-ray diffraction (Figures 2.2.2, 2.2.7 and 2.2.8).

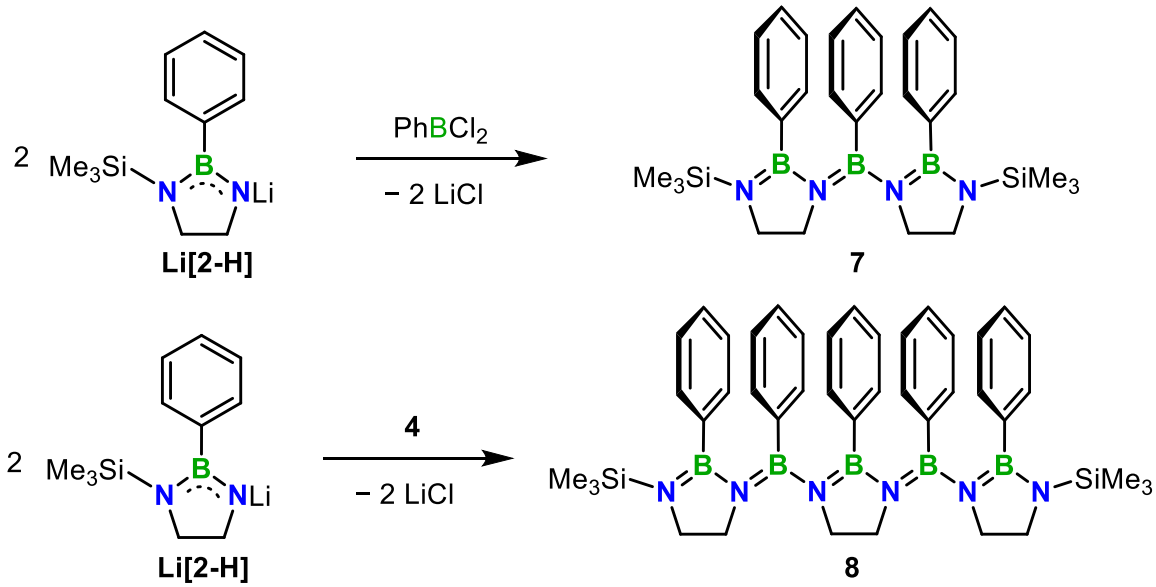

Scheme 2.2.2. Synthesis of monodisperse oligo(iminoborane)s **7** and **8**.

Silicon/boron exchange reactions of **7** and **8** in CH_2Cl_2 with PhB(NMe_2)Br at ambient temperature led to compounds **9** and **10**, respectively, featuring terminal NMe_2 groups (Scheme 2.2.3). We accomplished to isolate **9** in 80 % yield and the longest oligomer **10**, featuring a chain of 7 boron and 8 nitrogen atoms, in 95 % yield, both as colorless solids. The ^{1}H NMR spectra of **9** and **10** showed two singlets between 2.41 and 1.84 ppm for the N-CH_3 groups. The N-C_2H_4-N signals appeared as a broad singlet at 3.24 and a triplet at 2.62 ppm for **9** and as a very broad signal between 3.48 and 2.92 ppm and two broad singlets at 2.73 and 2.56 ppm for **10** at room temperature, respectively. At lower temperature (−40 °C) the three broad N-C_2H_4-N signals of **10** split into 6 signals, each with an integral of 2 (Figure S5.2.36). The ^{11}B NMR spectrum revealed a single broad resonance at around 35 ppm. We

were able to obtain suitable crystals of **9** for X-ray diffraction by slow crystallization from a mixture of THF and *n*-hexane (Figures 2.2.2 and 2.2.9).

In order to get some information about the electronic structure within the BN chain of the oligo(iminoborane)s studied herein, we determined the rotational barriers ($\Delta G^{\ddagger}$) of the terminal B–NMe_2 moieties for compounds **5**, **6**, **9**, and **10** using the dynamic NMR method.[27,28] We evaluated the no-exchange chemical shift difference $\Delta\nu$ (via extrapolation; Figure S5.2.47-S5.2.50) from the ^{1}H NMR data of compounds **5**, **6**, **9**, and **10** in toluene-d_8 and determined their coalescence temperatures (T_c). As a general trend, we observed a slight increase in $\Delta G^{\ddagger}$ with increasing BN chain length of the model oligomers. The lowest T_c, at 54 °C ± 1 °C, was observed for **5** (Figure S5.2.12) resulting in the lowest rotational barrier of 15.21 ± 0.05 kcal/mol. Compound **6** started to decompose at 60 °C while heating in toluene-d_8, nevertheless we were able to obtain the T_c with 78 °C ± 1 °C (Figure S5.2.19). This corresponds to a rotational barrier of 16.45 ± 0.05 kcal/mol, which is slightly increased compared to that of **5**. Also **9** and **10** showed some decomposition upon heating in toluene with an onset at 90 °C, making the determination of T_c more difficult, thus an inaccuracy of ±5 °C was applied. Thereby, however, we obtained a T_c of 100 °C for both **9** and **10**, indicating an upper limitation of T_c with increased BN chain length. Further heating to 115 °C led to appearance of a single broad signal for the NMe_2 signals at around 2.2 ppm (Figure S5.2.31 and S5.2.38). The rotational barrier of around 17.20 ± 0.24 kcal/mol for **9** and **10** indicates a stronger terminal B=N bond for longer oligo(iminoborane)s. This points to a slight decrease of the strength of the p-interaction between the BN units with increasing chain length. The free energies of activation $\Delta G^{\ddagger}$ for the hindered rotation about the B–NMe_2 bond of all model oligomers fit well with the calculated values (15.7 (**5**), 17.9 (**6**), 19.5 kcal mol^{-1}(**9**)) and are in the range of several mono-aminoboranes.[28]

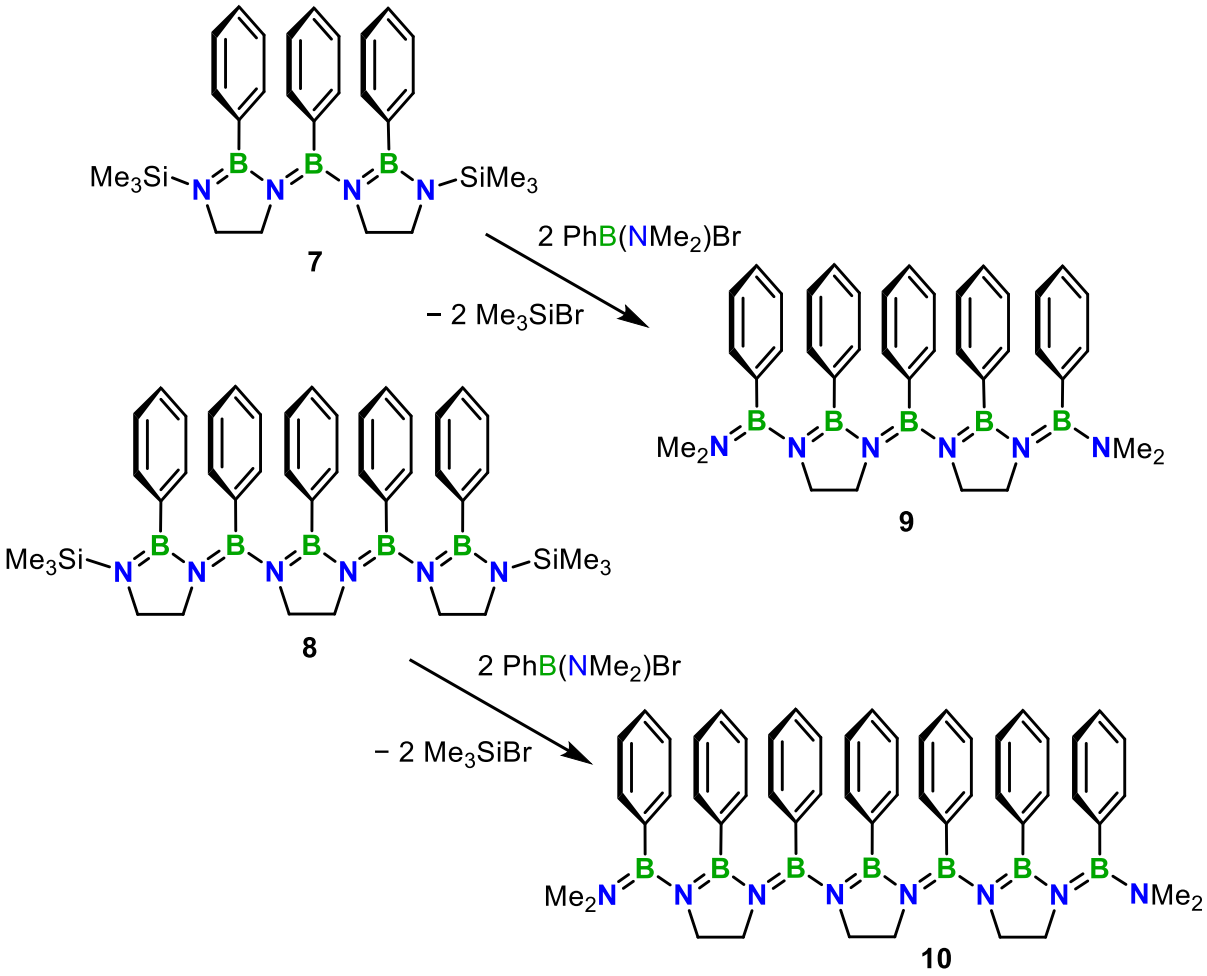

Scheme 2.2.3. Synthesis of monodisperse oligo(iminoborane)s **9** and **10**.

The crystal structures of compounds **4**–**9** were determined at 100 K using single-crystal X-ray diffraction. Crystal structure data are summarized in Table 2.2.2, while selected distances and angles are given in Tables 2.2.3–2.2.5. All the boron and nitrogen atoms are trigonal planar coordinated (∑(∠RBR) = ∑(∠RNR) = 360° within three standard deviations), with a slight deviation of ca. 3° only for the N2 nitrogen atoms in compounds **5** and **6** (∑(NR_3) ≈ 357.3(4)°). The individual average B–N bond lengths of the investigated compounds are in the range 1.428 – 1.446 Å, which is also the typical range for borazine compounds and, hence, for a B–N bond intermediate between a B–N single bond (1.48 – 1.51 Å) and double bond (1.38 – 1.41 Å).[29] The interplanar angle between the planar BR_3 and NR_3 planes of a B–N bond is supposed to be correlated with the degree of π-bonding, i.e., a small interplanar angle and, hence, high planarity of the $R_2B–NR_2$ moiety is expected to be indicative for a high degree of π-bonding and correlated with a short B–N bond length. The terminal B–N bonds that are not part of diazaborolidine rings have pronounced double-bond character (B–N = 1.406(3) – 1.414(3) Å) in **4**, **5**, **6**, and **9**, and their lengths are close to the B–N bond lengths observed in aminoboranes,[30] while the adjacent B–N bonds have more pronounced single-bond character (B–N = 1.449(2) – 1.477(3) Å). This is consistent with a higher rotational freedom for the latter,

longer B–N bonds (∠(BR_3, NR_3) = 31.02(10) – 45.18(11)°) than for the more planar $R_2B–NR_2$ moieties of the short, terminal B–N bonds (∠(BR_3, NR_3) = 10.97(10) – 25.08(5)°) (Figure S5.2.1). B–N bond lengths in the diazaborolidine rings and between the rings are in the intermediate range of 1.419(3) – 1.462(3) Å. For a comparison, B–N bond lengths of 1.435(2) – 1.468(4) Å were reported for the azadiborolane rings in our previous work.[8i] Again, the intermediate B–N bonds linking the rings (B–N = 1.422(3) – 1.452(3) Å), follow the trend in that interplanar angles ∠(BR_3, NR_3) = 27.8(2) – 38.49(2)° are intermediate between those of the terminal B–N bonds with more double bond character and the adjacent ones with more single-bond character. However, for the B–N bonds within the diazaborolidine rings (B–N = 1.419(3) – 1.462(3) Å), the interplanar angles ∠(BR_3, NR_3) are small and in the range 1.5313(7) – 14.50(8)°, while the B–N bond length variation is relatively large. Here, the higher planarity of the $R_2B–NR_2$ moieties is sterically determined by the geometry of the rings. Still, within the intraring B–N bonds, a slight positive correlation is observed between the B–N bond length and the interplanar angle ∠(BR_3, NR_3) (Figure S5.2.1). N–B–N angles within the diazaborolidine rings (108.7(1) – 110.6(1)°) are smaller than those linking the rings (118.8(2) – 122.6(1)°), which are close to the ideal value (120°) of a trigonal planar coordination. In contrast, B–N–B angles along the chain are stretched with angles of 128.6(2) – 136.7(2)°. The phenyl rings attached to boron are all significantly twisted by 34.43(8) – 84.33(6)° with respect to their respective planar BR_3 moieties (Table 2.2.4). Compound **4** shows a special configuration in that it is the only one of the investigated compounds for which all the adjacent phenyl groups are oriented in the same direction (Figure 2.2.2). Hence, they are aligned close to parallel, with phenyl C_{ipso} distances of 3.284(2) and 3.338(2) Å, respectively (Table 2.2.3). As a result, a weak intramolecular π–π interaction can be inferred between two phenyl rings (attached to B1 and B2, respectively) with a mean interplanar separation of 3.59 Å and a tilt of 32.45(5)° between the phenyl planes (Table 2.2.5). In all the other compounds, adjacent phenyl rings are oriented towards different directions with long phenyl C_{ipso} distances of 4.566(3) – 4.838(11) Å (Table 2.2.3). The phenyl C_{ipso} distances between next nearest neighbors in **7**, **8**, and **9** are actually shorter (3.578(4) – 3.853(1) Å), and these rings are approximately parallel aligned (angles of 2.37(8) – 21.555(7)° between phenyl planes, Table 2.2.4), however, also these rings point towards different directions, hence, there are no π–π interactions between them.

We also optimized the molecular structures of **4**–**9** computationally at the ωB97X-D/6-31+G(d,p) level of theory in the gas phase. The obtained structures are in good agreement with the experimental solid-state structures (Tables 2.2.8–2.2.10 and Figures S5.2.72–S5.2.74). The general trends of the B–N bond lengths and their correlation with the interplanar angles between the planar BR_3 and NR_3 planes, which are described above for the solid-state structures, are also evident in the optimized structures (Figure S5.2.72).

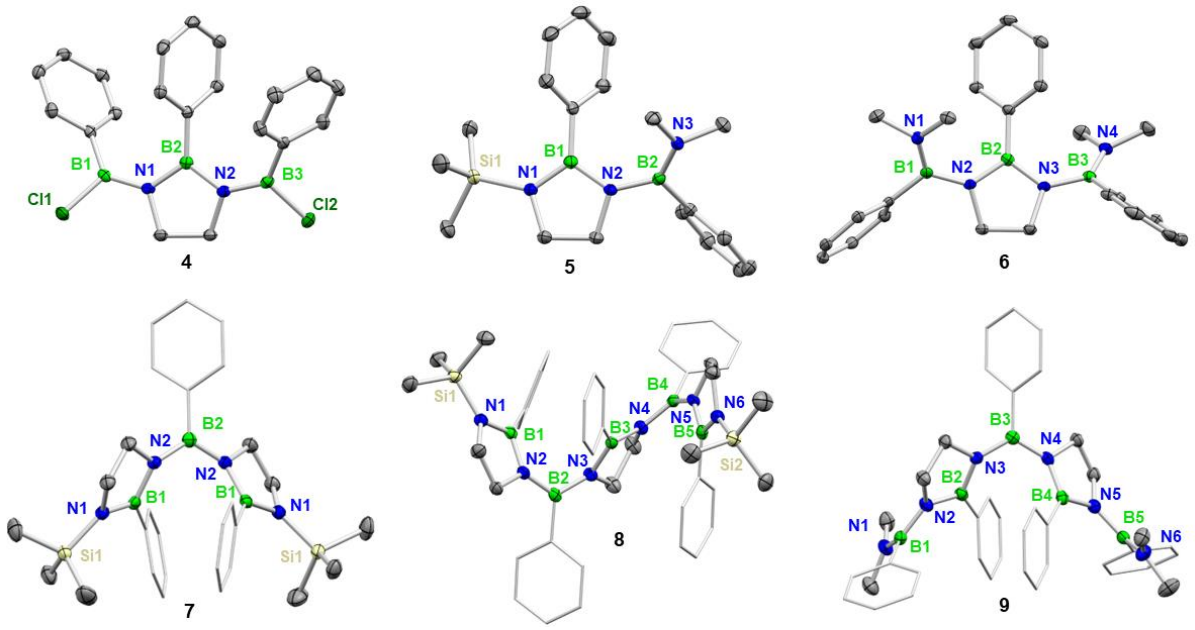

Figure 2.2.2. Molecular structures of **4**, **5**, **6**, **7**, **8**, and **9** in the solid state from single-crystal X-ray diffraction at 100 K (ellipsoids drawn at the 50 % probability level, except for the phenyl groups for **7**, **8**, and **9**; H atoms omitted for clarity).

The optimized bond lengths and interplanar angles are in a similar range as the experimental ones, while their variation is smaller, for instance, for the average B–N bond lengths (1.434 – 1.437 Å), the terminal B–N bonds (B–N = 1.413 – 1.420 Å, ∠(BR_3, NR_3) = 15.4 – 17.3°), the next-to-terminal B–N bonds (B–N = 1.453 – 1.456 Å, ∠(BR_3, NR_3) = 41.0 – 43.7°), and the B–N bonds linking the five-membered diazaborolidine rings (B–N = 1.432 – 1.437 Å, ∠(BR_3, NR_3) = 30.4 – 36.4°). However, the optimized intraring B–N bonds show a similar scatter and slight correlation between the bond length and the interplanar angle as in the solid-state structures (B–N = 1.426 – 1.453 Å, ∠(BR_3, NR_3) = 3.8 – 13.9°).

We previously reported the attempted synthesis of a poly(iminoborane) with exclusively phenyl side chains.[16b] This, however, led to an insoluble material – putatively the polymer **12** (Scheme 2.2.4). We herein repeated that experiment, with the same result. Thus, we installed solubility-enhancing *n*-butyl groups in *para* position with respect to the BN main chain, which resulted in soluble polymer **13**.[16b] For the present study, we repeated the synthesis of **13**, which yielded a higher-molecular-mass sample of it (see below), and we prepared the new polymers **14**–**16**, to increase the content of unsubstituted phenyl side groups. The synthesis of poly(iminoborane)s **13**–**15** we accomplished by Si/B exchange co-polycondensation of the respective disilylated diazaborolidine (**3** or **11**) and dichloroarylborane ($PhBCl_2$ or 4-(*n*-Bu)$C_6H_4BCl_2$) in dichloromethane at room temperature (Scheme 2.2.4). To obtain the polymer **16** with the highest phenyl-group content, we combined **11** with building block **4** under analogous conditions. After 24 h, the reactive B–Cl end groups were terminated with

Me_3SiNMe_2, and the desired polymers were isolated in moderate to good yields (57 – 88 %). We characterized the products obtained by multinuclear NMR spectroscopy, gel permeation chromatography (GPC), and thermogravimetric analysis (TGA).

Different from **12**, polymer **13** readily dissolved in most common organic solvents. It was even slightly soluble in *n*-pentane. Compounds **14** and **15** were mostly soluble in polar solvents (CH_2Cl_2, $CDCl_3$, THF), and formed cloudy suspensions at higher concentrations, whereas compound **16** showed notably poorer solubility in these solvents. The ^1H NMR spectra of **14**, **15**, and **16** showed broad peaks at room temperature, which was also the case for the N-C_2H_4-N signals of the longest monodisperse oligomer **10**. The signals for the aromatic protons of **14**–**16** appeared between 8.03 and 6.26 ppm and the signals for the N-C_2H_4-N moiety between 3.42 and 2.01 ppm. In the $^{11}B\{^1H\}$ NMR spectrum of **15** we observed a very broad and weak resonance at around 33 ppm, which was only evident after subtraction of the glass background stemming from the NMR tube (Figure S5.2.44).

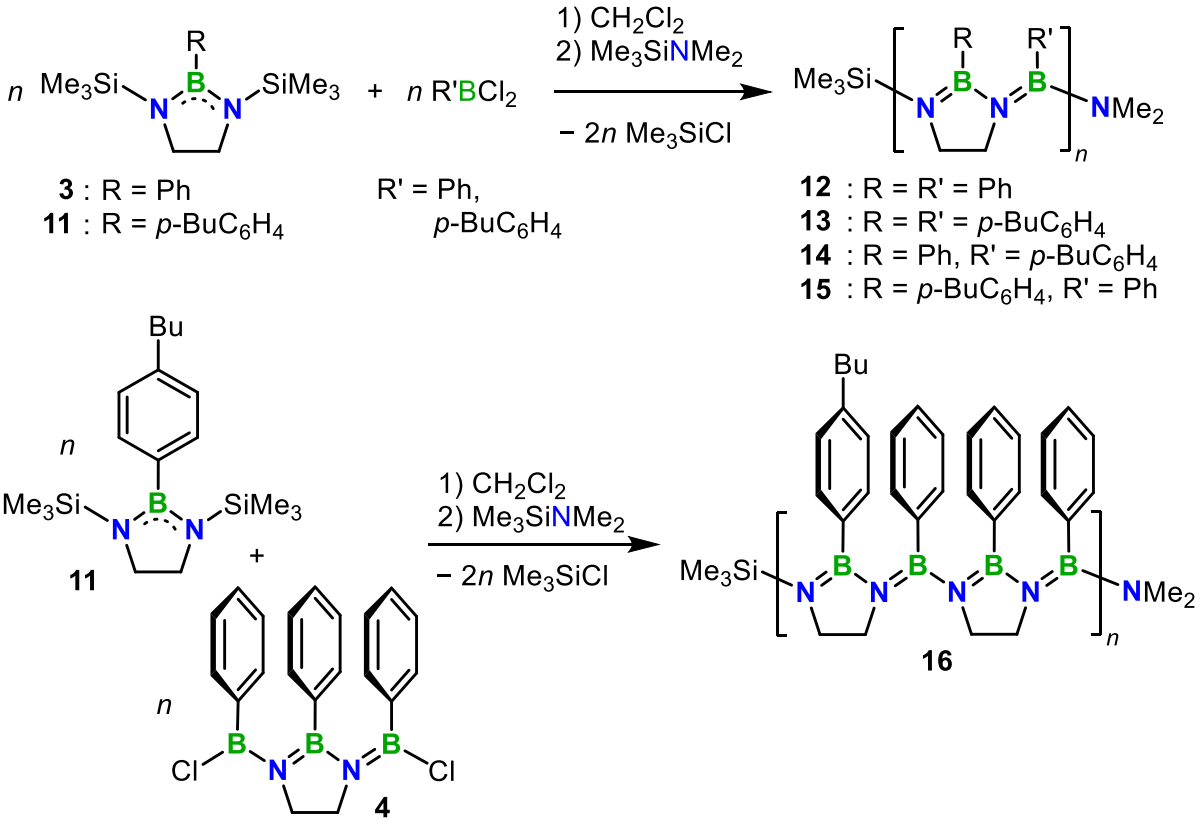

Scheme 2.2.4. Synthesis of poly(iminoborane)s **12**–**16**.

Analysis by GPC revealed that we had achieved to almost double the average molecular weight for the previously known derivative **13** from M_n = 2.2[16b] to 4.0 kDa, corresponding to a number average degree of polymerization DP_n of 23 (Table 2.2.1). The molecular-weight averages for **14** and **15** were slightly lower, but still in that same range, while that for **16** was

significantly lower, 1.9 kDa (DP_n = 7). This is probably due to precipitation during the polymerization because of the lower content of solubilizing butyl groups in this case.

Table 2.2.1. GPC data of **13**, **14**, **15**, and **16**.

	M_n [kDa]	M_w [kDa]	PDI	DP_n
13	4.0	6.1	1.5	23
14	2.5	2.8	1.2	17
15	3.3	4.8	1.5	22
16	1.9	2.2	1.2	7

The TGA measurements of the poly(iminoborane)s **12**, **13**, **14**, **15**, and **16** were performed with a heating rate of 10 K min^{-1} under nitrogen atmosphere, and that of **13**, additionally, at 5 K min^{-1} with addition of oxygen (ca. 71 %, Figure 2.2.3). A lower heating rate of 5 K min^{-1} for **13** led to slightly earlier onset temperatures for the main mass loss and a lower ceramic yield compared to the procedure at 10 K min^{-1} (Figure S5.2.63). In general, the process occurred in two steps, starting between 133 and 186 °C with the observation of a small mass loss (1.9–11.4 %). The main mass loss onsets for all samples were between 410 to 462 °C, on which they lose around 50 to 66 % of their mass. Gas analysis by mass spectrometry (MS) revealed the release of the (butyl)phenyl groups (see, Appendix 5.2, ion traces). The obtained ceramic yields of 30 to 36 % indicate incorporation of carbon atoms into the BN residue. By addition of O_2 to the residue of **13** at 1000 °C, we obtained a further decrease in ceramic yield of 8.3 % and MS confirmed CO_2 release during the process (Figure S5.2.61). This fits likewise well with the theoretical fraction of the C_2H_4 groups linking the nitrogen atoms of 8.2 % in **13**. The incorporation of the stabilizing C_2H_4 group into the BN ceramic during the combustion process seems to be a reasonable explanation. Thus, we decided to add O_2 directly at the start of the measurement at 30 °C (Figure S5.2.62). We observed a three-step process, in which the main mass loss of 66.6 % occurred at around 257 °C, which is at ca. 150 °C lower temperature than under pure nitrogen atmosphere, leading to the same residual mass of around 30.5 %. The third step started over a broad temperature range at about 550 °C and released further 11.9 % mass, which we have also previously assigned to the stabilizing C_2H_4 groups.[16b] The ion trace of *n*-butylbenzene was only observed at around 300 °C, whereas CO_2 showed a remarkable increase in the region around 550 °C, indicating the release of C_2H_4. However, the residual of 18.9 % is slightly higher than the theoretical fraction of BN of 14.2 %, which points to residual carbon content in the ceramic residue. Overall, these results demonstrate that the BN content

in the residue obtained can be increased using lower heating rates and increased O_2 content in the atmosphere.

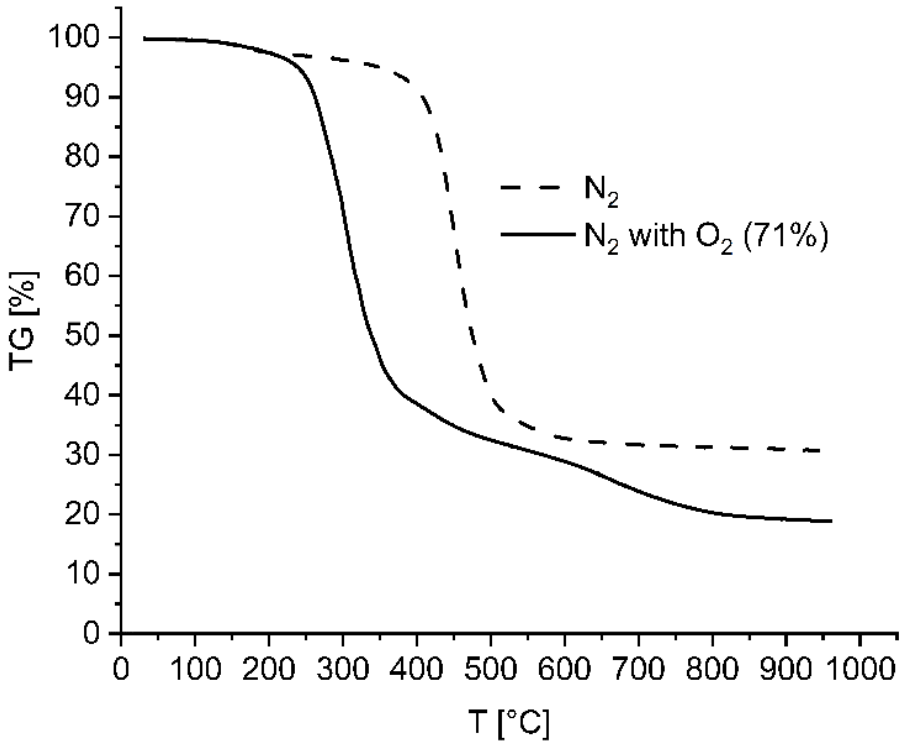

Figure 2.2.3. TG curves of **13** measured under nitrogen atmosphere (dashed line) and with addition of oxygen (solid line) with a heating rate of 5 K min^{-1}.

2.2.3 Conclusion

We herein presented a series of monodisperse oligo(iminoborane)s with increasing number of B=N units. Compound **10**, exhibiting 7 boron and 8 nitrogen atoms in the chain, represents the longest well-defined molecular $[>B=N<]_x$ chain to date. For the NMe_2-terminated derivatives **5**, **6**, **9**, and **10**, we were able to determine the barriers of rotation ($\Delta G^{\ddagger}$) about their terminal B=N bonds by dynamic VT-NMR measurements; the obtained data of which were found to be in line with those from DFT calculations. They revealed a slight increase in $\Delta G^{\ddagger}$ with increasing length of the oligomers, pointing to a slight decrease of the strength of the π-interaction between the individual BN units upon chain elongation. Our X-ray diffraction studies on 6 oligomers gave highly valuable insight into the structure of these cyclolinear species, thus allowing to draw conclusions for the structural arrangement of the respective polymers. The lengths of the B–N bonds along the chain are in between those of single and double bonds, and the observed twists between the BR_3 and the NR_3 planes appear to be caused by steric effects. The molecular structures are well reproduced by our DFT calculations.

In addition, we prepared the aryl-substituted poly(iminoborane) derivatives **12**–**16**. The new polymer **16** can still be dissolved to some extent, although only every fourth phenyl substituent carries a solubilizing butyl group in the *para*-position. The synthesis of polymer **13**, which we repeated here, furnished a sample with M_n = 4.0 kDa and DP_n = 23; this represents the highest-molecular-weight poly(iminoborane) to date. Our TGA measurements of the polymers revealed that the ceramic yields obtained are generally slightly higher than expected. However, we demonstrated that the BN content in the residue can be increased using lower heating rates and applying an O_2 atmosphere.

2.2.4 Experimental Section

General procedures. All manipulations were performed under an atmosphere of dry argon using standard Schlenk techniques or in an MBraun glovebox. Solvents (dichloromethane (DCM), tetrahydrofuran (THF), diethyl ether (Et_2O), toluene, *n*-hexane) were dried and degassed by means of an Innovative Technology solvent purification system (SPS). Deuterated solvents ($CDCl_3$, CD_2Cl_2, C_6D_6 and toluene-d_8) for NMR spectroscopy as well as triethylamine (NEt_3), trimethylsilyl chloride and *n*-pentane were dried and degassed at reflux over CaH_2 or Na, respectively, and freshly distilled prior to use. Pentamethylsilazane (Me_3SiNMe_2), and *n*-BuLi (2.5 M in *n*-hexane) were commercially purchased and used as received. Chloro(dimethylamino)phenylborane,[31] bromo(dimethylamino)phenylborane,[32] and dichlorophenylborane,[33] **1**[16b,34] and **3**[16b] were prepared according to literature procedures. NMR spectra were recorded at 25 °C on a Bruker Avance III HD spectrometer operating at 300 MHz, on a Bruker Avance 500 spectrometer operating at 500 MHz, or on a Bruker Avance Neo I 600 operating at 600 MHz. Chemical shifts were referenced to residual protic impurities in the solvent (^1H) or the deuterio solvent itself (^{13}C) and reported relative to external $SiMe_4$ (^1H, ^{13}C, ^{29}Si) and $BF_3{\cdot}OEt_2$ (^{11}B) standards. Mass spectra were obtained with the use of a Thermo Scientific Exactive Plus Orbitrap MS system employing liquid injection field desorption ionization (LIFDI) and atmospheric pressure chemical ionization (APCI). Elemental analyses were performed on an Elementar vario MICRO cube elemental analyzer. Thermogravimetric analysis (STA: DTA & TG) measurements were performed with a STA 449 F3 Perseus (Netzsch), connected to a QMS 403 Aeolos Quadro Mass Spectrometer for the analysis of the gaseous compounds in the temperature range of 30 to 1000 °C with heating rates of 5 or 10 K min^{-1} in an N_2 atmosphere or an O_2:N_2 mixture (ca. 71:29 %; flow rate: 70 mL min^{-1}). GPC chromatograms were recorded on an Agilent 1260 Infinity II Series, equipped with two PSS SDV 3 µm 1000 Å (300x8 mm) columns and one PSS SDV 3 µm 10000 Å (300x8 mm) column, at 25 °C with a flow rate of 1 mL min^{-1} and calibrated against polystyrene standards. The samples were diluted in THF and toluene as internal standard. Detection was carried out via

UV signal (λ = 254 nm). Evaluation of the chromatograms was performed by using WinGPC software.

Spectra. All spectra and other result figures are shown in Appendix 5.2.

Synthesis of 2. 2-Phenyl-1,3,2-diazaborolidine (**1**) (2.93 g, 20.1 mmol) in THF (200 mL) was stirred for 24 h until the suspension was completely dissolved. NEt_3 (2.03 g, 20.1 mmol) was added at −78 °C and stirred for 15 minutes. Subsequently, Me_3SiCl (2.33 g, 21.4 mmol) was added dropwise at −78 °C and the reaction mixture was warmed to room temperature overnight. After removing all volatiles *in vacuo*, the residue was washed with *n*-pentane (3 x 10 mL) to remove the formed salt. The *n*-pentane solution was stored for 24 h at −30 °C, and the resulting precipitate was removed by filtration at −30 °C. The solvent of the filtrate was removed *in vacuo* to obtain a colorless liquid (3.29 g, 15.1 mmol, 75 % yield). ^{1}H NMR (300 MHz, CD_2Cl_2): δ = 7.42-7.39 (m, 2H, Ph-*H*), 7.31-7.26 (m, 3H, Ph-*H*), 3.52-3.45 (m, 2H, N-CH_2), 3.43-3.37 (m, 2H, N-CH_2), 3.13 (br, 1H, N-*H*), -0.03 (s, 9H, SiCH_3) ppm; ^{11}B{^{1}H} NMR (96 MHz, CD_2Cl_2): δ = 34.8 (s) ppm; ^{13}C{^{1}H} NMR (76 MHz, CD_2Cl_2): δ = 132.9 (s, Ph-*C*), 128.3 (s, Ph-*C*), 127.6 (s, Ph-*C*), 48.6 (s, N-*C*H_2), 45.2 (s, N-*C*H_2), 0.7 (s, Si*C*H_3) ppm; ^{29}Si{^{1}H} NMR (60 MHz, CD_2Cl_2): δ = 4.6 ppm.

Synthesis of 4. To a solution of dichloro(phenyl)borane (369 mg, 2.33 mmol) in DCM (4.0 mL) a solution of **3** (290 mg, 1.0 mmol) in DCM (1.0 mL) was added dropwise at 0 °C. The reaction mixture was slowly warmed to ambient temperature overnight. The solvent was removed *in vacuo* and the residue was washed with *n*-pentane. The product **4** was isolated as an off-white solid (261 mg, 0.67 mmol, 67 % yield). ^{1}H NMR (500 MHz, $CDCl_3$): δ = 7.23-7.21 (m, 4H, Ph-*H*), 7.06-7.03 (m, 2H, Ph-*H*), 6.90-6.87 (m, 4H, Ph-*H*), 6.78-6.76 (m, 2H, Ph-*H*), 6.74-6.71 (m, 1H, Ph-*H*), 6.57-6.54 (m, 2H, Ph-*H*), 4.04 (s, 4H, N-CH_2) ppm; ^{11}B{^{1}H} NMR (160 MHz, $CDCl_3$): δ = 45.2 (s), 40.5 (s) ppm; ^{13}C{^{1}H} NMR (126 MHz, $CDCl_3$): δ = 136.6 (br, B-Ph-C_{ipso}), 134.4 (s, Ph-*C*), 133.6 (br, B-Ph-C_{ipso}) 130.1 (s, Ph-*C*), 128.3 (s, Ph-*C*), 126.7 (s, Ph-*C*), 126.2 (s, Ph-*C*), 51.3 (s, N-*C*H_2) ppm; HRMS (LIFDI): m/z calcd.: 390.1199, found: 390.1193.

Synthesis of 5. To a solution of **2** (546 mg, 2.50 mmol) in Et_2O (15 mL) was added dropwise 1.05 mL *n*-BuLi (2.5 M in *n*-hexane, 2.63 mmol) at −78 °C. After stirring for 2h at −78 °C, the reaction mixture was warmed to room temperature. Subsequently, $PhB(NMe_2)Br$ (563 mg, 2.66 mmol) was added dropwise at −78 °C and the mixture was slowly warmed to ambient temperature overnight. The solvent was removed *in vacuo* and the product **5** was isolated as off-white solid (860 mg, 2.46 mmol, 98 % yield). ^{1}H NMR (500 MHz, CD_2Cl_2): δ = 7.44-7.39 (m, 4H, Ph-*H*), 7.34-7.20 (m, 6H, Ph-*H*), 3.34 (t, 2H, N-CH_2), 3.15 (t, 2H, N-CH_2), 2.38 (s, 3H, N-

CH_3), 2.11 (s, 3H, N-CH_3), −0.03 (s, 9H, SiCH_3) ppm; $^{11}B\{^1H\}$ NMR (160 MHz, CD_2Cl_2): δ = 36.3 (s), 34.7 (s) ppm; $^{13}C\{^1H\}$ NMR (126 MHz, CD_2Cl_2): δ = 141.2 (br, B-Ph-C_{ipso}), 139.4 (br, B-Ph-C_{ipso}), 133.6 (s, Ph-*C*), 133.4 (s, Ph-*C*), 127.9 (s, Ph-*C*), 127.8 (s, Ph-*C*), 127.8 (s, Ph-*C*), 127.2 (s, Ph-*C*), 51.4 (s, N-CH_2), 48.9 (s, N-CH_2), 40.1 (s, N-CH_3), 1.0 (s, SiCH_3) ppm; $^{29}Si\{^1H\}$ NMR (99 MHz, CD_2Cl_2): δ = 4.5 ppm; HRMS (LIFDI): m/z calcd.: 349.2311, found: 349.2309.

Synthesis of 6. 2-Phenyl-1,3,2-diazaborolidine (**1**) (292 mg, 2.0 mmol) in THF (20.0 mL) was stirred for 24 h until the suspension was completely dissolved. Et_3N (445 mg, 4.4 mmol) was added slowly at ambient temperature and stirred for 30 minutes. Subsequently, $PhB(NMe_2)Br$ (687 mg, 4.1 mmol) was added dropwise and the mixture was stirred overnight. The formed salt was removed by filtration and the residue was washed with THF. The solvent was removed *in vacuo*. After washing the residue with cold *n*-pentane (−78°C), the product **6** was isolated as a colorless solid (572 mg, 1.40 mmol, 70 % yield). ^1H NMR (500 MHz, C_6D_6): δ = 7.72-7.70 (m, 2H, Ph-*H*), 7.62-7.60 (m, 4H, Ph-*H*), 7.35-7.31 (m, 4H, Ph-*H*), 7.27-7.24 (m, 2H, Ph-*H*), 7.22-7.20 (m, 3H, Ph-*H*), 3.08 (s, 4H, N-CH_2), 2.47 (s, 6H, N-CH_3), 2.20 (s, 6H, N-CH_3) ppm; $^{11}B\{^1H\}$ NMR (160 MHz, C_6D_6): δ = 35.4 (s) ppm; $^{13}C\{^1H\}$ NMR (126 MHz, C_6D_6): δ = 140.6 (br, Ph-C_{ipso}), 139.1 (br, Ph-C_{ipso}), 133.9 (s, Ph-*C*), 133.4 (s, Ph-*C*), 128.5 (s, Ph-*C*), 128.3 (s, Ph-*C*), 128.1 (s, Ph-*C*), 127.6 (s, Ph-*C*), 51.4 (s, N-CH_2), 40.2 (s, N-CH_3), 40.1 (s, N-CH_3) ppm; HRMS (LIFDI): m/z calcd.: 408.2822, found: 408.2815.

Alternative synthesis of 6. To a solution of $PhBCl_2$ (191 mg, 1.21 mmol) in DCM (2.0 mL) was added a solution of **3** (148 mg, 0.51 mmol) in DCM (1.0 mL) slowly at 0 °C. The solution was stirred at 0 °C for 1 h and another 3.5 h at room temperature. Subsequently, all volatiles were removed *in vacuo* to remove most of the $PhBCl_2$ excess. The residue was dissolved in DCM (2.5 mL) and Me_3SiNMe_2 (0.2 mL) was added at −78 °C. After 1h, the reaction mixture was warmed to room temperature and was stirred for another 2 h. After all volatiles were removed *in vacuo*, the residue was washed with cold *n*-pentane (−78 °C, 3 x 1.5 mL) to obtain an off-white solid (156 mg, 0.38 mmol, 75 % yield). ^1H NMR (500 MHz, CD_2Cl_2): δ = 7.52-7.51 (m, 4H, Ph-*H*), 7.49-7.48 (m, 2H, Ph-*H*), 7.36-7.33 (m, 4H, Ph-*H*), 7.31-7.28 (m, 2H, Ph-*H*), 7.26-7.23 (m, 1H, Ph-*H*), 7.21-7.19 (m, 1H, Ph-*H*), 3.07 (s, 4H, N-CH_2), 2.51 (s, 6H, N-CH_3), 2.13 (s, 6H, N-CH_3) ppm; $^{11}B\{^1H\}$ NMR (160 MHz, CD_2Cl_2): δ = 34.8 (s) ppm; $^{13}C\{^1H\}$ NMR (126 MHz, CD_2Cl_2): δ = 140.9 (br, Ph-C_{ipso}), 138.8 (br, Ph-C_{ipso}), 133.9 (s, Ph-*C*), 133.4 (s, Ph-*C*), 128.2 (s, Ph-*C*), 128.1 (s, Ph-*C*), 127.9 (s, Ph-*C*), 127.3 (s, Ph-*C*), 51.3 (s, N-CH_2), 40.2 (s, N-CH_3), 40.1 (s, N-CH_3) ppm; HRMS (APCI pos): m/z calcd.: 409.2901 $[M+H]^+$, found: 409.2900.

Synthesis of 7. To a solution of **2** (1.09 g, 5.0 mmol) in a mixture of Et_2O (10 mL) and *n*-pentane (20 mL) was added dropwise 2.1 mL *n*-BuLi (2.5 M in *n*-hexane, 5.25 mmol) at −78 °C. After stirring for 105 minutes at −78 °C, the reaction mixture was warmed to room temperature. Subsequently, $PhBCl_2$ (437 mg, 2.75 mmol) was added dropwise at −78 °C and the mixture was slowly warmed to ambient temperature overnight. The solvent was removed *in vacuo* and the residue was washed with *n*-pentane (3, 1.5, 1.5 mL). After recrystallization in *n*-pentane, **7** was obtained as colorless solid (831 mg, 1.59 mmol, 58 % yield). ^{1}H NMR (500 MHz, CD_2Cl_2): δ = 7.47-7.45 (m, 2H, Ph-*H*), 7.34-7.32 (m, 4H, Ph-*H*), 7.22-7.15 (m, 9H, Ph-*H*), 3.10 (t, 4H, N-CH_2), 2.78 (t, 4H, N-CH_2), –0.13 (s, 18H, SiCH_3) ppm; ^{11}B{^{1}H} NMR (160 MHz, CD_2Cl_2): δ = 37.5 (s) ppm; ^{13}C{^{1}H} NMR (126 MHz, CD_2Cl_2): δ = 140.7 (br, B-Ph-C_{ipso}), 139.1 (br, B-Ph-C_{ipso}), 134.2 (s, Ph-*C*), 134.0 (s, Ph-*C*), 128.8 (s, Ph-*C*), 127.7 (s, Ph-*C*), 127.6 (s, Ph-*C*), 126.9 (s, Ph-*C*), 50.8 (s, N-CH_2), 48.8 (s, N-CH_2), 0.9 (s, SiCH_3) ppm; ^{29}Si{^{1}H} NMR (99 MHz, CD_2Cl_2): δ = 4.7 ppm; HRMS (LIFDI): m/z calcd.: 522.3143, found: 522.3143; elem. anal. calcd. (%) for $C_{28}H_{41}B_3N_4Si_2$: C 64.39, H 7.91, N 10.73; found: C 64.38, H 8.05, N 10.38.

Synthesis of 8. To a solution of $PhBCl_2$ (375.4 mg, 2.36 mmol) in DCM (4.0 mL) a solution of **3** (290.6 mg, 1.0 mmol) in DCM (1.0 mL) was added dropwise at 0 °C. The reaction mixture was slowly warmed to ambient temperature overnight. The solvent was removed *in vacuo* and toluene (13 mL) was added. In a separate flask, *n*-BuLi (0.84 mL, 2.1 mmol, 2.5 M in *n*-hexane) was added to a solution of **2** (458.3 mg, 2.1 mmol) in Et_2O (10 mL) at −78 °C. The solution was warmed to room temperature after 2h. Subsequently, the lithiated species was added to the toluene solution dropwise at −78 °C. The reaction mixture was slowly warmed to room temperature overnight. After removing the solvent in *vacuo*, DCM (9 mL) was added and LiCl was removed by filtration at −30 °C. The solvent was removed in *vacuo* and the residue was washed with *n*-pentane to obtain the product **8** as an off-white solid (407 mg, 0.54 mmol, 54 % yield). ^{1}H NMR (500 MHz, $CDCl_3$): δ = 7.38-7.30 (m, 14H, Ph-*H*), 7.25-7.19 (m, 11H, Ph-*H*), 3.25 (t, 4H, N-CH_2), 2.83 (t, 4H, N-CH_2), 2.38 (s, 4H, N-CH_2), –0.23 (s, 18H, SiCH_3) ppm; ^{11}B{^{1}H} NMR (160 MHz, $CDCl_3$): δ = 37.3 (br) ppm; ^{13}C{^{1}H} NMR (126 MHz, $CDCl_3$): δ = 139.7 (br, B-Ph-C_{ipso}), 138.5 (br, B-Ph-C_{ipso}), 136.4 (s, Ph-*C*), 134.3 (s, Ph-*C*), 134.1 (s, Ph-*C*), 129.0 (s, Ph-*C*), 127.9 (s, Ph-*C*), 127.5 (Ph-*C*), 127.4 (s, Ph-*C*), 126.7 (s, Ph-*C*), 126.2 (s, Ph-*C*), 50.7 (s, N-CH_2), 50.1 (s, N-CH_2), 48.6 (s, N-CH_2), 0.9 (s, SiCH_3) ppm; ^{29}Si{^{1}H} NMR (99 MHz, CD_2Cl_2): δ = 4.7 ppm; HRMS (LIFDI): m/z calcd.: 753.4523, found: 753.4503; elem. anal. calcd. (%) for $C_{42}H_{55}B_5N_6Si_2$: C 66.89, H 7.35, N 11.14; found: C 66.51, H 7.57, N 11.11.

Synthesis of 9. To a solution of **7** (157 mg, 0.30 mmol) in DCM (3.0 mL) was added a solution of $PhB(NMe_2)Br$ (127 mg, 0.60 mmol) in DCM (7.0 mL) dropwise at 0 °C. After 2 h, the reaction

mixture was warmed to room temperature and stirred for another 1.5 h. Subsequently, Me_3SiNMe_2 (6.1 mg, 0.05 mmol) was added at ambient temperature to terminate all remaining B–Br groups. After 1 h, all volatiles were removed *in vacuo* and the residue was washed with cold *n*-pentane (−78 °C, 3.0 mL). After removing all volatiles *in vacuo*, **9** was obtained as a colorless solid (155 mg, 0.24 mmol, 80 % yield). ^{1}H NMR (500 MHz, CD_2Cl_2): δ = 7.70-7.69 (m, 2H, Ph-*H*), 7.41-7.22 (m, 19H, Ph-*H*), 7.09-7.07 (m, 4H, Ph-*H*), 3.24 (br, 4H, N-CH_2), 2.62 (t, 4H, N-CH_2), 2.41 (s, 6H, N-CH_3), 1.88 (s, 6H, N-CH_3) ppm; ^{11}B{^{1}H} NMR (160 MHz, CD_2Cl_2): δ = 35.2 (br) ppm; ^{13}C{^{1}H} NMR (126 MHz, CD_2Cl_2): δ = 140.6 (br, B-Ph-C_{ipso}), 140.0 (br, B-Ph-C_{ipso}), 138.2 (br, B-Ph-C_{ipso}), 135.1 (s, Ph-*C*), 134.4 (s, Ph-*C*), 134.3 (s, Ph-*C*), 129.1 (s, Ph-*C*), 128.1 (s, Ph-*C*), 128.1 (s, Ph-*C*), 128.0 (s, Ph-*C*), 127.6 (s, Ph-*C*), 126.9 (s, Ph-*C*), 51.3 (s, N-*C*H_2), 50.8 (s, N-*C*H_2), 40.0 (s, N-*C*H_3), 39.7 (s, N-*C*H_3) ppm; HRMS (LIFDI): m/z calcd.: 639.4202, found: 639.4190.

Synthesis of 10. To a solution of **8** (151 mg, 0.20 mmol) in DCM (3.0 mL) was added a solution of $PhB(NMe_2)Br$ (85 mg, 0.40 mmol) in DCM (6.0 mL) dropwise at 0 °C. After 2 h, the reaction mixture was warmed to room temperature and stirred for another 1 h. Subsequently, Me_3SiNMe_2 (7.1 mg, 0.06 mmol) was added at ambient temperature to terminate all remaining B–Br groups. After 1 h, all volatiles were removed *in vacuo* and the residue was washed with cold *n*-pentane (−78 °C, 2.0 mL). After removing all volatiles *in vacuo*, **10** was obtained as a colorless solid (165 mg, 0.19 mmol, 95 % yield). ^{1}H NMR (500 MHz, CD_2Cl_2): δ = 7.58 (t, 1H, Ph-*H*), 7.39-7.09 (m, 30H, Ph-*H*), 7.10 (m, 4H, Ph-*H*), 3.48-2.92 (br, 4H, N-CH_2), 2.73 (m, 4H, N-CH_2), 2.56 (m, 4H, N-CH_2), 2.37 (s, 6H, N-CH_3), 1.84 (s, 6H, N-CH_3) ppm; ^{11}B{^{1}H} NMR (160 MHz, CD_2Cl_2): δ = 35.3 (br) ppm; ^{13}C{^{1}H} NMR (126 MHz, CD_2Cl_2): δ = 140.0 (br, B-Ph-C_{ipso}), 138.4 (br, B-Ph-C_{ipso}), 137.0 (br, B-Ph-C_{ipso}), 134.9 (s, Ph-*C*), 134.6 (s, Ph-*C*), 134.3 (s, Ph-*C*), 129.2 (s, Ph-*C*), 128.3 (s, Ph-*C*), 128.1 (s, Ph-*C*), 127.9 (s, Ph-*C*), 127.7 (s, Ph-*C*), 127.5 (s, Ph-*C*), 126.9 (s, Ph-*C*), 126.6 (s, Ph-*C*), 51.1 (s, N-*C*H_2), 50.8 (s, N-*C*H_2), 50.5 (br, N-*C*H_2), 40.0 (s, N-*C*H_3), 39.7 (s, N-*C*H_3) ppm; HRMS (LIFDI): m/z calcd.: 871.5545, found: 871.5538.

Synthesis of 13.[16b] To a solution of **11** (347 mg, 1.0 mmol) in 0.5 mL was added a solution of *p*-$BuC_6H_4BCl_2$ (215 mg, 1.0 mmol) in 0.5 mL at ambient temperature. After stirring for 24 h, Me_3SiNMe_2 (20.5 mg, 0.17 mmol) was added to the cloudy reaction mixture to deactivate the reactive end groups. After another 45 min, the volatiles were removed *in vacuo* to obtain a colorless solid (303 mg, 0.88 mmol, 88 % yield). GPC (in THF, vs. polystyrene, detection by UV-vis signal): M_n = 4.0 kDa; M_w = 6.1 kDa.

Synthesis of 14. To a solution of **3** (290 mg, 1.0 mmol) in 0.5 mL was added a solution of *p*-$BuC_6H_4BCl_2$ (215 mg, 1.0 mmol) in 0.5 mL at ambient temperature. After stirring for 24 h, Me_3SiNMe_2 (22.0 mg, 0.19 mmol) was added to the cloudy reaction mixture to deactivate the reactive end groups. After another 45 min, the volatiles were removed *in vacuo* and the residue was washed with *n*-pentane (3 x 2 mL) to obtain a colorless solid (189 mg, 0.66 mmol, 66 % yield). ^{1}H NMR (500 MHz, CD_2Cl_2): δ = 7.54-6.85 (m, 9H, aryl), 3.34-2.28 (m, 6H, N-C_2H_4-N & butyl-CH_2), 1.78-1.27 (m, 4H, butyl-CH_2), 1.01-0.87 (m, 3H, butyl-CH_3), -0.26 (s, 0.8H, Si(CH_3)$_3$ end group) ppm; ^{11}B{^{1}H} NMR (160 MHz, CD_2Cl_2): δ = 32.8 (br) ppm; ^{13}C{^{1}H} NMR (126 MHz, CD_2Cl_2): δ = 144.4 (br, aryl), 136.6 (br, aryl), 134.9 (br, aryl), 127.6 (br, aryl), 126.5 (br, aryl), 50.2 (br, N-C_2H_4-N), 36.2 (m, butyl-CH_2), 34.2 (m, butyl-CH_2), 23.0 (m, butyl-CH_2), 14.2 (m, butyl-CH_3), 0.8 (s, Si(CH_3)$_3$ end group) ppm; GPC (in THF, vs. polystyrene, detection by UV-vis signal): M_n = 2.5 kDa; M_w = 2.8 kDa.

Synthesis of 15. To a solution of **11** (347 mg, 1.0 mmol) in 0.5 mL was added a solution of $PhBCl_2$ (159 mg, 1.0 mmol) in 0.5 mL at ambient temperature. After stirring for 24 h, Me_3SiNMe_2 (27.3 mg, 0.23 mmol) was added to the cloudy reaction mixture to deactivate the reactive end groups. After another 45 min, the volatiles were removed *in vacuo* and the residue was washed with *n*-pentane (3 x 2 mL) to obtain a colorless solid (165 mg, 0.57 mmol, 57 % yield). ^{1}H NMR (500 MHz, CD_2Cl_2): δ = 7.73-6.26 (m, 9H, aryl), 3.42-2.01 (m, 6H, N-C_2H_4-N & butyl-CH_2), 1.86-1.13 (m, 4H, butyl-CH_2), 0.94 (br, 3H, butyl-CH_3), −0.25 (s, 0.6H, Si(CH_3)$_3$ end group) ppm; ^{11}B{^{1}H} NMR (160 MHz, CD_2Cl_2): δ = 32.8 (br) ppm; ^{13}C{^{1}H} NMR (126 MHz, CD_2Cl_2): δ = 142.3 (br, aryl), 139.9 (br, aryl), 135.8 (br, aryl), 134.8 (br, aryl), 129.1 (br, aryl), 127.6 (br, aryl), 126.2 (br, aryl), 50.3 (br, N-C_2H_4-N), 36.2 (m, butyl-CH_2), 34.1 (m, butyl-CH_2), 22.9 (m, butyl-CH_2), 14.2 (m, butyl-CH_3), 0.9 (s, Si(CH_3)$_3$ end group) ppm; GPC (in THF, vs. polystyrene, detection by UV-vis signal): M_n = 3.3 kDa; M_w = 4.8 kDa.

Synthesis of 16. To a suspension of **4** (195 mg, 0.50 mmol) in 0.5 mL DCM was added a solution of **11** (173 mg, 0.50 mmol) in 0.5 mL DCM at ambient temperature. After stirring for 24 h, Me_3SiNMe_2 (13.2 mg, 0.11 mmol) was added to the cloudy reaction mixture to deactivate the reactive end groups. After 45 min, the volatiles were removed *in vacuo* and the residue was washed with *n*-pentane (3 x 2 mL) to obtain a colorless solid (170 mg, 0.32 mmol, 64 % yield). ^{1}H NMR (500 MHz, CD_2Cl_2): δ = 8.03-6.77 (m, 19H, aryl), 3.35-2.39 (m, 10H, N-C_2H_4-N & butyl-CH_2), 1.73-1.27 (m, 4H, butyl-CH_2), 0.94 (m, 3H, butyl-CH_3), -0.26 (s, 0.6H, Si(CH_3)$_3$ end group) ppm; ^{13}C{^{1}H} NMR: no signals were observed due to limited solubility; GPC (in THF, vs. polystyrene, detection by UV-vis signal): M_n = 1.9 kDa; M_w = 2.2 kDa.

Crystallographic data

Crystals suitable for single-crystal X-ray diffraction were selected, coated in perfluoropolyether oil, and mounted on MiTeGen micromounts or polyimide microloops. Diffraction data were collected on Bruker X8 Apex II 4-circle diffractometers with CCD area detectors using Mo-K_α radiation. The crystals were cooled using an Oxford Cryostreams low-temperature device. Data were collected at 100 K. The images were processed and corrected for Lorentz-polarization effects and absorption as implemented in the Bruker software packages. The structures were solved using the intrinsic phasing method (SHELXT)[35] and Fourier expansion technique. All non-hydrogen atoms were refined in anisotropic approximation, with hydrogen atoms 'riding' in idealized positions, by full-matrix least squares against F^2 of all data, using SHELXL[36] software and the SHELXLE graphical user interface.[37] Other structural information was extracted using OLEX2 software.[38] Crystal data and experimental details are listed in Table 2.2.2; full structural information has been deposited with the Cambridge Crystallographic Data Centre. CCDC-2314433 – 2314438.

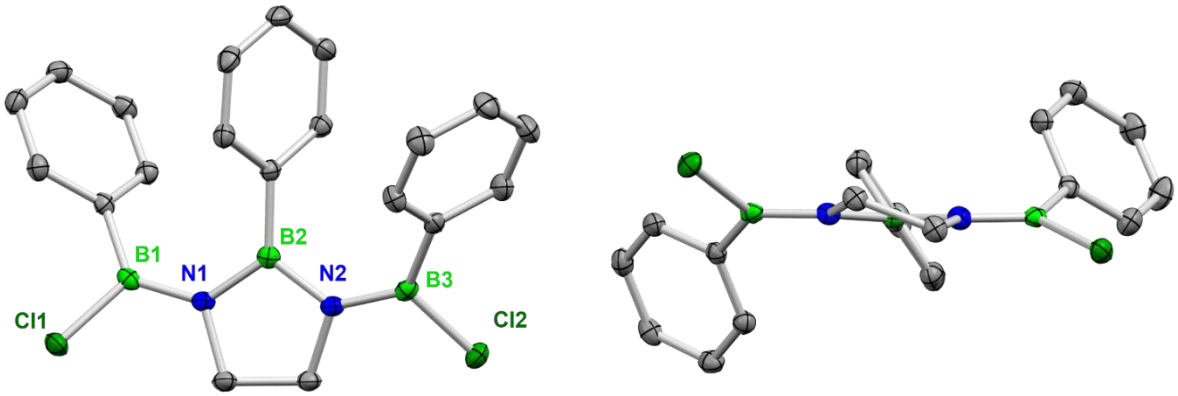

Figure 2.2.4. Molecular structure of **4** in the solid state determined by single-crystal X-ray diffraction at 100 K (H atoms omitted for clarity). Structure shown perpendicular (left) and parallel (right) to the N1-B2-N2 plane. All ellipsoids are drawn at the 50% probability level.

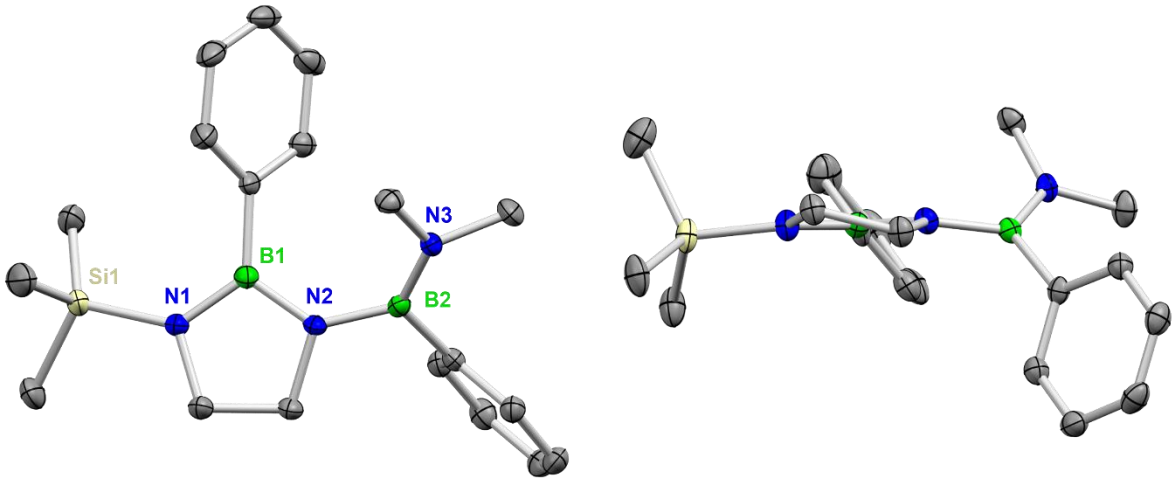

Figure 2.2.5. Molecular structure of **5** in the solid state determined by single-crystal X-ray diffraction at 100 K (H atoms omitted for clarity). Structure shown perpendicular (left) and parallel (right) to the N1-B1-N2 plane. All ellipsoids are drawn at the 50% probability level. There are two symmetry-independent molecules in the unit cell and only one is shown here.

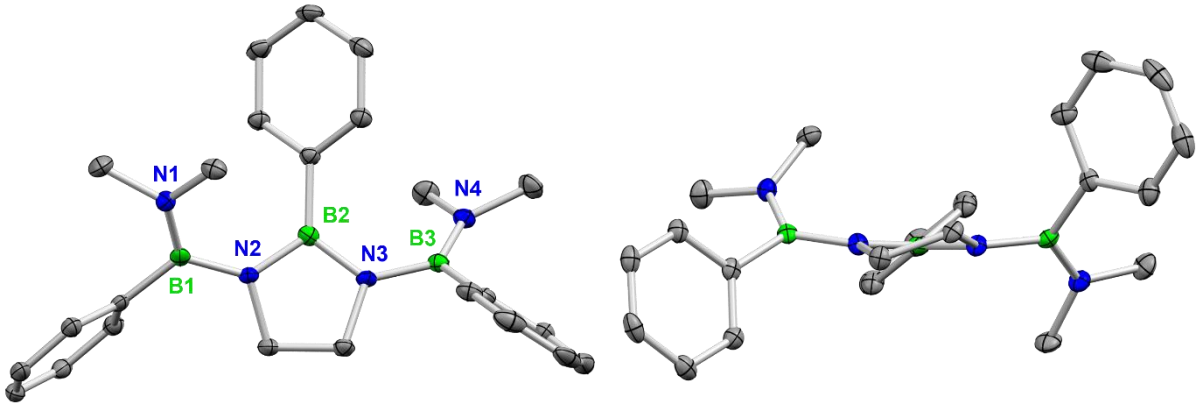

Figure 2.2.6. Molecular structure of **6** in the solid state determined by single-crystal X-ray diffraction at 100 K (H atoms omitted for clarity). Structure shown perpendicular (left) and parallel (right) to the N2-B2-N3 plane. All ellipsoids are drawn at the 50 % probability level.

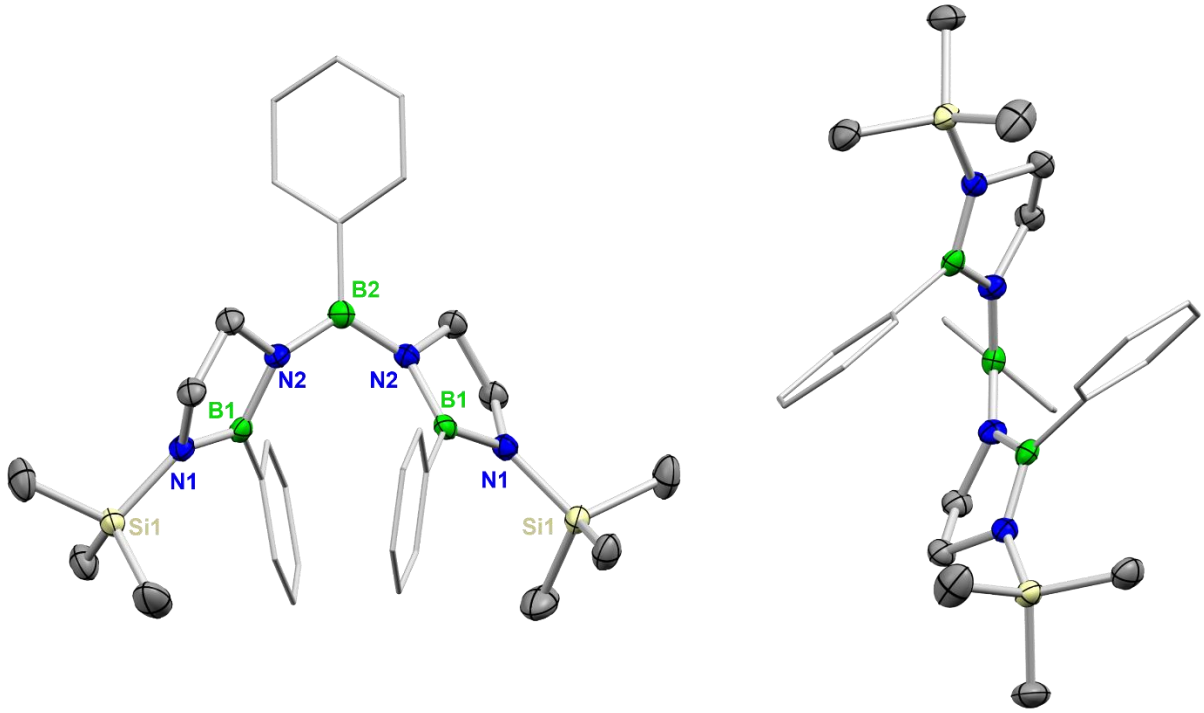

Figure 2.2.7. Molecular structure of **7** in the solid state determined by single-crystal X-ray diffraction at 100 K (H atoms omitted for clarity). Structure shown perpendicular (left) and parallel (right) to the N2-B2-N2 plane. All ellipsoids are drawn at the 50 % probability level. There are two symmetry-independent molecules in the unit cell and only one is shown here. Both molecules have two-fold rotational symmetry.

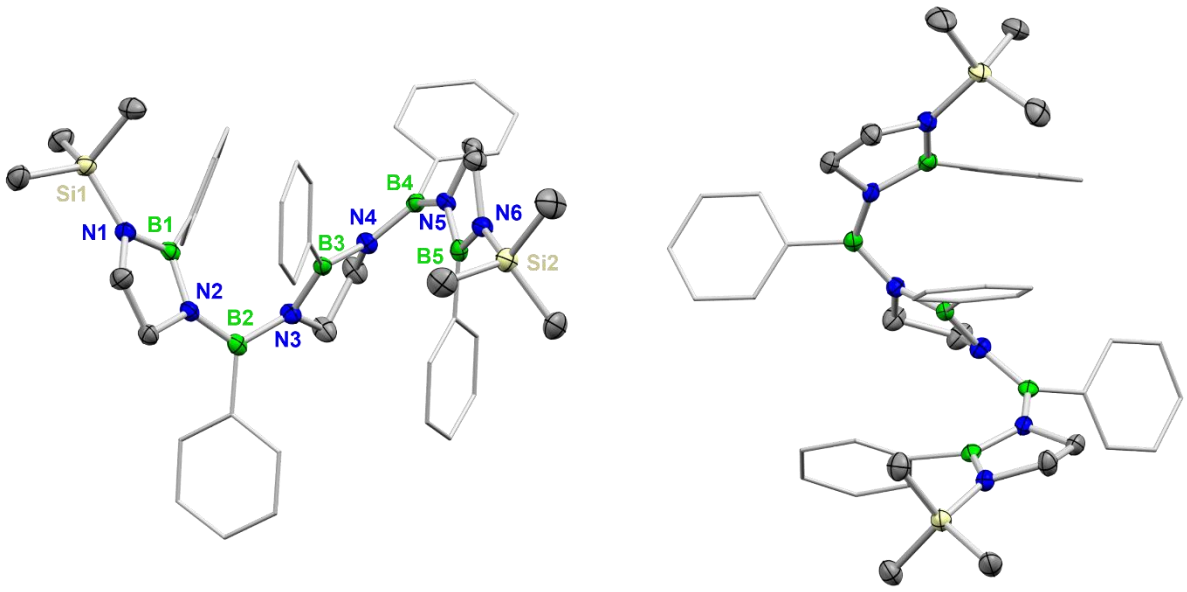

Figure 2.2.8. Molecular structure of **8** in the solid state determined by single-crystal X-ray diffraction at 100 K (H atoms and THF solvent molecules omitted for clarity). Structure shown perpendicular to the N2-B2-N3 plane (left) and approx. parallel to the N3-B3-N4 plane (right). All ellipsoids are drawn at the 50 % probability level.

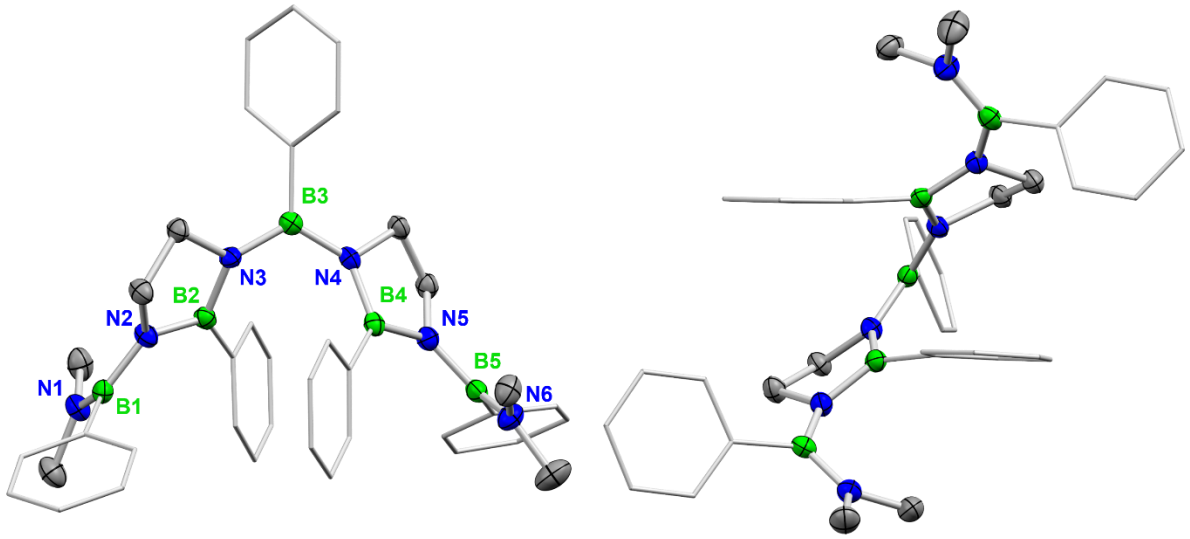

Figure 2.2.9. Molecular structure of **9** in the solid state determined by single-crystal X-ray diffraction at 100 K (H atoms and THF solvent molecules omitted for clarity). Structure shown perpendicular (left) and parallel (right) to the N3-B3-N4 plane. All ellipsoids are drawn at the 50 % probability level. The phenyl ring bonded to the B3 boron atom is disordered and only the major part (80%) is shown here.

Table 2.2.2. Single-crystal X-ray diffraction data and structure refinements.

Compound	**4**	**5**	**6**	**7**	**8**	**9**
CCDC number	2314433	2314434	2314435	2314436	2314437	2314438
Crystal size / mm³	0.40 x 0.46 x 0.71	0.16 x 0.23 x 0.37	0.20 x 0.29 x 0.43	0.40 x 0.40 x 0.43	0.23 x 0.32 x 0.32	0.24 x 0.25 x 0.30
Crystal color, habit	colorless block	colorless block	colorless block	colorless block	colorless block	colorless block
Empirical formula	$C_{20}H_{19}B_3Cl_2N_2$	$C_{19}H_{29}B_2N_3Si$	$C_{24}H_{31}B_3N_4$	$C_{28}H_{41}B_3N_4Si_2$	$C_{42}H_{55}B_5N_6Si_2 \cdot C_4H_8O$	$C_{38}H_{45}B_5N_6 \cdot C_4H_8O$
M_r	390.70	349.16	407.96	522.26	826.25	711.95
F(000)	808	752	436	2240	884	1520
Crystal system	monoclinic	triclinic	triclinic	orthorhombic	triclinic	monoclinic
Space group	$P2_1/c$	$P\bar{1}$	$P\bar{1}$	$Pbcn$	$P\bar{1}$	$P2_1/c$
a / Å	6.4201(13)	11.730(2)	7.8394(9)	14.782(5)	13.026(3)	13.366(9)
b / Å	19.327(7)	12.090(3)	9.5192(12)	28.766(6)	13.814(4)	22.871(16)
c / Å	15.793(3)	17.266(3)	16.4689(19)	14.542(2)	16.047(5)	15.186(12)
α / deg	90	109.591(16)	77.020(4)	90	105.790(13)	90
β / deg	95.70(3)	90.254(15)	79.163(4)	90	108.92(2)	115.638(19)
γ / deg	90	113.718(16)	82.686(4)	90	105.475(10)	90
V / Å³	1949.9(9)	2084.2(8)	1171.6(2)	6183(3)	2420.4(12)	4185(5)
Z	4	4	2	8	2	4
ρ_{calc} / g cm^{-3}	1.331	1.113	1.156	1.122	1.134	1.130
μ / mm^{-1}	0.340	0.119	0.067	0.138	0.113	0.067
T / K	100(2)	100(2)	100(2)	99(2)	100(2)	100(2)
$\theta_{min,max}$ / °	1.670, 26.431	1.268, 26.482	2.204, 26.838	1.416, 26.419	1.459, 26.474	1.690, 26.226
Reflections collected	30356	38935	19503	94009	33447	35236
Unique reflections	3996	8599	5009	6356	9968	8356
R_{int}	0.0354	0.0420	0.1025	0.0821	0.0459	0.0573
Parameters / restraints	244 / 0	461 / 0	284 / 0	343 / 12	553 / 85	592 / 577
GooF on F^2	1.034	1.021	0.998	1.053	1.040	1.026
R_1 [$I \geq 2\sigma(I)$]	0.0283	0.0404	0.0806	0.0434	0.0617	0.0553
wR_2 [all data]	0.0727	0.1062	0.2214	0.1198	0.1817	0.1540
Max. / min. residual electron density / e Å^{-3}	0.385 / -0.178	0.437 / -0.306	0.361 / -0.439	0.429 / -0.301	1.175 / -1.020	0.635 / -0.401

Table 2.2.3. Selected bond lengths and distances (Å), and angles (°). Atom labels are given according to atom assignments in Figures 2.2.4 – 2.2.9.

Compound	**4**	**5**[a]	**6**[b]
B1–N1	1.4064(18)	1.435(2) / 1.430(2)	1.409(3)
B1–N2		1.439(2) / 1.431(2)	1.450(3)
B2–N1	1.4486(18)		
B2–N2	1.4470(18)	1.452(2) / 1.453(2)	1.438(2)
B2–N3		1.407(2) / 1.407(2)	1.429(3)
B3–N2	1.4108(18)		
B3–N3			1.457(3)
B3–N4			1.406(3)
Average B–N	1.428	1.433 / 1.430	1.432
N–B–N	B2: 108.70(11)	B1_1: 110.27(13)	B2: 110.06(16)
N–B–C	126.22(12)	125.36(13)	124.72(18)
N–B–C	125.06(11)	124.33(13)	125.21(17)
N–B–N		B1_4: 110.58(12)	
N–B–C		126.43(13)	
N–B–C		122.99(13)	
B–N–B	N1: 130.10(11)	N2: 131.82(13) /	N2: 132.20(17)
	N2: 129.84(11)	131.56(12)	N3: 130.74(16)
N–B–N		B2: 122.61(14) /	B1: 122.16(18)
		122.26(13)	B3:121.38(17)
Sum ∠ RBR	N1: 359.6(1)	N1: 360.0(1) / 359.9(1)	N1: 359.7(2)
and	N2: 359.5(1)	N2: 357.0(1) / 357.3(1)	N2: 357.6(2)
Sum ∠ RNR	B1: 360.0(1)	N3: 359.9(1) / 359.9(1)	N3: 360.0(2)
	B2: 360.0(1)	B1: 360.0(1) / 360.0(1)	N4: 359.9(2)
	B3: 360.0(1)	B2: 360.0(1) / 360.0(1)	B1: 360.0(2)
			B2: 360.0(2)
			B3: 359.9(2)
C_{ipso}–C_{ipso}	3.2835(19)	4.647(3) / 4.591(3)	4.755(3)
	3.3377(19)		4.566(3)
Compound	**7**[a,c]	**8**	**9**[d,e]
B1–N1	1.428(2) / 1.425(2)	1.419(3)	1.414(3)
B1–N2	1.446(2) / 1.445(2)	1.443(3)	1.477(3)
B2–N1			
B2–N2	1.426(2) / 1.431(2)	1.422(3)	1.443(3)
B2–N3		1.439(3)	1.462(3)
B3–N2			
B3–N3		1.430(3)	1.452(3)
B3–N4		1.439(3)	1.439(3)
B4–N4		1.431(3)	1.457(3)
B4–N5		1.428(3)	1.437(3)
B5–N5		1.447(3)	1.465(3)
B5–N6		1.424(3)	1.409(3)
Average B–N	1.433 / 1.434	1.432	1.446

N–B–N N–B–C N–B–C N–B–N N–B–C N–B–C N–B–N N–B–C N–B–C	B1_1: 109.83(16) 126.60(16) 123.21(16) B1_5:109.73(15) 126.22(16) 123.95(16)	B1: 110.4(2) 125.7(2) 123.4(2) B3: 109.4(2) 124.1(2) 126.5(2) B5: 109.7(2) 122.2(2) 127.7(2)	B2: 109.67(17) 125.68(18) 124.48(19) B4: 109.38(18) 123.78(18) 126.64(18)
B–N–B	N2: 130.89(15) / 131.38(15)	N2: 128.6(2) N3: 130.7(2) N4: 131.7(2) N5: 130.2(2)	N2: 136.68(17) N3: 133.99(17) N4: 132.19(17) N5: 130.34(18)
N–B–N	B2: 119.9(2) / 120.6(2)	B2: 118.8(2) B4: 119.5(2)	B1: 122.1(2) B3: 120.59(18) B5: 120.71(19)
Sum ∠ RBR and Sum ∠ RNR	N1: 359.8(2) / 359.7(2) N2: 360.0(2) / 359.8(2) B1: 359.6(2) / 360.0(2) B2: 360.0(2) / 359.9(2)	N1: 359.6(2) N2: 360.0(2) N3: 360.0(2) N4: 360.0(2) N5: 360.0(2) N6: 359.4(2) B1: 359.5(2) B2: 360.0(2) B3: 360.0(2) B4: 360.0(2) B5: 359.6(2)	N1: 360.0(2) N2: 359.9(2) N3: 360.0(2) N4: 360.0(2) N5: 359.0(2) N6: 359.7(2) B1: 359.9(2) B2: 359.8(2) B3: 359.9(3) B4: 359.8(2) B5: 360.0(2)
C_{ipso}–C_{ipso}	4.670(3) / 4.676(3) 1,3: 3.578(4) / 3.623(4)	4.5854(19) 1,3: 3.8528(11) 4.6174(12) 4.7568(12) 3,5: 3.6768(9) 4.6007(18)	4.810(4) 4.838(11) 2,4: 3.579(3) 4.814(10) 4.573(3)

[a] There are two symmetry-independent molecules in the unit cell and values are given for both here.

[b] Atom labels in the table correspond to the respective atom labels in the cif-file according to: N1 ≡ N1_2, B1 ≡ B1_2, N2 ≡ N1_1, B2 ≡ B1_1, N3 ≡ N2_1, B3 ≡ B1_3, N4 ≡ N1_3.

[c] Atom labels of the second molecule correspond to the respective atom labels in the cif-file according to: N1 ≡ N2_5, N2 ≡ N1_5.

[d] The phenyl ring bonded to the B3 boron atom is disordered. Bond lengths and angles are given for the major part (80%) only.

[e] Atom labels in the table correspond to the respective atom labels in the cif-file according to: N1 ≡ N1_3, N2 ≡ N1_1, N3 ≡ N2_1, N4 ≡ N3_1, N5 ≡ N4_1, N6 ≡ N1_9, B1 ≡ B1_1, B2 ≡ B2_1, B3 ≡ B3_1, B4 ≡ B4_1, B5 ≡ B5_1.

Table 2.2.4. Selected interplanar angles (°). Atom labels are given according to atom assignments in Figures 2.2.4 – 2.2.9.

Compound	**4**	**5**[a]	**6**[b]
∠ BR_3-phenyl	B1: 40.16(4)	B1: 50.35(6) / 53.96(6)	B1: 48.80(7)
	B2: 54.77(5)	B2: 84.33(6) / 62.13(6)	B2: 40.53(7)
	B3: 36.34(4)		B3: 52.88(8)
∠ NBN-BNB	4.13(11)	10.22(13) / 10.25(11)	34.2(3)
	0.77(11)	50.9(2) / 52.3(2)	10.39(18)
			8.37(17)
			54.3(3)
∠ ph_{B1}-ph_{B2} [e]	32.45(5)	45.20(6) / 70.13(6)	79.81(7)
∠ ph_{B2}-ph_{B3}	41.58(4)		77.67(8)
∠ ph_{B3}-ph_{B4}			
∠ ph_{B4}-ph_{B5}			
∠ ph_{B1}-$ph_{B1'}$			
∠ ph_{B1}-ph_{B3}	73.35(5)		71.34(8)
∠ BR_3-NR_3			
B1/N1	18.82(5)	9.79(6) / 6.44(5)	22.28(11)
B1/N2		7.59(7) / 6.21(6)	31.02(10)
B2/N1	7.92(5)		
B2/N2	7.46(6)	37.44(7) / 39.55(7)	11.03(8)
B2/N3		12.44(7) / 12.86(8)	6.51(8)
B3/N2	25.08(5)		
B3/N3			43.64(9)
B3/N4			13.16(9)
Compound	**7**[a]	**8**	**9**[c,d]
∠ BR_3-phenyl	B1: 43.77(7) / 48.47(7)	B1: 57.15(2)	B1: 59.17(9)
	B2: 48.32(9) / 50.38(9)	B2: 45.989(10)	B2: 34.43(8)
		B3: 38.484(13)	B3: 52.44(16)
		B4: 45.641(17)	B4: 44.90(9)
		B5: 46.164(11)	B5: 43.52(10)
∠ NBN-BNB	11.40(14) / 3.67(15)	6.4514(19)	43.9(3)
	30.23(15) / 35.88(15)	35.603(14)	8.0(2)
		39.332(17)	13.95(18)
		10.732(5)	31.3(3)
		11.234(4)	27.1(3)
		32.152(12)	9.08(19)
		34.966(13)	0.2(2)
		8.2992(19)	52.3(4)
∠ ph_{B1}-ph_{B2} [e]	75.28(8) / 76.28(8)	72.79(2)	71.86(10)
∠ ph_{B2}-ph_{B3}		82.116(15)	69.93(16)
∠ ph_{B3}-ph_{B4}		80.009(17)	68.59(17)
∠ ph_{B4}-ph_{B5}		78.175(19)	89.91(9)
∠ ph_{B1}-$ph_{B1'}$	16.38(9)/16.94(10)		
∠ ph_{B1}-ph_{B3}		21.555(7)	86.77(19)

∠ ph_{B2}-ph_{B4}		60.50(2)	2.37(8)
∠ ph_{B3}-ph_{B5}		10.894(4)	59.07(18)
∠ BR_3-NR_3			
B1/N1	5.21(7) / 7.42(7)	1.5313(7)	10.97(10)
B1/N2	13.72(7) / 8.98(8)	11.957(4)	38.95(10)
B2/N1			
B2/N2	30.93(7) / 32.53(7)	34.387(13)	8.61(9)
B2/N3		38.492(16)	14.50(8)
B3/N2			
B3/N3		11.102(5)	30.76(17)
B3/N4		10.939(4)	27.81(18)
B4/N4		32.513(12)	12.75(9)
B4/N5		33.826(13)	5.21(10)
B5/N5		13.182(4)	45.18(11)
B5/N6		2.5204(12)	17.22(12)

[a] There are two symmetry-independent molecules in the unit cell and values are given for both here.
[b] Atom labels in the table correspond to the respective atom labels in the cif-file according to: B1 ≡ B1_2, B2 ≡ B1_1, B3 ≡ B1_3.
[c] The phenyl ring bonded to the B3 boron atom is disordered. Bond lengths and angles are given for the major part (80%) only.
[d] Atom labels in the table correspond to the respective atom labels in the cif-file according to: B1 ≡ B1_1, B2 ≡ B2_1, B3 ≡ B3_1, B4 ≡ B4_1, B5 ≡ B5_1.
[e] Interplanar angles between phenyl (ph) rings bonded to the boron atoms as given in the respective indices.

Table 2.2.5. Aryl···aryl (π···π) distances (Å) and tilt angle (°) in crystals of **4** at 100 K.

Compound	Aryl···Aryl	Centroid-centroid distance	Interplanar separation	Offset shift [a]	Tilt of planes
4	Phenyl(B1)···Phenyl(B2)	3.9641(14)	3.7174(17)	1.377(2)	32.45(5)
	intramolecular		3.4634(16)	1.929(2)	

[a] The offset shift, also called inter-centroid shift, is the distance within a plane of an aryl ring between the centroid of the respective aryl ring and the intersection point with the normal to the plane through the centroid of the other aryl ring.

Determination of the rotational barrier

The ^{1}H NMR spectra for these experiments were recorded at a Bruker Avance Neo I 600 operating at 600 MHz in toluene-d_8. The rotational barriers were estimated by extracting the coalescence temperature T_c and the no-exchange chemical shift differences $\Delta\nu$ from the ^{1}H NMR spectra. We were not able to reach the no-exchange temperature, thus we extrapolated the values using multiple $\Delta\nu$ between −95 and 70 °C. After using following equations, we were able to calculate the activation energy for the hindered rotation ΔG_c about the B–NMe_2 bonds. The quoted uncertainties represent possible inaccuracies in the determination of T_c. The uncertainties of the extrapolation of $\Delta\nu$ were negligible and thus were not considered.

eq 1: $k_c = \frac{\pi \cdot \Delta\nu}{\sqrt{2}}$

eq 2: $\Delta G_c = 4.58 \cdot T_c(10.32 + log\frac{T_c}{k_c})$ [kcal/mol]

Table 2.2.6. Determined values for estimating the rotational barriers for **5**, **6**, **9**, and **10**.

Compound	T_c [°C]	extrapolated $\Delta\nu$ [Hz]	ΔG_c [kcal/mol]
5	54 ± 1	217.5 ± 5.3	15.21 ± 0.05
6	78 ± 1	195.2 ± 1.1	16.45 ± 0.05
9	100 ± 5	300.6 ± 2.1	17.21 ± 0.24
10	100 ± 5	307.1 ± 2.4	17.19 ± 0.24

Computational information

DFT calculations were performed with the Gaussian 16, Revision C.01 program package[39] using the ωB97X-D[40] functional in combination with the 6-31+G(d,p)[41] basis sets for geometry optimizations and the 6-311+G(d,p)[41a,41d,41h,42] basis sets for single-point energy calculations. The molecules **4**, **5**, **6**, **7**, **8**, and **9** were optimized in gas phase starting from the crystal structures to get the differences between theory and experiment with respect to structural parameters. Regarding the rotational barriers, both calculations - geometry optimizations and singlepoint energies - were performed with the PCM[43] solvation model mimicking toluene (ε = 2.3741) as solvent. Their equilibrium geometries were determined by geometry optimization and proved by frequency computations. The connectivity between the obtained transition states and the corresponding intermediate was assessed by further geometry optimizations and visual inspection of the imaginary frequencies. Thermodynamic parameters were calculated at a temperature of 298.15 K and a pressure of 1.00 atm. A concentration correction of $\Delta G^{0\rightarrow *} = RT \cdot \ln(24.46) = 1.89$ kcal mol^{-1} (T = 298.15 K) was added to the free energies of all calculated species. This was done to change the 1.00 atm gas phase values to the condensed phase standard state concentration of 1.00 mol·L^{-1}, which leads to a proper description of associative/dissociative steps. This is necessary because pure gas estimations overestimate the entropy penalty for the formation of complexes.[44]

Table 2.2.7. Calculated rotational barriers of **5**, **6**, and **9** in toluene.

Compound	Rotational barriers [kcal mol^{-1}]
5	15.7
6	17.9
9	19.5

Table 2.2.8. Selected computed bond lengths and distances (Å), and angles (°). Atom labels are given according to atom assignments in Figures 2.2.4 – 2.2.9 for comparison with the related solid-state molecular structures.

Compound	**4**	**5**	**6**	**7**[a]	**8**	**9**
B1–N1	1.4203	1.4312	1.4139	1.4255 / 1.4256	1.4263	1.4133
B1–N2		1.4375	1.4531	1.4443 / 1.4443	1.4477	1.4564
B2–N1	1.4529					
B2–N2	1.4529	1.4539	1.4347	1.4352 / 1.4354	1.4324	1.4293
B2–N3		1.4133	1.4347		1.4373	1.4441
B3–N2	1.4203					
B3–N3			1.4531		1.4389	1.4328
B3–N4			1.4139		1.4388	1.4330
B4–N4					1.4374	1.4439
B4–N5					1.4324	1.4294
B5–N5					1.4477	1.4564
B5–N6					1.4263	1.4133
Average B–N	1.4366	1.4340	1.4339	1.4350 / 1.4351	1.4365	1.4352
N–B–N	B2: 108.44	B1: 110.22	B2: 109.74	B1: 109.78 / 109.78	B1: 109.75	B2: 109.25
N–B–C	125.78	125.68	125.13	127.28 / 127.35	126.60	123.81
N–B–C	125.78	124.08	125.13	122.72 / 122.66	123.29	126.80
N–B–N					B3: 109.07	B4: 109.25
N–B–C					125.47	126.80
N–B–C					125.47	123.81
N–B–N					B5: 109.75	
N–B–C					123.29	
N–B–C					126.60	
B–N–B	N1: 130.34	N2: 129.86	N2: 130.68	N2: 127.97 / 127.99	N2: 129.76	N2: 131.01
	N2: 130.33		N3: 130.68		N3: 130.77	N3: 130.38
					N4: 130.76	N4: 130.38
					N5: 129.76	N5: 131.02
N–B–N		B2: 121.70	B1: 121.44	B2: 117.95	B2: 119.77	B1: 121.25
			B3: 121.44		B4: 119.77	B3: 119.96
						B5: 121.25
Sum ∠RBR	N1: 359.7	N1: 360.0	N1: 359.8	N1: 359.7 / 359.7	N1: 359.8	N1: 359.7
and	N2: 359.7	N2: 357.8	N2: 358.8	N2: 360.0 / 360.0	N2: 360.0	N2: 359.2
Sum ∠RNR	B1: 360.0	N3: 359.8	N3: 358.8	B1: 359.8 / 359.8	N3: 360.0	N3: 360.0
	B2: 360.0	B1: 360.0	N4: 359.8	B2: 360.0	N4: 360.0	N4: 360.0
	B3: 360.0	B2: 360.0	B1: 360.0		N5: 360.0	N5: 359.2
			B2: 360.0		N6: 359.8	N6: 359.7
			B3: 360.0		B1: 359.6	B1: 360.0
					B2: 360.0	B2: 359.9
					B3: 360.0	B3: 360.0
					B4: 360.0	B4: 359.9
					B5: 359.6	B5: 360.0
C_{ipso}–C_{ipso}	3.2751	4.5726	4.6129	4.5749 / 4.5723	4.6726	4.5690
	3.2750		4.6128	1,3: 3.7820	1,3: 3.5610	4.7425

					4.7054 4.7048 3,5: 3.5617 4.6728	2,4: 3.5394 4.7411 4.5690

[a] Two values are given for the two symmetric distances and angles, respectively.

Table 2.2.9. Selected computed interplanar angles (°). Atom labels are given according to atom assignments in Figures 2.2.4 – 2.2.9 for comparison with the related solid-state molecular structures.

Compound	**4**	**5**	**6**	**7**[a]	**8**	**9**
∠ BR_3-phenyl	40.65 51.82 40.63	B1: 54.10 B2: 52.91	B1: 50.76 B2: 44.64 B3: 50.78	B1: 51.30 / 51.10 B2: 37.09	B1: 48.81 B2: 41.41 B3: 36.69 B4: 41.40 B5: 48.85	B1: 47.46 B2: 42.14 B3: 45.32 B4: 42.21 B5: 47.48
∠ NBN-BNB	3.25 3.23	8.61 52.13	49.09 2.51 2.54 49.13	11.40 / 11.09 35.06 / 35.23	12.12 29.44 33.71 10.73 10.70 33.78 29.42 12.13	50.45 1.58 6.87 32.60 32.44 6.95 1.56 50.46
∠ ph_{B1}-ph_{B2} [b]	28.77	76.12	77.98	85.65 / 85.80	79.62	87.30
∠ ph_{B2}-ph_{B3}	28.77		77.96		87.56	76.63
∠ ph_{B3}-ph_{B4}					87.60	76.59
∠ ph_{B4}-ph_{B5}					79.64	87.25
∠ ph_{B1}-$ph_{B1'}$				32.10		
∠ ph_{B1}-ph_{B3}	57.16		64.66		17.46	61.83
∠ ph_{B2}-ph_{B4}					60.28	1.80
∠ ph_{B3}-ph_{B5}					17.51	61.29
∠ BR_3-NR_3						
B1/N1	17.32	8.91	15.81	5.96 / 5.85	3.81	15.74
B1/N2		6.24	41.04	12.19 / 12.21	13.87	43.73
B2/N1	7.60					
B2/N2	7.60	41.46	6.57	36.43 / 36.26	30.42	6.70
B2/N3		15.42	6.57		33.82	10.16
B3/N2	17.32					
B3/N3			41.06		10.87	31.33
B3/N4			15.81		10.84	31.20
B4/N4					33.88	10.20
B4/N5					30.40	6.68
B5/N5					13.87	43.73
B5/N6					3.81	15.73

[a] Two values are given for the distances and angles, which are symmetry-equivalent in the experimentally determined structure.

[b] Interplanar angles between phenyl (ph) rings bonded to the boron atoms as given in the respective indices.

Table 2.2.10. Intramolecular aryl···aryl (π···π) distances (Å) and tilt angle (°) in the computed molecular structure of **4**.

Compound	Aryl···Aryl	Centroid-centroid distance	Interplanar separation	Offset shift [a]	Tilt of planes
4	Phenyl(B1)···Phenyl(B2)	3.8940	3.4522 3.5256	1.8016 1.6534	28.77
	Phenyl(B2)···Phenyl(B3)	3.8936	3.4520 3.5253	1.8010 1.6530	28.77

[a] The offset shift, also called inter-centroid shift, is the distance within a plane of an aryl ring between the centroid of the respective aryl ring and the intersection point with the normal to the plane through the centroid of the other aryl ring.

2.2.5 References

[1] a) S. J. Clarson, J. A. Semlyen, *Siloxane Polymers*, PTR Prentice Hall, Englewood Cliffs, NJ, **1993**; b) M. A. Brook, J. B. Grande, F. Ganachaud, *Adv. Polym. Sci.* **2010**, *235*, 161–183; c) J. E. Mark, D. W. Schaefer, G. Lin, *The Polysiloxanes*, Oxford University Press, New York, **2015**.

[2] a) H. R. Allcock, *Chemistry and Applications of Polyphosphazenes*, Wiley-Interscience, Hoboken, NJ, **2003**; b) M. Gleria, R. de Jaeger, *Phosphazenes: A Worldwide Insight*, Nova Science Publishers, New York, **2004**; c) V. Blackstone, A. Presa Soto, I. Manners, *Dalton Trans.* **2008**, 4363 –4371; d) V. Blackstone, S. Pfirrmann, H. Helten, A. Staubitz, A. Presa Soto, G. R. Whittell, I. Manners, *J. Am. Chem. Soc*. **2012**, *134*, 15293–15296; e) H. R. Allcock, *Dalton Trans.* **2016**, *45*, 1856–1862; f) S. Rothemund, I. Teasdale, *Chem. Soc. Rev.* **2016**, *45*, 5200–5215.

[3] a) R. West, *J. Organomet. Chem.* **1986**, *300*, 327–346; b) R. D. Miller, J. Michl, *Chem. Rev.* **1989**, *89*, 1359–1410; c) A. Feigl, A. Bockholt, J. Weis, B. Rieger, *Adv. Polym. Sci.* **2011**, *235*, 1–31; d) M. Majumdar, I. Bejan, V. Huch, A. J. P. White, G. R. Whittell, A. Schäfer, I. Manners, D. Scheschkewitz, *Chem. Eur. J.* **2014**, *20*, 9225–9229.

[4] a) F. Jäkle, *Chem. Rev.* **2010**, *110*, 3985–4022; b) F. Jäkle, *Top. Organomet. Chem.* **2015**, *49*, 297–325; c) Y. Ren, F. Jäkle, in *Main Group Strategies towards Functional Hybrid Materials* (Eds.: T. Baumgartner, F. Jäkle), Wiley, Hoboken, NJ **2017**, pp 79−110; d) H. Helten, *Chem. Asian J.* **2019**, *14*, 919–935; e) X. Yin, J. Liu, F. Jäkle, *Chem. Eur. J.* **2021**, *27*, 2973–2986; f) H. Helten, in *Comprehensive Organometallic Chemistry IV*, Vol. 14 (Eds: D. O'Hare, K. Meyer, G. Parkin), Elsevier, New York **2022**, 71-134; g) B. Chen, F. Jäkle, *Angew. Chem. Int. Ed.* **2023**, e202313379.

[5] W. L. A. Brooks, B. S. Sumerlin, *Chem. Rev.* **2016**, *116*, 1375–1397.

[6] a) A. Pitto-Barry, *Polym. Chem.* **2021**, *12*, 2035–2044; b) X. Zhang, Y. Lin, N. S. Hosmane, Y. Zhu, *Medical Review* **2023**, 1–19.

[7] a) M. J. D. Bosdet, W. E. Piers, *Can. J. Chem.* **2009**, *87*, 8–29; b) A. Staubitz, A. P. M. Robertson, M. E. Sloan, I. Manners, *Chem. Rev.* **2010**, *110*, 4023–4078; c) N. E. Stubbs, A. P.M. Robertson, E. M. Leitao, I. Manners, *J. Organomet. Chem.* **2013**, *730*, 84–89; d) H. C. Johnson, T. N. Hooper, A. S. Weller, *Top. Organomet. Chem.* **2015**, *49*, 153–220; e) D. Bonifazi, F. Fasano, M. M. Lorenzo-Garcia, D. Marinelli, H. Oubaha, J. Tasseroul, *Chem. Commun.* **2015**, *51*, 15222–15236; f) M. M. Morgan, W. E. Piers, *Dalton Trans.* **2016**, *45*, 5920–5924; g) H. Helten, *Chem. Eur. J.* **2016**, *22*, 12972–12982; h) G. Bélanger-Chabot, H. Braunschweig, D. K. Roy, *Eur. J. Inorg. Chem.* **2017**, 4353–4368; i) M. Stępień, E. Gońka, M. Żyła, N. Sprutta, *Chem. Rev.* **2017**, *117*, 3479–3716; j) Z. X. Giustra, S.-Y. Liu, *J. Am. Chem. Soc.* **2018**, *140*, 1184–1194; k) C. R. McConnell, S.-Y. Liu, *Chem. Soc. Rev.* **2019**, *48*, 3436–3453; l) X.-Y. Wang, X. Yao, A. Narita, K. Müllen, *Acc. Chem. Res.* **2019**, *52*, 2491–2505; m) F. Vidal, F. Jäkle, *Angew. Chem. Int. Ed.* **2019**, *58*, 5846–5870; *Angew. Chem.* **2019**, *131*, 5904–5929; n) D. Han, F. Anke, M. Trose, T. Beweries, *Coord. Chem. Rev.* **2019**, *380*, 260–286; o) K. Ota, R. Kinjo, *Chem. Asian J.* **2020**, *15*, 2558–2574; p) T. Beweries, H. Helten, "Poly(aminoborane)s and Poly(iminoborane)s". In *Encyclopedia of Inorganic and Bioinorganic Chemistry*; ed. R. A. Scott, Wiley, **2020**, DOI: 10.1002/9781119951438.eibc2717; q) R. Zhao, J. Liu, L. Wang, *Acc. Chem. Res.* **2020**, *53*, 1557–1567; r) J. Huang, X. Wang, Y. Xiang, L. Guo, G. Chen, *Adv. Energy Sustainability Res.* **2021**, *2*, 2100016; s) D. Marchionni, S. Basak, A. N. Khodadadi, A. Marrocchi, L. Vaccaro, *Adv. Funct. Mater.* **2023**, 2303635.

[8] a) T. Lorenz, A. Lik, F. A. Plamper, H. Helten, *Angew. Chem. Int. Ed.* **2016**, *55*, 7236–7241; *Angew. Chem.* **2016**, *128*, 7352–7357; b) T. Lorenz, M. Crumbach, T. Eckert, A. Lik, H. Helten, *Angew. Chem. Int. Ed.* **2017**, *56*, 2780–2784; *Angew. Chem.* **2017**, *129*, 2824–2828; c) N. A. Riensch, A. Deniz, S. Kühl, L. Müller, A. Adams, A. Pich, H. Helten, *Polym. Chem.* **2017**, *8*, 5264–5268, d) F. Brosge, T. Lorenz, H. Helten, C. Bolm, *Chem. Eur. J.* **2019**, *25*, 12708–12711, e) J. Chorbacher, M. Maier, J. Klopf, M. Fest, H. Helten, *Macromol. Rapid Commun.* **2023**, 2300278; f) M. Maier, J. Chorbacher, A. Hellinger, J. Klopf, J. Günther, H. Helten, *Chem. Eur. J.* **2023**, e202302767; g) J. S. Schneider, I.

Krummenacher, H. Braunschweig, H. Helten, *Chem. Commun.* **2023**, *59*, 8408–8411; h) V. Zeh, J. S. Schneider, J. Bachmann, I. Krummenacher, H. Braunschweig, H. Helten, *Chem. Commun.* **2023**, *59*, 13723–13726; i) M. Maier, V. Zeh, N. Munker, J. Glock., K. Oberdorf, O. Ayhan, C. Lichtenberg, H. Helten, *Eur. J. Inorg. Chem.* **2023**, *26*, e202300490.

[9] Examples from other groups: a) A. W. Baggett, F. Guo, B. Li, S.-Y. Liu, F. Jäkle, *Angew. Chem. Int. Ed.* **2015**, *54*, 11191; *Angew. Chem.* **2015***, 127*, 11343–11347; b) X.-Y. Wang, F.-D. Zhuang, J.-Y. Wang, J. Pei, *Chem. Commun.* **2015**, *51*, 17532–17535; c) D. Marinelli, F. Fasano, B. Najjari, N. Demitri, D. Bonifazi, *J. Am. Chem. Soc.* **2017**, *139*, 5503–5519; d) W. Zhang, G. Li, L. Xu, Y. Zhuo, W. Wan, N. Yan, G. He, *Chem. Sci.* **2018**, *9*, 4444–4450; e) H. Oubaha, N. Demitri, J. Rault-Berthelot, P. Dubois, O. Coulembier, D. Bonifazi, *J. Org. Chem.* **2019**, *84*, 9101–9116; f) Y. Fu, H. Yang, Y. Gao, L. Huang, R. Berger, J. Liu, H. Lu, Z. Cheng, S. Du, H.-J. Gao, X. Feng, *Angew. Chem. Int. Ed.* **2020**, *59*, 8873–8879; *Angew. Chem.* **2020**, 132, 8958–8964; g) S. Pang, Z. Wang, X. Yuan, L. Pan, W. Deng, H. Tang, H. Wu, S. Chen, C. Duan, F. Huang, Y. Cao, *Angew. Chem. Int. Ed.* **2021**, *60*, 8813–8817; *Angew. Chem.* **2021***, 133,* 8895–8899.

[10] For monomeric aminoboranes with interesting properties, see: a) K. K. Neena, P. Thilagar, *J. Mater. Chem. C* **2016**, *4*, 11465–11473; b) K. K. Neena, P. Thilagar, *Organometallics* **2017**, *36*, 2692–2701; c) K. K. Neena, P. Sudhakar, K. Dipak, P. Thilagar, *Chem. Commun.* **2017**, *53*, 3641–3644.

[11] A. Staubitz, A. Presa Soto, I. Manners, *Angew. Chem. Int. Ed.* **2008**, *47*, 6212–6215; *Angew. Chem.* **2008**, *120*, 6308–6311.

[12] Further examples: a) R. Dallanegra, A. P. M. Robertson, A. B. Chaplin, I. Manners, A. S. Weller, *Chem. Commun.* **2011**, *47*, 3763–3765; b) H. C. Johnson, A. P. M. Robertson, A. B. Chaplin, L. J. Sewell, A. L. Thompson, M. F. Haddow, I. Manners, A. S. Weller, *J. Am. Chem. Soc.* **2011**, *133*, 11076–11079; c) A. P. M. Robertson, R. Suter, L. Chabanne, G. R. Whittell, I. Manners, *Inorg. Chem.* **2011**, *50*, 12680–12691; d) A. P. M. Robertson, E. M. Leitao, T. Jurca, M. F. Haddow, H. Helten, G. C. Lloyd-Jones, I. Manners, *J. Am. Chem. Soc.* **2013**, *135*, 12670–12683; e) A. N. Marziale, A. Friedrich, I. Klopsch, M. Drees, V. R. Celinski, J. Schmedt auf der Günne, S. Schneider, *J. Am. Chem. Soc.* **2013**, *135*, 13342–13355; f) H. C. Johnson, E. M. Leitao, G. R. Whittell, I. Manners, G. C. Lloyd-Jones, A. S. Weller, *J. Am. Chem. Soc.* **2014**, *136*, 9078–9093; g) A. Glüer, M. Förster, V. R. Celinski, J. Schmedt auf der Günne, M. C. Holthausen, S. Schneider, *ACS Catal.* **2015**, *5*, 7214–7217; h) C. Lichtenberg, M. Adelhardt, T. L. Gianetti, K. Meyer, B. de Bruin, H. Grützmacher, *ACS Catal.* **2015**, *5*, 6230–6240; i) K. A. Erickson, J. P. W. Stelmach, N. T. Mucha, R. Waterman, *Organometallics* **2015**, *34*, 4693–4699; j) M. W. Lui, N. R. Paisley, R. McDonald, M. J. Ferguson, E. Rivard, *Chem. Eur. J.* **2016**, *22*, 2134–2145; k) N. T. Coles, M. F. Mahon, R. L. Webster, *Organometallics* **2017**, *36*, 2262–2268; l) D. A. Resendiz-Lara, N. E. Stubbs, M. I. Arz, N. E. Pridmore, H. A. Sparkes, I. Manners, *Chem. Commun.* **2017**, *53*, 11701–11704; m) F. Anke, D. Han, M. Klahn, A. Spannenberg, T. Beweries, *Dalton Trans.* **2017**, *46*, 6843–6847; n) M. Trose, M. Reiß, F. Reiß, F. Anke, A. Spannenberg, S. Boye, A. Lederer, P. Arndt, T. Beweries, *Dalton Trans.* **2018**, *47*, 12858–12862; o) G. M. Adams, A. L. Colebatch, J. T. Skornia, A. I. McKay, H. C. Johnson, G. C. Lloyd Jones, S. A. Macgregor, N. A. Beattie, A. S. Weller, *J. Am. Chem. Soc.* **2018**, *140*, 1481–1495; p) T. Jurca, T. Dellermann, N. E. Stubbs, D. A. Resendiz-Lara, G. R. Whittell, I. Manners, *Chem. Sci.* **2018**, *9*, 3360–3366; q) E. A. LaPierre, B. O. Patrick, I. Manners, *J. Am. Chem. Soc.* **2019**, *141*, 20009–20015; r) F. Anke, S. Boye, A. Spannenberg, A. Lederer, D. Heller, T. Beweries, *Chem. Eur. J.* **2020**, *26*, 7889–7899.

[13] a) K. Watanabe, T. Taniguchi, T. Niiyama, K. Miya, M. Taniguchi, *Nat. Photonics* **2009**, *3*, 591–594; b) L. Ci, L. Song, C. Jin, D. Jariwala, D. Wu, Y. Li, A. Srivastava, Z. F. Wang, K. Storr, L. Balicas, F. Liu, P. M. Ajayan, *Nat. Mater.* **2010**, *9*, 430–435; c) C. R. Dean, A. F. Young, I. Meric, C. Lee, L. Wang, S. Sorgenfrei, K. Watanabe, T. Taniguchi, P. Kim, K. L. Shepard, J. Hone, *Nat. Nanotechnol.* **2010**, *5*, 722–726; d) M. P.

Levendorf, C.-J. Kim, L. Brown, P. Y. Huang, R. W. Havener, D. A. Muller, J. Park, *Nature* **2012**, *488*, 627–632.

[14] For the generation of borazine-based boron nitride precursors: a) T. Wideman, P. J. Fazen, K. Su, E. E. Remsen, G. A. Zank, L. G. Sneddon, *Appl. Organomet. Chem.* **1998**, *12*, 681–693; b) S. Bernard, C. Salameh, P. Miele, *Dalton Trans.* **2016**, *45*, 861–873.

[15] a) D. R. Armstrong, J. Jamieson, P. G. Perkins, *Theor. Chim. Acta* **1978**, *49*, 55–65; b) A. Abdurahman, M. Albrecht, A. Shukla, M. Dolg, *J. Chem. Phys.* **1999**, *110*, 8819–8824; c) M. Côté, P. D. Haynes, C. Molteni, *Phys. Rev. B* **2001**, *63*, 125207; d) D. Jacquemin, *J. Phys. Chem. A* **2004**, *108*, 9260–9266; e) D. Jacquemin, A. Femenias, H. Chermette, J.-M. André, E. A. Perpète, *J. Phys. Chem. A* **2005**, *109*, 5734–5741.

[16] a) O. Ayhan, T. Eckert, F. A. Plamper, H. Helten, *Angew. Chem. Int. Ed.* **2016**, *55*, 13321–13325; *Angew. Chem.* **2016**, *128*, 13515–13519; b) O. Ayhan, N. A. Riensch, C. Glasmacher, H. Helten, *Chem. Eur. J.* **2018**, *24*, 5883–5894.

[17] See references in ref. [16].

[18] a) K. Shimoda, K. Doi, T. Nakagawa, Y. Zhang, H. Miyaoka, T. Ichikawa, M. Tansho, T. Shimizu, A. K. Burrell, Y. Kojima, *J. Phys. Chem. C* **2012**, *116*, 5957–5964; b) T. Kobayashi, S. Gupta, M. A. Caporini, V. K. Pecharsky, M. Pruski, *J. Phys. Chem. C* **2014**, *118*, 19548–19555.

[19] D. Bonifazi, F. Fasano, M. M. Lorenzo-Garcia, D. Marinelli, H. Oubaha, J. Tasseroul, *Chem. Commun.* **2015**, *51*, 15222–15236.

[20] J. E. Burch, W. Gerrard, E. F. Mooney, *J. Chem. Soc.* **1962**, 2200–2203.

[21] a) P. Paetzold, T. von Bennigsen-Mackiewicz, *Chem. Ber.* **1981**, *114*, 298–305; b) H.-U. Meier, P. Paetzold, E. Schröder, *Chem. Ber.* **1984**, *117*, 1954–1964.

[22] a) H. Braunschweig, C. Kollann, K. W. Klinkhammer, *Eur. J. Inorg. Chem.* **1999**, 1523–1529; b) C. Brunecker, M. Arrowsmith, F. Fantuzzi, H. Braunschweig, *Angew. Chem. Int. Ed.* **2021**, *60*, 16864–16868; *Angew. Chem.* **2021**, *133*, 17000–17004; c) L. C. Haufe, L. Endres, M. Arrowsmith, R. Bertermann, M. Dietz, F. Fantuzzi, M. Finze, H. Braunschweig, *J. Am. Chem. Soc.* **2023**, *145*, 23986–23993.

[23] For recent reports on coordinated iminoboranes, see: a) F. Dahcheh, D. Martin, D. W. Stephan, G. Bertrand, *Angew. Chem. Int. Ed.* **2014**, *53*, 13159–13163; *Angew. Chem.* **2014**, *126*, 13375–13379; b) H. Braunschweig, W. C. Ewing, K. Geetharani, M. Schäfer, *Angew. Chem. Int. Ed.* **2015**, *54*, 1662–1665; *Angew. Chem.* **2015**, *127*, 1682–1685; c) A. K. Swarnakar, C. Hering-Junghans, K. Nagata, M. J. Ferguson, R. McDonald, N. Tokitoh, E. Rivard, *Angew. Chem. Int. Ed.* **2015**, *54*, 10666–10669; *Angew. Chem.* **2015**, *127*, 10812–10816; d) A. K. Swarnakar, C. Hering-Junghans, M. J. Ferguson, R. McDonald, E. Rivard, *Chem. Sci.* **2017**, *8*, 2337–2343; e) B. L. Frenette, A. A. Omaña, M. J. Ferguson, Y. Zhou, E. Rivard, *Chem. Commun.* **2021**, *57*, 10895–10898; f) R. Guo, T. Li, R. Wei, X. Zhang, Q. Li, L. L. Liu, C.-H. Tung, L. Kong, *J. Am. Chem. Soc.* **2021**, *143*, 13483–13488; g) J. Wang, P. Jia, W. Sun, Y. Wie, Z. Lin, Q. Ye, *Inorg. Chem.* **2022**, *61*, 8879–8886; h) M. Bao, Y. Dai, C. Liu, Y. Su, *Inorg. Chem.* **2022**, *61*, 11137–11142.

[24] a) R. Köster, H. Bellut, S. Hattori, *Liebigs Ann. Chem.* **1968**, *720*, 1–22; b) H. Helten, A. P. M. Robertson, A. Staubitz, J. R. Vance, M. F. Haddow, I. Manners, *Chem. Eur. J.* **2012**, *18*, 4665–4680.

[25] a) X. Xie, M. F. Haddow, S. M. Mansell, N. C. Norman, C. A. Russell, *Chem. Commun.* **2011**, *47*, 3748–3750; b) X.-Y. Wang, A. Narita, X. Feng, K. Müllen, *J. Am. Chem. Soc.* **2015**, *137*, 7668–7676; c) K. Ota, R. Kinjo, *J. Am. Chem. Soc.* **2021**, *143*, 11152–11159; d) S. Zhou, Y. Liu, W. Jin, T. Qin, X. Liu, C. Zhao, Z. Liu, X. Yu, *Org. Lett.* **2023**, *25*, 1573–1577; S. Jeong, E. Park, J. Kim, S. B. Park, S. H. Kim, W. Choe, J. Kim, Y. S. Park, *Angew. Chem. Int. Ed.* **2023**, *62*, e202314148.

[26] Neilson *et al.* had followed related approaches previously, but the identification of a poly- or an extended oligo(iminoborane) has not been achieved in their studies; see: a) S. Y. Shaw, D. A. DuBois, W. H. Watson, R. H. Neilson, *Inorg. Chem.* **1988**, *27*, 974–976; b) S. Y. Shaw, G. M. Scheide, C. E. Davis, P. Mukherjee, R. H. Neilson, *Phosphorus, Sulfur Silicon Relat. Elem.* **1989**, *41*, 141–146; c) S. Y. Shaw, R. H.

Neilson, *Inorg. Chem.* **1994**, *33*, 3239–3245; d) N. Retta, R. H. Neilson, *Bull. Chem. Soc. Ethiop.* **1999**, *13*, 51–55; e) N. Retta, R. H. Neilson, *Bull. Chem. Soc. Ethiop.* **1999**, *13*, 121–125; f) N. Retta, R. H. Neilson, *Bull. Chem. Soc. Ethiop.* **2000**, *14*, 123–128.
[27] J. O. Sutherland, *Annu. Rep. NMR Spectrosc*. **1971**, *4*, 71–235.
[28] This has also been previously applied to a series of mono-aminoboranes; see: R. H. Neilson, R. L. Wells, *Inorg. Chem.* **1977**, *16*, 7-11.
[29] P. Paetzold, *Phosphorus Sulfur Silicon Relat. Elem.* **1994**, *93*, 39–50.
[30] a) R. A. Bartlett, X. Feng, M. M. Olmstead, P. P. Power, K. J. Weese, *J. Am. Chem. Soc.* **1987**, *109*, 4851; b) H. Chen, R. A. Bartlett, M. M. Olmstead, P. P. Power, S. C. Shoner, *J. Am. Chem. Soc.* **1990**, *112*, 1048; c) M. Maier, J. Klopf, C. Glasmacher, F. Fantuzzi, J. Bachmann, O. Ayhan, A. Koner, B. Engels, H. Helten, *Chem. Commun.* **2022**, *58*, 4464–4467.
[31] K. Niedenzu, S. S. Seelig, W. Weber, *Z. Anorg. Allg. Chem.* **1981**, *483*, 51–62.
[32] D. M. Spasyuk, S. H. Carpenter, C. E. Kefalidis, W. E. Piers, M. L. Neidig, L. Maron, *Chem. Sci.* **2016**, *7*, 5939–5944.
[33] D. Kaufmann, *Chem. Ber.* **1987**, *120*, 853–854.
[34] M. Pailer, W. Fenzl, *Monatsh. Chem. verw. Teile anderer Wiss.* **1961**, *92*, 1294–1299.
[35] G. M. Sheldrick, *Acta Crystallogr. A* **2015**, *71*, 3-8.
[36] G. M. Sheldrick, *Acta Crystallogr. C* **2015**, *71*, 3-8.
[37] C. B. Hübschle, G. M. Sheldrick, B. Dittrich, *J. Appl. Crystallogr.* **2011**, *44*, 1281-1284.
[38] O. V. Dolomanov, L. J. Bourhis, R. J. Gildea, J. A. K. Howard, H. Puschmann, *J. Appl. Crystallogr.* **2009**, *42*, 339-341.
[39] Gaussian 16 Revision C.01, M. J. Frisch, G. W. Trucks, H. B. Schlegel, G. E. Scuseria, M. A. Robb, J. R. Cheeseman, G. Scalmani, V. Barone, G. A. Petersson, H. Nakatsuji, M. Caricato X. Li, A. V. Marenich, J. Bloino, B. G. Janesko, R. Gomperts, B. Mennucci, H. P. Hratchian, J. V. Ortiz, A. F. Izmaylov, J. L. Sonnenberg, D. Williams-Young, F. Lipparini F. Ding, J. Goings F. Egidi, B. Peng, A. Petrone, T. Henderson, D. Ranasinghe, V. G. Zakrzewski, J. Gao, N. Rega, G. Zheng, W. Liang, M. Hada, M. Ehara, K. Toyota, R. Fukuda, J. Hasegawa, M. Ishida, T. Nakajima, Y. Honda, O. Kitao, H. Nakai, T. Vreven, K. Throssell, Jr. J. A. Montgomery, J. E. Peralta, F. Ogliaro, M. J. Bearpark, J. J. Heyd, E. N. Brothers, K. N. Kudin, V. N. Staroverov, T. A. Keith, R. Kobayashi, J. Normand, K. Raghavachari, A. P. Rendell, J. C. Burant, S. S. Iyengar, J. Tomasi, M. Cossi, J. M. Millam, M. Klene, C. Adamo, R. Cammi, J. W. Ochterski, R. L. Martin, K. Morokuma, O. Farkas, J. B. Foresman, D. J. Fox, Gaussian, Inc., Wallingford CT, **2016**.
[40] J.-D. Chai, M. Head-Gordon, *Phys. Chem. Chem. Phys.* **2008**, *10*, 6615–6620.
[41] a) T. Clark, J. Chandrasekhar, G. W. Spitznagel, P. v. R. Schleyer, *J. Comput. Chem.* **1983**, *4*, 294–301; b) J. D. Dill, J. A. Pople, *J. Chem. Phys.* **1975**, *62*, 2921–2923; c) R. Ditchfield, W. J. Hehre, J. A. Pople, *J. Chem. Phys.* **1971**, *54*, 724–728; d) M. M. Francl, W. J. Pietro, W. J. Hehre, J. S. Binkley, M. S. Gordon, D. J. DeFrees, J. A. Pople, *J. Chem. Phys.* **1982**, *77*, 3654–3665; e) M. S. Gordon, J. S. Binkley, J. A. Pople, W. J. Pietro, W. J. Hehre, *J. Am. Chem. Soc.* **1982**, *104*, 2797–2803; f) P. C. Hariharan, J. A. Pople, *Theor. Chim. Acta* **1973**, *28*, 213–222; g) W. J. Hehre, R. Ditchfield, J. A. Pople, *J. Chem. Phys.* **1972**, *56*, 2257–2261; h) G. W. Spitznagel, T. Clark, P. v. R. Schleyer, W. J. Hehre, *J. Comput. Chem.* **1987**, *8*, 1109–1116.
[42] a) R. Krishnan, J. S. Binkley, R. Seeger, J. A. Pople, *J. Chem. Phys.* **1980**, *72*, 650–654; b) A. D. McLean, G. S. Chandler, *J. Chem. Phys.* **1980**, *72*, 5639–5648.
[43] G. Scalmani, M. J. Frisch, *J. Chem. Phys.* **2010**, 114110.
[44] M. Sparta, C. Riplinger, F. Neese, *J. Chem. Theory Comput.* **2014**, *10*, 1099–1108.

2.3 Redistribution of Oligo(iminoborane)s

2.3.1 Introduction

Some years ago, our group reported the synthesis and characterization of cyclolinear poly(iminoborane)s (PIBs) comprising 1,3,2-diazaborolidine building blocks.[1] Building on that, in chapter 2.2 the synthesis of monodisperse cyclolinear oligo(iminoborane)s is described, where we linked 1,3,2-diazaborolidine-based building blocks and (di)haloboranes by silicon/boron exchange and salt elimination reactions. During the study, we observed redistribution reactions upon the addition of non-stoichiometric amounts of (di)haloboranes to longer oligomers, associated with the cleavage of exocyclic B–N bonds. Herein, first studies of the mechanistic details of these redistribution processes, which are supported computationally are reported.

2.3.2 Results and Discussion

We successfully synthesized compound **2** by the addition of 1,3-bis(trimethylsilyl)-2-phenyl-1,3,2-diazaborolidine **1** to an excess of dichloro(phenyl)borane in CH_2Cl_2 at room temperature (Scheme 2.3.1, top). The latter was used in excess to prevent uncontrolled oligo- or polymerization. After stirring the reaction mixture overnight, the ^{1}H and $^{11}B\{^{1}H\}$ NMR spectra revealed a clean conversion to **2**, confirming the formation of two new B–N bonds by Si/B exchange (see **4** in chapter 2.2).

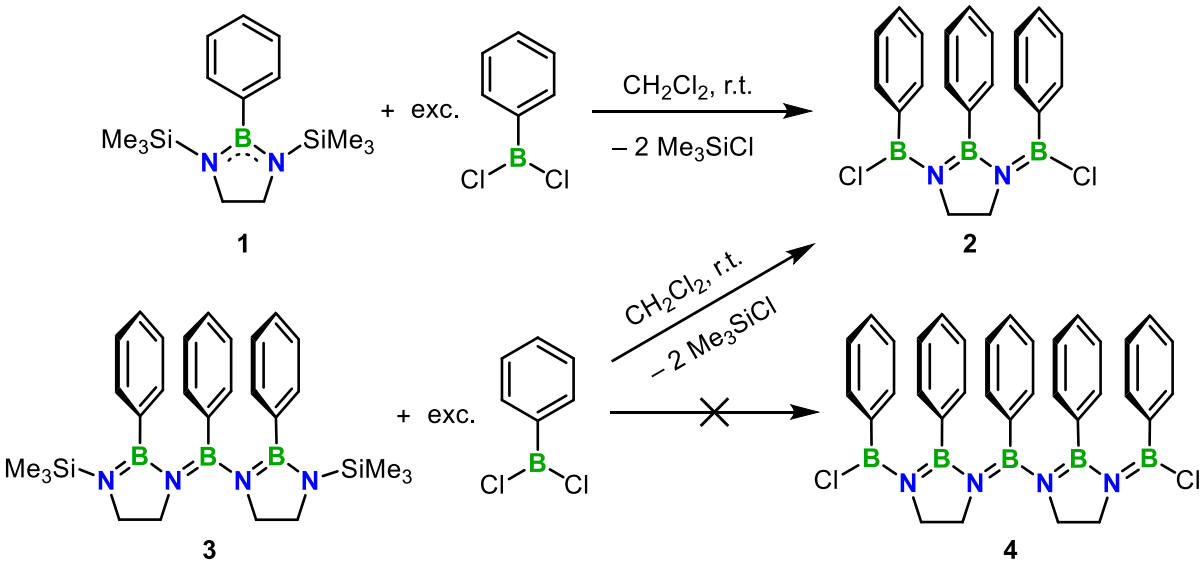

Scheme 2.3.1. Synthesis of **2** and the reaction of **3** with $PhBCl_2$ in CH_2Cl_2 at room temperature.

After we synthesized **3** (**7** in chapter 2.2, Scheme 2.2.2), we attempted to further extend the BN chain according to the procedure described above (for the synthesis of **2**). However, upon

addition of **3** to an excess of $PhBCl_2$ in CH_2Cl_2 we did not obtain the expected product **4** (Scheme 2.3.1, bottom). The ^{1}H NMR spectrum showed one singlet at 4.03 ppm instead of the expected set of two triplets for the ethylene moieties. In the $^{11}B\{^{1}H\}$ NMR spectrum we observed two resonances with similar shifts of 44.7 and 40.1 ppm. These ^{1}H and $^{11}B\{^{1}H\}$ NMR signals match the signals observed for compound **2**, which suggests that a redistribution process occurs in addition to the intended Si/B exchange reaction. We were able to isolate **2** from this reaction as an off-white solid in 65 % yield.

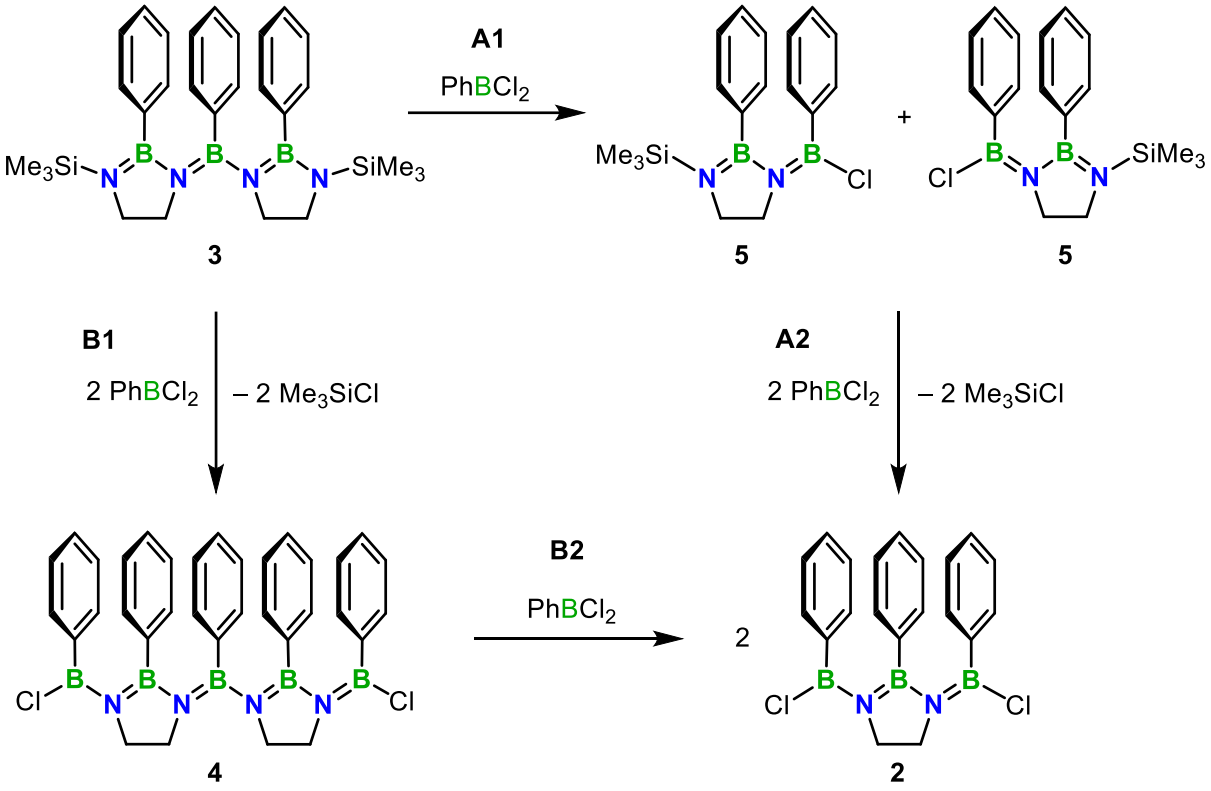

Scheme 2.3.2. Conceivable reaction paths **A** and **B** of the ligand scrambling reaction between **3** and $PhBCl_2$ to give **2**.

Considering that computational mechanistic studies of Si/B exchange reactions are scarce,[2] we decided to investigate whether the reaction proceeds via path **A** or **B** (Scheme 2.3.2) by DFT calculations. The crystal structures of **3** and **2** (Chapter 2.2, Figure 2.2.2) were used as starting points for the geometry optimizations (Figure 2.3.1). Since we could not find all energetically accessible barriers yet, we here use the Gibbs free energies of the minima for a preliminary assessment of the two alternative reaction pathways. This revealed that the reaction of **3** with $PhBCl_2$ to give compound **2** is overall exergonic with −40.1 kcal mol^{-1}. The calculations furthermore revealed that pathway **B1** is thermodynamically favored compared to pathway **A1** (−32.6 (**B1**) vs −7.1 kcal mol^{-1} (**A1**)). However, an unequivocal assessment of the relative contribution of the two alternative reaction paths is only possible with the knowledge of the respective reaction barriers (from the calculated transition states).

In chapter 2.2, we have for the first time mentioned the successful synthesis of oligomer **6** by the reaction of bromo(dimethylamino)phenylborane with compound **3** in a twofold Si/B exchange reaction with an exact 2:1 stoichiometry (path **C**, Scheme 2.3.3). However, the reaction of **3** with an excess of $PhB(NMe_2)Br$ did not result in a clean conversion to **6**. Under consideration of the previously observed cleavage of the exocyclic B–N bonds in compound **3** (path **A**, Scheme 2.3.2), an analogous redistribution process in the present case following formation of **6** is proposed (path **D**, Scheme 2.3.3) – even though $PhB(NMe_2)Br$ is less electrophilic compared to $PhBCl_2$.

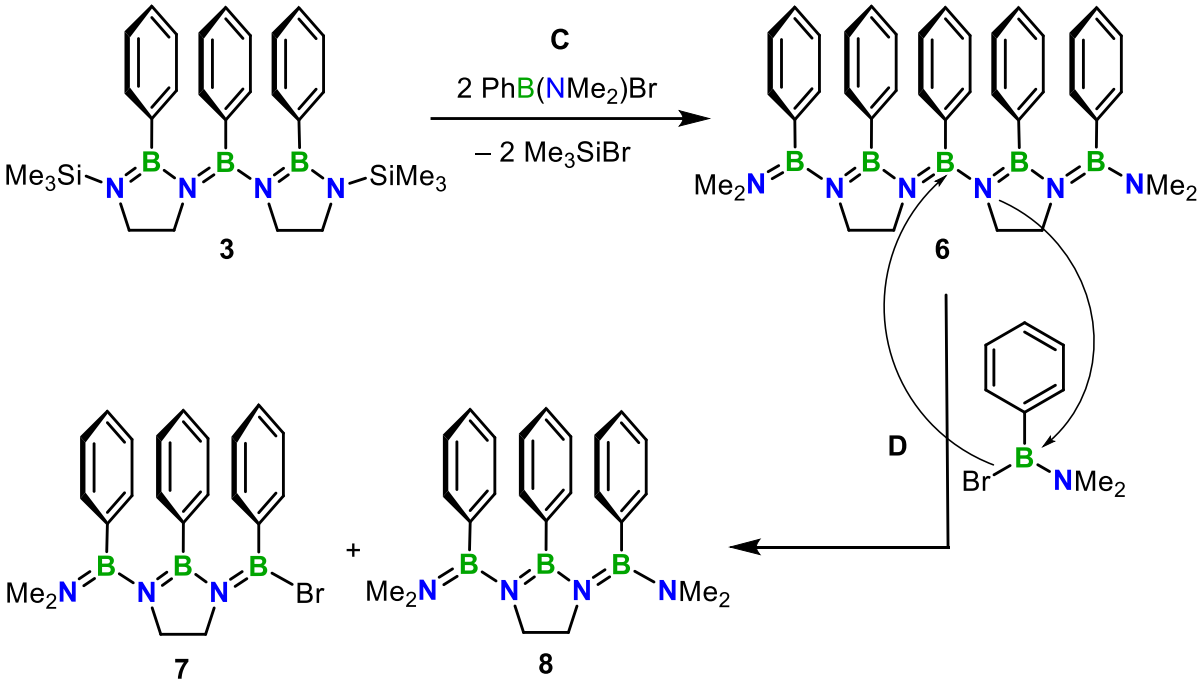

Scheme 2.3.3. Reaction of **6** (path **C**, or see chapter 2.2, Scheme 2.2.3) and the proposed reaction path **D** of the reaction of **6** with another equivalent $PhB(NMe_2)Br$.

However, the selective formation of **6** in the stoichiometric reaction indicates that the Si/B exchange reaction is favored compared to a redistribution process, suggesting that this should also be the first step when **3** is reacted with an excess of $PhB(NMe_2)Br$. Compound **6** can then react with another molecule $PhB(NMe_2)Br$ under cleavage of a central exocyclic B–N bond, resulting in the formation of **7** and **8** (path **D**, Scheme 2.2.3). While a further reaction of **8** is unlikely in this case, due to the excess of $PhB(NMe_2)Br$, compound **7** or $PhB(NMe_2)Br$ could further attack the inner exocyclic B–N bonds of **6** resulting in several products. The formation of both **6** and **8** was evidenced by ^1H NMR spectroscopy, confirming the proposed B–N cleavage (Figure S5.3.4). Additional resonances between 3.5 and 1.75 ppm indicate the presence of at least one other species (Figure S5.3.3). The presence of **6** and **8** was also confirmed by HRMS, while multiple other signals were also found (Figures S5.3.6 and S5.3.7). The signal at m/z = 872.5622 could be assigned to a known oligomer (**10** in chapter 2.2,

Scheme 2.2.3 and Figure S5.3.8), indicating recombination processes to even larger oligomers. This was further supported by the observation of two resonances at 2.37 and 1.82 ppm in the ^{1}H NMR spectrum corresponding to the N-CH_3 groups (see, chapter 2.2 and Figure S5.3.3).

An alternative attempt to accomplish the synthesis of **6** was the addition of $PhBCl_2$ to a solution of **9** (**5** in chapter 2.2) in CH_2Cl_2 at 0 °C (1:2 ratio, Scheme 2.3.4). After 3 h, the presence of the desired product **6** was evidenced by ^{1}H NMR spectroscopy, while multiple other resonances in the expected range for N-CH_2 and N-CH_3 moieties between 3.5 and 1.75 ppm were also detected (Figure S5.3.5). Under consideration of the above-mentioned redistribution processes, the presence of **8** as a by-product was confirmed. Therefore, this route also seemed unfavorable for a controlled BN catenation to **6**.

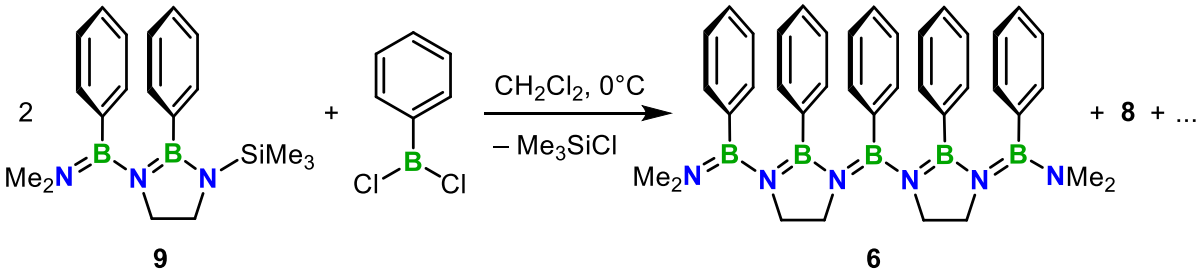

9 **6**

Scheme 2.3.4. Synthesis of **6** by reaction of **9** with $PhBCl_2$.

It is worth noting that the cleavage of exocyclic B–N bonds that was observed for the oligomeric compound **3** could also occur during the polymerization to poly(iminoborane)s (chapter 2.2). It is conceivable that cleavage processes in the polymer chains could lead to lower molecular weights and a higher polydispersity index. However, this was not observed and investigated in this work and thus further computational calculations and experiments would be necessary to fully understand these redistributions in the synthesis of oligo- and poly(iminoborane)s.

2.3.3 Conclusion

In conclusion, a study of the redistribution of oligo(iminoborane)s upon addition of (di)haloboranes was presented. While previous studies revealed that the stoichiometric reactions can lead to exclusively BN catenation, the excess of borane led to cleavage of exocyclic B–N bonds of the chain. First theoretical studies supported the assumption that Si/B exchange reactions used for BN catenation are thermodynamically favored over the redistribution processes. During an attempt to synthesize larger oligo(iminoborane)s by coupling of small oligomers with dichloro(phenyl)borane, instead of stepwise BN catenation, redistribution by-products were also observed. In general, our study reveal that the use of less

reactive borane species should favor controlled synthesis of monodisperse oligo(imino-borane)s, but exact stoichiometries are needed.

2.3.4 Experimental Section

General procedures. All manipulations were performed under an atmosphere of dry argon using standard Schlenk techniques or in an MBraun glovebox. Solvents (dichloromethane (DCM), *n*-hexane) were dried and degassed by means of an Innovative Technology solvent purification system (SPS). $CDCl_3$ for NMR spectroscopy was dried and degassed at reflux over CaH_2 and freshly distilled prior to use. Bromo(dimethylamino)phenylborane ($PhBBrNMe_2$)[3] and dichloro(phenyl)borane ($PhBCl_2$)[4] were prepared according to literature procedures. NMR spectra were recorded at 25 °C on a Bruker Avance III HD spectrometer operating at 300 MHz. Chemical shifts were referenced to residual protic impurities in the solvent (^1H) and reported relative to external $SiMe_4$ (^1H), $BF_3{\cdot}OEt_2$ (^{11}B) standards. Mass spectra were obtained with the use of a Thermo Scientific Exactive Plus Orbitrap MS system employing atmospheric pressure chemical ionization (APCI).

Spectra. All spectra and other result figures are shown in Appendix 5.3.

Reaction of 3 with an excess $PhBCl_2$.[5] To a solution of $PhBCl_2$ (24.7 mg, 0.16 mmol) in 0.4 mL DCM a solution of **3** (26.1 mg, 0.05 mmol) in 0.3 mL DCM was added dropwise at ambient temperature. The reaction mixture was stirred overnight and all volatiles were removed *in vacuo*. After recrystallization in an *n*-hexane/DCM mixture we obtained an off-white solid **2** (25.4 mg, 65 µmol, 65 % yield). ^1H NMR (300 MHz, $CDCl_3$): δ = 7.24-7.20 (m, 4H, Ph-*H*), 7.07-7.02 (m, 2H, Ph-*H*), 6.91-6.86 (m, 4H, Ph-*H*), 6.77-6.70 (m, 3H, Ph-*H*), 6.58-6.53 (m, 2H, Ph-*H*), 4.03 (s, 4H, N-CH_2) ppm; $^{11}B\{^1H\}$ NMR (96 MHz, $CDCl_3$): δ = 44.7, 40.1 (s) ppm.

Synthesis attempt of 6 by reaction of 9 with $PhBCl_2$. To a solution of **9** (70.6 mg, 0.20 mmol) in 1.0 mL DCM was added a solution of $PhBCl_2$ (16.0 mg, 0.10 mmol) in 1.0 mL DCM at 0 °C. After stirring for 2 h, the reaction mixture was warmed to room temperature and all volatiles were removed *in vacuo*.

Computational information

DFT calculations were performed with the Gaussian 16, Revision C.01 program package[6] using the ωB97X-D[7] functional in combination with the 6-31+G(d,p)[8] basis sets for geometry optimizations and the 6-311+G(d,p)[8a,8d,8h,9] basis sets for single-point energy calculations. Both calculations were performed with the PCM[10] solvation model mimicking dichloromethane (ε = 8.93) as solvent. Thermodynamic parameters were calculated at a temperature of

298.15 K and a pressure of 1.00 atm. A concentration correction of $\Delta G^{0\rightarrow *} = RT \cdot \ln(24.46) = 1.89$ kcal mol^{-1} (T = 298.15 K) was added to the free energies of all calculated species. This was done to change the 1.00 atm gas phase values to the condensed phase standard state concentration of 1.00 mol·L^{-1}, which leads to a proper description of associative/dissociative steps. This is necessary because pure gas estimations overestimate the entropy penalty for the formation of complexes.[11]

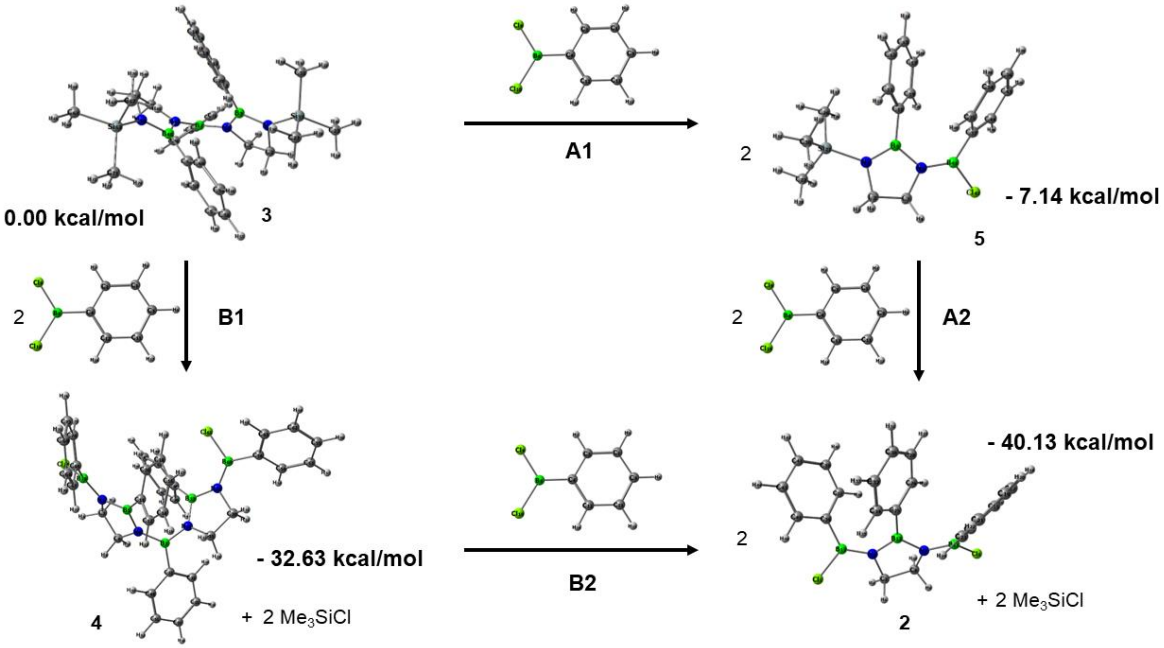

Figure 2.3.1. Proposed reaction paths and free energies of the reaction of **3** with $PhBCl_2$.

2.3.5 References

[1] a) O. Ayhan, T. Eckert, F. A. Plamper, H. Helten, *Angew. Chem. Int. Ed.* **2016**, *55*, 13321–13325; *Angew. Chem.* **2016**, *128*, 13515–13519; b) O. Ayhan, N. A. Riensch, C. Glasmacher, H. Helten, *Chem. Eur. J.* **2018**, *24*, 5883–5894.

[2] C. S. Qiu, N. P. Qiu, C. Flinn, Y. Zhao, *Phys. Chem. Chem. Phys.* **2023**, *25*, 6714–6725.

[3] D. M. Spasyuk, S. H. Carpenter, C. E. Kefalidis, W. E. Piers, M. L. Neidig, L. Maron, *Chem. Sci.* **2016**, *7*, 5939–5944.

[4] D. Kaufmann, *Chem. Ber.* **1987**, *120*, 853–854.

[5] For more analytical data of **2**, see: **4** in chapter 2.2.

[6] Gaussian 16 Revision C.01, M. J. Frisch, G. W. Trucks, H. B. Schlegel, G. E. Scuseria, M. A. Robb, J. R. Cheeseman, G. Scalmani, V. Barone, G. A. Petersson, H. Nakatsuji, M. Caricato X. Li, A. V. Marenich, J. Bloino, B. G. Janesko, R. Gomperts, B. Mennucci, H. P. Hratchian, J. V. Ortiz, A. F. Izmaylov, J. L. Sonnenberg, D. Williams-Young, F. Lipparini F. Ding, J. Goings F. Egidi, B. Peng, A. Petrone, T. Henderson, D. Ranasinghe, V. G. Zakrzewski, J. Gao, N. Rega, G. Zheng, W. Liang, M. Hada, M. Ehara, K. Toyota, R. Fukuda, J. Hasegawa, M. Ishida, T. Nakajima, Y. Honda, O. Kitao, H. Nakai, T. Vreven, K. Throssell, Jr. J. A. Montgomery, J. E. Peralta, F. Ogliaro, M. J. Bearpark, J. J. Heyd, E. N. Brothers, K. N. Kudin, V. N. Staroverov, T. A. Keith, R. Kobayashi, J. Normand, K. Raghavachari, A. P. Rendell, J. C. Burant, S. S. Iyengar, J. Tomasi, M. Cossi, J. M. Millam, M. Klene, C. Adamo, R. Cammi, J. W. Ochterski, R. L. Martin, K. Morokuma, O. Farkas, J. B. Foresman, D. J. Fox, Gaussian, Inc., Wallingford CT, **2016**.

[7] J.-D. Chai, M. Head-Gordon, *Phys. Chem. Chem. Phys.* **2008**, *10*, 6615–6620.

[8] a) T. Clark, J. Chandrasekhar, G. W. Spitznagel, P. v. R. Schleyer, *J. Comput. Chem.* **1983**, *4*, 294–301; b) J. D. Dill, J. A. Pople, *J. Chem. Phys.* **1975**, *62*, 2921–2923; c) R. Ditchfield, W. J. Hehre, J. A. Pople, *J. Chem. Phys.* **1971**, *54*, 724–728; d) M. M. Francl, W. J. Pietro, W. J. Hehre, J. S. Binkley, M. S. Gordon, D. J. DeFrees, J. A. Pople, *J. Chem. Phys.* **1982**, *77*, 3654–3665; e) M. S. Gordon, J. S. Binkley, J. A. Pople, W. J. Pietro, W. J. Hehre, *J. Am. Chem. Soc.* **1982**, *104*, 2797–2803; f) P. C. Hariharan, J. A. Pople, *Theor. Chim. Acta* **1973**, *28*, 213–222; g) W. J. Hehre, R. Ditchfield, J. A. Pople, *J. Chem. Phys.* **1972**, *56*, 2257–2261; h) G. W. Spitznagel, T. Clark, P. v. R. Schleyer, W. J. Hehre, *J. Comput. Chem.* **1987**, *8*, 1109–1116.

[9] a) R. Krishnan, J. S. Binkley, R. Seeger, J. A. Pople, *J. Chem. Phys.* **1980**, *72*, 650–654; b) A. D. McLean, G. S. Chandler, *J. Chem. Phys.* **1980**, *72*, 5639–5648.

[10] G. Scalmani, M. J. Frisch, *J. Chem. Phys.* **2010**, 114110.

[11] M. Sparta, C. Riplinger, F. Neese, *J. Chem. Theory Comput.* **2014**, *10*, 1099–1108.

2.4 Synthesis of 1,3,2-Benzodiazaborolines as Building Blocks for Oligo- and Poly(iminoborane)s

2.4.1 Introduction

Previous studies have shown that the class of 1,3,2-benzodiazaborolines proved to be suitable building blocks for organic light-emitting materials.[1] In literature, incorporation of these building blocks into a polymer backbone is only known across the boron atom and benzo unit[1d] or the 4,7-positions of the benzo core.[2] Our group reported the synthesis and characterization of cyclolinear poly(iminoborane)s (PIBs) comprising 1,3,2-diazaborolidine building blocks.[3] Herein, the synthesis 1,3,2-benzodiazaborolines based on the cyclic condensation reaction of *o*-phenylenediamine (**1**) with different borane reactants such as dihalo- or diaminoboranes or boronic acids is described.[4] In addition, the oligo- and polymerization of 1,3,2-benzodiazaborolines building blocks across the nitrogen moieties with dihaloboranes has been investigated.

2.4.2 Results and Discussion

The synthesis of the 1,3-dihydro-1,3,2-benzodiazaborolines **2** and **3** was performed by the reaction of **1** with dichloro(octyl)borane or bis(dimethylamino)methylborane, respectively (Scheme 2.4.1). The colorless solids **2** and **3** were obtained in moderate to good yields (74 and 59 %, respectively) and were characterized by NMR spectroscopy, high resolution mass spectrometry (HRMS), and elemental analysis. In the ^{1}H NMR spectra we observed new singlet signals for the NH protons at 6.31 ppm in both cases, confirming the cyclization. The ^{11}B{^{1}H} NMR spectra each showed a single resonance at around 31 ppm, which is slightly shifted to higher field compared to their 1,3,2-diazaborolidine congeners.[3a] The reaction of **2** and **3** with *n*-BuLi (1 or 2 equiv., respectively), in the presence of TMEDA, followed by addition of Me_3SiCl, yielded the mono- and bis-silylated compounds **4**, **5**, and **6**. Compound **4** was obtained as an orange oil in 80 % and **5** as a colorless liquid in 37 % yield, whereas **6** was isolated as a colorless solid in 89 % yield. In the ^{1}H NMR spectrum of **5**, a singlet at 6.36 ppm corresponding to the NH proton and a singlet at 0.47 ppm for the Me_3Si group confirmed the formation of the mono-silylated derivative (Figure S5.4.14). For **4** and **6** the Me_3Si proton signals appeared at 0.49 and 0.54 ppm, respectively. The ^{11}B{^{1}H} NMR spectra of **4**, **5**, and **6** each showed a single peak between 36.9 and 33.3 ppm. With increasing number of Me_3Si groups in the molecule a slight downfield shift of the ^{11}B NMR resonance was observed. The same trend was also observed for the broadened B-CH_3 signals in the ^{13}C{^{1}H} NMR spectra of **3** (−5.5 ppm), **5** (−2.6 ppm), and **6** (−0.1 ppm). For compounds **4**, **5**, and **6** we observed single signals in the ^{29}Si{^{1}H} NMR spectra between 7.3 and 6.3 ppm.

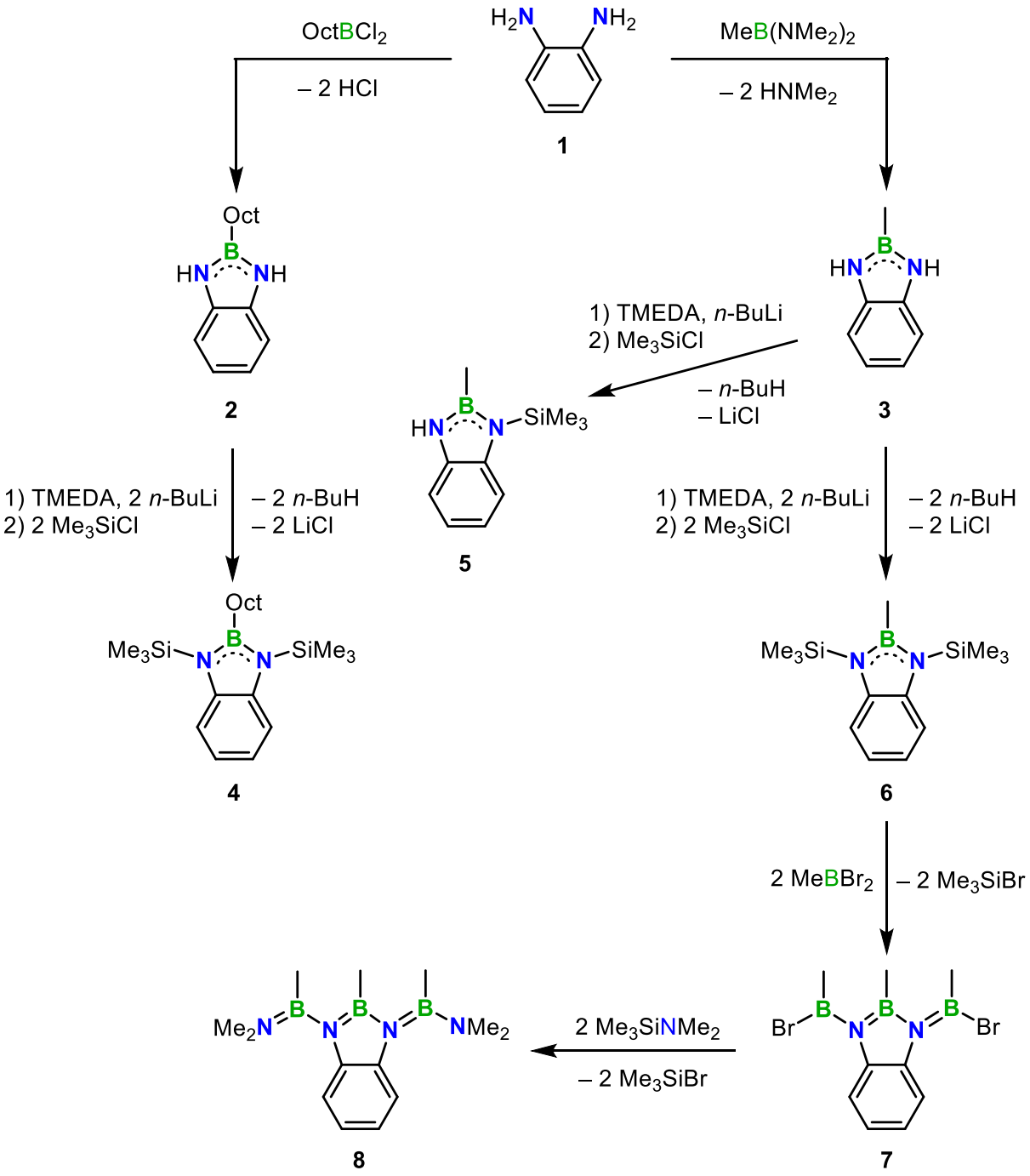

Scheme 2.4.1. Synthesis of 1,3,2-benzoazadiborolines **2**, **3**, **4**, **5**, and **6** and the oligomers **7** and **8**.

Upon slow crystallization of **6** from *n*-hexane, we obtained single crystals suitable for X-ray diffraction (Figure 2.4.1, table 2.4.1). The molecular structure of **6** in the solid-state features trigonal-planar coordinated boron and nitrogen centers (∑(NR$_3$) and ∑(BR$_3$) ≈ 360°). The B–N bond lengths N1–B1 (1.452(2) Å) and B1–N2 (1.454(2) Å) are intermediate between B=N double bonds and B–N single bonds.[5] The silicon atoms are both displaced off the N1B1N2 plane on the same side of the plane. Their orthogonal distance from the N1B1N2 plane is 0.129(3) Å (Si1) and 0.162(3) Å (Si2), which corresponds to a N1B1N2 plane to N-Si bond angle of 4.1° and 5.1°, respectively.

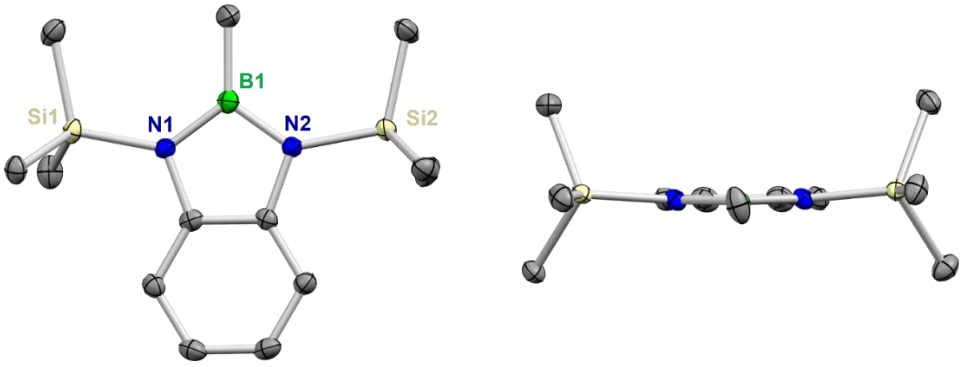

Figure 2.4.1. Molecular structure of **6** in the solid state determined by single-crystal X-ray diffraction at 100 K (H atoms omitted for clarity). The structure is shown perpendicular (left) and parallel (right) to the N1B1N2 plane. All ellipsoids are drawn at the 50 % probability level.

To probe the feasibility of the synthesis of 1,3,2-benzodiazaboroline-based poly(iminoborane)s, we aimed at the synthesis of monodisperse oligomers **8** (Scheme 2.4.1), **9**, and **10** (Scheme 2.4.2). For the synthesis of oligomer **8**, we first either isolated **7** or prepared it *in situ* by the Si/B exchange reaction of **6** with an excess of dibromo(methyl)borane. The ^{1}H NMR spectrum of **7** showed two doublets of doublets for the aromatic protons (7.76 and 6.95 ppm) and two singlets for the methyl protons at 1.07 (outer CH_3) and 0.73 ppm (inner CH_3). In the $^{11}B\{^{1}H\}$ NMR spectrum two signals, one for the two outer (51.9 ppm) and one for the inner (39.6 ppm) boron atoms, were observed. After addition of Me_3SiNMe_2 to a solution of **7** in CH_2Cl_2, **8** was isolated as a colorless oil in 72 % yield. In the ^{1}H NMR spectrum of **8** we observed four singlet signals for the NMe_2 groups between 2.55 and 2.43 ppm, which evidences pronouncedly hindered bond rotation about the outer BN bonds (Figure S5.4.25). The appearance of multiple signals for the B-CH_3 protons suggested the presence of a diastereomeric mixture of **8**. ^{1}H NMR measurements of **8** at elevated temperatures in toluene showed broadening but no coalescence of the signals up to 100 °C (Figure S5.4.29). The $^{11}B\{^{1}H\}$ NMR spectrum of **8** showed one signal for the two outer and one for the inner boron atoms at 37.7 and 32.6 ppm, respectively, which are highfield shifted compared to the signals of **7**. The $^{13}C\{^{1}H\}$ NMR spectrum showed three sets of signals in the aromatic region, each with two very close singlets for the different isomers (Figure S5.4.27).

The synthesis of **9** and **10** was attempted *via* the salt elimination procedure described in chapter 2.2 (Scheme 2.4.2). In the first step, we lithiated **5** with *n*-BuLi in the presence of TMEDA to give $\mathbf{5^{Li}}$ (not depicted). We completely removed the solvent, THF, used for this lithiation reaction afterwards to prevent its reaction with the (di)haloborane added in the following step. To synthesize **9**, we dissolved the $\mathbf{5^{Li}}$ in *n*-pentane and added $MeBBr_2$ (0.5 equiv.) at −78 °C. After the reaction mixture was warmed to room temperature overnight, we checked the reaction by NMR spectroscopy and HRMS.

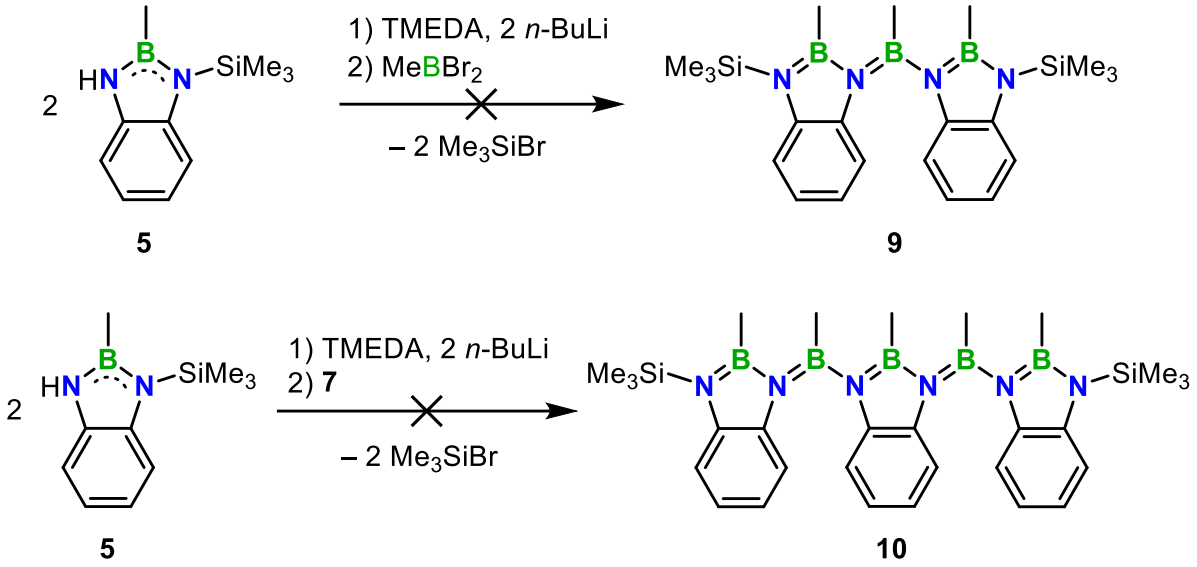

Scheme 2.4.2. Synthesis attempts of oligomers **9** and **10**.

In the ^{1}H NMR spectrum we observed multiple resonances which could not be assigned. In the ^{11}B{^{1}H} NMR spectrum, no remaining $MeBBr_2$ (63 ppm) was detected. However, three new signals at 46.8, 36.8, and 33.1 ppm were observed, and the latter two are in the range of the signals of **8**, which we tentatively regard as an indication of the formation of new B–N bonds. In the HRMS spectrum no signal for the desired product **9** (Figure S5.4.45) was detected but a signal at m/z = 276.1643 was observed, which can be assigned to compound **6** (Figure S5.4.46). The formation of **6** is conceivable when the Si/B exchange reaction between $\mathbf{5^{Li}}$ and $MeBBr_2$ competes with the salt elimination of LiBr. Then, the formed Me_3SiBr can react with the lithiated side to give **6**. However, the formation of **6** could not be confirmed by ^{1}H NMR spectroscopy. For the synthesis of **10**, we dissolved $\mathbf{5^{Li}}$ in toluene and added **7** (ca. 0.5 equiv.) at −40 °C. In the ^{1}H NMR spectrum we did not observe any remaining signals of **7** (Figure S5.4.33), and the integrals of the aromatic signals did not fit to any other resonance in the spectrum. The ^{11}B{^{1}H} NMR spectrum showed similar resonances as already observed for the attempted synthesis of **9**. It can be concluded that the syntheses of compounds **9** and **10** were not successful, which may be due to steric or electronic effects.

Polymerization attempts *via* Si/B exchange polycondensation with the disilylated compounds **4** and **6** in combination with a dihaloborane were conducted under various conditions. After 24 to 96 hours, Me_3SiNMe_2 was added to the reaction mixture to terminate the eventually remaining reactive B–X end groups (Scheme 2.4.3). The crude products obtained from these reactions were analyzed by NMR spectroscopy, HRMS, and gel permeation chromatography (GPC). We started our investigations with the reaction of **4** with $OctBCl_2$ in CH_2Cl_2 at room temperature or in *o*-DFB at 80 °C. After 4 d in CH_2Cl_2 we observed in the ^{11}B{^{1}H} NMR spectrum two signals at 52.2 and 38.0 ppm, which could correspond to a single coupling event between **4** and $OctBCl_2$ (Figure S5.4.35).[6]

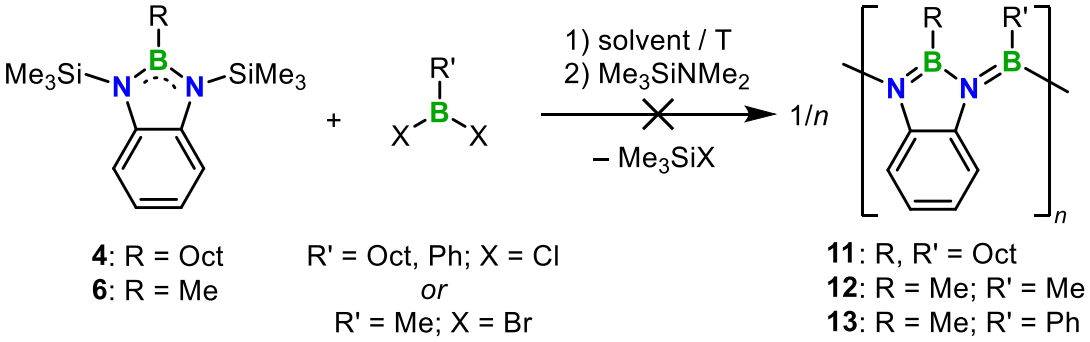

Scheme 2.4.3. Synthesis attempts of polymers **11**, **12**, and **13** in CH_2Cl_2 at room temperature or in *o*-DFB at 80 °C.

However, a signal at 61.9 ppm, which was detected in addition, indicates that there is remaining $OctBCl_2$ present in the reaction mixture and thus further BN catenation is hampered. The two $^{11}B\{^1H\}$ NMR signals corresponding to the single coupling product were also observed for the reaction in *o*-DFB at 80 °C. HRMS measurements after 12 d revealed the presence of oligomers **11a** and **11b** for the reaction in DCM and **11c** for the polymerization in *o*-DFB (Figures 2.4.2 and S5.4.47–S5.4.49).

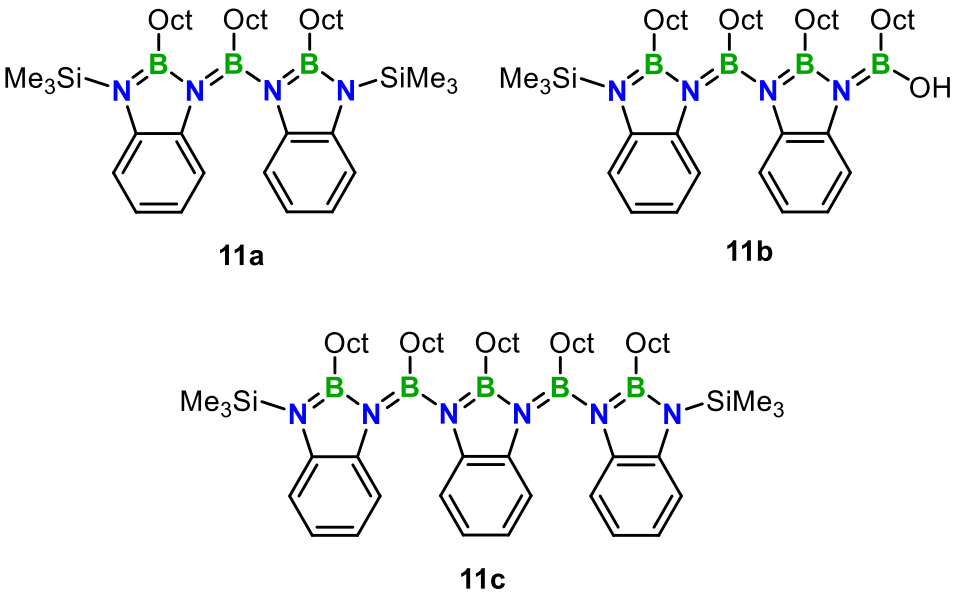

Figure 2.4.2. Structures of the detected species from the reaction of **4** with $OctBCl_2$ in HRMS measurements (LIFDI).

The GPC analysis of the crude products of the reactions of **6** with $MeBBr_2$ or $PhBCl_2$ revealed signals in the small-molecule range with number average molecular weights (M_n) between 126 and 273 g·mol^{-1} (Figures S5.4.50–S5.4.52). The number-average degree of polymerization of $DP_n = 1 – 2$, in combination with a polydispersity index of PDI = 1.0 – 1.3 confirmed the presence of low molecular weight species instead of the polymers **12** and **13**.

2.4.3 Conclusion

In conclusion, after the synthesis of 1,3,2-benzodiazaborolines, first small model compounds have been synthesized and characterized. Attempts to synthesize larger oligomers were not successful, which is presumably due to electronic or steric effects. An indication for this was that for the deprotonation of the N-H moieties of the 1,3,2-benzodiazaborolines using *n*-BuLi TMEDA was required as auxiliary base. In polymerization experiments, oligomers with up to three 1,3,2-benzodiazaboroline units were found in high resolution mass spectrometry. Overall, the polymerization involving 1,3,2-benzodiazaboroline seems to be significantly inhibited compared to the BN catenation using 1,3,2-diazaborolidines in chapter 2.2.

2.4.4 Experimental Section

General procedures. All manipulations were performed under an atmosphere of dry argon using standard Schlenk techniques or in an MBraun glovebox. Solvents (dichloromethane (DCM), tetrahydrofuran (THF), toluene) were dried and degassed by means of an Innovative Technology solvent purification system (SPS). $CDCl_3$ and C_6D_6 for NMR spectroscopy as well as *n*-pentane, *ortho*-difluorobenzene (*o*-DFB), *N*,*N*,*N'*,*N'*-tetramethylethylenediamine (TMEDA) and trimethylsilyl chloride (Me_3SiCl) were dried and degassed at reflux over CaH_2 or Na, respectively, and freshly distilled prior to use. *o*-Phenylenediamine (*o*-PDA), pentamethylsilazane (Me_3SiNMe_2), boron trichloride (BCl_3) and *n*-BuLi (2.5 M in *n*-hexane) were commercially purchased and used as received. Dichloro(octyl)borane (Oct-BCl_2)[7] was prepared according to methods described in the literature for boranes with other alkyl substituents.[8] Bis(dimethylamino)methylborane ($MeB(NMe_2)_2$),[9] dibromo(methyl)borane ($MeBBr_2$),[10] bromo(dimethylamino)phenylborane ($PhB(NMe_2)Br$)[11] and dichloro(phenyl)-borane ($PhBCl_2$)[12] were prepared according to literature procedures. NMR spectra were recorded at 25 °C on a Bruker Avance III HD spectrometer operating at 300 MHz or on a Bruker Avance 500 spectrometer operating at 500 MHz. Chemical shifts were referenced to residual protic impurities in the solvent (^1H) or the deuterio solvent itself (^{13}C) and reported relative to external $SiMe_4$ (^1H, ^{13}C, ^{29}Si), $BF_3{\cdot}OEt_2$ (^{11}B) standards. Mass spectra were obtained with the use of a Thermo Scientific Exactive Plus Orbitrap MS system employing liquid injection field desorption ionization (LIFDI), atmospheric pressure chemical ionization (APCI) and atmospheric sample analysis probe (ASAP). Elemental analyses were performed on an Elementar vario MICRO cube elemental analyzer. GPC chromatograms were recorded on an Agilent 1260 Infinity II Series, equipped with two PSS SDV 3 µm 1000 Å (300x8 mm) columns and one PSS SDV 3 µm 10000 Å (300x8 mm) column, at 25 °C with a flow rate of 1 mL min^{-1} and calibrated against polystyrene standards. The samples were diluted in THF and toluene

as internal standard. Detection was carried out via UV signal (λ = 254 nm). Evaluation of the chromatograms was performed by using WinGPC software.

Spectra. All spectra and other result figures are shown in Appendix 5.4.

Synthesis of chloro-bis(dimethylamino)borane.[9,13] To a solution of BCl_3 (1 M in *n*-hexane, 100 mmol) in 300 mL DCM was added Me_3SiNMe_2 (32 mL, 200 mmol) at −78 °C. The reaction mixture was warmed to room temperature overnight. All volatiles were removed under reduced pressure and after distillation a colorless liquid was obtained (10.6 g, 78.5 mmol, 79 % yield). ^{1}H NMR (300 MHz, $CDCl_3$): δ = 2.72 (s, 6H, N-C*H*$_3$) ppm; ^{11}B{^{1}H} NMR (96 MHz, $CDCl_3$): δ = 27.8 (s) ppm; ^{13}C{^{1}H} NMR (76 MHz, $CDCl_3$): δ = 40.1 (s, N-*C*H$_3$) ppm.

Synthesis of 2.[14] To a solution of **1** (2.16 g, 20.0 mmol) in 250 mL toluene was added a solution of $OctBCl_2$ (4.31 g, 22.1 mmol) in 100 mL toluene dropwise at −78 °C. Subsequently, the reaction mixture was warmed to room temperature and was refluxed for 4 h. The solvent was removed *in vacuo* and the crude product was recrystallized in *n*-pentane to obtain a colorless solid (3.41 g, 14.8 mmol, 74 % yield). ^{1}H NMR (500 MHz, $CDCl_3$): δ = 7.04-7.00 (m, 2H, Ph-C*H*), 6.94-6.90 (m, 2H, Ph-C*H*), 6.31 (s, 2H, N*H*), 1.59–1.52 (m, 2H, C*H*$_2$), 1.41–1.30 (m, 10H, C*H*$_2$), 1.20 (t, 2H, B-C*H*$_2$), 0.92 (t, 3H, C*H*$_3$) ppm; ^{11}B{^{1}H} NMR (160 MHz, $CDCl_3$): δ = 31.7 (s) ppm; ^{13}C{^{1}H} NMR (126 MHz, $CDCl_3$): δ = 136.3 (s, Ph-*C*-N), 118.9 (s, Ph-*C*H), 110.6 (s, Ph-*C*H), 32.8 (s, *C*H$_2$), 32.1 (s, *C*H$_2$), 29.7 (s, *C*H$_2$), 29.5 (s, *C*H$_2$), 26.2 (s, *C*H$_2$), 22.9 (s, *C*H$_2$), 14.3 (s, *C*H$_3$), 11.7 (br, B-*C*H$_2$) ppm; HRMS (LIFDI): m/z = 230.1947; calcd. for $C_{14}H_{23}BN_2$: 230.1949; elem. anal. calcd. (%) for $C_{14}H_{23}BN_2$: C 73.06, H 10.07, N 12.17; found: C 73.02, H 10.19, N 12.14.

Synthesis of 3.[15] To a solution of $MeB(NMe_2)_2$ (3.19 g, 28.0 mmol) in 60 mL THF was added a mixture of **1** (3.18 mg, 29.4 mmol) in 40 mL THF dropwise at −78°C. The reaction mixture was warmed to room temperature and was refluxed for 19 h. The solvent was removed in *vacuo* and the residue was filtered through a silica plug with a mixture of *n*-hexane and ethyl acetate (4:1). After removing the solvent and drying *in vacuo* a colorless solid was obtained. (2.18 g, 16.5 mmol, 59 % yield). ^{1}H-NMR (500 MHz, $CDCl_3$): δ = 7.03-7.00 (m, 2H, Ph-C*H*), 6.94-6.91 (m, 2H, Ph-C*H*), 6.31 (s, 2H, N*H*), 0.65 (s, 3H, B-C*H*$_3$) ppm; ^{11}B{^{1}H} NMR (160 MHz, $CDCl_3$): δ = 30.7 (s) ppm; ^{13}C{^{1}H} NMR (126 MHz, $CDCl_3$): δ = 136.4 (s, Ph-*C*-N), 118.9 (s, Ph-*C*H), 110.5 (s, Ph-*C*H), −5.5 (br, B-*C*H$_3$) ppm; HRMS (ASAP pos): m/z = 133.0930 $[M+H]^+$; calcd. for $C_7H_9BN_2$+H: 133.0932; elem. anal. calcd. (%) for $C_7H_9BN_2$: C 63.71, H 6.87, N 21.23; found: C 63.56, H 6.81, N 21.12.

Synthesis of 4.[14,16] To a solution of **2** (1.73 g, 7.5 mmol) in 75 mL THF was added TMEDA (2.18 g, 18.75 mmol, 2.83 mL) at room temperature and the reaction mixture was stirred for 5 minutes. After cooling to −78°C, *n*-BuLi (7.5 mL, 18.75 mmol) was slowly added and the reaction mixture was stirred for 2 h. Subsequently, Me_3SiCl (2.12 g, 19.5 mmol, 2.48 mL) was added and the reaction mixture was warmed to room temperature. The solvent was removed in *vacuo* and the residue was washed with *n*-pentane. After removing *n*-pentane *in vacuo* an orange cloudy oil was obtained (2.25 g, 6.0 mmol, 80 % yield). ^{1}H NMR (500 MHz, $CDCl_3$): δ = 7.25-7.21 (dd, 2H, Ph-C*H*), 6.96-6.92 (dd, 2H, Ph-C*H*), 1.40–1.30 (m, 12H, CH_2), 1.21 (m, 2H, B-CH_2), 0.91 (t, 3H, CH_3), 0.49 (s, 18H, Si(CH_3)$_3$) ppm; ^{11}B{^{1}H} NMR (160 MHz, $CDCl_3$): δ = 36.9 (s) ppm; ^{13}C{^{1}H} NMR (126 MHz, $CDCl_3$): δ = 142.2 (s, Ph-*C*-N), 118.7 (s, Ph-*C*H), 113.8 (s, Ph-*C*H), 33.4 (s, *C*H_2), 32.1 (s, *C*H_2), 29.7 (s, *C*H_2), 29.5 (s, *C*H_2), 28.7 (s, *C*H_2), 22.9 (s, *C*H_2), 14.3 (s, *C*H_3), 14.1 (br, B-*C*H_2), 1.9 (s, Si*C*H_3) ppm; ^{29}Si{^{1}H} NMR (99 MHz, CD_2Cl_2): δ = 6.3 (s) ppm; HRMS (LIFDI): m/z = 374.2731; calcd. for $C_{20}H_{39}BN_2Si_2$: 374.2739.

Synthesis of 5.[17] To a solution of **3** (1.00 g, 7.58 mmol) in THF (75 mL) was added TMEDA (1.26 mL, 8.34 mmol) and *n*-BuLi (2.5 M in *n*-hexane, 3.03 mL, 7.58 mmol) at −78 °C. The reaction mixture was stirred for 2 h at −78 °C. Subsequently, Me_3SiCl (1.16 mL, 9.10 mmol) was added at −78 °C and the reaction mixture was warmed to room temperature overnight. The solvent was removed *in vacuo* and the residue was washed with *n*-pentane (3 x 5 mL). After removing the solvent from the filtrate *in vacuo*, the crude product was purified by short path distillation (9 x 10^{-3} mbar, 85 °C) to obtain a colorless liquid (575 mg, 2.82 mmol, 37 % yield). ^{1}H NMR (300 MHz, $CDCl_3$): δ = 7.23-7.20 (m, 1H, Ph-C*H*), 7.02- 6.89 (m, 3H, Ph-C*H*), 6.36 (s, 1H, N*H*), 0.67 (s, 3H, B-CH_3), 0.47 (s, 9H, Si(CH_3)$_3$) ppm; ^{11}B{^{1}H} NMR (96 MHz, $CDCl_3$): δ = 33.3 (s) ppm; ^{13}C{^{1}H} NMR (76 MHz, $CDCl_3$): δ = 139.6 (s, NH-Ph-*C*), 139.0 (s, Me_3SiN-Ph-*C*), 119.3 (s, Ph-*C*H), 118.4 (s, Ph-*C*H), 113.6 (s, Ph-*C*H), 110.2 (s, Ph-*C*H), 1.5 (s, Si(*C*H_3)$_3$), −2.6 (br, B-*C*H_3) ppm; ^{29}Si{^{1}H} NMR (60 MHz, $CDCl_3$): δ = 7.3 (s) ppm; HRMS (ASAP pos): m/z = 204.1248 (mixture of [M] and [M+H]$^+$); calcd. for $C_{10}H_{17}BN_2Si$: 204.1249.

Synthesis of 6. To a solution of **3** (850 mg, 6.44 mmol) in THF (65 mL) was added TMEDA (2.47 mL, 16.1 mmol) and *n*-BuLi (2.5 M in *n*-hexane, 6.50 mL, 16.1 mmol) at −78 °C. After stirring for 90 min at −78 °C, Me_3SiCl (2.20 mL, 17.3 mmol) was added and the reaction mixture was warmed to room temperature overnight. The solvent was removed *in vacuo* and the residue was washed with *n*-pentane (3 x 10 mL). After removing *n*-pentane *in vacuo* and purification by distillation, a colorless solid was obtained (1.59 g, 5.75 mmol, 89 %). ^{1}H NMR (300 MHz, $CDCl_3$): δ = 7.32-7.26 (dd, 2H, Ph-C*H*), 7.02-6.96 (dd, 2H, Ph-C*H*), 0.79 (s, 3H, B-CH_3), 0.54 (s, 18H, Si(CH_3)$_3$) ppm; ^{11}B{^{1}H} NMR (96 MHz, $CDCl_3$): δ = 36.3 (s) ppm; ^{13}C{^{1}H} NMR (76 MHz, $CDCl_3$): δ = 142.2 (s, Ph-*C*-N), 118.7 (s, Ph-*C*H), 113.5 (s, Ph-*C*H), 2.0 (s,

Si(*C*H$_3$)$_3$), −0.1 (br, B-*C*H$_3$) ppm; ^{29}Si{^{1}H} NMR (60 MHz, CDCl$_3$): δ = 6.8 (s) ppm; HRMS (ASAP pos): m/z = 276.1640 (mixture of [M] and [M+H]$^+$); calcd. for $C_{13}H_{25}BN_2Si_2$: 276.1644; elem. anal. calcd. (%) for $C_{13}H_{25}BN_2Si_2$: C 56.50, H 9.12, N 10.14; found: C 56.58, H 9.19, N 10.06.

Synthesis of 7. To a solution of MeBBr$_2$ (166 mg, 0.89 mmol) in 2.0 mL DCM was added **6** (65.7 mg, 0.24 mmol) at −40 °C. After warming the reaction mixture to room temperature, all volatiles were removed *in vacuo* to obtain a brownish solid (no yield was determined). ^{1}H NMR (300 MHz, C$_6$D$_6$): δ = 7.76 (dd, 2H, Ph-C*H*), 6.95 (dd, 2H, Ph-C*H*), 1.07 (s, 6H, B-C*H$_3$*), 0.73 (s, 3H, B-C*H$_3$*) ppm; ^{11}B{^{1}H} NMR (96 MHz, C$_6$D$_6$): δ = 51.5, 39.6 (s) ppm; ^{13}C{^{1}H} NMR (76 MHz, C$_6$D$_6$): δ = 139.4 (s, Ph-*C*-N), 123.0 (s, Ph-*C*H), 117.8 (s, Ph-*C*H), 16.4 (br, B-*C*H$_3$), 2.7 (br, B-*C*H$_3$) ppm.

Synthesis of 8. To a solution of MeBBr$_2$ (483 mg, 2.6 mmol) in 5.0 mL DCM was added a solution of **6** (281 mg, 1.02 mmol) in 5.0 mL DCM at −78 °C. The reaction mixture was warmed to room temperature overnight and Me$_3$SiNMe$_2$ (586 mg, 5.0 mmol) was added at −78 °C. Subsequently, the reaction mixture was warmed to ambient temperature and the volatiles were removed *in vacuo*. After short path distillation, a colorless oil was obtained (193 mg, 0.72 mmol, 72 % yield). ^{1}H NMR (300 MHz, C$_6$D$_6$): δ = 7.11-6.99 (m, 4H, Ph-C*H*), 2.55-2.43 (4 s, 12H, N-C*H$_3$*), 0.72-0.67 (m, 9H, B-C*H$_3$*) ppm; ^{11}B{^{1}H} NMR (96 MHz, C$_6$D$_6$): δ = 37.7, 32.6 (s) ppm; ^{13}C{^{1}H} NMR (76 MHz, C$_6$D$_6$): δ = 141.1 (s, Ph-*C*-N), 140.9 (s, Ph-*C*-N), 119.2 (s, Ph-*C*H), 119.2 (s, Ph-*C*H), 113.1 (s, Ph-*C*H), 113.1 (s, Ph-*C*H), 39.1 (s, N*C*H$_3$), 39.0 (s, N*C*H$_3$), 38.9 (s, N*C*H$_3$), 38.9 (s, N*C*H$_3$), 2.5 (br, B-*C*H$_3$), −3.2 (br, B-*C*H$_3$) ppm; HRMS (APCI pos): m/z = 271.2424 [M+H]$^+$; calcd. for $C_{13}H_{25}B_3N_4$+H: 271.2431.

Synthesis attempt of 9. To a solution of **5** (51.2 mg, 0.25 mmol) in 2.5 mL THF was added TMEDA (0.04 mL, 0.275 mmol) and *n*-BuLi (2.5 M in *n*-hexane, 0.1 mL, 0.25 mmol) at −78 °C. After 2 h the reaction mixture was warmed to room temperature and all volatiles were completely removed *in vacuo*. The residue was dissolved in 2.0 mL *n*-pentane and a solution of MeBBr$_2$ (23.2 mg, 0.125 mmol) in 0.5 mL *n*-pentane was added at −78 °C. The reaction mixture was warmed to ambient temperature overnight and all volatiles were removed *in vacuo*.

Synthesis attempt of 10. To a solution of **5** (51.2 mg, 0.25 mmol) in 2.5 mL THF was added TMEDA (0.04 mL, 0.275 mmol) and *n*-BuLi (2.5 M in *n*-hexane, 0.1 mL, 0.25 mmol) at −78 °C. After 2 h the reaction mixture was warmed to room temperature and all volatiles were completely removed *in vacuo*. To around 0.21 mmol **5^{Li}** was added 0.5 mL toluene and a

solution of **7** (34.1 mg, 0.1 mmol) in 0.5 mL toluene at −40 °C. The reaction mixture was warmed to ambient temperature overnight and all volatiles were removed *in vacuo*.

General procedure for polymerization attempts. To a solution of disilylated 1,3,2-benzodiazaboroline (0.5 mmol) in 0.3 mL DCM or *o*-DFB was added a solution of dihaloborane (0.5 mmol) in 0.2 mL DCM or *o*-DFB at room temperature. The reaction was terminated by addition of Me_3SiNMe_2 (excess) and the solvent was removed *in vacuo* after 24 h.

Crystallographic data

Crystals suitable for single-crystal X-ray diffraction were selected, coated in perfluoropolyether oil, and mounted on MiTeGen micromounts or polyimide microloops. Diffraction data were collected on Bruker X8 Apex II 4-circle diffractometers with CCD area detectors using Mo-K_α radiation. The crystals were cooled using an Oxford Cryostreams low-temperature device. Data were collected at 100 K. The images were processed and corrected for Lorentz-polarization effects and absorption as implemented in the Bruker software packages. The structures were solved using the intrinsic phasing method (SHELXT)[18] and Fourier expansion technique. All non-hydrogen atoms were refined in anisotropic approximation, with hydrogen atoms 'riding' in idealized positions, by full-matrix least squares against F^2 of all data, using SHELXL[19] software and the SHELXLE graphical user interface.[20]

Table 2.4.2. Crystal structure and refinement data for **6**.

Compound	**6**
Crystal size / mm³	0.260 x 0.338 x 0.489
Empirical formula	$C_{13}H_{25}BN_2Si_2$
M / g mol^{-1}	276.34
F(000)	600
Crystal system	monoclinic
Space group	$P2_1/c$
a / Å	10.1315(17)
b / Å	13.038(4)
c / Å	12.387(6)
α / °	90
β / °	97.50(3)
γ / °	90
V / Å^3	1622.2(9)
Z	4
μ / mm^{-1}	0.205
T / K	100(2)
$\theta_{min,max}$ / °	2.027, 26.432
Completeness	0.998
Reflections: total / independent	3334, 2863
R_{int}	0.0460
Parameters / restraints	170 / 0
GooF on F^2	1.045
R_1 [$I \geq 2\sigma(I)$]	0.0374
Max. / min. residual electron density / e Å^{-3}	0.417, −0.283
ρ_{calc} / g cm^{-3}	1.131

2.4.5 References

[1] a) L. Weber, L. Böhling, *Coord. Chem. Rev.* **2015**, *284*, 236–275; b) S. Maruyama, Y. Kawanishi, *J. Mater. Chem.* **2002**, *12*, 2245–2249; c) L. Weber, V. Werner, I. Domke, H.-G. Stammler, B. Neumann, *Dalton Trans.* **2006**, 3777–3784; d) I. Yamaguchi, T. Tominaga, M. Sato, *Polym. Int.* **2009**, *58*, 17–21; e) J. H. Son, G. Jang, T. S. Lee, *Polymer* **2013**, *54*, 3542–3547.

[2] I. Yamaguchi, B.-J. Choi, T. Koizumi, K. Kubota, T. Yamamoto, *Macromolecules* **2007**, *40*, 438–443.

[3] a) O. Ayhan, T. Eckert, F. A. Plamper, H. Helten, *Angew. Chem. Int. Ed.* **2016**, *55*, 13321–13325; *Angew. Chem.* **2016**, *128*, 13515–13519; b) O. Ayhan, N. A. Riensch, C. Glasmacher, H. Helten, *Chem. Eur. J.* **2018**, *24*, 5883–5894.

[4] a) D. Ulmschneider, J. Goubeau, *Chem. Ber.* **1957**, *90*, 2733–2738; b) M. J. S. Dewar, V. P. Kubba, R. Pettit, *J. Chem. Soc.* **1958**, 3076–3079; c) H. Beyer, K. Niedenzu, J. W. Dawson, *J. Org. Chem.* **1962**, *27*, 4701–4702; d) G. Kaupp, M. R. Naimi-Jamal, V. Stepanenko, *Chem. Eur. J.* **2003**, *9*, 4156–4160.

[5] P. Paetzold, *Phosphorus Sulfur Silicon Relat. Elem.* **1994**, *93*, 39–50.

[6] For related molecular compounds, see: S. Y. Shaw, R. H. Neilson, *Inorg. Chem.* **1994**, *33*, 3239–3245.

[7] H. C. Brown, N. Ravindran, S. U. Kulkarni, *J. Org. Chem.* **1980**, *45*, 384–389.

[8] R. Soundararajan, D. S. Matteson, *Organometallics* **1995**, *14*, 4157–4166.

[9] H. Nöth, P. Fritz, *Z. Anorg. Allg. Chem.* **1963**, *322*, 297–309.

[10] W. Einholz, W. Gollinger, W. Haubold, *Z. Naturforsch.* **1990**, *45b*, 25–30.

[11] D. M. Spasyuk, S. H. Carpenter, C. E. Kefalidis, W. E. Piers, M. L. Neidig, L. Maron, *Chem. Sci.* **2016**, *7*, 5939–5944.

[12] D. Kaufmann, *Chem. Ber.* **1987**, *120*, 853–854.

[13] New synthetic approach to chloro-bis(dimethylamino)borane for the synthesis of $MeB(NMe_2)_2$.

[14] For another synthetic route, see: S. W. Hadebe, S. Sithebe, R. S. Robinson, *Tetrahedron* **2011**, *67*, 4277–4282.

[15] For another synthetic route and further analytical data, see: G. H. M. Davies, G. A. Molander, *J. Org. Chem.* **2016**, *81*, 3771–3779.

[16] Synthesis *via* metal catalyzed hydroboration: T. Ogawa, A. J. Ruddy, O. L. Sydora, M. Stradiotto, L. Turculet, *Organometallics* **2017**, *36*, 417–423.

[17] For another synthetic route and further analytical data, see: a) R. Goetze, H. Nöth, *Chem. Ber.* **1976**, *109*, 3247–3249; b) R. Goetze, H. Nöth, H. Pommerening, D. Sedlak, B. Wrackmeyer, *Chem. Ber.* **1981**, *114*, 1884–1893.

[18] G. M. Sheldrick, *Acta Crystallogr. A* **2015**, *71*, 3–8.

[19] G. M. Sheldrick, *Acta Crystallogr. A* **2008**, *64*, 112–122.

[20] C. B. Hübschle, G. M. Sheldrick, B. Dittrich, *J. Appl. Crystallogr.* **2011**, *44*, 1281–1284.

2.5 1,2,5-Azadiborolane as a Building Block for Inorganic–Organic Hybrid Polymers

The following section is slightly modified and reproduced from published article[†] with permission from John Wiley & Sons.

Abstract. The incorporation of BN units in organic scaffolds by isoelectronic/isosteric substitution of selected CC couples has emerged as an efficient tool to produce new materials with useful properties and functions. The knowledge about BN-doped inorganic–organic hybrid polymers, however, is still rather scarce. This is especially true for linear or cyclolinear macromolecules that feature longer inorganic chains. Herein, we introduce 1,2,5-azadiborolane as a polymer building block for the first time. An attempt to apply it for the synthesis of a cyclolinear poly(iminoborane) resulted after only two B–N coupling events in the formation of a molecular compound comprising a chain of three nitrogen and two boron atoms – as confirmed by single-crystal X-ray diffratometry. In combination with a *p*-phenylene diamine-based co-monomer, we accomplished to incorporate the 1,2,5-azadiborolane into a hybrid polymer of considerable molecular weight that features a B2N3 chain. We additionally synthesized a small molecular model compound for the polymer and characterized it crystallographically as well. Comparison of the UV-vis spectra of the monomer, the oligomer, and the polymer revealed systematic red-shifts of the longest-wavelength absorption band with increasing number of BN units in the chain.

2.5.1 Introduction

Making use of the isoelectronic and isosteric relationship between BN and CC couples, the incorporation of BN moieties in specific positions of organic compounds has evolved into a viable concept to produce new materials based on the structural frameworks of their carbonaceous parents but with significantly modified electronic characteristics.[1] This often results in fundamentally altered physical properties and chemical reactivities.

Boron-containing polymers and oligomers have attracted considerable attention in the past few decades.[2] In such cases where their backbone is composed of only boron and nitrogen – and no carbon atoms – they are formally classified as inorganic polymers. The first well-characterized poly(aminoborane)s (**PAB**, Figure 2.5.1), inorganic BN/CC isosteres of the polyolefins, comprising a main chain of tetracoordinate boron and nitrogen atoms, were presented by Manners and co-workers in 2008.[3,4] The unsaturated poly(iminoborane)s (**PIB**), which are

[†] M. Maier, V. Zeh, N. Munker, J. Glock, K. Oberdorf, O. Ayhan, C. Lichtenberg, H. Helten, *Eur. J. Inorg. Chem.* **2024**, *27*, e202300490. (M.M. and V.Z. contributed equally to this work)

polyacetylene isosteres, had been elusive until quite recently. First indications of their possible formation came from studies by Paetzold and co-workers in the 1980s, who obtained insoluble waxy materials via certain transient monomeric iminoboranes, RN≡BR'.[5-7] On the basis of elemental analysis, mass spectrometry, and a transformation reaction into a corresponding borazine, the authors proposed the constitution of linear **PIBs** for the substances obtained.[5]

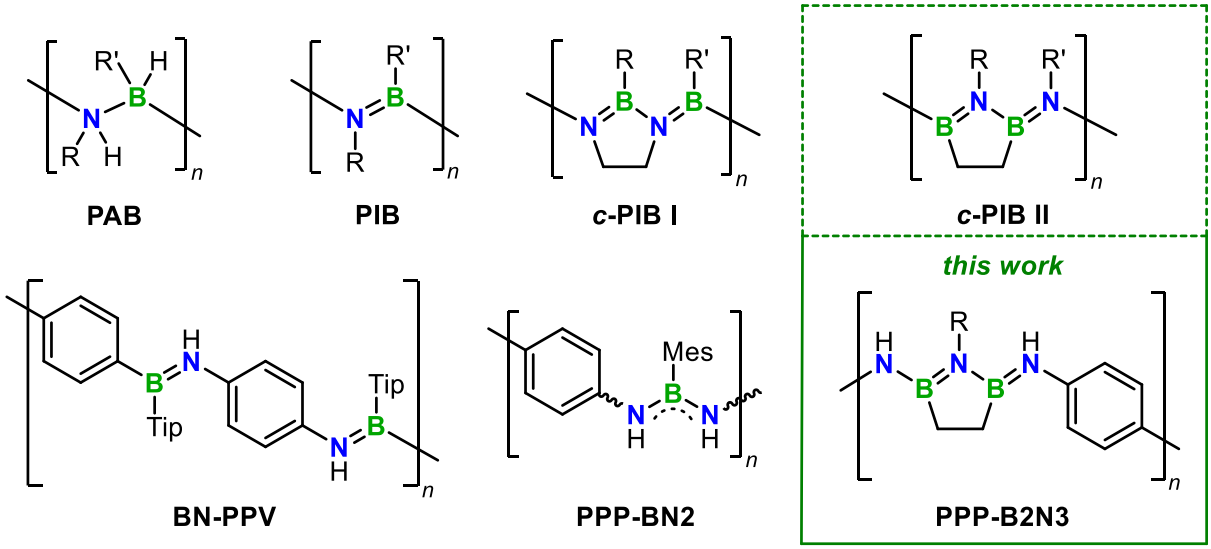

Figure 2.5.1. Generic structures of poly(aminoborane)s (**PAB**) and poly(iminoborane)s (**PIB**), cyclolinear poly- or oligo(iminoborane)s comprising 1,3,2-diazaborolidine rings (***c*-PIB I**) or 1,2,5-azadiborolane rings (***c*-PIB II**), and the BN-doped hybrid polymers **BN-PPV**, **PPP-BN2**, and **PPP-B2N3** (Tip = triisopropylphenyl; Mes = mesityl; R, R' = different organic substituents).

We recently devised a concept for the rational synthesis of well-defined cyclolinear species of type ***c*-PIB I** by introducing 1,3,2-diazaborolidine rings[8] into the backbone.[9] This approach eliminates competing reaction pathways leading to the unwanted formation of borazines. In this way, we accomplished to prepare examples of ***c*-PIB I** with up to 18 B=N units on average (DP_n).[9] These compounds represent the closest approach to poly(iminoborane)s to date.

Boron- and nitrogen-containing polymers that additionally contain organic building blocks in the backbone (i. e., inorganic–organic hybrid polymers) have attracted considerable attention in recent years.[10-13] Such materials have been used for various applications, including, for instance, organic electronics,[10a-k,11b] bioimaging,[10l] therapeutics,[10m] as well as hydrogen storage and transfer hydrogenations.[10n] If tricoordinate boron and nitrogen centers are incorporated in the main chain, π-conjugation can be extended over these atoms across the polymer backbone.[11-14] As most previous examples have the BN moieties embedded in cyclic frameworks,[11] we became interested in developing polymers that feature essentially linear B=N linkages in the main chain.[12] In such cases, potential π-conjugation is forced to involve the B=N bonds. In that respect, we presented the first poly(*p*-phenylene iminoborane) (**BN-PPV**),[12b] which can be regarded as an inorganic analog of poly(*p*-phenylene vinylene) (PPV), and the more nitrogen-rich NBN-linked hybrid polymer **PPP-BN2**.[12a] Very recently, we added

a BN congener of poly(thiophene vinylene) (PTV) to the family of conjugated BCN hybrid polymers.[12c]

We now introduce 1,2,5-azadiborolane as a building block for novel macromolecules. Whereas our initial attempt to construct a cyclolinear poly(iminoborane) of type ***c*-PIB II** stopped after two B–N bond formation events, we were successful in synthesizing an inorganic–organic hybrid polymer of type **PPP-B2N3**, which represents the example of a BCN hybrid macromolecule that comprises the longest inorganic BN chain part to date.

2.5.2 Results and Discussion

For the present study we chose 1-(*p*-bromophenyl)-2,5-dichloro-3,4-diisopropyl-1,2,5-azadiborolane (**4**) as the monomer, as this derivative was easily accessible via twofold hydroboration of 2,5-dimethyl-3,4-hexadiene (**1**) – taking advantage of the *anti*-Markovnikov selectivity of the hydroboration reaction – followed by ring closure of the intermediate, 2,5-dimethyl-3,4-bis(dichloroboryl)hexane (**2**), with disilazane **3** (Scheme 2.5.1). The bromo substituent was incorporated in the *para*-position of the *N*-aryl group as it potentially offers the opportunity of further modification via the side groups. Hydroboration of **1** in the desired manner proved feasible via Matteson's method[15] using a mixture of a hydrosilane, Et_3SiH, and BCl_3. We obtained bisborane **2** as a mixture of the *rac* (*R,R*/*S,S*) and the *meso* form (*R*,S**) in overall 84 % yield. We also synthesized compound **2** via regioselective twofold hydroboration of **1** with dichloroborane methyl sulfide complex in the presence of BCl_3.[16] Compound **2** was then converted with aryldisilazane **3** via ring closure to the corresponding 1,2,5-azadiborolane **4**, following the procedure described by Haubold *et al*. for the parent heterocycle.[17] Different from the latter, the reaction between **2** and **3** required reflux overnight to yield full conversion (*cf*. [18]). According to $^{11}B\{^1H\}$ NMR spectroscopy, compound **4** was formed quantitatively; its resonance was detected at 54.1 ppm. Upon repeated crystallization, we achieved to isolate exclusively the *rac* product of **4** using the bisborane **2** synthesized by Matteson's method in analytically pure form in 24 % yield. This sample was employed as the monomer in subsequent polymerization studies. Upon slow crystallization from a concentrated solution of **4** in *n*-pentane, we obtained single-crystals suitable for X-ray diffraction studies.

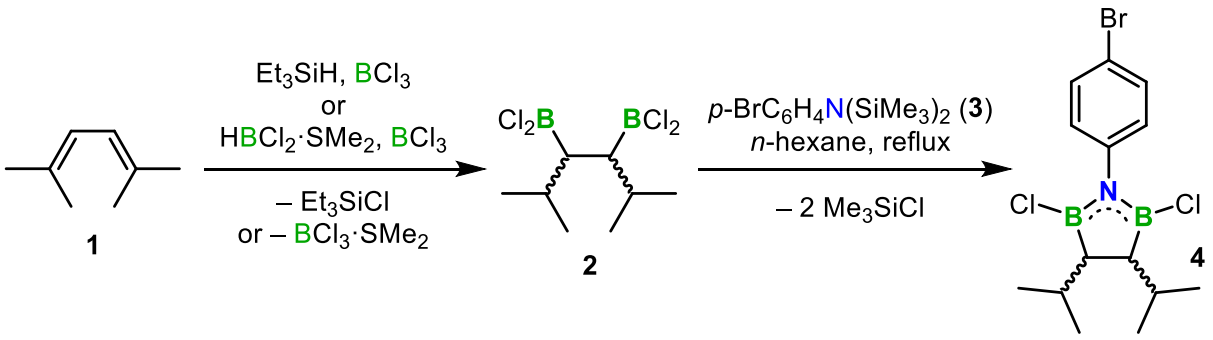

Scheme 2.5.1. Synthesis of monomer **4**.

To demonstrate the feasibility of a twofold amination of **4**, we added an excess of Me_3SiNMe_2 to a solution of **4** in dichloromethane (Scheme 2.5.2, left). After 24 h and after subsequent removal of all volatiles *in vacuo*, we obtained compound **5** as a colorless liquid in 65 % yield. Its ^{1}H NMR spectrum showed two broad peaks at 2.71 and 2.05 ppm confirming the incorporation of the NMe_2 groups (Figure S5.5.14). The $^{11}B\{^1H\}$ NMR spectrum showed a single signal at 37.7 ppm, clearly upfield-shifted compared to that of **4**.

Polymerization attempts via Si/B exchange polycondensation were conducted with *rac*-**4** in combination with *N*,*N*-bis(trimethylsilyl)butylamine (**6**) under various conditions. When the reaction was performed in *o*-difluorobenzene (*o*-DFB, 1 M) at 80 °C for 28 d (Scheme 2.5.2, right), gel permeation chromatography (GPC) analysis suggested a number average molecular weight (M_n) of 581 g mol^{-1} after deactivation of the reactive B–Cl groups with Me_3SiNMe_2 (Figure S5.5.48). After removing all volatiles, the residue crystallized, which allowed us to perform single crystal X-ray diffraction. Structure analysis revealed the formation of compound **7** (*vide infra*), which is the product of a single coupling event.

The ^{1}H NMR spectrum of **7** showed two broad peaks at 2.72 and 2.01 ppm for the NMe_2 group at ambient temperature, indicating hindered rotation around the B=N bond. While at 60 °C the NMe_2 signals nearly coalesced into one very broad peak at around 2.37 ppm, they gave rise to two sharp signals at –40 °C (Figures S5.5.17–S5.5.20). The $^{11}B\{^1H\}$ NMR spectrum showed a broad signal at 38.9 ppm, similar to **5**.

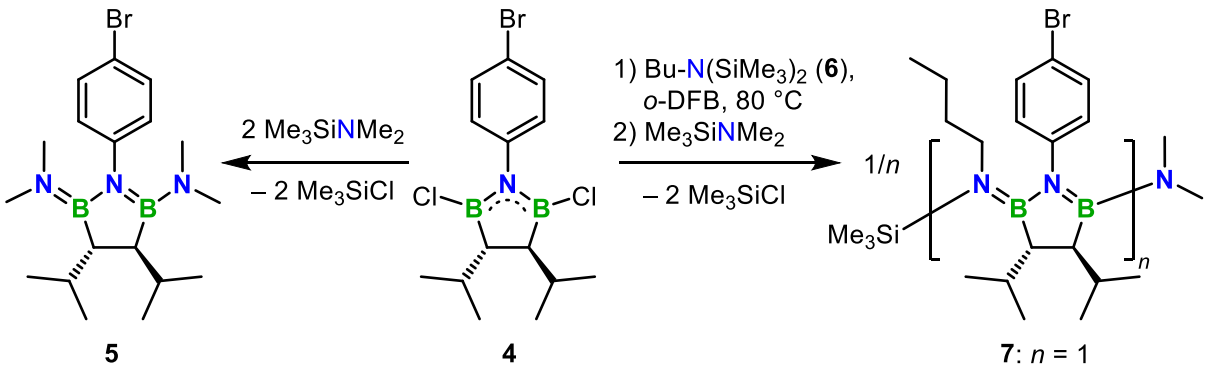

Scheme 2.5.2. Synthesis of **5**, and polymerization attempt of **4** with **6**.

Neither did further polymerization attempts between **4** and **6** in DCM at room temperature nor in *o*-DCB at 120 °C for 28 d increase the molecular weights, indicating that no further oligomerization had occurred. In order to investigate if a coupling reaction of **4** with two molecules of **6** is in principle possible, we additionally carried out the reaction in 1:2 ratio of the reactants in *o*-DFB at 80 °C for 2 days. We subsequently added Me_3SiNMe_2 to ensure that eventually remaining B–Cl are terminated. Inspection of the results from the NMR and GPC measurements revealed that they were almost identical to those from the 1:1 reaction (Figure S5.5.48). Additionally, a significant amount of **5** was detected as a by-product (Figure S5.5.28).

Obviously, the second B–N coupling event involving **4** and **6** is already severely hampered. We note that disilylamines such as **6** have relatively weak nucleophilic character compared to free or mono-silyl amines due to delocalization of the lone pair on nitrogen into the σ* orbitals of the adjacent silicon atoms.[19] It is furthermore expected that the first condensation event between **4** and **6** will cause a reduction of the electrophilicity of the remaining B–Cl bond in the intermediate formed, due to the +M effect of the amino group introduced at the other terminal position. In addition, steric hinderance between the side groups incorporated may also play a significant role. Overall, these results indicate that catenation of cyclolinear BN chains using **4** and **6** as co-monomers is rather unfeasible.

In the next step, we addressed the polymerization of our 1,2,5-azadiborolane monomer **4** with *N,N'*-bis(trimethylsilyl)-*p*-phenylenediamine (**10**) via Si/B exchange condensation to obtain a hybrid polymer of type **PPP-B2N3** (cf. Figure 2.5.1). For an initial assessment of the feasibility of the planned polymerization, we first attempted the synthesis of a model compound via the 1:2 reaction of **4** with **8** (Scheme 2.5.3).

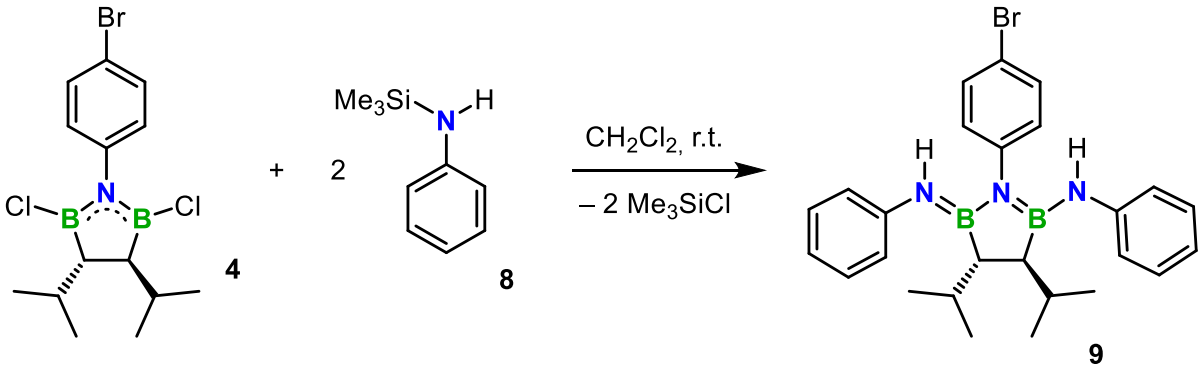

Scheme 2.5.3. Synthesis of **9**.

To this end, we dissolved **4** in dichloromethane and added **8** at room temperature. After 3 h, $^{11}B\{^1H\}$ NMR spectroscopy revealed the emergence of a single peak at around 39.0 ppm, significantly upfield-shifted compared to that of **4** and in the same range as that of **5**. In the ^1H NMR spectrum, the signal for the condensation by-product Me_3SiCl (0.43 ppm) and a new peak at 5.00 ppm for the N–H protons confirmed the formation of **9** (Figure S5.5.32). We isolated **9** in 70 % yield. In addition, we were able to obtain single-crystals of **9** suitable for X-ray diffraction studies by crystallization from a concentrated solution of **9** in Et_2O/*n*-hexane.

The molecular structures of **4**, **7**, and **9** in the solid state (Figure 2.5.2) show that their boron and nitrogen centers reside in trigonal-planar coordination spheres (sums of the bond angles ≈ 360° each). The B–N bond lengths within the azadiborolane rings are intermediate between B=N double bonds (1.38–1.41 Å) and B–N single bonds (1.48–1.51 Å).[20] The bonds of **4** (B1–N1 = 1.437(2) Å and B2–N1 = 1.435(2) Å) have more pronounced double bond character,

similar to that of another azadiborolane (B–N = 1.425(4) Å),[18] than those of **7** (B1–N2 = 1.450(2) Å and B2–N2 = 1.457(2) Å) and **9** (B1–N2 = 1.463(4) Å and B2–N2 = 1.468(4) Å) (Table 2.5.2). This points to a bond lengthening in the rings in case of further BN linkage to end-standing groups with shorter terminal B–N bond lengths having close to double-bond character (1.409(4)–1.434(4) Å), which is close to those observed in aminoboranes.[21] The phenyl groups of **4**, **7**, and **9** are twisted out of the plane of the BNB rings (**4**, ∢61.62(7)°), (**7**, ∢74.77(11)°), (**9**, ∢59.41(6)°), thus, conjugation between the aryl ring and the BNB unit is largely excluded.

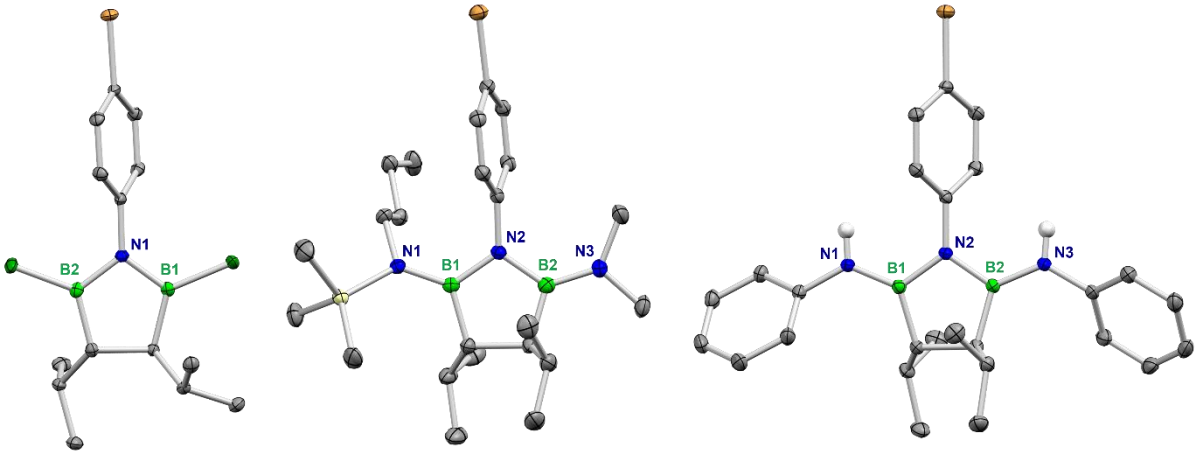

Figure 2.5.2. Molecular structures of **4**, **7**, and **9** (from left to right) in the solid state (ellipsoids drawn at the 50% probability level; H atoms omitted for clarity).

Encouraged by the successful synthesis of **9**, which demonstrates that **4** is capable of reacting with **8** at either side – with **8** being a substrate that has comparable steric and electronic demand with the designated co-monomer **10** – we attempted the synthesis of the corresponding polymer **11**. This, indeed, was achieved by Si/B exchange polycondensation of **4** and **10** in CH_2Cl_2 at ambient temperature (Scheme 2.5.4). We performed the polymerization at various reaction times, after which we added Me_3SiNMe_2 to deactivate possibly remaining B–Cl groups. The product was isolated as a white solid in 62 % yield. The polymer was characterized by NMR and UV–vis spectroscopy, and in terms of molecular weight by GPC.

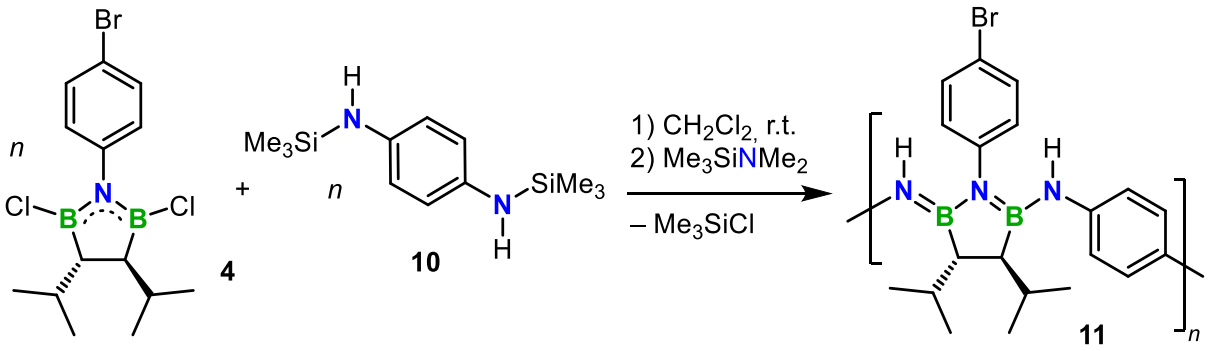

Scheme 2.5.4. Synthesis of **11** by Si/B exchange polycondensation of **4** and **10**.

Our different polymerization trials gave **11** in reasonably high molecular weights, as suggested by GPC analysis (Table 2.5.4). Overall, the data did not allow to derive a clear trend in terms of the reaction time, thus reflecting the expected variations in a step-growth process involving such air-sensitive compounds. Our best results obtained are listed in Table 2.5.1, and the associated GPC traces are depicted in Figure 2.5.3. Trial 1 resulted in a number-average degree of polymerization of DP_n = 91, together with a polydispersity index of PDI = 2.2, which is close to the ideal value of 2.0 for a step-growth polymerization. Remarkable is trial 2, in which we obtained **11** with a DP_n of 335. However, the molar mass distribution of the sample was quite broad (PDI = 6.0), which is indicative of the occurrence of intermolecular chain-transfer processes during the polymerization.

Table 2.5.1. Polymerization results.

	M_n [kDa]	M_w [kDa]	PDI	DP_n
trial 1[a]	18.7	40.4	2.2	91
trial 2[b]	68.6	414.5	6.0	335

[a] Reaction at r.t. in CH_2Cl_2 for 20 h. [b] Reaction at r.t. in CH_2Cl_2 for 72 h.

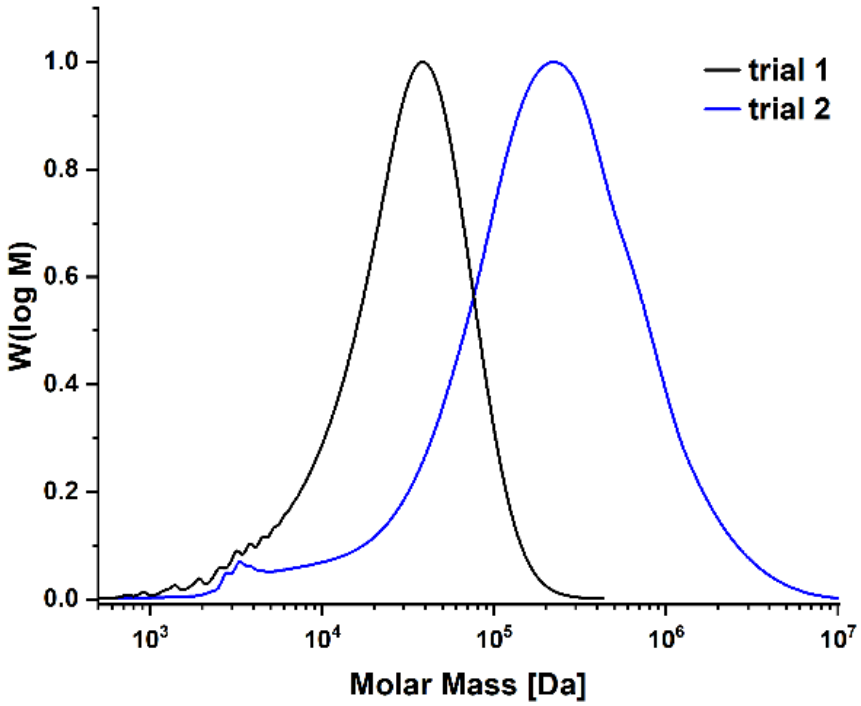

Figure 2.5.3. Normalized gel permeation chromatography (GPC) traces of **11** (trial 1 (black) and trial 2 (blue)) detected by a UV-vis detector at 280 nm.

The ^{1}H NMR spectrum of the isolated polymer **11** showed two broad doublets for the *p*-bromophenyl substituents and two singlets very close to each other at around 6.80 ppm for the phenylene units. The latter indicates different stereoisomeric linkages along the polymer backbone, which is also evidenced by the observation of two closely spaced signals for the N-H protons at 4.86 and 4.84 ppm (Figure S5.5.33). The ^{11}B{^{1}H} NMR spectrum showed a broad peak at 38.0 ppm, slightly upfield-shifted compared to that of compound **9** (Figure S5.5.34).

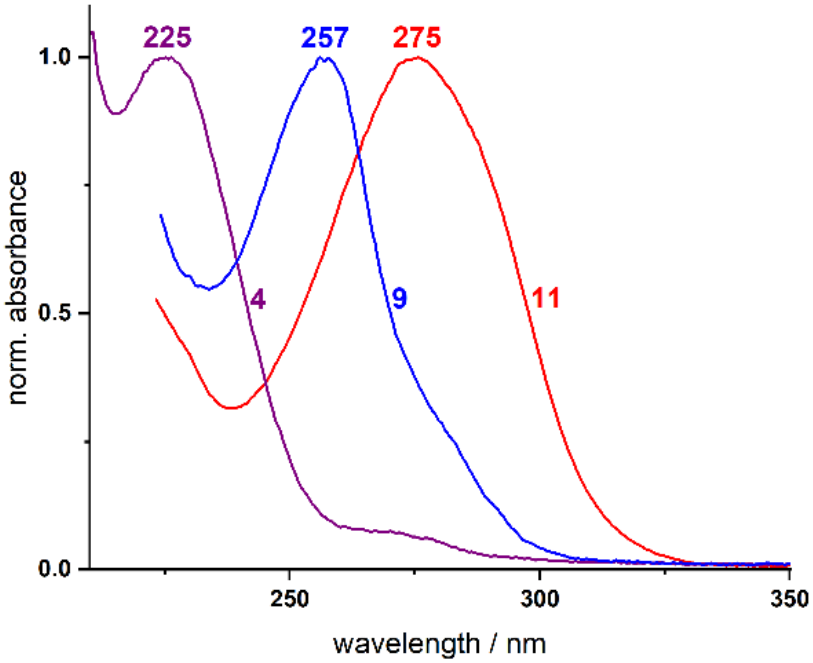

Figure 2.5.4. UV-vis absorption spectra of **4**, **9**, and **11** in THF.

The UV-vis spectra of the monomer **4**, the oligomer **9**, and the polymer **11** were recorded in THF (Figure 2.5.4). Their lowest-energy absorption band (though still being in the UV region) showed a systematic bathochromic shift with increasing number of BN units, thus, with increasing chain length, **4** (225 nm) < **9** (257 nm) < **11** (275 nm).

The electrochemical properties of the **4**, **9**, and **11** in DCM were investigated using cyclic voltammetry (CV). While the voltammograms of monomer **4** revealed one reversible redox event at $E_{1/2}$ = −505 mV (Figure S5.5.44), redox events under reducing conditions were neither observed for **11** nor for **9**. Instead, one reversible redox event was observed at $E_{1/2}$ = 815 mV for polymer **11**, while oligomer **9** showed one irreversible oxidation in DCM with a peak potential of 1096 mV. The reversibility of the redox events for **9** and **11** is presumably a result of the presence of the mono- or diaminoarene moieties[22] in these compounds, respectively, suggesting that these groups are involved in the oxidation processes.

2.5.3 Conclusion

Herein, we demonstrated the use of 1,2,5-azadiborolane as a building block for BCN hybrid polymers for the first time. We synthesized the new monomer 2,5-dichloro-1,2,5-azadiborolane **4** by taking advantage of the regiochemistry of twofold hydroboration of **1**. We were also able to isolate the pure *rac*-diastereomer of **4**, which we subsequently used for oligo- and polymerization studies. The reaction of **4** with an excess of Me_3SiNMe_2 to give **5** demonstrated that this heterocyclic compound, in principle, can undergo two consecutive B–N coupling reactions – one on either side. An attempt to apply **4** for the construction of a cyclolinear poly(iminoborane) corroborated this observation by the formation of **7**, but it also revealed that further catenation is unfeasible.

Application of **4** in combination with **10** as the co-monomer, on the other hand, allowed the successful synthesis of the unprecedented BCN hybrid polymer **11**. Thereby, *p*-phenylene groups are incorporated into the polymer backbone. We additionally prepared oligomer **9** as a molecular model for **11**. Studies of the monomer **4** and oligomers **7** and **9** by X-ray crystallography provided first indications of delocalization of the π-electrons, to some extent, over the B–N chain in such species. Investigations by UV-vis absorption spectroscopy further revealed that the longest-wavelength absorption band shifts bathochromically with increasing number of BN units in the chain.

We are now exploring the application potential of the novel hybrid macromolecule obtained and the possiblity of its post-modification. In addition, we aim at designing further new building blocks for inorganic and organic–inorganic hybrid materials.

2.5.4 Experimental Section

General procedures. All manipulations before the aqueous workup were performed under an atmosphere of dry argon using standard Schlenk techniques or in an MBraun glovebox. Solvents (dichloromethane (DCM), *n*-hexane) were dried and degassed by means of an Innovative Technology solvent purification system (SPS). $CDCl_3$ for NMR spectroscopy as well as *o*-difluorobenzene (*o*-DFB) and *n*-pentane were dried and degassed at reflux over CaH_2 and Na, respectively, and freshly distilled prior to use. *N,N*-Dimethyltrimethylsilylamine (Me_3SiNMe_2), 2,5-dimethyl-2,4-hexadiene and dichloroborane-dimethyl sulfide were commercially purchased and used as received. *p*-Bromo-*N*,*N*-bis(trimethylsilyl)aniline (**3**)[23], *N*,*N*-bis(trimethylsilyl)butylamine (**6**)[24], **8**[24] and **10**[25] were prepared according to literature procedures. Unless otherwise stated, NMR spectra were recorded at 25 °C on a Bruker Avance III HD spectrometer operating at 300 MHz, on a Bruker Avance 500 spectrometer operating at 500 MHz, or on an Avance Neo I 600 operating at 600 MHz. Chemical shifts were referenced to residual protic impurities in the solvent (^1H) or the deuterio solvent itself (^{13}C)

and reported relative to external $SiMe_4$ (^1H, ^{13}C, ^{29}Si), $BF_3{\cdot}OEt_2$ (^{11}B), $MeNO_2$ (^{15}N) standards. Mass spectra were obtained using a Thermo Scientific Exactive Plus Orbitrap MS system employing liquid injection field desorption ionization (LIFDI) and atmospheric pressure chemical ionization (APCI). Elemental analyses were performed on an Elementar vario MICRO cube elemental analyzer. UV/vis spectra were obtained using a Mettler Toledo UV7 UV/Vis spectrophotometer under inert conditions. Cyclic voltammetry experiments were performed using a Gamry Interface 1010B potentiostat. A standard three-electrode cell configuration was employed using a platinum disk working electrode, a platinum wire counter electrode, and a silver wire, separated by a Vycor tip, serving as the reference electrode. Tetra-*n*-butylammonium hexafluorophosphate ([*n*-Bu_4N][PF_6]) (0.1 M) was employed as the supporting electrolyte. The scans were referenced after the addition of a small amount of ferrocene as internal standard. The potentials are reported relative to the ferrocene/ferrocenium couple. All experiments were measured at room temperature under an argon atmosphere. GPC chromatograms were recorded on an Agilent 1260 Infinity II Series, equipped with two PSS SDV 3 µm 1000 Å (300x8 mm) columns and one PSS SDV 3 µm 10000 Å (300x8 mm) column, at 25 °C with a flow rate of 1 mL min^{-1} and calibrated against polystyrene standards. The samples were diluted in THF and toluene as internal standard. Detection was carried out via UV signal (λ = 280 nm). Evaluation of the chromatograms was performed using WinGPC software.

Spectra. All spectra and other result figures are shown in Appendix 5.5.

Synthesis of 2 (via Kulkarni's method[16]). To a solution of dichloroborane-dimethyl sulfide (19.5 g, 134 mmol) in *n*-hexane (43 mL) was added **1** (7.38 g, 67.0 mmol) dropwise at 25 °C (water bath). Subsequently, a solution of BCl_3 (26.7 g, 228 mmol, 3.4 equiv.) in *n*-hexane (43 mL) was added and the mixture was stirred at room temperature overnight. The volatiles were removed *in vacuo* and the formed precipitate was filtered off with *n*-pentane. After removal of the solvent, the crude product was distilled to obtain a colorless liquid (7.63 g, 27.7 mmol, 41 % yield). ^1H NMR (500 MHz, $CDCl_3$): Isomer 1: δ = 2.11 (m, 4H, C*H*), 1.15 (d, 6H, $^3J_{HH}$ = 6.8 Hz, CH_3), 0.96 (d, 6H, $^3J_{HH}$ = 6.8 Hz, CH_3) ppm; Isomer 2: δ = 2.34 (m, 2H, B-C*H*), 1.85 (m, 2H, *i*-Pr-C*H*), 1.05 (d, 6H, $^3J_{HH}$ = 6.9 Hz, CH_3), 1.03 (d, 6H, $^3J_{HH}$ = 6.9 Hz, CH_3) ppm; $^{11}B\{^1H\}$ NMR (96 MHz, $CDCl_3$): δ = 64.1 (s) ppm; $^{13}C\{^1H\}$ NMR (126 MHz, $CDCl_3$): Isomer 1: δ = 46.9 (br, B-*C*H), 28.3 (s, *i*-Pr-*C*H), 23.5 (s, *C*H_3), 20.7 (s, *C*H_3) ppm; Isomer 2: δ = 48.3 (br, B-*C*H), 31.9 (s, *i*-Pr-*C*H), 24.6 (s, *C*H_3), 20.0 (s, *C*H_3) ppm.

Synthesis of 2 (via Matteson's method[15]). To BCl_3 (1 M in toluene, 21.0 mmol, 21 mL) was added **1** (1.11 g, 10.0 mmol) at –78 °C. Subsequently, Et_3SiH (2.33 g, 20.0 mmol) was added

dropwise at −78 °C and the reaction mixture was stirred for 1.5 h at −78 °C. The reaction mixture was stirred for another 1.5 h at room temperature. All volatiles were removed *in vacuo* to obtain a colorless liquid (2.32 g, 8.42 mmol, 84 %). ^{1}H NMR (300 MHz, $CDCl_3$): Isomer 1: δ = 2.11 (m, 4H, C*H*), 1.15 (d, 6H, $^{3}J_{HH}$ = 6.8 Hz, CH_3), 0.96 (d, 6H, $^{3}J_{HH}$ = 6.8 Hz, CH_3) ppm; ^{11}B{^{1}H} NMR (96 MHz, $CDCl_3$): δ = 64.0 (s) ppm; ^{13}C{^{1}H} NMR (75 MHz, $CDCl_3$): Isomer 1: δ = 47.1 (br, B-*C*H), 28.3 (s, *i*-Pr-*C*H), 23.5 (s, *C*H_3), 20.7 (s, *C*H_3) ppm.

Synthesis of 4. To a solution of **2** (2.15 g, 7.80 mmol) in *n*-hexane (80 mL) was added *p*-bromo-*N*,*N*-bis(trimethylsilyl)aniline **3** (2.47 g, 7.80 mmol) dropwise. Subsequently, the reaction mixture was refluxed at 100 °C overnight. After removal of the solvent *in vacuo*, a colorless solid was obtained. The solid was recrystallized multiple times to obtain colorless crystals of exclusively the *rac*-isomer (702 mg, 1.87 mmol, 24 % yield). ^{1}H NMR (500 MHz, $CDCl_3$): 7.49 (m, 2H, N-Ph-C*H*), 6.84 (m, 2H, Br-Ph-C*H*), 2.09 (dsept, 2H, $^{3}J_{HH}$ = 6.9 Hz, $^{3}J_{HH}$ = 3.0 Hz, *i*-Pr-C*H*), 1.43 (d, 2H, $^{3}J_{HH}$ = 2.8 Hz, B-C*H*), 1.00 (d, 6H, $^{3}J_{HH}$ = 6.9 Hz, CH_3), 0.98 (d, 6H, $^{3}J_{HH}$ = 6.9 Hz, CH_3) ppm; ^{11}B{^{1}H} NMR (160 MHz, $CDCl_3$): δ = 54.1 (s) ppm; ^{13}C{^{1}H} NMR (126 MHz, $CDCl_3$): δ = 139.7 (s, N-*C*), 132.2 (s, *o*-*C*H), 128.4 (s, *m*-*C*H), 120.2 (s, Br-*C*), 40.3 (br, B-*C*H), 30.4 (*i*-Pr-*C*H), 21.4 (s, *C*H_3), 21.4 (s, *C*H_3) ppm; HRMS (LIFDI): m/z calcd. for $C_{14}H_{20}B_2BrCl_2N$: 375.0316, found: 375.0308; UV/Vis (THF): $\lambda_{abs,\ max}$ = 225 nm.

Synthesis of 5. To a solution of **4** (74.9 mg, 0.20 mmol) in DCM (1.0 mL) was added Me_3SiNMe_2 (53.8 mg, 0.45 mmol) dropwise at room temperature. The reaction mixture was stirred at room temperature for 24 h. Removing all volatiles *in vacuo* yielded a colorless liquid (50 mg, 0.13 mmol, 65 % yield). ^{1}H NMR (500 MHz, $CDCl_3$): 7.32 (m, 2H, N-Ph-C*H*), 6.85 (m, 2H, Br-Ph-C*H*), 2.71 (br, 6H, N-CH_3), 2.05 (br, 6H, N-CH_3), 1.78 (m, 2H, *i*-Pr-C*H*), 0.97 (d, 2H, B-C*H*), 0.95 (d, 6H, *i*-Pr-CH_3), 0.85 (d, 6H, *i*-Pr-CH_3) ppm; ^{11}B{^{1}H} NMR (160 MHz, $CDCl_3$): δ = 37.7 (s) ppm; ^{13}C{^{1}H} NMR (126 MHz, $CDCl_3$): δ = 148.5 (s, Ph-*C*), 131.6 (s, Ph-*C*H), 130.1 (s, Ph-*C*H), 116.9 (s, Ph-*C*), 42.0 (s, N-*C*H_3), 38.9 (s, N-*C*H_3), 36.4 (br, B-*C*H), 30.4 (s, *i*-Pr-*C*H), 23.3 (s, *i*-Pr-*C*H_3), 21.0 (s, *i*-Pr-*C*H_3) ppm; HRMS (LIFDI): m/z calcd. for $C_{18}H_{32}B_2BrN_3$: 391.1960, found: 391.1948.

Polymerization attempt of 4 with 6 resulting in 7.

To a solution of **4** (375 mg, 1.0 mmol) in *o*-DFB (0.5 mL) was added a solution of **6** (218 mg, 1.0 mmol) in *o*-DFB (0.5 mL). The reaction mixture was stirred for 28 d at 80 °C. After removal of all volatiles, DCM (2.0 mL) was added and the reactive B–Cl bonds were terminated by addition of $TMSNMe_2$ (0.25 mL) at −78 °C. After the reaction was warmed to room temperature overnight, all volatiles were removed *in vacuo*. ^{1}H NMR (600 MHz, $CDCl_3$, 233.15 K): 7.31 (m, 2H, N-Ph-C*H*), 6.92 (m, 2H, Br-Ph-C*H*), 2.68 (s, 3H, N-CH_3), 2.35 (m, 1H, butyl-N-CH_2), 2.23

(m, 1H, butyl-N-C*H*$_2$), 1.94 (s, 3H, N-C*H*$_3$), 1.87 (m, 1H, *i*-Pr-C*H*), 1.79 (m, 1H, *i*-Pr-C*H*), 1.04 (m, 2H, butyl-C*H*$_2$), 0.97 (m, 1H, B-C*H*), 0.92 (m, 1H, B-C*H*), 0.90-0.88 (m, 6H, *i*-Pr-C*H*$_3$), 0.77 (m, 3H, *i*-Pr-C*H*$_3$), 0.72-0.69 (m, 6H, *i*-Pr-C*H*$_3$, butyl-C*H*$_3$), 0.65 (m, 2H, butyl-C*H*$_2$) 0.09 (s, 9H, Si(C*H*$_3$)$_3$) ppm; ^{11}B{^{1}H} NMR (193 MHz, $CDCl_3$, 233.15 K): δ = 38.9 (br) ppm; ^{13}C{^{1}H} NMR (151 MHz, $CDCl_3$, 233.15 K): δ = 147.9 (s, Ph-*C*), 131.2 (s, Ph-*C*H), 129.9 (s, Ph-*C*H), 117.0 (s, Ph-*C*), 44.0 (s, butyl-N-*C*H$_2$), 42.3 (s, N-*C*H$_3$), 38.8 (s, N-*C*H$_3$), 37.0 (s, butyl-*C*H$_2$), 34.3 (br, B-*C*H), 33.1 (br, B-*C*H), 29.8 (s, *i*-Pr-*C*H), 29.5 (s, *i*-Pr-*C*H), 23.3 (s, *i*-Pr-*C*H$_3$), 20.7 (s, *i*-Pr-*C*H$_3$), 20.0 (s, butyl-*C*H$_2$), 19.1 (s, *i*-Pr-*C*H$_3$), 14.2 (s, butyl-*C*H$_3$), 2.4 (s, Si(*C*H$_3$)$_3$) ppm; ^{29}Si{^{1}H} NMR (119 MHz, $CDCl_3$, 233.15 K): δ = 7.0 (s) ppm; ^{15}N{^{1}H} NMR (61 MHz, $CDCl_3$, 233.15 K): δ = −245.8 (s, B-*N*-B), −307.2 (s, *N*-Si(CH$_3$)$_3$), −322.9 (s, *N*-CH$_3$) ppm; HRMS (APCI pos): m/z calcd. for $C_{23}H_{44}B_2BrN_3Si$: 492.2747 $[M+H]^+$, found: 492.2728.

Synthesis of 9. To a solution of **4** (112 mg, 0.30 mmol) in DCM (3.0 mL) was added **8** (100 mg, 0.60 mmol) dropwise at room temperature. The reaction was stirred at room temperature for 3 h. Subsequently, all volatiles were removed *in vacuo* and after recrystallization in *n*-pentane a colorless solid was obtained (101 mg, 0.21 mmol, 70 % yield). ^{1}H NMR (500 MHz, $CDCl_3$): 7.58-7.55 (m, 2H, B_2N-Ph-C*H*), 7.24-7.20 (m, 4H, NH-Ph-C*H*), 6.99-6.91 (m, 8H, Br-Ph-C*H* and NH-Ph-C*H*), 5.00 (s, 2H, N*H*), 2.03 (dsept, 2H, $^3J_{HH}$ = 6.8 Hz, $^3J_{HH}$ = 3.3 Hz, *i*-Pr-C*H*), 1.74 (d, 2H, $^3J_{HH}$ = 3.2 Hz, B-C*H*), 1.00 (d, 6H, $^3J_{HH}$ = 6.8 Hz, C*H*$_3$), 0.82 (d, 6H, $^3J_{HH}$ = 6.8 Hz, C*H*$_3$) ppm; ^{11}B{^{1}H} NMR (160 MHz, $CDCl_3$): δ = 39.0 (s) ppm; ^{13}C{^{1}H} NMR (126 MHz, $CDCl_3$): δ = 144.1 (s, NH-*C*), 141.9 (s, B_2N-*C*), 133.3 (s, B_2N-Ph-*C*H), 129.2 (s, Ph-*C*H), 129.1 (s, Br-Ph-*C*H), 121.5 (s, Ph-*C*H), 119.7 (s, Ph-*C*H), 119.1 (s, Br-*C*), 33.3 (br, B-*C*H), 28.3 (s, *i*-Pr-*C*H), 23.1 (s, *C*H$_3$), 20.3 (s, *C*H$_3$) ppm; HRMS (APCI): m/z calcd. For $C_{26}H_{32}B_2BrN_3$: 487.1960, found: 487.1951; elem. anal. calcd. (%) for $C_{26}H_{32}B_2BrN_3$: C 63.98, H 6.61, N 8.61; found: C 64.20, H 6.75, N 8.53; UV/Vis (THF): $\lambda_{abs,\,max}$ = 257 nm.

Synthesis of 11 (trial 1). To a solution of **4** (37.5 mg, 0.10 mmol) in DCM (0.25 mL), a solution of **10** (25.3 mg, 0.10 mmol) in DCM (0.25 mL) was added. The reaction mixture was stirred for 20 h at room temperature. $TMSNMe_2$ (11 mg, 0.09 mmol) was added, and the reaction mixture stirred for another 3 hours. After removing all volatiles *in vacuo*, the product was obtained as a colorless powder (30 mg, 0.06 mmol, 62 % yield). ^{1}H NMR (500 MHz, $CDCl_3$): 7.51 (d, 2H, N-Ph-C*H*), 6.94 (d, 2H, Br-Ph-C*H*), 6.81 (s, 2H, NH-Ph-C*H*), 6.80 (s, 2H, NH-Ph-C*H*), 4.86 (s, 1H, N-*H*), 4.84 (s, 1H, N-*H*), 1.89 (m, 2H, *i*-Pr-C*H*$_3$), 1.61 (m, 2H, B-C*H*), 0.93 (m, 6H, C*H*$_3$), 0.79 (m, 6H, C*H*$_3$) ppm; ^{11}B{^{1}H} NMR (160 MHz, $CDCl_3$): δ = 38.0 ppm; ^{13}C{^{1}H} NMR (126 MHz, $CDCl_3$): δ = 142.3 (s, B_2N-*C*), 138.2 (s, NH-*C*), 133.1 (s, Br-Ph-*C*H), 129.0 (s, Br-Ph-*C*H), 121.1 (s, Ph-*C*H), 118.8 (s, Br-Ph-*C*H), 33.2 (s, B-*C*H), 28.7 (s, *i*-Pr-*C*H), 23.0 (m,

CH_3), 20.5 (m, CH_3) ppm; GPC (in THF, vs. polystyrene, detection by UV-Vis signal): M_n = 18736 Da; M_w = 40405 Da; UV/Vis (THF): $\lambda_{abs,\ max}$ = 275 nm.

Crystallographic data

Crystals suitable for single-crystal X-ray diffraction were selected, coated in perfluoropolyether oil, and mounted on MiTeGen micromounts or polyimide microloops. Diffraction data were collected on a Bruker X8 Apex II 4-circle diffractometer with a CCD area detector (**4**) or on a Bruker D8 Quest 4-circle diffractometer with a CMOS area detector (**7**, **9**) using multi-layer mirror monochromated Mo-K_α radiation. The crystals were cooled using an Oxford Cryo-streams low-temperature device. Data were collected at 100 K. The images were processed and corrected for Lorentz-polarization effects and absorption as implemented in the Bruker software packages. The structures were solved using the intrinsic phasing method (SHELXT)[26] and Fourier expansion technique. All non-hydrogen atoms were refined in anisotropic approximation, with hydrogen atoms 'riding' in idealized positions, by full-matrix least squares against F^2 of all data, using SHELXL[27] software and the SHELXLE graphical user interface.[28] Crystal data and experimental details are listed in Table 2.5.3; full structural information has been deposited with the Cambridge Crystallographic Data Centre. CCDC-2143337, 2285237 and 2285238.

Table 2.5.2. Selected bond lengths (Å) and angles (°).

Compound	**4**	**7**	**9**
B1–N1	1.437(2)	1.434(4)	1.4183(17)
B1–N2		1.463(4)	1.4503(18)
B2–N1	1.435(2)		
B2–N2		1.468(4)	1.4574(18)
B2–N3		1.409(4)	1.4177(18)
∠ B_2C_2N-phenyl (twist)	61.62(7)	74.77(11)	59.41(6)

Table 2.5.3. Single crystal X-ray diffraction data and structure refinements of **4**, **7** and **9**.

Compound	**4**	**7**	**9**
CCDC number	2143337	2285237	2285238
Empirical formula	$C_{14}H_{20}B_2BrCl_2N$	$C_{23}H_{44}B_2BrN_3Si$	$C_{26}H_{32}B_2BrN_3 \cdot C_4H_{10}O$
M_r	374.74	492.23	562.19
T / K	101(2)	100(2)	100(2)
Radiation, λ / Å	Mo-K_α, 0.71073	Mo-K_α, 0.71073	Mo-K_α, 0.71073
Crystal size / mm³	0.155 x 0.247 x 0.355	0.086 x 0.233x 0.280	0.126 x 0.223 x 0.256
Crystal color, habit	colorless block	colorless plate	colorless block
Crystal system	triclinic	monoclinic	monoclinic
Space group	*P*1	$P2_1/c$	$P2_1/c$
a / Å	5.826(2)	8.3415(13)	14.928(2)
b / Å	11.8272(12)	35.712(9)	11.953(2)
c / Å	12.722(4)	9.268(4)	18.134(4)
α / °	75.954(13)	90	90
β / °	78.41(4)	91.394(11)	113.092(12)
γ / °	86.873(14)	90	90
Volume / Å³	833.0(4)	2760.0(14)	2976.6(10)
Z	2	4	4
ρ_{calc} / g cm^{-3}	1.494	1.185	1.255
μ / mm^{-1}	2.776	1.547	1.408
F(000)	380	1048	1184
θ range / °	1.682 – 26.478	2.271 – 28.400	2.096 – 30.529
Reflections collected	15425	43900	59245
Unique reflections	3208	5603	7804
R_{int}	0.0398	0.0700	0.0633
Parameters / restraints	185 / 0	281 / 0	338 / 4
GooF on F^2	1.026	1.129	1.037
R_1 [$I \geq 2\sigma(I)$]	0.0221	0.0485	0.0327
wR_2 [all data]	0.0567	0.1042	0.0874
Max. / min. residual electron density / e Å^{-3}	0.446 / –0.226	0.601 / –1.048	0.765 / –0.493

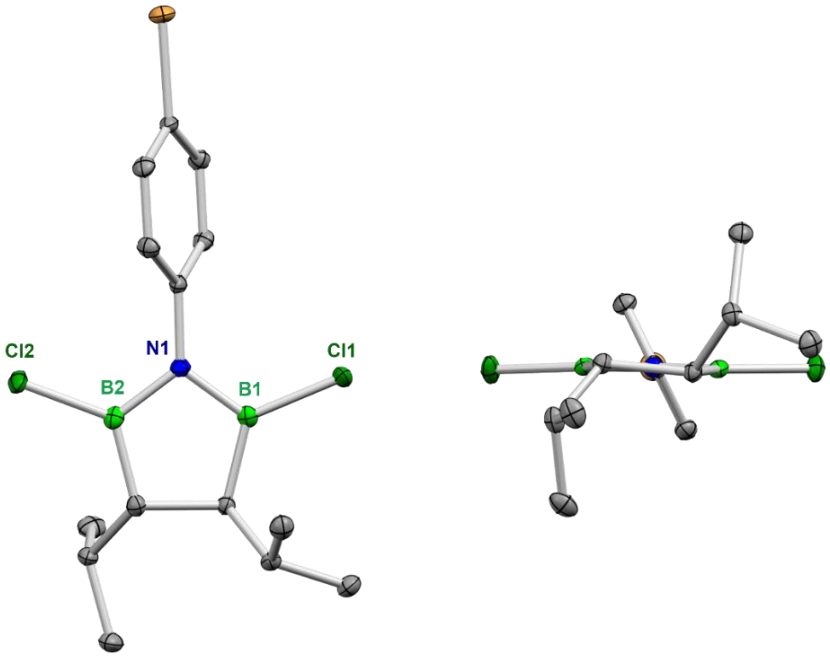

Figure 2.5.5. Molecular structure of **4** in the solid state determined by single-crystal X-ray diffraction at 100 K (H atoms omitted for clarity). Structure shown perpendicular (left) and parallel (right) to the NB_2 plane. All ellipsoids are drawn at the 50% probability level.

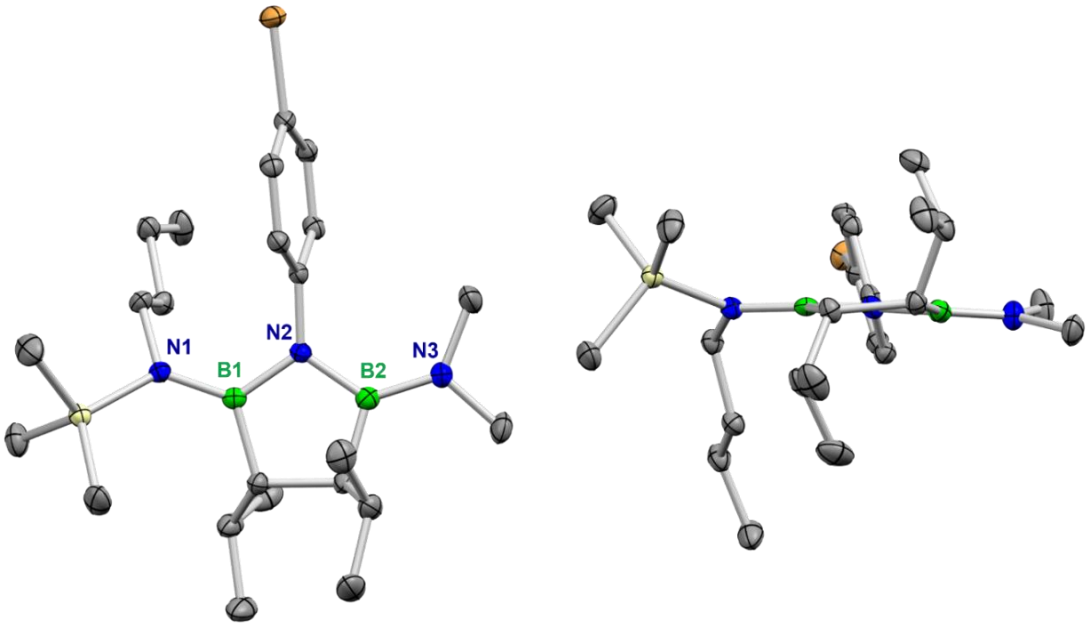

Figure 2.5.6. Molecular structure of **7** in the solid state determined by single-crystal X-ray diffraction at 100 K (H atoms omitted for clarity). Structure shown perpendicular (left) and parallel (right) to the NB_2 plane. All ellipsoids are drawn at the 50% probability level.

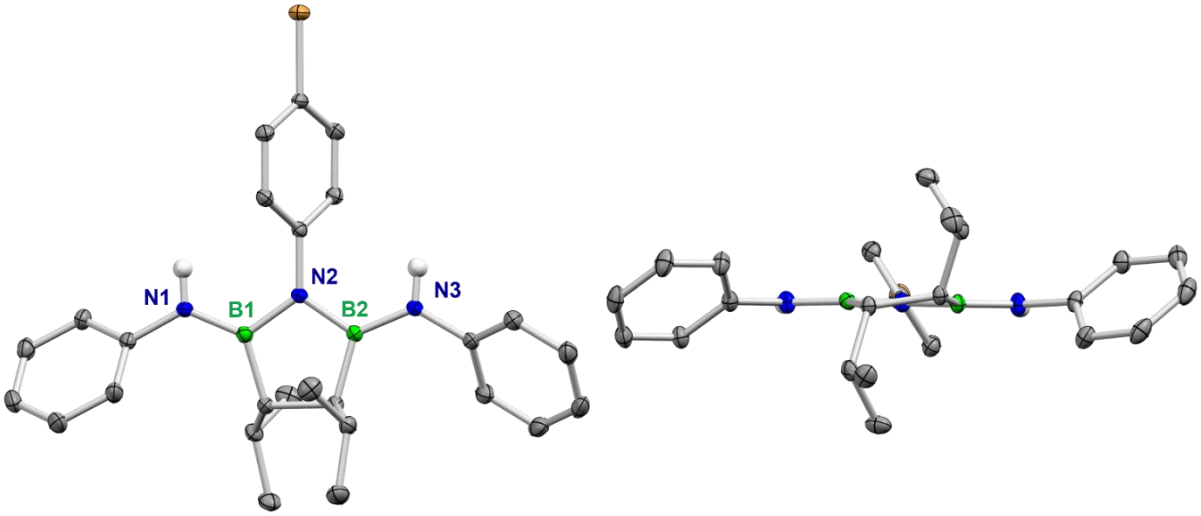

Figure 2.5.7. Molecular structure of **9** in the solid state determined by single-crystal X-ray diffraction at 100 K (H atoms and THF solvent molecule omitted for clarity). Structure shown perpendicular (left) and parallel (right) to the NB_2 plane. All ellipsoids are drawn at the 50% probability level.

Gel permeation chromatography data

Table 2.5.4. Reaction conditions for the polymerizations of **4** with **10** via silicon/boron exchange reaction to **11**.

	solvent	time [h]	T [°C]	M_n [Da]	M_w [Da]	PDI	DP_n
trial 1	DCM	20	r.t.	18736	40405	2.2	91
trial 2	DCM	72	r.t.	68642	414520	6.0	335
trial 3	DCM	24	r.t.	8892	20919	2.4	43
trial 4	DCM	7 d	r.t.	10165	25272	2.5	50

2.5.5 References

[1] a) M. J. D. Bosdet, W. E. Piers, *Can. J. Chem.* **2009**, *87*, 8–29; b) A. Staubitz, A. P. M. Robertson, M. E. Sloan, I. Manners, *Chem. Rev.* **2010**, *110*, 4023–4078; c) N. E. Stubbs, A. P.M. Robertson, E. M. Leitao, I. Manners, *J. Organomet. Chem.* **2013**, *730*, 84–89; d) H. C. Johnson, T. N. Hooper, A. S. Weller, *Top. Organomet. Chem.* **2015**, *49*, 153–220; e) D. Bonifazi, F. Fasano, M. M. Lorenzo-Garcia, D. Marinelli, H. Oubaha, J. Tasseroul, *Chem. Commun.* **2015**, *51*, 15222–15236; f) M. M. Morgan, W. E. Piers, *Dalton Trans.* **2016**, *45*, 5920–5924; g) H. Helten, *Chem. Eur. J.* **2016**, *22*, 12972–12982; h) G. Bélanger-Chabot, H. Braunschweig, D. K. Roy, *Eur. J. Inorg. Chem.* **2017**, 4353–4368; i) M. Stępień, E. Gońka, M. Żyła, N. Sprutta, *Chem. Rev.* **2017**, *117*, 3479–3716; j) Z. X. Giustra, S.-Y. Liu, *J. Am. Chem. Soc.* **2018**, *140*, 1184–1194; k) C. R. McConnell, S.-Y. Liu, *Chem. Soc. Rev.* **2019**, *48*, 3436–3453; l) X.-Y. Wang, X. Yao, A. Narita, K. Müllen, *Acc. Chem. Res.* **2019**, *52*, 2491–2505; m) F. Vidal, F. Jäkle, *Angew. Chem. Int. Ed.* **2019**, *58*, 5846–5870; *Angew. Chem.* **2019**, *131*, 5904–5929; n) D. Han, F. Anke, M. Trose, T. Beweries, *Coord. Chem. Rev.* **2019**, *380*, 260–286; o) K. Ota, R. Kinjo, *Chem. Asian J.* **2020**, *15*, 2558–2574; p) T. Beweries, H. Helten, "Poly(aminoborane)s and Poly(iminoborane)s". In *Encyclopedia of Inorganic and Bioinorganic Chemistry*; ed. R. A. Scott, Wiley, **2020**, DOI: 10.1002/9781119951438.eibc2717; q) R. Zhao, J. Liu, L. Wang, *Acc. Chem. Res.* **2020**, *53*, 1557–1567; r) J. Huang, X. Wang, Y. Xiang, L. Guo, G. Chen, *Adv. Energy Sustainability Res.* **2021**, *2*, 2100016.

[2] a) F. Jäkle, *Chem. Rev.* **2010**, *110*, 3985–4022; b) F. Jäkle, *Top. Organomet. Chem.* **2015**, *49*, 297–325; c) W. L. A. Brooks, B. S. Sumerlin, *Chem. Rev.* **2016**, *116*, 1375–1397; d) Y. Ren, F. Jäkle, in *Main Group Strategies towards Functional Hybrid Materials* (Eds.: T. Baumgartner, F. Jäkle), Wiley, Hoboken, NJ **2017**, pp 79−110; e) H. Helten, *Chem. Asian J.* **2019**, *14*, 919–935; f) X. Yin, J. Liu, F. Jäkle, *Chem. Eur. J.* **2021**, *27*, 2973–2986; g) H. Helten, in *Comprehensive Organometallic Chemistry IV*, Vol. 14 (Eds: D. O'Hare, K. Meyer, G. Parkin), Elsevier, New York **2022**, pp. 71-134.

[3] a) A. Staubitz, A. Presa Soto, I. Manners, *Angew. Chem. Int. Ed.* **2008**, *47*, 6212–6215; *Angew. Chem.* **2008**, *120*, 6308–6311; b) A. Staubitz, M. E. Sloan, A. P. M. Robertson, A. Friedrich, S. Schneider, P. J. Gates, J. Schmedt auf der Günne, I. Manners, *J. Am. Chem. Soc.* **2010**, *132*, 13332–13345.

[4] Further examples of poly(aminoborane) syntheses: a) R. Dallanegra, A. P. M. Robertson, A. B. Chaplin, I. Manners, A. S. Weller, *Chem. Commun.* **2011**, *47*, 3763–3765; b) H. C. Johnson, A. P. M. Robertson, A. B. Chaplin, L. J. Sewell, A. L. Thompson, M. F. Haddow, I. Manners, A. S. Weller, *J. Am. Chem. Soc.* **2011**, *133*, 11076–11079; c) A. P. M. Robertson, R. Suter, L. Chabanne, G. R. Whittell, I. Manners, *Inorg. Chem.* **2011**, *50*, 12680–12691; d) A. P. M. Robertson, E. M. Leitao, T. Jurca, M. F. Haddow, H. Helten, G. C. Lloyd-Jones, I. Manners, *J. Am. Chem. Soc.* **2013**, *135*, 12670–12683; e) A. N. Marziale, A. Friedrich, I. Klopsch, M. Drees, V. R. Celinski, J. Schmedt auf der Günne, S. Schneider, *J. Am. Chem. Soc.* **2013**, *135*, 13342–13355; f) H. C. Johnson, E. M. Leitao, G. R. Whittell, I. Manners, G. C. Lloyd-Jones, A. S. Weller, *J. Am. Chem. Soc.* **2014**, *136*, 9078–9093; g) A. Glüer, M. Förster, V. R. Celinski, J. Schmedt auf der Günne, M. C. Holthausen, S. Schneider, *ACS Catal.* **2015**, *5*, 7214–7217; h) C. Lichtenberg, M. Adelhardt, T. L. Gianetti, K. Meyer, B. de Bruin, H. Grützmacher, *ACS Catal.* **2015**, *5*, 6230–6240; i) K. A. Erickson, J. P. W. Stelmach, N. T. Mucha, R. Waterman, *Organometallics* **2015**, *34*, 4693–4699; j) M. W. Lui, N. R. Paisley, R. McDonald, M. J. Ferguson, E. Rivard, *Chem. Eur. J.* **2016**, *22*, 2134–2145; k) N. T. Coles, M. F. Mahon, R. L. Webster, *Organometallics* **2017**, *36*, 2262–2268; l) D. A. Resendiz-Lara, N. E. Stubbs, M. I. Arz, N. E. Pridmore, H. A. Sparkes, I. Manners, *Chem. Commun.* **2017**, *53*, 11701–11704; m) F. Anke, D. Han, M. Klahn, A. Spannenberg, T. Beweries, *Dalton Trans.* **2017**, *46*, 6843–6847; n) M. Trose, M. Reiß, F. Reiß, F. Anke, A. Spannenberg, S. Boye, A. Lederer, P. Arndt, T. Beweries, *Dalton Trans.* **2018**, *47*, 12858–12862; o) G. M. Adams, A. L. Colebatch, J. T. Skornia, A. I. McKay, H. C. Johnson, G. C. Lloyd Jones, S. A. Macgregor, N. A. Beattie, A. S. Weller,

J. Am. Chem. Soc. **2018**, *140*, 1481–1495; p) T. Jurca, T. Dellermann, N. E. Stubbs, D. A. Resendiz-Lara, G. R. Whittell, I. Manners, *Chem. Sci.* **2018**, *9*, 3360–3366; q) E. A. LaPierre, B. O. Patrick, I. Manners, *J. Am. Chem. Soc.* **2019**, *141*, 20009–20015; r) F. Anke, S. Boye, A. Spannenberg, A. Lederer, D. Heller, T. Beweries, *Chem. Eur. J.* **2020**, *26*, 7889–7899.

[5] a) P. Paetzold, T. von Bennigsen-Mackiewicz, *Chem. Ber.* **1981**, *114*, 298–305; b) H.-U. Meier, P. Paetzold, E. Schröder, *Chem. Ber.* **1984**, *117*, 1954–1964.

[6] For recent reports on trapped iminoboranes, see: a) F. Dahcheh, D. Martin, D. W. Stephan, G. Bertrand, *Angew. Chem. Int. Ed.* **2014**, *53*, 13159–13163; *Angew. Chem.* **2014**, *126*, 13375–13379; b) H. Braunschweig, W. C. Ewing, K. Geetharani, M. Schäfer, *Angew. Chem. Int. Ed.* **2015**, *54*, 1662–1665; *Angew. Chem.* **2015**, *127*, 1682–1685; c) A. K. Swarnakar, C. Hering-Junghans, K. Nagata, M. J. Ferguson, R. McDonald, N. Tokitoh, E. Rivard, *Angew. Chem. Int. Ed.* **2015**, *54*, 10666–10669; *Angew. Chem.* **2015**, *127*, 10812–10816; d) A. K. Swarnakar, C. Hering-Junghans, M. J. Ferguson, R. McDonald, E. Rivard, *Chem. Sci.* **2017**, *8*, 2337–2343; e) B. L. Frenette, A. A. Omaña, M. J. Ferguson, Y. Zhou, E. Rivard, *Chem. Commun.* **2021**, *57*, 10895–10898.

[7] Further examples of molecules comprising catenated B=N units: a) H. Braunschweig, C. Kollann, K. W. Klinkhammer, *Eur. J. Inorg. Chem.* **1999**, 1523–1529; b) X. Xie, M. F. Haddow, S. M. Mansell, N. C. Norman, C. A. Russell, *Chem. Commun.* **2011**, *47*, 3748–3750; c) C. Brunecker, M. Arrowsmith, F. Fantuzzi, H. Braunschweig, *Angew. Chem. Int. Ed.* **2021**, *60*, 16864–16868; *Angew. Chem.* **2021**, *133*, 17000–17004; d) K. Ota, R. Kinjo, *J. Am. Chem. Soc.* **2021**, *143*, 11152–11159.

[8] a) N. Retta, R. H. Neilson, *Bull. Chem. Soc. Ethiop.* **1999**, *13*, 121–125; b) N. Retta, R. H. Neilson, *Bull. Chem. Soc. Ethiop.* **2000**, *14*, 123–128; c) C. J. Wallis, H. Dyer, L. Vendier, G. Alcaraz, S. Sabo-Etienne, *Angew. Chem. Int. Ed.* **2012**, *51*, 3646–3648; *Angew. Chem.* **2012**, *124*, 3706–3708; d) M. Kaaz, C. Bäucker, M. Deimling, S. König, S. H. Schlindwein, J. Bender, M. Nieger, D. Gudat, *Eur. J. Inorg. Chem.* **2017**, 4525–4532.

[9] a) O. Ayhan, T. Eckert, F. A. Plamper, H. Helten, *Angew. Chem. Int. Ed.* **2016**, *55*, 13321–13325; *Angew. Chem.* **2016**, *128*, 13515–13519; b) O. Ayhan, N. A. Riensch, C. Glasmacher, H. Helten, *Chem. Eur. J.* **2018**, *24*, 5883–5894.

[10] Examples: a) P. Zalar, Z. B. Henson, G. C. Welch, G. C. Bazan, T.-Q. Nguyen, *Angew. Chem. Int. Ed.* **2012**, *51*, 7495–7498; b) D. L. Crossley, I. A. Cade, E. R. Clark, A. Escande, M. J. Humphries, S. M. King, I. Vitorica-Yrezabal, M. J. Ingleson, M. L. Turner, *Chem. Sci.* **2015**, *6*, 5144–5151; c) R. Zhao, C. Dou, Z. Xie, J. Liu, L. Wang, *Angew. Chem. Int. Ed.* **2016**, *55*, 5313–5317; *Angew. Chem.* **2016**, *128*, 5399–5403; d) S. M. Barbon, J. B. Gilroy, *Polym. Chem.* **2016**, *7*, 3589–3598; e) J. S. Dhindsa, R. R. Maar, S. M. Barbon, M. Olivia Avilés, Z. K. Powell, F. Lagugné-Labarthet, J. B. Gilroy, *Chem. Commun.* **2018**, *54*, 6899–6902; f) A. F. Alahmadi, R. A. Lalancette, F. Jäkle, *Macromol. Rapid Commun.* **2018**, *39*, e1800456; g) Y. Li, H. Meng, T. Liu, Y. Xiao, Z. Tang, B. Pang, Y. Li, Y. Xiang, G. Zhang, X. Lu, G. Yu, H. Yan, C. Zhan, J. Huang, J. Yao, *Adv. Mater.* **2019**, *31*, e1904585; h) Z. Ding, R. Zhao, Y. Yu, J. Liu, *J. Mater. Chem. A* **2019**, *7*, 26533–26539; i) R. Zhao, N. Wang, Y. Yu, J. Liu, *Chem. Mater.* **2020**, *32*, 1308–1314; j) R. Zhao, Y. Min, C. Dou, B. Lin, W. Ma, J. Liu, L. Wang, *ACS Appl. Polym. Mater.* **2020**, *2*, 19–25; k) B. Liu, Z. Ma, Y. Xu, Y. Guo, F. Yang, D. Xia, C. Li, Z. Tang, W. Li, *J. Mater. Chem. C* **2020**, *8*, 2232–2237; l) L. Chen, D. Chen, Y. Jiang, J. Zhang, J. Yu, C. C. DuFort, S. R. Hingorani, X. Zhang, C. Wu, D. T. Chiu, *Angew. Chem. Int. Ed.* **2019**, *58*, 7008–7012; *Angew. Chem.* **2019**, 131, 7082–7086; m) W. Zhang, W. Lin, C. Li, S. Liu, X. Hu, Z. Xie, *ACS Appl. Mater. Interfaces* **2019**, *11*, 32720–32728; n) A. Ledoux, P. Larini, C. Boisson, V. Monteil, J. Raynaud, E. Lacôte, *Angew. Chem. Int. Ed.* **2015**, *54*, 15744–15749; *Angew. Chem.* **2015**, *127*, 15970–15975.

[11] a) A. W. Baggett, F. Guo, B. Li, S.-Y. Liu, F. Jäkle, *Angew. Chem. Int. Ed.* **2015**, *54*, 11191; *Angew. Chem.* ***2015****, 127, 11343–11347;* b) X.-Y. Wang, F.-D. Zhuang, J.-Y. Wang, J. Pei, *Chem. Commun.* **2015**, *51*, 17532–17535; e) D. Marinelli, F. Fasano, B. Najjari, N. Demitri, D. Bonifazi, *J. Am. Chem. Soc.* **2017**, *139*, 5503–5519; g) W. Zhang, G. Li, L. Xu, Y. Zhuo, W. Wan, N. Yan, G. He, *Chem. Sci.* **2018**, *9*, 4444–4450; i) H.

Oubaha, N. Demitri, J. Rault-Berthelot, P. Dubois, O. Coulembier, D. Bonifazi, *J. Org. Chem.* **2019**, *84*, 9101–9116; j) Y. Fu, H. Yang, Y. Gao, L. Huang, R. Berger, J. Liu, H. Lu, Z. Cheng, S. Du, H.-J. Gao, X. Feng, *Angew. Chem. Int. Ed.* **2020**, *59*, 8873–8879; *Angew. Chem.* **2020**, 132, 8958–8964; k) S. Pang, Z. Wang, X. Yuan, L. Pan, W. Deng, H. Tang, H. Wu, S. Chen, C. Duan, F. Huang, Y. Cao, *Angew. Chem. Int. Ed.* **2021**, *60*, 8813–8817; *Angew. Chem.* **2021***, 133, 8895–8899*.

[12] a) T. Lorenz, A. Lik, F. A. Plamper, H. Helten, *Angew. Chem. Int. Ed.* **2016**, *55*, 7236–7241; *Angew. Chem.* **2016**, *128*, 7352–7357; b) T. Lorenz, M. Crumbach, T. Eckert, A. Lik, H. Helten, *Angew. Chem. Int. Ed.* **2017**, *56*, 2780–2784; *Angew. Chem.* **2017**, *129*, 2824–2828; c) J. Chorbacher, M. Maier, J. Klopf, M. Fest, H. Helten, *Macromol. Rapid Commun.* **2023**, 2300278.

[13] Examples from our group on B=N-containing hybrid polymers with interrupted π-conjugation: a) N. A. Riensch, A. Deniz, S. Kühl, L. Müller, A. Adams, A. Pich, H. Helten, *Polym. Chem.* **2017**, *8*, 5264–5268; b) F. Brosge, T. Lorenz, H. Helten, C. Bolm, *Chem. Eur. J.* **2019**, *25*, 12708–12711.

[14] Previous examples of polymers with linear BN linkages, showing limited conjugation: a) N. Matsumi, K. Kotera, K. Naka, Y. Chujo, *Macromolecules* **1998**, *31*, 3155–3157; b) N. Matsumi, Y. Chujo, *Macromolecules* **1998**, *31*, 3802–3806; c) N. Matsumi, K. Kotera, Y. Chujo, *Macromolecules* **2000**, *33*, 2801–2806.

[15] R. Soundararajan, D. S. Matteson, *J. Org. Chem.* **1990**, *55*, 2274–2275.

[16] H. C. Brown, N. Ravindran, S. U. Kulkarni, *J. Org. Chem.* **1980**, *45*, 384–389.

[17] W. Haubold, U. Kraatz, *Chem. Ber.* **1979**, *112*, 1083–1087.

[18] P. Greiwe, V. Beez, H. Pritzkow, W. Siebert, *Eur. J. Inorg. Chem.* **2001**, 381–386.

[19] For N-silylamines: V. Verma, A. Koperniku, P. M. Edwards, L. L. Schafer, *Chem. Commun.* **2022**, *58*, 9174–9189.

[20] P. Paetzold, *Phosphorus, Sulfur Silicon Relat. Elem.* **1994**, *93*, 39–50.

[21] a) R. A. Bartlett, X. Feng, M. M. Olmstead, P. P. Power, K. J. Weese, *J. Am. Chem. Soc.* **1987**, *109*, 4851–4854; b) H. Chen, R. A. Bartlett, M. M. Olmstead, P. P. Power, S. C. Shoner, *J. Am. Chem. Soc.* **1990**, *112*, 1048–1055; c) M. Maier, J. Klopf, C. Glasmacher, F. Fantuzzi, J. Bachmann, O. Ayhan, A. Koner, B. Engels, H. Helten, *Chem. Commun.* **2022**, *58*, 4464–4467.

[22] A. G. Macdiarmid, J. C. Chiang, M. Halpern, W. S. Huang, S. L. Mu, L. D. Nanaxakkara, S. W. Wu, S. I. Yaniger, *Mol. Cryst. Liq. Cryst.* **1985**, *121*, 173–180.

[23] J. R. Pratt, W. D. Massey, F. H. Pinkerton, S. F. Thames, *J. Org. Chem.* **1975**, *40*, 1090–1094.

[24] Compound **6** was synthesized analogous to *N,N*-bis(trimethylsilyl)hexylamine and compound **8** as described in literature; see M. J. Fuchter, C. J. Smith, M. W. Tsang, A. Boyer, S. Saubern, J. H. Ryan, A. B. Holmes, *Chem. Commun.* **2008**, *18*, 2152–2154.

[25] H. Bock, J. Meuret, C. Näther, U. Krynitz, *Chem. Ber.* **1994**, *127*, 55–65.

[26] G. M. Sheldrick, *Acta Crystallogr. A* **2015**, *71*, 3–8.

[27] G. M. Sheldrick, *Acta Crystallogr. C* **2015**, *71*, 3–8.

[28] C. B. Hübschle, G. M. Sheldrick, B. Dittrich, *J. Appl. Crystallogr.* **2011**, *44*, 1281–1284.

2.6 Synthesis of 1,2,5-Azadiborolanes as Building Blocks for Oligo- and Poly(iminoborane)s

2.6.1 Introduction

Some years ago, our group reported the synthesis and characterization of cyclolinear poly(iminoborane)s (PIBs) comprising 1,3,2-diazaborolidine building blocks.[1] The introduction of the five-membered rings turned out to be an effective method to achieve linear BN catenation and prevent unwanted side reactions to borazines. Very recently, we reported the introduction of 1,2,5-azadiborolane as a polymer building block for the first time.[2] The boron atoms of the five-membered ring were linked by a hydrocarbon bridge bearing two isopropyl substituents (B-CH(^{i}Pr)–CH(^{i}Pr)-B). While the reaction to a cyclolinear PIB was inhibited and stopped after two B–N bond formation events, we successfully synthesized an inorganic–organic hybrid polymer (Chapter 2.5). In this chapter, the synthesis of a 1,2,5-azadiborolane building block with ethylene-linked boron atoms and a followed polymerization attempt to cyclolinear poly(iminoborane)s is described.

2.6.2 Results and Discussion

We started the synthesis with the reaction of tetrakis(dimethylamino)diborane[3] **1** with methanol and hydrochloric acid to obtain tetramethoxydiborane(4) **2** (Scheme 2.6.1).[4] By addition of boron tribromide to **2** at room temperature, we were able to obtain tetrabromodiborane(4) **3**.[5] It was found that the by-product dibromo(methoxy)borane decomposes to bromomethane, boron tribromide and boron trioxide under these reaction conditions. The highly reactive compound **3** was stored at low temperature (−78 °C). The synthesis of compound **4**[6] was realized by halogen exchange reaction of **3** with gallium trichloride, and it was stored as *n*-hexane solution at −30 °C.[7] Further reactions were performed with the B_2Cl_4 stock solution under the assumption of complete conversion. We were able to synthesize 1,2-bis(dichloroboryl)ethane **5**[8] by addition of ethylene to the stock solution of **4**,[9,10] which resulted in the insertion of ethylene into the B–B bond. The reactions from **1** to **5** were performed as described in the literature and thus are not discussed here in further detail. Unfortunately, upscaling of the synthesis of **5** was not successful and we therefore performed the reaction to **6** on a small scale.

We added *N*,*N*-bis(trimethylsilyl)butylamine to a solution of **5** in CD_2Cl_2 at low temperature to achieve a twofold Si/B exchange reaction. This yielded the desired product **6** after warming to ambient temperature overnight. The ^{1}H NMR spectrum showed a new signal at 0.43 ppm corresponding to the formation of Me_3SiCl as a by-product and a singlet at 1.26 ppm which can be assigned to the B-C_2H_4-B group (Figure S5.6.1). This shift is very similar to that observed for 2,5-dichloro-1-methyl-1,2,5-azadiborolane.[11] The resonance of the N-CH_2 group

(3.34 ppm) is significantly downfield shifted compared to the other CH_2 group signals of the butyl rest (1.51 – 1.30 ppm). In the $^{11}B\{^1H\}$ NMR spectrum of **6** a single signal at 54.3 ppm was observed, which is shifted to higher field compared to the signal of **5** (63.3 ppm) in agreement with the literature.[11]

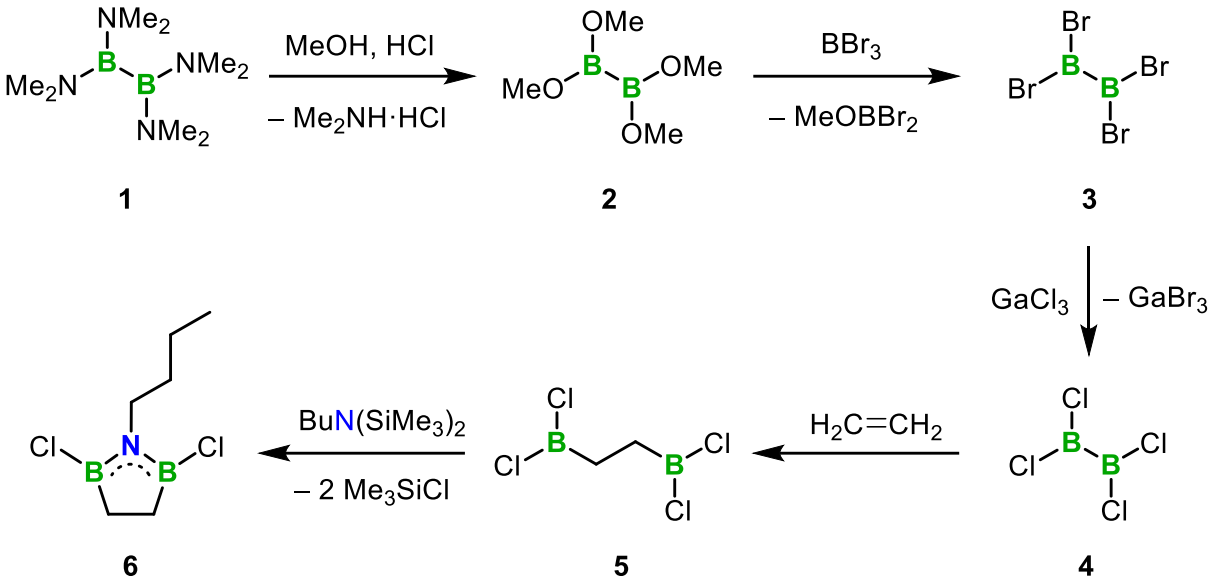

Scheme 2.6.1. Synthetic route to 1,2,5-azadiborolane **6**.

For further reactivity studies we added 1-2 drops of $BuN(SiMe_3)_2$ to **6** in a sealed J. Young tube with a view to obtain oligomer **7** (Scheme 2.6.2). In the ^1H NMR spectrum after a reaction time of 30 minutes, we observed the formation of further Me_3SiCl by comparison of the integrals of the N-CH_2 signal and the Me_3SiCl signal (Figure S5.6.3). The formation of another 2 equivalents of Me_3SiCl indicated the reaction of **6** with further 2 equivalents of $BuN(SiMe_3)_2$. The $^{11}B\{^1H\}$ NMR spectrum showed the emergence of new highfield-shifted peaks, as expected for BN catenation. After stirring the reaction mixture overnight, the signals in the ^1H and $^{11}B\{^1H\}$ NMR spectra showed further broadening (Figures S5.6.5 and S5.6.6), which indicates oligomerization to **7**. This was previously observed in the spectra of 1,3,2-diazaborolidine-based poly(iminoborane)s.[1b] These observations indicate enhanced reactivity of **6** compared to its isopropyl-substituted congener (**4**, Scheme 2.5.1) discussed in chapter 2.5.

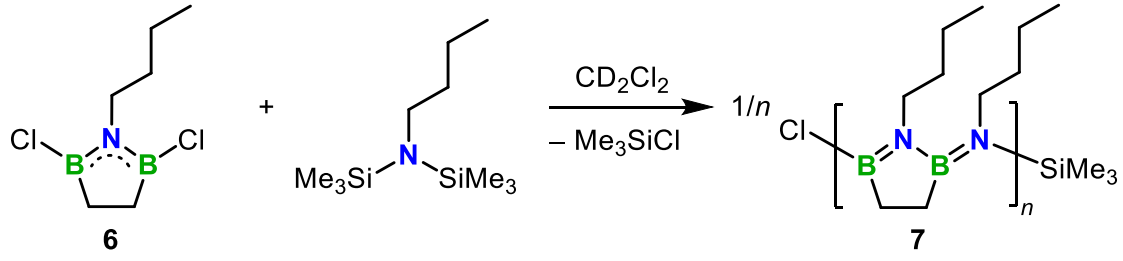

Scheme 2.6.2. Polymerization attempt of **6** with $BuN(SiMe_3)_2$ by Si/B exchange polycondensation.

2.6.3 Conclusion

Herein, the successful multi-step synthesis to an 1,2,5-azadiborolane (**6**) with ethylene-bridged boron atoms was reported. A subsequent polymerization attempt indicated BN catenation and an enhanced reactivity of **6**, compared to 1,2,5-azadiborolanes with sterically demanding groups attached on the ethylene linker.

2.6.4 Experimental Section

General procedures. All manipulations were performed under an atmosphere of dry argon using standard Schlenk techniques or in an MBraun glovebox. CD_2Cl_2 for NMR spectroscopy was dried and degassed at reflux over CaH_2 and freshly distilled prior to use. *N*,*N*-Bis(trimethylsilyl)butylamine ($BuN(SiMe_3)_2$) was prepared according to literature procedure.[12] NMR spectra were recorded at 25 °C on a Bruker Avance III HD spectrometer operating at 300 MHz. Chemical shifts were referenced to residual protic impurities in the solvent (^1H) and reported relative to external $SiMe_4$ (^1H), $BF_3{\cdot}OEt_2$ (^{11}B) standards.

Spectra. All spectra and other result figures are shown in Appendix 5.6.

Synthesis of 6. To a solution of **5** (21.7 mg, 0.11 mmol) in 1.5 mL CD_2Cl_2 was added $BuN(SiMe_3)_2$ (26.0 mg, 0.12 mmol) at −78 °C. After warming to room temperature overnight, the product could be assigned by NMR measurement in a sealed J. Young tube. ^1H NMR (300 MHz, CD_2Cl_2): δ = 3.34 (t, 2H, Bu-C*H*$_2$), 1.53-1.43 (m, 2H, Bu-C*H*$_2$), 1.35-1.30 (m, 2H, Bu-C*H*$_2$), 1.26 (s, 4H, B-C*H*$_2$), 0.92 (t, 3H, Bu-C*H*$_3$), 0.43 (s, 18H, (C*H*$_3$)$_3$SiCl) ppm; $^{11}B\{^1H\}$ NMR (96 MHz, CD_2Cl_2): δ = 54.3 (s) ppm.

Synthesis attempt of 7. To the J. Young tube with **6** in CD_2Cl_2 was added $BuN(SiMe_3)_2$ (1-2 drops) and after 30 min the formation of Me_3SiCl was observed. After reaction overnight, a broadening of the $^{11}B\{^1H\}$ NMR signal was observed. $^{11}B\{^1H\}$ NMR (96 MHz, CD_2Cl_2): δ = 44.9 (br) ppm.

2.6.5 References

[1] a) O. Ayhan, T. Eckert, F. A. Plamper, H. Helten, *Angew. Chem. Int. Ed.* **2016**, *55*, 13321–13325; *Angew. Chem.* **2016**, *128*, 13515–13519; b) O. Ayhan, N. A. Riensch, C. Glasmacher, H. Helten, *Chem. Eur. J.* **2018**, *24*, 5883–5894.

[2] M. Maier, V. Zeh, N. Munker, J. Glock, K. Oberdorf, O. Ayhan, C. Lichtenberg, H. Helten, *Eur. J. Inorg. Chem.* **2023**, e202300490.

[3] R. J. Brotherton, A. L. McCloskey, L. L. Petterson, H. Steinberg, *J. Am. Chem. Soc.* **1960**, *82*, 6242–6245.

[4] R. J. Brotherton, A. L. McCloskey, J. L. Boone, H. M. Manasevit, *J. Am. Chem. Soc.* **1960**, *82*, 6245–6248.

[5] H. Nöth, H. Pommerening, *Chem. Ber.* **1981**, *114*, 398–399.

[6] G. Urry, T. Wartik, R. E. Moore, H. I. Schlesinger, *J. Am. Chem. Soc.* **1954**, *76*, 5293–5298.

[7] M. Arrowsmith, J. Böhnke, H. Braunschweig, A. Deißenberger, R. D. Dewhurst, W. C. Ewing, C. Hörl, J. Mies, J. H. Muessig, *Chem. Commun.* **2017**, *53*, 8265–8267.

[8] Alternative route: J.-K. Uhm, H. Römich, H. Wadepohl, W. Siebert, *Z. Naturforsch. B* **1988**, *43*, 306–308.

[9] G. Urry, J. Kerrigan, T. D. Parsons, H. I. Schlesinger, *J. Am. Chem. Soc.* **1954**, *76*, 5299–5301.

[10] Reactions of B_2Cl_4 with other alkenes and alkynes are also known, see: a) P. Ceron, A. Finch, J. Frey, J. Kerrigan, T. Parsons, G. Urry, H. I. Schlesinger, *J. Am. Chem. Soc.* **1959**, *81*, 6368–6371; b) C. Chambers, A. K. Holliday, *J. Chem. Soc.* **1965**, 3459–3462; c) C. N. Welch, S. G. Shore, *Inorg. Chem.* **1969**, *8*, 2810–2812; d) W. Siebert, M. Hildenbrand, P. Hornbach, G. Karger, H. Pritzkow, *Z. Naturforsch. B* **1989**, *43*, 1179–1186.

[11] W. Haubold, U. Kraatz, *Chem. Ber.* **1979**, *112*, 1083–1087.

[12] Synthesis analog to *N*,*N*-bis(trimethylsilyl)hexylamine, see: M. J. Fuchter, C. J. Smith, M. W. Tsang, A. Boyer, S. Saubern, J. H. Ryan, A. B. Holmes, *Chem. Commun.* **2008**, *18*, 2152–2154.

2.7 Poly(thiophene iminoborane): A Poly(thiophene vinylene) (PTV) Analogue with a Fully B=N-Doped Backbone

The following section is slightly modified and reproduced from published article[‡] with permission from John Wiley & Sons.

Abstract. An unprecedented poly(thiophene iminoborane) – a boron–nitrogen analogue of the well-established conjugated organic polymer poly(thiophene vinylene) (PTV) – is presented. The polymer synthesis has been achieved by selective Si/B exchange polycondensation of a 2,5-diborylthiophene with a 2,5-diaminothiophene derivative. For the latter, a facile synthetic strategy has been devised, which makes this versatile, strongly electron-releasing building block easily accessible. The novel polymer and a series of monodisperse thiophene iminoborane oligomers reveal systematic bathochromic shifts in their absorption with increasing chain length, and thus extended π-conjugation over the B=N units along the backbone, which is further supported by TD-DFT calculations.

2.7.1 Introduction

π-Conjugated organic polymers attract continuing tremendous research interest, due to their facile processability, thus enabling roll-to-roll production of active coatings for optoelectronic devices, such as organic/polymer light emitting diodes (OLEDs/PLEDs), organic field-effect transistors (OFETs), and organic photovoltaics (OPVs). Furthermore they show applicability in sensory, imaging, and therapeutic purposes.[1] Amongst the most extensively studied classes of conjugated polymers are poly(*p*-phenylene vinylene)s (PPVs, Figure 2.7.1).[2] In addition, thiophene-comprising building blocks have developed over the last decades into a further class of highly versatile, popular components for organic electronic materials.[3] It is therefore not surprising that the thiophene congeners of PPV, namely, poly(thiophene vinylene)s (PTVs), have proven useful in optoelectronic applications as well.[4] Although PTVs had initially received somewhat less consideration as compared with, for instance, PPVs or polythiophenes (PTs), recent studies have uncovered a great potential for this versatile class of materials.[5]
In recent times, the incorporation of main group elements beyond those from the standard repertoire of classical organic chemistry has come into the focus of organic electronic materials' research.[6,7] Particularly, boron offers exciting opportunities due to the effects that result from incorporation of the vacant p-orbital of tricoordinate boron into the backbone of π-conjugated polymers.[8,9] The substitution of selected CC units by isoelectronic and isosteric

[‡] J. Chorbacher, M. Maier, J. Klopf, M. Fest, H. Helten, *Macromol. Rapid Commun.* **2023**, *44*, 2300278.
(J.C. and M.M. contributed equally to this work)

BN units in organic, especially in polyaromatic compounds has evolved into a powerful approach for accessing novel materials with modified, often intriguing properties and functions.[10,11] Application of this BN/CC isosterism concept to conjugated polymers, however, is still in its infancy.[12-16]

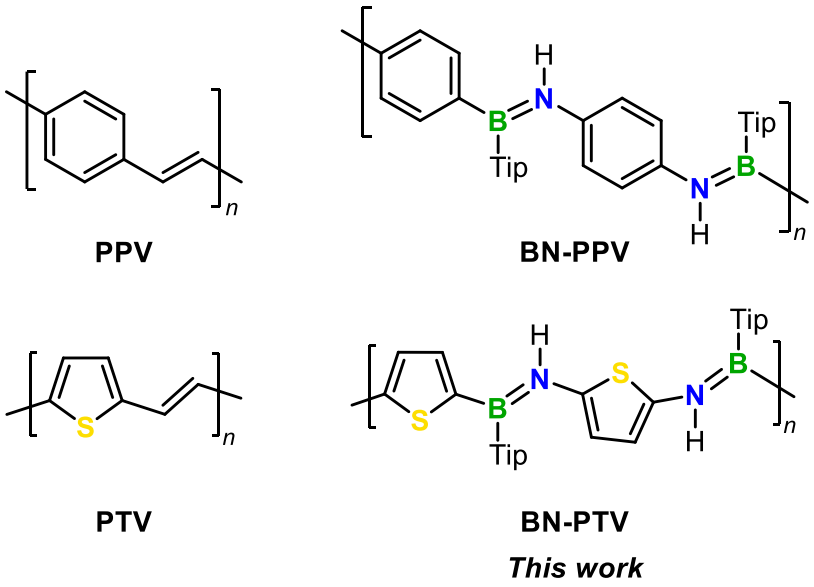

Figure 2.7.1. Poly(*p*-phenylene vinylene) (PPV) and poly(thiophene vinylene) (PTV) and BN isosters thereof (Tip = 2,4,6-triisopropylphenyl).

We recently reported the first poly(*p*-phenylene iminoborane), which is derived from PPV through replacement of its vinylene groups by B=N moieties (i.e., BN-PPV).[15] In contrast to previously known and most other BN-containing polymers,[12-14] the π-conjugation over the backbone of this BN-PPV is forced to involve the B=N linkages, since any alternative conjugation pathways are absent.[16] Building on that, it appeared to us as a logical extension to target a BN/CC isostere of PTV next, namely, a poly(thiophene iminoborane) (BN-PTV). Our investigations on the polymer and a series of monodisperse oligomers, which are reported herein, reveal even more pronounced π-conjugation over the B=N units, as evidenced by photophysical studies and supported by TD-DFT calculations.

2.7.2 Results and Discussion

The planned syntheses using Si/B exchange condensations required as starting materials 2-mono- and 2,5-bis-bromoborylthiophenes **4** and **8** and *N*-silylated 2-monoamino- and *N*,*N'*-disilylated 2,5-diaminothiophenes **7** and **3**, respectively. Especially the synthesis of the latter turned out to be quite challenging. As reported previously, 2-aminothiophene is unstable above its melting point. It has been speculated that this highly electron-rich species undergoes spontaneous Diels–Alder-like diene polymerization.[17] To access 2,5-diaminothiophene

derivatives thus proved to be even more challenging. However, we successfully obtained the previously unknown tetrasilylated thiophene diamine **1** in 88 % isolated yield by using a nickel-catalyzed variant of the Buchwald–Hartwig amination (i) (Scheme 2.7.1), following a procedure demonstrated by Fout and co-workers for related substrates.[18]

The solid-state structure of **1** was determined by single-crystal X-ray diffractometry (see inset in Scheme 2.7.1). The four trimethylsilyl groups on the nitrogen atoms effectively stabilize the compound, making it safely storable under inert atmosphere at −40 °C. Reaction of **1** with an excess of anhydrous HCl (ii) led to 2,5-diaminothiophene bis-hydrochloride **2** as an off-white solid in 81 % yield. As compound **2** is insoluble in common solvents suitable for our follow up chemistry, we did not attempt to characterize it further. However, we succeeded in transforming it into the bis-silylated compound **3** (iii) via release of the free 2,5-thiophenediamine by deprotonation with NEt_3 at −78 °C, followed by twofold silylation with Me_3SiCl in 83 % isolated yield. We additionally found an even more convenient way to **3** in 79 % overall yield by a one-pot process directly from **1** (iv): reaction of **1** with $HCl{\cdot}Et_2O$, followed by silylation through *in situ* generated Me_3SiCl upon addition of NEt_3. Compound **3** proved to be stable for more than four weeks under inert conditions at −40 °C.

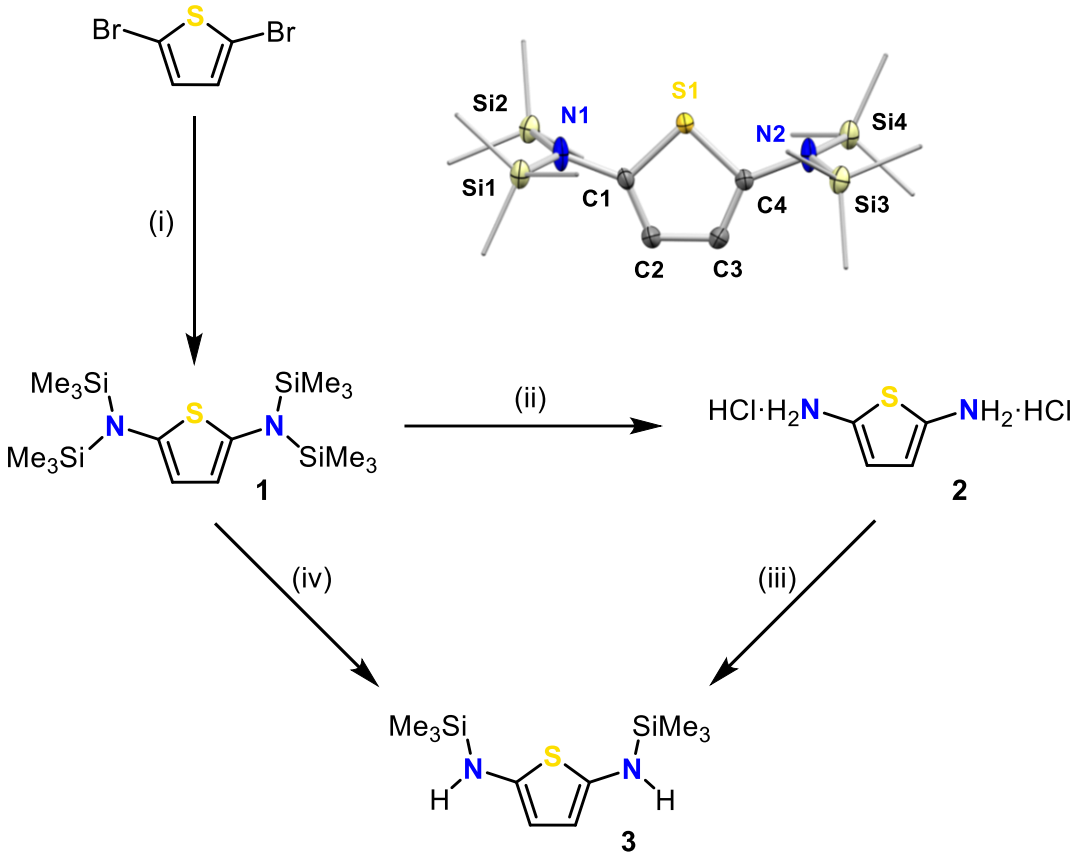

Scheme 2.7.1. Synthesis of 2,5-diaminothiophenes **1**, **2**, and **3**. Reagents and conditions: (i) $(Ph_3P)_2NiCl_2$, $LiN(SiMe_3)_2$, toluene, 100 °C. (ii) $HCl{\cdot}Et_2O$, CH_2Cl_2, −78 °C. (iii) NEt_3, Me_3SiCl, CH_2Cl_2, −78 °C. (iv) $HCl{\cdot}Et_2O$, CH_2Cl_2, −78 °C then NEt_3, CH_2Cl_2, −78 °C. Inset: Molecular structure of **1** in the solid state (ellipsoids drawn at the 50% probability level, except for the CH_3 groups; H atoms omitted for clarity).

We used the *N*-silyl mono- and diaminothiophenes **7** and **3** in combination with the respective di- and mono(bromoboryl)thiophenes **8** and **4** to prepare oligo(thiophene iminoborane)s **9** and **10** (i.e., the "dimers") via selective silicon/boron exchange reactions, while we applied salt elimination for the coupling of **4** with **5** in the presence of NEt_3 as auxiliary base to obtain the "monomeric" model compound **6** (Scheme 2.7.2). For kinetic stabilization of the tricoordinate boron centers we attached 2,4,6-triisopropylphenyl (Tip) substituents to them.

Compounds **6**, **9**, and **10** were purified by column chromatography on neutral aluminum oxide and were obtained and characterized as mixtures of diastereomers that differ by the configuration at the B=N double bonds. In the cases of **6** and **9**, the (*E*)- and the (*E*/*E*)-diastereomer, respectively, was by far the most abundant isomer, as proven by NOESY measurements (Figure S5.7.16 and S5.7.27). In the case of **10**, additionally, significant amounts of the (*E*/*Z*)-isomer and minor quantities of the (*Z*/*Z*)-isomer were present. No coalescence of the signals for the different isomers of **10** was observed up to 110 °C in toluene by variable-temperature NMR measurements (Figure S5.7.37). This evidences pronouncedly hindered bond rotation, and thus significant B=N π bonding. In the ^{1}H NMR spectra the aromatic β-protons of the *N*-bound thiophene moieties appear significantly high field shifted (6.63 – 5.68 ppm) compared to the protons of the *B*-bound thiophene rings (7.64 – 7.38 ppm). The ^{11}B{^{1}H} NMR spectra of the oligomers showed each a single, broad peak at about 40 ppm, slightly upfield from those of their oligo(*p*-phenylene iminoborane) congeners (43 – 45 ppm).[15]

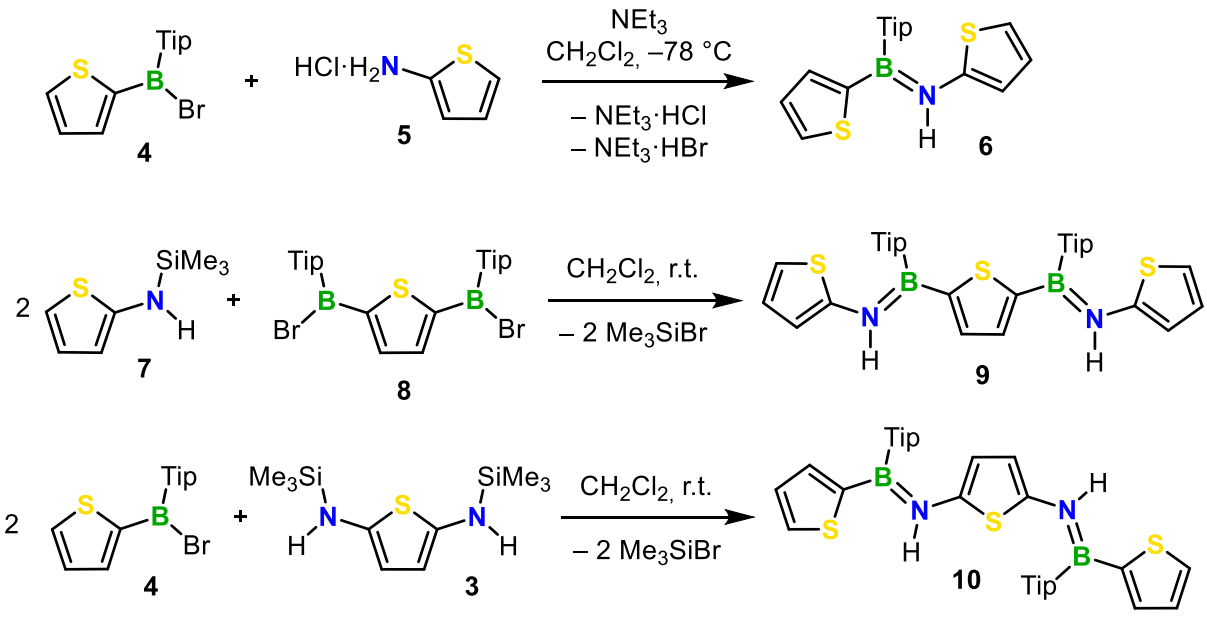

Scheme 2.7.2. Synthesis of monodisperse oligomers **6**, **9**, and **10** (Tip = 2,4,6-triisopropylphenyl).

Upon slow crystallization of **6**, **9**, and **10** from *n*-hexane, we obtained single crystals suitable for X-ray diffractometry of exclusively the all-(*E*)-configured isomers (Figure 2.7.2). Their molecular structures feature perfectly trigonal-planar coordinated boron and nitrogen centers

(both $\sum(NR_3)$ and $\sum(BR_3)$ = 360.0°). The B–N bond lengths of **6** (1.408(2) Å), **10** (B1–N1: 1.412(3) Å and B2–N2: 1.410(3) Å), and **9** (B1–N1: 1.407(4) Å, B2–N2: 1.410(4) Å for conformer I and B1–N1: 1.410(4) Å and B2–N2: 1.401(3) Å) for conformer II; Table 2.7.2) are in the same range with those of the BN-PPV model dimers[15] and related aminoboranes, having pronounced double bond character.[19]

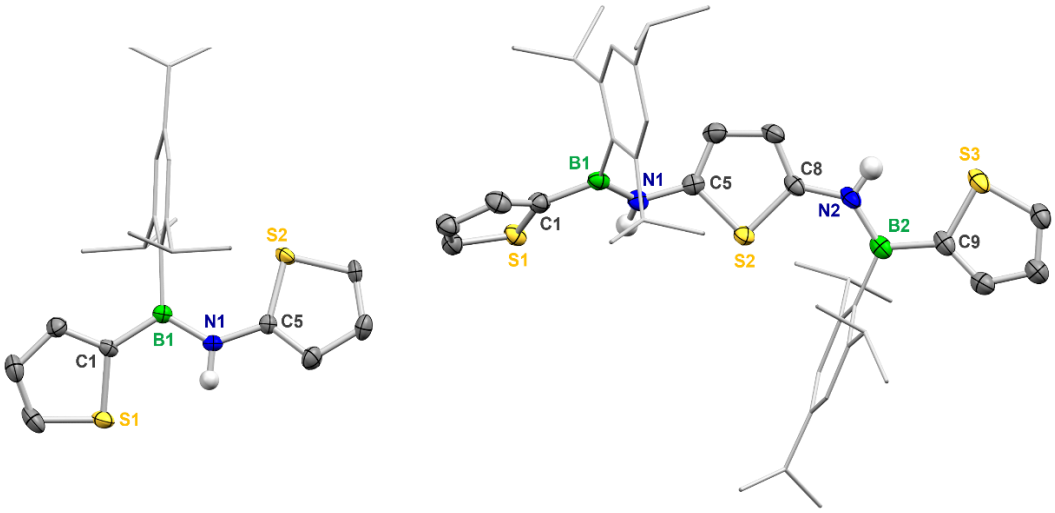

Figure 2.7.2. Molecular structures of **6** and **10** in the solid state (ellipsoids drawn at the 50% probability level, except for the Tip groups; H atoms and disorders of the thiophene units and Tip groups omitted for clarity).

The triisopropylphenyl groups are largely perpendicular to the plane of the C_2BNC moiety; thus providing effective steric shielding of the boron center. Whereas compound **6** features a rather planar backbone, with only a slight twisting between the thiophene ring planes and the BN moiety (10.4 and 12.4°, defined by C_2BNC), the solid-state molecular structure of **10** shows one major twist between the B1=N1 unit and the central thiophene ring (torsion angles between the thiophene ring planes and the BN moieties from left to right, Figure 2.7.2: 16.9, 50.1, 9.1, and 8.9°). The unit cell of **9** contains two conformers, which show quite different degrees of twisting about their ring planes. Conformer I features a highly planar backbone with small torsion angles of 6.2, 4.8, 2.5, and 3.0° between the thiophene ring planes and the adjacent BN moieties from left to right (Figure 2.7.7). Conformer II shows a strong twist between the B2=N2 unit and the outer thiophene ring of 34.0° beside its otherwise quite planar backbone structure (torsion angles: 7.3, 4.4, 2.9 and 34.0° from left to right; Figure 2.7.8).[20]

The synthesis of the corresponding polymer, poly(thiophene iminoborane) **11** was achieved by Si/B exchange co-polycondensation of **3** with **8** in CH_2Cl_2 at ambient temperature (Scheme 2.7.3). After 48 h, Me_3SiNMe_2 was added to terminate the eventually remaining reactive B–Br end groups of the polymer.

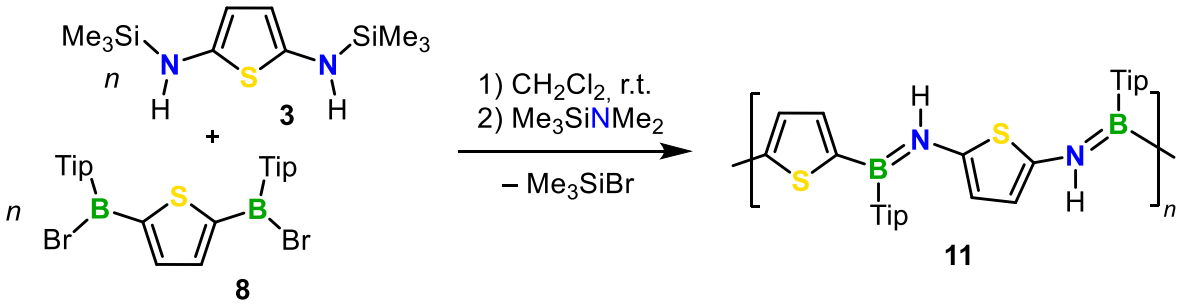

Scheme 2.7.3. Synthesis of BN-PTV **11** by Si/B exchange polycondensation of **3** and **8**.

Gel permeation chromatography (GPC) of the crude product showed a major broad signal for a distribution around higher molecular weights (at around 15 kDa) and some minor signals in the small-molecule range (between 1.3 kDa and 5.0 kDa). After twofold precipitation into cold methanol (−78 °C), to remove smaller oligomers, the desired poly(thiophene iminoborane) **11** was obtained in 38 % yield. The polymer, which is soluble in common solvents such as THF and chloroform, was characterized by NMR and UV-vis spectroscopy, and in terms of molecular weight by GPC. The ^{1}H NMR spectrum of **11** showed multiple peaks in the aromatic region between 5.50 and 7.50 ppm indicating different *E*/*Z* arrangements around the B=N bonds along the polymer chain. The main peaks appear at 5.64 and 7.20 ppm, which we assign to the *N*- and the *B*-bonded thiophene moieties at (*E*)-configured B=N bonds, based on the observations made on the model oligomers. GPC analysis of purified **11** revealed molecular-weight averages of M_n = 14.2 kDa and M_w = 23.0 kDa, which corresponds to a number average degree of polymerization of DP_n = 46. The polydispersity index of PDI = 1.6 is slightly lower than the theoretical value for ideal polycondensation reactions (PDI = 2).

The UV-vis spectra of the monodisperse oligomers **6**, **9**, and **10** and the polymer **11** in THF (Figure 2.7.3) displayed each a strong low-energy absorption band with a systematic bathochromic shift with increasing number of B=N units. The maxima appear at 305 nm (**6**), 340 nm (**9**), 348 nm (**10**), and 388 nm (**11**), thus significantly red-shifted, by 33 – 47 nm, compared with their respective phenylene analogues[15] (Table 2.7.3). However, the compounds showed no emission in THF and DCM.

Based on TD-DFT calculations of the vertical singlet excitations of the all *E*/(*E*/*E*)-isomers of **6**, **9**, and **10** we assign the lowest energy absorption to a π–π* process, which corresponds to a HOMO→LUMO excitation (Figure 2.7.4 and Table 2.7.4). The calculations also revealed that the HOMO of these molecules tends to have the strongest contribution on the electron-donating aminothiophene units, whereas the LUMO is more confined in the thiophenylborane sequences, reflecting some degree of intramolecular charge transfer character of this transition.

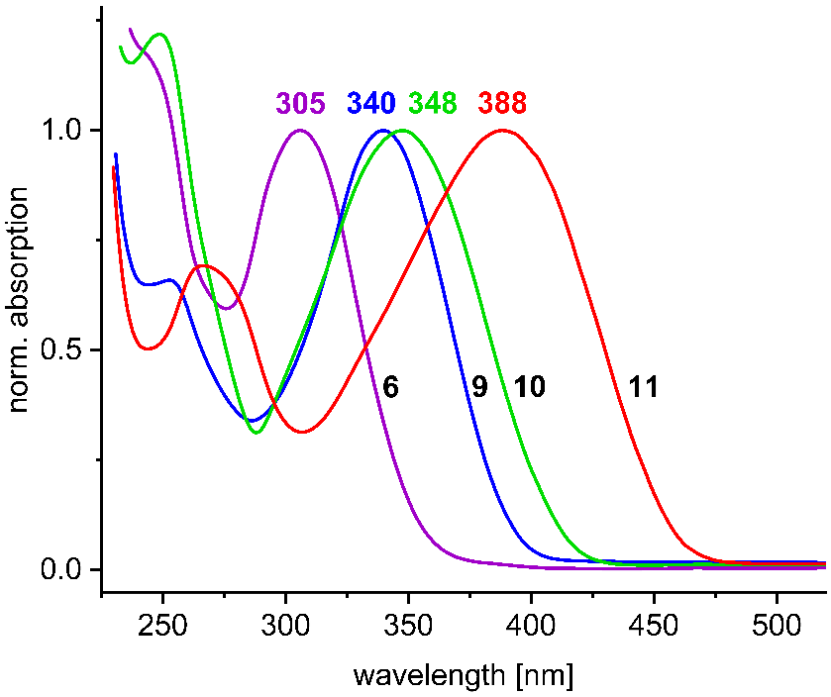

Figure 2.7.3. UV-vis absorption spectra of **6**, **9**, **10** and **11** in THF.

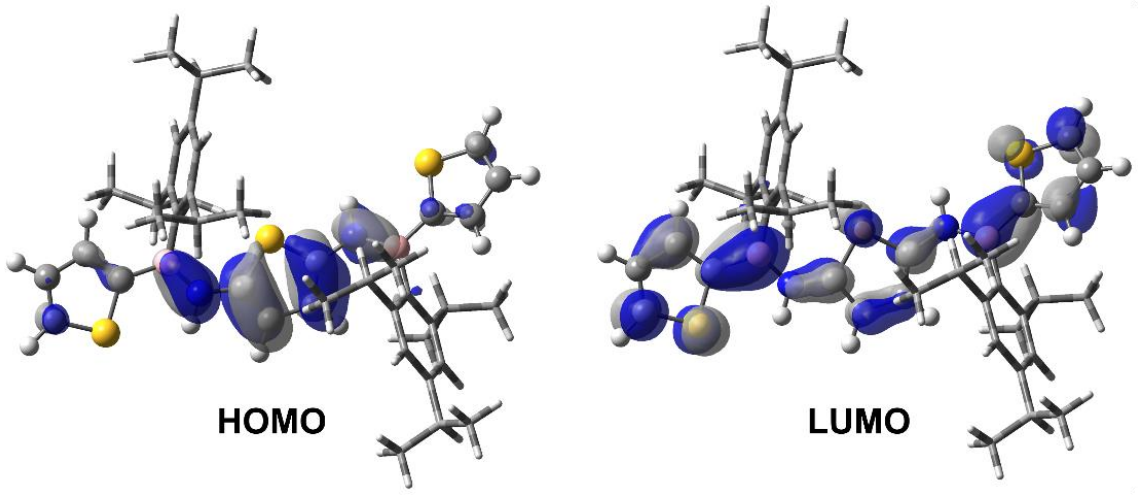

Figure 2.7.4. Calculated frontier orbitals of **10** (isovalue 0.03 a.u.; ω_TB97X-D3/def2-SVP, CPCM(THF), ω_T = 0.14).

Cyclic voltammetry (CV) of the oligomers and the polymer in CH_2Cl_2 revealed multiple irreversible oxidation events. For compound **10** one reversible oxidation event was observed at $E_{1/2}$ = 0.32 V (vs Fe/Fe^+) (Figure S5.7.57, right). From the CV curves, we determined the oxidation onset potentials of **6**, **9**, **10** and **11**, displaying the tendency to decrease from **6** (0.62 V) to **9** (0.61 V), over **10** (0.25 V) to **11** (0.24 V). The same trend is observed in DFT calculations of the HOMO energies of **6**, **9** and **10** (Table 2.7.5). The highest HOMO energy was calculated for compound **10** (–6.65 eV) which fits to its lowest oxidation onset potential of the oligomers. It is plausible that compound **10** has the lowest oxidation potential of our series as it contains the strongly electron-releasing diaminothiophene subunit.

2.7.3 Conclusion

In conclusion, we herein presented the first derivative of a novel class of conjugated polymers, namely poly(thiophene iminoborane). This species can be regarded, on the one hand, as a BN analogue of poly(thiophene vinylene) (PTV) and, on the other hand, as a hybrid of polythiophene and poly(iminoborane). In the course of our investigations on the synthesis of the required monomers, we devised a convenient method to access 2,5-diaminothiophene derivates. Our findings should offer new opportunities for the use of these extremely electron-rich species as versatile building blocks for further organic electronic materials in the future.
The series of the monodisperse oligomers and the polymer revealed systematic red-shifts in their low-energy absorption band with increasing chain length, thus evidencing effective π-conjugation over the B=N units. This is more pronounced than in the related BN congeners of PPV. We are now investigating the full potential of this novel class of polymers and extending our research to further B=N-linked polymer materials.

2.7.4 Experimental Section

General Procedures. All manipulations before the aqueous workup were performed under an atmosphere of dry argon using standard Schlenk techniques or in an MBraun glovebox. Solvents (dichloromethane (DCM), toluene, tetrahydrofuran (THF)) were dried and degassed by means of an Innovative Technology solvent purification system (SPS). $CDCl_3$ and toluene-d_8 for NMR spectroscopy as well as triethylamine (NEt_3), *n*-pentane and methanol were dried and degassed at reflux over CaH_2, Na or Mg respectively, and freshly distilled prior to use. Solvents for aqueous work-up (DCM, *n*-hexane), hydrogen chloride (2M in diethyl ether), 2-bromothiophene, 2,5-dibromothiophene, pentamethylsilazane, dichlorobis(triphenyl-phosphine)nickel(II) and lithium-bis(trimethylsilyl)amide were commercially purchased and used as received. Trimethylsilyl chloride was purified by inert-gas distillation. 2-Dibromoborylthiophene,[21] 2,5-bis(dibromoboryl)thiophene,[22] 2,4,6-triisopropylphenyllithium (TipLi),[23] were prepared according to literature procedures. NMR spectra were recorded at 25 °C on a Bruker Avance III HD spectrometer operating at 300 MHz, on a Bruker Avance 500 spectrometer operating at 500 MHz or on a Avance Neo I 600 operating at 600 MHz. Chemical shifts were referenced to residual protic impurities in the solvent (^1H) or the deuterio solvent itself (^{13}C) and reported relative to external $SiMe_4$ (^1H, ^{13}C, ^{29}Si), $BF_3{\cdot}OEt_2$ (^{11}B) standards. Mass spectra were obtained with the use of a Thermo Scientific Exactive Plus Orbitrap MS system employing liquid injection field desorption ionization (LIFDI) and atmospheric sample analysis probe (ASAP). Elemental analyses were performed on an Elementar vario MICRO cube elemental analyzer. UV–vis spectra were obtained using a Perkin Elmer LAMDA 465 UV/Vis spectrophotometer. Cyclic voltammetry experiments were performed using a Gamry

Interface 1010B potentiostat. A standard three-electrode cell configuration was employed using a platinum disk working electrode, a platinum wire counter electrode, and a silver wire, separated by a Vycor tip, serving as the reference electrode. Tetra-*n*-butylammonium hexafluorophosphate ([*n*-Bu_4N][PF_6]) was employed as the supporting electrolyte. The scans were referenced after the addition of a small amount of ferrocene as internal standard. The potentials are reported relative to the ferrocene/ferrocenium couple. All experiments were measured at room temperature under an argon atmosphere. GPC chromatograms were recorded on an Agilent 1260 Infinity II Series, equipped with two PSS SDV 3 µm 1000 Å (300x8 mm) columns and one PSS SDV 3 µm 10000 Å (300x8 mm) column, at 25 °C with a flow rate of 1 mL min^{-1} and calibrated against polystyrene standards. The samples were diluted in THF and toluene as internal standard. Detection was carried out via UV signal (λ = 254 nm). Evaluation of the chromatograms was performed by using WinGPC software.

Spectra. All spectra and other result figures are shown in Appendix 5.7.

Synthesis of *N,N*-bis(trimethylsilyl)-2-aminothiophene.[24] To a solution of 2-bromothiophene (3.46 g, 21.2 mmol, 1 equiv.) in toluene (130 mL) was added $(Ph_3P)_2NiCl_2$ (694 mg, 1.06 mmol, 0.05 equiv.) at room temperature. Subsequently lithium-bis(trimethylsilyl)amide (3.90 g, 23.3 mmol, 1.1 equiv.) was added and the reaction mixture was stirred at 100 °C overnight. After removal of all volatiles, the product was obtained by distillation *in vacuo* at 120 °C as yellowish oil (2.78 g, 11.4 mmol, 54 % yield). ^{1}H NMR (300 MHz, $CDCl_3$): δ = 6.78 (dd, *J* = 5.8 Hz, *J* = 1.4 Hz, 1H, Thi-C*H*), 6.74 (dd, *J* = 5.8 Hz, *J* = 3.5 Hz, 1H, Thi-C*H*), 6.29 (dd, *J* = 3.5 Hz, *J* = 1.4 Hz, 1H, Thi-C*H*), 0.11 (s, 18H, Si(CH_3)$_3$) ppm.

Synthesis of 1. To a solution of 2,5-dibromothiophene (9.68 g, 40.0 mmol, 1 equiv.) in toluene (480 mL) was added $(Ph_3P)_2NiCl_2$ (2.62 g, 2.00 mmol, 0.05 equiv.) at room temperature. Subsequently lithium-bis(trimethylsilyl)amide (14.7 g, 87.9 mmol, 2.2 equiv.) was added and the reaction was stirred at 100 °C overnight. The residue was filtered off and all volatiles were removed *in vacuo*. The product was purified by distillation *in vacuo* at 160 °C to give **1** as colorless solid (14.1 g, 35.1 mmol, 88 % yield). ^{1}H NMR (300 MHz, $CDCl_3$): δ = 5.94 (s, 2H, Thi-C*H*), 0.10 (s, 36H, Si(CH_3)$_3$) ppm; ^{13}C{^{1}H} NMR (76 MHz, $CDCl_3$): δ = 145.8 (s, Thi-*C*N(SiMe$_3$)$_2$), 120.0 (s, Thi-*C*H), 1.6 (s, Si-*C*H_3) ppm; ^{29}Si{^{1}H} NMR (60 MHz, $CDCl_3$): δ = 6.3 ppm; HRMS (LIFDI): m/z calcd.: 402.1827, found: 402.1827.

Synthesis of 2. To a solution of **1** (2.04 g, 5.06 mmol, 1 equiv.) in DCM (50 mL) was added a solution of HCl (2M in Et_2O, 40.8 mmol, 8 equiv.) at −78 °C. The suspension was stirred for 90

minutes at –78 °C. Subsequently the solvent and excess of HCl was removed *in vacuo* by warming the reaction mixture to room temperature. After washing with DCM (3 x 15 mL) and removing the volatiles *in vacuo*, **2** was obtained as off-white solid (771 mg, 4.12 mmol, 81 % yield). The product was insoluble in common NMR solvents, and its formation was confirmed by further reaction.

Synthesis of 3. To a solution of **1** (2.01 g, 5.00 mmol, 1 equiv.) in DCM (40 mL) was added a solution of HCl (2M in Et_2O, 35.0 mmol, 7 equiv.) at −78 °C. The resulting suspension was stirred for 2 h at –78 °C and NEt_3 (17.5 mL) was added. The mixture was stirred for 2 h at −78 °C and all volatiles were removed *in vacuo* by slowly warming the reaction mixture to room temperature. The salt formed in the reaction was precipitated in THF (10.0 mL) and filtered off and the residue was washed with THF (3 x 10 mL). All volatiles were removed *in vacuo* to give **3** as off-white solid (1.02 g, 3.95 mmol, 79 % yield). ^{1}H NMR (300 MHz, $CDCl_3$): δ = 5.78 (s, 2H, Thi-C*H*), 3.01 (s, 2H, Thi-N*H*) 0.17 (s, 18H, Si(CH_3)$_3$) ppm; ^{13}C{^{1}H} NMR (76 MHz, $CDCl_3$): δ = 140.3 (s, Thi-*C*NH(SiMe$_3$)$_2$), 110.5 (s, Thi-*C*H), 0.0 (s, Si-*C*H$_3$) ppm; ^{29}Si{^{1}H} NMR (60 MHz, $CDCl_3$): δ = 5.5 ppm; HRMS (LIFDI): m/z calcd.: 258.1037, found: 258.1035.

Alternative synthesis of 3. To a suspension of **2** (187 mg, 1 mmol, 1 equiv.) in DCM (10 mL) was added TMSCl (435 mg, 4 mmol, 4 equiv.) at –78 °C. Subsequently, NEt_3 (2 mL) was added and the reaction mixture was stirred at –78 °C for 90 minutes. All volatiles were removed *in vacuo* at −78 °C to room temperature. The formed salt was removed by filtration with THF (3 x 3 mL) and after solvent removal a red solid was obtained (214 mg, 0.83 mmol, 83 % yield).

Synthesis of 4. To a solution of 2-dibromoborylthiophene (5.12 g, 20.2 mmol, 1 equiv.) in toluene (30 mL) was added a solution of TipLi (4.59 g, 21.8 mmol, 1.1 equiv.) in toluene (30 mL) at 0 °C. The mixture was warmed to room temperature overnight. The formed salt was removed by filtration and all volatiles were removed *in vacuo*. After recrystallization in *n*-pentane at −30 °C, an orange solid was obtained (5.77 g, 15.3 mmol, 76 % yield). ^{1}H NMR (300 MHz, $CDCl_3$): δ = 8.03 (dd, *J* = 4.7 Hz, *J* = 1.0 Hz, 1H, Thi-C*H*), 7.89 (dd, *J* = 3.6 Hz, *J* = 1.0 Hz, 1H, Thi-C*H*), 7.31 (dd, *J* = 4.7 Hz, *J* = 3.6 Hz, 1H, Thi-C*H*), 6.99 (s, 2H, Tip-Ar-C*H*), 2.92 (sept, 1H, *p*-Tip-C*H*), 2.63 (sept, 2H, *o*-Tip-C*H*), 1.29 (d, 6H, *p*-Tip-CH_3), 1.24 (d, 6H, *o*-Tip-CH_3), 1.12 (d, 6H, *o*-Tip-CH_3) ppm; ^{11}B{^{1}H} NMR (96 MHz, $CDCl_3$): δ = 61.9 (s) ppm; ^{13}C{^{1}H} NMR (76 MHz, $CDCl_3$): δ = 150.2 (s, *p*-Tip-*C*), 149.2 (s, *o*-Tip-*C*), 143.3 (s, Thi-*C*H), 140.7 (s, Thi-*C*H), 129.9 (s, Thi-*C*H), 120.7 (s, Tip-*C*H$_{Ar}$), 35.6 (s, *o*-Tip-*C*H), 34.5 (s, *p*-Tip-*C*H), 24.5 (s, *o*-Tip-*C*H$_3$), 24.2 (s, *p*-Tip-*C*H$_3$), 24.0 (s, *o*-Tip-*C*H$_3$) ppm; HRMS (ASAP pos): m/z calcd.: 377.1105, found: 377.1096.

Synthesis of 5.[25] To a solution of *N,N*-bis(trimethylsilyl)-2-aminothiophene (1.26 g, 5.17 mmol, 1 equiv.) in DCM (42 mL) was added a solution of HCl (2M in Et_2O, 20.7 mmol, 4 equiv.) at −78 °C. The mixture was stirred for 90 minutes at –78°C. Subsequently the solvent and excess of HCl was removed *in vacuo* by warming the reaction mixture to room temperature. After washing with DCM (3 x 5 mL) and removing the volatiles *in vacuo*, an off-white solid was obtained (651 mg, 4.80 mmol, 93 % yield). The formation of the product was confirmed by generating 2-aminothiophene in presence of NEt_3 in $CDCl_3$. ^{1}H NMR (300 MHz, $CDCl_3$) of 2-aminothiophene: δ = 6.65 (dd, *J* = 5.5 Hz, *J* = 3.5 Hz, 1H, Thi-C*H*), 6.47 (dd, *J* = 5.5 Hz, *J* = 1.4 Hz, 1H, Thi-C*H*), 6.17 (dd, *J* = 3.5 Hz, *J* = 1.4 Hz, 1H, Thi-C*H*), 3.79 (br, 2H, NH_2) ppm.

Synthesis of 6. To a suspension of **5** (75.3 mg, 0.56 mmol, 1.1 equiv.) in DCM (3 mL) was added NEt_3 (0.55 mL) at −78 °C. After 15 min, a solution of **4** (190 mg, 0.50 mmol, 1 equiv.) in DCM (3 mL) was added and the reaction mixture was warmed to room temperature overnight. After removing the volatiles *in vacuo*, the residue was purified by column chromatography (neutral AlO_x, *n*-hexane/DCM 5:1) to obtain **6** as yellowish solid (137 mg, 0.35 mmol, 69 % yield). ^{1}H NMR (500 MHz, $CDCl_3$): δ = 7.64 (dd, *J* = 4.7 Hz, *J* = 0.9 Hz, 1H, B-Thi-C*H*), 7.37 (dd, *J* = 3.5 Hz, *J* = 0.9 Hz, 1H, B-Thi-C*H*), 7.18 (dd, *J* = 4.7 Hz, *J* = 3.5 Hz, 1H, B-Thi-C*H*), 7.12 (s, 1H, N*H*), 7.01 (s, 2H, Tip-Ar-C*H*), 6.63 (dd, *J* = 5.5 Hz, *J* = 3.7 Hz, 1H, N-Thi-C*H*), 6.51 (dd, *J* = 5.5 Hz, *J* = 1.3 Hz, 1H, N-Thi-C*H*), 6.29 (dd, *J* = 3.7 Hz, *J* = 1.3 Hz, 1H, N-Thi-C*H*), 2.94 (sept, 1H, *p*-Tip-C*H*), 2.71 (sept, 2H, *o*-Tip-C*H*), 1.31 (d, 6H, *p*-Tip-CH_3), 1.08 (d, 6H, *o*-Tip-CH_3), 1.05 (d, 6H, *o*-Tip-CH_3) ppm; ^{11}B{^{1}H} NMR (160 MHz, $CDCl_3$): δ = 39.8 (s) ppm; ^{13}C{^{1}H} NMR (126 MHz, $CDCl_3$): δ = 150.7 (s, *o*-Tip-*C*), 149.9 (s, *p*-Tip-*C*), 148.0 (s, N-Thi-C_{ipso}), 142.7 (br, B-Thi-C_{ipso}), 136.7 (s, B-Thi-*C*H), 133.8 (br, B-Tip-C_{ipso}), 131.7 (s, B-Thi-*C*H), 128.8 (s, B-Thi-*C*H), 124.8 (s, N-Thi-*C*H), 120.6 (s, Tip-CH_{Ar}), 116.4 (s, N-Thi-*C*H), 113.2 (s, N-Thi-*C*H), 35.0 (s, *o*-Tip-*C*H), 34.5 (s, *p*-Tip-*C*H), 25.0 (s, *o*-Tip-CH_3), 24.3 (s, *o*-Tip-CH_3), 24.3 (s, *p*-Tip-CH_3) ppm; HRMS (LIFDI): m/z calcd.: 395.1907, found: 395.1903; elem. anal. calcd. (%) for $C_{23}H_{30}BNS_2$: C 69.86, H 7.65, N 3.54, S 16.22; found: C 70.03, H 7.79, N 3.63, S 16.82; UV/Vis (THF): $\lambda_{abs,\,max}$ = 305 nm ($\varepsilon = 1.3 \cdot 10^4$ L mol^{-1} cm^{-1}).

Synthesis of 7.[26] To a suspension of **5** (616 mg, 4.54 mmol, 1 equiv.) in DCM (45 mL) was added NEt_3 (4.5 mL) at −78°C. The mixture was stirred for 1 hour at –78 °C. Subsequently, TMSCl (1.03 g, 9.48 mmol, 1.2 mL, 2.1 equiv.) was added and the mixture was warmed to room temperature after 20 minutes. After removing the volatiles *in vacuo*, the product was condensed and was obtained as a colorless liquid (714 mg, 4.17 mmol, 92 % yield). ^{1}H NMR (500 MHz, $CDCl_3$): δ = 6.69 (ddd, *J* = 5.6 Hz, *J* = 3.6 Hz, *J* = 0.3 Hz, 1H, Thi-C*H*), 6.44 (ddd, *J* = 5.6 Hz, *J* = 1.4 Hz, *J* = 0.3 Hz, 1H, Thi-C*H*), 6.08 (ddd, *J* = 3.6 Hz, *J* = 1.4 Hz, *J* =

0.6 Hz, 1H, Thi-C*H*), 3.60 (s, 1H, N*H*), 0.25 (s, 9H, Si(CH_3)$_3$) ppm; ^{13}C{^{1}H} NMR (126 MHz, $CDCl_3$): δ = 152.2 (s, Thi-*C*NHSiMe$_3$), 126.3 (s, Thi-*C*H), 111.6 (s, Thi-*C*H), 108.3 (s, Thi-*C*H), −0.2 (s, Si-*C*H$_3$) ppm; ^{29}Si{^{1}H} NMR (99 MHz, $CDCl_3$): δ = 6.2 ppm.

Synthesis of 8. To a suspension of 2,5-bis(dibromoboryl)thiophene (8.47 g, 20.0 mmol, 1 equiv.) in toluene (40 mL) was added a solution of TipLi (8.82 g, 42.0 mmol, 2.1 equiv.) in toluene (40 mL) at 0 °C. The mixture was warmed to room temperature overnight. The formed salt was removed by filtration and all volatiles were removed *in vacuo*. After recrystallization in *n*-pentane at −30 °C, an off-white solid was obtained (6.87 g, 10.2 mmol, 51 % yield). ^{1}H NMR (300 MHz, $CDCl_3$): δ = 8.06 (s, 2H, Thi-C*H*), 6.98 (s, 4H, Tip-Ar-C*H*), 2.91 (sept, 2H, *p*-Tip-C*H*), 2.55 (sept, 4H, *o*-Tip-C*H*), 1.28 (d, 12H, *p*-Tip-CH_3), 1.23 (d, 12H, *o*-Tip-CH_3), 1.09 (d, 12H, *o*-Tip-CH_3) ppm; ^{11}B{^{1}H} NMR (96 MHz, $CDCl_3$): δ = 61.4 (br) ppm; ^{13}C{^{1}H} NMR (76 MHz, $CDCl_3$): δ = 150.6 (s, *p*-Tip-*C*), 149.1 (s, *o*-Tip-*C*), 143.2 (s, Thi-*C*H), 120.9 (s, Tip-*C*H$_{Ar}$), 36.0 (s, *o*-Tip-*C*H), 34.4 (s, *p*-Tip-*C*H), 24.5 (s, *o*-Tip-*C*H$_3$), 24.1 (s, *p*-Tip-*C*H$_3$), 24.0 (s, *o*-Tip-*C*H$_3$) ppm; HRMS (LIFDI): m/z calcd.: 670.2003, found: 670.1984.

Synthesis of 9. To a solution of **8** (337 mg, 0.50 mmol, 1 equiv.) in DCM (4 mL) was added a solution of **7** (193 mg, 1.13 mmol, 2.3 equiv.) in DCM (3 mL) at room temperature. After stirring the mixture overnight, all volatiles were removed *in vacuo*. The residue was purified by column chromatography (neutral AlO_x, *n*-hexane/DCM 2:1) to obtain **9** as off-white solid (296 mg, 0.42 mmol, 85 % yield). ^{1}H NMR (500 MHz, $CDCl_3$): δ = 7.38 (s, 2H, B-Thi-C*H*), 7.18 (s, 2H, N*H*), 7.00 (s, 4H Tip-Ar-C*H*), 6.63 (dd, *J* = 5.5 Hz, *J* = 3.7 Hz, 2H, N-Thi-C*H*), 6.52 (dd, *J* = 5.5 Hz, *J* = 1.4 Hz, 2H, N-Thi-C*H*), 6.28 (dd, *J* = 3.7 Hz, *J* = 1.4 Hz, 2H, N-Thi-C*H*), 2.94 (sept, 2H, *p*-Tip-C*H*), 2.71 (sept, 4H, *o*-Tip-C*H*), 1.31 (d, 12H, *p*-Tip-CH_3), 1.08 (d, 12H, *o*-Tip-CH_3), 1.03 (d, 12H, *o*-Tip-CH_3) ppm; ^{11}B{^{1}H} NMR (160 MHz, $CDCl_3$): δ = 39.8 (br) ppm; ^{13}C{^{1}H} NMR (126 MHz, $CDCl_3$): δ = 150.7 (s, *o*-Tip-*C*), 149.9 (s, *p*-Tip-*C*), 149.4 (br, B-Thi-*C*$_{ipso}$), 147.9 (s, N-Thi-*C*$_{ipso}$), 137.5 (s, B-Thi-*C*H), 133.9 (br, B-Tip-*C*$_{ipso}$), 124.8 (s, N-Thi-*C*H), 120.6 (s, Tip-*C*H$_{Ar}$), 116.5 (s, N-Thi-*C*H), 113.4 (s, N-Thi-*C*H), 35.0 (s, *o*-Tip-*C*H), 34.5 (s, *p*-Tip-*C*H), 25.0 (s, *o*-Tip-*C*H$_3$), 24.3 (s, *p*-Tip-*C*H$_3$), 24.3 (s, *o*-Tip-*C*H$_3$) ppm; HRMS (LIFDI): m/z calcd.: 706.3787, found: 706.3779; elem. anal. calcd. (%) for $C_{42}H_{56}B_2N_2S_3$: C 71.38, H 7.99, N 3.96, S 13.61; found: C 71.47, H 8.12, N 4.01, 13.83; UV/Vis (THF): $\lambda_{abs,\ max}$ = 340 nm ($\varepsilon = 3.0 \cdot 10^4$ L mol^{-1} cm^{-1}).

Synthesis of 10. To a solution of **4** (377 mg, 1.00 mmol, 2 equiv.) in DCM (3 mL) was added a solution of **3** (129 mg, 0.50 mmol, 1 equiv.) in DCM (2 mL) at room temperature. The mixture was stirred overnight and all volatiles were removed *in vacuo*. The crude product was purified by column chromatography (neutral AlO_x, *n*-hexane/DCM 4:1) and recrystallised in *n*-pentane

at −30 °C to give **10** as off-white solid (244 mg, 0.33 mmol, 66 % yield). ^{1}H NMR (500 MHz, $CDCl_3$): δ = 7.58 (dd, *J* = 4.7 Hz, *J* = 0.84 Hz, 2H, B-Thi-C*H*), 7.25 (dd, *J* = 3.6 Hz, *J* = 0.95 Hz, 2H, B-Thi-C*H*), 7.13 (dd, *J* = 4.7 Hz, *J* = 3.5 Hz, 2H, B-Thi-C*H*), 6.96 (s, 4H Tip-Ar-C*H*), 6.68 (s, 2H, N*H*), 5.68 (s, 2H, N-Thi-C*H*), 2.93 (sept, 2H, *p*-Tip-C*H*), 2.65 (sept, 4H, *o*-Tip-C*H*), 1.31 (d, 12H, *p*-Tip-CH_3), 1.03 (d, 12H, *o*-Tip-CH_3), 1.01 (d, 12H, *o*-Tip-CH_3) ppm; ^{11}B{^{1}H} NMR (160 MHz, $CDCl_3$): δ = 39.0 (br) ppm; ^{13}C{^{1}H} NMR (126 MHz, $CDCl_3$): δ = 150.5 (s, *o*-Tip-*C*), 149.4 (s, *p*-Tip-*C*), 142.9 (br, B-Thi-C_{ipso}), 138.5 (s, N-Thi-C_{ipso}), 136.3 (s, B-Thi-*C*H), 134.0 (br, B-Tip-C_{ipso}), 131.4 (s, B-Thi-*C*H), 128.6 (s, B-Thi-*C*H), 120.4 (s, Tip-CH_{Ar}), 111.8 (s, N-Thi-*C*H), 34.9 (s, *o*-Tip-*C*H), 34.4 (s, *p*-Tip-*C*H), 24.9 (s, *o*-Tip-*C*H_3), 24.5 (s, *o*-Tip-*C*H_3), 24.3 (s, *p*-Tip-*C*H_3) ppm; HRMS (LIFDI): m/z calcd.: 706.3787, found: 706.3777; elem. anal. calcd. (%) for $C_{44}H_{64}B_2N_2S_3$: C 71.53, H 8.73, N 3.79, S 13.02; found: C 71.76, H 8.39, N 3.73, 13.27; UV/Vis (THF): $\lambda_{abs,\ max}$ = 348 nm ($\varepsilon = 2.0 \cdot 10^4$ L mol^{-1} cm^{-1}).

Synthesis of 11. To a stirred suspension of **8** (168 mg, 0.25 mmol, 1 equiv.) in DCM (2.5 mL) was added a solution of **3** (66.4 mg, 0.25 mmol, 1 equiv.) in DCM (1.0 mL) at room temperature. The mixture was stirred for 2 d and $TMSNMe_2$ (0.25 mL) was added. The mixture was stirred overnight and all volatiles were removed *in vacuo*. The crude product was solved in THF (2.5 mL) and precipitated into cooled (−78 °C) methanol (25 mL). The supernatant liquid was removed by filtration at −78 °C and dried *in vacuo*. The precipitation process was repeated for complete purification to give **11** as a pale yellow solid. (63.4 mg, 38 % yield). ^{1}H NMR (500 MHz, $CDCl_3$): δ = 7.20 (m, 2H, B-Thi-C*H*), 6.94 (m, 4H Tip-Ar-C*H*), 6.70 (m, 2H, N*H*), 5.64 (m, 2H, N-Thi-C*H*), 2.92 (m, 2H, *p*-Tip-C*H*), 2.61 (m, 4H, *o*-Tip-C*H*), 1.29 (m, 12H, *p*-Tip-CH_3), 1.01 (m, 12H, *o*-Tip-CH_3), 0.96 (m, 12H, *o*-Tip-CH_3) ppm; ^{11}B{^{1}H} NMR (160 MHz, $CDCl_3$): δ = to broad; ^{13}C{^{1}H} NMR (126 MHz, $CDCl_3$): δ = 150.5 (s, *o*-Tip-*C*), 149.4 (s, *p*-Tip-*C*), 149.3 (br, B-Thi-C_{ipso}), 138.5 (s, N-Thi-C_{ipso}), 137.2 (s, B-Thi-*C*H), 134.0 (br, B-Tip-C_{ipso}), 120.4 (s, Tip-CH_{Ar}), 111.9 (s, N-Thi-*C*H), 34.9 (s, *o*-Tip-*C*H), 34.3 (s, *p*-Tip-*C*H), 24.9 (s, *o*-Tip-*C*H_3), 24.4 (s, *o*-Tip-*C*H_3), 24.3 (s, *p*-Tip-*C*H_3) ppm; GPC (in THF, vs. polystyrene, detection by UV-Vis signal): M_n = 14 231 Da; M_w = 23 040 Da; UV/Vis (THF): $\lambda_{abs,\ max}$ = 388 nm ($\varepsilon = 1.6 \cdot 10^4$ L mol^{-1} cm^{-1}).

Crystallographic data

Crystals suitable for single-crystal X-ray diffraction were selected, coated in perfluoropolyether oil, and mounted on MiTeGen sample holders. Diffraction data were collected on Bruker X8 Apex II 4-circle diffractometers with CCD area detectors using Mo-Kα radiation. The crystals were cooled using an Oxford Cryostreams low-temperature device. Data were collected at 100 K. The images were processed and corrected for Lorentz-polarization effects and absorption as implemented in the Bruker software packages. The structures were solved using

the intrinsic phasing method (SHELXT)[27] and Fourier expansion technique. All non-hydrogen atoms were refined in anisotropic approximation, with hydrogen atoms 'riding' in idealized positions, by full-matrix least squares against F^2 of all data, using SHELXL[28] software and the SHELXLE graphical user interface.[29]

Table 2.7.1. X-ray crystallographic information.

No.	**1**	**6**	**9**	**10**
CCDC number	2251073	2251074	2251076	2251075
Size / mm	0.242 x 0.256 x 0.353	0.195 x 0.224 x 0.296	0.153 x 0.168 x 0.420	0.170 x 0.206 x 0.367
Empiric Formula	$C_{16}H_{38}N_2SSi_4$	$C_{23}H_{30}BNS_2$	$C_{90}H_{126}B_4N_4S_6$	$C_{42}H_{56}B_2N_2S_3$
M / g mol^{-1}	402.90	395.41	1499.54	706.68
Crystal system	triclinic	monoclinic	triclinic	triclinic
Space group	P -1	P 21/n	P -1	P -1
a / Å	6.5623(11)	9.859(3)	14.405(4)	9.306(2)
b / Å	12.287(4)	17.534(5)	18.274(5)	14.618(3)
c / Å	16.576(5)	12.873(6)	18.671(5)	15.880(3)
α / deg	72.790(14)	90	68.77(2)	76.449(13)
β / deg	83.609(17)	97.12(3)	82.359(13)	78.815(15)
γ / deg	79.86(3)	90	76.084(16)	77.766(19)
V / Å^3	1254.2(6)	2208.3(14)	4441(2)	2028.6(7)
Z	2	4	2	2
μ / mm^{-1}	0.322	0.249	0.199	0.214
T / K	100(2)	100(2)	100(2)	100(2)
$\theta_{min,max}$	1.289, 28.407	1.972, 27.132	1.172, 28.403	1.334, 28.355
Completeness	0.982	0.999	0.993	0.997
Reflections: total / independent	6181, 5170	4878, 4107	22158, 14104	10122, 7363
R_{int}	0.0344	0.0475	0.0594	0.0455
Final R1 and wR2	0.0485, 0.1218	0.0452, 0.1180	0.0754, 0.2237	0.0555, 0.1498
Largest peak and hole / e Å^{-3}	1.064, –0.631	0.820, –0.344	1.188, –1.003	0.607, –0.417
ρ_{calc} / g cm^{-3}	1.067	1.189	1.121	1.157

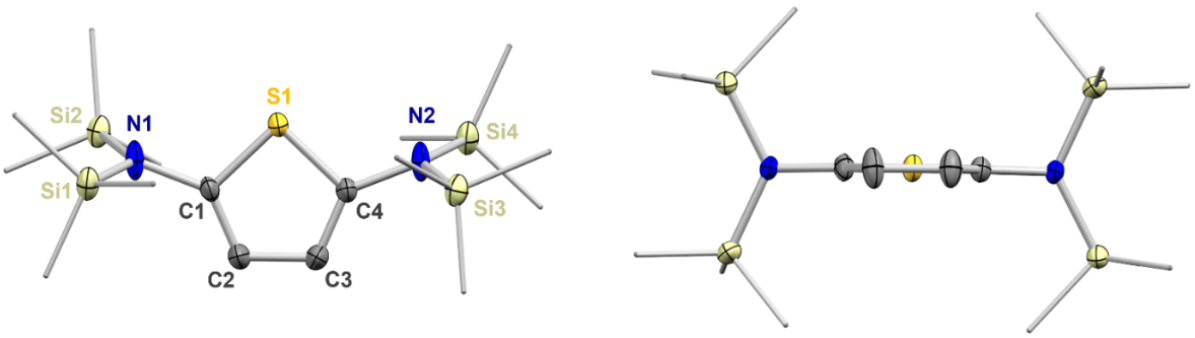

Figure 2.7.5. Molecular structure of **1** in the solid state by single-crystal X-ray diffraction (H atoms and disorders of the thiophene unit omitted for clarity). Structure shown perpendicular (left) and parallel (right) to the thiophene backbone. All ellipsoids are drawn at the 50% probability level.

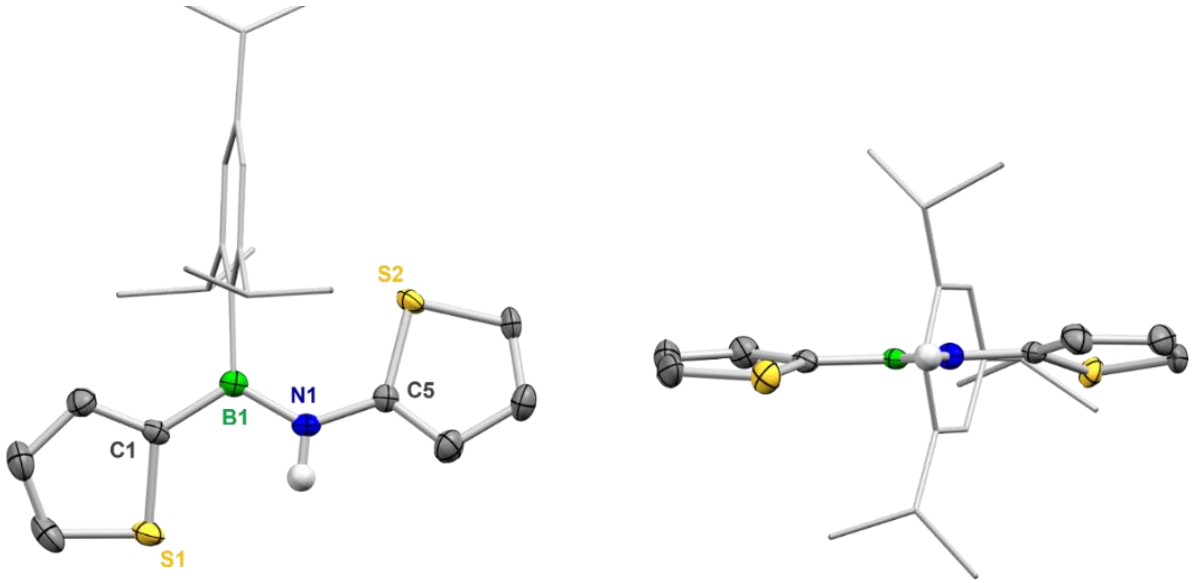

Figure 2.7.6. Molecular structure of **6** in the solid state by single-crystal X-ray diffraction (H atoms and disorders of the thiophene unit and Tip group omitted for clarity). Structure shown perpendicular (left) and parallel (right) to the thiophene backbone. All ellipsoids are drawn at the 50% probability level.

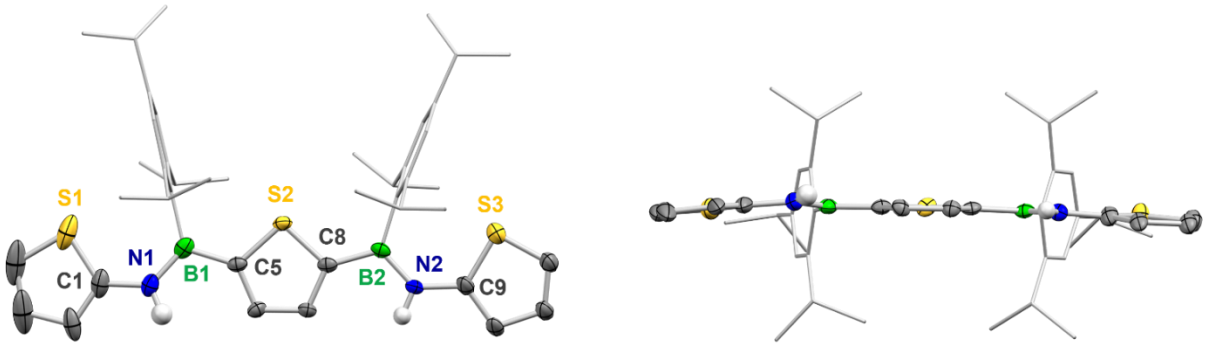

Figure 2.7.7. Molecular structure of **9** (conformer I) in the solid state by single-crystal X-ray diffraction (H atoms and disorders of the thiophene units and Tip groups omitted for clarity). Structure shown perpendicular (left) and parallel (right) to the thiophene backbone. All ellipsoids are drawn at the 50% probability level.

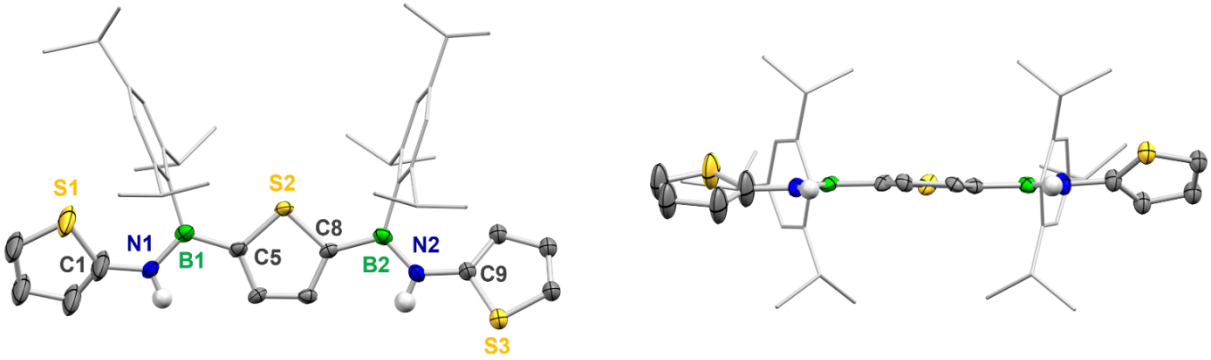

Figure 2.7.8. Molecular structure of **9** (conformer II) in the solid state by single-crystal X-ray diffraction (H atoms and disorders of the thiophene units and Tip groups omitted for clarity). Structure shown perpendicular (left) and parallel (right) to the thiophene backbone. All ellipsoids are drawn at the 50% probability level.

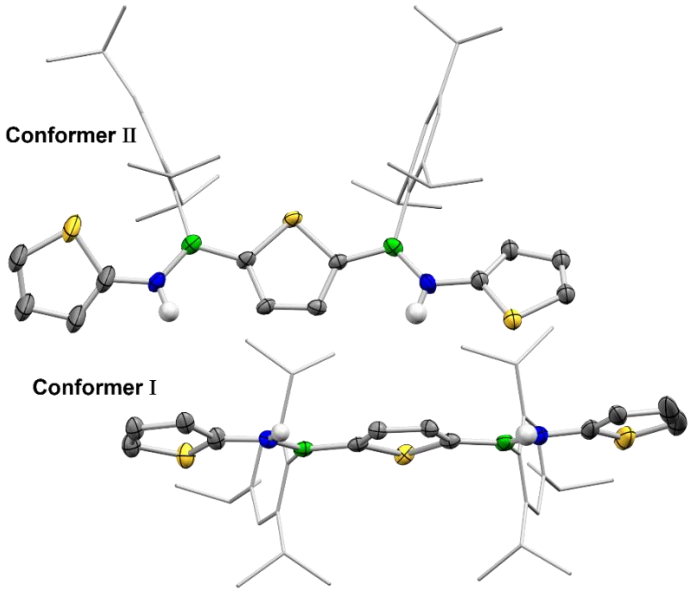

Figure 2.7.9. Molecular structure of **9** (conformer I and II in one unit cell) in the solid state by single-crystal X-ray diffraction (H atoms and disorders of the thiophene units and Tip groups omitted for clarity). All ellipsoids are drawn at the 50% probability level.

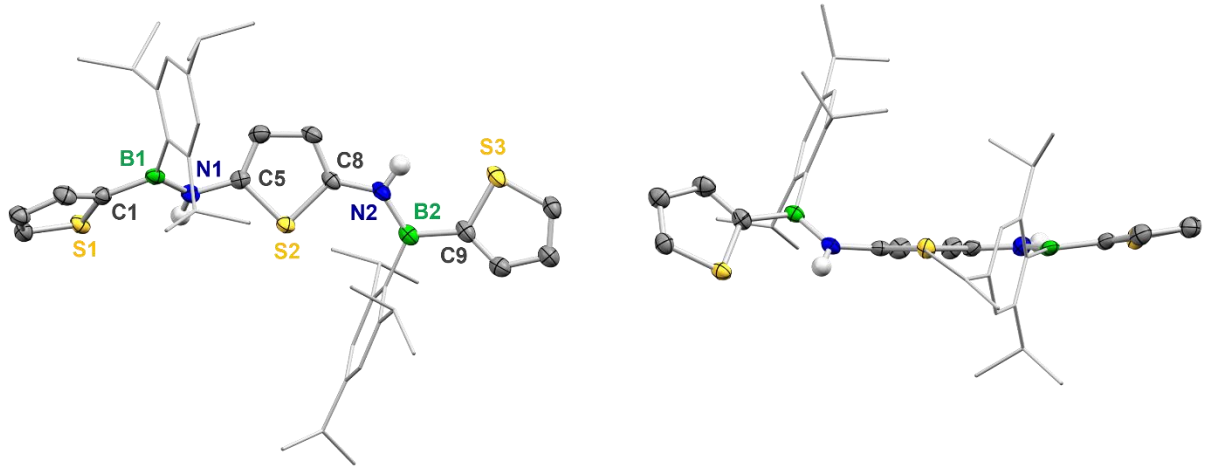

Figure 2.7.10. Molecular structure of **10** in the solid state by single-crystal X-ray diffraction (H atoms and disorders of the thiophene units and Tip groups omitted for clarity). Structure shown perpendicular (left) and parallel (right) to the thiophene backbone. All ellipsoids are drawn at the 50% probability level.

Table 2.7.2. Selected values from the crystallographic data.

	6	**9** (I)	**9** (II)	**10**
∑∠Twist thiophene and BN planes (defined by C_2BNC plane)	Thi1-BN: 10.4° BN-Thi2: 12.4°	Thi1-NB: 6.2° NB-Thi2: 4.8° Thi2-BN: 2.5° BN-Thi3: 3.0°	Thi1-NB: 7.3° NB-Thi2: 4.4° Thi2-BN: 2.9° BN-Thi3: 34.0°	Thi1-BN: 16.9° BN-Thi2: 50.1° Thi2-NB: 9.1° NB-Thi3: 8.9°
∑∠Twist thiophene planes	Thi1-Thi2: 22.4°	Thi1-Thi2: 6.4° Thi2-Thi3: 3.4° Thi1-Thi3: 9.7°	Thi1-Thi2: 8.3° Thi2-Thi3: 33.1° Thi1-Thi3: 41.4°	Thi1-Thi2: 66.9° Thi2-Thi3: 9.4° Thi1-Thi3: 71.1°
B−N distances [Å]	B1–N1: 1.408(2)	B1–N1: 1.407(4) B2–N2: 1.410(4)	N1–B1: 1.410(4) N2–B2: 1.401(4)	B1–N1: 1.412(3) B2–N2: 1.410(3)

Photophysical properties

Table 2.7.3. Photophysical properties of compound **6**, **9**, **10**, **11**, **PhBNPh***, **PhNBPhBNPh***, **PhBNPhNB*** and **BN-PPV*** in THF.

	$\lambda_{abs,\ max}$ **[nm]**	**ε [10^4 L mol^{-1} cm^{-1}]**		$\lambda_{abs,\ max}$ **[nm]**	**ε [10^4 L mol^{-1} cm^{-1}]**
6	305	1.3	**PhBNPh***	272	1.6
9	340	3.0	**PhNBPhBNPh***	298	2.6
10	348	2.0	**PhBNPhNB***	308	1.9
11	388	1.5	**BN-PPV***	341	2.2
*In THF measured phenylene analogues from literature[15]					

Computational information

DFT geometry optimizations were carried out with the Gaussian 16, Revision C.01 program package[30] using the ωB97X-D[31] functional in combination with the def2-SVP[32] basis set in gas phase. The equilibrium geometries were characterized as minima by frequency computations. Vertical singlet excitations were calculated by means of time-dependent DFT with the program ORCA 5.0.3[33] using the ωB97X-D3[34] functional with optimal tuned ω parameters[35], the def2-SVP[32] basis set and the CPCM[36] solvation model mimicking tetrahydrofuran (ε = 7.58) as solvent.

Table 2.7.4. Results from TD-DFT calculations for the compounds **6**, **9** and **10**.

Compound	λ / nm	Oscillator strength *f*	Orbital contributions	$\|c\|^2$ / %
6	286.6	0.5928	**HOMO → LUMO**	88.4
9	320.8	1.1693	**HOMO → LUMO**	85.8
10	327.4	0.8883	**HOMO → LUMO**	89.6
Trimer	340.9	1.1529	**HOMO → LUMO** **HOMO → LUMO+1**	74.2 12.1

Table 2.7.5. Calculated HOMO and LUMO energies for the compounds **6**, **9** and **10**.

Compound	HOMO energy (eV)	LUMO energy (eV)	HOMO-LUMO gap (eV)	LUMO+1 energy (eV)	HOMO-LUMO+1 gap (eV)
6	-7.3487	0.2782	7.6269		
9	-6.9712	-0.2684	6.7028		
10	-6.6506	0.0436	6.6942		
Trimer	-6.5069	-0.262	6.2449	0.0984	6.6053

Frontier orbitals

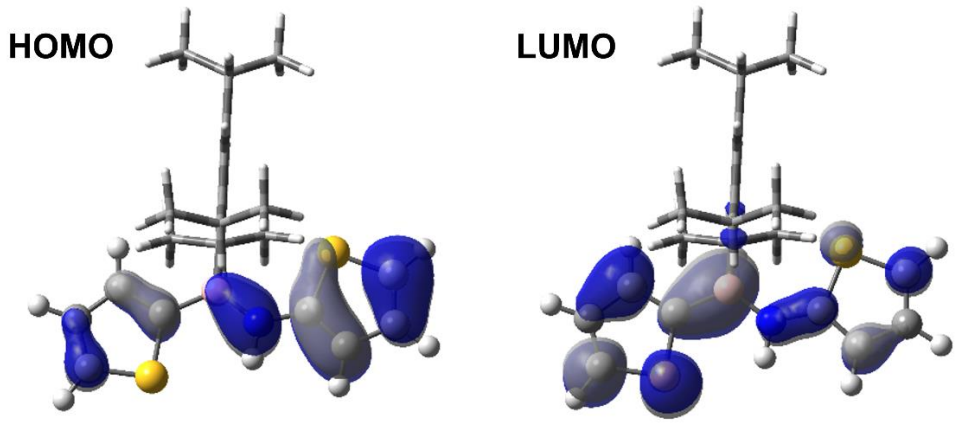

Figure 2.7.11. Calculated frontier orbitals (isovalue 0.03 a.u.) of **6** (ω_TB97X-D3/def2-SVP, CPCM(THF), ω_T = 0.17).

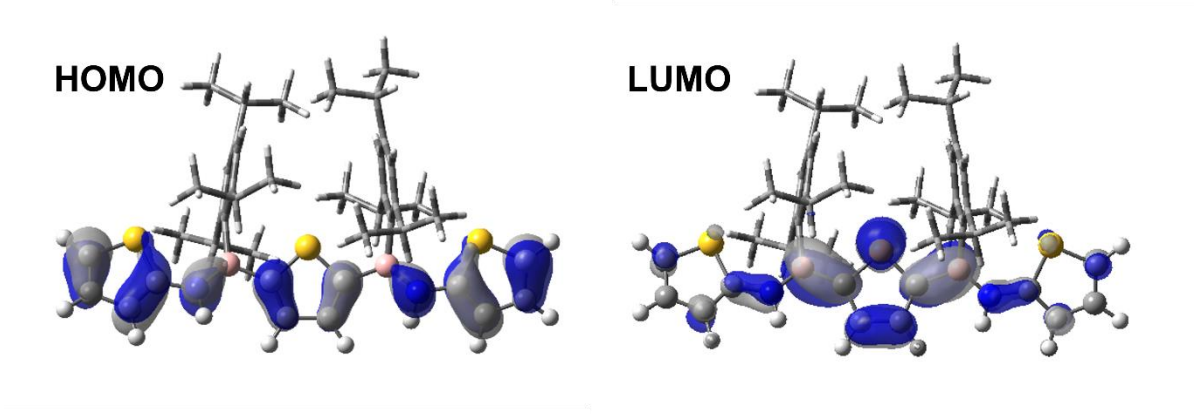

Figure 2.7.12. Calculated frontier orbitals (isovalue 0.03 a.u.) of **9** (ω_TB97X-D3/def2-SVP, CPCM(THF), ω_T = 0.14).

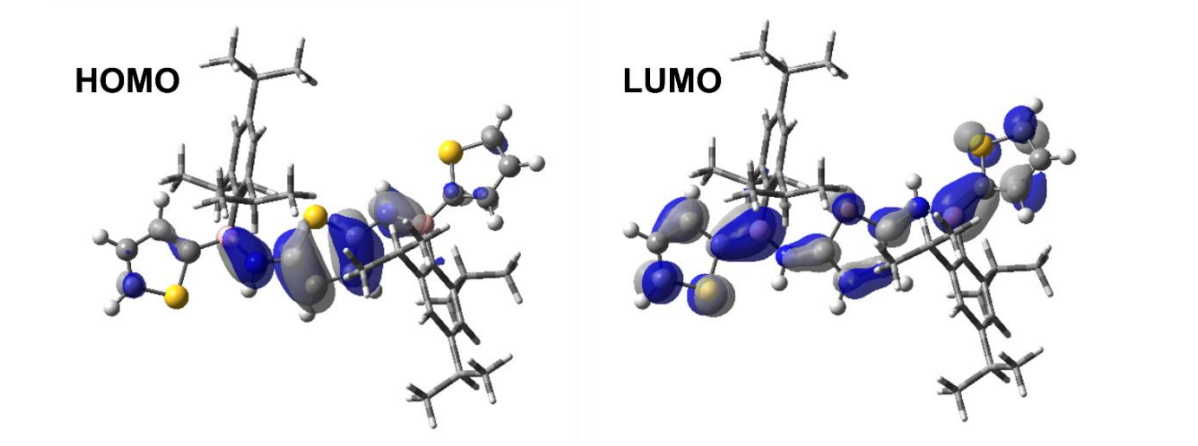

Figure 2.7.13. Calculated frontier orbitals (isovalue 0.03 a.u.) of **10** (ω_TB97X-D3/def2-SVP, CPCM(THF), ω_T = 0.14).

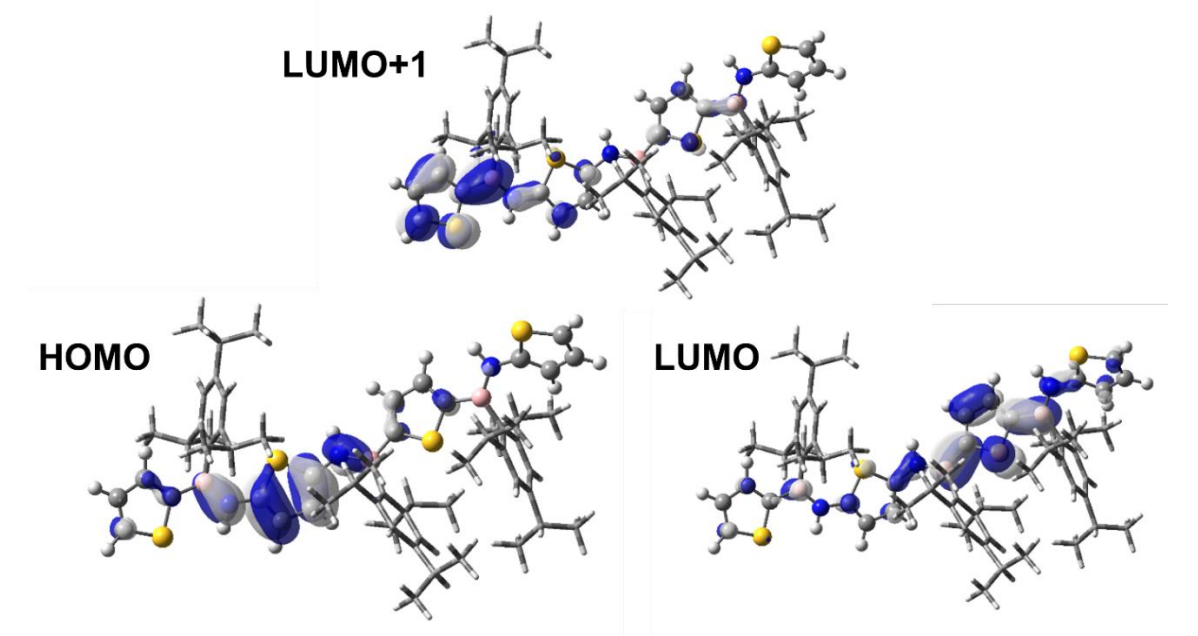

Figure 2.7.14. Calculated frontier orbitals (isovalue 0.03 a.u.) of **Trimer** (ω_TB97X-D3/def2-SVP, CPCM(THF), ω_T = 0.125).

2.7.5 References

[1] a) T. Mikie, I. Osaka, *J. Mater. Chem. C* **2020**, *8*, 14262–14288; b) J. Li, K. Pu, *Chem. Soc. Rev.* **2019**, *48*, 38–71; c) O. Inganäs, *Adv. Mater.* **2018**, *30*, 1800388; d) T. M. Swager, *Macromolecules* **2017**, *50*, 4867–4886.

[2] a) J. Banerjee, K. Dutta, *Chem. Pap.* **2021**, *75*, 5139–5151; b) C. Li, M. Liu, N. G. Pschirer, M. Baumgarten, K. Müllen, *Chem. Rev.* **2010**, *110*, 6817–6855.

[3] a) G. Zhang, F. R. Lin, F. Qi, T. Heumüller, A. Distler, H.-J. Egelhaaf, N. Li, P. C. Y. Chow, C. J. Brabec, A. K.-Y. Jen, H.-L. Yip, *Chem. Rev.* **2022**, *122*, 14180−14274; b) Q. Wang, Y. Qin, M. Li, L. Ye, Y. Geng, *Adv. Energy Mater.* **2020**, *10*, 2002572; c) F. A. Larik, M. Faisal, A. Saeed, Q. Abbas, M. A. Kazi, N. Abbas, A. A. Thebo, D. M. Khan, P. A. Channar, *J. Mater. Sci.: Mater. Electron.* **2018**, *29*, 17975–18010; d) T. P. Kaloni, P. K. Giesbrecht, G. Schreckenbach, M. S. Freund, *Chem. Mater.* **2017**, *29*, 10248–10283; e) J. Qian, X. Li, D. J. Lunn, J. Gwyther, Z. M. Hudson, E. Kynaston, P. A. Rupar, M. A. Winnik, I. Manners, *J. Am. Chem. Soc.* **2014**, *136*, 4121–4124.

[4] a) G. Manecke, M. Hartel, G. Koßmehl, *Makromol. Chem.* **1970**, *131*, 15–36; b) R. Toyoshima, K. Akagi, H. Shirakawa, *Synth. Met.* **1997**, *84*, 431–432.

[5] a) Q. Wang, X. Dong, M. He, M. Li, H. Tian, J. Liu, Y. Geng, *Polymer* **2018**, *140*, 89−95; b) C. Yang, S. Zhang, J. Hou, *Aggregate* **2022**, *3*, e111; c) P. Bi, J. Ren, S. Zhang, J. Wang, Z. Chen, M. Gao, Y. Cui, T. Zhang, J. Qin, Z. Zheng, L. Ye, X. Hao, J. Hou, *Nano Energy* **2022**, *100*, 107463; d) L. Ma, S. Zhang, J. Ren, G. Wang, J. Li, Z. Chen, H. Yao, J. Hou, *Angew. Chem. Int. Ed.* **2023**, *62*, e202214088.

[6] a) F. Vidal, F. Jäkle, *Angew. Chem. Int. Ed.* **2019**, *58*, 5846–5870; b) H. Helten in *Encyclopedia of Inorganic and Bioinorganic Chemistry* (Ed.: R. A. Scott), Wiley, Chichester, **2017**; c) A. M. Priegert, B. W. Rawe, S. C. Serin, D. P. Gates, *Chem. Soc. Rev.* **2016**, *45*, 922–953; d) X. He, T. Baumgartner, *RSC Adv.* **2013**, *3*, 11334–11350.

[7] E.g., for main group analogues of PPV or respective oligomers, see: a) V. A. Wright, D. P. Gates, *Angew. Chem. Int. Ed.* **2002**, *41*, 2389–2392; b) R. C. Smith, J. D. Protasiewicz, *J. Am. Chem. Soc.* **2004**, *126*, 2268–2269; c) I. Bejan, D. Scheschkewitz, *Angew. Chem. Int. Ed.* **2007**, *46*, 5783–5786; d) A. Fukazawa, Y. Li, S. Yamaguchi, H. Tsuji, K. Tamao, *J. Am. Chem. Soc.* **2007**, *129*, 14164-14165; e) L. Li, T. Matsuo, D. Hashizume, H. Fueno, K. Tanaka, K. Tamao, *J. Am. Chem. Soc.* **2015**, *137*, 15026−15035; for model compounds for silicon analogues of PTV, see: f) N. Hayakawa, S. Nishimura, N. Kazusa, N. Shintani, T. Nakahodo, H. Fujihara, M. Hoshino, D. Hashizume, T. Matsuo, *Organometallics* **2017**, *36*, 3226−3233; g) T. Matsuo, N. Hayakawa, *Sci. Technol. Adv. Mater.* **2018**, *19*, 108–129.

[8] a) H. Helten in *Comprehensive Organometallic Chemistry IV*, *Vol. 14* (Eds.: D. O'Hare, K. Meyer, G. Parkin), Elsevier, **2022**, pp. 71−134; b) X. Yin, J. Liu, F. Jäkle, *Chem. Eur. J.* **2021**, *27*, 2973–2986; c) H. Helten, *Chem. Asian J.* **2019**, *14*, 919–935; d) Y. Ren, F. Jäkle in *Main Group Strategies towards Functional Hybrid Materials* (Eds.: T. Baumgartner, F. Jäkle), Wiley: Hoboken, **2017**; pp 79−110; e) F. Jäkle, *Top. Organomet. Chem.* **2015**, *49*, 297–325; f) F. Jäkle, *Chem. Rev.* **2010**, *110*, 3985–4022.

[9] Selected examples: a) A. Sundararaman, M. Victor, R. Varughese, F. Jäkle, *J. Am. Chem. Soc.* **2005**, *127*, 13748–13749; b) A. Nagai, T. Murakami, Y. Nagata, K. Kokado, Y. Chujo, *Macromolecules* **2009**, *42*, 7217–7220; c) H. Li, F. Jäkle, *Angew. Chem. Int. Ed.* **2009**, *48*, 2313–2316; *Angew. Chem.* **2009**, *121*, 2349–2352; d) A. Lorbach, M. Bolte, H. Li, H.-W. Lerner, M. C. Holthausen, F. Jäkle, M. Wagner, *Angew. Chem. Int. Ed.* **2009**, *48*, 4584–4588; e) X. Yin, F. Guo, R. A. Lalancette, F. Jäkle, *Macromolecules* **2016**, *49*, 537–546; f) K. Hu, Z. Zhang, J. Burke, Y. Qin, *J. Am. Chem. Soc.* **2017**, *139*, 11004–11007; g) A. Lik, L. Fritze, L. Müller, H. Helten, *J. Am. Chem. Soc.* **2017**, *139*, 5692–5695; h) A. Lik, S. Jenthra, L. Fritze, L. Müller, K.-N. Truong, H. Helten, *Chem. Eur. J.* **2018**, *24*, 11961–11972; i) B. Meng, Y. Ren, J. Liu, F. Jäkle, L. Wang, *Angew. Chem. Int. Ed.* **2018**, *57*, 2183–2187; j) Y. Adachi, Y. Ooyama, Y. Ren, X. Yin, F. Jäkle, J. Ohshita, *Polym. Chem.* **2018**, *9*, 291–299; k) L. Fritze, M. Fest, A. Helbig, T. Bischof, I. Krummenacher, H. Braunschweig, M. Finze, H. Helten, *Macromolecules* **2021**, *54*, 7653−7665.

[10] a) X. Chen, D. Tan, D.-T. Yang, *J. Mater. Chem. C* **2022**, 10, 13499–13532; b) C. R. McConnell, S.-Y. Liu, *Chem. Soc. Rev.* **2019**, *48*, 3436–3453; c) Z. X. Giustra, S.-Y. Liu, *J. Am. Chem. Soc.* **2018**, *140*, 1184–1194; d) G. Bélanger-Chabot, H. Braunschweig, D. K. Roy, *Eur. J. Inorg. Chem.* **2017**, 4353–4368; e) H. Helten, *Chem. Eur. J.* **2016**, *22*, 12972–12982; f) M. M. Morgan, W. E. Piers, *Dalton Trans.* **2016**, *45*, 5920–5924; g) X.-Y. Wang, J.-Y. Wang, J. Pei, *Chem. Eur. J.* **2015**, *21*, 3528–3539; h) P. G. Campbell, A. J. V. Marwitz, S.-Y. Liu, *Angew. Chem. Int. Ed.* **2012**, *51*, 6074–6092; i) M. J. D. Bosdet, W. E. Piers, *Can. J. Chem.* **2009**, *87*, 8–29; for BN isosteres of non-conjugated compounds, see, e.g.: j) A. Staubitz, A. P. M. Robertson, M. E. Sloan, I. Manners, *Chem. Rev.* **2010**, *110*, 4023–4078; k) H. C. Johnson, T. N. Hooper, A. S. Weller, *Top. Organomet. Chem.* **2015**, *49*, 153–220.

[11] Selected recent examples: a) K. Matsui, S. Oda, K. Yoshiura, K. Nakajima, N. Yasuda, T. Hatakeyama, *J. Am. Chem. Soc.* **2018**, *140*, 1195–1198; b) A. S. Scholz, J. G. Massoth, M. Bursch, J.-M. Mewes, T. Hetzke, B. Wolf, M. Bolte, H.-W. Lerner, S. Grimme, M. Wagner, *J. Am. Chem. Soc.* **2020**, *142*, 11072–11083; c) Y. Chen, W. Chen, Y. Qiao, X. Lu, G. Zhou, *Angew. Chem. Int. Ed.* **2020**, *59*, 7122–7130; d) K. Ota, R. Kinjo, *J. Am. Chem. Soc.* **2021**, *143*, 11152–11159; e) M. Chen, K. S. Unikela, R. Ramalakshmi, B. Li, C. Darrigan, A. Chrostowska, S.-Y. Liu, *Angew. Chem. Int. Ed.* **2021**, *60*, 1556–1560; f) D. Tian, W. Zhang, G. Shi, S. Luo, Y. Chen, W. Chen, H. Huang, S. Xing, B. Zhu, *Org. Chem. Front.* **2021**, *8*, 4124–4130; g) S. Hagspiel, M. Arrowsmith, F. Fantuzzi, A. Vargas, A. Rempel, A. Hermann, T. Brückner, H. Braunschweig, *Angew. Chem. Int. Ed.* **2021**, *60*, 6446–6450; h) S. Akahori, T. Sasamori, H. Shinokubo, Y. Miyake, *Chem. Eur. J.* **2021**, *27*, 8178–8184; i) M. Crumbach, O. Ayhan, L. Fritze, J. A. P. Sprenger, L. Zapf, M. Finze, H. Helten, *Chem. Commun.* **2021**, *57*, 2408–2411; j) M. Zhao, Q. Miao, *Angew. Chem. Int. Ed.* **2021**, *60*, 21289–21294; k) M. Crumbach, J. Bachmann, L. Fritze, A. Helbig, I. Krummenacher, H. Braunschweig, H. Helten, *Angew. Chem. Int. Ed.* **2021**, *60*, 9290–9295; l) J. Wu, G. Zhang, *Angew. Chem. Int. Ed.* **2022**, *61*, e202208061; m) M. R. Rapp, W. Leis, F. Zinna, L. Di Bari, T. Arnold, B. Speiser, M. Seitz, H. F. Bettinger, *Chem. Eur. J.* **2022**, *28*, e202104161; n) K. Zhao, Z.-F. Yao, Z.-Y. Wang, J.-C. Zeng, L. Ding, M. Xiong, J.-Y. Wang, J. Pei, *J. Am. Chem. Soc.* **2022**, *144*, 3091–3098; o) J. Bachmann, A. Helbig, M. Crumbach, I. Krummenacher, H. Braunschweig, H. Helten, *Chem. Eur. J.* **2022**, *28*, e202202455; p) W. Li, C.-Z. Du, X.-Y. Chen, L. Fu, R.-R. Gao, Z.-F. Yao, J.-Y. Wang, W. Hu, J. Pei, X.-Y. Wang, *Angew. Chem. Int. Ed.* **2022**, e202201464; q) J. Guo, Z. Li, X. Tian, T. Zhang, Y. Wang, C. Dou, *Angew. Chem. Int. Ed.* **2023**, *62*, e202217470.

[12] a) I. Yamaguchi, B.-J. Choi, T.-a. Koizumi, K. Kubota, T. Yamamoto, *Macromolecules* **2007**, *40*, 438–443; b) I. Yamaguchi, T. Tominaga, M. Sato, *Polym. Int.* **2009**, *58*, 17–21; c) S. Hayashi, T. Koizumi, *Polym. Chem.* **2012**, *3*, 613–616; d) A. W. Baggett, F. Guo, B. Li, S.-Y. Liu, F. Jäkle, *Angew. Chem. Int. Ed.* **2015**, *54*, 11191–11195; e) X.-Y. Wang, F.-D. Zhuang, J.-Y. Wang, J. Pei, *Chem. Commun.* **2015**, *51*, 17532–17535; f) W. Zhang, G. Li, L. Xu, Y. Zhuo, W. Wan, N. Yan, G. He, *Chem. Sci.* **2018**, *9*, 4444–4450; g) S. Pang, Z. Wang, X. Yuan, L. Pan, W. Deng, H. Tang, H. Wu, S. Chen, C. Duan, F. Huang, Y. Cao, *Angew. Chem. Int. Ed.* **2021**, *60*, 8813–8817.

[13] Chujo and co-workers reported as series of poly(boronic carbamate)s and related BN-linked polymers, however, with no significant conjugation over the B=N units, presumably due to either the boronic carbamate groups, meta-phenylene linkages or cross-links in the polymer backbone; see: a) N. Matsumi, Y. Chujo, *Macromolecules* **1998**, *31*, 3802–3806; b) N. Matsumi, K. Kotera, K. Naka, Y. Chujo, *Macromolecules* **1998**, *31*, 3155–3157; c) N. Matsumi, K. Kotera, Y. Chujo, *Macromolecules* **2000**, *33*, 2801–2806.

[14] For borazine-containing polymers and other BN-linked polymer networks, see: a) T. E. Reich, K. T. Jackson, S. Li, P. Jena, H. M. El-Kaderi, *J. Mater. Chem.* **2011**, *21*, 10629–10632; b) T. E. Reich, S. Behera, K. T. Jackson, P. Jena, H. M. El-Kaderi, *J. Mater. Chem.* **2012**, *22*, 13524–13528; c) C. Sánchez-Sánchez, S. Brüller, H. Sachdev, K. Müllen, M. Krieg, H. F. Bettinger, A. Nicolaï, V. Meunier, L. Talirz, R. Fasel, P. Ruffieux, *ACS nano* **2015**, *9*, 9228–9235; d) D. Marinelli, F. Fasano, B. Najjari, N. Demitri, D.

Bonifazi, *J. Am. Chem. Soc.* **2017**, *139*, 5503–5519; e) N. A. Riensch, A. Deniz, S. Kühl, L. Müller, A. Adams, A. Pich, H. Helten, *Polym. Chem.* **2017**, *8*, 5264–5268; f) H. Oubaha, N. Demitri, J. Rault-Berthelot, P. Dubois, O. Coulembier, D. Bonifazi, *J. Org. Chem.* **2019**, *84*, 9101–9116; g) Y. Fu, H. Yang, Y. Gao, L. Huang, R. Berger, J. Liu, H. Lu, Z. Cheng, S. Du, H.-J. Gao, X. Feng, *Angew. Chem. Int. Ed.* **2020**, *59*, 8873–8879; h) F. Fasano, J. Dosso, C. G. Bezzu, M. Carta, F. Kerff, N. Demitri, B.-L. Su, D. Bonifazi, *Chem. Eur. J.* **2021**, *27*, 4124–4133; i) J. Dosso, H. Oubaha, F. Fasano, S. Melinte, J.-F. Gohy, C. E. Hughes, K. D. M. Harris, N. Demitri, M. Abrami, M. Grassi, D. Bonifazi, *Chem. Mater.* **2022**, *34*, 10670–10680.

[15] T. Lorenz, M. Crumbach, T. Eckert, A. Lik, H. Helten, *Angew. Chem. Int. Ed.* **2017**, *56*, 2780–2784.

[16] We also prepared related polymers with linear BN linkages in collaboration with the Bolm group (a), as well as polymers with NBN units in the main chain (b), and poly(iminoborane)s (c and d): a) F. Brosge, T. Lorenz, H. Helten, C. Bolm, *Chem. Eur. J.* **2019**, *25*, 12708–1271; b) T. Lorenz, A. Lik, F. A. Plamper, H. Helten, *Angew. Chem. Int. Ed.* **2016**, *55*, 7236–7241; c) O. Ayhan, T. Eckert, F. A. Plamper, H. Helten, *Angew. Chem. Int. Ed.* **2016**, *55*, 13321–13325 d) O. Ayhan, N. A. Riensch, C. Glasmacher, H. Helten, *Chem. Eur. J.* **2018**, *24*, 5883–5894.

[17] D. L. Eck, G. W. Stacy, *J. Heterocycl. Chem.* **1969**, *6*, 147–151.

[18] G. E. Martinez, J. W. Nugent, A. R. Fout, *Organometallics* **2018**, *37*, 2941-2944.

[19] a) R. A. Bartlett, X. Feng, M. M. Olmstead, P. P. Power, K. J. Weese, *J. Am. Chem. Soc.* **1987**, *109*, 4851–4854; b) H. Chen, R. A. Bartlett, M. M. Olmstead, P. P. Power, S. C. Shoner, *J. Am. Chem. Soc*. **1990**, *112*, 1048–1055.

[20] The twisting of the thiophene ring planes is also observed in the computed structures.

[21] X. Yin, J. Chen, R. A. Lalancette, T. B. Marder, F. Jäkle, *Angew. Chem. Int. Ed.* **2014**, *53*, 9761-9765.

[22] L. Weber, V. Werner, I. Domke, H.-G. Stammler, B. Neumann, *Dalton Trans.* **2006**, 3777-3784.

[23] K. Ruhlandt-Senge, J. J. Ellison, R. J. Wehmschulte, F. Pauer, P. P. Power, *J. Am. Chem. Soc.* **1993**, *115*, 11353-11357.

[24] For more analytical data, see reference [18].

[25] Further examples for the synthesis of 2-aminothiophene hydrochloride, see a) reference [17]; b) D. Binder, G. Habison, C. R. Noe, *Synthesis* **1977**, *4*, 255-256.

[26] For more analytical data, see: A. Casarini, P. Dembech, D. Lazzari, E. Marini, G. Reginato, A. Ricci, G. Seconi, *J. Org. Chem.* **1993**, *58*, 5620-5623.

[27] G. M. Sheldrick, *Acta Crystallogr. A* **2015**, *71*, 3-8.

[28] G. M. Sheldrick, *Acta Crystallogr. A* **2008**, *64*, 112-122.

[29] C. B. Hübschle, G. M. Sheldrick, B. Dittrich, *J. Appl. Crystallogr.* **2011**, *44*, 1281-1284.

[30] Gaussian 16 Revision C.01, M. J. Frisch, G. W. Trucks, H. B. Schlegel, G. E. Scuseria, M. A. Robb, J. R. Cheeseman, G. Scalmani, V. Barone, G. A. Petersson, H. Nakatsuji, M. Caricato X. Li, A. V. Marenich, J. Bloino, B. G. Janesko, R. Gomperts, B. Mennucci, H. P. Hratchian, J. V. Ortiz, A. F. Izmaylov, J. L. Sonnenberg, D. Williams-Young, F. Lipparini F. Ding, J. Goings F. Egidi, B. Peng, A. Petrone, T. Henderson, D. Ranasinghe, V. G. Zakrzewski, J. Gao, N. Rega, G. Zheng, W. Liang, M. Hada, M. Ehara, K. Toyota, R. Fukuda, J. Hasegawa, M. Ishida, T. Nakajima, Y. Honda, O. Kitao, H. Nakai, T. Vreven, K. Throssell, Jr. J. A. Montgomery, J. E. Peralta, F. Ogliaro, M. J. Bearpark, J. J. Heyd, E. N. Brothers, K. N. Kudin, V. N. Staroverov, T. A. Keith, R. Kobayashi, J. Normand, K. Raghavachari, A. P. Rendell, J. C. Burant, S. S. Iyengar, J. Tomasi, M. Cossi, J. M. Millam, M. Klene, C. Adamo, R. Cammi, J. W. Ochterski, R. L. Martin, K. Morokuma, O. Farkas, J. B. Foresman, D. J. Fox, Gaussian, Inc., Wallingford CT, **2016**.

[31] J.-D. Chai, M. Head-Gordon, *Phys. Chem. Chem. Phys.* **2008**, *10*, 6615.

[32] F. Weigend, R. Ahlrichs, *Phys. Chem. Chem. Phys.* **2005**, *7*, 3297-3305.

[33] a) F. Neese, F. Wennmohs, U. Becker, C. Riplinger, *J. Chem. Phys.* **2020**, *152*, 224108; b) F. Neese, *WIREs Comput Mol Sci.* **2022**, *12:e1606*.

[34] Y.-S. Lin, G.-D. Li, S.-P. Mao and J.-D. Chai, *J. Chem. Theory Comput.* **2013**, *9*, 263-272.
[35] a) T. Stein, L. Kronik, R. Baer, *J. Am. Chem. Soc.* **2009**, *131*, 2818-2820; b) T. Stein, H. Eisenberg, L. Kronik, R. Baer, *Phys. Rev. Lett.*, **2010**, *105*, 266802; c) A. Karolewski, L. Kronik, S. Kümmel, *J. Chem. Phys.* **2013**, *138*, 204115.
[36] V. Barone, M. Cossi, *J. Phys. Chem. A* 1**998**, *102*, *11*, 1995–2001.

2.8 Poly(arylene iminoborane)s, Analogues of Poly(arylene vinylene) with a BN-Doped Backbone: A Comprehensive Study

The following section is slightly modified and reproduced from published article[§] with permission from John Wiley & Sons.

Abstract. Despite the great success of the concept of doping organic compounds with BN units to access new materials with tailored properties, its use in polymer chemistry has only been realized quite recently. Herein, we present a comprehensive study of oligo- and poly-(arylene iminoborane)s comprising a backbone of phenylene or thiophene moieties, as well as combinations thereof, linked via B=N units. The novel polymers can be regarded as BN analogues of poly(*p*-phenylene vinylene) (PPV) or poly(thiophene vinylene) (PTV) or their copolymers, respectively. Our modular synthetic approach allowed us to prepare four polymers and twelve monodisperse oligomers with modulated electronic properties. Alternating electron-releasing diaminoarylene and electron-accepting diborylarylene building blocks give rise to a pronounced donor–acceptor character. Effective π-conjugation over the arylene iminoborane backbone is evidenced by systematic bathochromic shifts of the low-energy UV-vis absorption maximum with increasing chain length, which is furthermore supported by crystallographic and computational investigations. Furthermore, all compounds investigated show emission of visible light in the solid state and aggregation-induced emission (AIE) behavior, due to the presence of partially flexible linear B=N linkages in the backbone.

2.8.1 Introduction

π-Conjugated polymers are subject of continuing tremendous research activity due to their versatility in various fields of application such as (opto)electronics, sensors, and biomedicine, to mention but a few.[1] In recent times, the incorporation of inorganic main group elements into the backbone of conjugated organic macromolecules has led to significant advances.[2,3] Boron, for instance, opens up exciting opportunities, especially if it is embedded into the π-system of a conjugated polymer via its vacant p-orbital.[4,5] Of particular note is also the use of B=N units as isoelectronic substitutes for selected C=C entities in organic frameworks. This isosteric substitution conserves the basic structural features of the parent carbonaceous system, but it usually results in modified, often intriguing electronic and photophysical properties, as well as altered chemical reactivity.[6,7] While this concept has been extensively

[§] M. Maier, J. Chorbacher, A. Hellinger, J. Klopf, J. Günther, H. Helten, *Chem. Eur. J.* **2023**, *29*, e202302767. (M.M. and J.C. contributed equally to this work)

applied to polyaromatic molecules,[6,7] application of this concept to polymer chemistry has come into the focus of active research only quite recently.[8-16]

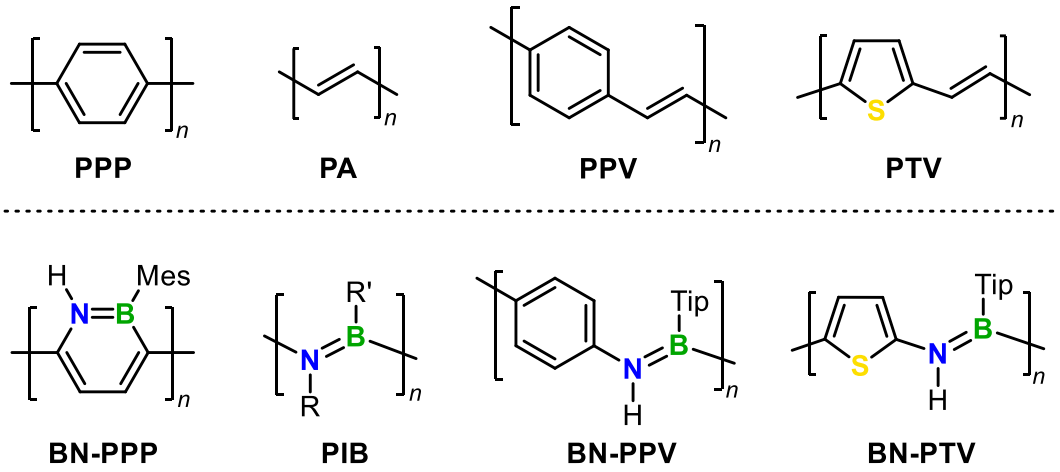

Figure 2.8.1. Top: Representative examples of π-conjugated organic polymers: poly(*p*-phenylene) (PPP), polyacetylene (PA), poly(*p*-phenylene vinylene) (PPV), and poly(thiophene vinylene) (PTV). Bottom: BN isosters thereof (partly stylized structural formulae). Mes = 2,4,6-trimethylphenyl, mesityl; R,R' = organic substituents or H; Tip = 2,4,6-triisopropylphenyl, tripyl.

Jäkle and Liu and co-workers presented a polymer composed of regioregularly concatenated 1,2-azaborinine rings, herein abbreviated as BN-PPP (Figure 2.8.1).[11] This species is formally derived from poly(*p*-phenylene) (PPP), but in contrast to the latter, structural studies on a model oligomer indicated that the adjacent rings in BN-PPP are largely coplanar. In fact, its electronic structure resembles more closely that of poly(cyclohexadiene) or trans-*cisoid* poly(acetylene) (PA) than that of PPP. This behavior was partly ascribed to the limited contribution of the B=N units to the frontier orbitals compared to the C atoms along the chain in PPP and BN-PPP.[11] Reports on several further exciting examples of polymers comprising 1,2-azaborinine as part of a polycyclic structural element followed subsequently.[12] A general observation was that the B=N moiety is involved to a lesser extent, as compared to the carbon chain, in the major conjugation path along the polymer backbone. This led us to target polymers with essentially linear B=N linkages, thus excluding alternative conjugation paths.

We exploited B–N coupling by silicon/boron exchange condensation as a new polymerization strategy, which we first applied to access novel hybrid polymers featuring linear N–B–N linkages.[13] Our photophysical investigations revealed a certain extent of π-conjugation across this moiety. We then targeted a poly(iminoborane) (PIB, Figure 2.8.1), which is a B=N isostere of polyacetylene (PA).[14] To this end, we had to incorporate a cyclic 1,3,2-diazaborolidine building block in the polymer chain to prevent the formation of the respective borazine derivatives, which would otherwise compete with polycondensation in a linear fashion.

Derivatives of poly(*p*-phenylene vinylene) (PPV) are amongst the most extensively studied semiconducting polymers for organic electronic applications.[17] The vinylene bridges ensure

good coplanarity between the adjacent rings along the chain.[18] In light of the versatility of many thiophene-based organic materials,[19] on the other hand, it is not surprising that thiophene congeners of PPV, namely, poly(thiophene vinylene)s (PTVs), have recently been recognized as an emergent class of organic electronic materials as well.[20]

In a short communication, a few years ago, we presented the first poly(*p*-phenylene iminoborane) (BN-PPV) and some molecular model oligomers of that type.[15] These species are derived from poly(*p*-phenylene vinylene) (PPV) through isosteric replacement of its vinylene by B=N moieties.[21] Very recently, we also briefly communicated the synthesis and characterization of the first poly(thiophene iminoborane) (BN-PTV), which can be regarded as a BN/CC isostere of poly(thiophene vinylene) (PTV).[16] Herein, we report full details of these studies, and we add alternating copolymers of both BN-PPV and BN-PTV, as well as monodisperse homo- and mixed oligomers in all possible variations. Our investigations reveal that these species are efficiently conjugated along the arylene iminoborane backbone. The copolymer composition of alternating electron-rich diaminoarylene and electron-poor diborylarylene moieties results in pronounced donor–acceptor characteristics, as reflected in the photophysical properties of the polymers and oligomers. Furthermore, the flexible linear B=N linkage causes interesting aggregation-induced emission (AIE) behavior as a result of the formation of nanoaggregates, as well as efficient solid-state fluorescence.

2.8.2 Results and Discussion

We synthesized the mono-aminoboranes **3**,[15] **5**, **7**, and **8**[16] (i. e., the “monomers”) by salt elimination reactions between the appropriate bromoborane **1** or **4** and aniline (**2**) or 2-amino-thiophene hydrochloride (**6**), respectively, using NEt_3 as auxiliary base (Scheme 2.8.1). 2,4,6-Triisopropylphenyl (Tip) was chosen as the third substituent at the tricoordinate boron center for kinetic stabilization. In our previous report, we described the synthesis of the diphenyl derivative **3**, as well as the phenylene iminoborane dimers **10** and **17** (see Schemes 2.8.2 and 2.8.3), via Si/B exchange condensation reactions.[15] For the present study, we found salt elimination to be feasible in these cases as well, thereby saving us one reaction step each. For the synthesis of **7** and **8**,[16] free 2-aminothiophene was generated *in situ* via deprotonation of **6**. To avoid decomposition of this highly reactive species, these reactions were conducted at −78 °C. We obtained all products after purification by column chromatography on neutral aluminum oxide as mixtures of diastereomers in good yields (as indicated in the scheme below the molecules). In each case, the respective main diastereomer was the one in which the thienyl and/or phenyl groups adopt *trans* positions at the B=N double bonds (i. e., the (*E*)-isomer in the case of **5** and **8**, and the (*Z*)-isomer of **3** and **7**). We estimated the amounts of the minor isomers as 5 % (**3**), 8 % (**5**), <3 % (**7**), and 12 % (**8**).

The $^{11}B\{^1H\}$ NMR spectra of these mono-aminoboranes show each a single, broad signal, whereas the ones of the *B*–phenyl derivatives **3** and **7** appear slightly downfield (at 44 and 43 ppm, respectively) from those of their *B*–thienyl congeners **5** and **8** (at 39 and 40 ppm). The ^1H NMR resonances for the protons on the *B*-bound aryl rings generally appear at significantly lower field than those on the *N*-bound arenes in all compounds. For instance, the protons of the *B*-thiophene rings of **5** and **8** give rise to three doublets of doublets at 7.64 – 7.17 ppm, while those of the *N*-bound thiophene rings of **7** and **8** resonate at 6.64 – 6.29 ppm. The protons of the phenyl groups split into three sets of signals and, similarly, show a downfield shift for the *B*-bound phenyl protons of **3** and **7** (7.63 – 7.36 ppm) compared to the *N*-bound phenyl signals of **3** and **5** (7.09 – 6.77 ppm). Comparison of the NMR data for the minor isomers with those of the major species revealed the general trend that the N-*H* protons are significantly more shielded in the former, wherein they are *cis* to the Tip substituent. For example, the N-*H* signal of the (*Z*)-diastereomer of **5** was detected at 6.20 ppm, that is, significantly highfield shifted compared to that of its (*E*)-isomer (6.80 ppm).

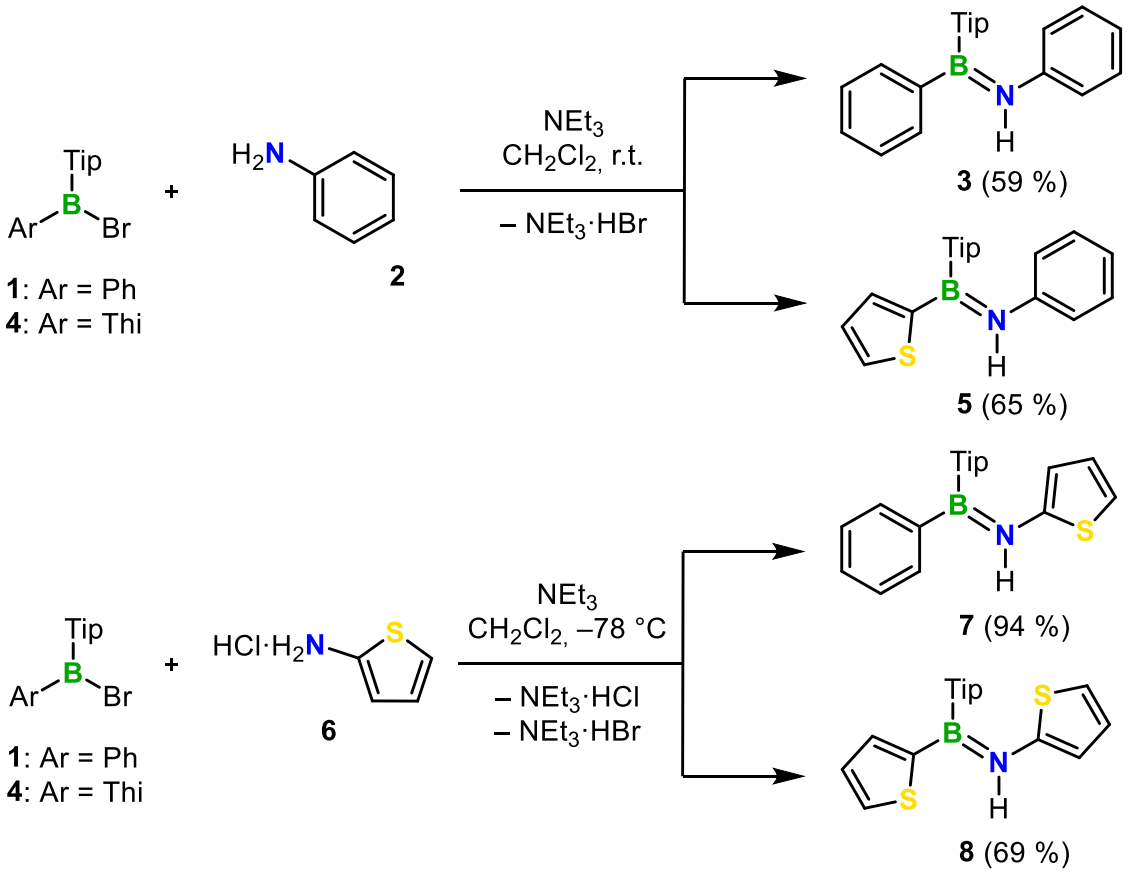

Scheme 2.8.1. Synthesis of monodisperse oligomers **3**, **5**, **7**, and **8** with one B=N unit (Tip = 2,4,6-triisopropylphenyl, Thi = 2-thienyl).

The synthesis of the dimers comprising NBBN sequence (Scheme 2.8.2) or BNNB sequence (Scheme 2.8.3) of the heteroatoms along the chain was achieved via either salt elimination (for **10**, **12**, **17**, and **18**) or silicon/boron exchange reactions (for **14**, **15**, **20**, and **21**), respectively.

Each synthesis was performed in DCM at room temperature, and after purification by column chromatography on neutral aluminum oxide these dimers were obtained in moderate to good yields (as indicated in the schemes).

Compounds **10**, **12**, **14**, and **15** (Scheme 2.8.2) as well as **17**, **18**, **20**, and **21** (Scheme 2.8.3) were each obtained as mixtures of diastereomers. In each case, the main isomer exhibited *trans* configuration of the B=N bonds with respect to the thienyl(ene) and/or phenyl(ene) units. Thus, in the case of **12**, **15**, **18**, and **21** the (*E*,*E*)-diastereomer and in the case of **10**, **14**, **17**, and **20** the (*Z*,*Z*)-diastereomer was by far the most abundant species in the mixture.

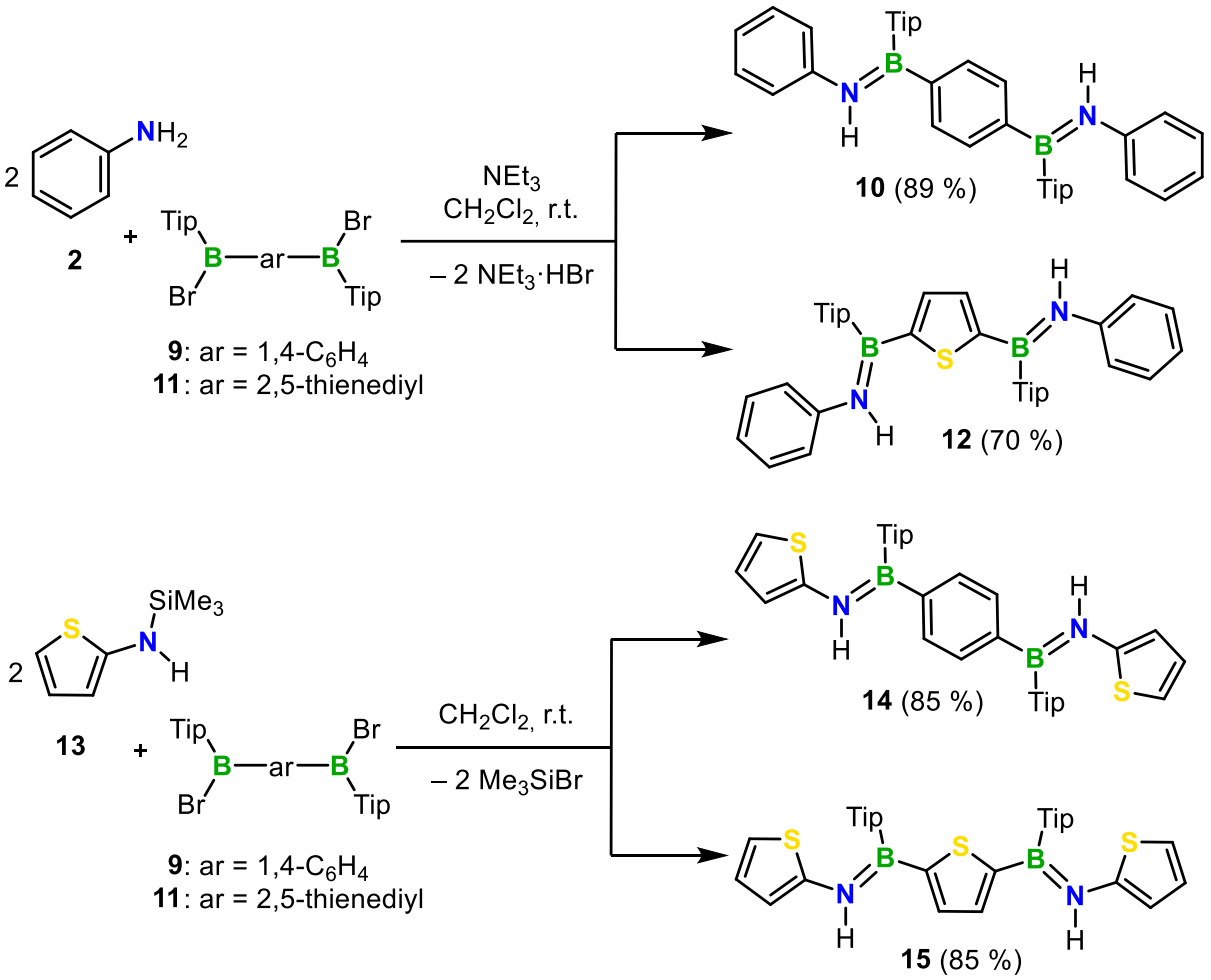

Scheme 2.8.2. Synthesis of monodisperse oligomers **10**, **12**, **14**, and **15** with NBBN sequence.

In the ^{1}H NMR spectra we observed singlet signals for the protons of the *B*-bound inner arenes of the dimers **10**, **12**, **14**, and **15** between 7.60 and 7.32 ppm, that is, significantly downfield shifted from the *N*-bound inner arene protons of **17**, **18**, **20**, and **21** (6.45 – 5.68 ppm). The major isomers of the dimers **14** and **15** show three doublets of doublets between 6.65 and 6.28 ppm for the protons of the outer *N*-bound thienyl rings. These signals are significantly highfield shifted compared to those of the outer *B*-bound thienyl rings of **18** and **21** (7.58 – 7.13 ppm), which also appear as doublet of doublets. The same trend is observed for the signals of dimer **10** and **12** with outer *N*-bound phenyl moieties (multiplets between 7.09 and 6.77 ppm) and for **17** and **20**, containing outer *B*-bound phenyl moieties (multiplets, 7.58 – 7.32 ppm). The N-*H* signals for the major isomers (*Z*,*Z*)-**14** and (*E*,*E*)-**15** with outer *N*-bound thiophene rings appear downfield shifted at around 7.25 ppm, compared to (*E*,*E*)-**18** and (*E*,*E*)-**21** with outer *B*-bound thiophene rings (ca. 6.65 ppm). The N-*H* signals of (*E*,*E*)-**12** and (*Z*,*Z*)-**20** appear at 6.86 ppm.

For compounds **10**, **12**, **15**, **17**, **18**, **20**, and **21** the respective (*E*,*Z*)-isomer was also found, as proven by NOESY and ROESY measurements (Appendix 5.8). The N-*H* signals of the *Z*-configured double bond of the (*E*,*Z*)-isomers of **12**, **15**, **18**, and **21** can be assigned due to cross peaks with the Tip-*o*-^{i}Pr-C*H*$_3$ and Tip-*o*-^{i}Pr-C*H* signals, whereas the N-*H* signals at the *E*-configured double bond show cross peaks with the aromatic thiophene protons. However, the major isomer of compound **10**, **17**, and **20** is the (*Z*,*Z*)-diastereomer and thus the N-*H* signals at the *E*-configured double bond of the (*E*,*Z*)-isomer show cross signals with the Tip-C*H*$_3$ and Tip-^{i}Pr-C*H* signals. In the case of **14**, only minor quantities of another isomer (ca. 7 %) were found. The ^{1}H NMR spectrum shows six small doublet of doublet signals for the thiophene protons and two doublets for the phenylene protons, what indicates the formation of the (*E*,*Z*)-isomer (inset Figure S5.8.31). In general, we observe for dimers with BNNB sequence significantly larger ratios of the corresponding (*E,Z*)-isomer (**17**: 11 %, **18**: 19 %, **20**: 14 %, **21**: 40 %) than for the dimers with NBBN sequence (**10**: 10 %, **12**: 11 %, **14**: 7 %, **15**: 13 %). Only compound **21** showed beside the major (*E*,*E*)-isomer and significant amounts of the (*E*,*Z*)-isomer, additionally minor amounts of a third isomer, that is, the (*Z*,*Z*)-form (ca. 3 %). The N-*H* signal of (*Z*,*Z*)-**21** appears as a single peak at 5.93 ppm and shows in the NOESY cross signals with the Tip-*o*-^{i}Pr-C*H*$_3$, Tip-*o*-^{i}Pr-C*H* and one *N*-bound aromatic thiophene proton signal (Figure S5.8.63).

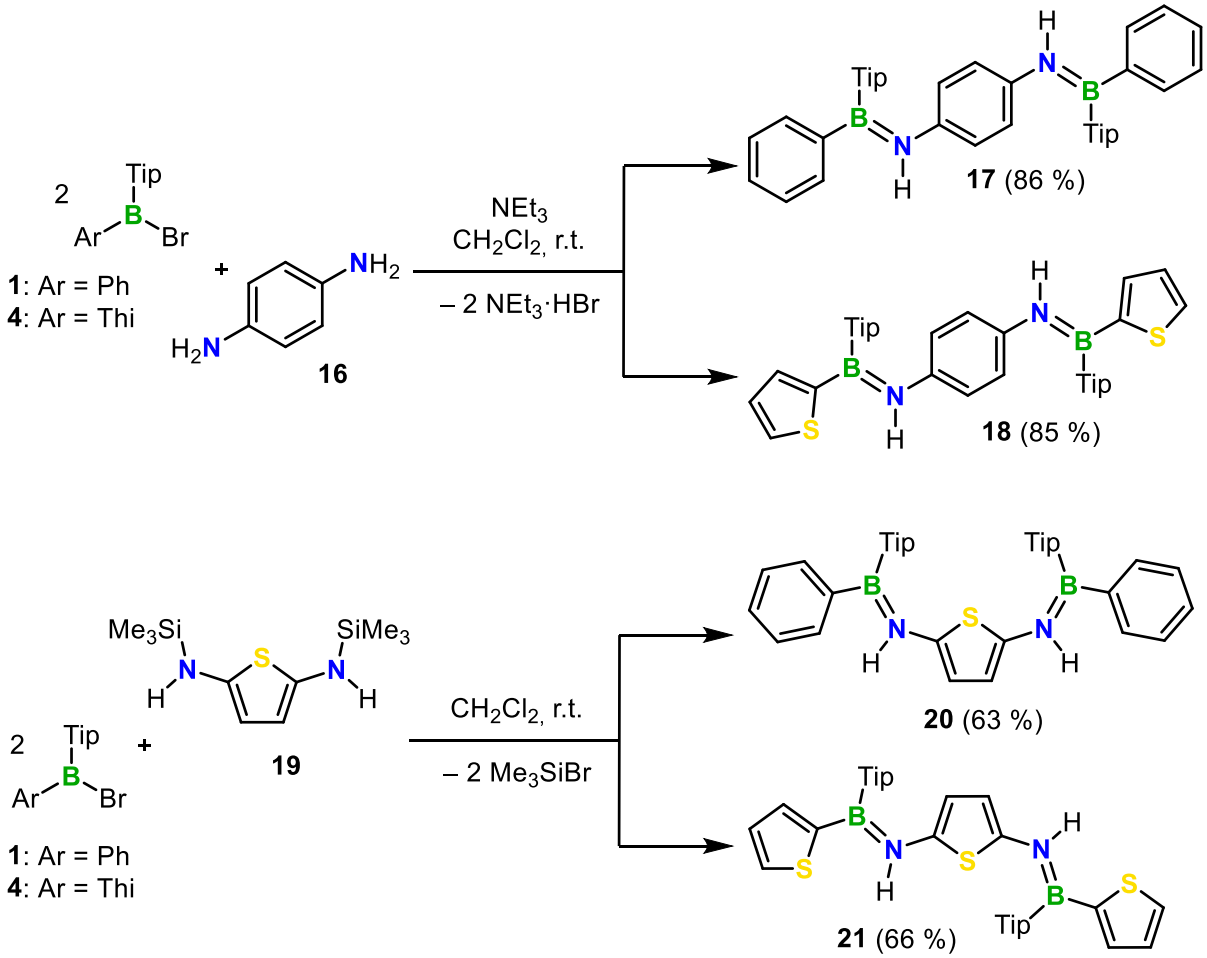

Scheme 2.8.3. Synthesis of monodisperse oligomers **17**, **18**, **20**, and **21** with BNNB sequence.

The $^{11}B\{^1H\}$ NMR spectra of the dimers showed each a single, broad peak. The signals of compounds **10**, **14**, **17**, and **20** (42 – 44 ppm) are slightly downfield shifted compared to the signals of the *B*-thiophene congeners **12**, **15**, **18**, and **21** (38 – 40 ppm).

Upon slow crystallization of **5**, **12**, **18**, and **20** from *n*-hexane, and of **14** from a mixture of DCM and *n*-hexane, we obtained single crystals suitable for X-ray diffractometry of exclusively the major isomers showing *trans* arrangement of the thienyl(ene) and/or phenyl(ene) moieties at each B=N unit along the backbone (Figures 2.8.2 and 2.8.8–2.8.12), similar to the all-phenyl(ene)[15] and all-thienyl(ene)[16] congeners. The molecular structures of all compounds feature perfectly trigonal-planar coordinated boron and nitrogen centers (both ∑(NR_3) and ∑(BR_3) = 360.0°). The B–N bond lengths of **5**, **12**, **14**, **18**, and **20** are between 1.396(3) – 1.414(2) Å (Table 2.8.4), thus, in the same range with those of the BN-PPV[15] and BN-PTV[16] model oligomers and related aminoboranes having pronounced double bond character.[22] Furthermore, the phenyl(ene) and thienyl(ene) rings are rotated in a way that they are, to a certain degree, coplanar with the >B=N< moieties they are bound to. The monomeric compounds **5** and **8**[16] feature rather planar backbones, with only a slight twisting between the thiophene and the phenyl ring planes and the >B=N< moiety in **5** (5.2 and 12.0°, defined by

C_2BNC), and between the thienyl rings and the >B=N< moiety in **8** (10.4 and 12.4°).[16] The solid-state molecular structures of **12**, **14**, **18**, and **20** show overall slightly larger backbone twists (Table 2.8.4). Within the series of these dimeric species, the torsion angles between a BN unit and an adjacent thiophene plane are somewhat larger than those between a phenylene and a BN plane. This is the case both if thiophene is in the center (e.g., **12**, Figure 2, torsion angles between the thiophene and phenylene ring planes and the BN moieties from left to right: 7.3, 15.0, 22.4, and 18.0°) or at the outer position (e.g., **14**; 22.6, 18.4, 6.0, and 22.8°) of the oligomer backbone structure.

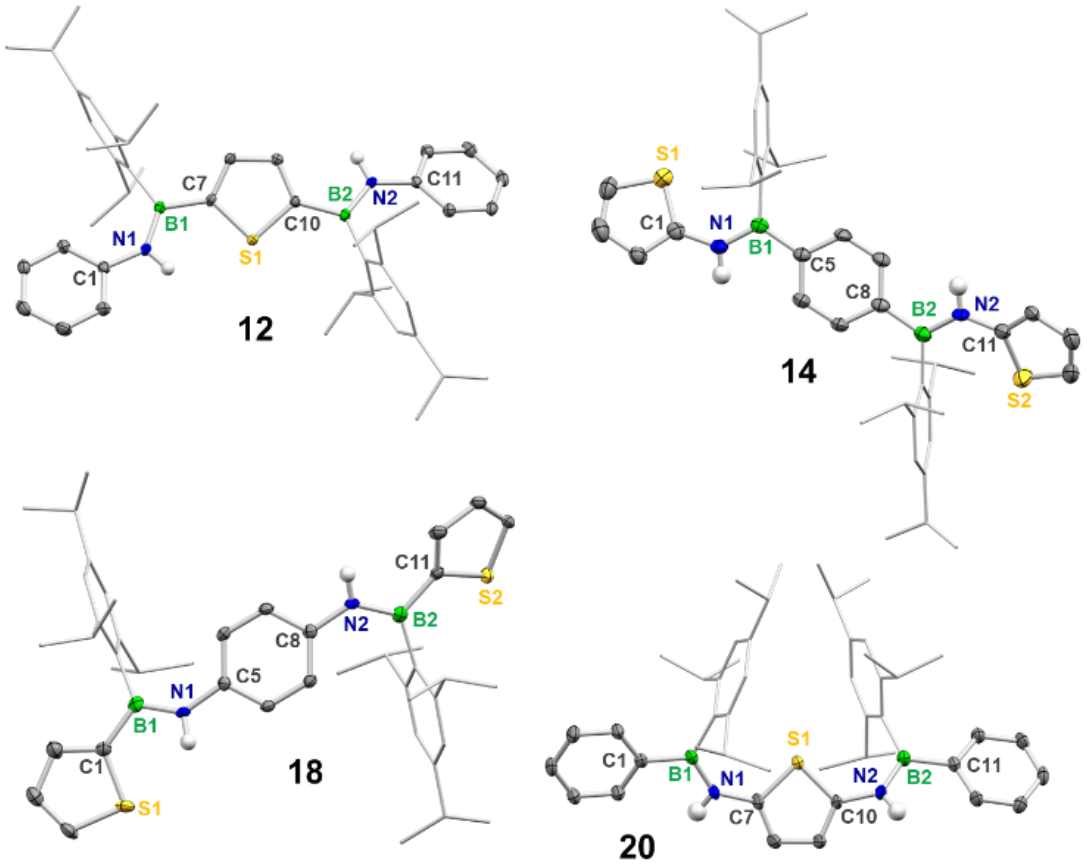

Figure 2.8.2. Molecular structures of **12**, **14**, **18**, and **20** in the solid state by single-crystal X-ray diffraction (ellipsoids drawn at the 50% probability level, except for the Tip groups; H atoms and disorders of the thiophene units and Tip groups omitted for clarity).

We previously reported the synthesis of poly(*p*-phenylene iminoborane) (BN-PPV) **22** via silicon/boron exchange co-polycondensation of **9** and *N,N'*-bis(trimethylsilyl)-*p*-phenylene-diamine (**24**).[15] Now, we demonstrate that **22** can also be prepared by polycondensation of **9** with *p*-phenylenediamine (**16**) via salt elimination in the presence of NEt_3 (Scheme 2.8.4). In each polymerization, Me_3SiNMe_2 was added after 48 – 72 h to terminate the eventually remaining reactive B–Br end groups of the polymer. This procedure afforded **22** with appreciable molecular weight (Table 2.8.1). We synthesized the all-thiophene analogue, poly(thiophene iminoborane) (BN-PTV) **23**, by silicon/boron exchange co-polycondensation of **11** and **19**.[16] In this case, a controlled polymerization to **23** via salt elimination was not successful due to the instability of the, thus required, highly electron rich diaminothiophene.

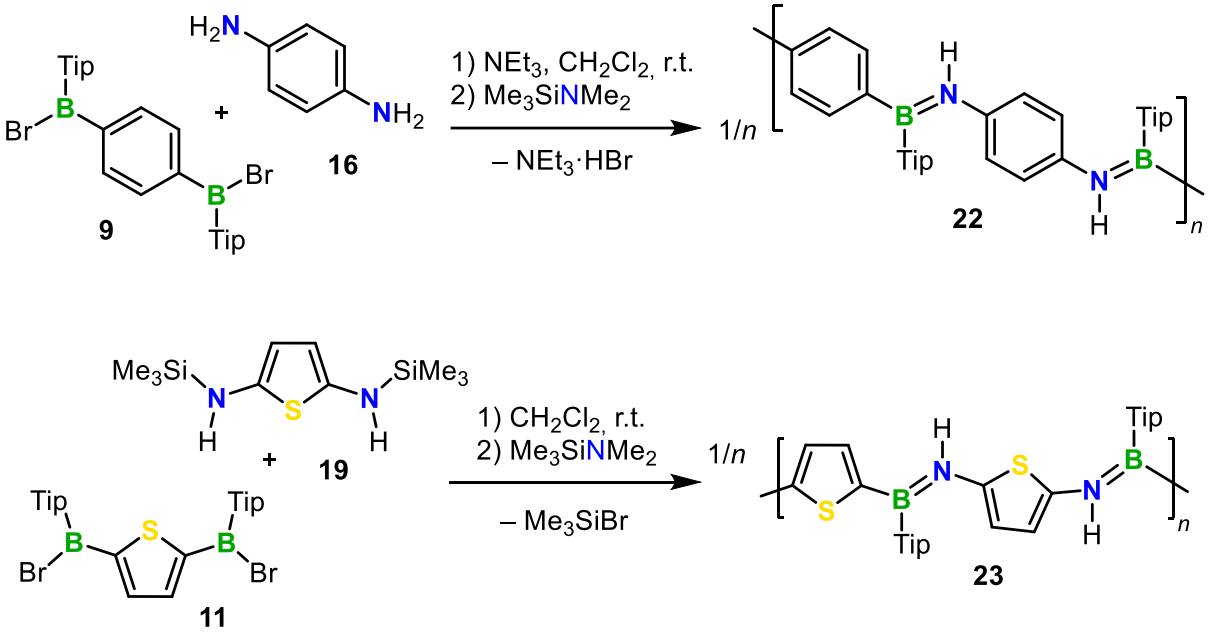

Scheme 2.8.4. Synthesis of BN-PPV **22** and BN-PTV **23**.

Next, we performed copolymerizations to obtain the mixed copolymers poly[(*p*-phenylene iminoborane)-*alt*-(2,5-thiophene iminoborane)]s **25** and **26**, which differ from each other as they are composed of diborylthiophene and diaminobenzene or diborylbenzene and diaminothiophene building blocks, respectively (Scheme 2.8.5). Copolymer **25** was obtained via either Si/B exchange co-polycondensation of **11** with **24** or via salt elimination of **11** with **16**. Silicon/boron exchange polycondensation of **9** with **19** yielded copolymer **26**.

Gel permeation chromatography (GPC) of the crude products showed major broad signals for a distribution around higher molecular weights and some minor signals in the small-molecule range (between 1.3 kDa and 5.0 kDa). The latter were removed through precipitation of the crude products into cold methanol (−78 °C), whereby we accomplished to isolate the desired polymers in moderate yields (35 – 45 %).

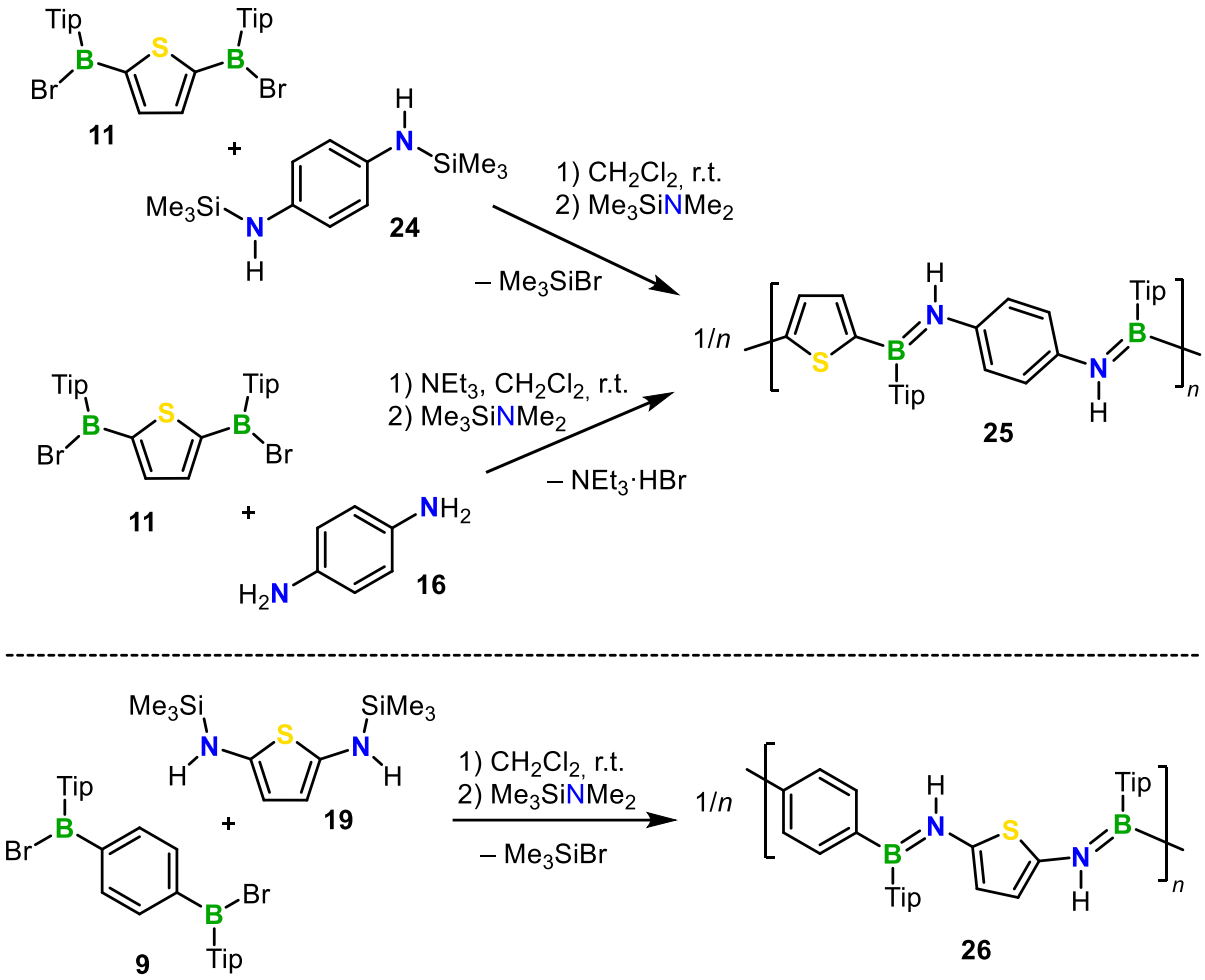

Scheme 2.8.5. Synthesis of alternating copolymers **25** and **26**.

GPC analysis of the purified polymers revealed molecular-weight averages ranging from M_n = 14.2 kDa for **23** and 21.2 kDa for **22**, corresponding to number-average degrees of polymerization of DP_n = 46 – 70 (Table 2.8.1, Figure 2.8.3). The polydispersity indices (PDI) are in the range of 1.4 to 1.9, as expected for step growth-type polycondensation reactions.

Table 2.8.1. GPC data of **22**, **23**, **25**, and **26**.

Polymer	M_n [kDa]	M_w [kDa]	PDI	DP_n
22[a]	21.2	39.9	1.9	70
23[b]	14.2	23.0	1.6	46
25[a]	19.5	27.2	1.4	63
25[b]	17.0	23.3	1.4	55
26[b]	20.4	38.9	1.9	66

[a] by salt elimination [b] by Si/B exchange.

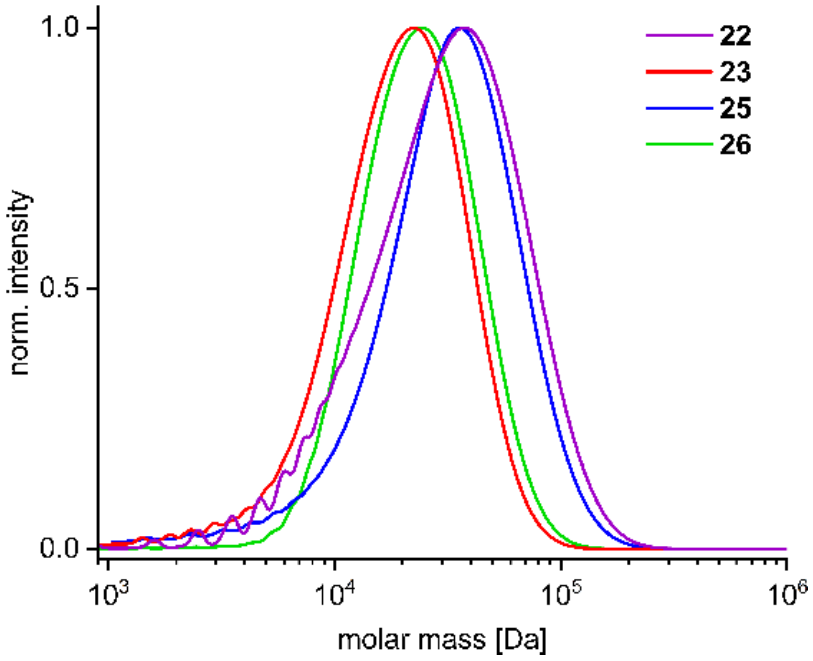

Figure 2.8.3. Normalized gel permeation chromatography (GPC) traces of the polymers detected by UV-vis detector at 254 nm.

The ^{1}H NMR spectra of **25** and **26** showed multiple signals in the aromatic region between 5.69 and 7.43 ppm, indicating different *E*/*Z* arrangements at the B=N bonds along the polymer chains. The main peaks of **25** appear at 7.24 and 6.40 ppm, which we assign to the *B*-bonded thiophene and the *N*-bonded phenylene moieties at *trans*-configured B=N bonds along the backbone, respectively, by comparison with the observations made for the model oligomers. The main resonances of **26** appear at 7.43 ppm (*B*-bonded phenylene groups) and 5.69 ppm (*N*-bonded thiophene moieties) at *trans*-configured B=N moieties.

We investigated the photophysical properties of the oligomers and polymers reported herein by UV-vis absorption and fluorescence emission spectroscopy in THF (Figure S5.8.82–S5.8.89 and Table 2.8.5) and as poly(methyl methacrylate) (PMMA) films (Figure 2.8.5 and Table 2.8.2). The UV-vis spectra of all compounds display a strong low-energy absorption band, which shows two clear trends: i) Within each series of comparable compounds (i. e., having the same type of constituent rings) it undergoes a systematic bathochromic shift when going from the monomers to the dimers and further to the respective polymers, thus with increasing length of the π-conjugated system. ii) Within each series of compounds of comparable chain length (i. e., monomers, dimers, or polymers) it shows a bathochromic shift with increasing ratio of thiophene to phenylene moieties in the backbone. In THF, the absorption maxima of the monomeric compounds appear at 272 nm (**3**), 288 nm (**5**), 296 nm (**7**), and 305 nm (**8**), thus red-shifted by 33 nm (32 nm in the PMMA film) for the dithienyl-substituted compound **8** with respect to the diphenyl derivative **3**. For the dimers and the polymers, the shift for the pure thiophene systems compared to their respective derivatives

featuring only phenylene groups in the backbone is even larger: 42 nm (**10** to **15**), 40 nm (**17** to **21**), and 47 nm (**22** to **23**). The mixed phenylene–thiophene compounds show intermediate values, which clearly fits the trend.

Among the mixed oligomers and polymers the relative position of the thiophene and the phenylene moieties actually plays an important role. The absorption maxima of the compounds featuring nitrogen–thiophene and boron–phenyl(ene) linkages (**7**, **14**, and **20**) are significantly bathochromic shifted compared to those of the inversely linked ones (**5**, **12**, and **18**). This points to a certain donor–acceptor character in the systems involving strongly electron-releasing aminothiophene units and electron-accepting borylbenzene moieties.

Our calculations of vertical singlet excitations by TD-DFT on the mixed oligomers **18** and **20** (Figure 2.8.4; Table 2.8.9) further confirm what we have derived from our previous calculations on compound series with only phenyl(ene) groups in the backbone **3**, **10**, and **17**,[15] and on the thiophene congeners **8**, **15**, and **21**:[16] the lowest energy absorption is unambiguously assigned to a π–π* transition within the arylene iminoborane backbone. This process corresponds to the respective HOMO→LUMO excitation in each case. As we have already noted for the pure thiophene species,[16] the HOMO of these compounds also tends to have the strongest contribution on the electron-donating aminoarylene units, whereas the LUMO is more polarized towards the aryleneborane sequences. This is particularly clearly seen in the diaminothiophene–phenylborane derivative **20**, thus reflecting the certain intermolecular charge transfer character of this transition.

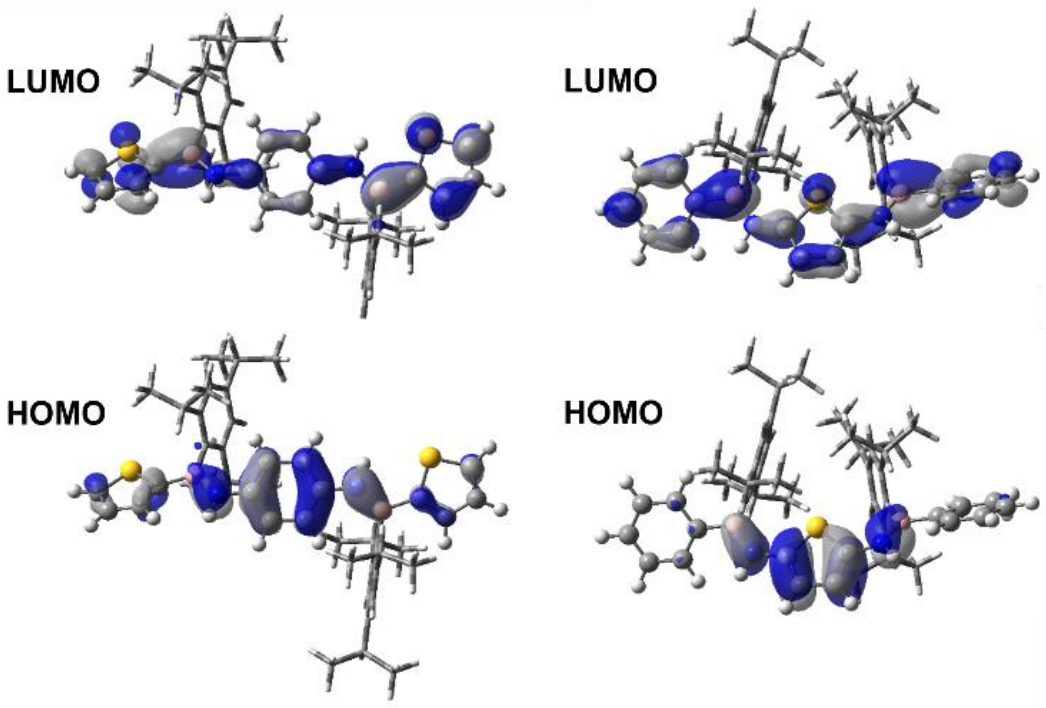

Figure 2.8.4. Calculated frontier orbitals of **18** (left) and **20** (right; isovalue 0.03 a.u.; ωTB97X-D3/def2-SVP, CPCM(THF), ωT = 0.14).

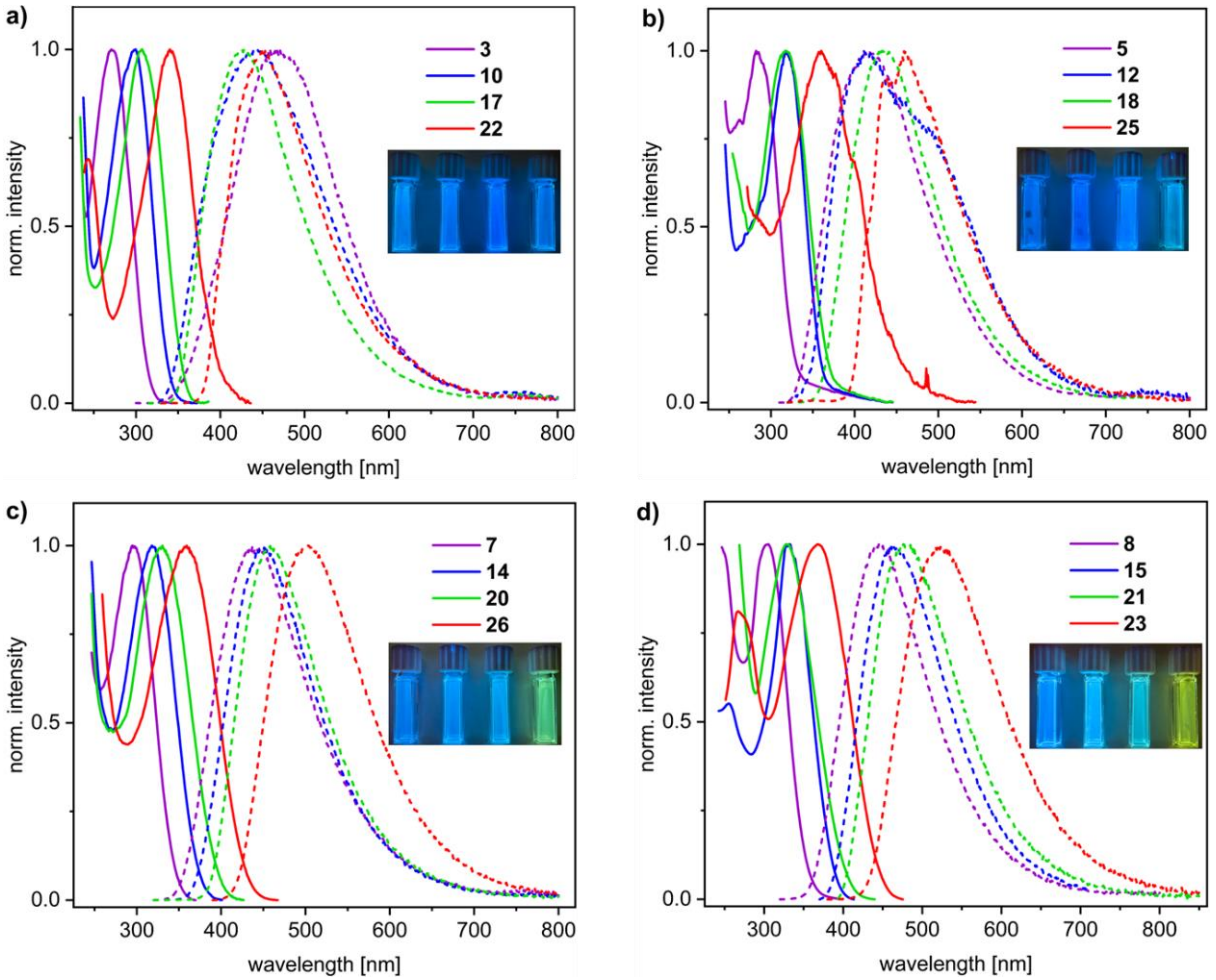

Figure 2.8.5. UV-vis absorption (solid lines) and emission (dashed lines) spectra of a) all-phenylene- b) *B*-thiophene–*N*-phenylene- c) *B*-phenylene–*N*-thiophene- and d) all-thiophene-linked iminoborane compounds as PMMA films. Inset: Photograph of PMMA films under UV light (sequence of the films analogous to the sequence of numbers).

Table 2.8.2. Photophysical data of the iminoborane oligomers and polymers as PMMA films.

No.[a]	λ_{max} abs | em [nm]	Φ_{fl}[e] [%]	No.[b]	λ_{max} abs | em [nm]	Φ_{fl}[e] [%]	No.[c]	λ_{max} abs | em [nm]	Φ_{fl}[e] [%]	No.[d]	λ_{max} abs | em [nm]	Φ_{fl}[e] [%]
3	272 | 466	36	**10**	298 | 442	31	**17**	306 | 426	42	**22**	341 | 450	25
5	282 | 415	9	**12**	319 | 415	15	**18**	318 | 435	29	**25**	359 | 460	15
7	296 | 440	10	**14**	318 | 449	10	**20**	329 | 459	13	**26**	360 | 502	10
8	304 | 445	6	**15**	331 | 462	10	**21**	329 | 479	9	**23**	368 | 521	5

[a] Monomeric compounds. [b] Dimeric compounds with NBBN sequence. [c] Dimeric compounds with BNNB sequence. [d] Polymers. [e] Fluorescence quantum yields, determined using an integration sphere.

All compounds showed no or marginal light emission upon excitation in polar solvents such as THF and DCM, which implies that mostly non-radiative decay processes must take place. They partly showed moderate fluorescence in *n*-hexane (see Appendix). In the solid state, however, significantly enhanced luminescence was observed. To investigate the photophysical properties of the compounds in the aggregated state more detailed, we prepared homogeneous PMMA films of them. To this end, a DCM solution of PMMA and the sample was slowly evaporated to one layer in the cuvettes under ambient conditions and then dried at 60 °C. All compounds gave rise to a broad emission band showing a bathochromic shift with increasing chain length (Figure 2.8.5; Table 2.8.2); only that of **3** was further bathochromic shifted. From the phenylene-bridged aminoboranes to the pure thiophene-bridged compounds, a clear red-shift was observed. This trend is particularly evident at the polymers, starting from the deep blue luminescent BN-PPV **22** (450 nm) through the light blue mixed polymer **25** (460 nm) and the green luminescent **26** (502 nm) to the BN-PTV **23** (521 nm) which emits yellowish-green. The highest fluorescence quantum yields are actually observed for the compounds with the highest phenylene content (e. g., for the BNNB linked oligomers: **21** (9 %) < **20** (13 %) < **18** (29 %) < **17** (42 %)).

The observation of such aggregated-state dependent photophysics suggested that these cyclolinear species might exhibit aggregation-induced emission (AIE)[23] properties. Therefore, we decided to investigate the best solid-state emitters (BNNB linked oligomers **17**, **18**, **20**, and **21**) of each series for their AIE behavior in more detail. In pure THF, all compounds show almost no emission. However, if up to 90 % water was added to the solution, an increasingly intense luminescence was observed (Figure 2.8.6). For compounds **17**, **18**, **20**, and **21**, the fluorescence intensity was increased about 71, 118, 57, and 39-fold, respectively, in a solvent with 90 % water content compared to the pure THF solution. Another striking feature of the spectra of **17** and **18** is a clear hypsochromic shift as the water content was increased from 0 to 90 %, by 142 (from 632 to 490 nm) for **17** and by 177 nm (from 648 to 471 nm) for **18**. The spectra of **20** and **21** show a blue-shift as well, but only by about 10 nm. This could be explained by two opposing effects. Hypsochromic effects upon AIE have been observed previously, and they were attributed to the physical restriction of the intramolecular motions due to the increase in the hydrophobicity of the local environment of the nanoaggregates formed.[24] On the other hand, the enhanced polarity of the solvent environment with increasing water content leads to a positive solvatochromic effect in donor–acceptor species – such as the ones that are subject of this study – which form charge-separated excited states. This effect is most pronounced for derivatives **20** and **21**, featuring the strong diaminothiophene donor moieties; herein, both effects nearly cancel each other out.

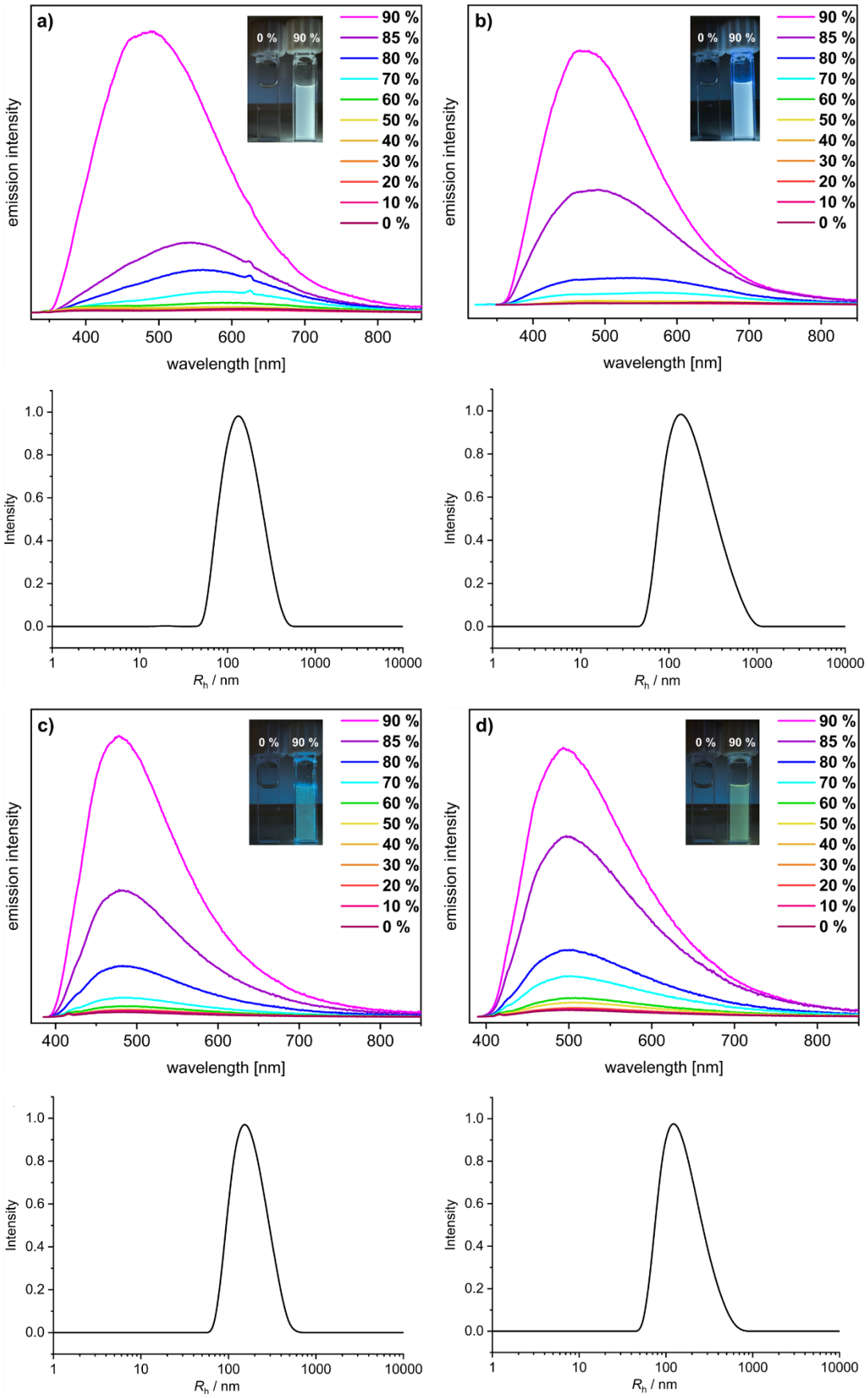

Figure 2.8.6. Emission spectra of a) **17**, b) **18**, c) **20**, and d) **21** in THF/water mixtures (conc. $5 \cdot 10^{-5}$ M) with different water fractions (0 – 90 %) and corresponding DLS measurements on the bottom. Inset: Photographs of cuvettes of the samples with 0 % (left) and 90 % (right) water fraction under UV light.

The observation of this AIE effect indicates the formation of emissive nanoaggregates. To confirm this hypothesis, we additionally performed dynamic light scattering (DLS) measurements in THF/water (10/90) mixtures. This confirmed the formation of particles of **17**, **18**, **20**, and **21** with hydrodynamic radii (R_h) of 133.7, 153.2, 163.0, and 136.5 nm, respectively (Figure 2.8.6).

Thilagar and co-workers recently discovered that certain tetraaryl-substituted aminoboranes exhibit AIE properties.[25] Their studies revealed that this is due to the restricted intramolecular rotation (RIR) of the aryl substituents at the aminoborane moiety in the aggregated state. It is suggested that similar effects are operative in the polymers and oligomers presented herein as well. This is enabled by the partially flexible backbone through the linear B=N linkages along the chain.

Cyclic voltammetry (CV) of the oligomers containing BN or NBBN sequences and the polymers in CH_2Cl_2 revealed multiple irreversible oxidation events. In general, for the compounds the feature *N*-phenyl groups, that is, **3**, **5**, **10**, and **12**, the oxidation process started at around 1.0 V, whereas the *N*-thienyl derivatives **7**, **8**, **14**, and **15** showed an oxidation onset potential at around 0.6 V. The polymers with the most electron-rich diaminothiophene subunits showed the lowest oxidation onset, of ~0.25 V, and those with di(bromoboryl)thiophene subunits showed their onset at ~0.6 V (Table 2.8.8).

The CV curves of compounds **17**, **18**, **20**, and **21**, containing BNNB sequences, showed each one reversible oxidation wave (Figure 2.8.7). Compound **21** has the lowest oxidation potential of our series as it contains, in addition to the strongly electron-releasing diaminothiophene subunit, further electron rich thiophene units at the outer boron centers. An increased oxidation potential was observed for the compounds **17** and **18** containing inner diaminophenylene moieties. The oxidation half-wave potentials thus increase in the order: **21** (0.32 V) < **20** (0.34 V) < **18** (0.68 V) < **17** (0.72 V). The DFT-calculated HOMO energies of these compounds are consistent with this trend (Table 2.8.10).

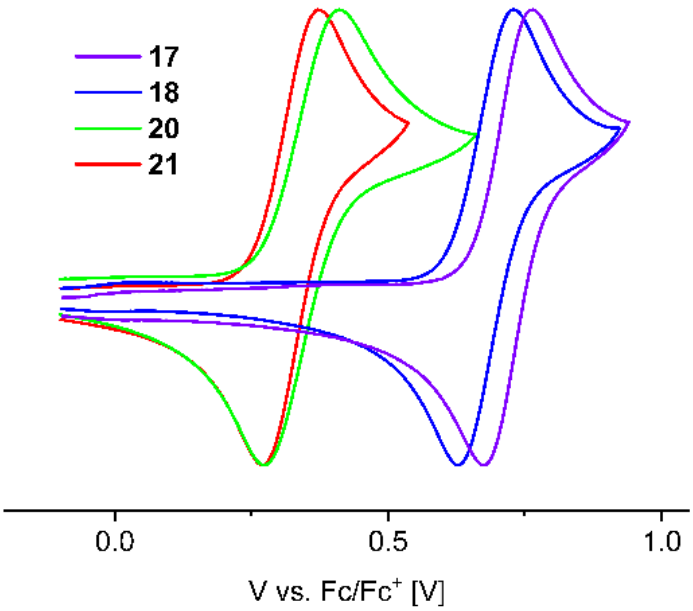

Figure 2.8.7. Cyclic voltammograms of **17**, **18**, **20**, and **21** in DCM (vs. $[Cp_2Fe]^{0/+}$, scan rate: 150 mV s^{-1}).

2.8.3 Conclusion

We herein presented a comprehensive study of oligo- and poly(arylene iminoborane)s comprising cyclolinear chains of B=N-linked phenylene or thiophene rings, as well as mixed oligomers and copolymers of that type in all possible combinations. These species can be regarded, on the one hand, as inorganic–organic hybrid variants of the well-established conjugated organic polymers PPV and PTV, respectively, or combinations thereof. Alternatively, the novel polymers can be described as hybrids of polyarylenes and poly(iminoborane)s.

Via a modular approach using either salt elimination or silicon/boron exchange (poly)condensation protocols, we succeeded in the synthesis of four polymers and twelve monodisperse oligomers, the properties of which are effectively tailored through the sequence of their components. We found that the compounds obtained are preferentially formed with a *trans* arrangement of the thienyl(ene) and/or phenyl(ene) moieties at the doubly-bonded B=N groups along the backbone. Structural studies of some of the oligomers revealed that the rings in the chain are only slightly twisted with respect to each other, with a certain degree of coplanarity between these rings and the >B=N< moieties they are bound to. These features indicate possible π-conjugation over the arylene iminoborane backbone. Our photophysical investigations confirm this. The UV-vis spectra show systematic bathochromic shifts with increasing chain length. In addition, the combination of alternating strongly electron-releasing diaminoarylene and electron-accepting diborylarylene moieties results in a pronounced donor–acceptor backbone structure, which is reflected in the photophysical properties and is further supported by TD-DFT calculations. Thus, the largest red-shifts of the absorption are observed

for compounds featuring N–thiophene and B–phenyl(ene) linkages. Our electrochemical investigations revealed reversible oxidation processes for the oligomers that feature diaminoarylene moieties, with the lowest half-wave potentials for the derivatives comprising the strongly electron-releasing diaminothiophene building block.

While the oligo- and poly(arylene iminoborane)s reported herein are only weakly to non-emissive in dilute solution, they show efficient solid-state fluorescence as well as AIE properties. The formation of nanoaggregates was confirmed by DLS studies. This effect is enabled by the partially flexible backbone of the polymers and oligomers through the linear B=N linkages. In future studies, we are planning to explore the full potential of this novel class of polymers and oligomers, and we aim at extending our investigations to further B=N-linked molecular and macromolecular materials.

2.8.4 Experimental Section

General procedures. All manipulations before the aqueous workup were performed under an atmosphere of dry argon using standard Schlenk techniques or in an MBraun glovebox. Solvents (dichloromethane (DCM), tetrahydrofuran (THF)) were dried and degassed by means of an Innovative Technology solvent purification system (SPS). $CDCl_3$ for NMR spectroscopy as well as triethylamine (NEt_3), aniline, n-pentane and methanol were dried and degassed at reflux over CaH_2, Na or Mg respectively, and freshly distilled prior to use. Solvents for aqueous work-up (DCM, n-hexane), *p*-phenylenediamine (PPD) and pentamethylsilazane (Me_3SiNMe_2) were commercially purchased and used as received. **1**,[15] **4**,[16] **6**,[16] **9**,[15] **11**,[16] **13**,[16] **19**,[16] **24**,[26] were prepared according to literature procedures. NMR spectra were recorded at 25 °C on a Bruker Avance III HD spectrometer operating at 300 MHz, on a Bruker Avance 500 spectrometer operating at 500 MHz or on a Avance Neo I 600 operating at 600 MHz. Chemical shifts were referenced to residual protic impurities in the solvent (^1H) or the deuterio solvent itself (^{13}C) and reported relative to external SiMe4 (^1H, ^{13}C, ^{29}Si), $BF_3{\cdot}OEt_2$ (^{11}B) standards. Mass spectra were obtained with the use of a Thermo Scientific Exactive Plus Orbitrap MS system employing liquid injection field desorption ionization (LIFDI). Elemental analyses were performed on an Elementar vario MICRO cube elemental analyzer. UV–vis spectra were obtained using a Perkin Elmer LAMDA 465 UV/Vis spectrophotometer. The emission spectra were recorded using an Edinburgh Instruments FLSP920 spectrometer equipped with a double monochromator for both excitation and emission, operating in right-angle geometry mode, and all spectra were fully corrected for the spectral response of the instrument. Fluorescence quantum yields were measured using a calibrated integrating sphere from Edinburgh Instruments combined with the FLSP920 spectrometer described above. Thin films of the iminoborane oligomers and polymers were prepared from a solution of 60 mg poly(methyl methacrylate) (PMMA) and 0.25 mg of the compounds (stock solution) in 1.0 mL DCM by slow

evaporation on the side of the cuvettes under normal conditions and then drying at 60 °C. Dynamic light scattering (DLS) experiments were performed using a ALV/CGS-3 Compact Goniometer System with a scattering electronics and multiple tau digital correlator and a 22 mW HeNe-Laser (632.8 nm). Measurements were performed at 25 °C with a scattering angle of 90° and the concentration of the samples kept at $5 \cdot 10^{-5}$ M. Cyclic voltammetry experiments were performed using a Gamry Interface 1010B potentiostat. A standard three-electrode cell configuration was employed using a platinum disk working electrode, a platinum wire counter electrode, and a silver wire, separated by a Vycor tip, serving as the reference electrode. Tetra-n-butylammonium hexafluorophosphate ([n-Bu_4N][PF_6]) was employed as the supporting electrolyte. The scans were referenced after the addition of a small amount of ferrocene as internal standard. The potentials are reported relative to the ferrocene/ferrocenium couple. All experiments were measured at room temperature under an argon atmosphere. GPC chromatograms were recorded on an Agilent 1260 Infinity II Series, equipped with two PSS SDV 3 µm 1000 Å (300x8 mm) columns and one PSS SDV 3 µm 10000 Å (300x8 mm) column, at 25 °C with a flow rate of 1 mL min-1 and calibrated against polystyrene standards. The samples were diluted in THF and toluene as internal standard. Detection was carried out via UV signal (λ = 254 nm). Evaluation of the chromatograms was performed by using WinGPC software.

Spectra. All spectra and other result figures are shown in Appendix 5.8.

Synthesis of 3.[15] To a solution of **6** (93 mg, 0.25 mmol, 1 equiv.) in DCM (2.5 mL) was added NEt_3 (0.2 mL) at room temperature. Subsequently, aniline (**2**) (26 mg, 0.28 mmol, 1.1 equiv.) was added and the reaction mixture was stirred overnight. The volatiles were removed *in vacuo* and the formed salt was removed by filtration with THF. After removing the solvent *in vacuo*, the residue was purified by column chromatography (neutral AlO_x, *n*-hexane/DCM 10:1) to obtain **3** as colorless solid (57 mg, 0.147 mmol, 59 % yield). ^{1}H NMR (500 MHz, $CDCl_3$): δ = 7.63-7.61 (m, 2H, B-*o*-Ph-C*H*), 7.44-7.36 (m, 3H, B-*m/p*-Ph-C*H*), 7.09-7.06 (m, 2H, N-*m*-Ph-C*H*), 7.01 (s, 2H, Tip-Ar-C*H*), 6.96 (br, 1H; N*H*), 6.91-6.88 (m, 1H, N-*p*-Ph-C*H*), 6.80-6.78 (m, 2H, N-*o*-Ph-C*H*), 2.95 (sept, 1H, *p*-Tip-C*H*), 2.69 (sept, 2H, *o*-Tip-C*H*), 1.32 (d, 6H, *p*-Tip-CH_3), 0.99 (d, 6H, *o*-Tip-CH_3), 0.96 (d, 6H, *o*-Tip-CH_3) ppm; ^{11}B{^{1}H} NMR (160 MHz, $CDCl_3$): δ = 43.5 ppm; ^{13}C{^{1}H} NMR (126 MHz, $CDCl_3$): δ = 149.8 (s, *o*-Tip-*C*), 149.1 (s, *p*-Tip-*C*), 143.9 (s, N-Ph-C_{ipso}), 140.6 (br, B-Ph-C_{ipso}), 135.9 (br, B-Tip-C_{ipso}), 133.3 (s, B-*o*-Ph-*C*H), 130.4 (s, B-*p*-Ph-*C*H), 128.9 (s, N-*m*-Ph-*C*H), 128.1 (s, B-*m*-Ph-*C*H), 122.6 (s, N-*p*-Ph-*C*H), 120.5 (s, Tip-CH_{Ar}), 120.5 (s, N-*o*-Ph-*C*H), 34.9 (s, *o*-Tip-*C*H), 34.4 (s, *p*-Tip-*C*H), 24.7 (s, *o*-Tip-CH_3), 24.3 (s, *p*-Tip-CH_3), 24.3 (s, *o*-Tip-CH_3) ppm; UV/Vis (THF): $\lambda_{abs,\,max}$ = 272 nm ($\varepsilon = 0.9 \cdot 10^4$ L

mol^{-1} cm^{-1}), UV/Vis (PMMA): $\lambda_{abs,\ max}$ = 272 nm; fluorescence (PMMA): $\lambda_{em,\ max}$ = 466 nm (Φ_{fl} = 36 %).

Synthesis of 5. To a solution of **4** (754.0 mg, 2.0 mmol, 1 equiv.) in DCM (20 mL) was added NEt_3 (1 mL) at −30°C. Subsequently, aniline (**2**) (200.4 mg, 2.15 mmol, 1.1 equiv.) was added and the reaction mixture was warmed to room temperature overnight. The volatiles were removed *in vacuo* and the formed salt was removed by filtration with THF (3 x 5 mL). After removing the solvent *in vacuo*, the residue was purified by column chromatography (neutral AlO_x, *n*-hexane/DCM 5:1). After recrystallisation in *n*-pentane, **5** was obtained as a yellowish solid (506.0 mg, 1.30 mmol, 65 % yield). ^{1}H NMR (600 MHz, $CDCl_3$): δ = 7.62 (dd, *J* = 4.7 Hz, *J* = 0.9 Hz, 1H; Thi-C*H*), 7.34 (dd, *J* = 3.5 Hz, *J* = 0.9 Hz, 1H, Thi-C*H*), 7.17 (dd, *J* = 4.7 Hz, *J* = 3.5 Hz, 1H, Thi-C*H*), 7.08-7.05 (m, 2H, Ph-C*H*), 7.00 (s, 2H, Tip-Ar-C*H*), 6.90-6.87 (m, 1H, Ph-C*H*), 6.80 (s, 1H, N*H*), 6.79-6.77 (m, 2H, Ph-C*H*), 2.94 (sept, 1H, *p*-Tip-C*H*), 2.75 (sept, 2H, *o*-Tip-C*H*), 1.31 (d, 6H, *p*-Tip-CH_3), 1.05 (d, 6H, *o*-Tip-CH_3), 0.99 (d, 6H, *o*-Tip-CH_3) ppm; ^{11}B{^{1}H} NMR (193 MHz, $CDCl_3$): δ = 39.3 (s) ppm; ^{13}C{^{1}H} NMR (151 MHz, $CDCl_3$): δ = 149.9 (s, *o*-Tip-*C*), 149.3 (s, *p*-Tip-*C*), 144.0 (br, B-Thi-C_{ipso}), 143.6 (s, N-Ph-C_{ipso}), 136.1 (s, B-Thi-*C*H), 135.4 (br, B-Tip-C_{ipso}), 131.4 (s, B-Thi-*C*H), 128.9 (s, Ph-*C*H), 128.7 (s, B-Thi-*C*H), 122.5 (s, Ph-*C*H), 120.6 (s, Tip-CH_{Ar}), 120.1 (s, Ph-*C*H), 35.0 (s, *o*-Tip-*C*H), 34.5 (s, *p*-Tip-*C*H), 24.7 (s, *o*-Tip-CH_3), 24.4 (s, *o*-Tip-CH_3), 24.3 (s, *p*-Tip-CH_3) ppm; HRMS (LIFDI): m/z calcd.: 389.2343, found: 389.2337; elem. anal. calcd. (%) for $C_{25}H_{32}BNS$: C 77.11, H 8.28, N 3.60, S 8.23; found: C 77.38, H 8.42, N 3.59, S 8.51; UV/Vis (THF): $\lambda_{abs,\ max}$ = 288 nm ($\varepsilon = 1.8 \cdot 10^4$ L mol^{-1} cm^{-1}), UV/Vis (PMMA): $\lambda_{abs,\ max}$ = 282 nm; fluorescence (PMMA): $\lambda_{em,\ max}$ = 415 nm (Φ_{fl} = 9 %).

Synthesis of 7. To a suspension of **6** (75.5 mg, 0.56 mmol, 1.1 equiv.) in DCM (3 mL) was added NEt_3 (0.55 mL) at −78 °C. After 15 min, a solution of **1** (186 mg, 0.50 mmol, 1 equiv.) in DCM (3 mL) was added and the reaction mixture was warmed to room temperature overnight. After removing the volatiles *in vacuo*, the residue was purified by column chromatography (neutral AlO_x, *n*-hexane/DCM 5:1) to obtain **7** as colorless solid (183 mg, 0.47 mmol, 94 % yield). ^{1}H NMR (500 MHz, $CDCl_3$): δ = 7.63-7.61 (m, 2H, Ph-C*H*), 7.44-7.41 (m, 1H, Ph-C*H*), 7.39-7.37 (m, 2H, Ph-C*H*), 7.30 (s, 1H, N*H*), 7.01 (s, 2H, Tip-Ar-C*H*), 6.64 (dd, *J* = 5.5 Hz, *J* = 3.6 Hz, 1H, Thi-C*H*), 6.53 (dd, *J* = 5.5 Hz, *J* = 1.4 Hz, 1H, Thi-C*H*), 6.30 (dd, *J* = 3.6 Hz, *J* = 1.4 Hz, 1H, Thi-C*H*), 2.95 (sept, 1H, *p*-Tip-C*H*), 2.66 (sept, 2H, *o*-Tip-C*H*), 1.32 (d, 6H, *p*-Tip-CH_3), 1.07 (d, 6H, *o*-Tip-CH_3), 1.00 (d, 6H, *o*-Tip-CH_3) ppm; ^{11}B{^{1}H} NMR (160 MHz, $CDCl_3$): δ = 43.2 (s) ppm; ^{13}C{^{1}H} NMR (126 MHz, $CDCl_3$): δ = 150.6 (s, *o*-Tip-*C*), 149.7 (s, *p*-Tip-*C*), 148.4 (s, N-Thi-C_{ipso}), 139.2 (br, B-Ph-C_{ipso}), 134.3 (br, B-Tip-C_{ipso}), 133.5 (s, Ph-C*H*), 130.6 (s, Ph-*C*H), 128.1 (s, Ph-C*H*), 124.8 (s, N-Thi-*C*H), 120.5 (s, Tip-CH_{Ar}), 116.4 (s, N-Thi-

*C*H), 113.4 (s, N-Thi-*C*H), 35.0 (s, *o*-Tip-*C*H), 34.5 (s, *p*-Tip-*C*H), 25.0 (s, *o*-Tip-*C*H_3), 24.4 (s, *p*-Tip-*C*H_3), 24.3 (s, *o*-Tip-*C*H_3) ppm; HRMS (LIFDI): m/z calcd.: 389.2343, found: 389.2336; elem. anal. calcd. (%) for $C_{25}H_{32}BNS$: C 77.11, H 8.28, N 3.60, S 8.23; found: C 77.31, H 8.28, N 3.60, S 8.28; UV/Vis (THF): $\lambda_{abs,\,max}$ = 296 nm ($\varepsilon = 0.9 \cdot 10^4$ L mol^{-1} cm^{-1}), UV/Vis (PMMA): $\lambda_{abs,\,max}$ = 296 nm; fluorescence (PMMA): $\lambda_{em,\,max}$ = 440 nm (Φ_{fl} = 10 %).

Synthesis of 8.[16] To a suspension of **6** (75.3 mg, 0.56 mmol, 1.1 equiv.) in DCM (3 mL) was added NEt_3 (0.55 mL) at −78 °C. After 15 min, a solution of **4** (190 mg, 0.50 mmol, 1 equiv.) in DCM (3 mL) was added and the reaction mixture was warmed to room temperature overnight. After removing the volatiles *in vacuo*, the residue was purified by column chromatography (neutral AlO_x, *n*-hexane/DCM 5:1) to obtain **8** as yellowish solid (137 mg, 0.35 mmol, 69 % yield). ^{1}H NMR (500 MHz, $CDCl_3$): δ = 7.64 (dd, *J* = 4.7 Hz, *J* = 0.9 Hz, 1H, B-Thi-C*H*), 7.37 (dd, *J* = 3.5 Hz, *J* = 0.9 Hz, 1H, B-Thi-C*H*), 7.18 (dd, *J* = 4.7 Hz, *J* = 3.5 Hz, 1H, B-Thi-C*H*), 7.12 (s, 1H, N*H*), 7.01 (s, 2H, Tip-Ar-C*H*), 6.63 (dd, *J* = 5.5 Hz, *J* = 3.7 Hz, 1H, N-Thi-C*H*), 6.51 (dd, *J* = 5.5 Hz, *J* = 1.3 Hz, 1H, N-Thi-C*H*), 6.29 (dd, *J* = 3.7 Hz, *J* = 1.3 Hz, 1H, N-Thi-C*H*), 2.94 (sept, 1H, *p*-Tip-C*H*), 2.71 (sept, 2H, *o*-Tip-C*H*), 1.31 (d, 6H, *p*-Tip-C*H*$_3$), 1.08 (d, 6H, *o*-Tip-C*H*$_3$), 1.05 (d, 6H, *o*-Tip-C*H*$_3$) ppm; ^{11}B{^{1}H} NMR (160 MHz, $CDCl_3$): δ = 39.8 (s) ppm; ^{13}C{^{1}H} NMR (126 MHz, $CDCl_3$): δ = 150.7 (s, *o*-Tip-*C*), 149.9 (s, *p*-Tip-*C*), 148.0 (s, N-Thi-*C*$_{ipso}$), 142.7 (br, B-Thi-*C*$_{ipso}$), 136.7 (s, B-Thi-*C*H), 133.8 (br, B-Tip-*C*$_{ipso}$), 131.7 (s, B-Thi-*C*H), 128.8 (s, B-Thi-*C*H), 124.8 (s, N-Thi-*C*H), 120.6 (s, Tip-*C*H$_{Ar}$), 116.4 (s, N-Thi-*C*H), 113.2 (s, N-Thi-*C*H), 35.0 (s, *o*-Tip-*C*H), 34.5 (s, *p*-Tip-*C*H), 25.0 (s, *o*-Tip-*C*H_3), 24.3 (s, *o*-Tip-*C*H_3), 24.3 (s, *p*-Tip-*C*H_3) ppm; HRMS (LIFDI): m/z calcd.: 395.1907, found: 395.1903; elem. anal. calcd. (%) for $C_{23}H_{30}BNS_2$: C 69.86, H 7.65, N 3.54, S 16.22; found: C 70.03, H 7.79, N 3.63, S 16.82; UV/Vis (THF): $\lambda_{abs,\,max}$ = 305 nm ($\varepsilon = 1.3 \cdot 10^4$ L mol^{-1} cm^{-1}), UV/Vis (PMMA): $\lambda_{abs,\,max}$ = 305 nm; fluorescence (PMMA): $\lambda_{em,\,max}$ = 445 nm (Φ_{fl} = 6 %).

Synthesis of 10.[15] To a suspension of **9** (332 mg, 0.50 mmol, 1 equiv.) in DCM (10 mL) was added NEt_3 (0.5 mL) at room temperature. Subsequently, aniline (**2**) (101 mg, 1.10 mmol, 2.2 equiv.) was added and the reaction mixture was stirred overnight. All volatiles were removed *in vacuo* and the residue was purified by column chromatography (neutral AlO_x, *n*-hexane/DCM 3:1) to obtain **10** as colorless solid (305 mg, 0.443 mmol, 89 % yield). ^{1}H NMR (500 MHz, $CDCl_3$): δ = 7.60 (s, 4H, B-C$_6$*H*$_4$), 7.09-7.06 (m, 4H, N-*m*-Ph-C*H*), 6.99 (br, 4H, Tip-Ar-C*H*), 6.99 (br, 2H; N*H*), 6.91-6.88 (m, 2H, N-*p*-Ph-C*H*), 6.83-6.81 (m, 4H, N-*o*-Ph-C*H*), 2.93 (sept, 2H, *p*-Tip-C*H*), 2.68 (sept, 4H, *o*-Tip-C*H*), 1.30 (d, 12H, *p*-Tip-C*H*$_3$), 0.96 (d, 24H, *o*-Tip-C*H*$_3$) ppm; ^{11}B{^{1}H} NMR (160 MHz, $CDCl_3$): δ = 43.8 ppm; ^{13}C{^{1}H} NMR (126 MHz, $CDCl_3$): δ = 149.7 (s, *o*-Tip-*C*), 149.0 (s, *p*-Tip-*C*), 143.9 (s, N-Ph-*C*$_{ipso}$), 142.7 (br, B-Ph-*C*$_{ipso}$), 135.9 (br, B-Tip-*C*$_{ipso}$), 132.7 (s, B-C$_6$H$_4$-*C*H), 128.9 (s, N-*m*-Ph-*C*H), 122.6 (s, N-*p*-Ph-*C*H), 120.5 (s,

Tip-*C*H_{Ar}), 120.5 (s, N-*o*-Ph-*C*H), 34.9 (s, *o*-Tip-*C*H), 34.4 (s, *p*-Tip-*C*H), 24.7 (s, *o*-Tip-*C*H_3), 24.3 (s, *p*-Tip-*C*H_3), 24.3 (s, *o*-Tip-*C*H_3) ppm; UV/Vis (THF): $\lambda_{abs,\ max}$ = 298 nm ($\varepsilon = 2.6 \cdot 10^4$ L mol^{-1} cm^{-1}), UV/Vis (PMMA): $\lambda_{abs,\ max}$ = 298 nm; fluorescence (PMMA): $\lambda_{em,\ max}$ = 442 nm (Φ_{fl} = 31 %).

Synthesis of 12. To a solution of **11** (1.34 g, 2.0 mmol, 1 equiv.) in DCM (20 mL) was added NEt_3 (2 mL) at −30°C. Subsequently, **2** (441 mg, 4.74 mmol, 2.4 equiv.) was added and the reaction mixture was warmed to room temperature overnight. The volatiles were removed *in vacuo* and the formed salt was removed by filtration with THF (3 x 5 mL). After removing the solvent *in vacuo*, the residue was purified by column chromatography (neutral AlO_x, *n*-hexane/DCM 3:1). After recrystallisation in *n*-pentane, **12** was obtained as a colorless solid (910 mg, 1.40 mmol, 70 % yield). ^{1}H NMR (600 MHz, $CDCl_3$): δ = 7.32 (s, 2H; Thi-C*H*), 7.08-7.05 (m, 4H, Ph-C*H*), 7.00 (s, 4H, Tip-Ar-C*H*), 6.90-6.87 (m, 2H, Ph-C*H*), 6.86 (s, 2H, N*H*), 6.79-6.77 (m, 4H, Ph-C*H*), 2.94 (sept, 2H, *p*-Tip-C*H*), 2.75 (sept, 4H, *o*-Tip-C*H*), 1.31 (d, 12H, *p*-Tip-CH_3), 1.03 (d, 12H, *o*-Tip-CH_3), 0.99 (d, 12H, *o*-Tip-CH_3) ppm; ^{11}B{^{1}H} NMR (193 MHz, $CDCl_3$): δ = 39.7 (br) ppm; ^{13}C{^{1}H} NMR (151 MHz, $CDCl_3$): δ = 150.3 (br, B-Thi-C_{ipso}), 149.9 (s, *o*-Tip-*C*), 149.3 (s, *p*-Tip-*C*), 143.6 (s, N-Ph-C_{ipso}), 137.3 (s, B-Thi-*C*H), 135.5 (br, B-Tip-C_{ipso}), 128.9 (s, Ph-*C*H), 122.6 (s, Ph-*C*H), 120.6 (s, Tip-*C*H_{Ar}), 120.2 (s, Ph-*C*H), 35.0 (s, *o*-Tip-*C*H), 34.4 (s, *p*-Tip-*C*H), 24.7 (s, *o*-Tip-*C*H_3), 24.3 (s, *o*-Tip-*C*H_3), 24.3 (s, *p*-Tip-*C*H_3) ppm; HRMS (LIFDI) m/z calcd.: 694.4673, found: 694.4645; elem. anal. calcd. (%) for $C_{46}H_{60}B_2N_2S$: C 79.53, H 8.71, N 4.03, S 4.62; found: C 79.82, H 8.85, N 4.13, S 4.50; UV/Vis (THF): $\lambda_{abs,\ max}$ = 323 nm ($\varepsilon = 3.6 \cdot 10^4$ L mol^{-1} cm^{-1}), UV/Vis (PMMA): $\lambda_{abs,\ max}$ = 319 nm; fluorescence (PMMA): $\lambda_{em,\ max}$ = 415 nm (Φ_{fl} = 15 %).

Synthesis of 14. To a suspension of **9** (332 mg, 0.50 mmol, 1 equiv.) in DCM (4 mL) was added a solution of **13** (193 mg, 1.13 mmol, 2.3 equiv.) in DCM (3 mL) at room temperature. After stirring the reaction mixture overnight, all volatiles were removed *in vacuo*. The residue was purified by column chromatography (neutral AlO_x, *n*-hexane/DCM 2:1) to obtain **14** as colorless solid (296 mg, 0.42 mmol, 85 % yield). ^{1}H NMR (500 MHz, $CDCl_3$): δ = 7.60 (s, 4H, Ph-C*H*), 7.32 (s, 2H, N*H*), 6.99 (s, 4H Tip-Ar-C*H*), 6.64 (dd, *J* = 5.5 Hz, *J* = 3.7 Hz, 2H, N-Thi-C*H*), 6.53 (dd, *J* = 5.5 Hz, *J* = 1.4 Hz, 2H, N-Thi-C*H*), 6.31 (dd, *J* = 3.7 Hz, *J* = 1.4 Hz, 2H, N-Thi-C*H*), 2.93 (sept, 2H, *p*-Tip-C*H*), 2.65 (sept, 4H, *o*-Tip-C*H*), 1.31 (d, 12H, *p*-Tip-CH_3), 1.06 (d, 12H, *o*-Tip-CH_3), 0.96 (d, 12H, *o*-Tip-CH_3) ppm; ^{11}B{^{1}H} NMR (160 MHz, $CDCl_3$): δ = 43.2 (br) ppm; ^{13}C{^{1}H} NMR (126 MHz, $CDCl_3$): δ = 150.5 (s, *o*-Tip-*C*), 149.7 (s, *p*-Tip-*C*), 148.4 (s, N-Thi-C_{ipso}), 141.6 (br, B-Ph-C_{ipso}), 134.3 (br, B-Tip-C_{ipso}), 133.0 (s, Ph-*C*H), 124.8 (s, N-Thi-*C*H), 120.5 (s, Tip-*C*H_{Ar}), 116.6 (s, N-Thi-*C*H), 113.5 (s, N-Thi-*C*H), 35.0 (s, *o*-Tip-*C*H), 34.5 (s, *p*-Tip-*C*H), 24.9 (s, *o*-Tip-*C*H_3), 24.4 (s, *p*-Tip-*C*H_3), 24.2 (s, *o*-Tip-*C*H_3) ppm; HRMS (LIFDI):

m/z calcd.: 700.4222, found: 700.4217; elem. anal. calcd. (%) for $C_{44}H_{58}B_2N_2S_2$: C 75.42, H 8.34, N 4.00, S 9.15; found: C 74.97, H 8.41, N 4.14, S 9.22; UV/Vis (THF): $\lambda_{abs,\,max}$ = 322 nm ($\varepsilon = 2.3 \cdot 10^4$ L mol^{-1} cm^{-1}), UV/Vis (PMMA): $\lambda_{abs,\ max}$ = 318 nm; fluorescence (PMMA): $\lambda_{em,\,max}$ = 449 nm (Φ_{fl} = 10 %).

Synthesis of 15.[16] To a solution of **11** (337 mg, 0.50 mmol, 1 equiv.) in DCM (4 mL) was added a solution of **13** (193 mg, 1.13 mmol, 2.3 equiv.) in DCM (3 mL) at room temperature. After stirring the reaction mixture overnight, all volatiles were removed *in vacuo*. The residue was purified by column chromatography (neutral AlO_x, *n*-hexane/DCM 2:1) to obtain **15** as off-white solid (296 mg, 0.42 mmol, 85 % yield). ^{1}H NMR (500 MHz, $CDCl_3$): δ = 7.38 (s, 2H, B-Thi-C*H*), 7.18 (s, 2H, N*H*), 7.00 (s, 4H Tip-Ar-C*H*), 6.63 (dd, *J* = 5.5 Hz, *J* = 3.7 Hz, 2H, N-Thi-C*H*), 6.52 (dd, *J* = 5.5 Hz, *J* = 1.4 Hz, 2H, N-Thi-C*H*), 6.28 (dd, *J* = 3.7 Hz, *J* = 1.4 Hz, 2H, N-Thi-C*H*), 2.94 (sept, 2H, *p*-Tip-C*H*), 2.71 (sept, 4H, *o*-Tip-C*H*), 1.31 (d, 12H, *p*-Tip-CH_3), 1.08 (d, 12H, *o*-Tip-CH_3), 1.03 (d, 12H, *o*-Tip-CH_3) ppm; ^{11}B{^{1}H} NMR (160 MHz, $CDCl_3$): δ = 39.8 (br) ppm; ^{13}C{^{1}H} NMR (126 MHz, $CDCl_3$): δ = 150.7 (s, *o*-Tip-*C*), 149.9 (s, *p*-Tip-*C*), 149.4 (br, B-Thi-C_{ipso}), 147.9 (s, N-Thi-C_{ipso}), 137.5 (s, B-Thi-*C*H), 133.9 (br, B-Tip-C_{ipso}), 124.8 (s, N-Thi-*C*H), 120.6 (s, Tip-CH_{Ar}), 116.5 (s, N-Thi-*C*H), 113.4 (s, N-Thi-*C*H), 35.0 (s, *o*-Tip-*C*H), 34.5 (s, *p*-Tip-*C*H), 25.0 (s, *o*-Tip-CH_3), 24.3 (s, *p*-Tip-CH_3), 24.3 (s, *o*-Tip-CH_3) ppm; HRMS (LIFDI): m/z calcd.: 706.3787, found: 706.3779; elem. anal. calcd. (%) for $C_{42}H_{56}B_2N_2S_3$: C 71.38, H 7.99, N 3.96, S 13.61; found: C 71.47, H 8.12, N 4.01, 13.83; UV/Vis (THF): $\lambda_{abs,\,max}$ = 340 nm ($\varepsilon = 3.0 \cdot 10^4$ L mol^{-1} cm^{-1}), UV/Vis (PMMA): $\lambda_{abs,\ max}$ = 331 nm; fluorescence (PMMA): $\lambda_{em,\,max}$ = 462 nm (Φ_{fl} = 10 %).

Synthesis of 17.[15] To a solution of **1** (228 mg, 0.615 mmol, 2.05 equiv.) in DCM (3 mL) was added NEt_3 (0.3 mL). Subsequently, **16** (32.4 mg, 0.3 mmol, 1 equiv.) was added at room temperature and the reaction mixture was stirred overnight. The volatiles were removed *in vacuo* and the formed salt was removed by filtration with THF. After removing the solvent *in vacuo*, the residue was purified by column chromatography (neutral AlO_x, *n*-hexane/DCM 4:1) to obtained **17** as a colorless solid (177 mg, 0.257 mmol, 86 % yield). ^{1}H NMR (500 MHz, $CDCl_3$): δ = 7.58-7.56 (m, 4H, B-*o*-Ph-C*H*), 7.40-7.33 (m, 6H, B-*m/p*-Ph-C*H*), 6.95 (s, 4H, Tip-Ar-C*H*), 6.80 (br, 2H; N*H*), 6.45 (s, 4H, N-C_6H_4), 2.92 (sept, 2H, *p*-Tip-C*H*), 2.63 (sept, 4H, *o*-Tip-C*H*), 1.30 (d, 12H, *p*-Tip-CH_3), 0.97 (d, 12H, *o*-Tip-CH_3), 0.90 (d, 12H, *o*-Tip-CH_3) ppm; ^{11}B{^{1}H} NMR (160 MHz, $CDCl_3$): δ = 43.3 ppm; ^{13}C{^{1}H} NMR (126 MHz, $CDCl_3$): δ = 149.8 (s, *o*-Tip-*C*), 149.0 (s, *p*-Tip-*C*), 140.5 (s, B-Ph-C_{ipso}), 138.8 (s, N-Ph-C_{ipso}), 135.9 (br, B-Tip-C_{ipso}), 133.2 (s, B-*o*-Ph-*C*H), 130.2 (s, B-*p*-Ph-*C*H), 128.0 (s, B-*m*-Ph-*C*H), 120.7 (s, N-C_6H_4-*C*H), 120.4 (s, Tip-CH_{Ar}), 34.8 (s, *o*-Tip-*C*H), 34.5 (s, *p*-Tip-*C*H), 24.7 (s, *o*-Tip-CH_3), 24.4 (s, *p*-Tip-

CH_3), 24.2 (s, *o*-Tip-CH_3) ppm; UV/Vis (THF): $\lambda_{abs,\ max}$ = 308 nm ($\varepsilon = 1.9 \cdot 10^4$ L mol^{-1} cm^{-1}), UV/Vis (PMMA): $\lambda_{abs,\ max}$ = 306 nm; fluorescence (PMMA): $\lambda_{em,\ max}$ = 426 nm (Φ_{fl} = 42 %).

Synthesis of 18. To a solution of **4** (1.55 g, 4.1 mmol, 2.04 equiv.) in DCM (20 mL) was added NEt_3 (2 mL) and **16** (217 mg, 2.01 mmol, 1 equiv.) at room temperature. After stirring the reaction mixture overnight and removing all volatiles *in vacuo*, the residue was purified by column chromatography (neutral AlO_x, *n*-hexane/DCM 3:1). After recrystallisation in *n*-hexane and DCM, **18** was obtained as yellowish solid (1.18 g, 1.69 mmol, 85 % yield). ^{1}H NMR (500 MHz, $CDCl_3$): δ = 7.58 (dd, *J* = 4.7 Hz, *J* = 1.0 Hz, 2H; Thi-C*H*), 7.28 (dd, *J* = 3.5 Hz, *J* = 1.0 Hz, 2H, Thi-C*H*), 7.14 (dd, *J* = 4.7 Hz, *J* = 3.5 Hz, 2H, Thi-C*H*), 6.95 (s, 4H, Tip-Ar-C*H*), 6.63 (s, 2H, N*H*), 6.44 (s, 4H, Ph-C*H*), 2.91 (sept, 2H, *p*-Tip-C*H*), 2.69 (sept, 4H, *o*-Tip-C*H*), 1.29 (d, 12H, *p*-Tip-CH_3), 1.02 (d, 12H, *o*-Tip-CH_3), 0.92 (d, 12H, *o*-Tip-CH_3) ppm; ^{11}B{^{1}H} NMR (160 MHz, $CDCl_3$): δ = 38.2 (br) ppm; ^{13}C{^{1}H} NMR (126 MHz, $CDCl_3$): δ = 149.9 (s, *o*-Tip-*C*), 149.2 (s, *p*-Tip-*C*), 144.0 (br, B-Thi-C_{ipso}), 138.5 (s, N-Ph-C_{ipso}), 135.9 (s, B-Thi-*C*H), 135.4 (br, B-Tip-C_{ipso}), 131.1 (s, B-Thi-*C*H), 128.6 (s, B-Thi-*C*H), 120.4 (s, Tip-CH_{Ar}), 120.4 (s, Ph-*C*H), 34.8 (s, *o*-Tip-*C*H), 34.5 (s, *p*-Tip-*C*H), 24.7 (s, *o*-Tip-CH_3), 24.3 (s, *p*-Tip-CH_3), 24.3 (s, *o*-Tip-CH_3) ppm; HRMS (LIFDI) m/z calcd.: 700.4237, found: 700.4206; elem. anal. calcd. (%) for $C_{44}H_{58}B_2N_2S_2$: C 75.42, H 8.34, N 4.00, S 9.15; found: C 75.53, H 8.41, N 4.01, S 9.15; UV/Vis (THF): $\lambda_{abs,\ max}$ = 320 nm ($\varepsilon = 2.8 \cdot 10^4$ L mol^{-1} cm^{-1}), UV/Vis (PMMA): $\lambda_{abs,\ max}$ = 318 nm; fluorescence (PMMA): $\lambda_{em,\ max}$ = 435 nm (Φ_{fl} = 29 %).

Synthesis of 20. To a solution of **1** (371 mg, 1.00 mmol, 2 equiv.) in DCM (3 mL) was added a solution of **19** (129 mg, 0.50 mmol, 1 equiv.) in DCM (2 mL) at room temperature. The reaction mixture was stirred overnight and all volatiles were removed *in vacuo*. The crude product was purified by column chromatography (neutral AlO_x, *n*-hexane/DCM 4:1) and washed with *n*-pentane (3 x 4 mL) at −30 °C to give **20** as colorless solid (219 mg, 0.32 mmol, 63 % yield). ^{1}H NMR (500 MHz, $CDCl_3$): δ = 7.52-7.51 (m, 4H, Ph-C*H*), 7.39-7.32 (m, 6H, Ph-C*H*), 6.97 (s, 4H, Tip-Ar-C*H*), 6.86 (s, 2H, N*H*), 5.68 (s, 2H; Thi-C*H*), 2.94 (sept, 2H, *p*-Tip-C*H*), 2.60 (sept, 4H, *o*-Tip-C*H*), 1.32 (d, 12H, *p*-Tip-CH_3), 1.03 (d, 12H, *o*-Tip-CH_3), 0.96 (d, 12H, *o*-Tip-CH_3) ppm; ^{11}B{^{1}H} NMR (160 MHz, $CDCl_3$): δ = 42.3 (br) ppm; ^{13}C{^{1}H} NMR (126 MHz, $CDCl_3$): δ = 150.4 (s, *o*-Tip-*C*), 149.2 (s, *p*-Tip-*C*), 139.5 (br, B-Tip-C_{ipso}), 139.0 (s, N-Thi-C_{ipso}), 134.5 (br, B-Tip-C_{ipso}), 133.3 (s, Ph-*C*H), 130.4 (s, Ph-*C*H), 128.0 (s, Ph-*C*H), 120.4 (s, Tip-CH_{Ar}), 111.8 (s, Thi-*C*H), 34.9 (s, *o*-Tip-*C*H), 34.4 (s, *p*-Tip-*C*H), 24.9 (s, *o*-Tip-CH_3), 24.5 (s, *o*-Tip-CH_3), 24.3 (s, *p*-Tip-CH_3) ppm; HRMS (LIFDI): m/z calcd.: 694.4658, found: 694.4650; elem. anal. calcd. (%) for $C_{46}H_{60}B_2N_2S$: C 79.53, H 8.71, N 4.03, S 4.62; found: C 79.55, H 8.71, N 4.03, S 4.53; UV/Vis (THF): $\lambda_{abs,\ max}$ = 341 nm ($\varepsilon = 1.5 \cdot 10^4$ L mol^{-1} cm^{-1}), UV/Vis (PMMA): $\lambda_{abs,\ max}$ = 329 nm; fluorescence (PMMA): $\lambda_{em,\ max}$ = 459 nm (Φ_{fl} = 13 %).

Synthesis of 21.[16] To a solution of **19** (377 mg, 1.00 mmol, 2 equiv.) in DCM (3 mL) was added a solution of **4** (129 mg, 0.50 mmol, 1 equiv.) in DCM (2 mL) at room temperature. The reaction mixture was stirred overnight and all volatiles were removed *in vacuo*. The crude product was purified by column chromatography (neutral AlO_x, *n*-hexane/DCM 4:1) and recrystallised in *n*-pentane at −30 °C to give **21** as off-white solid (244 mg, 0.33 mmol, 66 % yield). ^{1}H NMR (500 MHz, $CDCl_3$): δ = 7.58 (dd, *J* = 4.7 Hz, *J* = 0.84 Hz, 2H, B-Thi-C*H*), 7.25 (dd, *J* = 3.6 Hz, *J* = 0.95 Hz, 2H, B-Thi-C*H*), 7.13 (dd, *J* = 4.7 Hz, *J* = 3.5 Hz, 2H, B-Thi-C*H*), 6.96 (s, 4H Tip-Ar-C*H*), 6.68 (s, 2H, N*H*), 5.68 (s, 2H, N-Thi-C*H*), 2.93 (sept, 2H, *p*-Tip-C*H*), 2.65 (sept, 4H, *o*-Tip-C*H*), 1.31 (d, 12H, *p*-Tip-CH_3), 1.03 (d, 12H, *o*-Tip-CH_3), 1.01 (d, 12H, *o*-Tip-CH_3) ppm; ^{11}B{^{1}H} NMR (160 MHz, $CDCl_3$): δ = 39.0 (br) ppm; ^{13}C{^{1}H} NMR (126 MHz, $CDCl_3$): δ = 150.5 (s, *o*-Tip-*C*), 149.4 (s, *p*-Tip-*C*), 142.9 (br, B-Thi-C_{ipso}), 138.5 (s, N-Thi-C_{ipso}), 136.3 (s, B-Thi-*C*H), 134.0 (br, B-Tip-C_{ipso}), 131.4 (s, B-Thi-*C*H), 128.6 (s, B-Thi-*C*H), 120.4 (s, Tip-*C*H_{Ar}), 111.8 (s, N-Thi-*C*H), 34.9 (s, *o*-Tip-*C*H), 34.4 (s, *p*-Tip-*C*H), 24.9 (s, *o*-Tip-*C*H_3), 24.5 (s, *o*-Tip-*C*H_3), 24.3 (s, *p*-Tip-*C*H_3) ppm; HRMS (LIFDI): m/z calcd.: 706.3787, found: 706.3777; elem. anal. calcd. (%) for $C_{44}H_{64}B_2N_2S_3$: C 71.53, H 8.73, N 3.79, S 13.02; found: C 71.76, H 8.39, N 3.73, 13.27; UV/Vis (THF): $\lambda_{abs,\ max}$ = 348 nm ($\varepsilon = 2.0 \cdot 10^4$ L mol^{-1} cm^{-1}), UV/Vis (PMMA): $\lambda_{abs,\ max}$ = 329 nm; fluorescence (PMMA): $\lambda_{em,\ max}$ = 479 nm (Φ_{fl} = 9 %).

Synthesis of polymer 22.[15] To a stirred solution of **9** (266 mg, 0.40 mmol, 1 equiv.) in DCM (4 mL) was added NEt_3 (0.4 mL). Subsequently, **16** (43.0 mg, 0.40 mmol, 1 equiv.) was added and the reaction mixture was stirred for 3 d. Me_3SiNMe_2 (0.10 mL) was added and the reaction mixture was stirred overnight. The volatiles were removed *in vacuo* and the formed salt was removed by filtration with THF (3 x 5 mL). Subsequently, the yellowish solid was washed with n-pentane (2 x 2 mL) at 0 °C. The crude product was dried *in vacuo*, solved in THF (3 mL) and precipitated into cooled (–30 °C) methanol (15 mL). The supernatant liquid was removed by filtration and the product was washed with cooled n-pentane (3 x 3 mL) at –30 °C. All volatiles were removed *in vacuo* to give **22** as colorless solid (111 mg, 45 % yield). ^{1}H NMR (500 MHz, $CDCl_3$): δ = 7.50 (br, 4H, B-Ph-C*H*), 6.91 (br, 4H, Tip-Ar-C*H*), 6.79 (br, 2H; N*H*), 6.44 (br, 4H, N-Ph-C*H*), 2.88 (br, 2H, *p*-Tip-C*H*), 2.59 (br, 4H, *o*-Tip-C*H*), 1.26 (br, 12H, *p*-Tip-CH_3), 0.90 (br, 12H, *o*-Tip-CH_3), 0.87 (br, 12H, *o*-Tip-CH_3) ppm; ^{11}B{^{1}H} NMR (160 MHz, $CDCl_3$): δ = broad signal; ^{13}C{^{1}H} NMR (126 MHz, $CDCl_3$): δ = 149.7 (s, *o*-Tip-*C*), 148.9 (s, *p*-Tip-*C*), 142.4 (br, B-Ph-C_{ipso}), 138.8 (s, N-Ph-C_{ipso}), 136.0 (br, B-Tip-C_{ipso}), 132.6 (s, B-Ph-*C*H), 120.7 (s, N-Ph-*C*H), 120.4 (s, Tip-*C*H_{Ar}), 34.8 (s, *o*-Tip-*C*H), 34.5 (s, *p*-Tip-*C*H), 24.6 (s, *o*-Tip-*C*H_3), 24.3 (s, *p*-Tip-*C*H_3), 24.2 (s, *o*-Tip-*C*H_3) ppm; GPC (in THF, vs. polystyrene, detection by UV-vis signal): M_n = 21 220 Da; M_w = 39 885 Da; UV/Vis (THF): $\lambda_{abs,\ max}$ = 341 nm ($\varepsilon = 2.2 \cdot 10^4$ L mol^{-1} cm^{-1}), UV/Vis (PMMA): $\lambda_{abs,\ max}$ = 341 nm; fluorescence (PMMA): $\lambda_{em,\ max}$ = 450 nm (Φ_{fl} = 25 %).

Synthesis of polymer 23.[16] To a stirred suspension of **11** (168 mg, 0.25 mmol, 1 equiv.) in DCM (2.5 mL) was added a solution of **19** (66.4 mg, 0.25 mmol, 1 equiv.) in DCM (1.0 mL) at room temperature. The mixture was stirred for 2 d and $TMSNMe_2$ (0.25 mL) was added. The mixture was stirred overnight and all volatiles were removed *in vacuo*. The crude product was solved in THF (2.5 mL) and precipitated into cooled (−78 °C) methanol (25 mL). The supernatant liquid was removed by filtration at −78 °C and dried *in vacuo*. The precipitation process was repeated for complete purification to give **23** as a pale yellow solid. (63.4 mg, 38 % yield). ^{1}H NMR (500 MHz, $CDCl_3$): δ = 7.20 (m, 2H, B-Thi-C*H*), 6.94 (m, 4H Tip-Ar-C*H*), 6.70 (m, 2H, N*H*), 5.64 (m, 2H, N-Thi-C*H*), 2.92 (m, 2H, *p*-Tip-C*H*), 2.61 (m, 4H, *o*-Tip-C*H*), 1.29 (m, 12H, *p*-Tip-CH_3), 1.01 (m, 12H, *o*-Tip-CH_3), 0.96 (m, 12H, *o*-Tip-CH_3) ppm; ^{11}B{^{1}H} NMR (160 MHz, $CDCl_3$): δ = to broad; ^{13}C{^{1}H} NMR (126 MHz, $CDCl_3$): δ = 150.5 (s, *o*-Tip-*C*), 149.4 (s, *p*-Tip-*C*), 149.3 (br, B-Thi-C_{ipso}), 138.5 (s, N-Thi-C_{ipso}), 137.2 (s, B-Thi-*C*H), 134.0 (br, B-Tip-C_{ipso}), 120.4 (s, Tip-*C*H_{Ar}), 111.9 (s, N-Thi-*C*H), 34.9 (s, *o*-Tip-*C*H), 34.3 (s, *p*-Tip-*C*H), 24.9 (s, *o*-Tip-*C*H_3), 24.4 (s, *o*-Tip-*C*H_3), 24.3 (s, *p*-Tip-*C*H_3) ppm; GPC (in THF, vs. polystyrene, detection by UV-Vis signal): M_n = 14 231 Da; M_w = 23 040 Da; UV/Vis (THF): $\lambda_{abs,\,max}$ = 388 nm ($\varepsilon = 1.5 \cdot 10^4$ L mol^{-1} cm^{-1}), UV/Vis (PMMA): $\lambda_{abs,\,max}$ = 368 nm; fluorescence (PMMA): $\lambda_{em,\,max}$ = 521 nm (Φ_{fl} = 5 %).

Synthesis of polymer 25 (by salt elimination). To a stirred solution of **11** (268 mg, 0.40 mmol, 1 equiv.) in DCM (4 mL) was added NEt_3 (0.4 mL). Subsequently, **16** (43.2 mg, 0.40 mmol, 1 equiv.) was added and the reaction mixture was stirred for 2 d at ambient temperature. Me_3SiNMe_2 (0.2 mL) was added and the reaction mixture was stirred overnight. The volatiles were removed *in vacuo* and the formed salt was removed by filtration with THF (3 x 3 mL). Subsequently, all volatiles were removed *in vacuo* and the crude product was solved in THF (3 mL) and precipitated twice into cooled (−78 °C) methanol (35 mL). The supernatant liquid was removed by filtration at −78 °C and the product was dried *in vacuo* to give **25** as a pale yellow solid (98 mg, 39 % yield). ^{1}H NMR (600 MHz, $CDCl_3$): δ = 7.26-7.24 (br, 2H; Thi-C*H*), 6.91 (br, 4H, Tip-Ar-C*H*), 6.64 (s, 2H, N*H*), 6.40 (br, 4H, Ph-C*H*), 2.89 (br, 2H, *p*-Tip-C*H*), 2.65 (br, 4H, *o*-Tip-C*H*), 1.27 (br, 12H, *p*-Tip-CH_3), 0.97 (br, 12H, *o*-Tip-CH_3), 0.89 (br, 12H, *o*-Tip-CH_3) ppm; ^{11}B{^{1}H} NMR (193 MHz, $CDCl_3$): δ = 38.2 (br) ppm; ^{13}C{^{1}H} NMR (151 MHz, $CDCl_3$): δ = 150.1 (br, B-Thi-C_{ipso}), 149.8 (s, *o*-Tip-*C*), 149.1 (s, *p*-Tip-*C*), 138.5 (s, N-Ph-C_{ipso}), 136.8 (s, B-Thi-*C*H), 135.5 (br, B-Tip-C_{ipso}), 120.5 (s, Ph-*C*H), 120.4 (s, Tip-*C*H_{Ar}), 34.9 (s, *o*-Tip-*C*H), 34.4 (s, *p*-Tip-*C*H), 24.7 (s, *o*-Tip-*C*H_3), 24.3 (s, *p*-Tip-*C*H_3), 24.2 (s, *o*-Tip-*C*H_3) ppm; GPC (in THF, vs. polystyrene, detection by UV-vis signal): M_n = 19 546 Da; M_w = 27 169 Da; UV/Vis (THF): $\lambda_{abs,\,max}$ = 362 nm ($\varepsilon = 2.3 \cdot 10^4$ L mol^{-1} cm^{-1}), UV/Vis (PMMA): $\lambda_{abs,\,max}$ = 359 nm; fluorescence (PMMA): $\lambda_{em,\,max}$ = 460 nm (Φ_{fl} = 15 %).

Synthesis of polymer 25 (by Si/B exchange). To a stirred solution of **11** (268 mg, 0.40 mmol, 1 equiv.) in DCM (3 mL) was added a solution of **24** (101 mg, 0.40 mmol, 1 equiv.) in DCM (1 mL) and the reaction mixture was stirred for 2 d at ambient temperature. Me_3SiNMe_2 (0.2 mL) was added and the reaction mixture was stirred for 1 h. After solvent removal *in vacuo*, the residue was dissolved in THF (4 mL) and precipitated into cooled (−78 °C) methanol (40 mL). The precipitation was repeated one more time. The supernatant liquid was removed by filtration at –78 °C and the product was dried *in vacuo* to give **25** as an off-white solid (87 mg, 35 % yield). ^{1}H NMR (300 MHz, $CDCl_3$): δ = 7.26-7.24 (br, 2H; Thi-C*H*), 6.91 (br, 4H, Tip-Ar-C*H*), 6.63 (s, 2H, N*H*), 6.40 (br, 4H, Ph-C*H*), 2.88 (br, 2H, *p*-Tip-C*H*), 2.65 (br, 4H, *o*-Tip-C*H*), 1.27 (br, 12H, *p*-Tip-CH_3), 0.97 (br, 12H, *o*-Tip-CH_3), 0.88 (br, 12H, *o*-Tip-CH_3) ppm; GPC (in THF, vs. polystyrene, detection by UV-vis signal): M_n = 16 992 Da; M_w = 23 293 Da.

Synthesis of polymer 26. To a stirred suspension of **9** (166 mg, 0.25 mmol, 1 equiv.) in DCM (1.5 mL) was added a solution of **19** (66.4 mg, 0.25 mmol, 1 equiv.) in DCM (1.0 mL) at room temperature. The reaction mixture was stirred for 2 d and Me_3SiNMe_2 (0.25 mL) was added. The reaction mixture was stirred overnight and all volatiles were removed *in vacuo*. The crude product was solved in DCM (2.5 mL) and precipitated twice into cooled (−78 °C) methanol (25 mL). The supernatant liquid was removed by filtration at −78 °C and the product was dried *in vacuo* to give **26** as a pale yellow solid (54 mg, 35 % yield). ^{1}H NMR (500 MHz, $CDCl_3$): δ = 7.43 (br, 4H, Ph-C*H*), 6.92 (br, 4H, Tip-Ar-C*H*), 6.85 (br, 2H, N*H*), 5.69 (br, 2H; Thi-C*H*), 2.90 (br, 2H, *p*-Tip-C*H*), 2.55 (br, 4H, *o*-Tip-C*H*), 1.28 (br, 12H, *p*-Tip-CH_3), 0.99 (br, 12H, *o*-Tip-CH_3), 0.89 (br, 12H, *o*-Tip-CH_3) ppm; ^{11}B{^{1}H} NMR (160 MHz, $CDCl_3$): δ = broad signal; ^{13}C{^{1}H} NMR (126 MHz, $CDCl_3$): δ = 150.3 (s, *o*-Tip-*C*), 149.2 (s, *p*-Tip-*C*), 141.6 (br, B-Ph-C_{ipso}), 139.0 (s, N-Thi-C_{ipso}), 134.5 (br, B-Tip-C_{ipso}), 132.7 (s, Ph-*C*H), 120.3 (s, Tip-*C*H_{Ar}), 111.8 (s, Thi-*C*H), 34.9 (s, *o*-Tip-*C*H), 34.4 (s, *p*-Tip-*C*H), 24.8 (s, *o*-Tip-*C*H_3), 24.5 (s, *o*-Tip-*C*H_3), 24.3 (s, *p*-Tip-*C*H_3) ppm; GPC (in THF, vs. polystyrene, detection by UV-vis signal): M_n = 20 440; M_w = 38 934; UV/Vis (THF): $\lambda_{abs,\ max}$ = 372 nm ($\varepsilon = 1.6 \cdot 10^4$ L mol^{-1} cm^{-1}), UV/Vis (PMMA): $\lambda_{abs,\ max}$ = 360 nm; fluorescence (PMMA): $\lambda_{em,\ max}$ = 502 nm (Φ_{fl} = 10 %).

Crystallographic data

Crystals suitable for single-crystal X-ray diffraction were selected, coated in perfluoropolyether oil, and mounted on MiTeGen sample holders. Diffraction data were collected on Bruker X8 Apex II 4-circle diffractometers with CCD area detectors using Mo-Kα radiation. The crystals were cooled using an Oxford Cryostreams low-temperature device. Data were collected at 100 K. The images were processed and corrected for Lorentz-polarization effects and absorption as implemented in the Bruker software packages. The structures were solved using the intrinsic phasing method (SHELXT)[27] and Fourier expansion technique. All non-hydrogen

atoms were refined in anisotropic approximation, with hydrogen atoms 'riding' in idealized positions, by full-matrix least squares against F2 of all data, using SHELXL[28] software and the SHELXLE graphical user inter-face.[29]

Table 2.8.3. X-ray crystallographic information.

No.	**5**	**12**	**14**	**18**	**20**
CCDC number	2289519	2289521	2289523	2289522	2289531
Size / mm	0.094 x 0.205 x 0.343	0.149 x 0.206 x 0.279	0.101 x 0.157 x 0.301	0.188 x 0.345 x 0.456	0.144 x 0.340 x 0.349
Empiric Formula	$C_{25}H_{32}BNS$	$C_{46}H_{60}B_2N_2S$	$C_{44}H_{58}B_2N_2S_2$	$C_{44}H_{58}B_2N_2S_2$	$C_{46}H_{60}B_2N_2S$
M / g mol^{-1}	389.38	694.64	700.66	700.66	694.64
Crystal system	triclinic	triclinic	monoclinic	triclinic	triclinic
Space group	P -1	P -1	P 21/c	P -1	P -1
a / Å	9.3937(16)	9.304(2)	18.160(6)	9.696(3)	15.830(3)
b / Å	9.933(3)	10.903(3)	11.010(3)	14.465(4)	15.898(3)
c / Å	13.519(3)	21.021(3)	20.518(9)	15.321(5)	28.112(7)
α / deg	69.162(10)	77.299(17)	90	102.475(16)	74.829(14)
β / deg	81.78(2)	88.579(15)	91.104(18)	103.180(14)	76.14(2)
γ / deg	72.854(8)	77.497(19)	90	95.651(10)	69.016(15)
V / Å^3	1125.5(4)	2030.2(8)	4102(2)	2018.0(11)	6292(3)
Z	2	2	4	2	6
μ / mm^{-1}	0.154	0.113	0.162	0.164	0.110
T / K	100(2)	100(2)	100(2)	100(2)	99(2)
$\theta_{min,max}$	1.613, 28.198	0.993, 28.469	1.121, 26.741	1.408, 25.508	0.760, 26.532
Completeness	0.995	0.988	0.997	0.975	0.994
Reflections: total / independent	5521, 4356	10141, 8076	8676, 4897	7339, 4909	25998, 15839
R_{int}	0.0496	0.0436	0.0921	0.0771	0.0885
Final R1 and wR2	0.0426, 0.1084	0.0412, 0.1120	0.0742, 0.2093	0.0503, 0.1162	0.0702, 0.2002
Largest peak and hole / e Å^{-3}	0.344, -0.263	0.417, -0.259	0.645, -0.524	0.370, -0.219	0.639, -0.597
ρ_{calc} / g cm^{-3}	1.149	1.136	1.135	1.153	1.100

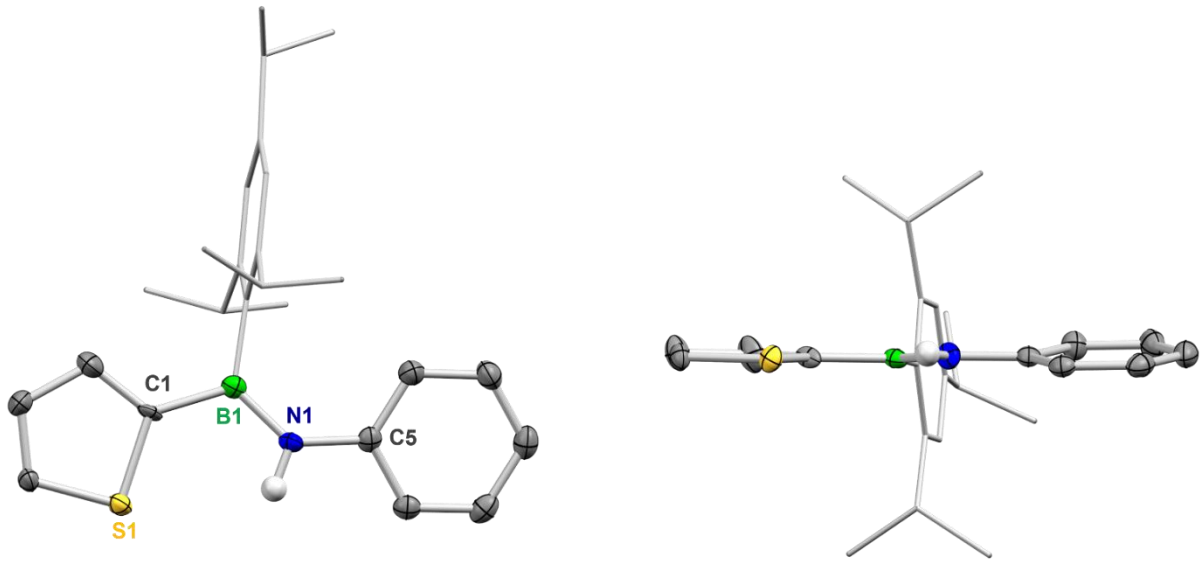

Figure 2.8.8. Molecular structure of **5** in the solid state by single-crystal X-ray diffraction (H atoms and disorders of the thiophene unit omitted for clarity). Structure shown perpendicular (left) and parallel (right) to the arylene backbone. All ellipsoids are drawn at the 50% probability level.

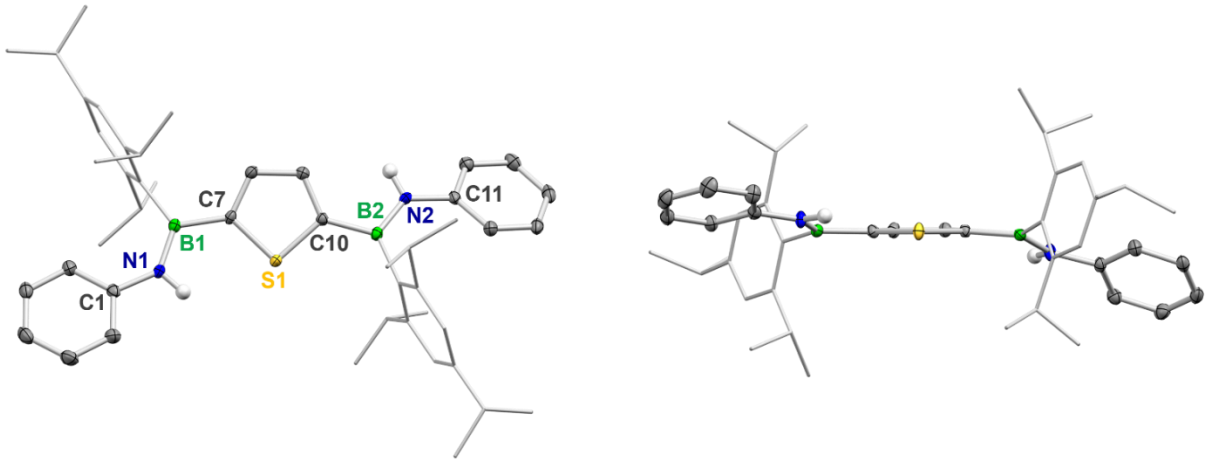

Figure 2.8.9. Molecular structure of **12** in the solid state by single-crystal X-ray diffraction (H atoms and disorders of the thiophene units omitted for clarity). Structure shown perpendicular (left) and parallel (right) to the arylene backbone. All ellipsoids are drawn at the 50% probability level.

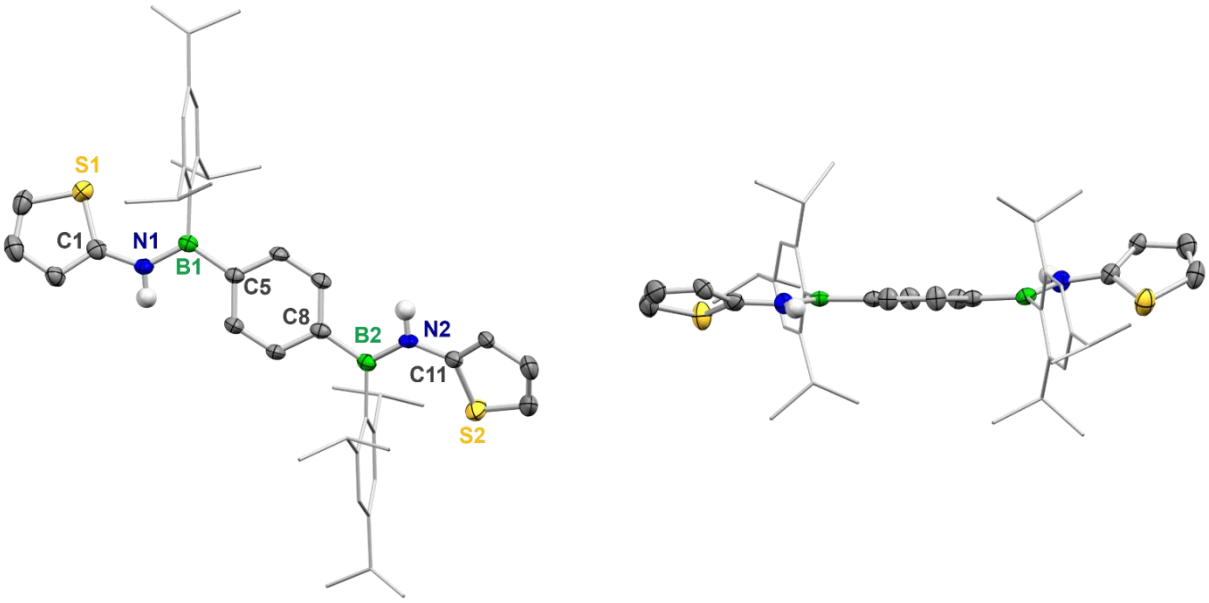

Figure 2.8.10. Molecular structure of **14** in the solid state by single-crystal X-ray diffraction (H atoms and disorders of the thiophene units omitted for clarity). Structure shown perpendicular (left) and parallel (right) to the arylene backbone. All ellipsoids are drawn at the 50% probability level.

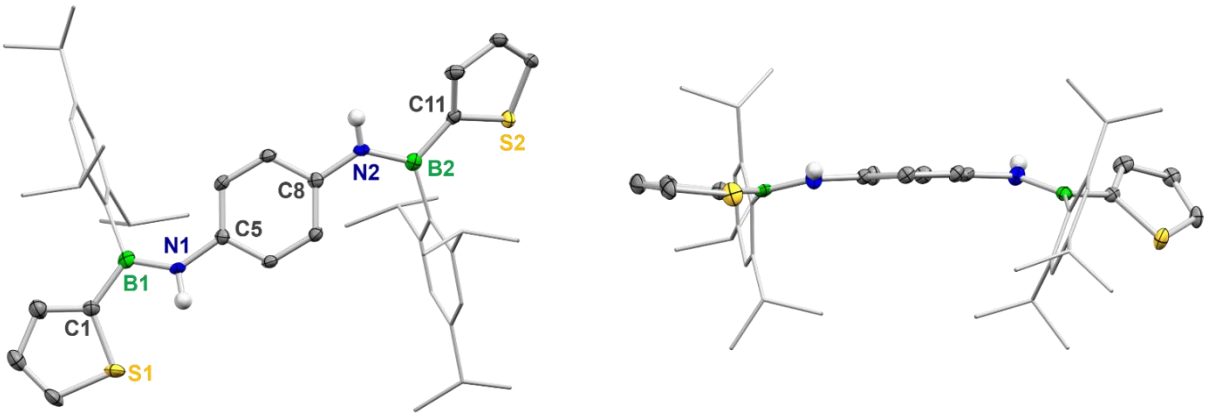

Figure 2.8.11. Molecular structure of **18** in the solid state by single-crystal X-ray diffraction (H atoms and disorders of the thiophene units omitted for clarity). Structure shown perpendicular (left) and parallel (right) to the arylene backbone. All ellipsoids are drawn at the 50% probability level.

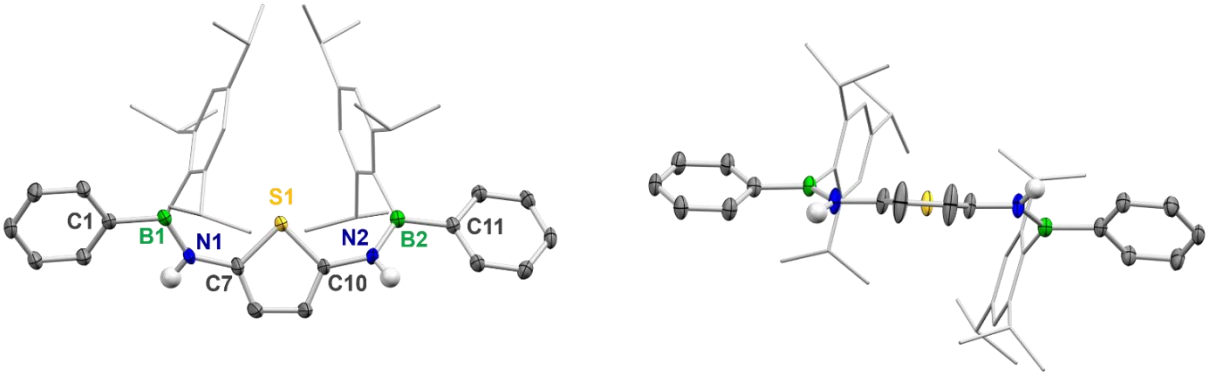

Figure 2.8.12. Molecular structure of **20** in the solid state by single-crystal X-ray diffraction (H atoms and disorders of the thiophene units omitted for clarity). Structure shown perpendicular (left) and parallel (right) to the arylene backbone. All ellipsoids are drawn at the 50% probability level. Only one of three independent molecules with similar structural data is shown.

Table 2.8.4. Selected values from the crystallographic data.

	5	12	14	18	20
∑∠Twist thiophene and BN planes (defined by C_2BNC plane)	Thi-BN: 5.2° BN-Ph: 12.0°	Ph1-NB: 7.3° NB-Thi: 15.0° Thi-BN: 22.4° BN-Ph2: 18.0°	Thi1-NB: 22.6° NB-Ph: 18.4° Ph-BN: 6.0° BN-Thi2: 22.8°	Thi1-BN: 18.8° BN-Ph: 12.5° Ph-NB: 20.4° NB-Thi2: 29.6°	Ph1-BN: 12.3° BN-Thi: 20.5° Thi-NB: 29.3° NB-Ph2: 12.4°
∑∠Twist thiophene/ phenylene planes	Thi-Ph: 7.4°	Ph1-Thi: 22.0° Thi-Ph2: 39.9° Ph1-Ph2: 21.7°	Thi1-Ph: 40.1° Ph-Thi2: 16.9° Thi1-Thi2: 56.9°	Thi1-Ph: 7.2° Ph-Thi2: 50.0° Thi1-Thi2: 44.2°	Ph1-Thi: 31.5° Thi-Ph2: 38.7° Ph1-Ph2: 69.9°
B−N distances [Å]	B1–N1: 1.4117(18)	B1–N1: 1.4095(17) B2–N2: 1.4138(17)	N1–B1: 1.410(4) N2–B2: 1.401(4)	B1–N1: 1.412(3) B2–N2: 1.412(3)	B1–N1: 1.403(4) B2–N2: 1.396(3)

Photophysical properties

Table 2.8.5. UV-vis absorption data of the iminoborane oligomers and polymers in THF.

No.[a]	λ_{abs} [nm]	ε[e]	No.[b]	λ_{abs} [nm]	ε[e]	No.[c]	λ_{abs} [nm]	ε[e]	No.[d]	λ_{abs} [nm]	ε [e]
3	272	1.6	**10**	298	2.6	**17**	308	1.9	**22**	341	2.2
5	288	1.8	**12**	323	3.6	**18**	320	2.8	**25**	362	2.3
7	296	0.9	**14**	322	2.3	**20**	341	1.5	**26**	372	1.6
8	305	1.3	**15**	340	3.0	**21**	348	2.0	**23**	388	1.5

[a] Monomeric compounds. [b] Dimeric compounds with NBBN sequence. [c] Dimeric compounds with BNNB sequence. [d] Polymers. [e] 10^4 L mol^{-1} cm^{-1}.

Table 2.8.6. Fluorescence data of the iminoborane oligomers and polymers as PMMA-films.

No.[a]	λ_{max} abs | em [nm]	Φ_{fl} [e] [%]	No.[b]	λ_{max} abs | em [nm]	Φ_{fl} [e] [%]	No.[c]	λ_{max} abs | em [nm]	Φ_{fl} [e] [%]	No.[d]	λ_{max} abs | em [nm]	Φ_{fl} [e] [%]
3	272 | 466	36	**10**	298 | 442	31	**17**	306 | 426	42	**22**	341 | 450	25
5	282 | 415	9	**12**	319 | 415	15	**18**	318 | 435	29	**25**	359 | 460	15
7	296 | 440	10	**14**	318 | 449	10	**20**	329 | 459	13	**26**	360 | 502	10
8	304 | 445	6	**15**	331 | 462	10	**21**	329 | 479	9	**23**	368 | 521	5

[a] Monomeric compounds. [b] Dimeric compounds with NBBN sequence. [c] Dimeric compounds with BNNB sequence. [d] Polymers. [e] Fluorescence quantum yields, determined using an integration sphere.

Table 2.8.7. Fluorescence data of the iminoborane oligomers and polymers in *n*-hexane.

No.[a]	λ_{em} [nm]	Φ_{fl}[e] [%]	No.[b]	λ_{em} [nm]	Φ_{fl}[e] [%]	No.[c]	λ_{em} [nm]	Φ_{fl}[e] [%]	No.[d]	λ_{em} [nm]	Φ_{fl}[e] [%]
3	503	5	**10**	528	11	**17**	554	4	**22**	578	-
5	501	2	**12**	528	3	**18**	551	3	**25**	427	-
7	580	-	**14**	608	-	**20**	621	-	**26**	498	-
8	579	-	**15**	608	-	**21**	581	-	**23**	507	-

[a] Monomeric compounds. [b] Dimeric compounds with NBBN sequence. [c] Dimeric compounds with BNNB sequence. [d] Polymers. [e] Fluorescence quantum yields, determined using an integration sphere.

Electrochemical properties

Table 2.8.8. Oxidation onset potentials.

Compound	Oxidation Onset [V]	Compound	Oxidation Onset [V]
3	1.07	**17**	0.65
5	1.01	**18**	0.61
7	0.63	**20**	0.27
8	0.62	**21**	0.25
10	1.06	**22**	0.63
12	1.00	**23**	0.24
14	0.62	**25**	0.56
15	0.61	**26**	0.25

Computational information

DFT geometry optimizations were carried out with the Gaussian 16, Revision C.01 program package[30] using the ωB97X-D[31] functional in combination with the def2-SVP[32] basis set in gas phase. The equilibrium geometries were characterized as minima by frequency computations. Vertical singlet excitations were calculated by means of time-dependent DFT with the program ORCA 5.0.3[33] using the ωB97X-D3[34] functional with optimal tuned ω parameters[35], the def2-SVP[32] basis set and the CPCM[36] solvation model mimicking tetrahydrofuran (ε = 7.58) as solvent.

Table 2.8.9. Results from TD-DFT calculations for the model compounds for **17**, **18**, **20** and **21**.

Compound	λ / nm	Oscillator strength *f*	Orbital contributions	$\|c\|^2$ / %
17	293.1	1.1090	**HOMO → LUMO**	88.8
18	303.5	1.1592	**HOMO → LUMO**	87.3
20	325.6	0.7286	**HOMO → LUMO**	90.7
21	327.4	0.8883	**HOMO → LUMO**	89.6

Table 2.8.10. Calculated HOMO and LUMO energies for the compounds **17**, **18**, **20** and **21**.

Compound	HOMO energy (eV)	LUMO energy (eV)	HOMO-LUMO gap (eV)
17	-6.9169	0.2007	7.1176
18	-6.8974	0.0971	6.9945
20	-6.6413	0.1451	6.7864
21	-6.6506	0.0436	6.6942

Frontier orbitals

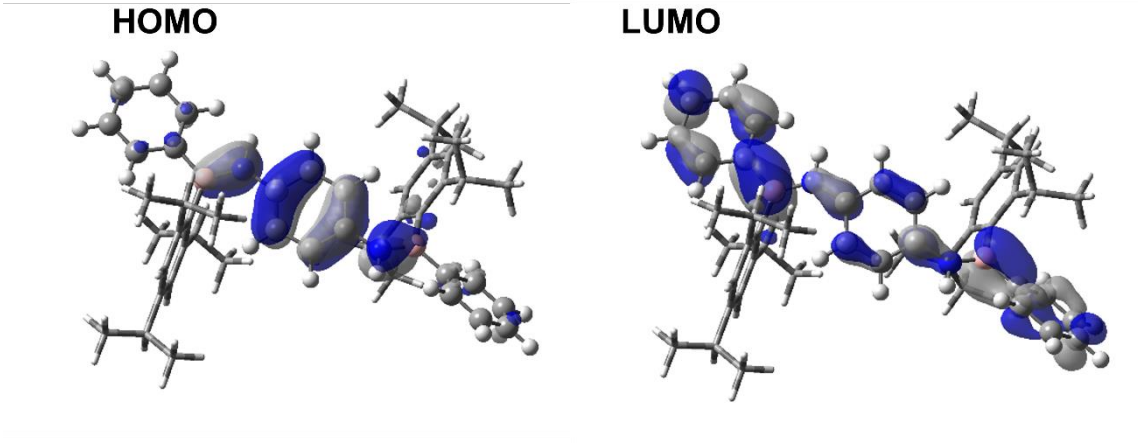

Figure 2.8.13. Calculated frontier orbitals (isovalue 0.03 a.u.) of **17** (ω_TB97X-D3/def2-SVP, CPCM(THF), ω_T = 0.135).

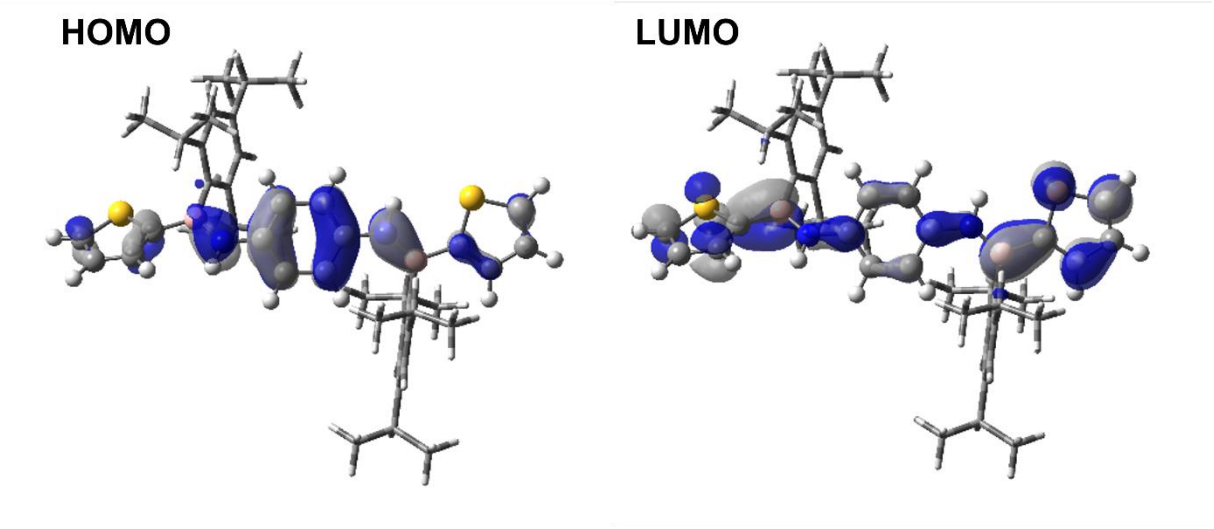

Figure 2.8.14. Calculated frontier orbitals (isovalue 0.03 a.u.) of **18** (ω_TB97X-D3/def2-SVP, CPCM(THF), ω_T = 0.14).

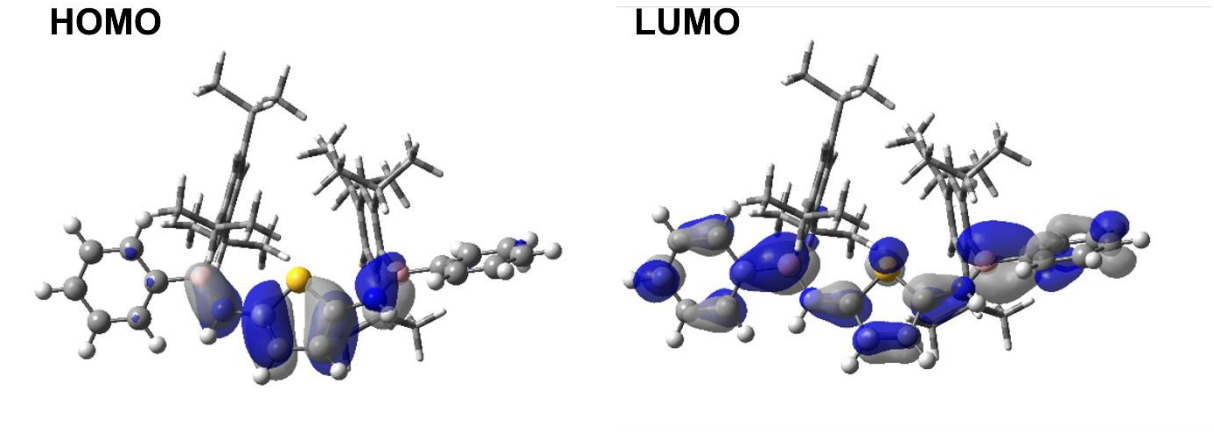

Figure 2.8.15. Calculated frontier orbitals (isovalue 0.03 a.u.) of **20** (ω_TB97X-D3/def2-SVP, CPCM(THF), ω_T = 0.14).

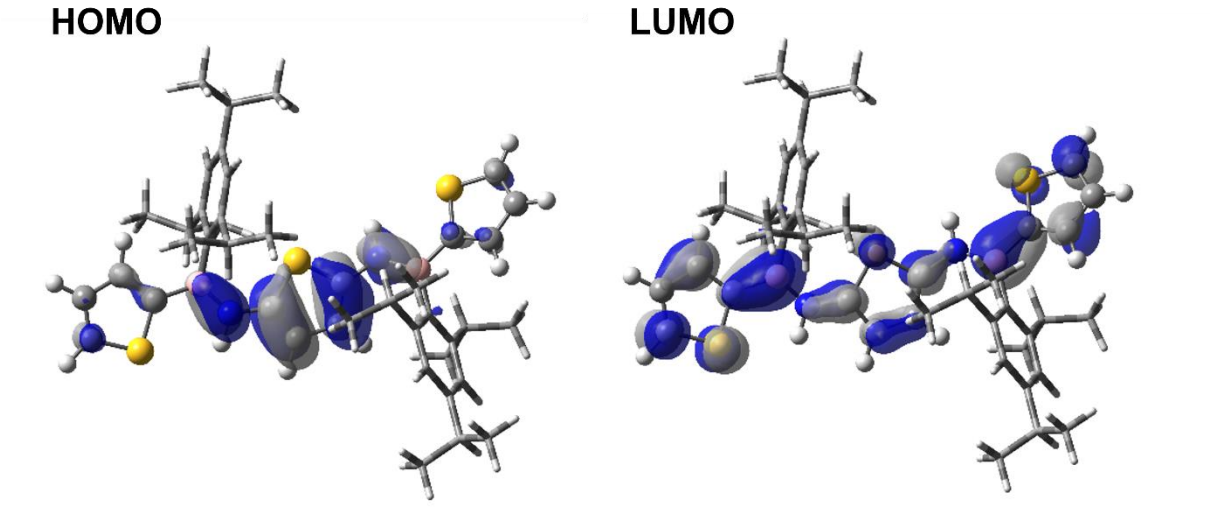

Figure 2.8.16. Calculated frontier orbitals (isovalue 0.03 a.u.) of **21** (ω_TB97X-D3/def2-SVP, CPCM(THF), ω_T = 0.14).

2.8.5 References

[1] a) T. Mikie, I. Osaka, *J. Mater. Chem. C* **2020**, *8*, 14262–14288; b) J. Li, K. Pu, *Chem. Soc. Rev.* **2019**, *48*, 38–71; c) O. Inganäs, *Adv. Mater.* **2018**, *30*, 1800388; d) T. M. Swager, *Macromolecules* **2017**, *50*, 4867–4886.

[2] a) E. Rivard, *Chem. Rec.* **2020**, *20*, 640–648; b) F. Vidal, F. Jäkle, *Angew. Chem. Int. Ed.* **2019**, *58*, 5846–5870; *Angew. Chem.* **2019**, *131*, 5904–5929; c) H. Helten in *Encyclopedia of Inorganic and Bioinorganic Chemistry* (Ed.: R. A. Scott), Wiley, Chichester, **2017**; d) A. M. Priegert, B. W. Rawe, S. C. Serin, D. P. Gates, *Chem. Soc. Rev.* **2016**, *45*, 922–953; e) E. I. Carrera, D. S. Seferos, *Macromolecules* **2015**, *48*, 297–308; f) X. He, T. Baumgartner, *RSC Adv.* **2013**, *3*, 11334–11350.

[3] E.g., for main group analogues of PPV or respective oligomers, see: a) V. A. Wright, D. P. Gates, *Angew. Chem. Int. Ed.* **2002**, *41*, 2389–2392; b) R. C. Smith, J. D. Protasiewicz, *J. Am. Chem. Soc.* **2004**, *126*, 2268–2269; c) I. Bejan, D. Scheschkewitz, *Angew. Chem. Int. Ed.* **2007**, *46*, 5783–5786; d) A. Fukazawa, Y. Li, S. Yamaguchi, H. Tsuji, K. Tamao, *J. Am. Chem. Soc.* **2007**, *129*, 14164-14165; e) L. Li, T. Matsuo, D. Hashizume, H. Fueno, K. Tanaka, K. Tamao, *J. Am. Chem. Soc.* **2015**, *137*, 15026−15035; for model compounds for silicon analogues of PTV, see: f) N. Hayakawa, S. Nishimura, N. Kazusa, N. Shintani, T. Nakahodo, H. Fujihara, M. Hoshino, D. Hashizume, T. Matsuo, *Organometallics* **2017**, *36*, 3226−3233; g) T. Matsuo, N. Hayakawa, *Sci. Technol. Adv. Mater.* **2018**, *19*, 108–129.

[4] a) H. Helten in *Comprehensive Organometallic Chemistry IV*, *Vol. 14* (Eds.: D. O'Hare, K. Meyer, G. Parkin), Elsevier, **2022**, pp. 71−134; b) D. Shimoyama, F. Jäkle, *Aggregate* **2022**, *3*, e149; c) X. Yin, J. Liu, F. Jäkle, *Chem. Eur. J.* **2021**, *27*, 2973–2986; d) H. Helten, *Chem. Asian J.* **2019**, *14*, 919–935; e) Y. Ren, F. Jäkle in *Main Group Strategies towards Functional Hybrid Materials* (Eds.: T. Baumgartner, F. Jäkle), Wiley: Hoboken, **2017**; pp 79−110; f) F. Jäkle, *Top. Organomet. Chem.* **2015**, *49*, 297–325; g) F. Jäkle, *Chem. Rev.* **2010**, *110*, 3985–4022.

[5] Selected examples: a) A. Sundararaman, M. Victor, R. Varughese, F. Jäkle, *J. Am. Chem. Soc.* **2005**, *127*, 13748–13749; b) A. Nagai, T. Murakami, Y. Nagata, K. Kokado, Y. Chujo, *Macromolecules* **2009**, *42*, 7217–7220; c) H. Li, F. Jäkle, *Angew. Chem. Int. Ed.* **2009**, *48*, 2313–2316; *Angew. Chem.* **2009**, *121*, 2349–2352; d) A. Lorbach, M. Bolte, H. Li, H.-W. Lerner, M. C. Holthausen, F. Jäkle, M. Wagner, *Angew. Chem. Int. Ed.* **2009**, *48*, 4584–4588; e) X. Yin, F. Guo, R. A. Lalancette, F. Jäkle, *Macromolecules* **2016**, *49*, 537–546; f) K. Hu, Z. Zhang, J. Burke, Y. Qin, *J. Am. Chem. Soc.* **2017**, *139*, 11004–11007; g) A. Lik, L. Fritze, L. Müller, H. Helten, *J. Am. Chem. Soc.* **2017**, *139*, 5692–5695; h) A. Lik, S. Jenthra, L. Fritze, L. Müller, K.-N. Truong, H. Helten, *Chem. Eur. J.* **2018**, *24*, 11961–11972; i) B. Meng, Y. Ren, J. Liu, F. Jäkle, L. Wang, *Angew. Chem. Int. Ed.* **2018**, *57*, 2183–2187; *Angew. Chem.* **2018**, *130*, 2205–2209; j) Y. Adachi, Y. Ooyama, Y. Ren, X. Yin, F. Jäkle, J. Ohshita, *Polym. Chem.* **2018**, *9*, 291–299; k) L. Fritze, M. Fest, A. Helbig, T. Bischof, I. Krummenacher, H. Braunschweig, M. Finze, H. Helten, *Macromolecules* **2021**, *54*, 7653−7665; l) A. F. Alahmadi, X. Yin, R. A. Lalancette, F. Jäkle, *Chem. Eur. J.* **2023**, *29*, e202203619.

[6] a) D. Marchionni, S. Basak, A. N. Khodadadi, A. Marrocchi, L. Vaccaro, *Adv. Funct. Mater.* **2023**, 2303635; b) X. Chen, D. Tan, D.-T. Yang, *J. Mater. Chem. C* **2022**, 10, 13499–13532; c) C. R. McConnell, S.-Y. Liu, *Chem. Soc. Rev.* **2019**, *48*, 3436–3453; d) Z. X. Giustra, S.-Y. Liu, *J. Am. Chem. Soc.* **2018**, *140*, 1184–1194; e) G. Bélanger-Chabot, H. Braunschweig, D. K. Roy, *Eur. J. Inorg. Chem.* **2017**, 4353–4368; f) H. Helten, *Chem. Eur. J.* **2016**, *22*, 12972–12982; g) M. M. Morgan, W. E. Piers, *Dalton Trans.* **2016**, *45*, 5920–5924; h) D. Bonifazi, F. Fasano, M. M. Lorenzo-Garcia, D. Marinelli, H. Oubaha, J. Tasseroul, *Chem. Commun.* **2015**, *51*, 15222–15236; i) X.-Y. Wang, J.-Y. Wang, J. Pei, *Chem. Eur. J.* **2015**, *21*, 3528–3539; j) P. G. Campbell, A. J. V. Marwitz, S.-Y. Liu, *Angew. Chem. Int. Ed.* **2012**, *51*, 6074–6092; k) M. J. D. Bosdet, W. E. Piers, *Can. J. Chem.* **2009**, *87*, 8–29; for BN isosteres of non-conjugated compounds, see, e.g.: l) A. Staubitz, A. P. M. Robertson, M. E. Sloan, I. Manners,

Chem. Rev. **2010**, *110*, 4023–4078; m) H. C. Johnson, T. N. Hooper, A. S. Weller, *Top. Organomet. Chem.* **2015**, *49*, 153–220.

[7] Selected recent examples: a) K. Matsui, S. Oda, K. Yoshiura, K. Nakajima, N. Yasuda, T. Hatakeyama, *J. Am. Chem. Soc.* **2018**, *140*, 1195–1198; b) T. Kaehler, M. Bolte, H.-W. Lerner, M. Wagner, *Angew. Chem. Int. Ed.* **2019**, *58*, 11379–11384; *Angew. Chem.* **2019**, *131*, 11501–11506; c) A. S. Scholz, J. G. Massoth, M. Bursch, J.-M. Mewes, T. Hetzke, B. Wolf, M. Bolte, H.-W. Lerner, S. Grimme, M. Wagner, *J. Am. Chem. Soc.* **2020**, *142*, 11072–11083; d) Y. Chen, W. Chen, Y. Qiao, X. Lu, G. Zhou, *Angew. Chem. Int. Ed.* **2020**, *59*, 7122–7130; *Angew. Chem.* **2020**, *132*, 7188–7196; e) K. Ota, R. Kinjo, *Angew. Chem. Int. Ed.* **2020**, *59*, 6572–6575; f) K. Ota, R. Kinjo, *J. Am. Chem. Soc.* **2021**, *143*, 11152–11159; g) M. Chen, K. S. Unikela, R. Ramalakshmi, B. Li, C. Darrigan, A. Chrostowska, S.-Y. Liu, *Angew. Chem. Int. Ed.* **2021**, *60*, 1556–1560; *Angew. Chem.* **2021**, *133*, 1580–1584; h) D. Tian, W. Zhang, G. Shi, S. Luo, Y. Chen, W. Chen, H. Huang, S. Xing, B. Zhu, *Org. Chem. Front.* **2021**, *8*, 4124–4130; i) S. Hagspiel, M. Arrowsmith, F. Fantuzzi, A. Vargas, A. Rempel, A. Hermann, T. Brückner, H. Braunschweig, *Angew. Chem. Int. Ed.* **2021**, *60*, 6446–6450; *Angew. Chem.* **2021**, *133*, 6519–6524; j) C. Brunecker, M. Arrowsmith, F. Fantuzzi, H. Braunschweig, *Angew. Chem. Int. Ed.* **2021**, *60*, 16864–16868; *Angew. Chem.* **2021**, *60*, 16864–16868; k) S. Akahori, T. Sasamori, H. Shinokubo, Y. Miyake, *Chem. Eur. J.* **2021**, *27*, 8178–8184; l) M. Crumbach, O. Ayhan, L. Fritze, J. A. P. Sprenger, L. Zapf, M. Finze, H. Helten, *Chem. Commun.* **2021**, *57*, 2408–2411; m) M. Zhao, Q. Miao, *Angew. Chem. Int. Ed.* **2021**, *60*, 21289–21294; *Angew. Chem.* **2021**, *133*, 21459–21464; n) M. Crumbach, J. Bachmann, L. Fritze, A. Helbig, I. Krummenacher, H. Braunschweig, H. Helten, *Angew. Chem. Int. Ed.* **2021**, *60*, 9290–9295; *Angew. Chem.* **2021**, *133*, 9376–9381; o) M. Fingerle, J. Dingerkus, H. Schubert, K. M. Wurst, M. Scheele, H. F. Bettinger, *Angew. Chem. Int. Ed.* **2021**, *60*, 15798–15802; *Angew. Chem.* **2021**, *60*, 15798–15802; p) Y. Zhang, C. Zhang, Y. Guo, J. Ye, B. Zhen, Y. Chen, X. Liu, *J. Org. Chem.* **2021**, *86*, 6322–6330; q) J. Wu, G. Zhang, *Angew. Chem. Int. Ed.* **2022**, *61*, e202208061; *Angew. Chem.* **2022**, *134*, e202208061; r) M. R. Rapp, W. Leis, F. Zinna, L. Di Bari, T. Arnold, B. Speiser, M. Seitz, H. F. Bettinger, *Chem. Eur. J.* **2022**, *28*, e202104161; s) K. Zhao, Z.-F. Yao, Z.-Y. Wang, J.-C. Zeng, L. Ding, M. Xiong, J.-Y. Wang, J. Pei, *J. Am. Chem. Soc.* **2022**, *144*, 3091–3098; t) J. Bachmann, A. Helbig, M. Crumbach, I. Krummenacher, H. Braunschweig, H. Helten, *Chem. Eur. J.* **2022**, *28*, e202202455; u) W. Li, C.-Z. Du, X.-Y. Chen, L. Fu, R.-R. Gao, Z.-F. Yao, J.-Y. Wang, W. Hu, J. Pei, X.-Y. Wang, *Angew. Chem. Int. Ed.* **2022**, *61*, e202201464; *Angew. Chem.* **2022**, *134*, e202201464; v) J. Guo, Z. Li, X. Tian, T. Zhang, Y. Wang, C. Dou, *Angew. Chem. Int. Ed.* **2023**, *62*, e202217470; *Angew. Chem.* **2023**, *135*, e202217470; w) R. P. Nandi, N. K. Kalluvettukuzhy, S. Pagidi, P. Thilagar, *Inorg. Chem.* **2023**, *62*, 1122–1134.

[8] a) I. Yamaguchi, B.-J. Choi, T.-a. Koizumi, K. Kubota, T. Yamamoto, *Macromolecules* **2007**, *40*, 438–443; b) I. Yamaguchi, T. Tominaga, M. Sato, *Polym. Int.* **2009**, *58*, 17–21; c) S. Hayashi, T. Koizumi, *Polym. Chem.* **2012**, *3*, 613–616.

[9] Chujo and co-workers reported as series of poly(boronic carbamate)s and related BN-linked polymers, however, with no significant conjugation over the B=N units, presumably due to either the boronic carbamate groups, meta-phenylene linkages or cross-links in the polymer backbone; see: a) N. Matsumi, Y. Chujo, *Macromolecules* **1998**, *31*, 3802–3806; b) N. Matsumi, K. Kotera, K. Naka, Y. Chujo, *Macromolecules* **1998**, *31*, 3155–3157; c) N. Matsumi, K. Kotera, Y. Chujo, *Macromolecules* **2000**, *33*, 2801–2806.

[10] For borazine-containing polymers and other BN-linked polymer networks, see: a) T. E. Reich, K. T. Jackson, S. Li, P. Jena, H. M. El-Kaderi, *J. Mater. Chem.* **2011**, *21*, 10629–10632; b) T. E. Reich, S. Behera, K. T. Jackson, P. Jena, H. M. El-Kaderi, *J. Mater. Chem.* **2012**, *22*, 13524–13528; c) C. Sánchez-Sánchez, S. Brüller, H. Sachdev, K. Müllen, M. Krieg, H. F. Bettinger, A. Nicolaï, V. Meunier, L. Talirz, R. Fasel, P. Ruffieux, *ACS nano* **2015**, *9*, 9228–9235; d) D. Marinelli, F. Fasano, B. Najjari, N. Demitri, D. Bonifazi, *J. Am. Chem. Soc.* **2017**, *139*, 5503–5519; e) N. A. Riensch, A. Deniz, S.

Kühl, L. Müller, A. Adams, A. Pich, H. Helten, *Polym. Chem.* **2017**, *8*, 5264–5268; f) H. Oubaha, N. Demitri, J. Rault-Berthelot, P. Dubois, O. Coulembier, D. Bonifazi, *J. Org. Chem.* **2019**, *84*, 9101–9116; g) Y. Fu, H. Yang, Y. Gao, L. Huang, R. Berger, J. Liu, H. Lu, Z. Cheng, S. Du, H.-J. Gao, X. Feng, *Angew. Chem. Int. Ed.* **2020**, *59*, 8873–8879; *Angew. Chem.* **2020**, *132*, 8958–8964; h) F. Fasano, J. Dosso, C. G. Bezzu, M. Carta, F. Kerff, N. Demitri, B.-L. Su, D. Bonifazi, *Chem. Eur. J.* **2021**, *27*, 4124–4133; i) J. Dosso, H. Oubaha, F. Fasano, S. Melinte, J.-F. Gohy, C. E. Hughes, K. D. M. Harris, N. Demitri, M. Abrami, M. Grassi, D. Bonifazi, *Chem. Mater.* **2022**, *34*, 10670–10680.

[11] A. W. Baggett, F. Guo, B. Li, S.-Y. Liu, F. Jäkle, *Angew. Chem. Int. Ed.* **2015**, *54*, 11191–11195; *Angew. Chem.* **2015**, *127*, 11343–11347.

[12] a) X.-Y. Wang, F.-D. Zhuang, J.-Y. Wang, J. Pei, *Chem. Commun.* **2015**, *51*, 17532–17535; b) W. Zhang, G. Li, L. Xu, Y. Zhuo, W. Wan, N. Yan, G. He, *Chem. Sci.* **2018**, *9*, 4444–4450; c) S. Pang, Z. Wang, X. Yuan, L. Pan, W. Deng, H. Tang, H. Wu, S. Chen, C. Duan, F. Huang, Y. Cao, *Angew. Chem. Int. Ed.* **2021**, *60*, 8813–8817; *Angew. Chem.* **2021**, *133*, 8895–8899.

[13] T. Lorenz, A. Lik, F. A. Plamper, H. Helten, *Angew. Chem. Int. Ed.* **2016**, *55*, 7236–7241; *Angew. Chem.* **2016**, *128*, 7352–7357.

[14] a) O. Ayhan, T. Eckert, F. A. Plamper, H. Helten, *Angew. Chem. Int. Ed.* **2016**, *55*, 13321–13325; *Angew. Chem.* **2016**, *128*, 13515–13519; b) O. Ayhan, N. A. Riensch, C. Glasmacher, H. Helten, *Chem. Eur. J.* **2018**, *24*, 5883–5894.

[15] T. Lorenz, M. Crumbach, T. Eckert, A. Lik, H. Helten, *Angew. Chem. Int. Ed.* **2017**, *56*, 2780–2784; *Angew. Chem.* **2017**, *129*, 2824–2828.

[16] J. Chorbacher, M. Maier, J. Klopf, M. Fest, H. Helten, *Macromol. Rapid Commun.* **2023**, 2300278.

[17] a) C. Li, M. Liu, N. G. Pschirer, M. Baumgarten, K. Müllen, *Chem. Rev.* **2010**, *110*, 6817–6855; b) J. Banerjee, K. Dutta, *Chem. Pap.* **2021**, *75*, 5139–5151.

[18] W. Zhang, G. Yu, *J. Polym. Sci. Part A: Polym. Chem.* **2017**, *55*, 585–603.

[19] a) G. Zhang, F. R. Lin, F. Qi, T. Heumüller, A. Distler, H.-J. Egelhaaf, N. Li, P. C. Y. Chow, C. J. Brabec, A. K.-Y. Jen, H.-L. Yip, *Chem. Rev.* **2022**, *122*, 14180−14274; b) Q. Wang, Y. Qin, M. Li, L. Ye, Y. Geng, *Adv. Energy Mater.* **2020**, *10*, 2002572; c) F. A. Larik, M. Faisal, A. Saeed, Q. Abbas, M. A. Kazi, N. Abbas, A. A. Thebo, D. M. Khan, P. A. Channar, *J. Mater. Sci.: Mater. Electron.* **2018**, *29*, 17975–18010; d) T. P. Kaloni, P. K. Giesbrecht, G. Schreckenbach, M. S. Freund, *Chem. Mater.* **2017**, *29*, 10248–10283; e) J. Qian, X. Li, D. J. Lunn, J. Gwyther, Z. M. Hudson, E. Kynaston, P. A. Rupar, M. A. Winnik, I. Manners, *J. Am. Chem. Soc.* **2014**, *136*, 4121–4124.

[20] a) Q. Wang, X. Dong, M. He, M. Li, H. Tian, J. Liu, Y. Geng, *Polymer* **2018**, *140*, 89−95; b) C. Yang, S. Zhang, J. Hou, *Aggregate* **2022**, *3*, e111; c) P. Bi, J. Ren, S. Zhang, J. Wang, Z. Chen, M. Gao, Y. Cui, T. Zhang, J. Qin, Z. Zheng, L. Ye, X. Hao, J. Hou, *Nano Energy* **2022**, *100*, 107463; d) L. Ma, S. Zhang, J. Ren, G. Wang, J. Li, Z. Chen, H. Yao, J. Hou, *Angew. Chem. Int. Ed.* **2023**, *62*, e202214088; *Angew. Chem.* **2023**, *135*, e202214088.

[21] We also prepared a related polymer with linear BN linkages in collaboration with the Bolm group: F. Brosge, T. Lorenz, H. Helten, C. Bolm, *Chem. Eur. J.* **2019**, *25*, 12708–1271.

[22] a) R. A. Bartlett, X. Feng, M. M. Olmstead, P. P. Power, K. J. Weese, *J. Am. Chem. Soc.* **1987**, *109*, 4851–4854; b) H. Chen, R. A. Bartlett, M. M. Olmstead, P. P. Power, S. C. Shoner, *J. Am. Chem. Soc.* **1990**, *112*, 1048–1055.

[23] a) J. Luo, Z. Xie, J. W. Lam, L. Cheng, H. Chen, C. Qiu, H. S. Kwok, X. Zhan, Y. Liu, D. Zhu, B. Z. Tang, *Chem. Commun.* **2001**, 1740–1741; b) B.-K. An, S.-K. Kwon, S.-D. Jung, S. Y. Park, *J. Am. Chem. Soc.* **2002**, *124*, 14410–14415; c) Y. Hong, J. W. Y. Lam, B. Z. Tang, *Chem. Soc. Rev.* **2011**, *40*, 5361–5388; d) B.-K. An, J. Gierschner, S. Y. Park, *Acc. Chem. Res.* **2012**, *45*, 544–554; e) J. Mei, N. L. C. Leung, R. T. K. Kwok, J. W. Y. Lam, B. Z. Tang, *Chem. Rev.* **2015**, *115*, 11718–11940; f) J. Li, J. Wang, H. Li, N. Song, D. Wang, B. Z. Tang, *Chem. Soc. Rev.* **2020**, *49*, 1144–1172.

[24] a) C. Arivazhagan, A. Maity, K. Bakthavachalam, A. Jana, S. K. Panigrahi, E. Suresh, A. Das, S. Ghosh, *Chem. Eur. J.* **2017**, *23*, 7046–7051; b) R. Hu, E. Lager, A. Aguilar-Aguilar, J. Liu, J. W. Y. Lam, H. H. Y. Sung, I. D. Williams, Y. Zhong, K. S. Wong, E. Pena-Cabrera, B. Z. Tang, *J. Phys. Chem. C* **2009**, *113*, 15845–15853.

[25] a) K. K. Neena, P. Thilagar, *J. Mater. Chem. C* **2016**, *4*, 11465–11473; b) K. K. Neena, P. Thilagar, *Organometallics* **2017**, *36*, 2692–2701; c) K. K. Neena, P. Sudhakar, K. Dipak, P. Thilagar, *Chem. Commun.* **2017**, *53*, 3641–3644.

[26] H. Bock, J. Meuret, C. Näther, U. Krynitz, *Chem. Ber.* **1994**, *127*, 55–65.

[27] G. M. Sheldrick, *Acta Crystallogr. A* **2015**, *71*, 3-8.

[28] G. M. Sheldrick, *Acta Crystallogr. A* **2008**, *64*, 112-122.

[29] C. B. Hübschle, G. M. Sheldrick, B. Dittrich, *J. Appl. Crystallogr.* **2011**, *44*, 1281-1284.

[30] Gaussian 16 Revision C.01, M. J. Frisch, G. W. Trucks, H. B. Schlegel, G. E. Scuseria, M. A. Robb, J. R. Cheeseman, G. Scalmani, V. Barone, G. A. Petersson, H. Nakatsuji, M. Caricato X. Li, A. V. Marenich, J. Bloino, B. G. Janesko, R. Gomperts, B. Mennucci, H. P. Hratchian, J. V. Ortiz, A. F. Izmaylov, J. L. Sonnenberg, D. Williams-Young, F. Lipparini F. Ding, J. Goings F. Egidi, B. Peng, A. Petrone, T. Henderson, D. Ranasinghe, V. G. Zakrzewski, J. Gao, N. Rega, G. Zheng, W. Liang, M. Hada, M. Ehara, K. Toyota, R. Fukuda, J. Hasegawa, M. Ishida, T. Nakajima, Y. Honda, O. Kitao, H. Nakai, T. Vreven, K. Throssell, Jr. J. A. Montgomery, J. E. Peralta, F. Ogliaro, M. J. Bearpark, J. J. Heyd, E. N. Brothers, K. N. Kudin, V. N. Staroverov, T. A. Keith, R. Kobayashi, J. Normand, K. Raghavachari, A. P. Rendell, J. C. Burant, S. S. Iyengar, J. Tomasi, M. Cossi, J. M. Millam, M. Klene, C. Adamo, R. Cammi, J. W. Ochterski, R. L. Martin, K. Morokuma, O. Farkas, J. B. Foresman, D. J. Fox, Gaussian, Inc., Wallingford CT, **2016**.

[31] J.-D. Chai, M. Head-Gordon, *Phys. Chem. Chem. Phys.* **2008**, *10*, 6615.

[32] F. Weigend, R. Ahlrichs, *Phys. Chem. Chem. Phys.* **2005**, *7*, 3297-3305.

[33] a) F. Neese, F. Wennmohs, U. Becker, C. Riplinger, *J. Chem. Phys.* **2020**, *152*, 224108; b) F. Neese, *WIREs Comput Mol Sci.* **2022**, *12:e1606*.

[34] Y.-S. Lin, G.-D. Li, S.-P. Mao and J.-D. Chai, *J. Chem. Theory Comput.* **2013**, *9*, 263-272.

[35] a) T. Stein, L. Kronik, R. Baer, *J. Am. Chem. Soc.* **2009**, *131*, 2818-2820; b) T. Stein, H. Eisenberg, L. Kronik, R. Baer, *Phys. Rev. Lett.*, **2010**, *105*, 266802; c) A. Karolewski, L. Kronik, S. Kümmel, *J. Chem. Phys.* **2013**, *138*, 204115.

[36] V. Barone, M. Cossi, *J. Phys. Chem. A* 1**998**, *102*, *11*, 1995–2001.

2.9 BN- and BO-Doped Inorganic–Organic Hybrid Polymers Based on Sulfur-Containing Building Blocks

The following section is slightly modified and reproduced from a manuscript[+] in preparation.

2.9.1 Introduction

Synthetic polymers in pharmaceutical applications can be classified in polymer-drug conjugates, micro-, nanoparticulate- and macroscopic drug carriers as well as coatings, matrix excipients and polymeric drugs.[1] The polymer often serves as a protection and transport medium for the active ingredient. Boron-containing macromolecular materials are attracting considerable current research interest. While polymers having the vacant p-orbital of trivalent boron incorporated in a π-conjugated backbone have been used for electronic, optoelectronic, and sensory applications,[2] various boronic acid based polymers are noted for their well-established biomedical activities.[3] The incorporation of BN units into organic molecules or polymers to replace selected isoelectronic and isosteric CC units has evolved into a viable approach for accessing materials with special properties and functions.[4] Some of us recently reported of a series of BN-doped inorganic–organic hybrid polymers,[5] including BN analogs of poly(phenylene vinylene)[6] (PPV) and poly(thiophene vinylene)[7] (PTV). In a collaborative effort with the Pich group, we prepared borazine-based hybrid cyclomatrix polymers that self-assemble into microspheres, where we incorporated a dapsone-type diaryl sulfone as a building block.[8] Such dapsone-type moieties are of special interest as they have produced advantageous effects in polymer conjugates because of their anti-inflammatory and bioactive properties.[9] The first polysulfoximines, reported by Takata and co-workers, were prepared via Friedel–Crafts reactions.[10] In another study, they also reported the first well-characterized example of main chain type polysulfilimines, which is quite rarely studied.[11] However, the class of polysulfoxides has been described more intensively in the literature.[12] We recently communicated a series of novel inorganic–organic hybrid sulfoximine-containing copolymers featuring B=N and B–O linkages.[13] While the B=N-linked polymers were synthesized via Si/B exchange polycondensation, the favorable route to the B–O linked polymers followed a salt elimination approach. We now expanded our work to further sulfur-containing building blocks. Herein, we present a detailed study aimed at obtaining sulfone-, sulfoximine-, sulfoxide-, and sulfilimine-containing polymers. In addition, we prepared a series of oligomers that serve as molecular model systems for these polymers. We also studied the pH-triggered degradation

[+] M. Maier, F. Brosge, J. S. Schneider, J. Bachmann, S. Schmidt, C. Bolm, H. Helten, **2024**, *in preparation*.
(M.M. and F.B. contributed equally to this work)

of the oligomers and one polymer, as a proof-of-concept, which occurs under release of the intact sulfur-containing block.

2.9.2 Results and Discussion

The sulfur-containing building blocks **1**-**3** were provided by Bolm and co-workers, therefore, the synthesis thereof is not discussed in this work (Figure 2.9.1).

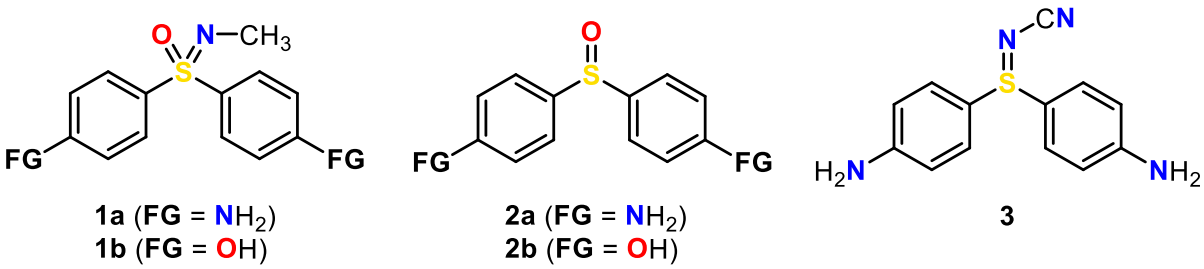

Figure 2.9.1. Sulfur-containing building blocks **1**-**3** provided by Bolm and co-workers.

For the planned polymer synthesis via silicon boron exchange polycondensation, the corresponding *N*,*N'*-bis-silylated derivatives of the sulfur-containing components **1**-**3** were required. These compounds were readily synthesized by treating the respective diamines with Me_3SiCl in the presence of NEt_3 as auxiliary base at 45 °C, similar to the synthesis of **4**[14] (Scheme 2.9.1).

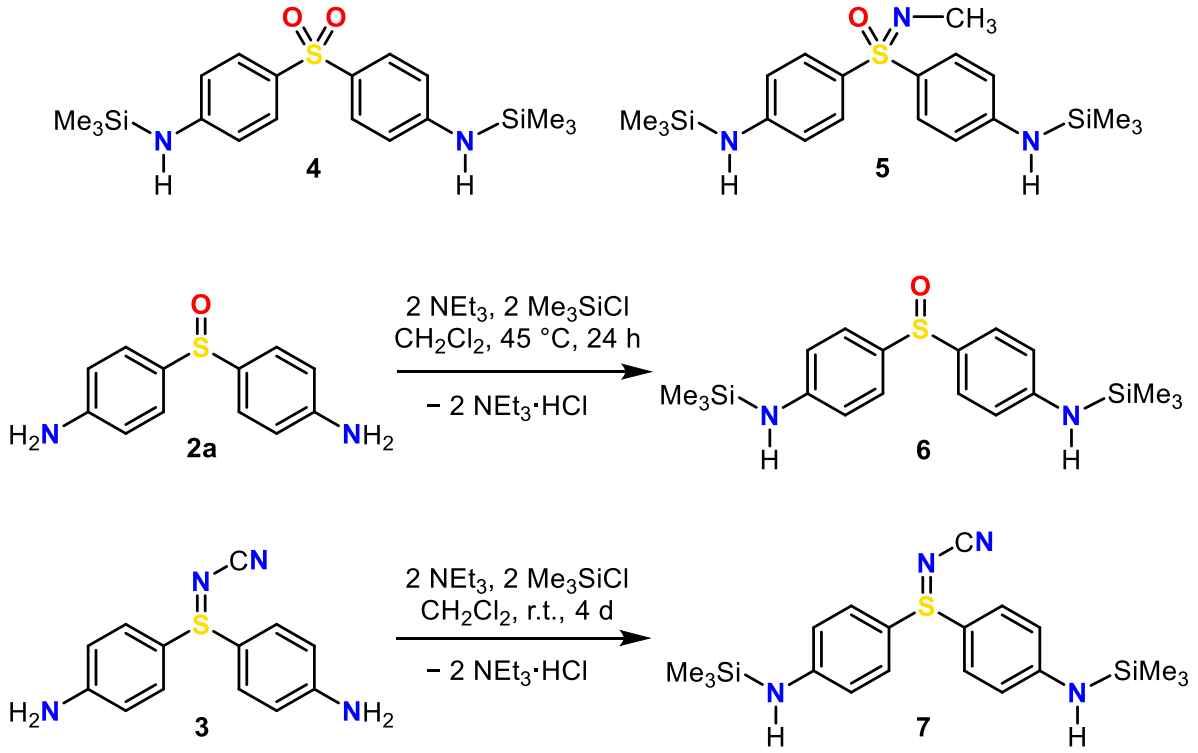

Scheme 2.9.1. Bis-silylated monomers **4** and **5** and synthesis of the **6** and **7**.

In our previous communication we already described synthesis of compound **5**.[13] Similarly, we synthesized **6** by the reaction of **2a** with NEt_3 and Me_3SiCl for 24 h at 45 °C in 67 % yield. An attempt to synthesize compound **7** under these conditions, however, produced several by-products, but we were able to synthesize **7** in 61 % yield under milder conditions, that is, by the reaction at room temperature for 4 d. In the ^1H NMR spectrum the signal for the Me_3Si groups appear between 0.28 and 0.25 ppm for **5**, **6**, and **7**. The N-*H* resonance of **7** appears at 4.01 ppm, which is slightly downfield shifted compared to that of **5** (3.81 ppm) and **6** (3.72 ppm). A downfield shift is also observed in the $^{29}Si\{^1H\}$ NMR spectrum of **7**, wherein the signal was detected at 5.1 ppm, while those for **5** and **6** appear at 4.6 and 4.2 ppm, respectively. Because compounds **6** and **7** showed poor long-term stability, we synthesized them freshly prior use.

Next, we decided to perform a series of model reactions of the sulfur-containing building blocks each with two equivalents of the mono-functional bromoborane TipB(Ph)Br to obtain the resulting “trimers” as model compounds for the corresponding polymers and to test the feasibility of the planned polymerization reactions (Scheme 2.9.2). For the synthesis of **8** we applied silicon/boron exchange condensation, while we used salt elimination reactions to obtain **9b** and **10b** because we had previously found for the reaction of a bis-bromoborane with *O*-trimethylsilylphenol that B–O bond formation using Si/B exchange progresses too slowly.[13] We also directly synthesized the compounds **9a** and **10a** via salt elimination reactions of **1a** and **2a**, respectively, with TipB(Ph)Br to avoid using the less stable bis-silylated compounds **5** and **6**. We obtained the resulting trimers in good to moderate yields (**8** (87 %), **9a** (90 %), **10a** (44 %), **9b** (80 %) and **10b** (54 %)). Their constitution was assured by multi-nuclear NMR spectroscopy and high-resolution mass spectrometry (HRMS); degradation experiments further corroborate our structural assignment (see below). Upon slow crystallization from a concentrated solution of **10b** in *n*-hexane, we obtained single-crystals suitable for X-ray diffraction studies (Figure 2.9.2). In the ^1H NMR spectra of the B=N-linked compounds **8**, **9a**, and **10a** the signal of the N–*H* groups appeared as singlets between 7.14 and 7.05 ppm. In the $^{11}B\{^1H\}$ NMR spectrum these oligomers show a broad peak between 45 and 43 ppm, in the same range as those of their oligo(*p*-phenylene iminoborane) congeners.[5a] As proven by ^1H, ^1H ROESY measurements for **8**, the (*Z*/*Z*)-diastereomer is the exclusively formed isomer for the compounds with B=N double bonds (Figure S5.9.13). The B–O-linked trimers, **9b** and **10b**, showed in the $^{11}B\{^1H\}$ NMR spectra a single broad resonance at around 48 ppm, which is slightly downfield shifted compared to their BN congeners. The $^{13}C\{^1H\}$ NMR spectra of **9b** and **10b** showed each two broad signals for the *o*-CH_3 groups of the triisopropylphenyl (Tip) substituents (Figure S5.9.19 and S5.9.25), indicating hindered rotation of the B–C(Tip) bond, in contrast to **9a** and **10a**.

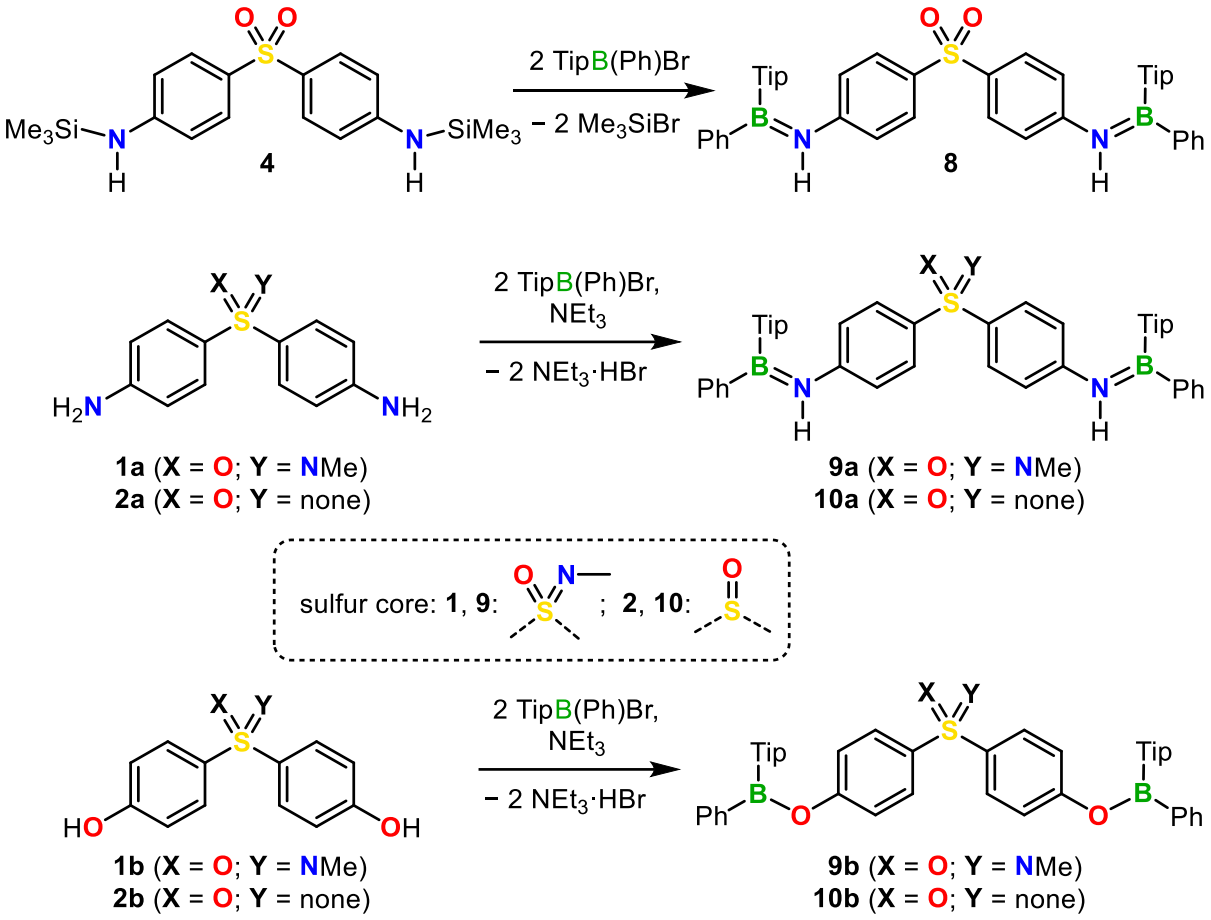

Scheme 2.9.2. Synthesis of oligomers **8**, **9**, and **10** containing different sulfur core units and B–N or B–O linkages (Tip = 2,4,6-triisopropylphenyl).

The molecular structure of **10b** features perfectly trigonal–planar coordinated boron centers ($\sum(\angle BR_3) = 360.0°$), a trigonal–pyramidal sulfur atom and the B–O bond lengths of 1.375(5) Å are in the same range with those in BO doped polycyclic aromatic hydrocarbons (Figure 2.9.2, left).[15] The triisopropylphenyl groups are largely perpendicular to the plane of the C_2BNC moiety; thus providing effective steric shielding of the boron center.

An attempt to prepare a corresponding trimer **11** from **3** and TipB(Ph)Br via an analogous salt elimination protocol, however, was unsuccessful (Scheme 2.9.3, top). In this case, we observed an immediate color change from colorless to brown after addition of the borane to a mixture of **3** and NEt_3 in CH_2Cl_2. After 24 h the ^1H NMR spectrum of the thus formed purple reaction mixture showed beside expected signals of the triethylammonium bromide by-product, unexpected multiple signals for aromatic phenyl(ene) and Tip-CH_3 moieties (Figure S5.9.26). In the $^{11}B\{^1H\}$ NMR spectrum we observed a broad peak at 45.1 ppm in the same range with that of **9a** and **10a**. In HRMS measurements we observed the signals for the expected product **11** and various other signals indicating side reactions (Figure S5.9.77). It is well-known that haloboranes can undergo haloboration reactions with cyano groups.[16]

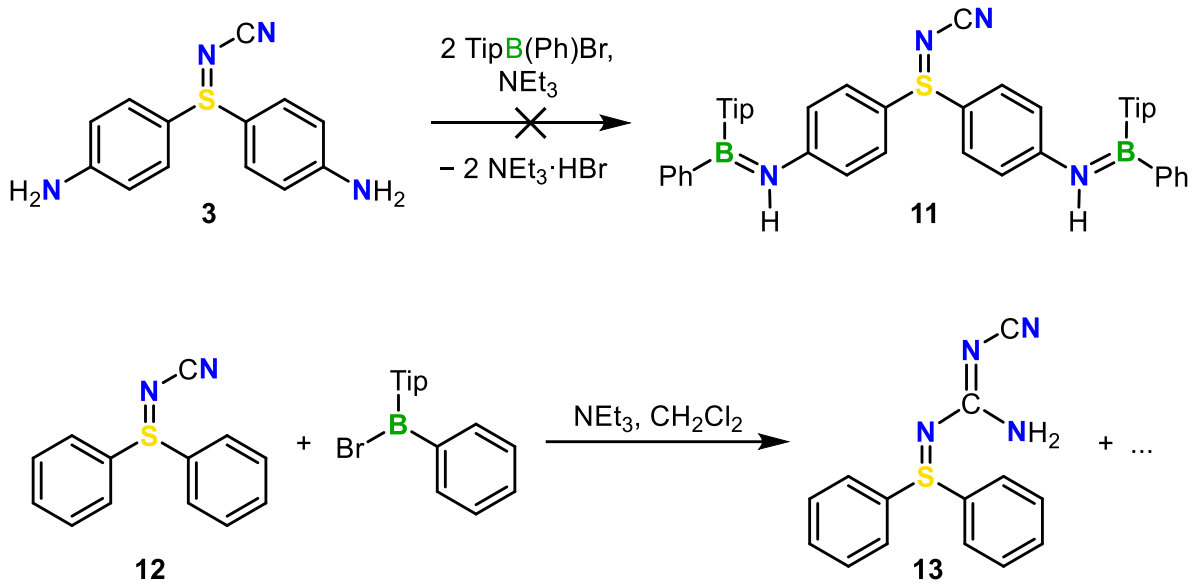

Scheme 2.9.3. Synthesis attempt of **11** (top) and model reaction of **12** with TipB(Ph)Br (Tip = 2,4,6-triisopropylphenyl).

In order to examine if the cyano group might play a role in the above reaction, we synthesized **12**,[17] which lacks reactive amino groups, and reacted it with TipB(Ph)Br under the same conditions (Scheme 2.9.3, bottom). After stirring overnight, we observed a clear brown solution. After extraction with *n*-hexane, the ^{1}H NMR spectrum of the *n*-hexane phase revealed the presence of multiple species (Figure S5.9.28). The residue, however, showed signals that point to the formation of two different triethylammonium species indicated by their two triplets at 1.47 and 1.42 ppm and corresponding quartet signals at 3.65 and 3.13 ppm, respectively (ratio 1.5:1, see Figure S5.9.29).

From the *n*-hexane phase we obtained a single crystal suitable for X-ray diffraction of compound **13** (Figure 2.9.2, right). This result confirms the reaction of the cyano group through addition of an amino and cyano group to molecule **12**. The unit cell contains three symmetry-independent molecules with similar structural parameters which are connected by hydrogen bonds with lengths between 2.128 and 2.207 Å (Figure 2.9.5, Table 2.9.2). The molecular structure of **13** in the solid state features a carbon atom that is trigonal–planar coordinated by three nitrogen atoms ($\sum(\angle CN_3) = 360.0°$, for each of the three independent molecules) with C1–N bond lengths between a single and a double bond (1.334(2) to 1.359(2) Å). The C1–NH_2 bond is shortened and shows double bond character, probably due to conjugation into the other C1–N bonds. The structure also reveals a similar bond length for the C2–N3 bond (ca. 1.320 Å) and the terminal cyano group (C2≡N4) has triple bond character with a bond length of about 1.160 Å.

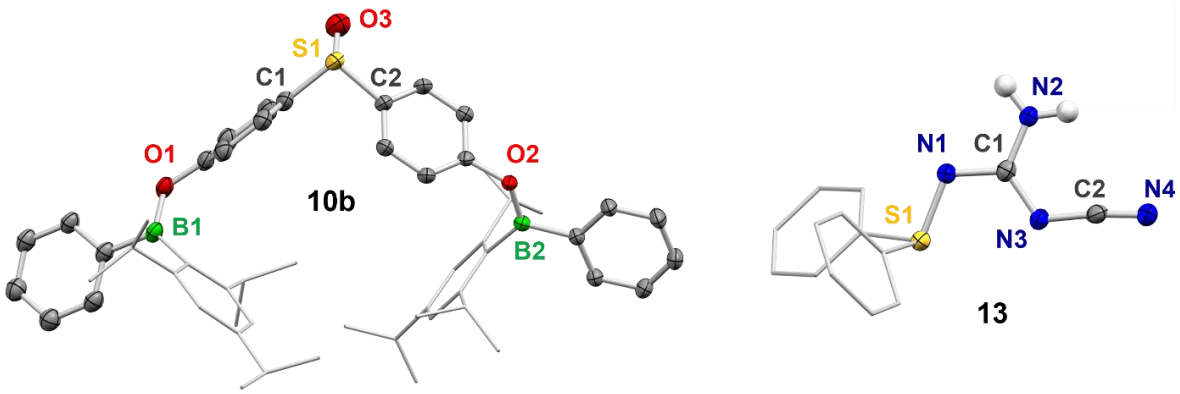

Figure 2.9.2. Molecular structures of **10b** (left) and one molecule of **13** (right) in the solid state by single-crystal X-ray diffraction (ellipsoids drawn at the 50 % probability level, except for the Tip groups of **10b** and phenyl groups of **13**; H atoms omitted for clarity).

Then, we aimed at the synthesis of the corresponding BN- and BO-doped inorganic–organic hybrid polymers. This was achieved by Si/B exchange co-polycondensation or salt elimination of the sulfur-containing monomers with bis(bromoborane) **14** in CH_2Cl_2 at room temperature or in *o*-difluorobenzene (*o*-DFB) at 80 °C for 3 days (Scheme 2.9.4).

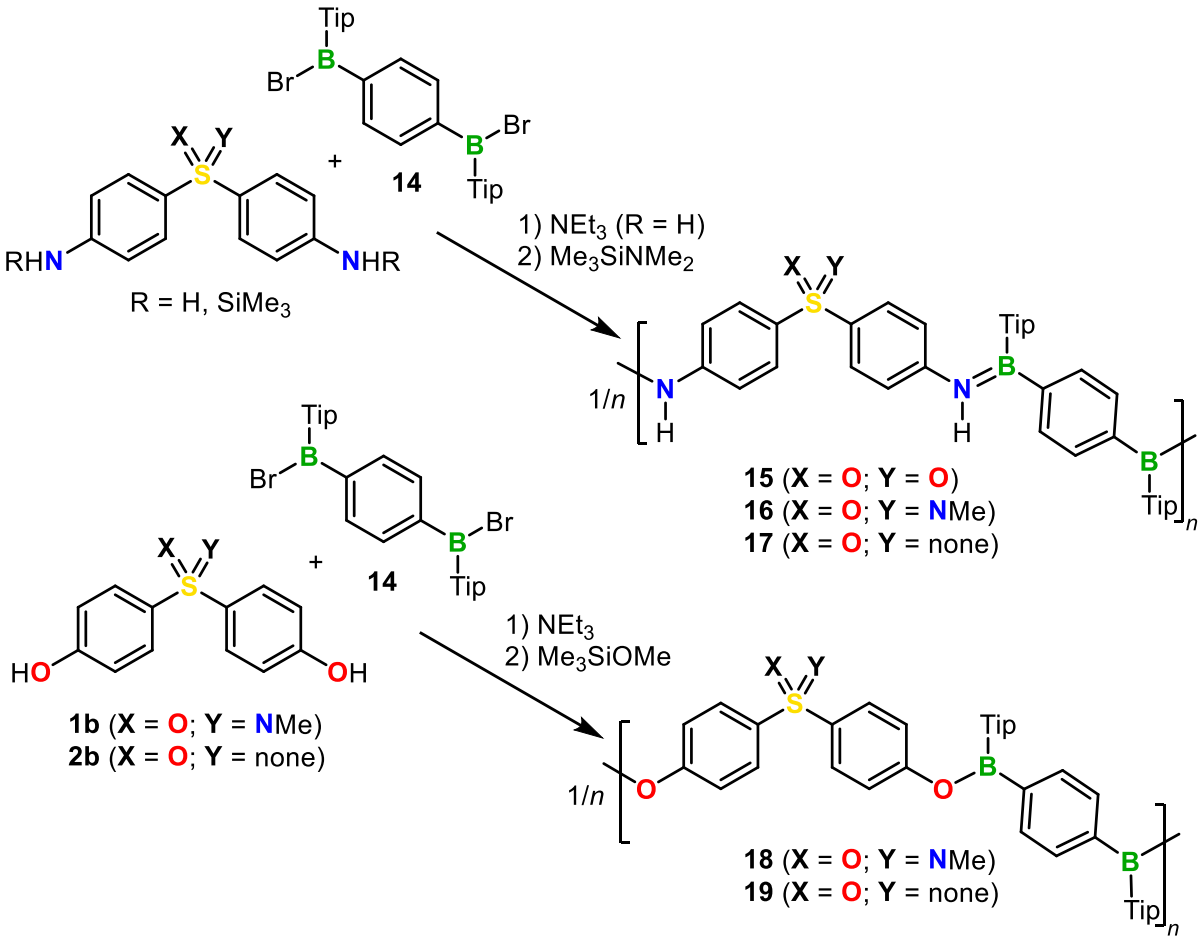

Scheme 2.9.4. Synthesis of polymers **15**, **16**, **17**, **18**, and **19** in DCM (r.t.) or *o*-DFB (80 °C) for 3 d (see Table 2.9.1 for the specific reaction conditions).

All salt elimination reactions were performed with NEt_3 as auxiliary base. The eventually remaining reactive B–Br end groups were terminated by addition of Me_3SiNMe_2 to the BN-linked **15**-**17** and of Me_3SiOMe to the BO-linked polymers **18** and **19**, respectively. After precipitation in cold *n*-pentane (−40 °C) and/or filtering off the triethylammonium bromide we accomplished to isolate the desired polymers in moderate to excellent yields (40–96 %). The polymers, which are soluble in the most common solvents such as THF, DCM, and chloroform, were characterized by NMR spectroscopy and in terms of molecular weight by gel permeation chromatography (GPC).

The ^{1}H NMR spectra showed the expected signals for the polymers, which we can assign based on the observations made on the model oligomers (Appendix 5.9). In the $^{11}B\{^{1}H\}$ NMR spectra the signals are very broad, overlaid by the glass background. After reducing the latter, we observed for **17** a signal at 42.6 ppm, close to that of its corresponding model oligomer **10a** (43.2 ppm).

GPC analysis of the isolated polymers revealed molecular-weight averages ranging from M_n = 3.0 to 12.2 kDa for the BN linked polymers, corresponding to number-average degrees of polymerization of DP_n = 8 – 33 (Table 2.9.1). The BO linked polymers, however, only reached M_n values between 1.5 and 2.9 kDa, corresponding to a DP_n of 4 – 8. The polydispersity indices (PDI) are in the range of 1.6 to 2.6, as expected for step growth-type polycondensation reactions. Only **18** showed a lower PDI of 1.2, which indicates the presence of a monodisperse oligomer species, consistent with a low determined molecular weight of around M_n = 1.5 kDa.

That we achieved higher molecular weights for the BN-linked than for the BO-linked polymers is consistent with our previous findings.[13] Furthermore, by silicon/boron exchange polycondensation in dichloromethane at room temperature we generally achieved higher molecular weights than by salt elimination reactions. While we did not observe any significant difference between Si/B exchange reactions in either DCM at room temperature or in *o*-DFB at 80 °C for **15** in terms of the molecular weight obtained, we accomplished to reproduce the increased M_n for **16** in the reaction in *o*-DFB (Table 2.9.1).[13] The best polymerization result was obtained for **17** in DCM with a M_n of 12.2 kDa (Table 2.9.1, entry 7), which corresponds to a DP_n of 33. Neither the Si/B exchange reaction in *o*-DFB nor that by salt elimination showed higher molecular weights. The BO-linked polymer **19** also showed a slightly increased degree of polymerization (DP_n = 7 – 8) compared to **18** (DP_n = 4).

Table 2.9.1. GPC data of the synthesized polymers **15**-**19**.

Entry	Polymer	M_n [kDa]	M_w [kDa]	PDI	DP_n
1	**15**[a, i]	7.5	14.3	1.9	20
2	**15**[a, ii]	7.7	15.1	2.0	20
3	**15**[b, i]	6.3	14.9	2.4	17
4	**16**[a, i]	8.8	15.2	1.7	23
5	**16**[a, ii]	11.3	21.7	1.9	30
6	**16**[b, i]	4.2	7.2	1.7	11
7	**17**[a, i]	12.2	28.2	2.3	33
8	**17**[a, ii]	3.0	5.4	1.8	8
9	**17**[b, i]	6.0	15.5	2.6	16
10	**18**[b, i]	1.5	1.7	1.2	4
11	**18**[b, ii]	1.6	1.9	1.2	4
12	**19**[b, i]	2.7	4.2	1.6	7
13	**19**[b, ii]	2.9	4.5	1.6	8

[a] Si/B exchange. [b] salt elimination in the presence of NEt_3. Reaction conditions: [i] CH_2Cl_2, r.t.; [ii] *o*-DFB, 80 °C.

As *Dapson* has been used as a drug with an anti-inflammatory effect,[9] it was of interest to investigate the possibility of a pH-triggered degradation of the species presented herein, potentially associated with the release of the respective sulfur-based agent. Therefore, we performed degradation experiments on the monodisperse oligomers under acidic and basic conditions, monitored by ^1H and $^{13}C\{^1H\}$ NMR spectroscopy and HRMS. In a typical NMR experiment, we dissolved the respective oligomer in DMSO-d_6 and added a drop of aqueous 1M NaOH or HCl, respectively. While we employed the base for degradation experiments of the BN-linked oligomers, for the BO species we additionally applied acidic conditions. To ensure the identification of the sulfur compound formed, we additionally treated the respective monomeric building blocks with base or acid, respectively, and analyzed the resulting solutions by NMR spectroscopy – under the same conditions as we monitored the oligomer degradation reactions. After the addition of a drop of 1M NaOH to a **2a** solution, the amine proton resonances at around 5.6 ppm disappeared, but the aromatic doublet signals remained nearly unchanged at δ = 7.19 and 6.59 ppm, with a coupling constant of $^3J_{HH}$ = 8.7 Hz (Figure 2.9.3). When we performed this experiment with **10a**, its aromatic proton resonances at δ = 7.20 and 6.99 ppm vanished immediately in favor of the appearance of the doublet signals of **2a** at δ = 7.18 and 6.60 ppm, confirming the successful release of that building block. In the $^{13}C\{^1H\}$ NMR spectrum we observed four signals which match the carbon signals of **2a**, and an HRMS

measurement showed the presence of the molecular ion of **2a** at *m/z* = 233.0740 (Figure S5.9.62 & S5.9.82).

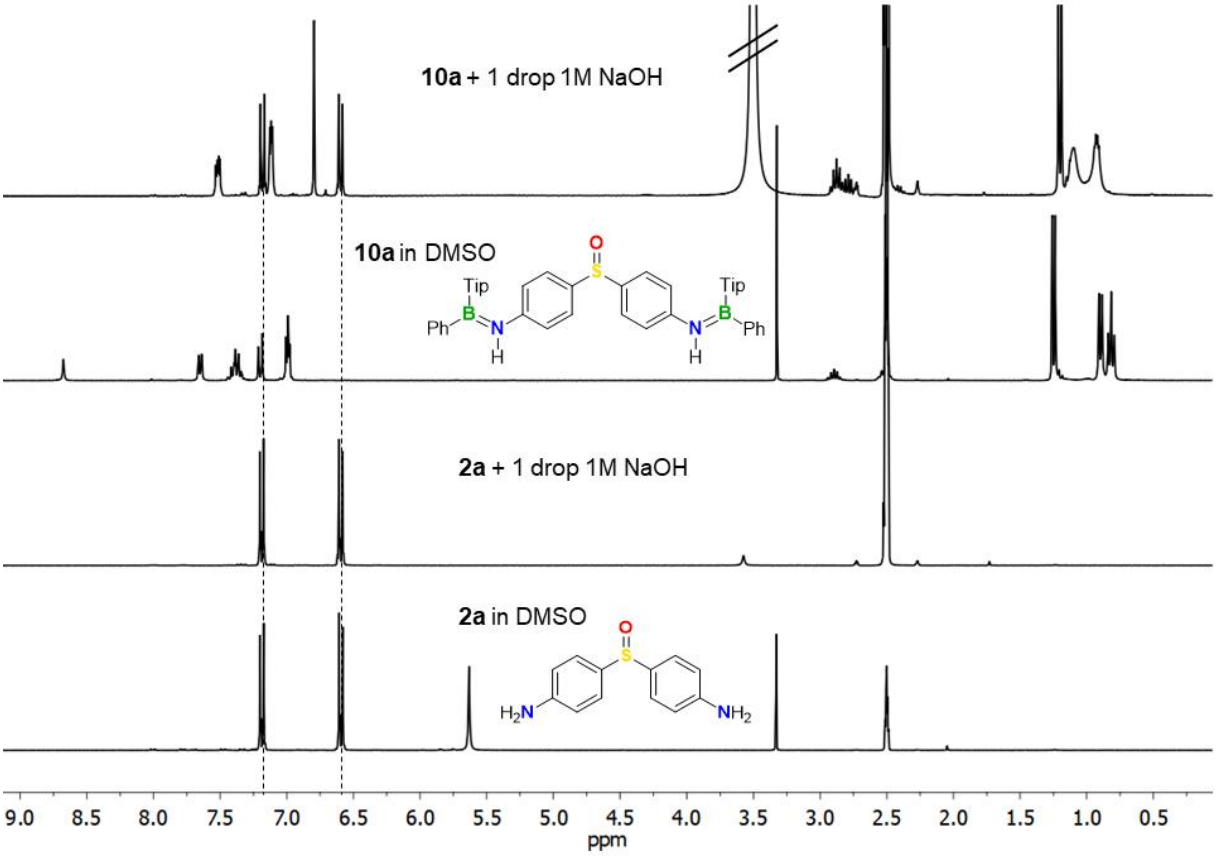

Figure 2.9.3. ^{1}H NMR spectra of the pH-triggered degradation of **10a** with **2a** reference in DMSO-d_6.

In the case of the BO reference **2b**, we observed after addition of one drop of NaOH in the ^{1}H NMR spectrum the disappearance of the hydroxy protons associated with a highfield shift of the aromatic resonances from δ = 7.42 and 6.87 ppm to δ = 7.23 and 6.66 ppm, respectively. After subsequent addition of HCl we observed the reverse reaction, indicated by re-formation of the downfield-shifted signals for **2b** at δ = 7.42 and 6.88 ppm with a coupling constant of $^{3}J_{HH}$ = 8.8 Hz (Figure S5.9.65). We assume the formation of a phenoxide derivative as an intermediate product after addition of the base, which is protonated upon addition of the acid to form the respective phenol species. By treating **9b** and **10b** the same reagents sequentially, analogous signal-shifts were also observed (Figure S5.9.59 and S5.9.65). After basic degradation of **10b** and subsequent addition of HCl, we obtained two aromatic signals at 7.41 and 6.87 ppm with a coupling constant of $^{3}J_{HH}$ = 8.8 Hz, which perfectly match those of the reference **2b**. On the other hand, when we added a drop of 1M aqueous HCl to the BO species **9b** and **10b** in DMSO we observed the direct release of the respective sulfur-based monomers (see SI). As a good case in point, we studied the degradation of polymer **18** upon addition of HCl. Immediately after the addition, two new aromatic resonances at δ = 7.98 and 7.12 ppm

and one at 2.75 ppm for the N-CH_3 group were detected, which match the signals of degraded **9b** and thus are consistent with the release of the sulfur-containing compound **1b** (Figure S5.9.67).

2.9.3 Conclusion

We presented an extensive study of inorganic–organic hybrid polymers and oligomers composed of different sulfur-based building blocks and B=N- or B–O-linkages, respectively. We successfully prepared unprecedented polymers of this type featuring sulfone (**15**) and sulfoxide groups (**17** and **19**), and we studied the sulfoximine-containing polymers **16** and **18**, previously reported by us, in more detail. For each new polymer, we synthesized a corresponding trimer (**8**, **9a**,**b**, and **10a**,**b**) as a molecular model system in addition. The incorporation of a sulfilimine building block into such structures was not successful. The formation of compound **13** in a model reaction involving sulfilimine **12** that is devoid of polymerizable end groups, suggests the competing reactivity of the cyano group in the sulfilimine-based monomer **3**. The pH-triggered degradation of all oligomers and polymer **18**, which occurred under release of the sulfur-containing blocks, showed promising results for possible applicability in drug delivery systems.

2.9.4 Experimental Section

General procedures. Unless otherwise stated, all reagents were purchased from commercial suppliers and used without further purification. All solvents were distilled prior to using and for inert reactions degassed solvents (DCM, THF, *n*-hexane) by means of an Innovative Technology solvent purification system (SPS) was used. When required, solvents (*n*-pentane, *o*-DFB, $CDCl_3$, CD_2Cl_2) were dried according to general purification methods. **4**,[14] **12**,[17] **14**,[5a] TipB(Ph)Br[5a] were prepared according to literature procedures. NMR spectra were recorded either on a Bruker Avance III HD, Bruker Avance 400 Nanobay or on a Bruker Avance 500 spectrometer in deuterated solvents. The chemical shifts (δ) are given in ppm relative to the residual peak of the non-deuterated solvent as internal standard (^{1}H: $CDCl_3$, 7.26 ppm; DMSO-d_6, 2.50 ppm; ^{13}C: $CDCl_3$, 77.16 ppm; DMSO-d_6, 39.52 ppm) or external $BF_3{\cdot}OEt_2$ (^{11}B) and $SiMe_4$ (^{29}Si). High resolution mass spectra (HRMS) were recorded on a Thermo Scientific Exactive Plus Orbitrap MS system. Elemental analyses were performed on an Elementar vario MICRO cube elemental analyzer. GPC chromatograms were recorded on an Agilent 1260 Infinity II Series, equipped with two PSS SDV 3 µm 1000 Å (300 x 8 mm) columns and one PSS SDV 3 µm 10000 Å (300x8 mm) column, at 25 °C with a flow rate of 1 mL min^{-1} and calibrated against polystyrene standards. The samples were diluted in THF and toluene as

internal standard. Detection was carried out via UV signal (λ = 280 nm). Evaluation of the chromatograms was performed by using WinGPC software.

Spectra. All spectra and other result figures are shown in Appendix 5.9.

Synthesis of 5. To a solution of bis(4-aminophenyl)(methylimino)-λ^6-sulfanone (736 mg, 2.8 mmol) in THF (22 mL) was added NEt_3 (5.6 mL) and Me_3SiCl (1.43 mL, 11.2 mmol). The reaction mixture was heated at 45 °C for 24 h. The solvent was removed *in vacuo*. The product was extracted with THF (3 x 8 mL) and the solvent was removed *in vacuo*. After washing with *n*-pentane to remove THF residues the product **5** was isolated as a white solid (950 mg, 2.34 mmol, 84 % yield). ^{1}H NMR (500 MHz, $CDCl_3$): δ = 7.66-7.64 (m, 4H, N-Ph-C*H*), 6.63-6.61 (m, 4H, S-Ph-C*H*), 3.81 (s, 2H, N*H*), 2.77 (s, 3H, NCH_3), 0.25 (s, 18H, Si(CH_3)$_3$) ppm; ^{13}C{^{1}H} NMR (125 MHz, $CDCl_3$): δ = 151.4 (s, N-Ph-*C*), 130.1 (s, N-Ph-*C*H), 128.9 (s, S-Ph-*C*), 115.9 (s, S-Ph-*C*H), 29.8 (s, N*C*H$_3$), 0.0 (s, Si(*C*H$_3$)$_3$) ppm; ^{29}Si{^{1}H} NMR (99.4 MHz, $CDCl_3$): δ = 4.6 ppm; HRMS (ASAP pos): *m/z* calcd. for $[M+H]^+$: 406.1799; found: 406.1790.

Synthesis of 6. To a suspension of **2a** (465 mg, 2.0 mmol) in THF (16.0 mL) was added NEt_3 (4.0 mL) and Me_3SiCl (1.02 mL, 8.0 mmol). The reaction mixture was heated at 45 °C for 24 h and after full conversion the salt was removed by filtration. The solvent was removed *in vacuo* and the product **6** was isolated as a yellowish solid (500 mg, 1.33 mmol, 67 % yield). ^{1}H NMR (500 MHz, $CDCl_3$): δ = 7.36-7.34 (m, 4H, N-Ph-C*H*), 6.67-6.65 (m, 4H, S-Ph-C*H*), 3.72 (s, 2H, N*H*), 0.26 (s, 18H, Si(CH_3)$_3$) ppm; ^{13}C{^{1}H} NMR (125 MHz, $CDCl_3$): δ = 150.4 (s, N-Ph-*C*), 133.3 (s, S-Ph-*C*), 127.3 (s, N-Ph-*C*H), 116.4 (s, S-Ph-*C*H), 0.0 (s, Si(*C*H$_3$)$_3$) ppm; ^{29}Si{^{1}H} NMR (99.4 MHz, $CDCl_3$): δ = 4.2 ppm; HRMS (ASAP pos): *m/z* calcd. for $[M+H]^+$: 377.1534; found: 377.1524; elem. anal. calcd. % for $C_{18}H_{28}N_2OSSi_2$: C 57.40, H 7.49, N 7.44, S 8.51; found: C 57.12, H 7.66, N 7.43, S 8.17.

Synthesis of 7. To a suspension of **3** (256 mg, 1.0 mmol) in THF (8.0 mL) was added NEt_3 (2.0 mL) and Me_3SiCl (0.51 mL, 4.0 mmol). The reaction mixture was stirred at room temperature for 4 d and after full conversion the salt was removed by filtration. The solvent was removed in vacuo and the product **7** was isolated as an off-white solid (244 mg, 0.61 mmol, 61 % yield). ^{1}H NMR (500 MHz, $CDCl_3$): δ = 7.39-7.37 (m, 4H, N-Ph-C*H*), 6.71-6.69 (m, 4H, S-Ph-C*H*), 4.01 (s, 2H, N*H*), 0.28 (s, 18H, Si(CH_3)$_3$) ppm; ^{13}C{^{1}H} NMR (125 MHz, $CDCl_3$): δ = 152.2 (s, N-Ph-*C*), 129.6 (s, N-Ph-*C*H), 122.4 (s, S-Ph-C), 122.0 (s, N-*C*N), 116.9 (s, S-Ph-*C*H), −0.1 (s, Si(*C*H$_3$)$_3$) ppm; ^{29}Si{^{1}H} NMR (99.4 MHz, $CDCl_3$): δ = 5.1 ppm; HRMS (ASAP pos): *m/z* calcd. for $[M+H]^+$: 401.1646; found: 401.1641; elem. anal. calcd. % for $C_{19}H_{28}N_4SSi_2$: C 56.95, H 7.04, N 13.98, S 8.00; found: C 56.66, H 7.09, N 14.00, S 7.60.

Synthesis of 8. To a solution of **4** (393 mg, 1.00 mmol) in DCM (2.5 mL) was added a solution of TipB(Ph)Br (762 mg, 2.05 mmol) in 6.0 mL DCM, dropwise at −78 °C. The reaction mixture was warmed to room temperature overnight. After removing the solvent and washing with *n*-pentane (3 x 5 mL), an off-white solid was obtained (723 mg, 0.87 mmol, 87 % yield). ^{1}H NMR (500 MHz, $CDCl_3$): δ = 7.62- 7.60 (m, 4H, B-*o*-Ph-C*H*), 7.57-7.55 (m, 4H, S-Ph-C*H*), 7.46-7.43 (m, 2H, B-*p*-Ph-C*H*), 7.40-7.37 (m, 4H, B-*m*-Ph-C*H*), 7.09 (s, 2H, N*H*), 7.01 (s, 4H, Tip-CH_{Ar}), 6.83-6.82 (m, 4H, N-Ph-C*H*), 2.95 (sept, 2H, *p*-Tip-C*H*), 2.56 (sept, 4H, *o*-Tip-C*H*), 1.33 (d, 12H, *p*-Tip-CH_3), 0.98 (d, 12H, *o*-Tip-CH_3), 0.90 (d, 12H, *o*-Tip-CH_3) ppm; ^{11}B{^{1}H} NMR (160 MHz, $CDCl_3$): δ = 45.1 (br) ppm; ^{13}C{^{1}H} NMR (125 MHz, $CDCl_3$): δ = 149.7 (s, *p*-Tip-*C*), 149.5 (s, *o*-Tip-*C*), 148.3 (s, S-Ph-*C*), 139.4 (br, B-Ph-C_{ipso}), 135.2 (s, N-Ph-*C*), 134.9 (br, B-Tip-C_{ipso}), 133.4 (s, B-Ph-C_{ortho}), 131.1 (s, B-Ph-C_{para}), 128.7 (s, S-Ph-*C*H), 128.2 (s, B-Ph-C_{meta}), 120.9 (s, Tip-*C*H_{Ar}), 120.3 (s, N-Ph-*C*H), 35.1 (s, *o*-Tip-*C*H), 34.5 (s, *p*-Tip-*C*H), 24.6 (s, *o*-Tip-*C*H_3), 24.3 (s, *o*-Tip-*C*H_3), 24.3 (s, *p*-Tip-*C*H_3) ppm; HRMS (LIFDI): *m/z* calcd. for [M]: 828.5026; found: 828.5014; elem. anal. calcd. % for $C_{54}H_{66}B_2N_2O_2S$: C 78.26, H 8.03, N 3.38, S 3.87; found: C 77.30, H 8.00, N 3.38, S 3.84.

Synthesis of 9a. To a suspension of **1a** (65.5 mg, 0.25 mmol) in DCM (1.0 mL) was added NEt_3 (0.25 mL) and a solution of TipB(Ph)Br (194 mg, 0.51 mmol) in 2.0 mL DCM at room temperature. After stirring overnight, the solvent was removed *in vacuo*. Subsequently, the salt was removed by filtration with *n*-hexane (2, 1.5, 1.5 mL). After removing the solvent, the product was dried and isolated as an off-white solid (189 mg, 0.22 mmol, 90 % yield). ^{1}H NMR (500 MHz, $CDCl_3$): δ = 7.61 (d, 4H, B-*o*-Ph-C*H*), 7.58 (d, 2H, S-Ph-C*H*), 7.45-7.42 (m, 2H, B-*p*-Ph-C*H*), 7.39-7.37 (m, 4H, B-*m*-Ph-C*H*), 7.05 (s, 2H, N*H*), 7.00 (s, 4H, Tip-CH_{Ar}), 6.82-6.80 (d, 4H, N-Ph-C*H*), 2.94 (sept, 2H, *p*-Tip-C*H*), 2.68 (s, 3H, NCH_3), 2.56 (sept, 4H, *o*-Tip-C*H*), 1.32 (d, 12H, *p*-Tip-CH_3), 0.97 (d, 12H, *o*-Tip-CH_3), 0.89 (m, 12H, *o*-Tip-CH_3) ppm; ^{11}B{^{1}H} NMR (160 MHz, $CDCl_3$): δ = 45.0 (br) ppm; ^{13}C{^{1}H} NMR (125 MHz, $CDCl_3$): δ = 149.6 (s, *p*-Tip-*C*), 149.6 (s, *o*-Tip-*C*), 149.6 (s, *o*-Tip-*C*), 147.6 (s, S-Ph-*C*), 139.6 (br, B-Ph-C_{ipso}), 135.1 (br, B-Tip-C_{ipso}), 133.8 (s, N-Ph-*C*), 133.4 (s, B-Ph-C_{ortho}), 131.0 (s, B-Ph-C_{para}), 129.6 (s, S-Ph-*C*H), 128.2 (s, B-Ph-C_{meta}), 120.8 (s, Tip-*C*H_{Ar}), 120.4 (s, N-Ph-*C*H), 35.1 (s, *o*-Tip-*C*H), 34.5 (s, *p*-Tip-*C*H), 29.6 (s, N*C*H_3), 24.6 (s, *o*-Tip-*C*H_3), 24.3 (s, *p*-Tip-*C*H_3), 24.3 (s, *o*-Tip-*C*H_3) ppm; HRMS (APCI pos): *m/z* calcd. for $[M+H]^+$: 842.5420; found: 842.5404.

Synthesis of 9b. To a suspension of **1b** (26.3 mg, 0.10 mmol) in DCM (1.0 mL) was added NEt_3 (0.1 mL) and a solution of TipB(Ph)Br (76.3 mg, 0.21 mmol) in 1.5 mL DCM at room temperature. The reaction mixture was warmed to room temperature overnight and the solvent was removed *in vacuo*. Subsequently, the salt was removed by filtration with *n*-hexane (3 x 1.0 mL). After removing the solvent, the product was dried and isolated as a colorless solid

(66.2 mg, 0.08 mmol, 80 % yield). ^{1}H NMR (500 MHz, $CDCl_3$): δ = 7.82- 7.79 (m, 4H, B-*o*-Ph-C*H*), 7.71-6.69 (m, 4H, O-Ph-C*H*), 7.52-7.47 (m, 2H, B-*p*-Ph-C*H*), 7.41-7.38 (m, 4H, B-*m*-Ph-C*H*), 7.00-6.98 (m, 4H, S-Ph-C*H*), 6.89 (s, 4H, Tip-CH_{Ar}), 2.87 (sept, 2H, *p*-Tip-C*H*), 2.66 (s, 3H, NCH_3), 2.50 (sept, 4H, *o*-Tip-C*H*), 1.26 (d, 12H, *p*-Tip-CH_3), 0.98 (d, 24H, *o*-Tip-CH_3) ppm; ^{11}B{^{1}H} NMR (160 MHz, $CDCl_3$): δ = 48.2 (br) ppm; ^{13}C{^{1}H} NMR (125 MHz, $CDCl_3$): δ = 159.1 (s, O-Ph-C_{ipso}), 150.2 (s, *p*-Tip-*C*), 150.0 (s, *o*-Tip-*C*), 137.5 (br, B-Ph-C_{ipso}), 136.2 (s, B-Ph-C_{Ortho}), 135.1 (s, S-Ph-C_{ipso}), 132.5 (s, B-Ph-C_{Para}), 131.9 (br, B-Tip-C_{ipso}), 130.0 (s, O-Ph-*C*H), 127.8 (s, B-Ph-C_{Meta}), 121.1 (s, S-Ph-*C*H), 120.6 (s, Tip-*C*H_{Ar}), 35.5 (s, *o*-Tip-*C*H), 34.4 (s, *p*-Tip-*C*H), 29.5 (s, N*C*H_3), 25.0 (br, *o*-Tip-*C*H_3), 24.1 (s, *p*-Tip-*C*H_3), 24.0 (br, *o*-Tip-*C*H_3) ppm; HRMS (APCI pos): *m/z* calcd. for $[M+H]^+$: 844.5101; found: 844.5080.

Synthesis of 10a. To a suspension of **2a** (117 mg, 0.50 mmol) in DCM (3.5 mL) was added NEt_3 (0.5 mL) and a solution of TipB(Ph)Br (382 mg, 1.03 mmol) in 2.0 mL DCM at 0 °C. The reaction mixture was warmed to room temperature overnight and the solvent was removed *in vacuo*. Subsequently, the salt was removed by filtration with *n*-hexane (2, 1, 1 mL). After removing the solvent and washing the crude product with cold *n*-pentane (3 x 1 mL) at −78 °C the product was dried and isolated as an orange solid (180 mg, 0.22 mmol, 44 % yield). ^{1}H NMR (500 MHz, CD_2Cl_2): δ = 7.61- 7.59 (m, 4H, B-*o*-Ph-C*H*), 7.45-7.42 (m, 2H, B-*p*-Ph-C*H*), 7.40-7.37 (m, 4H, B-*m*-Ph-C*H*), 7.25-7.23 (m, 4H, S-Ph-C*H*), 7.14 (s, 2H, N*H*), 7.03 (m, 4H, Tip-CH_{Ar}), 6.87-6.86 (m, 4H, N-Ph-C*H*), 2.94 (sept, 2H, *p*-Tip-C*H*), 2.61 (sept, 2H, *o*-Tip-C*H*), 2.61 (sept, 2H, *o*-Tip-C*H*), 1.32 (d, 12H, *p*-Tip-CH_3), 0.98 (d, 12H, *o*-Tip-CH_3), 0.91 (d, 6H, *o*-Tip-CH_3), 0.90 (d, 6H, *o*-Tip-CH_3) ppm; ^{11}B{^{1}H} NMR (160 MHz, CD_2Cl_2): δ = 43.2 (br) ppm; ^{13}C{^{1}H} NMR (125 MHz, CD_2Cl_2): δ = 150.0 (s, *o*-Tip-*C*), 149.9 (s, *o*-Tip-*C*), 149.9 (s, *p*-Tip-*C*), 146.9 (s, S-Ph-C_{ipso}), 140.2 (br, B-Ph-C_{ipso}), 139.6 (s, N-Ph-C_{ipso}), 135.7 (br, B-Tip-C_{ipso}), 133.6 (s, B-Ph-C_{ortho}), 131.0 (s, B-Ph-C_{para}), 128.4 (s, B-Ph-C_{meta}), 126.2 (s, S-Ph-*C*H), 121.2 (s, N-Ph-*C*H), 121.0 (s, Tip-*C*H_{Ar}), 35.3 (s, *o*-Tip-*C*H), 34.8 (s, *p*-Tip-*C*H), 24.6 (s, *o*-Tip-*C*H_3), 24.3 (s, *o*-Tip-*C*H_3), 24.3 (s, *p*-Tip-*C*H_3) ppm; HRMS (APCI pos): *m/z* calcd. for $[M+H]^+$: 813.5155; found: 813.5134.

Synthesis of 10b. To a suspension of **2b** (117 mg, 0.50 mmol) in DCM (3.5 mL) was added NEt_3 (0.5 mL) and a solution of TipB(Ph)Br (383 mg, 1.03 mmol) in 2.0 mL DCM at 0 °C. The reaction mixture was warmed to room temperature overnight and the solvent was removed *in vacuo*. Subsequently, the salt was removed by filtration with *n*-pentane (3, 1, 1 mL) After removing the solvent and washing the crude product with *n*-pentane (3 x 2 mL) the product was dried and isolated as an off-white solid (220 mg, 0.27 mmol, 54 % yield). ^{1}H NMR (500 MHz, $CDCl_3$): δ = 7.82- 7.81 (m, 4H, B-*o*-Ph-C*H*), 7.52-7.48 (m, 2H, B-*p*-Ph-C*H*), 7.41-7.39 (m, 4H, B-*m*-Ph-C*H*), 7.38-7.36 (m, 4H, O-Ph-C*H*), 7.00-6.99 (m, 4H, S-Ph-C*H*), 6.90 (s,

4H, Tip-CH_{Ar}), 2.87 (sept, 2H, *p*-Tip-C*H*), 2.52 (sept, 4H, *o*-Tip-C*H*), 1.26 (d, 12H, *p*-Tip-CH_3), 1.00-0.97 (m, 24H, *o*-Tip-CH_3) ppm; $^{11}B\{^1H\}$ NMR (160 MHz, $CDCl_3$): δ = 48.1 (br) ppm; $^{13}C\{^1H\}$ NMR (125 MHz, $CDCl_3$): δ = 158.1 (s, O-Ph-C_{ipso}), 150.1 (s, *p*-Tip-*C*), 150.0 (s, *o*-Tip-*C*), 139.9 (s, S-Ph-C_{ipso}), 137.6 (br, B-Ph-C_{ipso}), 136.2 (s, B-Ph-C_{Ortho}), 132.4 (s, B-Ph-C_{Para}), 132.0 (br, B-Tip-C_{ipso}), 127.8 (s, B-Ph-C_{Meta}), 126.5 (s, O-Ph-*C*H), 121.4 (s, S-Ph-*C*H), 120.5 (s, Tip-*C*H_{Ar}), 35.5 (s, *o*-Tip-*C*H), 34.4 (s, *p*-Tip-*C*H), 25.1 (br, *o*-Tip-*C*H_3), 24.1 (s, *p*-Tip-*C*H_3), 24.0 (br, *o*-Tip-*C*H_3) ppm; HRMS (APCI pos): *m/z* calcd. for $[M+H]^+$: 815.4835; found: 815.4814.

Synthesis of 15 (Si/B exchange, CH_2Cl_2, r.t.). To a suspension of **14** (166 mg, 0.25 mmol) in DCM (2.5 mL) was added **4** (98 mg, 0.25 mmol) and the reaction mixture was stirred for 3 d at room temperature. Subsequently, Me_3SiNMe_2 (5.1 mg, 0.04 mmol) was added to deactivate reactive B–Br groups and after 2 h the reaction mixture was precipitated in cold *n*-pentane (25 mL, −40 °C). The residue was washed with *n*-pentane (3 x 5 mL) and after all volatiles were removed *in vacuo* an off-white solid was obtained (184 mg, 0.24 mmol, 96 % yield). ^1H NMR (500 MHz, $CDCl_3$): δ = 7.57 (s, 4H, B-Ph-C*H*), 7.55 (d, 4H, S-Ph-C*H*), 7.07 (s, 2H, N*H*), 6.97 (s, 4H, Tip-CH_{Ar}), 6.83 (d, 4H, N-Ph-C*H*), 2.92 (sept, 2H, *p*-Tip-C*H*), 2.52 (sept, 4H, *o*-Tip-C*H*), 1.30 (d, 12H, *p*-Tip-CH_3), 0.92 (d, 12H, *o*-Tip-CH_3), 0.87 (d, 12H, *o*-Tip-CH_3) ppm; $^{11}B\{^1H\}$ NMR (160 MHz, $CDCl_3$): δ = no signal; $^{13}C\{^1H\}$ NMR (125 MHz, $CDCl_3$): δ = 149.8 (s, *p*-Tip-*C*), 149.4 (s, *o*-Tip-*C*), 148.2 (s, S-Ph-*C*), 142.2 (br, B-Ph-*C*), 135.4 (s, N-Ph-*C*), 134.8 (br, B-Tip-*C*), 133.0 (s, B-Ph-*C*H), 128.7 (s, S-Ph-*C*H), 120.9 (s, Tip-*C*H_{Ar}), 120.4 (s, N-Ph-*C*H), 35.2 (s, *o*-Tip-*C*H), 34.5 (s, *p*-Tip-*C*H), 24.6 (s, *o*-Tip-*C*H_3), 24.3 (s, *o*-Tip-*C*H_3), 24.3 (s, *p*-Tip-*C*H_3) ppm; GPC (in THF, vs. polystyrene, detection by UV-Vis signal): M_n = 7 513 Da; M_w = 14 294 Da.

Synthesis of 15 (Si/B exchange, *o*-DFB, 80 °C). To a suspension of **14** (166 mg, 0.25 mmol) in *o*-DFB (2.5 mL) was added **4** (98 mg, 0.25 mmol) and the mixture was stirred for 3 d at 80 °C. Subsequently, Me_3SiNMe_2 (5.0 mg, 0.04 mmol) was added to deactivate reactive B–Br groups and after 2 h the reaction mixture was precipitated in cold *n*-pentane (25 mL, −40 °C). The residue was washed with *n*-pentane (3 x 5 mL) and after all volatiles were removed *in vacuo* an off-white solid was obtained (134 mg, 0.18 mmol, 72 % yield). ^1H NMR (300 MHz, $CDCl_3$): δ = 7.57 (s, 4H, B-Ph-C*H*), 7.56 (d, 4H, S-Ph-C*H*), 7.08 (s, 2H, N*H*), 6.97 (s, 4H, Tip-CH_{Ar}), 6.83 (d, 4H, N-Ph-C*H*), 2.92 (sept, 2H, *p*-Tip-C*H*), 2.52 (sept, 4H, *o*-Tip-C*H*), 1.30 (d, 12H, *p*-Tip-CH_3), 0.92 (d, 12H, *o*-Tip-CH_3), 0.87 (d, 12H, *o*-Tip-CH_3) ppm; GPC (in THF, vs. polystyrene, detection by UV-Vis signal): M_n = 7 693 Da; M_w = 15 115 Da.

Synthesis of 15 (salt elimination, CH_2Cl_2, r.t.). To a suspension of **14** (166 mg, 0.25 mmol) in DCM (2.5 mL) was added NEt_3 (0.25 mL). Subsequently, *Dapson* (62.1 mg, 0.25 mmol) was

added and the reaction mixture was stirred at room temperature. After 3 d, Me_3SiNMe_2 (10.8 mg, 0.09 mmol) was added to deactivate reactive B–Br groups and after 2 h the reaction mixture was precipitated in cold *n*-pentane (25 mL, −40 °C). The residue was washed with *n*-pentane (2 x 5 mL) and dried *in vacuo*. The polymer was dissolved in THF (15 mL) and was removed from the formed triethylammonium bromide by filtration. The precipitation was repeated two more times and after removing all volatiles *in vacuo* an off-white solid was obtained (114 mg, 0.15 mmol, 61 % yield). GPC (in THF, vs. polystyrene, detection by UV-Vis signal): M_n = 6 278 Da; M_w = 14 862 Da.

Synthesis of 16 (Si/B exchange, CH_2Cl_2, r.t.). To a suspension of **14** (166 mg, 0.25 mmol) in DCM (2.5 mL) was added **5** (101 mg, 0.25 mmol) and the reaction mixture was stirred for 3 d at room temperature. Subsequently, Me_3SiNMe_2 (10.0 mg, 0.09 mmol) was added to deactivate reactive B–Br groups and after 2 h the reaction mixture was precipitated twice in cold *n*-pentane (25 mL, −40 °C). The residue was washed with *n*-pentane (3 x 5 mL) and after all volatiles were removed *in vacuo* an off-white solid was obtained (128 mg, 0.17 mmol, 68 % yield). ^{1}H NMR (500 MHz, $CDCl_3$): δ = 7.57 (s, 4H, B-Ph-C*H*), 7.57 (d, 4H, S-Ph-C*H*), 7.06 (s, 2H, N*H*), 6.96 (s, 4H, Tip-CH_{Ar}), 6.83 (d, 4H, N-Ph-C*H*), 2.91 (sept, 2H, *p*-Tip-C*H*), 2.66 (s, 3H, NCH_3), 2.52 (sept, 4H, *o*-Tip-C*H*), 1.29 (d, 12H, *p*-Tip-CH_3), 0.92 (d, 12H, *o*-Tip-CH_3), 0.87 (d, 6H, *o*-Tip-CH_3), 0.86 (d, 6H, *o*-Tip-CH_3) ppm; ^{11}B{^{1}H} NMR (160 MHz, $CDCl_3$): δ = no signal; ^{13}C{^{1}H} NMR (125 MHz, $CDCl_3$): δ = 149.7 (s, *p*-Tip-*C*), 149.5 (s, *o*-Tip-*C*), 147.6 (s, S-Ph-*C*), 142.3 (br, B-Ph-*C*), 135.0 (s, N-Ph-*C*), 133.7 (br, B-Tip-*C*), 132.9 (s, B-Ph-*C*H), 129.6 (s, S-Ph-*C*H), 120.8 (s, Tip-*C*H$_{Ar}$), 120.5 (s, N-Ph-*C*H), 35.1 (s, *o*-Tip-*C*H), 34.4 (s, *p*-Tip-*C*H), 29.6 (s, N-*C*H$_3$), 24.6 (s, *o*-Tip-*C*H$_3$), 24.3 (s, *p*-Tip-*C*H$_3$), 24.3 (s, *o*-Tip-*C*H$_3$) ppm; GPC (in THF, vs. polystyrene, detection by UV-Vis signal): M_n = 8 799 Da; M_w = 15 181 Da.

Synthesis of 16 (Si/B exchange, *o*-DFB, 80 °C). To a suspension of **14** (166 mg, 0.25 mmol) in *o*-DFB (2.5 mL) was added **5** (101 mg, 0.25 mmol) and the reaction mixture was stirred for 3 d at 80 °C. Subsequently, Me_3SiNMe_2 (7.4 mg, 0.06 mmol) was added to deactivate reactive B–Br groups and after 2 h the reaction mixture was precipitated three times in cold *n*-pentane (25 mL, −40 °C). The residue was washed with *n*-pentane (3 x 5 mL) and after all volatiles were removed *in vacuo* an off-white solid was obtained (76.2 mg, 0.10 mmol, 40 % yield). GPC (in THF, vs. polystyrene, detection by UV-Vis signal): M_n = 11 331 Da; M_w = 21 672 Da.

Synthesis of 16 (salt elimination, CH_2Cl_2, r.t.). To a suspension of **14** (166 mg, 0.25 mmol) in DCM (2.5 mL) was added NEt_3 (0.25 mL). Subsequently, **1a** (65.3 mg, 0.25 mmol) was added and the reaction mixture was stirred at room temperature. After 3 d, Me_3SiNMe_2 (7.0 mg, 0.05 mmol) was added to deactivate reactive B–Br groups and after 2 h the reaction

mixture was precipitated in cold *n*-pentane (25 mL, –40 °C). The residue was washed with *n*-pentane (2 x 5 mL) and dried *in vacuo*. The polymer was dissolved in THF (15 mL) and was removed from the formed triethylammonium bromide by filtration. The precipitation was repeated two more times and after removing all volatiles *in vacuo* an off-white solid was obtained (108 mg, 0.14 mmol, 57 % yield). GPC (in THF, vs. polystyrene, detection by UV-Vis signal): M_n = 4 174 Da; M_w = 7 225 Da.

Synthesis of 17 (Si/B exchange, CH_2Cl_2, r.t.). To a suspension of **14** (66.4 mg, 0.10 mmol) in DCM (1.0 mL) was added **6** (37.7 mg, 0.10 mmol) and the reaction mixture was stirred for 3 d at room temperature. Subsequently, Me_3SiNMe_2 (5.9 mg, 0.05 mmol) was added to deactivate reactive B–Br groups and after 2.5 h the reaction mixture was precipitated in cold *n*-pentane (10 mL, −40 °C). The *n*-pentane was removed by syringe and after drying the product *in vacuo* a slightly orange solid was obtained (46.2 mg, 62.9 µmol, 63 % yield). ^{1}H NMR (500 MHz, $CDCl_3$): δ = 7.57 (s, 4H, B-Ph-C*H*), 7.25 (d, 4H, S-Ph-C*H*), 7.03 (s, 2H, N*H*), 6.96 (2s, 4H, Tip-CH_{Ar}), 6.84 (d, 4H, N-Ph-C*H*), 2.91 (sept, 2H, *p*-Tip-C*H*), 2.56 (dsept, 2H, *o*-Tip-C*H*), 1.29 (d, 12H, *p*-Tip-CH_3), 0.93 (d, 12H, *o*-Tip-CH_3), 0.89 (d, 6H, *o*-Tip-CH_3), 0.87 (d, 6H, *o*-Tip-CH_3) ppm; ^{11}B{^{1}H} NMR (160 MHz, $CDCl_3$): δ = 42.6 (br) ppm; ^{13}C{^{1}H} NMR (125 MHz, $CDCl_3$): δ = 149.5 (s, *o*-Tip-*C*), 149.5 (s, *p*-Tip-*C*), 146.5 (s, S-Ph-C_{ipso}), 142.4 (br, B-Ph-C_{ipso}), 138.8 (s, N-Ph-C_{ipso}), 135.1 (br, B-Tip-C_{ipso}), 132.9 (s, B-Ph-*C*H), 126.3 (s, S-Ph-*C*H), 120.9 (s, N-Ph-*C*H), 120.7 (s, Tip-*C*H_{Ar}), 35.1 (s, *o*-Tip-*C*H), 34.4 (s, *p*-Tip-*C*H), 24.6 (s, *o*-Tip-*C*H_3), 24.3 (s, *p*-Tip-*C*H_3) ppm; GPC (in THF, vs. polystyrene, detection by UV-Vis signal): M_n = 12 166 Da; M_w = 28 164 Da.

Synthesis of 17 (Si/B exchange, *o*-DFB, 80 °C). To a suspension of **14** (166 mg, 0.25 mmol) in *o*-DFB (2.5 mL) was added **6** (94.2 mg, 0.25 mmol) and the reaction mixture was stirred for 3 d at 80 °C. Subsequently, Me_3SiNMe_2 (9.9 mg, 0.08 mmol) was added to deactivate reactive B–Br groups at room temperature and after 2 h the reaction mixture was precipitated twice in cold *n*-pentane (25 mL, −40°C). The residue was washed with *n*-pentane (3 x 5 mL) and after all volatiles were removed *in vacuo* an orange solid was obtained (86.3 mg, 0.12 mmol, 48 % yield). GPC (in THF, vs. polystyrene, detection by UV-Vis signal): M_n = 3 001 Da; M_w = 5 399 Da.

Synthesis of 17 (salt elimination, CH_2Cl_2, r.t.). To a suspension of **14** (166 mg, 0.25 mmol) in DCM (2.5 mL) was added NEt_3 (0.25 mL). Subsequently, **2a** (58.1 mg, 0.25 mmol) was added and the reaction mixture was stirred at room temperature. After 3 d, Me_3SiNMe_2 (12.1 mg, 0.10 mmol) was added to deactivate reactive B–Br groups and after 2 h the reaction mixture was precipitated in cold *n*-pentane (25 mL, −40°C). The residue was washed with *n*-

pentane (2 x 5 mL) and dried *in vacuo*. The polymer was dissolved in THF (15 mL) and was removed from the formed triethylammonium bromide by filtration. The precipitation was repeated two more times and after removing all volatiles *in vacuo* a yellow solid was obtained (107 mg, 0.15 mmol, 60 % yield). GPC (in THF, vs. polystyrene, detection by UV-Vis signal): M_n = 5 977 Da; M_w = 15 494 Da.

Synthesis of 18 (salt elimination, CH_2Cl_2, r.t.). To a suspension of **14** (66.4 mg, 0.10 mmol) in DCM (2.0 mL) was added NEt_3 (0.1 mL). Subsequently, **1b** (26.3 mg, 0.10 mmol) was added and the reaction mixture was stirred for 3 d at room temperature. After all volatiles were removed *in vacuo* the residue was dissolved in DCM (2.0 mL) and Me_3SiOMe (17.1 mg, 0.16 mmol) was added to deactivate reactive B–Br groups. After 2 h the volatiles were removed *in vacuo*. The polymer was dissolved in THF (6.0 mL) and was removed from the formed triethylammonium bromide by filtration. After removing all volatiles *in vacuo* an off-white solid was obtained (66.4 mg, 86.7 µmol, 87 % yield). GPC (in THF, vs. polystyrene, detection by UV-Vis signal): M_n = 1 468 Da; M_w = 1 713 Da.

Synthesis of 18 (salt elimination, *o*-DFB, 80 °C). To a suspension of **14** (66.4 mg, 0.10 mmol) in *o*-DFB (2.0 mL) was added NEt_3 (0.1 mL). Subsequently, **1b** (26.3 mg, 0.10 mmol) was added and the reaction mixture was stirred for 3 d at 80 °C. After all volatiles were removed *in vacuo* the residue was dissolved in DCM (2.0 mL) and Me_3SiOMe (12.9 mg, 0.12 mmol) was added to deactivate reactive B–Br groups. After 2 h the volatiles were removed *in vacuo*. The polymer was dissolved in THF (6.0 mL) and was removed from the formed triethylammonium bromide by filtration. After removing all volatiles *in vacuo* an off-white solid was obtained (65.1 mg, 85.0 µmol, 85 % yield). ^{1}H NMR (500 MHz, $CDCl_3$): δ = 7.82-7.79 (m, 4H, B-Ph-C*H*), 7.71-6.69 (m, 4H, O-Ph-C*H*), 7.00-6.99 (m, 4H, S-Ph-C*H*), 6.86 (s, 4H, Tip-CH_{Ar}), 2.84 (sept, 2H, *p*-Tip-C*H*), 2.65 (s, 3H, NCH_3), 2.47 (sept, 4H, *o*-Tip-C*H*), 1.23 (d, 12H, *p*-Tip-CH_3), 0.95 (d, 24H, *o*-Tip-CH_3) ppm; ^{11}B{^{1}H} NMR (160 MHz, $CDCl_3$): δ = no signal; ^{13}C{^{1}H} NMR (125 MHz, $CDCl_3$): δ = 159.0 (s, O-Ph-C_{ipso}), 150.3 (s, *p*-Tip-*C*), 149.9 (s, *o*-Tip-*C*), 141.3 (br, B-Ph-C_{ipso}), 135.2 (s, S-Ph-C_{ipso}), 135.1 (s, B-Ph-*C*H), 131.7 (br, B-Tip-C_{ipso}), 130.0 (s, O-Ph-*C*H), 121.1 (s, S-Ph-*C*H), 120.6 (s, Tip-*C*H_{Ar}), 35.6 (s, *o*-Tip-*C*H), 34.4 (s, *p*-Tip-*C*H), 29.5 (s, N*C*H_3), 24.8 (br, *o*-Tip-*C*H_3), 24.1 (s, *p*-Tip-*C*H_3), 24.0 (br, *o*-Tip-*C*H_3) ppm; GPC (in THF, vs. polystyrene, detection by UV-Vis signal): M_n = 1 586 Da; M_w = 1 877 Da.

Synthesis of 19 (salt elimination, CH_2Cl_2, r.t.). To a suspension of **14** (166 mg, 0.25 mmol) in DCM (5.0 mL) was added NEt_3 (0.25 mL). Subsequently, **2b** (58.6 mg, 0.25 mmol) was added and the reaction mixture was stirred for 3 d at room temperature. After all volatiles were removed *in vacuo* the residue was dissolved in DCM (2.0 mL) and Me_3SiOMe (9.7 mg,

0.09 mmol) was added to deactivate reactive B–Br groups. After 2 h the volatiles were removed *in vacuo*. The polymer was dissolved in THF (5.0 mL) and was removed from the formed triethylammonium bromide by filtration. After removing all volatiles *in vacuo* an off-white solid was obtained (162 mg, 0.22 mmol, 88 % yield). ^{1}H NMR (500 MHz, $CDCl_3$): δ = 7.80-7.79 (m, 4H, B-Ph-C*H*), 7.37-7.36 (m, 4H, O-Ph-C*H*), 7.01-6.99 (m, 4H, S-Ph-C*H*), 6.87 (s, 4H, Tip-CH_{Ar}), 2.84 (sept, 2H, *p*-Tip-C*H*), 2.49 (sept, 4H, *o*-Tip-C*H*), 1.24-1.22 (m, 12H, *p*-Tip-CH_3), 0.97-0.95 (m, 24H, *o*-Tip-CH_3) ppm; ^{11}B{^{1}H} NMR (160 MHz, $CDCl_3$): δ = no signal; ^{13}C{^{1}H} NMR (125 MHz, $CDCl_3$): δ = 158.1 (s, O-Ph-C_{ipso}), 150.2 (s, *p*-Tip-*C*), 149.9 (s, *o*-Tip-*C*), 141.4 (s, B-Ph-C_{ipso}), 140.0 (br, S-Ph-C_{ipso}), 135.1 (s, B-Ph-*C*H), 131.9 (br, B-Tip-C_{ipso}), 126.5 (s, O-Ph-*C*H), 121.4 (s, S-Ph-*C*H), 120.5 (s, Tip-*C*H_{Ar}), 35.6 (s, *o*-Tip-*C*H), 34.4 (s, *p*-Tip-*C*H), 24.8 (br, *o*-Tip-*C*H_3), 24.1 (s, *p*-Tip-*C*H_3), 24.0 (br, *o*-Tip-*C*H_3) ppm; GPC (in THF, vs. polystyrene, detection by UV-Vis signal): M_n = 2 692 Da; M_w = 4 194 Da.

Synthesis of 19 (salt elimination, *o*-DFB, 80 °C). To a suspension of **14** (166 mg, 0.25 mmol) in *o*-DFB (5.0 mL) was added NEt_3 (0.25 mL). Subsequently, **2b** (58.8 mg, 0.25 mmol) was added and the reaction mixture was stirred for 3 d at 80 °C. After all volatiles were removed *in vacuo* the residue was dissolved in DCM (2.0 mL) and Me_3SiOMe (10.8 mg, 0.10 mmol) was added to deactivate reactive B–Br groups. After 2 h the volatiles were removed *in vacuo*. The polymer was dissolved in THF (5.0 mL) and was removed from the formed triethylammonium bromide by filtration. After removing all volatiles *in vacuo* an off-white solid was obtained (163 mg, 0.22 mmol, 88 % yield). GPC (in THF, vs. polystyrene, detection by UV-Vis signal): M_n = 2 868 Da; M_w = 4 533 Da.

Crystallographic data

Crystals suitable for single-crystal X-ray diffraction were selected, coated in perfluoropolyether oil, and mounted on MiTeGen micromounts or polyimide microloops. Diffraction data were collected on Bruker X8 Apex II 4-circle diffractometers with CCD area detector (**10b**) or on a Bruker D8 Quest 4-circle diffractometer with a CMOS area detector (**13**) using multi-layer mirror monochromated Mo-K_α radiation. The crystals were cooled using an Oxford Cryostreams low-temperature device. Data were collected at 100 K. The images were processed and corrected for Lorentz-polarization effects and absorption as implemented in the Bruker software packages. The structures were solved using the intrinsic phasing method (SHELXT)[18] and Fourier expansion technique. All non-hydrogen atoms were refined in anisotropic approximation, with hydrogen atoms 'riding' in idealized positions, by full-matrix least squares against F^2 of all data, using SHELXL[19] software and the SHELXLE graphical user interface.[20] Crystal data and experimental details are listed in Table 2.9.3.

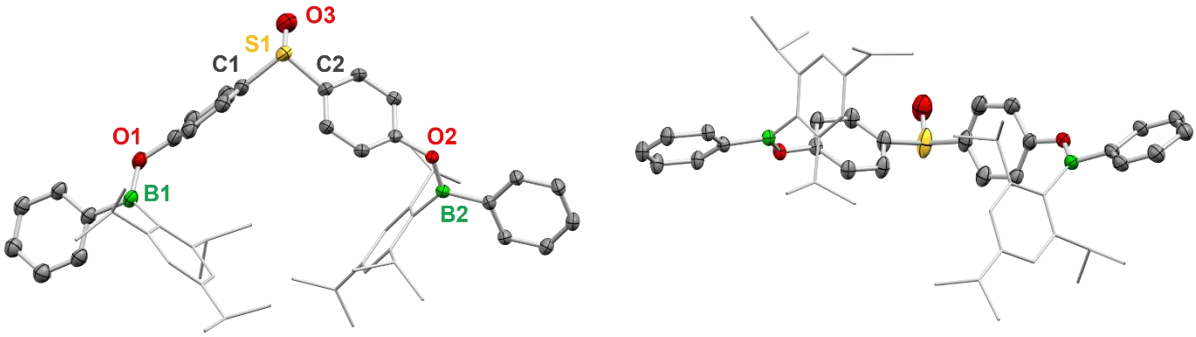

Figure 2.9.4. Molecular structure of **10b** in the solid state determined by single-crystal X-ray diffraction at 100 K (H atoms omitted for clarity). Structure shown perpendicular (left) and parallel (right) to the C1-S1-C2 plane. All ellipsoids are drawn at the 50 % probability level.

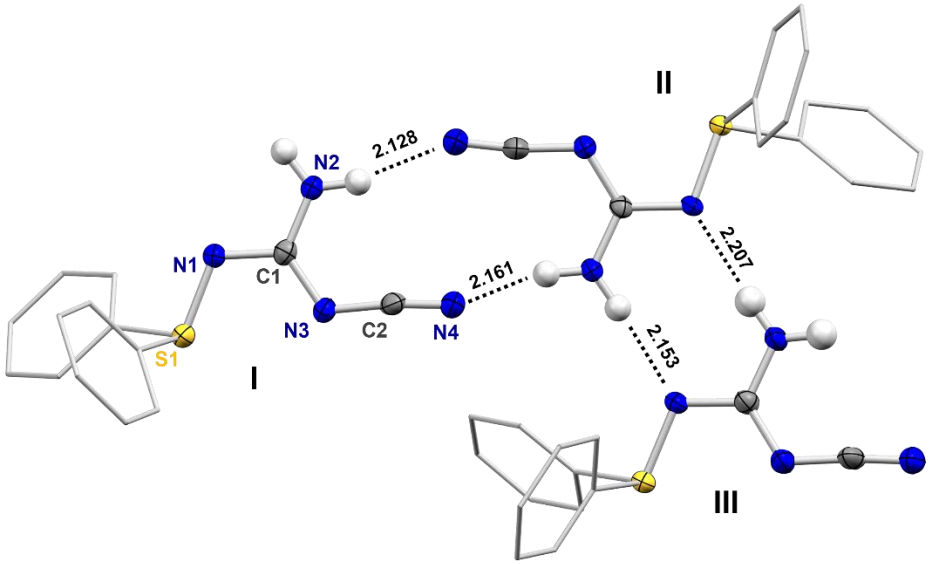

Figure 2.9.5. Molecular structure of the three symmetry-independent molecules of **13** in the solid state determined by single-crystal X-ray diffraction at 100 K (H atoms of the phenyl groups omitted for clarity). All ellipsoids are drawn at the 50 % probability level. All three symmetry-independent molecules and the intermolecular hydrogen bonds are shown.

Table 2.9.2. Selected bond lengths and distances (Å), and angles (°) of **13**. Atom labels are given according to atom assignments in Figure 2.9.5.

Molecule	**I**	**II**	**III**
S1–N1	1.6387(14)	1.6446(13)	1.6394(13)
C1–N1	1.358(2)	1.359(2)	1.358(2)
C1–N2	1.337(2)	1.334(2)	1.335(2)
C1–N3	1.336(2)	1.340(2)	1.341(2)
N3–C2	1.318(2)	1.318(2)	1.322(2)
C2–N4	1.160(2)	1.158(2)	1.162(2)
∑(∠CN_3)	359.99(15)	360.0(14)	360.0(15)

Table 2.9.3. Single-crystal X-ray diffraction data and structure refinements.

Compound	**10b**	**13**
Empirical formula	$C_{54}H_{64}B_2O_3S$	$C_{14}H_{12}N_4S$
M_r	814.73	268.34
T / K	100(2)	100(2)
Radiation, λ / Å	MoK\a, 0.71073	MoK\a, 0.71073
Crystal size / mm³	0.194 x 0.289 x 0.543	0.206 x 0.330 x 0.349
Crystal color, habit	colorless block	colorless block
Crystal system	monoclinic	monoclinic
Space group	P 21/c	P 21/n
a / Å	18.819(4)	8.3228(10)
b / Å	10.503(2)	27.687(5)
c / Å	25.010(6)	17.713(2)
α / °	90	90
β / °	103.253(15)	99.813(10)
γ / °	90	90
Volume / Å³	4811.7(18)	4021.9(10)
Z	4	12
ρ_{calc} / g cm^{-3}	1.125	1.329
μ / mm^{-1}	0.108	0.232
F(000)	1752	1680
θ range / °	1.112 – 26.473	1.878 – 26.395
Completeness	0.997	0.999
Reflections collected	95396	112959
Unique reflections	7776	7268
R_{int}	0.0853	0.0590
Parameters / restraints	554 / 1098	514 / 0
GooF on F^2	1.034	1.042
R_1 [$I \geq 2\sigma(I)$]	0.1048	0.0375
wR_2 [all data]	0.2791	0.0965
Max. / min. residual electron density / e Å^{-3}	2.416 / –1.135	0.430 / -0.391

2.9.5 References

[1] C. Englert, J. C. Brendel, T. C. Majdanski, T. Yildrim, S. Schubert, M. Gottschaldt, N. Windhab, U. S. Schubert, *Prog. Polym. Sci.* **2018**, *87*, 107–164.

[2] a) F. Jäkle, *Chem. Rev.* **2010**, *110*, 3985–4022; b) F. Jäkle, *Top. Organomet. Chem.* **2015**, *49*, 297–325; c) Y. Ren, F. Jäkle, in *Main Group Strategies towards Functional Hybrid Materials* (Eds.: T. Baumgartner, F. Jäkle), Wiley, Hoboken, NJ **2017**, 79−110; d) H. Helten, *Chem. Asian J.* **2019**, *14*, 919–935; e) X. Yin, J. Liu, F. Jäkle, *Chem. Eur. J.* **2021**, *27*, 2973–2986; f) H. Helten, in *Comprehensive Organometallic Chemistry IV*, Vol. 14 (Eds: D. O'Hare, K. Meyer, G. Parkin), Elsevier, New York **2022**, 71-134; g) B. Chen, F. Jäkle, *Angew. Chem. Int. Ed.* **2023**, e202313379.

[3] a) J. N. Cambre, B. S. Sumerlin, *Polymer* **2011**, *52*, 4631–4643; W. L. A. Brooks, B. S. Sumerlin, *Chem. Rev.* **2016**, *116*, 1375–1397.

[4] a) M. M. Morgan, W. E. Piers, *Dalton Trans.* **2016**, *45*, 5920–5924; b) H. Helten, *Chem. Eur. J.* **2016**, *22*, 12972–12982; c) G. Bélanger-Chabot, H. Braunschweig, D. K. Roy, *Eur. J. Inorg. Chem.* **2017**, 4353–4368; d) M. Stępień, E. Gońka, M. Żyła, N. Sprutta, *Chem. Rev.* **2017**, *117*, 3479–3716; e) Z. X. Giustra, S.-Y. Liu, *J. Am. Chem. Soc.* **2018**, *140*, 1184–1194; f) C. R. McConnell, S.-Y. Liu, *Chem. Soc. Rev.* **2019**, *48*, 3436–3453; g) X.-Y. Wang, X. Yao, A. Narita, K. Müllen, *Acc. Chem. Res.* **2019**, *52*, 2491–2505; h) F. Vidal, F. Jäkle, *Angew. Chem. Int. Ed.* **2019**, *58*, 5846–5870; *Angew. Chem.* **2019**, *131*, 5904–5929; i) D. Han, F. Anke, M. Trose, T. Beweries, *Coord. Chem. Rev.* **2019**, *380*, 260–286; j) K. Ota, R. Kinjo, *Chem. Asian J.* **2020**, *15*, 2558–2574; k) T. Beweries, H. Helten, "Poly(aminoborane)s and Poly(iminoborane)s". In *Encyclopedia of Inorganic and Bioinorganic Chemistry*; ed. R. A. Scott, Wiley, **2020**, DOI: 10.1002/9781119951438.eibc2717; l) R. Zhao, J. Liu, L. Wang, *Acc. Chem. Res.* **2020**, *53*, 1557–1567; m) J. Huang, X. Wang, Y. Xiang, L. Guo, G. Chen, *Adv. Energy Sustainability Res.* **2021**, *2*, 2100016; n) D. Marchionni, S. Basak, A. N. Khodadadi, A. Marrocchi, L. Vaccaro, *Adv. Funct. Mater.* **2023**, 2303635.

[5] a) T. Lorenz, M. Crumbach, T. Eckert, A. Lik, H. Helten, *Angew. Chem. Int. Ed.* **2017**, *56*, 2780–2784; *Angew. Chem.* **2017**, *129*, 2824–2828; b) J. Chorbacher, M. Maier, J. Klopf, M. Fest, H. Helten, *Macromol. Rapid Commun.* **2023**, *44*, 2300278; c) M. Maier, J. Chorbacher, A. Hellinger, J. Klopf, J. Günther, H. Helten, *Chem. Eur. J.* **2023**, e202302767.

[6] a) C. Li, M. Liu, N. G. Pschirer, M. Baumgarten, K. Müllen, *Chem. Rev.* **2010**, *110*, 6817–6855; b) J. Banerjee, K. Dutta, *Chem. Pap.* **2021**, *75*, 5139–5151.

[7] a) Q. Wang, X. Dong, M. He, M. Li, H. Tian, J. Liu, Y. Geng, *Polymer* **2018**, *140*, 89–95; b) C. Yang, S. Zhang, J. Hou, *Aggregate* **2022**, *3*, e111; c) P. Bi, J. Ren, S. Zhang, J. Wang, Z. Chen, M. Gao, Y. Cui, T. Zhang, J. Qin, Z. Zheng, L. Ye, X. Hao, J. Hou, *Nano Energy* **2022**, *100*, 107463; d) L. Ma, S. Zhang, J. Ren, G. Wang, J. Li, Z. Chen, H. Yao, J. Hou, *Angew. Chem. Int. Ed.* **2023**, *62*, e202214088; *Angew. Chem.* **2023**, *135*, e202214088.

[8] N. A. Riensch, A. Deniz, S. Kühl, L. Müller, A. Adams, A. Pich, H. Helten, *Polym. Chem.* **2017**, *8*, 5264–5268.

[9] L. Rojo, M. Fernandesz-Gutierrez, S. Deb, M. M. Stevens, J. San Roman, *Acta Biomater.* **2015**, *27*, 32–41.

[10] T. Takata, K. Nakamura, T. Endo, *Macromolecules* **1996**, *29*, 2696–2697.

[11] S. Matsumura, N. Kihara, T. Takata, *J. Polym. Sci., Part A: Polym. Chem.* **2003**, *41*, 1330–1334.

[12] a) V. A. Nikonov, G. V. Leplyanin, *Sulfur Rep.* **1989**, *9*, 1–23; b) T. Oyama, J. Ozaki, Y. Chujo, *Polym. Bull.* **1998**, *40*, 503–508; c) F. E. Mohtadi, R. d'Arcy, X. Yang, Z. Y. Turhan, A. Alshamsan, N. Tirelli, *Int. J. Mol. Sci.* **2019**, *20*, 4583.

[13] F. Brosge, T. Lorenz, H. Helten, C. Bolm, *Chem. Eur. J.* **2019**, *25*, 12708–12711.

[14] X. Lin, F. Zhang, Y. Luo, C. Xu, *J. Organomet. Chem.* **2014**, *749*, 251–254.

[15] O. Ouadoudi, T. Kaehler, M. Bolte, H.-L. Lerner, M. Wagner, *Chem. Sci.* **2021**, *12*, 5898–5909.

[16] F. Matsumoto, Y. Chujo, *J. Organomet. Chem.* **2003**, *680*, 27–30.

[17] O. García Mancheño, O. Bistri, C. Bolm, *Org. Lett.* **2007**, *9*, 3809–3811.
[18] G. M. Sheldrick, *Acta Crystallogr. A* **2015**, *71*, 3-8.
[19] G. M. Sheldrick, *Acta Crystallogr. C* **2015**, *71*, 3-8.
[20] C. B. Hübschle, G. M. Sheldrick, B. Dittrich, *J. Appl. Crystallogr.* **2011**, *44*, 1281-1284.

3 Summary

In this work, potential catalytic routes for B–N coupling, routes for the formation of BN-containing macromolecules, and the synthesis of inorganic polymers comprising a backbone of exclusively boron and nitrogen atoms (poly(iminoborane)s) and their monodisperse oligomers is described. In addition, novel inorganic–organic hybrid polymers were synthesized and characterized that represent BN analogs of conjugated poly(arylene vinylene)s or hybrid polymers comprising longer $(BN)_x$ chains or BN/BO-doped congeners of poly(phenylene sulfide) derivatives, respectively.

In the first chapter 2.1, we aimed at the development of catalytic B–N coupling routes for the controlled synthesis of macromolecular materials. The model reaction of an *N*-silyl-*B*-chloro-aminoborane with the electrophilic reagent trimethylsilyl triflate led to effective B–N coupling and the formation of the expected borazine **2a** (Scheme 3.1, left).

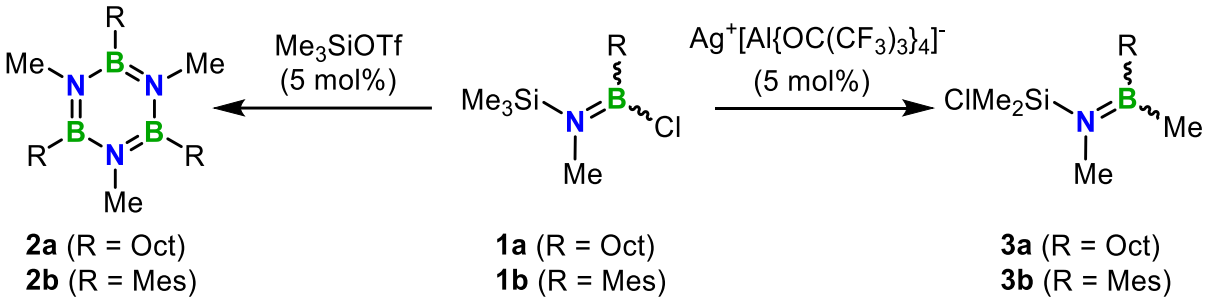

Scheme 3.1. Reaction of **1** with Me_3SiOTf and a silver(I) salt (OTf = OSO_2CF_3).

When a silver(I) salt $Ag[Al\{OC(CF_3)_3\}_4]$ was used, an intramolecular Cl/Me exchange between the boron and silicon centers was observed (Scheme 3.1, right). For the mesityl-substituted **1b**, the methyl migration was investigated using NMR spectroscopy. The experimental studies were complemented by detailed theoretical investigations leading to a proposed reaction cycle (Figure 3.1).

An induction phase was observed at the start of the reaction to **3b**, which can be attributed to inhibited chloride abstraction due to the slow nucleation of silver chloride, and thus inhibited precipitation thereof. In various experiments, the length of the induction phase differed apparently randomly, which can be attributed to the difficult-to-control nucleation. The subsequent methyl migration after initiation occurs through the cationic intermediate **4**, resulting in **5**. The cycle is completed by the abstraction of a chloride ion from another molecule **1b**. After the induction phase, the conversion of **1b** to **3b** shows an almost linear progress, indicating zero-order kinetics (determined by ^1H NMR spectroscopy).

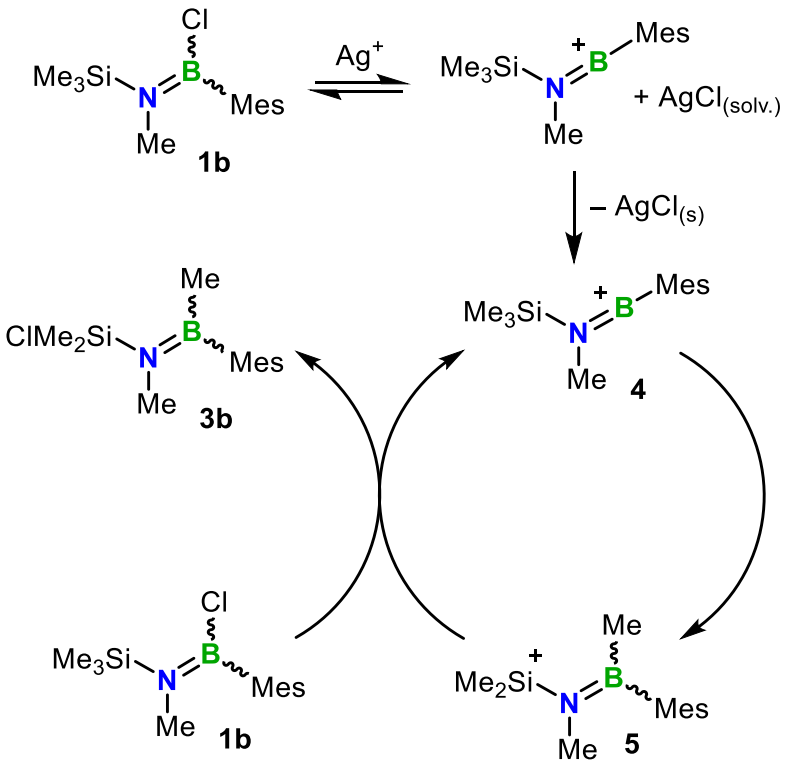

Figure 3.1. Proposed reaction cycle of the reaction of **1b** with a silver(I) salt.

In the second chapter 2.2, the synthesis and characterization of poly(iminoborane)s with aromatic side groups (**I**) and their corresponding monodisperse oligomers (**II**) was presented (Figure 3.2).

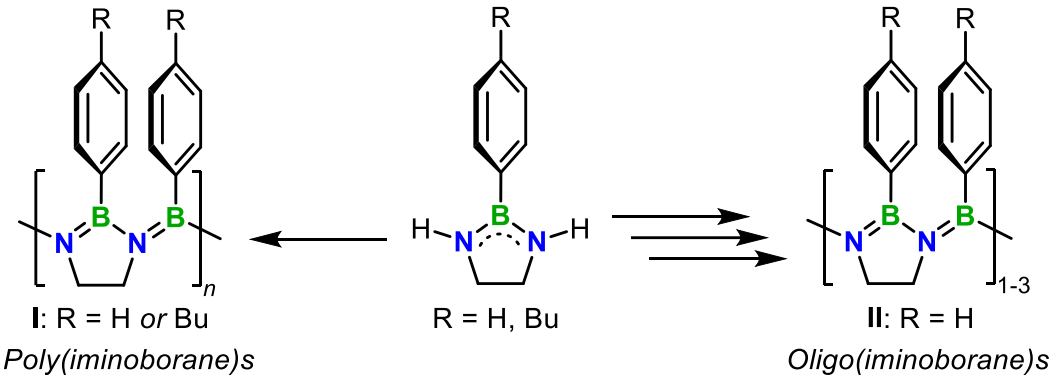

Figure 3.2. Visualization of poly(iminoborane)s (**I**) and monodisperse oligo(iminoborane)s (**II**).

An oligo(iminoborane) with 7 boron and 8 nitrogen atoms was synthesized by successively extending the B–N main chain. X-ray diffraction analysis of six oligomers provided crystal structures of compounds with up to 5 boron and 6 nitrogen atoms (**6**, **7**), which contributed to the structural analysis of these cyclolinear species (Figure 3.3). The bond lengths of the B–N bonds along the main chain were between those of typical BN single and double bonds. The observed twists between adjacent BR_3 and NR_3 planes were attributed to steric effects.

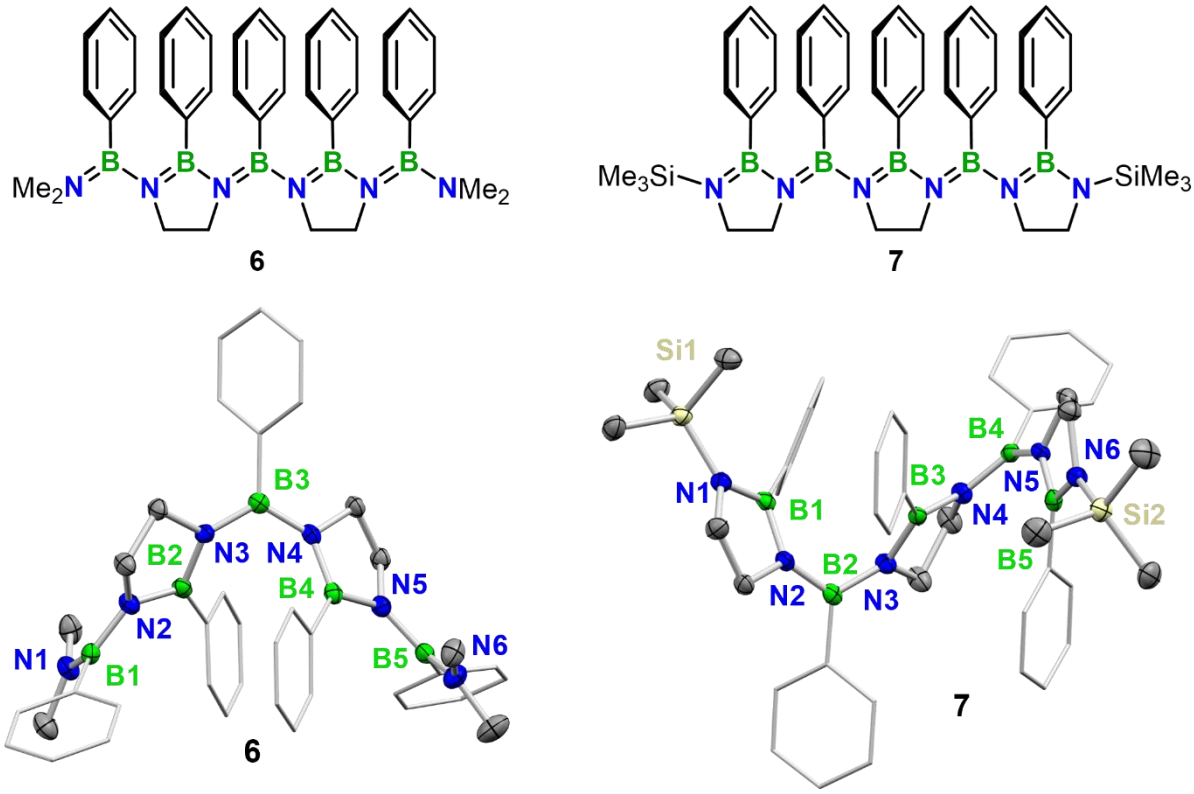

Figure 3.3. Oligo(iminoborane)s **6** and **7** (top) and their solid-state structures (bottom; H atoms are omitted for clarity).

The NMe_2-terminated compounds (e.g. **6**) were examined with regard to possible conjugation between the BN units by temperature-dependent NMR measurements. The degree of conjugation can be estimated by investigation of the rotational barrier $\Delta G^{\ddagger}$ of the terminal B=N moieties which is expected to be lower for systems with stronger conjugation throughout the BN-chain. Our investigations revealed a slight increase of $\Delta G^{\ddagger}$ with increasing chain length, which led to the assumption of weaker conjugation between the B–N units. This trend was supported by theoretical studies.

Furthermore, various poly(iminoborane)s **8**–**11** and **13** with different aromatic contents were synthesized (Scheme 3.2). For better comparability, we repeated the synthesis of the literature known polymers **8** and **9**. For **9**, a degree of polymerization (DP_n) of 23 was achieved, which represents the highest-molecular-weight poly(iminoborane) to date. The lowest number-average molecular weight (M_n) was observed for **13**, which was attributed to a significantly lower solubility. The thermogravimetric analyses of polymers **8**–**11** and **13** revealed that the ceramic yields are higher than expected, with the main mass loss occurred between 400 and 500 °C. By using an O_2 atmosphere and a lower heating rate, the BN content of the ceramic yield of **9** could be significantly increased.

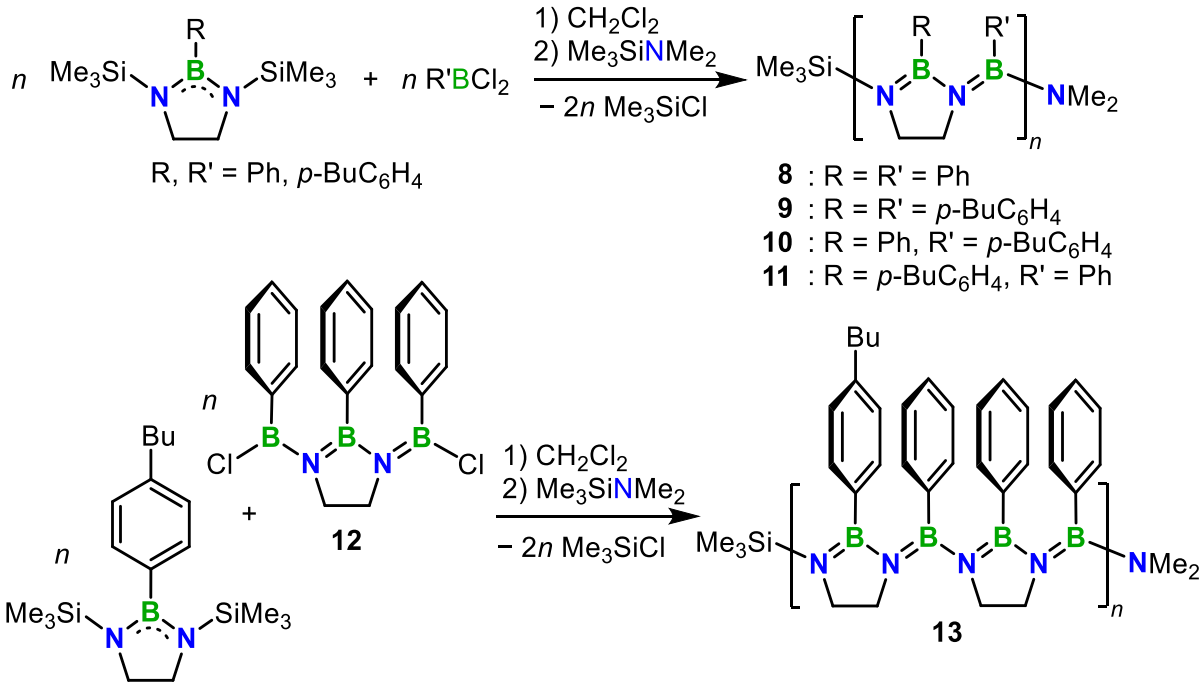

Scheme 3.2. Synthesis of poly(iminoborane)s **8**–**11** and **13**.

In chapter 2.3, the redistribution processes resulting from the reaction of longer oligo(iminoborane)s with non-stoichiometric amounts of (di)halogenated boranes was reported. In the reaction of **14** with an excess of $PhBCl_2$ quantitative formation of **12** instead of the targeted B–N coupling to give **15** was observed (Scheme 3.3).

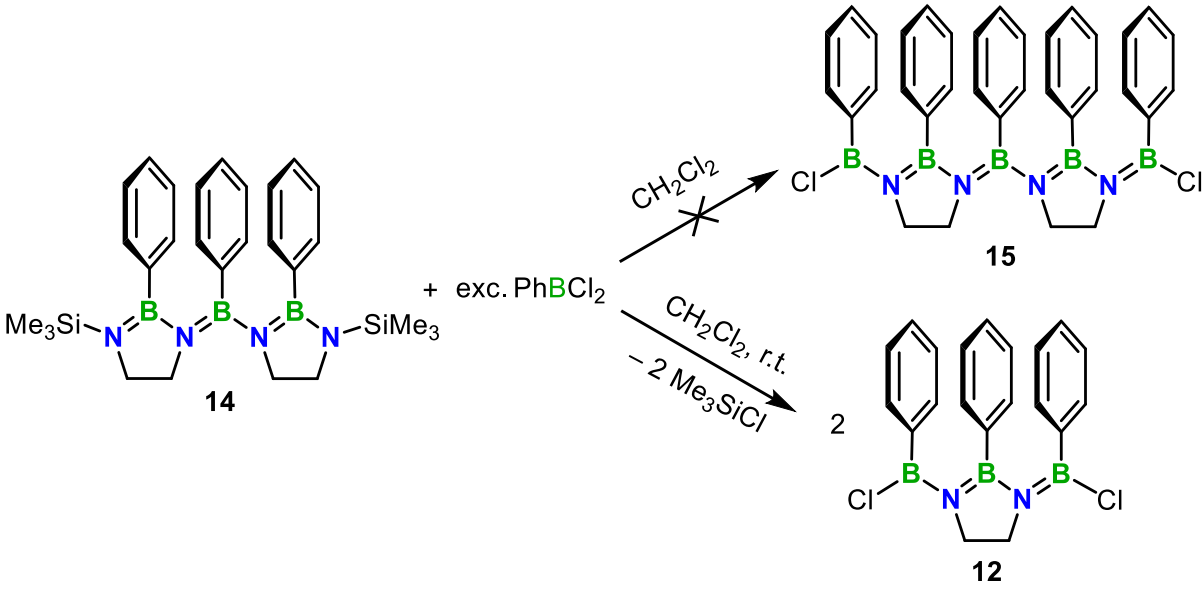

Scheme 3.3. Reaction of **14** with an excess of $PhBCl_2$.

However, compound **12** can only be formed by the cleavage of exocyclic B–N bonds. Computational mechanistic studies indicate that **15** is formed in the first step, which subsequently reacts with $PhBCl_2$ to give two molecules of **12**. When a less reactive

monohalogenated borane ($PhB(NMe_2)Br$) was used in excess, redistribution processes were also observed.

In chapter 2.4, the synthesis of 1,3,2-benzodiazaborolines **16** and their polymerizations via the nitrogen atoms to poly(iminoborane)s was investigated. The consecutive reaction of **16** with $MeBBr_2$ and Me_3SiNMe_2 successfully yielded oligomer **17** (Scheme 3.4), whereas attempts to synthesize larger model systems (see chapter 2.2) were unsuccessful.

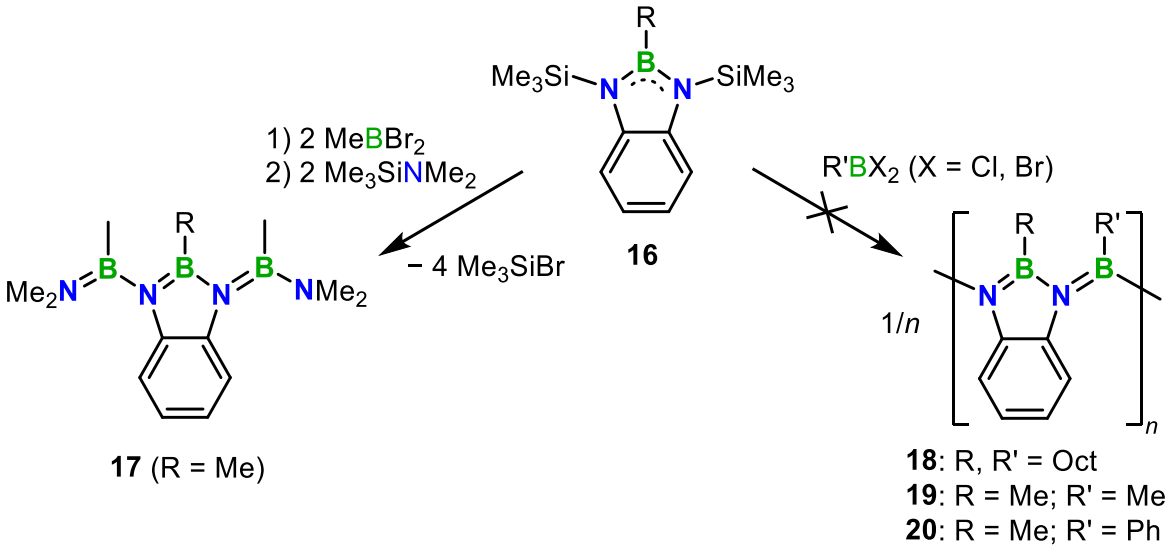

Scheme 3.4. Synthesis of oligomer **17** and polymerization attempts of **16** with dihaloboranes.

Polymerization attempts to **18**–**20** by Si/B exchange polycondensation of **16** with various dihaloboranes also did not lead to BN catenation. Analyzing the residue of the polymerization attempt of **16** with $OctylBCl_2$ in *o*-DFB at 80 °C for 12 days by mass spectrometry revealed the formation of oligomers with up to three 1,3,2-benzodiazaboroline units. This indicated a significantly lower reactivity of benzodiazaborolines compared to the diazaborolidines described in chapter 2.2.

In the chapters 2.5 and 2.6, the syntheses of 1,2,5-azadiborolanes as building blocks for the synthesis of poly(iminoborane)s and inorganic–organic hybrid polymers are described. In chapter 2.5, a 1,2,5-azadiborolane with sterically demanding groups on the boron-bridging ethylene unit was used. After the successful isolation of **21**, a twofold B–N bond formation to **22** was demonstrated by reaction with Me_3SiNMe_2 (Scheme 3.5). The polymerization attempt of **21** with $BuN(SiMe_3)_2$, however, only led to the single coupling product **23**. Elevated temperatures and longer reaction times did not lead to any further B–N coupling events.

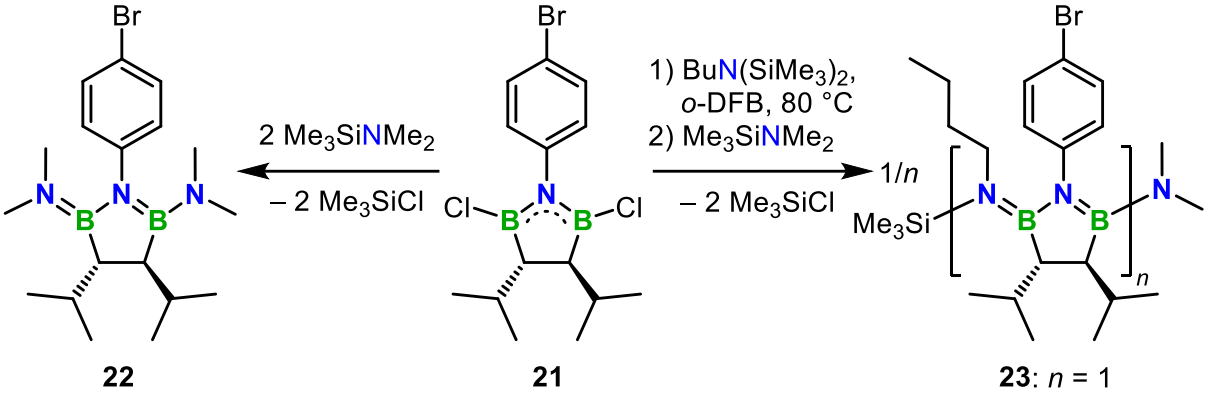

Scheme 3.5. Synthesis of **22** and polymerization attempt of **21** with $BuN(SiMe_3)_2$.

The polymerization attempts of **21** with the co-monomer **24** led to successful synthesis of the hybrid polymer **25** and the incorporation of phenylene units into the polymer backbone (Scheme 3.6). In one attempt, a M_n of 68.6 kDa was obtained, corresponding to a DP_n of 335. In photophysical studies, a bathochromic shift of the absorption maximum with increasing number of BN units was observed, indicating π-conjugation along the polymer chain. Cyclic voltammetry revealed a reversible oxidation event for **25**, which was attributed to the oxidation of the diaminoarylene group.

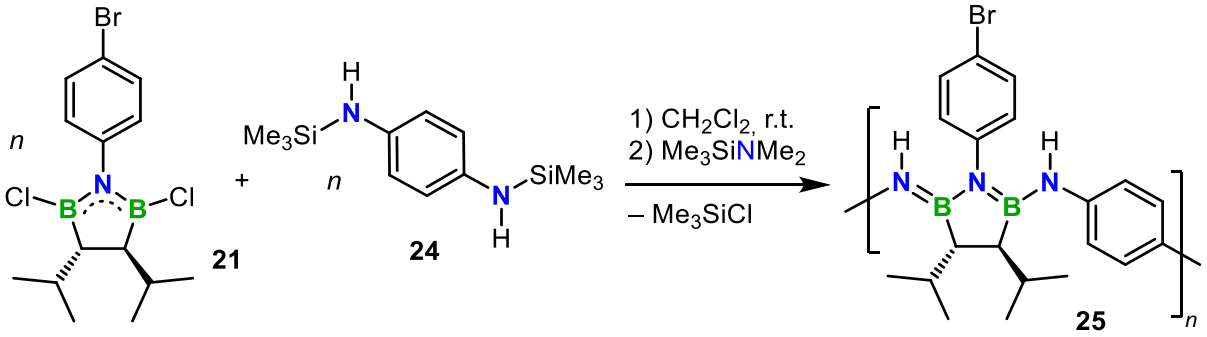

Scheme 3.6. Synthesis of **25** by Si/B exchange polycondensation of **21** and **24**.

In chapter 2.6, the synthesis of 1,2,5-azadiborolane based poly(iminoborane)s was attempted in which the boron atoms are bridged by an unsubstituted ethylene unit. After multi-step synthesis, **26** was obtained and subsequently reacted with **27** on NMR scale (Scheme 3.7). ^{1}H NMR spectroscopy revealed the formation of two equivalents of Me_3SiCl indicating a twofold B–N coupling event. Broadening of the signals over time evidenced further chain growth. These results indicated increased reactivity of the azadiborolane **26** compared to the sterically demanding **21**.

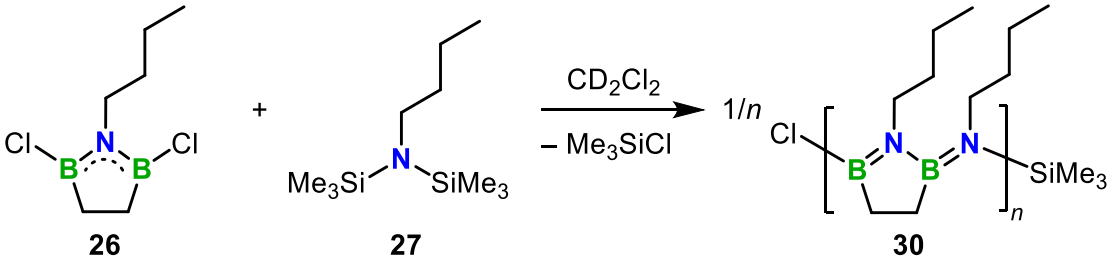

Scheme 3.7. Polymerization of **26** and **27** by Si/B exchange polycondensation.

The chapters 2.7 and 2.8 describe a comprehensive study of poly(arylene iminoborane)s, which are BN analogs of poly(arylene vinylene)s. In chapter 2.7, the first synthesis of poly(thiophene iminoborane) (BN-PTV), a BN analog of poly(thiophene vinylene) (PTV), was described. In addition to the successful synthesis of the highly reactive diaminothiophene species **31**, a series of monodisperse oligomers was synthesized. BN-PTV **33** was obtained by Si/B exchange polycondensation of **31** and **32** (Scheme 3.8). The oligomers and **33** showed good solubility in common organic solvents and air and moisture stability. GPC analysis of **33** showed an M_n = 14.2 kDa, corresponding to a DP_n of 46. Investigations of the absorption behavior in solution revealed a systematic red-shift of the absorption maximum with increasing chain length of the oligomers to **33**, indicating pronounced conjugation across the B=N units.

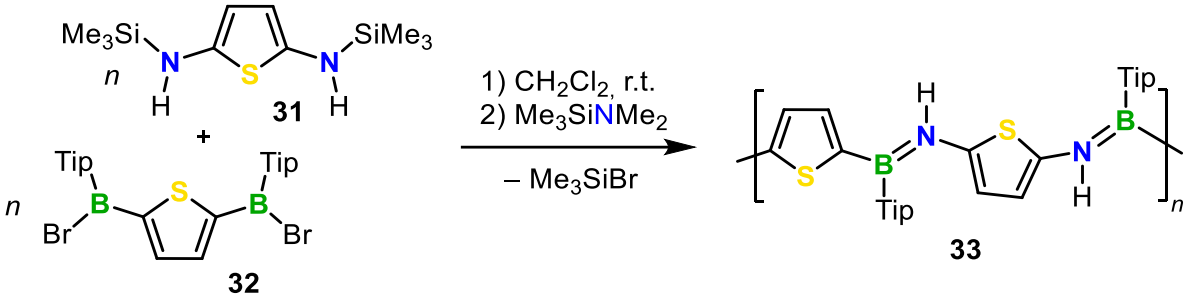

Scheme 3.8. Synthesis of BN-PTV **33** by Si/B exchange polycondensation (Tip = 2,4,6-triisopropylphenyl).

Based on TD-DFT calculations of the model oligomers the lowest-energy absorption band could be assigned to HOMO to LUMO transitions with π-π* character. In chapter 2.8, the exclusively thienyl-based oligo- and polymers were compared with the poly(*p*-phenylene iminoborane)s (BN-PPV). In addition, mixed compounds featuring alternating thiophene and phenylene moieties between the B=N units were synthesized. In our study, the properties of four polymers and twelve monodisperse oligomers were investigated. The model compounds with two B=N units (dimers) were categorized based on their BN sequence into NBBN (e.g. **35**) and BNNB dimers (e.g. **36**–**39**) (Scheme 3.9).

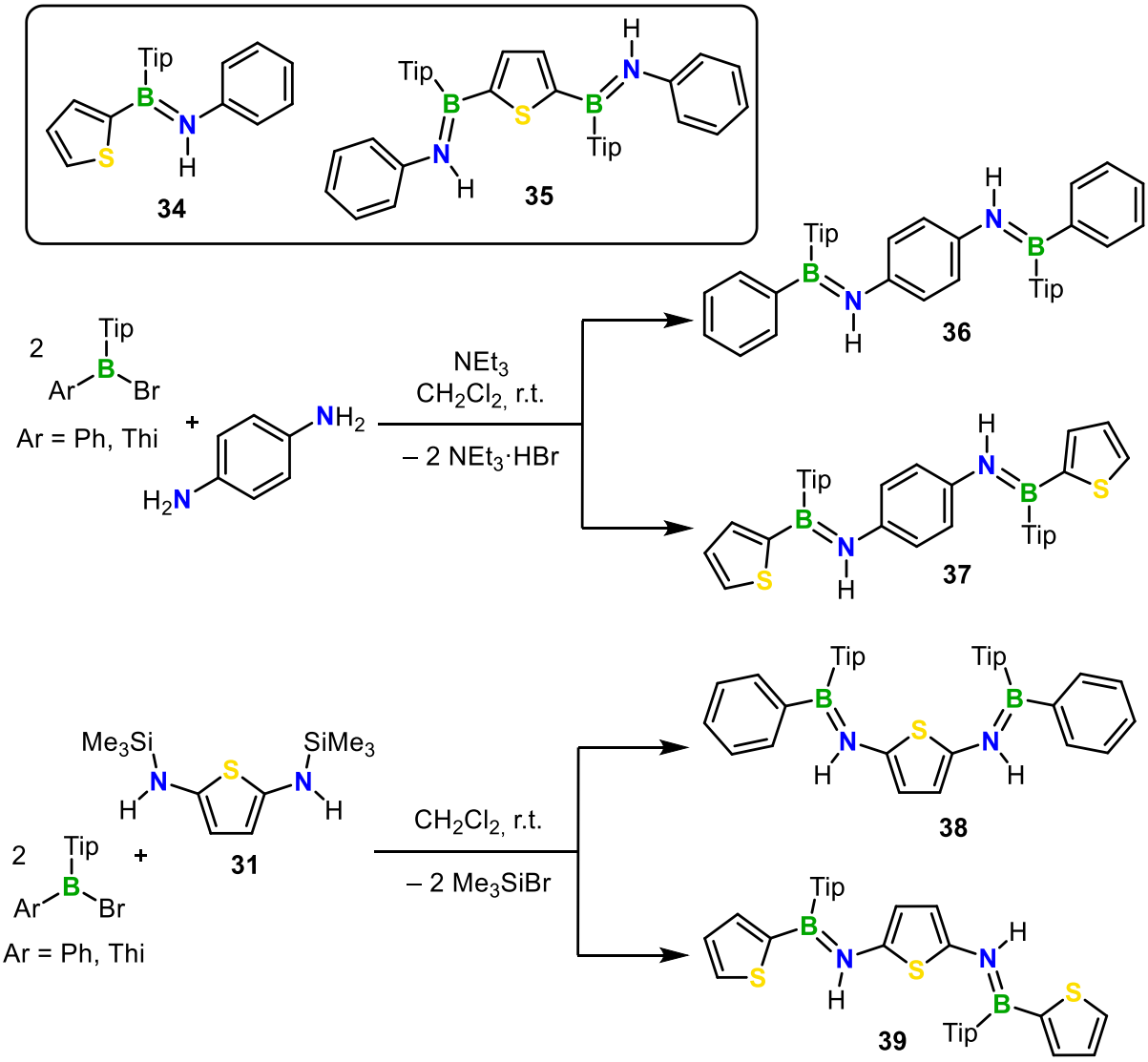

Scheme 3.9. Synthesis of monodisperse oligomers **36**–**39** with BNNB sequence and molecular structure of **34** with BN and **35** with NBBN sequence by Si/B exchange condensation or salt elimination (Tip = 2,4,6-triisopropylphenyl).

The monomers and dimers were synthesized either by salt elimination (e.g., **36**, **37**) or Si/B exchange condensation (e.g., **38**, **39**). All oligomers were obtained as mixtures of diastereomers, while the main isomer showed *trans*-arrangement of the aryl(ene) groups at the B=N units, which was evidenced by 2D NMR spectroscopy and X-ray diffraction analysis (Figure 3.4). The solid-state structures showed that the adjacent rings in the chain are only slightly twisted with respect to each other, which enables π-conjugation across the B=N and aryl(ene) units. This was confirmed by photophysical investigations as well as theoretical studies.

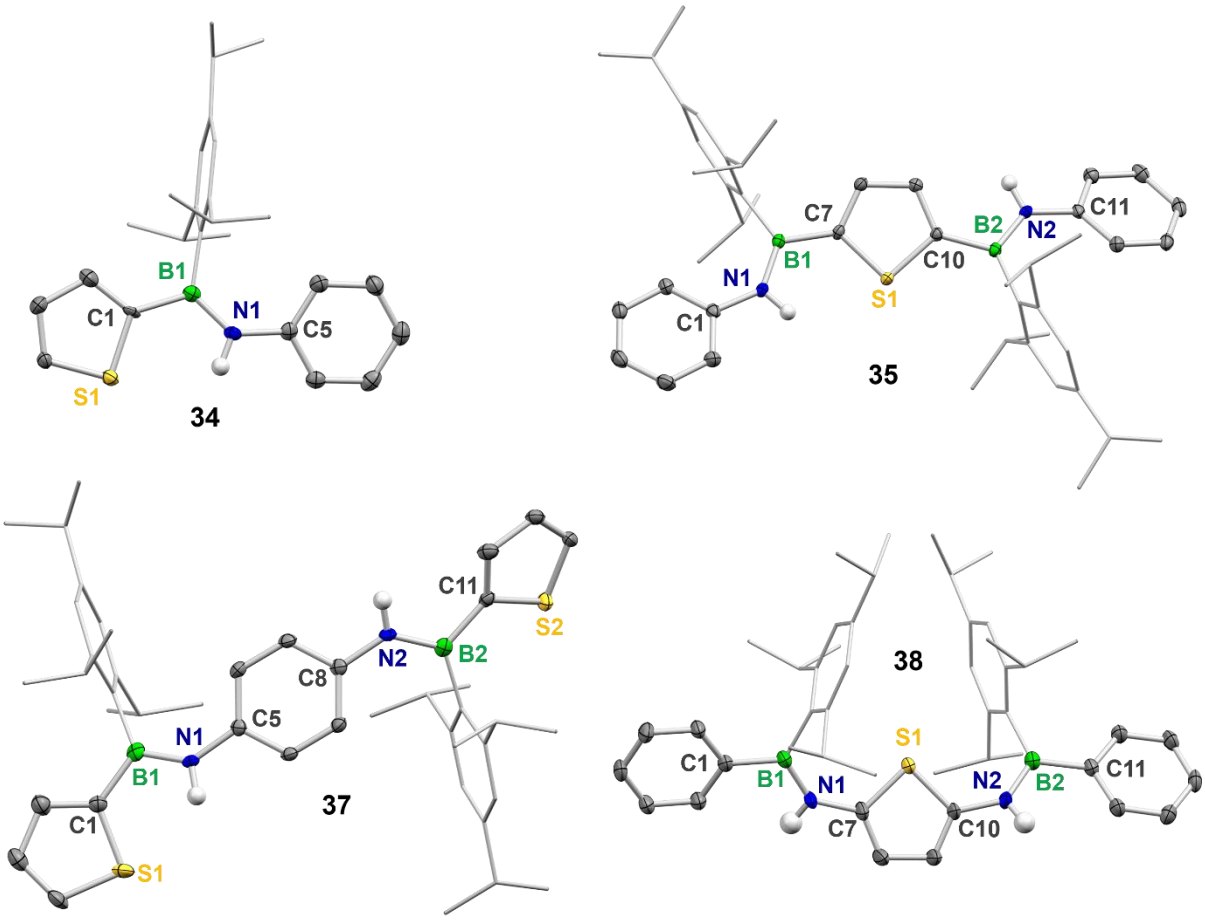

Figure 3.4. Solid-state structures of monomer **34**, NBBN dimer **35**, and BNNB dimers **37** und **38** (H atoms are omitted for clarity).

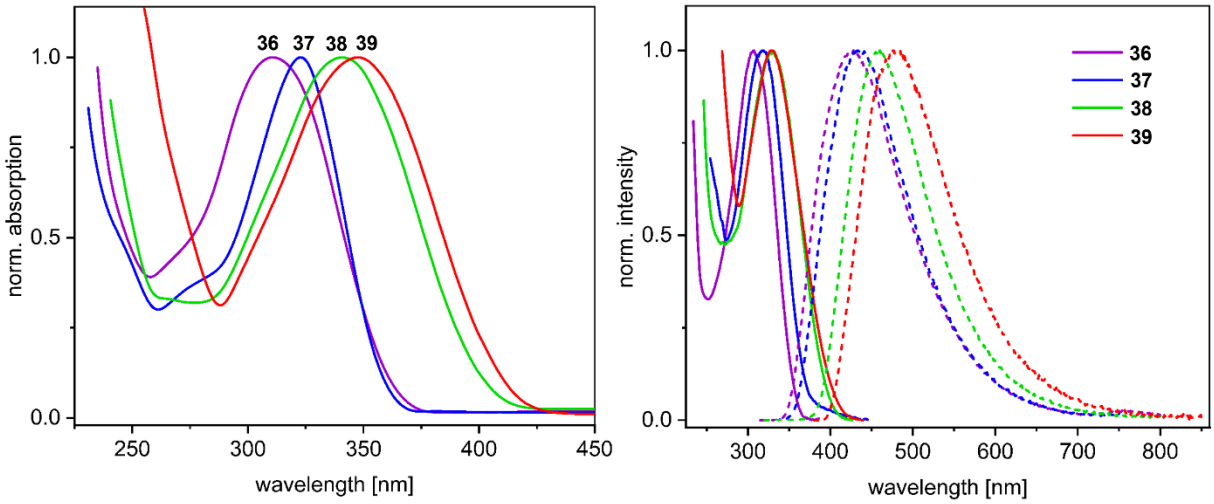

Figure 3.5. Normalized absorption spectra of **36**–**39** in THF (left) and normalized absorption and emission spectra of **36**–**39** as PMMA film (right).

Photophysical investigations of the monomers, dimers and polymers showed a systematic bathochromic shift of the absorption maximum with increasing chain length. In the series of **36**–**39**, the dimers **38** and **39** were red-shifted, which is related to their increased donor-

acceptor character (Figure 3.5, left). The same trend was observed in the absorption and emission spectra of **36**–**39** as PMMA film (Figure 3.5, right).

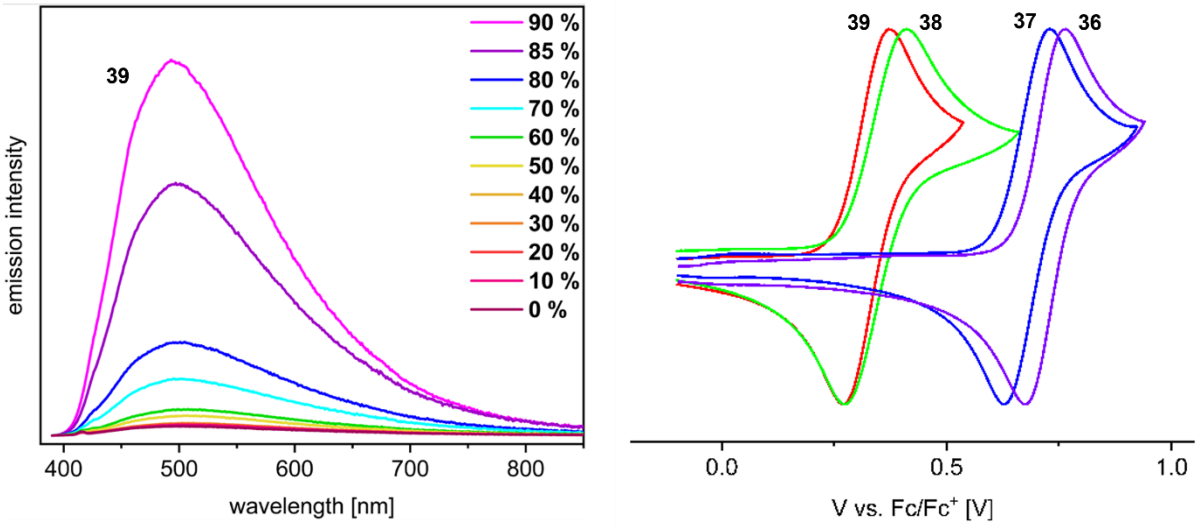

Figure 3.6. Emission spectra of **39** in THF/water mixtures (conc. $5x10^{-5}$ M) with different water contents (0-90 %; left) and cyclic voltammograms of **36**–**39** in CH_2Cl_2 (scan rate: 150 mV s^{-1}; right).

The oligo- and poly(arylene iminoborane)s (e.g. **39**) showed only very weak to no emission in solution, but the BNNB dimers exhibited aggregation induced emission (AIE) in a THF/water mixture (Figure 3.6, left). Electrochemical investigations revealed reversible oxidation events for compounds with diaminoarylene groups (e.g., **36**–**39**), whereas the compounds with the electron-rich diaminothiophene units (e.g., **38**, **39**) showed the lowest oxidation potentials (Figure 3.6, right). Polymers **39** and **40** were synthesized by Si/B exchange polycondensation (Figure 3.7). While the absorption maxima of **39** and **40** were in a similar range, **40** showed a 42 nm red-shifted maximum, which was attributed to the more pronounced donor-acceptor structure of the polymer backbone.

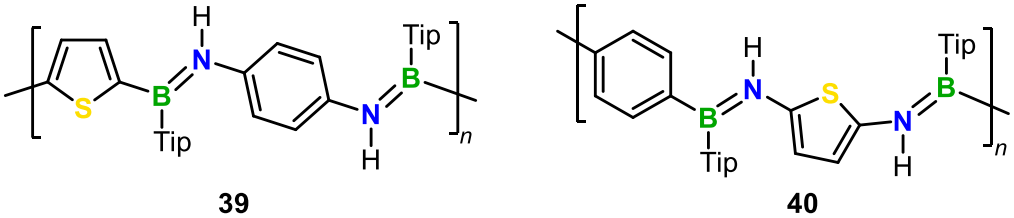

Figure 3.7. Structures of the mixed polymers **39** and **40** (Tip = 2,4,6-triisopropylphenyl).

In chapter 2.9, the functionalization of sulfur-containing building blocks, their oligo- and polymerization and the subsequent pH-triggered degradation of the model compounds and a polymer were investigated. In this study, we attempted to incorporate sulfone, sulfoximine, sulfoxide, and sulfilimine building blocks via B=N or B–O linkages into polymers. In a feasibility

study, model systems were synthesized, whereas the sulfone-, sulfoximine-, and sulfoxide-containing molecular oligomers could be successfully synthesized by Si/B exchange condensation or salt elimination (e.g. **42**, Scheme 3.10). The sulfilimine-containing oligomer could not be isolated due to a competing reaction of the cyano group, which was confirmed by X-ray diffraction analysis.

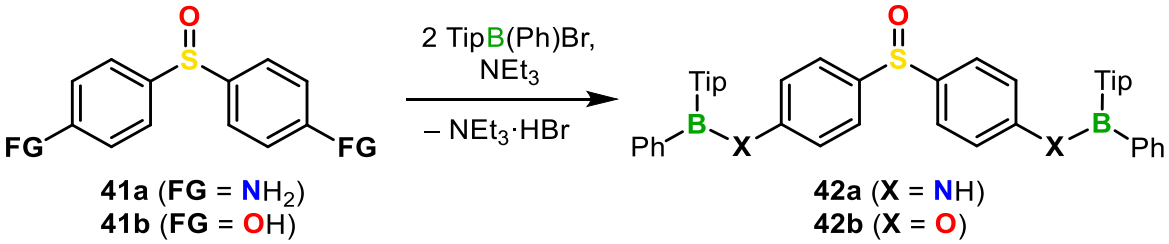

Scheme 3.10. Reaction to sulfoxide-containing oligomers **42** (Tip = 2,4,6-triisopropylphenyl).

Subsequently, the B=N linked polymers were synthesized by Si/B exchange polycondensation or salt elimination and the B–O linked polymers by salt elimination of the sulfone, sulfoximine, and sulfoxide building blocks. In general, the B=N linked polymers showed significantly higher molecular weights, whereas the polymers synthesized by Si/B exchange polycondensation showed higher molecular weights than those synthesized by salt elimination. As *Dapson* has been used in biomedicine, degradation experiments of the model compounds and a polymer **43** were performed. The sulfur-containing building blocks were successfully released under acidic or basic conditions (Scheme 3.11), which was confirmed by NMR spectroscopy and mass spectrometry.

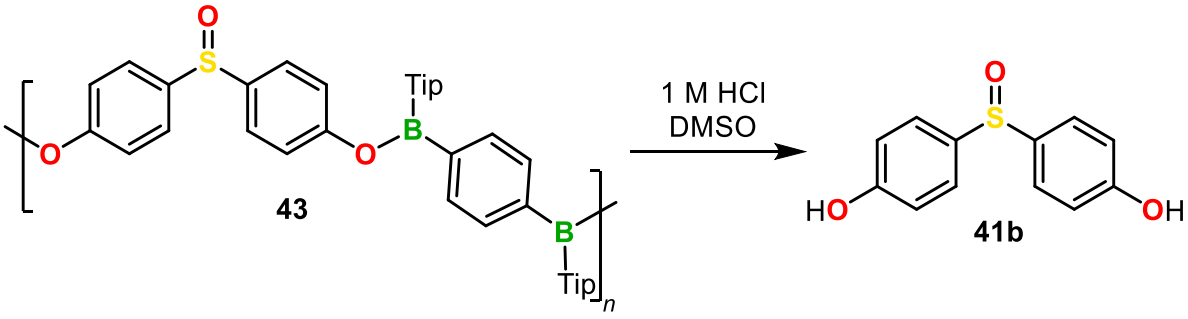

Scheme 3.11. Degradation of the sulfoxide-containing polymer **43** with aqueous HCl to **41b** (Tip = 2,4,6-triisopropylphenyl).

In summary, the results in this work provide valuable insights into compounds that have one or more linearly arranged B=N units. Oligomers and polymers with purely inorganic main chains of BN units and inorganic–organic hybrid polymers and their monodisperse oligomers were studied.

4 Zusammenfassung

In dieser Arbeit wurde neben potenziellen katalytischen Routen zur B–N-Knüpfung für die gezielte Synthese von BN-haltigen Makromolekülen auch die Synthese von anorganischen Polymeren, die ausschließlich Bor und Stickstoff in der Hauptkette enthalten (Poly(imino-boran)e) sowie deren monodispersen Oligomeren beschrieben. Außerdem wurden neuartige anorganisch–organische Hybridpolymere, die BN-Analoge zu konjugierten organischen Poly(arylen vinylen)en darstellen, sowie Hybridpolymere mit längeren $(BN)_x$-Ketten und BN/BO-dotierte Artverwandte von Poly(phenylen sulfid) Derivaten synthetisiert und charakterisiert.

Im ersten Kapitel 2.1 wurde die Entwicklung von Methoden zur katalytischen Knüpfung von B–N Bindungen angestrebt, die für die kontrollierte Synthese von makromolekularen Materialien geeignet sind. Die Umsetzung eines *N*-Silyl-*B*-chloro-Aminoborans mit dem elektrophilen Reagenz Trimethylsilyltriflat führte zur effektiven B–N Knüpfung und der Bildung des erwarteten Borazins **2a** (Schema 4.1, links).

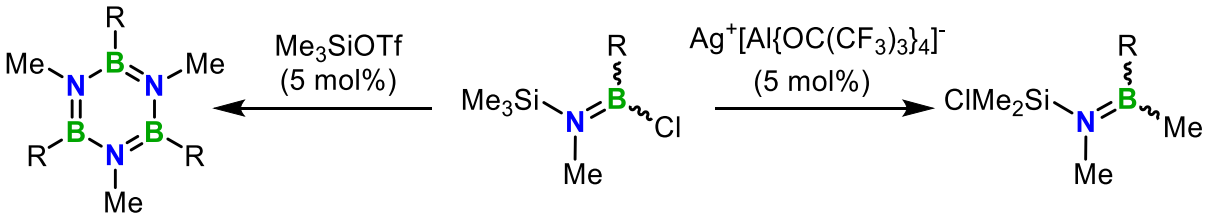

Schema 4.1. Umsetzung von **1** mit Me_3SiOTf und einem Silber(I)salz (OTf = OSO_2CF_3).

Bei der Verwendung des Silber(I)salzes $Ag[Al\{OC(CF_3)_3\}_4]$ wurde hingegen ein intramolekularer Cl/Me-Austausch zwischen dem Bor- und Siliziumatom beobachtet (Schema 4.1, rechts). Im Fall der mesityl-substituierten Verbindung **1b** wurde die Methylmigration durch NMR-Spektroskopie untersucht. Die experimentellen Studien wurden durch detaillierte theoretische Untersuchungen ergänzt, die zu einem Vorschlag für einen Reaktionszyklus führten (Abbildung 4.1).

Zu Beginn der Reaktion zu **3b** konnte eine Induktionsphase beobachtet werden, die auf eine gehemmte Chlorid Abspaltung durch die langsame Keimbildung von Silberchlorid zurück-zuführen ist. In verschiedenen Versuchen trat die Induktionsphase in unterschiedlichen Längen auf, was auf die schwer kontrollierbare Keimbildung zurückzuführen ist. Die anschließende Methylwanderung nach Initiation erfolgt ausgehend von dem kationischen Intermediat **4** unter Bildung von **5**. Der Zyklus wird durch die Abspaltung eines Chlorids von

einem weiteren Molekül **1b** geschlossen. Der Reaktionsumsatz von **1b** zu **3b** zeigt einen nahezu linearen Verlauf nach der Induktionsphase, entsprechend einer Reaktion 0. Ordnung (ermittelt durch ^{1}H NMR-Spektroskopie).

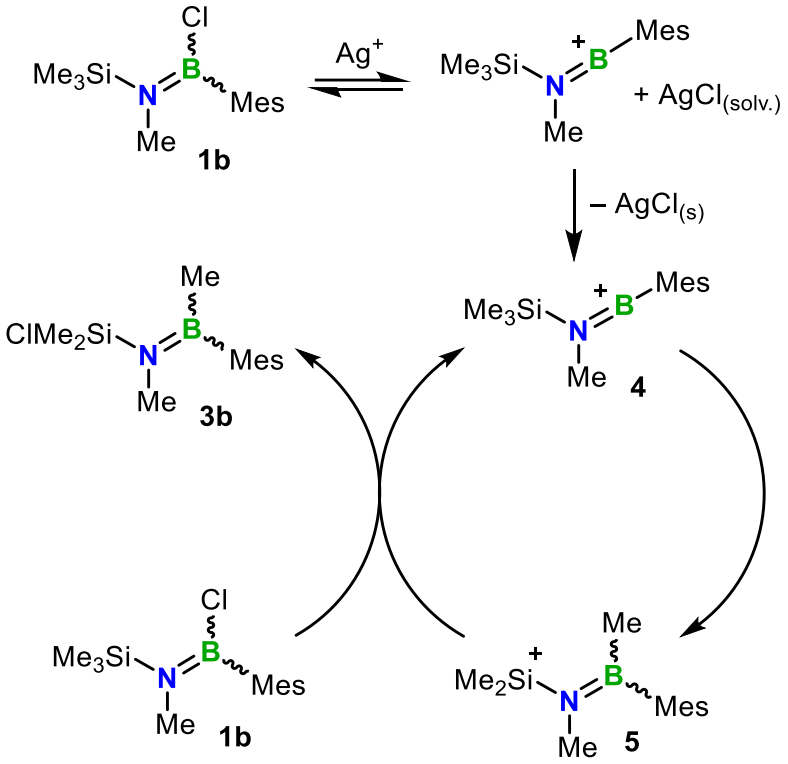

Abbildung 4.1. Vorgeschlagener Reaktionszyklus der Reaktion von **1b** mit einem Silber(I)salz.

Im zweiten Kapitel 2.2 wurde die Synthese und Charakterisierung von Poly(iminoboran)en mit aromatischen Seitengruppen (**I**) und deren zugehörigen monodispersen Oligomeren (**II**) beschrieben (Abbildung 4.2).

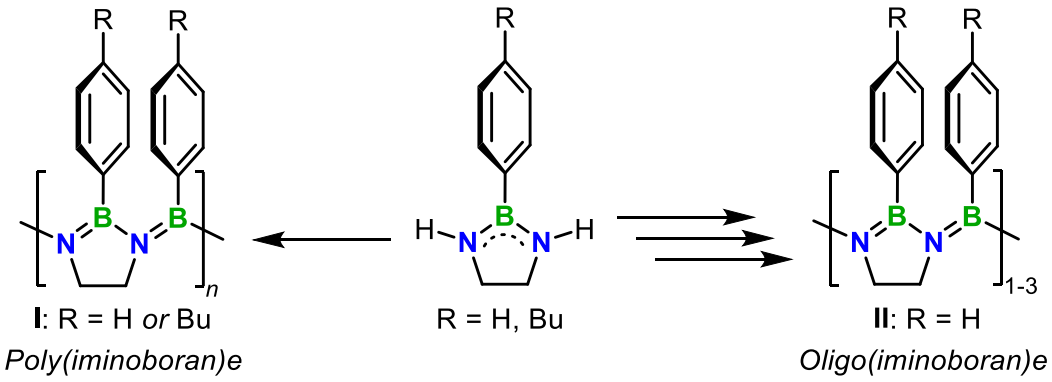

Abbildung 4.2. Darstellung von Poly(iminoboran)en (**I**) und monodispersen Oligo(iminoboran)en (**II**).

Durch die sukzessive Verlängerung der B–N Hauptkette wurde ein Oligo(iminoboran) mit 7 Bor- und 8 Stickstoffatomen synthetisiert. Mittels Röntgenstrukturanalyse konnten die Festkörperstrukturen von sechs Oligomeren, mit bis zu 5 Bor- und 6 Stickstoffatomen (**6**, **7**), aufgeklärt werden (Abbildung 4.3). Die B–N Bindungslängen entlang der Hauptkette befinden sich dabei in einem typischen Bereich zwischen Einfach- und Doppelbindungen. Die beobachteten Verdrehungen zwischen den benachbarten BR_3 und NR_3 Ebenen wurden auf sterische Effekte zurückgeführt.

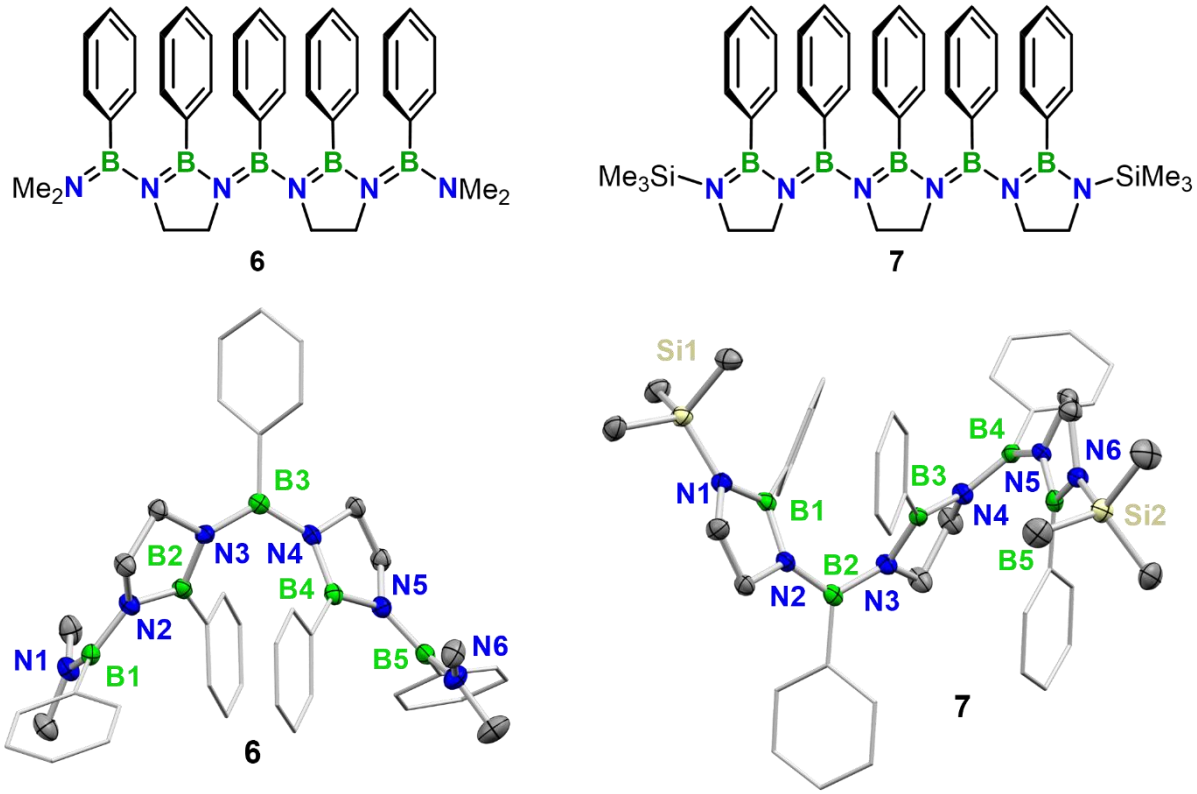

Abbildung 4.3. Oligo(iminoboran)e **6** und **7** (oben) und deren Festkörperstrukturen (unten; H-Atome sind zur besseren Übersichtlichkeit nicht dargestellt).

Die Verbindungen mit endständigen NMe_2-Gruppen (z.B. **6**) wurden auf eine mögliche Konjugation zwischen den B–N Einheiten durch temperaturabhängige NMR-Messungen untersucht. Ein Maß für die Konjugation zwischen den B–N Einheiten ist die Rotationsbarriere ($\Delta G^{\ddagger}$) der terminalen B=N Einheiten, die geringere Energien für konjugierte Systeme aufweisen sollte. In unseren Untersuchungen konnte eine leichte Erhöhung von $\Delta G^{\ddagger}$ mit zunehmender Kettenlänge beobachtet werden, wodurch von einer schwächeren Konjugation zwischen den B–N Einheiten ausgegangen wurde. Dieser Trend konnte durch theoretische Studien unterstützt werden.

Des Weiteren konnten verschiedene Poly(iminoboran)e **8**–**11** und **13** mit unterschiedlichen aromatischen Anteilen synthetisiert werden (Schema 4.2). Für eine bessere Vergleichbarkeit wurden dabei die Synthesen der literaturbekannten Polymere **8** und **9** wiederholt. Mit einem

Polymerisationsgrad (DP_n) von 23 konnte für **9** das bis dato höchstmolekulare Poly(iminoboran) erhalten werden. Das geringste zahlenmittlere Molekulargewicht (M_n) zeigte **13**, was auf eine deutlich geringere Löslichkeit zurückgeführt wurde. Die thermogravimetrischen Analysen der Polymere **8**–**11** und **13** zeigten eine höhere keramische Ausbeute als erwartet, wobei der Hauptmassenverlust im Bereich zwischen 400 und 500 °C auftrat. Durch Verwendung einer O_2 Atmosphäre und einer geringeren Heizrate konnte der BN-Anteil des keramischen Rückstands von **9** signifikant erhöht werden.

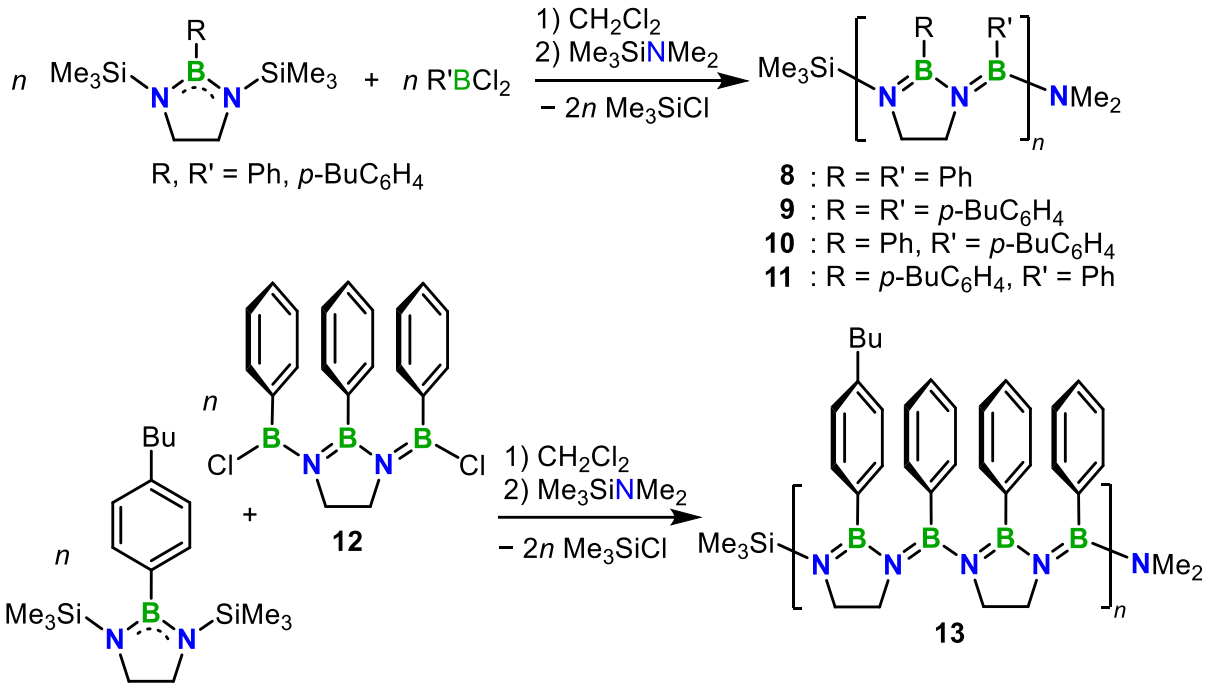

Schema 4.2. Synthese der Poly(iminoboran)e **8**–**11** und **13**.

In Kapitel 2.3 wurde über Umverteilungsprozesse berichtet, die bei der Umsetzung von längeren Oligo(iminoboran)en mit nicht stöchiometrischen Mengen von (di)halogenierten Boranen resultierten. Bei der Reaktion von **14** mit einem Überschuss von $PhBCl_2$ wurde, anstelle der angestrebten B–N Bindungsbildung zu Verbindung **15**, die quantitative Bildung von **12** beobachtet (Schema 4.3). Verbindung **12** kann dabei nur durch die Spaltung von exozyklischen B–N Bindungen entstehen. Dabei weisen quantenchemische mechanistische Studien darauf hin, dass erst **15** gebildet wird, welches mit $PhBCl_2$ zu zwei Molekülen **12** weiterreagiert. Bei Verwendung eines weniger reaktiven monohalogenierten Borans ($PhB(NMe_2)Br$) im Überschuss wurde das Auftreten von Umverteilungsprozessen ebenfalls beobachtet.

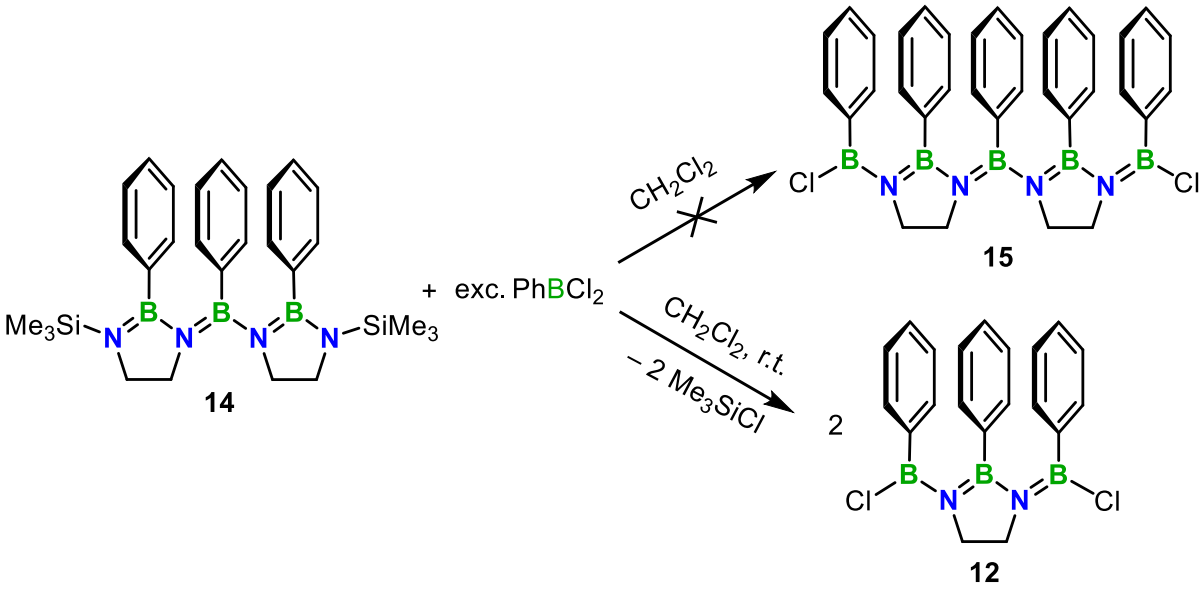

Schema 4.3. Reaktion von **14** mit einem Überschuss $PhBCl_2$.

In Kapitel 2.4 wurde die Synthese von 1,3,2-Benzodiazaborolinen **16** und deren Polymerisation, über deren Stickstoffeinheiten zu Poly(iminoboran)en angestrebt. Durch die Reaktion von **16** mit $MeBBr_2$ und Me_3SiNMe_2 konnte erfolgreich das Oligomer **17** dargestellt werden (Schema 4.4), während Syntheseversuche zu größeren Modellsystemen (siehe Kapitel 2.2) ohne Erfolg blieben.

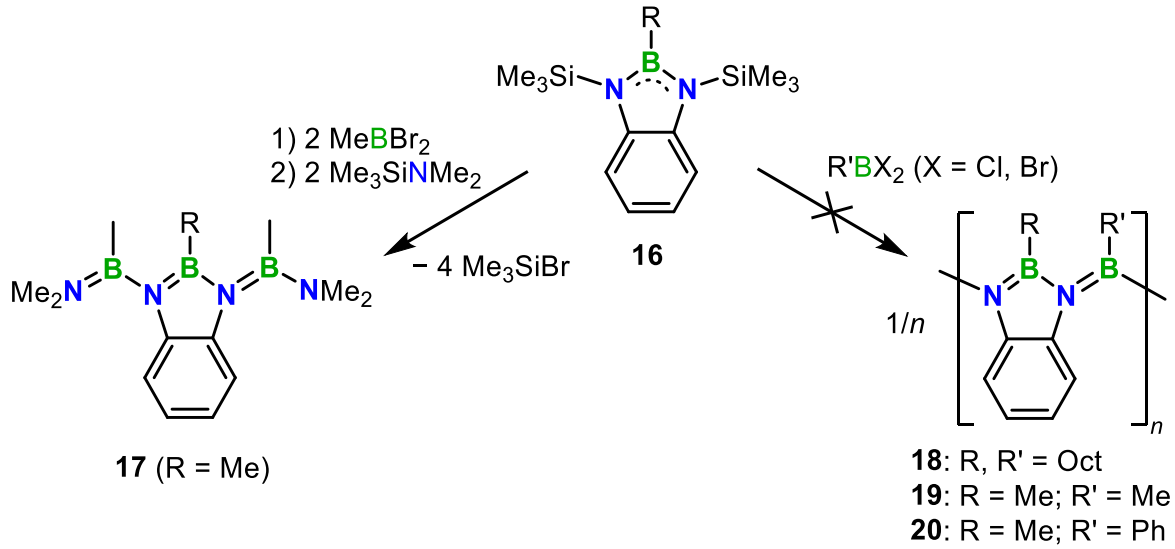

Schema 4.4. Synthese von Oligomer **17** und Polymerisationsversuche von **16** mit Dihaloboranen.

Polymerisationsversuche zu **18**–**20** mittels Si/B Austauschpolykondensation von **16** mit verschiedenen Dihaloboranen führten ebenfalls nicht zu BN-Bindungsknüpfungen. Nach dem Polymerisationsversuch von **16** mit Octyl-BCl_2 in *o*-DFB bei 80 °C für 12 Tage konnten durch hochaufgelöste Massenspektrometrie Oligomere mit bis zu drei 1,3,2-Benzodiazaborolin-

Einheiten nachgewiesen werden. Dadurch wurde auf eine deutlich geringere Reaktivität von Benzodiazaborolinen gegenüber den im Kapitel 2.2 beschriebenen Diazaborolidinen geschlossen.

In den Kapiteln 2.5 und 2.6 wurde die Synthese von 1,2,5-Azadiborolanen als Bausteine für die Synthese von Poly(iminoboran)en und anorganisch–organischen Hybridpolymeren beschrieben. In Kapitel 2.5 wurde ein 1,2,5-Azadiborolan mit sterisch anspruchsvolleren Gruppen an der Bor-verbrückenden Ethyleneinheit verwendet. Die Reaktion von **21** mit Me_3SiNMe_2 führt unter zweifacher B–N Bindungsbildung zu **22** (Schema 4.5). Bei dem Polymerisationsversuch von **21** mit $BuN(SiMe_3)_2$ konnte allerdings nur eine einfache Kupplung der Monomere zu **23** beobachtet werden. Die Verwendung von höheren Temperaturen sowie längeren Reaktionszeiten führte nicht zu einem weiteren Kettenwachstum.

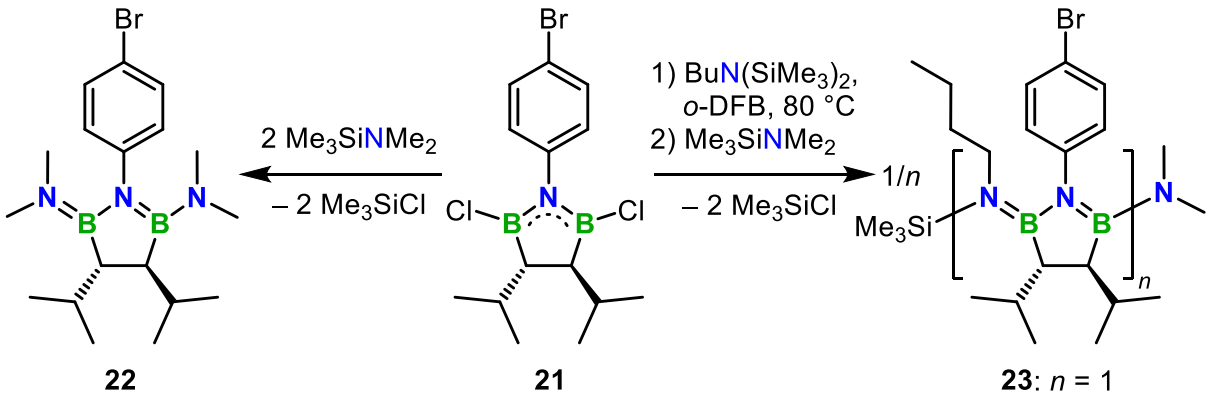

Schema 4.5. Synthese von **22** und Polymerisationsversuch von **21** mit $BuN(SiMe_3)_2$.

Polymerisationsversuche von **21** mit dem Co-Monomer **24** führten zu der erfolgreichen Synthese des Hybridpolymers **25** und den Einbau von Phenyleneinheiten in das Polymerrückgrat (Schema 4.6). In einem Versuch konnte ein M_n von 68.6 kDa erhalten werden, was einem DP_n von 335 entspricht. In photophysikalischen Untersuchungen konnte eine bathochrome Verschiebung des Absorptionsmaximums mit zunehmender Anzahl von BN-Einheiten beobachtet werden, was auf eine π-Konjugation entlang der Polymerkette hinweist. Die Untersuchung der elektrochemischen Eigenschaften von **25** durch Cyclovoltammetrie zeigte ein reversibles Oxidationsereignis für **25**, was der Oxidation der Diaminoarylengruppe zugeordnet wurde.

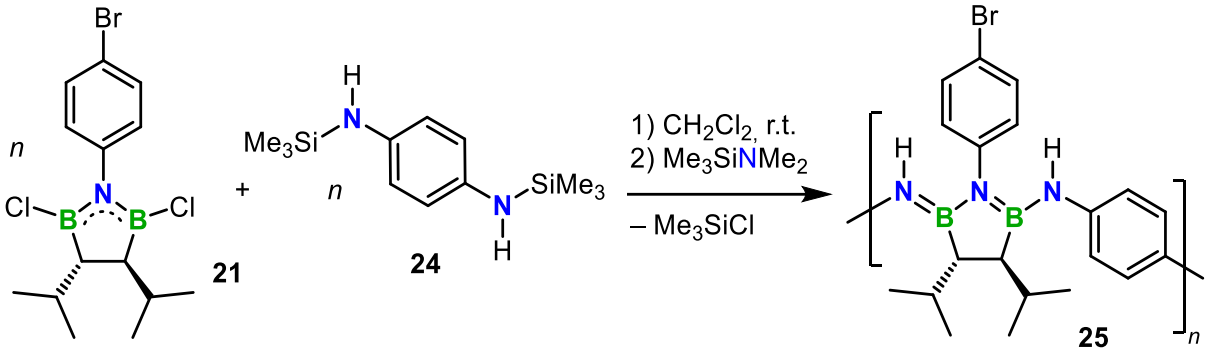

Schema 4.6. Synthese von **25** durch Si/B Austauschpolykondensation von **21** und **24**.

In Kapitel 2.6 wurde die Synthese eines Poly(iminoboran)s mit 1,2,5-Azadiborolan-Baugruppen angestrebt, dessen Boratome durch eine unsubstituierte Ethyleneinheit verbrückt sind. Nach mehrstufiger Synthese konnte **26** erhalten werden, welches anschließend im NMR-Maßstab mit **27** umgesetzt wurde (Schema 4.7). Durch ^{1}H NMR-Spektroskopie konnte die Bildung von zwei Äquivalenten Me_3SiCl nachgewiesen werden, was auf eine zweifache B–N Kupplung hinwies. Aufgrund der zunehmenden Verbreiterung der ^{1}H NMR-Signale über die Zeit konnte von einem fortschreitenden Kettenwachstum ausgegangen werden. Dies wies auf eine höhere Reaktivität des Azadiborolans **26** im Vergleich zum sterisch anspruchsvolleren **21** hin.

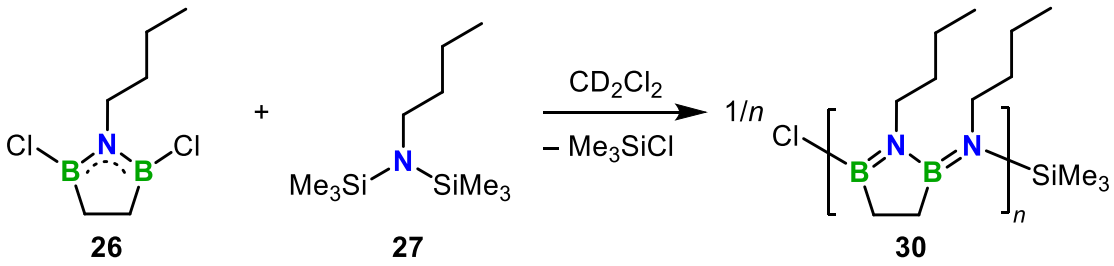

Schema 4.7. Polymerisation von **26** und **27** über Si/B Austauschpolykondensation.

In den Kapiteln 2.7 und 2.8 wurde die umfassende Untersuchung von Poly(arylen iminoboran)en beschrieben, die die BN Analoga von Poly(arylen vinylen)en darstellen. Dabei wurde in Kapitel 2.7 die erstmalige Synthese von Poly(thiophen iminoboran) (BN-PTV), einem BN Analogon des in der Literatur bekannten Poly(thiophen vinylen) (PTV), beschrieben. Neben der erfolgreichen Synthese der hochreaktiven Diaminothiophen-Spezies **31**, konnte eine Serie von monodispersen Oligomeren dargestellt werden. Das BN-PTV **33** konnte durch die Si/B Austausch-Polykondensation von **31** und **32** erhalten werden (Schema 4.8). Die Oligomere und **33** zeigten neben guter Löslichkeit in den gängigen Lösungsmitteln, eine gute Luft- und Feuchtebeständigkeit. Die Analyse von **33** durch GPC ergab ein M_n = 14.2 kDa was einem DP_n von 46 entspricht. Die Untersuchung des Absorptionsverhalten in Lösung zeigte eine systematische Rotverschiebung des Absorptionsmaximums mit zunehmender Kettenlänge der Oligomere zu **33**, was auf eine ausgeprägte Konjugation über die B=N Einheiten hinwies.

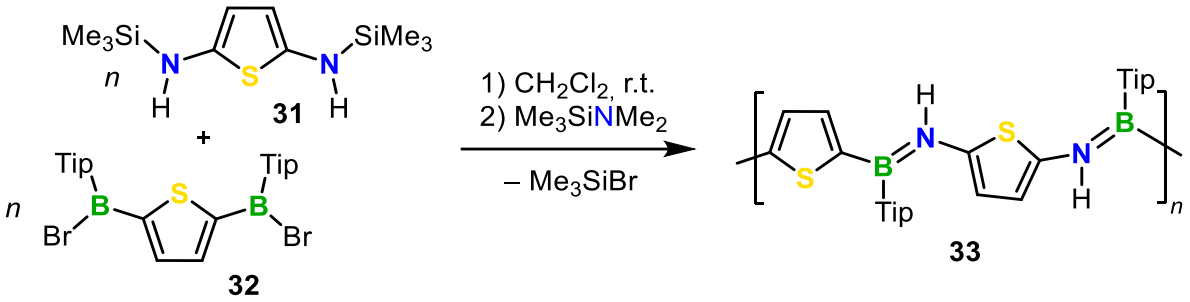

Schema 4.8. Synthese von BN-PTV **33** mittels Si/B Austausch-Polykondensation (Tip = 2,4,6-Triisopropylphenyl).

Durch TD-DFT-Rechnungen der monodispersen Oligomere konnte die Absorptionsbande mit niedrigster Energie HOMO–LUMO Anregungen mit π-π* Charakter zugeordnet werden. In Kapitel 2.8 wurden die rein Thiophen-basierenden Oligo- und Polymere mit den Poly(*p*-phenylen iminoboran)en (BN-PPV) verglichen. Zusätzlich wurden gemischte Verbindungen synthetisiert, die abwechselnd Thienyl- und Phenyleneinheiten zwischen den B=N Einheiten aufweisen. Innerhalb dieser Studie wurden vier Polymere und zwölf monodisperse Oligomere auf ihre Eigenschaften untersucht. Die Modellverbindungen mit zwei B=N Einheiten (Dimere) wurden entsprechend ihrer BN-Sequenz in NBBN- (z.B. **35**) und BNNB-Dimere (z.B. **36**–**39**) unterteilt (Schema 4.9).

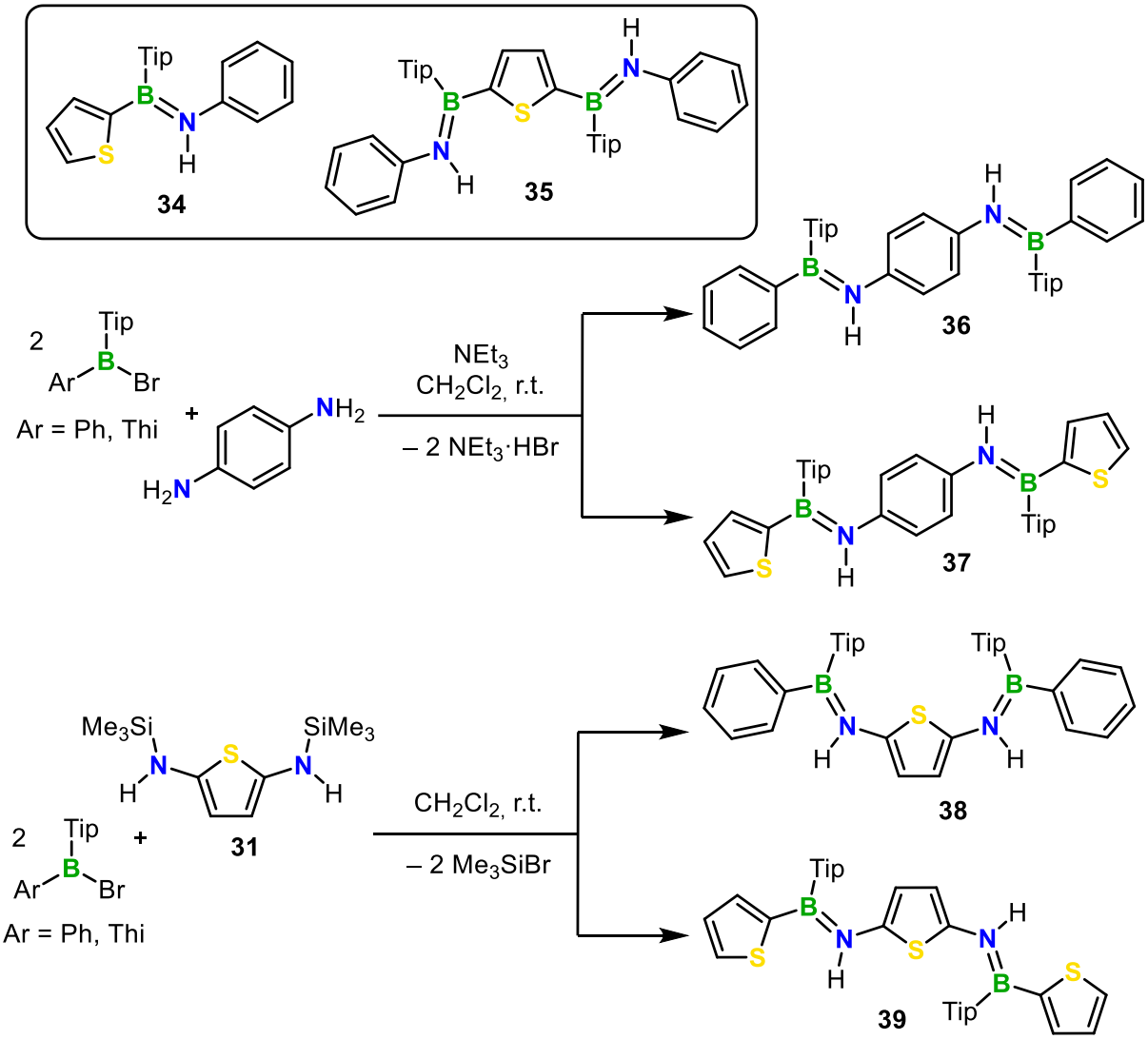

Schema 4.9. Synthese der monodispersen Oligomere **36**–**39** mit BNNB-Sequenz sowie Molekülstruktur von **34** mit BN- und **35** mit NBBN-Sequenz über Si/B Austauschkondensation oder Salzeliminierungsreaktion (Tip = 2,4,6-Triisopropylphenyl).

Die monomeren und dimeren Verbindungen konnten entweder mittels Salzeliminierungsreaktion (**36**, **37**) oder Si/B Austauschkondensation (**38**, **39**) synthetisiert werden. Alle Oligomere wurden als Diastereomerengemische erhalten, wobei in jedem Fall das Hauptisomer *trans*-Konfiguration der Aryl(en)gruppen an den B=N Einheiten zeigte. Dies konnte mittels 2D NMR-Spektroskopie und Röntgenstrukturanalyse (Abbildung 4.4) nachgewiesen werden. Die Untersuchung der Festkörperstrukturen zeigte, dass die benachbarten Ringe in der Kette nur leicht gegeneinander verdreht sind, was eine π-Konjugation über die B=N und Aryl(en)-einheiten ermöglicht. Dies konnte durch photophysikalische Untersuchungen bestätigt und durch theoretische Rechnungen unterstützt werden.

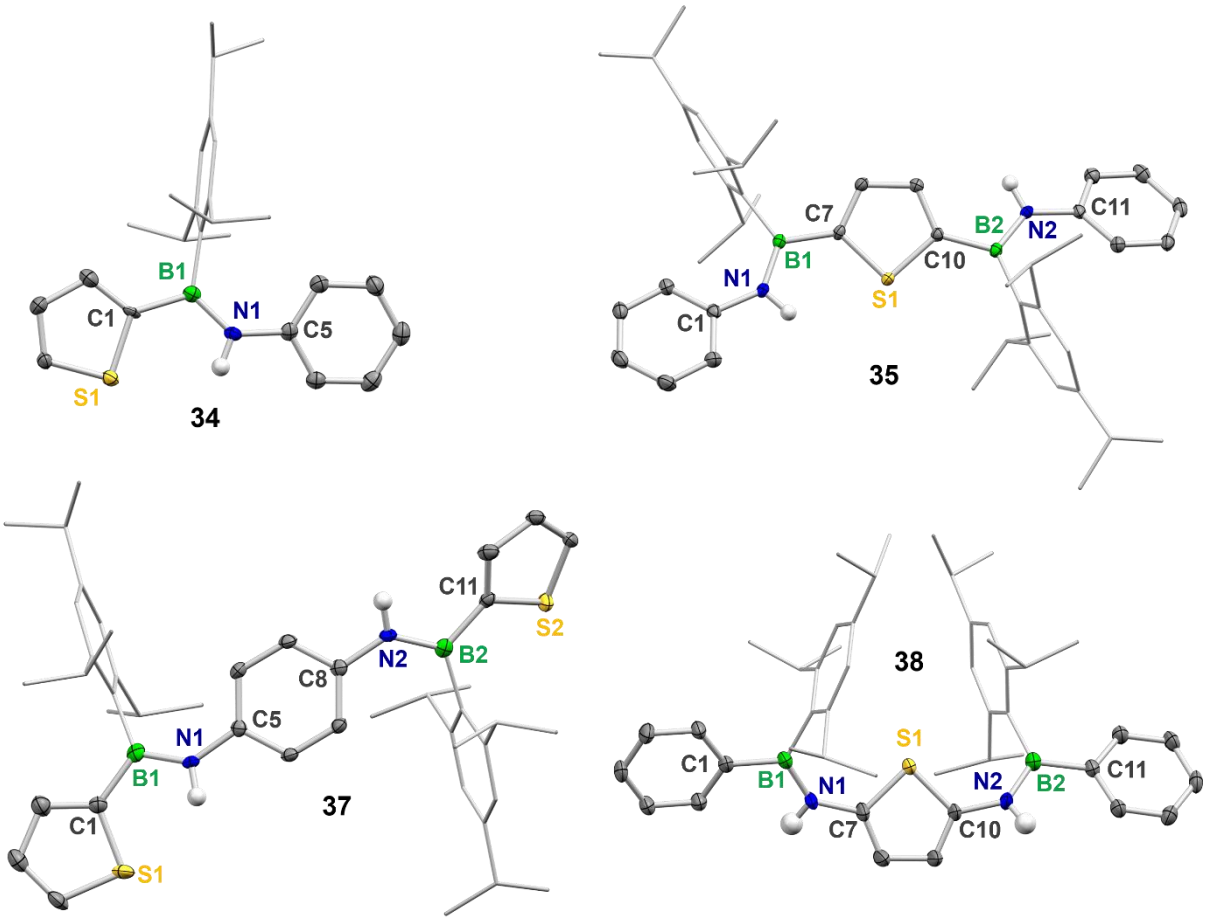

Abbildung 4.4. Festkörperstrukturen des Monomers **34**, NBBN-Dimers **35**, und der BNNB-Dimere **37** und **38** (H-Atome sind zur besseren Übersichtlichkeit nicht dargestellt).

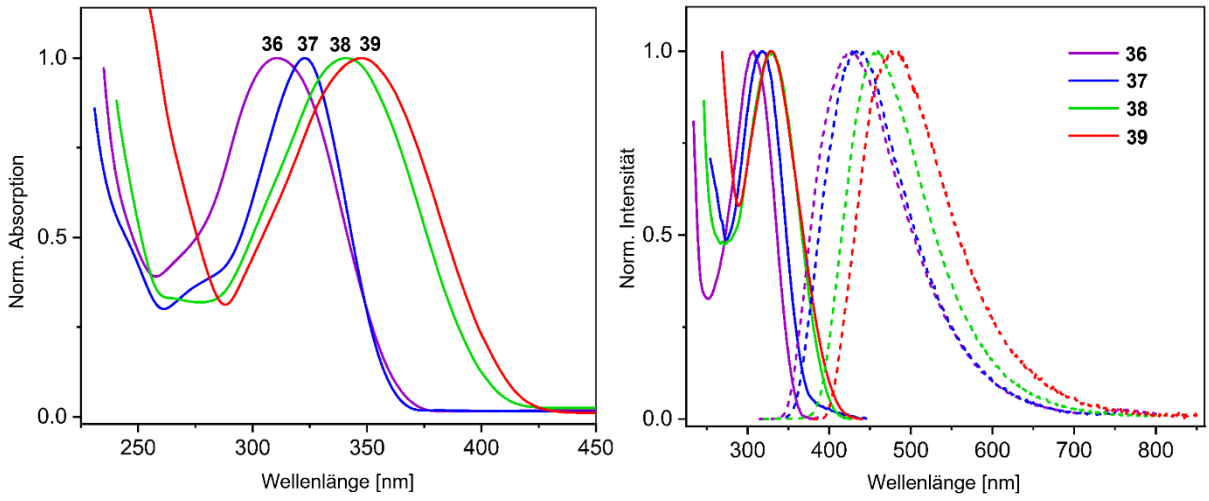

Abbildung 4.5. Normierte Absorptionsspektren von **36**–**39** in THF (links) und normierte Absorptionsspektren und Emissionsspektren von **36**–**39** als PMMA-Film (rechts).

Photophysikalische Untersuchungen der Monomere, Dimere und Polymere zeigten eine systematische bathochrome Verschiebung des Absorptionsmaximums mit zunehmender Kettenlänge. In der Reihe von **36**–**39** zeigten **38** und **39** eine rotverschobene Absorption, was

mit der ausgeprägteren Donor-Akzeptor Struktur der Verbindungen zusammenhängt (Abbildung 4.5, links). Der gleiche Trend konnte in den Absorptions- und Emissionsspektren von **36**–**39** als PMMA-Film beobachtet werden (Abbildung 4.5, rechts).

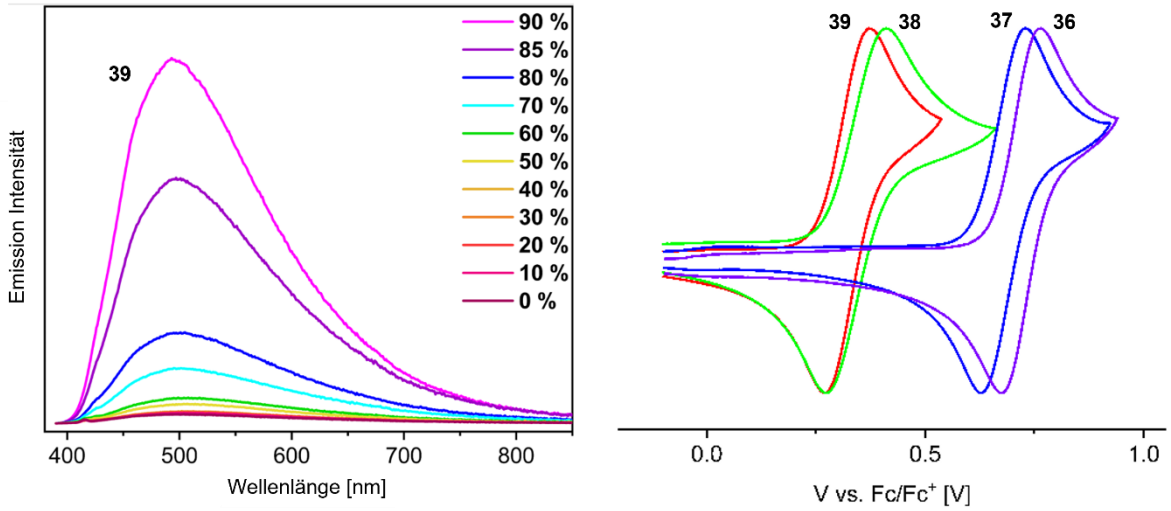

Abbildung 4.6. Emissionsspektren von **39** in THF/Wasser Mischungen (Konz. $5x10^{-5}$ M) mit verschiedenen Wasseranteilen (0-90 %; links) und Cyclovoltammogramme von **36**–**39** in CH_2Cl_2 (Scanrate: 150 mV s^{-1}; rechts).

Die Oligo- und Poly(arylen iminoboran)e (z.B. **39**) zeigten nur sehr schwache oder keine Emission in Lösung, wobei die BNNB Dimere durch Aggregation induzierte Emission in einem THF/Wasser Gemisch zeigten (Abbildung 4.6, links). Elektrochemische Untersuchungen zeigten reversible Oxidationen für Verbindungen mit Diaminoarylen-Gruppen (z.B. **36**–**39**), wobei die Verbindungen mit den elektronenreichen Diaminothiophen-Einheiten (z.B. **38**, **39**) die geringsten Oxidationspotentiale aufwiesen (Abbildung 4.6, rechts). Die synthetisierten Polymere **39** und **40** konnten mittels Si/B Austauschpolykondensation hergestellt werden (Abbildung 4.7). Während die Absorptionsmaxima von **39** und **40** im gleichen Bereich lagen, zeigte **40** ein um 42 nm rotverschobenes Emissionsmaximum, was auf die ausgeprägtere Donor-Akzeptor Struktur der Polymerhauptkette zurückzuführen ist.

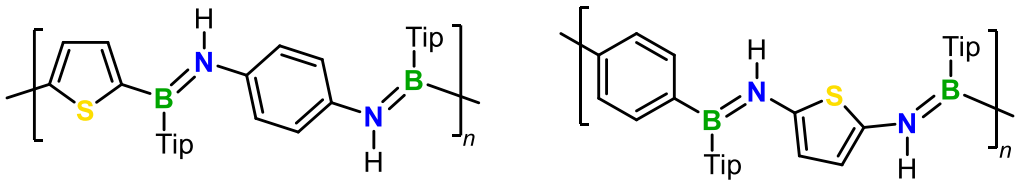

Abbildung 4.7. Struktur der gemischten Polymere **39** und **40** (Tip = 2,4,6-Triisopropylphenyl).

In Kapitel 2.9 wurde die Funktionalisierung von schwefelhaltigen Bausteinen, deren Oligo- und Polymerisierung, sowie die anschließende pH-gesteuerte Degradierung von den Modellverbindungen und eines Polymers untersucht. In dieser Studie wurde versucht, Sulfon-, Sulfoximin-, Sulfoxid- und Sulfilimin-Bausteine über eine B=N- oder B–O-Brücke in Polymere einzubauen. In einer Machbarkeitsstudie wurden Modellsysteme synthetisiert, wobei die Sulfon-, Sulfoximin- und Sulfoxid-haltigen molekularen Oligomere erfolgreich durch Si/B-Austauschkondensation oder Salzeliminierung dargestellt werden konnten (z.B. **42**, Schema 4.10). Der Versuch, die Sulfilimin-haltigen Oligomere zu synthetisieren führte aufgrund einer Konkurrenzreaktion an der Cyanogruppe nicht zum gewünschten Produkt, was mittels Röntgenstrukturanalyse bestätigt wurde.

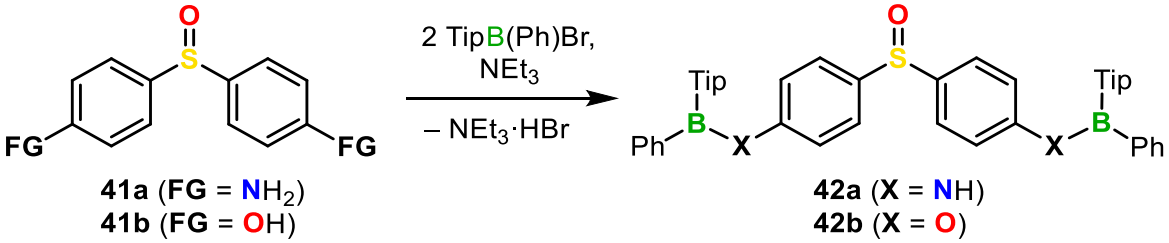

Schema 4.10. Exemplarische Reaktion zu Sulfoxid-haltigen Oligomeren **42** (Tip = 2,4,6-Triisopropylphenyl).

Anschließend konnten die B=N-verknüpften Polymere mittels Si/B Austauschpolykondensation oder Salzeliminierung und die B–O verknüpften Polymere über Salzeliminierungen der Sulfon-, Sulfoximin- und Sulfoxid-Bausteine dargestellt werden. Die B=N verknüpften Polymere zeigten deutlich höhere Molekulargewichte als die B–O Polymere. Polymerisationen mittels Si/B Austauschkondensation führten zu höher molekularen Polymeren als die mittels Salzeliminierung. Da der Sulfonbaustein *Dapson* in der Biomedizin Anwendung findet, wurden Freisetzungsversuche der Modellverbindungen und eines Polymers **43** untersucht. Die schwefelhaltigen Bausteine konnten dabei alle erfolgreich unter sauren oder basischen Bedingungen freigesetzt werden (Schema 4.11), was NMR-spektroskopisch und mittels Massenspektrometrie bestätigt wurde.

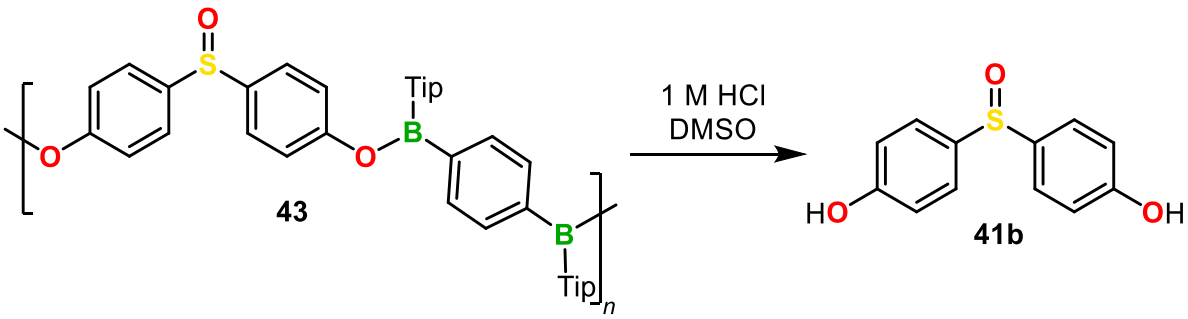

Schema 4.11. Degradierung des Sulfoxid-haltigen Polymers **43** mit wässriger HCl zu **41b** (Tip = 2,4,6-Triisopropylphenyl).

Zusammenfassend liefern die Ergebnisse in dieser Arbeit wertvolle Erkenntnisse über Verbindungen die eine oder mehrere linear angeordnete B=N Einheiten besitzen. Dabei wurde einerseits auf Oligo- und Polymere, die eine rein anorganische Hauptkette aus B=N Einheiten besitzen und andererseits auf anorganisch–organische Hybridpolymere und deren monodispersen Oligomere eingegangen.

5 Appendix

5.1 Electrophilic activation of difunctional aminoboranes: B–N coupling versus intramolecular Cl/Me exchange

NMR spectra

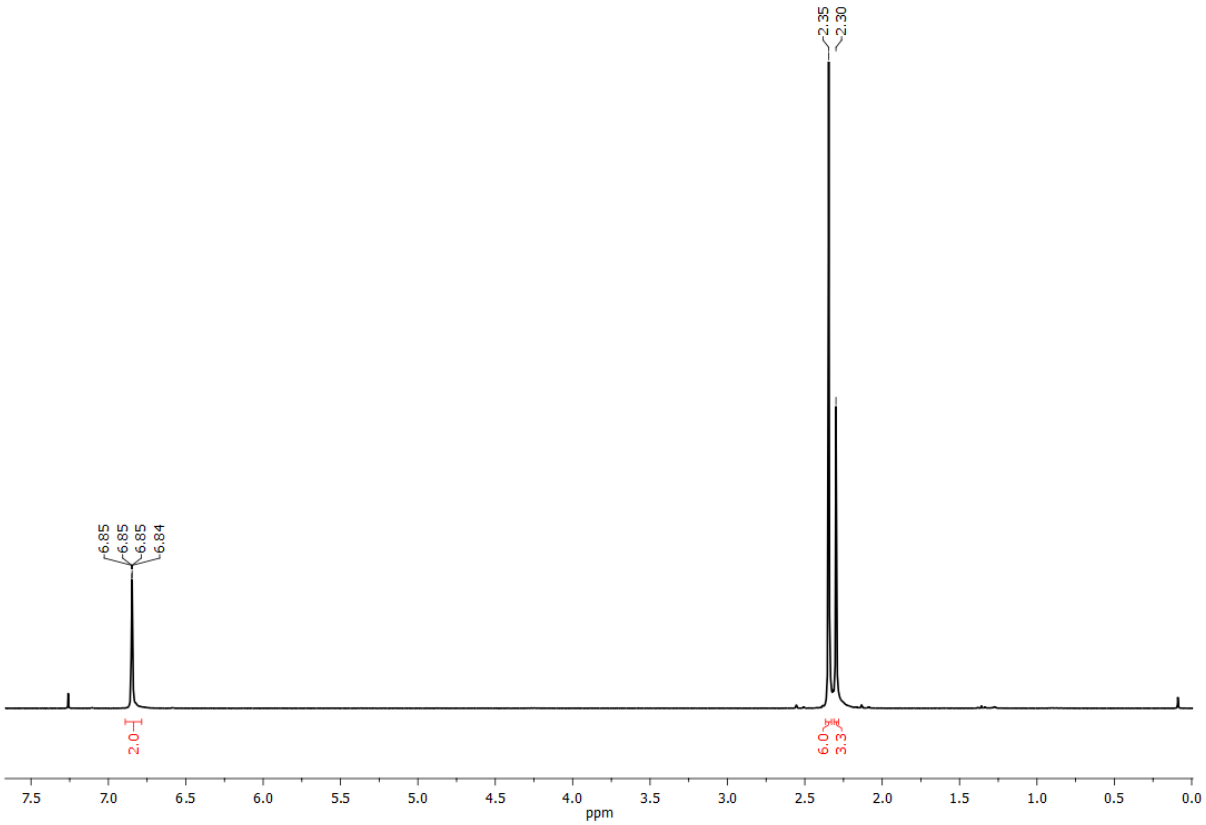

Figure S5.1.1. ^{1}H NMR spectrum (300 MHz) of $MesBCl_2$ in $CDCl_3$.

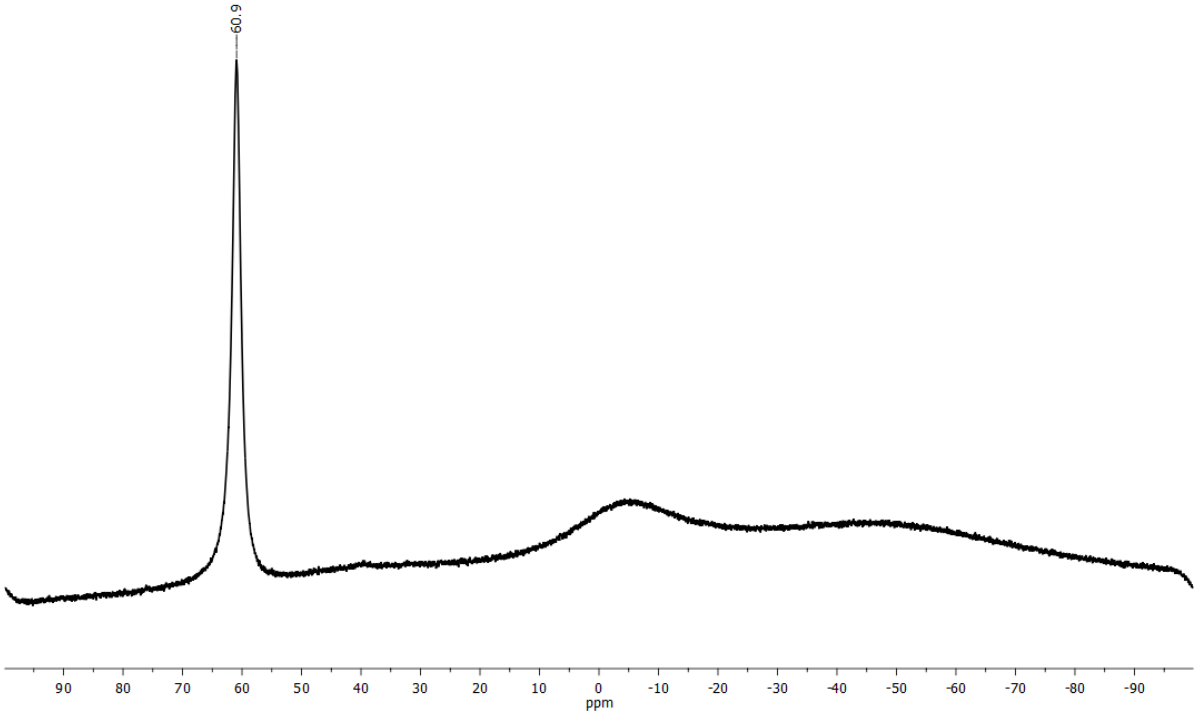

Figure S5.1.2. $^{11}B\{^{1}H\}$ NMR spectrum (96 MHz) of $MesBCl_2$ in $CDCl_3$.

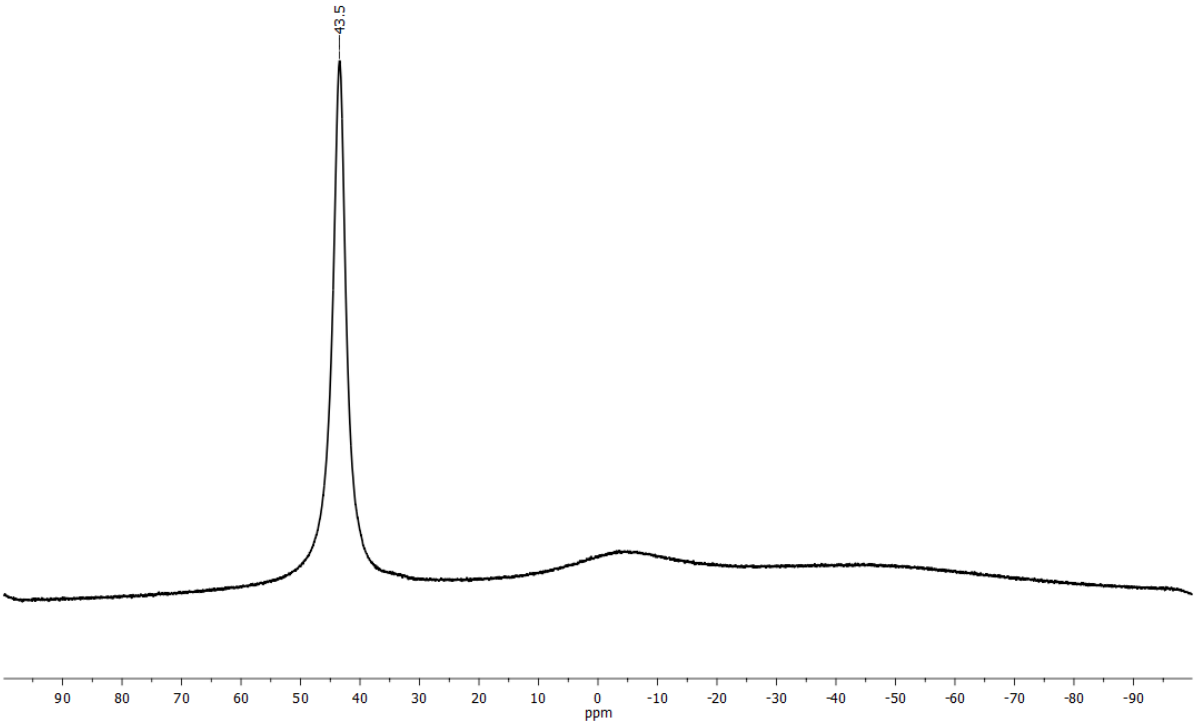

Figure S5.1.3. $^{11}B\{^{1}H\}$ NMR spectrum (96 MHz) of **1a** in CH_2Cl_2.

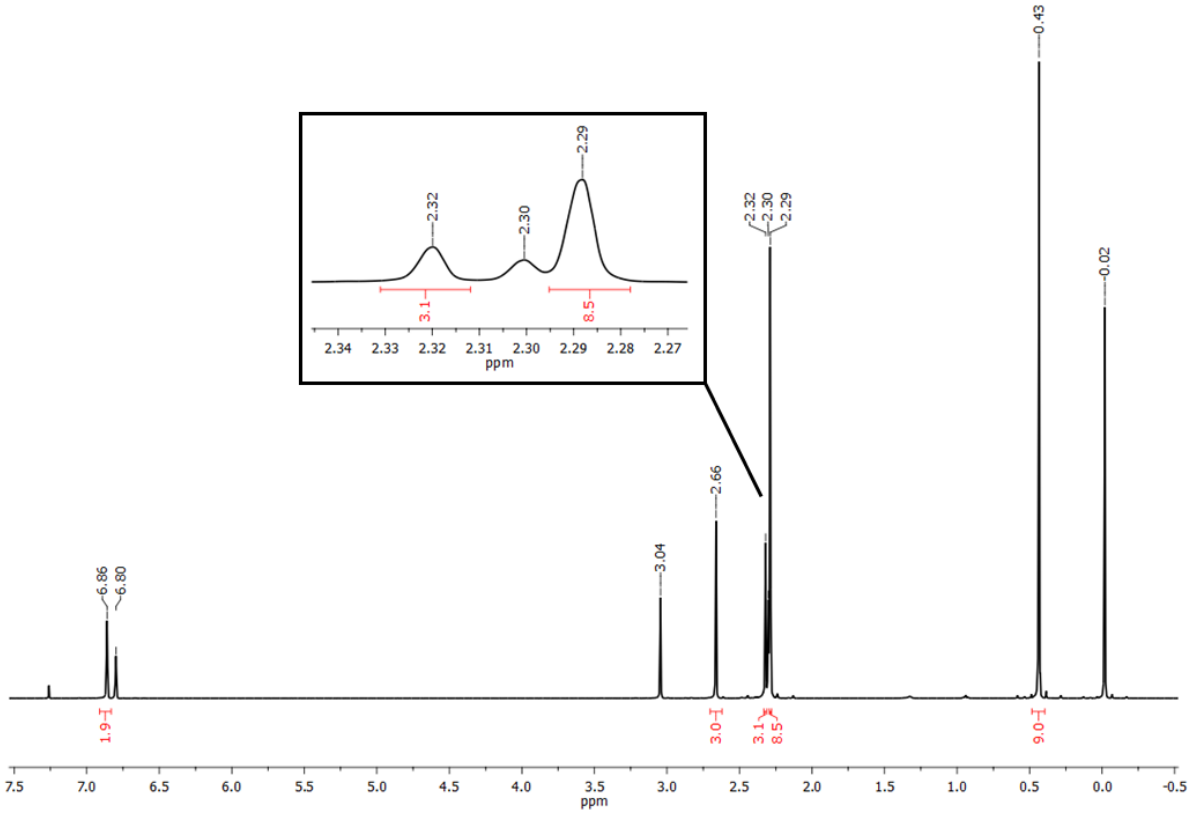

Figure S5.1.4. ^{1}H NMR spectrum (400 MHz) of **1b** in $CDCl_3$ with integrals for (*Z*)-**1b**.

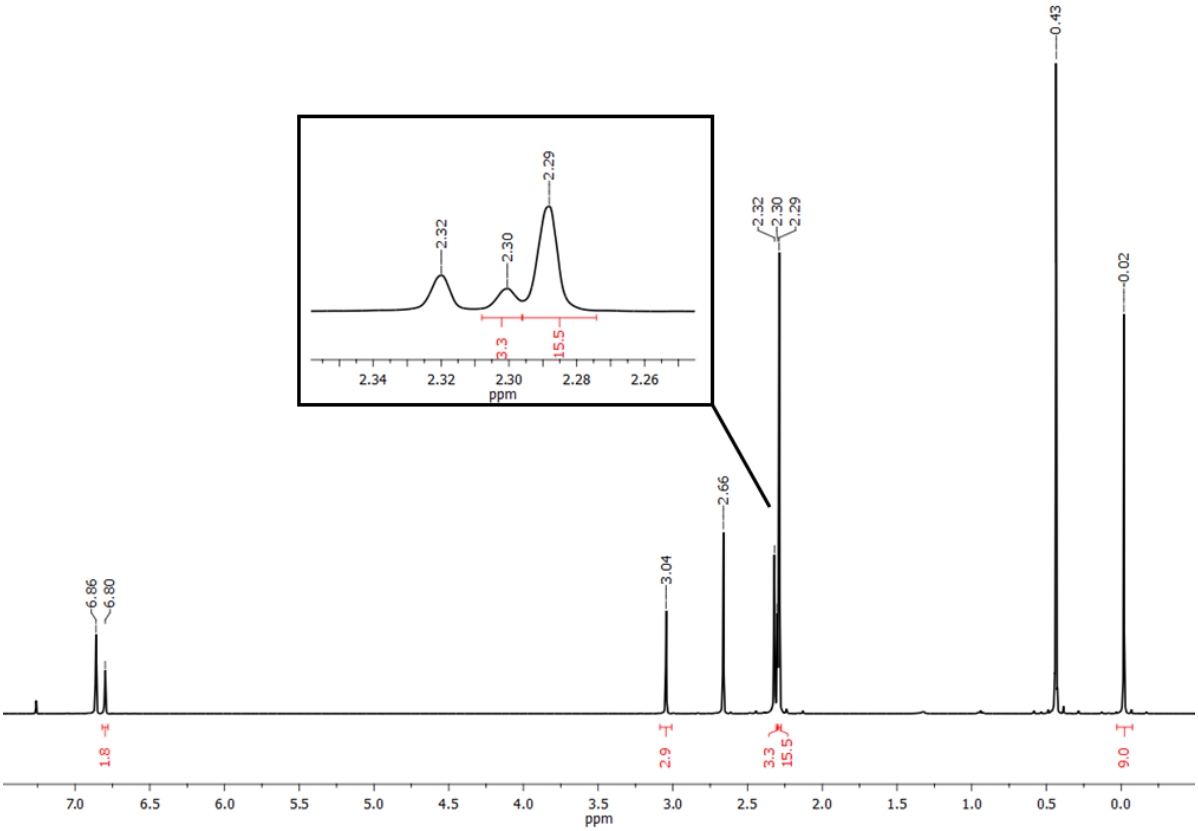

Figure S5.1.5. ^{1}H NMR spectrum (400 MHz) of **1b** in $CDCl_3$ with integrals for (*E*)-**1b**.

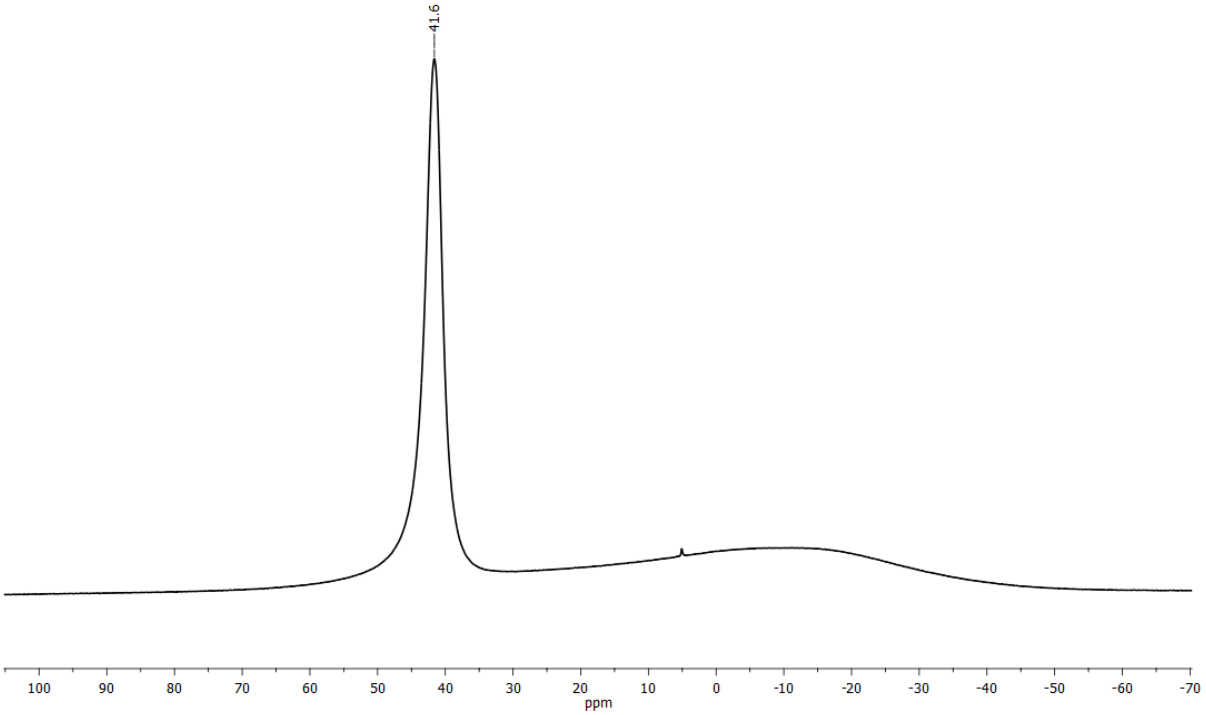

Figure S5.1.6. $^{11}B\{^{1}H\}$ NMR spectrum (128 MHz) of **1b** in $CDCl_3$.

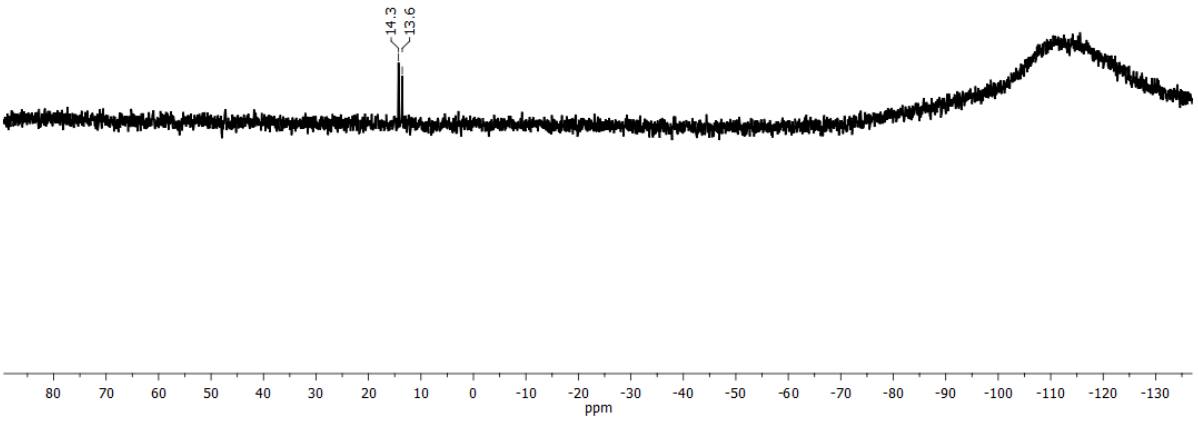

Figure S5.1.7. $^{29}Si\{^{1}H\}$ NMR spectrum (60 MHz) of **1b** in $CDCl_3$.

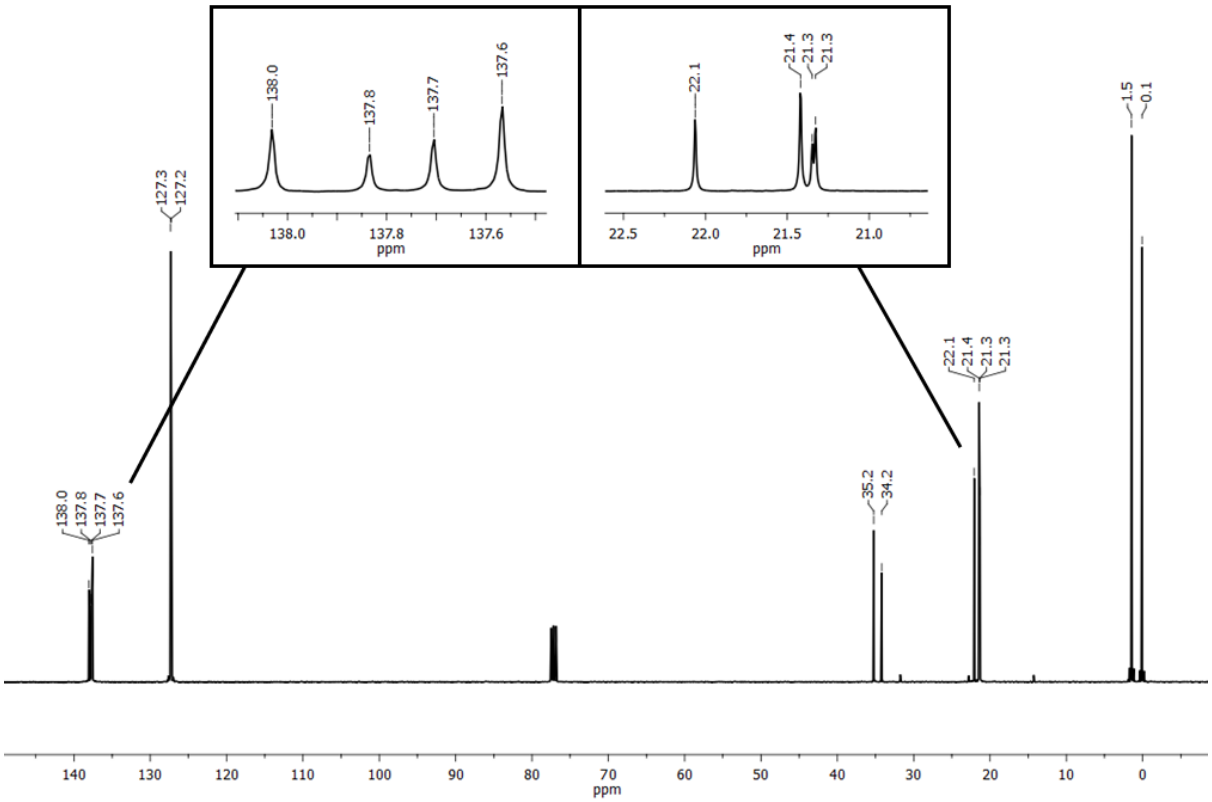

Figure S5.1.8. $^{13}C\{^{1}H\}$ NMR spectrum (100 MHz) of **1b** in $CDCl_3$.

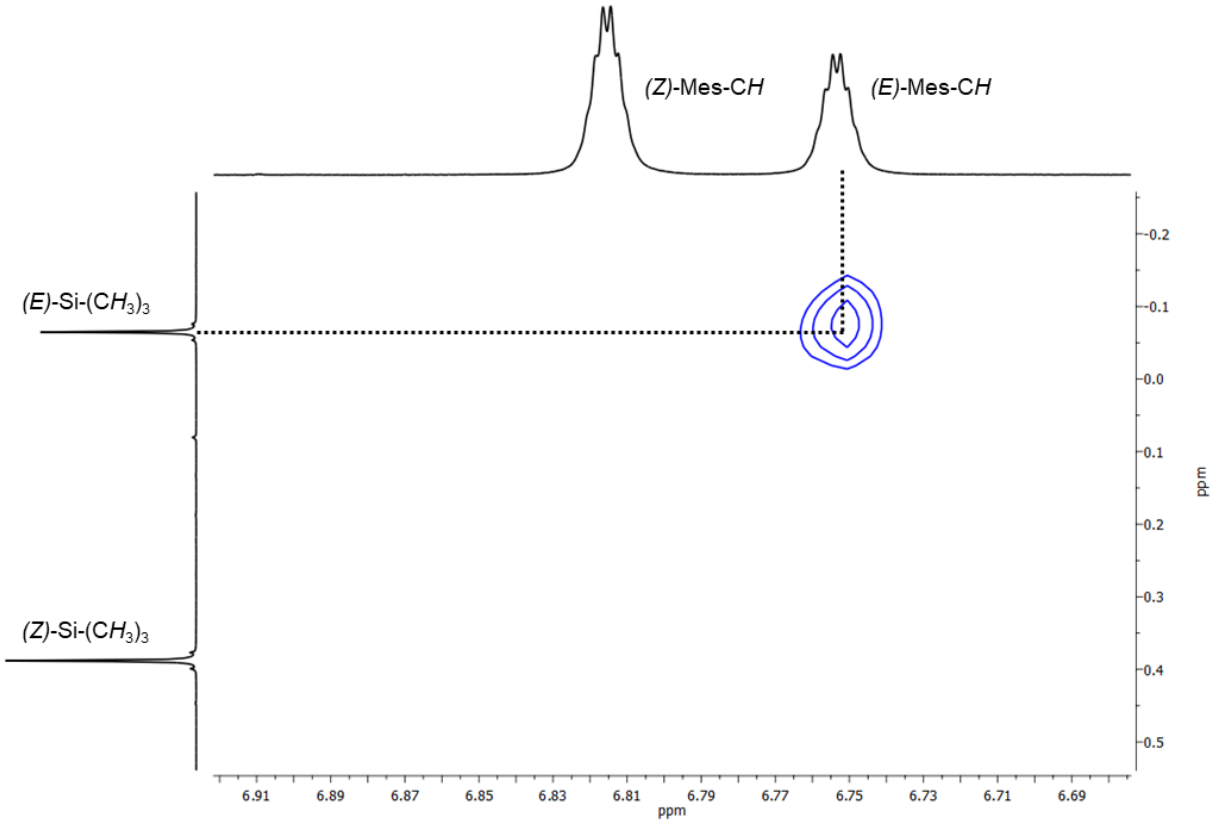

Figure S5.1.9. Detail of $^{1}H,^{1}H$ NOESY spectrum of **1b** in $CDCl_3$.

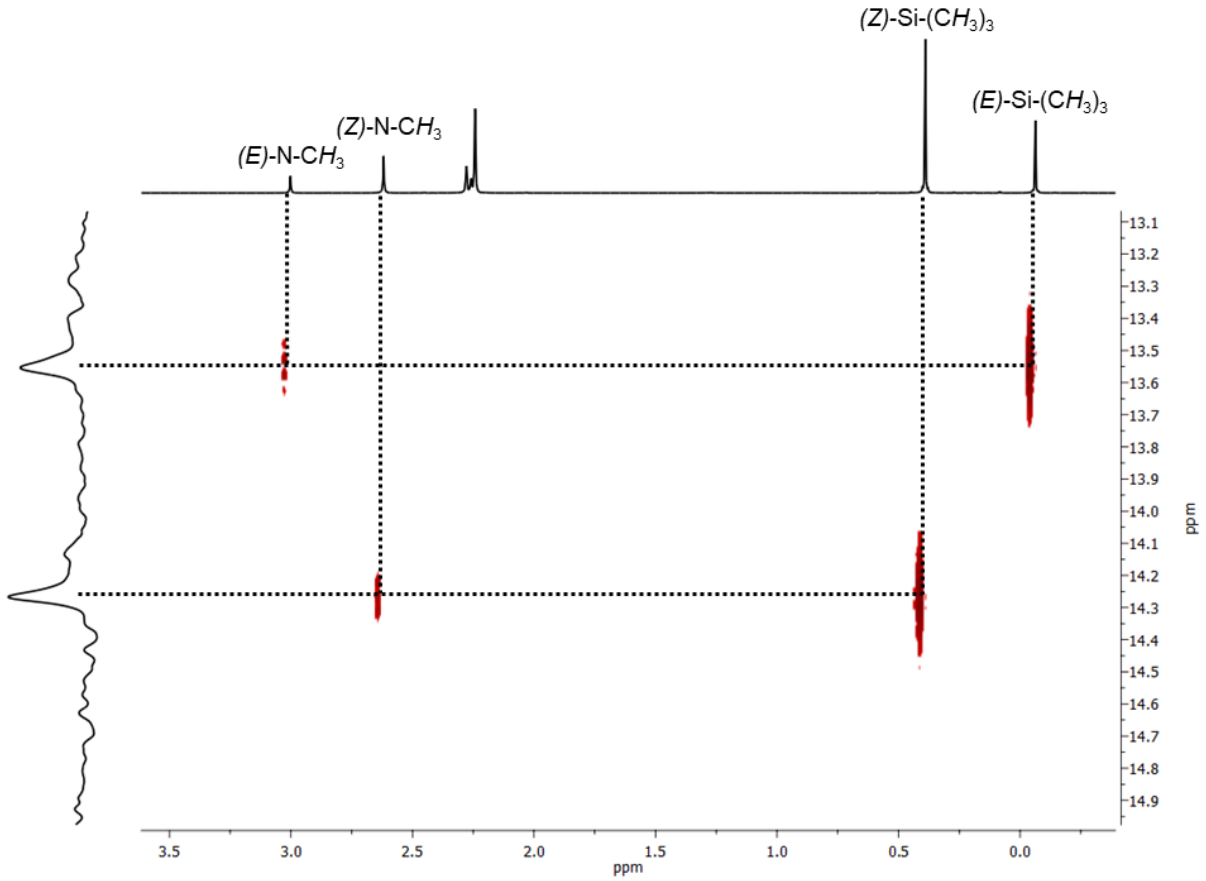

Figure S5.1.10. Detail of $^{1}H,^{29}Si$ HMQC spectrum of **1b** in $CDCl_3$.

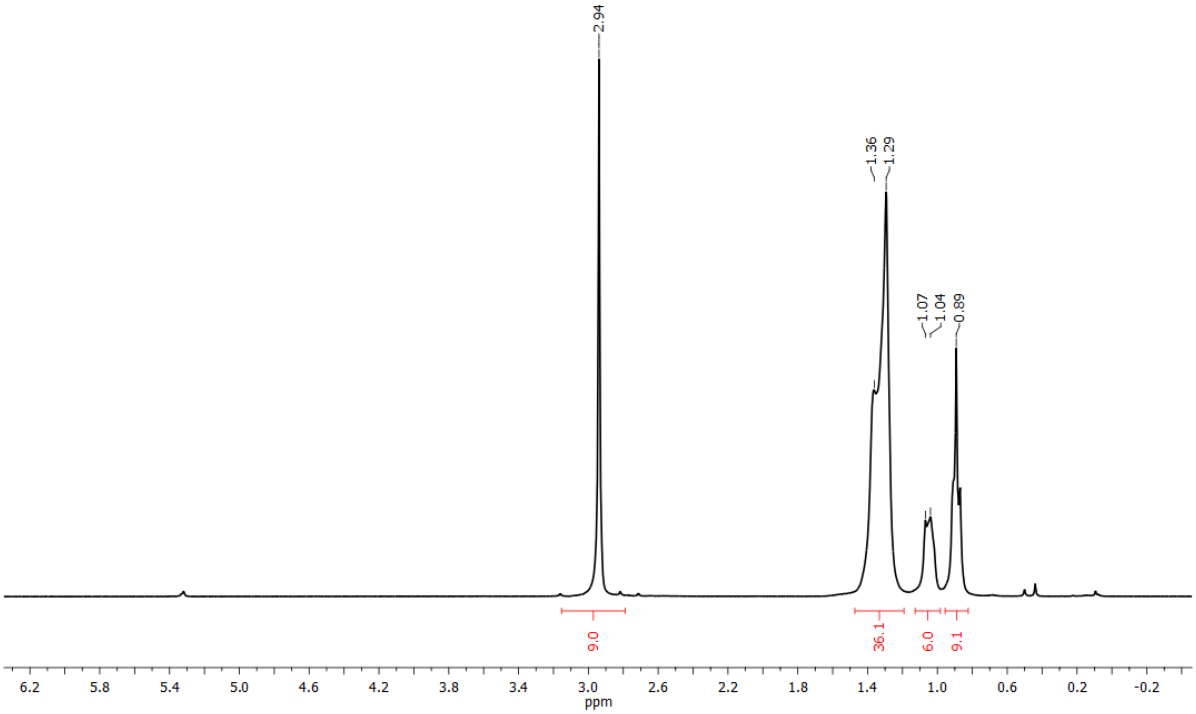

Figure S5.1.11. ^{1}H NMR spectrum (300 MHz) of **2a** in CD_2Cl_2.

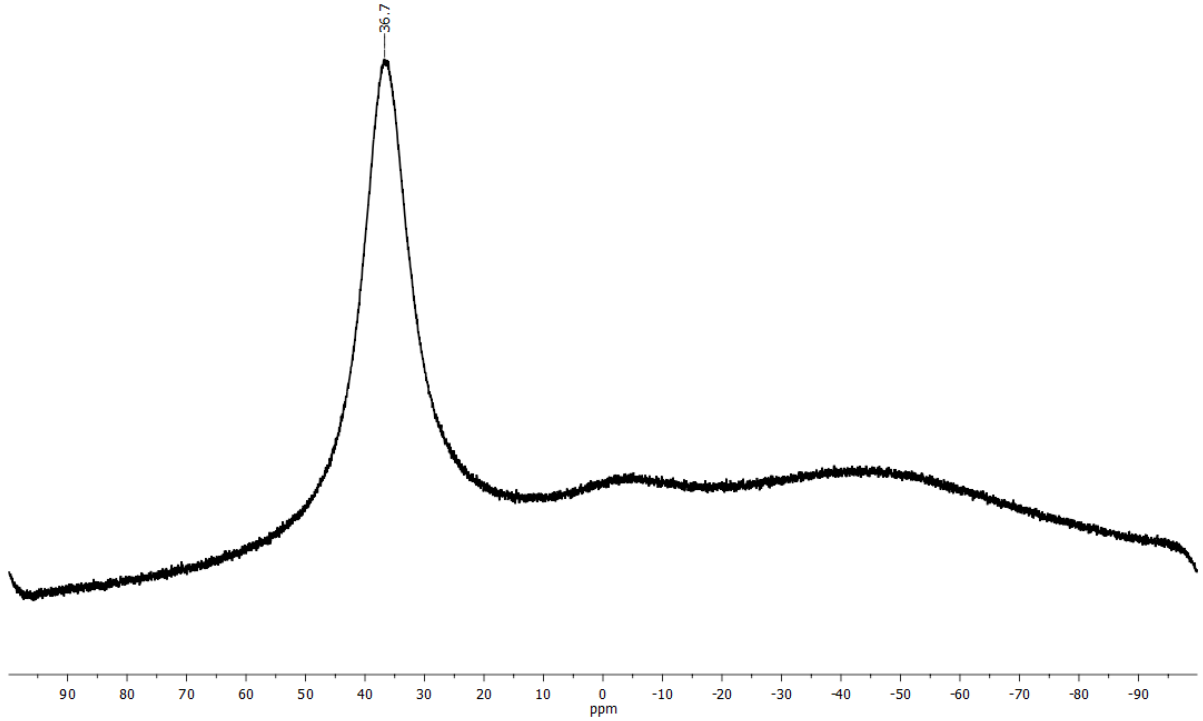

Figure S5.1.12. $^{11}B\{^{1}H\}$ NMR spectrum (96 MHz) of **2a** in CD_2Cl_2.

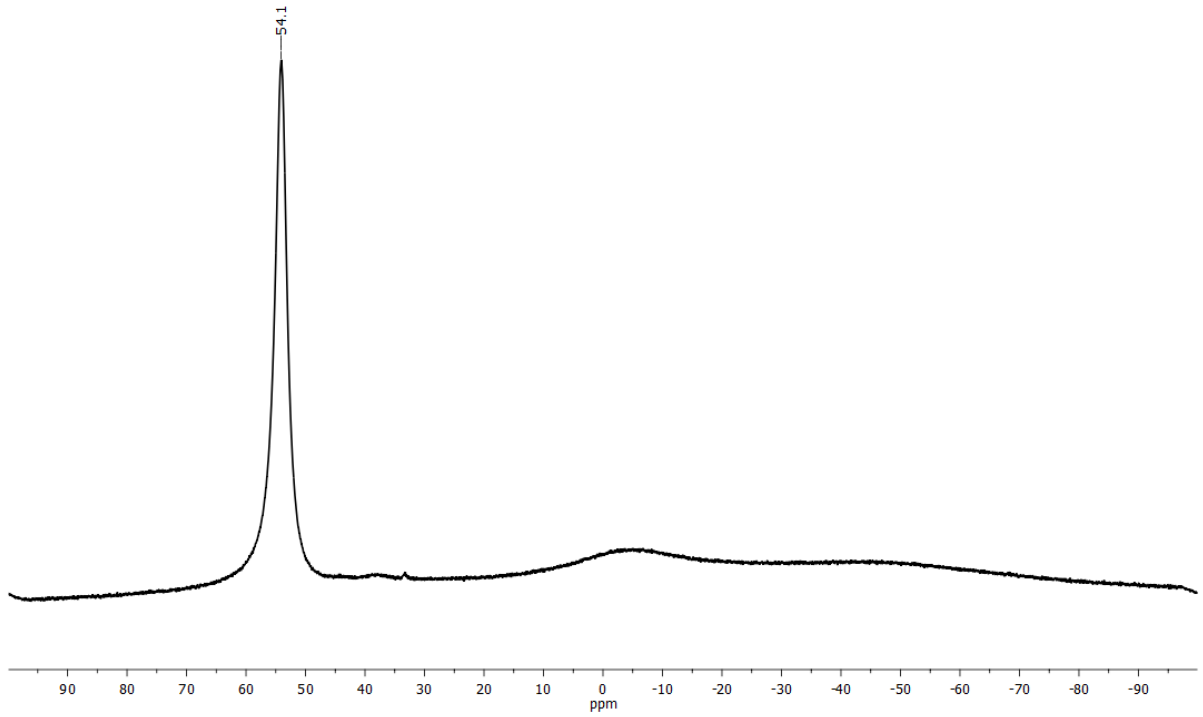

Figure S5.1.13. $^{11}B\{^{1}H\}$ NMR spectrum (96 MHz) of the reaction of **1a** to **3a** in the presence of 5 mol% $Ag[Al\{OC(CF_3)_3\}_4]$ in CH_2Cl_2 after 10 min.

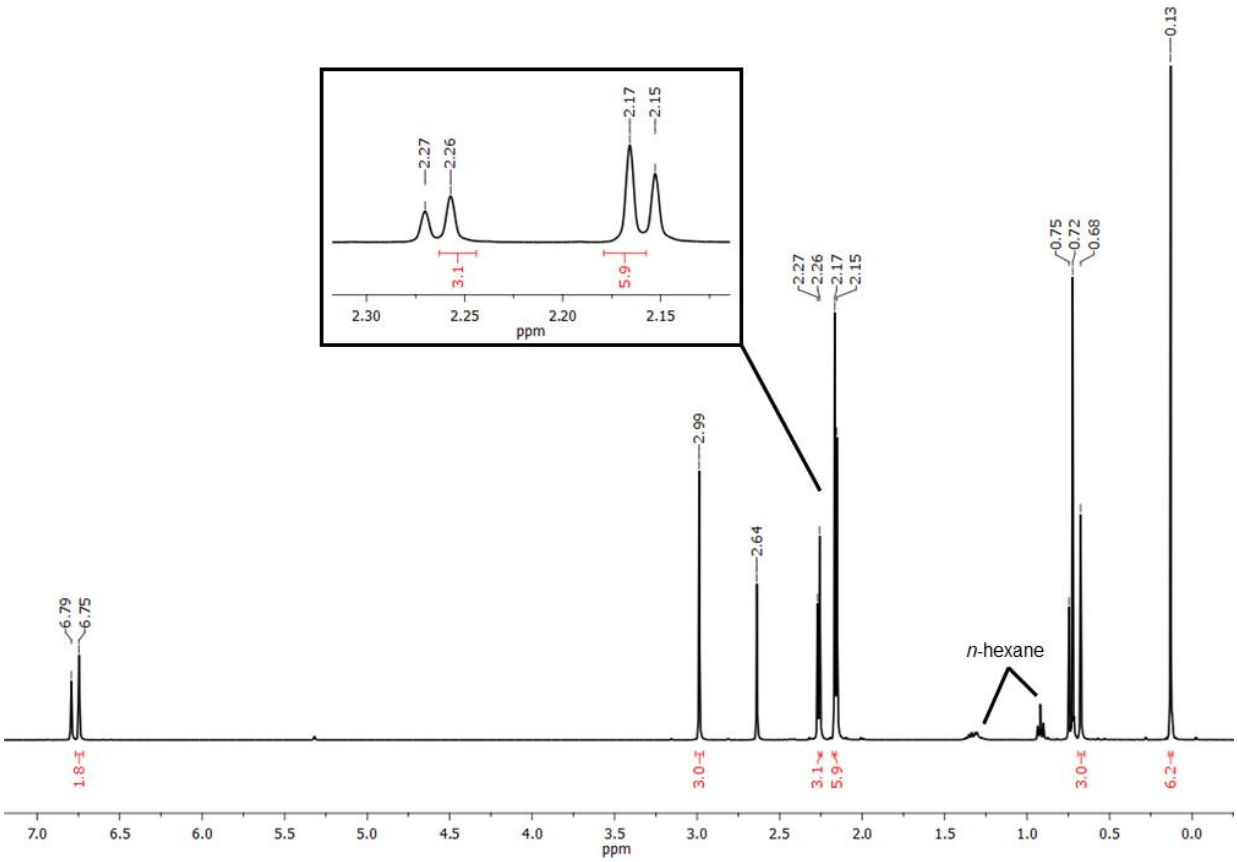

Figure S5.1.14. ^{1}H NMR spectrum (400 MHz) of **3b** in CD_2Cl_2 with integrals for (*Z*)-**3b**.

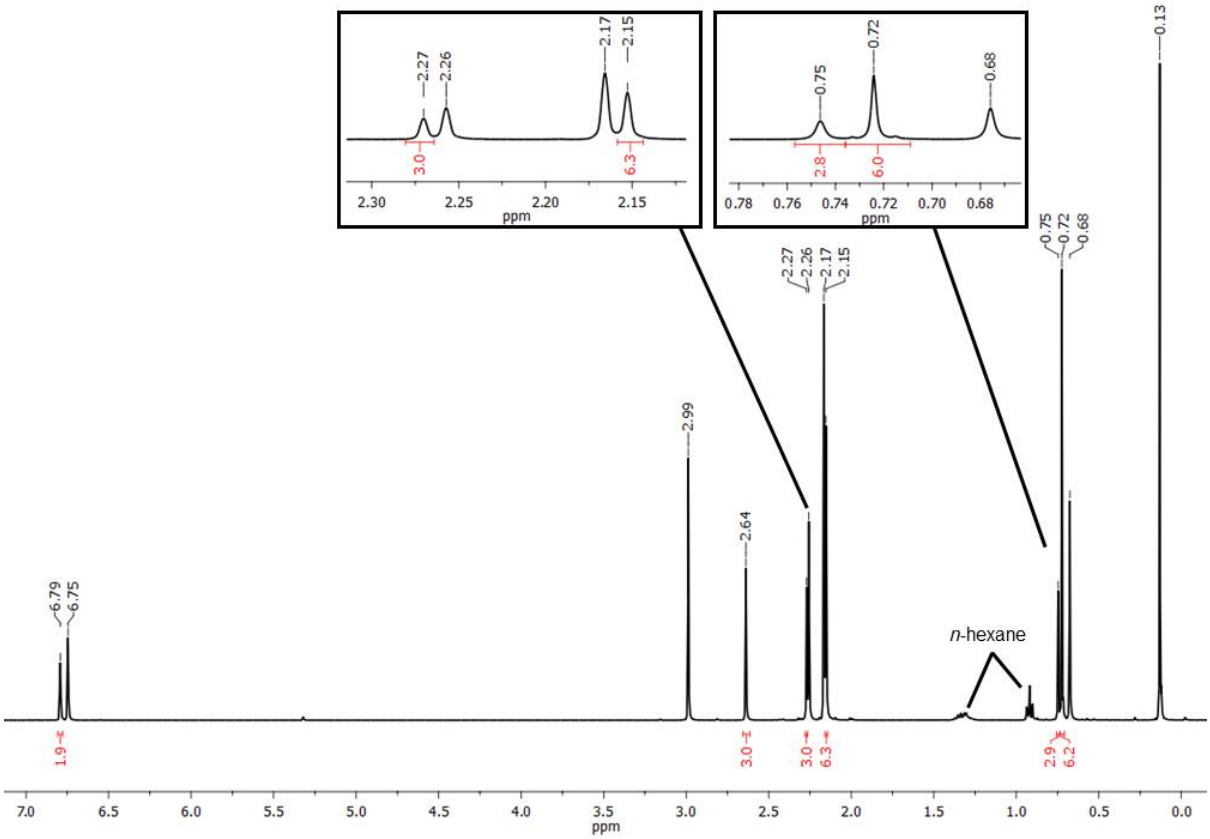

Figure S5.1.15. ^{1}H NMR spectrum (400 MHz) of **3b** in CD_2Cl_2 with integrals for (*E*)-**3b**.

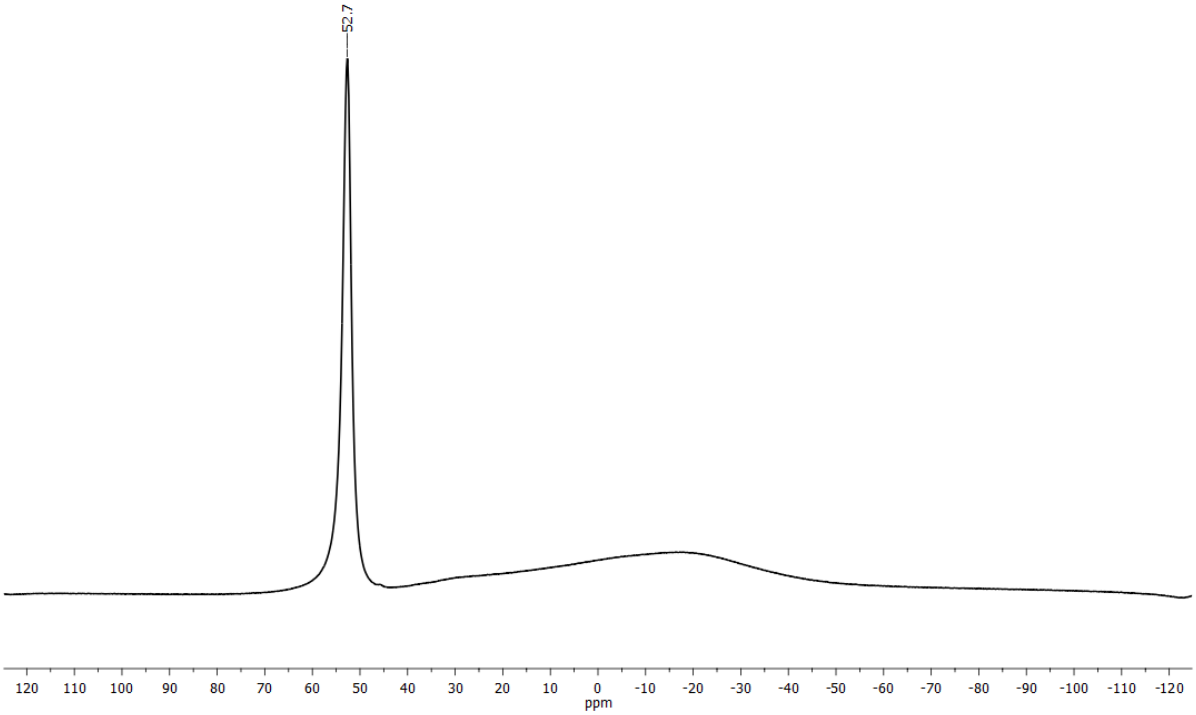

Figure S5.1.16. $^{11}B\{^{1}H\}$ NMR spectrum (128 MHz) of **3b** in CD_2Cl_2.

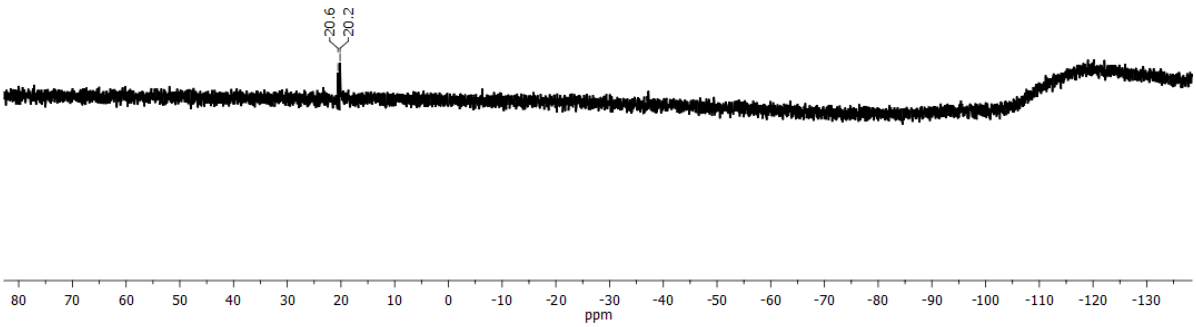

Figure S5.1.17. $^{29}Si\{^{1}H\}$ NMR spectrum (60 MHz) of **3b** in CD_2Cl_2.

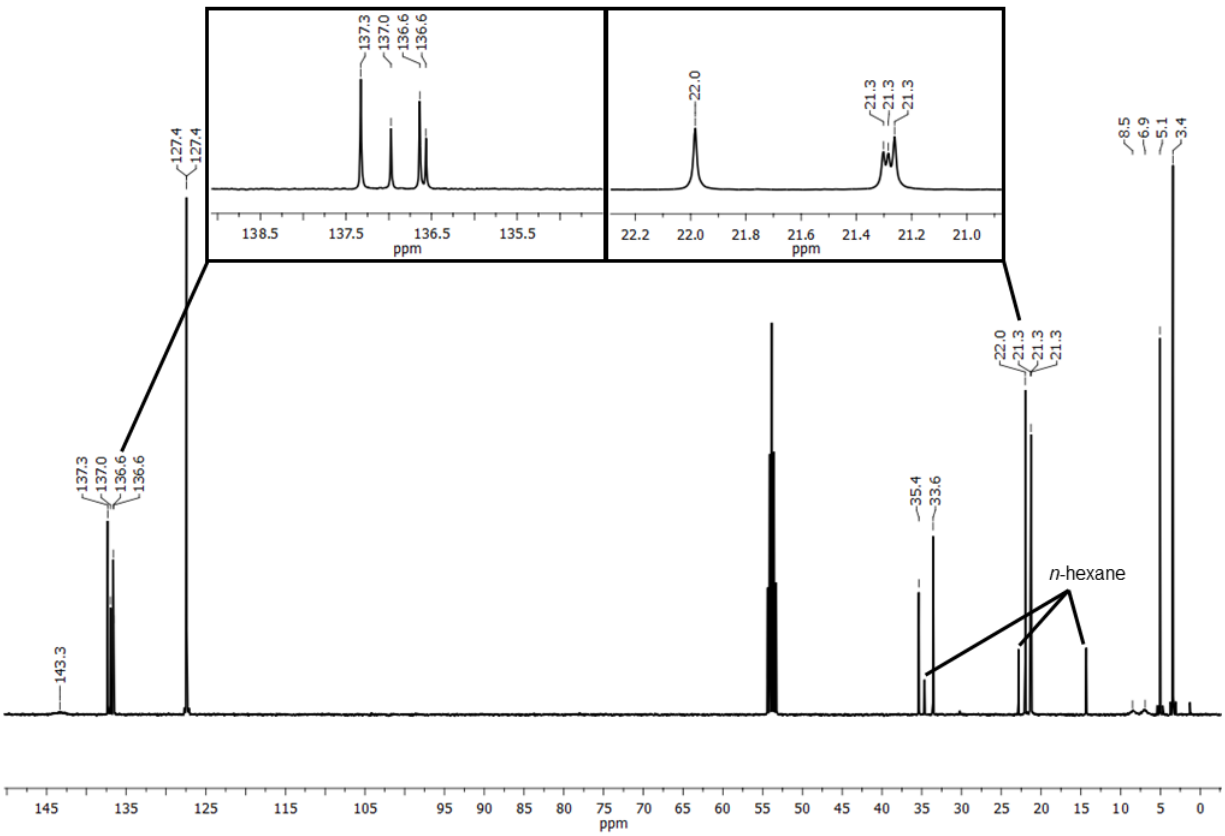

Figure S5.1.18. $^{13}C\{^{1}H\}$ NMR spectrum (100 MHz) of **3b** in CD_2Cl_2.

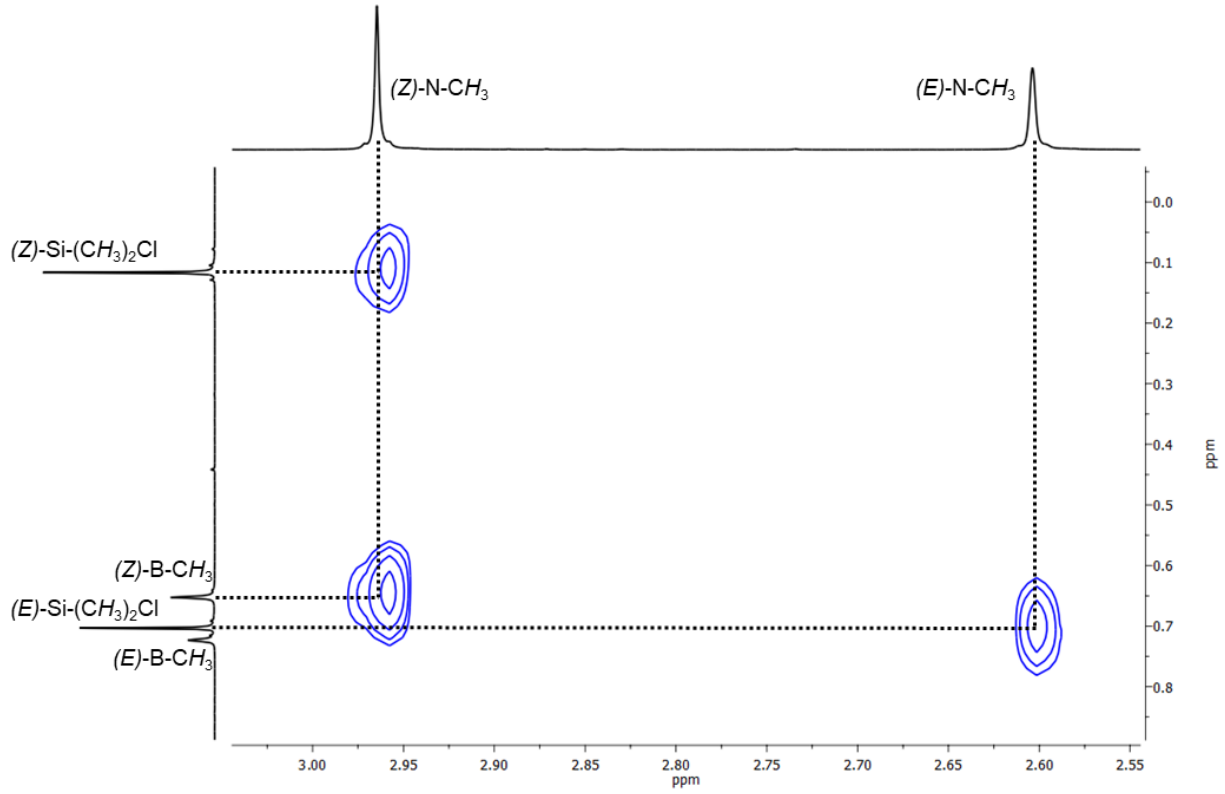

Figure S5.1.19. Detail of $^{1}H,^{1}H$ NOESY spectrum of **3b** in CD_2Cl_2.

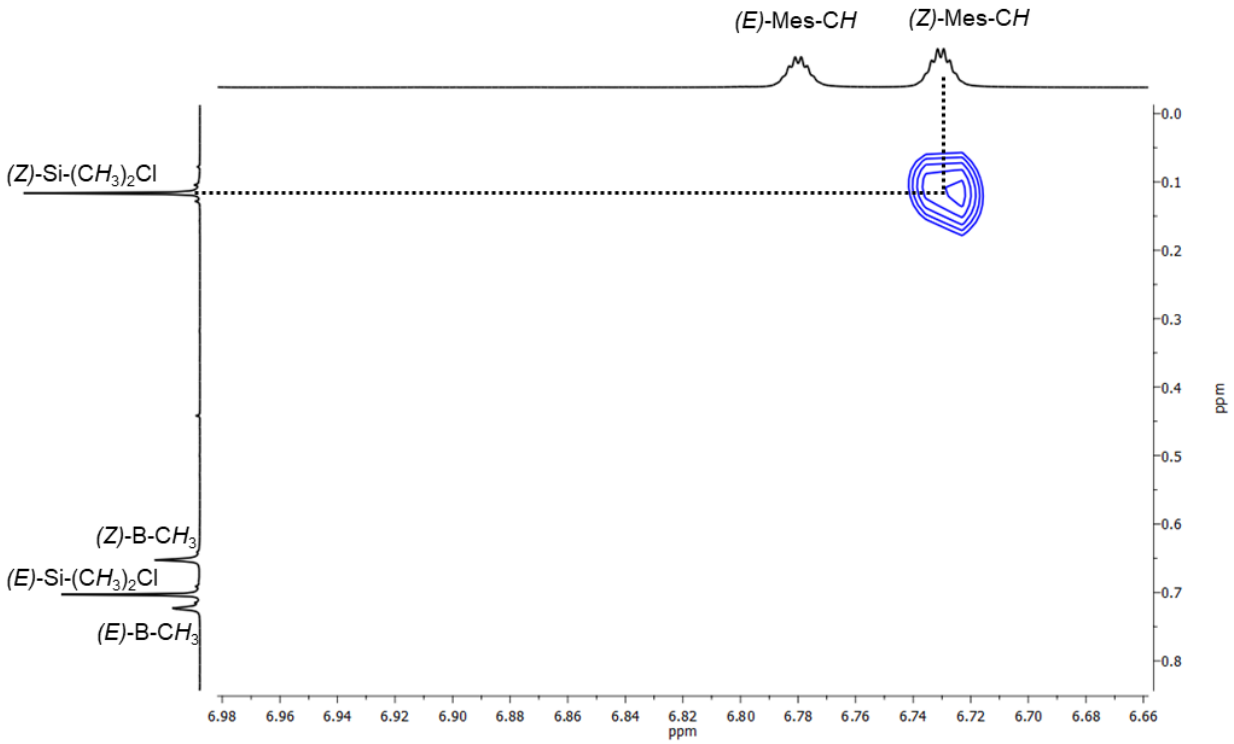

Figure S5.1.20. Detail of $^{1}H,^{1}H$ NOESY spectrum of **3b** in CD_2Cl_2.

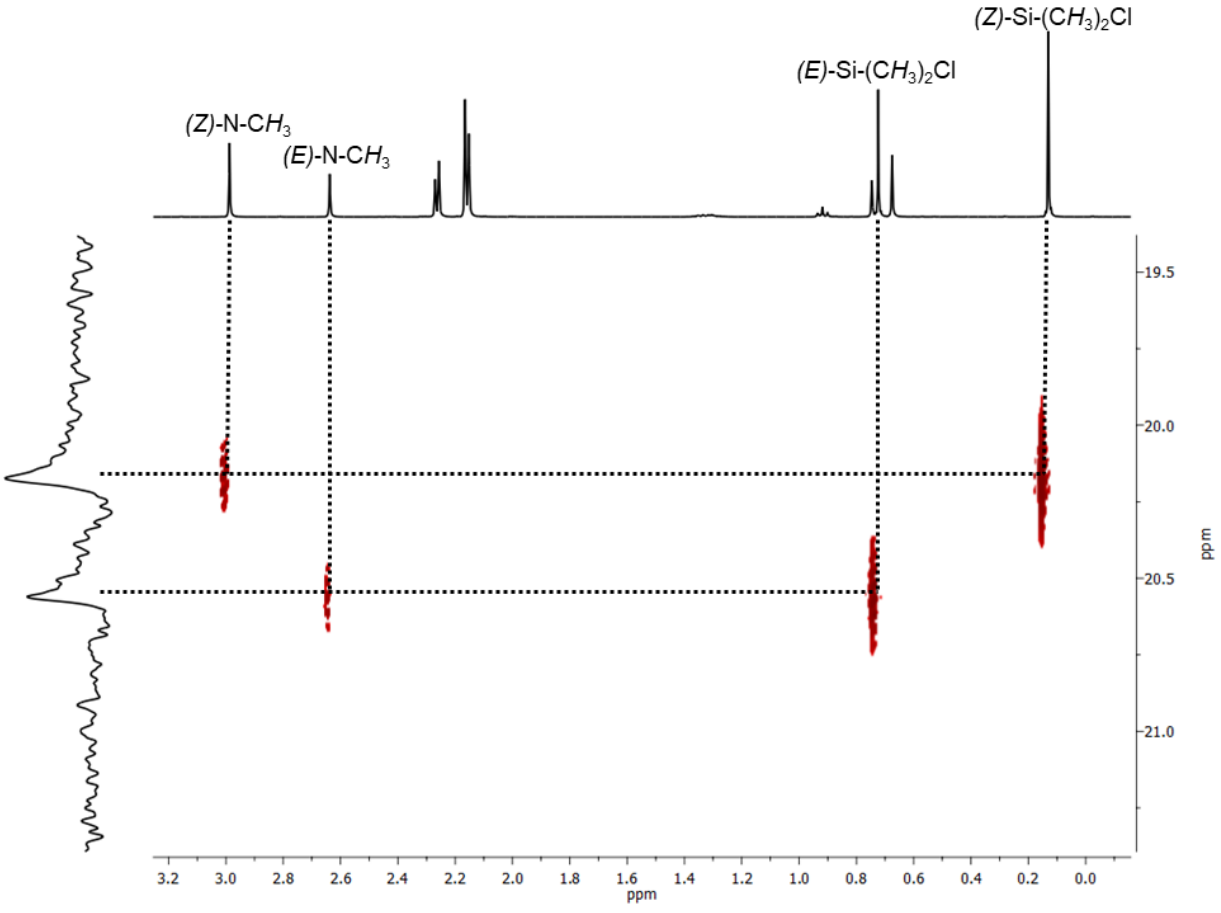

Figure S5.1.21. Detail of $^{1}H,^{29}Si$ HMQC spectrum of **3b** in CD_2Cl_2.

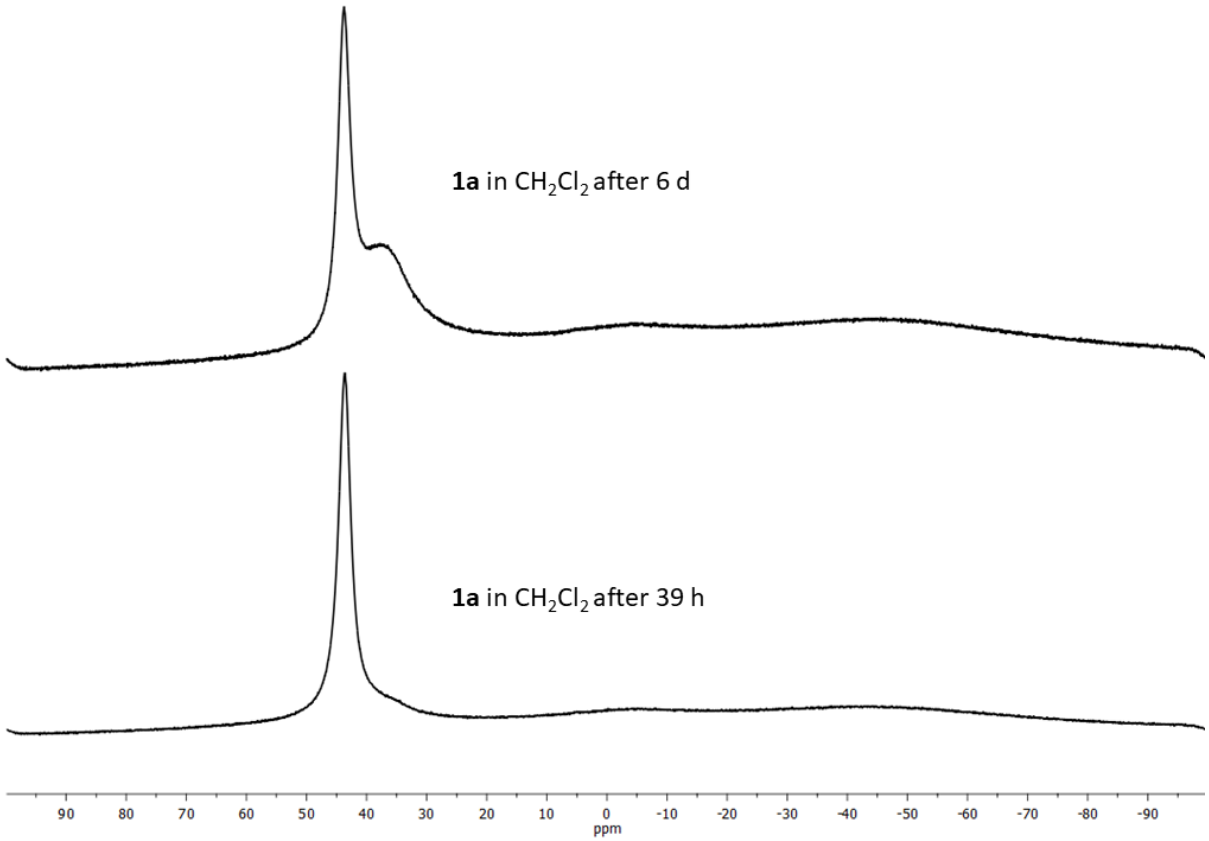

Figure S5.1.22. $^{11}B\{^{1}H\}$ NMR spectra (96 MHz) of **1a** in CH_2Cl_2 after 39 h and 6 d.

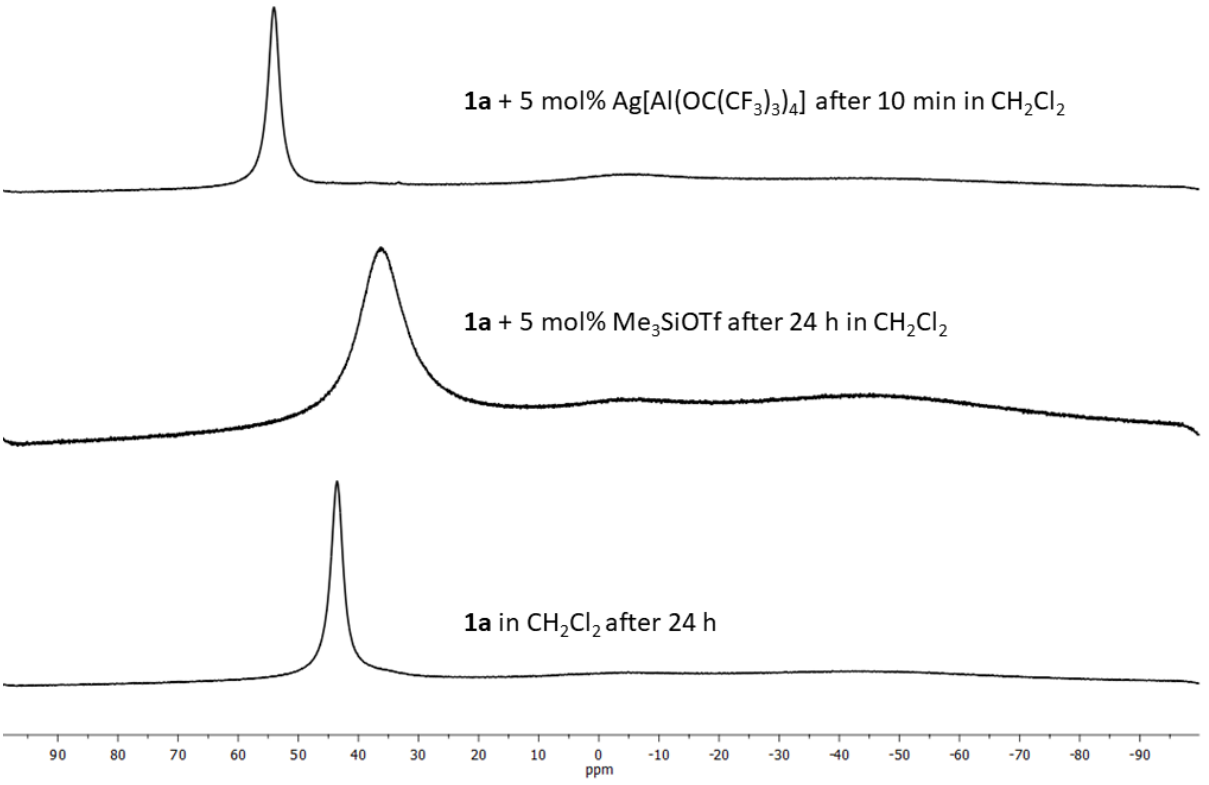

Figure S5.1.23. $^{11}B\{^{1}H\}$ NMR spectra (96 MHz) of **1a** in CH_2Cl_2 and of **1a** in the presence of 5 mol% Me_3SiOTf or $Ag[Al\{OC(CF_3)_3\}_4]$ in CH_2Cl_2.

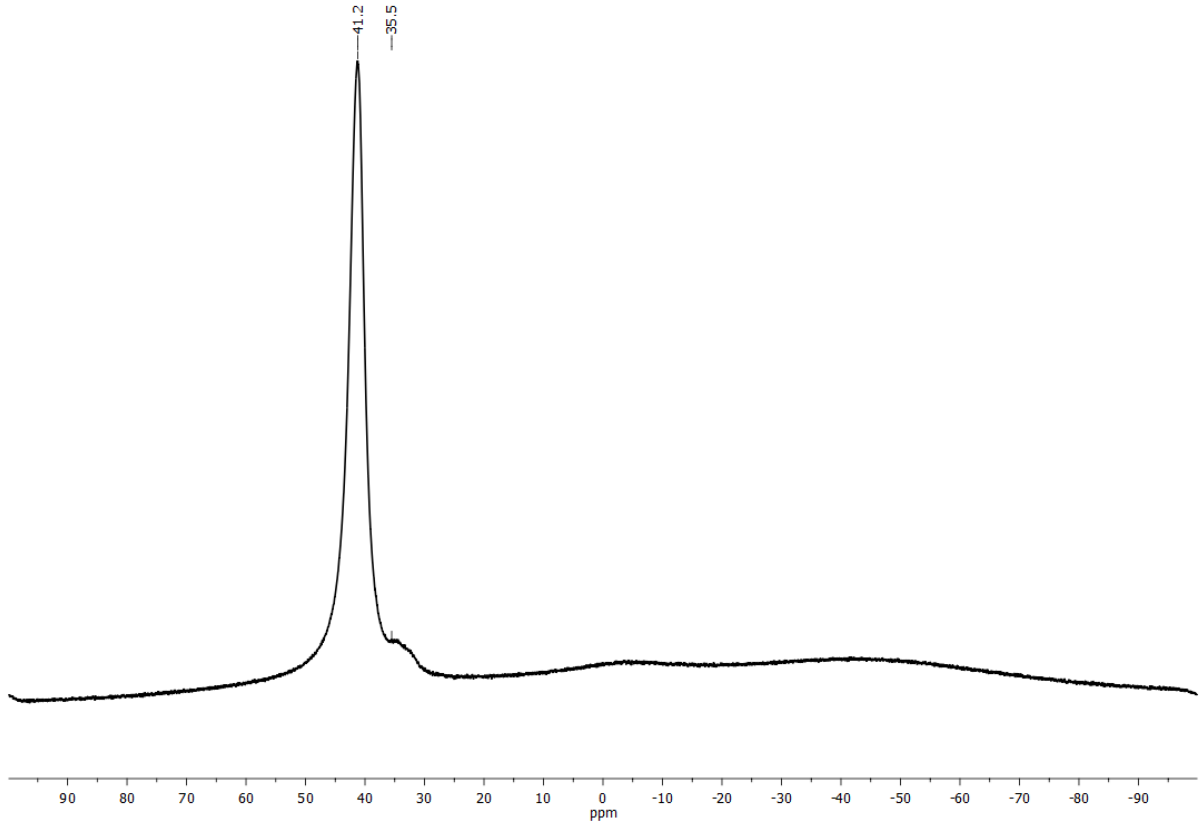

Figure S5.1.24. $^{11}B\{^{1}H\}$ NMR spectrum (96 MHz) of the reaction of **1b** in the presence of 5 mol% Me_3SiOTf in CD_2Cl_2 after 14 d.

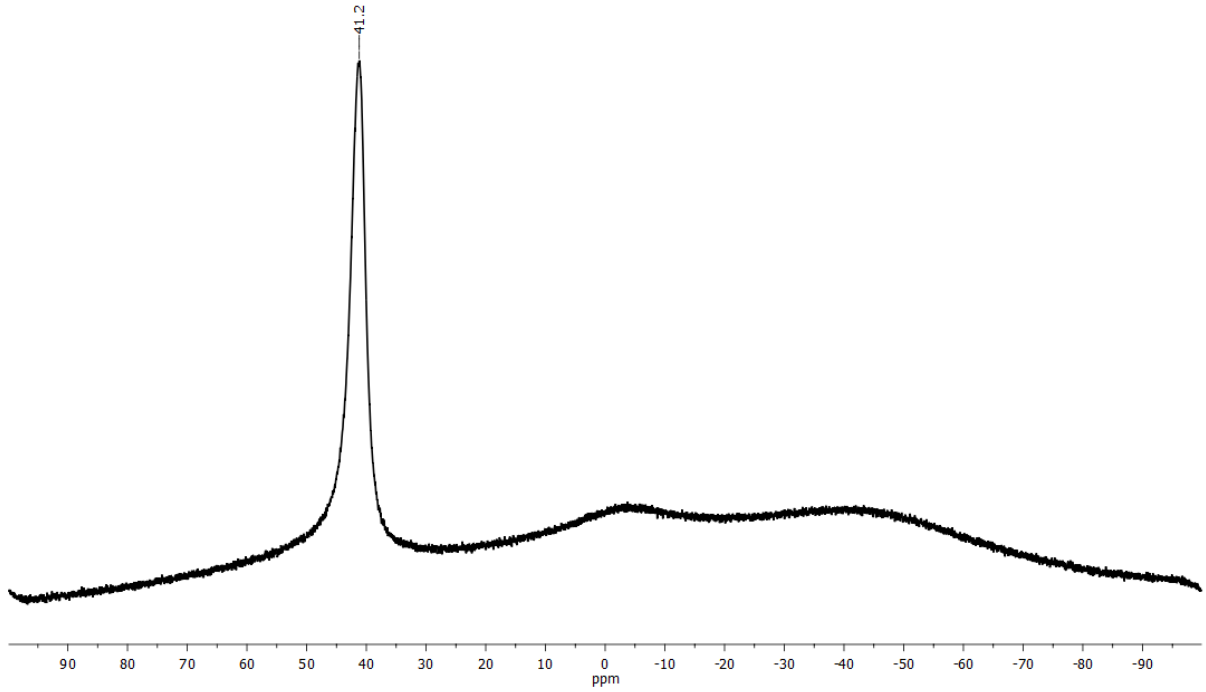

Figure S5.1.25. $^{11}B\{^{1}H\}$ NMR spectrum (96 MHz) of the reaction of **1b** in the presence of 1 mol% $Ag[Al\{OC(CF_3)_3\}_4]$ in CD_2Cl_2 after 12 d.

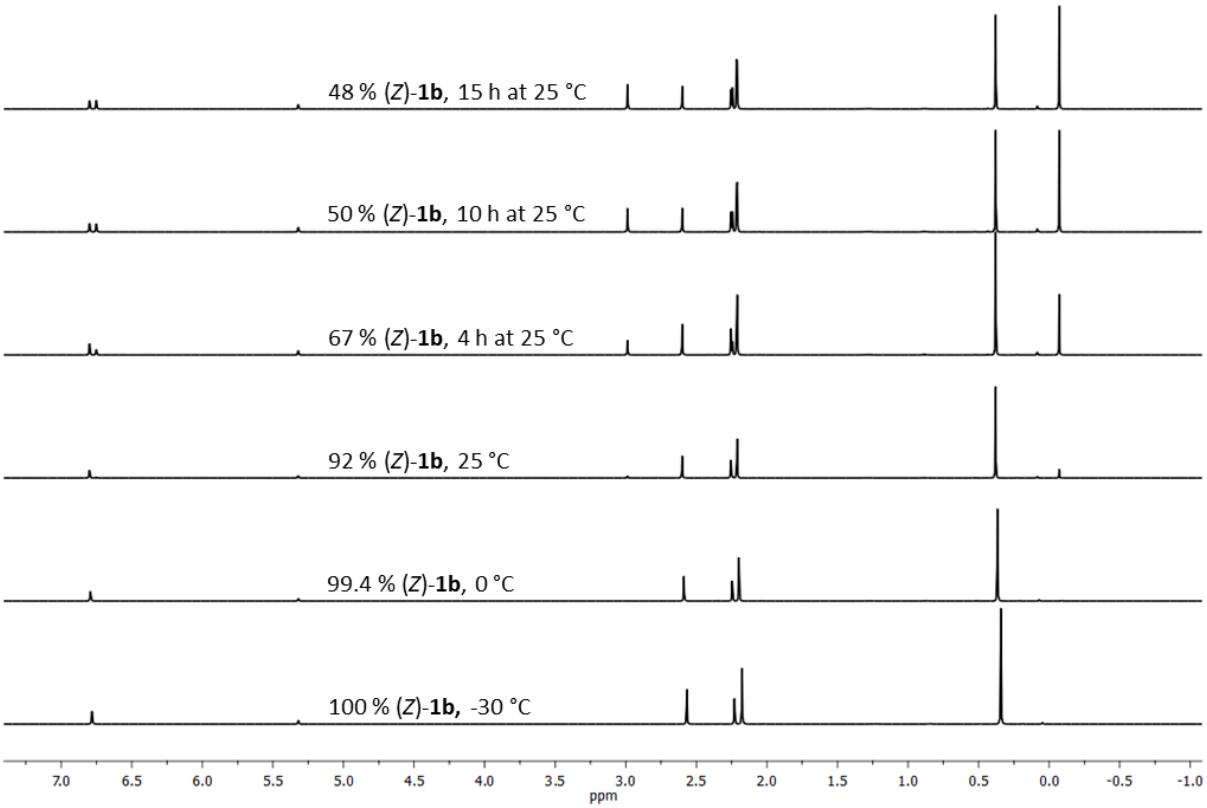

Figure S5.1.26. Isomerization of (*Z*)-**1b** to (*E*/*Z*)-**1b** between −30 °C and 25 °C in CD_2Cl_2.

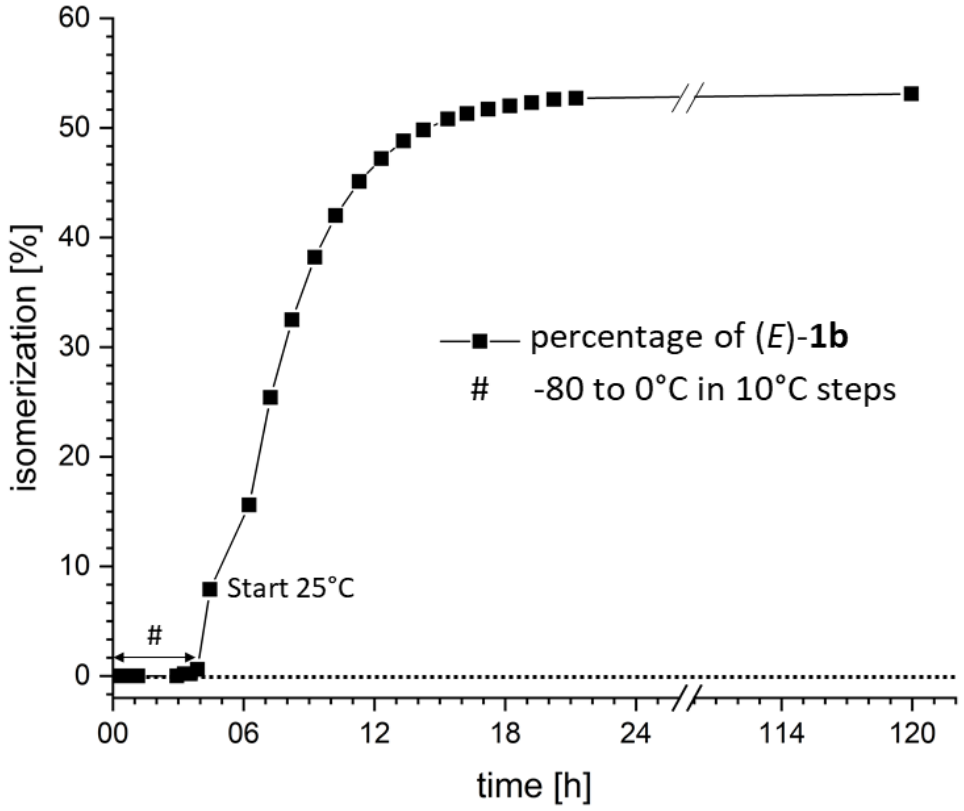

Figure S5.1.27. Progress of the isomerization of (*Z*)-**1b** to (*E*/*Z*)-**1b** between −80 °C and 25 °C in CD_2Cl_2.

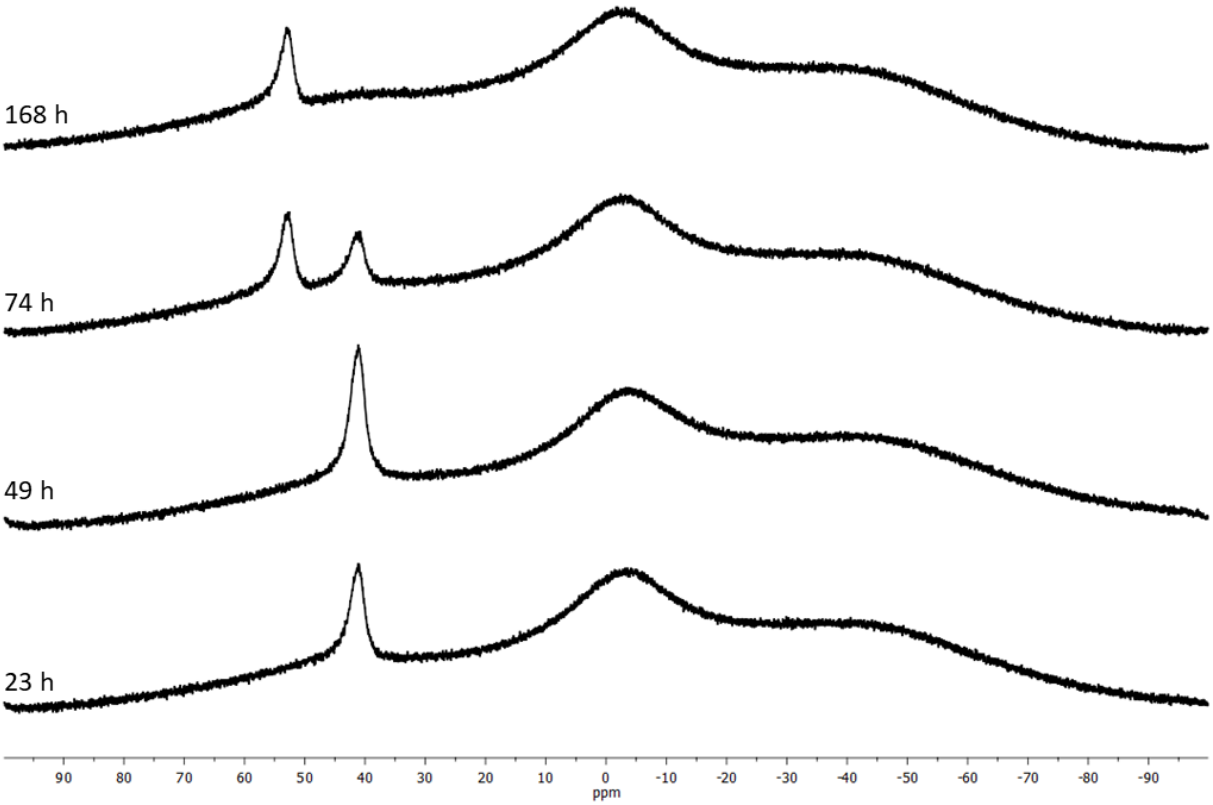

Figure S5.1.28. $^{11}B\{^{1}H\}$ NMR spectra (96 MHz) of a stirred reaction of **1b** in the presence of 5 mol% $Ag[Al\{OC(CF_3)_3\}_4]$ in CD_2Cl_2 (0.15 M).

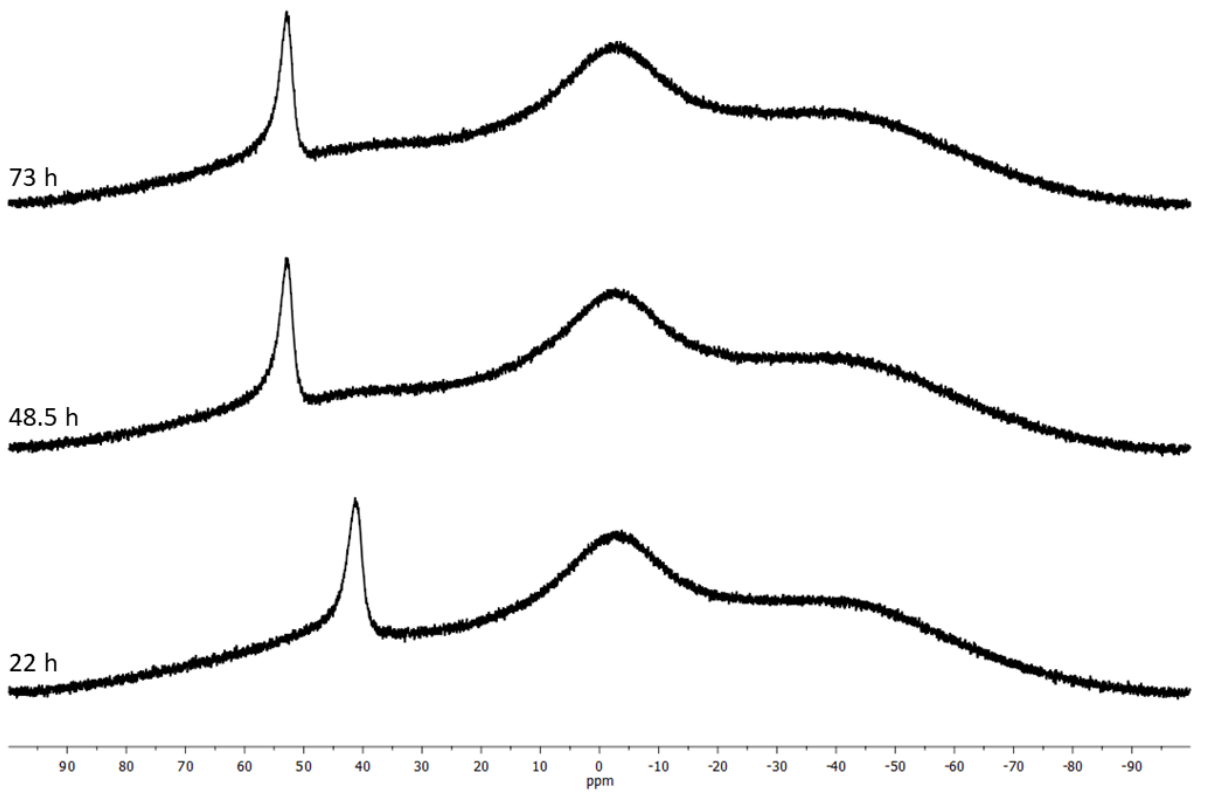

Figure S5.1.29. $^{11}B\{^{1}H\}$ NMR spectra (96 MHz) of a stirred reaction of **1b** in the presence of 5 mol% $Ag[Al\{OC(CF_3)_3\}_4]$ in CD_2Cl_2 (0.075 M).

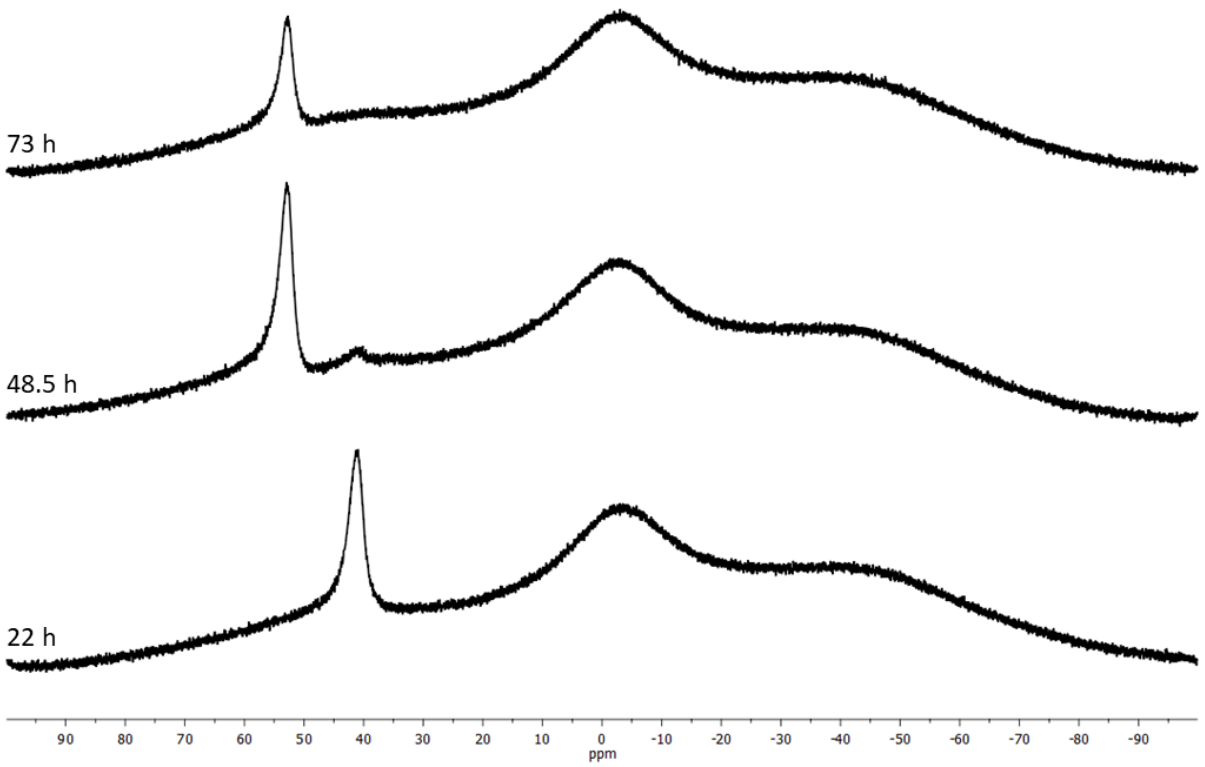

Figure S5.1.30. $^{11}B\{^{1}H\}$ NMR spectra (96 MHz) of a stirred reaction of **1b** in the presence of 5 mol% $Ag[Al\{OC(CF_3)_3\}_4]$ in CD_2Cl_2 (0.3 M).

HRMS spectra

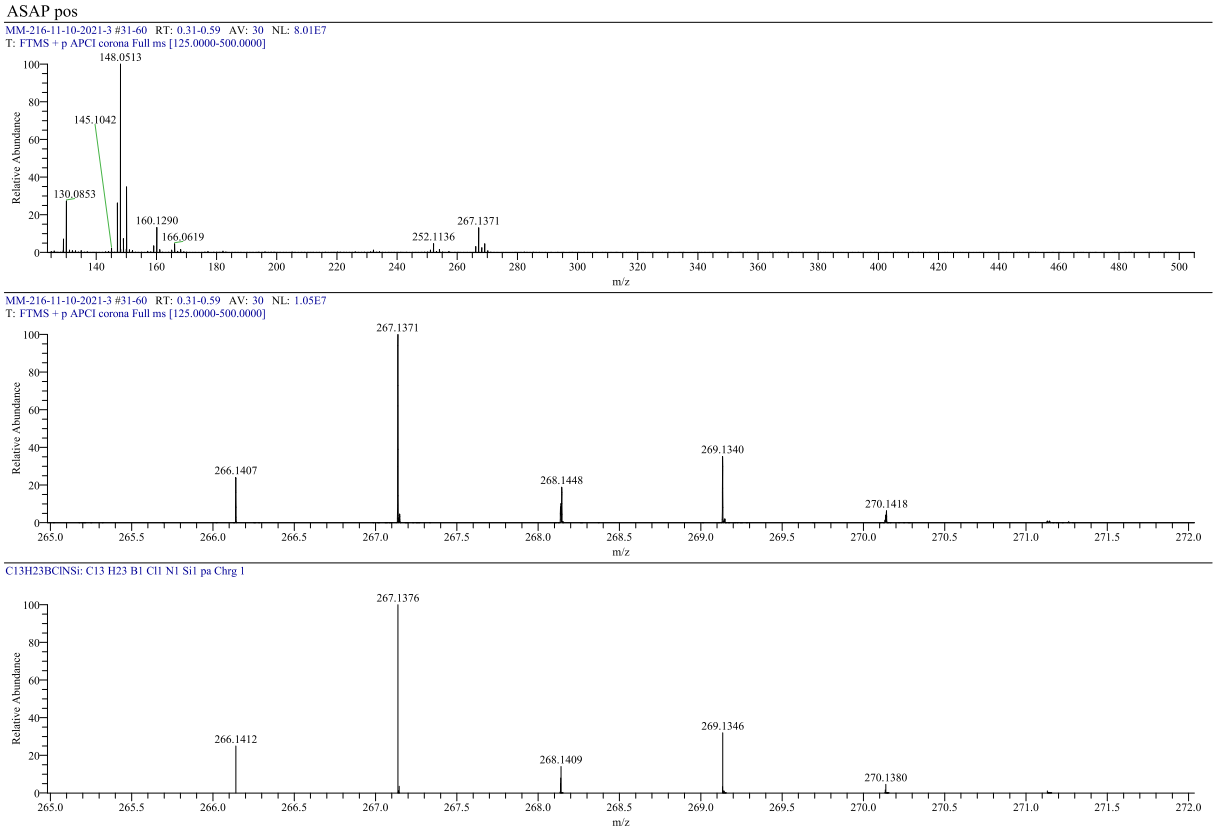

Figure S5.1.31. ASAP spectrum of **1b**.

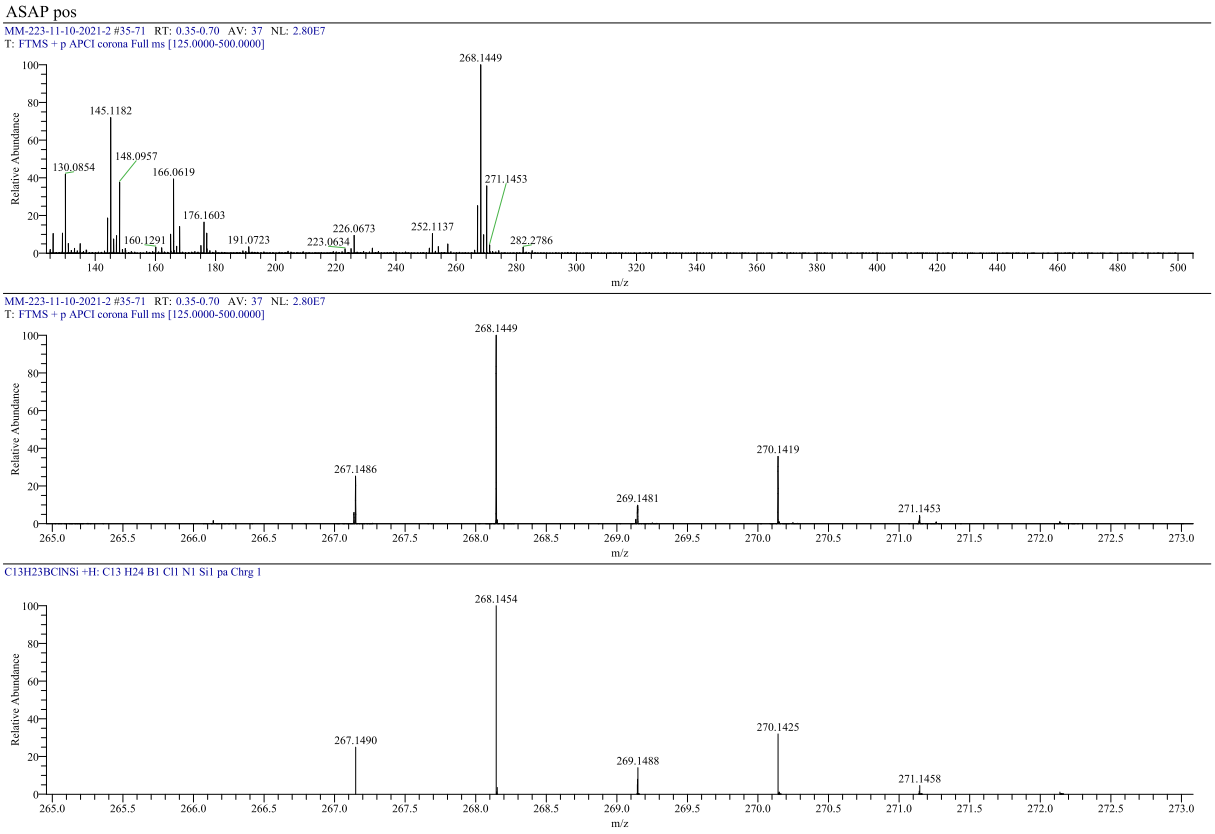

Figure S5.1.32. ASAP spectrum of **3b**.

Cartesian coordinates (Å) and total energies (a.u.) of optimized stationary points

The molecular species were optimized at the ωB97X-D/6-31+G(d,p) level. The total energy is given as the sum of the electronic energy (ωB97X-D/6-311+G(d,p), PCM), the thermal correction to Gibbs Free Energy (ωB97X-D/6-31+G(d,p)), and the concentration correction (1.89 kcal/mol).

(*Z*)-**1b**: Total energy: -1338.40525983326

B	3.075931000	-2.491253000	-0.073385000
N	2.098980000	-3.478685000	0.103692000
C	1.308484000	-3.895509000	-1.066122000
H	1.621834000	-3.340309000	-1.951409000
H	1.438591000	-4.963167000	-1.270404000
H	0.241246000	-3.709420000	-0.908018000
Si	1.719637000	-4.294214000	1.661944000
C	0.336772000	-5.527915000	1.334134000
H	0.622599000	-6.302305000	0.615400000
H	0.096115000	-6.030278000	2.278095000
H	-0.580158000	-5.050152000	0.975105000
C	3.212355000	-5.247023000	2.278918000
H	4.037540000	-4.586568000	2.555248000
H	2.939198000	-5.841072000	3.158493000
H	3.571301000	-5.936730000	1.507256000
C	1.098300000	-3.045599000	2.915563000
H	1.872159000	-2.329715000	3.202220000
H	0.249307000	-2.485476000	2.508780000
H	0.756758000	-3.561818000	3.820004000
C	3.398517000	-1.784686000	-1.443155000
C	4.363375000	-2.325226000	-2.310437000
C	2.719974000	-0.610853000	-1.813152000
C	4.639089000	-1.687804000	-3.520443000
C	3.016889000	0.004463000	-3.029611000
C	3.978340000	-0.517609000	-3.895292000
H	5.385998000	-2.114045000	-4.187442000
H	2.485340000	0.911881000	-3.309751000
C	5.090343000	-3.595641000	-1.936394000
H	5.656285000	-3.466964000	-1.007085000
H	4.387838000	-4.421891000	-1.776639000
H	5.792047000	-3.899077000	-2.717549000
C	1.667709000	-0.025359000	-0.900855000
H	0.862880000	-0.745041000	-0.711018000
H	2.095252000	0.246652000	0.070573000
H	1.218851000	0.872485000	-1.333367000
C	4.314446000	0.179793000	-5.189603000
H	5.122352000	0.905093000	-5.040891000
H	4.646408000	-0.531878000	-5.950929000
H	3.451696000	0.723692000	-5.584681000
Cl	4.068437000	-1.952094000	1.345538000

(*Z*)-**1b^{Ag}**:

Total energy (SDD/ECP for Ag): -1485.27118810326

B	-0.790987000	0.037122000	-0.011389000

N	-1.890542000	0.861594000	0.062200000
C	-1.663142000	2.315645000	0.176856000
H	-0.595691000	2.543886000	0.192221000
H	-2.112410000	2.844780000	-0.667605000
H	-2.107161000	2.704239000	1.096951000
Si	-3.643194000	0.328730000	0.028224000
C	-4.693483000	1.873834000	0.141684000
H	-4.543031000	2.557586000	-0.699119000
H	-5.744775000	1.564924000	0.120978000
H	-4.540348000	2.429665000	1.071559000
C	-3.966295000	-0.531604000	-1.601389000
H	-3.441736000	-1.485728000	-1.695718000
H	-5.038776000	-0.733196000	-1.699646000
H	-3.674352000	0.106413000	-2.442412000
C	-3.958450000	-0.756643000	1.519041000
H	-3.431490000	-1.712997000	1.473161000
H	-3.664494000	-0.245116000	2.441818000
H	-5.030068000	-0.973214000	1.591354000
C	0.731364000	0.499237000	0.004489000
C	1.368695000	0.907467000	-1.205780000
C	1.427577000	0.659828000	1.238644000
C	2.656254000	1.440263000	-1.156201000
C	2.725655000	1.190817000	1.232487000
C	3.349732000	1.593626000	0.051453000
H	3.129737000	1.759708000	-2.081515000
H	3.244108000	1.316696000	2.179557000
C	0.613651000	0.852979000	-2.512212000
H	0.045007000	-0.075204000	-2.627185000
H	-0.104783000	1.678776000	-2.563272000
H	1.287096000	0.946139000	-3.366495000
C	0.729930000	0.396263000	2.553565000
H	0.152004000	1.280638000	2.843977000
H	0.028994000	-0.442291000	2.501420000
H	1.446118000	0.194113000	3.352968000
C	4.732810000	2.187394000	0.060712000
H	5.420216000	1.586004000	-0.542371000
H	4.721659000	3.194599000	-0.366668000
H	5.136200000	2.253047000	1.073156000
Cl	-1.006270000	-1.797743000	-0.146750000
Ag	1.710472000	-1.687776000	-0.052895000

4b: Total energy: -877.951005113263

B	0.400904000	0.046753000	0.667361000
N	1.707287000	0.048437000	0.876087000
C	2.316800000	0.085414000	2.226564000
H	2.932852000	-0.804049000	2.370685000
H	2.939196000	0.977260000	2.319613000
H	1.547573000	0.110524000	2.999236000
Si	2.825786000	-0.001944000	-0.596897000
C	3.853271000	1.548882000	-0.501033000
H	4.503291000	1.561557000	0.379109000
H	4.501951000	1.615828000	-1.381103000
H	3.228108000	2.447043000	-0.482407000
C	3.821126000	-1.566496000	-0.418788000
H	3.177350000	-2.448900000	-0.349967000
H	4.466407000	-1.694823000	-1.294515000
H	4.472491000	-1.544877000	0.460195000
C	1.677820000	-0.027161000	-2.070364000
H	1.028629000	-0.908720000	-2.088119000
H	1.049186000	0.867303000	-2.130610000
H	2.281542000	-0.056487000	-2.984106000
C	-1.042490000	0.021227000	0.384648000
C	-1.716829000	-1.233906000	0.287402000
C	-1.744933000	1.240289000	0.193533000
C	-3.067697000	-1.232250000	0.000152000
C	-3.103640000	1.184475000	-0.093096000
C	-3.778192000	-0.034050000	-0.191761000
H	-3.598015000	-2.177087000	-0.080941000
H	-3.651844000	2.110209000	-0.244297000
C	-0.973967000	-2.527447000	0.503810000
H	-0.074969000	-2.587248000	-0.119126000
H	-0.665355000	-2.633559000	1.549340000
H	-1.600763000	-3.386167000	0.258217000
C	-1.063650000	2.579240000	0.300620000
H	-1.440414000	3.128984000	1.168571000
H	0.022405000	2.497183000	0.406355000
H	-1.268560000	3.187537000	-0.584493000
C	-5.246819000	-0.083180000	-0.499012000
H	-5.428804000	-0.670466000	-1.404342000
H	-5.789884000	-0.569679000	0.317353000
H	-5.665939000	0.913718000	-0.644456000

$TS_{4\rightarrow5}$: Total energy: -877.926654057263

B	0.590848000	0.001242000	0.095424000
N	1.679879000	-0.003173000	0.981070000
C	1.541694000	-0.007860000	2.438011000
H	2.016538000	-0.904679000	2.881999000
H	2.018933000	0.884730000	2.887951000
H	0.479445000	-0.007405000	2.755230000
Si	2.915060000	-0.000592000	-0.276288000
C	3.918562000	1.524908000	-0.394506000
H	4.574509000	1.621993000	0.496542000
H	4.595894000	1.518978000	-1.270396000
H	3.333477000	2.458898000	-0.447122000
C	3.914066000	-1.528141000	-0.405487000
H	3.326174000	-2.460003000	-0.464259000
H	4.590956000	-1.518152000	-1.281682000
H	4.570172000	-1.633298000	0.484519000
C	1.424181000	0.006126000	-1.564877000
H	0.852547000	-0.889327000	-1.892582000
H	0.853159000	0.904459000	-1.885883000
H	2.269764000	0.009109000	-2.328448000
C	-0.929415000	0.002852000	0.000992000
C	-1.621003000	-1.220103000	-0.026775000
C	-1.620019000	1.224882000	-0.025237000
C	-3.018179000	-1.212431000	-0.081851000
C	-3.018814000	1.218259000	-0.080478000
C	-3.723976000	0.003899000	-0.110155000
H	-3.569654000	-2.151974000	-0.102234000
H	-3.567168000	2.159604000	-0.099791000
C	-0.889411000	-2.522776000	-0.012914000
H	0.086429000	-2.483970000	0.484013000
H	-1.463986000	-3.305476000	0.512871000
H	-0.738444000	-2.900989000	-1.036031000
C	-0.890379000	2.528534000	-0.009253000
H	-1.451190000	3.299610000	0.547814000
H	0.100401000	2.484529000	0.456265000
H	-0.771716000	2.925825000	-1.029618000
C	-5.211821000	-0.006740000	-0.164377000
H	-5.590067000	-0.645493000	-0.978145000
H	-5.643378000	-0.401316000	0.770450000
H	-5.649944000	0.990193000	-0.316593000

(*E*)-**5b**: Total energy: -877.930722751263

B	2.614670000	-2.709315000	-0.273437000
N	2.053072000	-3.975065000	-0.195933000
C	1.722541000	-4.908099000	-1.266128000
H	2.315262000	-5.820902000	-1.169860000
H	0.662426000	-5.167912000	-1.231417000
H	1.941583000	-4.440082000	-2.227641000
Si	1.997458000	-3.891600000	1.516446000
C	3.239870000	-4.884308000	2.455353000
H	4.235554000	-4.806019000	2.009749000
H	3.294612000	-4.578344000	3.504654000
H	2.949204000	-5.940930000	2.436994000
C	0.342993000	-3.634722000	2.296252000

H	-0.233933000	-4.564937000	2.241043000
H	0.430514000	-3.366054000	3.353564000
H	-0.228813000	-2.858843000	1.779249000
C	2.842697000	-1.987226000	1.288235000
H	2.660009000	-2.163314000	2.368371000
H	3.919958000	-1.801699000	1.254537000
H	2.294059000	-1.055606000	1.121075000
C	3.103208000	-1.859044000	-1.467915000
C	4.335729000	-2.177609000	-2.078373000
C	2.330735000	-0.792421000	-1.956881000
C	4.771273000	-1.419341000	-3.158627000
C	2.796960000	-0.058811000	-3.048545000
C	4.014363000	-0.353815000	-3.659265000
H	5.720573000	-1.661414000	-3.630478000
H	2.193344000	0.759514000	-3.433190000
C	5.170255000	-3.331012000	-1.570329000
H	5.401359000	-3.228587000	-0.502573000
H	4.656494000	-4.289308000	-1.708055000
H	6.123666000	-3.393518000	-2.098372000
C	1.013190000	-0.418146000	-1.317470000
H	0.517774000	-1.277970000	-0.851305000
H	1.148602000	0.355121000	-0.551312000
H	0.318075000	-0.012376000	-2.056077000
C	4.514971000	0.444976000	-4.833237000
H	5.461486000	0.937831000	-4.590386000
H	4.695654000	-0.203035000	-5.696159000
H	3.799389000	1.214434000	-5.130389000

(*Z*)-**5b**: Total energy: -877.955903011263

B	2.565277000	-2.631704000	-0.564046000
N	2.101556000	-3.921877000	-0.267563000
C	1.693394000	-5.013278000	-1.139490000
H	2.317759000	-5.894913000	-0.971631000
H	0.650774000	-5.285305000	-0.954382000
H	1.791748000	-4.714843000	-2.184675000
Si	2.200300000	-3.711581000	1.457370000
C	3.468577000	-4.718729000	2.370796000
H	4.375122000	-4.910784000	1.795221000
H	3.746572000	-4.226626000	3.308796000
H	3.022599000	-5.685280000	2.631513000
C	0.602787000	-3.679558000	2.408270000
H	0.333241000	-4.709252000	2.669351000
H	0.725262000	-3.128764000	3.346814000
H	-0.229773000	-3.244050000	1.853962000
C	2.804395000	-1.917932000	-1.932962000
H	2.570512000	-2.540130000	-2.800457000
H	2.200913000	-1.004710000	-1.997532000
H	3.848562000	-1.594462000	-2.018306000
C	2.857153000	-1.880595000	0.891569000
C	1.906668000	-0.895042000	1.354457000
C	4.229144000	-1.737178000	1.323257000
C	2.281020000	0.025672000	2.316220000
C	4.554761000	-0.798746000	2.285457000
C	3.591653000	0.073883000	2.811928000
H	1.552387000	0.747172000	2.675734000
H	5.584772000	-0.714665000	2.621227000
C	0.525126000	-0.812623000	0.763978000
H	0.483389000	0.053910000	0.094692000
H	0.255867000	-1.689491000	0.171799000
H	-0.233339000	-0.663488000	1.536453000
C	5.327811000	-2.554319000	0.699284000
H	4.958189000	-3.395073000	0.108861000
H	5.899050000	-1.910390000	0.021349000
H	6.023969000	-2.932339000	1.452080000
C	3.962474000	1.055839000	3.881969000
H	3.340223000	1.952048000	3.837917000
H	3.811961000	0.596899000	4.866005000
H	5.012277000	1.348162000	3.812301000

(*Z*,*E*)-**6b**: Total energy: -2216.340817213260

B	2.469251000	0.711232000	-0.169597000
N	3.774387000	0.793678000	0.239954000
C	4.163421000	2.089871000	0.849546000
H	3.319589000	2.779752000	0.850022000
H	4.493715000	1.939049000	1.879862000
H	4.978533000	2.546597000	0.284219000
Si	5.140239000	-0.413608000	0.047422000
C	6.652869000	0.320539000	0.865101000
H	6.508202000	0.516691000	1.931627000
H	7.465031000	-0.410044000	0.778285000
H	6.997272000	1.242333000	0.388213000
C	4.706887000	-2.011072000	0.926263000
H	3.903479000	-2.574989000	0.446492000
H	5.594715000	-2.653298000	0.934180000
H	4.435226000	-1.826689000	1.971136000
C	5.450267000	-0.645351000	-1.782082000
H	4.628602000	-1.142503000	-2.304264000
H	5.629412000	0.319395000	-2.268139000
H	6.348371000	-1.256074000	-1.925752000
C	1.270496000	1.691807000	-0.147767000
C	0.588669000	1.984900000	1.047867000
C	0.871483000	2.316098000	-1.350324000
C	-0.506494000	2.848095000	1.013030000
C	-0.218313000	3.180780000	-1.341739000
C	-0.938639000	3.439995000	-0.172219000
H	-1.034101000	3.066841000	1.938350000
H	-0.520907000	3.661497000	-2.268865000
C	1.026047000	1.430203000	2.382734000
H	1.808806000	0.672857000	2.289967000
H	1.420362000	2.231102000	3.016923000
H	0.183587000	0.983197000	2.920246000
C	1.597074000	2.047390000	-2.647558000
H	2.675056000	1.919767000	-2.499774000
H	1.220508000	1.139636000	-3.134180000
H	1.459165000	2.871069000	-3.351285000
C	-2.164876000	4.312535000	-0.191469000
H	-3.064005000	3.693101000	-0.286526000
H	-2.257361000	4.890442000	0.731681000
H	-2.149482000	5.008667000	-1.033247000
Cl	2.022009000	-0.993717000	-1.062941000
B	-2.220796000	-1.781988000	0.476537000
N	-1.084269000	-1.350451000	-0.288757000
C	-1.269775000	-0.298250000	-1.306999000
H	-1.403359000	0.673742000	-0.827514000
H	-0.410648000	-0.237748000	-1.975637000
H	-2.155062000	-0.511758000	-1.907386000
Si	0.394762000	-2.169564000	0.038348000
C	0.997723000	-2.119310000	1.797465000
H	0.354471000	-1.477976000	2.404375000
H	0.975890000	-3.127756000	2.222318000
H	2.025420000	-1.755788000	1.871583000
C	0.659540000	-3.765357000	-0.866636000
H	0.505509000	-3.644648000	-1.942696000
H	1.659160000	-4.174660000	-0.693502000
H	-0.074224000	-4.495750000	-0.508518000
C	-2.140304000	-2.979912000	1.514971000
H	-1.264775000	-3.639475000	1.510456000
H	-2.235896000	-2.578745000	2.532104000
H	-3.017642000	-3.619737000	1.370775000
C	-3.593463000	-1.035496000	0.282142000
C	-3.892722000	0.093329000	1.061355000
C	-4.524985000	-1.477263000	-0.674170000
C	-5.098615000	0.769154000	0.869531000
C	-5.721937000	-0.783335000	-0.844149000
C	-6.027990000	0.344700000	-0.079710000
H	-5.320524000	1.644754000	1.476443000
H	-6.434498000	-1.126892000	-1.591099000

C	-2.924726000	0.560288000	2.123972000
H	-2.971650000	-0.084208000	3.009942000
H	-1.892772000	0.551892000	1.754617000
H	-3.149653000	1.579206000	2.449935000
C	-4.229536000	-2.699975000	-1.512922000
H	-3.244220000	-2.637314000	-1.991515000
H	-4.237057000	-3.610504000	-0.902453000
H	-4.970629000	-2.832068000	-2.304518000
C	-7.341121000	1.062517000	-0.259579000
H	-7.291549000	2.087463000	0.116999000
H	-7.633326000	1.099438000	-1.312703000
H	-8.139878000	0.547625000	0.285010000

TS$_{6\rightarrow3}$: Total energy: -2216.333177853260

B	-2.477250000	-1.153725000	-0.072626000
N	-3.779041000	-1.271902000	0.227366000
C	-4.162169000	-2.703645000	0.430647000
H	-3.304696000	-3.359130000	0.266792000
H	-4.524671000	-2.853599000	1.448217000
H	-4.948023000	-2.974008000	-0.277457000
Si	-5.123671000	-0.034015000	0.487809000
C	-6.519752000	-0.959650000	1.317273000
H	-6.241025000	-1.363170000	2.295418000
H	-7.333052000	-0.244518000	1.485815000
H	-6.928412000	-1.771071000	0.708596000
C	-4.473946000	1.274081000	1.651342000
H	-3.682959000	1.882055000	1.209929000
H	-5.294343000	1.943229000	1.933247000
H	-4.092312000	0.819041000	2.571409000
C	-5.663718000	0.589138000	-1.185029000
H	-4.894222000	1.175588000	-1.691940000
H	-5.945117000	-0.245007000	-1.836148000
H	-6.547976000	1.225206000	-1.067293000
C	-1.092966000	-1.727890000	-0.193641000
C	-0.209713000	-1.608657000	0.901942000
C	-0.689445000	-2.381839000	-1.380193000
C	1.066585000	-2.143917000	0.790179000
C	0.598170000	-2.900515000	-1.448134000
C	1.495027000	-2.773163000	-0.382062000
H	1.757640000	-2.057240000	1.622331000
H	0.921216000	-3.401987000	-2.356483000
C	-0.627612000	-0.870155000	2.147636000
H	-0.461602000	0.206916000	2.020362000
H	-1.687956000	-1.016780000	2.379569000
H	-0.050304000	-1.193856000	3.015874000
C	-1.628031000	-2.486304000	-2.555543000
H	-2.563378000	-2.987835000	-2.283193000
H	-1.885394000	-1.493138000	-2.941691000
H	-1.178237000	-3.053308000	-3.372541000
C	2.915048000	-3.249752000	-0.501324000
H	3.577079000	-2.391261000	-0.668606000
H	3.248648000	-3.735247000	0.419583000
H	3.039725000	-3.948477000	-1.331307000
Cl	-2.152889000	1.123218000	-1.000023000
B	2.019925000	1.789125000	0.508769000
N	0.931555000	1.539692000	-0.402972000
C	1.118704000	0.608035000	-1.535898000
H	1.898293000	-0.112144000	-1.294539000
H	0.204456000	0.052282000	-1.742753000
H	1.412836000	1.142648000	-2.444866000
Si	-0.513374000	2.500921000	-0.528312000
C	-1.158047000	3.347398000	0.994962000
H	-1.227902000	2.675056000	1.854140000
H	-0.535559000	4.200018000	1.275414000
H	-2.160466000	3.727317000	0.771517000
C	-0.504736000	3.585741000	-2.036122000
H	-0.291840000	3.015617000	-2.944533000
H	-1.461560000	4.098736000	-2.168397000
H	0.277399000	4.345282000	-1.923305000
C	1.934980000	2.923864000	1.621531000
H	1.770550000	3.914956000	1.179582000
H	1.136318000	2.764954000	2.354434000
H	2.873079000	2.985659000	2.177678000
C	3.350630000	0.932496000	0.409699000
C	3.707242000	0.092722000	1.489532000
C	4.220475000	1.002332000	-0.692798000
C	4.843922000	-0.706724000	1.409665000
C	5.363836000	0.197140000	-0.738435000
C	5.683564000	-0.679807000	0.292810000
H	5.093835000	-1.360039000	2.243820000
H	6.023697000	0.268163000	-1.600955000
C	2.906273000	0.077630000	2.772702000
H	3.242847000	0.874115000	3.445287000
H	1.838084000	0.231112000	2.602310000
H	3.029592000	-0.868482000	3.308304000
C	3.995116000	1.967682000	-1.835906000
H	3.131798000	2.618605000	-1.671111000
H	4.869041000	2.613764000	-1.962742000
H	3.845224000	1.438428000	-2.783195000
C	6.892294000	-1.576499000	0.219214000
H	7.564468000	-1.276328000	-0.588176000
H	7.456548000	-1.558009000	1.156080000
H	6.595029000	-2.615464000	0.037179000

(*E*)-**3b**: Total energy: -1338.40713455326

B	0.103014000	0.133818000	0.703332000
N	1.114670000	0.005969000	-0.284347000
C	0.754373000	-0.170118000	-1.701244000
H	-0.330105000	-0.131146000	-1.809021000
H	1.192972000	0.617039000	-2.321803000
H	1.107097000	-1.132448000	-2.084532000
Si	2.821071000	0.044946000	0.166486000
C	3.271968000	-1.338872000	1.336481000
H	2.996801000	-2.301226000	0.893782000
H	4.351535000	-1.344768000	1.516969000
H	2.761057000	-1.247968000	2.298551000
C	3.353904000	1.741446000	0.737146000
H	3.158804000	2.475113000	-0.051173000
H	2.813809000	2.056923000	1.634233000
H	4.426393000	1.754174000	0.955275000
C	0.399296000	0.342403000	2.253911000
H	0.081402000	-0.559669000	2.793549000
H	1.424611000	0.560612000	2.562292000
H	-0.239057000	1.147372000	2.636219000
C	-1.430362000	0.053089000	0.303243000
C	-2.156484000	1.222984000	0.020938000
C	-2.092542000	-1.185965000	0.254653000
C	-3.515722000	1.143482000	-0.285921000
C	-3.452757000	-1.237476000	-0.053583000
C	-4.184417000	-0.080190000	-0.320981000
H	-4.065454000	2.056482000	-0.507654000
H	-3.953476000	-2.203318000	-0.091001000
C	-1.456316000	2.562663000	0.017999000
H	-1.004487000	2.782503000	0.992097000
H	-0.648939000	2.583225000	-0.723189000
H	-2.147645000	3.375915000	-0.217810000
C	-1.325836000	-2.463464000	0.510688000
H	-0.502844000	-2.579192000	-0.203906000
H	-0.885501000	-2.473548000	1.514317000
H	-1.970959000	-3.341626000	0.423879000
C	-5.661725000	-0.148649000	-0.617701000
H	-6.247938000	-0.084382000	0.306036000
H	-5.976288000	0.674566000	-1.265566000
H	-5.925630000	-1.088861000	-1.110465000
Cl	3.926518000	-0.328463000	-1.572464000

TS_{Rot3}: Total energy: -1338.372666013260

B	0.235587000	1.131005000	0.821950000
N	1.450531000	1.005952000	-0.019086000
C	1.479485000	2.071775000	-1.033807000
H	0.835406000	1.846044000	-1.893485000
H	1.146860000	3.023272000	-0.601702000
H	2.495703000	2.231869000	-1.400623000
Si	2.565772000	-0.293337000	-0.139146000
C	3.001303000	-0.962723000	1.550522000
H	2.127207000	-1.235807000	2.144784000
H	3.630196000	-1.853136000	1.453933000
H	3.563467000	-0.200928000	2.101560000
C	4.107490000	0.233720000	-1.056891000
H	3.912618000	0.446750000	-2.111579000
H	4.560044000	1.117805000	-0.595114000
H	4.835975000	-0.582456000	-1.016200000
C	0.341685000	2.028188000	2.112502000
H	-0.612121000	2.398652000	2.497848000
H	0.764931000	1.366352000	2.886456000
H	1.057898000	2.849825000	2.003938000
C	-1.147373000	0.455182000	0.431418000
C	-2.095636000	1.211040000	-0.285323000
C	-1.492420000	-0.853945000	0.818936000
C	-3.317460000	0.639986000	-0.648647000
C	-2.721576000	-1.394481000	0.443989000
C	-3.644493000	-0.669495000	-0.308481000
H	-4.036631000	1.241768000	-1.201656000
H	-2.970019000	-2.406670000	0.757619000
C	-1.834608000	2.649665000	-0.677661000
H	-2.772983000	3.204650000	-0.761887000
H	-1.214065000	3.172486000	0.057822000
H	-1.328419000	2.717310000	-1.646480000
C	-0.558363000	-1.688329000	1.661985000
H	0.239125000	-2.126372000	1.053259000
H	-0.098628000	-1.093444000	2.459382000
H	-1.092024000	-2.512568000	2.142597000
C	-4.951277000	-1.286150000	-0.738779000
H	-5.717324000	-0.523007000	-0.903007000
H	-4.828512000	-1.839620000	-1.676528000
H	-5.325913000	-1.988866000	0.011204000
Cl	1.798483000	-1.908851000	-1.259342000

TS_{Rot5}: Total energy: -877.897654831263

B	0.492964000	1.275397000	-0.384648000
N	1.708438000	0.747102000	0.309560000
C	2.278522000	1.718314000	1.286000000
H	3.034981000	1.244743000	1.916927000
H	2.742917000	2.560523000	0.767520000
H	1.493943000	2.092341000	1.947570000
Si	2.560209000	-0.674258000	0.075272000
C	3.365161000	-1.458689000	1.542520000
H	4.366896000	-1.036909000	1.689184000
H	2.788184000	-1.309243000	2.458019000
H	3.496237000	-2.532016000	1.372551000
C	3.295115000	-1.104825000	-1.563192000
H	3.263818000	-2.181443000	-1.757395000
H	2.821450000	-0.572414000	-2.391319000
H	4.351842000	-0.810269000	-1.536473000
C	0.650252000	2.695971000	-1.044318000
H	1.645633000	2.795770000	-1.493806000
H	-0.096967000	2.888687000	-1.816789000
H	0.564247000	3.511806000	-0.315355000
C	-0.844198000	0.452600000	-0.294925000
C	-0.898732000	-0.963294000	-0.349307000
C	-2.055706000	1.128697000	0.008870000
C	-2.077803000	-1.662489000	-0.121250000
C	-3.222011000	0.393916000	0.242505000
C	-3.265681000	-0.994915000	0.177699000
H	-2.081823000	-2.747984000	-0.187638000
H	-4.134779000	0.932139000	0.484442000
C	0.303236000	-1.778848000	-0.729860000
H	0.787154000	-1.424968000	-1.640780000
H	1.031143000	-1.841139000	0.136456000
H	0.073594000	-2.836785000	-0.880275000
C	-2.167986000	2.632102000	0.138825000
H	-3.146194000	2.903395000	0.539468000
H	-1.416601000	3.051115000	0.812820000
H	-2.063318000	3.130851000	-0.828126000
C	-4.549001000	-1.749659000	0.391566000
H	-4.366174000	-2.729260000	0.840343000
H	-5.232841000	-1.196430000	1.039223000
H	-5.057155000	-1.912874000	-0.564853000

Ag^+: Total energy (SDD/ECP): -146.854492474263

Ag	-0.201774000	0.000000000	-1.767258000

AgCl:

Total energy (SDD/ECP for Ag): -607.291749383263

Ag	0.000000000	0.000000000	0.614540000
Cl	0.000000000	0.000000000	-1.699023000

5.2 Poly(iminoborane)s with Aromatic Side Groups: Insights into the Microstructure from Monodisperse Model Oligomers

Crystallographic data

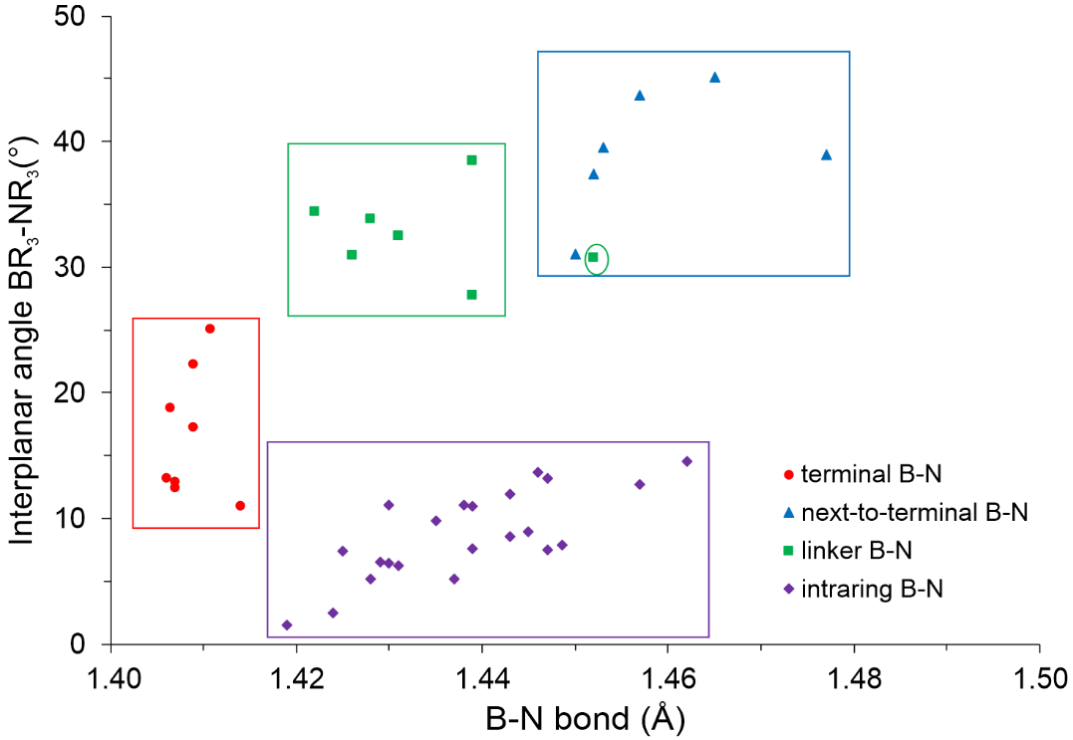

Figure S5.2.1. Correlation of the B–N bonds with the interplanar angle BR_3-NR_3 (°).

NMR spectra

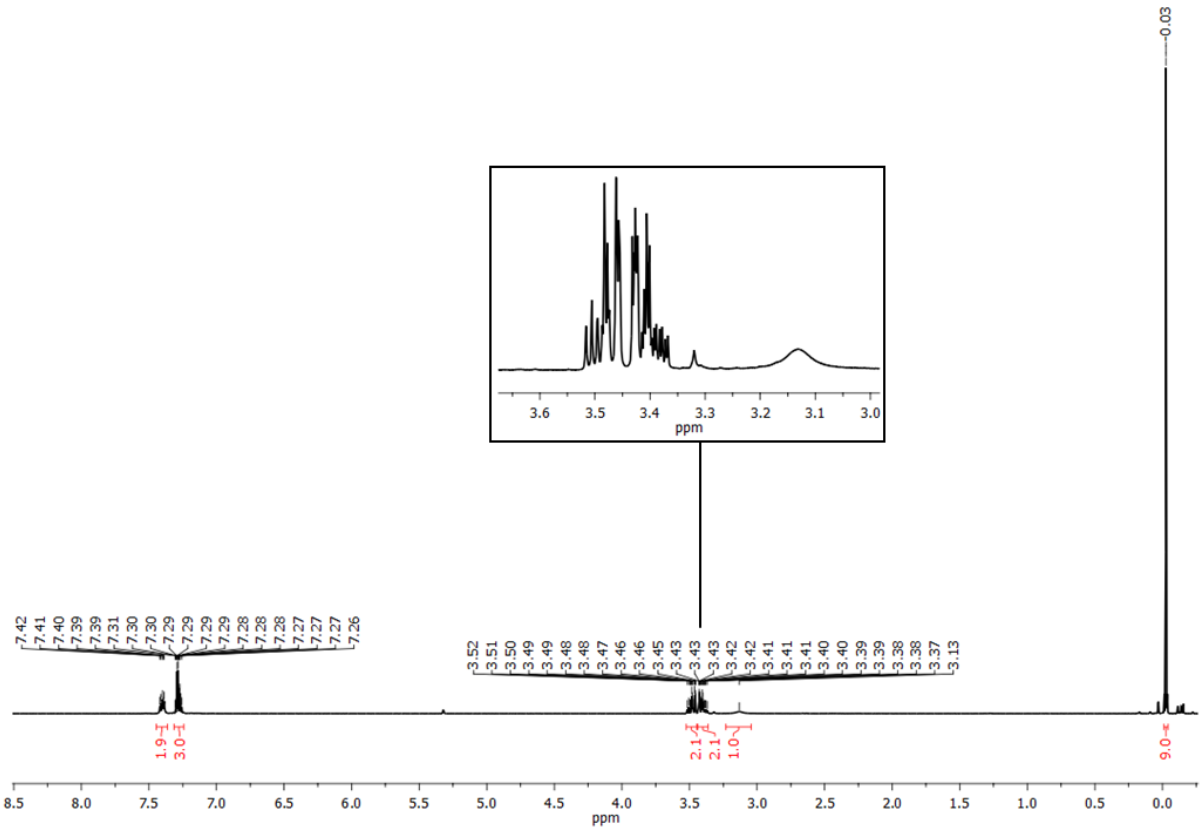

Figure S5.2.2. ^{1}H NMR spectrum (300 MHz) of **2** in CD_2Cl_2.

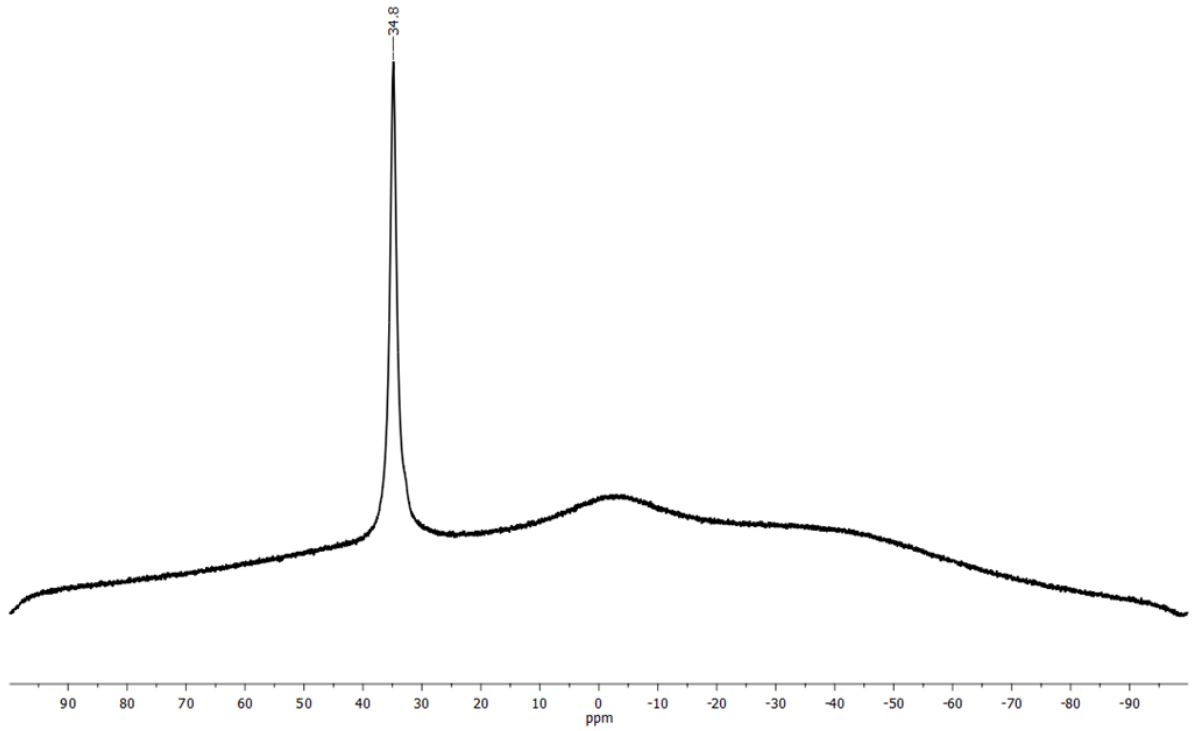

Figure S5.2.3. $^{11}B\{^{1}H\}$ NMR spectrum (96 MHz) of **2** in CD_2Cl_2.

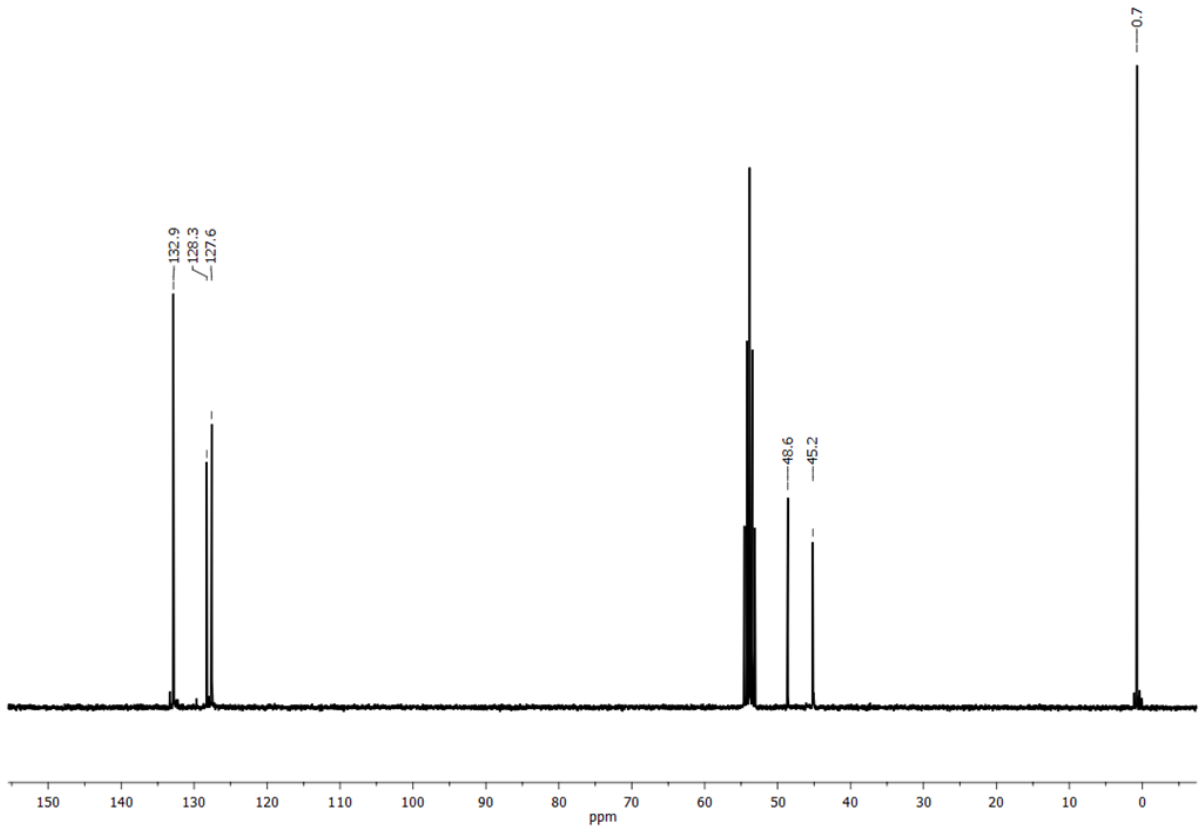

Figure S5.2.4. $^{13}C\{^{1}H\}$ NMR spectrum (76 MHz) of **2** in CD_2Cl_2.

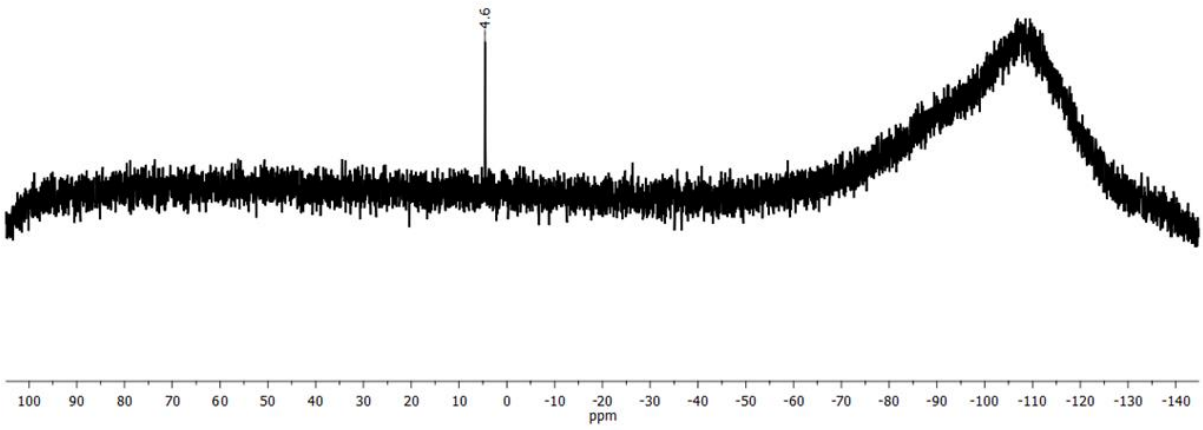

Figure S5.2.5. $^{29}Si\{^{1}H\}$ NMR spectrum (60 MHz) of **2** in CD_2Cl_2.

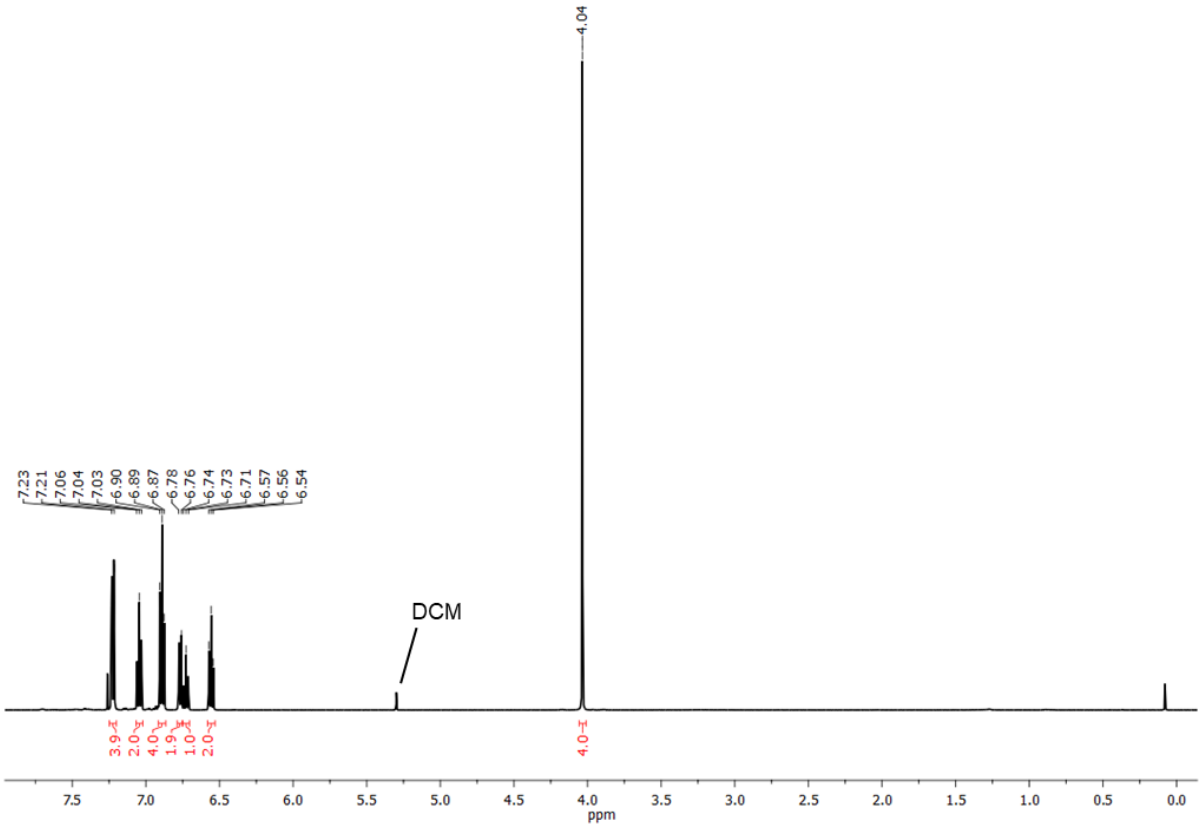

Figure S5.2.6. ^{1}H NMR spectrum (500 MHz) of **4** in $CDCl_3$.

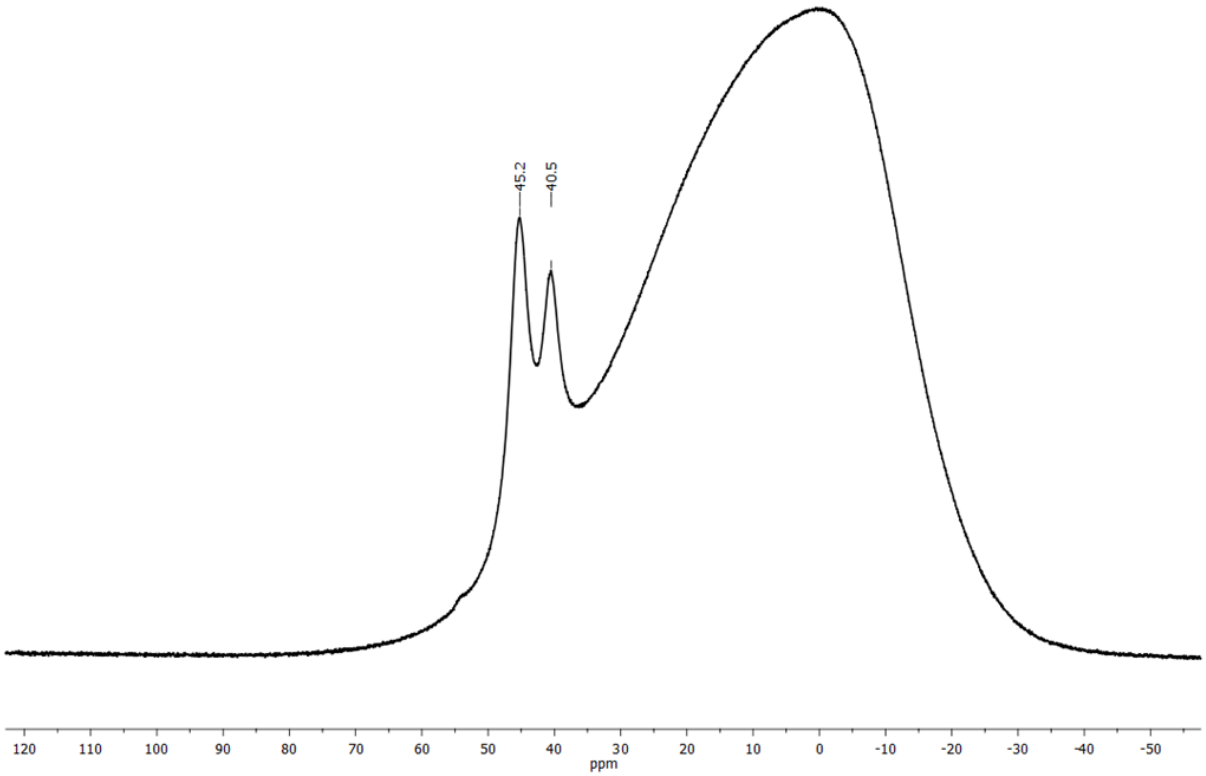

Figure S5.2.6. $^{11}B\{^{1}H\}$ NMR spectrum (160 MHz) of **4** in $CDCl_3$.

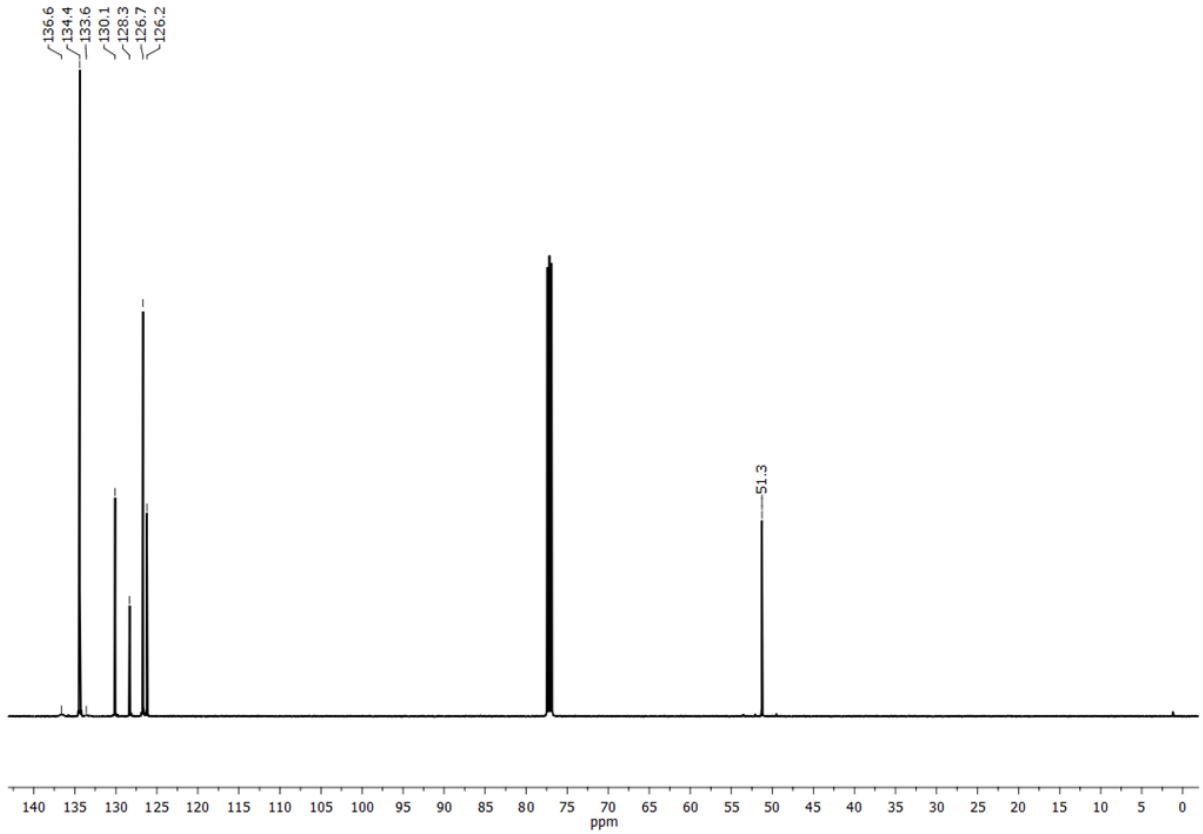

Figure S5.2.7. $^{13}C\{^{1}H\}$ NMR spectrum (126 MHz) of **4** in $CDCl_3$.

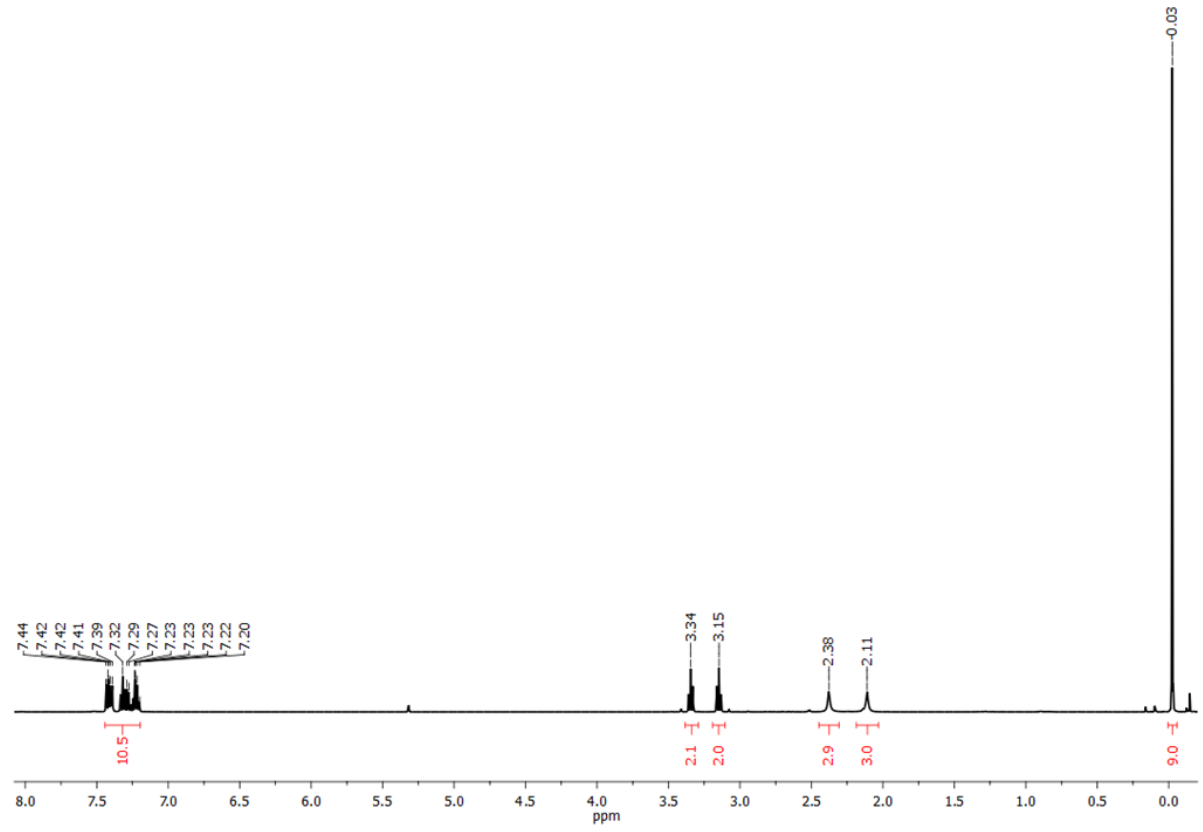

Figure S5.2.8. ^{1}H NMR spectrum (500 MHz) of **5** in CD_2Cl_2.

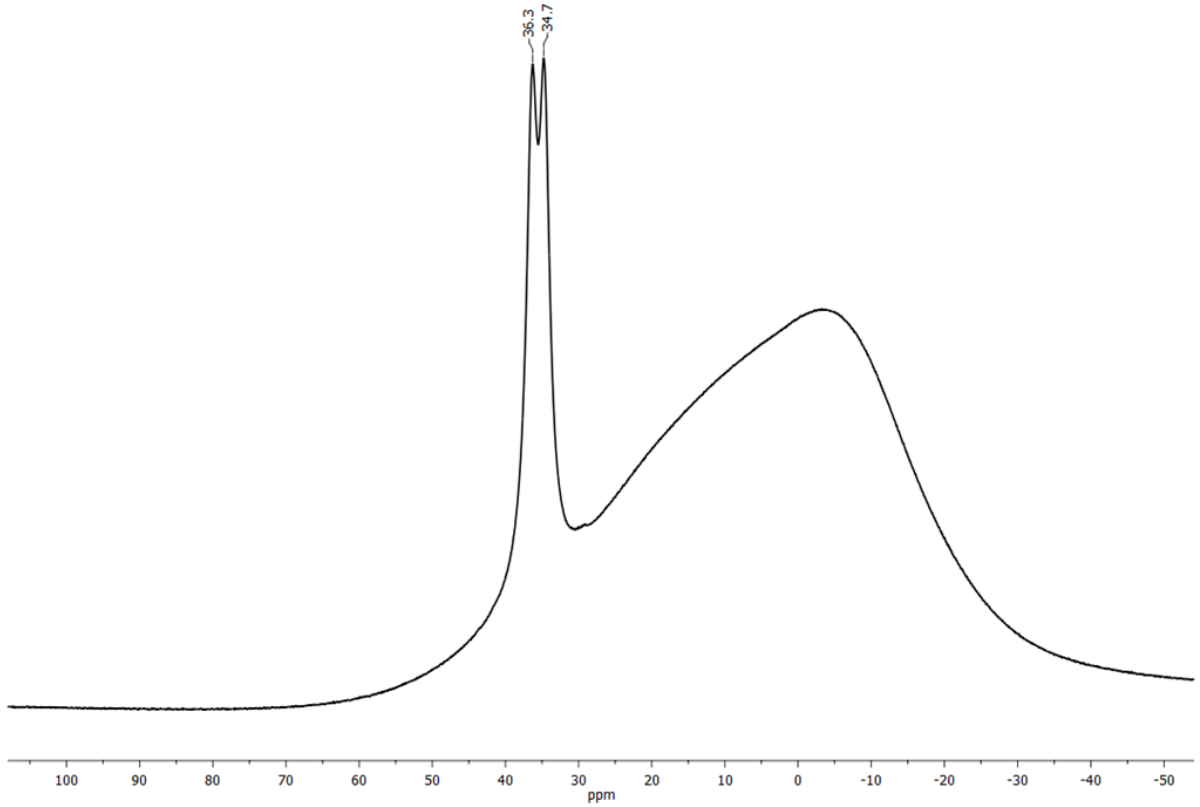

Figure S5.2.9. $^{11}B\{^{1}H\}$ NMR spectrum (160 MHz) of **5** in CD_2Cl_2.

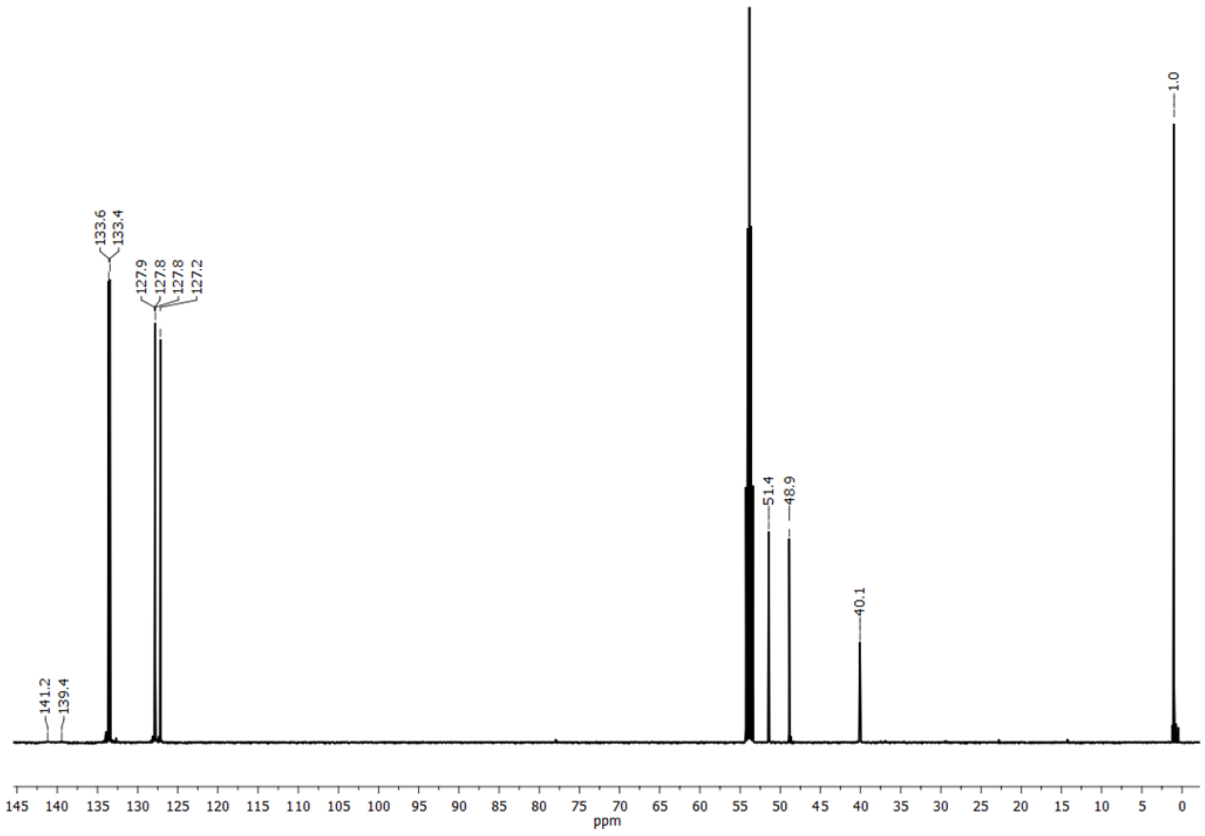

Figure S5.2.10. $^{13}C\{^{1}H\}$ NMR spectrum (126 MHz) of **5** in CD_2Cl_2.

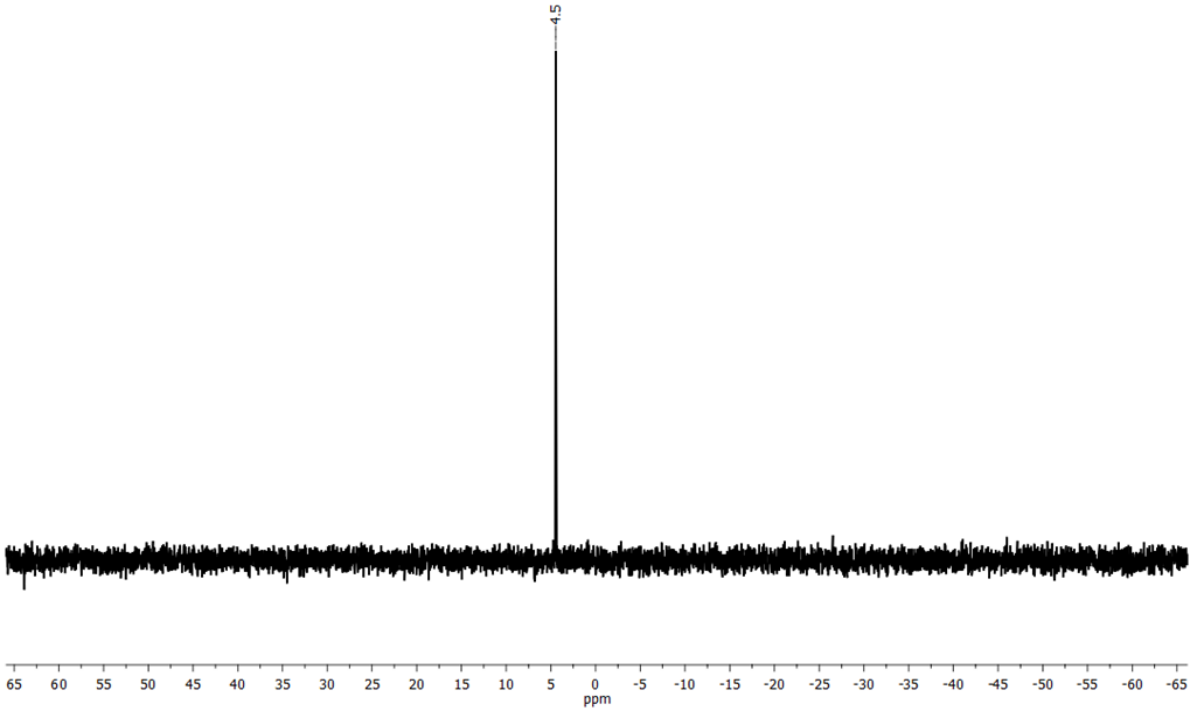

Figure S5.2.11. $^{29}Si\{^{1}H\}$ NMR spectrum (99 MHz) of **5** in CD_2Cl_2.

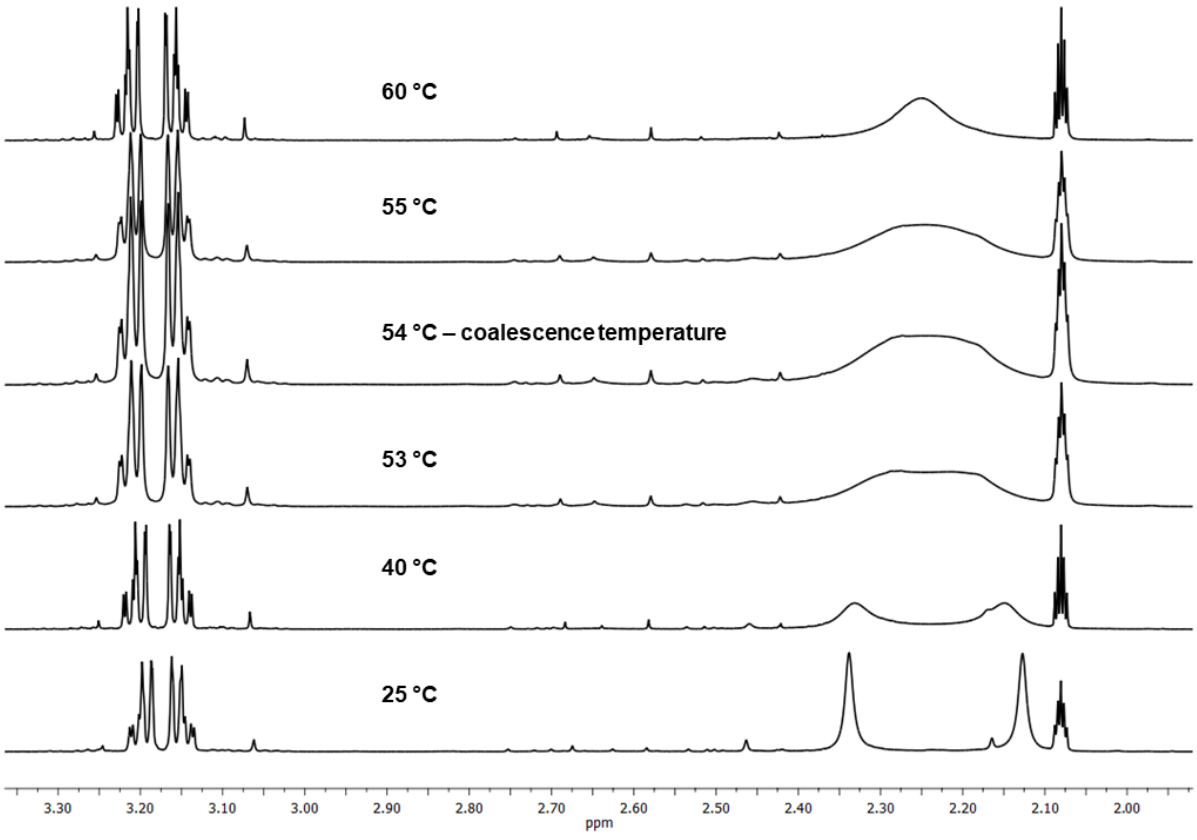

Figure S5.2.12. ^{1}H NMR spectra (600 MHz) of the determination of the coalescence temperature of **5** from 25 to 60 °C in toluene-d_8.

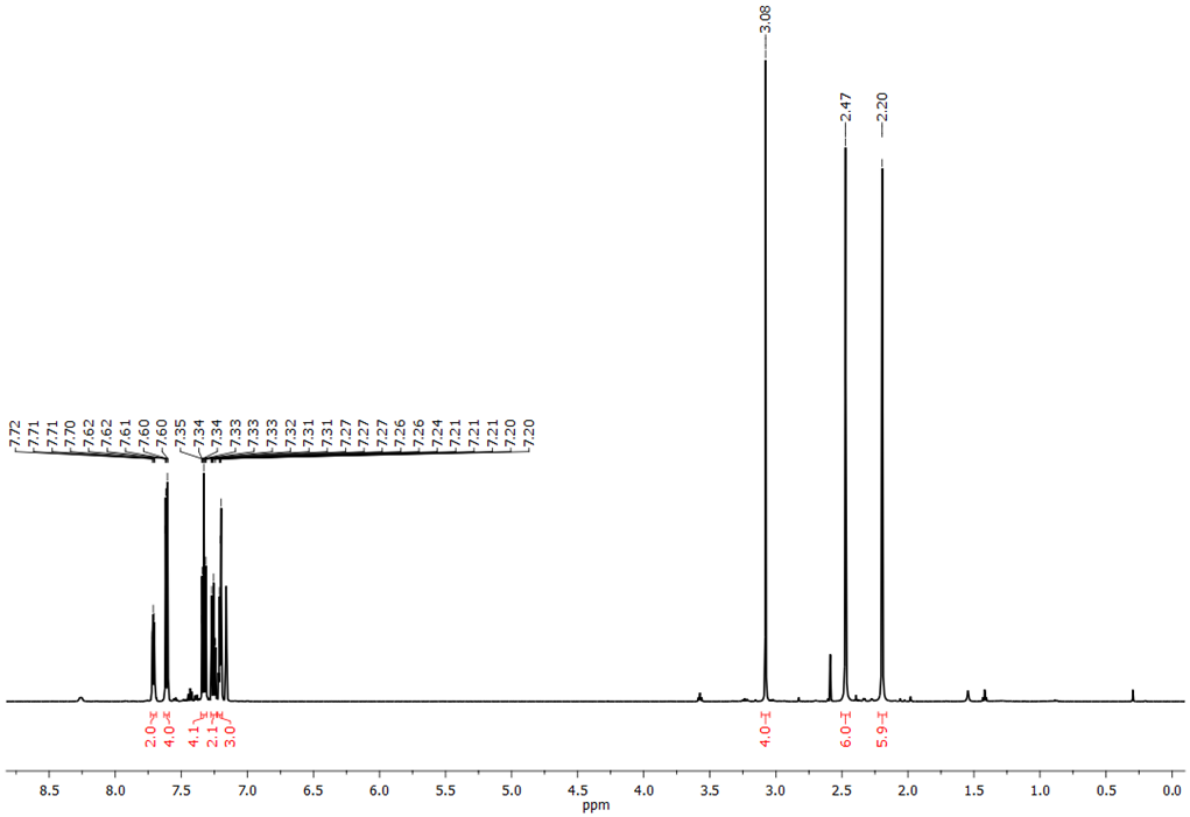

Figure S5.2.13. ^{1}H NMR spectrum (500 MHz) of **6** in C_6D_6.

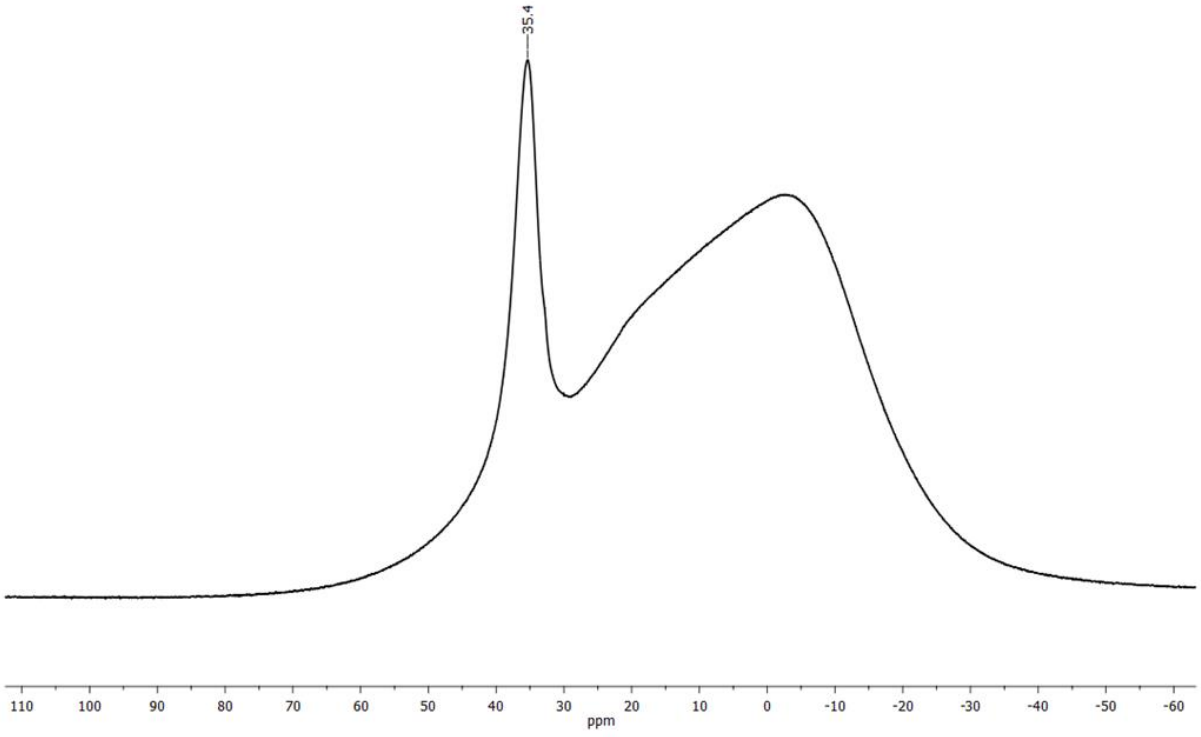

Figure S5.2.14. $^{11}B\{^{1}H\}$ NMR spectrum (160 MHz) of **6** in C_6D_6.

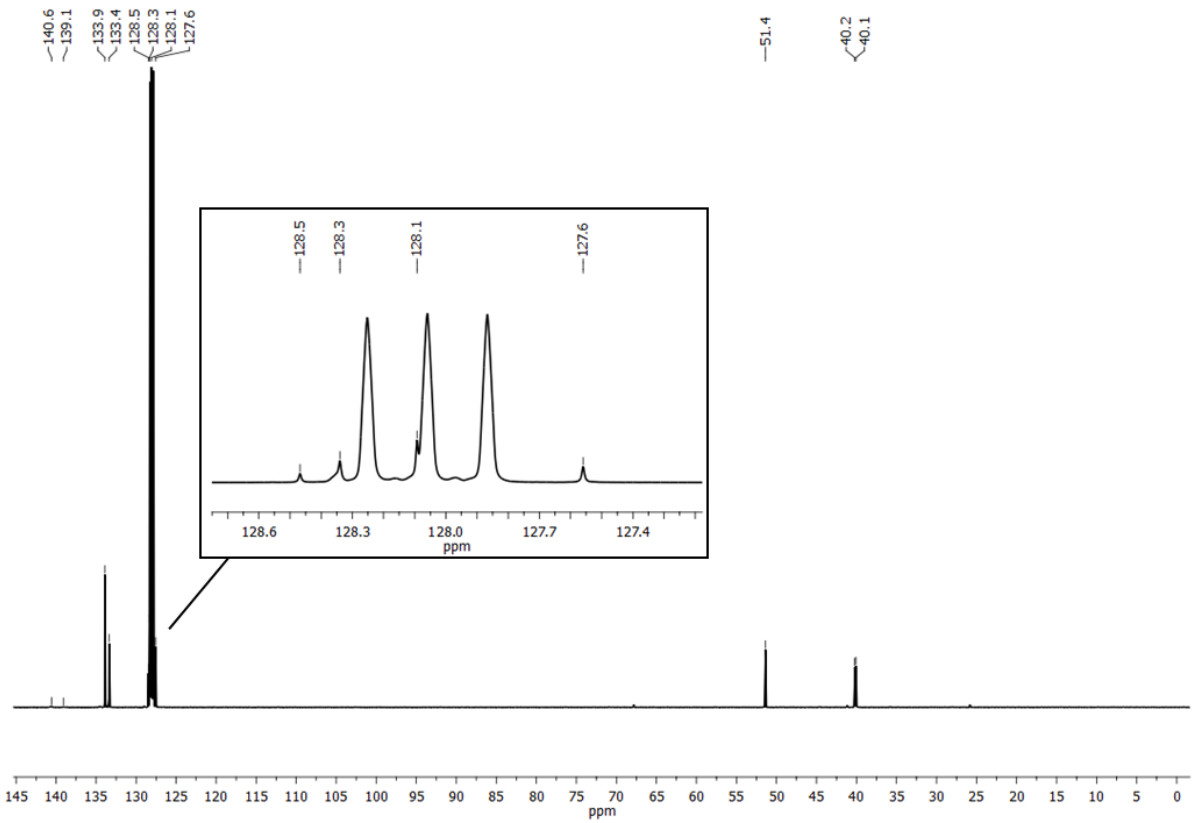

Figure S5.2.15. $^{13}C\{^{1}H\}$ NMR spectrum (126 MHz) of **6** in C_6D_6.

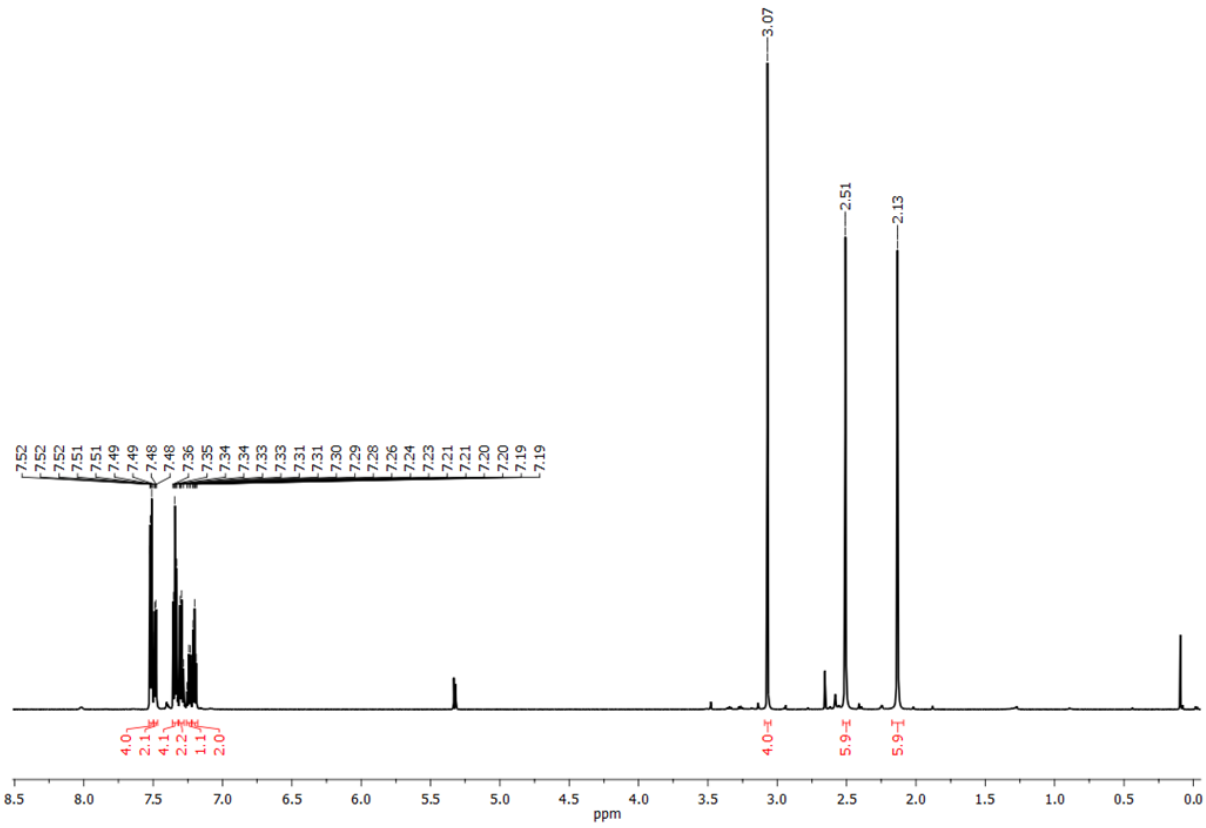

Figure S5.2.16. ^{1}H NMR spectrum (500 MHz) of **6** in CD_2Cl_2 (alternative synthesis).

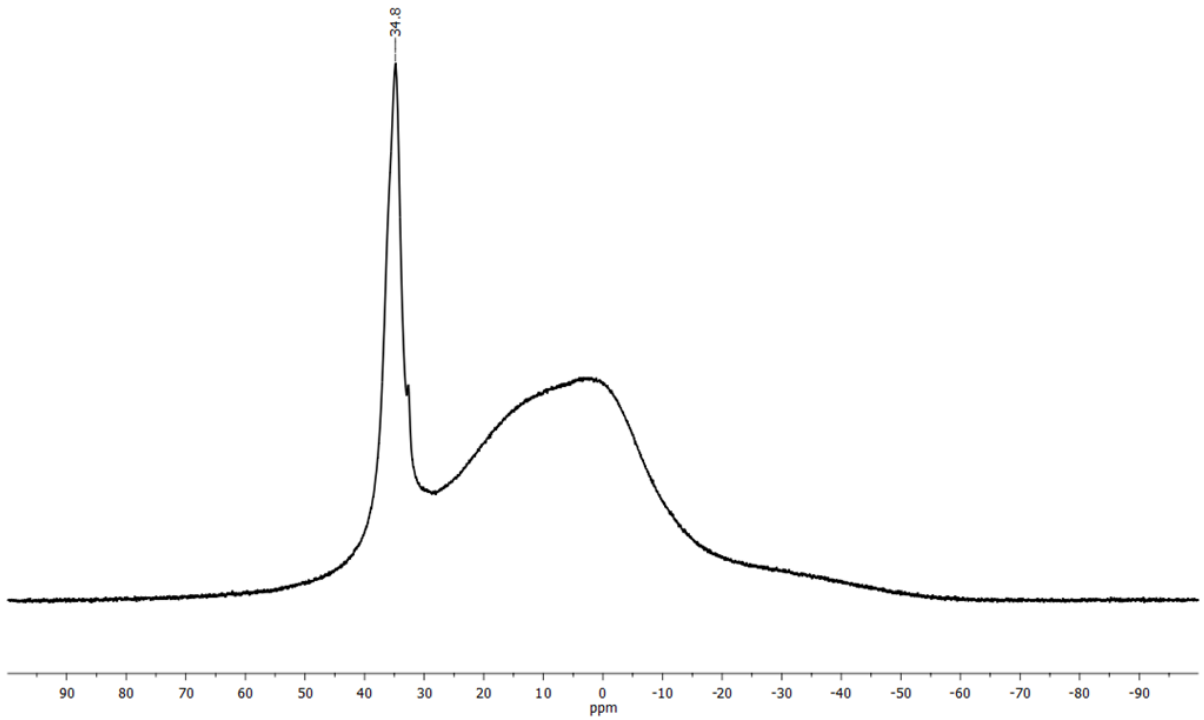

Figure S5.2.17. $^{11}B\{^{1}H\}$ NMR spectrum (160 MHz) of **6** in CD_2Cl_2 (alternative synthesis).

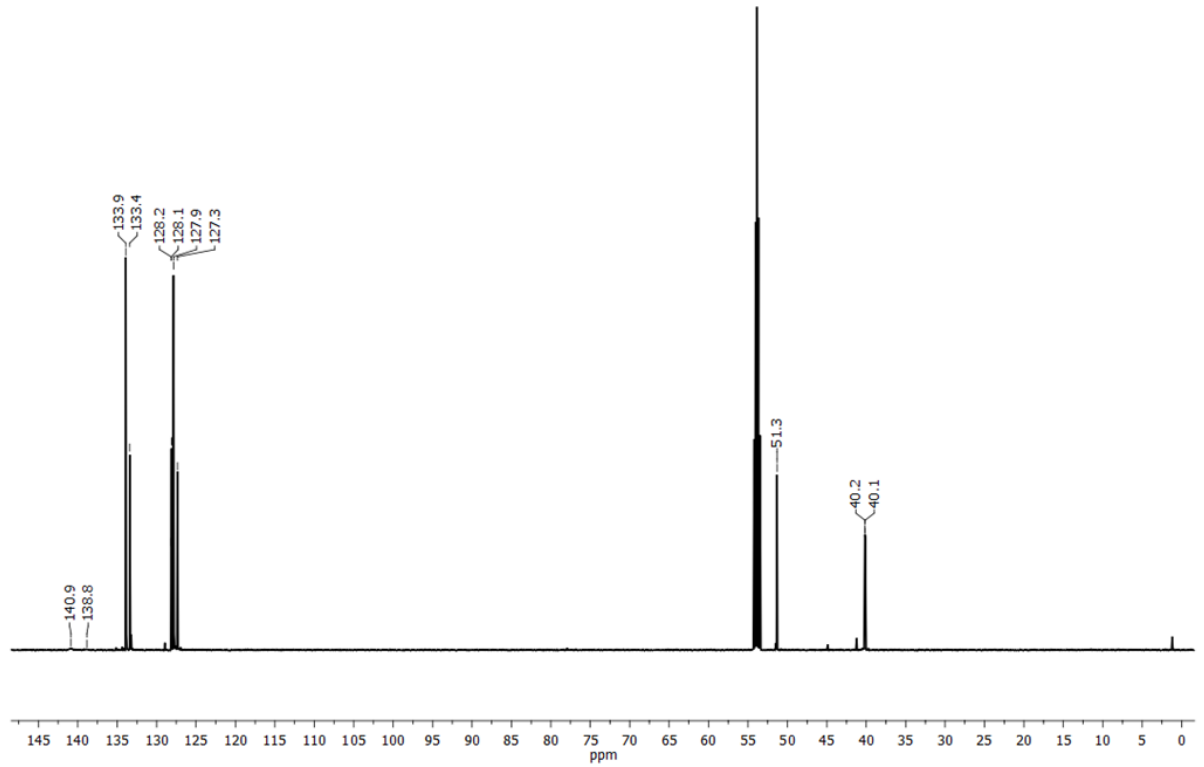

Figure S5.2.18. $^{13}C\{^{1}H\}$ NMR spectrum (126 MHz) of **6** in CD_2Cl_2 (alternative synthesis).

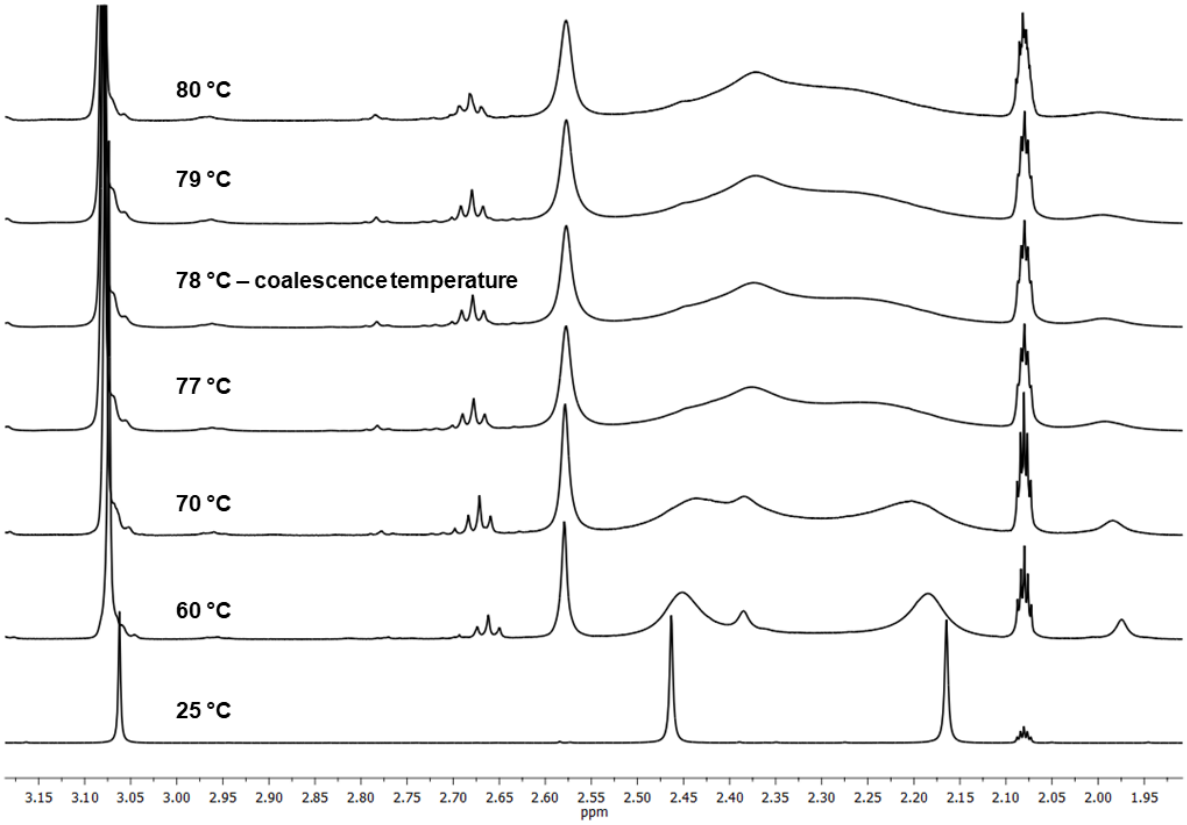

Figure S5.2.19. ^{1}H NMR spectra (600 MHz) of the determination of the coalescence temperature of **6** from 25 to 80 °C in toluene-d_8.

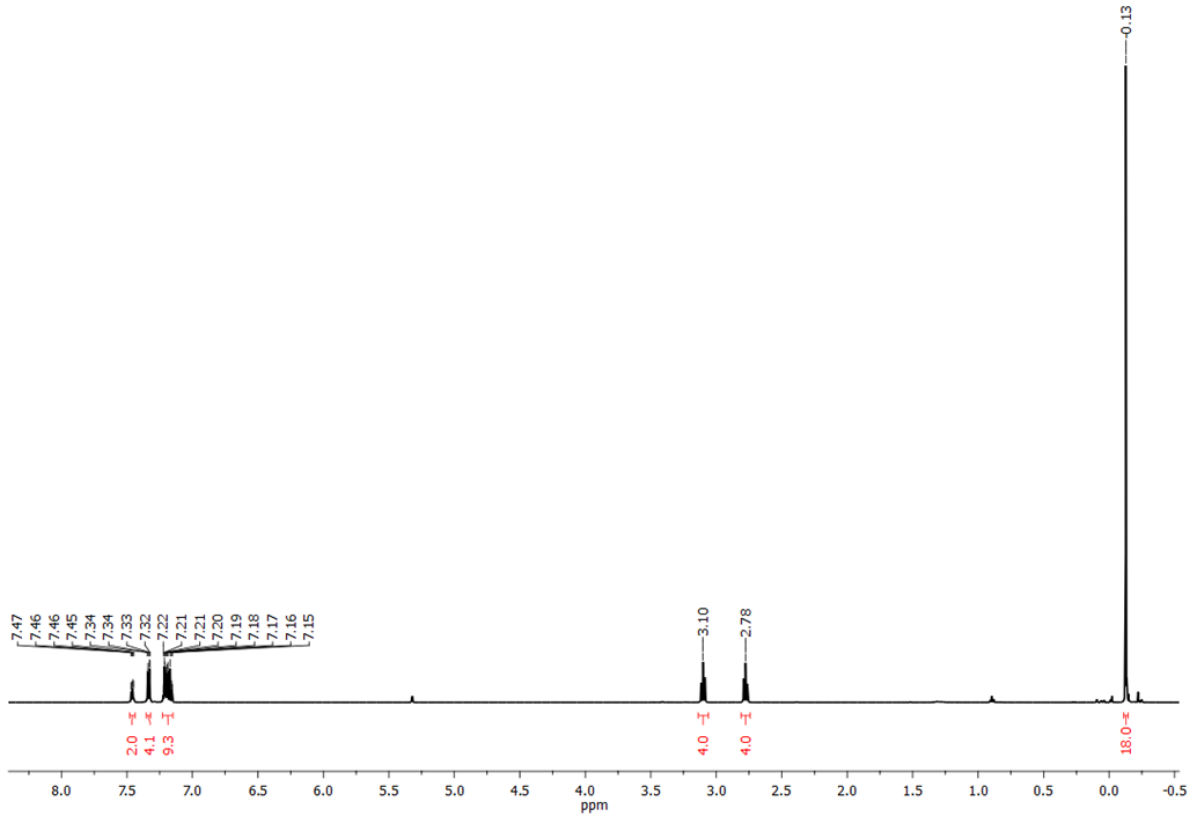

Figure S5.2.20. ^{1}H NMR spectrum (500 MHz) of **7** in CD_2Cl_2.

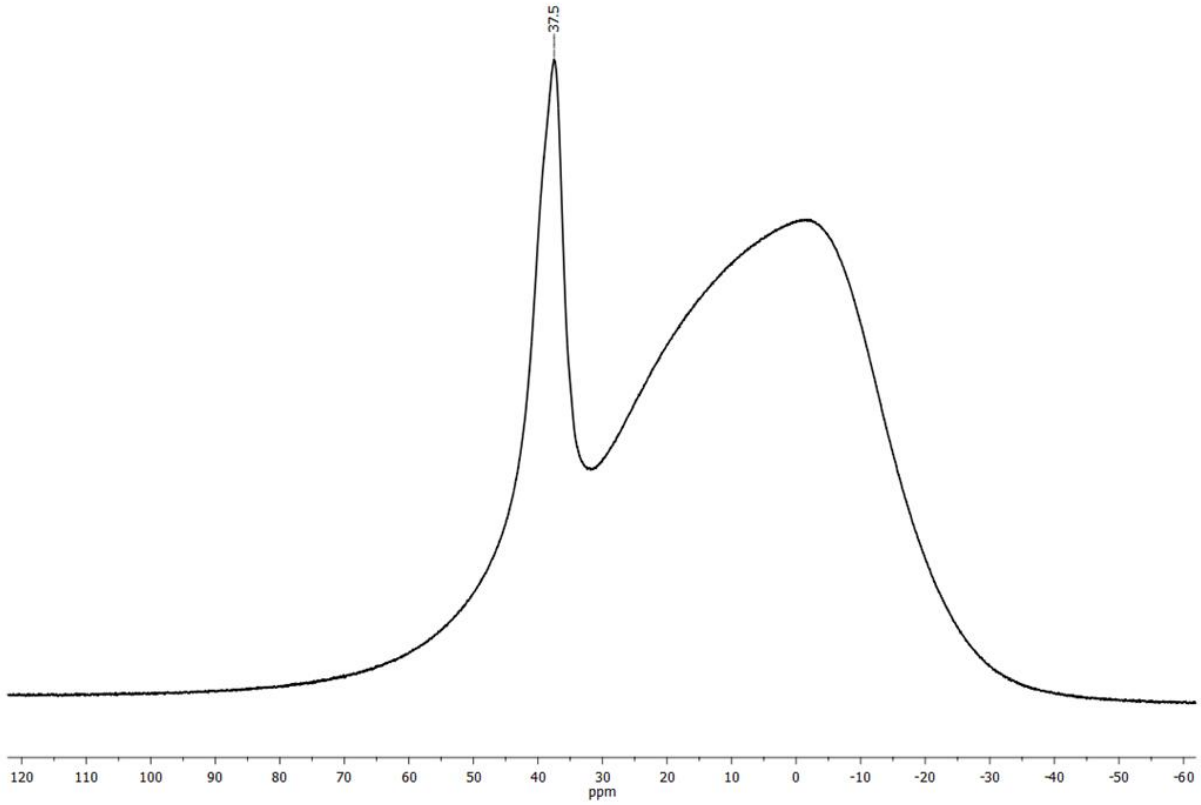

Figure S5.2.21. $^{11}B\{^{1}H\}$ NMR spectrum (160 MHz) of **7** in CD_2Cl_2.

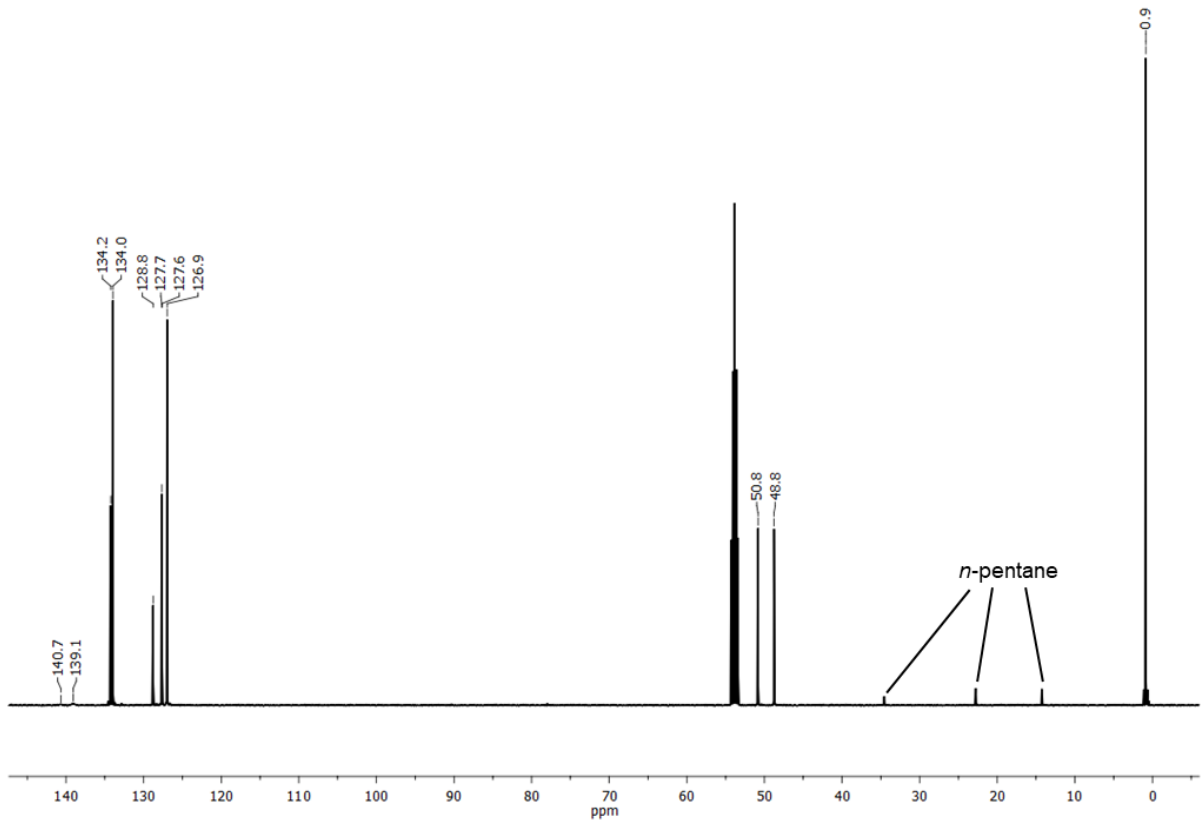

Figure S5.2.22. $^{13}C\{^{1}H\}$ NMR spectrum (126 MHz) of **7** in CD_2Cl_2.

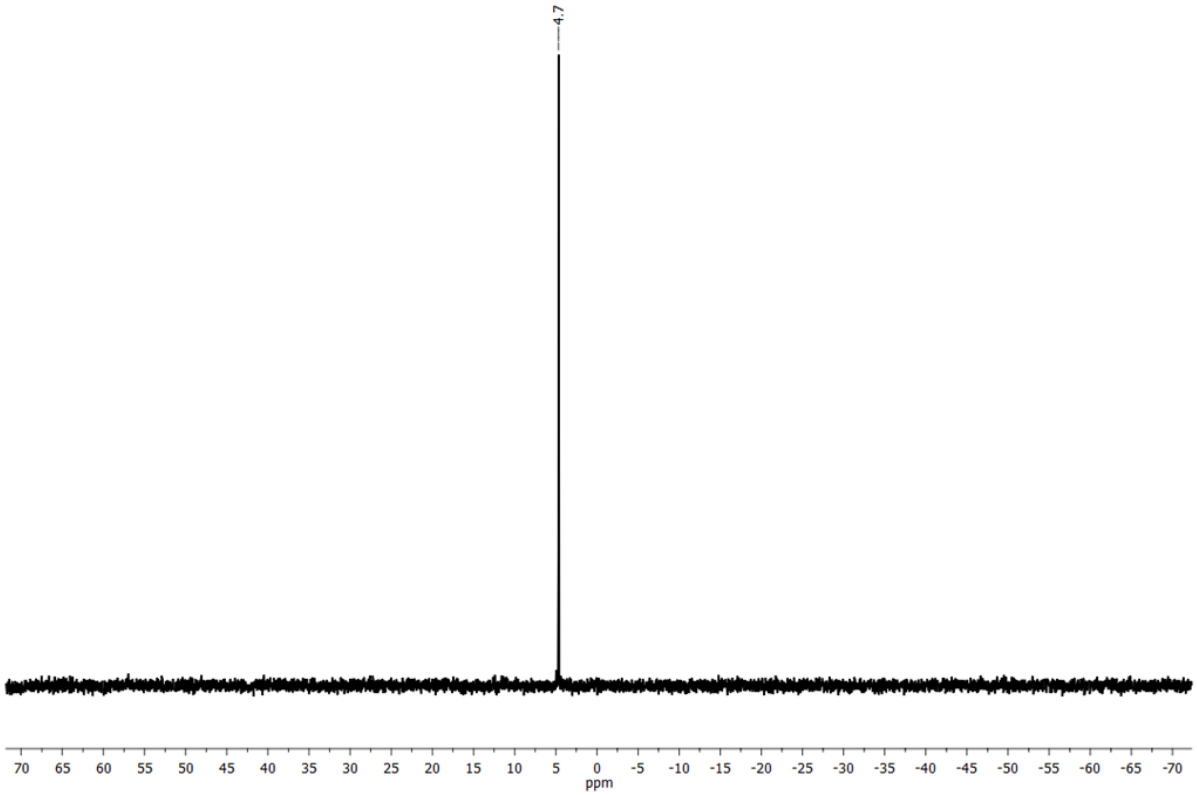

Figure S5.2.23. $^{29}Si\{^{1}H\}$ NMR spectrum (99 MHz) of **7** in CD_2Cl_2.

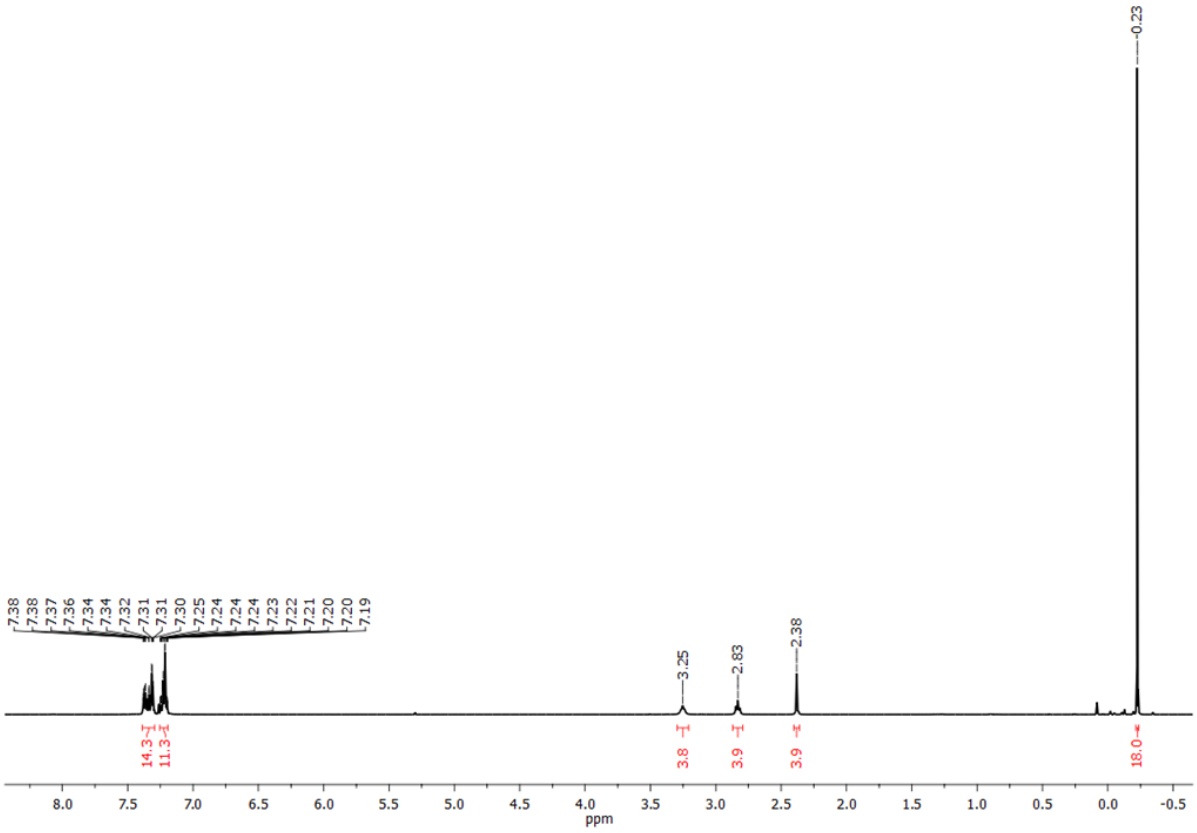

Figure S5.2.24. ^{1}H NMR spectrum (500 MHz) of **8** in $CDCl_3$.

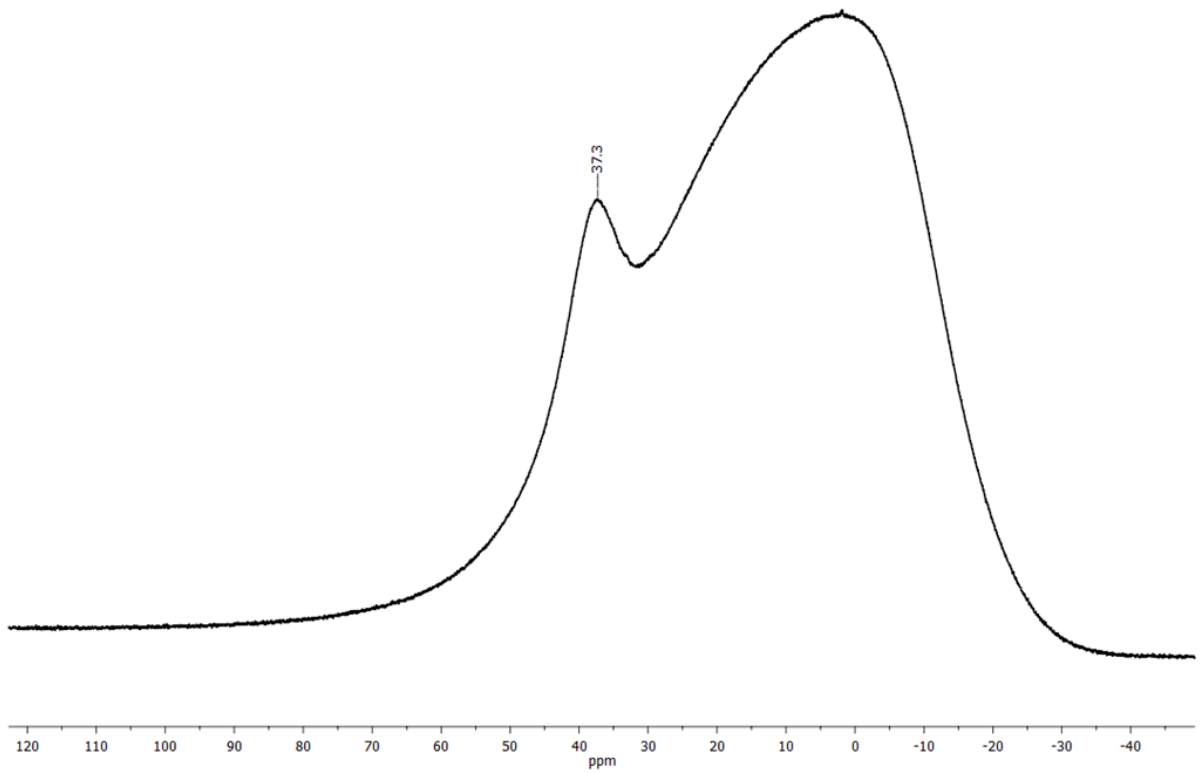

Figure S5.2.25. $^{11}B\{^{1}H\}$ NMR spectrum (160 MHz) of **8** in $CDCl_3$.

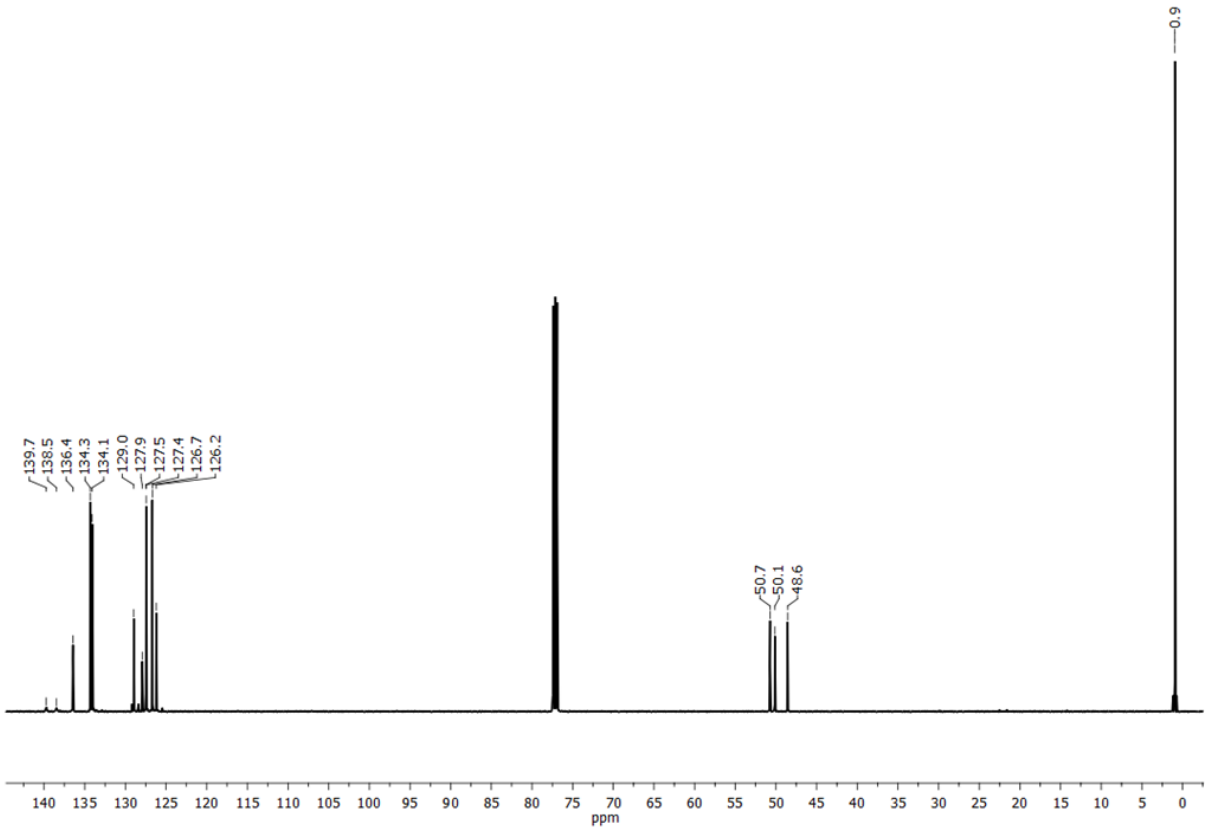

Figure S5.2.26. $^{13}C\{^{1}H\}$ NMR spectrum (126 MHz) of **8** in $CDCl_3$.

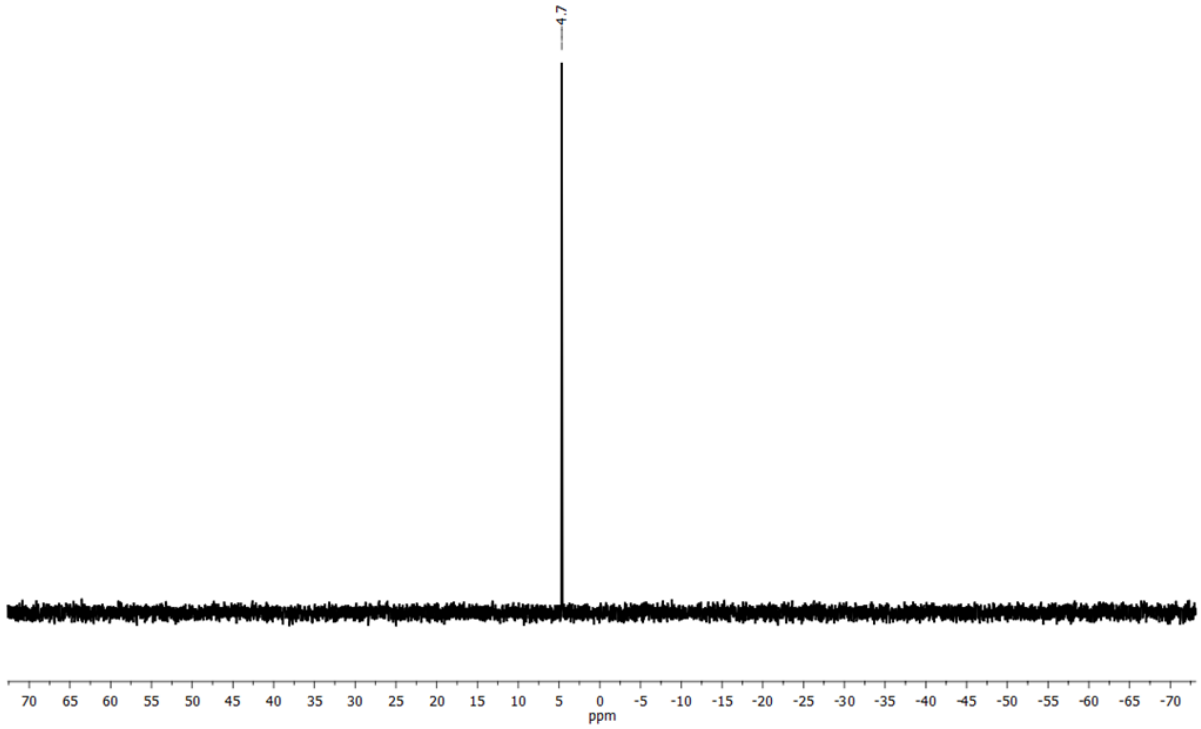

Figure S5.2.27. $^{29}Si\{^{1}H\}$ NMR spectrum (99 MHz) of **8** in $CDCl_3$.

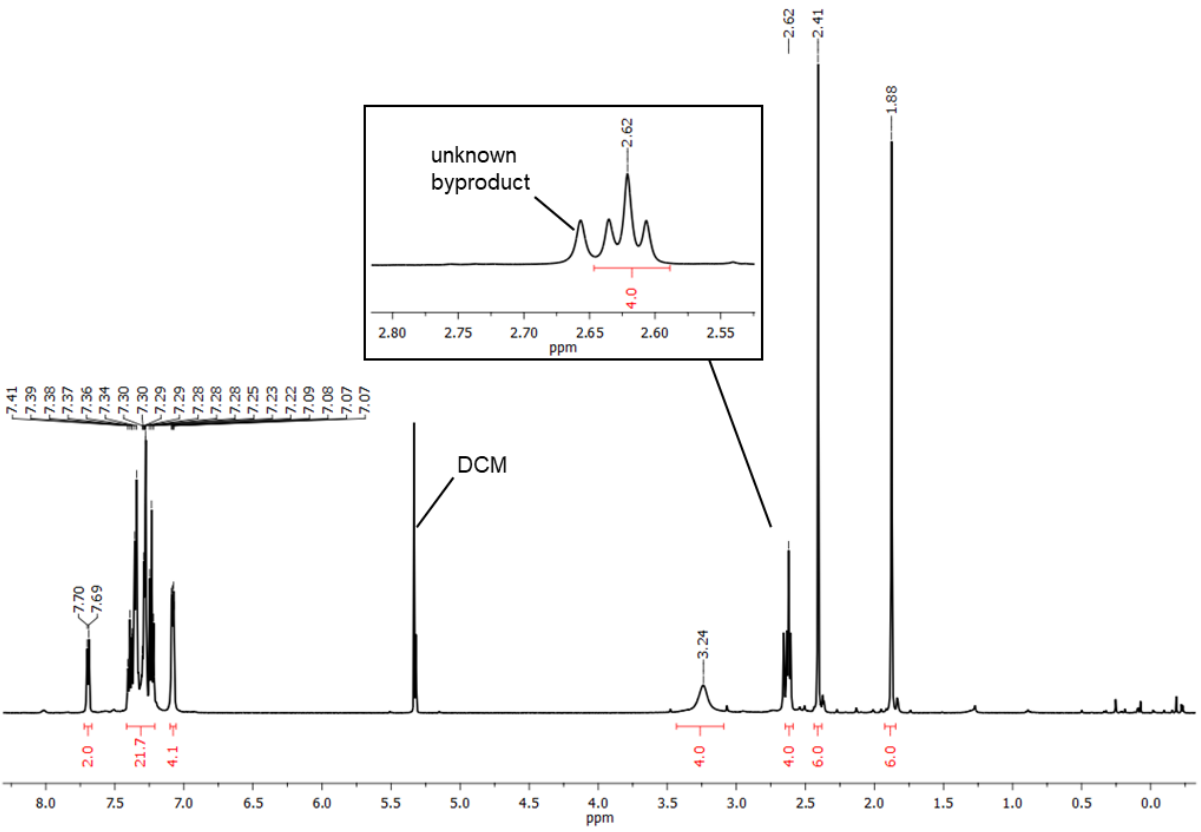

Figure S5.2.28. ^{1}H NMR spectrum (500 MHz) of **9** in CD_2Cl_2.

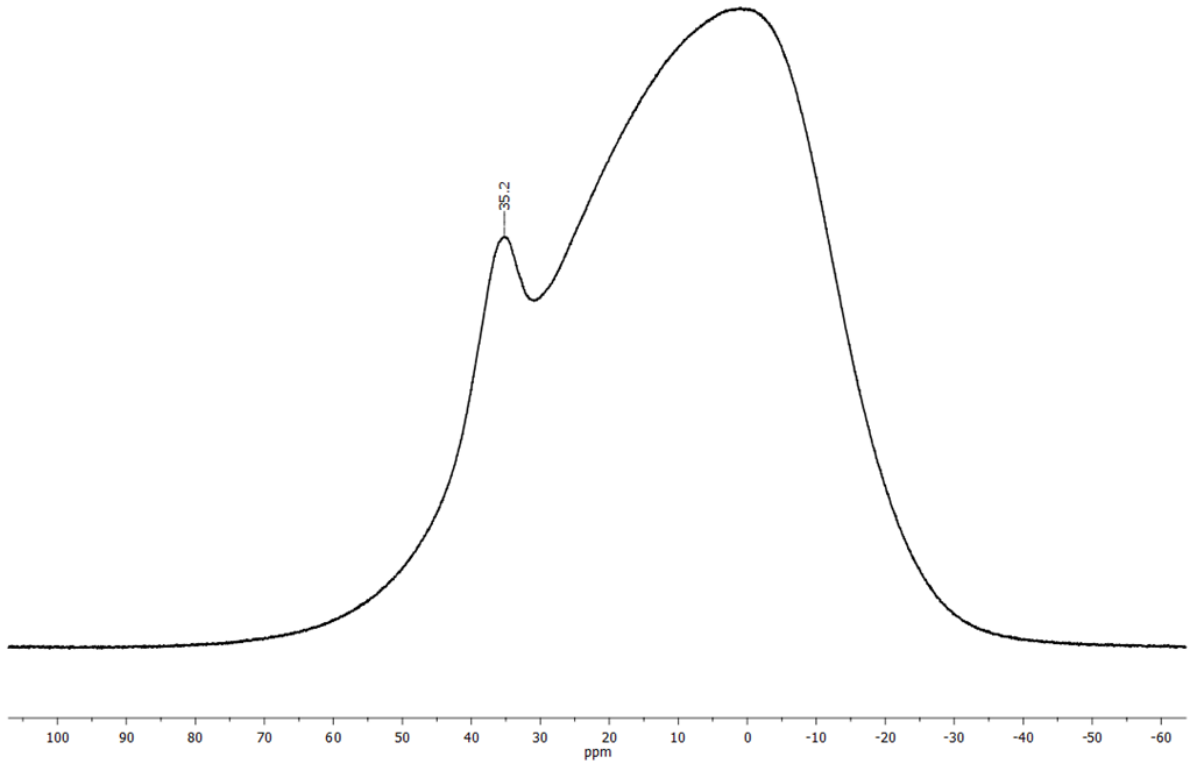

Figure S5.2.29. $^{11}B\{^{1}H\}$ NMR spectrum (160 MHz) of **9** in CD_2Cl_2.

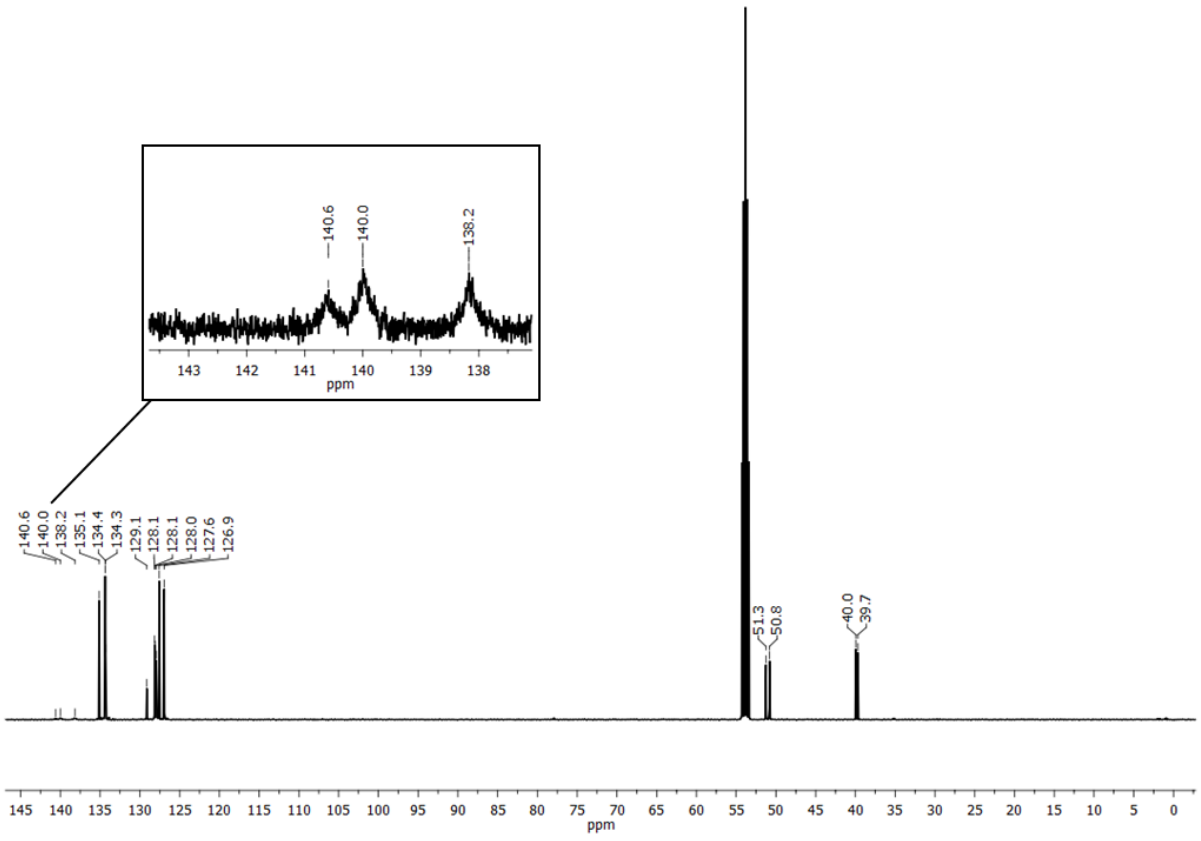

Figure S5.2.30. $^{13}C\{^{1}H\}$ NMR spectrum (126 MHz) of **9** in CD_2Cl_2.

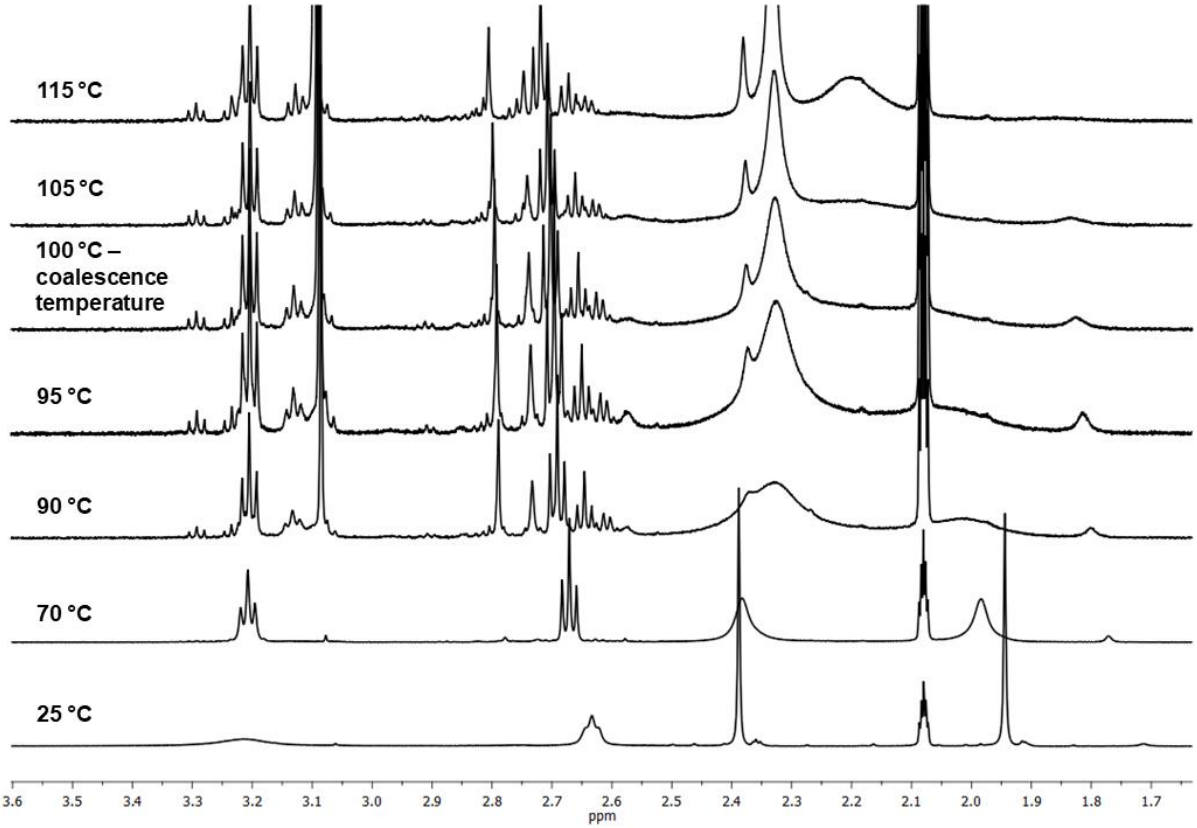

Figure S5.2.31. ^{1}H NMR spectra (600 MHz) of the determination of the coalescence temperature of **9** from 25 to 115 °C in toluene-d_8.

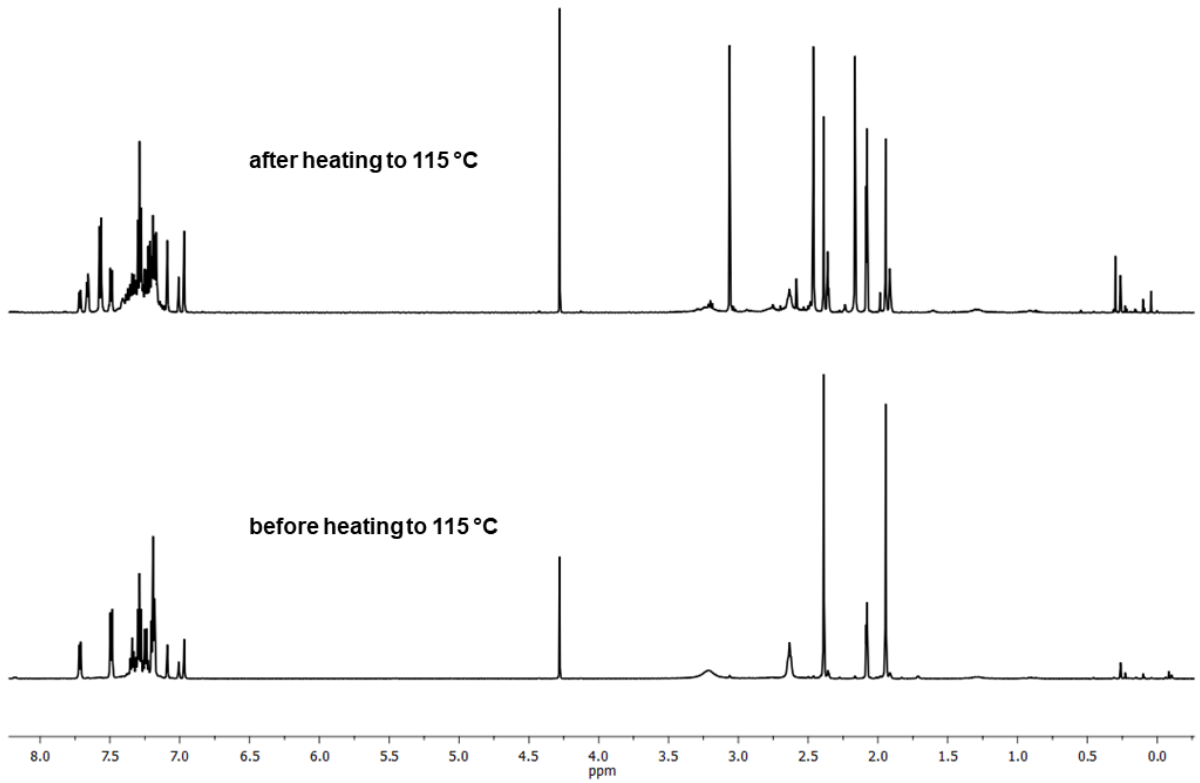

Figure S5.2.32. ^{1}H NMR spectra (600 MHz) of **9** before and after heating to 115 °C in toluene-d_8.

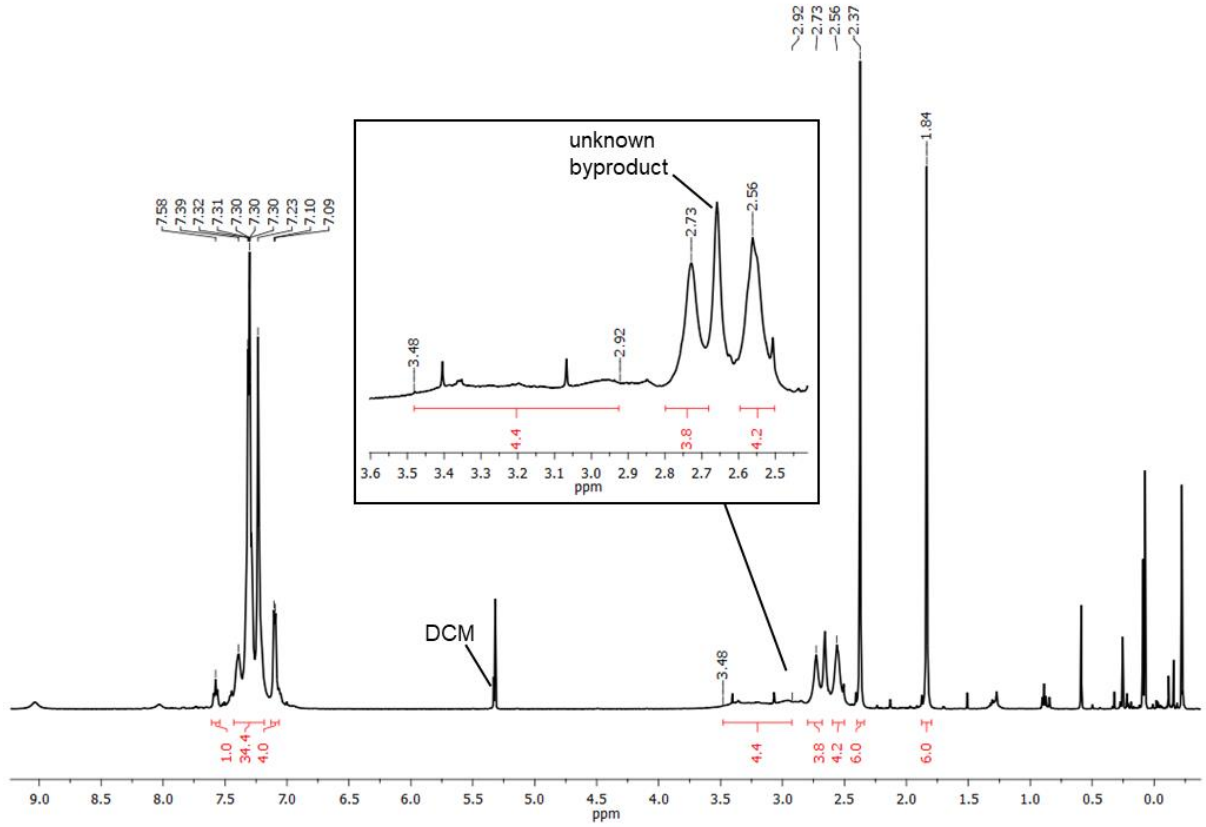

Figure S5.2.33. ^{1}H NMR spectrum (500 MHz) of **10** in CD_2Cl_2.

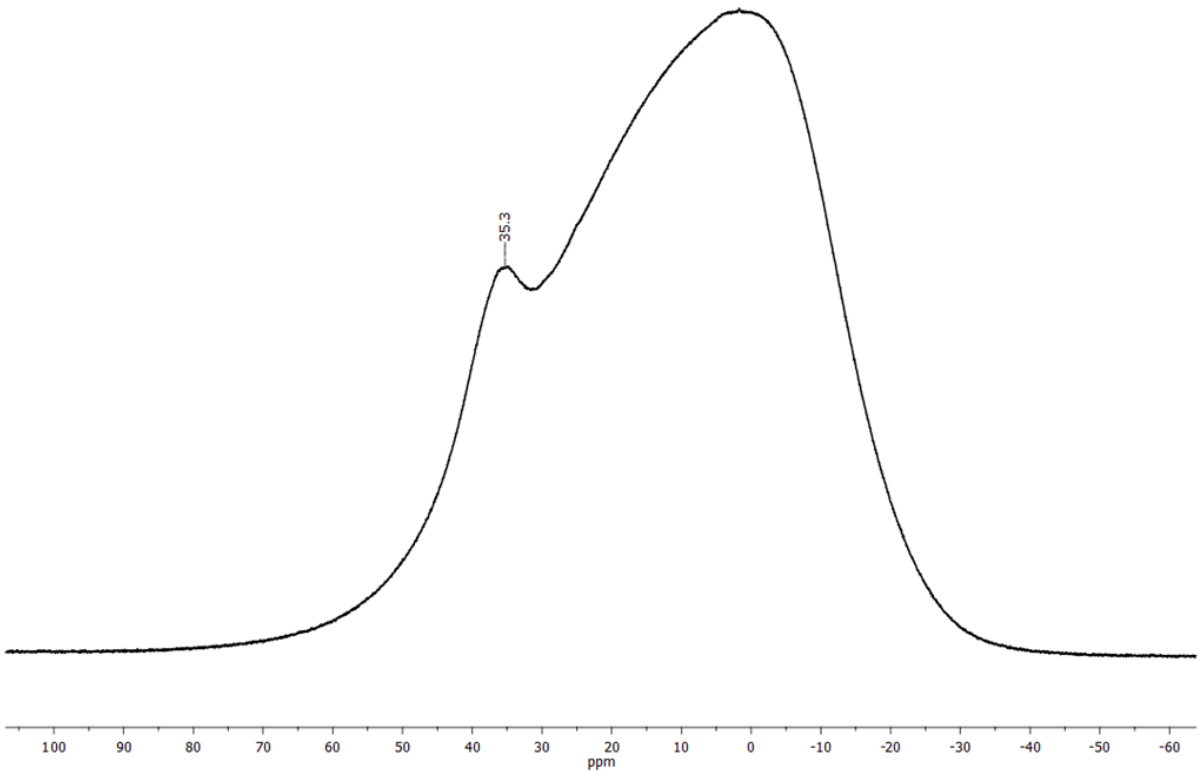

Figure S5.2.34. $^{11}B\{^{1}H\}$ NMR spectrum (160 MHz) of **10** in CD_2Cl_2.

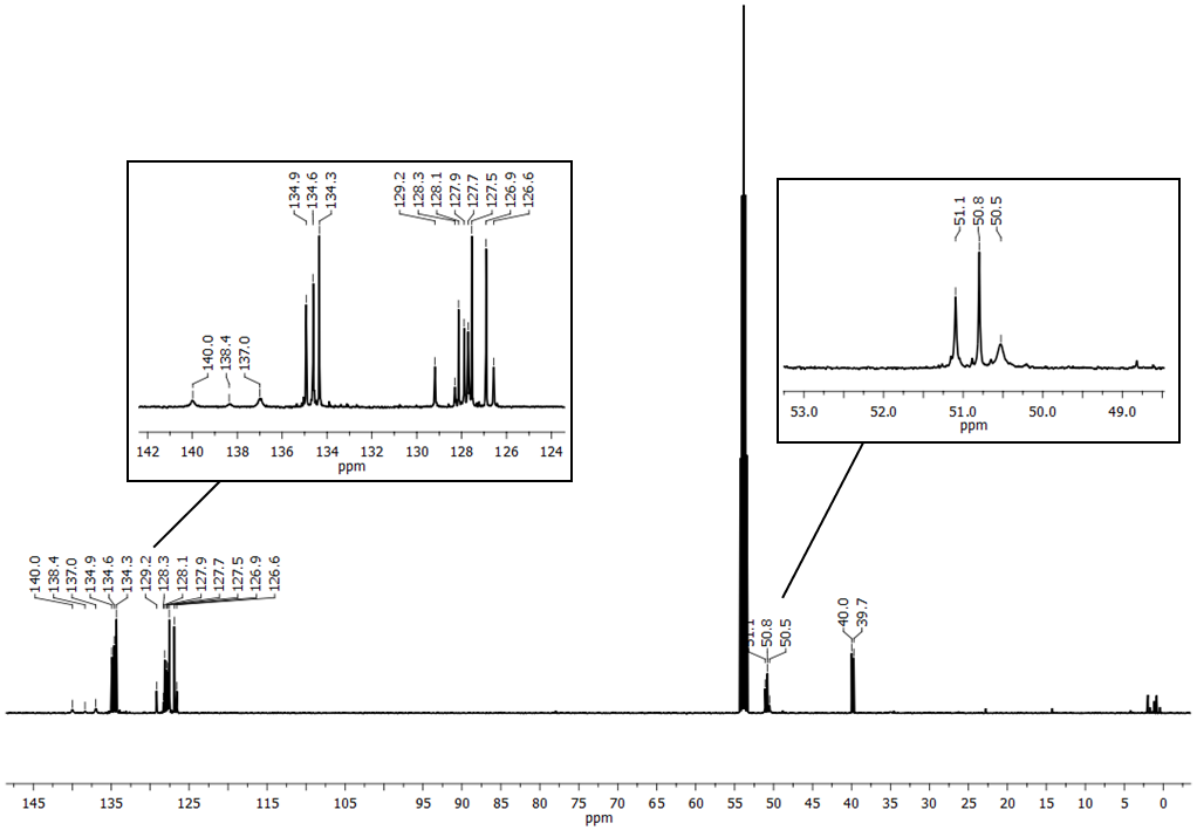

Figure S5.2.35. $^{13}C\{^{1}H\}$ NMR spectrum (126 MHz) of **10** in CD_2Cl_2.

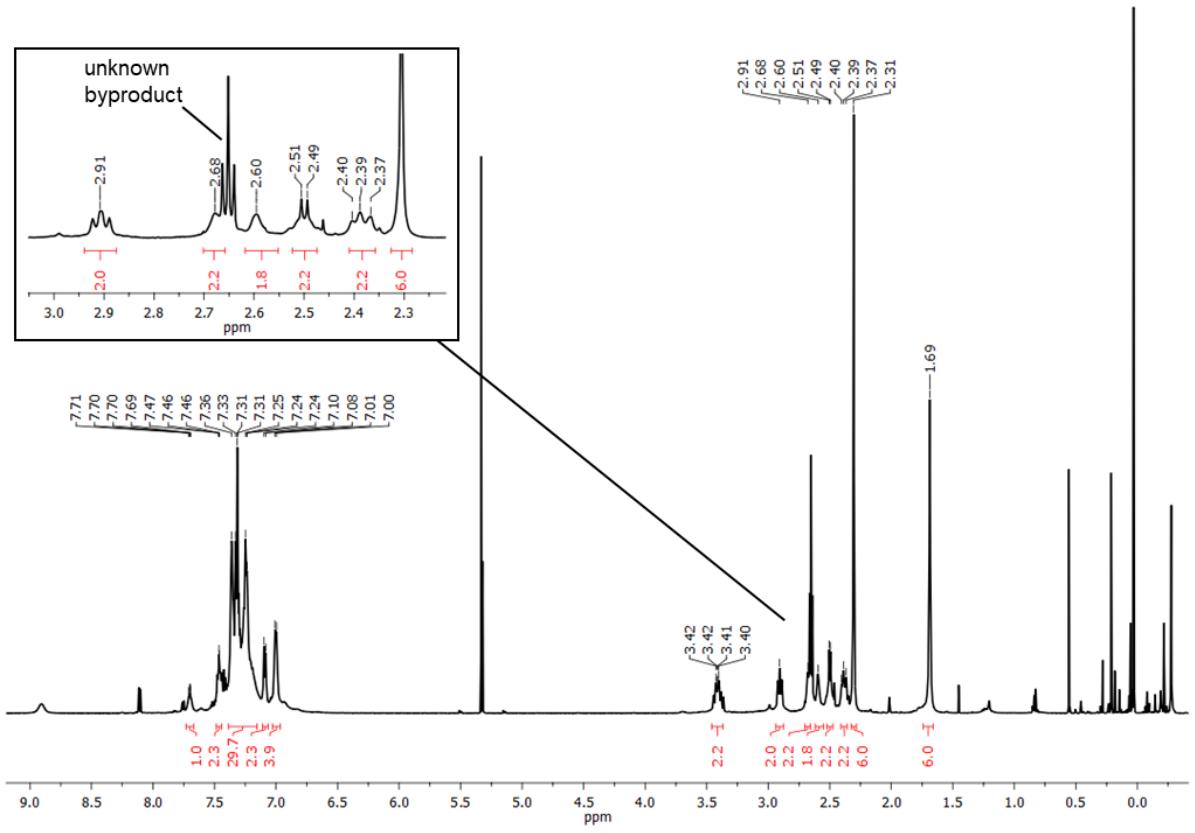

Figure S5.2.36. ^{1}H NMR spectrum (500 MHz) of **10** at −40 °C in CD_2Cl_2.

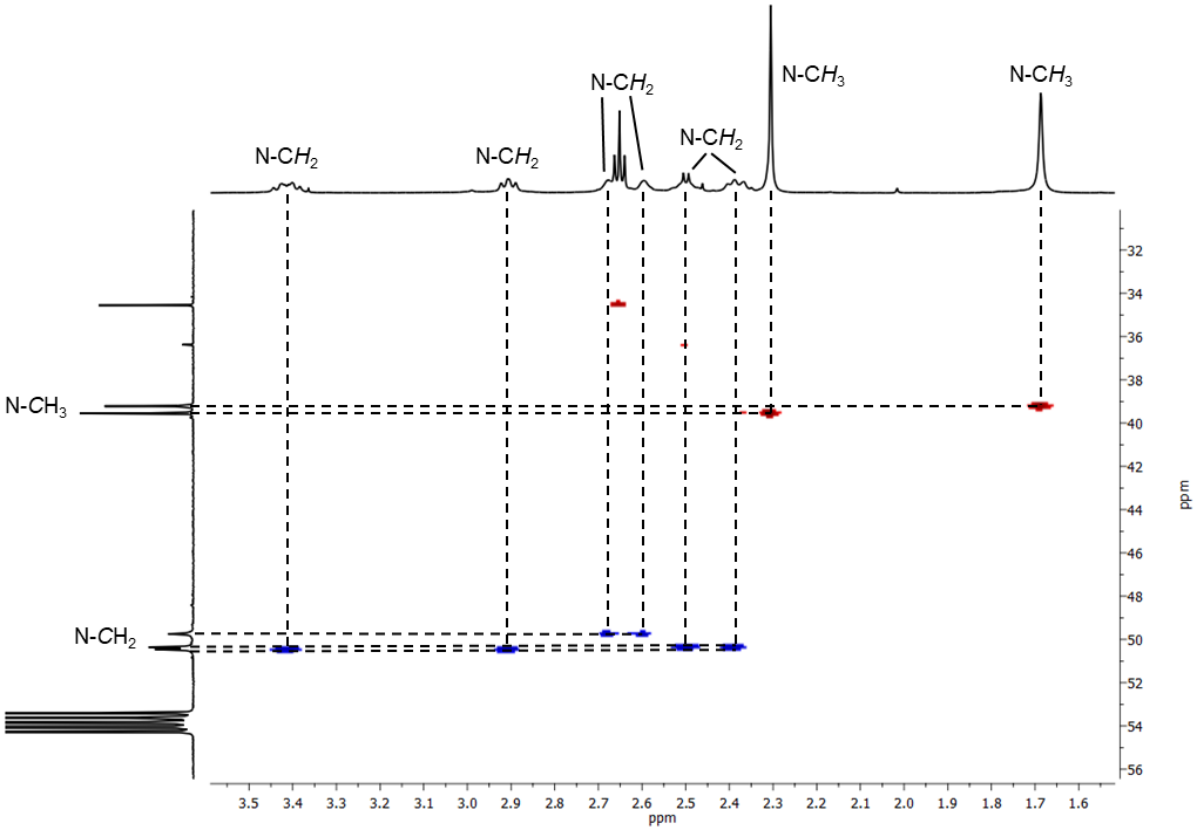

Figure S5.2.37. Detail of ^{1}H, ^{13}C HSQC spectrum of **10** at −40 °C in CD_2Cl_2.

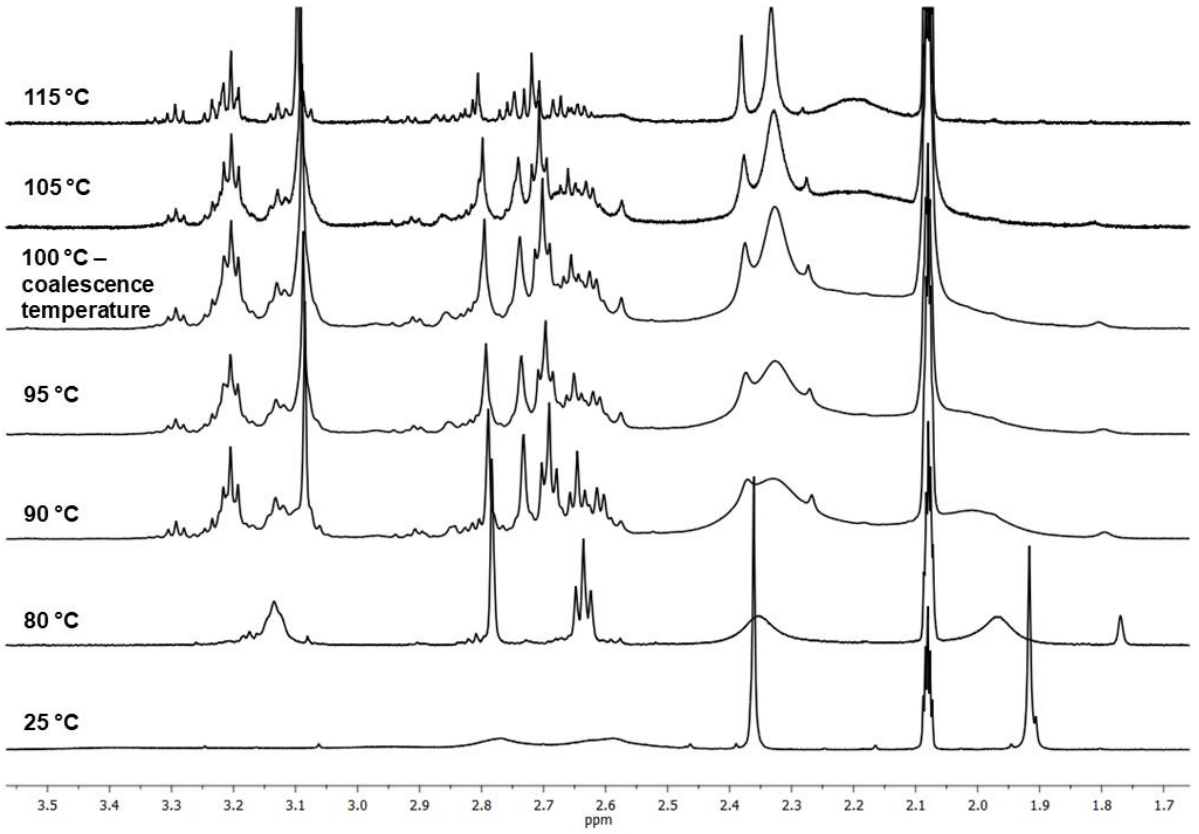

Figure S5.2.38. ^{1}H NMR spectra (600 MHz) of the determination of the coalescence temperature of **10** from 25 to 115 °C in toluene-d_8.

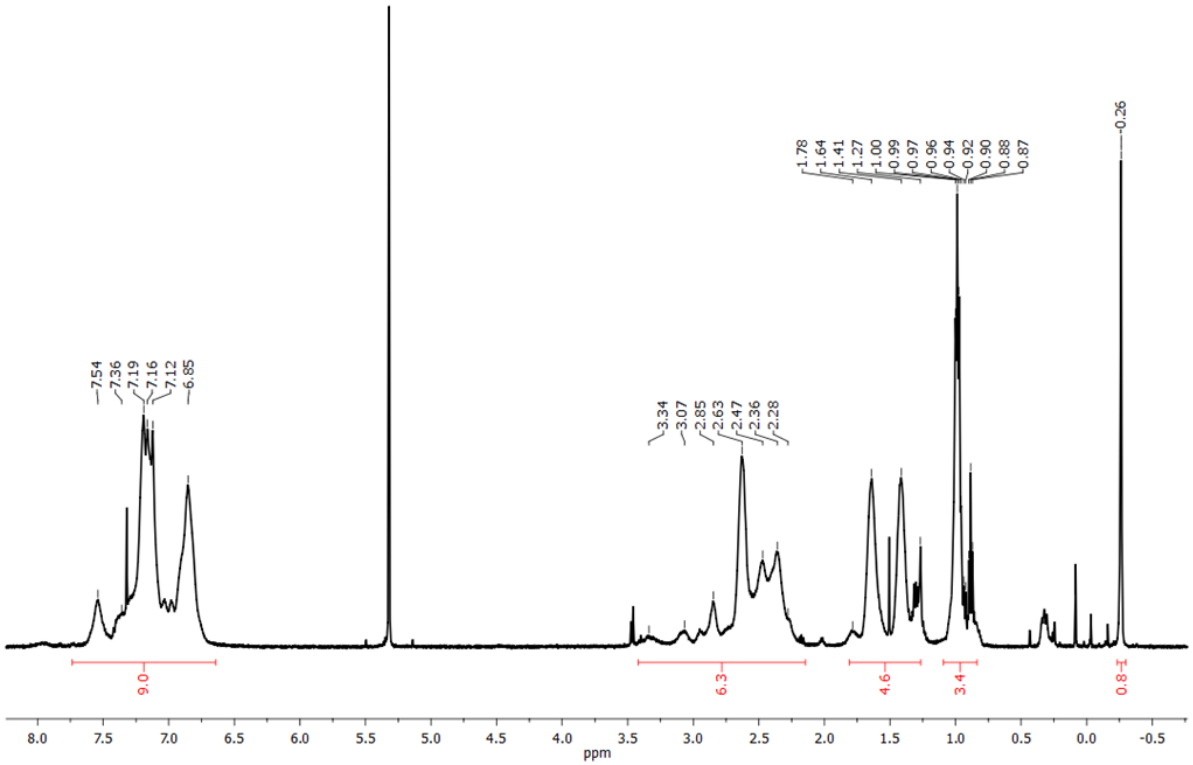

Figure S5.2.39. ^{1}H NMR spectrum (500 MHz) of **14** in CD_2Cl_2.

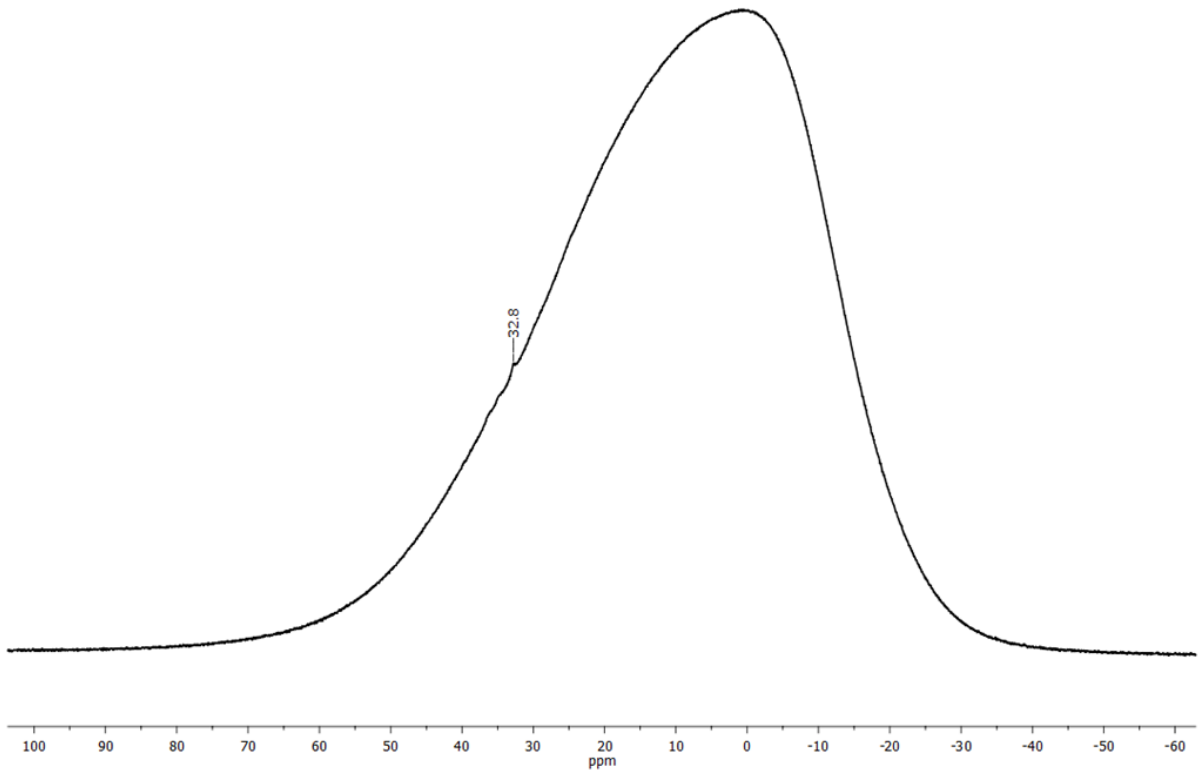

Figure S5.2.40. $^{11}B\{^{1}H\}$ NMR spectrum (160 MHz) of **14** in CD_2Cl_2.

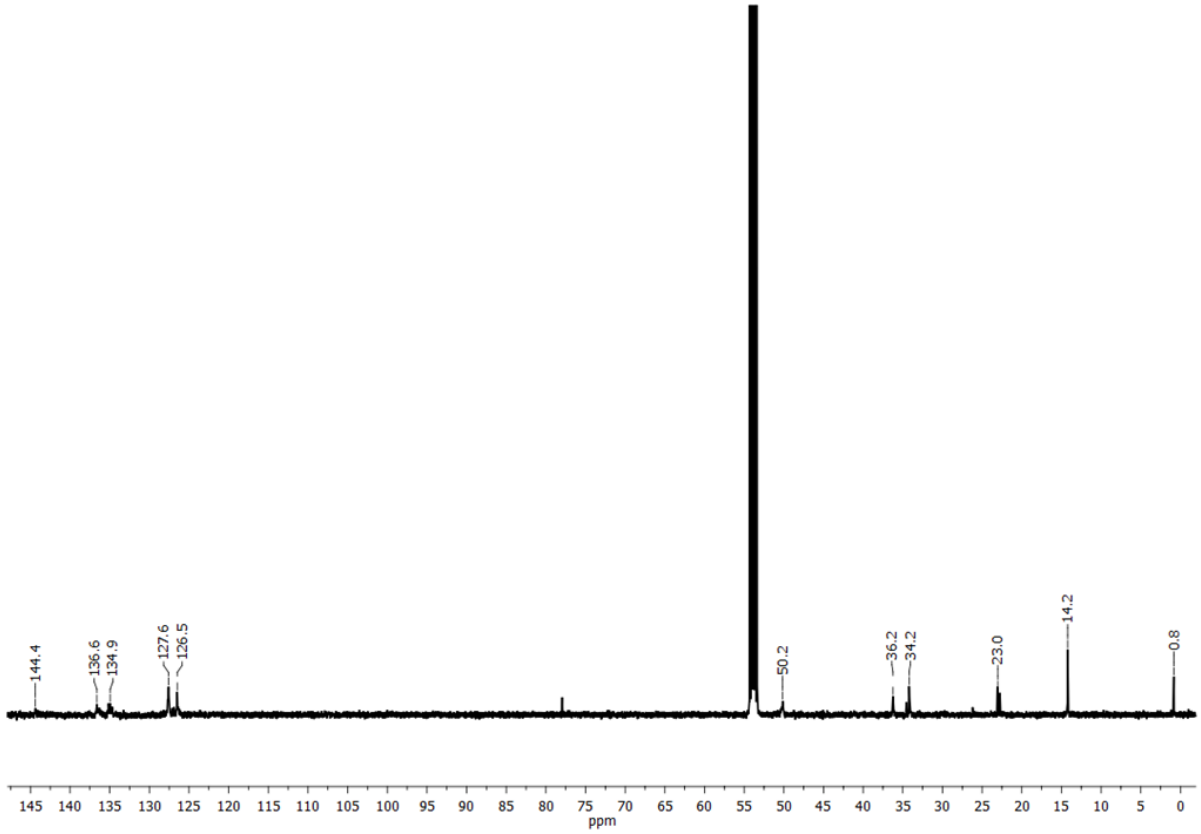

Figure S5.2.41. $^{13}C\{^{1}H\}$ NMR spectrum (126 MHz) of **14** in CD_2Cl_2.

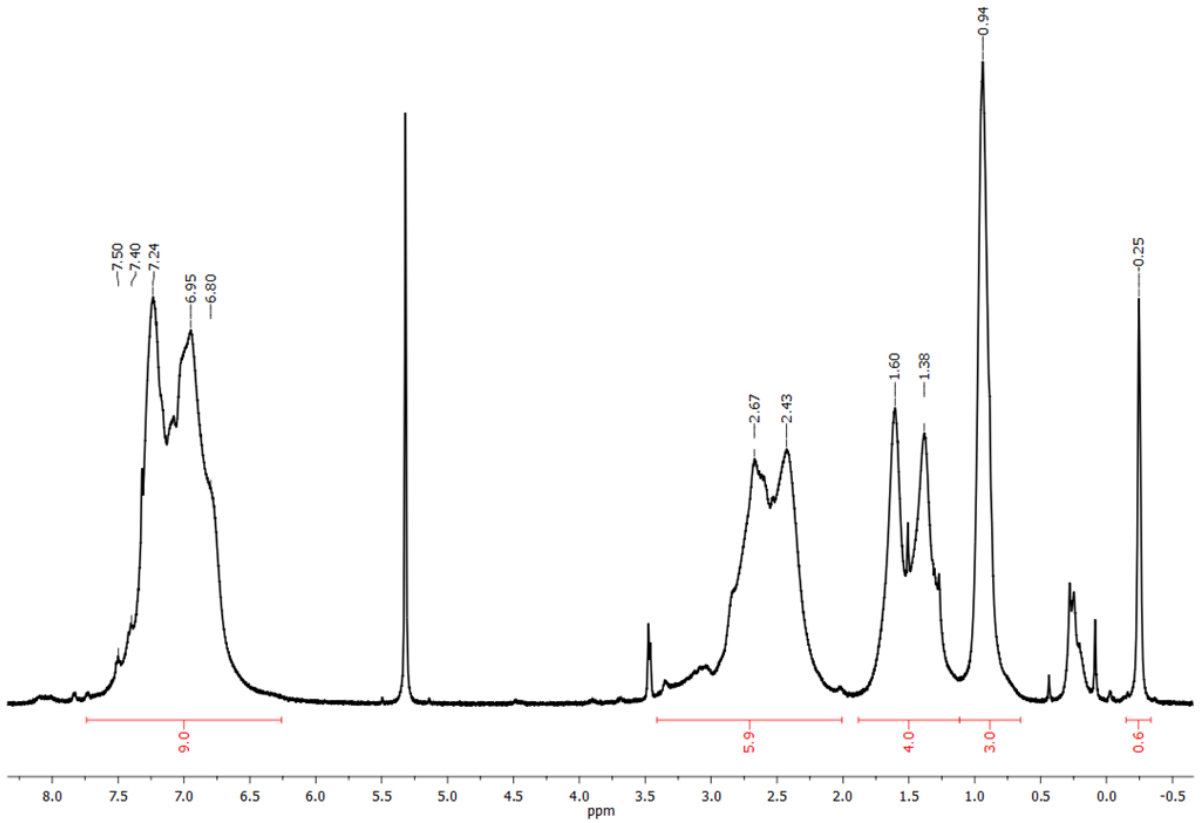

Figure S5.2.42. ^{1}H NMR spectrum (500 MHz) of **15** in CD_2Cl_2.

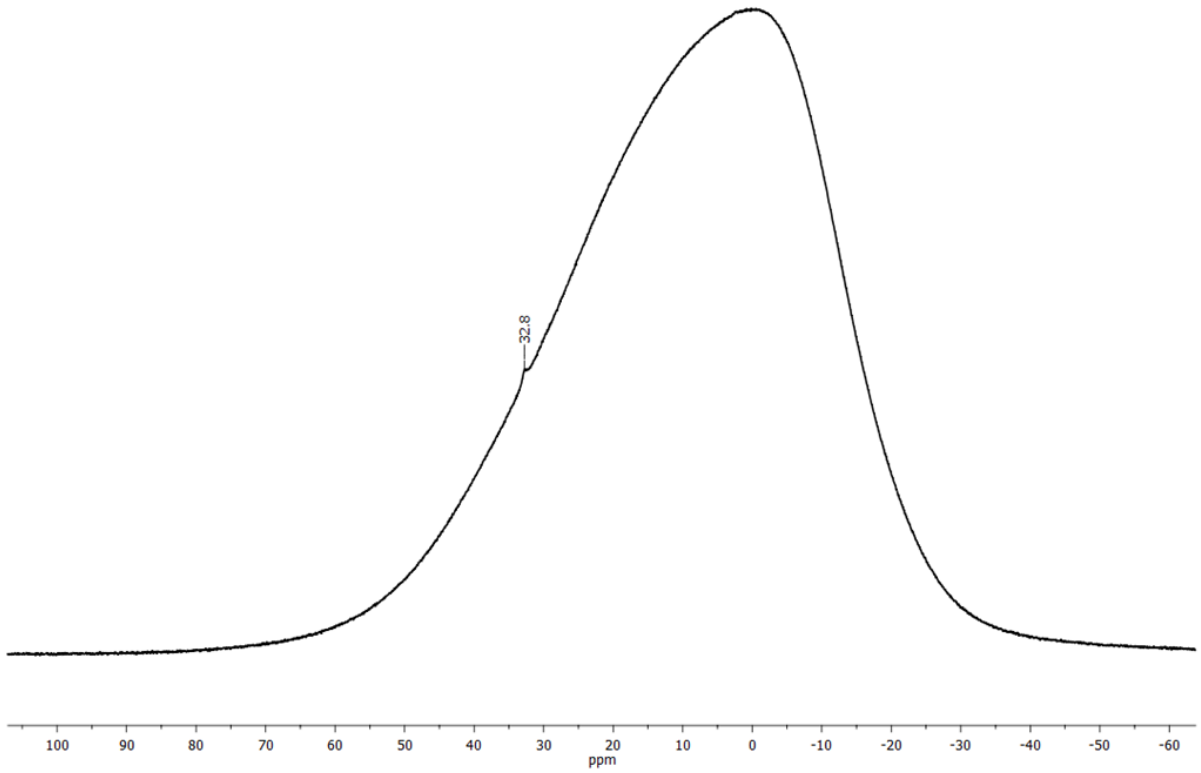

Figure S5.2.43. $^{11}B\{^{1}H\}$ NMR spectrum (160 MHz) of **15** in CD_2Cl_2.

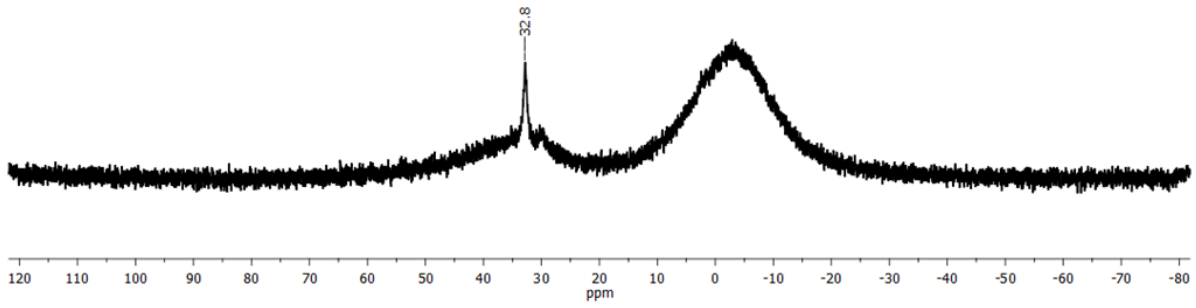

Figure S5.2.44. $^{11}B\{^{1}H\}$ NMR spectrum (160 MHz) of **15** in CD_2Cl_2 with reduced glass background.

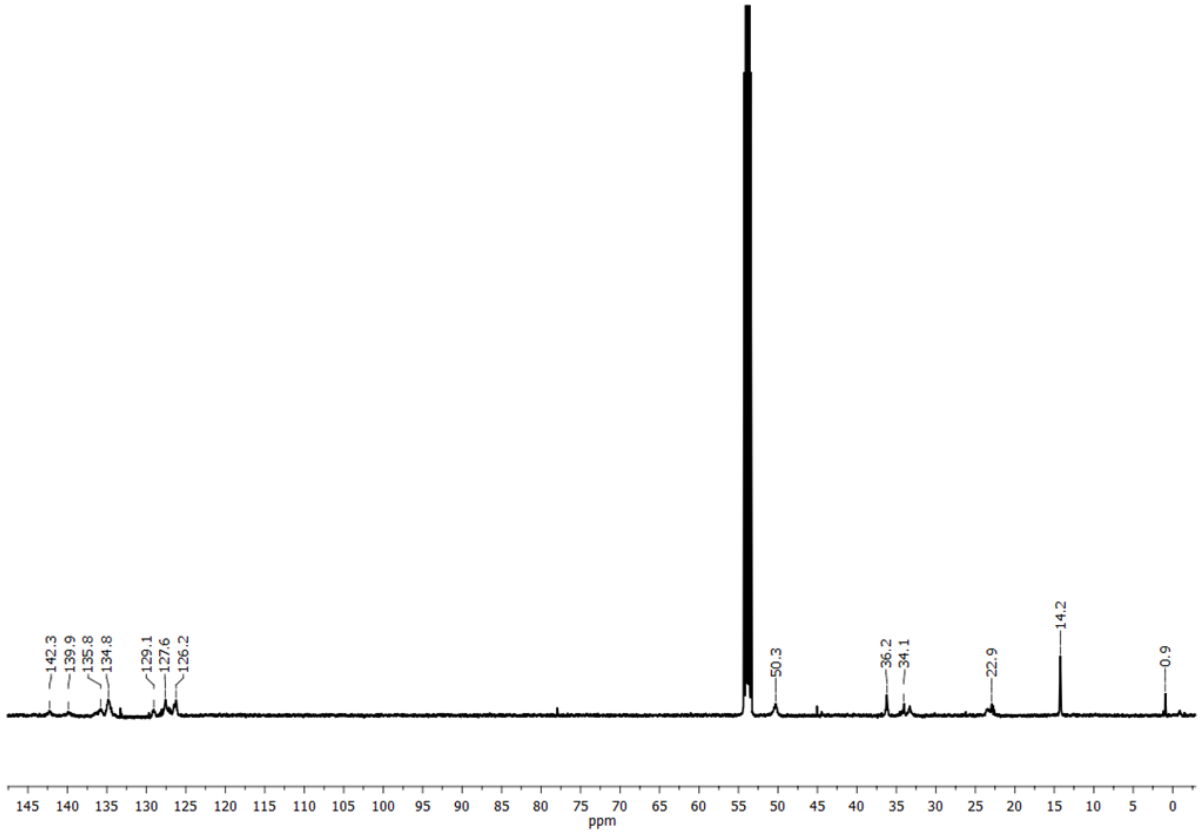

Figure S5.2.45. $^{13}C\{^{1}H\}$ NMR spectrum (126 MHz) of **15** in CD_2Cl_2.

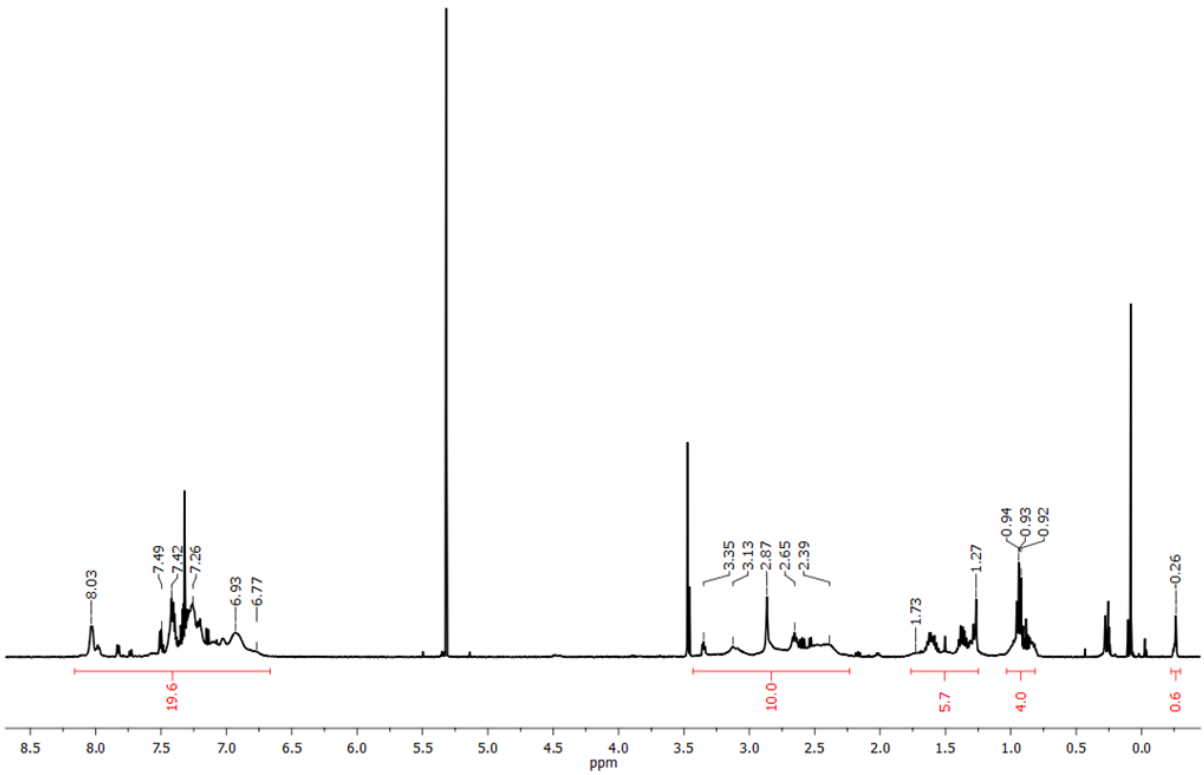

Figure S5.2.46. ^{1}H NMR spectrum (500 MHz) of **16** in CD_2Cl_2.

Determination of the rotational barrier

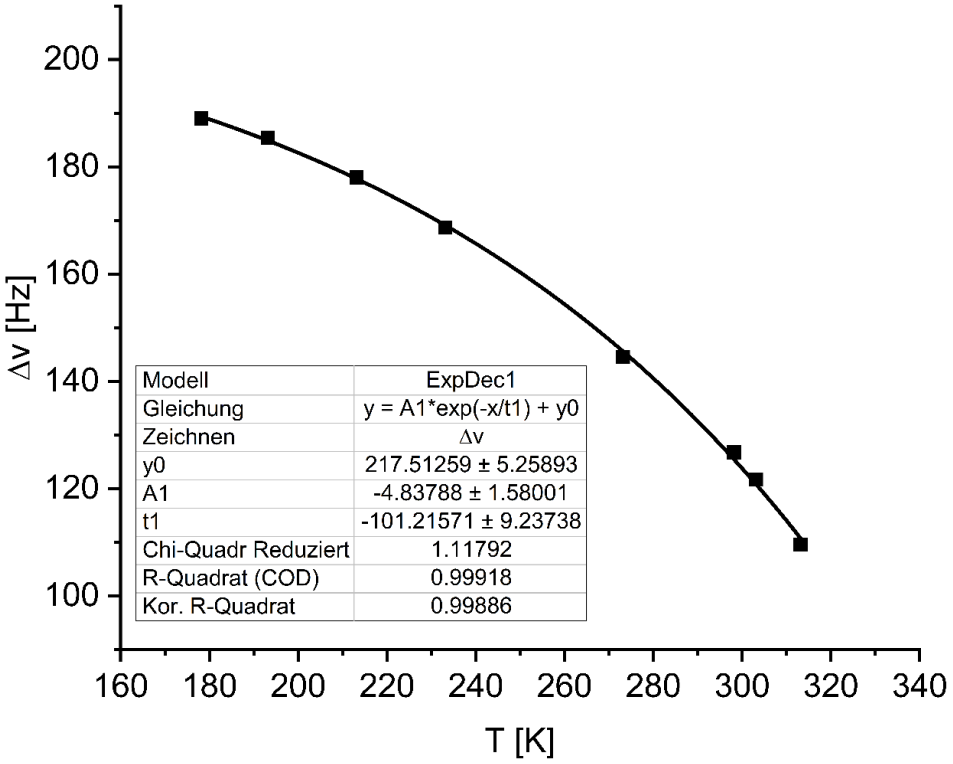

Figure S5.2.47. Extrapolation function of the no-exchange chemical shift difference Δν of **5**.

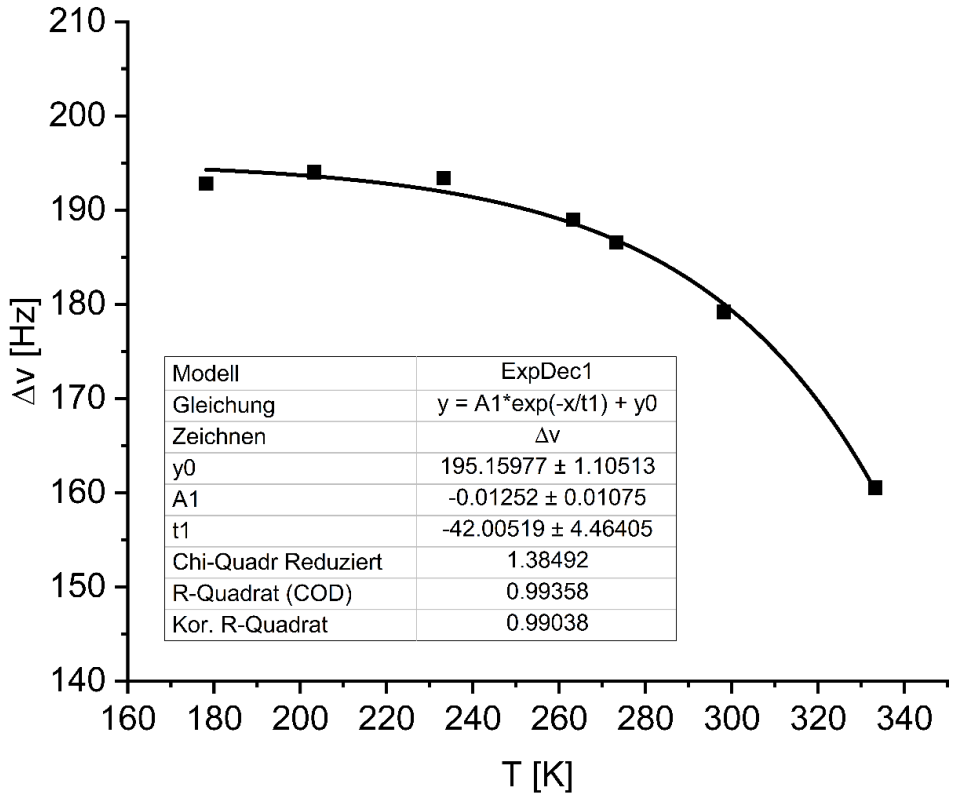

Figure S5.2.48. Extrapolation function of the no-exchange chemical shift difference Δν of **6**.

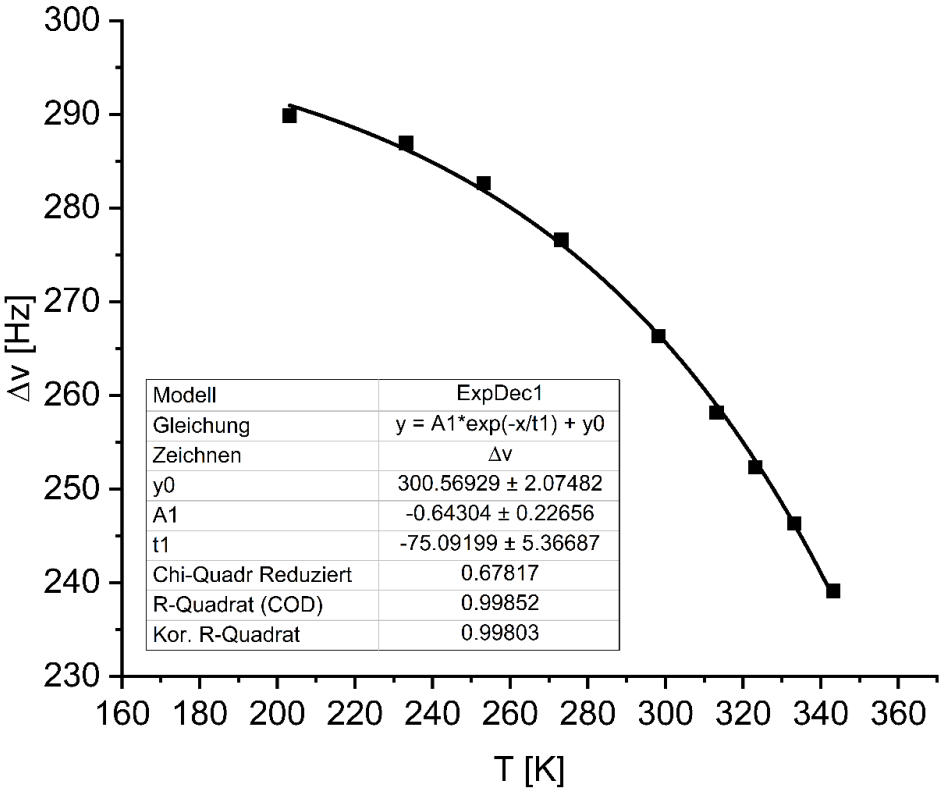

Figure S5.2.49. Extrapolation function of the no-exchange chemical shift difference Δν of **9**.

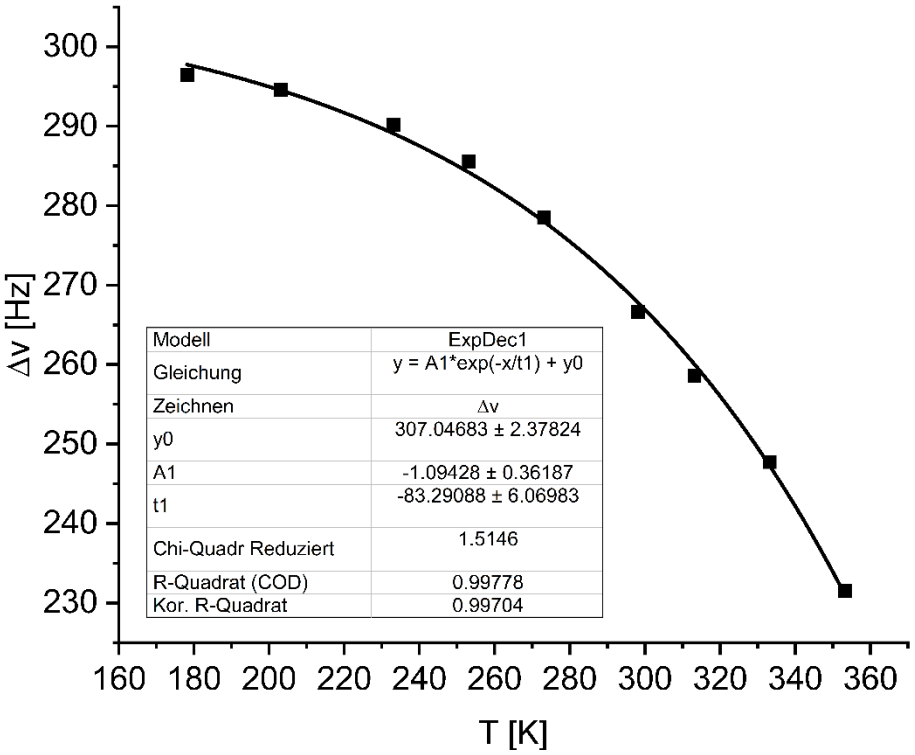

Figure S5.2.50. Extrapolation function of the no-exchange chemical shift difference Δν of **10**.

HRMS spectra

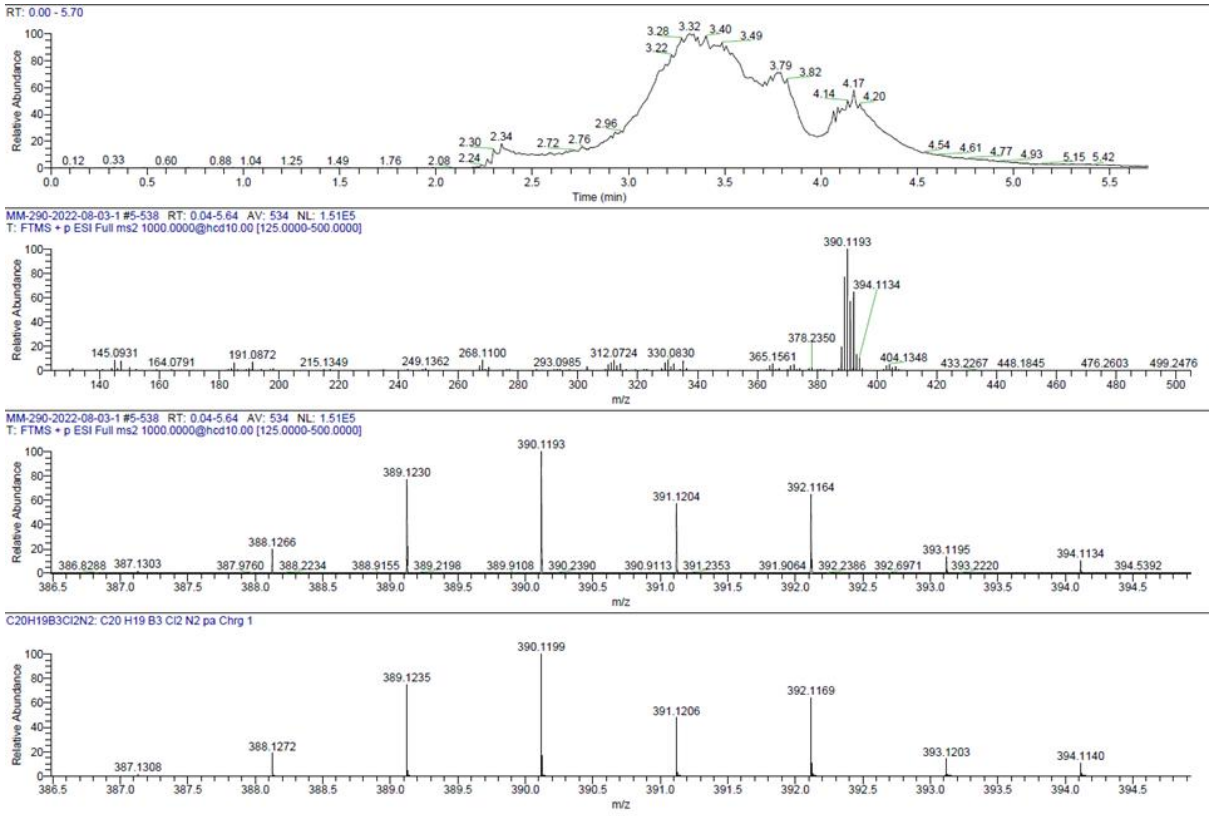

Figure S5.2.51. HRMS spectrum (LIFDI) of **4**.

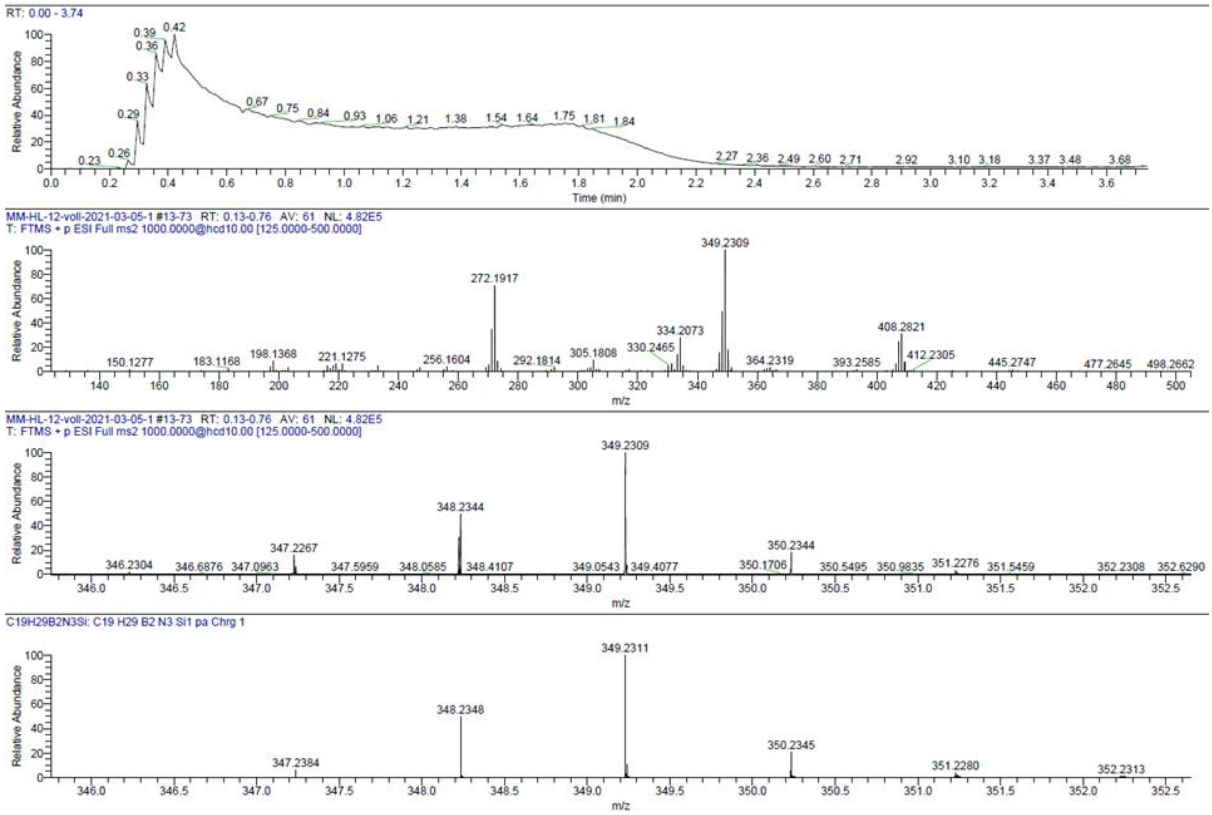

Figure S5.2.52. HRMS spectrum (LIFDI) of **5**.

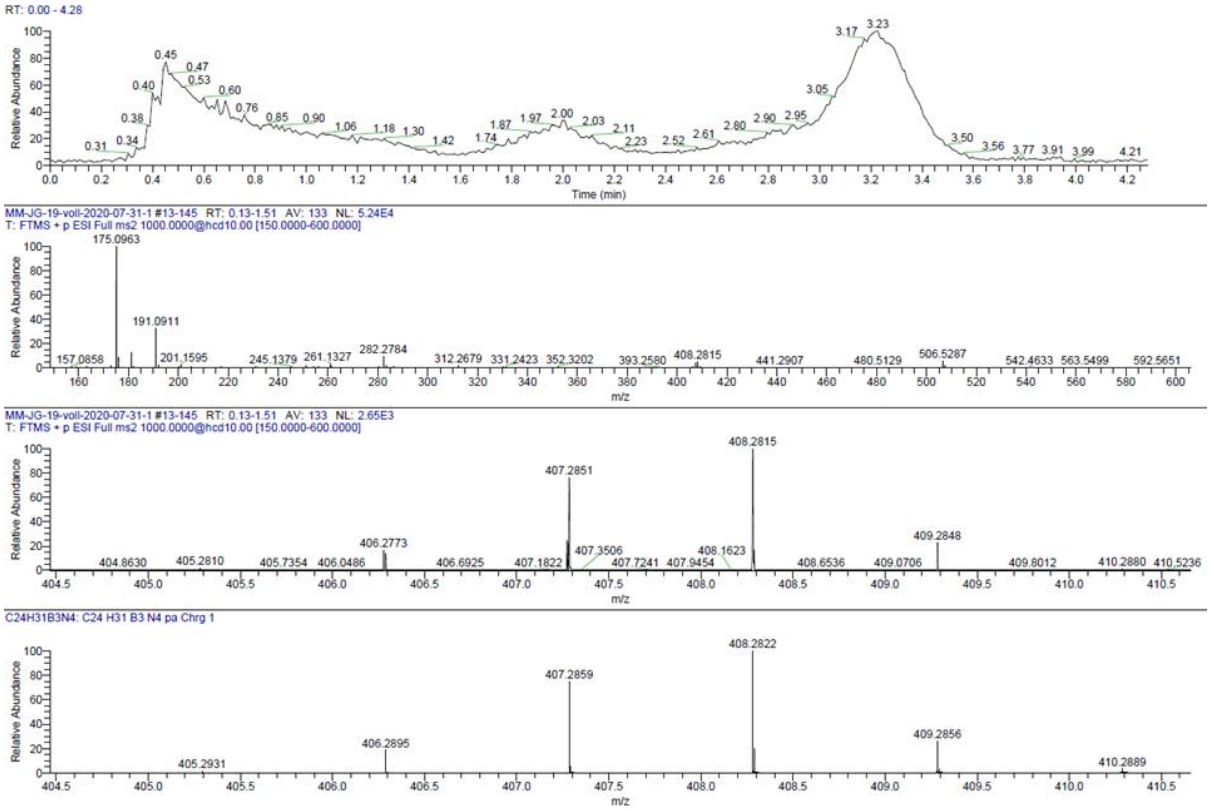

Figure S5.2.53. HRMS spectrum (LIFDI) of **6**.

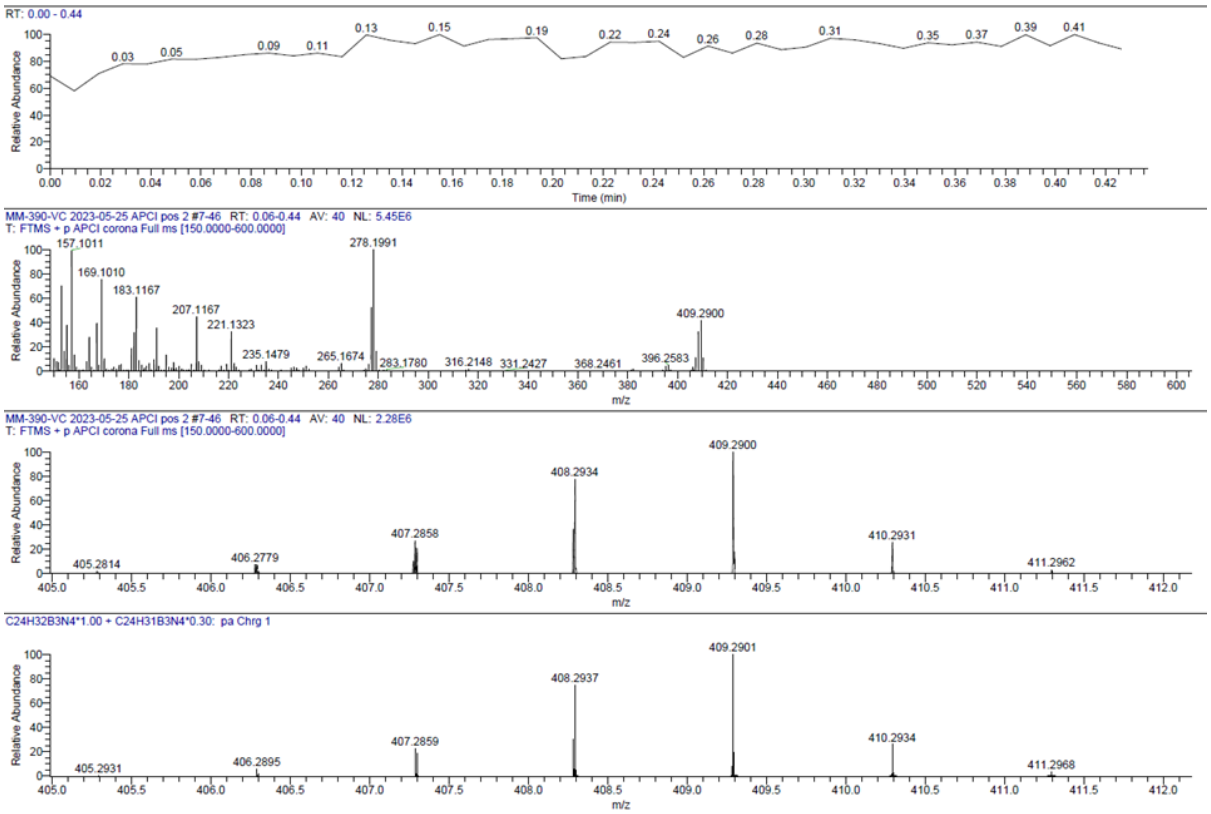

Figure S5.2.54. HRMS spectrum (APCI pos) of **6** (alternative route; mixture [M] and $[M+H]^+$).

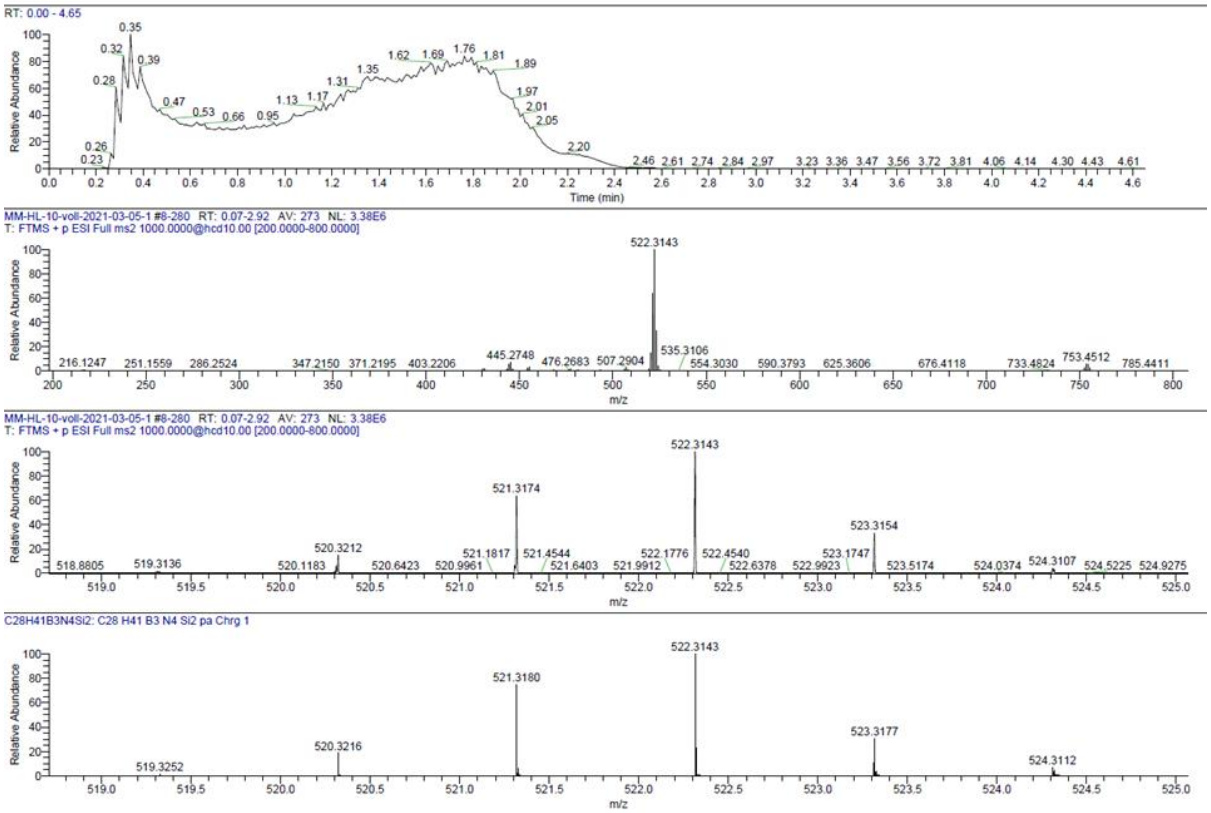

Figure S5.2.55. HRMS spectrum (LIFDI) of **7**.

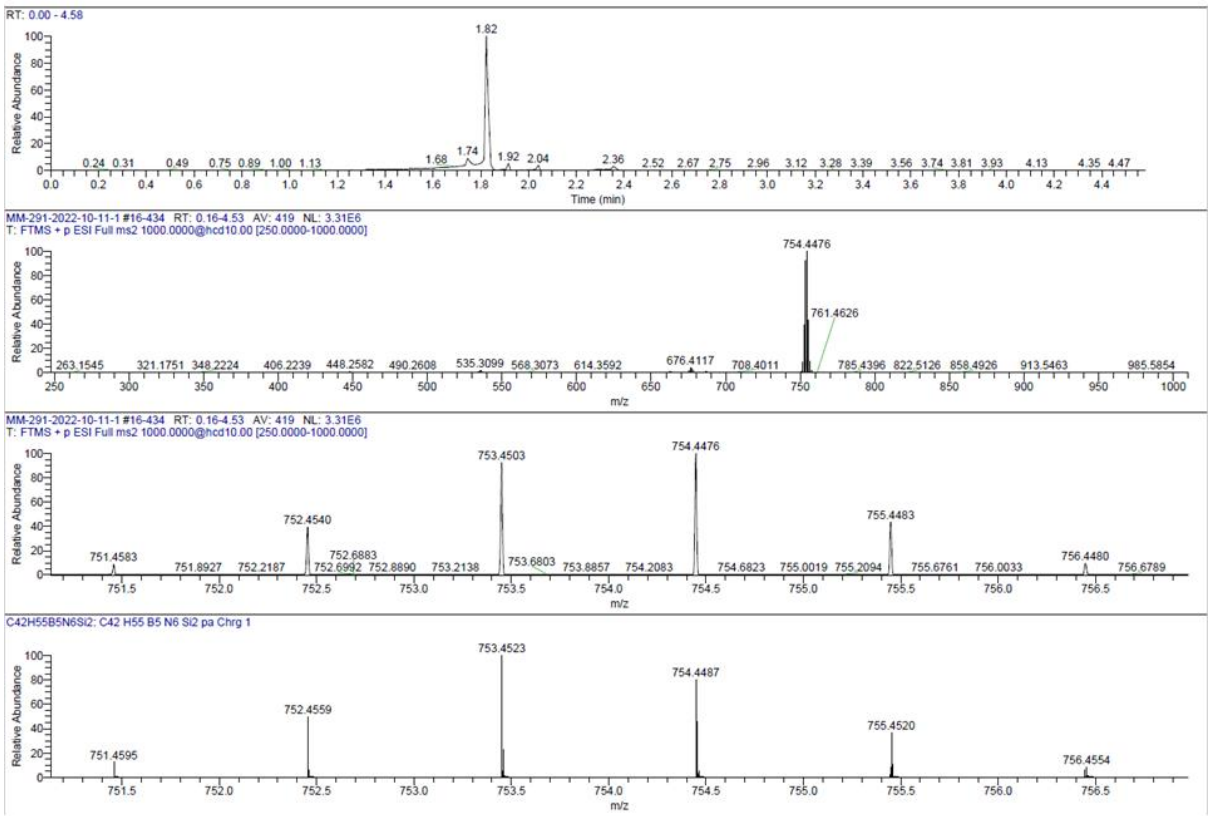

Figure S5.2.56. HRMS spectrum (LIFDI) of **8**.

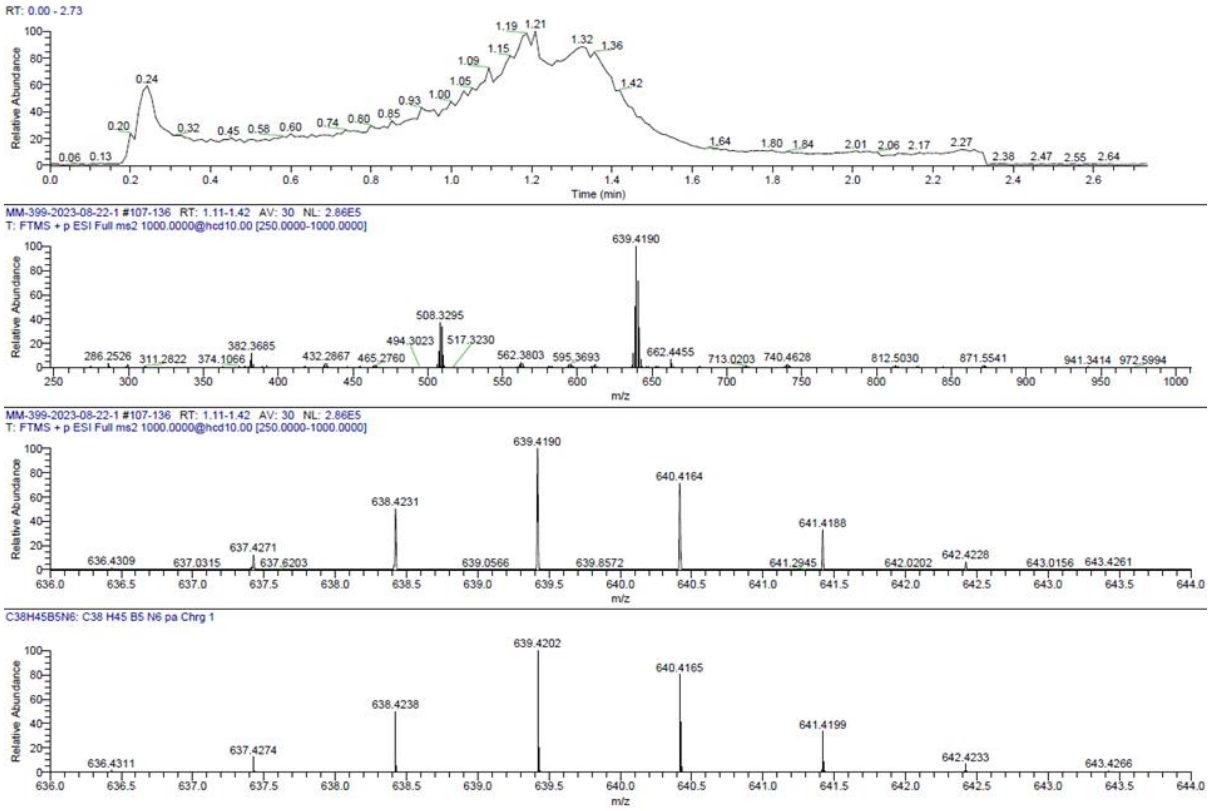

Figure S5.2.57. HRMS spectrum (LIFDI) of **9**.

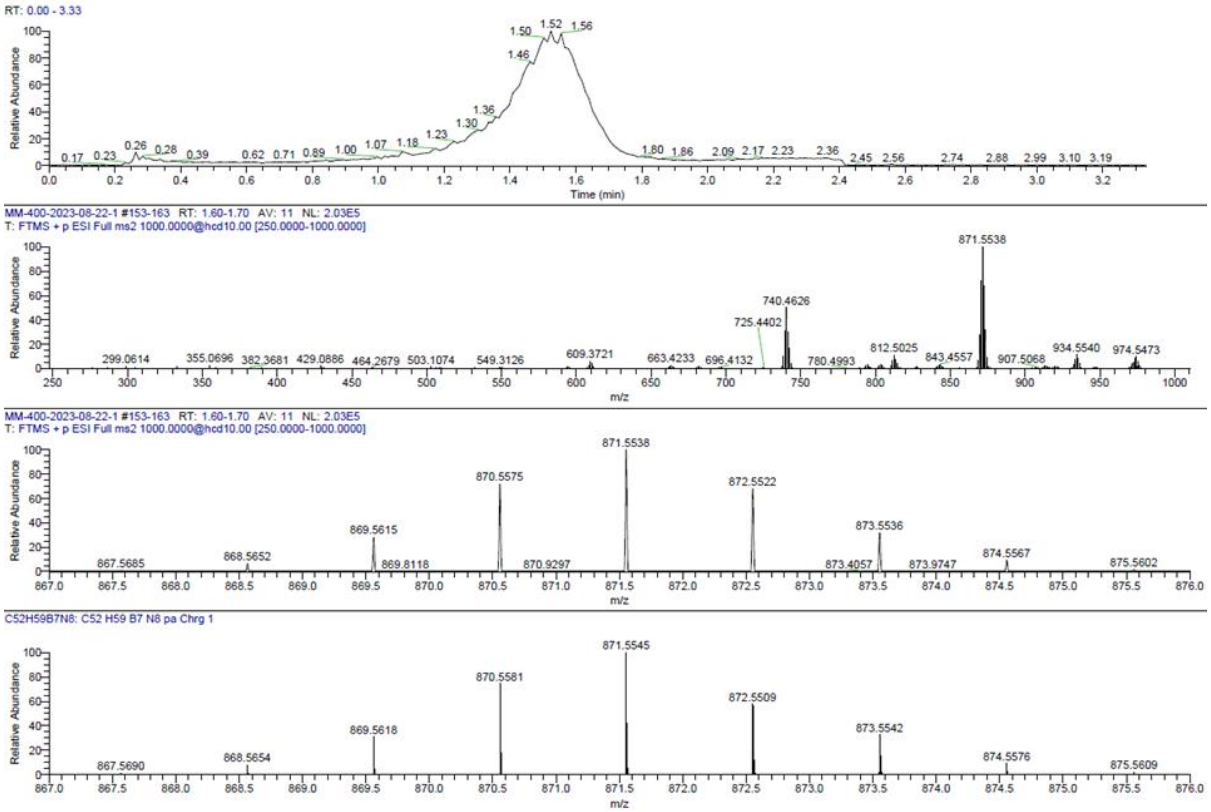

Figure S5.2.58. HRMS spectrum (LIFDI) of **10**

Thermogravimetric analysis

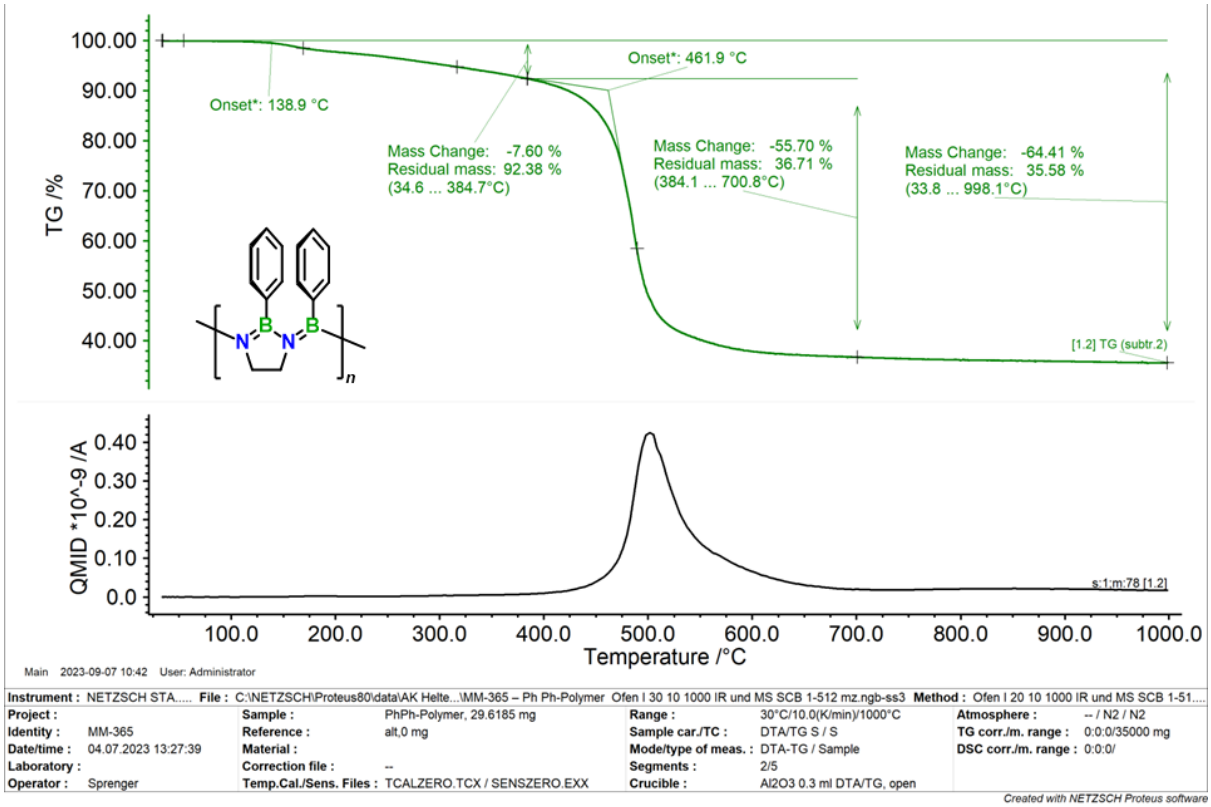

Figure S5.2.59. TG curve of **12** (top) with ion trace (bottom) of benzene.

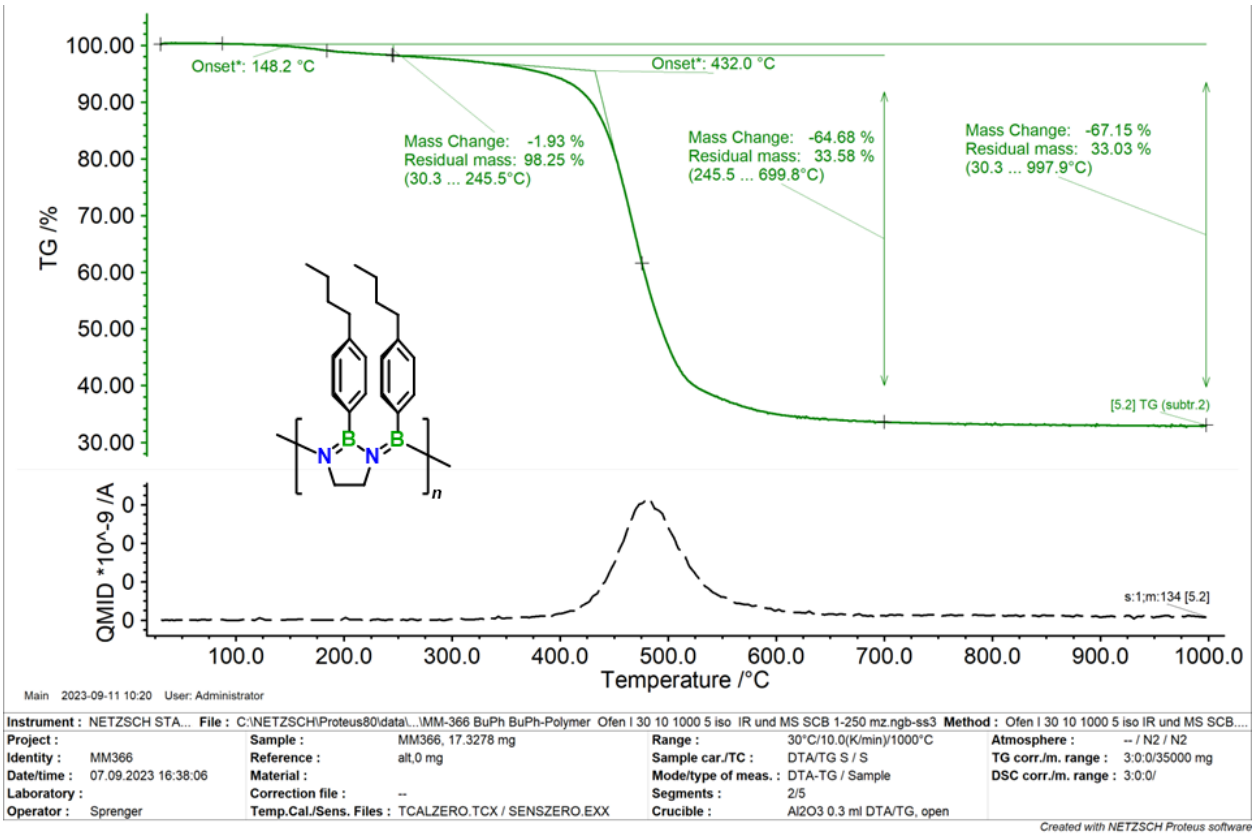

Figure S5.2.60. TG curve of **13** under N_2 atmosphere (10 K min^{-1}, top) with ion trace (bottom) of *n*-butylbenzene.

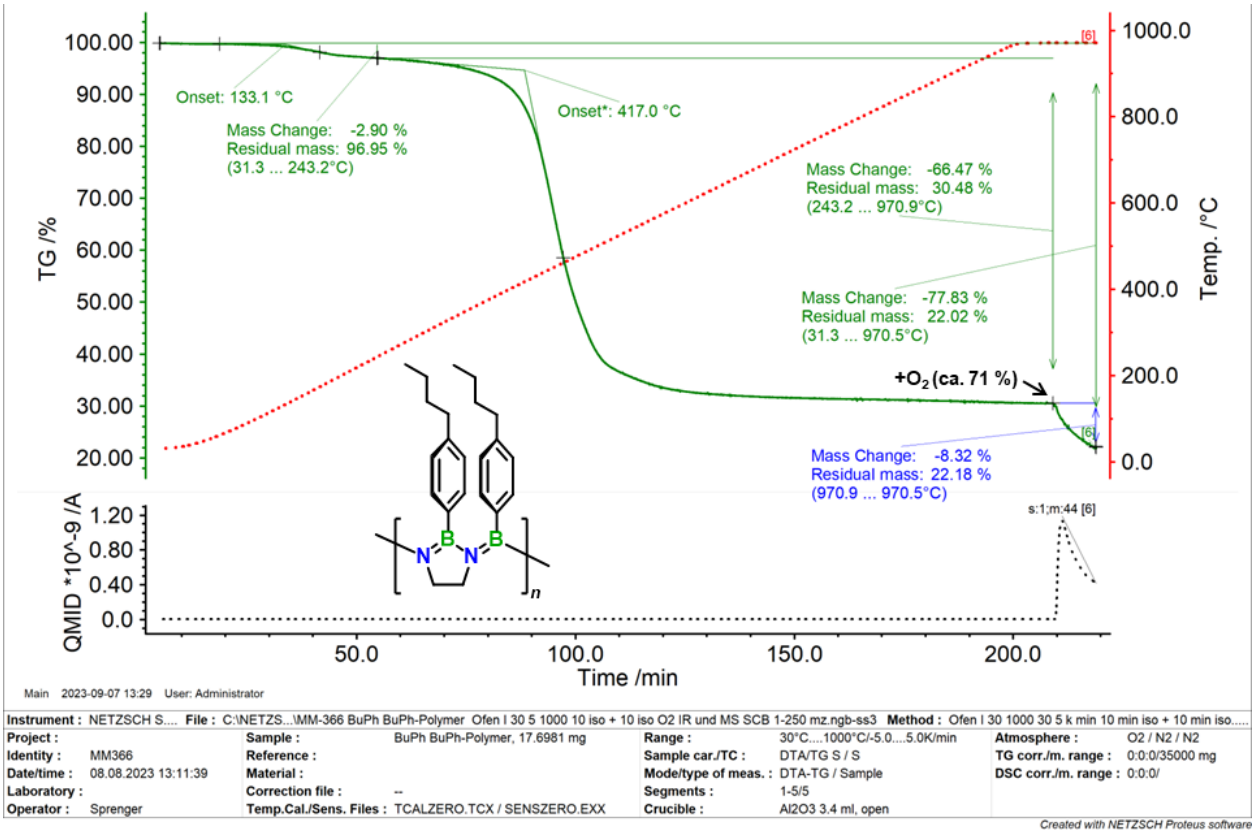

Figure S5.2.61. TG curve of **13** under N_2 atmosphere (5 K min^{-1}) while heating followed of an isothermic period and addition of O_2 (ca. 71 %) at 1000 °C (top) with ion trace (bottom) of CO_2.

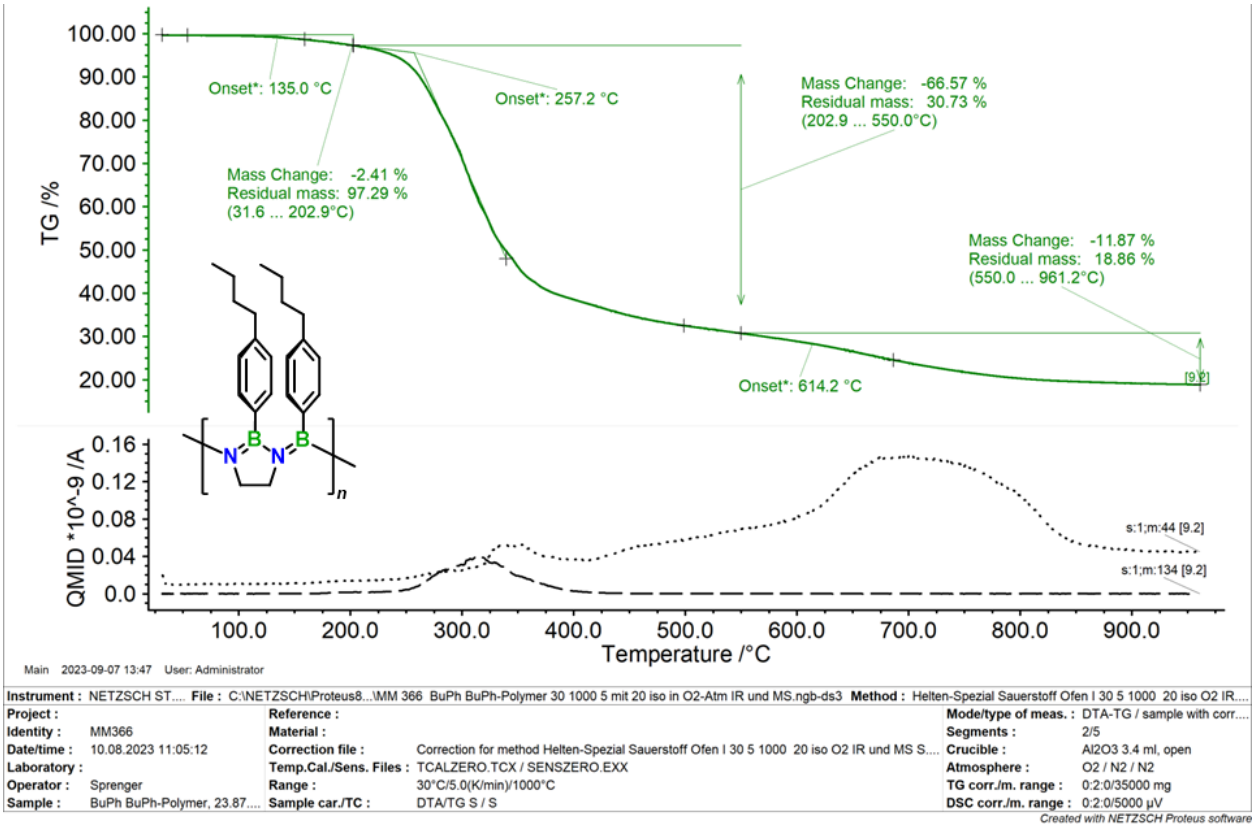

Figure S5.2.62. TG curve of **13** under a mixed O_2:N_2 atmosphere (ca. 71:29 %, 5 K min^{-1}, top) with the ion traces (bottom) of *n*-butylbenzene (dashed line) and CO_2 (dotted line).

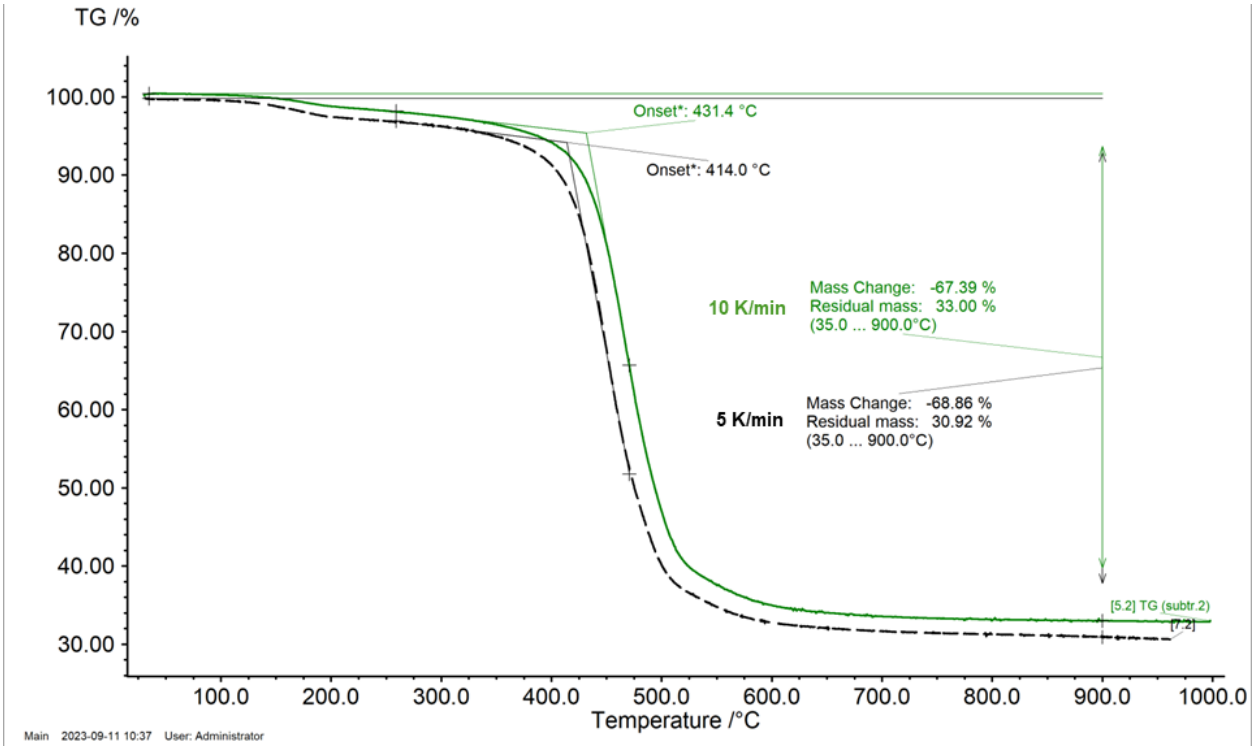

Figure S5.2.63. TG curve of **13** under N_2 atmosphere with a heating rate of 5 K min^{-1} (dashed line) and 10 K min^{-1} (solid line).

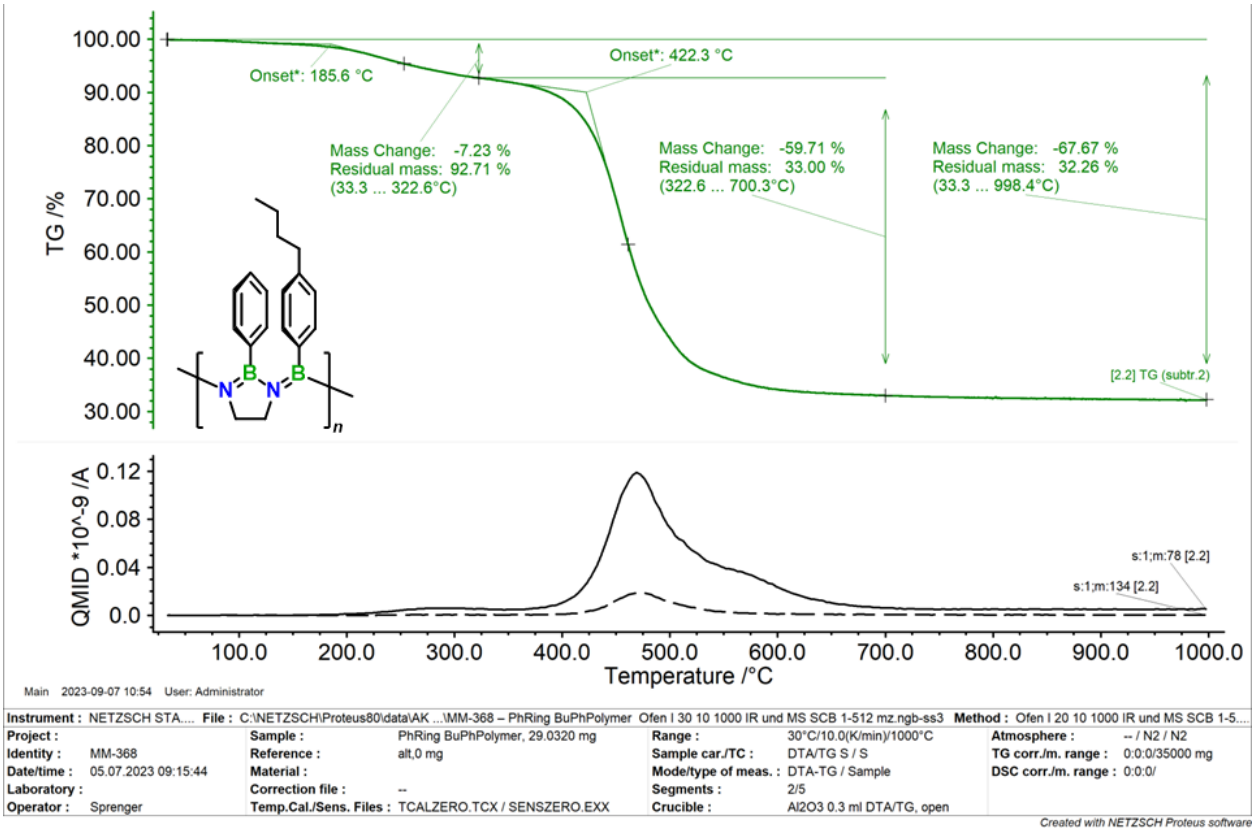

Figure S5.2.64. TG curve of **14** (top) with the ion traces (bottom) of benzene (solid line) and *n*-butylbenzene (dashed line).

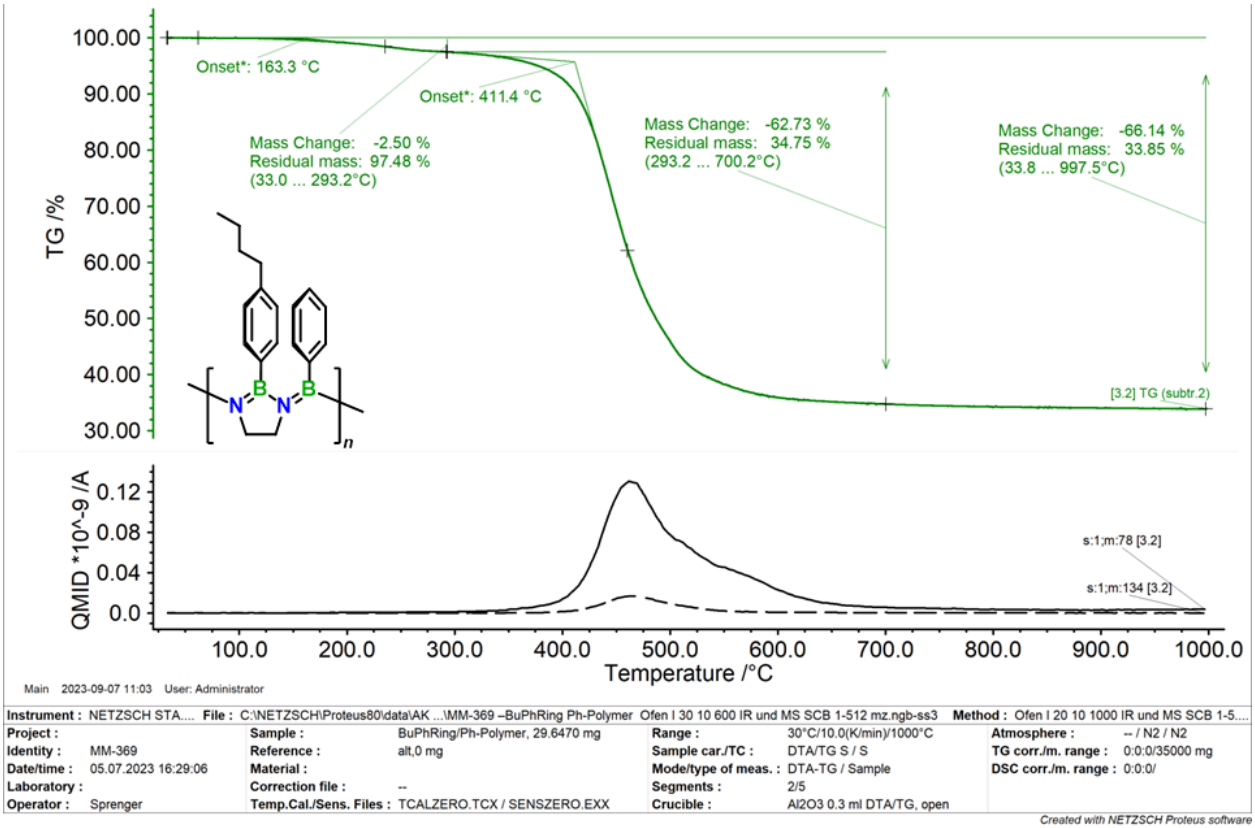

Figure S5.2.65. TG curve of **15** (top) with the ion traces (bottom) of benzene (solid line) and *n*-butylbenzene (dashed line).

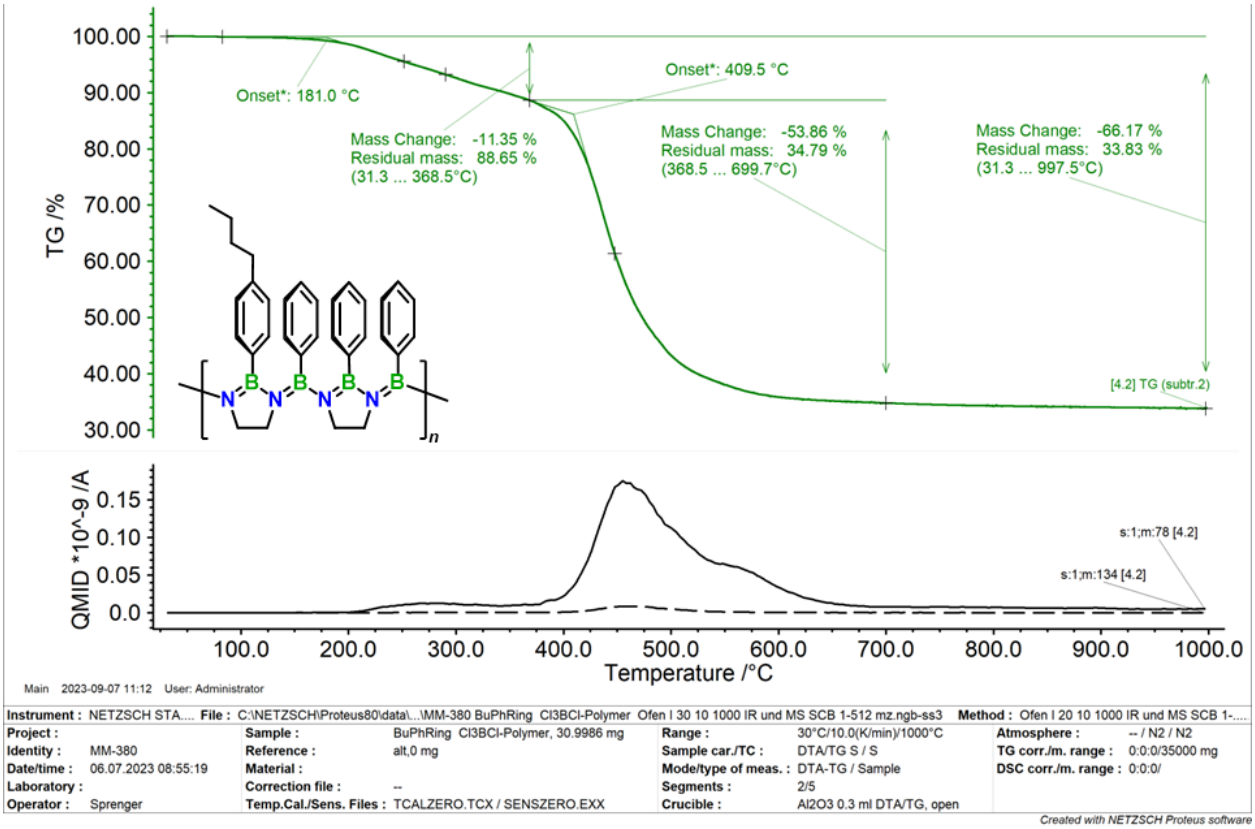

Figure S5.2.66. TG curve of **16** (top) with the ion traces (bottom) of benzene (solid line) and *n*-butylbenzene (dashed line).

GPC traces

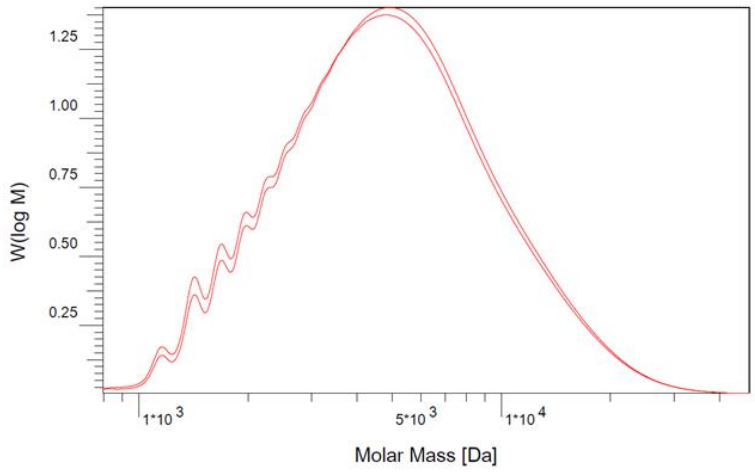

	I1: VWD 1, Signal A	Unsicherheit [%]	I1: VWD 1, Signal B	Unsicherheit [%]	
Mn :	3.8497e3	0.16	3.9917e3	0.14	g/mol
Mw :	5.9407e3	0.11	6.0802e3	0.06	g/mol
Mz :	9.2163e3	0.15	9.2873e3	0.13	g/mol
Mv :	0.000000	0.16	0.000000	0.14	g/mol
D :	1.5431e0	0.19	1.5232e0	0.15	
[n]:	0.000000	0.00	0.000000	0.00	ml/g
Vp :	2.4848e1	0.09	2.4798e1	0.03	ml
Mp :	4.8381e3	0.19	4.9396e3	0.16	g/mol
FI :	1.3835e3	0.09	9.5002e2	0.03	ml*V
< 794	0.00	0.09	0.00	0.03	
w% :	100.00	0.09	100.00	0.03	
> 48314	0.00	0.09	0.00	0.03	

Figure S5.2.67. Original GPC data of **13** (1 M) (in THF, vs. polystyrene standard).

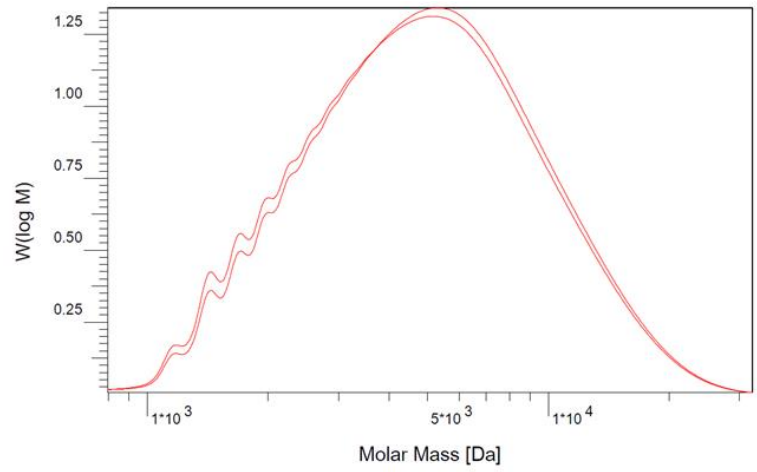

	I1: VWD 1, Signal A	Unsicherheit [%]	I1: VWD 1, Signal B	Unsicherheit [%]	
Mn :	3.8386e3	0.30	3.9813e3	0.31	g/mol
Mw :	5.8559e3	0.27	6.0128e3	0.28	g/mol
Mz :	8.6306e3	0.29	8.7690e3	0.30	g/mol
Mv :	0.000000	0.30	0.000000	0.31	g/mol
D :	1.5255e0	0.40	1.5103e0	0.41	
[n]:	0.000000	0.00	0.000000	0.00	ml/g
Vp :	2.4687e1	0.26	2.4637e1	0.27	ml
Mp :	5.1731e3	0.31	5.2817e3	0.32	g/mol
FI :	2.1085e3	0.26	1.4568e3	0.27	ml*V
< 794	0.00	0.26	0.00	0.27	
w% :	100.00	0.26	100.00	0.27	
> 32284	0.00	0.26	0.00	0.27	

Figure S5.2.68. Original GPC data of **13** (0.5 M) (in THF, vs. polystyrene standard).

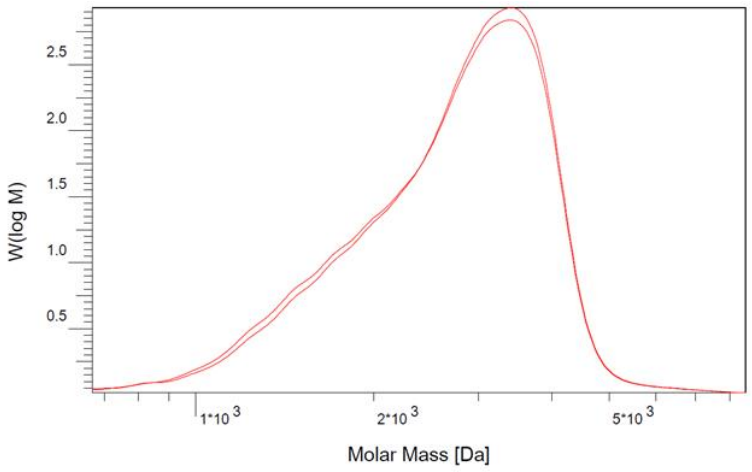

	I1: VWD 1, Signal A	Unsicherheit [%]	I1: VWD 1, Signal B	Unsicherheit [%]	
Mn :	2.4080e3	0.15	2.4524e3	0.14	g/mol
Mw :	2.7973e3	0.07	2.8338e3	0.07	g/mol
Mz :	3.1428e3	0.13	3.1690e3	0.13	g/mol
Mv :	0.000000	0.15	0.000000	0.14	g/mol
D :	1.1617e0	0.16	1.1555e0	0.15	
[n]:	0.000000	0.00	0.000000	0.00	ml/g
Vp :	2.5692e1	0.05	2.5692e1	0.04	ml
Mp :	3.4121e3	0.17	3.4121e3	0.17	g/mol
FI :	1.0214e3	0.05	7.7459e2	0.04	ml*V
< 667	0.00	0.05	0.00	0.04	
w% :	100.00	0.05	100.00	0.04	
> 8497	0.00	0.05	0.00	0.04	

Figure S5.2.69. Original GPC data of **14** (in THF, vs. polystyrene standard).

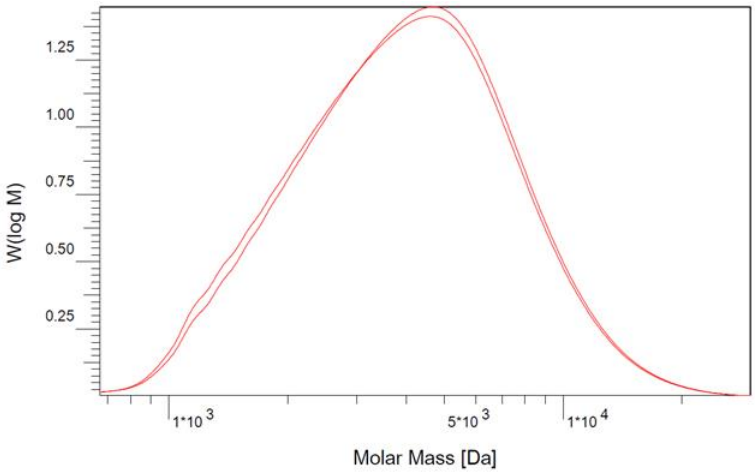

	I1: VWD 1, Signal A	Unsicherheit [%]	I1: VWD 1, Signal B	Unsicherheit [%]	
Mn :	3.1741e3	0.15	3.2767e3	0.14	g/mol
Mw :	4.6656e3	0.09	4.7715e3	0.06	g/mol
Mz :	6.6551e3	0.14	6.7439e3	0.12	g/mol
Mv :	0.000000	0.15	0.000000	0.14	g/mol
D :	1.4699e0	0.17	1.4562e0	0.15	
[n]:	0.000000	0.00	0.000000	0.00	ml/g
Vp :	2.4962e1	0.06	2.4912e1	0.03	ml
Mp :	4.6156e3	0.17	4.7125e3	0.16	g/mol
FI :	1.5896e3	0.06	1.2178e3	0.03	ml*V
< 667	0.00	0.06	0.00	0.03	
w% :	100.00	0.06	100.00	0.03	
> 29812	0.00	0.06	0.00	0.03	

Figure S5.2.70. Original GPC data of **15** (in THF, vs. polystyrene standard).

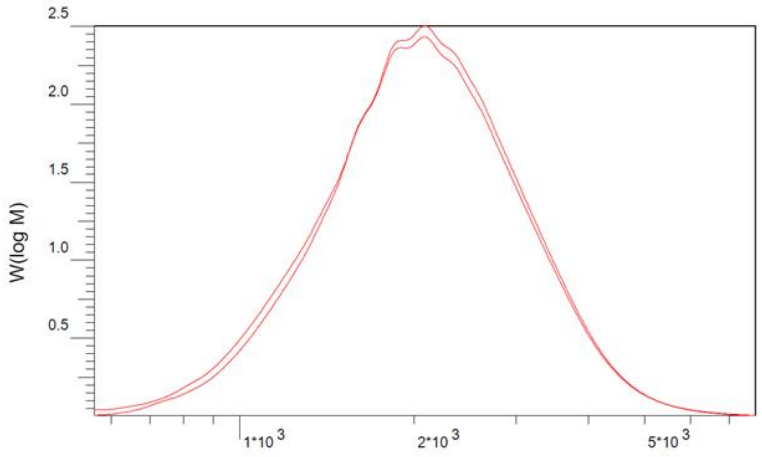

	I1: VWD 1, Signal A	Unsicherheit [%]	I1: VWD 1, Signal B	Unsicherheit [%]	
Mn :	1.8696e3	1.04	1.9192e3	0.33	g/mol
Mw :	2.1856e3	1.03	2.2198e3	0.30	g/mol
Mz :	2.5334e3	1.04	2.5513e3	0.32	g/mol
Mv :	0.000000	1.04	0.000000	0.33	g/mol
D :	1.1690e0	1.46	1.1566e0	0.44	
[n]:	0.000000	0.00	0.000000	0.00	ml/g
Vp :	2.6900e1	1.03	2.6900e1	0.30	ml
Mp :	2.0930e3	1.04	2.0930e3	0.34	g/mol
FI :	9.9319e1	1.03	7.6996e1	0.30	ml*V
< 560	0.00	1.03	0.00	0.30	
w% :	100.00	1.03	100.00	0.30	
> 7766	0.00	1.03	0.00	0.30	

Figure S5.2.71. Original GPC data of **16** (in THF, vs. polystyrene standard).

Computational information

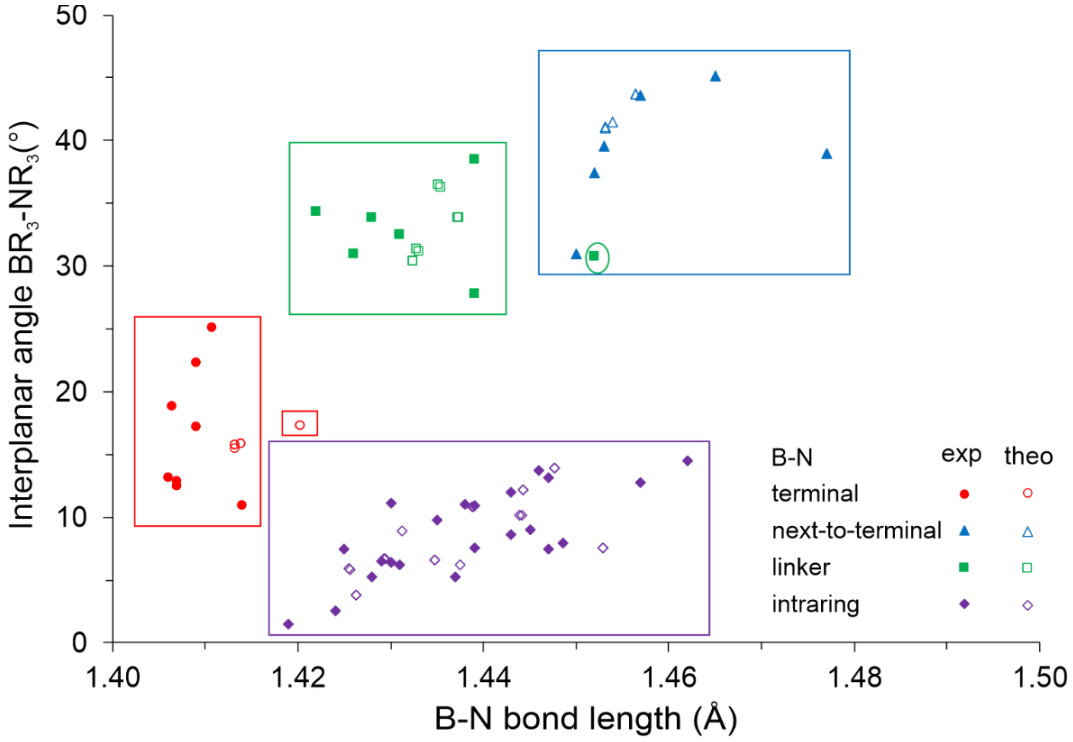

Figure S5.2.72. Relation between the B–N bond lengths (Å) and the interplanar angles ∠(BR_3,NR_3) (°) of the experimentally determined (exp, filled symbols) and theoretically computed (theo, open symbols) molecular structures of compounds **4**, **5**, **6**, **7**, **8**, and **9**.

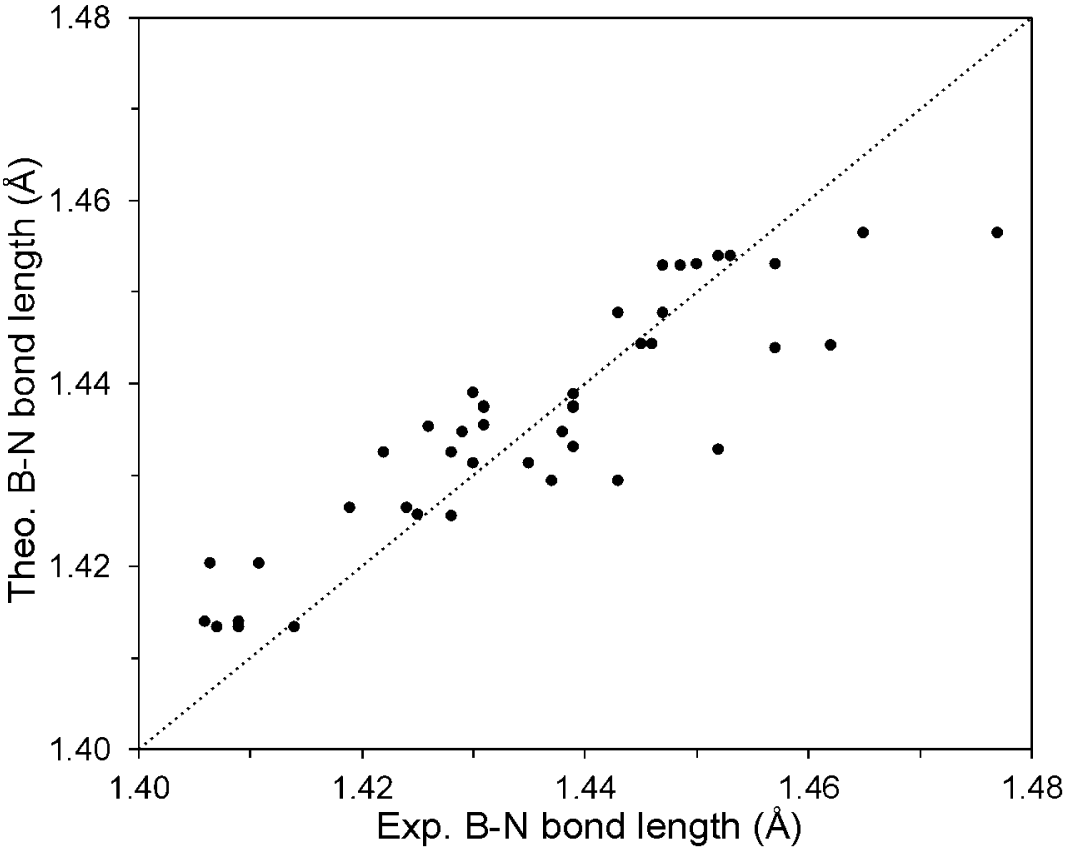

Figure S5.2.73. Correlation between the B–N bond lengths (Å) obtained from experimental and theoretical data of **4**, **5**, **6**, **7**, **8**, and **9**.

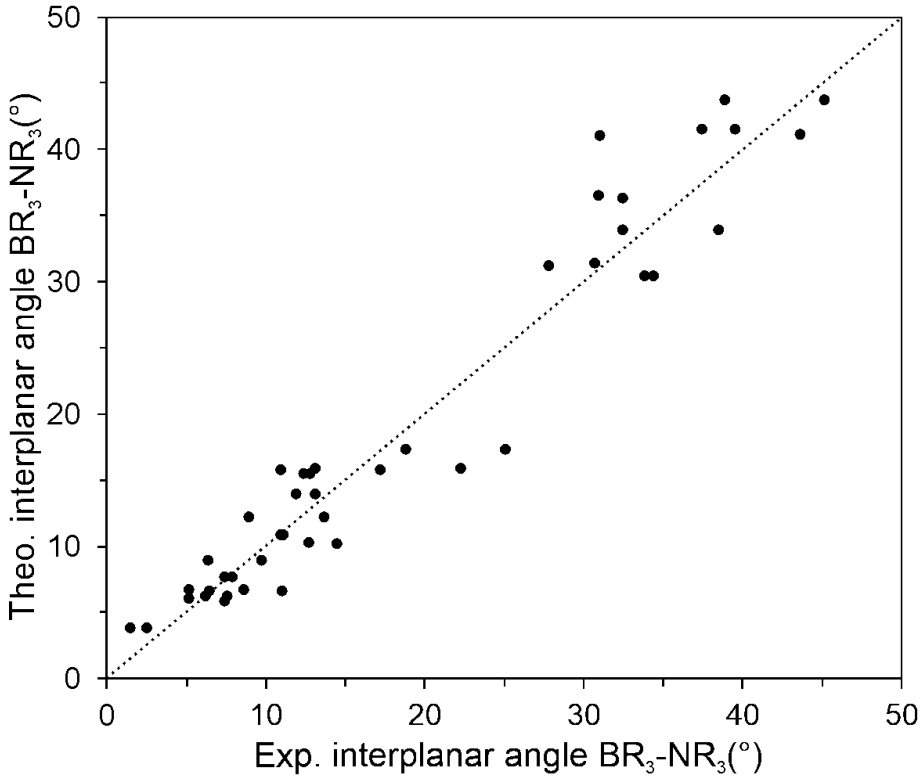

Figure S5.2.74. Correlation between the interplanar angles ∠(BR_3,NR_3) (°) obtained from experimental and theoretical data of **4**, **5**, **6**, **7**, **8**, and **9**.

Cartesian coordinates (Å) and total energies (a.u.) of optimized stationary points

The following molecular species were optimized at the ωB97X-D/6-31+G(d,p) level with PCM. The total energy is given as the sum of the electronic energy (ωB97X-D/6-311+G(d,p), PCM), the thermal correction to Gibbs Free Energy (ωB97X-D/6-31+G(d,p), PCM), and the concentration correction (1.89 kcal/mol).

5: Total energy: -1244.708357793260

B	-0.773966000	-0.162957000	-0.327832000
Si	-3.273013000	-1.595815000	0.111342000
N	0.559990000	-0.493524000	-0.751104000
C	0.601821000	-1.954475000	-0.938547000
H	0.998009000	-2.450777000	-0.042775000
H	1.235133000	-2.237200000	-1.784271000
N	-1.625063000	-1.308309000	-0.435536000
C	-0.862784000	-2.339281000	-1.164940000
H	-1.110793000	-2.311567000	-2.235943000
H	-1.072102000	-3.347749000	-0.798008000
B	1.786327000	0.282292000	-0.665752000
N	1.864179000	1.606641000	-1.153055000
C	0.856805000	2.230965000	-1.992535000
H	0.162735000	1.482629000	-2.375466000
H	1.342995000	2.724910000	-2.844092000
H	0.282357000	2.985952000	-1.439965000
C	2.909128000	2.544334000	-0.778913000
H	2.470723000	3.410645000	-0.264400000
H	3.442408000	2.914820000	-1.664759000
H	3.629720000	2.077480000	-0.108072000
C	-3.451787000	-3.435948000	0.465334000
H	-3.378883000	-4.042798000	-0.443409000
H	-4.434633000	-3.627510000	0.910407000
H	-2.690443000	-3.784621000	1.171579000
C	-4.522276000	-1.134843000	-1.220113000
H	-4.542577000	-0.055333000	-1.400364000
H	-5.532285000	-1.443479000	-0.926604000
H	-4.281895000	-1.630799000	-2.167147000
C	-3.617073000	-0.633440000	1.685623000
H	-2.853029000	-0.840694000	2.442189000
H	-4.589199000	-0.935882000	2.092067000
H	-3.638934000	0.446425000	1.517421000
C	-1.202913000	1.250977000	0.215209000
C	-2.275737000	1.952563000	-0.351666000
H	-2.831160000	1.506146000	-1.172691000
C	-2.638354000	3.219217000	0.101253000
H	-3.469887000	3.744014000	-0.359949000
C	-1.931270000	3.811603000	1.146483000
H	-2.210994000	4.797489000	1.505593000
C	-0.860973000	3.131947000	1.726916000
H	-0.304808000	3.587382000	2.541060000
C	-0.501442000	1.869579000	1.259127000
H	0.344541000	1.359100000	1.713445000
C	3.059088000	-0.407577000	-0.011770000
C	4.296420000	-0.474266000	-0.668325000
H	4.402893000	-0.018900000	-1.650489000
C	5.394240000	-1.110533000	-0.090813000
H	6.339462000	-1.154589000	-0.624144000
C	5.279243000	-1.685950000	1.173764000
H	6.133623000	-2.177185000	1.629857000
C	4.060370000	-1.629472000	1.848714000
H	3.963105000	-2.075816000	2.834166000
C	2.965249000	-1.006397000	1.253454000
H	2.014019000	-0.985022000	1.782230000

TS-5: Total energy: -1244.683322173260

B	0.767106000	-0.273591000	-0.063840000
Si	3.260811000	-1.728942000	0.079685000
N	-0.660794000	-0.580838000	-0.063521000
C	-0.786291000	-2.040293000	-0.221678000
H	-0.969671000	-2.284376000	-1.275284000
H	-1.615203000	-2.441204000	0.365283000
N	1.510904000	-1.481396000	-0.002410000
C	0.571001000	-2.595354000	0.221595000
H	0.554055000	-2.874358000	1.284796000
H	0.844467000	-3.484643000	-0.352913000
B	-1.758981000	0.294467000	0.113524000
N	-1.497740000	1.729925000	0.318092000
C	-1.878258000	2.295616000	1.595571000
H	-1.576305000	1.630167000	2.411927000
H	-2.964167000	2.485536000	1.689919000
H	-1.360764000	3.252246000	1.745309000
C	-1.885272000	2.572107000	-0.796856000
H	-1.409603000	3.556663000	-0.702066000
H	-2.978509000	2.724030000	-0.870220000
H	-1.539972000	2.134950000	-1.739857000
C	3.600658000	-3.494186000	-0.473121000
H	3.167584000	-4.231234000	0.211474000
H	4.681870000	-3.668547000	-0.504849000
H	3.201639000	-3.683538000	-1.475628000
C	3.856792000	-1.513995000	1.849904000
H	3.735223000	-0.476180000	2.176817000
H	4.917420000	-1.774332000	1.940975000
H	3.292177000	-2.155273000	2.535720000
C	4.153746000	-0.531915000	-1.053829000
H	3.738521000	-0.563464000	-2.066357000
H	5.212739000	-0.809574000	-1.110974000
H	4.088738000	0.499232000	-0.695665000
C	1.414429000	1.156303000	-0.143001000
C	1.994863000	1.753246000	0.983143000
H	1.953868000	1.243395000	1.942851000
C	2.617989000	2.997137000	0.902774000
H	3.056611000	3.442154000	1.791315000
C	2.682910000	3.666960000	-0.318039000
H	3.173324000	4.633391000	-0.386259000
C	2.113682000	3.086904000	-1.451167000
H	2.160426000	3.601429000	-2.406697000
C	1.485842000	1.847124000	-1.359317000
H	1.047299000	1.408983000	-2.252932000
C	-3.242189000	-0.271431000	0.032878000
C	-4.142640000	-0.184039000	1.106076000
H	-3.816887000	0.240696000	2.051833000
C	-5.453196000	-0.647269000	0.995319000
H	-6.125012000	-0.578382000	1.846013000
C	-5.903054000	-1.191781000	-0.206105000
H	-6.925566000	-1.545760000	-0.296906000
C	-5.030951000	-1.279221000	-1.290058000
H	-5.372924000	-1.700319000	-2.231091000
C	-3.717076000	-0.831934000	-1.163783000
H	-3.047837000	-0.918594000	-2.017508000

6: Total energy: -1226.469320743260

N	-1.122437000	-0.645895000	0.342042000
C	-0.764298000	-2.027735000	-0.028197000
H	-1.115831000	-2.263774000	-1.041631000
H	-1.202282000	-2.758434000	0.657006000
B	0.000011000	0.179994000	-0.000018000
N	1.122419000	-0.645920000	-0.342147000
C	0.764237000	-2.027763000	0.028022000
H	1.115767000	-2.263866000	1.041443000
H	1.202195000	-2.758442000	-0.657220000
B	-2.483852000	-0.292404000	0.706990000
N	-2.754170000	0.681266000	1.695573000
C	-4.037113000	1.347014000	1.843999000
H	-4.756709000	0.971879000	1.116802000
H	-3.920096000	2.428212000	1.686399000
H	-4.445709000	1.197599000	2.852421000
C	-1.758763000	1.220954000	2.605669000
H	-0.853465000	0.613881000	2.583409000
H	-2.156473000	1.217322000	3.628865000
H	-1.489794000	2.253043000	2.344947000
B	2.483848000	-0.292437000	-0.707056000
N	2.754205000	0.681272000	-1.695592000
C	4.037136000	1.347070000	-1.843894000
H	4.756739000	0.971815000	-1.116767000
H	3.920104000	2.428239000	-1.686100000
H	4.445731000	1.197840000	-2.852343000
C	1.758810000	1.221054000	-2.605649000
H	0.853547000	0.613924000	-2.583530000
H	2.156572000	1.217608000	-3.628825000
H	1.489765000	2.253084000	-2.344767000
C	-3.669032000	-1.045535000	-0.033256000
C	-4.712703000	-1.672915000	0.662615000
H	-4.731272000	-1.626510000	1.749229000
C	-5.727016000	-2.355935000	-0.006545000
H	-6.519623000	-2.840107000	0.556590000
C	-5.725534000	-2.413603000	-1.399572000
H	-6.517234000	-2.939464000	-1.924898000
C	-4.700509000	-1.795183000	-2.114493000
H	-4.692420000	-1.836828000	-3.199818000
C	-3.682141000	-1.130912000	-1.433591000
H	-2.877344000	-0.667247000	-2.001090000
C	0.000047000	1.752215000	0.000030000
C	-1.064472000	2.478335000	-0.552363000
H	-1.907621000	1.947454000	-0.987785000
C	-1.067850000	3.871507000	-0.558667000
H	-1.902441000	4.410275000	-0.997730000
C	0.000106000	4.572543000	0.000083000
H	0.000130000	5.658475000	0.000101000
C	1.068027000	3.871441000	0.558813000
H	1.902639000	4.410157000	0.997900000
C	1.064589000	2.478269000	0.552462000
H	1.907712000	1.947340000	0.987876000
C	3.668993000	-1.045603000	0.033210000
C	4.712721000	-1.672917000	-0.662636000
H	4.731365000	-1.626431000	-1.749245000
C	5.726995000	-2.355975000	0.006544000
H	6.519648000	-2.840094000	-0.556571000
C	5.725415000	-2.413750000	1.399567000
H	6.517084000	-2.939641000	1.924909000
C	4.700329000	-1.795401000	2.114462000
H	4.692161000	-1.837133000	3.199784000
C	3.682001000	-1.131091000	1.433538000
H	2.877154000	-0.667487000	2.001015000

TS-6: Total energy: -1226.440869953260

N	-1.234521000	-0.185473000	-0.543244000
C	-1.011181000	-1.422066000	-1.316505000
H	-1.177218000	-1.223271000	-2.382850000
H	-1.688654000	-2.220708000	-1.010561000
B	0.070913000	0.464890000	-0.422904000
N	1.082634000	-0.450350000	-0.832968000
C	0.454824000	-1.765016000	-1.058962000
H	0.560566000	-2.403884000	-0.172714000
H	0.908782000	-2.288205000	-1.905037000
B	-2.453222000	0.098272000	0.120504000
N	-2.581750000	1.321595000	0.934077000
C	-3.388097000	2.350562000	0.298332000
H	-3.115545000	2.455471000	-0.756464000
H	-3.209693000	3.319307000	0.782311000
H	-4.471958000	2.136591000	0.345497000
C	-2.973674000	1.124503000	2.317533000
H	-2.348716000	0.356142000	2.785202000
H	-4.032511000	0.828273000	2.437456000
H	-2.821940000	2.055226000	2.878049000
B	2.537137000	-0.337682000	-0.718990000
N	3.236389000	0.753686000	-1.270201000
C	4.594560000	1.114281000	-0.897478000
H	5.000180000	0.408755000	-0.173273000
H	4.603756000	2.115446000	-0.445755000
H	5.251791000	1.134837000	-1.776626000
C	2.646269000	1.735429000	-2.164459000
H	1.683746000	1.383280000	-2.535190000
H	3.313084000	1.900091000	-3.020415000
H	2.492128000	2.696099000	-1.656512000
C	-3.692864000	-0.880904000	-0.064707000
C	-4.205093000	-1.674384000	0.972679000
H	-3.720659000	-1.671165000	1.945807000
C	-5.322051000	-2.487528000	0.782230000
H	-5.690931000	-3.099485000	1.600254000
C	-5.966750000	-2.512565000	-0.452922000
H	-6.840067000	-3.140474000	-0.601472000
C	-5.480980000	-1.726770000	-1.496833000
H	-5.975862000	-1.739650000	-2.463673000
C	-4.354977000	-0.928959000	-1.302102000
H	-3.982628000	-0.332773000	-2.132978000
C	0.373793000	1.920236000	0.078834000
C	-0.206664000	3.036085000	-0.538064000
H	-0.926474000	2.889102000	-1.338588000
C	0.128052000	4.332478000	-0.158455000
H	-0.331979000	5.180384000	-0.657695000
C	1.053454000	4.541309000	0.864300000
H	1.315431000	5.550951000	1.166461000
C	1.641088000	3.446109000	1.494561000
H	2.362847000	3.599073000	2.291671000
C	1.308309000	2.152290000	1.096355000
H	1.789743000	1.310277000	1.588613000
C	3.302370000	-1.498580000	0.044595000
C	4.406794000	-2.162762000	-0.508527000
H	4.773322000	-1.862851000	-1.487721000
C	5.045683000	-3.200605000	0.168024000
H	5.894515000	-3.703739000	-0.285801000
C	4.596519000	-3.589809000	1.429086000
H	5.095266000	-4.393881000	1.961919000
C	3.501056000	-2.943970000	2.000995000
H	3.144316000	-3.243080000	2.982238000
C	2.859403000	-1.919877000	1.307452000
H	1.992895000	-1.436685000	1.755380000

9: Total energy: -1927.480891273260

N	2.854712000	0.319522000	0.563051000
B	3.622575000	-0.834124000	1.010180000
C	3.375613000	1.224541000	-0.478688000
H	3.227202000	0.792381000	-1.477013000
H	4.442541000	1.423821000	-0.347826000
N	1.229843000	1.959025000	0.161848000
B	1.493996000	0.690329000	0.798241000

N	-1.229979000	1.959016000	-0.163143000
C	-2.527023000	2.484318000	0.299761000
H	-2.974165000	3.145341000	-0.454406000
H	-2.424735000	3.051613000	1.228472000
B	-0.000085000	2.676048000	-0.000643000
N	-2.854660000	0.319094000	-0.563441000
C	-3.375665000	1.224629000	0.477803000
H	-3.227161000	0.793049000	1.476366000
H	-4.442622000	1.423691000	0.346859000
B	-1.493996000	0.689921000	-0.798842000
B	-3.622486000	-0.834786000	-1.010041000
C	2.526804000	2.484226000	-0.301378000
H	2.973873000	3.145781000	0.452365000
H	2.424427000	3.050931000	-1.230443000
C	4.430723000	-1.644574000	-0.085841000
C	3.793198000	-1.986931000	-1.287110000
H	2.757614000	-1.693223000	-1.440949000
C	4.457301000	-2.691551000	-2.288383000
H	3.935287000	-2.953095000	-3.204504000
C	5.793474000	-3.051149000	-2.116073000
H	6.318697000	-3.593565000	-2.896746000
C	6.454258000	-2.706163000	-0.937397000
H	7.497251000	-2.976696000	-0.800181000
C	5.774287000	-2.017059000	0.065659000
H	6.299254000	-1.761027000	0.983353000
N	3.651447000	-1.214686000	2.370699000
C	4.054240000	-2.531955000	2.832657000
H	4.357781000	-3.161727000	1.996939000
H	3.214279000	-3.021609000	3.345000000
H	4.887906000	-2.464293000	3.544395000
C	3.156792000	-0.391598000	3.460870000
H	2.982362000	0.628780000	3.119274000
H	3.898990000	-0.367947000	4.269389000
H	2.216819000	-0.786108000	3.869192000
C	0.504065000	-0.132811000	1.703347000
C	0.483002000	-1.534625000	1.668582000
H	1.081936000	-2.060132000	0.929270000
C	-0.279935000	-2.273341000	2.569634000
H	-0.277097000	-3.358344000	2.521298000
C	-1.045826000	-1.618249000	3.533387000
H	-1.634370000	-2.190097000	4.244771000
C	-1.064012000	-0.225257000	3.569608000
H	-1.670106000	0.292236000	4.307370000
C	-0.299538000	0.502756000	2.660283000
H	-0.315920000	1.589006000	2.708046000
C	-0.504026000	-0.133620000	-1.703531000
C	0.299433000	0.501481000	-2.660894000
H	0.315704000	1.587704000	-2.709275000
C	1.063902000	-0.226977000	-3.569868000
H	1.669890000	0.290153000	-4.307971000
C	1.045846000	-1.619949000	-3.532859000
H	1.634361000	-2.192146000	-4.243984000
C	0.280099000	-2.274567000	-2.568669000
H	0.277372000	-3.359543000	-2.519718000
C	-0.482830000	-1.535413000	-1.667973000
H	-1.081627000	-2.060551000	-0.928289000
C	-0.000094000	4.258488000	-0.000553000
C	0.733361000	4.985454000	0.949051000
H	1.313158000	4.449363000	1.697327000
C	0.729046000	6.378903000	0.960347000
H	1.296348000	6.919157000	1.712581000
C	-0.000106000	7.078818000	-0.000255000
H	-0.000112000	8.164787000	-0.000140000
C	-0.729249000	6.379097000	-0.961004000
H	-1.296555000	6.919505000	-1.713126000
C	-0.733552000	4.985646000	-0.950004000
H	-1.313343000	4.449713000	-1.698397000
C	-4.430623000	-1.644717000	0.086368000
C	-3.793093000	-1.986538000	1.287780000
H	-2.757495000	-1.692798000	1.441451000
C	-4.457201000	-2.690657000	2.289400000
H	-3.935165000	-2.951784000	3.205629000
C	-5.793393000	-3.050278000	2.117288000
H	-6.318625000	-3.592302000	2.898228000
C	-6.454186000	-2.705820000	0.938462000
H	-7.497194000	-2.976374000	0.801396000
C	-5.774207000	-2.017217000	-0.064935000
H	-6.299181000	-1.761595000	-0.982739000
N	-3.651358000	-1.215990000	-2.370379000
C	-4.054169000	-2.533470000	-2.831718000
H	-4.357635000	-3.162878000	-1.995699000
H	-3.214239000	-3.023337000	-3.343907000
H	-4.887891000	-2.466140000	-3.543422000
C	-3.156706000	-0.393425000	-3.460947000
H	-2.982217000	0.627105000	-3.119839000
H	-3.898925000	-0.370122000	-4.269458000
H	-2.216761000	-0.788168000	-3.869107000

TS-9: Total energy: -1927.449862693260

N	2.688875000	0.014577000	0.374538000
B	3.423291000	-1.123721000	0.793025000
C	3.274538000	0.960032000	-0.602885000
H	3.131916000	0.570599000	-1.616355000
H	4.345025000	1.091120000	-0.436745000
N	1.192787000	1.806263000	0.100261000
B	1.370118000	0.528968000	0.731645000
N	-1.254454000	1.925084000	-0.330852000
C	-2.550982000	2.530392000	0.028449000
H	-2.930844000	3.152920000	-0.792079000
H	-2.470386000	3.154590000	0.921381000
B	-0.007441000	2.581652000	-0.089481000
N	-2.932526000	0.331201000	-0.717652000
C	-3.459773000	1.321410000	0.241949000
H	-3.372318000	0.948483000	1.270618000
H	-4.510460000	1.553889000	0.050384000
B	-1.547071000	0.627461000	-0.903826000
B	-3.734726000	-0.809006000	-1.138312000
C	2.495755000	2.258665000	-0.409865000
H	2.993954000	2.912683000	0.317356000
H	2.395581000	2.817126000	-1.344502000
C	4.867913000	-1.382104000	0.179161000
C	4.964766000	-1.828708000	-1.148959000
H	4.059829000	-1.931768000	-1.746022000
C	6.195321000	-2.139293000	-1.724212000
H	6.241257000	-2.486664000	-2.752465000
C	7.367068000	-1.998634000	-0.981691000
H	8.328736000	-2.234423000	-1.427423000
C	7.295120000	-1.553030000	0.336633000
H	8.203067000	-1.438911000	0.921818000
C	6.058058000	-1.257223000	0.909391000
H	6.026711000	-0.914350000	1.940767000
N	2.837592000	-2.121333000	1.704725000
C	2.458684000	-3.341400000	1.007754000
H	1.908305000	-3.102336000	0.090877000
H	1.802653000	-3.948937000	1.645576000
H	3.328004000	-3.963010000	0.725285000
C	3.609225000	-2.414936000	2.899186000
H	3.879038000	-1.487702000	3.415119000
H	4.537210000	-2.980307000	2.694837000
H	2.999647000	-3.008775000	3.591462000
C	0.331471000	-0.005007000	1.790724000
C	-0.107562000	-1.330802000	1.897475000
H	0.269447000	-2.072055000	1.206382000
C	-1.024393000	-1.719653000	2.869639000
H	-1.349972000	-2.755046000	2.920090000
C	-1.529274000	-0.784488000	3.772550000

H	-2.244809000	-1.086646000	4.531779000
C	-1.112462000	0.541323000	3.687879000
H	-1.498764000	1.281448000	4.382506000
C	-0.198930000	0.919368000	2.705312000
H	0.110417000	1.960759000	2.654008000
C	-0.529866000	-0.309347000	-1.656298000
C	0.396864000	0.200020000	-2.576199000
H	0.441290000	1.272340000	-2.750959000
C	1.268568000	-0.634834000	-3.270914000
H	1.975045000	-0.213047000	-3.980114000
C	1.239720000	-2.010657000	-3.048498000
H	1.922255000	-2.665452000	-3.582439000
C	0.323926000	-2.541816000	-2.141360000
H	0.290562000	-3.613164000	-1.965282000
C	-0.551363000	-1.697836000	-1.462282000
H	-1.264147000	-2.128128000	-0.763953000
C	0.074391000	4.159848000	-0.037110000
C	0.827622000	4.803034000	0.956720000
H	1.358808000	4.203053000	1.692687000
C	0.905441000	6.192428000	1.026325000
H	1.485808000	6.666704000	1.812252000
C	0.242164000	6.972666000	0.080116000
H	0.305914000	8.055781000	0.125404000
C	-0.502401000	6.356989000	-0.925334000
H	-1.017067000	6.960250000	-1.667428000
C	-0.589615000	4.967152000	-0.972729000
H	-1.179103000	4.499221000	-1.757854000
C	-4.691587000	-1.470983000	-0.061745000
C	-4.195372000	-1.746296000	1.220638000
H	-3.160614000	-1.506385000	1.450861000
C	-4.998065000	-2.314101000	2.207221000
H	-4.583198000	-2.524355000	3.189191000
C	-6.335075000	-2.600820000	1.934378000
H	-6.968752000	-3.035928000	2.701607000
C	-6.856709000	-2.320784000	0.671588000
H	-7.899349000	-2.534882000	0.455086000
C	-6.038944000	-1.768554000	-0.313245000
H	-6.457287000	-1.561918000	-1.295873000
N	-3.674700000	-1.302637000	-2.461564000
C	-4.128020000	-2.627754000	-2.849153000
H	-4.526420000	-3.169080000	-1.991629000
H	-3.288301000	-3.204941000	-3.260496000
H	-4.906017000	-2.570257000	-3.622252000
C	-3.054006000	-0.602306000	-3.572573000
H	-2.846059000	0.433509000	-3.303580000
H	-3.732513000	-0.608897000	-4.435576000
H	-2.111281000	-1.077736000	-3.873962000

The following molecular species were optimized at the ωB97X-D/6-31+G(d,p) level in gas phase. The total energy is given as the electronic energy (ωB97X-D/6-31+G(d,p)).

4: Total energy: -1878.01670016

Cl	-0.317123000	4.419907000	13.934828000
N	1.955210000	5.828507000	13.267800000
C	1.861025000	6.473536000	14.594270000
H	1.703061000	5.739548000	15.385670000
H	1.019392000	7.175799000	14.608343000
Cl	5.538215000	9.148227000	14.423726000
N	3.565824000	7.547593000	13.355936000
C	3.190024000	7.203763000	14.743366000
H	3.103022000	8.094773000	15.366689000
H	3.952649000	6.552125000	15.185524000
B	4.521391000	8.556641000	13.062776000
B	2.904516000	6.595802000	12.479752000
B	1.114928000	4.745495000	12.895960000
C	4.749871000	9.204636000	11.660442000
C	6.042181000	9.485507000	11.193480000
H	6.898419000	9.285466000	11.831878000
C	6.249338000	10.001819000	9.917659000
H	7.259142000	10.193826000	9.568029000
C	5.160206000	10.277514000	9.093484000
H	5.319199000	10.681475000	8.098198000
C	3.865917000	10.041201000	9.552411000
H	3.012982000	10.260956000	8.918097000
C	3.667758000	9.506708000	10.820508000
H	2.654593000	9.309264000	11.157931000
C	3.169813000	6.425715000	10.948795000
C	4.469664000	6.253784000	10.456611000
H	5.310802000	6.248798000	11.145041000
C	4.710462000	6.096363000	9.095828000
H	5.726696000	5.965575000	8.737094000
C	3.647632000	6.119863000	8.195345000
H	3.832149000	6.001812000	7.131889000
C	2.347273000	6.295350000	8.663669000
H	1.514022000	6.308992000	7.967949000
C	2.115284000	6.440553000	10.027326000
H	1.093737000	6.560966000	10.378627000
C	1.341874000	3.805577000	11.669688000
C	2.629786000	3.371749000	11.322102000
H	3.479690000	3.673919000	11.926841000
C	2.844928000	2.572317000	10.205126000
H	3.851499000	2.254071000	9.952774000
C	1.769046000	2.195935000	9.403587000
H	1.935217000	1.583587000	8.522409000
C	0.478806000	2.600454000	9.739930000
H	-0.363649000	2.301199000	9.123870000
C	0.268892000	3.384045000	10.870929000
H	-0.742898000	3.683654000	11.130228000

5: Total energy: -1244.91951601

B	-0.775039000	-0.163149000	-0.334948000
Si	-3.271124000	-1.591249000	0.117415000
N	0.556968000	-0.494752000	-0.761848000
C	0.595841000	-1.954035000	-0.957800000
H	0.996051000	-2.456458000	-0.067240000
H	1.225757000	-2.232212000	-1.807698000
N	-1.628972000	-1.306367000	-0.445802000
C	-0.870778000	-2.335080000	-1.180939000
H	-1.121805000	-2.302655000	-2.251309000
H	-1.081207000	-3.344839000	-0.817546000
B	1.784399000	0.279075000	-0.670485000
N	1.862980000	1.606150000	-1.150196000
C	0.858776000	2.233840000	-1.990513000
H	0.168585000	1.486110000	-2.381543000
H	1.348453000	2.733259000	-2.837070000
H	0.279868000	2.984369000	-1.436455000
C	2.902944000	2.542847000	-0.762019000
H	2.459050000	3.403158000	-0.241901000
H	3.439977000	2.923104000	-1.641710000
H	3.621326000	2.071390000	-0.091926000
C	-3.451186000	-3.433613000	0.462317000
H	-3.389175000	-4.036598000	-0.449816000
H	-4.429532000	-3.627281000	0.916214000
H	-2.684306000	-3.788784000	1.159255000
C	-4.534080000	-1.120811000	-1.198081000
H	-4.555975000	-0.039989000	-1.369828000
H	-5.541954000	-1.430182000	-0.898224000
H	-4.304533000	-1.608488000	-2.152011000
C	-3.595406000	-0.636969000	1.700139000
H	-2.823413000	-0.849837000	2.446904000
H	-4.563454000	-0.937602000	2.117468000

H	-3.615391000	0.444054000	1.539661000
C	-1.199495000	1.250054000	0.212154000
C	-2.272628000	1.954350000	-0.350117000
H	-2.832541000	1.508644000	-1.168495000
C	-2.628850000	3.222353000	0.103334000
H	-3.460622000	3.749586000	-0.354573000
C	-1.914956000	3.813136000	1.144214000
H	-2.189670000	4.800294000	1.503577000
C	-0.844597000	3.130598000	1.720295000
H	-0.283510000	3.584797000	2.531696000
C	-0.491438000	1.867037000	1.252319000
H	0.355055000	1.354030000	1.702740000
C	3.053814000	-0.413152000	-0.014597000
C	4.294458000	-0.474019000	-0.664749000
H	4.404254000	-0.013941000	-1.644335000
C	5.390147000	-1.110228000	-0.084284000
H	6.338316000	-1.149975000	-0.612626000
C	5.269550000	-1.691504000	1.176556000
H	6.122603000	-2.182755000	1.635025000
C	4.047412000	-1.641118000	1.845051000
H	3.946047000	-2.092061000	2.827951000
C	2.954424000	-1.018010000	1.246982000
H	2.000132000	-1.000551000	1.770526000

6: Total energy: -1226.72028678

N	-1.122483000	-0.648386000	0.341304000
C	-0.764613000	-2.030328000	-0.027611000
H	-1.118607000	-2.268200000	-1.039728000
H	-1.202560000	-2.759804000	0.659035000
B	0.000058000	0.177145000	-0.000411000
N	1.122429000	-0.648520000	-0.342323000
C	0.764330000	-2.030470000	0.026437000
H	1.118311000	-2.268515000	1.038511000
H	1.202144000	-2.759911000	-0.660333000
B	-2.483582000	-0.292998000	0.705364000
N	-2.752000000	0.685333000	1.690223000
C	-4.032291000	1.356289000	1.832192000
H	-4.751131000	0.980696000	1.104372000
H	-3.910446000	2.436534000	1.670864000
H	-4.444695000	1.212454000	2.840179000
C	-1.756704000	1.223701000	2.600797000
H	-0.854121000	0.612475000	2.582065000
H	-2.156606000	1.223430000	3.623348000
H	-1.482498000	2.253970000	2.338408000
B	2.483707000	-0.293230000	-0.705777000
N	2.752576000	0.685147000	-1.690487000
C	4.032843000	1.356298000	-1.831695000
H	4.751863000	0.979490000	-1.104695000
H	3.911115000	2.436308000	-1.668628000
H	4.444907000	1.214032000	-2.840033000
C	1.757572000	1.223798000	-2.601223000
H	0.854936000	0.612636000	-2.582909000
H	2.157786000	1.223771000	-3.623654000
H	1.483335000	2.254019000	-2.338668000
C	-3.669473000	-1.045840000	-0.032231000
C	-4.714882000	-1.667089000	0.665866000
H	-4.732705000	-1.615941000	1.752292000
C	-5.730380000	-2.350028000	-0.000585000
H	-6.524427000	-2.829801000	0.564234000
C	-5.728283000	-2.413858000	-1.392807000
H	-6.521133000	-2.939934000	-1.916130000
C	-4.701712000	-1.801707000	-2.109918000
H	-4.693467000	-1.848142000	-3.195019000
C	-3.682221000	-1.137342000	-1.431831000
H	-2.875792000	-0.677979000	-2.000601000
C	0.000122000	1.749153000	-0.000244000
C	-1.062583000	2.475253000	-0.555678000
H	-1.904430000	1.944114000	-0.993310000
C	-1.065618000	3.868083000	-0.561926000
H	-1.898529000	4.406924000	-1.004016000
C	0.000189000	4.568747000	0.000341000
H	0.000194000	5.654652000	0.000582000
C	1.065967000	3.867814000	0.562319000
H	1.898888000	4.406435000	1.004658000
C	1.062868000	2.474987000	0.555492000
H	1.904653000	1.943654000	0.992996000
C	3.669277000	-1.046178000	0.032232000
C	4.714776000	-1.667745000	-0.665441000
H	4.732912000	-1.616833000	-1.751874000
C	5.729964000	-2.350713000	0.001448000
H	6.524085000	-2.830754000	-0.563040000
C	5.727460000	-2.414246000	1.393686000
H	6.520076000	-2.940347000	1.917338000
C	4.700796000	-1.801765000	2.110372000
H	4.692232000	-1.847959000	3.195482000
C	3.681607000	-1.137367000	1.431853000
H	2.875093000	-0.677766000	2.000314000

7: Total energy: -1964.25059988

N	2.660485000	-0.880495000	-0.093784000
C	3.059841000	-0.108421000	-1.289008000
H	2.553793000	-0.504006000	-2.180638000
H	4.139650000	-0.143020000	-1.458960000
B	1.561538000	-0.187238000	0.492824000
N	1.410395000	1.106412000	-0.131274000
B	0.316575000	2.026944000	-0.002956000
C	2.583226000	1.316994000	-0.989075000
H	3.364402000	1.881239000	-0.461632000
H	2.324950000	1.863680000	-1.900251000
C	0.687900000	-0.645787000	1.723478000
C	0.530319000	0.219896000	2.817174000
H	1.013321000	1.194389000	2.798419000
C	-0.231634000	-0.136337000	3.925940000
H	-0.328663000	0.551141000	4.761191000
C	-0.876551000	-1.372337000	3.959356000
H	-1.478177000	-1.652695000	4.818829000
C	-0.741016000	-2.245838000	2.883230000
H	-1.239904000	-3.210308000	2.897229000
C	0.039031000	-1.884305000	1.786830000
H	0.142107000	-2.583301000	0.962209000
Si	3.412784000	-2.422977000	0.287936000
C	5.191135000	-2.367901000	-0.327636000
H	5.250043000	-2.311303000	-1.419750000
H	5.716787000	-3.278099000	-0.017905000
H	5.733149000	-1.511583000	0.088228000
C	2.536986000	-3.831556000	-0.603112000
H	1.496951000	-3.934959000	-0.277226000
H	3.043624000	-4.786789000	-0.423719000
H	2.528110000	-3.648938000	-1.683137000
C	3.418463000	-2.710249000	2.142082000
H	3.842534000	-1.846570000	2.664759000
H	4.036655000	-3.585055000	2.375041000
H	2.417961000	-2.884467000	2.545421000
C	0.561523000	3.585853000	-0.003581000
C	-0.342711000	4.463870000	-0.619596000
H	-1.226982000	4.058018000	-1.105968000
C	-0.127127000	5.839837000	-0.630418000
H	-0.836508000	6.499005000	-1.122188000
C	0.999821000	6.370315000	-0.004307000
H	1.168680000	7.443115000	-0.004605000
N	-2.803876000	-0.024193000	0.092174000
C	-2.950241000	0.837641000	1.283766000
H	-2.591498000	0.309713000	2.178320000
H	-3.989199000	1.135852000	1.450306000
B	-1.545085000	0.297935000	-0.494224000
N	-1.006466000	1.485808000	0.126108000

C	-2.059704000	2.047732000	0.980921000
H	-2.629952000	2.822382000	0.450370000
H	-1.647528000	2.491997000	1.891176000
C	-0.853698000	-0.410897000	-1.722026000
C	-0.442916000	0.359542000	-2.821162000
H	-0.606203000	1.434924000	-2.808041000
C	0.171252000	-0.218209000	-3.928379000
H	0.470700000	0.402249000	-4.768042000
C	0.409014000	-1.592096000	-3.954634000
H	0.894169000	-2.047277000	-4.812924000
C	0.016986000	-2.376677000	-2.872897000
H	0.198359000	-3.447334000	-2.881314000
C	-0.612968000	-1.788508000	-1.778186000
H	-0.922200000	-2.418104000	-0.949264000
Si	-3.988624000	-1.267531000	-0.284141000
C	-5.666511000	-0.672597000	0.328470000
H	-5.705721000	-0.596460000	1.420283000
H	-6.443642000	-1.381415000	0.021297000
H	-5.922821000	0.306208000	-0.091332000
C	-3.581160000	-2.871050000	0.614664000
H	-2.621157000	-3.286194000	0.291127000
H	-4.353307000	-3.628819000	0.438888000
H	-3.517490000	-2.694297000	1.693832000
C	-4.080612000	-1.547650000	-2.137070000
H	-4.224173000	-0.598367000	-2.663604000
H	-4.934012000	-2.195996000	-2.367427000
H	-3.179166000	-2.017201000	-2.538326000
C	1.691858000	4.143969000	0.611971000
H	2.408866000	3.486321000	1.098390000
C	1.909376000	5.519637000	0.622121000
H	2.787039000	5.929272000	1.113525000

8: Total energy: -2665.38552083

N	-3.900435000	0.085967000	1.610871000
C	-3.861305000	-1.324370000	2.046917000
H	-4.790418000	-1.628230000	2.536723000
H	-3.033657000	-1.481493000	2.751862000
B	-3.197486000	0.162924000	0.372201000
N	-2.889604000	-1.170742000	-0.099287000
B	-2.012381000	-1.590978000	-1.150800000
N	-0.859031000	-0.798047000	-1.477745000
C	-0.342324000	-0.685422000	-2.854780000
H	-1.146383000	-0.747978000	-3.592657000
H	0.384632000	-1.480114000	-3.063906000
B	0.000116000	-0.000534000	-0.643342000
N	0.859418000	0.795736000	-1.478693000
C	0.343294000	0.680925000	-2.855751000
H	1.147701000	0.742191000	-3.593361000
H	-0.383493000	1.475331000	-3.066543000
B	2.012376000	1.589636000	-1.152420000
N	2.889885000	1.170593000	-0.100720000
C	3.632410000	2.111363000	0.750655000
H	3.072445000	3.035362000	0.919966000
H	4.593695000	2.380219000	0.293002000
B	3.198148000	-0.162655000	0.371798000
N	3.901094000	-0.084538000	1.610368000
C	3.861689000	1.326123000	2.045315000
H	4.790804000	1.630545000	2.534782000
H	3.034079000	1.483604000	2.750214000
C	-3.632309000	-2.110672000	0.752854000
H	-3.072569000	-3.034686000	0.922861000
H	-4.593676000	-2.379662000	0.295456000
C	-2.924705000	1.464652000	-0.474497000
C	-2.352753000	2.623722000	0.063858000
H	-2.052045000	2.632057000	1.106853000
C	-2.148357000	3.764115000	-0.708987000
H	-1.692665000	4.645196000	-0.266159000
C	-2.525051000	3.772120000	-2.050457000
H	-2.369237000	4.659689000	-2.656812000
C	-3.097626000	2.631465000	-2.610354000
H	-3.392017000	2.627305000	-3.655761000
C	-3.286129000	1.494112000	-1.829612000
H	-3.722809000	0.607380000	-2.283385000
C	-2.299707000	-2.926380000	-1.945130000
C	-3.596561000	-3.285152000	-2.340778000
H	-4.428258000	-2.626881000	-2.099221000
C	-3.841241000	-4.460909000	-3.046871000
H	-4.852695000	-4.712526000	-3.352316000
C	-2.785471000	-5.316902000	-3.357239000
H	-2.973155000	-6.237855000	-3.901458000
C	-1.488630000	-4.984830000	-2.968436000
H	-0.661969000	-5.647838000	-3.207971000
C	-1.252707000	-3.797712000	-2.279486000
H	-0.237312000	-3.540240000	-1.989952000
C	0.000141000	0.000433000	0.933346000
C	-0.222401000	-1.174288000	1.664707000
H	-0.403401000	-2.104194000	1.132002000
C	-0.212622000	-1.182825000	3.056417000
H	-0.373901000	-2.112442000	3.595001000
C	0.000623000	0.001976000	3.757456000
H	0.000849000	0.002558000	4.843638000
C	0.213544000	1.186021000	3.055051000
H	0.374942000	2.116241000	3.592557000
C	0.222850000	1.175966000	1.663344000
H	0.403547000	2.105329000	1.129590000
C	2.298639000	2.924685000	-1.947691000
C	1.250871000	3.794843000	-2.282678000
H	0.235711000	3.536708000	-1.992906000
C	1.485736000	4.981652000	-2.972513000
H	0.658489000	5.643760000	-3.212514000
C	2.782279000	5.314565000	-3.361598000
H	2.969145000	6.235272000	-3.906515000
C	3.838805000	4.459724000	-3.050627000
H	4.850028000	4.711994000	-3.356300000
C	3.595173000	3.284278000	-2.343653000
H	4.427455000	2.626910000	-2.101660000
C	2.925479000	-1.465044000	-0.473917000
C	3.287459000	-1.495650000	-1.828856000
H	3.724723000	-0.609441000	-2.283090000
C	3.098696000	-2.633467000	-2.608856000
H	3.393518000	-2.630220000	-3.654145000
C	2.525230000	-3.773399000	-2.048394000
H	2.369178000	-4.661309000	-2.654187000
C	2.148039000	-3.764256000	-0.707070000
H	1.691728000	-4.644795000	-0.263793000
C	2.352768000	-2.623440000	0.065065000
H	2.051713000	-2.630889000	1.107974000
Si	-4.616660000	1.320596000	2.643897000
C	-5.441481000	2.654149000	1.613416000
H	-4.727072000	3.262359000	1.053804000
H	-6.015369000	3.319414000	2.269158000
H	-6.135258000	2.207518000	0.893494000
C	-3.324397000	2.054846000	3.797971000
H	-2.802102000	1.257816000	4.338522000
H	-3.789148000	2.720470000	4.534520000
H	-2.565618000	2.627365000	3.255938000
C	-5.930226000	0.488935000	3.706760000
H	-6.677327000	-0.028418000	3.095006000
H	-6.453359000	1.248565000	4.298488000
H	-5.501862000	-0.234822000	4.408176000
Si	4.617412000	-1.318364000	2.644289000
C	3.325268000	-2.050666000	3.799714000
H	2.805613000	-1.253012000	4.341892000
H	3.789434000	-2.718234000	4.534876000
H	2.564356000	-2.620687000	3.258036000
C	5.932121000	-0.486142000	3.705284000

H	6.679326000	0.029602000	3.092298000
H	6.454924000	-1.245236000	4.297996000
H	5.504723000	0.239104000	4.405744000
C	5.440811000	-2.653523000	1.614752000
H	4.725554000	-3.263072000	1.057688000
H	6.016235000	-3.317296000	2.270647000
H	6.132988000	-2.208026000	0.892588000

9: Total energy: -1927.85532028

N	2.854708000	0.323646000	0.569647000
B	3.620408000	-0.832756000	1.014110000
C	3.379047000	1.231982000	-0.466957000
H	3.236292000	0.802051000	-1.467070000
H	4.445443000	1.431040000	-0.330945000
N	1.229002000	1.961334000	0.164658000
B	1.492390000	0.690955000	0.798444000
N	-1.229822000	1.961466000	-0.169529000
C	-2.528837000	2.490505000	0.283083000
H	-2.970710000	3.147970000	-0.477434000
H	-2.430813000	3.064370000	1.208319000
B	-0.000450000	2.678240000	-0.002397000
N	-2.854971000	0.322483000	-0.571573000
C	-3.379806000	1.232680000	0.463122000
H	-3.237142000	0.804788000	1.464125000
H	-4.446233000	1.431177000	0.326490000
B	-1.492783000	0.689653000	-0.800921000
B	-3.620180000	-0.835207000	-1.013659000
C	2.527740000	2.489909000	-0.289281000
H	2.969564000	3.149111000	0.469759000
H	2.429336000	3.061806000	-1.215702000
C	4.434187000	-1.636485000	-0.081086000
C	3.803838000	-1.972866000	-1.287474000
H	2.768610000	-1.680330000	-1.445447000
C	4.475054000	-2.670345000	-2.288321000
H	3.958707000	-2.927241000	-3.208900000
C	5.810227000	-3.028789000	-2.110275000
H	6.340826000	-3.565788000	-2.891019000
C	6.463524000	-2.690109000	-0.926199000
H	7.506109000	-2.959820000	-0.784648000
C	5.777013000	-2.007882000	0.076431000
H	6.295772000	-1.755279000	0.998620000
N	3.639593000	-1.221261000	2.372836000
C	4.035078000	-2.542594000	2.827566000
H	4.343306000	-3.166516000	1.989087000
H	3.189790000	-3.033583000	3.330195000
H	4.863795000	-2.482826000	3.546176000
C	3.141934000	-0.403209000	3.464968000
H	2.970655000	0.619022000	3.127362000
H	3.881647000	-0.383995000	4.276158000
H	2.199844000	-0.797815000	3.868471000
C	0.501046000	-0.137868000	1.696762000
C	0.486064000	-1.539591000	1.657291000
H	1.088486000	-2.059355000	0.916742000
C	-0.274048000	-2.284176000	2.555411000
H	-0.266637000	-3.368967000	2.503685000
C	-1.042781000	-1.635556000	3.520922000
H	-1.628253000	-2.212368000	4.230812000
C	-1.067599000	-0.243174000	3.561322000
H	-1.675930000	0.269132000	4.300802000
C	-0.306246000	0.491004000	2.654603000
H	-0.326539000	1.577025000	2.705713000
C	-0.501262000	-0.140488000	-1.697779000
C	0.304654000	0.486909000	-2.657742000
H	0.323608000	1.572812000	-2.711674000
C	1.066258000	-0.248668000	-3.563120000
H	1.673532000	0.262483000	-4.304266000
C	1.043025000	-1.640972000	-3.519244000
H	1.628715000	-2.218899000	-4.228047000
C	0.275661000	-2.288029000	-2.551596000
H	0.269503000	-3.372697000	-2.497143000
C	-0.484659000	-1.542070000	-1.654792000
H	-1.085708000	-2.060668000	-0.912321000
C	-0.000318000	4.260012000	-0.001891000
C	0.724749000	4.986351000	0.954107000
H	1.297666000	4.449289000	1.707015000
C	0.720403000	6.379283000	0.965896000
H	1.281043000	6.919234000	1.723272000
C	-0.000040000	7.079309000	-0.000440000
H	0.000074000	8.165247000	0.000107000
C	-0.720619000	6.380411000	-0.967492000
H	-1.281153000	6.921252000	-1.724311000
C	-0.725243000	4.987465000	-0.957138000
H	-1.298276000	4.451325000	-1.710607000
C	-4.433780000	-1.636956000	0.083111000
C	-3.803277000	-1.970991000	1.290081000
H	-2.768080000	-1.678008000	1.447427000
C	-4.474338000	-2.666674000	2.292281000
H	-3.957893000	-2.921822000	3.213286000
C	-5.809491000	-3.025572000	2.115043000
H	-6.339971000	-3.561141000	2.896851000
C	-6.462937000	-2.689180000	0.930397000
H	-7.505509000	-2.959253000	0.789459000
C	-5.776577000	-2.008800000	-0.073584000
H	-6.295429000	-1.757990000	-0.996210000
N	-3.639189000	-1.226522000	-2.371576000
C	-4.034606000	-2.548790000	-2.823653000
H	-4.342221000	-3.171305000	-1.983898000
H	-3.189462000	-3.040454000	-3.325841000
H	-4.863739000	-2.490559000	-3.541921000
C	-3.141829000	-0.410651000	-3.465461000
H	-2.970467000	0.612259000	-3.129997000
H	-3.881739000	-0.393083000	-4.276520000
H	-2.199841000	-0.806101000	-3.868365000

5.3 Redistribution of Oligo(iminoborane)s

NMR spectra

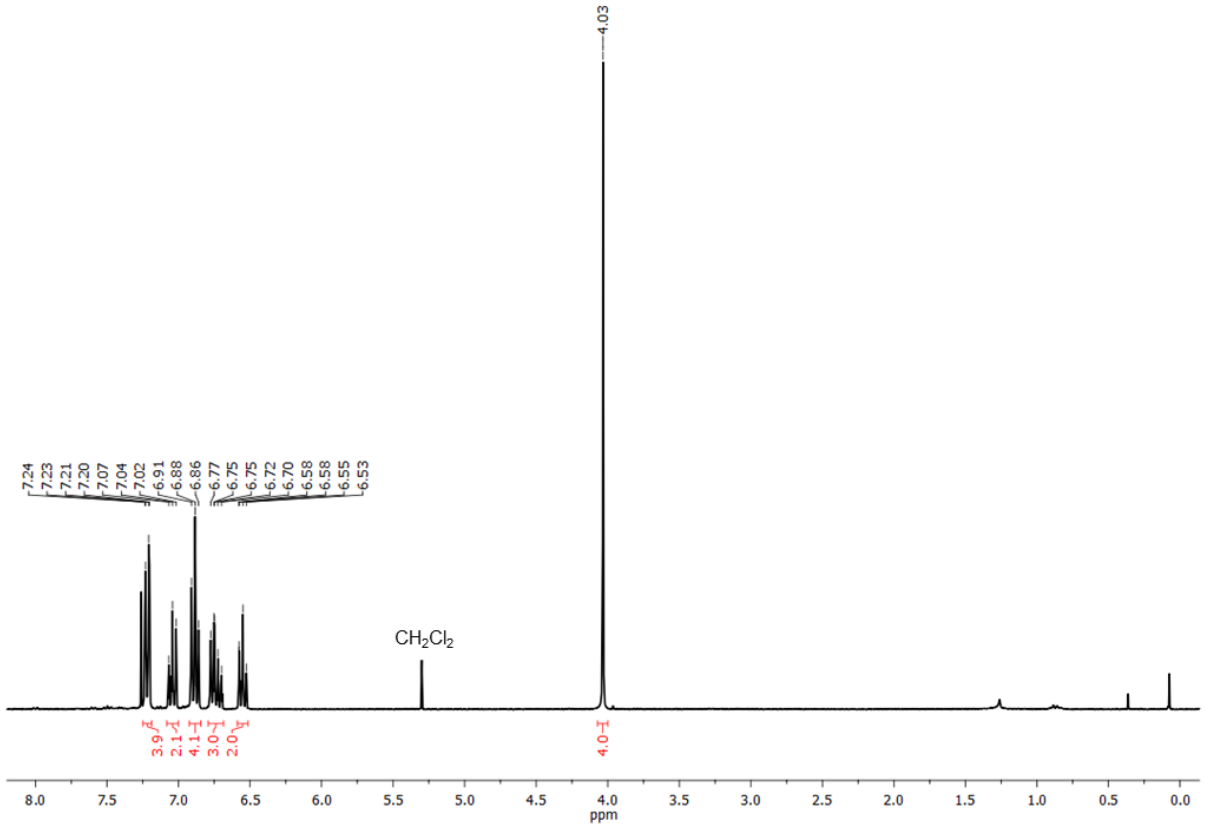

Figure S5.3.1. ^{1}H NMR spectrum (300 MHz) of **2** in $CDCl_3$ (reaction of **3** with excess $PhBCl_2$).

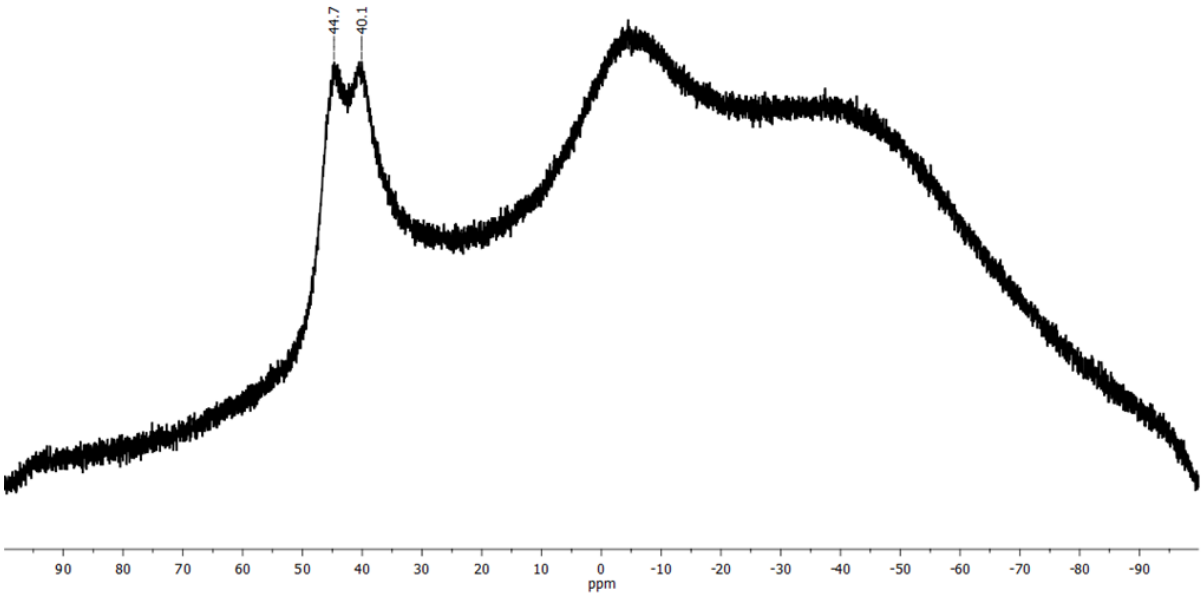

Figure S5.3.2. $^{11}B\{^{1}H\}$ NMR spectrum (96 MHz) of **2** in $CDCl_3$ (reaction of **3** with excess $PhBCl_2$).

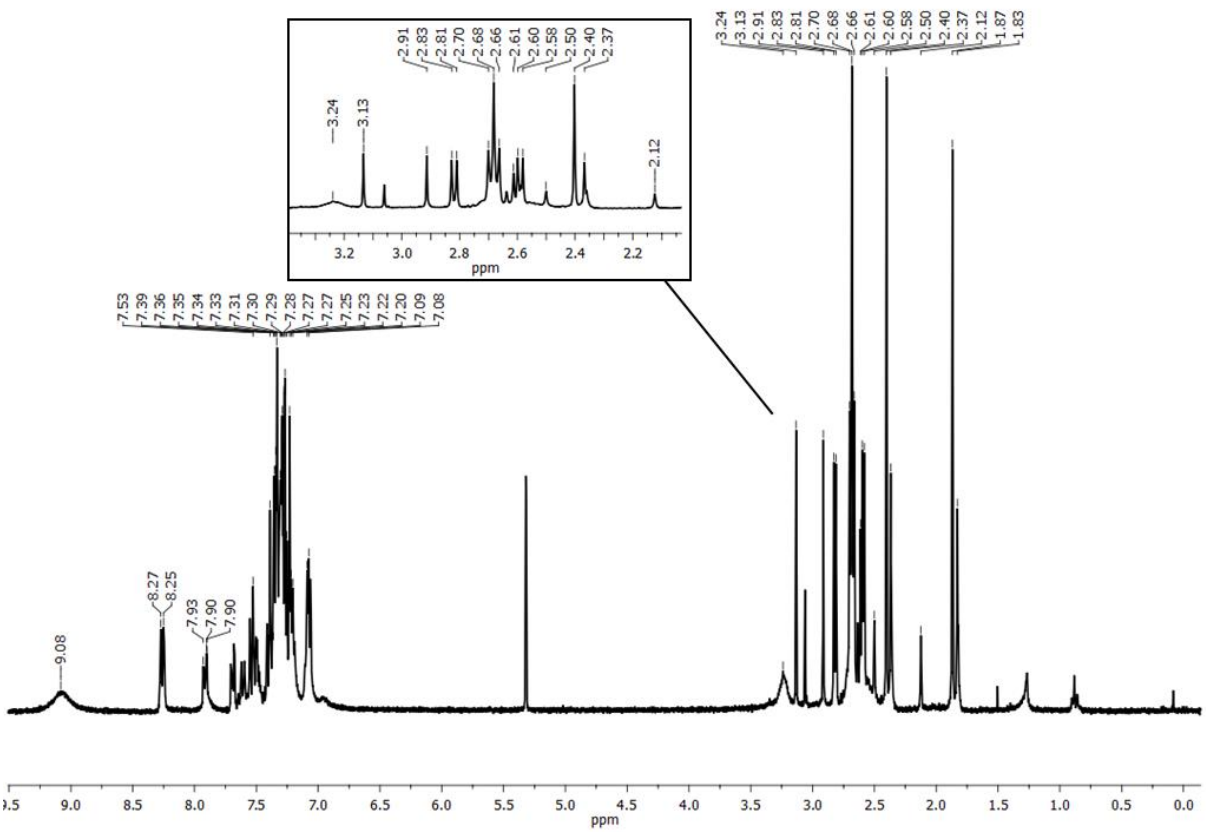

Figure S5.3.3. ^{1}H NMR spectrum (300 MHz) of the reaction of **3** with an excess of $PhB(NMe_2)Br$ in CD_2Cl_2.

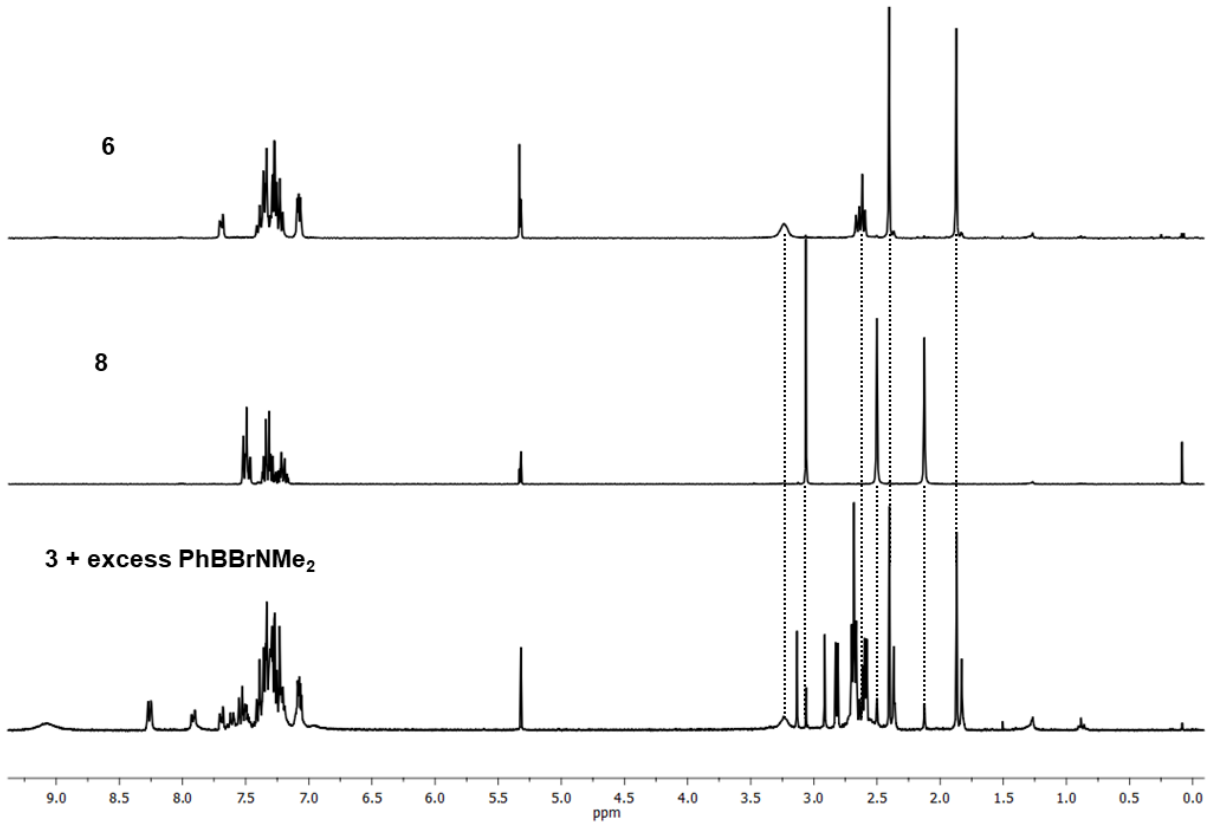

Figure S5.3.4. ^{1}H NMR spectra (300 MHz) of **6**, **8** and the reaction of **3** with an excess of $PhB(NMe_2)Br$ in CD_2Cl_2.

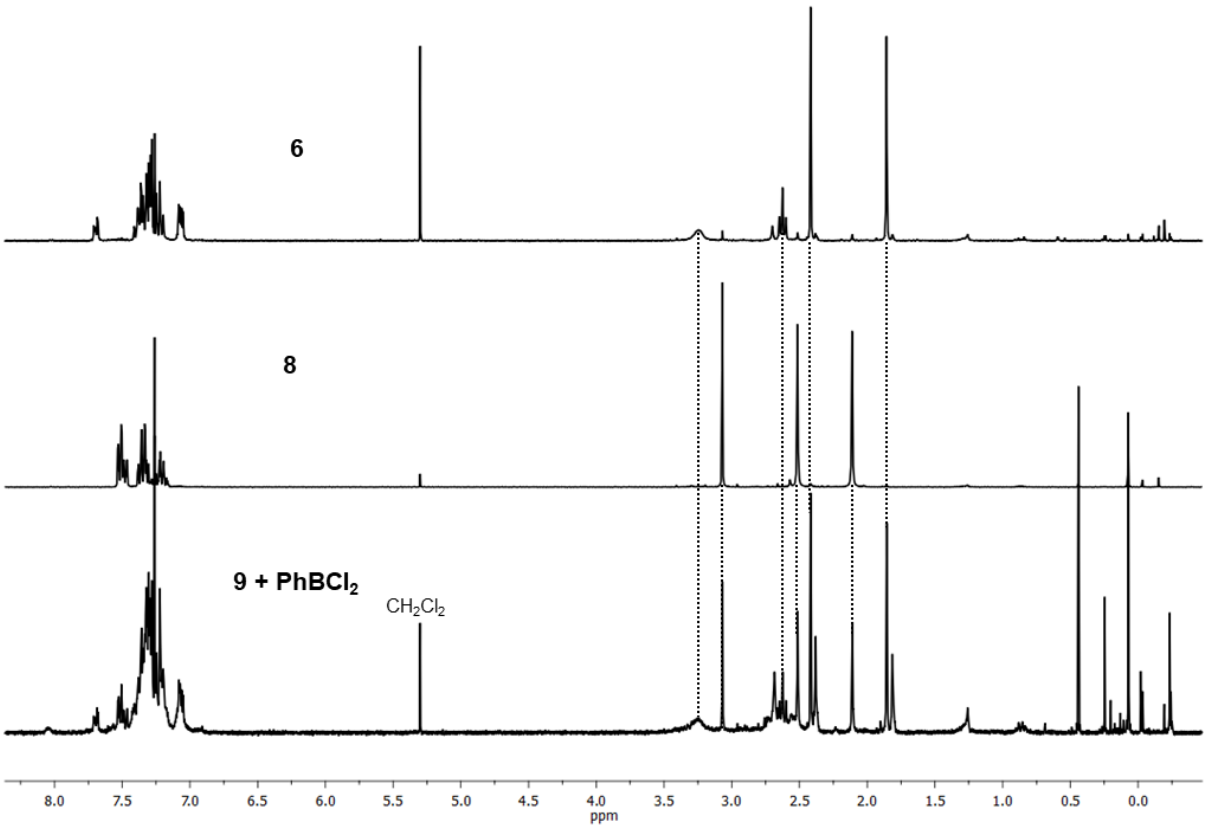

Figure S5.3.5. ^{1}H NMR spectra (300 MHz) of **6**, **8** and the reaction of **9** (2 equiv.) with $PhBCl_2$ in $CDCl_3$.

HRMS spectra

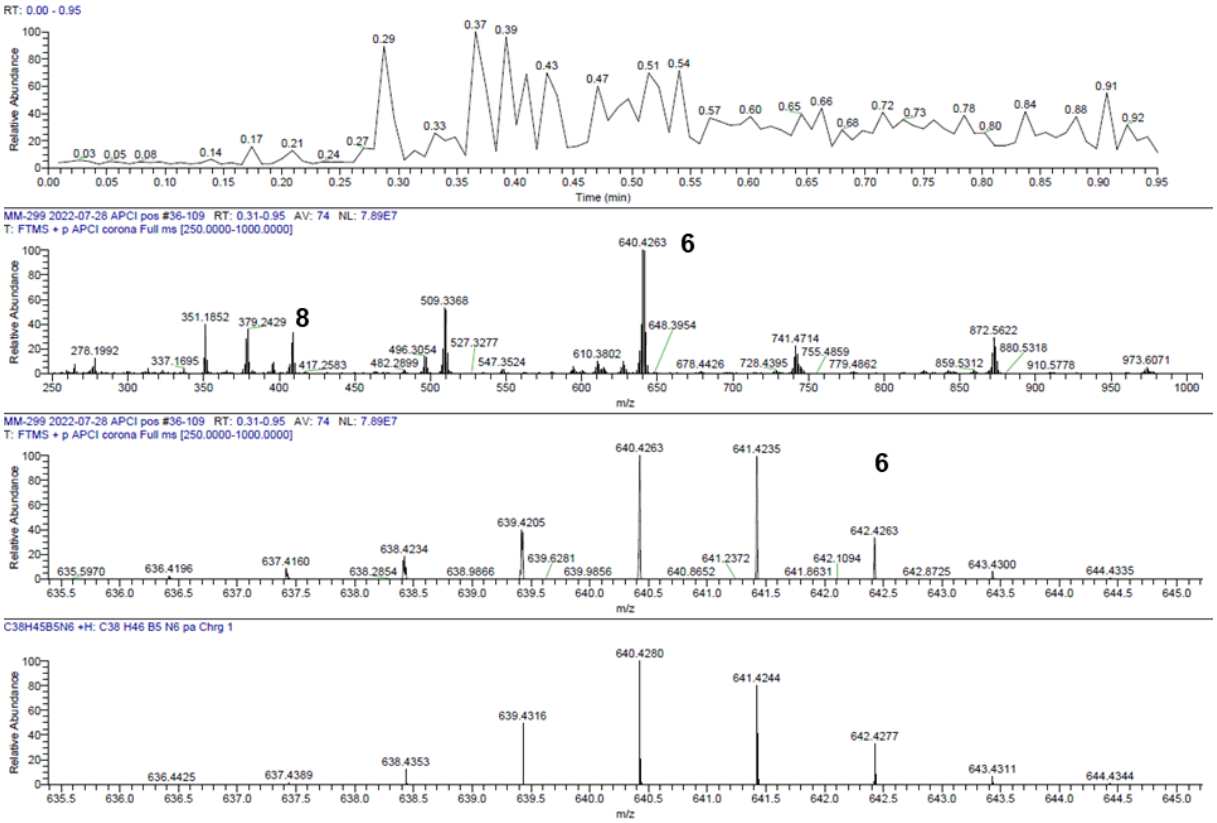

Figure S5.3.6. HRMS spectrum (APCI pos) of the reaction of **3** with an excess of $PhB(NMe_2)Br$ (calc. of **6**).

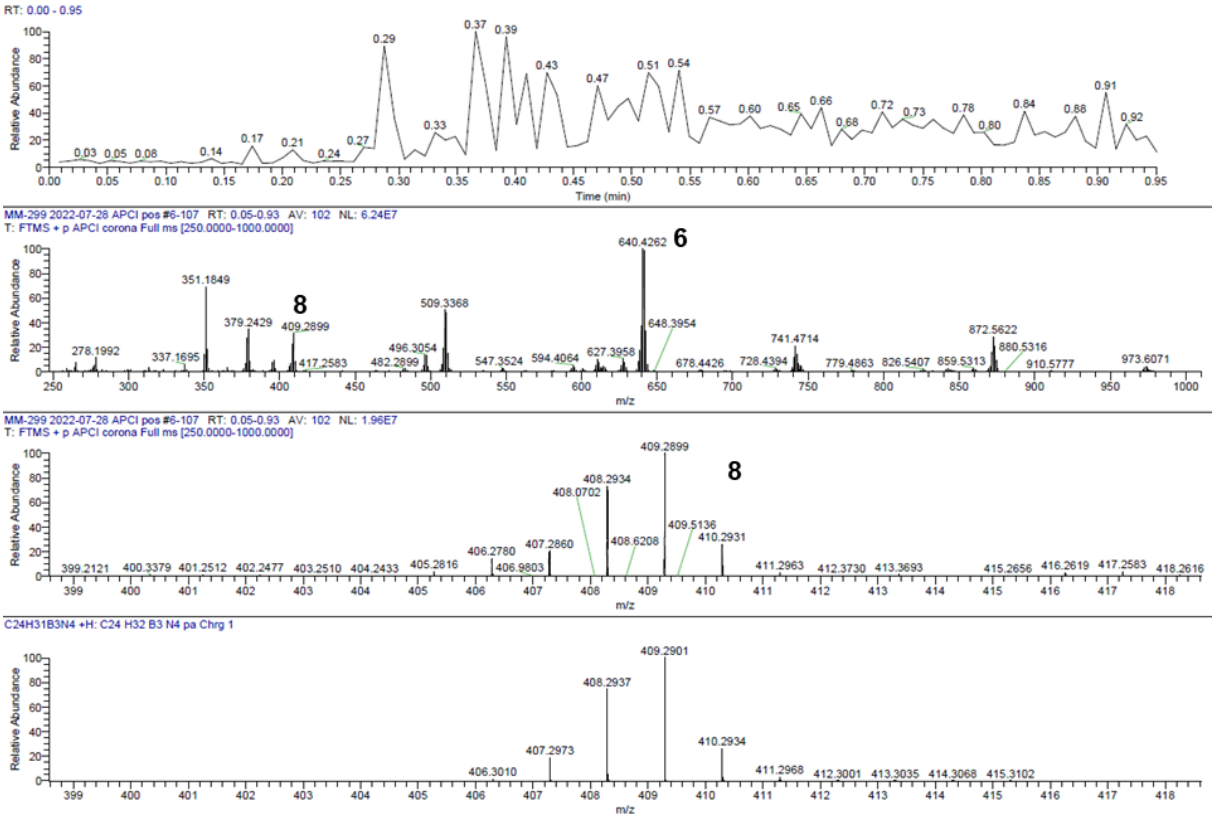

Figure S5.3.7. HRMS spectrum (APCI pos) of the reaction of **3** with an excess of PhB(NMe_2)Br (calc. of **8**).

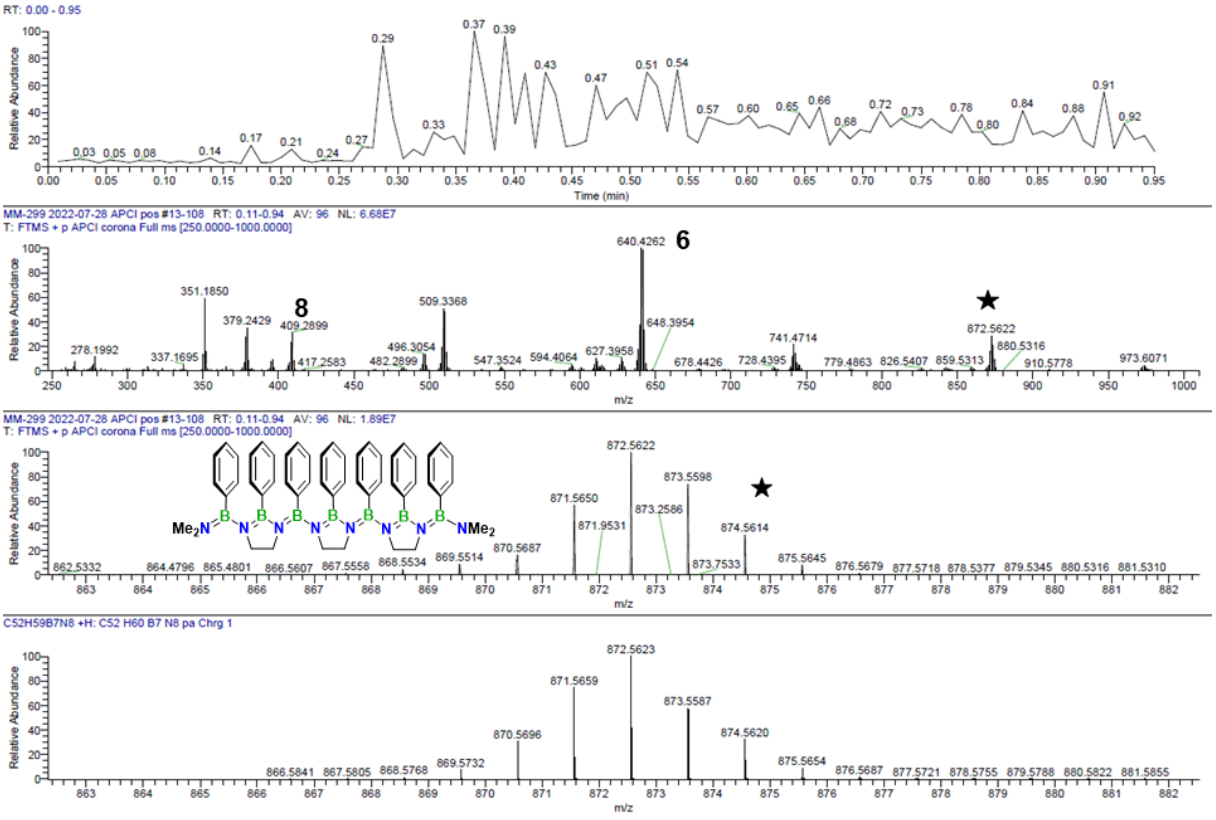

Figure S5.3.8. HRMS spectrum (APCI pos) of the reaction of **3** with an excess of PhB(NMe_2)Br.

Cartesian coordinates (Å) and total energies (a.u.) of optimized stationary points

The molecular species were optimized at the ωB97X-D/6-31+G(d,p) level. The total energy is given as the sum of the electronic energy (ωB97X-D/6-311+G(d,p), PCM), the thermal correction to Gibbs Free Energy (ωB97X-D/6-31+G(d,p)), and the concentration correction (1.89 kcal/mol).

Compound 3: Total energy: -1963.958568683260

N	-2.828484000	-0.337842000	0.067417000
C	-3.099903000	0.537224000	1.228445000
H	-2.723145000	0.072084000	2.149662000
H	-4.167737000	0.734588000	1.353782000
B	-1.594571000	0.099233000	-0.499483000
N	-1.196282000	1.351331000	0.102999000
B	0.054261000	2.044427000	-0.008991000
C	-2.325094000	1.821629000	0.918110000
H	-2.954613000	2.523127000	0.354476000
H	-1.985732000	2.324092000	1.828098000
C	-0.803371000	-0.562028000	-1.693617000
C	-0.405119000	0.228265000	-2.783797000
H	-0.653726000	1.287223000	-2.794162000
C	0.310095000	-0.307536000	-3.851461000
H	0.601655000	0.327885000	-4.682720000
C	0.664758000	-1.656863000	-3.844772000
H	1.233946000	-2.077234000	-4.668571000
C	0.282908000	-2.461289000	-2.773175000
H	0.556043000	-3.512180000	-2.755888000
C	-0.450086000	-1.916800000	-1.720050000
H	-0.746064000	-2.562101000	-0.898525000
Si	-3.875566000	-1.709178000	-0.284722000
C	-5.617701000	-1.264743000	0.269900000
H	-5.689913000	-1.158924000	1.357481000
H	-6.309169000	-2.059570000	-0.031743000
H	-5.958352000	-0.329982000	-0.188739000
C	-3.327456000	-3.231086000	0.677233000
H	-2.331951000	-3.570675000	0.373560000
H	-4.029729000	-4.059171000	0.526980000
H	-3.287006000	-3.007988000	1.749153000
C	-3.899537000	-2.061557000	-2.128596000
H	-4.126113000	-1.150524000	-2.692695000
H	-4.681919000	-2.798527000	-2.344301000
H	-2.948627000	-2.457085000	-2.493883000
C	0.102648000	3.624923000	-0.004199000
C	1.113153000	4.317946000	0.680242000
H	1.874522000	3.754593000	1.215216000
C	1.156946000	5.711044000	0.697394000
H	1.943414000	6.224902000	1.242407000
C	0.191015000	6.444618000	0.008319000
H	0.224997000	7.530077000	0.013092000
N	2.802529000	-0.494336000	-0.071083000
C	3.121835000	0.355726000	-1.238458000
H	2.723581000	-0.097090000	-2.156845000
H	4.198750000	0.496283000	-1.362606000
B	1.591577000	0.011499000	0.488683000
N	1.261945000	1.278277000	-0.122945000
C	2.414256000	1.681381000	-0.941052000
H	3.078611000	2.355373000	-0.383804000
H	2.101791000	2.191510000	-1.856467000
C	0.764612000	-0.600583000	1.684736000
C	0.408809000	0.214136000	2.771497000
H	0.712175000	1.258795000	2.777105000
C	-0.331853000	-0.279417000	3.842243000
H	-0.589322000	0.373807000	4.670953000
C	-0.755353000	-1.608770000	3.842056000
H	-1.344270000	-1.995580000	4.668409000
C	-0.417136000	-2.436500000	2.773505000
H	-0.744557000	-3.471818000	2.761003000
C	0.341436000	-1.935051000	1.717174000
H	0.602236000	-2.598007000	0.897853000
Si	3.774983000	-1.915278000	0.297330000
C	5.536333000	-1.574670000	-0.269920000
H	5.608877000	-1.485369000	-1.358976000
H	6.184096000	-2.403191000	0.038038000
H	5.930589000	-0.655075000	0.176275000
C	3.142149000	-3.419554000	-0.640347000
H	2.134474000	-3.706859000	-0.323326000
H	3.804392000	-4.279338000	-0.486293000
H	3.102448000	-3.207884000	-1.714608000
C	3.787065000	-2.239390000	2.146430000
H	4.087787000	-1.338853000	2.692531000
H	4.511838000	-3.030785000	2.370312000
H	2.810983000	-2.553310000	2.524584000
C	-0.862254000	4.385780000	-0.682316000
H	-1.657207000	3.876368000	-1.222440000
C	-0.818652000	5.779014000	-0.687065000
H	-1.571190000	6.345891000	-1.227381000

$PhBCl_2$: Total energy: -1176.921670783260

C	2.507840000	-1.208521000	0.000007000
C	1.117286000	-1.206884000	0.000089000
C	3.204362000	0.000000000	-0.000032000
C	0.392021000	0.000000000	0.000138000
H	3.048678000	-2.149049000	-0.000027000
H	4.289827000	-0.000001000	-0.000097000
H	0.586987000	-2.153837000	0.000120000
B	-1.153904000	0.000000000	0.000239000
Cl	-2.087742000	-1.502921000	-0.000393000
Cl	-2.087742000	1.502922000	-0.000387000
C	2.507840000	1.208520000	0.000012000
C	1.117287000	1.206884000	0.000094000
H	3.048679000	2.149048000	-0.000019000
H	0.586988000	2.153837000	0.000128000

Compound 4: Total energy: -2578.939000443260

N	-3.084920000	0.064381000	0.339501000
C	-3.404991000	1.294049000	1.100630000
H	-2.966397000	1.229677000	2.102665000
H	-4.482648000	1.435142000	1.194478000
B	-1.852438000	0.336075000	-0.389081000
N	-1.562561000	1.738755000	-0.288334000
B	-0.322096000	2.408412000	-0.554111000
C	-2.742219000	2.405209000	0.289370000
H	-3.415658000	2.763027000	-0.498586000
H	-2.458923000	3.255058000	0.913524000
C	-0.977384000	-0.670560000	-1.218844000
C	-0.592404000	-0.317331000	-2.521096000
H	-0.906944000	0.639443000	-2.932238000
C	0.182201000	-1.167450000	-3.307152000
H	0.457469000	-0.872305000	-4.315339000
C	0.613426000	-2.389197000	-2.792895000
H	1.227159000	-3.050501000	-3.397017000

C	0.249734000	-2.757216000	-1.498440000
H	0.578711000	-3.706966000	-1.087781000
C	-0.546619000	-1.911537000	-0.731697000
H	-0.845190000	-2.236673000	0.259055000
C	-0.286290000	3.921907000	-0.983973000
C	0.742713000	4.766215000	-0.537353000
H	1.521187000	4.360000000	0.105110000
C	0.783682000	6.112169000	-0.894011000
H	1.583757000	6.748795000	-0.528514000
C	-0.203710000	6.639004000	-1.726782000
H	-0.172728000	7.686103000	-2.012619000
N	2.554148000	0.165885000	0.375881000
C	3.171403000	1.027754000	-0.665078000
H	3.792367000	0.448380000	-1.349047000
H	3.801937000	1.781687000	-0.180784000
B	1.233885000	0.748200000	0.654758000
N	0.914999000	1.669029000	-0.384423000
C	1.997140000	1.695777000	-1.374117000
H	2.238252000	2.712526000	-1.693794000
H	1.695850000	1.120386000	-2.258116000
C	0.369696000	0.704235000	1.979249000
C	0.240506000	1.932182000	2.653705000
H	0.751484000	2.811979000	2.269108000
C	-0.533326000	2.059970000	3.805336000
H	-0.605978000	3.022270000	4.303248000
C	-1.220801000	0.956385000	4.306892000
H	-1.835687000	1.050433000	5.196728000
C	-1.116057000	-0.268460000	3.650731000
H	-1.654496000	-1.134248000	4.024487000
C	-0.324483000	-0.389887000	2.510433000
H	-0.255067000	-1.357030000	2.029896000
C	-1.271068000	4.476717000	-1.815984000
H	-2.077300000	3.846665000	-2.183590000
C	-1.230133000	5.817547000	-2.192909000
H	-1.997278000	6.223234000	-2.845561000
C	7.038041000	-0.822739000	0.131128000
C	5.740633000	-0.464945000	0.492200000
C	7.298606000	-2.104979000	-0.350040000
C	4.680752000	-1.381219000	0.403243000
H	7.843662000	-0.100527000	0.221662000
H	8.306799000	-2.383627000	-0.641113000
H	5.556577000	0.540933000	0.859845000
B	3.219592000	-0.984248000	0.828143000
Cl	2.389589000	-2.147529000	1.928571000
C	6.259685000	-3.029660000	-0.451051000
C	4.969796000	-2.672986000	-0.063983000
H	6.456068000	-4.030617000	-0.823026000
H	4.174117000	-3.410465000	-0.129950000
C	-3.598345000	-3.244797000	-2.732475000
C	-3.701611000	-2.172321000	-1.851390000
C	-3.485652000	-4.542970000	-2.235903000
C	-3.708269000	-2.370162000	-0.461995000
H	-3.594774000	-3.068238000	-3.803651000
H	-3.390794000	-5.381186000	-2.919588000
Cl	-4.879155000	-1.293675000	1.940404000
C	-3.500956000	-4.762763000	-0.858776000
C	-3.627529000	-3.686362000	0.016012000
H	-3.645177000	-3.871761000	1.086787000
H	-3.418273000	-5.772288000	-0.467815000
H	-3.766005000	-1.163752000	-2.249710000
B	-3.783365000	-1.146621000	0.508766000

Compound 5: Total energy: -1570.445808153260

N	2.074387000	-0.816507000	-0.145550000
C	2.153546000	-2.242286000	-0.513313000
H	2.979730000	-2.751618000	-0.011829000
H	2.299113000	-2.349210000	-1.596431000
B	0.709187000	-0.461801000	-0.026497000
N	-0.121352000	-1.672522000	-0.110410000
C	0.806863000	-2.822820000	-0.080167000
H	0.471989000	-3.624016000	-0.740994000
H	0.865187000	-3.221015000	0.939438000
C	0.180293000	0.998939000	0.203580000
C	0.427041000	2.005265000	-0.739526000
H	0.970331000	1.765799000	-1.650094000
C	-0.024643000	3.308744000	-0.543610000
H	0.172767000	4.070255000	-1.292269000
C	-0.731542000	3.632152000	0.613670000
H	-1.085587000	4.646439000	0.771574000
C	-0.986545000	2.645071000	1.565747000
H	-1.540708000	2.889216000	2.467132000
C	-0.536829000	1.343525000	1.356841000
H	-0.756086000	0.582346000	2.101383000
Si	3.544850000	0.162319000	0.018736000
C	4.926720000	-0.989900000	0.561915000
H	4.663785000	-1.530306000	1.477734000
H	5.826828000	-0.399682000	0.767043000
H	5.181773000	-1.724102000	-0.209404000
C	3.300985000	1.490091000	1.320610000
H	2.593529000	2.260297000	1.002578000
H	4.264161000	1.971567000	1.525502000
H	2.932663000	1.055099000	2.255590000
C	4.011406000	0.924819000	-1.634515000
H	4.060729000	0.158199000	-2.415643000
H	4.995127000	1.403630000	-1.569927000
H	3.288416000	1.684301000	-1.947871000
C	-3.386009000	1.219837000	-1.554958000
C	-2.462141000	0.196709000	-1.358342000
C	-4.433146000	1.394856000	-0.651408000
C	-2.571104000	-0.681614000	-0.270310000
H	-3.281820000	1.887652000	-2.404664000
H	-5.146911000	2.200639000	-0.793947000
H	-1.637828000	0.085937000	-2.057018000
B	-1.516357000	-1.817597000	-0.048127000
Cl	-2.177320000	-3.470736000	0.302917000
C	-4.564088000	0.527875000	0.432997000
C	-3.650684000	-0.508698000	0.608688000
H	-5.380320000	0.656601000	1.137392000
H	-3.771509000	-1.183911000	1.451808000

Compound 2: Total energy: -1877.936311393260

Cl	-0.345843000	4.444080000	13.902868000
N	1.944479000	5.840951000	13.254875000
C	1.859306000	6.484345000	14.584176000
H	1.687024000	5.751805000	15.373258000
H	1.035964000	7.207058000	14.595999000
Cl	5.583117000	9.112378000	14.408888000
N	3.586025000	7.527903000	13.351637000
C	3.204414000	7.182937000	14.738580000
H	3.133112000	8.071201000	15.366950000
H	3.950965000	6.509312000	15.173597000
B	4.542005000	8.528022000	13.053709000
B	2.908448000	6.592869000	12.470120000
B	1.104643000	4.766611000	12.876239000
C	4.752745000	9.195541000	11.657230000
C	6.036677000	9.454831000	11.154802000
H	6.909147000	9.208122000	11.753867000
C	6.215456000	10.003479000	9.887463000
H	7.217818000	10.176084000	9.507768000
C	5.106468000	10.334764000	9.109647000
H	5.243517000	10.765774000	8.122537000
C	3.821366000	10.118063000	9.605293000
H	2.954404000	10.382191000	9.007723000
C	3.650665000	9.547644000	10.863153000
H	2.644393000	9.364652000	11.228792000
C	3.171907000	6.424475000	10.937759000

C	4.469456000	6.231787000	10.445588000
H	5.309284000	6.203868000	11.135010000
C	4.708502000	6.075671000	9.083094000
H	5.721951000	5.924152000	8.724215000
C	3.645968000	6.121593000	8.181264000
H	3.828934000	6.004700000	7.117379000
C	2.347654000	6.318168000	8.650433000
H	1.515759000	6.353697000	7.953641000
C	2.117556000	6.461795000	10.015837000
H	1.098785000	6.604050000	10.366921000
C	1.342309000	3.812357000	11.662542000
C	2.631072000	3.340653000	11.369799000
H	3.466323000	3.632878000	11.999658000
C	2.864275000	2.511910000	10.276396000
H	3.869619000	2.159110000	10.068328000
C	1.807669000	2.149299000	9.442005000
H	1.988368000	1.515075000	8.579424000
C	0.516996000	2.596993000	9.721895000
H	-0.309548000	2.312121000	9.078185000
C	0.287491000	3.406750000	10.831285000
H	-0.724178000	3.742646000	11.042587000

Me_3SiCl: Total energy: -869.457458485263

Si	-0.357322000	0.000293000	0.000022000
C	-0.890565000	0.906459000	-1.544062000
C	-0.890875000	-1.789903000	-0.013078000
C	-0.890712000	0.883891000	1.557101000
H	-0.521443000	1.936474000	-1.545121000
H	-1.984883000	0.935627000	-1.594067000
H	-0.521301000	0.404684000	-2.443553000
H	-0.521684000	-2.318500000	0.870938000
H	-1.985183000	-1.847765000	-0.013368000
H	-0.521878000	-2.305328000	-0.904905000
H	-0.521548000	0.369247000	2.449313000
H	-0.521655000	1.913791000	1.572988000
H	-1.985013000	0.912285000	1.607421000
Cl	1.760135000	-0.000056000	0.000132000

5.4 Synthesis of 1,3,2-Benzodiazaborolines as Building Blocks for Oligo- and Poly(iminoborane)s

NMR spectra

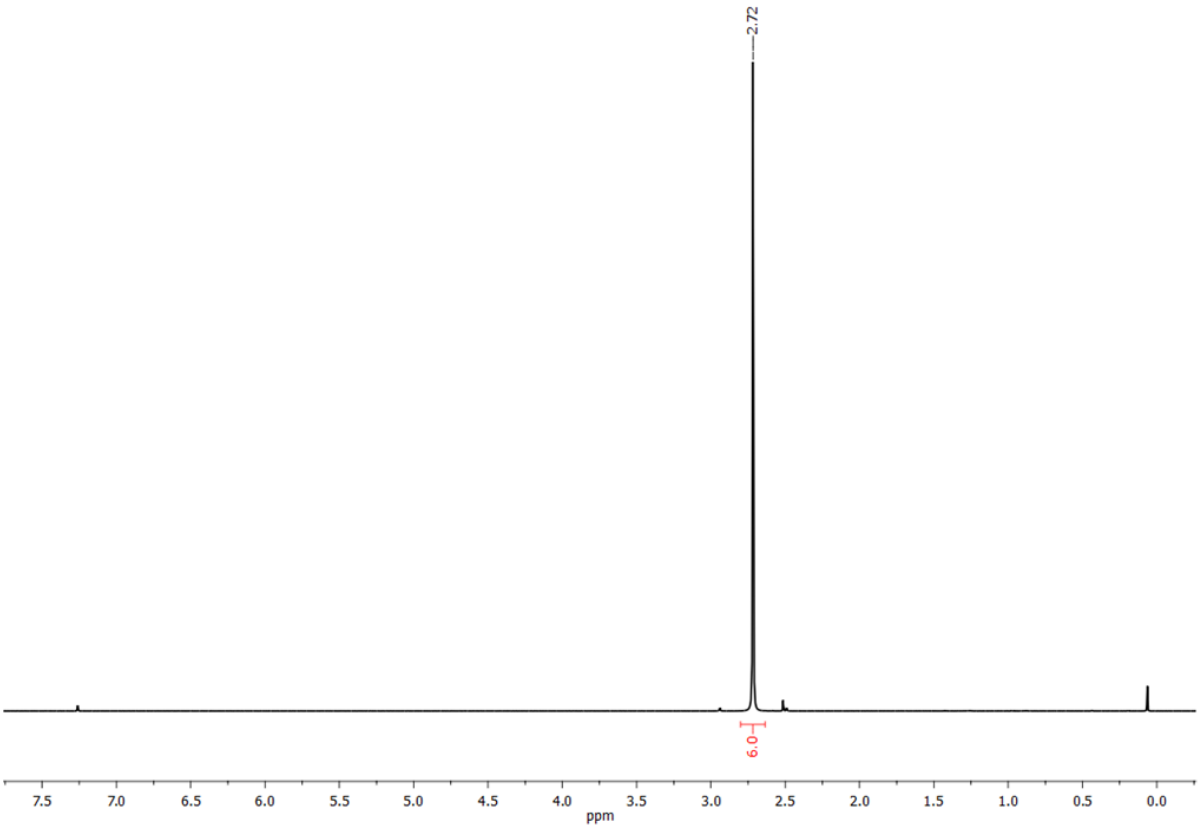

Figure S5.4.1. ^{1}H NMR spectrum (300 MHz) of chloro-bis(dimethylamino)borane in $CDCl_3$.

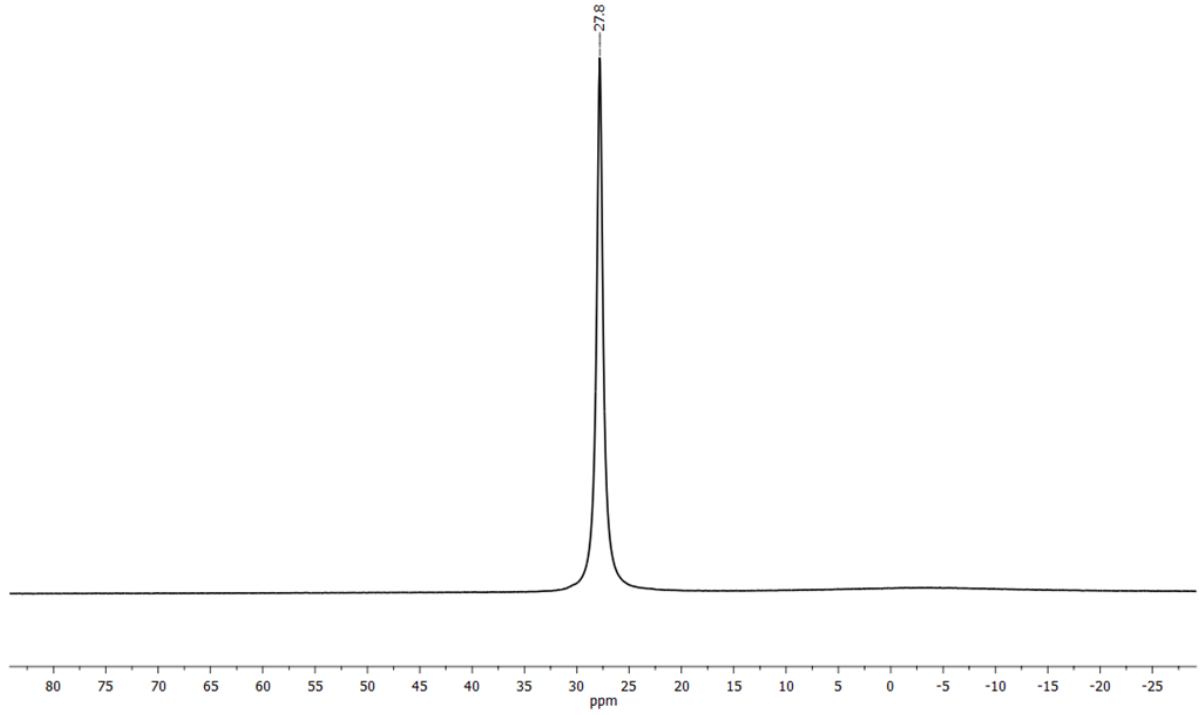

Figure S5.4.2. $^{11}B\{^{1}H\}$ NMR spectrum (96 MHz) of chloro-bis(dimethylamino)borane in $CDCl_3$.

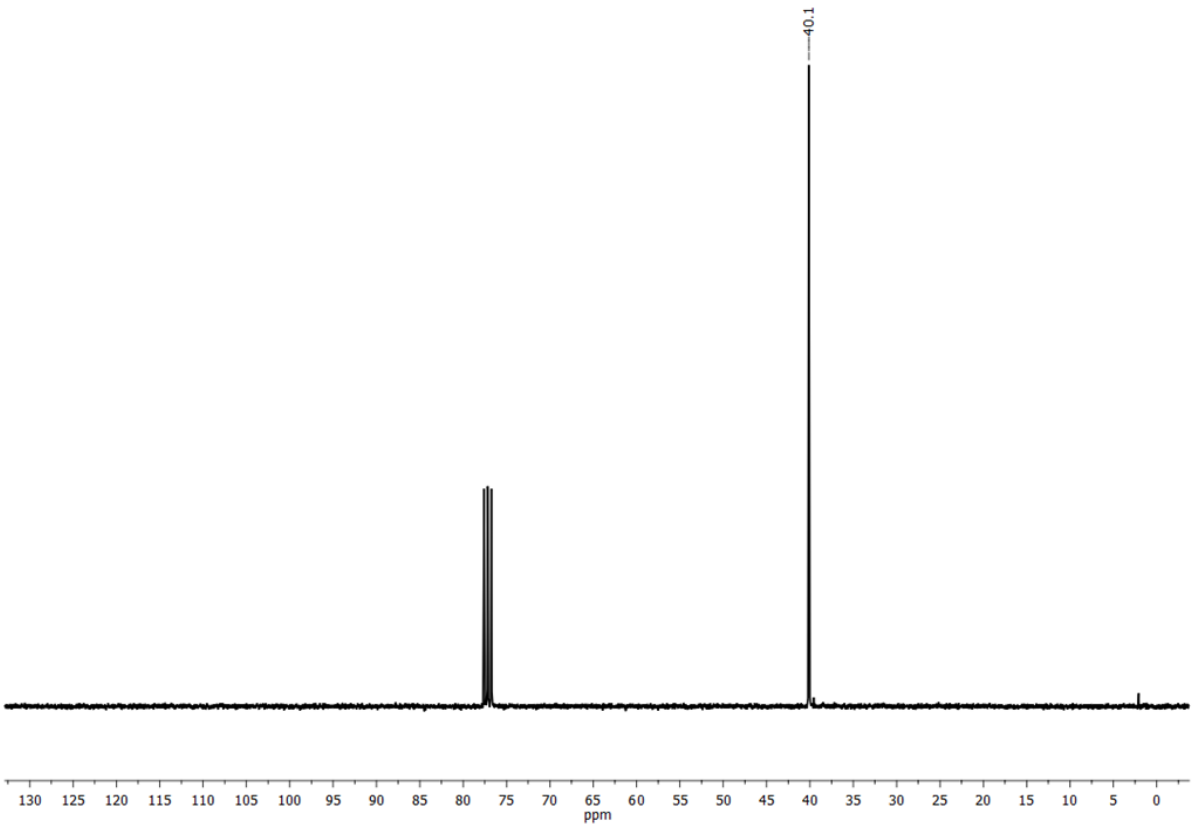

Figure S5.4.3. $^{13}C\{^{1}H\}$ NMR spectrum (76 MHz) of chloro-bis(dimethylamino)borane in $CDCl_3$.

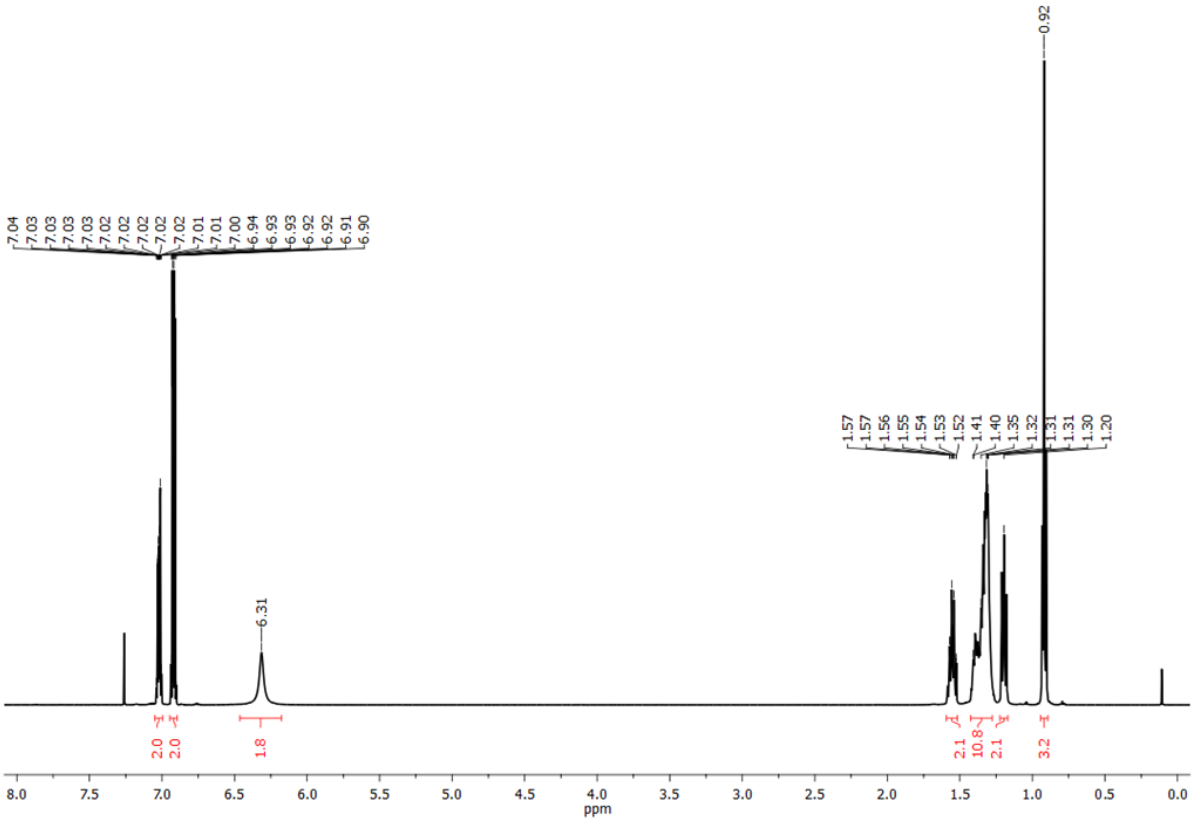

Figure S5.4.4. ^{1}H NMR spectrum (500 MHz) of **2** in $CDCl_3$.

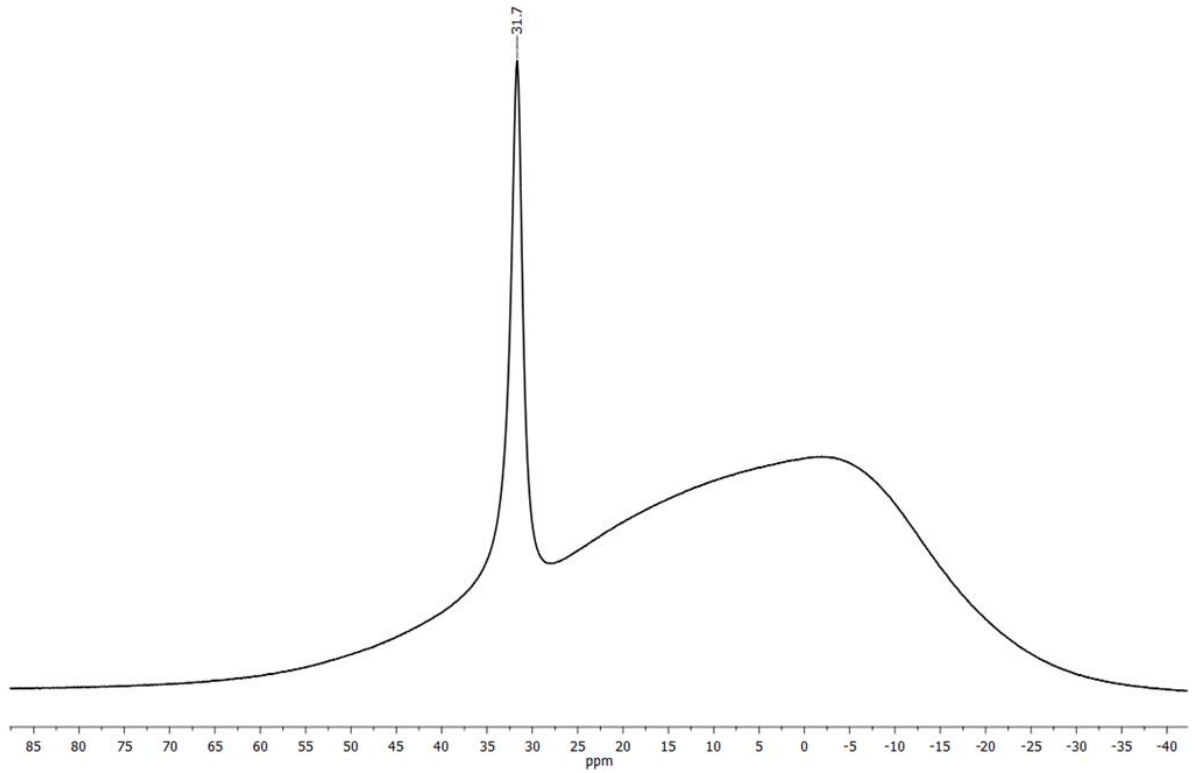

Figure S5.4.5. $^{11}B\{^{1}H\}$ NMR spectrum (160 MHz) of **2** in $CDCl_3$.

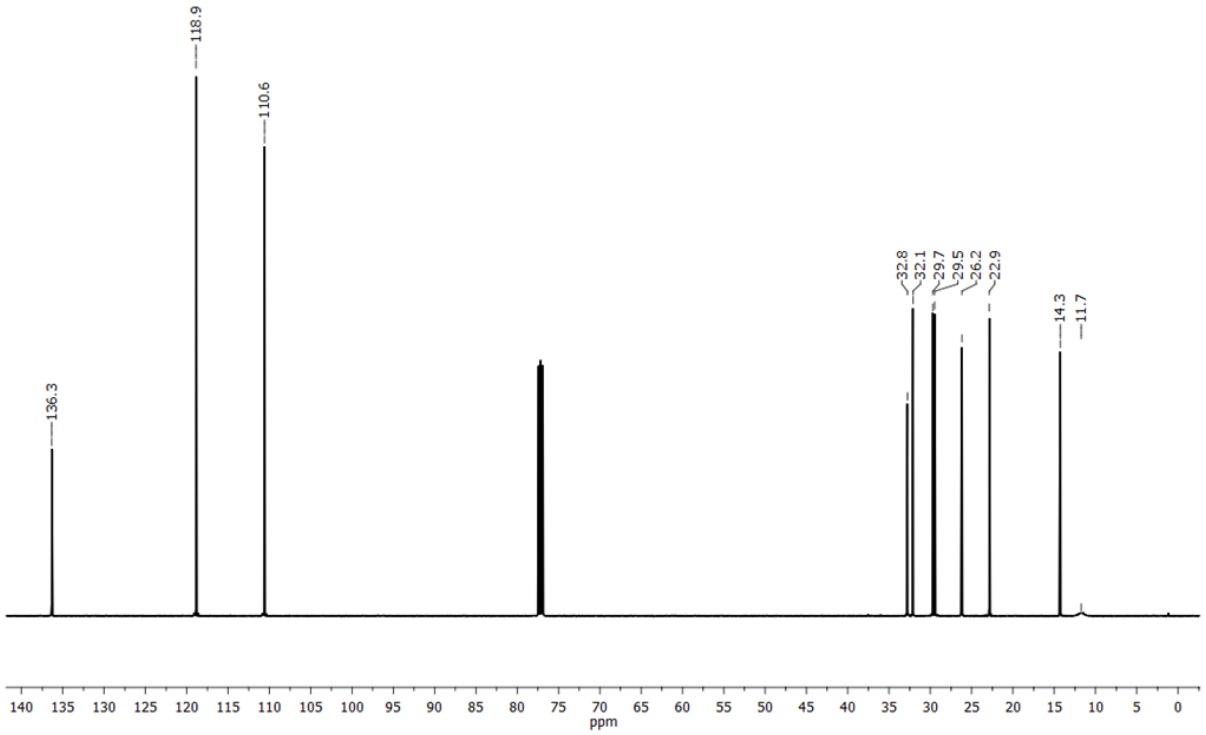

Figure S5.4.6. $^{13}C\{^{1}H\}$ NMR spectrum (126 MHz) of **2** in $CDCl_3$.

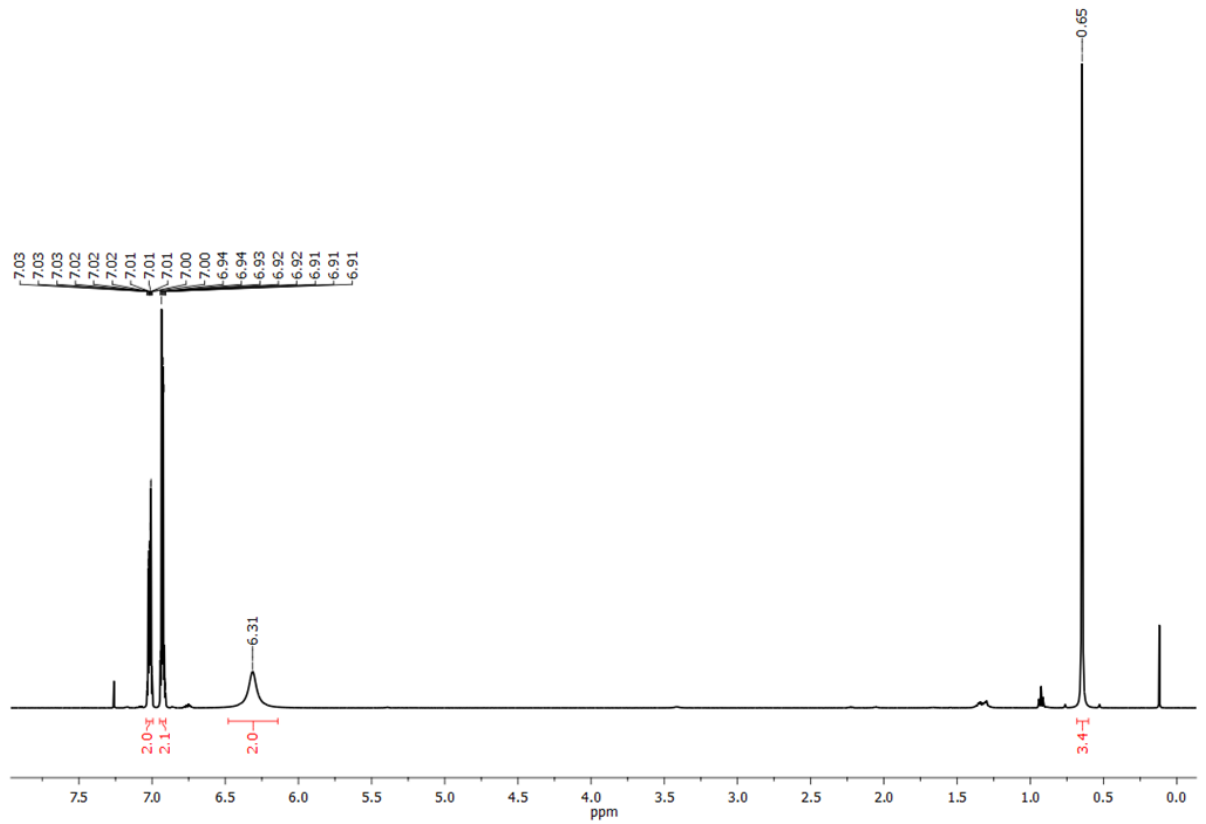

Figure S5.4.7. ^{1}H NMR spectrum (500 MHz) of **3** in $CDCl_3$.

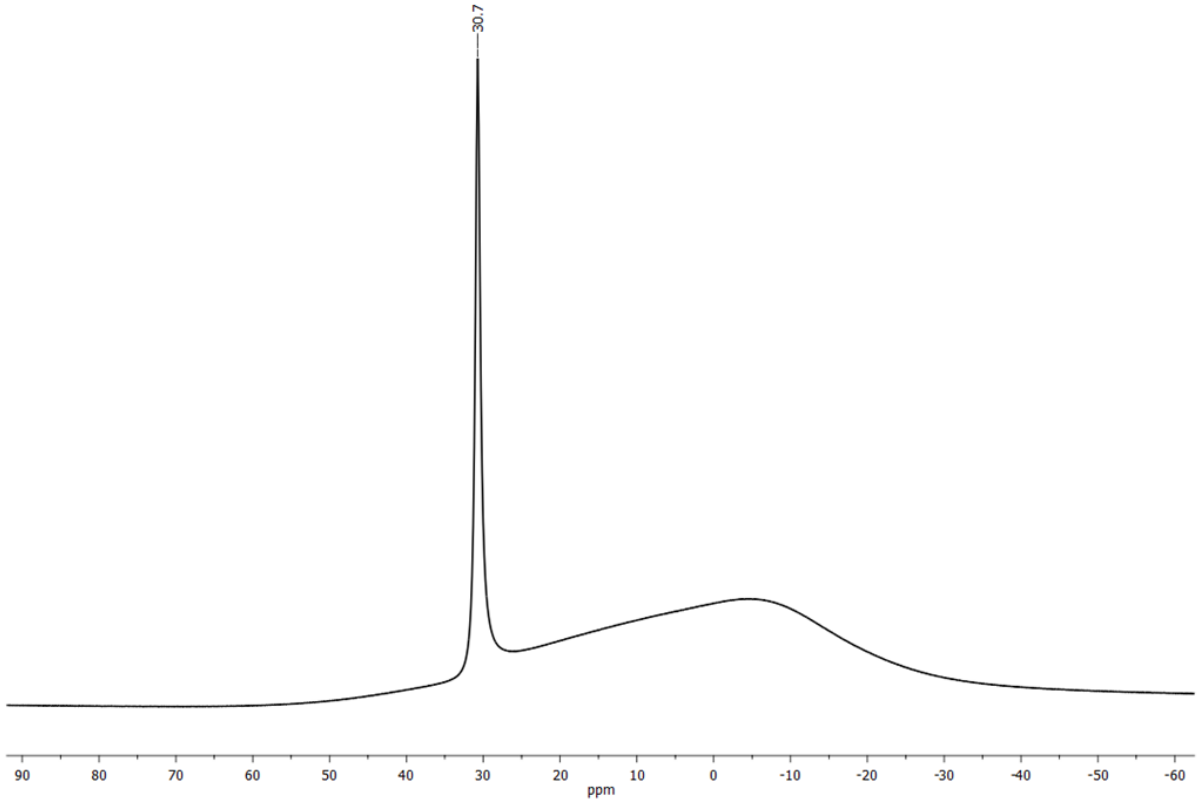

Figure S5.4.8. $^{11}B\{^{1}H\}$ NMR spectrum (160 MHz) of **3** in $CDCl_3$.

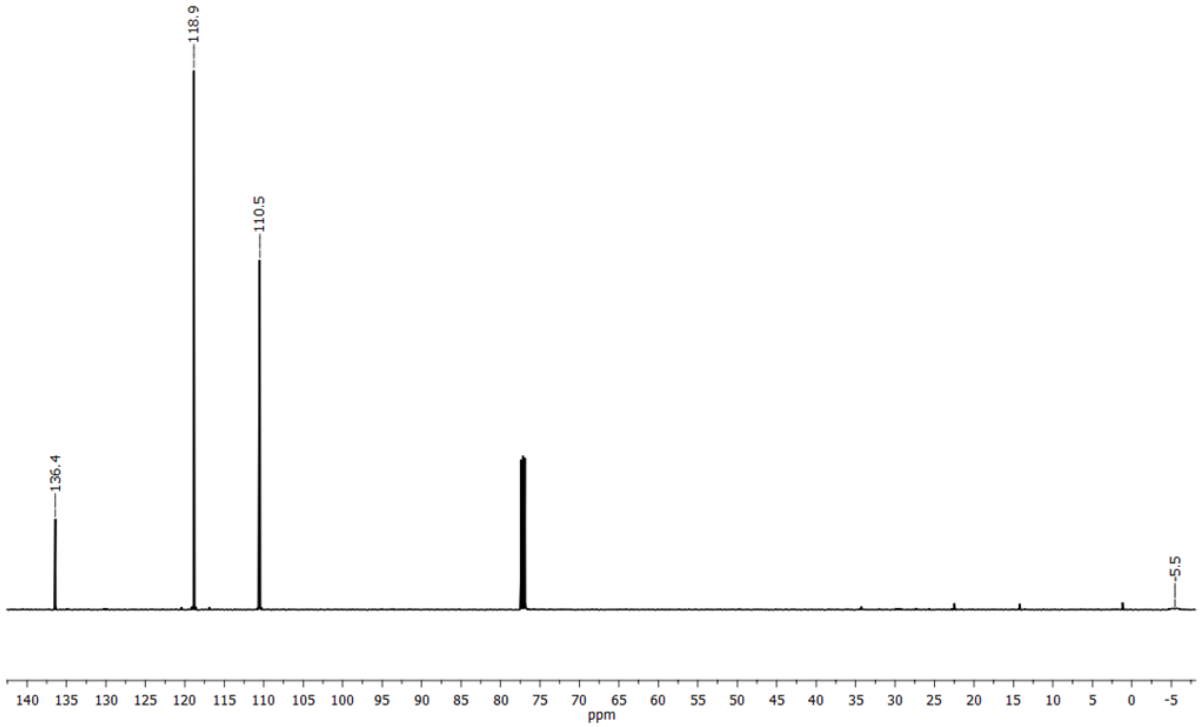

Figure S5.4.9. $^{13}C\{^{1}H\}$ NMR spectrum (126 MHz) of **3** in $CDCl_3$.

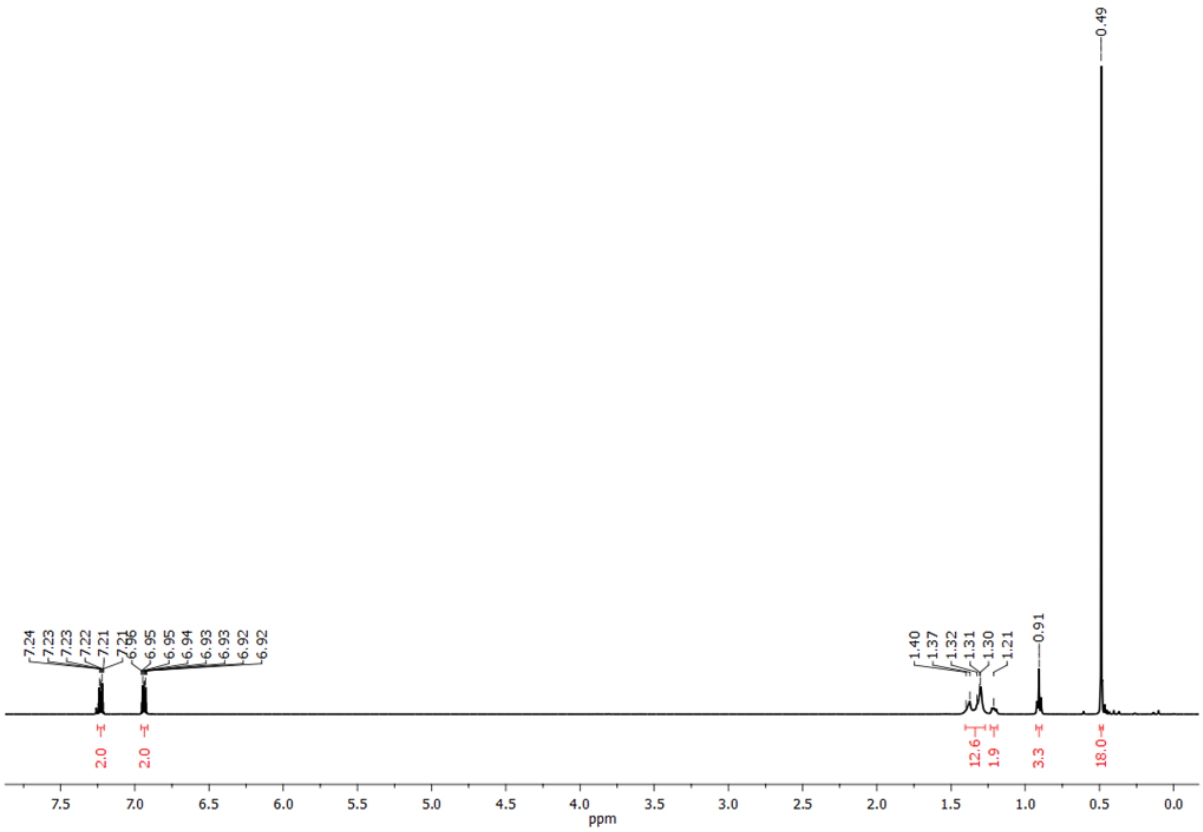

Figure S5.4.10. ^{1}H NMR spectrum (500 MHz) of **4** in $CDCl_3$.

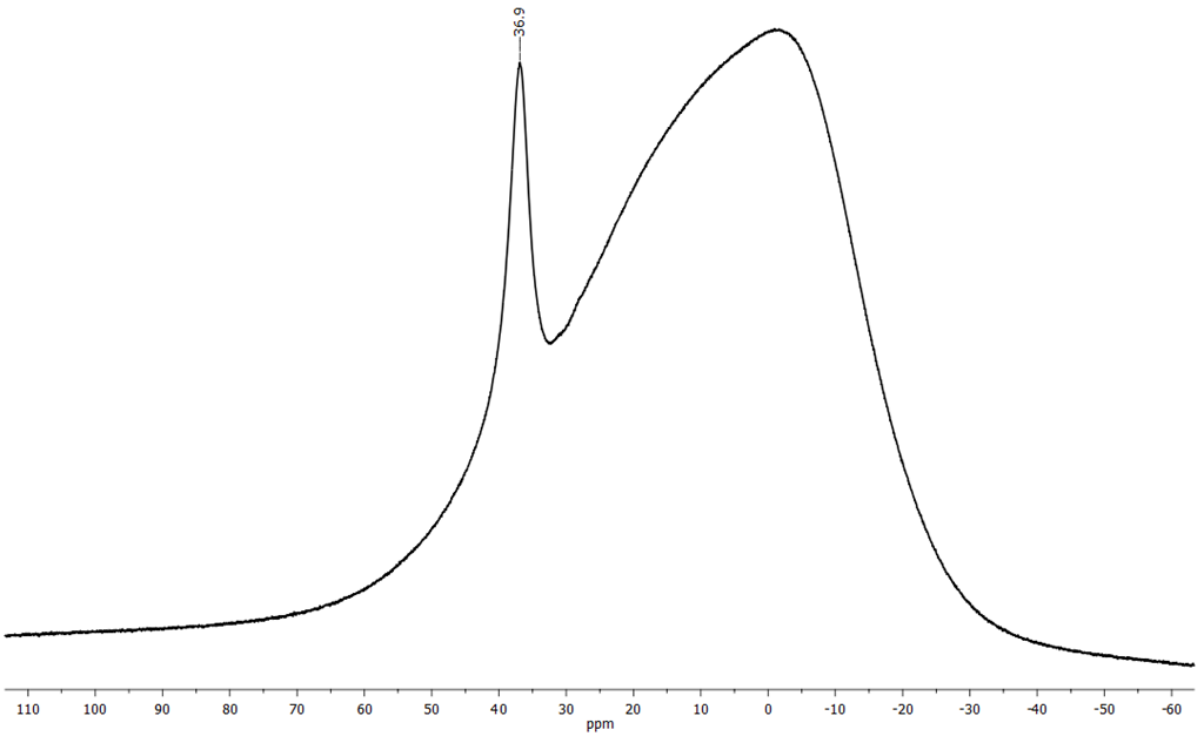

Figure S5.4.11. $^{11}B\{^{1}H\}$ NMR spectrum (160 MHz) of **4** in $CDCl_3$.

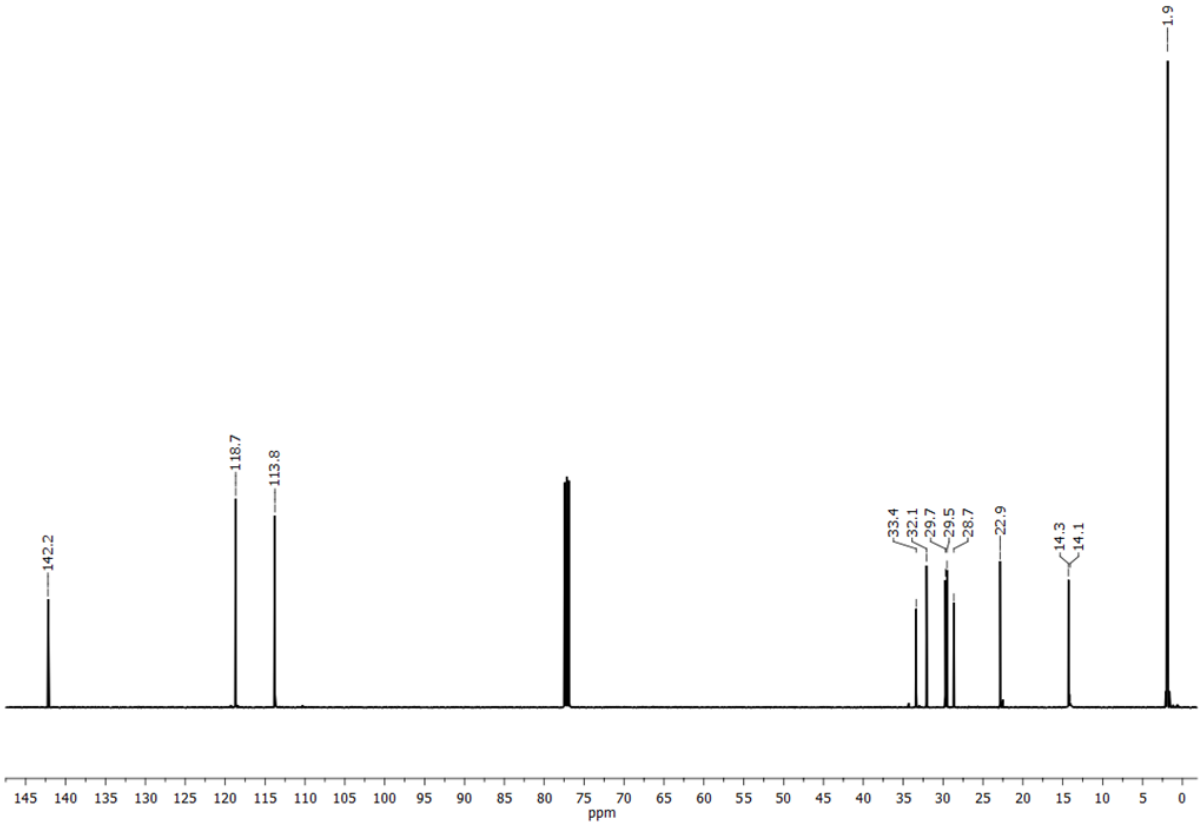

Figure S5.4.12. $^{13}C\{^{1}H\}$ NMR spectrum (126 MHz) of **4** in $CDCl_3$.

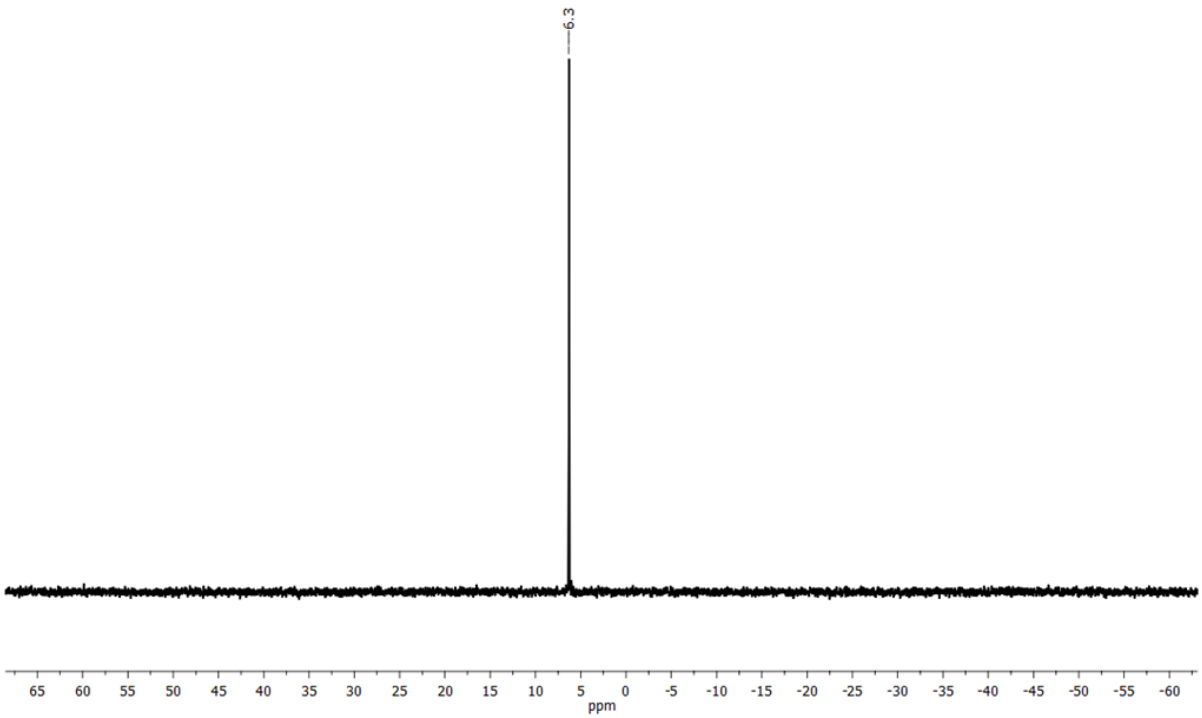

Figure S5.4.13. $^{29}Si\{^{1}H\}$ NMR spectrum (99 MHz) of **4** in $CDCl_3$.

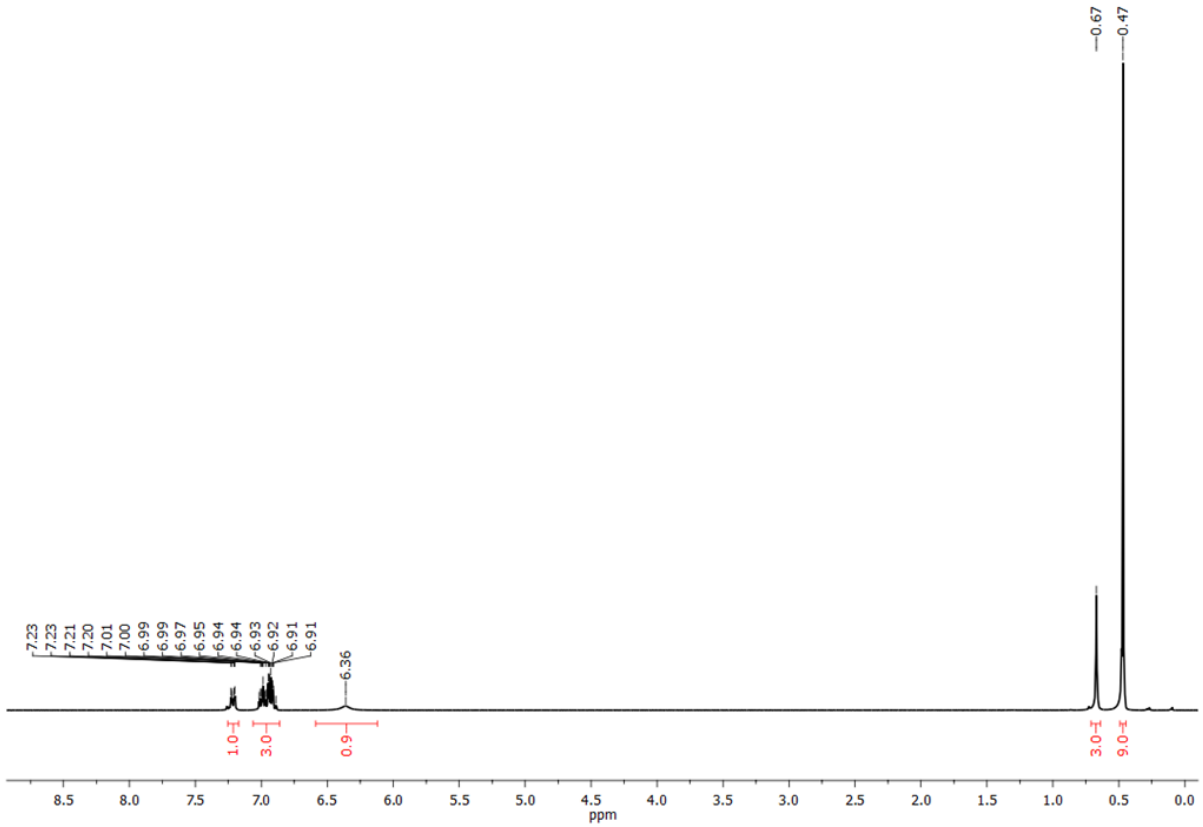

Figure S5.4.14. ^{1}H NMR spectrum (300 MHz) of **5** in $CDCl_3$.

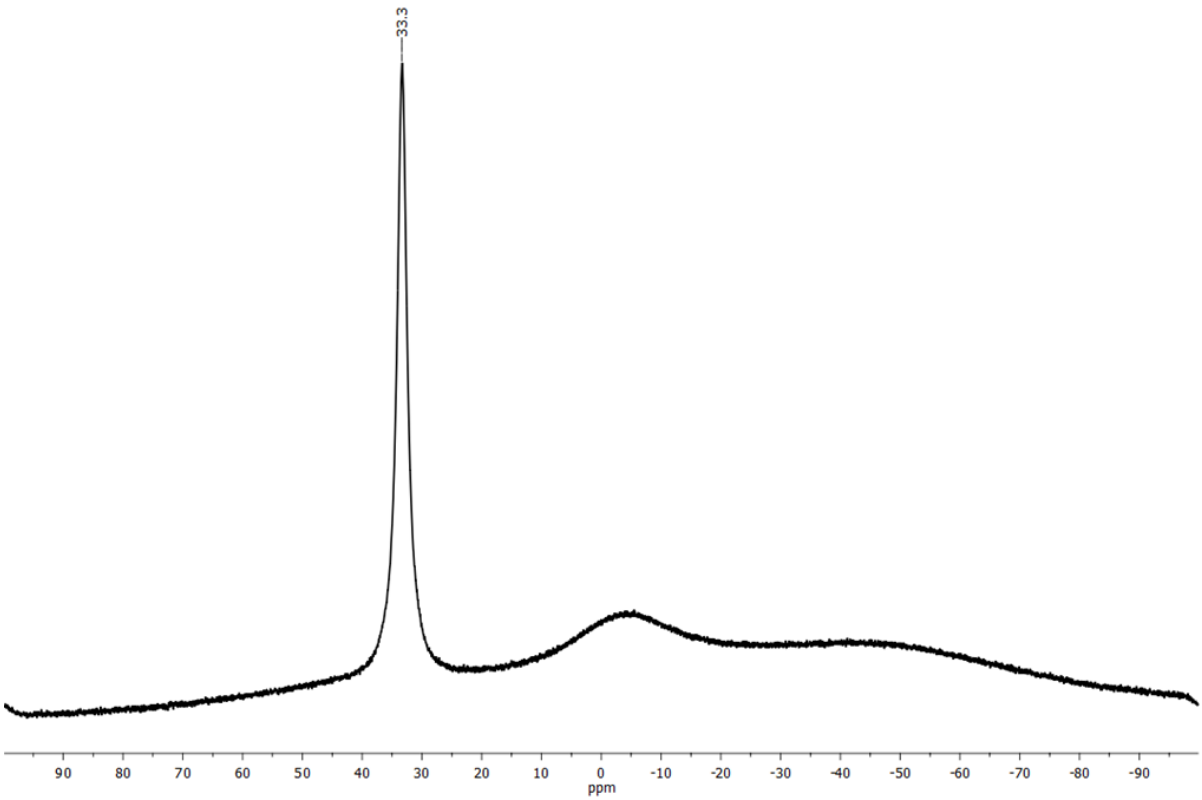

Figure S5.4.15. $^{11}B\{^{1}H\}$ NMR spectrum (96 MHz) of **5** in $CDCl_3$.

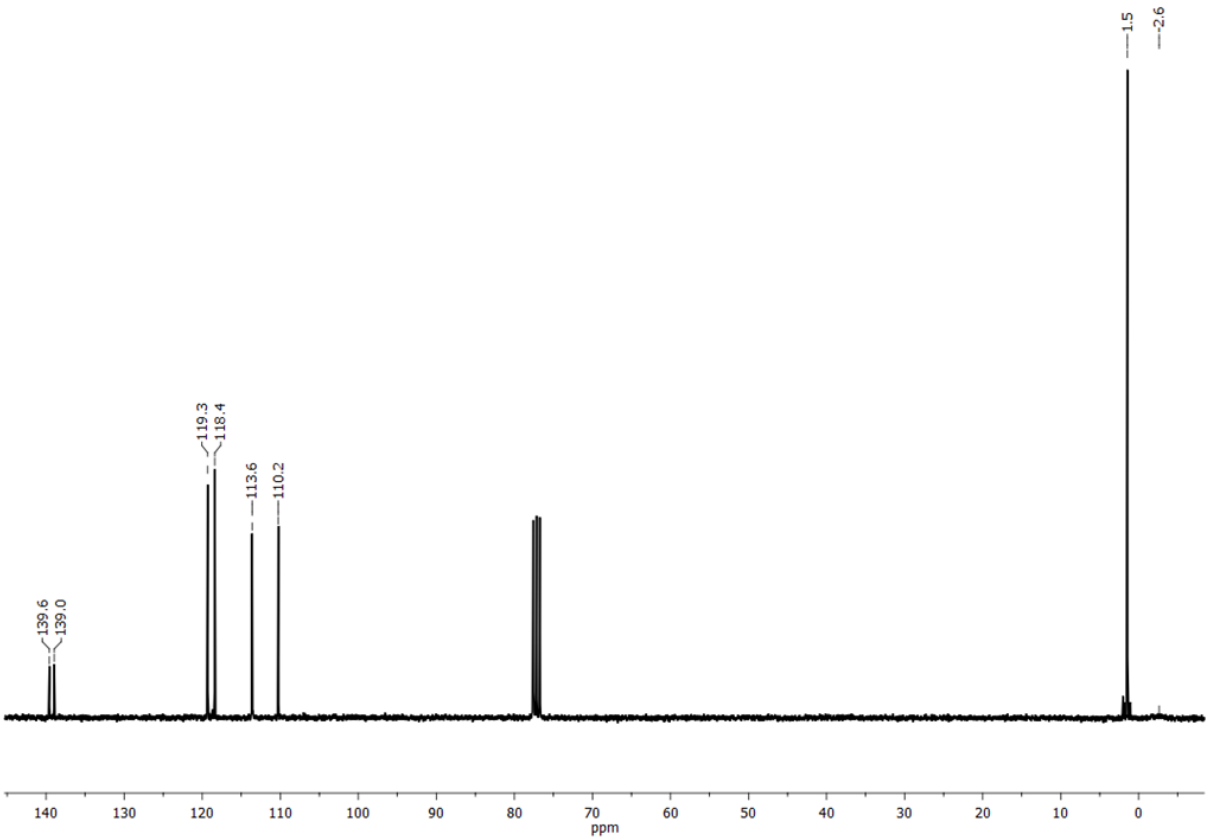

Figure S5.4.16. $^{13}C\{^{1}H\}$ NMR spectrum (76 MHz) of **5** in $CDCl_3$.

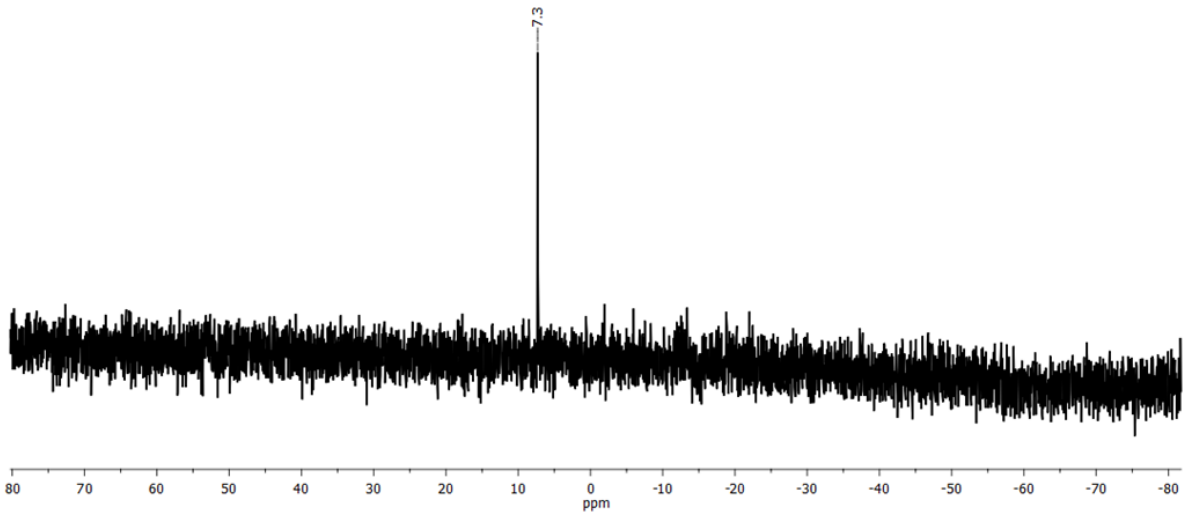

Figure S5.4.17. $^{29}Si\{^{1}H\}$ NMR spectrum (60 MHz) of **5** in $CDCl_3$.

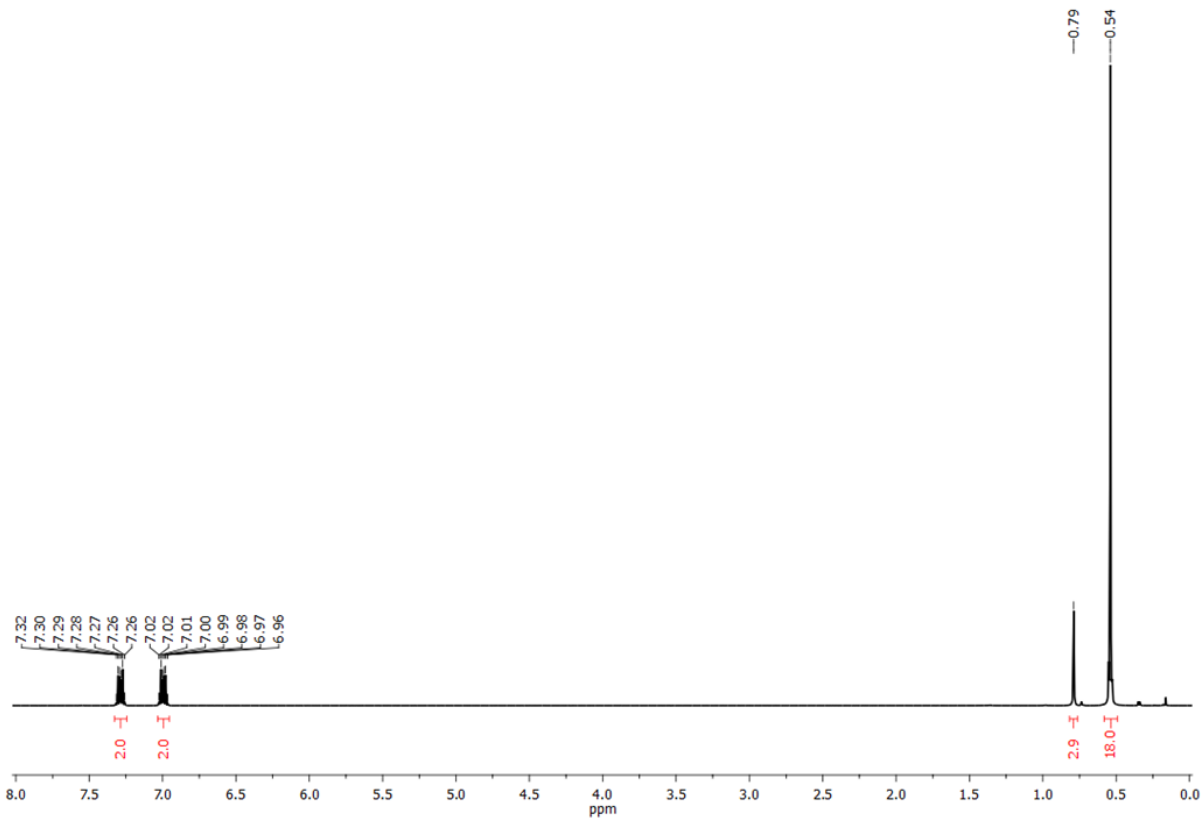

Figure S5.4.18. ^{1}H NMR spectrum (300 MHz) of **6** in $CDCl_3$.

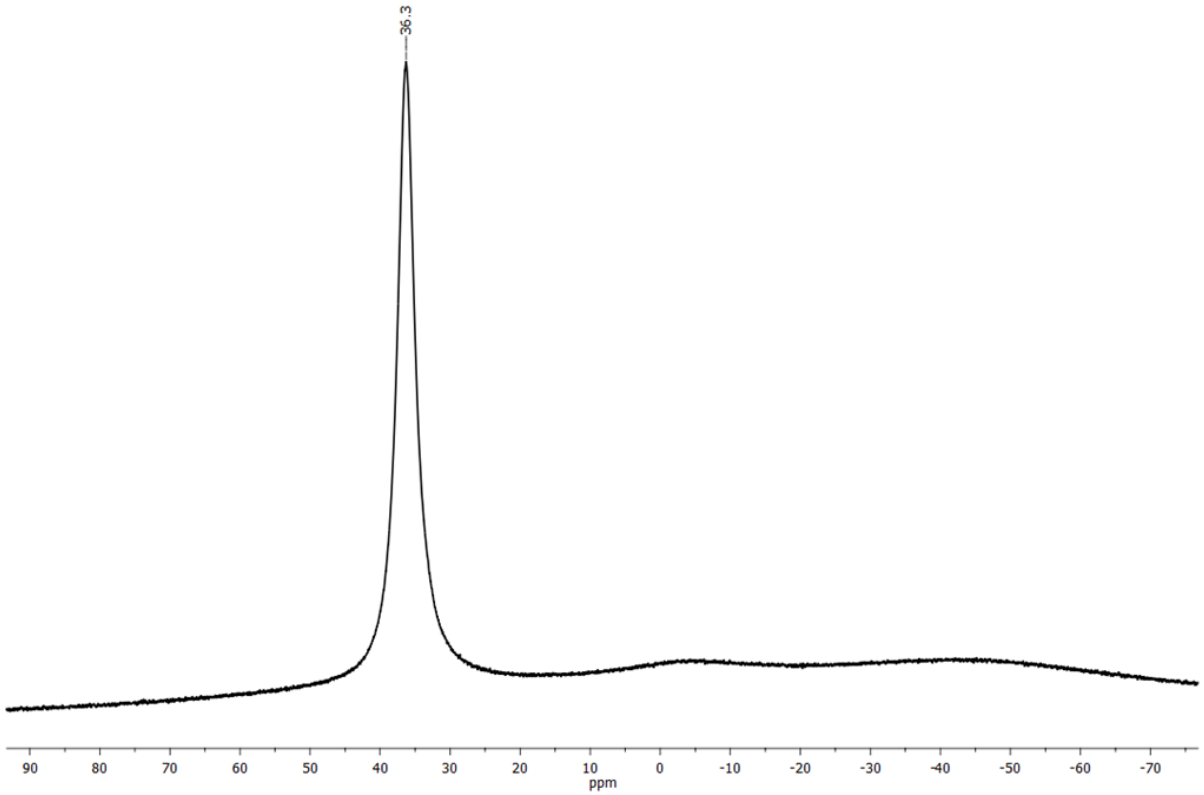

Figure S5.4.18. $^{11}B\{^{1}H\}$ NMR spectrum (96 MHz) of **6** in $CDCl_3$.

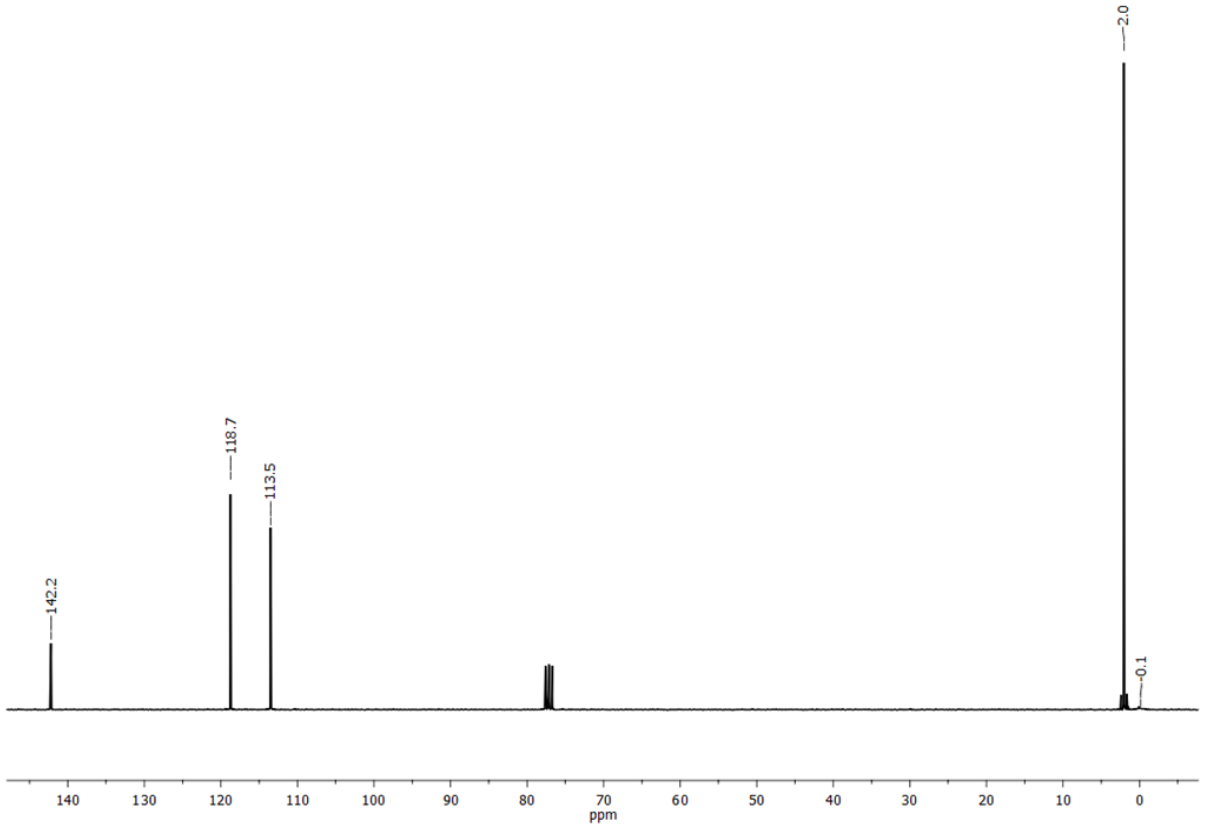

Figure S5.4.19. $^{13}C\{^{1}H\}$ NMR spectrum (76 MHz) of **6** in $CDCl_3$.

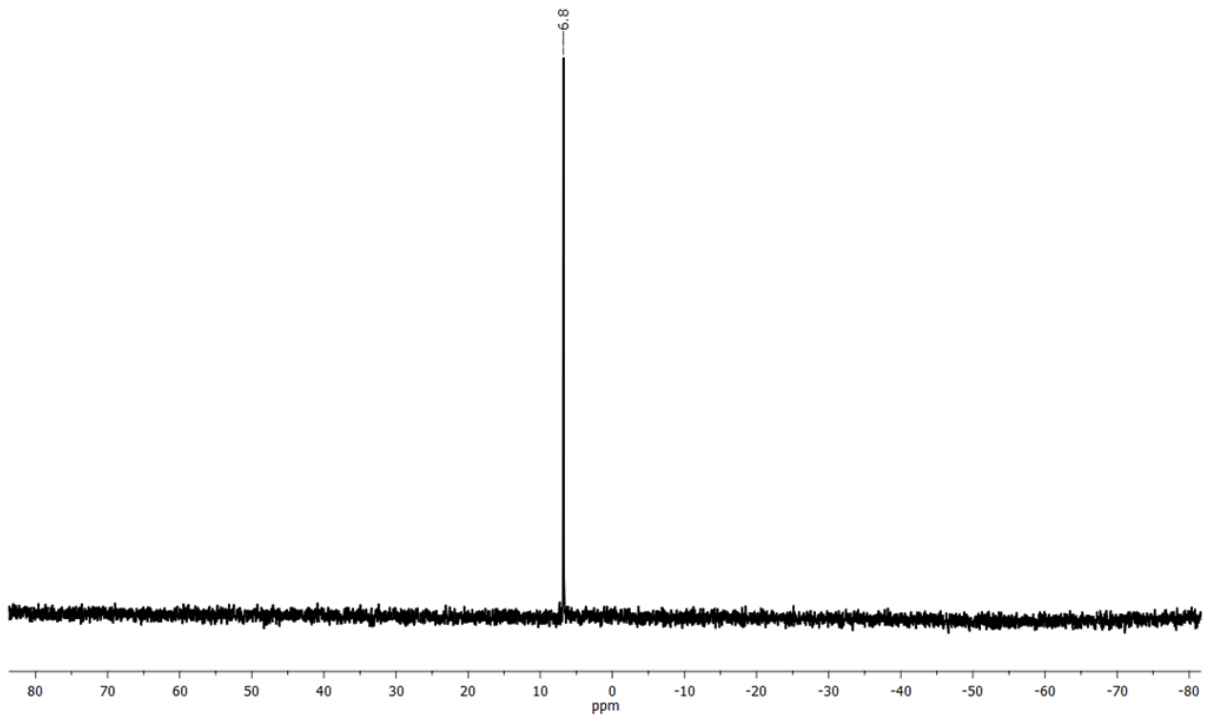

Figure S5.4.20. $^{29}Si\{^{1}H\}$ NMR spectrum (60 MHz) of **6** in $CDCl_3$.

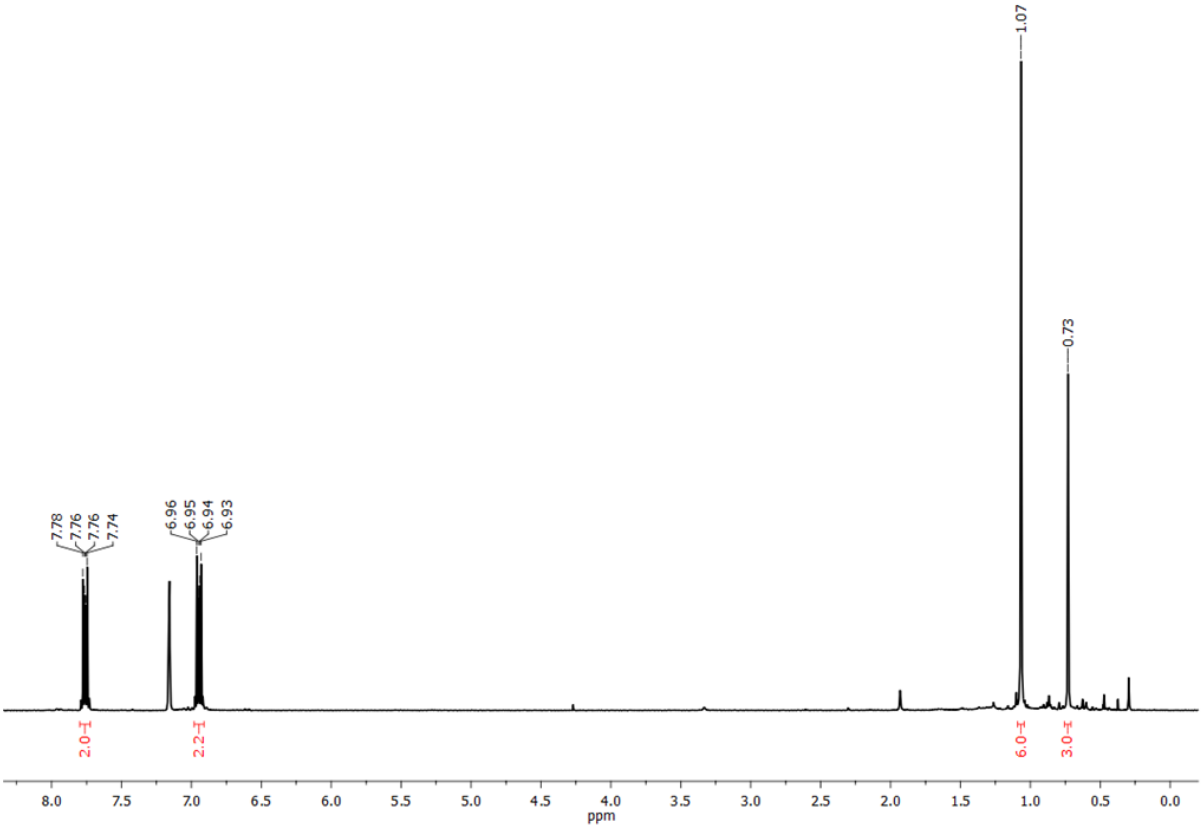

Figure S5.4.21. ^{1}H NMR spectrum (300 MHz) of **7** in C_6D_6.

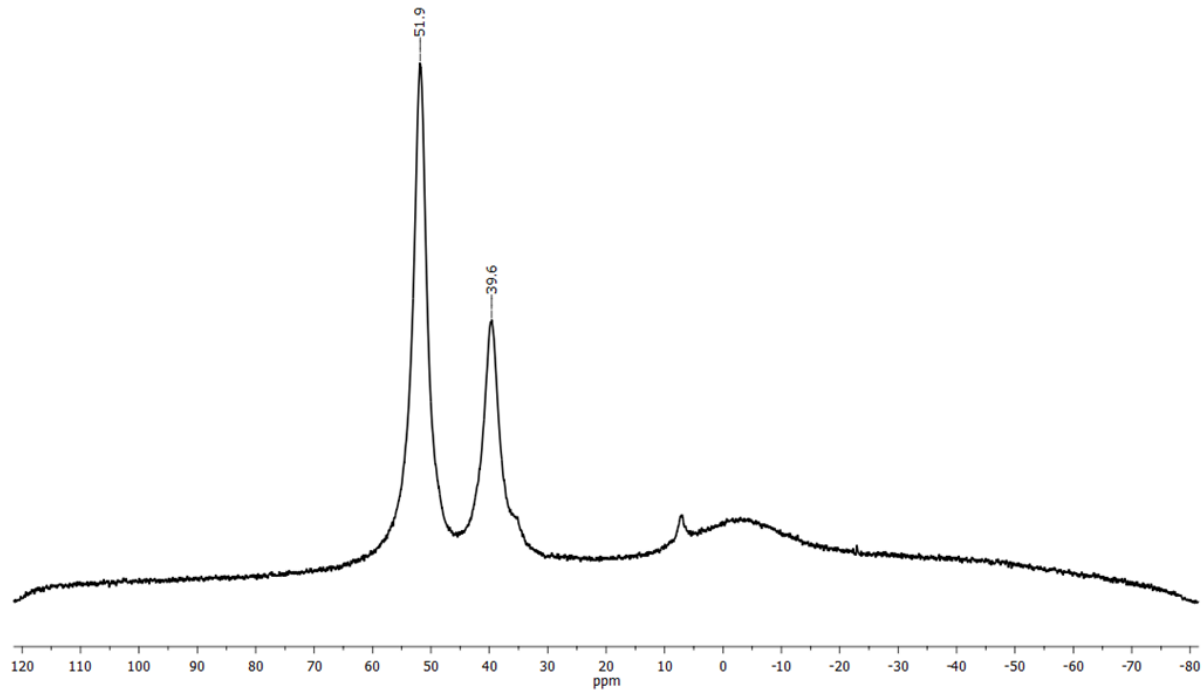

Figure S5.4.22. $^{11}B\{^{1}H\}$ NMR spectrum (96 MHz) of **7** in C_6D_6.

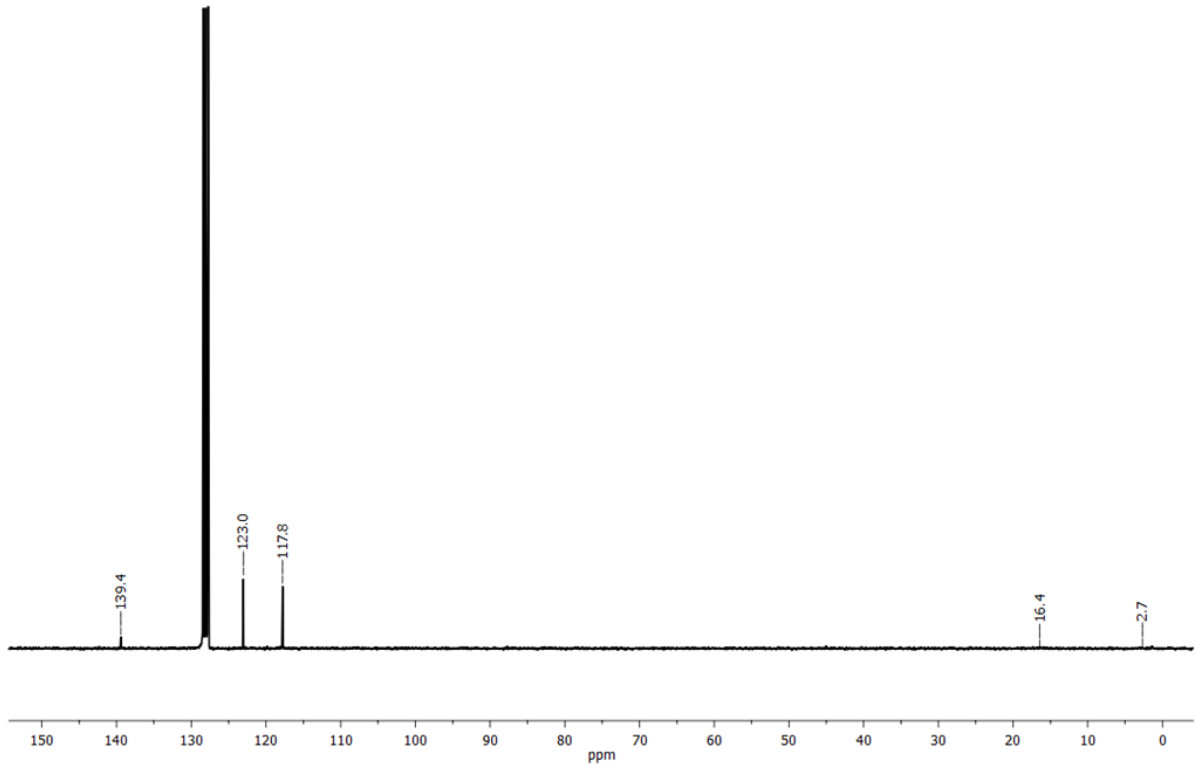

Figure S5.4.23. $^{13}C\{^{1}H\}$ NMR spectrum (76 MHz) of **7** in C_6D_6.

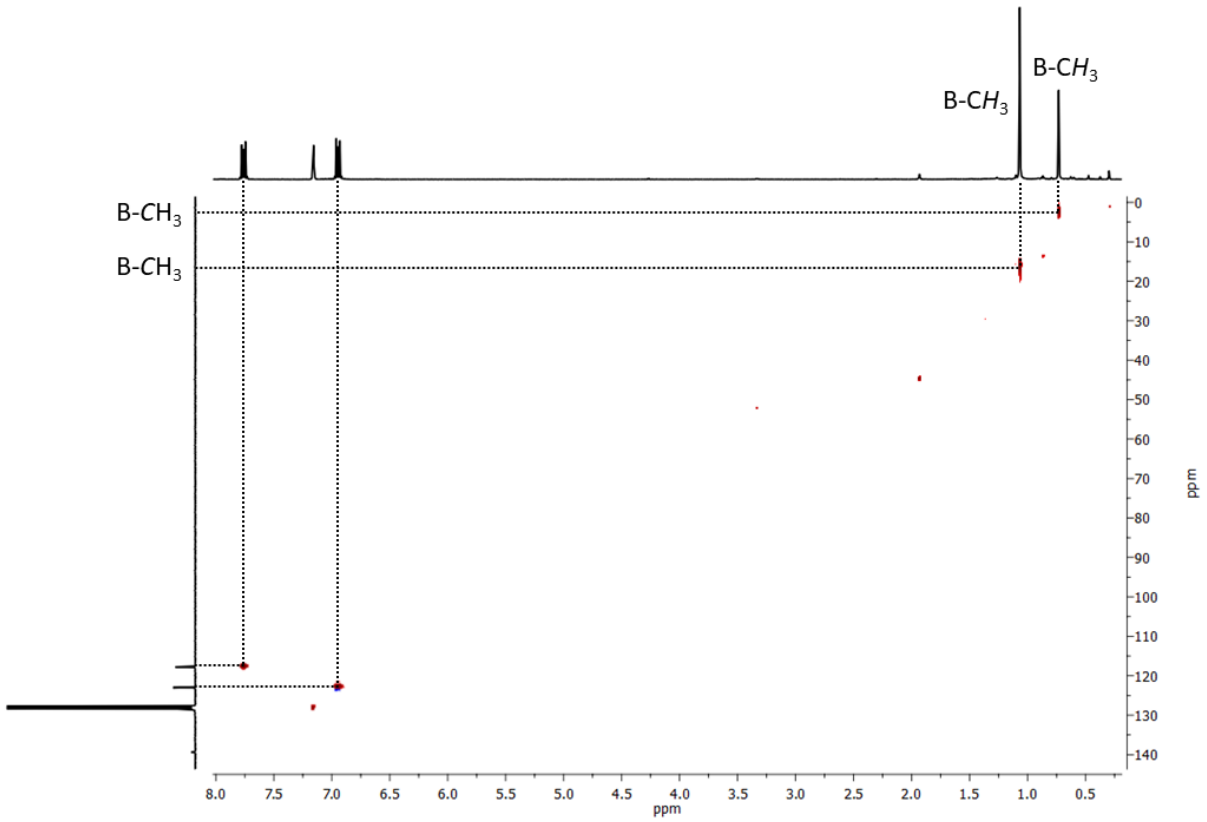

Figure S5.4.24. Detail of ^{1}H, ^{13}C HSQC spectrum of **7** in C_6D_6.

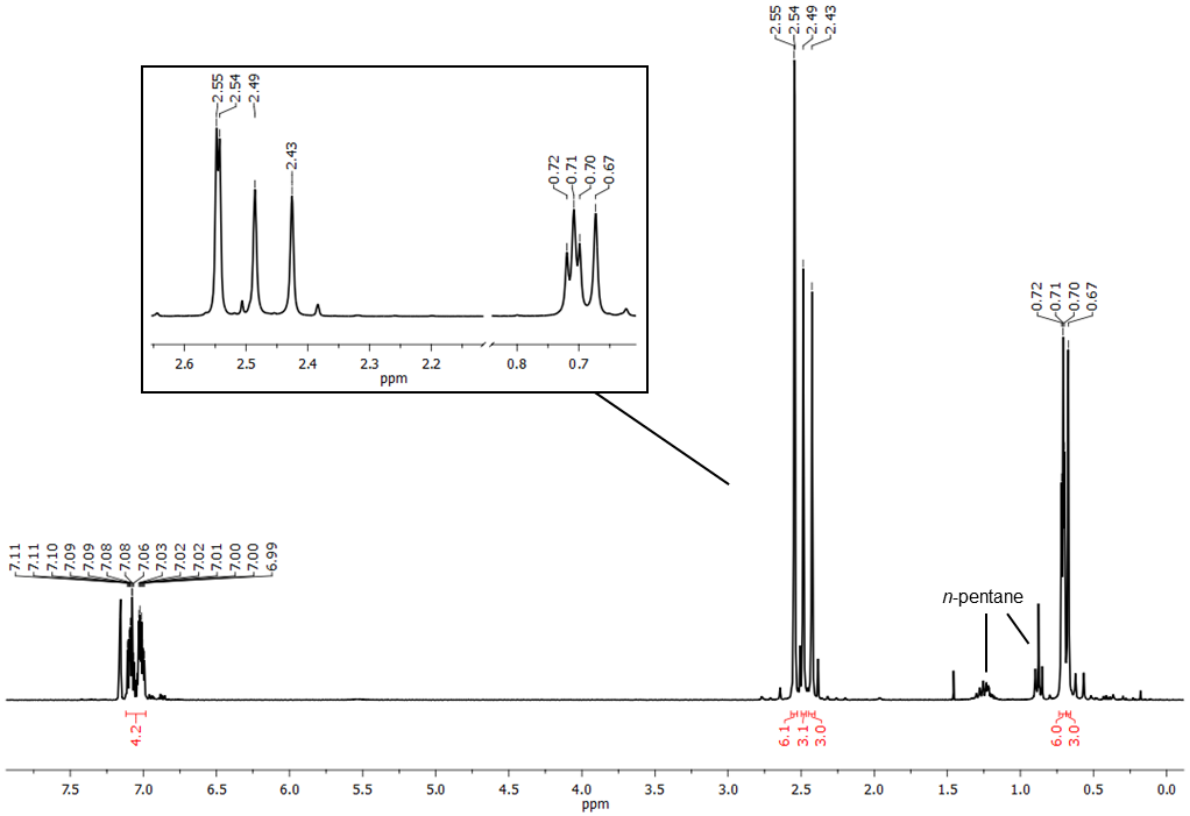

Figure S5.4.25. ^{1}H NMR spectrum (300 MHz) of **8** in C_6D_6.

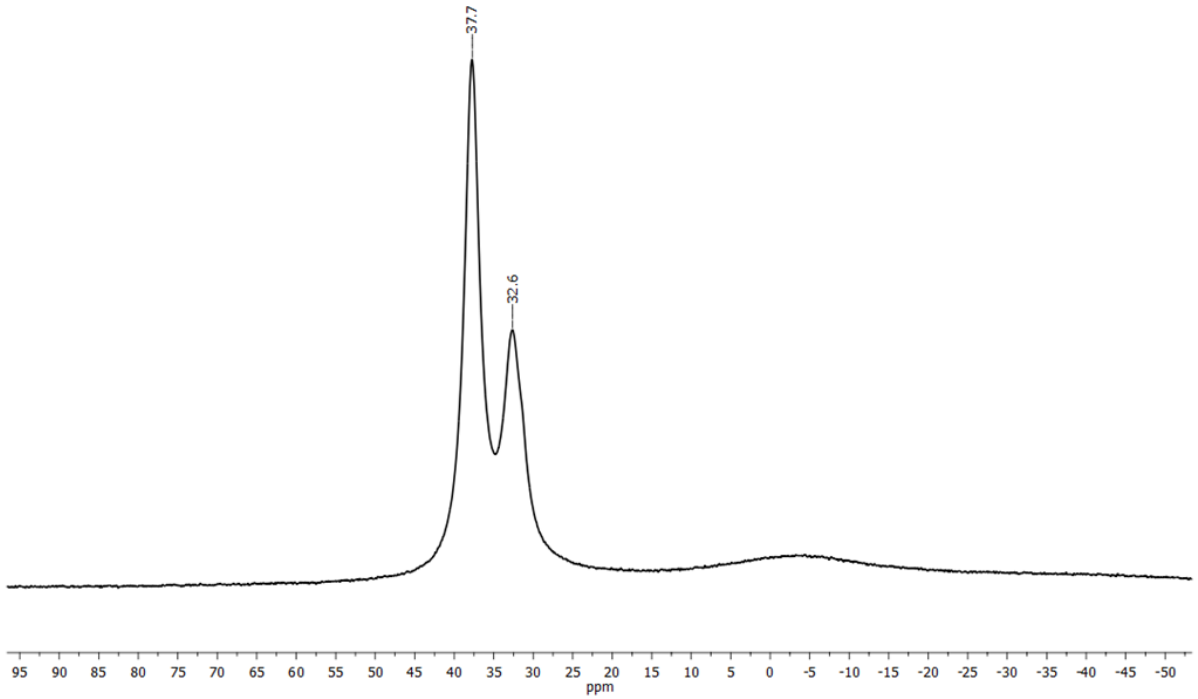

Figure S5.4.26. $^{11}B\{^{1}H\}$ NMR spectrum (96 MHz) of **8** in C_6D_6.

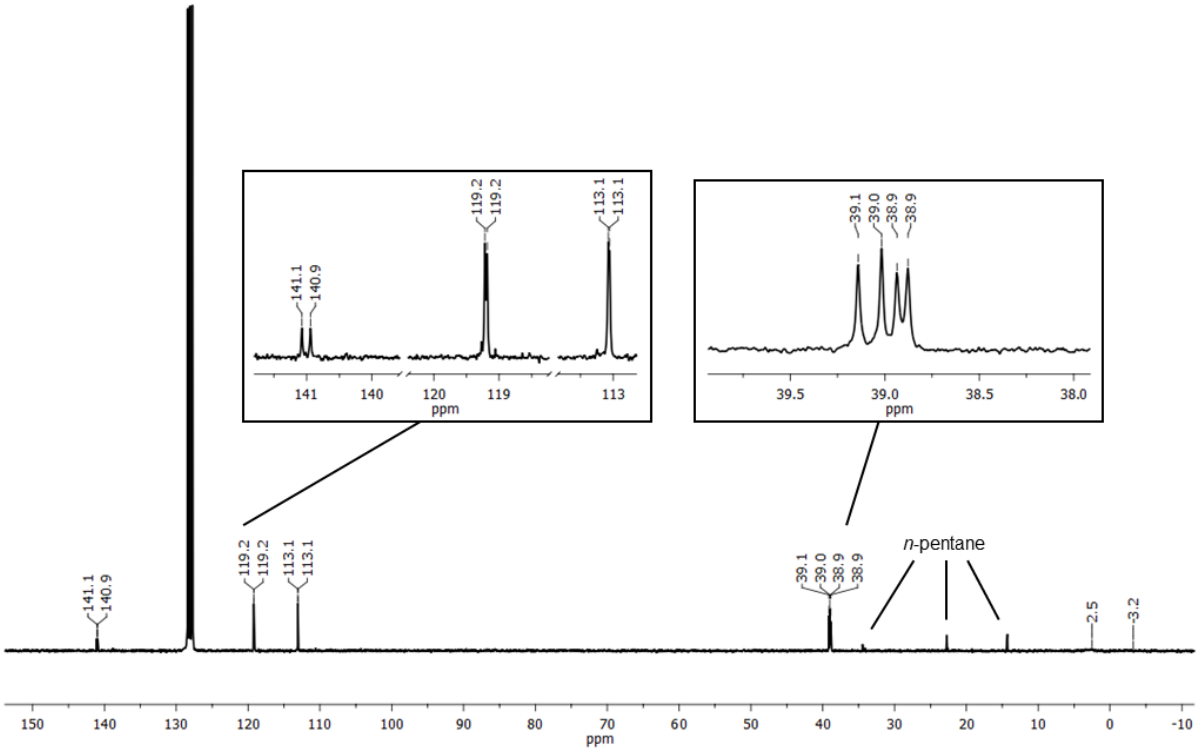

Figure S5.4.27. $^{13}C\{^{1}H\}$ NMR spectrum (76 MHz) of **8** in C_6D_6.

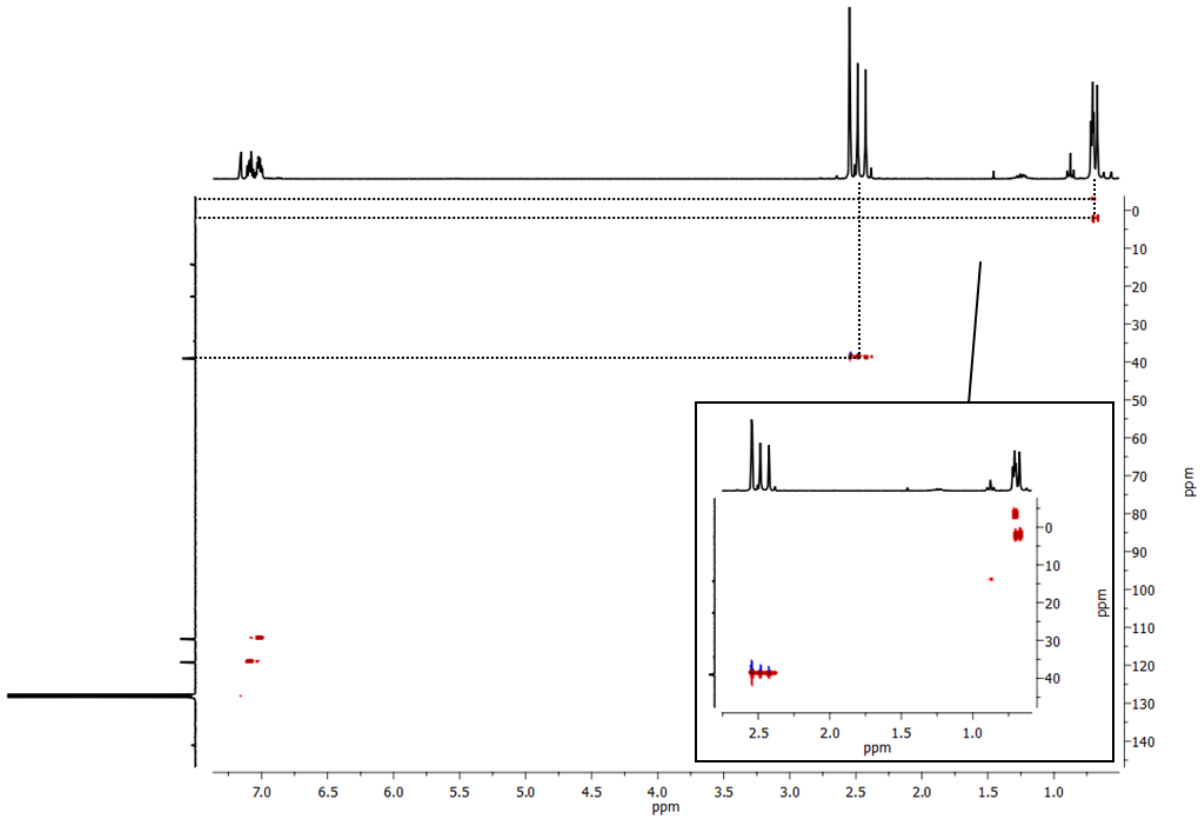

Figure S5.4.28. Detail of ^{1}H, ^{13}C HSQC spectrum of **8** in C_6D_6.

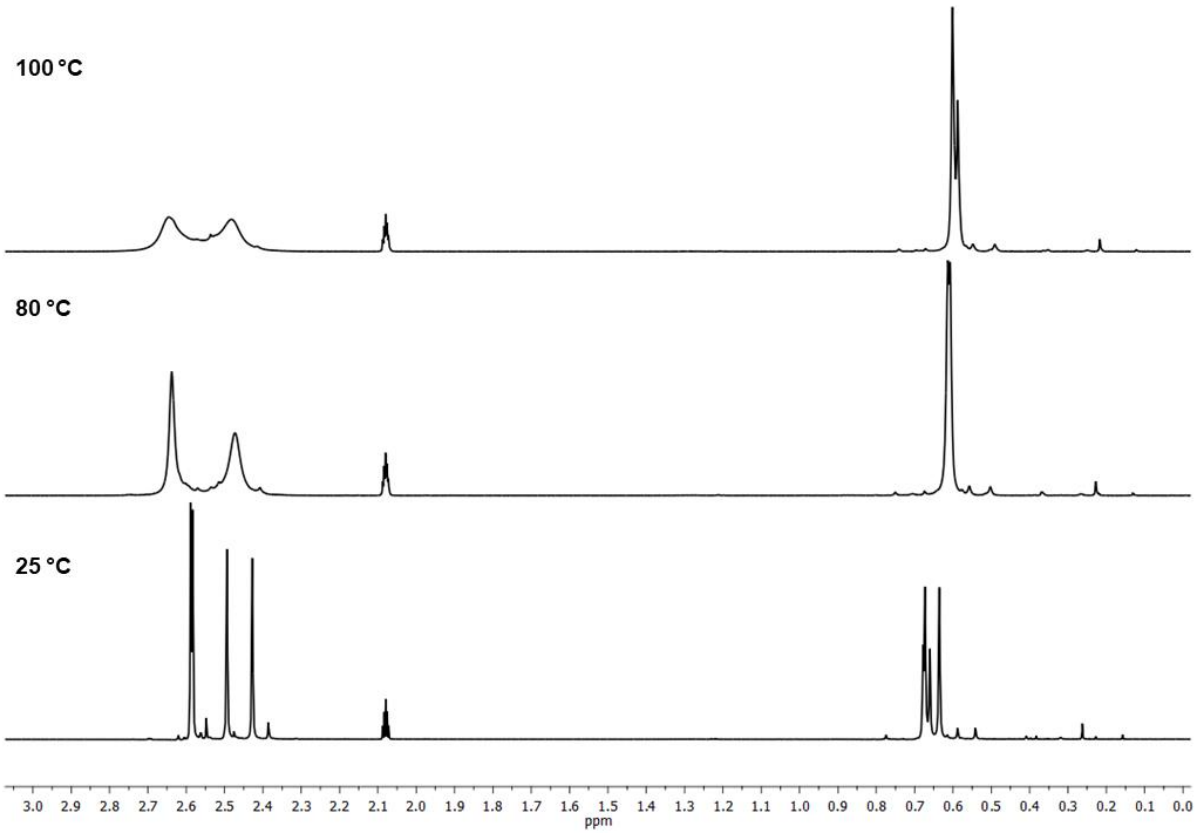

Figure S5.4.29. Isomerization attempt of **8** from 25 to 100 °C in toluene-d_8.

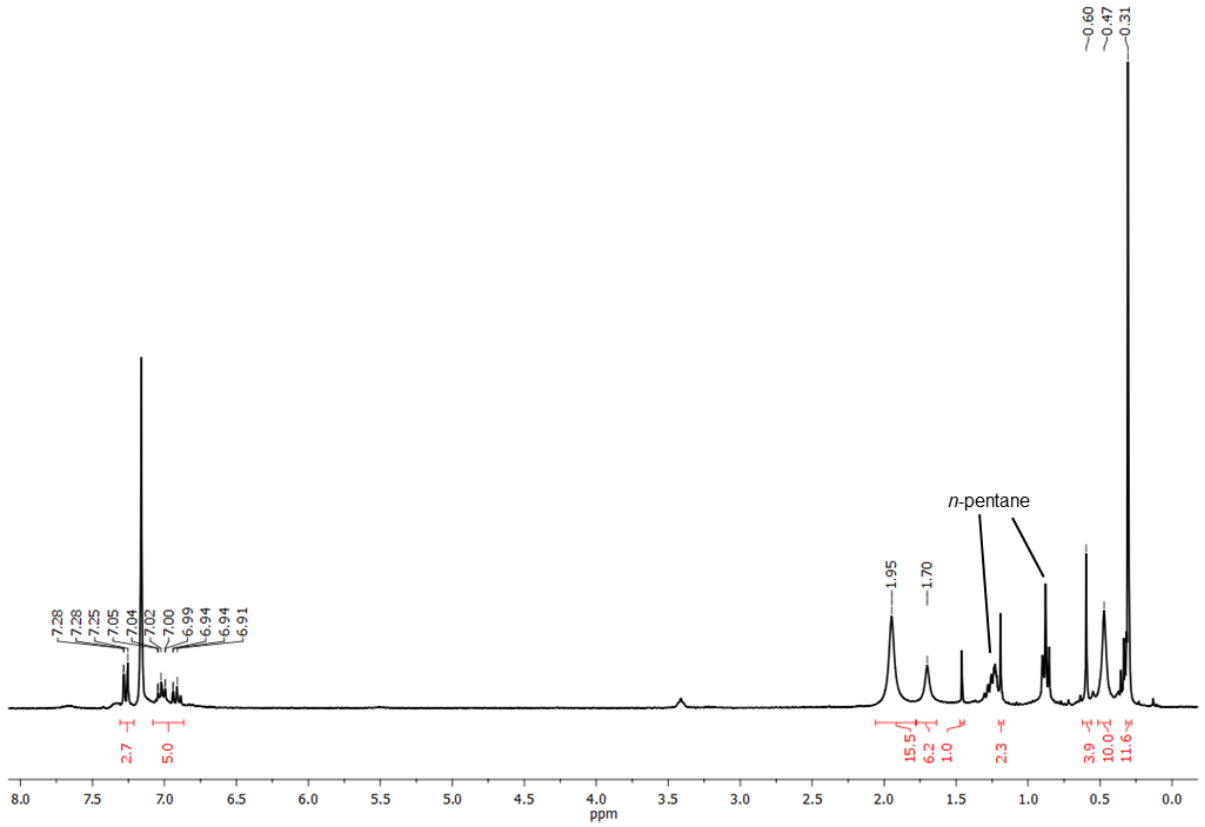

Figure S5.4.30. ^{1}H NMR spectrum (300 MHz) of the synthesis attempt of **9** in C_6D_6.

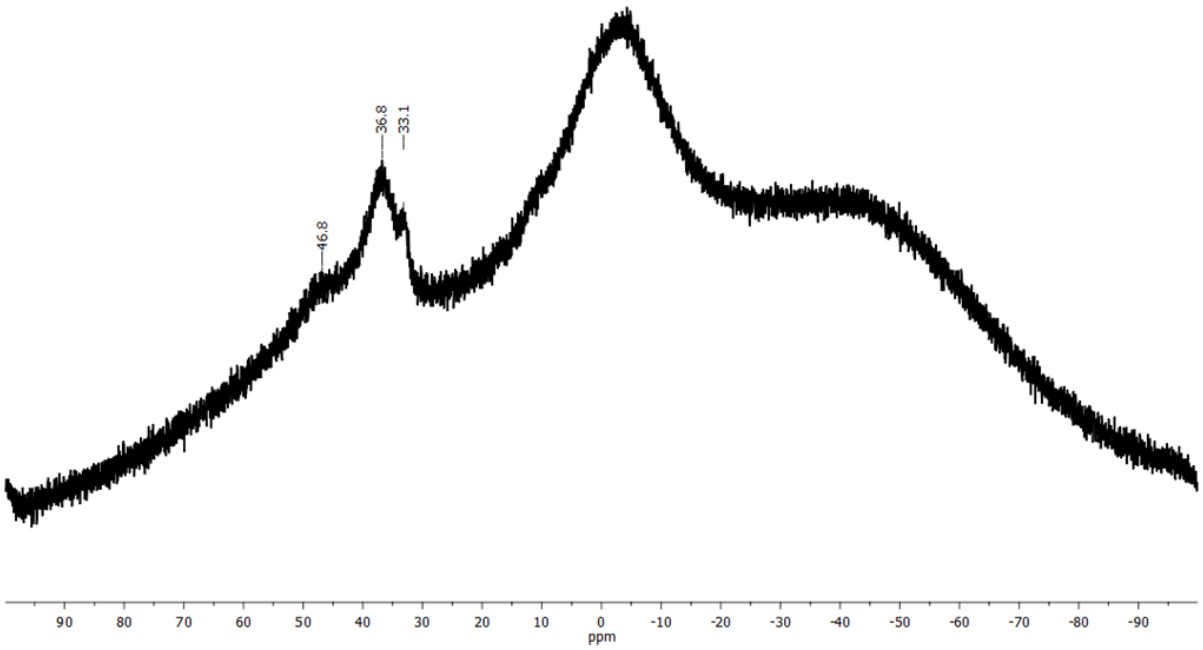

Figure S5.4.31. $^{11}B\{^{1}H\}$ NMR spectrum (96 MHz) of the synthesis attempt of **9** in C_6D_6.

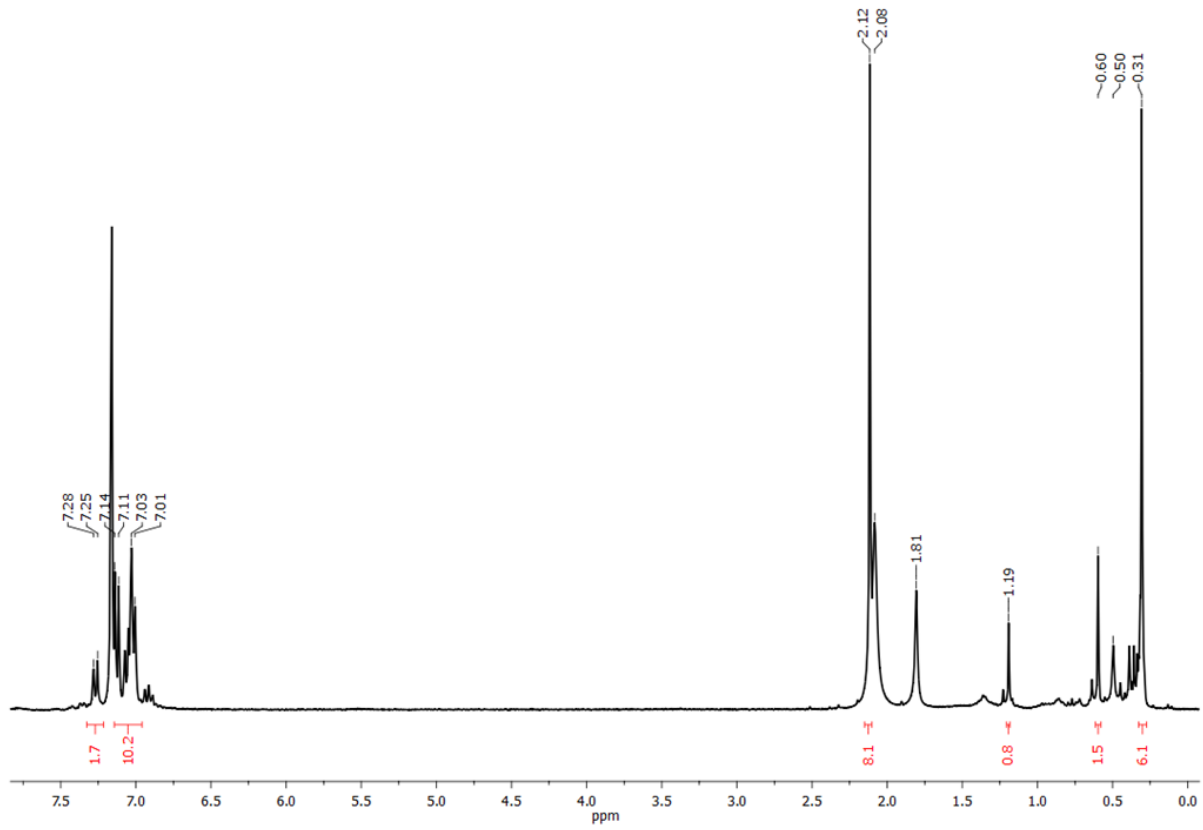

Figure S5.4.32. ^{1}H NMR spectrum (300 MHz) of the synthesis attempt of **10** in C_6D_6.

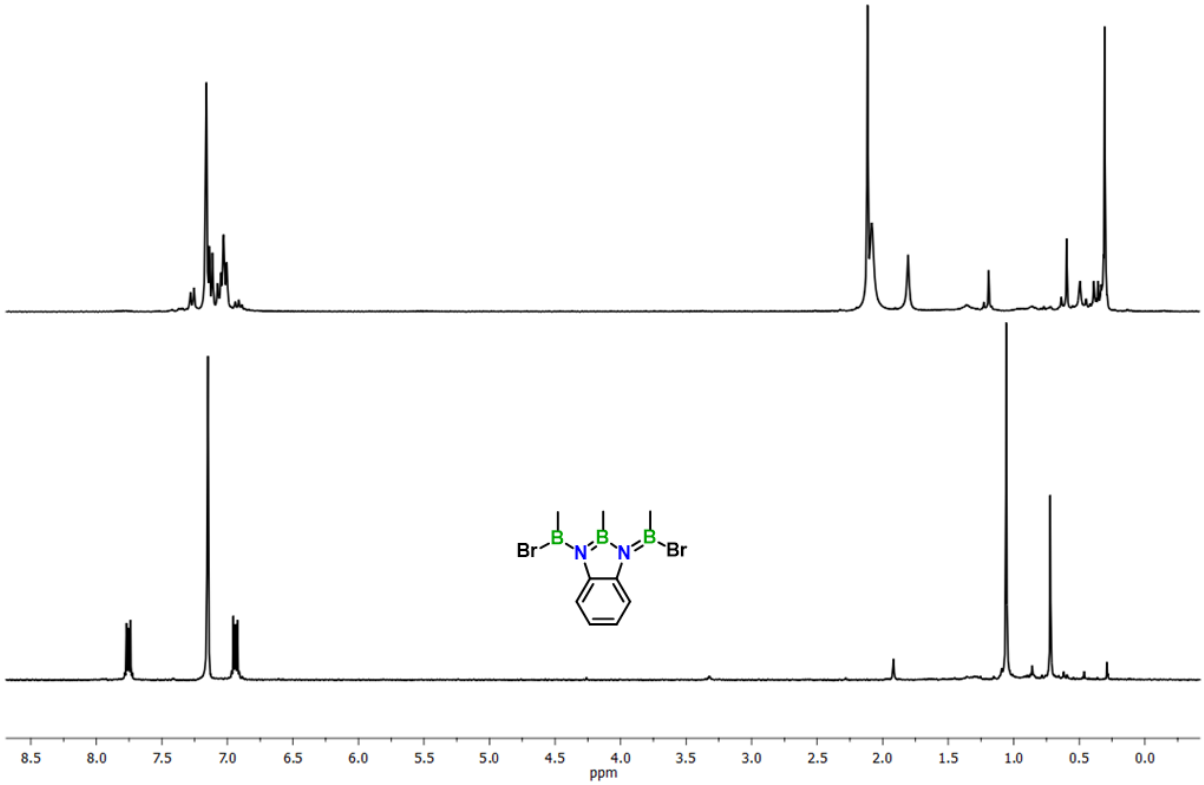

Figure S5.4.33. Comparison of the ^{1}H NMR spectra of the synthesis attempt of **10** (top) and **7** (bottom) in C_6D_6.

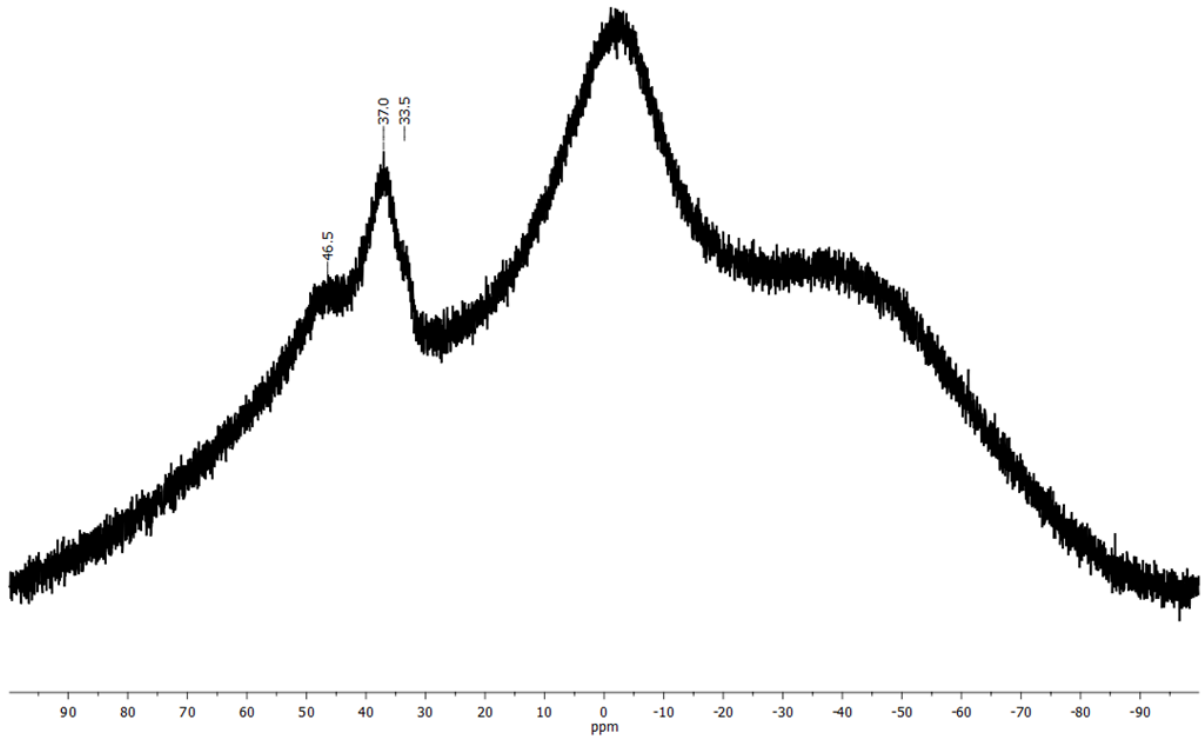

Figure S5.4.34. $^{11}B\{^{1}H\}$ NMR spectrum (96 MHz) of the synthesis attempt of **10** in C_6D_6.

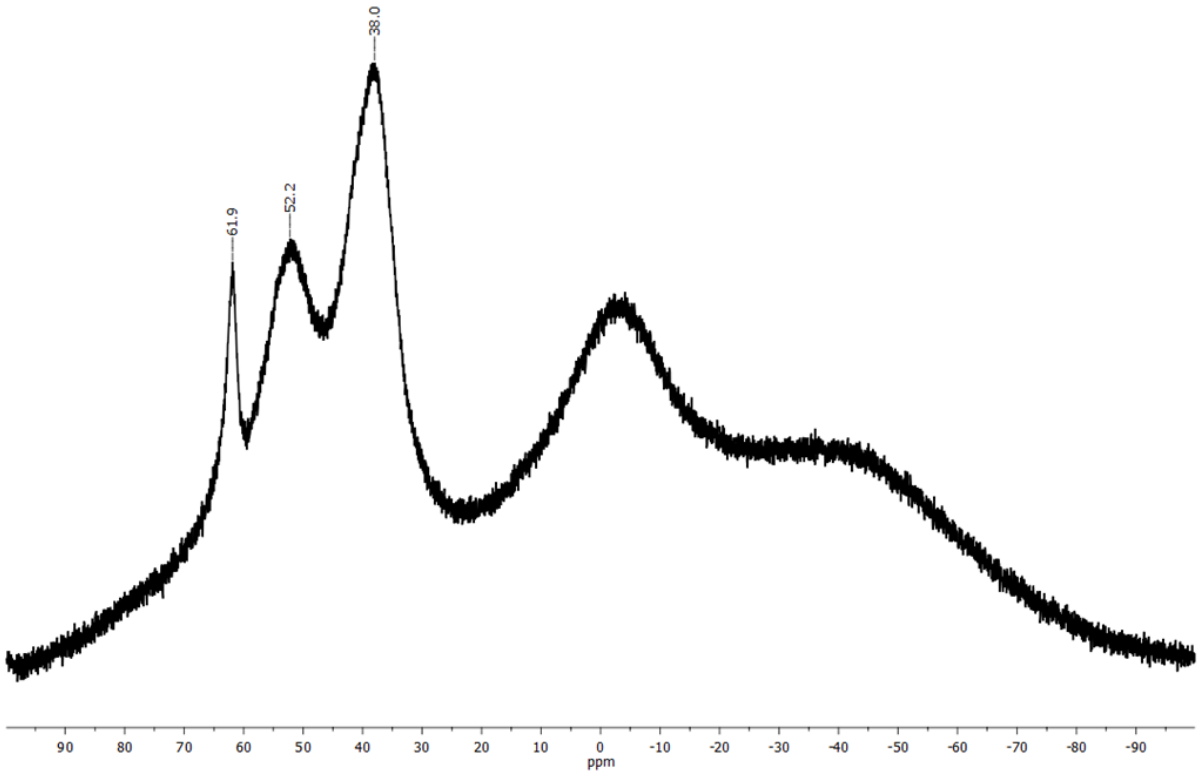

Figure S5.4.35. $^{11}B\{^{1}H\}$ NMR spectrum (96 MHz) of the polymerization attempt to **11** (in DCM) in $CDCl_3$.

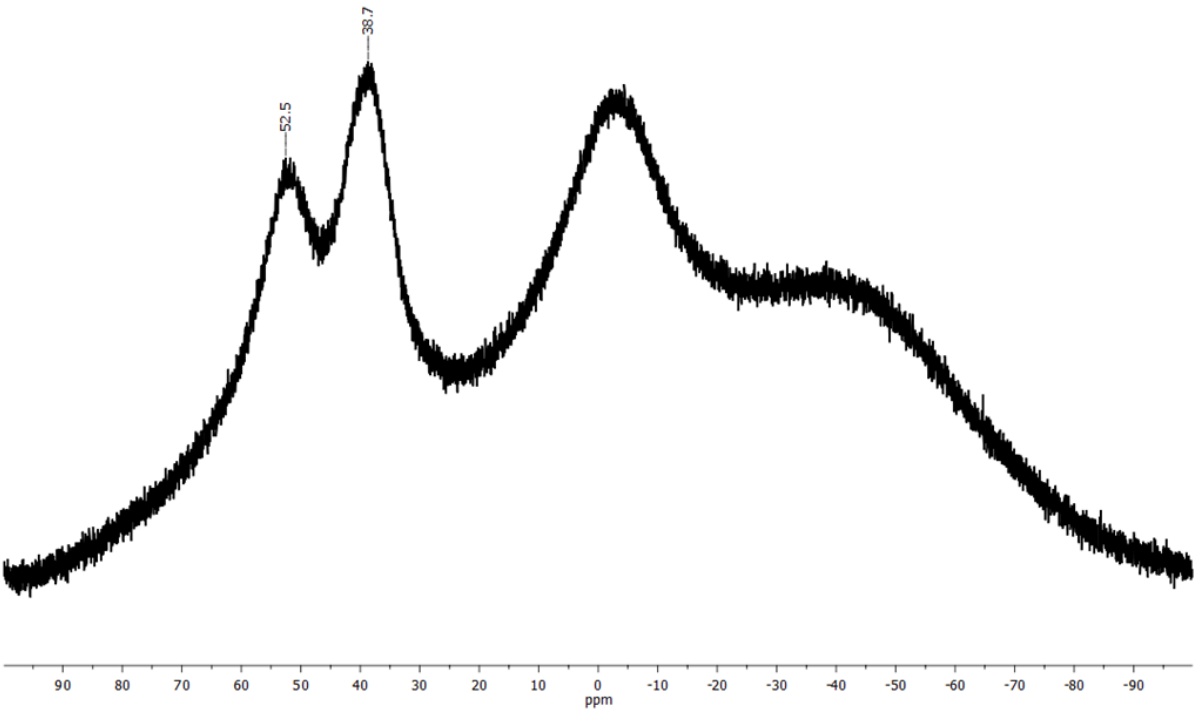

Figure S5.4.36. $^{11}B\{^{1}H\}$ NMR spectrum (96 MHz) of the polymerization attempt to **11** (in *o*-DFB) in $CDCl_3$.

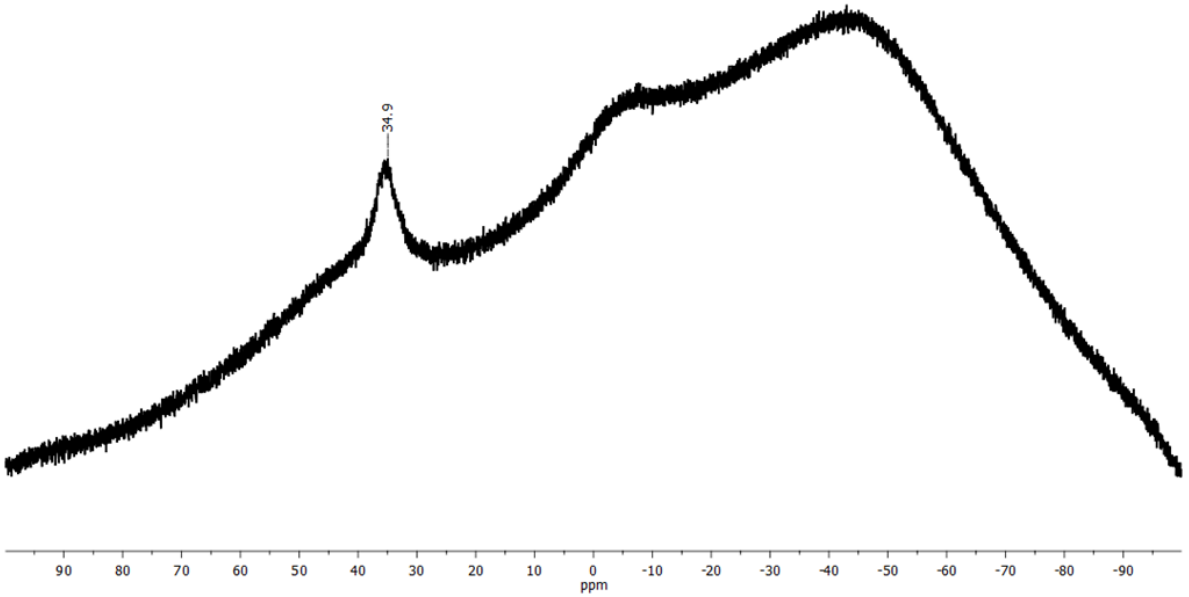

Figure S5.4.37. $^{11}B\{^{1}H\}$ NMR spectrum (96 MHz) of the polymerization attempt to **13** (in DCM) in $CDCl_3$.

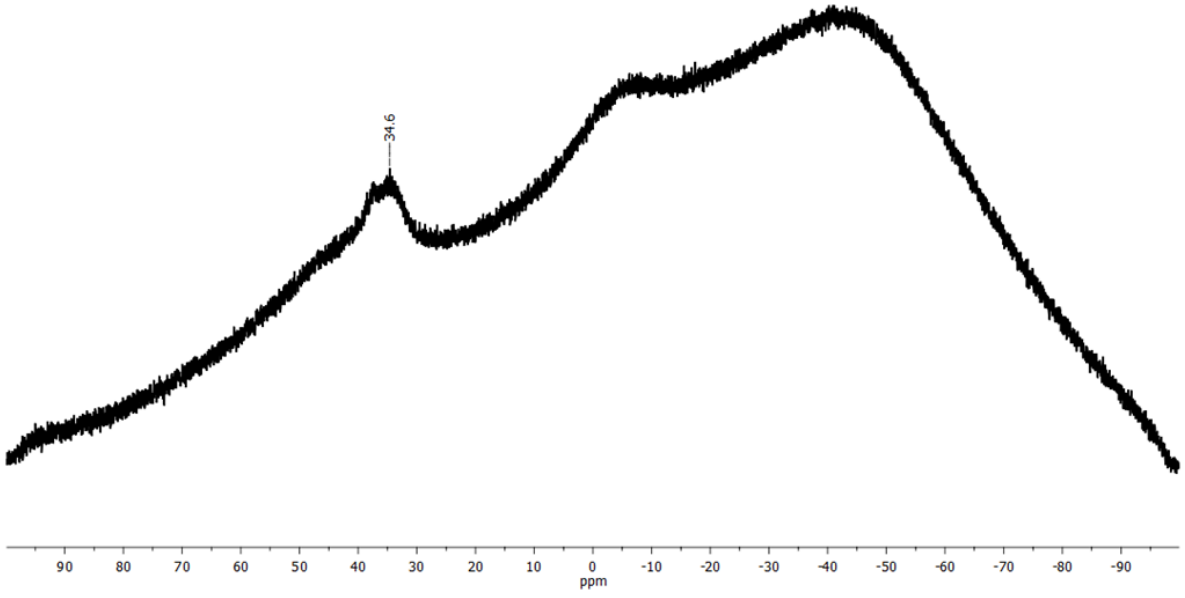

Figure S5.4.38. $^{11}B\{^{1}H\}$ NMR spectrum (96 MHz) of the polymerization attempt to **13** (in *o*-DFB) in $CDCl_3$.

HRMS spectra

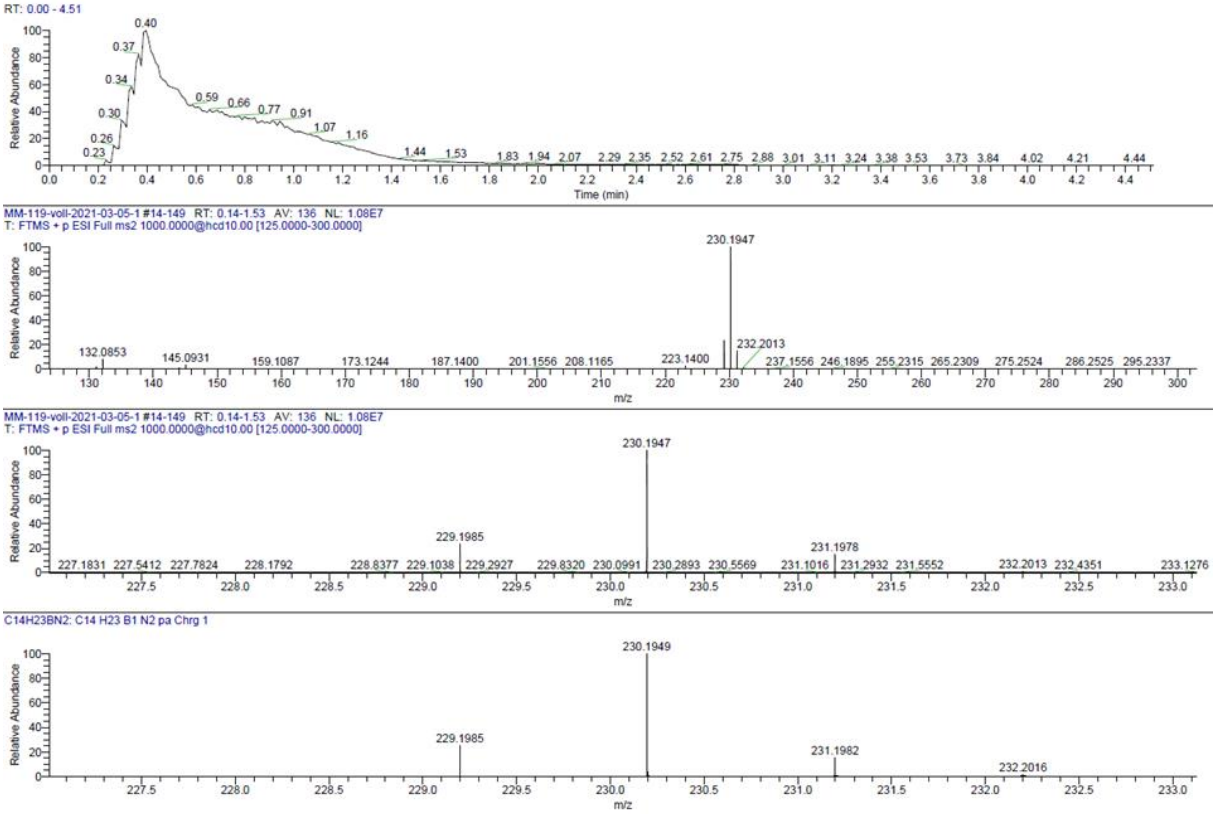

Figure S5.4.39. HRMS spectrum (LIFDI) of **2**.

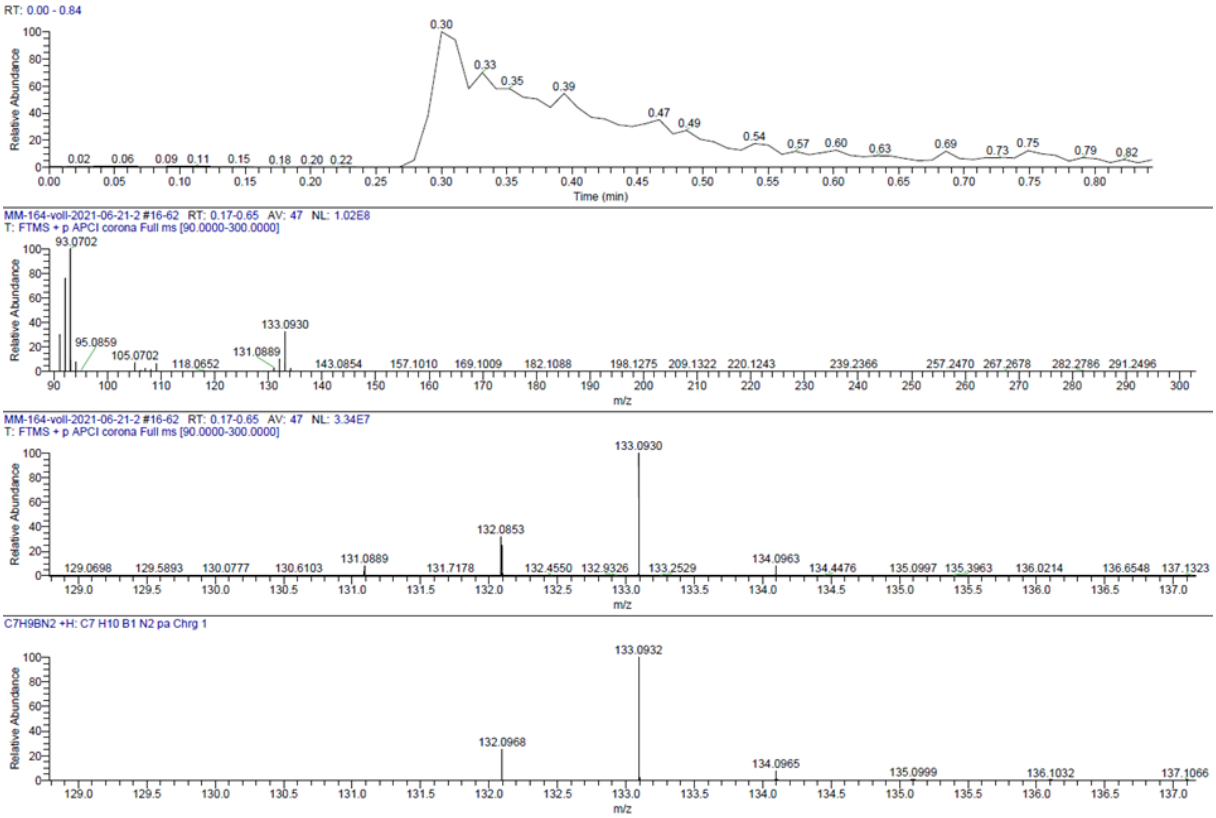

Figure S5.4.40. HRMS spectrum (ASAP pos) of **3**.

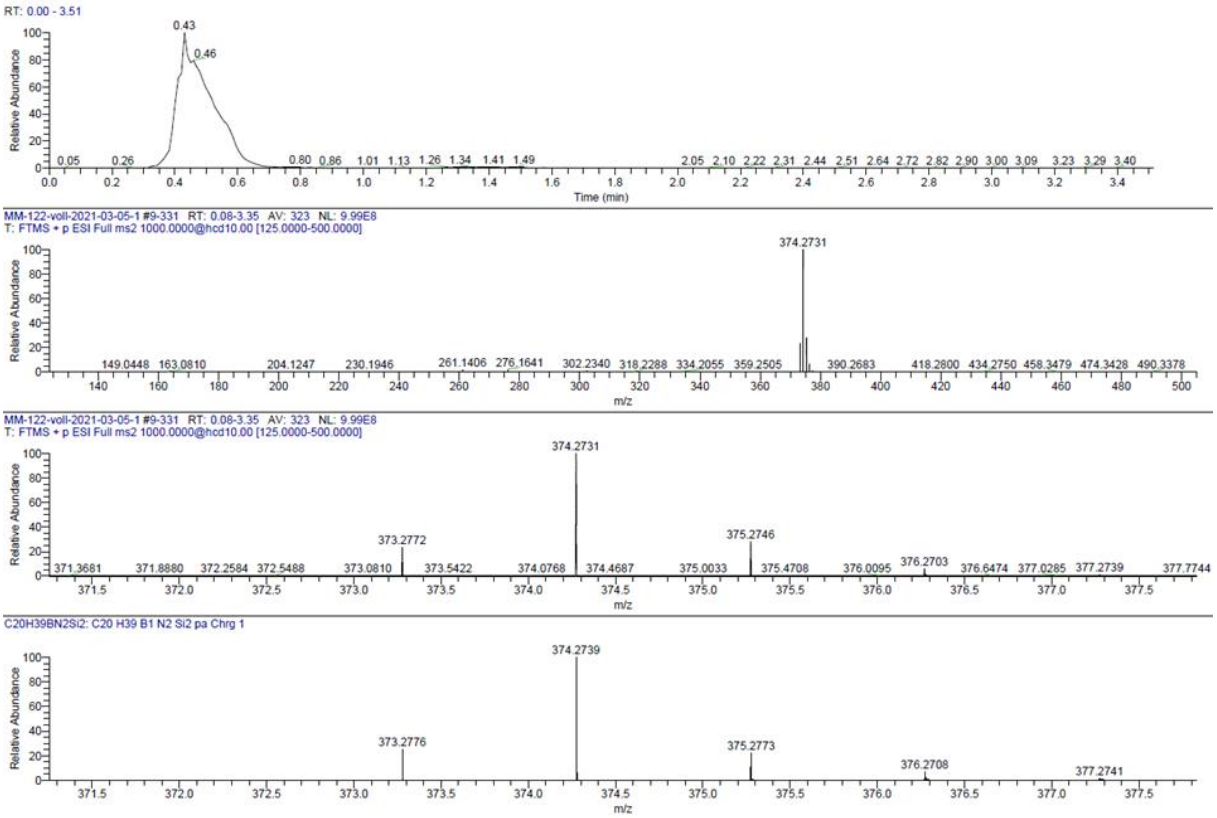

Figure S5.4.41. HRMS spectrum (LIFDI) of **4**.

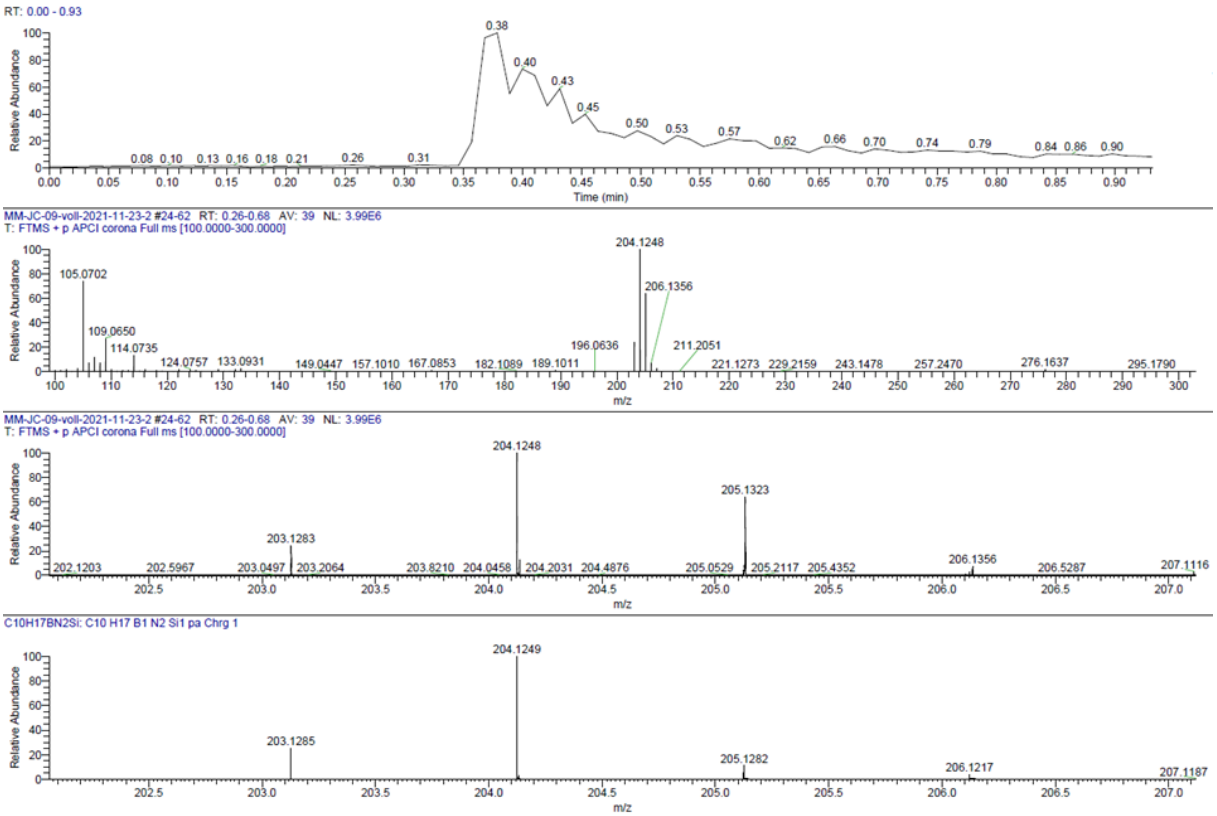

Figure S5.4.42. HRMS spectrum (ASAP pos) of **5**.

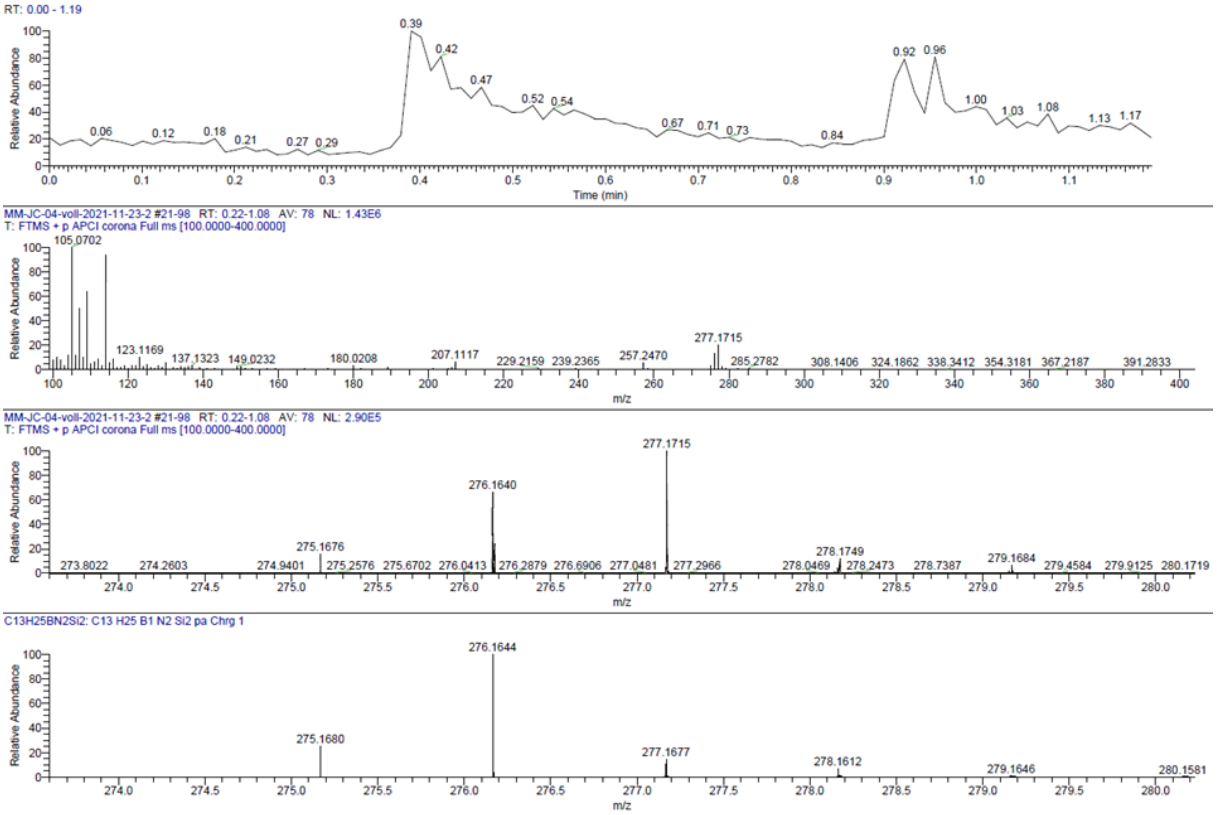

Figure S5.4.43. HRMS spectrum (ASAP pos) of **6**.

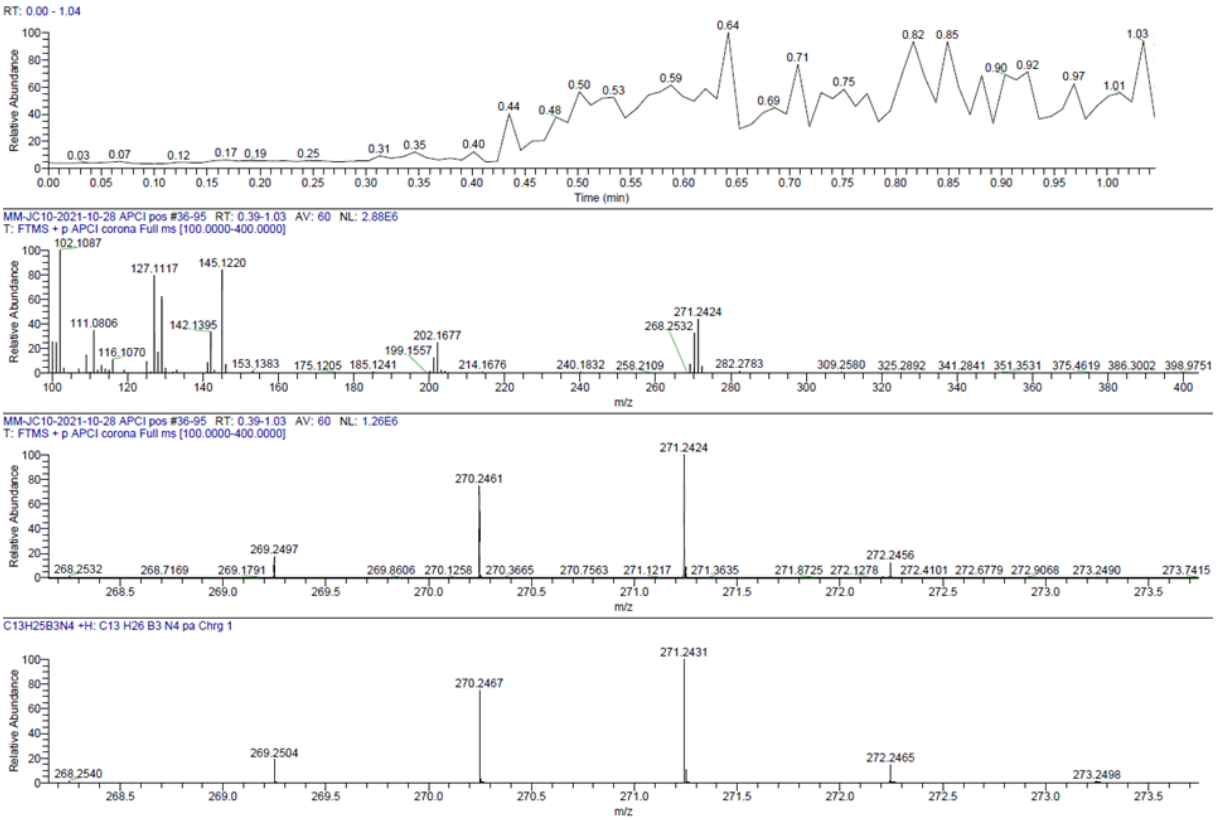

Figure S5.4.44. HRMS spectrum (APCI pos) of **8**.

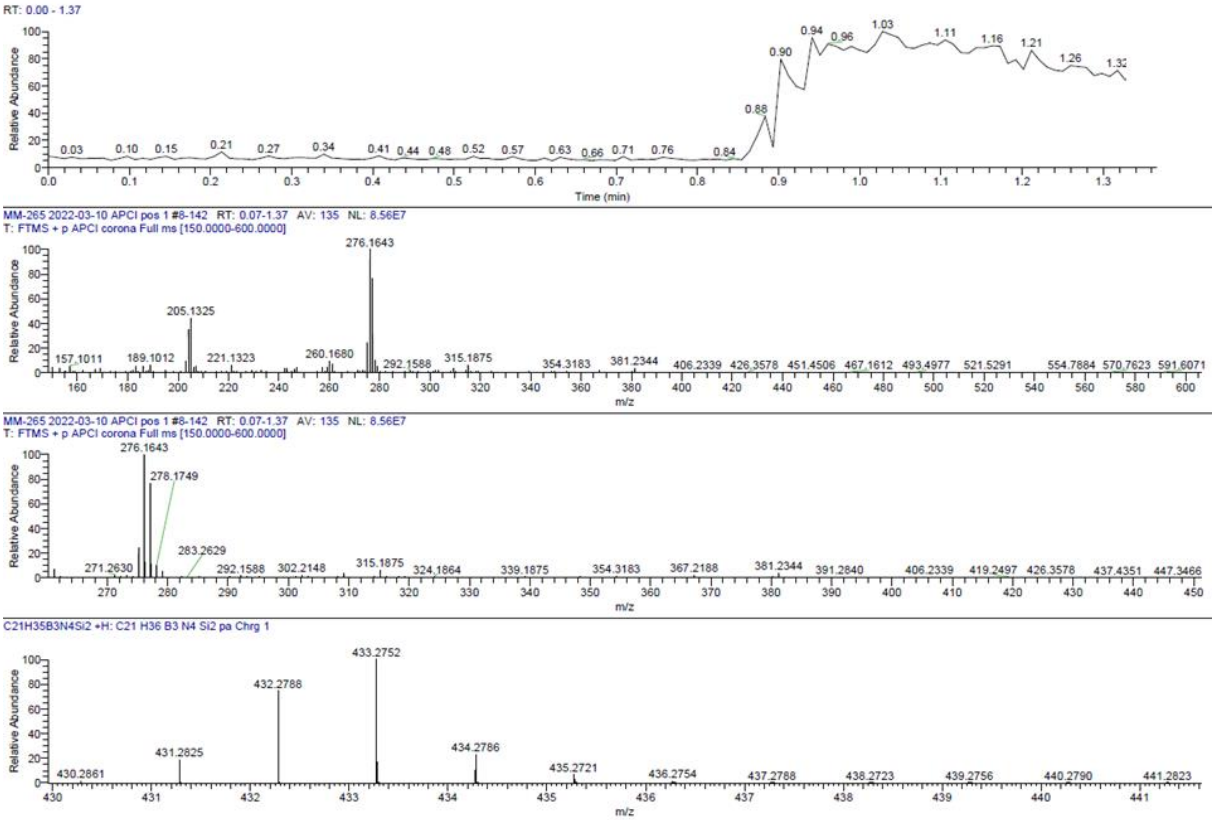

Figure S5.4.45. HRMS spectrum (APCI pos) of the synthesis attempt of **9** (calc. of **9** bottom).

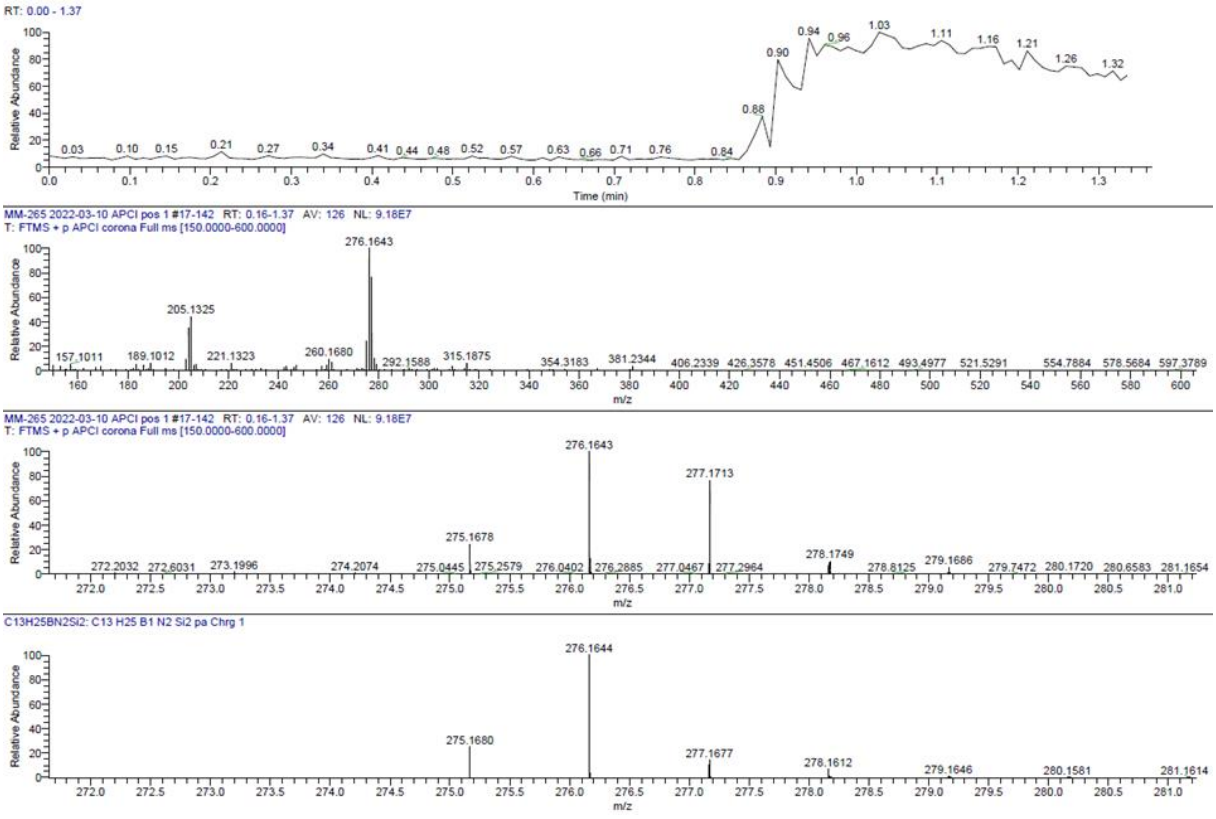

Figure S5.4.46. HRMS spectrum (APCI pos) of the synthesis attempt of **9** (calc. of **6** bottom).

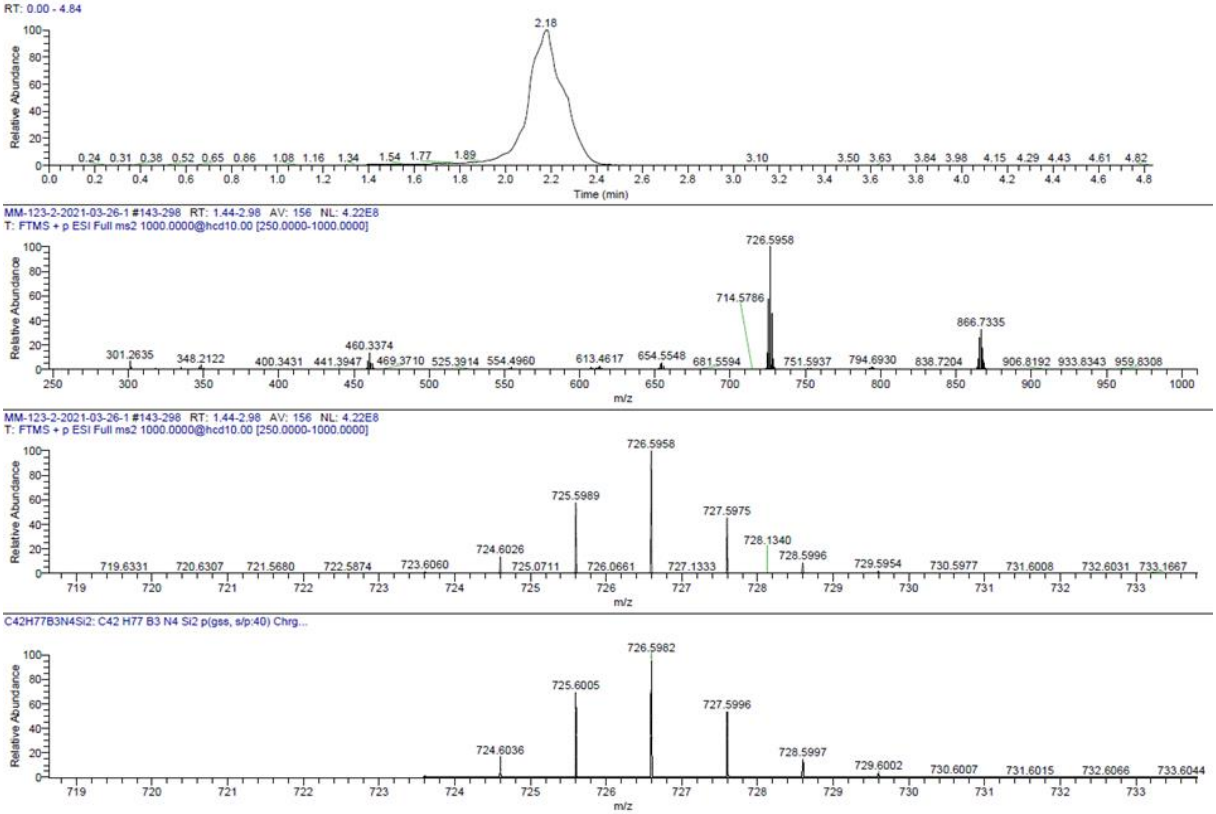

Figure S5.4.47. HRMS spectrum (LIFDI) of the synthesis attempt of **11a**.

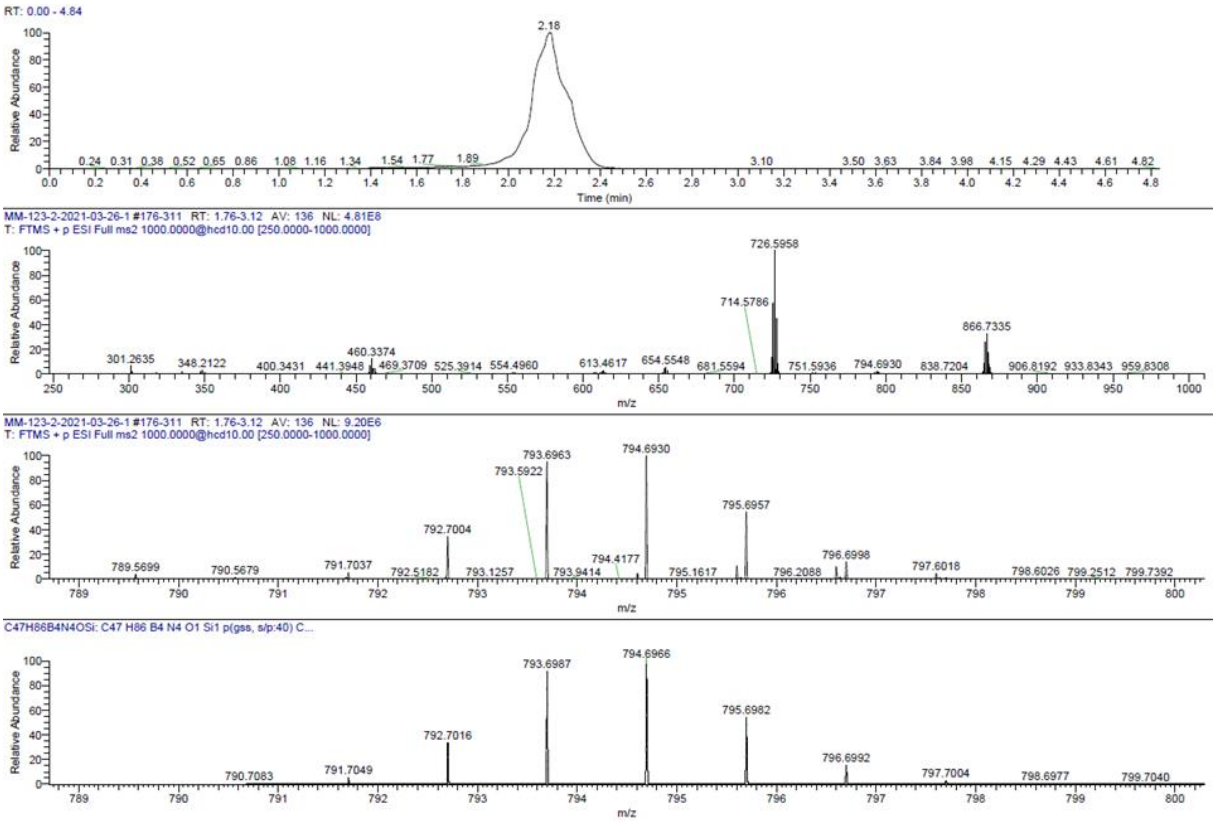

Figure S5.4.48. HRMS spectrum (LIFDI) of the synthesis attempt of **11b**.

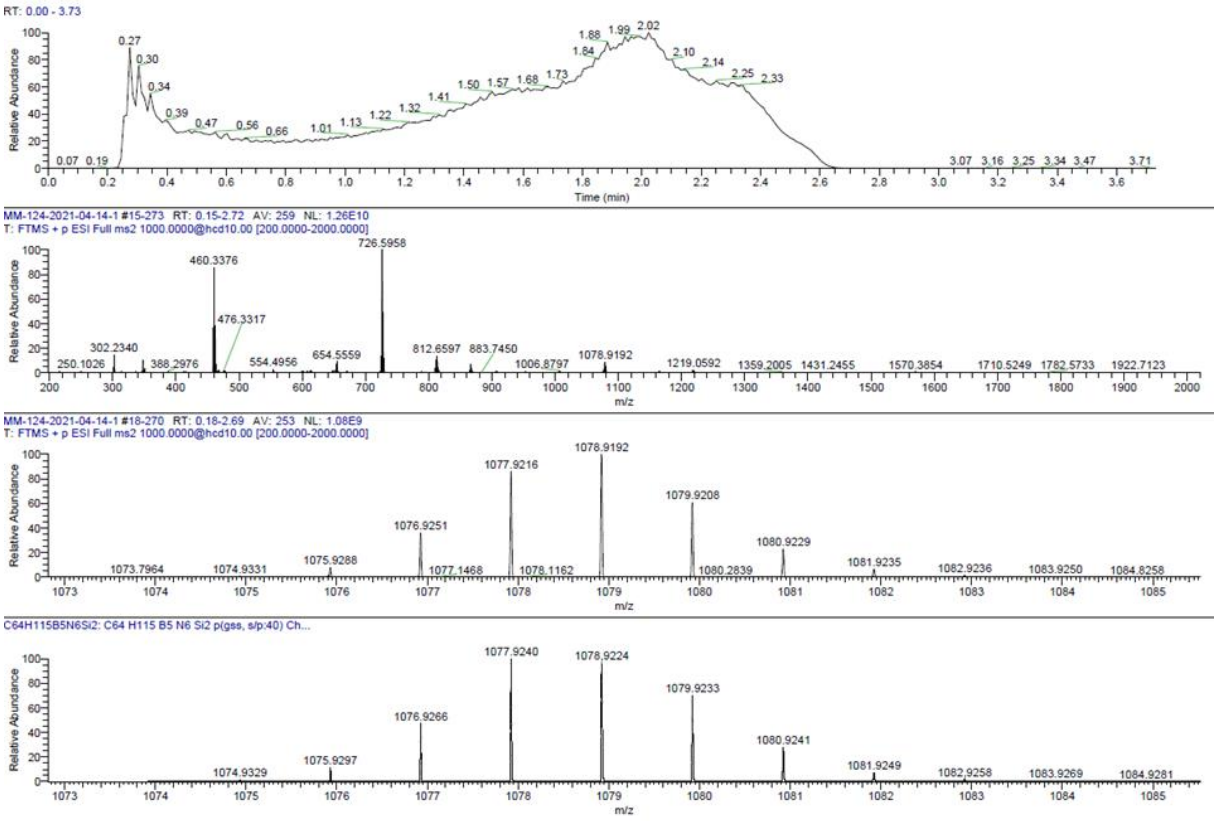

Figure S5.4.49. HRMS spectrum (LIFDI) of the synthesis attempt of **11c**.

GPC traces

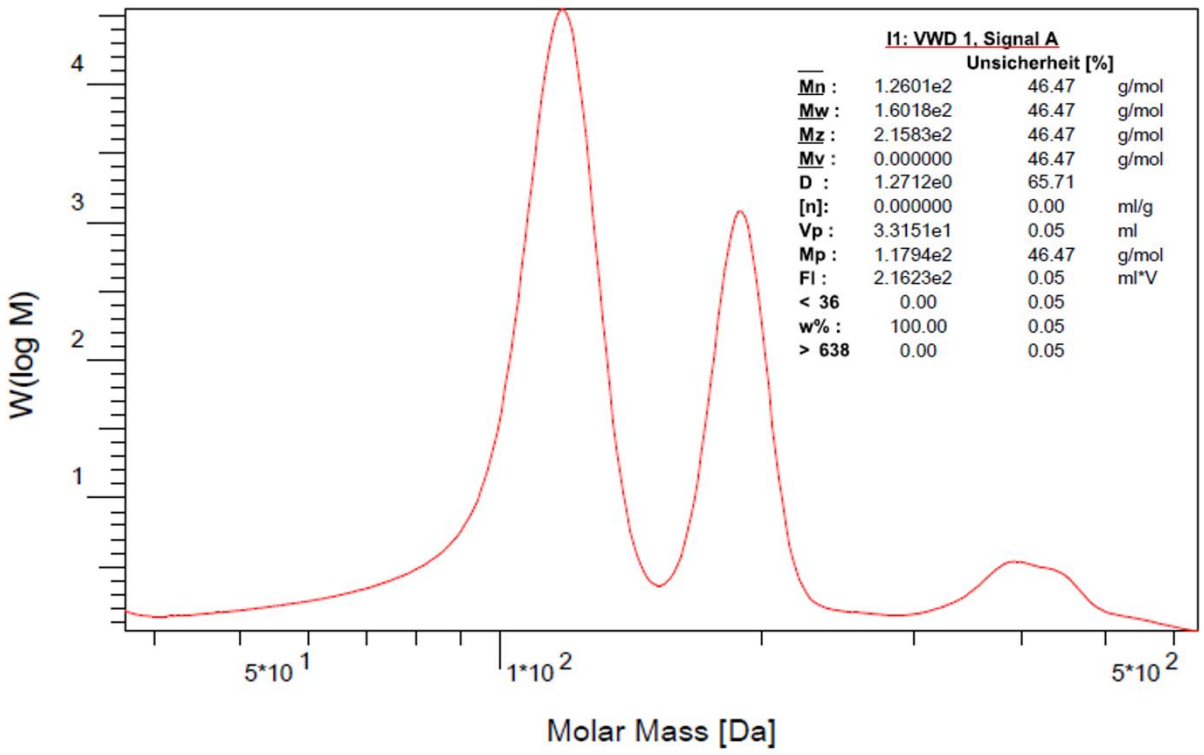

Figure S5.4.50. Original GPC data of **12** (in THF, vs polystyrene standard).

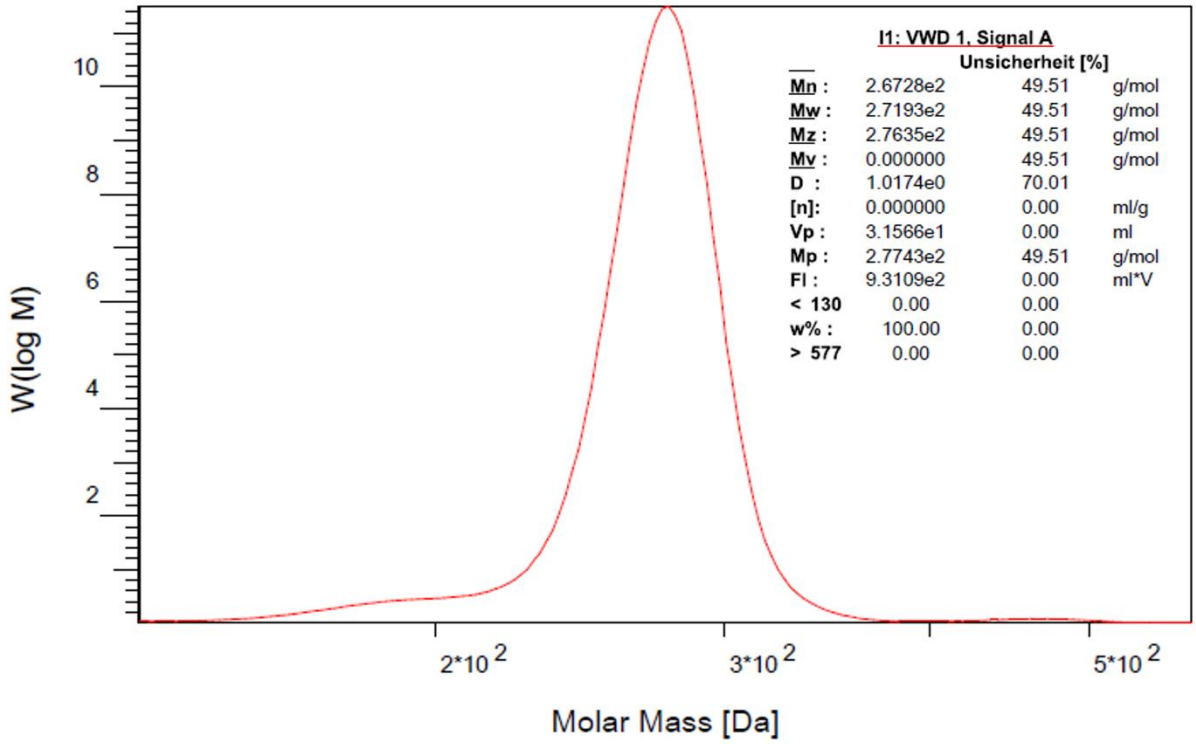

Figure S5.4.51. Original GPC data of **13** (reaction in DCM) (in THF, vs polystyrene standard).

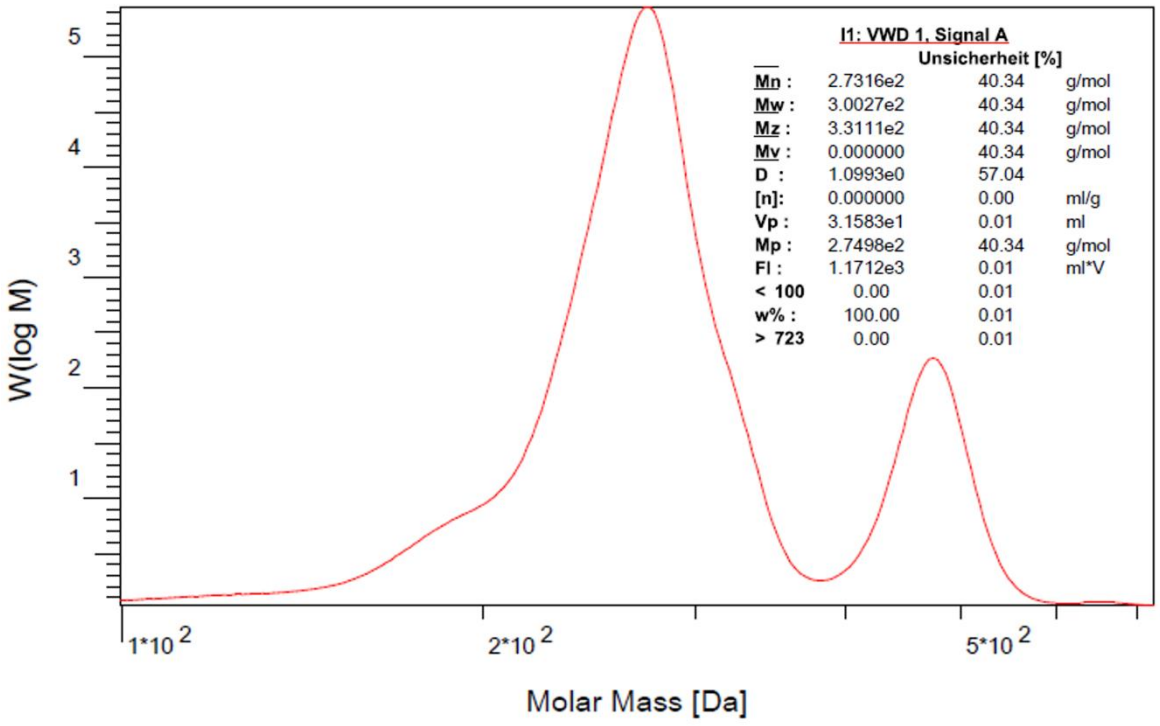

Figure S5.4.52. Original GPC data of **13** (reaction in *o*-DFB) (in THF, vs polystyrene standard).

5.5 1,2,5-Azadiborolane as a Building Block for Inorganic–Organic Hybrid Polymers

NMR spectra

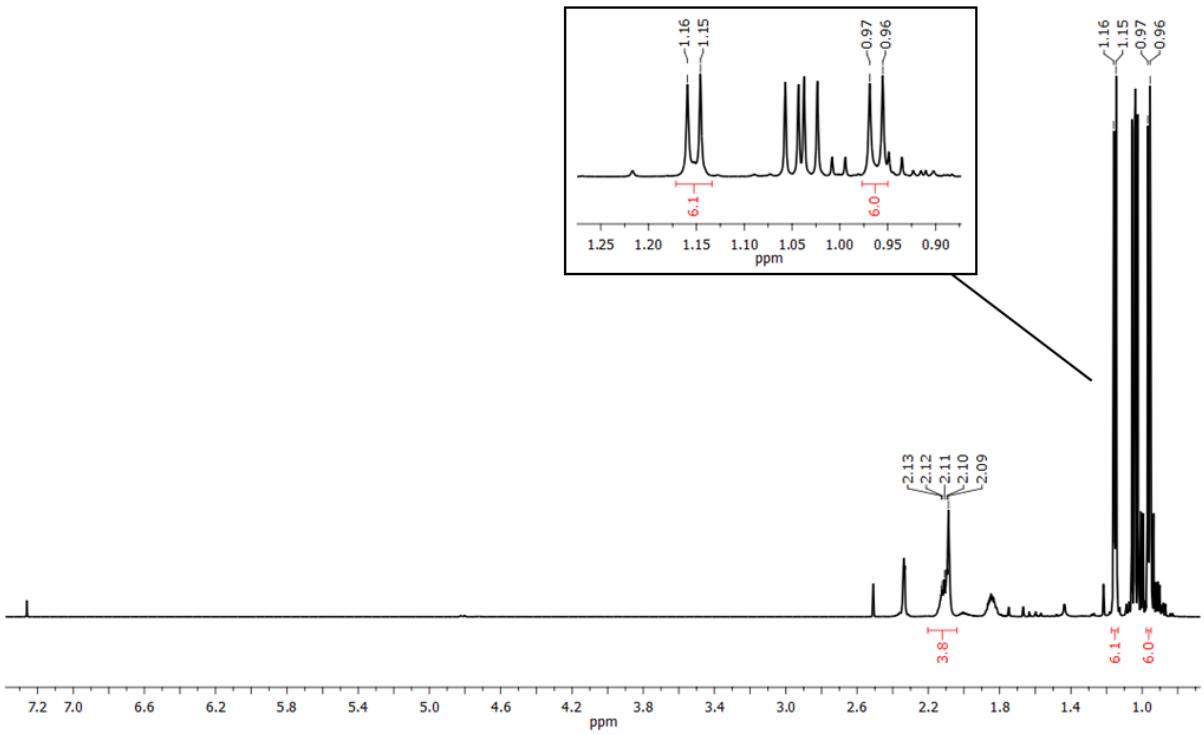

Figure S5.5.1. ^{1}H NMR spectrum (500 MHz) of **2** (integration of Isomer 1 – synthesized via Kulkarni's method) in $CDCl_3$.

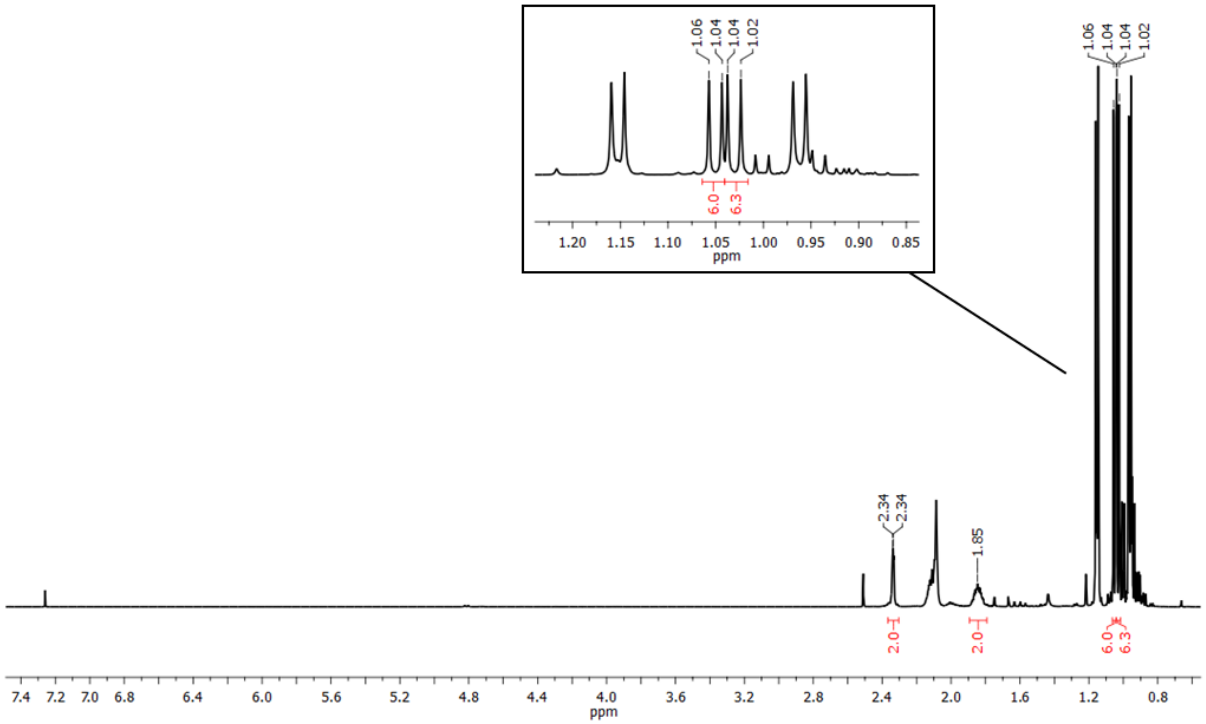

Figure S5.5.2. ^{1}H NMR spectrum (500 MHz) of **2** (integration of Isomer 2 – via Kulkarni's method) in $CDCl_3$.

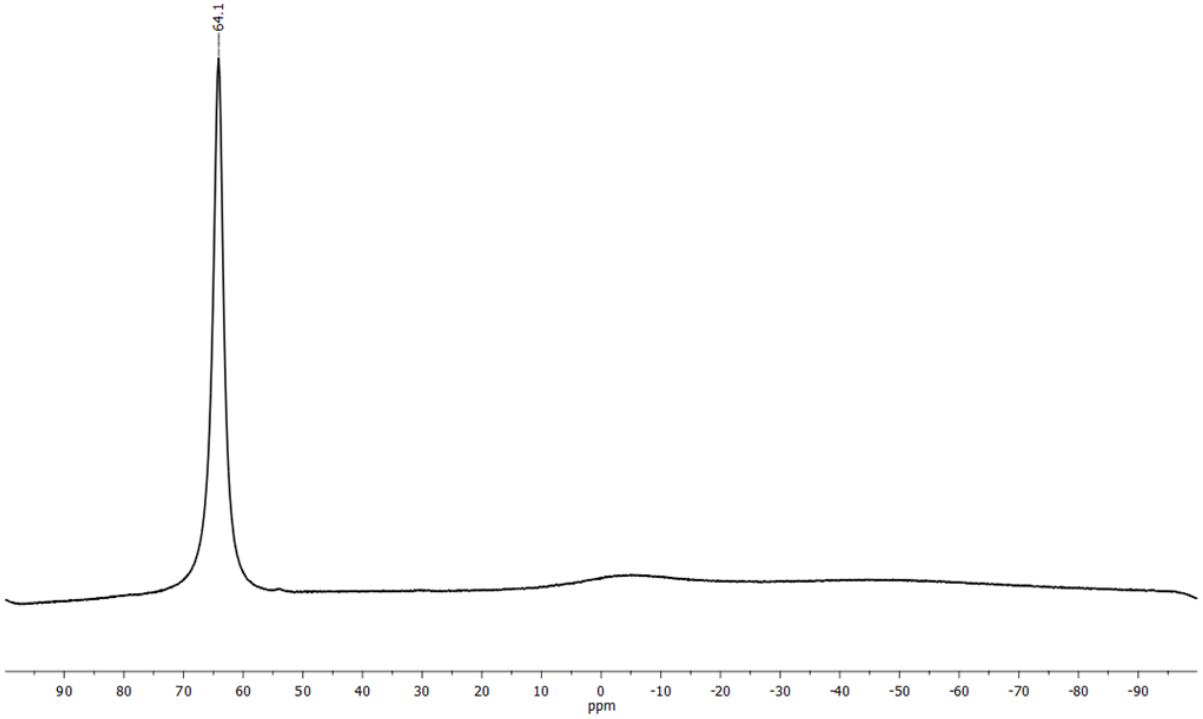

Figure S5.5.3. $^{11}B\{^{1}H\}$ NMR spectrum (96 MHz) of **2** (synthesized via Kulkarni's method in $CDCl_3$.

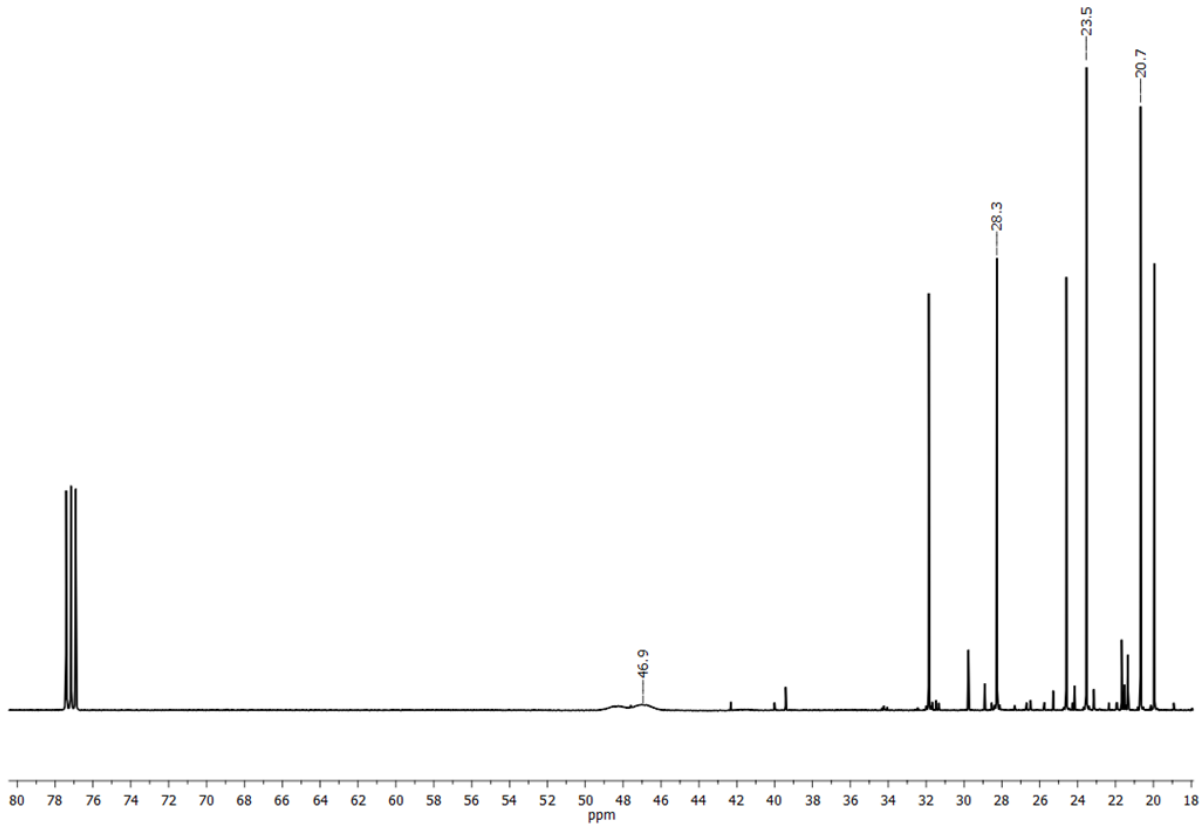

Figure S5.5.4. $^{13}C\{^{1}H\}$ NMR spectrum (126 MHz) of **2** (Isomer 1 – via Kulkarni's method) in $CDCl_3$.

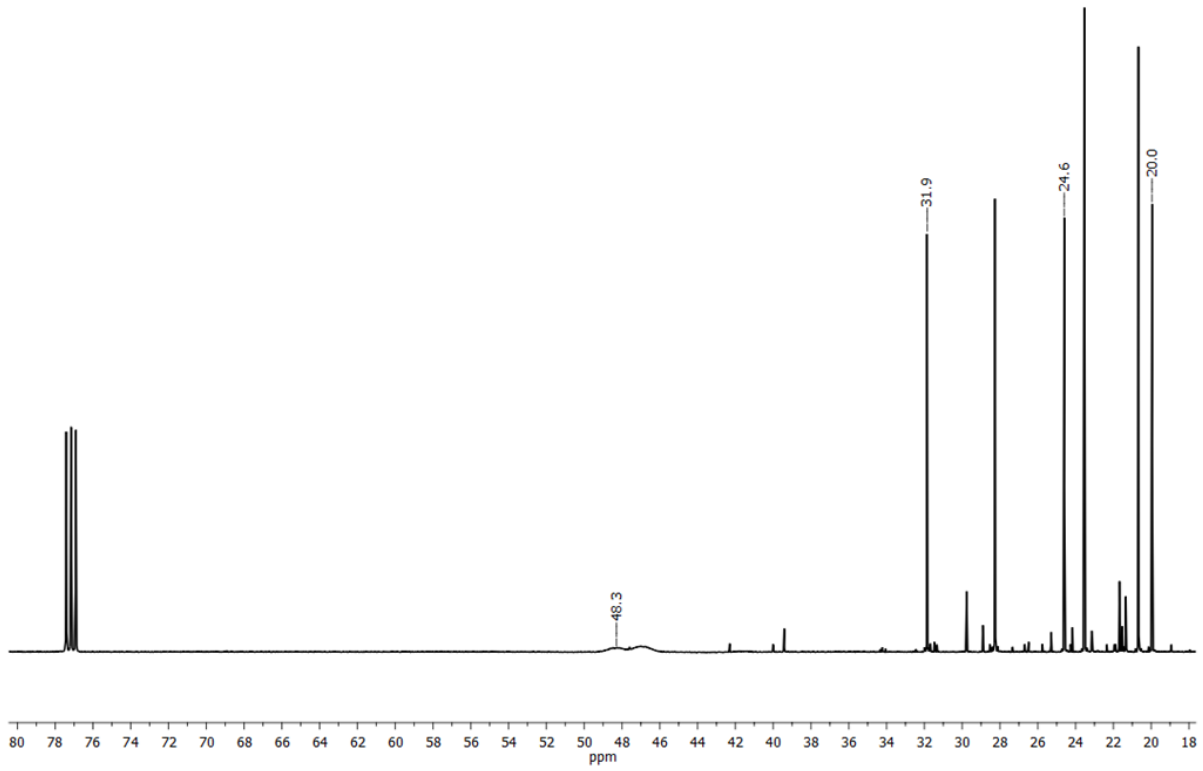

Figure S5.5.5. $^{13}C\{^{1}H\}$ NMR spectrum (126 MHz) of **2** (Isomer 2 – via Kulkarni's method) in $CDCl_3$.

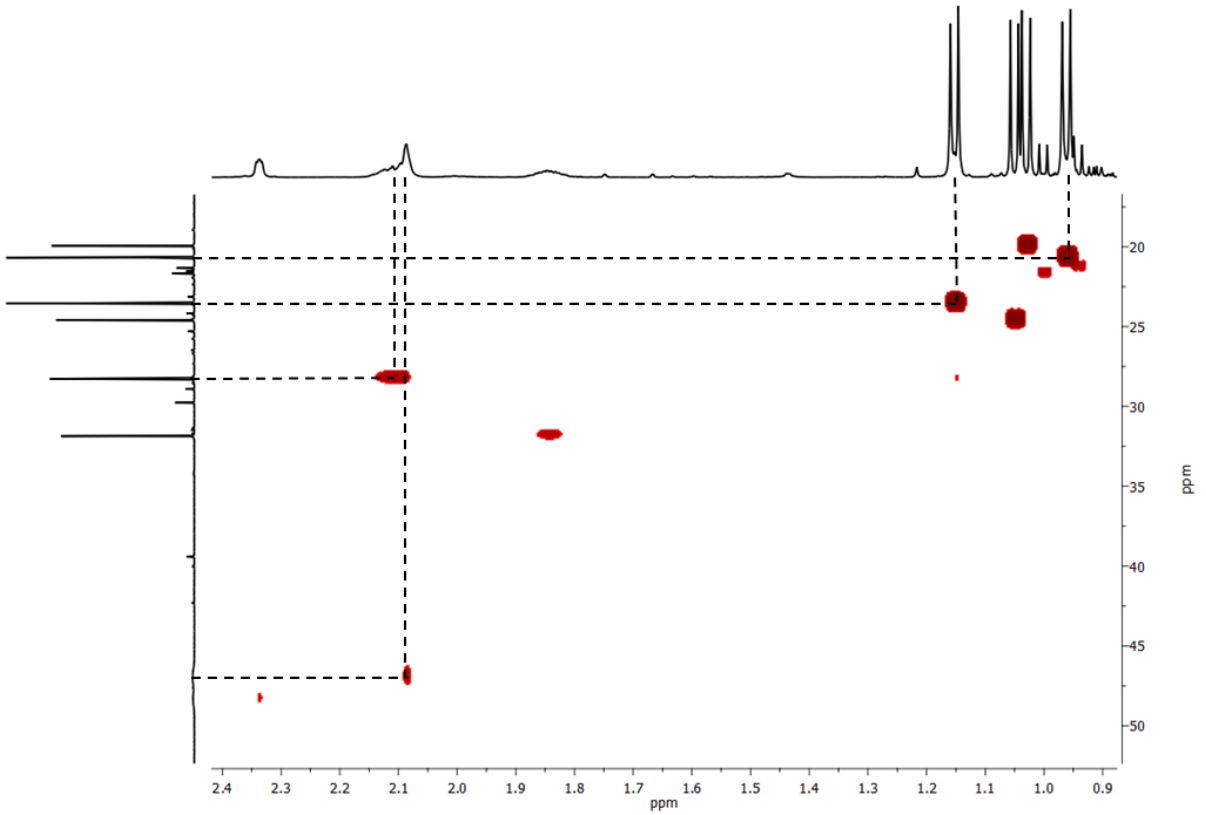

Figure S5.5.6. Detail of ^{1}H, ^{13}C HSQC spectrum of **2** (Isomer 1 – via Kulkarni's method) in $CDCl_3$.

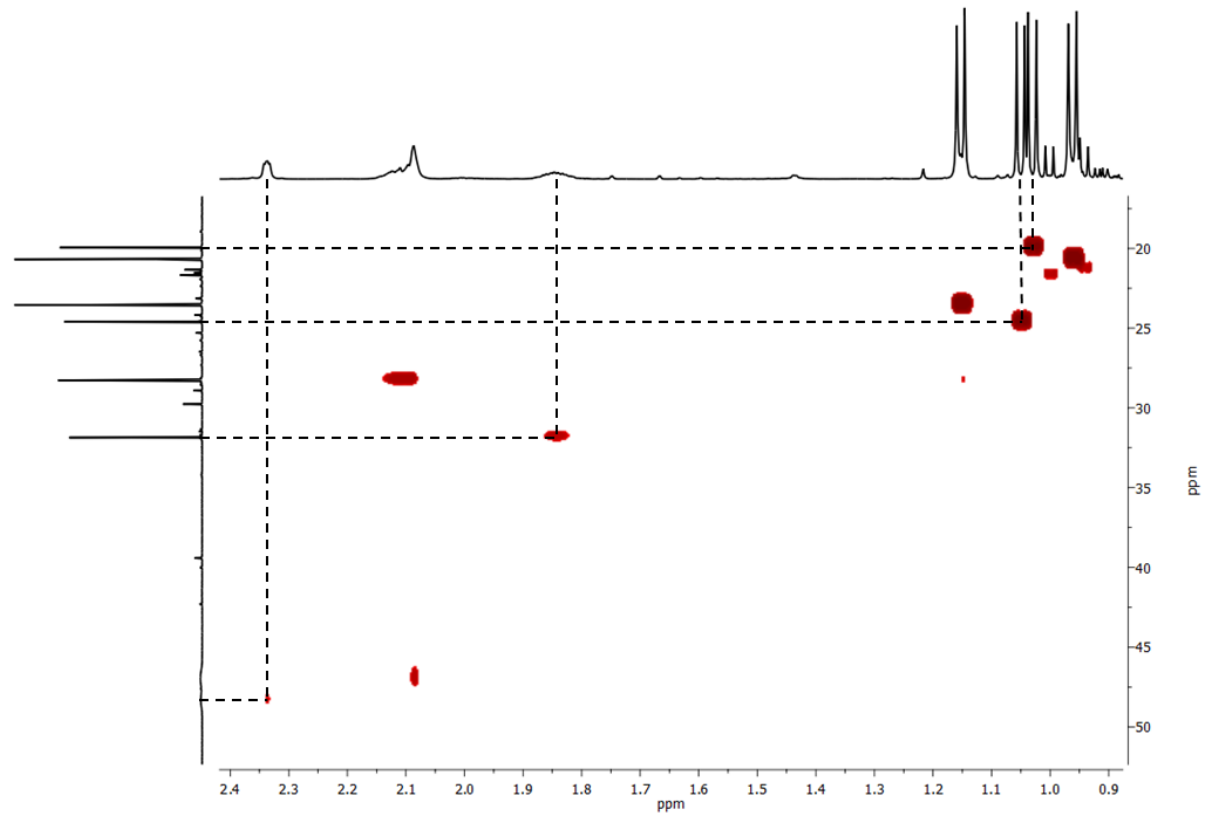

Figure S5.5.7. Detail of ^{1}H, ^{13}C HSQC spectrum of **2** (Isomer 2 – via Kulkarni's method) in $CDCl_3$.

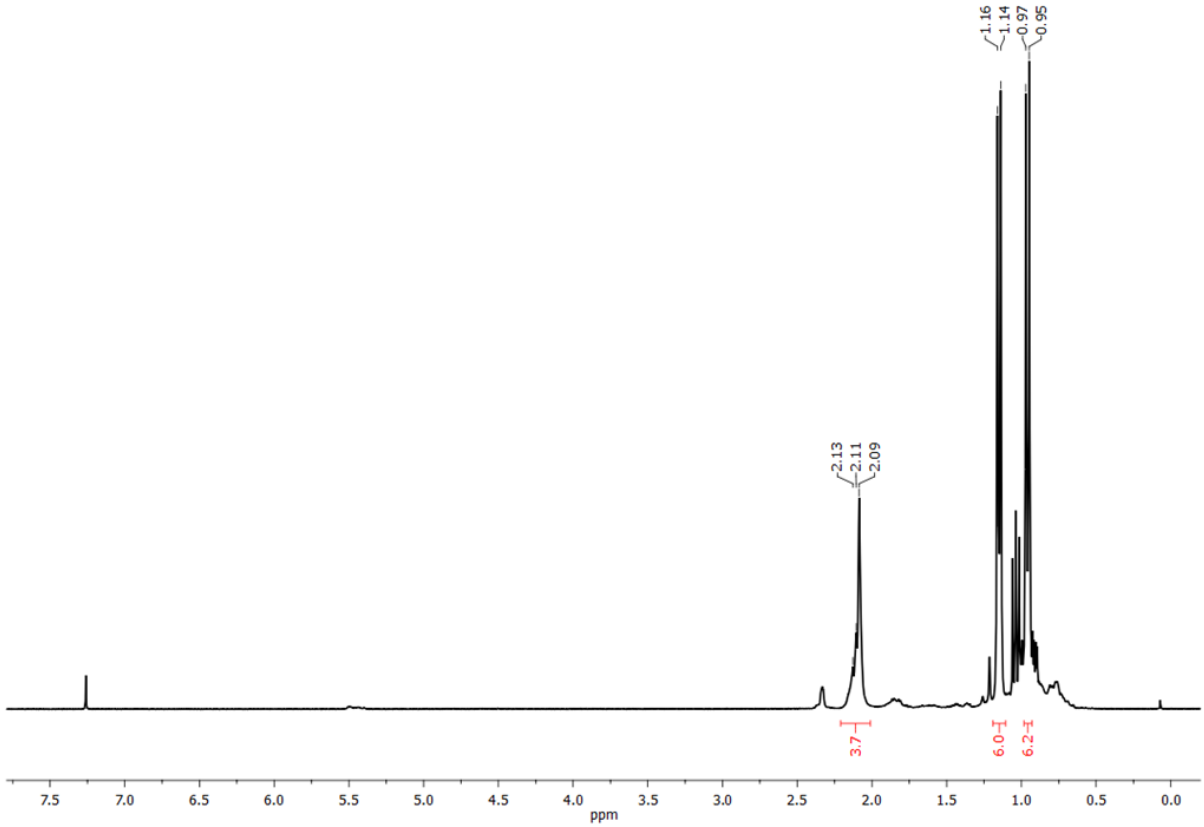

Figure S5.5.8. ^{1}H NMR spectrum (300 MHz) of **2** (integration of Isomer 1 – synthesized via Matteson's method) in $CDCl_3$.

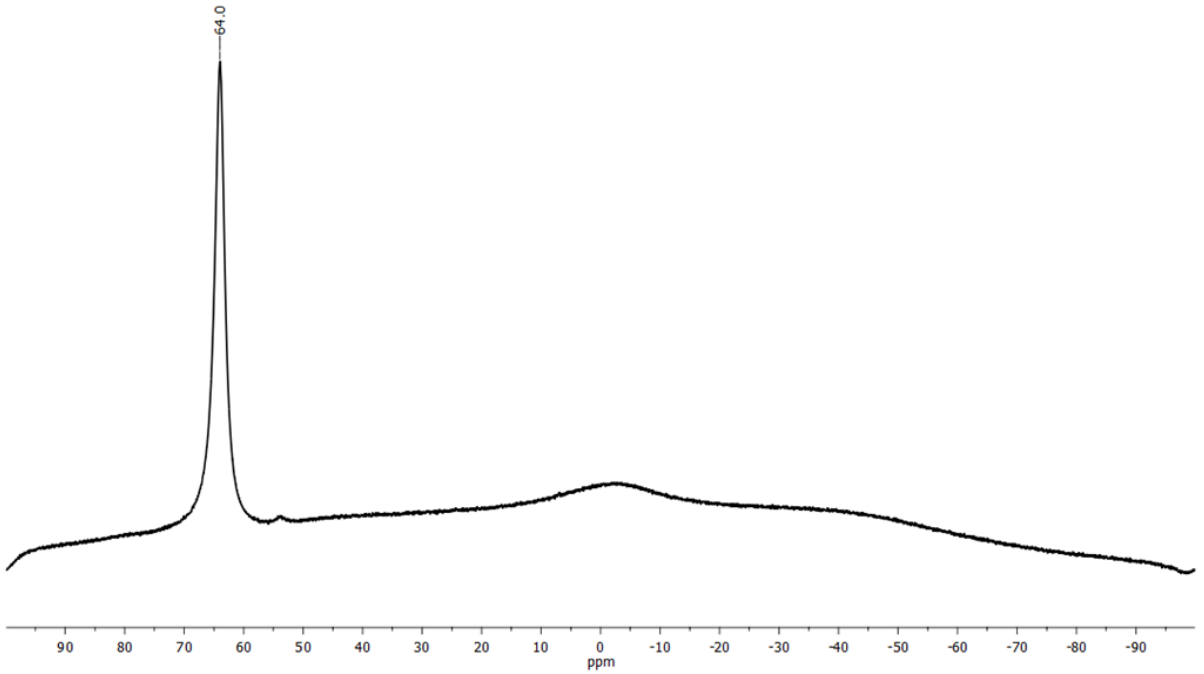

Figure S5.5.9. $^{11}B\{^{1}H\}$ NMR spectrum (96 MHz) of **2** (synthesized via Matteson's method) in $CDCl_3$.

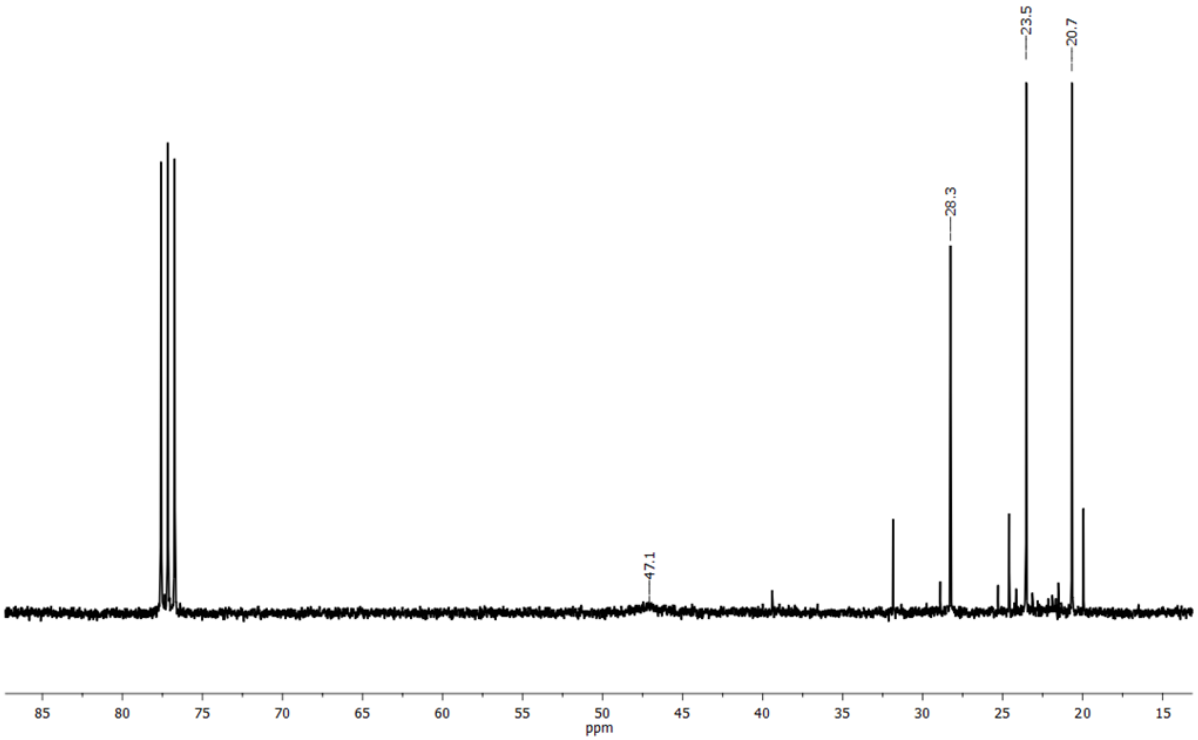

Figure S5.5.10. $^{13}C\{^{1}H\}$ NMR spectrum (75 MHz) of **2** (synthesized via Matteson's method) in $CDCl_3$.

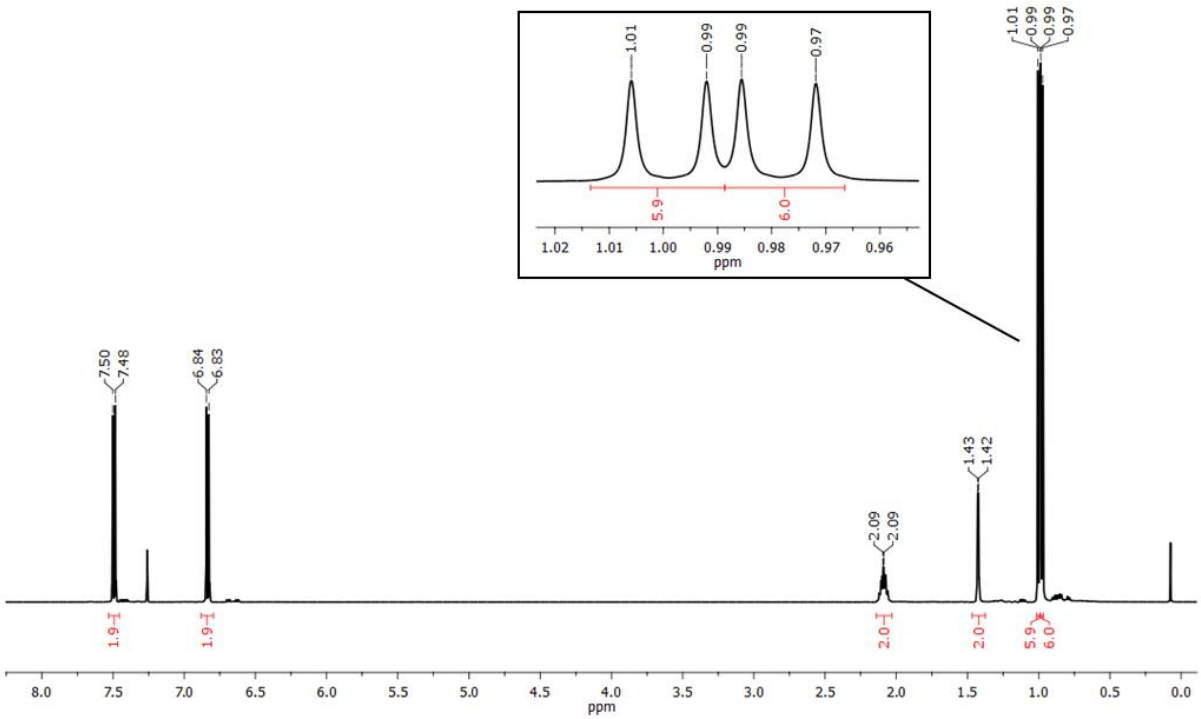

Figure S5.5.11. ^{1}H NMR spectrum (500 MHz) of **4** in $CDCl_3$.

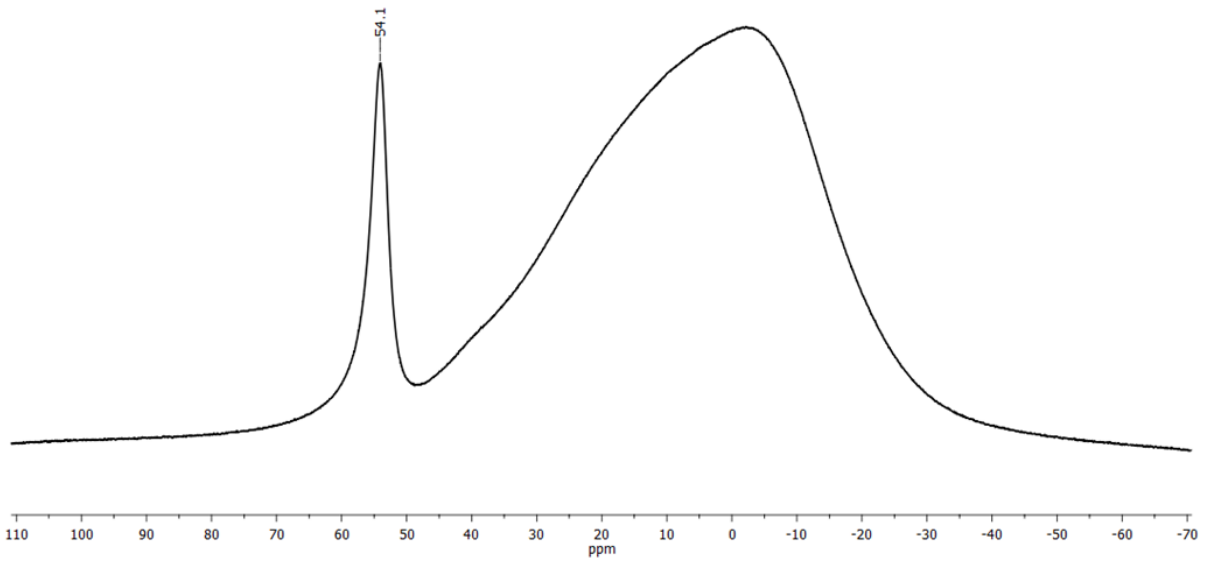

Figure S5.5.12. $^{11}B\{^{1}H\}$ NMR spectrum (160 MHz) of **4** in $CDCl_3$.

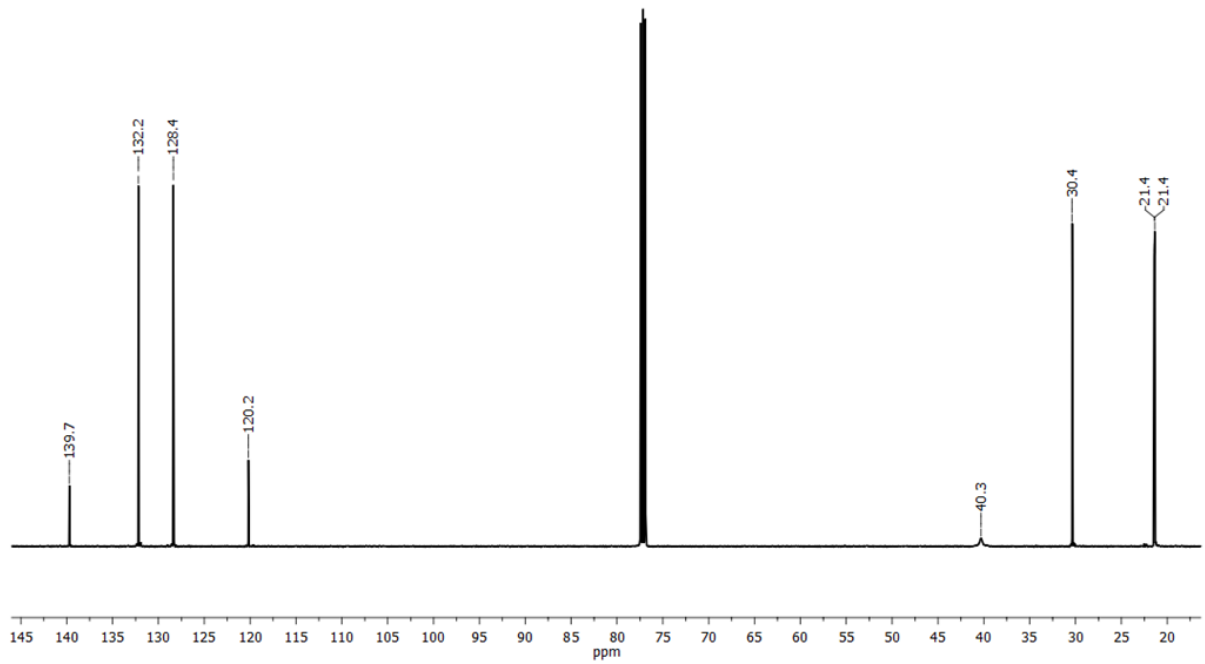

Figure S5.5.13. $^{13}C\{^{1}H\}$ NMR spectrum (126 MHz) of **4** in $CDCl_3$.

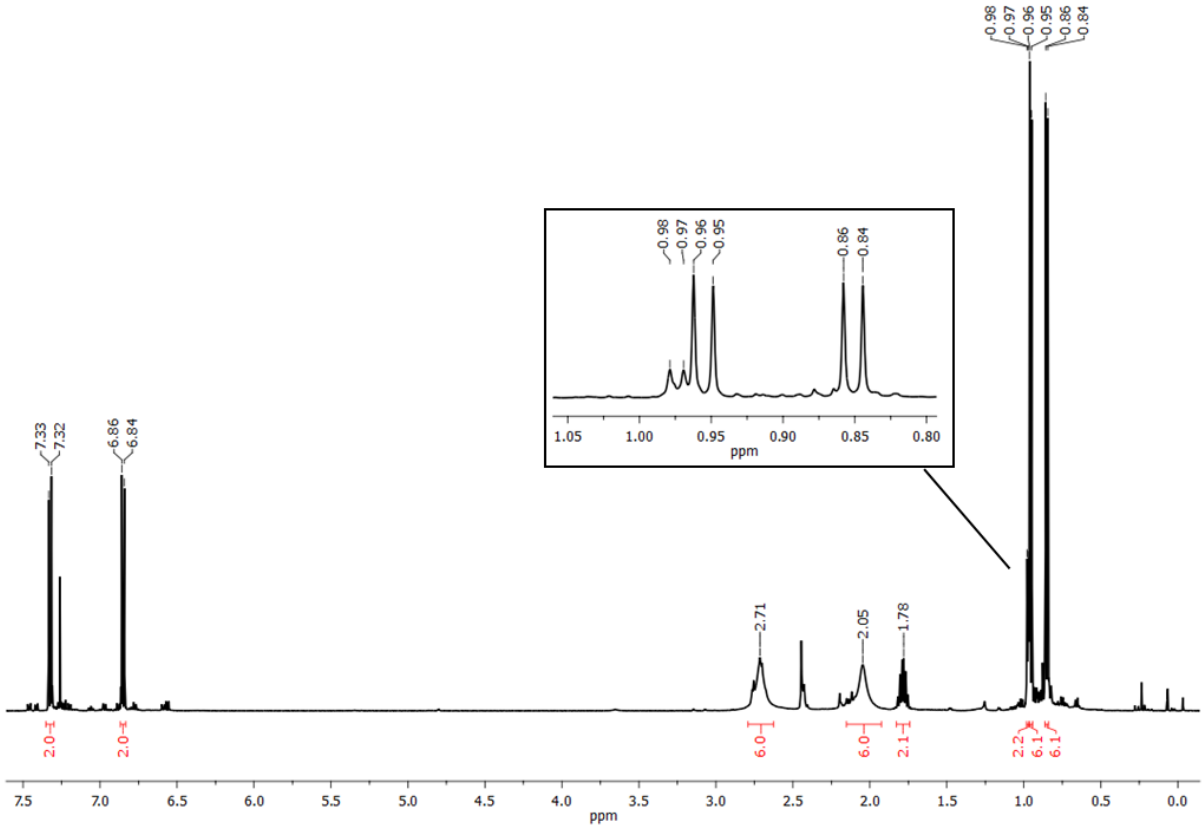

Figure S5.5.14. ^{1}H NMR spectrum (500 MHz) of **5** in $CDCl_3$.

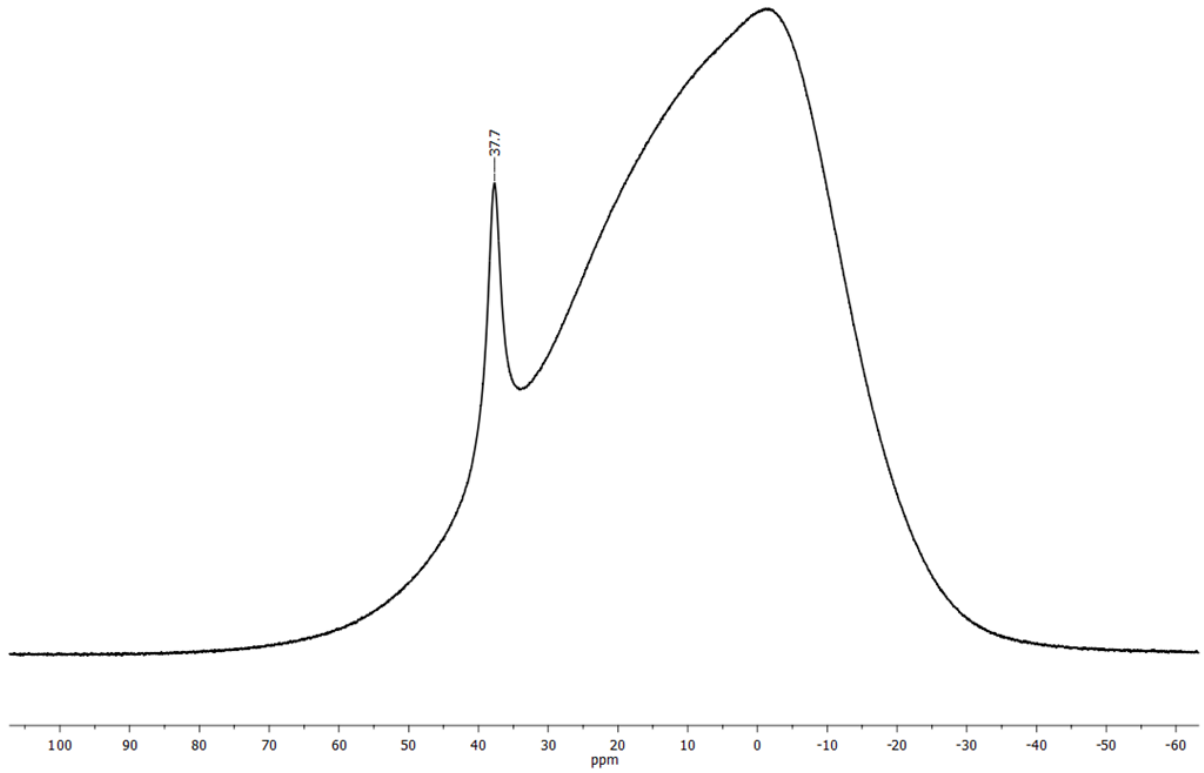

Figure S5.5.15. $^{11}B\{^{1}H\}$ NMR spectrum (160 MHz) of **5** in $CDCl_3$.

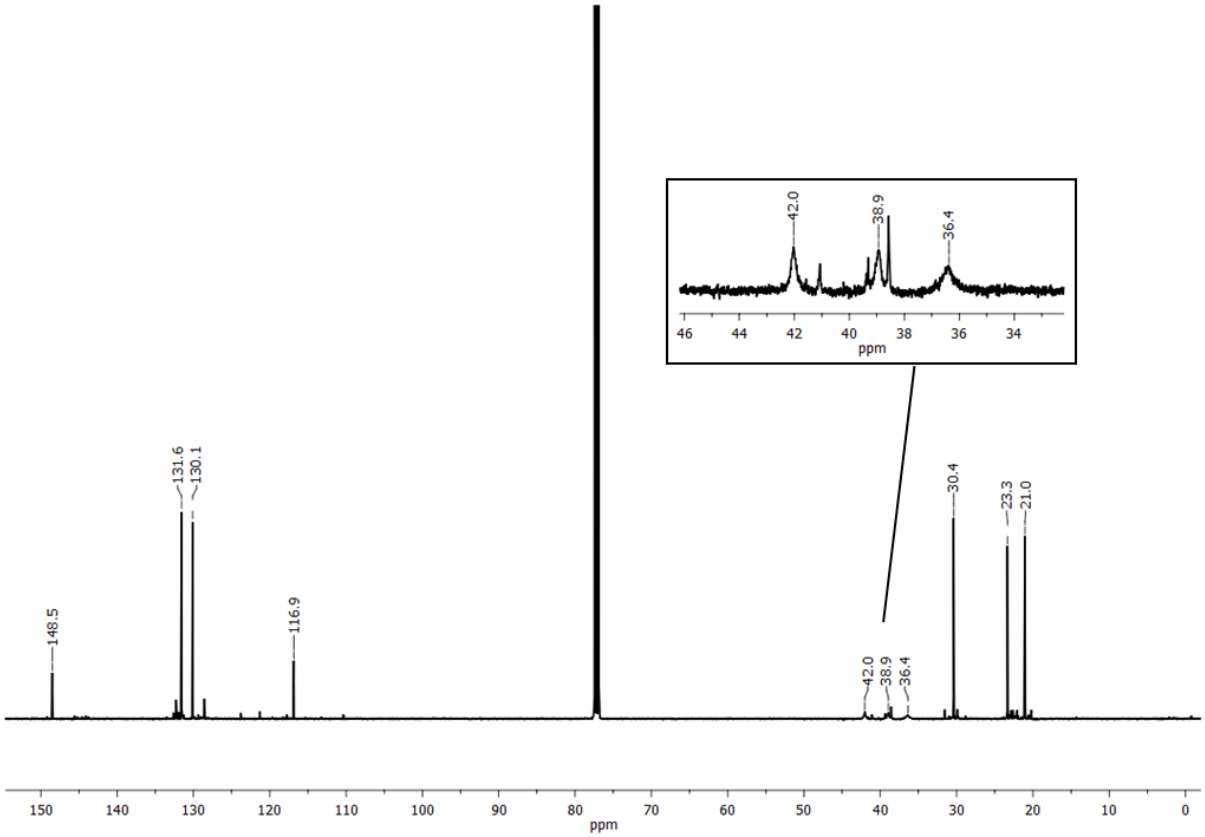

Figure S5.5.16. $^{13}C\{^{1}H\}$ NMR spectrum (126 MHz) of **5** in $CDCl_3$.

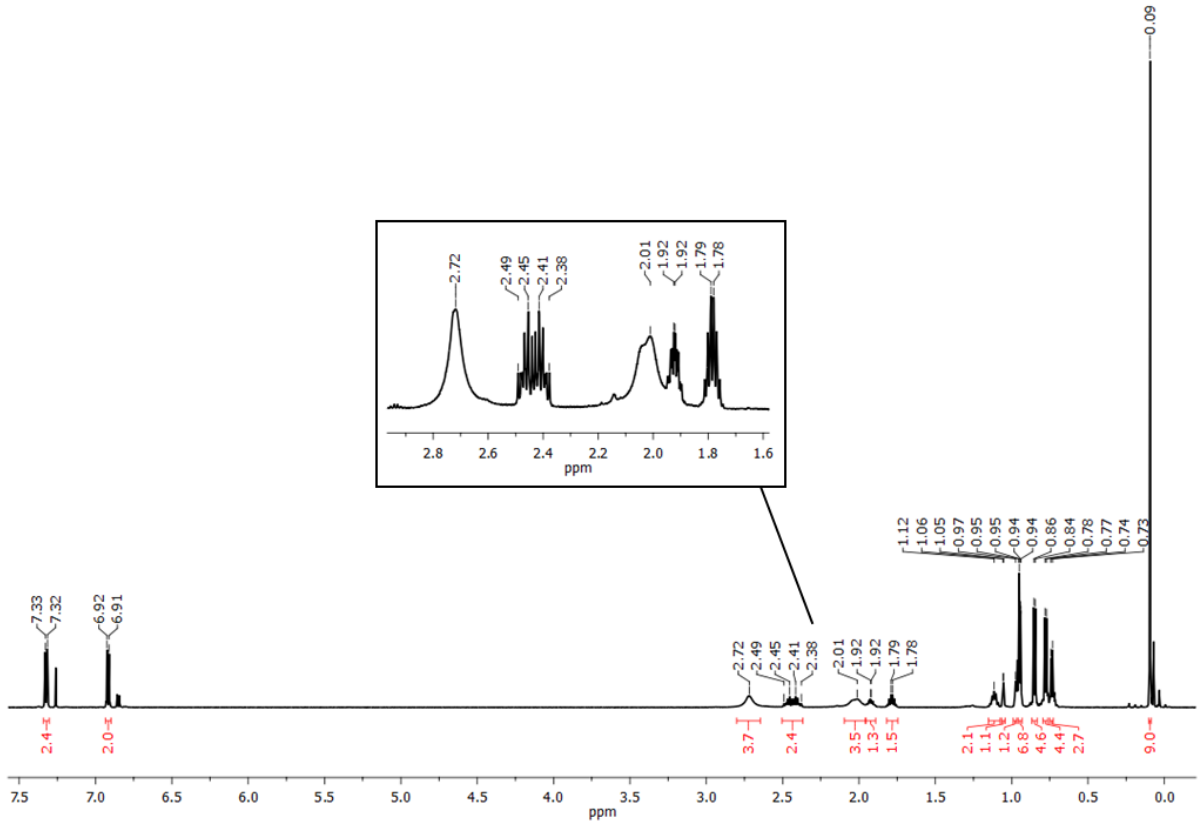

Figure S5.5.17. ^{1}H NMR spectrum (600 MHz) of **7** at room temperature in $CDCl_3$.

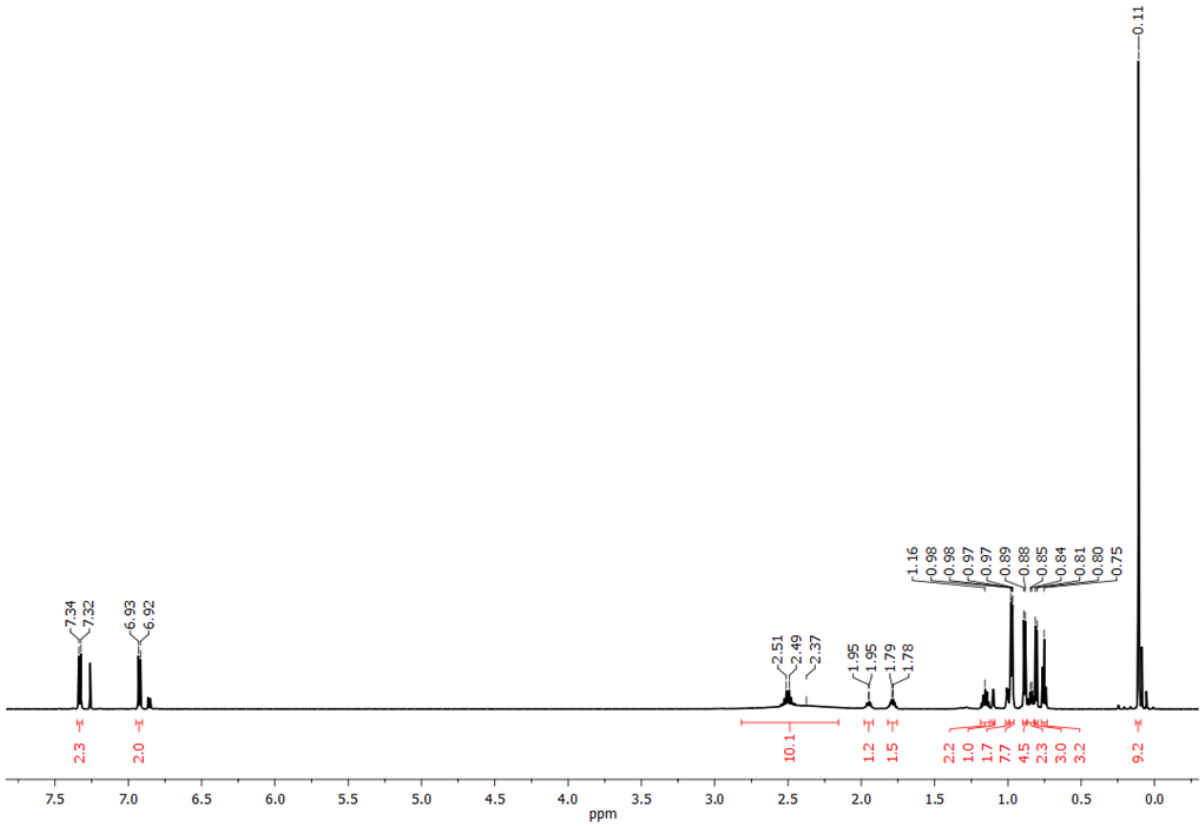

Figure S5.5.18. ^{1}H NMR spectrum (600 MHz) of **7** at +60 °C in $CDCl_3$.

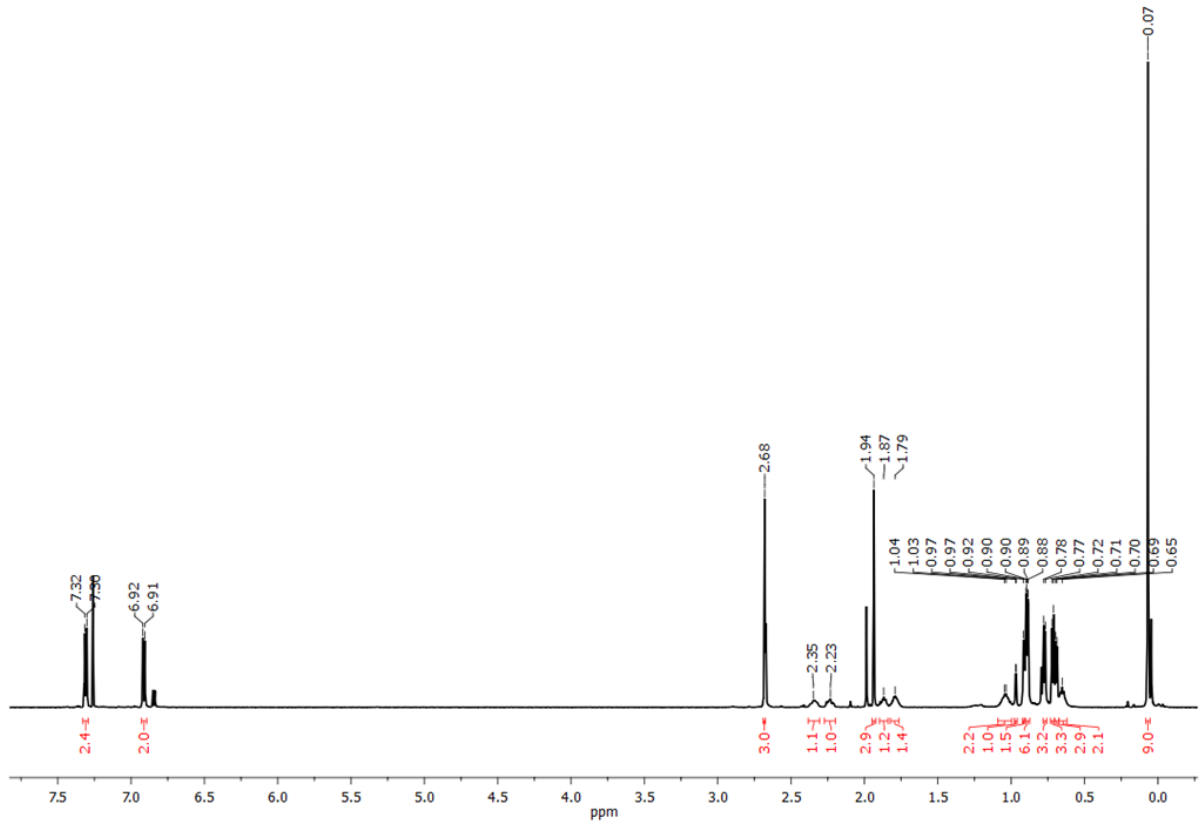

Figure S5.5.19. ^{1}H NMR spectrum (600 MHz) of **7** at –40 °C in $CDCl_3$.

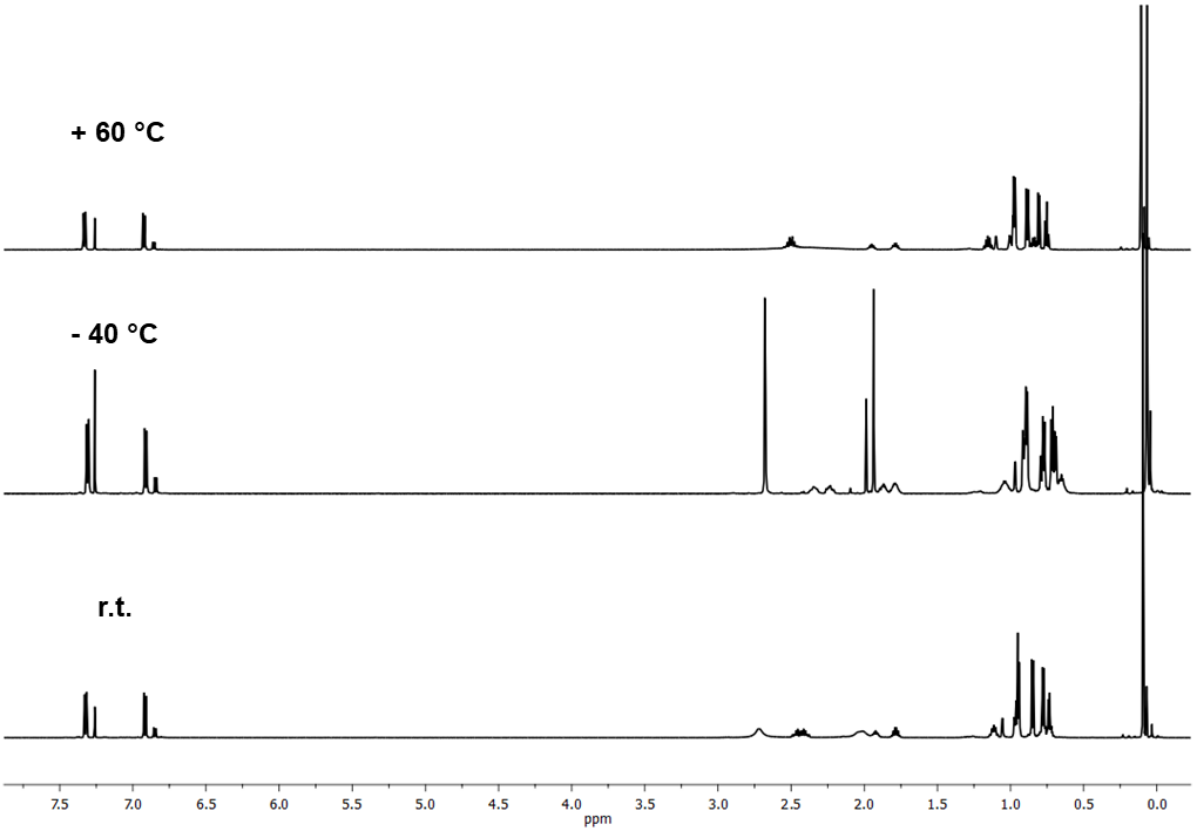

Figure S5.5.20. ^{1}H NMR spectra (600 MHz) of **7** at –40 °C, room temperature and +60 °C in $CDCl_3$.

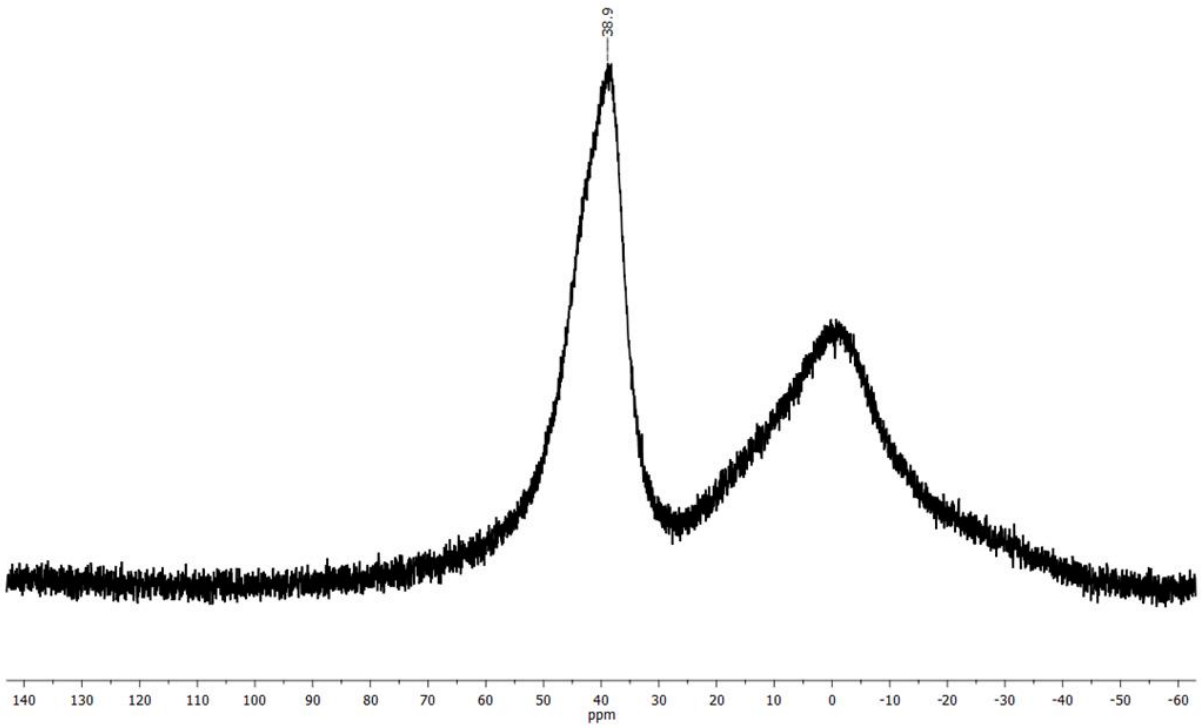

Figure S5.5.21. $^{11}B\{^{1}H\}$ NMR spectrum (193 MHz) of **7** at –40 °C in $CDCl_3$ with reduced glass background.

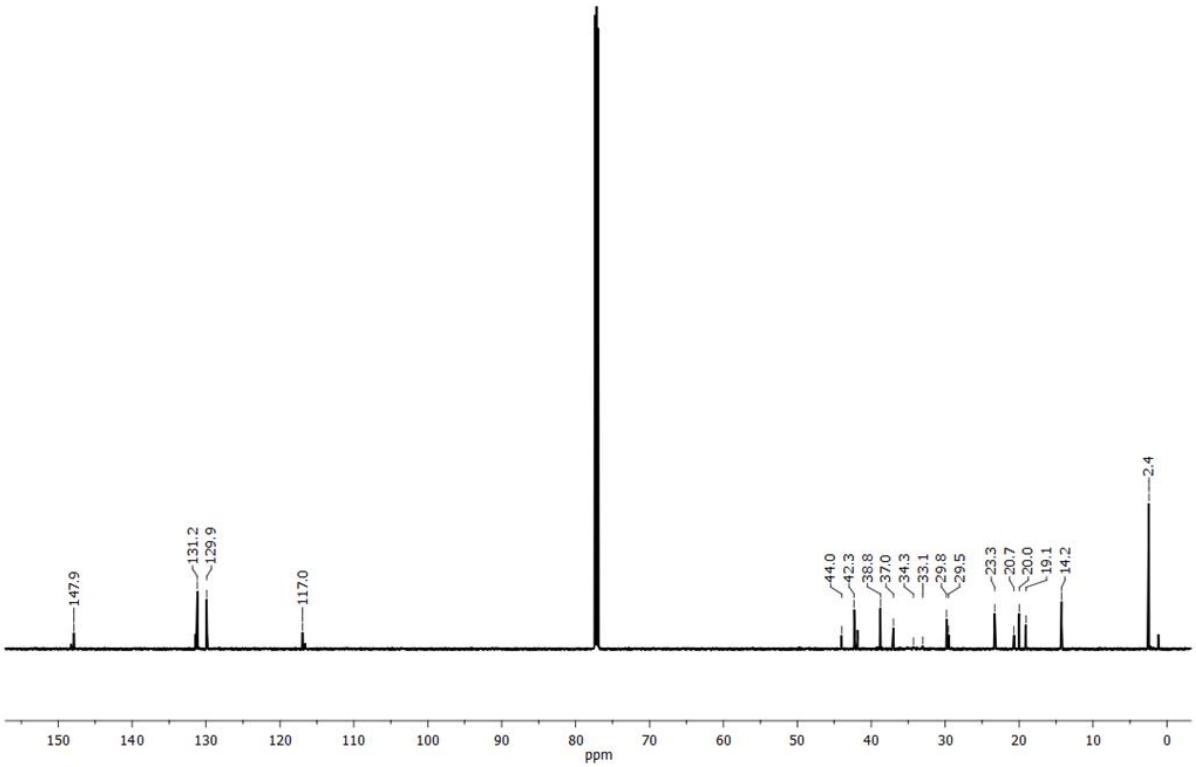

Figure S5.5.22. $^{13}C\{^{1}H\}$ NMR spectrum (151 MHz) of **7** at –40 °C in $CDCl_3$.

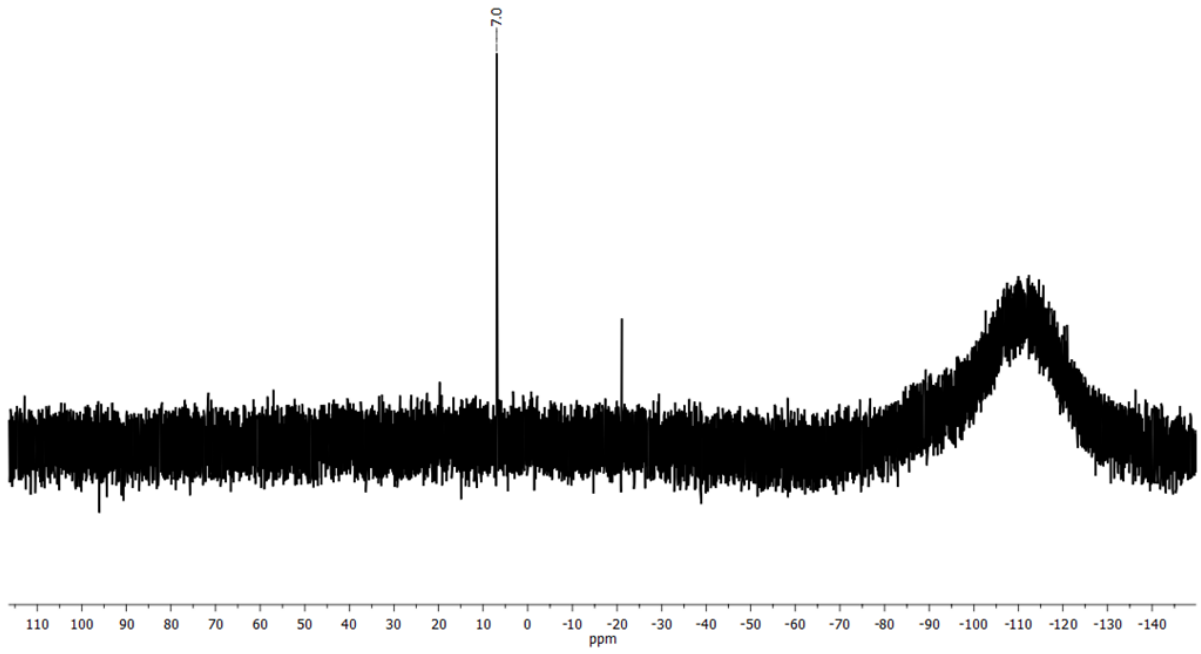

Figure S5.5.23. $^{29}Si\{^{1}H\}$ NMR spectrum (119 MHz) of **7** at –40 °C in $CDCl_3$.

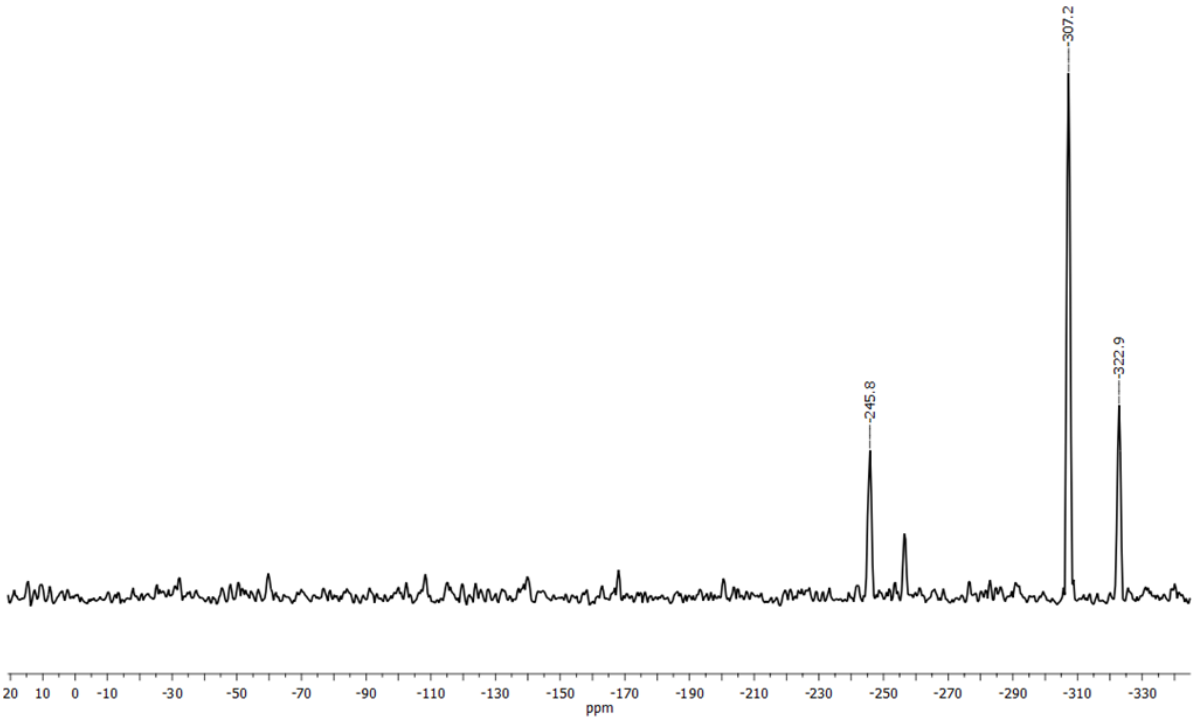

Figure S5.5.24. ^{15}N NMR spectrum (61 MHz) of **7** at –40 °C in $CDCl_3$.

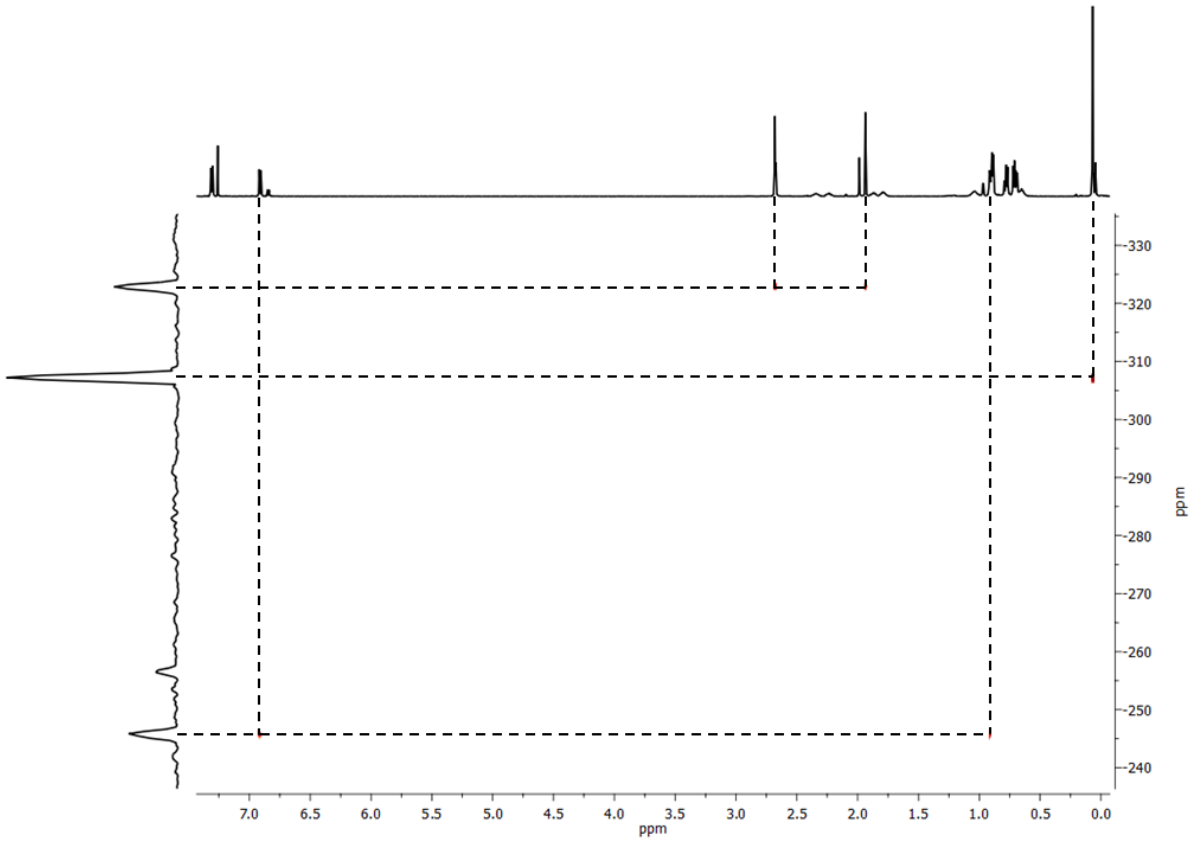

Figure S5.5.25. Detail of ^{1}H, ^{15}N HMBC spectrum of **7** at –40 °C in $CDCl_3$.

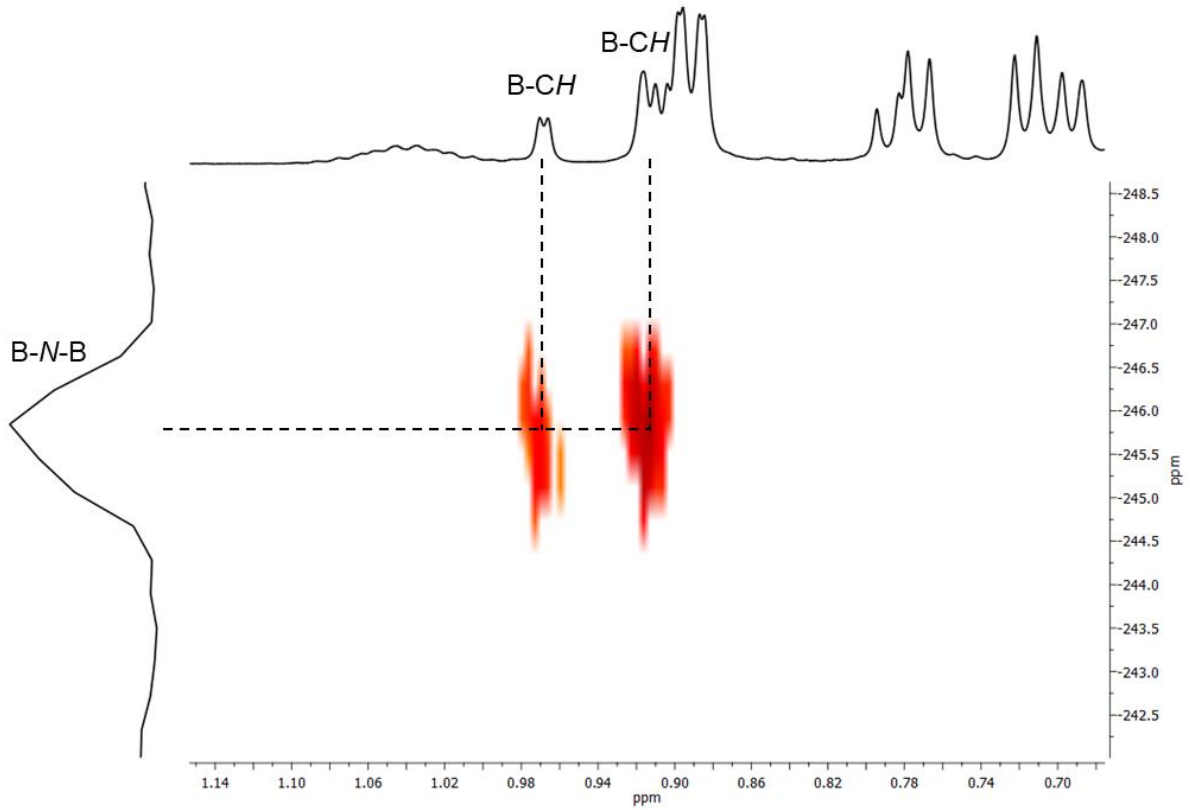

Figure S5.5.26. Sequence of ^{1}H, ^{15}N HMBC spectrum of **7** at –40 °C in $CDCl_3$.

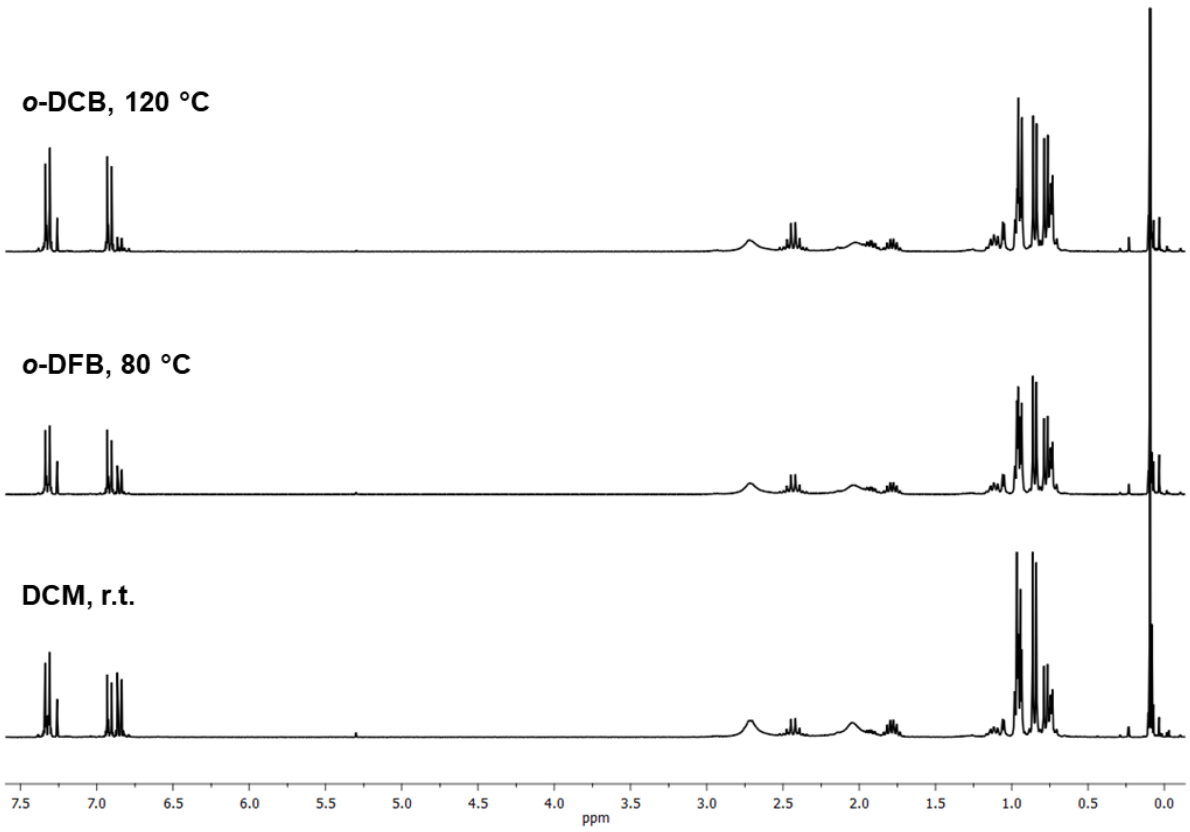

Figure S5.5.27. ^{1}H NMR spectra after the reaction of **4** with **6** in different solvents at different temperatures for 28 days in $CDCl_3$.

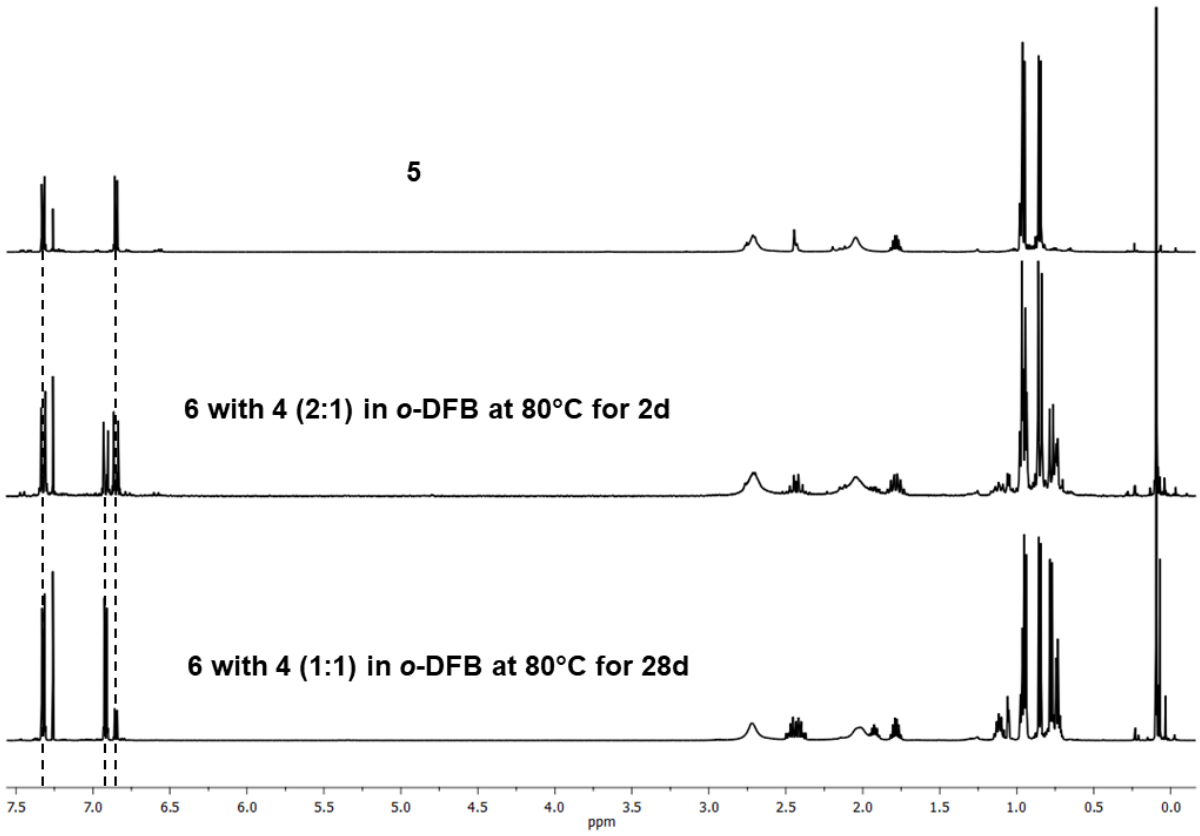

Figure S5.5.28. ^{1}H NMR spectra of the reaction of **4** with **6** in different stoichiometry and **5** in $CDCl_3$.

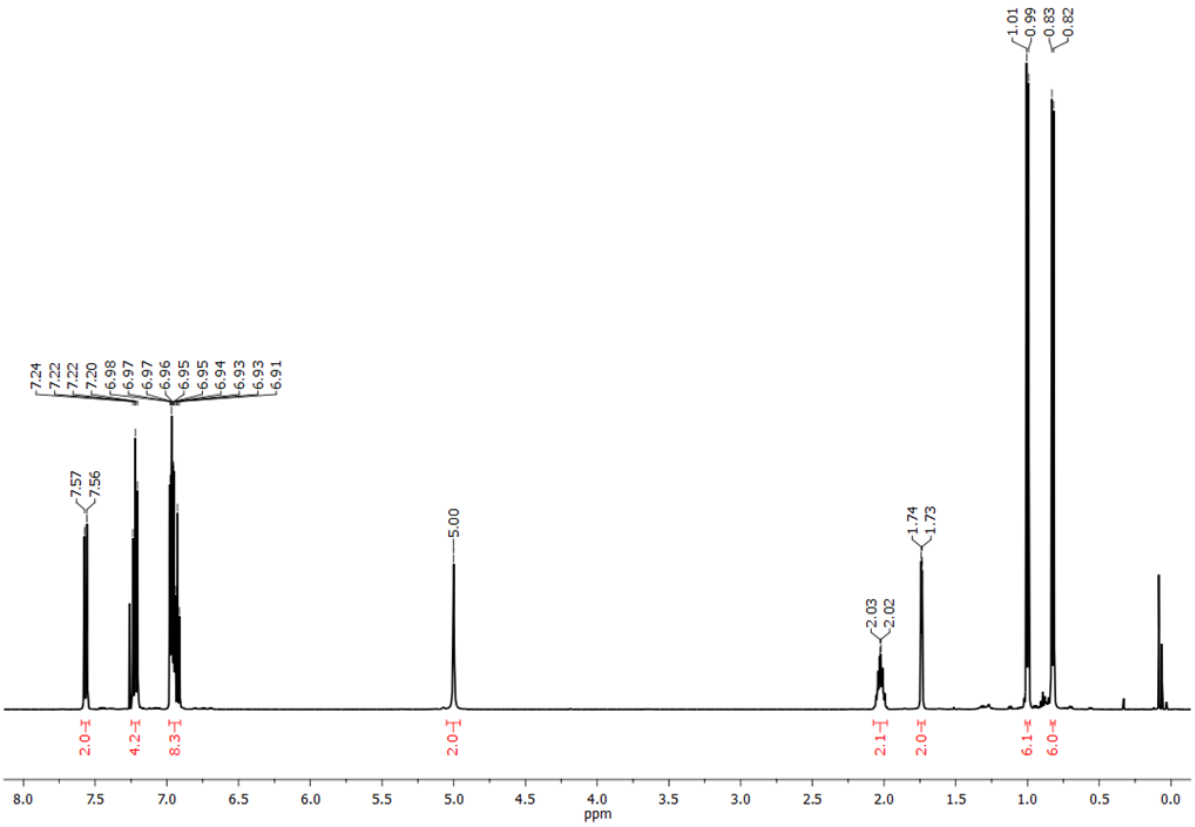

Figure S5.5.29. ^{1}H NMR spectrum (500 MHz) of **9** in $CDCl_3$.

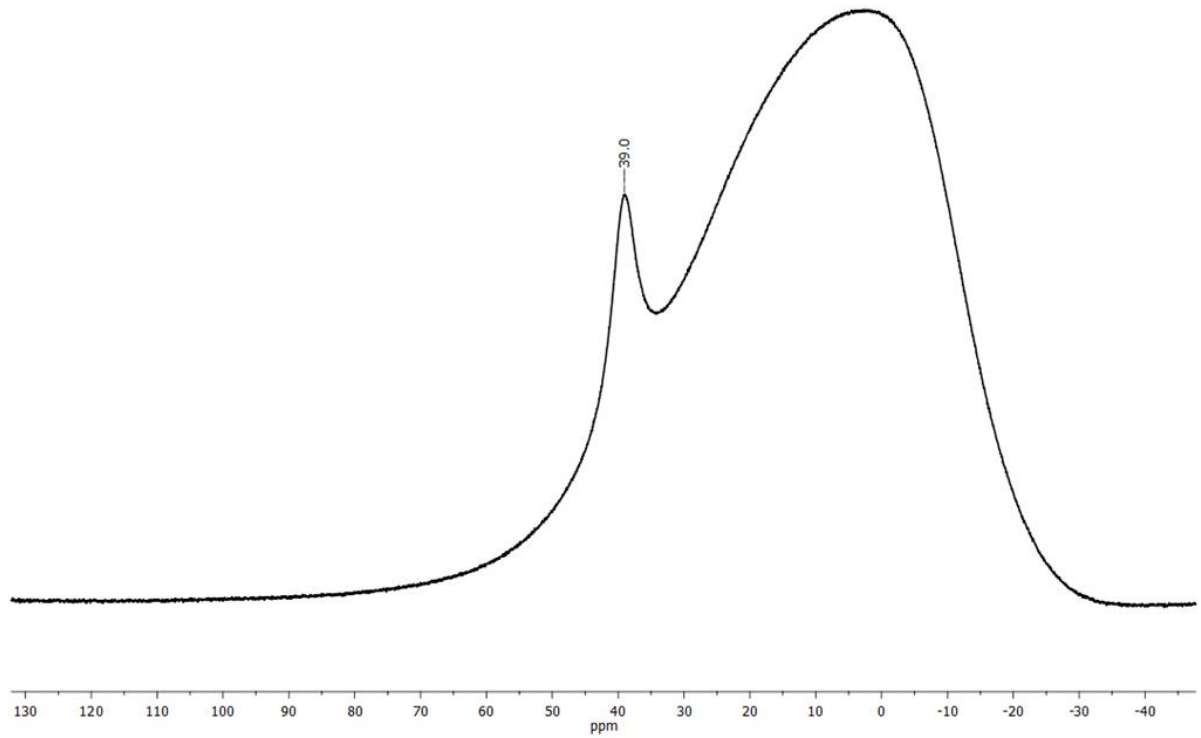

Figure S5.5.30. $^{11}B\{^{1}H\}$ NMR spectrum (160 MHz) of **9** in $CDCl_3$.

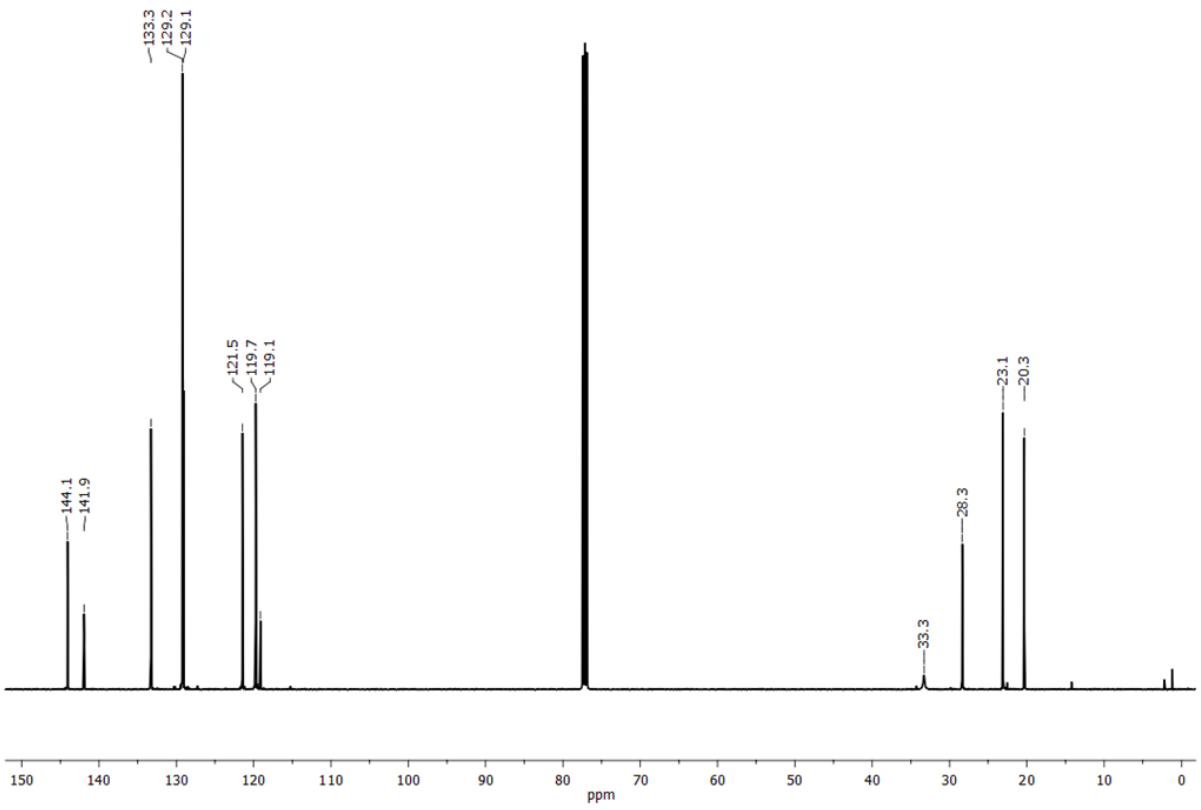

Figure S5.5.31. $^{13}C\{^{1}H\}$ NMR spectrum (126 MHz) of **9** in $CDCl_3$.

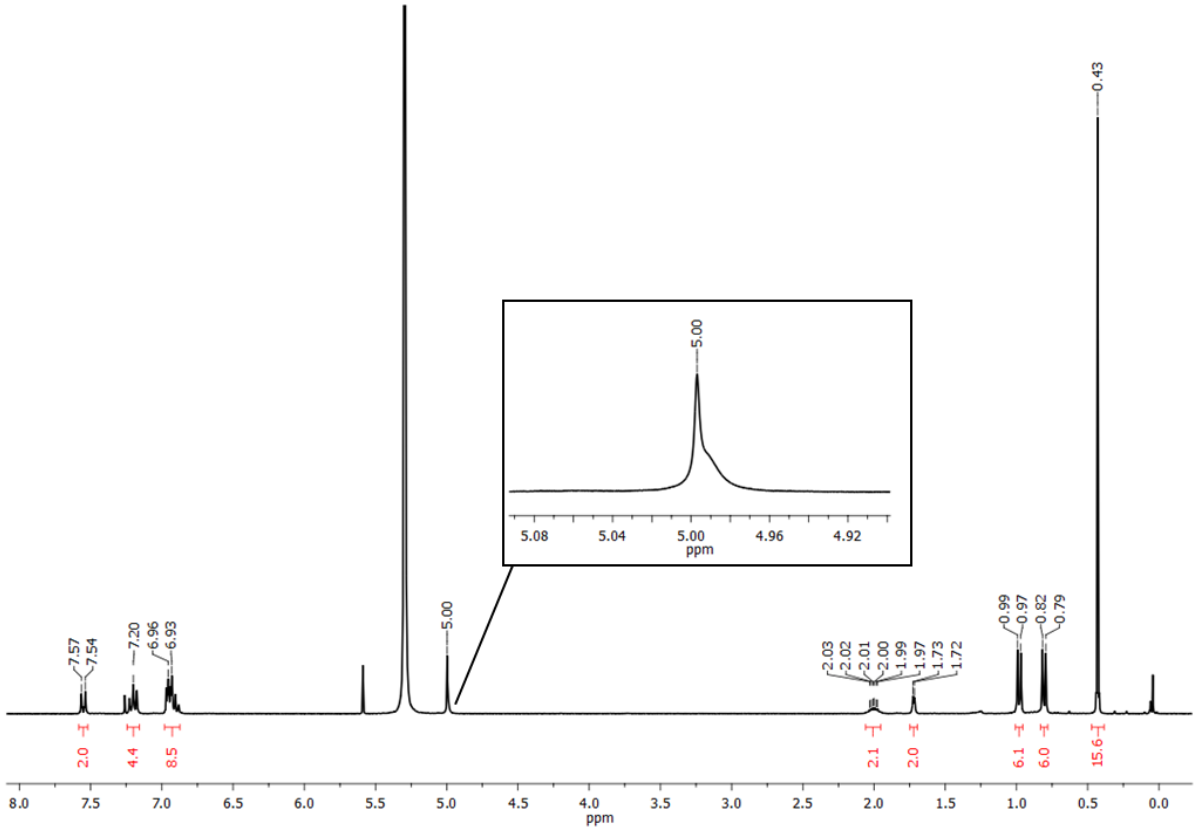

Figure S5.5.32. ^{1}H NMR spectrum (300 MHz) for the reaction control after 3 h of **9** in $CDCl_3$.

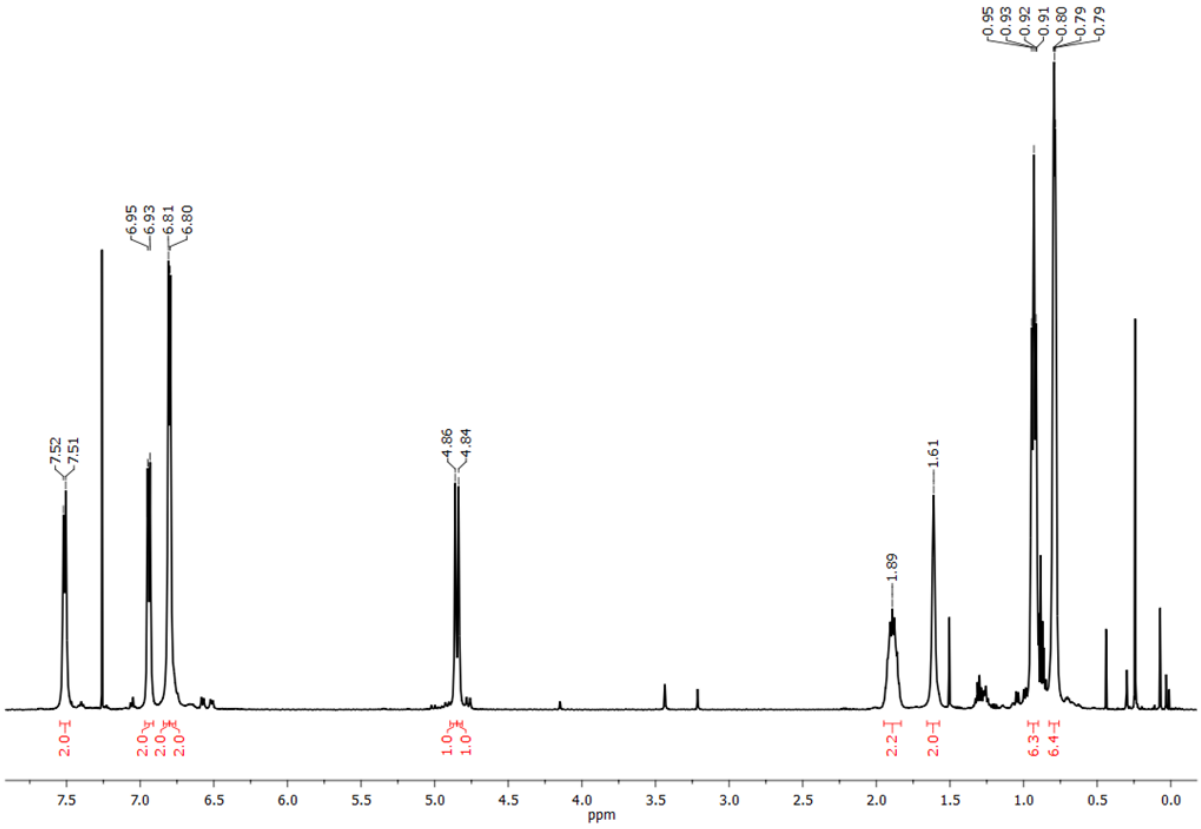

Figure S5.5.33. ^{1}H NMR spectra (500 MHz) of **11** in $CDCl_3$.

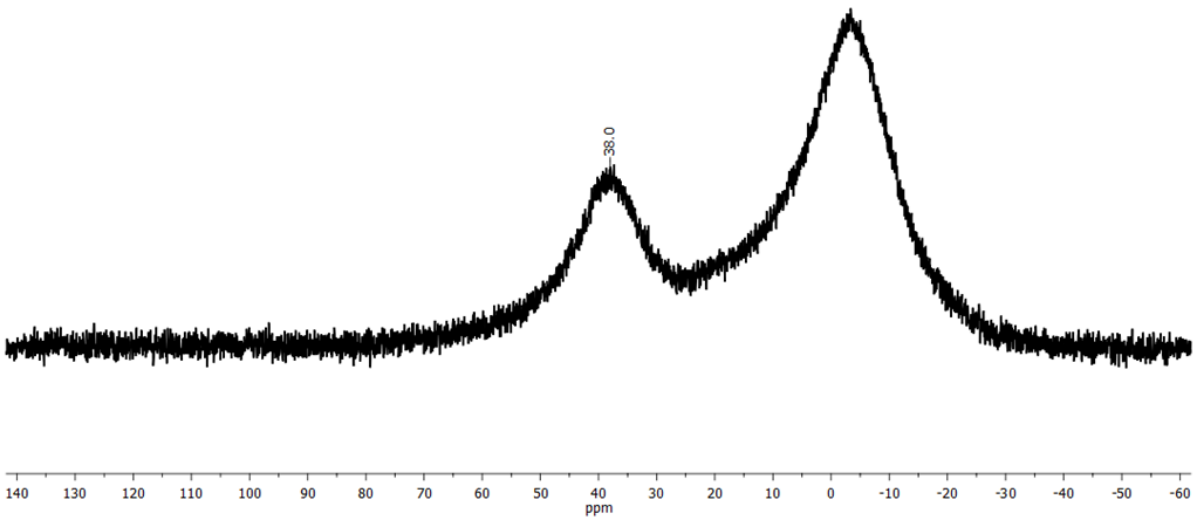

Figure S5.5.34. $^{11}B\{^{1}H\}$ NMR spectrum (160 MHz) of **11** with reduced glass background in $CDCl_3$.

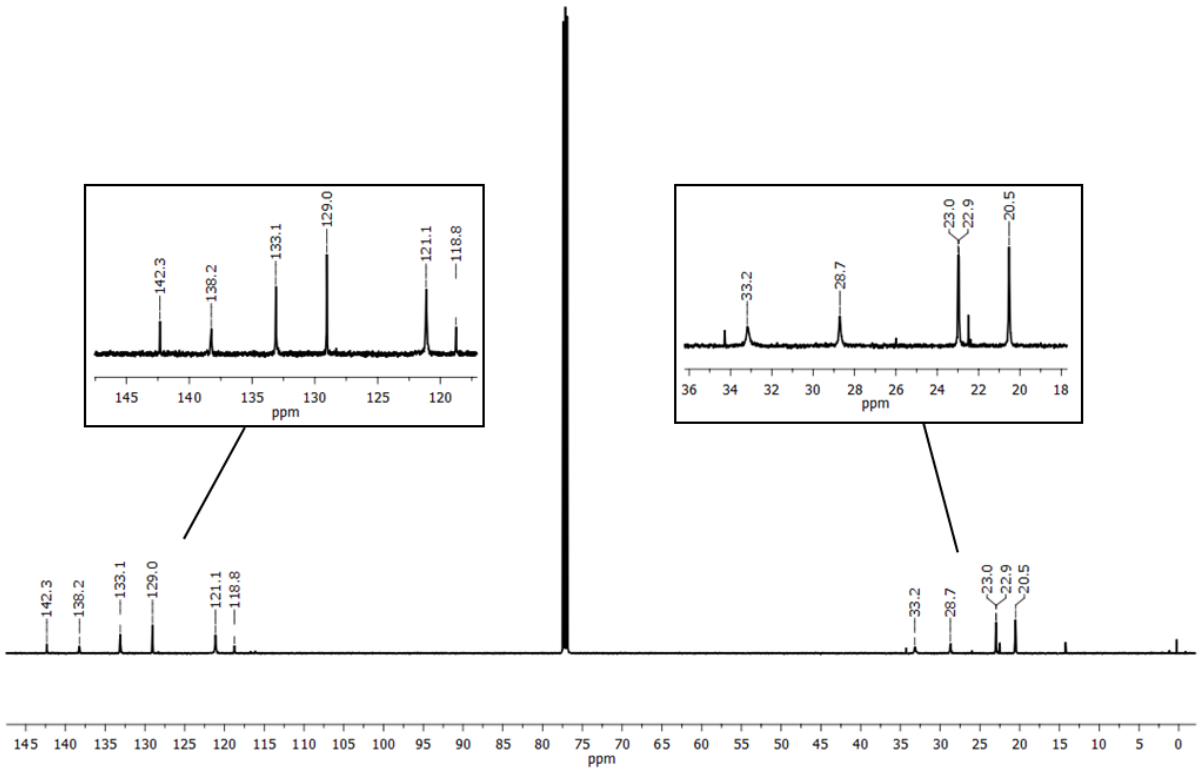

Figure S5.5.35. $^{13}C\{^{1}H\}$ NMR spectrum (126 MHz) of **11** in $CDCl_3$.

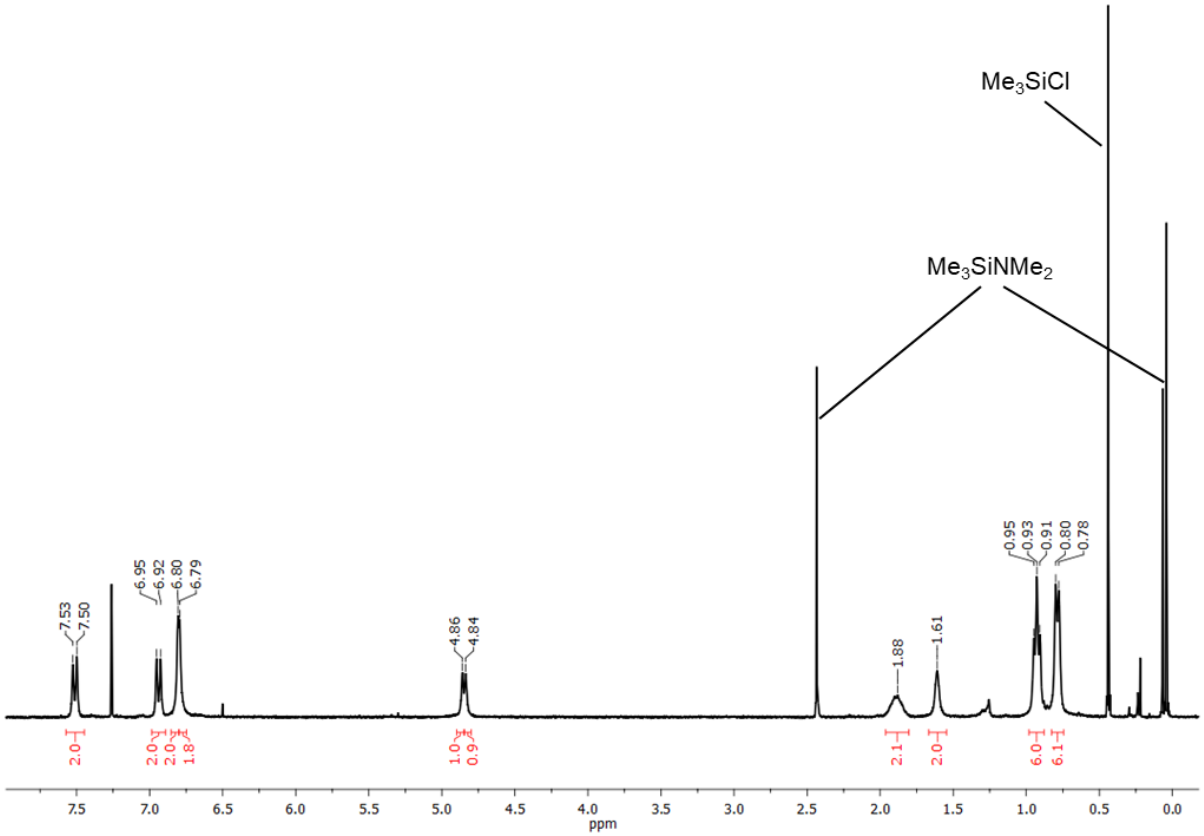

Figure S5.5.36. ^{1}H NMR spectra (300 MHz) of **11** (with M_n = 68.6 kDa) in $CDCl_3$.

HRMS spectra

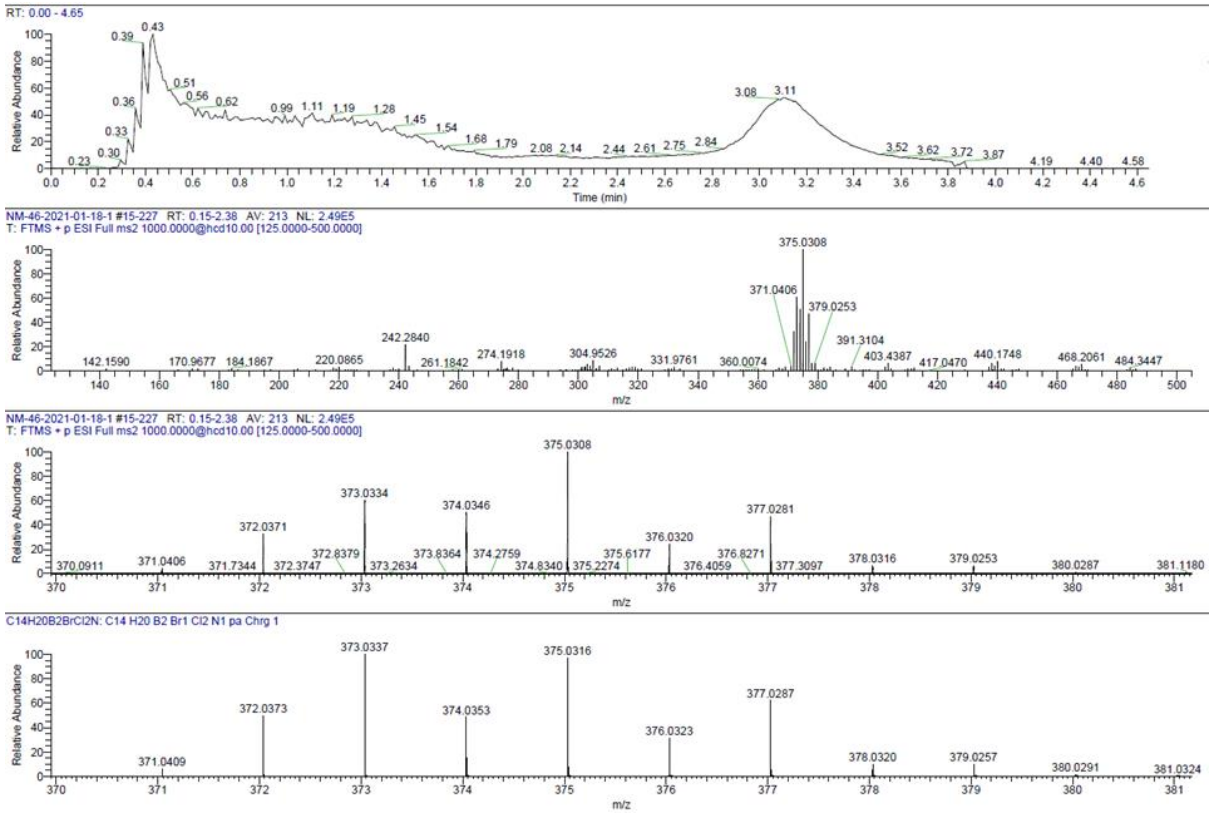

Figure S5.5.37. HRMS spectrum (LIFDI) of **4**.

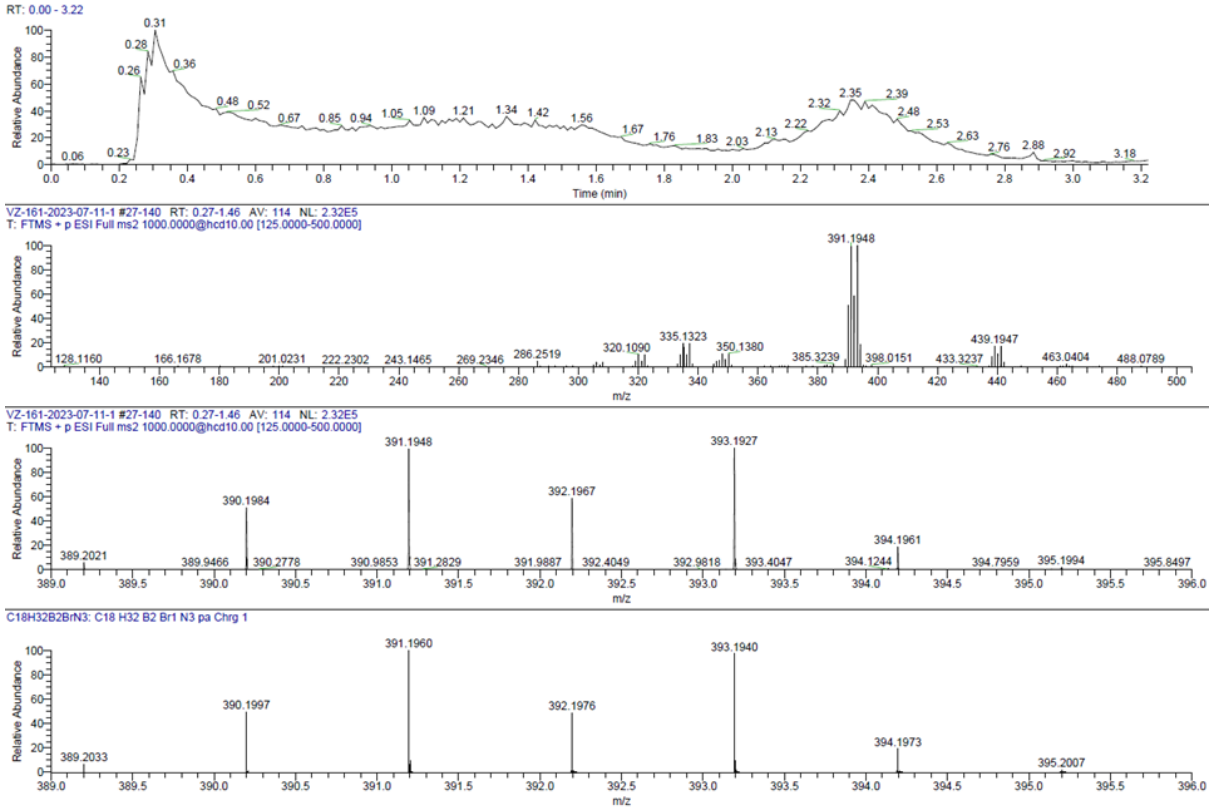

Figure S5.5.38. HRMS spectrum (LIFDI) of **5**.

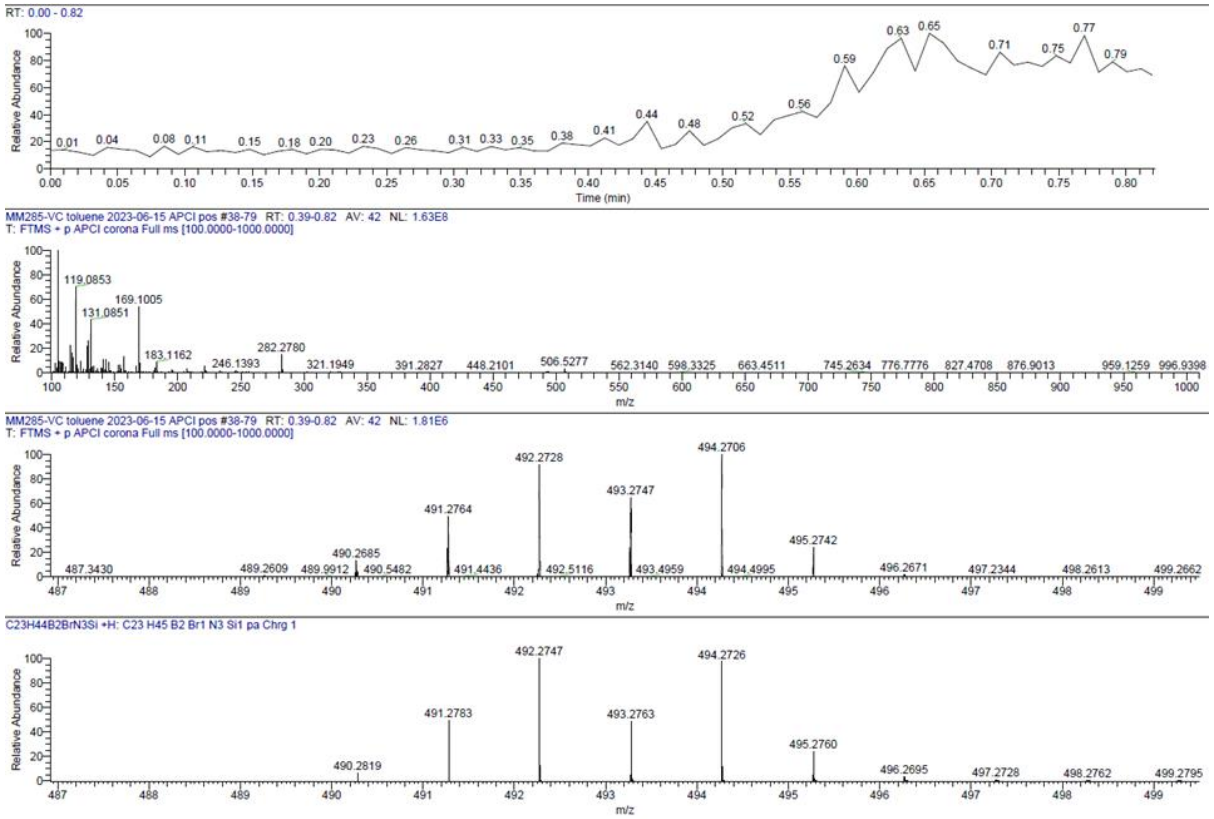

Figure S5.5.39. HRMS spectrum (APCI pos) of **7**.

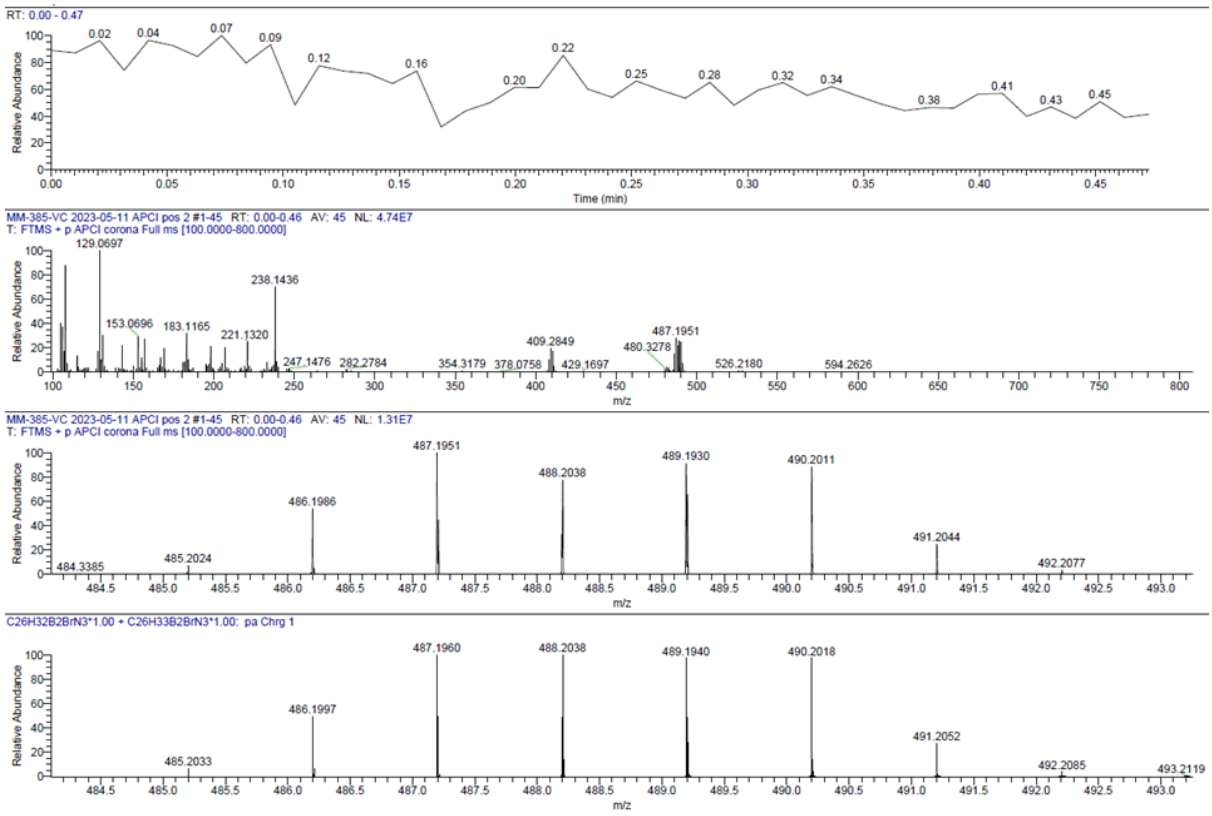

Figure S5.5.40. HRMS spectrum (APCI pos) of **9** (approx. 1:1 mixture [M] and $[M+H]^+$).

UV-vis spectra

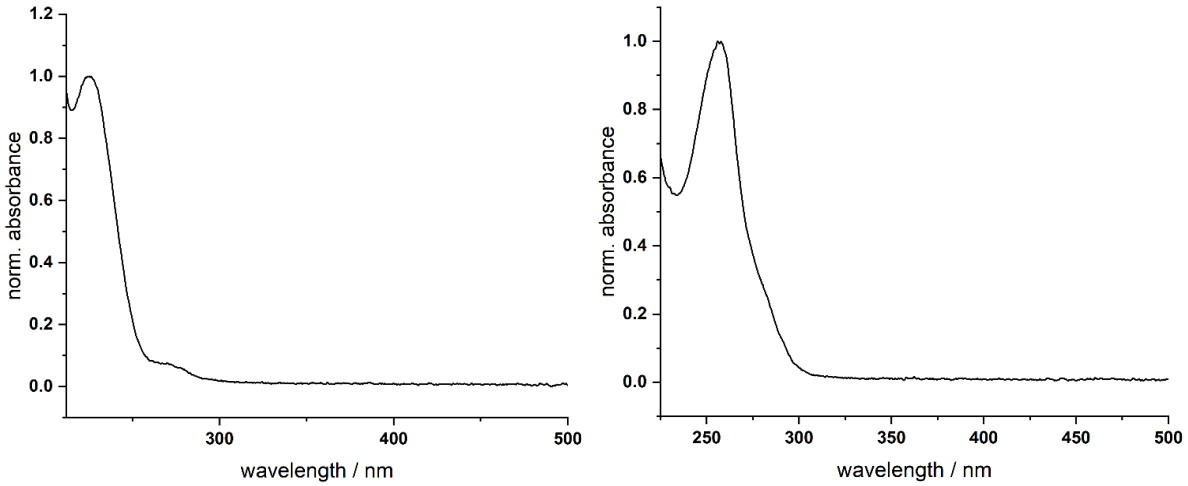

Figure S5.5.41. Normalized absorption spectra of **4** (left) and **9** (right) in THF.

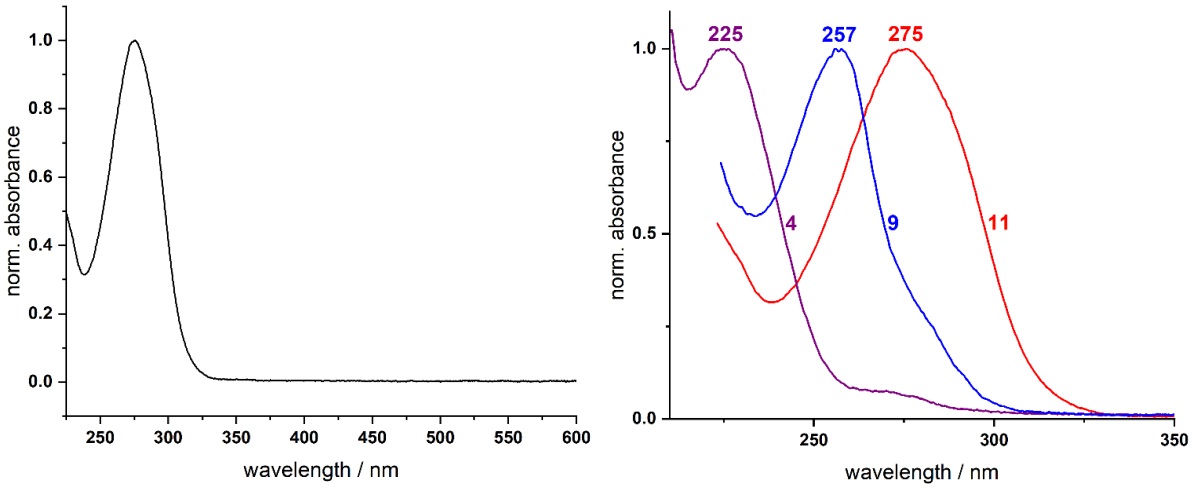

Figure S5.5.42. Normalized absorption spectrum of **11** (left) and comparison of the normalized absorption spectra of **4** (black), **9** (blue) and **11** (red) in THF (right).

Cyclic voltammorgrams

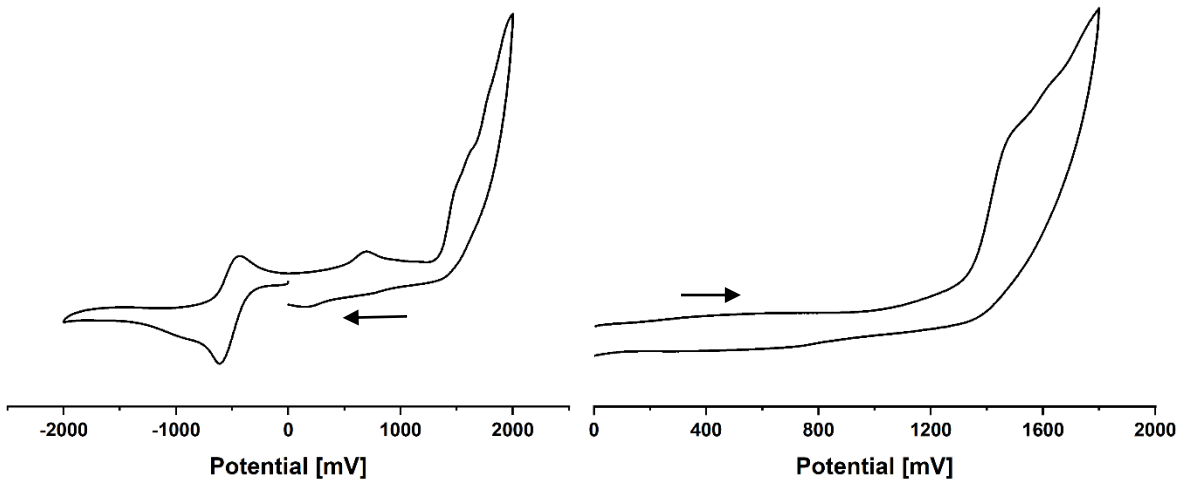

Figure S5.5.43. Cyclic voltammograms of **4** in DCM (vs. $[Cp_2Fe]^{0/+}$, scan rate: 250 mV s^{-1}).

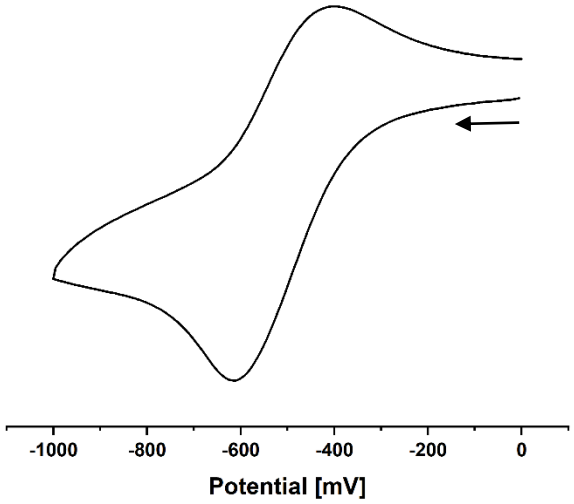

Figure S5.5.44. Cyclic voltammogram of the reduction process of **4** in DCM (vs. $[Cp_2Fe]^{0/+}$, scan rate: 250 mV s^{-1}).

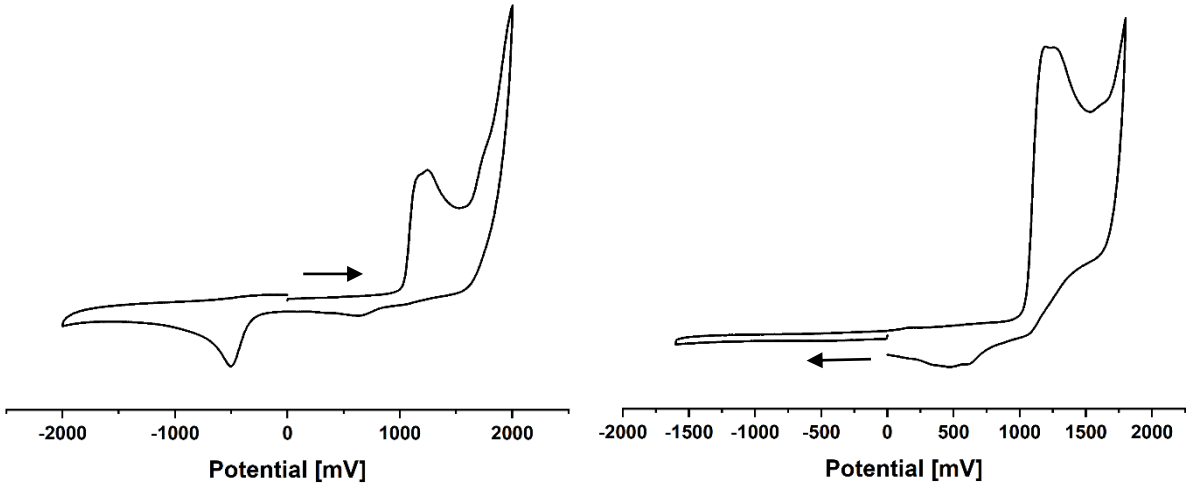

Figure S5.5.45. Cyclic voltammograms of **9** in DCM (vs. $[Cp_2Fe]^{0/+}$, scan rate: 250 mV s^{-1}).

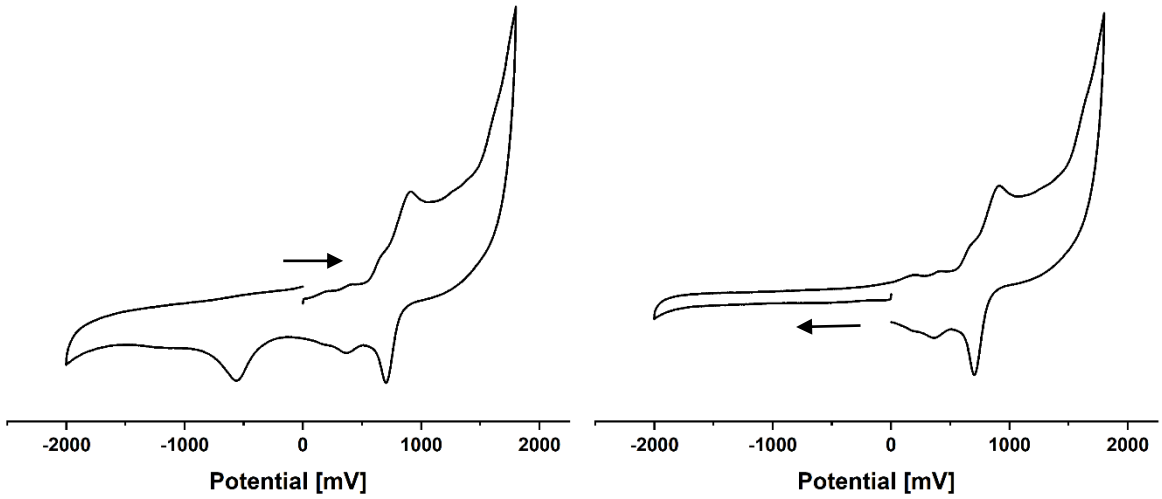

Figure S5.5.46. Cyclic voltammograms of **11** in DCM (vs. $[Cp_2Fe]^{0/+}$, scan rate: 250 mV s^{-1}).

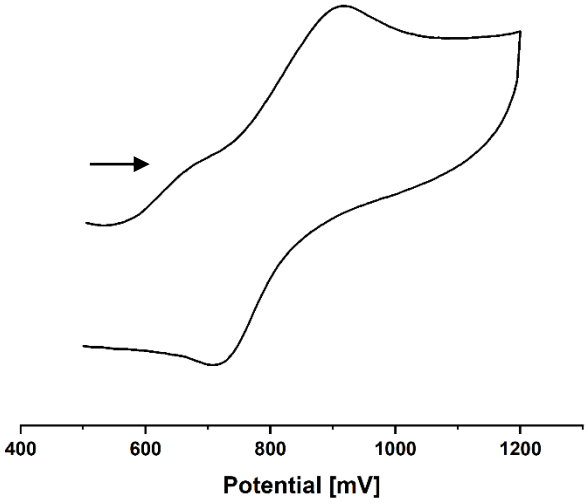

Figure S5.5.47. Cyclic voltammogram of **11** in DCM (vs. $[Cp_2Fe]^{0/+}$, scan rate: 250 mV s^{-1}).

GPC traces

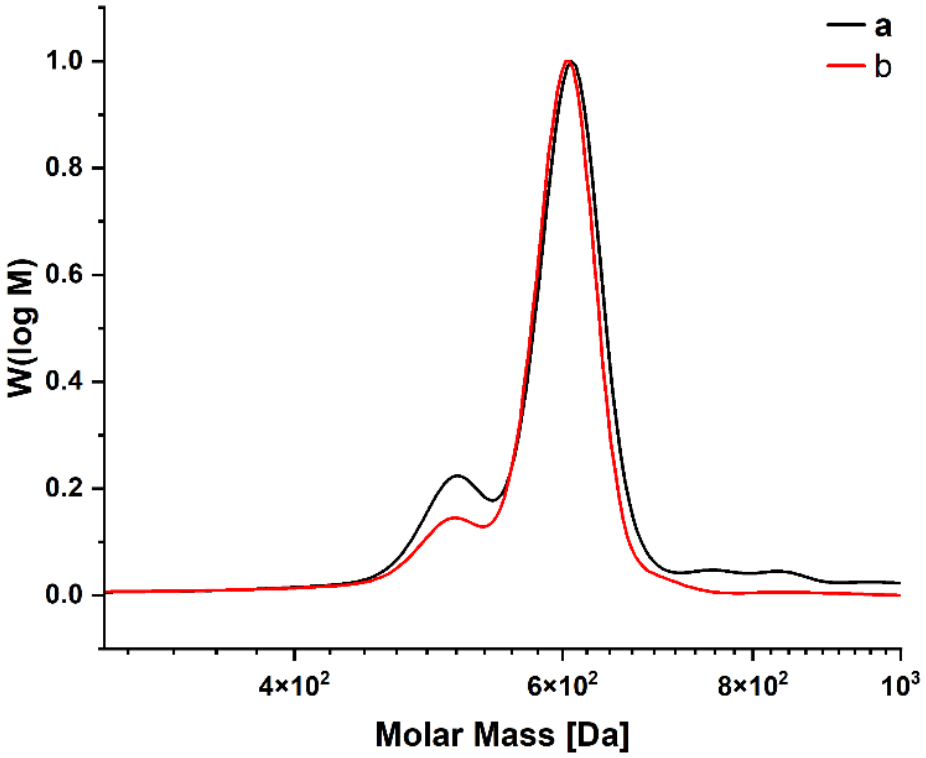

Figure S5.5.48. Normalized gel permeation chromatography (GPC) traces of **7** (a) and of the reaction of **4** with **6** (1:2 ratio) (b) detected by UV-vis detector at 280 nm.

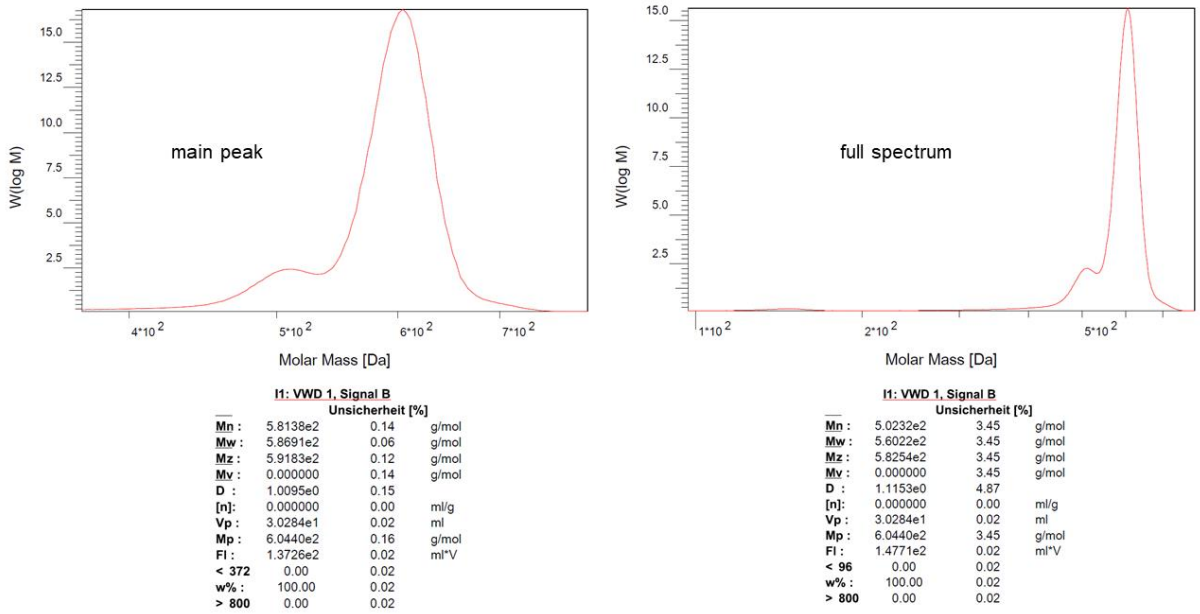

Figure S5.5.49. Original GPC data of **7** (in THF, vs polystyrene standard).

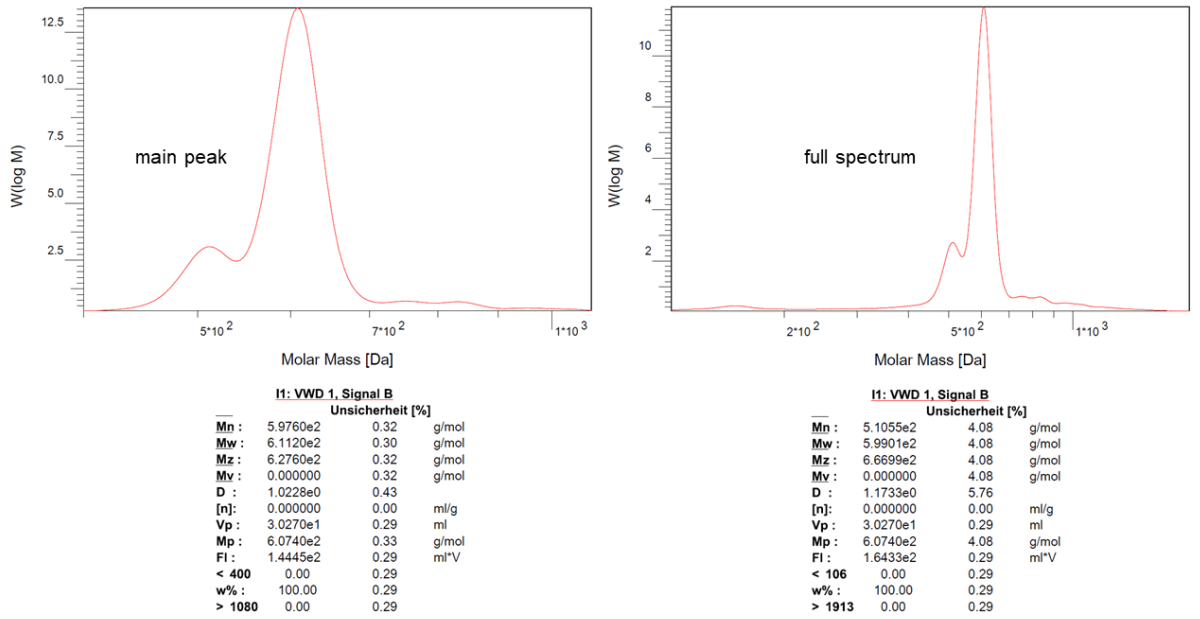

Figure S5.5.50. Original GPC data of the reaction of **4** with **6** (1:2 ratio) in *o*-DFB at 80 °C for 1 week (in THF, vs polystyrene standard).

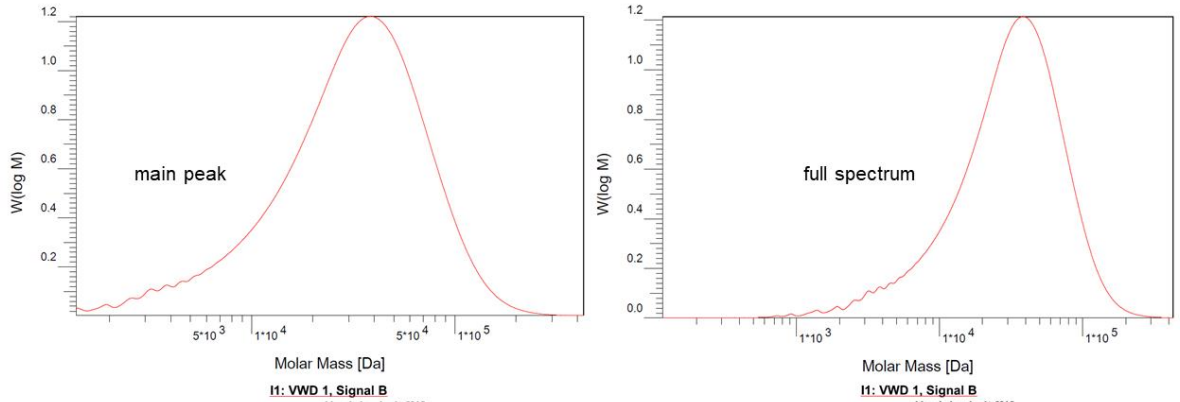

I1: VWD 1, Signal B

		Unsicherheit [%]	
Mn :	1.8736e4	0.14	g/mol
Mw :	4.0405e4	0.05	g/mol
Mz :	6.6037e4	0.12	g/mol
Mv :	0.000000	0.14	g/mol
D :	2.1565e0	0.14	
[n]:	0.000000	0.00	ml/g
Vp :	1.9647e1	0.00	ml
Mp :	4.4811e4	0.16	g/mol
FI :	8.2005e3	0.00	ml*V
< 1368	0.00	0.00	
w% :	100.00	0.00	
> 429205	0.00	0.00	

I1: VWD 1, Signal B

		Unsicherheit [%]	
Mn :	1.6349e4	0.14	g/mol
Mw :	4.0184e4	0.06	g/mol
Mz :	6.6029e4	0.12	g/mol
Mv :	0.000000	0.14	g/mol
D :	2.4579e0	0.15	
[n]:	0.000000	0.00	ml/g
Vp :	1.9647e1	0.00	ml
Mp :	4.4811e4	0.16	g/mol
FI :	8.2465e3	0.00	ml*V
< 115	0.00	0.00	
w% :	100.00	0.00	
> 429205	0.00	0.00	

Figure S5.5.51. Original GPC data of **11** (trial 1) (in THF, vs polystyrene standard).

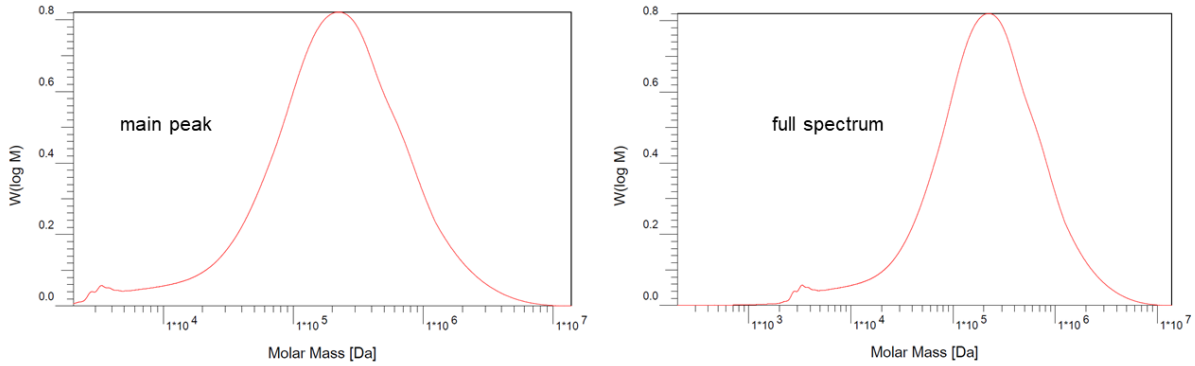

I1: VWD 1, Signal B

		Unsicherheit [%]	
Mn :	6.8642e4	3.15	g/mol
Mw :	4.1452e5	3.15	g/mol
Mz :	1.4131e6	3.15	g/mol
Mv :	0.000000	3.15	g/mol
D :	6.0388e0	4.45	
[n]:	0.000000	0.00	ml/g
Vp :	1.6954e1	0.01	ml
Mp :	3.0491e5	3.16	g/mol
FI :	6.6954e3	0.01	ml*V
< 2024	0.00	0.01	
w% :	100.00	0.01	
> 13809596	0.00	0.01	

I1: VWD 1, Signal B

		Unsicherheit [%]	
Mn :	5.7418e4	3.16	g/mol
Mw :	4.1358e5	3.16	g/mol
Mz :	1.4131e6	3.16	g/mol
Mv :	0.000000	3.16	g/mol
D :	7.2030e0	4.46	
[n]:	0.000000	0.00	ml/g
Vp :	1.6954e1	0.01	ml
Mp :	3.0491e5	3.16	g/mol
FI :	6.7107e3	0.01	ml*V
< 200	0.00	0.01	
w% :	100.00	0.01	
> 13809596	0.00	0.01	

Figure S5.5.52. Original GPC data of **11** (trial 2) (in THF, vs polystyrene standard).

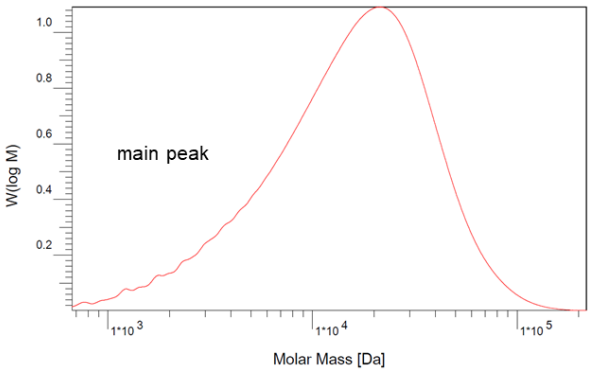

I1: VWD 1, Signal B

		Unsicherheit [%]	
Mn :	8.8916e3	8.32	g/mol
Mw :	2.0919e4	8.32	g/mol
Mz :	3.6528e4	8.32	g/mol
Mv :	0.000000	8.32	g/mol
D :	2.3526e0	11.76	
[n]:	0.000000	0.00	ml/g
Vp :	2.1071e1	8.32	ml
Mp :	2.3183e4	8.32	g/mol
FI :	5.5051e3	8.32	ml*V
< 667	0.00	8.32	
w% :	100.00	8.32	
> 218430	0.00	8.32	

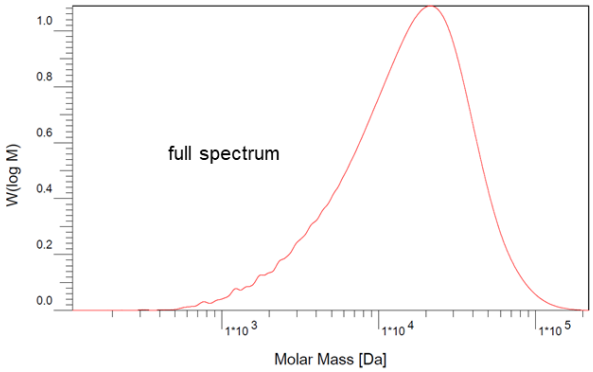

I1: VWD 1, Signal B

		Unsicherheit [%]	
Mn :	8.4494e3	8.32	g/mol
Mw :	2.0869e4	8.32	g/mol
Mz :	3.6526e4	8.32	g/mol
Mv :	0.000000	8.32	g/mol
D :	2.4699e0	11.76	
[n]:	0.000000	0.00	ml/g
Vp :	2.1071e1	8.32	ml
Mp :	2.3183e4	8.32	g/mol
FI :	5.5184e3	8.32	ml*V
< 110	0.00	8.32	
w% :	100.00	8.32	
> 218430	0.00	8.32	

Figure S5.5.53. Original GPC data of **11** (trial 3) (in THF, vs polystyrene standard).

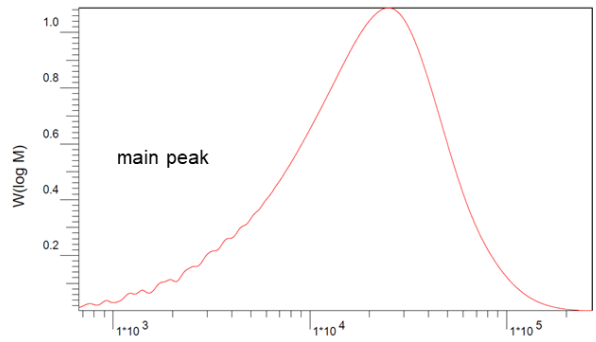

I1: VWD 1, Signal B

		Unsicherheit [%]	
Mn :	1.0165e4	0.14	g/mol
Mw :	2.5272e4	0.05	g/mol
Mz :	4.5600e4	0.12	g/mol
Mv :	0.000000	0.14	g/mol
D :	2.4863e0	0.14	
[n]:	0.000000	0.00	ml/g
Vp :	2.0691e1	0.00	ml
Mp :	2.7373e4	0.16	g/mol
FI :	9.4121e3	0.00	ml*V
< 667	0.00	0.00	
w% :	100.00	0.00	
> 271600	0.00	0.00	

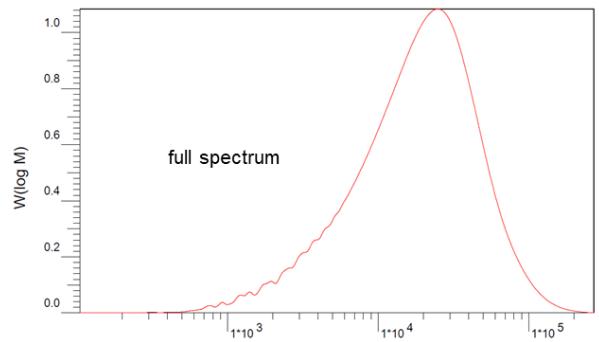

I1: VWD 1, Signal B

		Unsicherheit [%]	
Mn :	9.5272e3	0.14	g/mol
Mw :	2.5212e4	0.07	g/mol
Mz :	4.5598e4	0.13	g/mol
Mv :	0.000000	0.14	g/mol
D :	2.6463e0	0.15	
[n]:	0.000000	0.00	ml/g
Vp :	2.0691e1	0.00	ml
Mp :	2.7373e4	0.17	g/mol
FI :	9.4351e3	0.00	ml*V
< 104	0.00	0.00	
w% :	100.00	0.00	
> 271600	0.00	0.00	

Figure S5.5.54. Original GPC data of **11** (trial 4) (in THF, vs polystyrene standard).

5.6 Synthesis of 1,2,5-Azadiborolanes as Building Blocks for Oligo- and Poly(iminoborane)s

NMR spectra

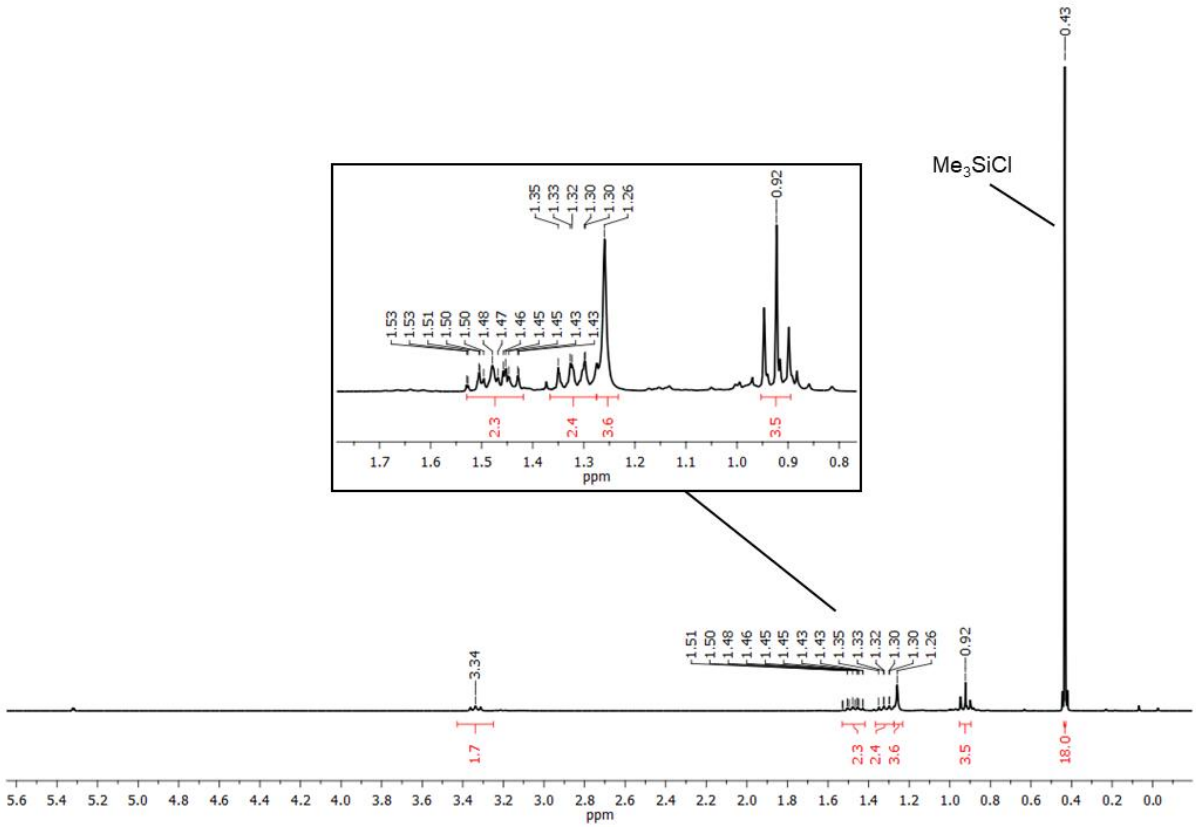

Figure S5.6.1. ^{1}H NMR spectrum (300 MHz) of **6** in CD_2Cl_2.

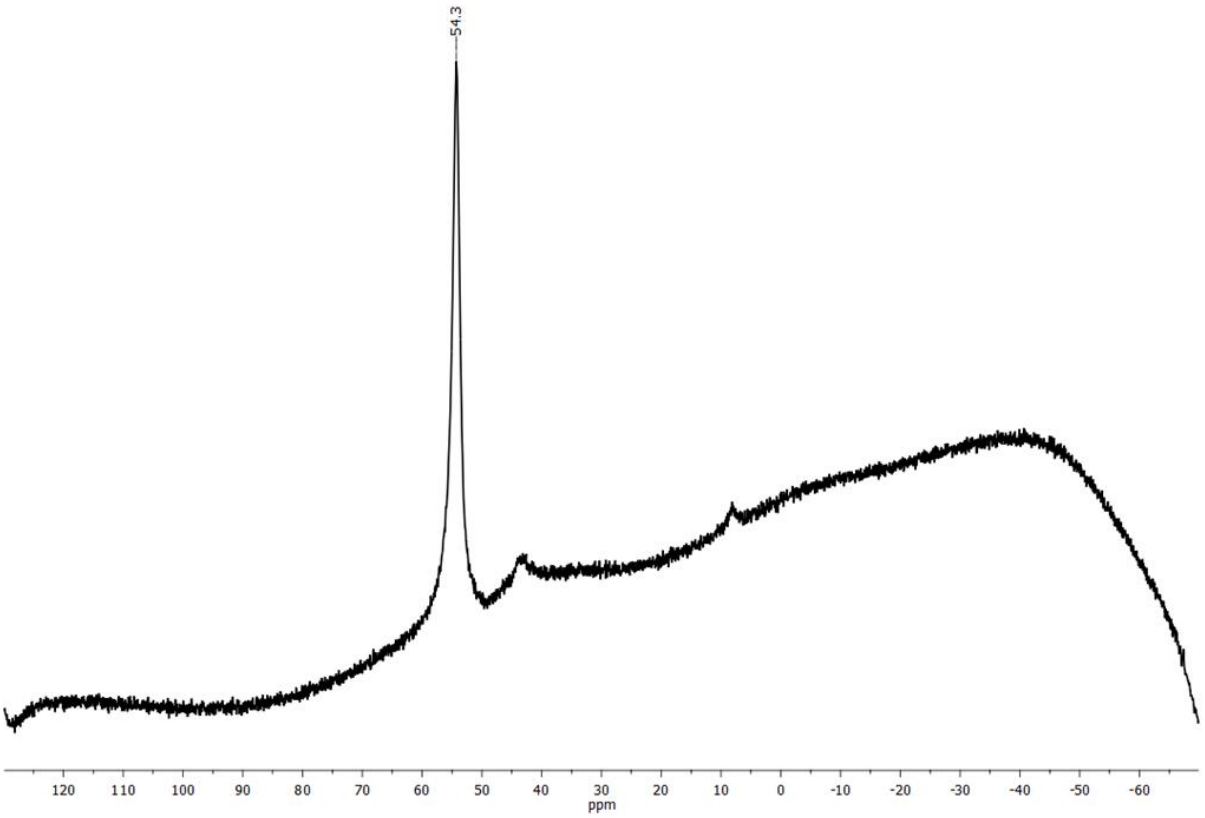

Figure S5.6.2. $^{11}B\{^{1}H\}$ NMR spectrum (96 MHz) of **6** in CD_2Cl_2.

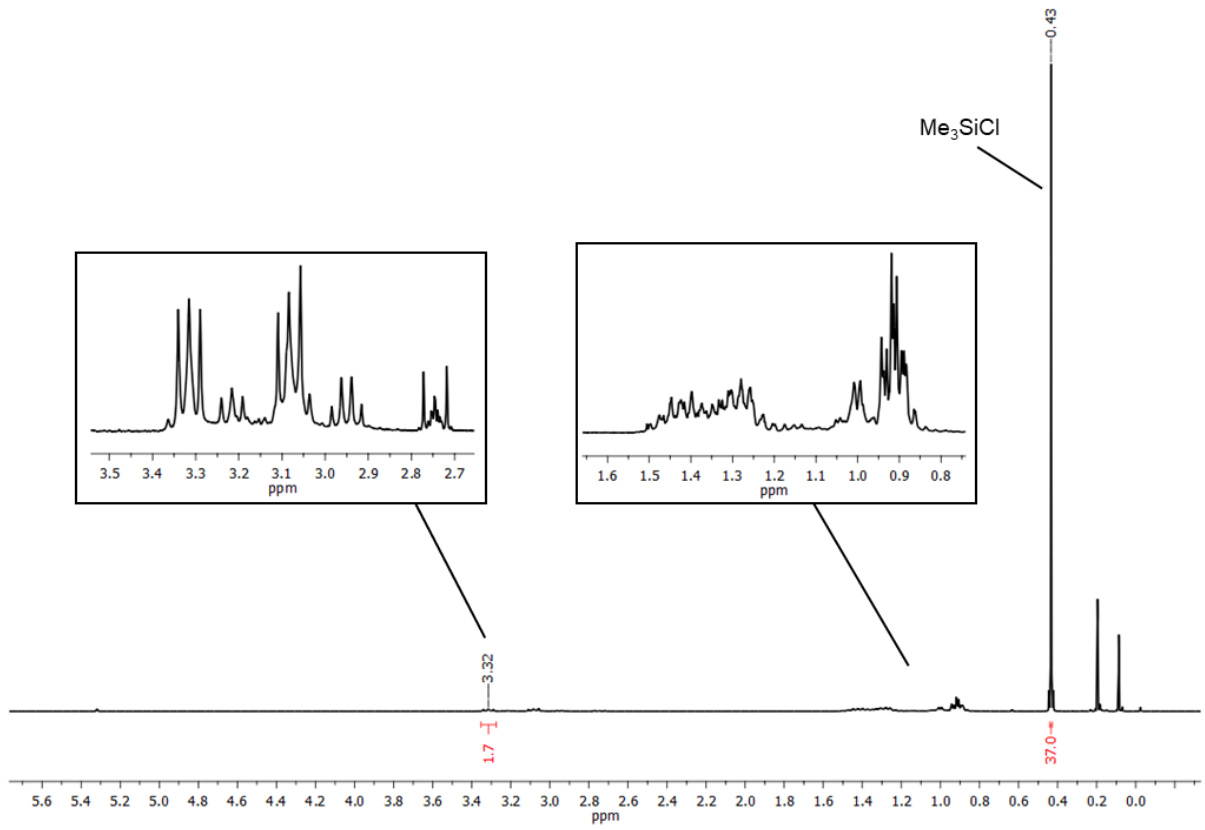

Figure S5.6.3. ^{1}H NMR spectrum (300 MHz) of **6** with $BuN(SiMe_3)_2$ after 30 min in CD_2Cl_2.

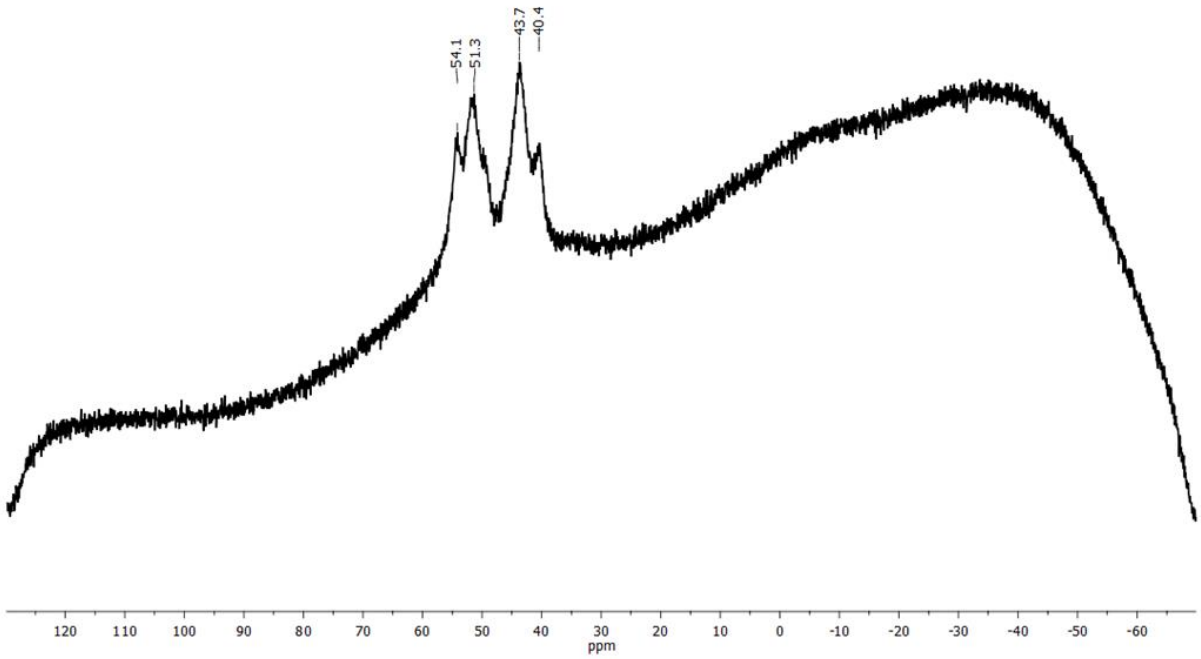

Figure S5.6.4. $^{11}B\{^{1}H\}$ NMR spectrum (96 MHz) of **6** with $BuN(SiMe_3)_2$ after 30 min in CD_2Cl_2.

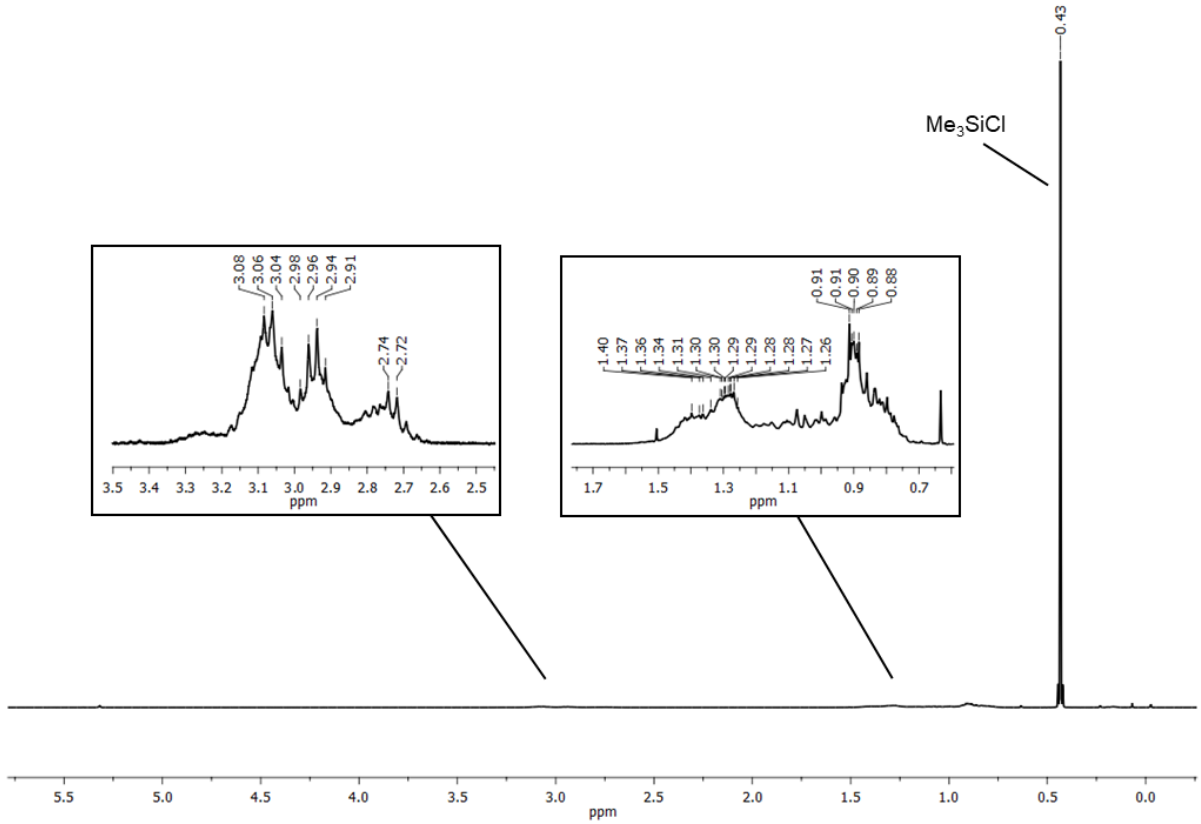

Figure S5.6.5. ^{1}H NMR spectrum (300 MHz) of **6** with $BuN(SiMe_3)_2$ after one night in CD_2Cl_2.

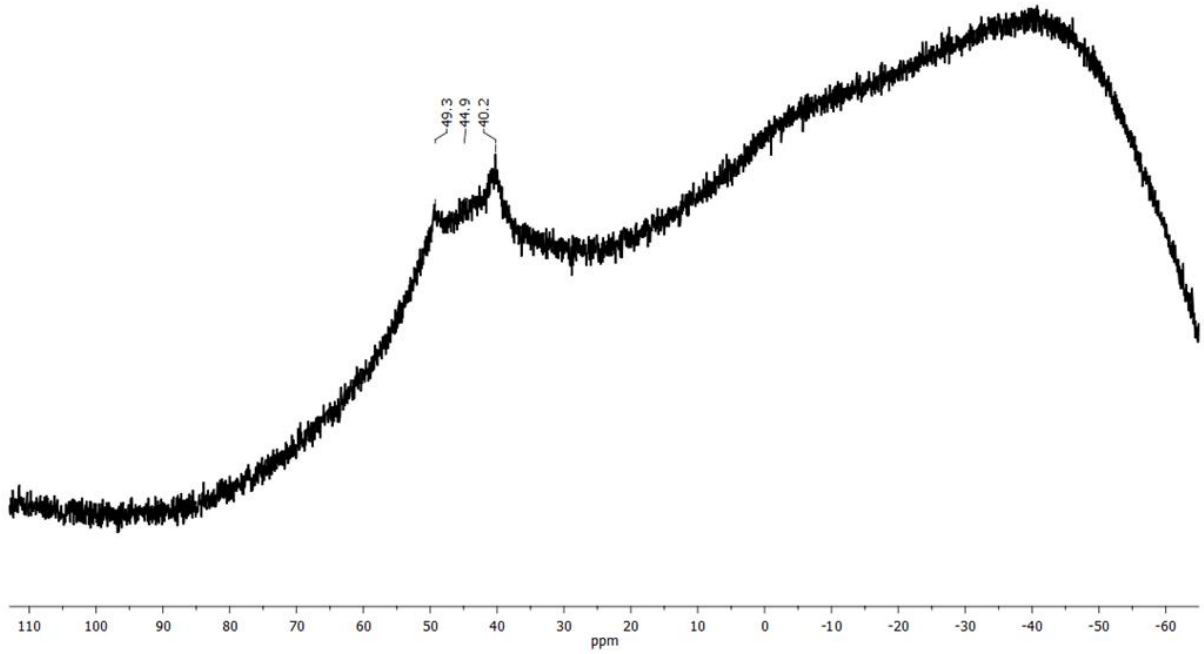

Figure S5.6.6. $^{11}B\{^{1}H\}$ NMR spectrum (96 MHz) of **6** with $BuN(SiMe_3)_2$ after one night in CD_2Cl_2.

5.7 Poly(thiophene iminoborane): A Poly(thiophene vinylene) (PTV) Analogue with a Fully B=N-Doped Backbone

NMR spectra

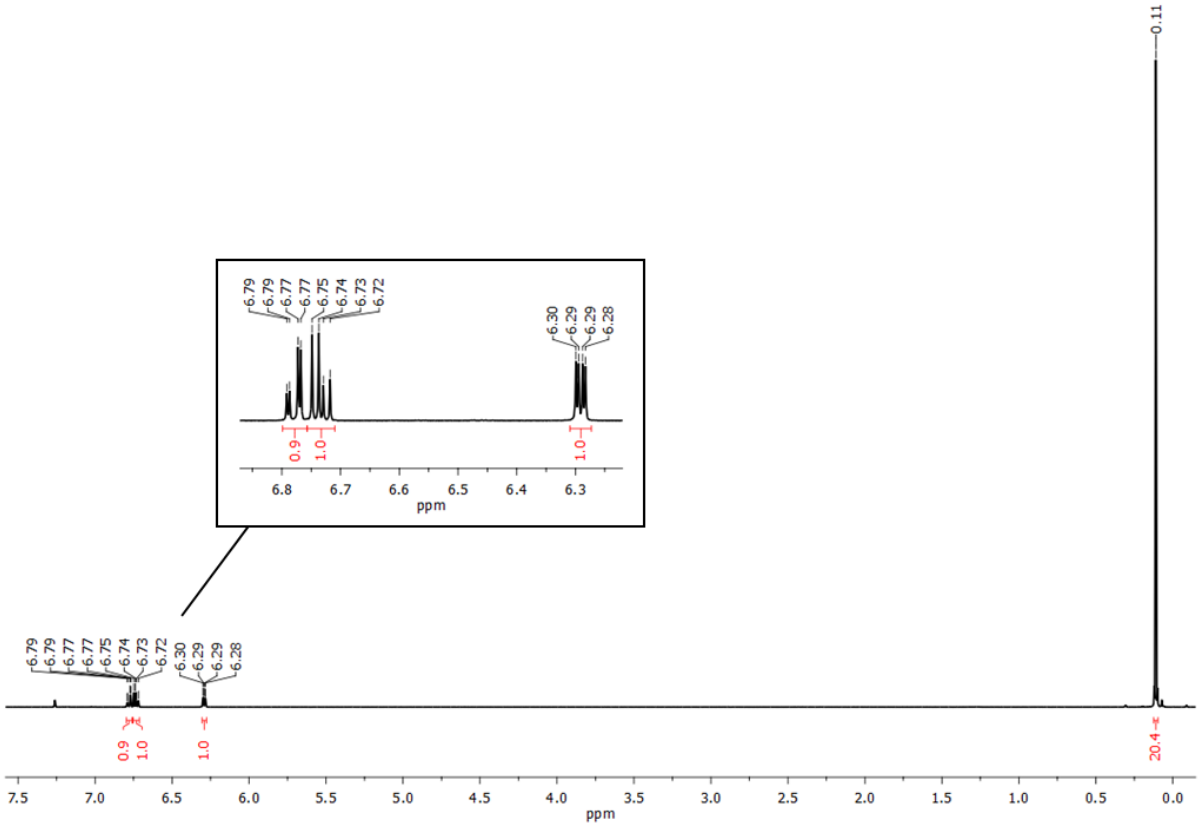

Figure S5.7.1. ^{1}H NMR spectrum (300 MHz) of *N,N*-bis(trimethylsilyl)-2-aminothiophene in $CDCl_3$.

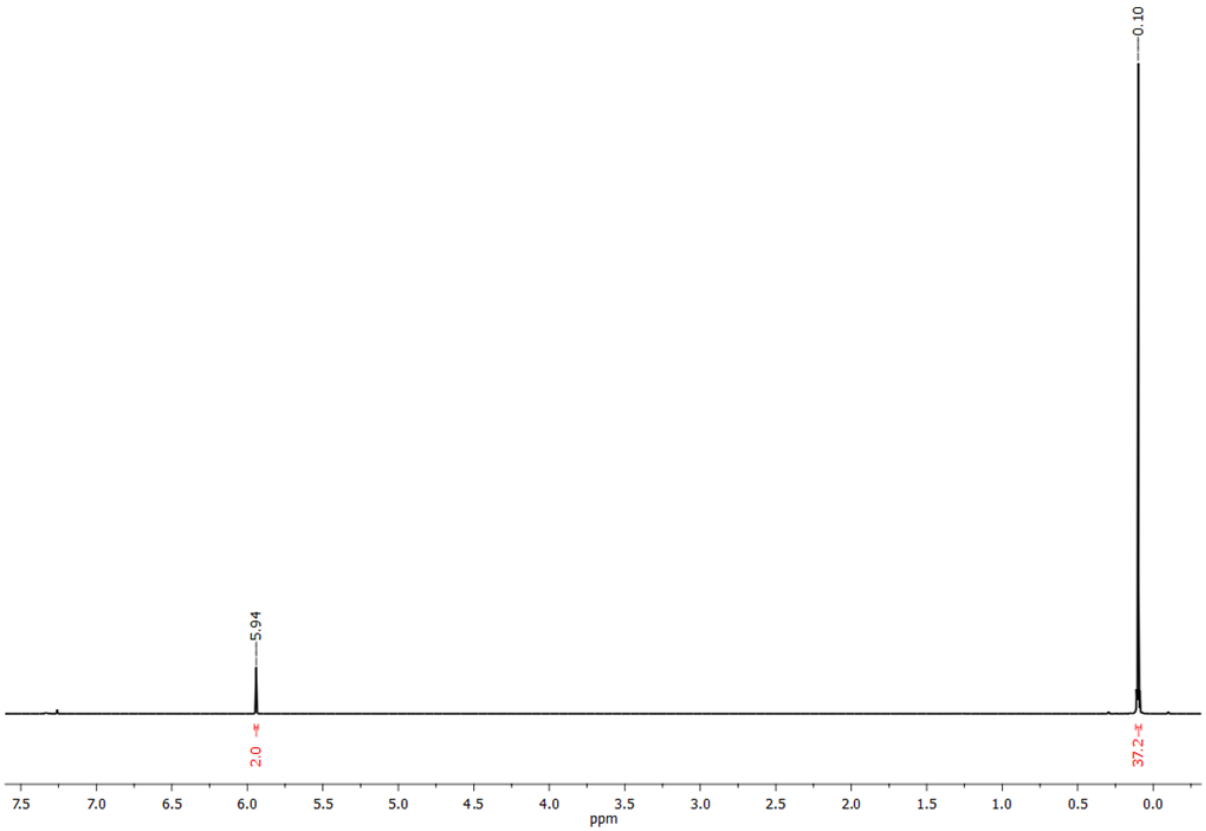

Figure S5.7.2. ^{1}H NMR spectrum (300 MHz) of **1** in $CDCl_3$.

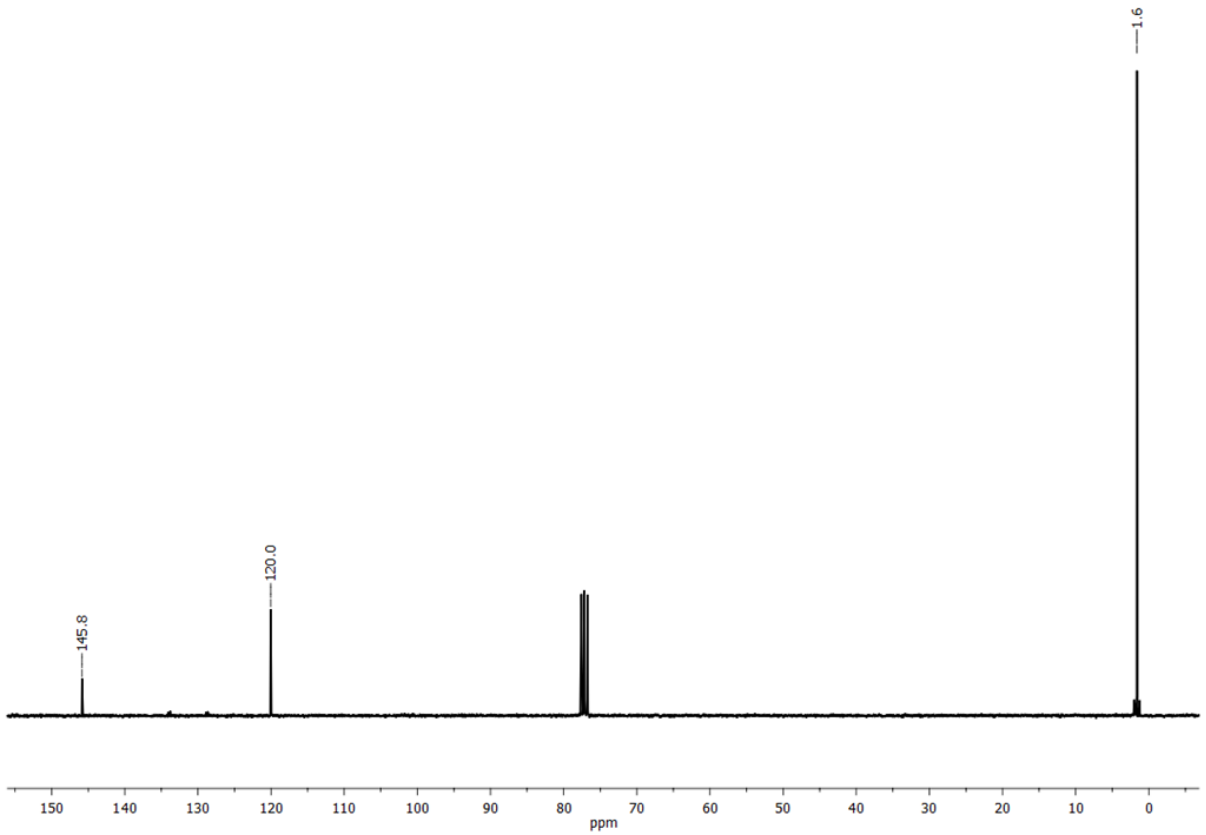

Figure S5.7.3. $^{13}C\{^{1}H\}$ NMR spectrum (76 MHz) of **1** in $CDCl_3$.

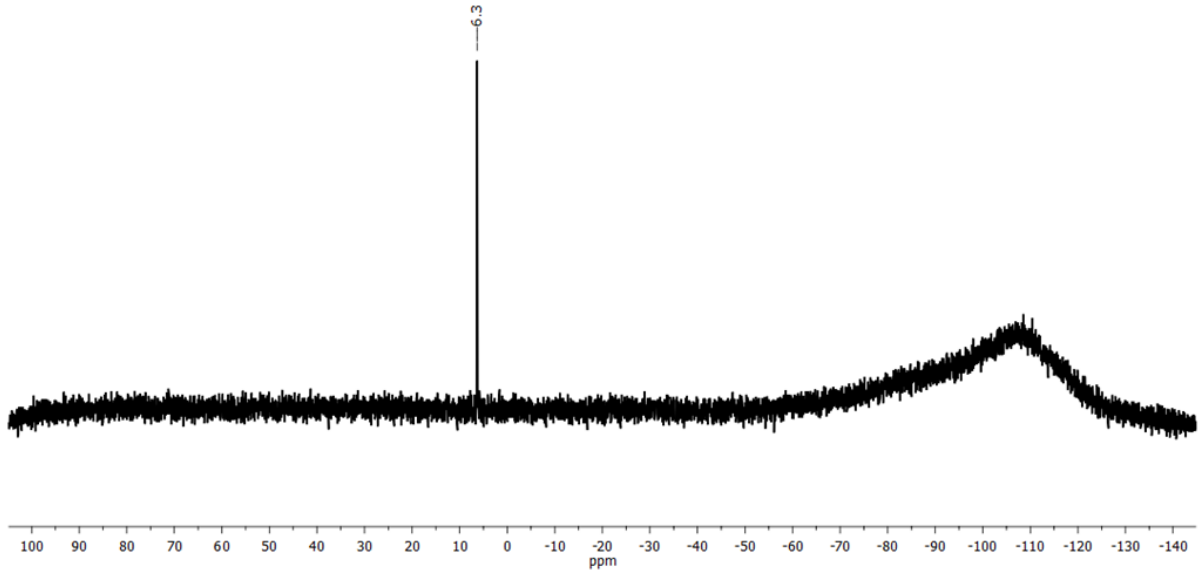

Figure S5.7.4. $^{29}Si\{^{1}H]$ NMR spectrum (60 MHz) of **1** in $CDCl_3$.

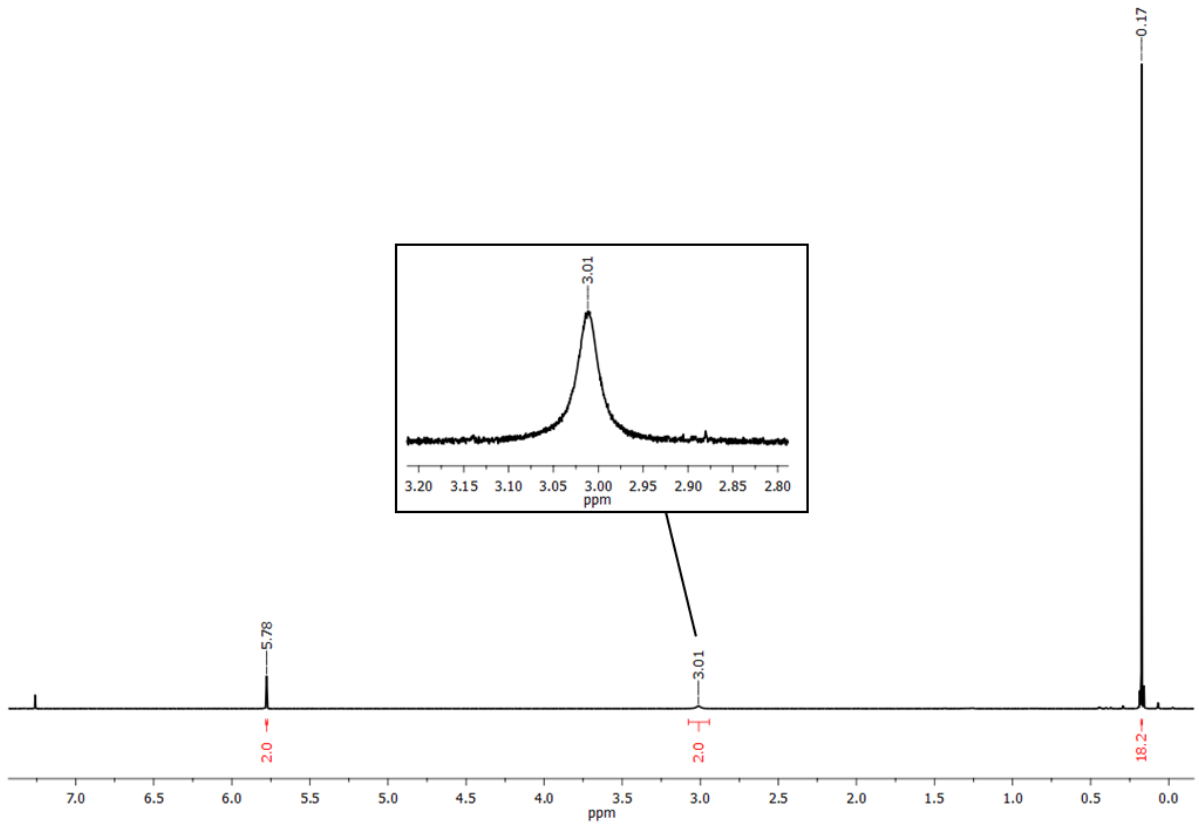

Figure S5.7.5. ^{1}H NMR spectrum (300 MHz) of **3** in $CDCl_3$.

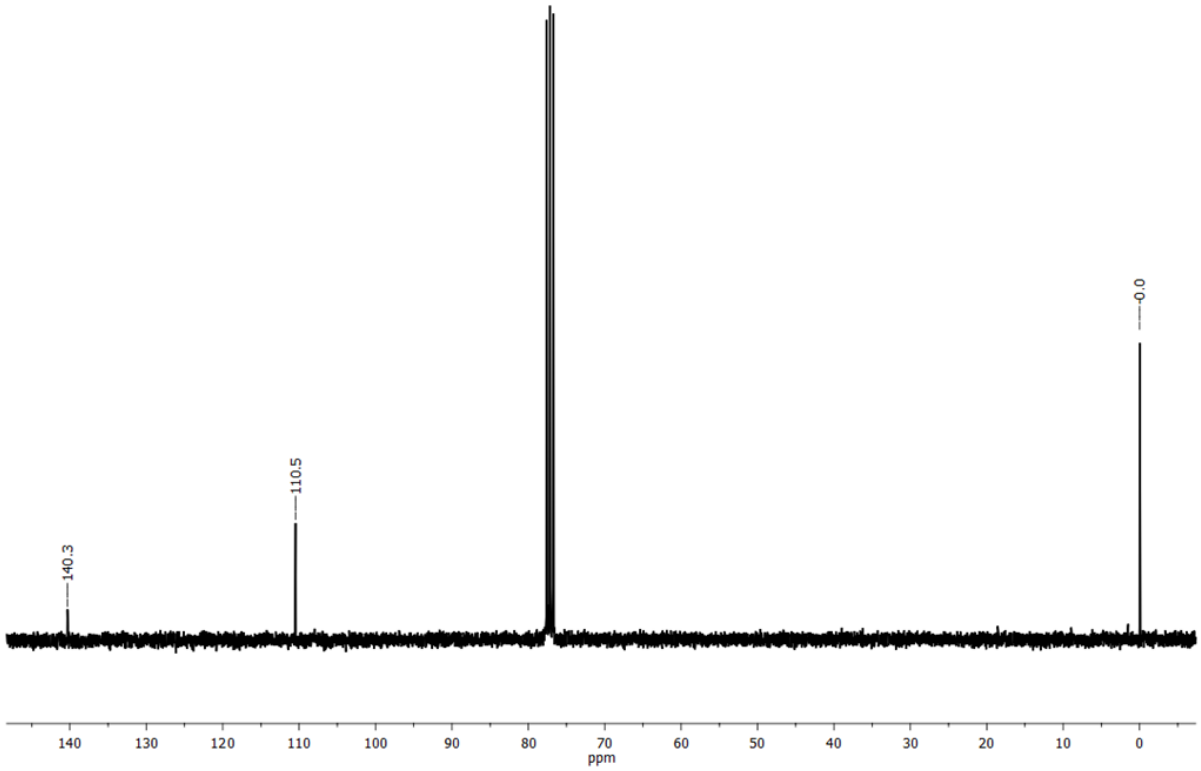

Figure S5.7.6. $^{13}C\{^{1}H\}$ NMR spectrum (76 MHz) of **3** in $CDCl_3$.

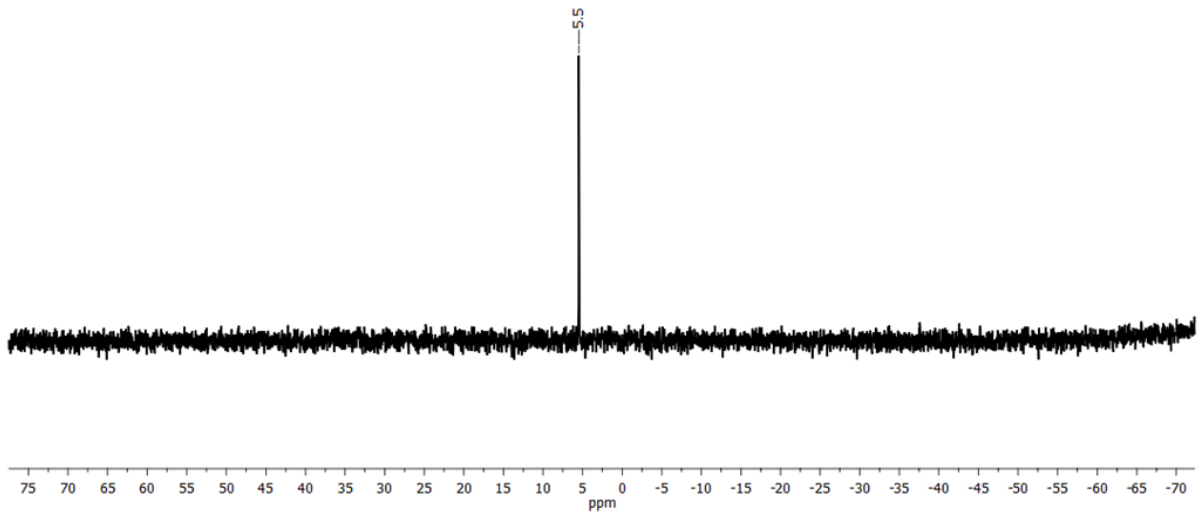

Figure S5.7.7. $^{29}Si\{^{1}H]$ NMR spectrum (60 MHz) of **3** in $CDCl_3$.

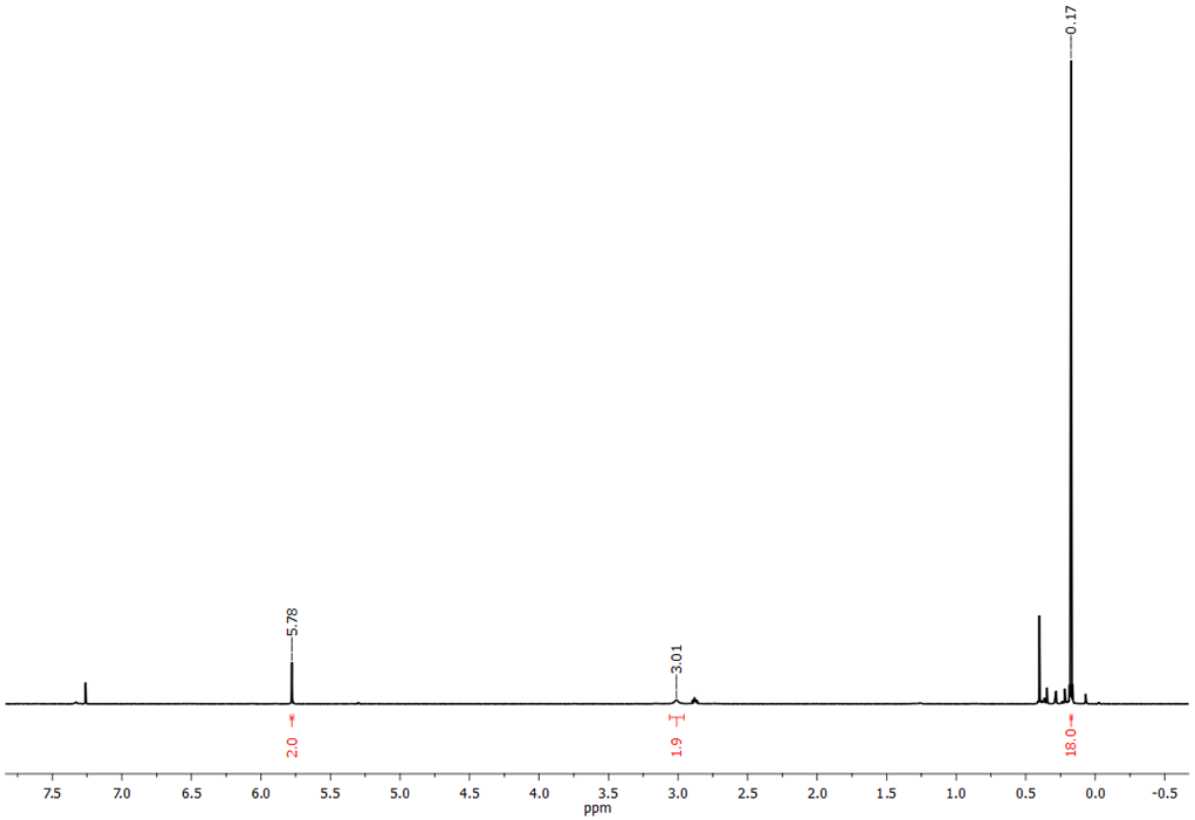

Figure S5.7.8. ^{1}H NMR spectrum (300 MHz) of **3** after synthesis from **2** in $CDCl_3$.

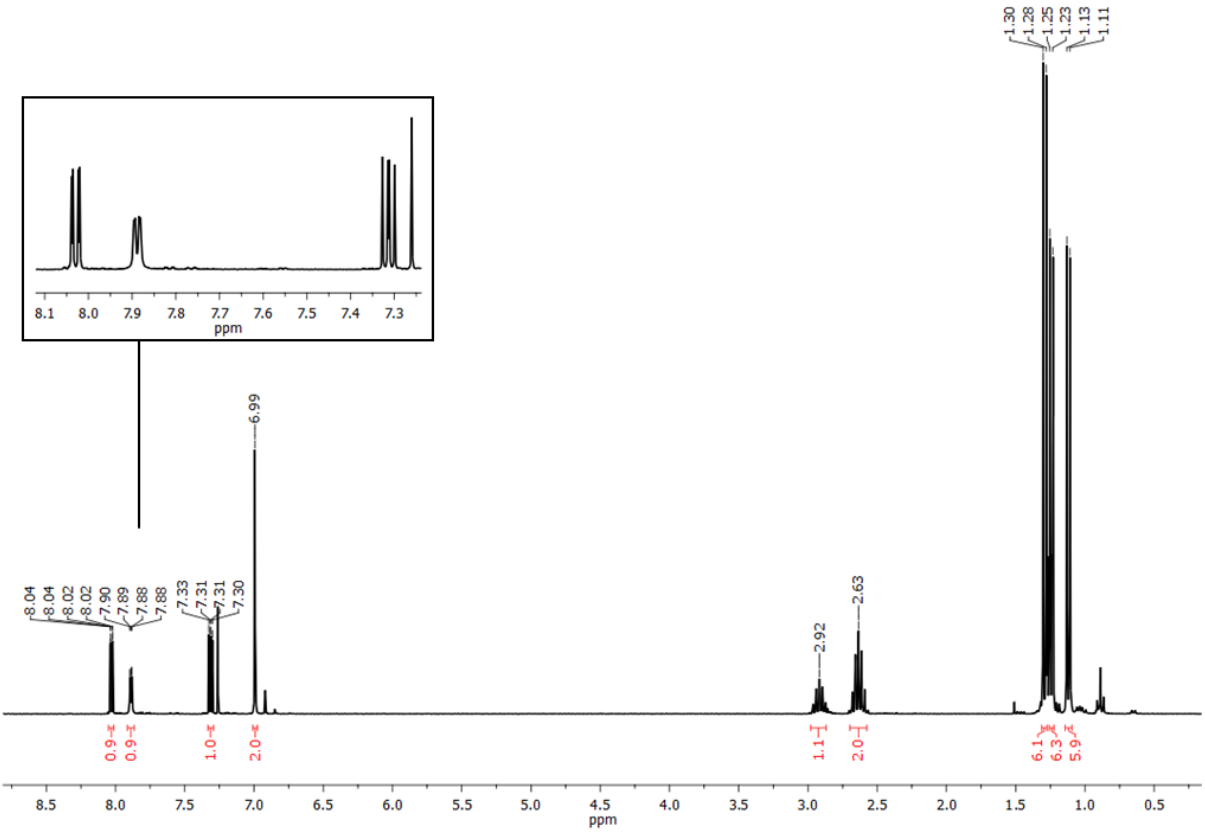

Figure S5.7.9. ^{1}H NMR spectrum (300 MHz) of **4** in $CDCl_3$.

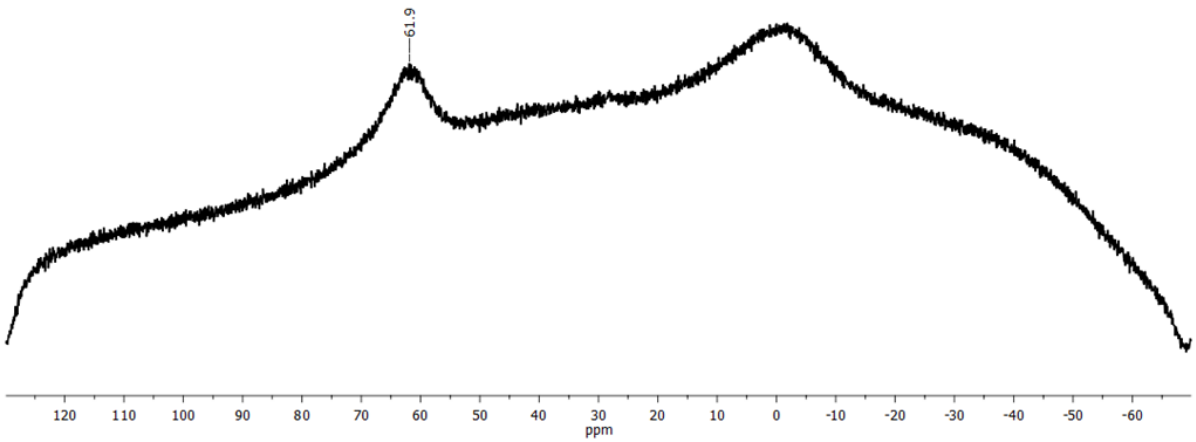

Figure S5.7.10. $^{11}B\{^{1}H\}$ NMR spectrum (96 MHz) of **4** in $CDCl_3$.

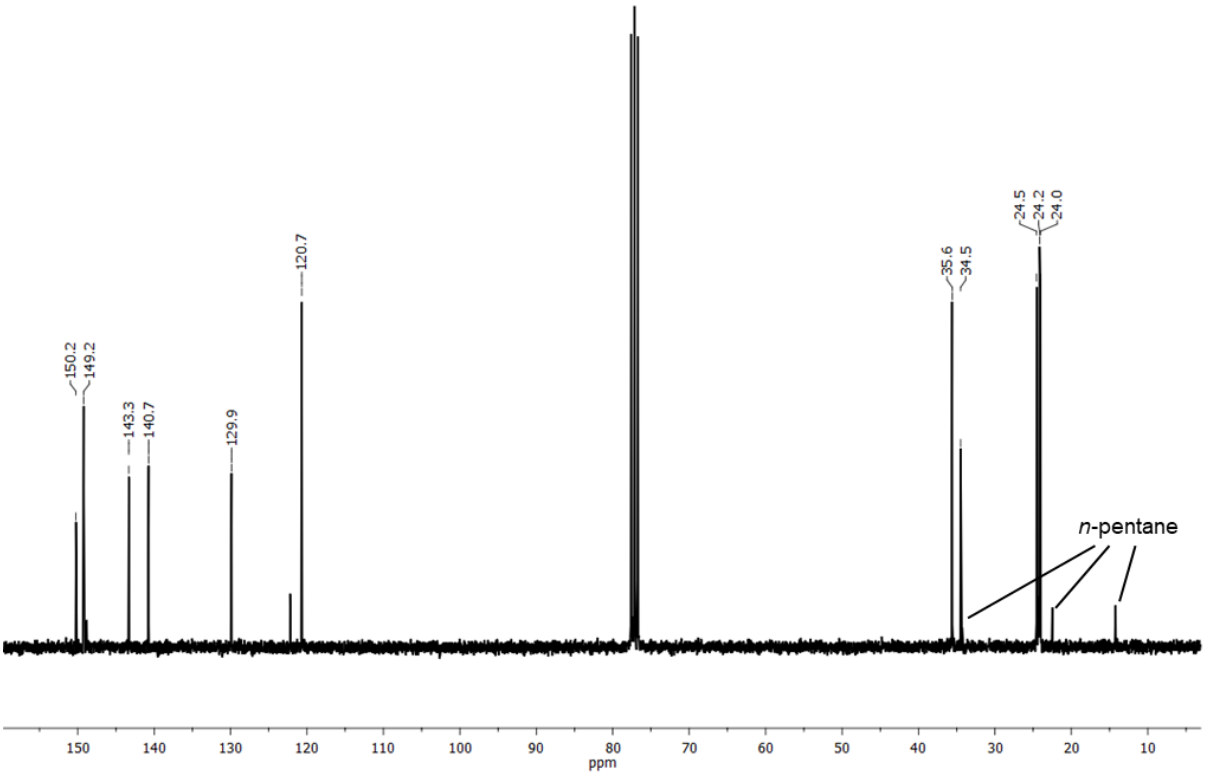

Figure S5.7.11. $^{13}C\{^{1}H\}$ NMR spectrum (76 MHz) of **4** in $CDCl_3$.

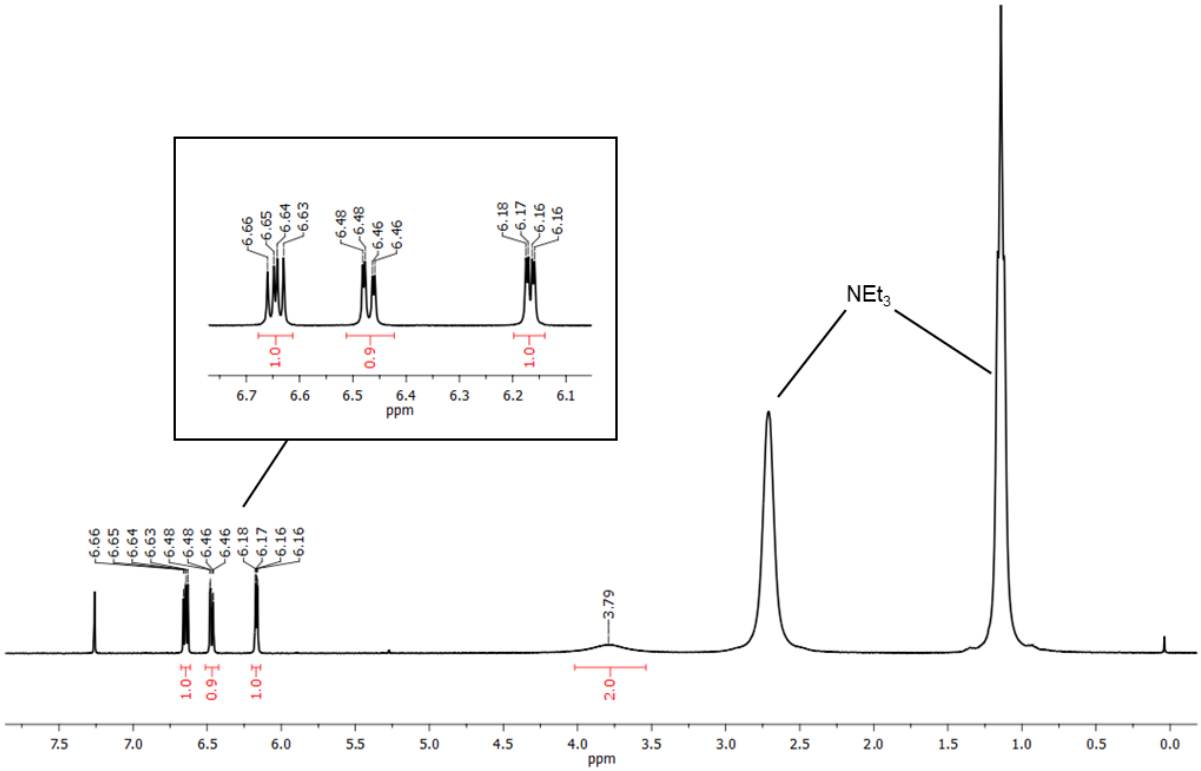

Figure S5.7.12. ^{1}H NMR spectrum (300 MHz) of 2-aminothiophene after generation from **5** in presence of NEt_3 in $CDCl_3$.

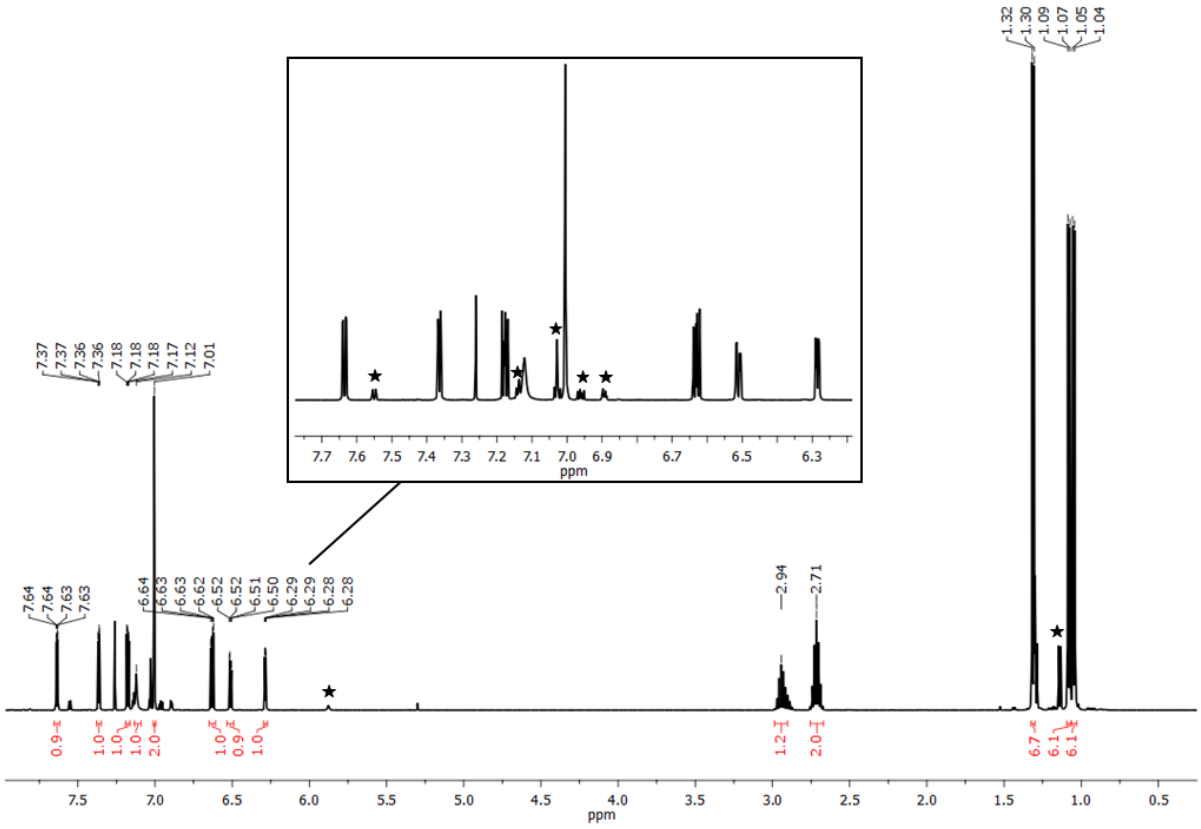

Figure S5.7.13. ^{1}H NMR spectrum (500 MHz) of **6** in $CDCl_3$. The signals marked with an asterisk belong to the minor isomer.

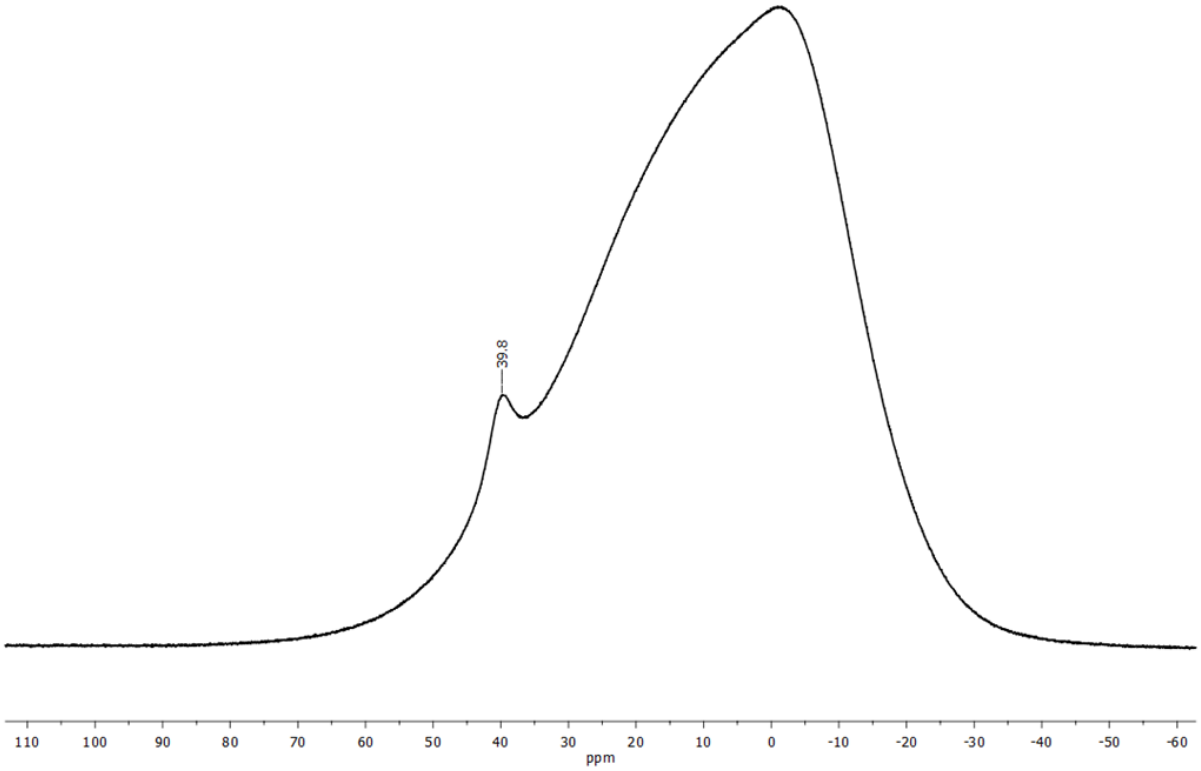

Figure S5.7.14. $^{11}B\{^{1}H\}$ NMR spectrum (160 MHz) of **6** in $CDCl_3$.

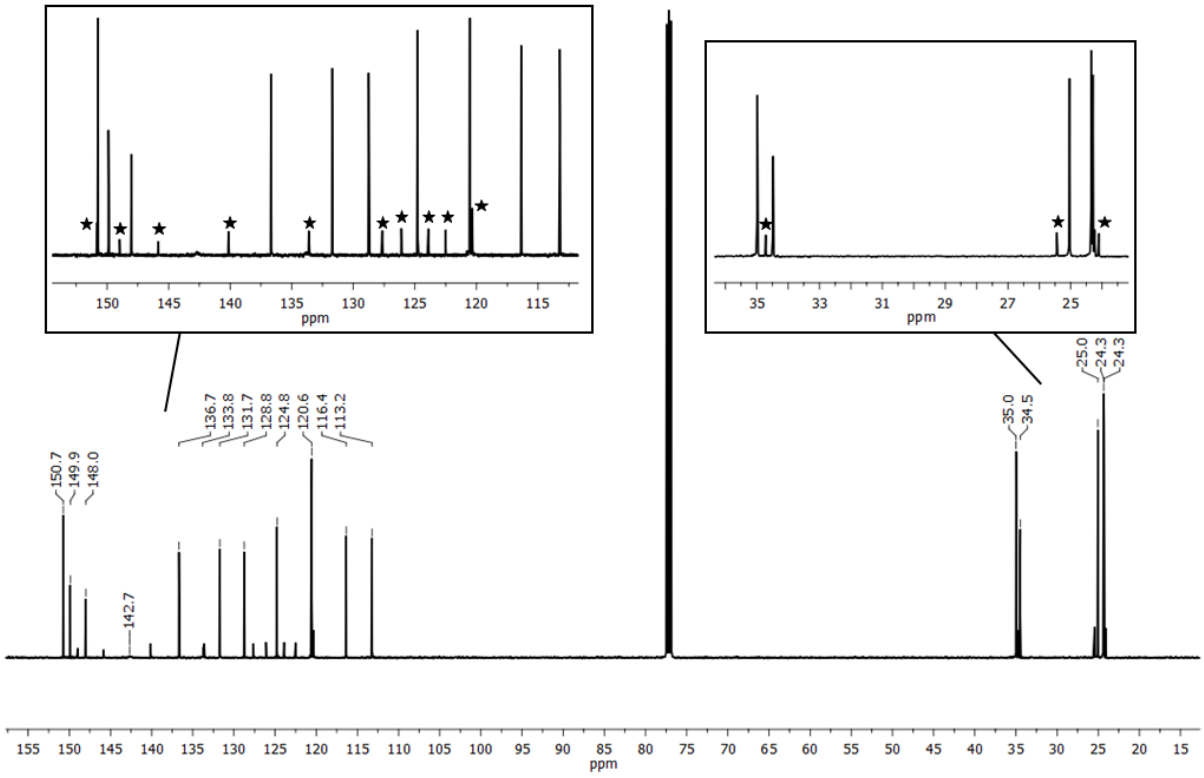

Figure S5.7.15. $^{13}C\{^{1}H\}$ NMR spectrum (126 MHz) of **6** in $CDCl_3$. The signals marked with an asterisk belong to the minor isomer.

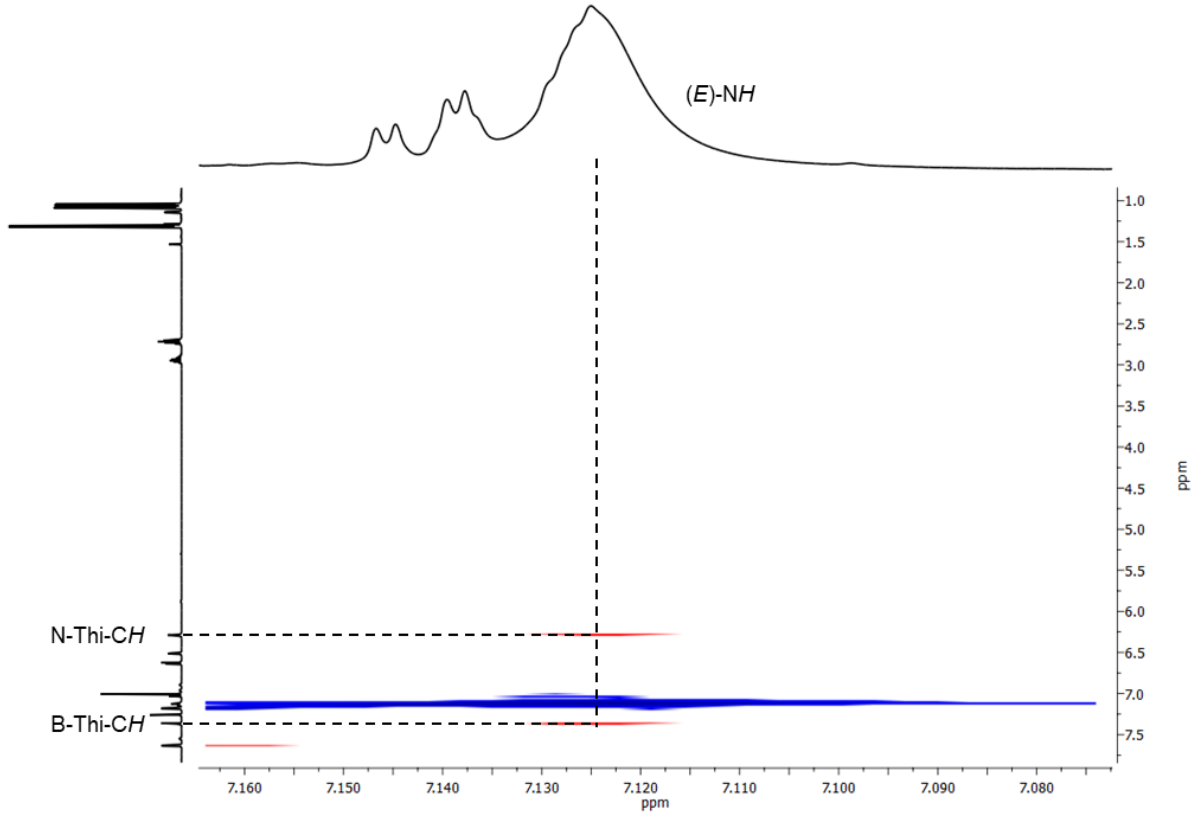

Figure S5.7.16. Detail of ^{1}H, ^{1}H NOESY spectrum of **6** ((*E*)-Isomer) in $CDCl_3$.

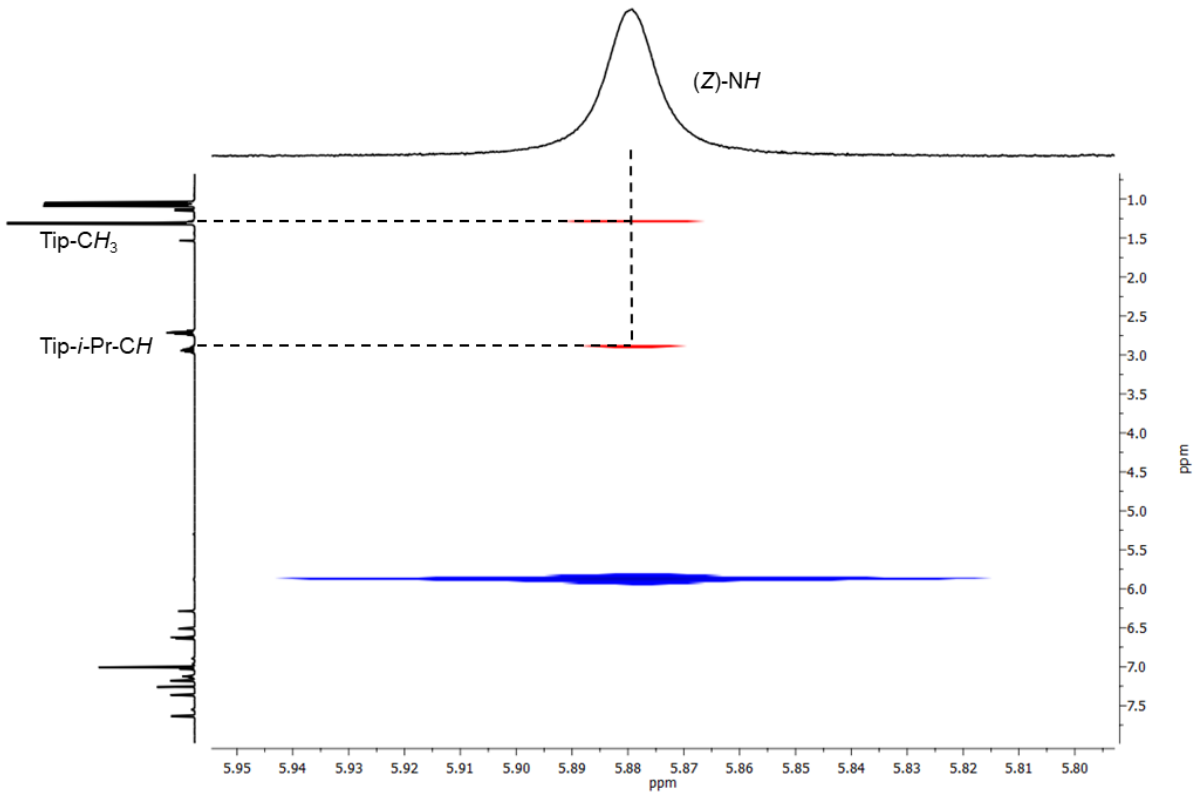

Figure S5.7.17. Detail of ^{1}H, ^{1}H NOESY spectrum of **6** ((*Z*)-Isomer) in $CDCl_3$.

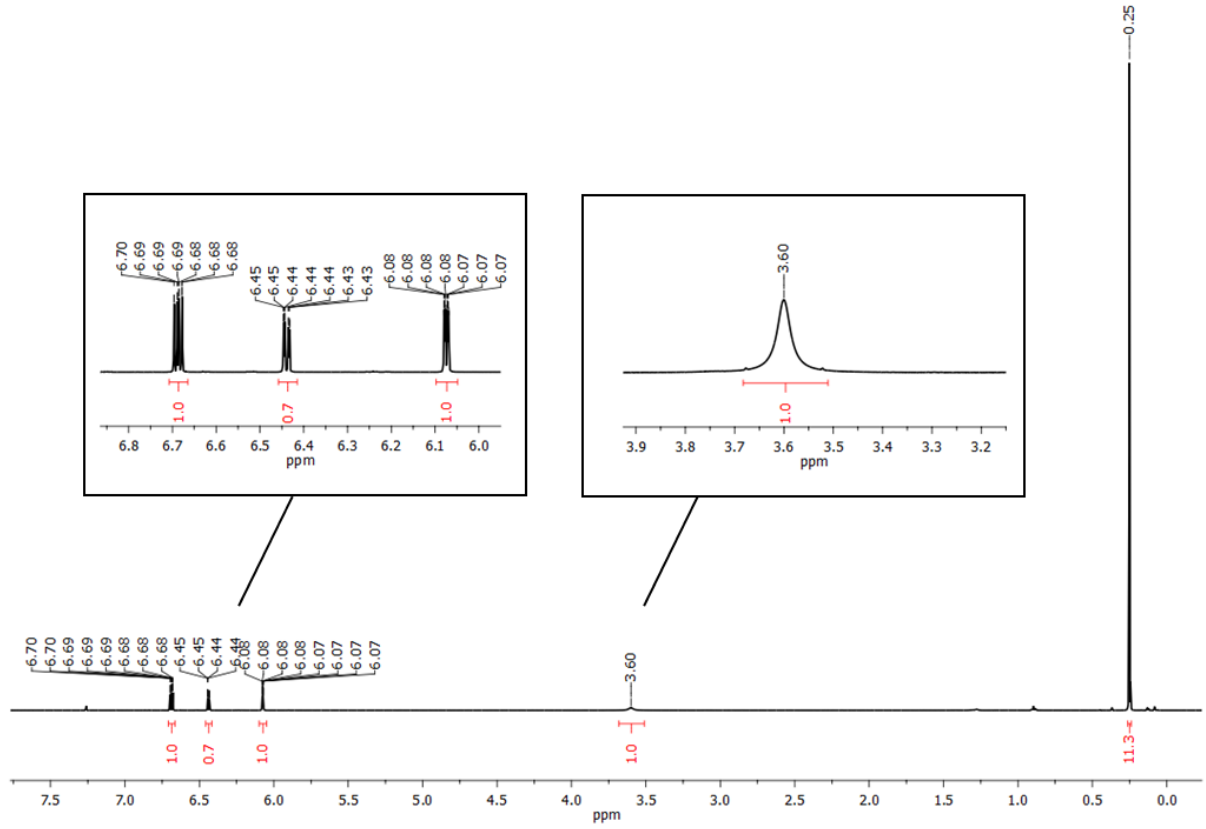

Figure S5.7.18. ^{1}H NMR spectrum (500 MHz) of **7** in $CDCl_3$.

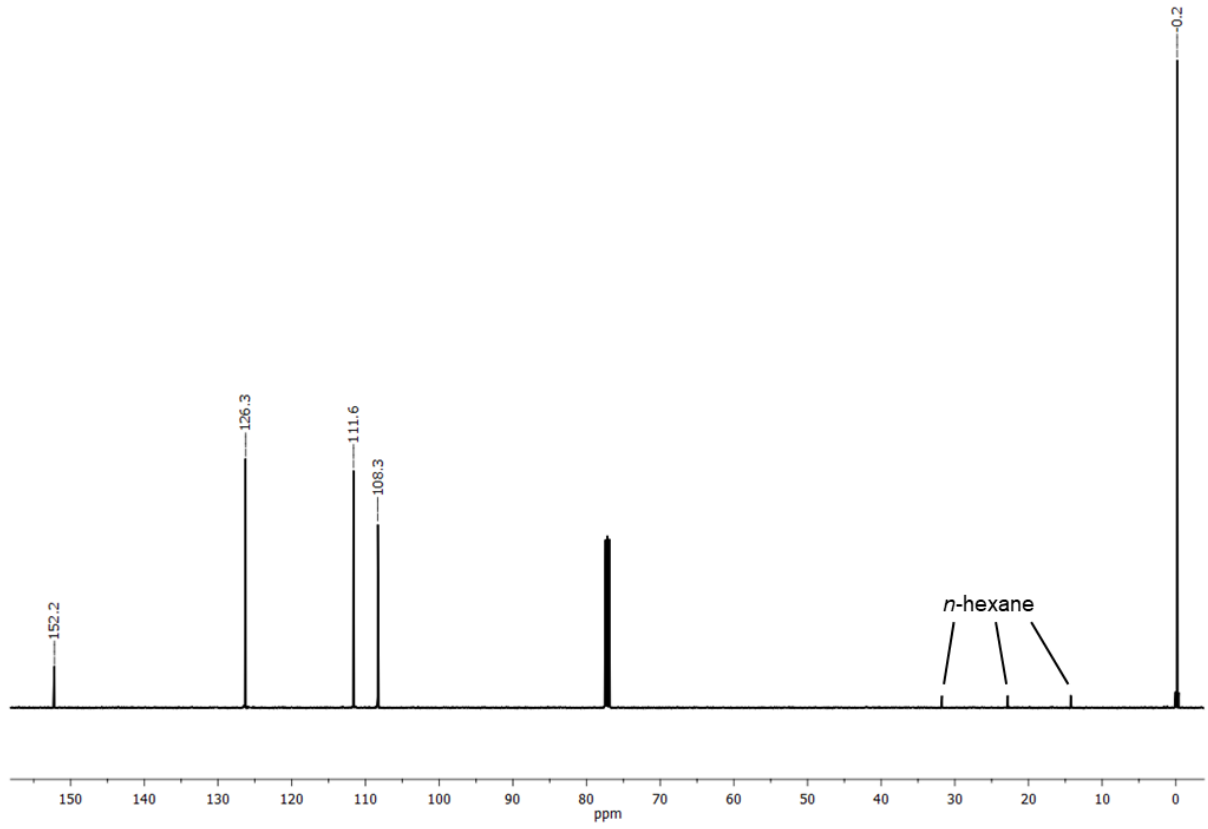

Figure S5.7.19. $^{13}C\{^{1}H\}$ NMR spectrum (126 MHz) of **7** in $CDCl_3$.

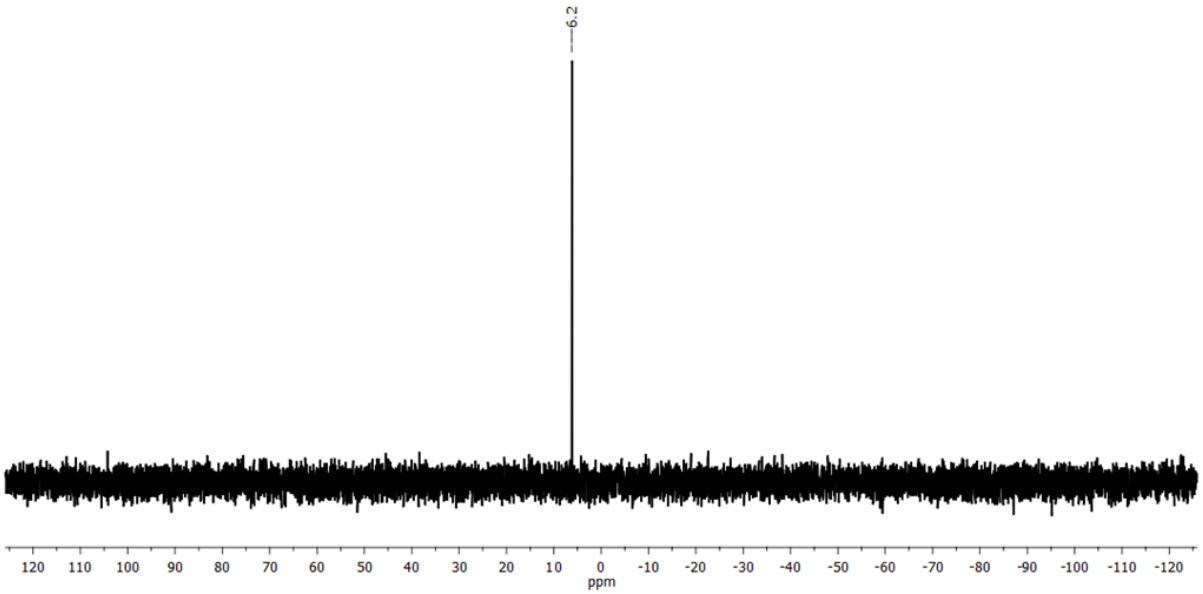

Figure S5.7.20. $^{29}Si\{^{1}H\}$ NMR spectrum (99 MHz) of **7** in $CDCl_3$.

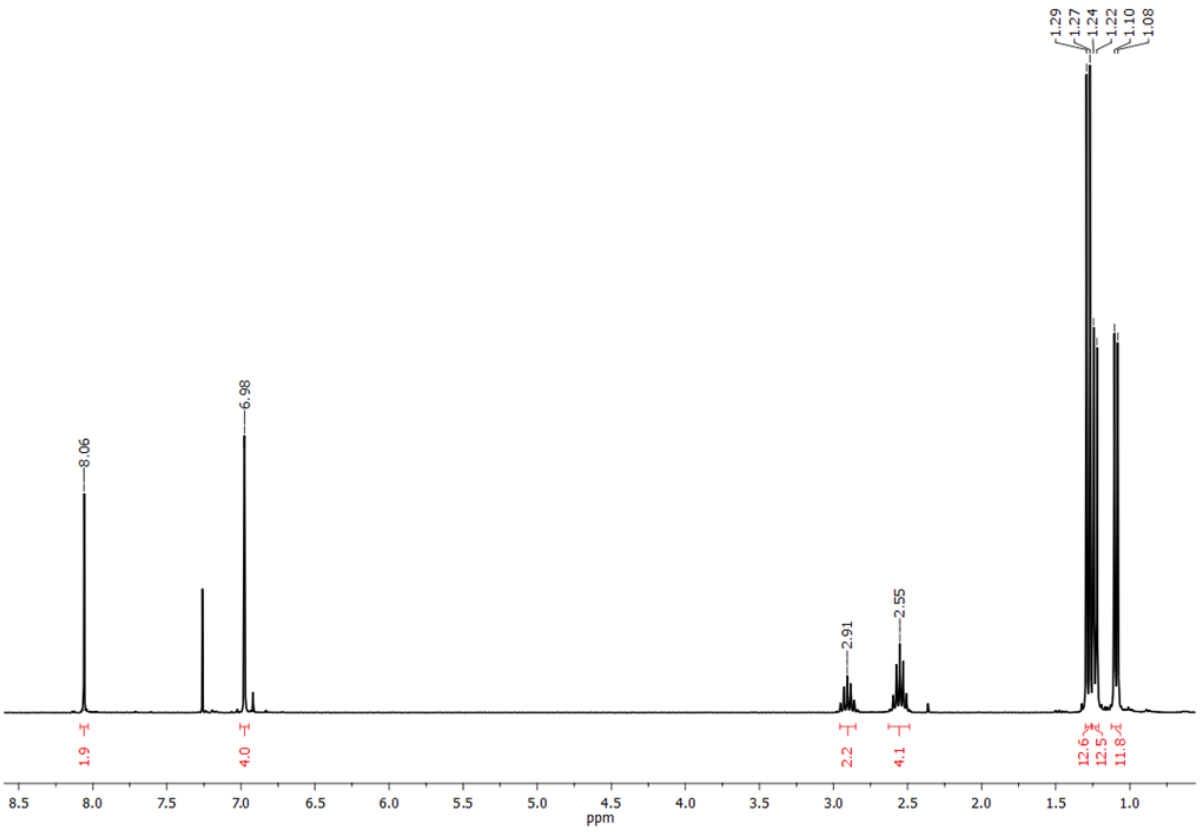

Figure S5.7.21. ^{1}H NMR spectrum (300 MHz) of **8** in $CDCl_3$.

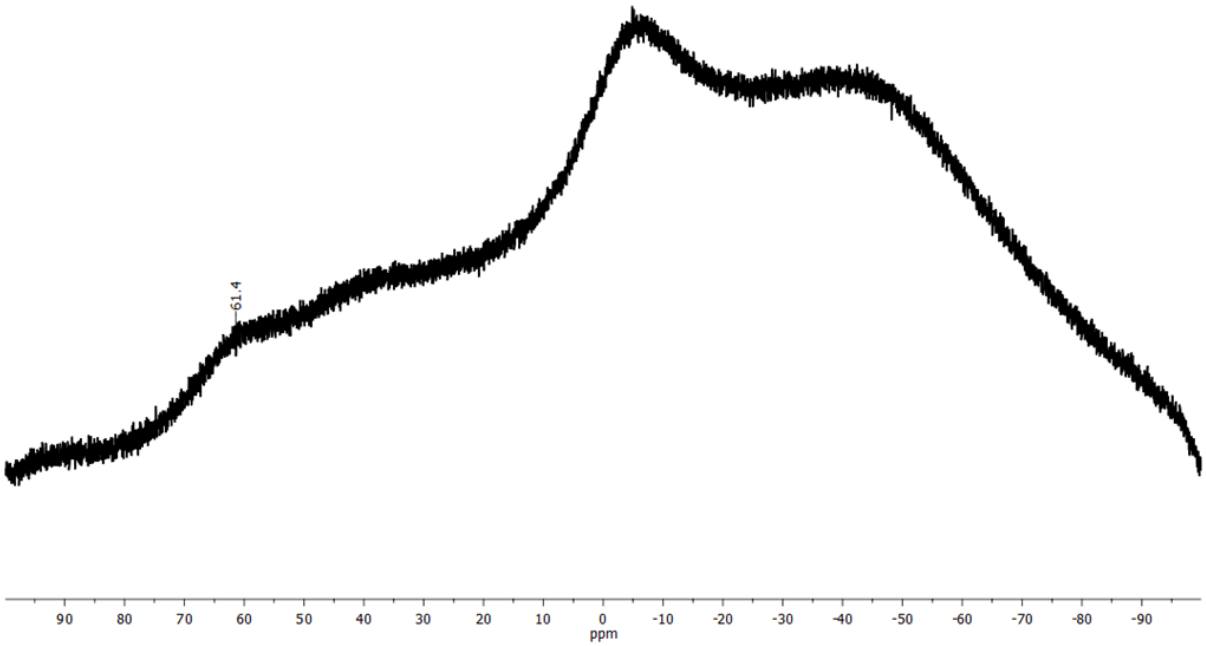

Figure S5.7.22. $^{11}B\{^{1}H\}$ NMR spectrum (96 MHz) of **8** in $CDCl_3$.

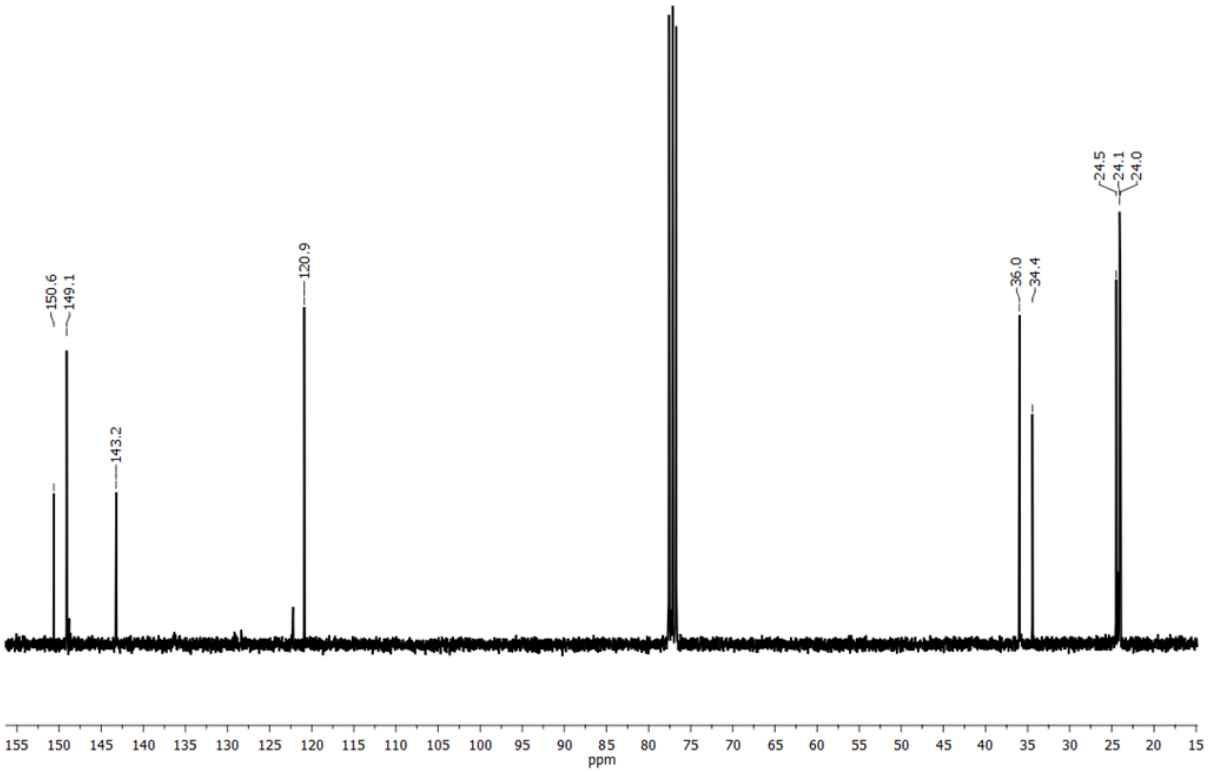

Figure S5.7.23. $^{13}C\{^{1}H\}$ NMR spectrum (76 MHz) of **8** in $CDCl_3$.

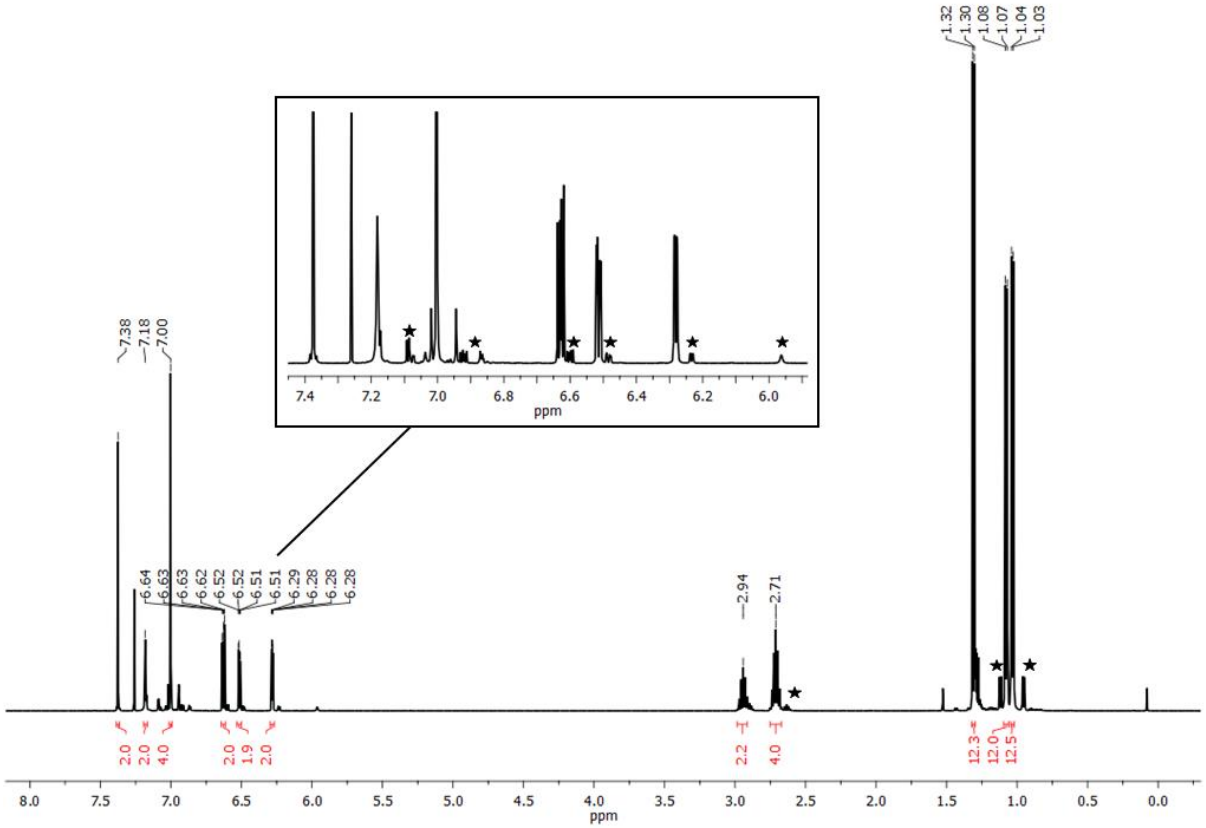

Figure S5.7.24. ^{1}H NMR spectrum (500 MHz) of **9** in $CDCl_3$. The signals marked with an asterisk belong to the minor isomer.

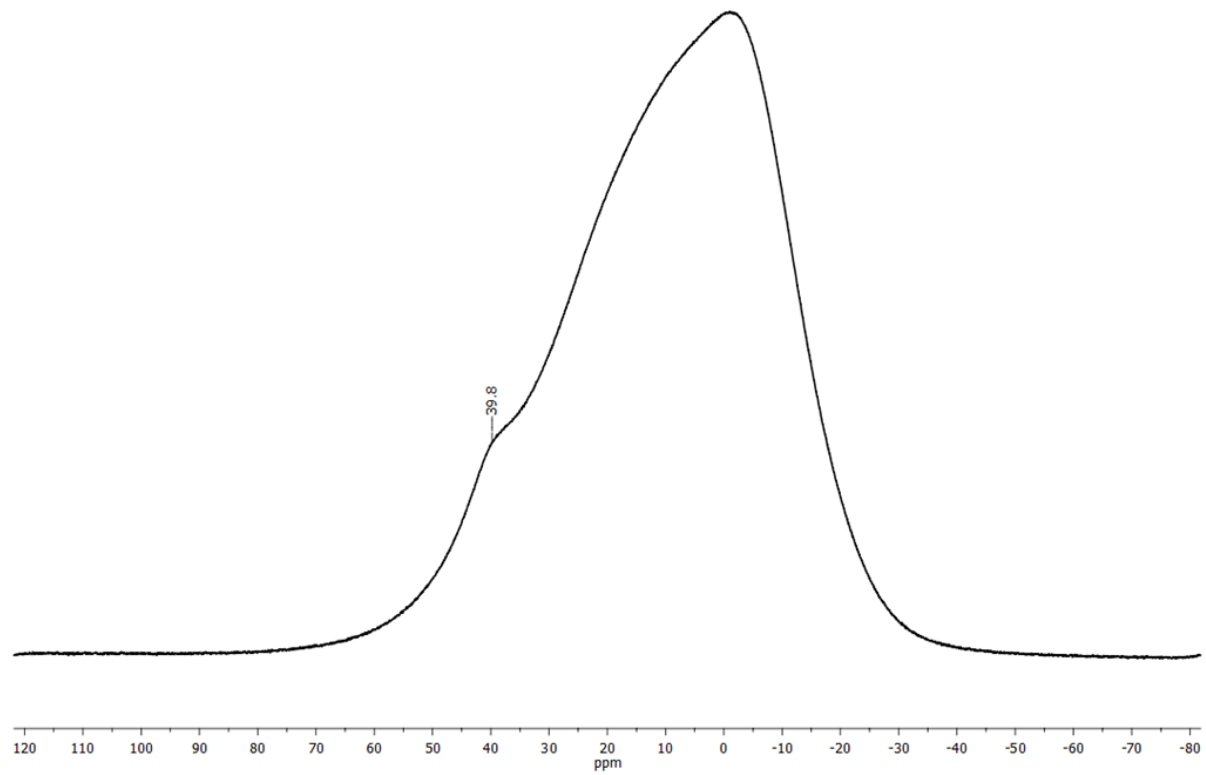

Figure S5.7.25. $^{11}B\{^{1}H\}$ NMR spectrum (160 MHz) of **9** in $CDCl_3$.

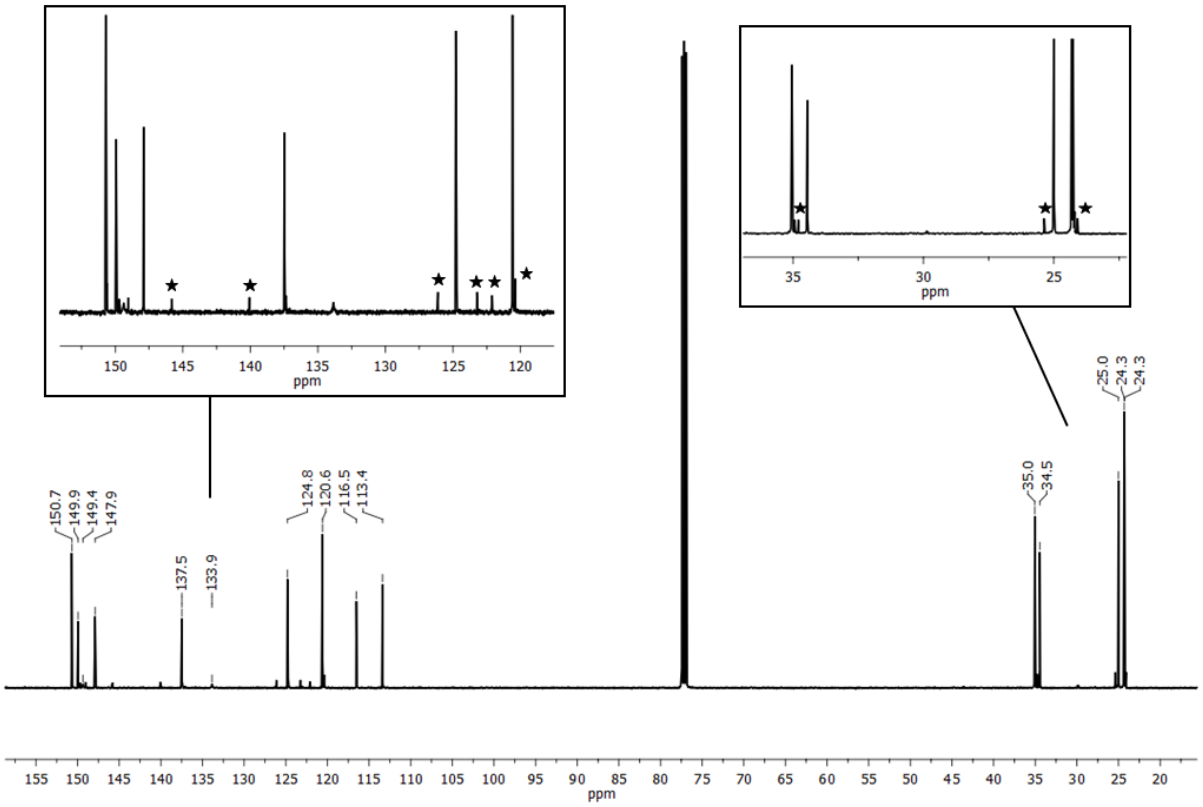

Figure S5.7.26. $^{13}C\{^{1}H\}$ NMR spectrum (126 MHz) of **9** in $CDCl_3$. The signals marked with an asterisk belong to the minor isomer.

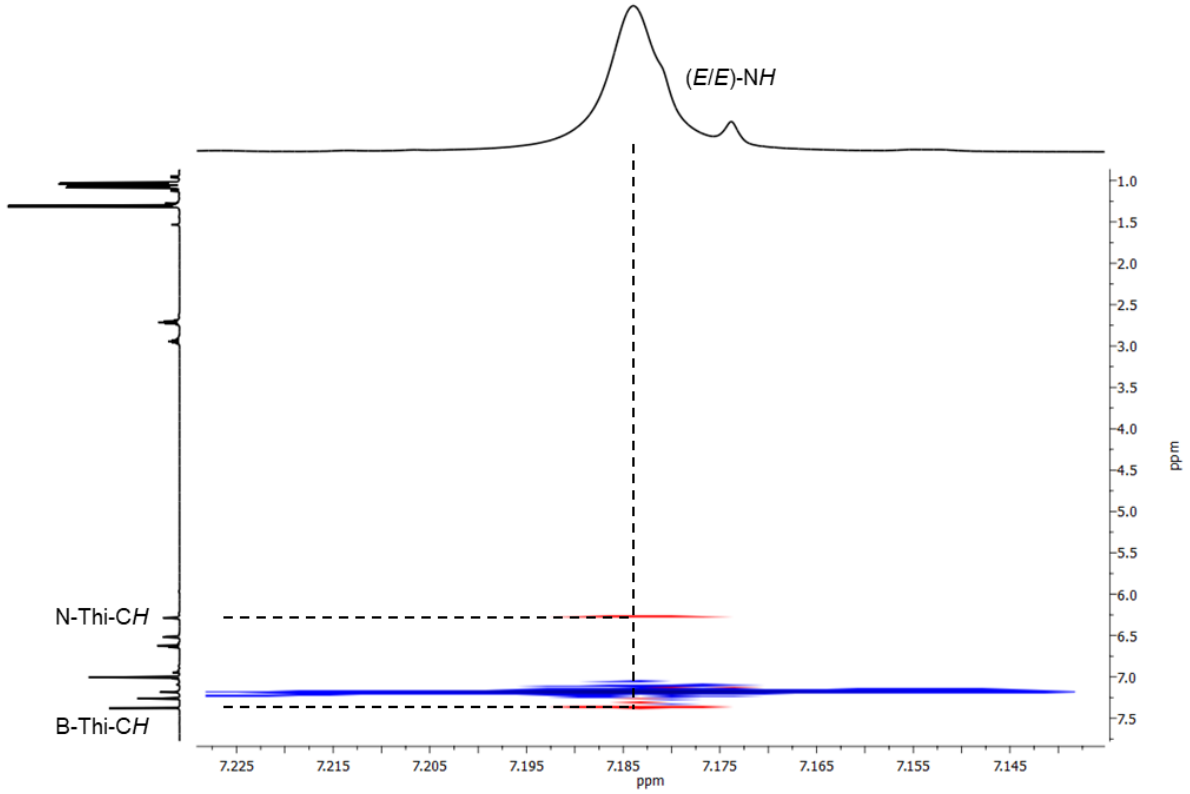

Figure S5.7.27. Detail of ^{1}H, ^{1}H NOESY spectrum of **9** ((*E*/*E*)-Isomer) in $CDCl_3$.

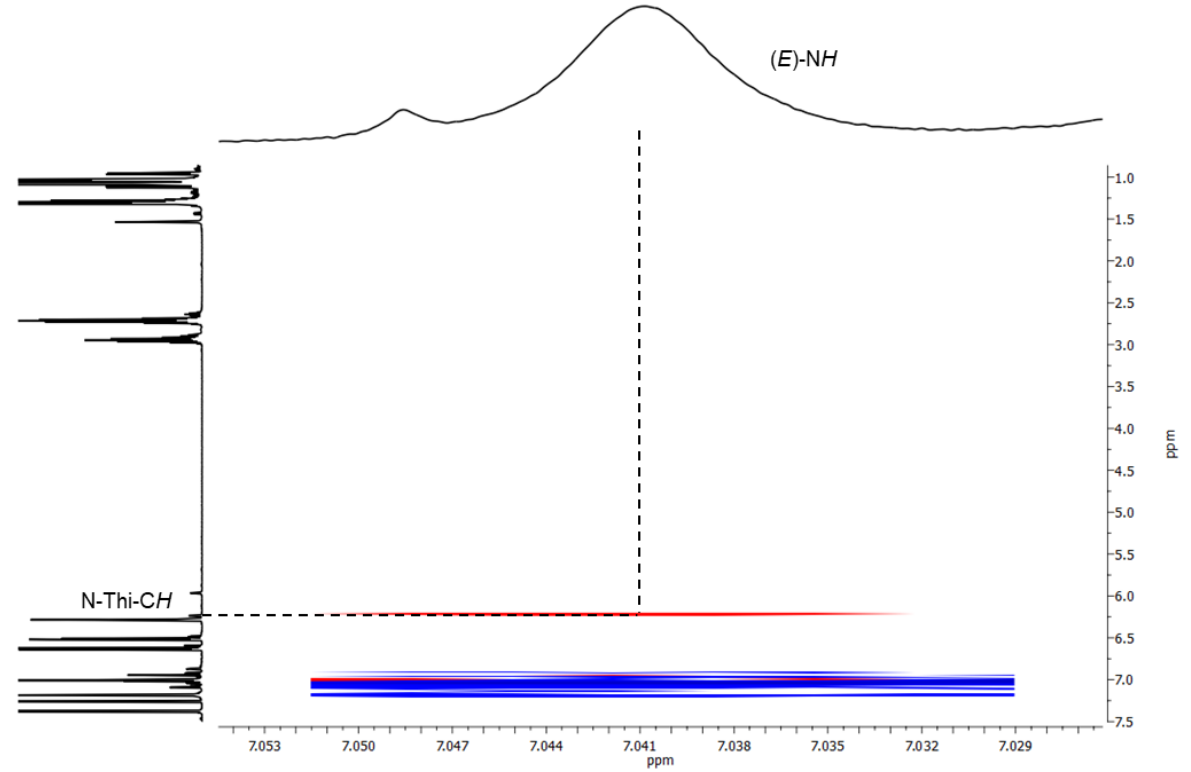

Figure S5.7.28. Detail of ^{1}H, ^{1}H NOESY spectrum of **9** ((*E*/*Z*)-Isomer) in $CDCl_3$. The N*H* signal of the *E*-configured double bond is shown.

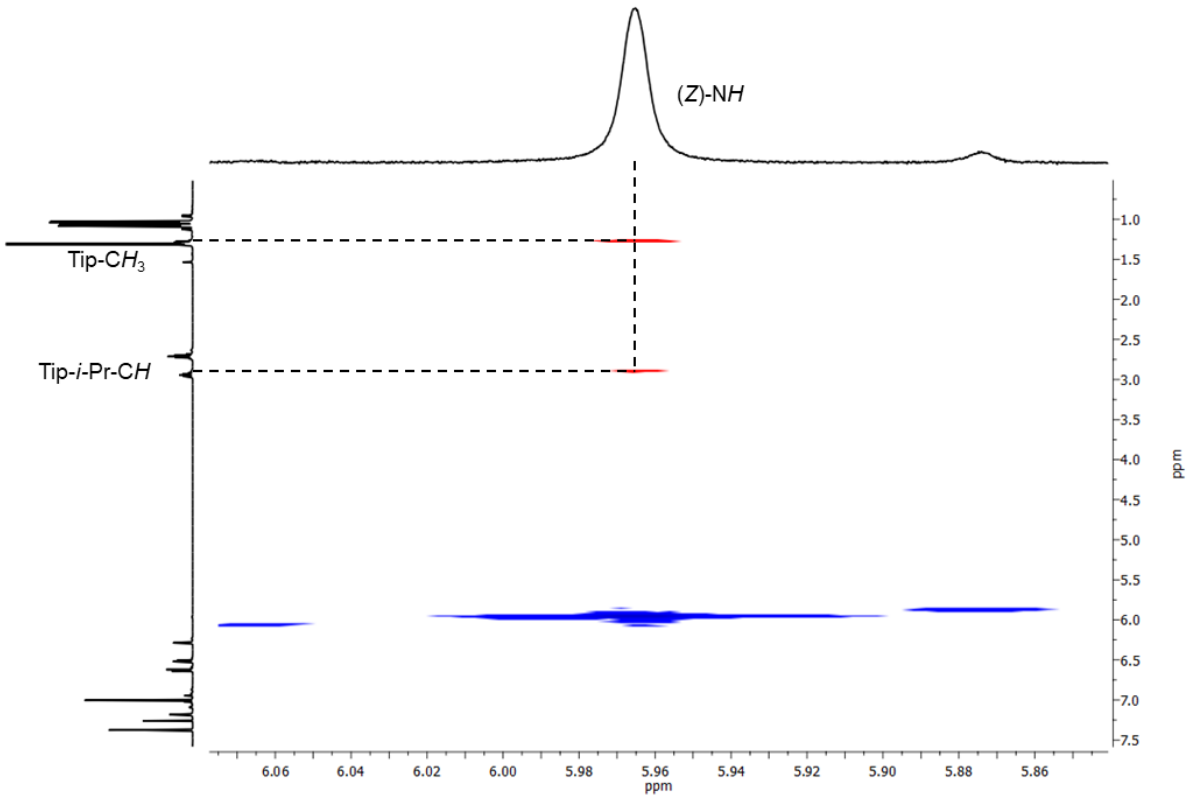

Figure S5.7.29. Detail of ^{1}H, ^{1}H NOESY spectrum of **9** ((*E*/*Z*)-Isomer) in $CDCl_3$. The N*H* signal of the *Z*-configured double bond is shown.

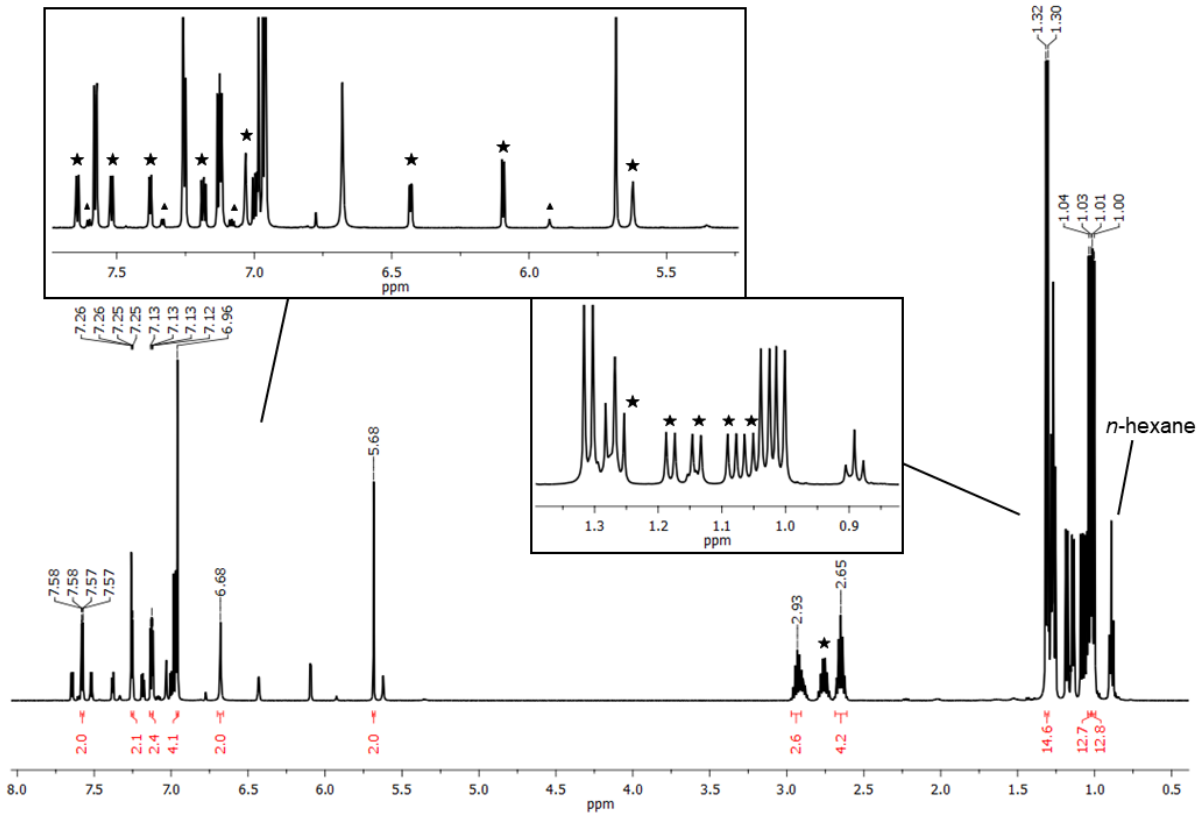

Figure S5.7.30. ^{1}H NMR spectrum (500 MHz) of **10** in $CDCl_3$. The signals marked with an asterisk and a triangle, respectively, belong to the minor isomers.

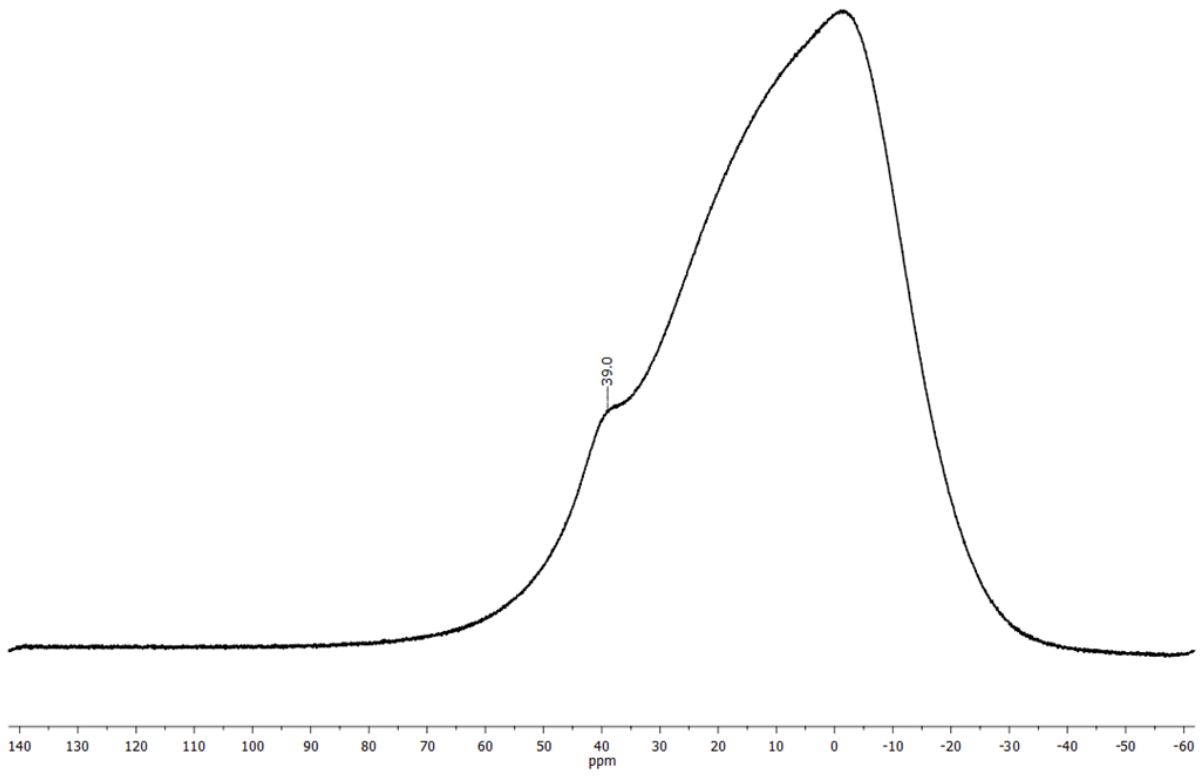

Figure S5.7.31. $^{11}B\{^{1}H\}$ NMR spectrum (160 MHz) of **10** in $CDCl_3$.

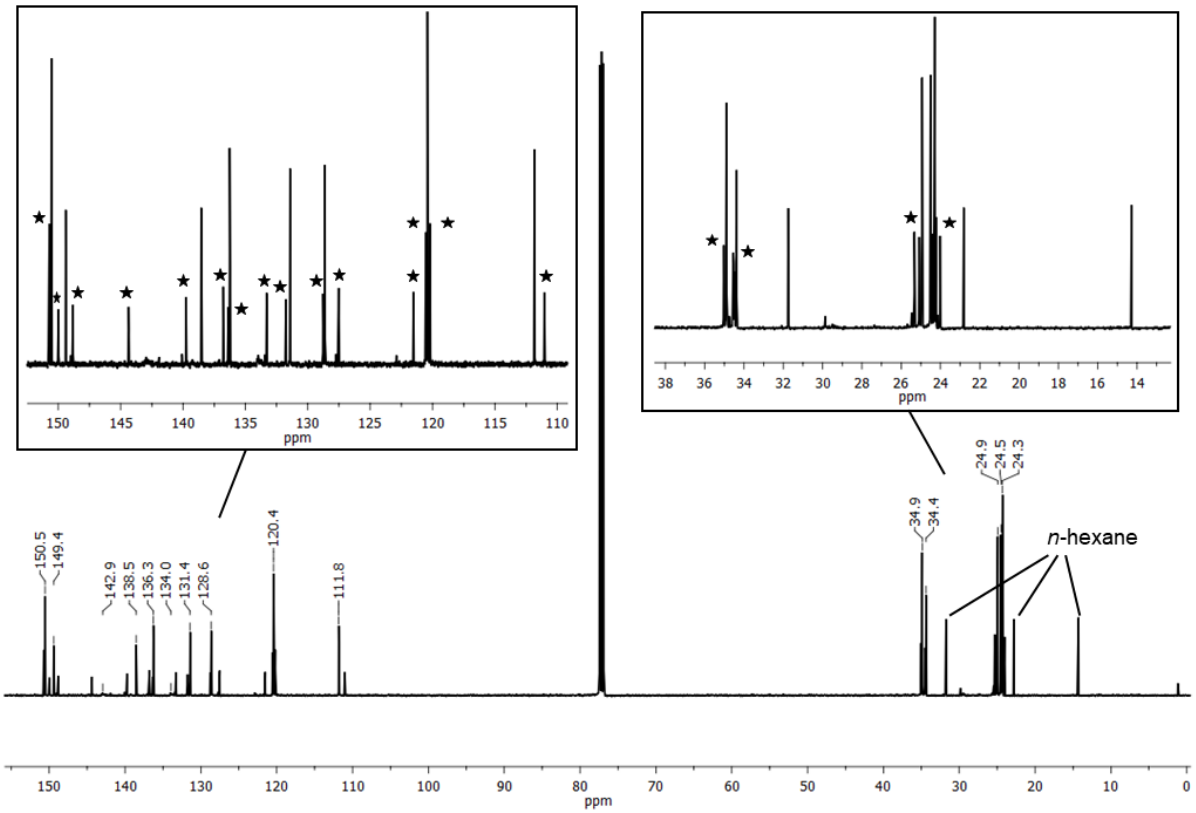

Figure S5.7.32. $^{13}C\{^{1}H\}$ NMR spectrum (126 MHz) of **10** in $CDCl_3$. The signals marked with an asterisk belong to the minor isomer.

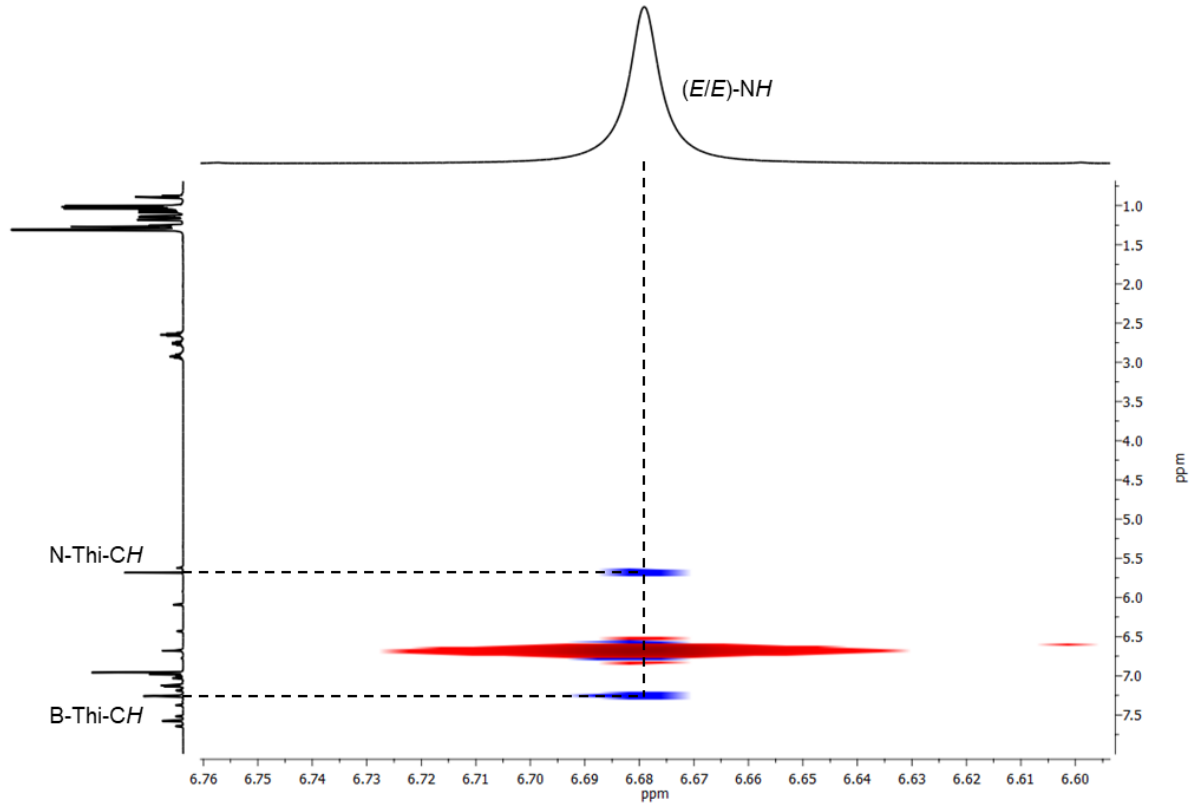

Figure S5.7.33. Detail of ^{1}H, ^{1}H ROESY spectrum of **10** ((*E*/*E*)-Isomer) in $CDCl_3$.

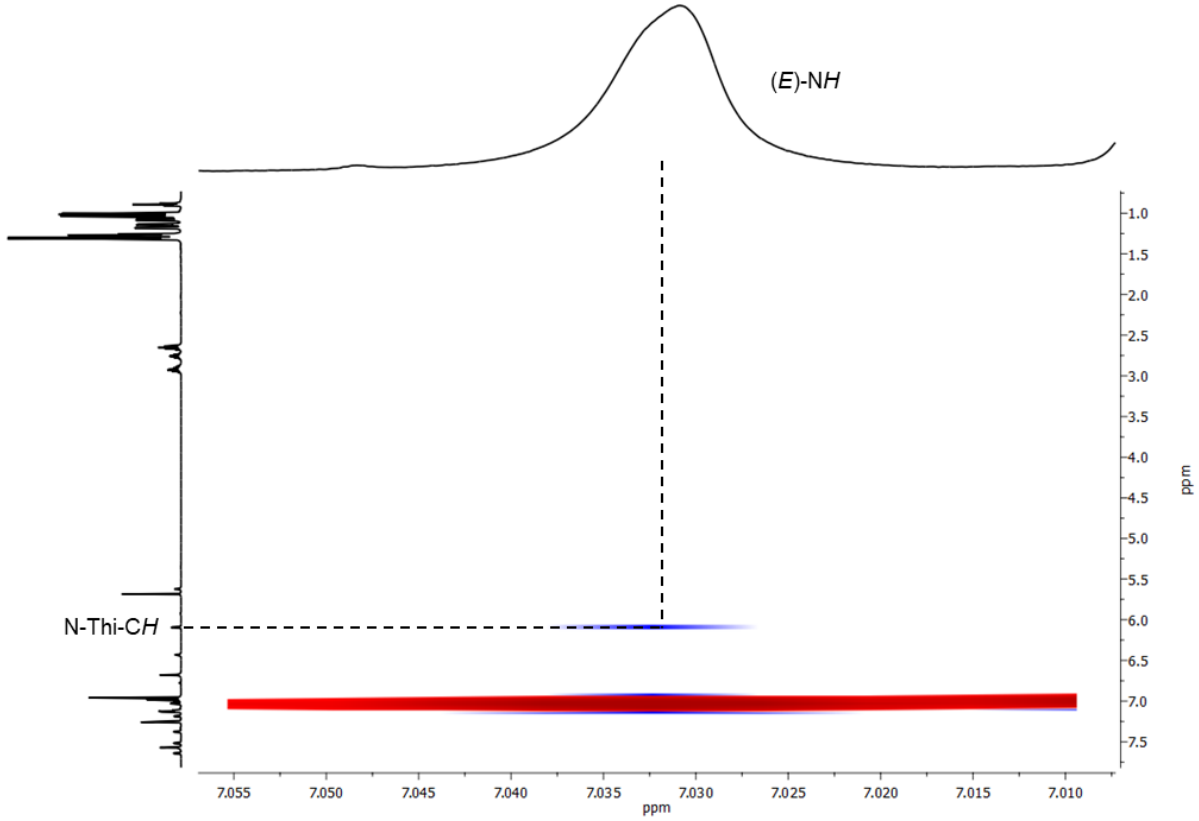

Figure S5.7.34. Detail of ^{1}H, ^{1}H ROESY spectrum of **10** ((*E*/*Z*)-Isomer) in $CDCl_3$. The N*H* signal of the *E*-configured double bond is shown.

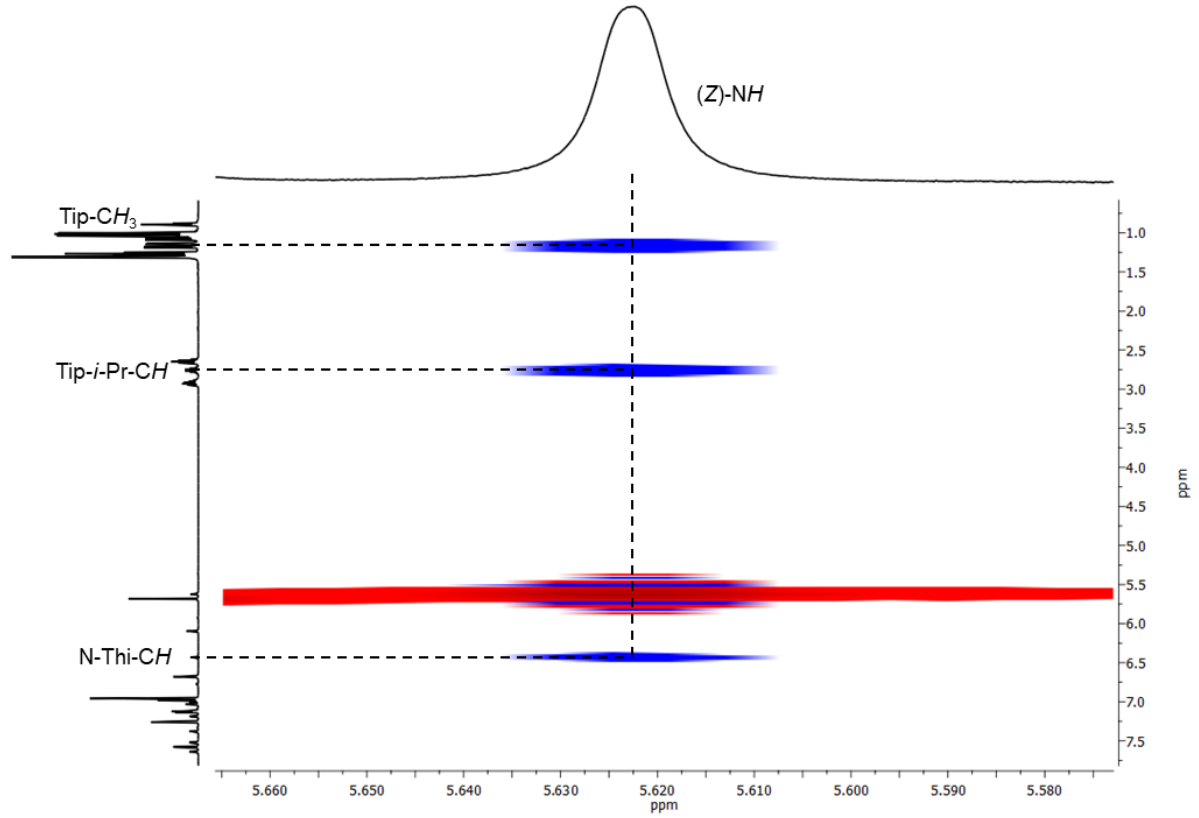

Figure S5.7.35. Detail of ^{1}H, ^{1}H ROESY spectrum of **10** ((*E*/*Z*)-Isomer) in $CDCl_3$. The N*H* signal of the *Z*-configured double bond is shown.

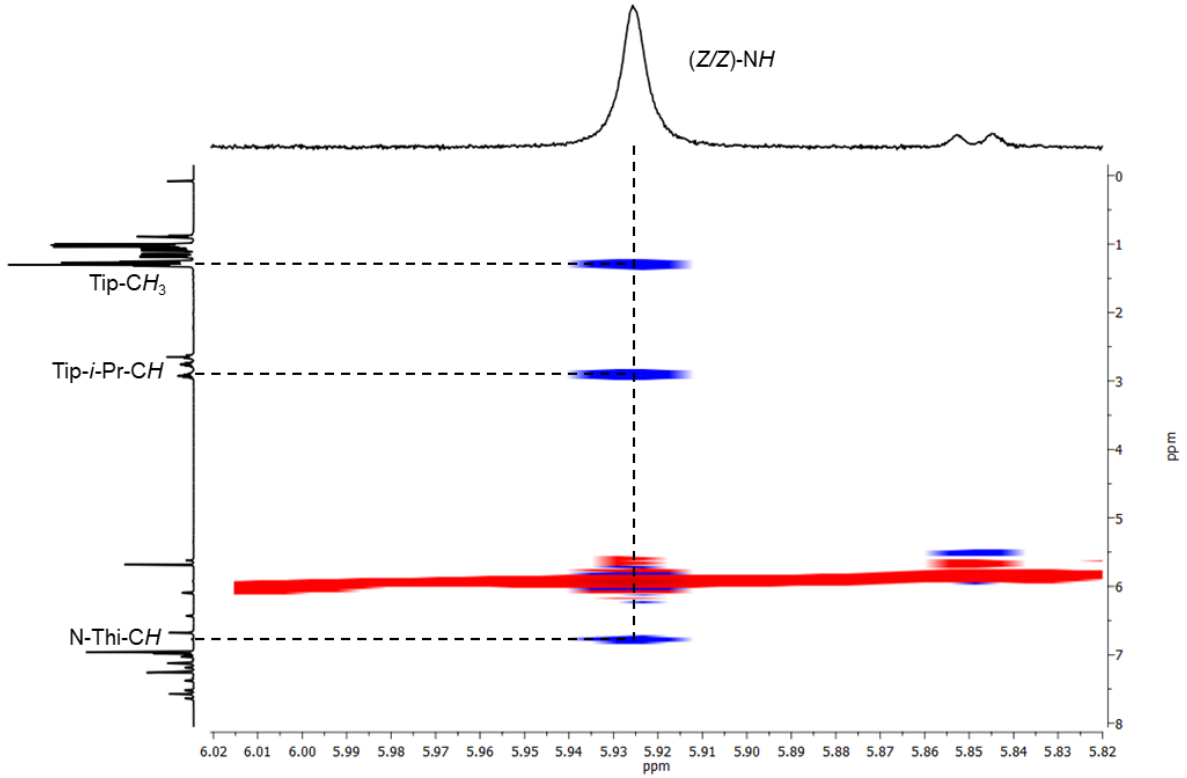

Figure S5.7.36. Detail of ^{1}H, ^{1}H ROESY spectrum of **10** ((*Z*/*Z*)-Isomer) in $CDCl_3$.

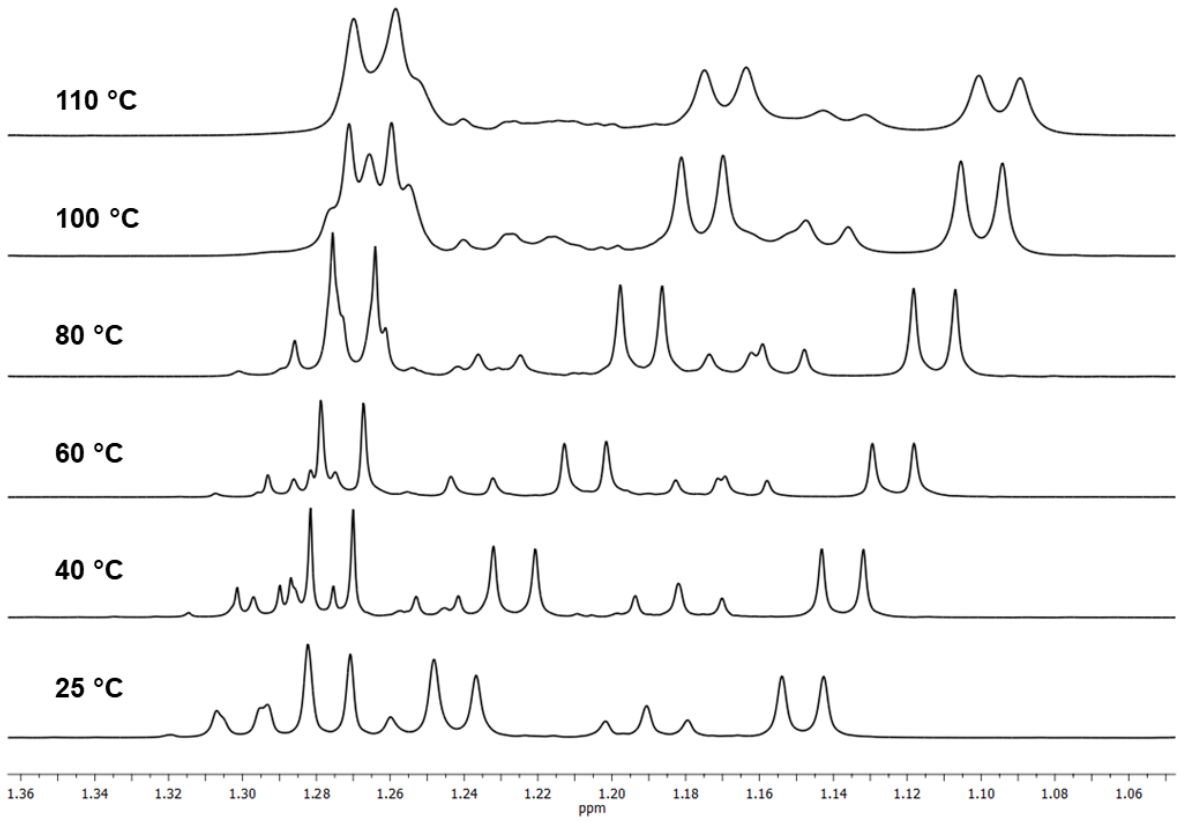

Figure S5.7.37. Isomerization attempt of **10** from 25 °C to 110 °C in toluene-d_8.

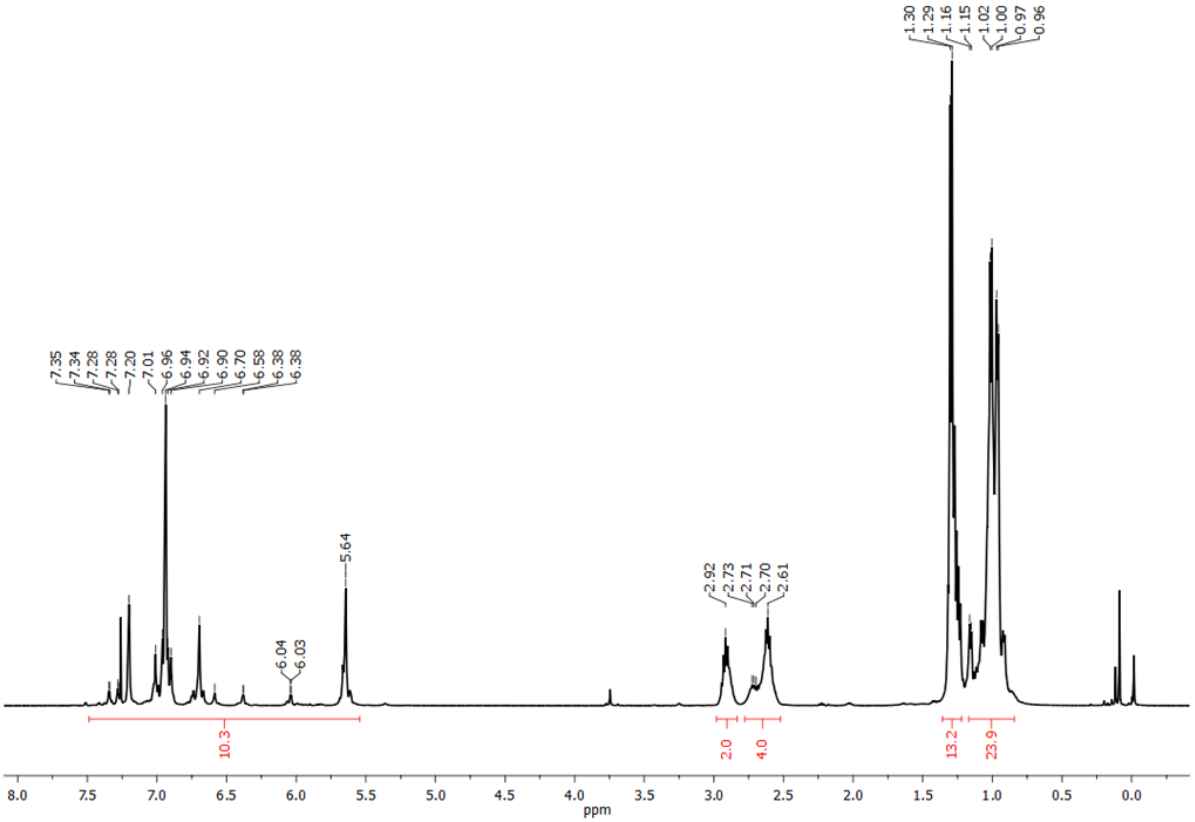

Figure S5.7.38. ^{1}H NMR spectrum (500 MHz) of **11** in $CDCl_3$.

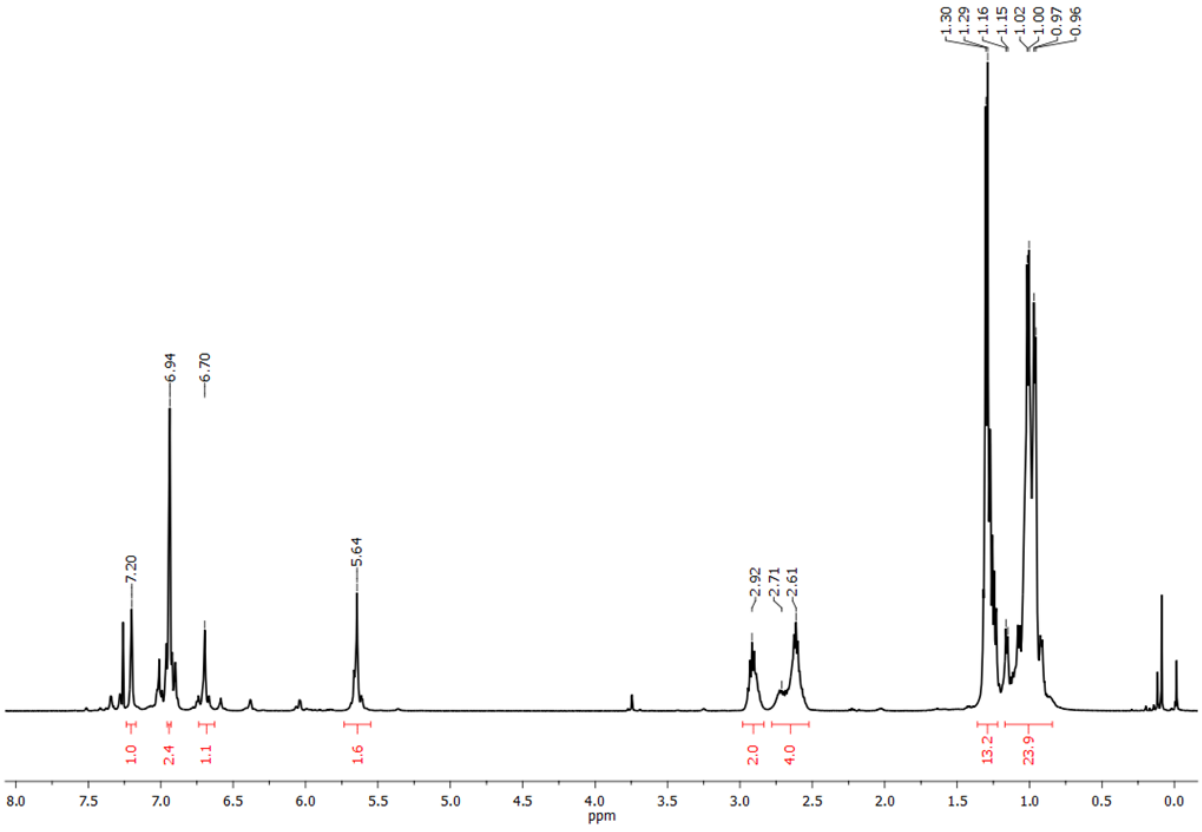

Figure S5.7.39. ^{1}H NMR spectrum (500 MHz) of **11** with integration of the main peaks in $CDCl_3$.

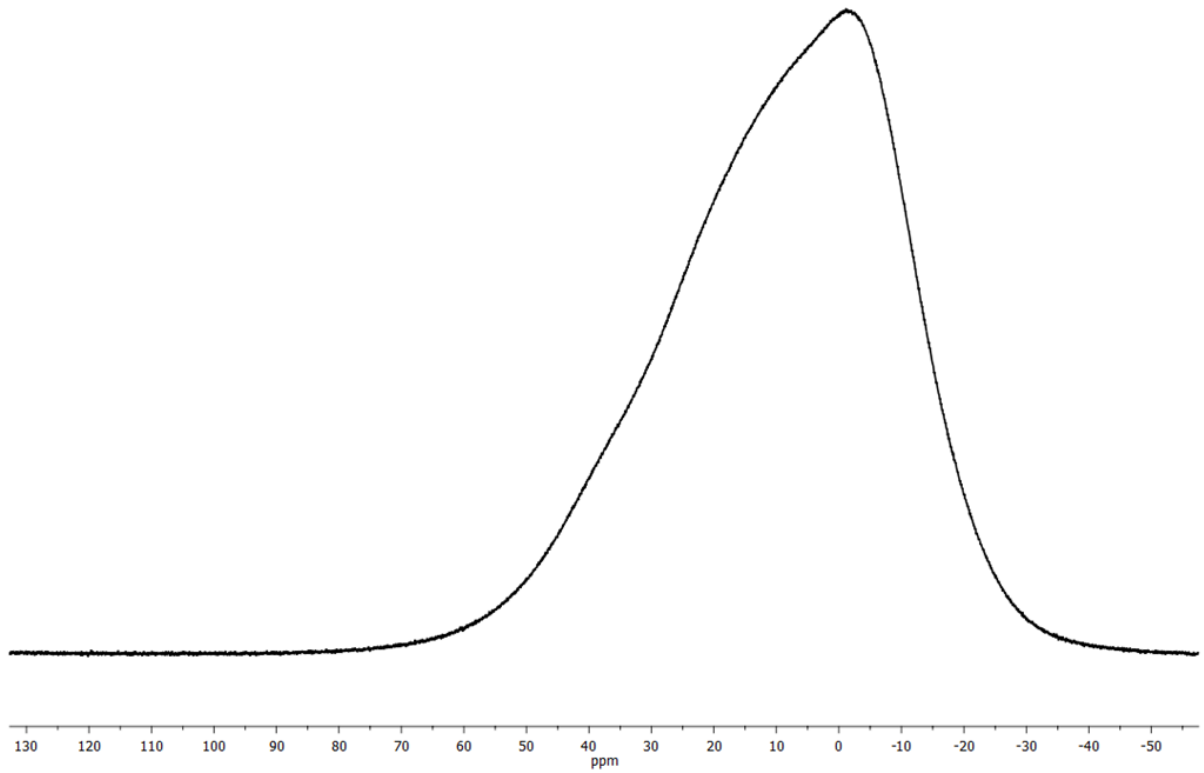

Figure S5.7.40. $^{11}B\{^{1}H\}$ NMR spectrum (160 MHz) of **11** in $CDCl_3$. No signal was detected.

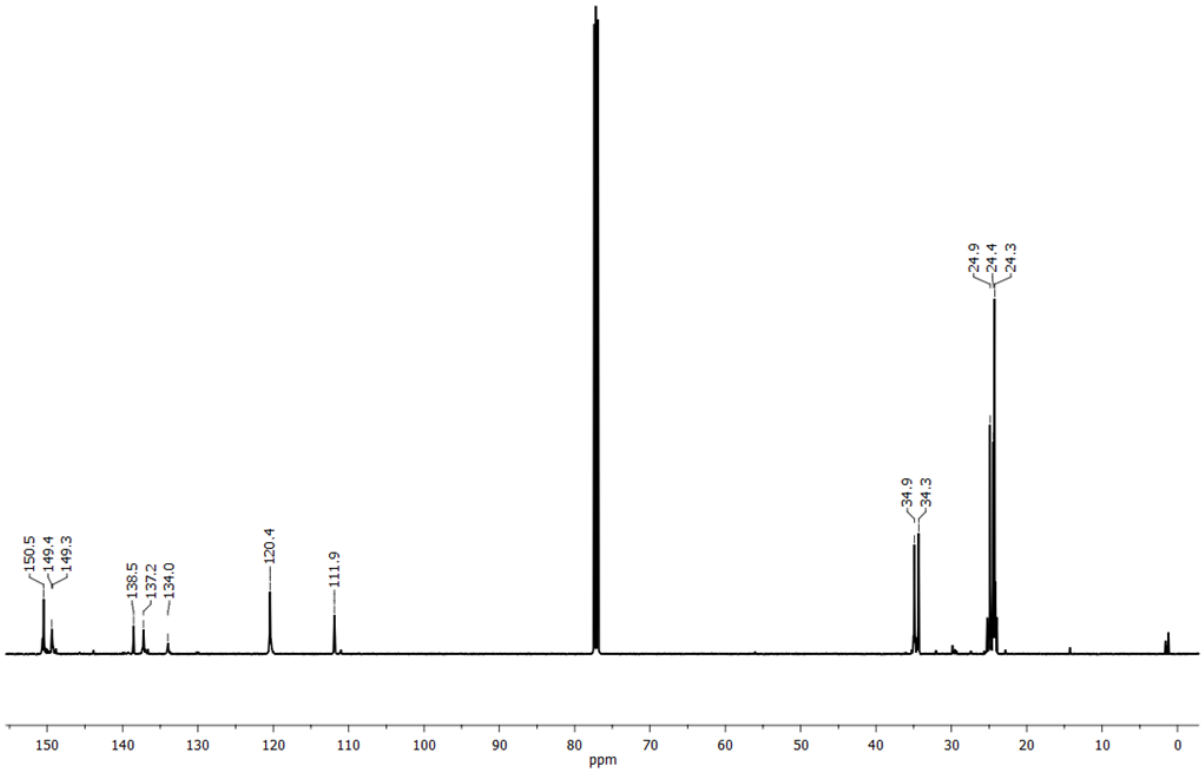

Figure S5.7.41. $^{13}C\{^{1}H\}$ NMR spectrum (126 MHz) of **11** in $CDCl_3$.

HRMS spectra

The mass spectra were processed using the Qual Browser of the XCalibur software. The figures show the total spectrum in the upper part, the product peak with isotope distribution in the middle and a corresponding simulation in the lower part.

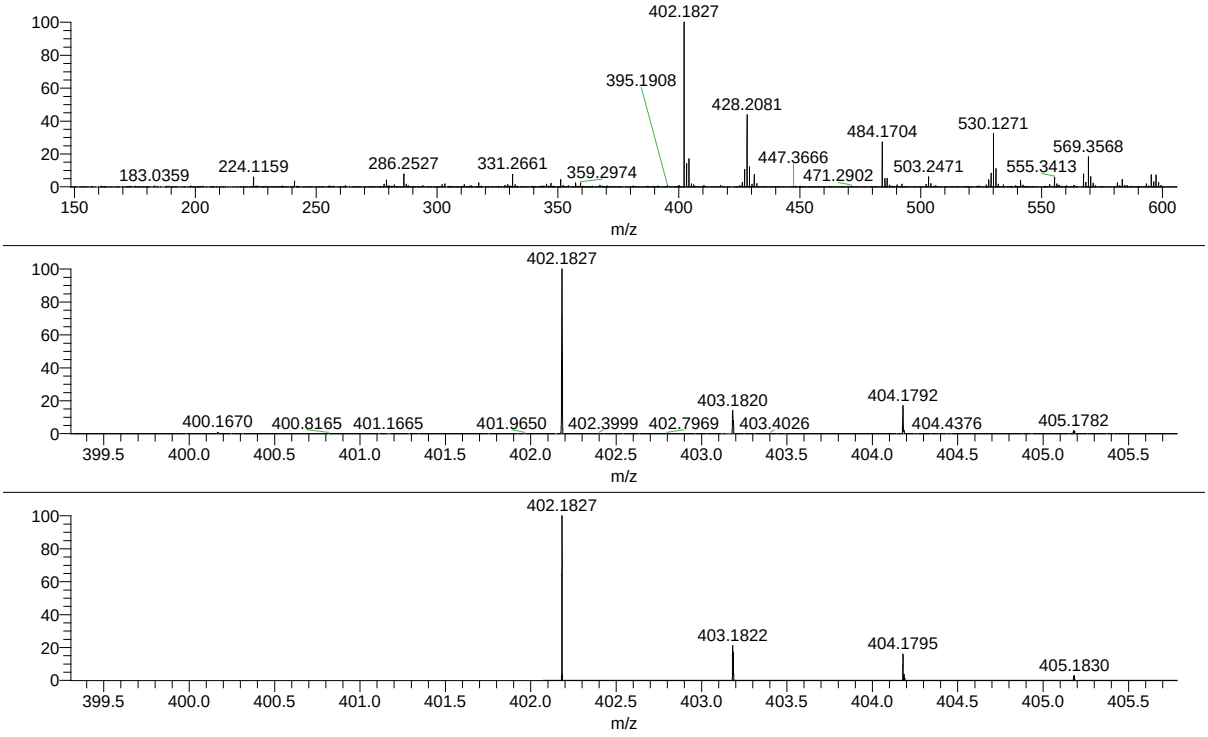

Figure S5.7.42. HRMS spectrum (LIFDI) of **1**.

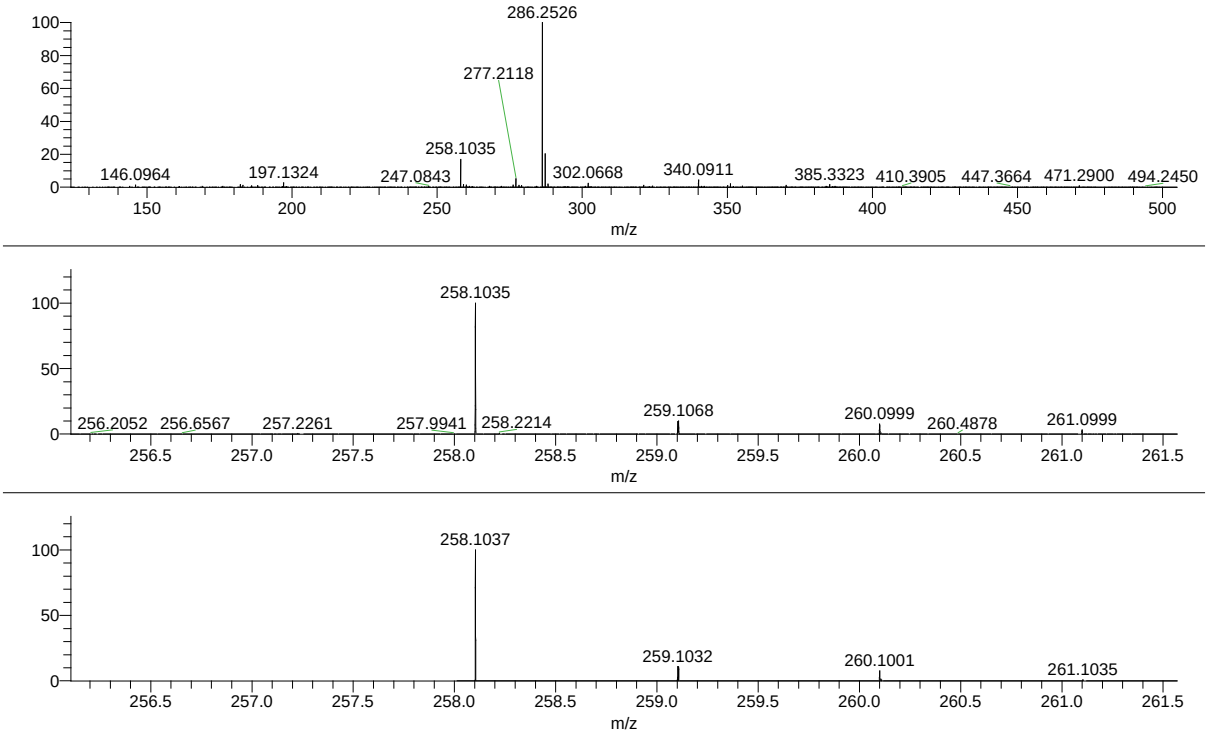

Figure S5.7.43. HRMS spectrum (LIFDI) of **3**.

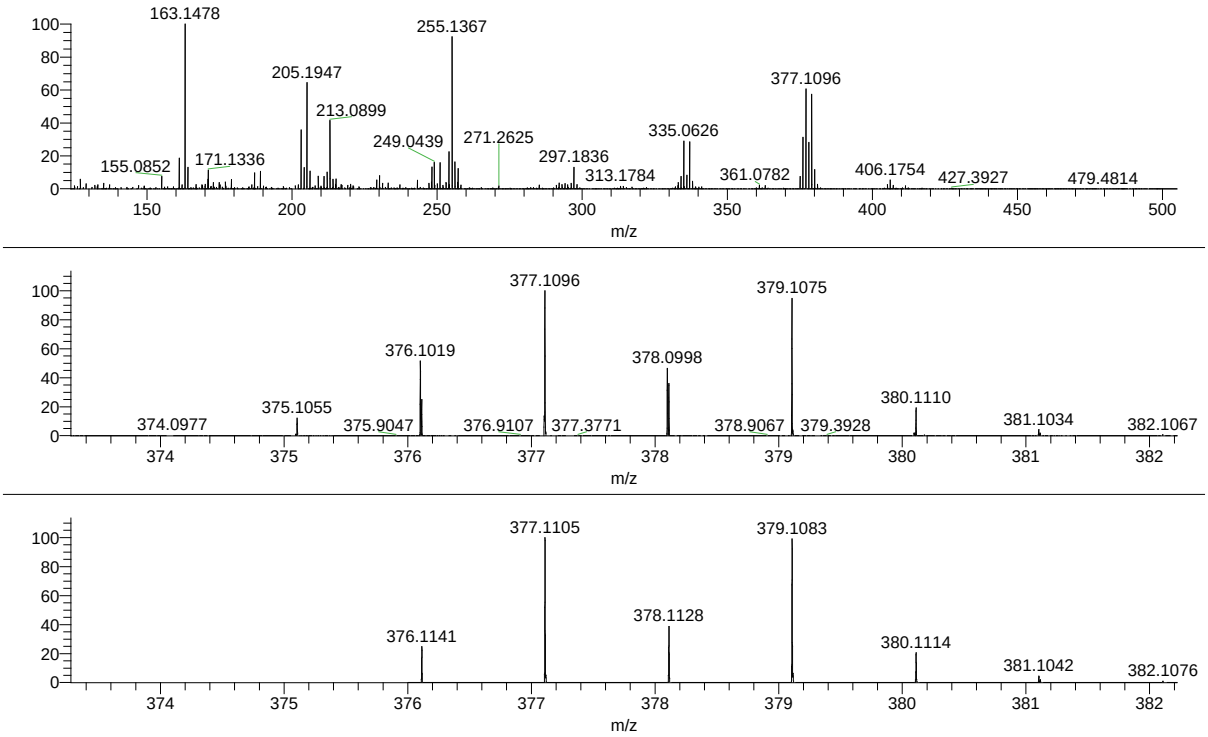

Figure S5.7.44. HRMS spectrum (ASAP pos) of **4**.

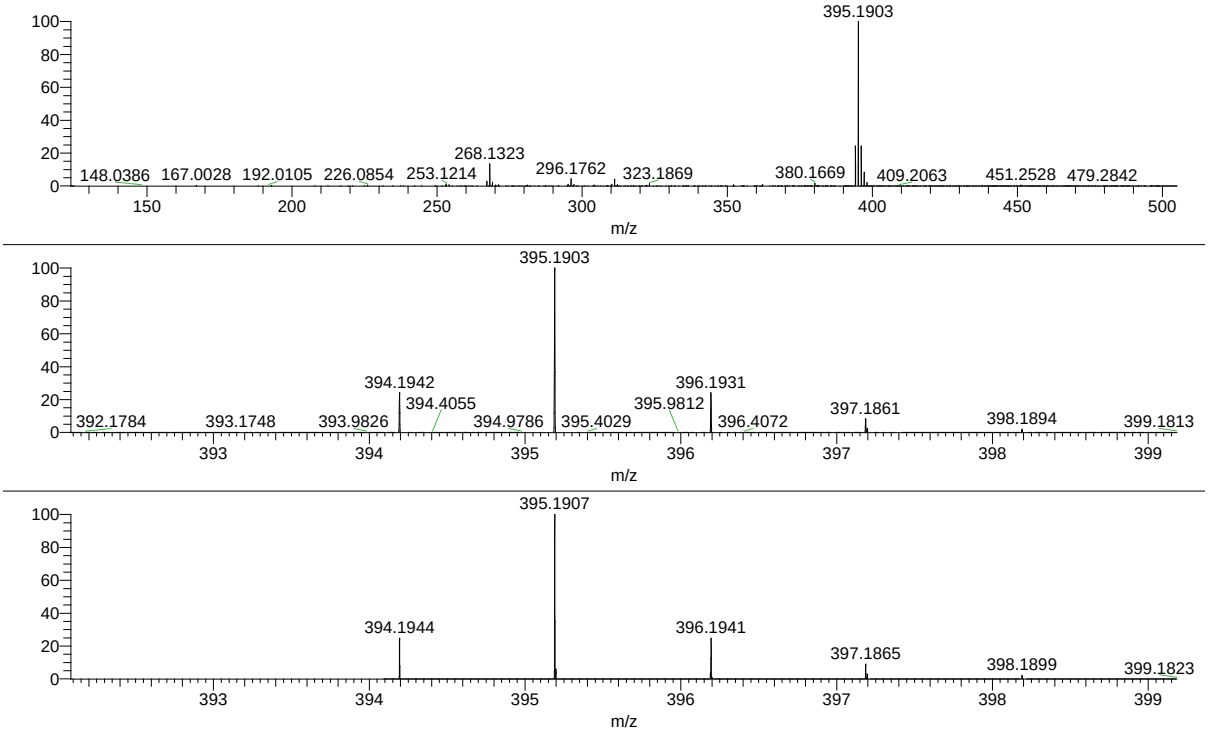

Figure S5.7.45. HRMS spectrum (LIFDI) of **6**.

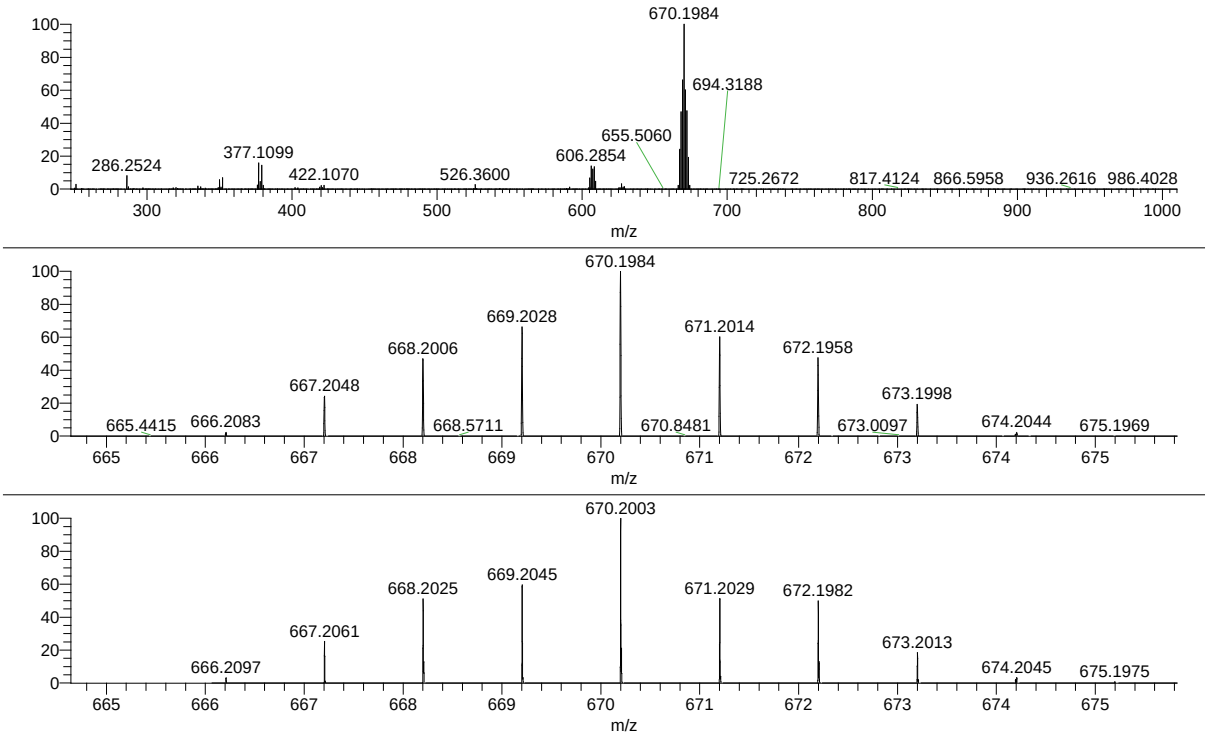

Figure S5.7.46. HRMS spectrum (LIFDI) of **8**.

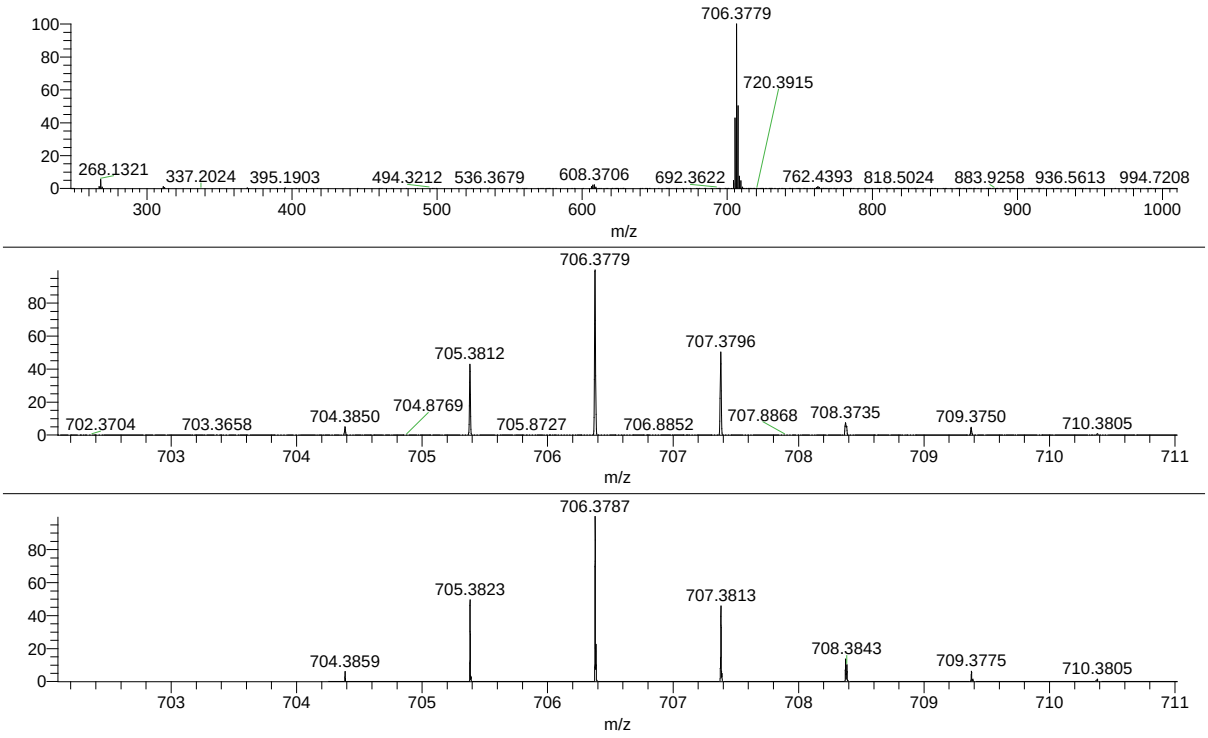

Figure S5.7.47. HRMS spectrum (LIFDI) of **9**.

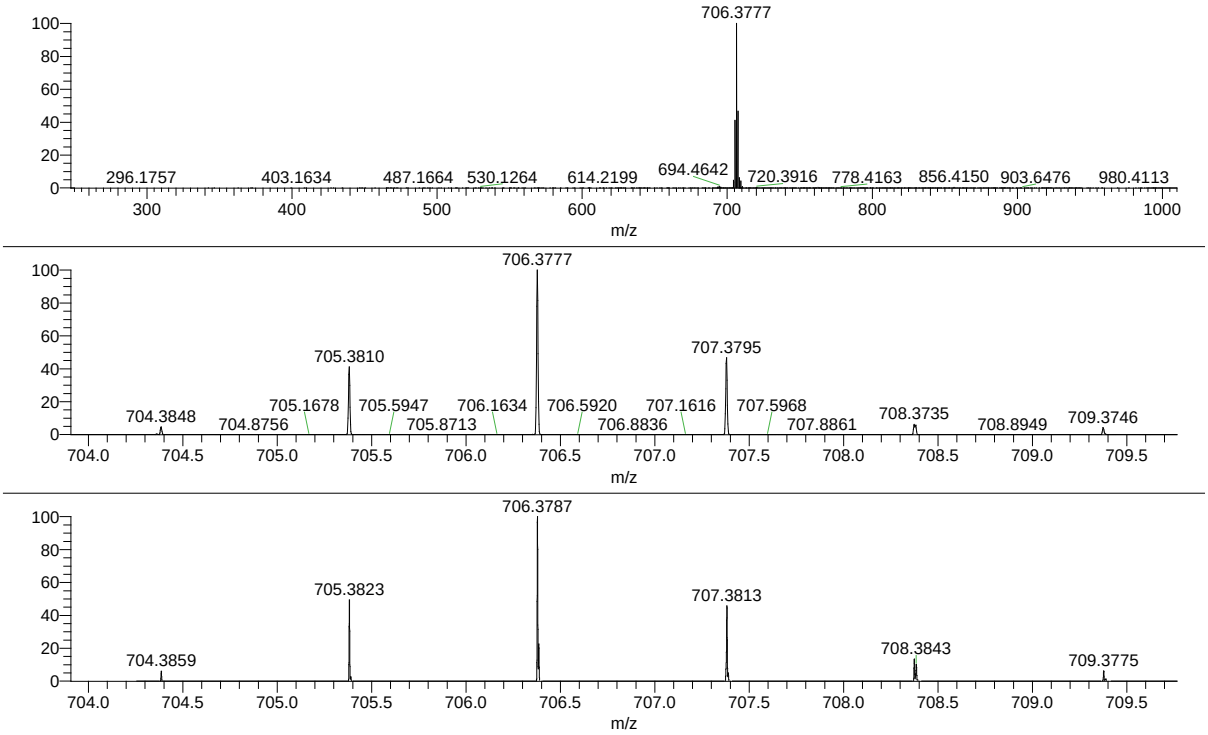

Figure S5.7.48. HRMS spectrum (LIFDI) of **10**.

UV-vis spectra

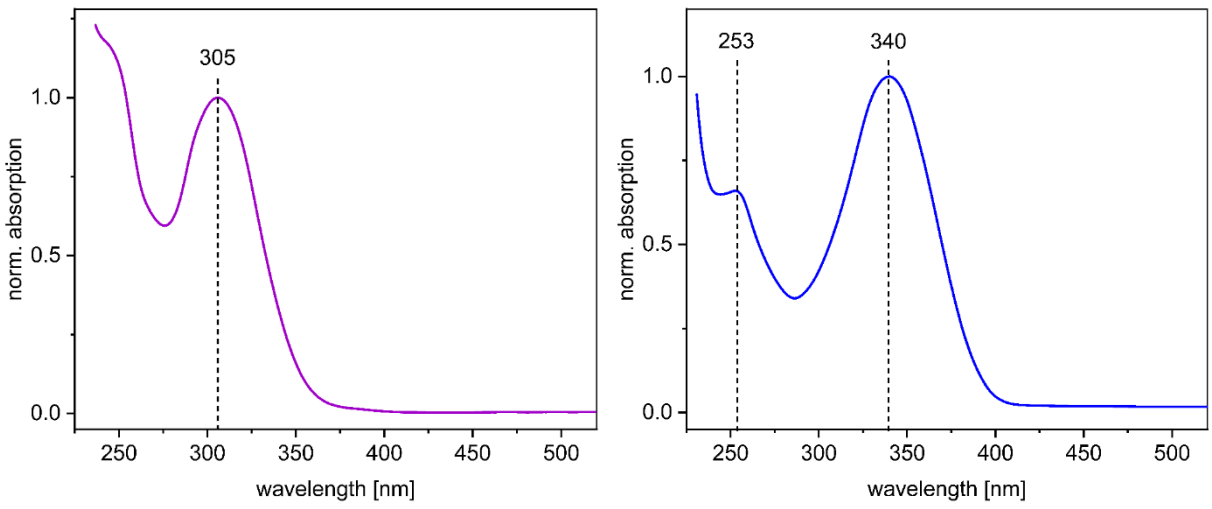

Figure S5.7.49. Normalized absorption spectra of **6** (left) and **9** (right) in THF.

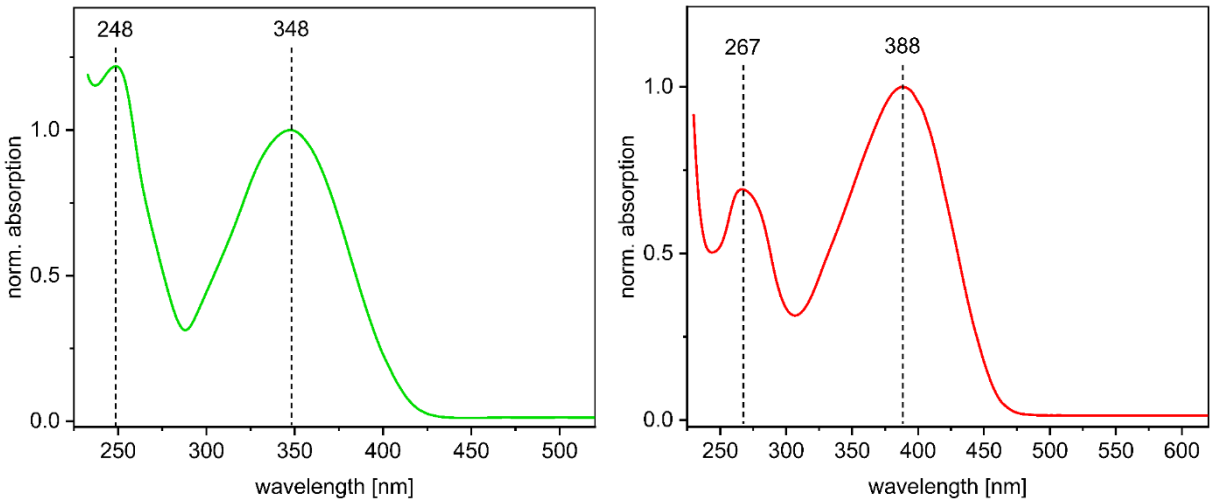

Figure S5.7.50. Normalized absorption spectra of **10** (left) and **11** (right) in THF.

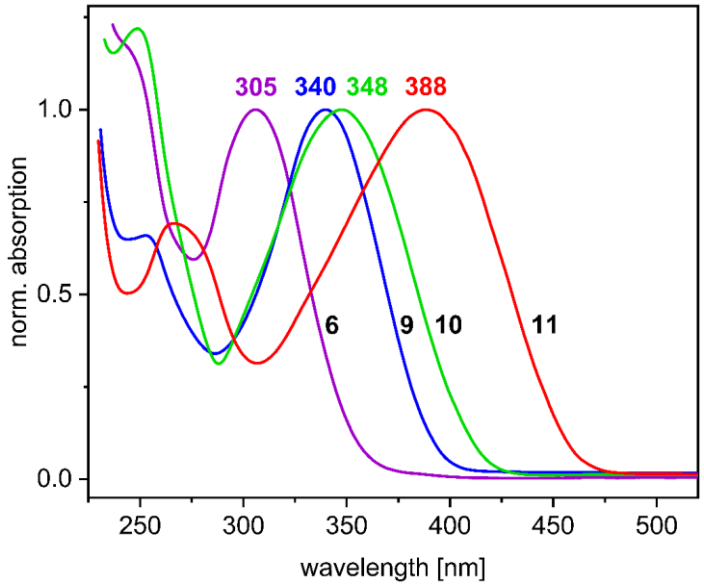

Figure S5.7.51. Normalized absorption spectra of **6** (purple), **9** (blue), **10** (green) and **11** (red) in THF.

Cyclic voltammograms

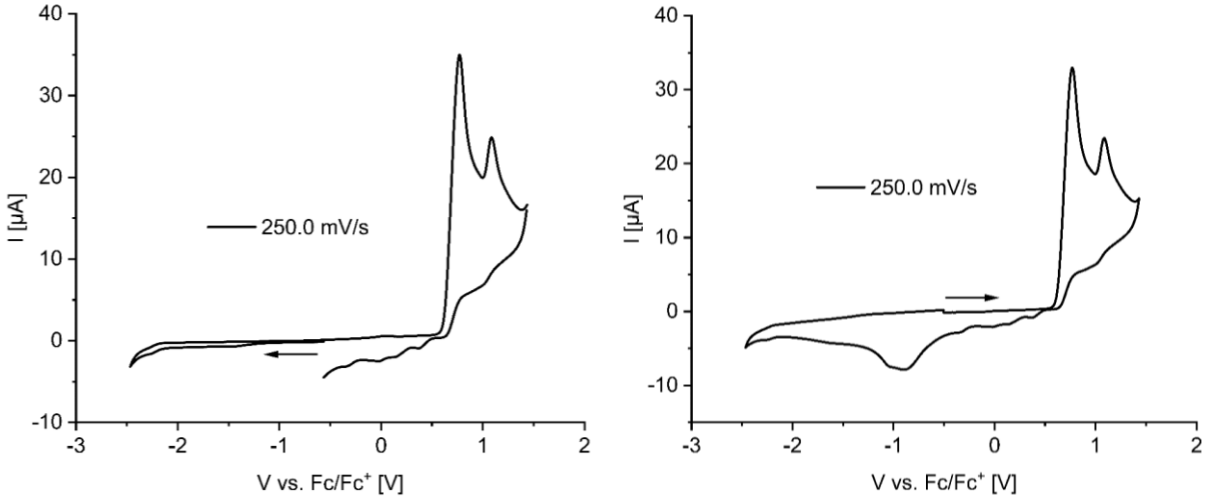

Figure S5.7.52. Cyclic voltammograms of **6** in DCM (vs. $[Cp_2Fe]^{0/+}$, scan rate: 250 mV s^{-1}).

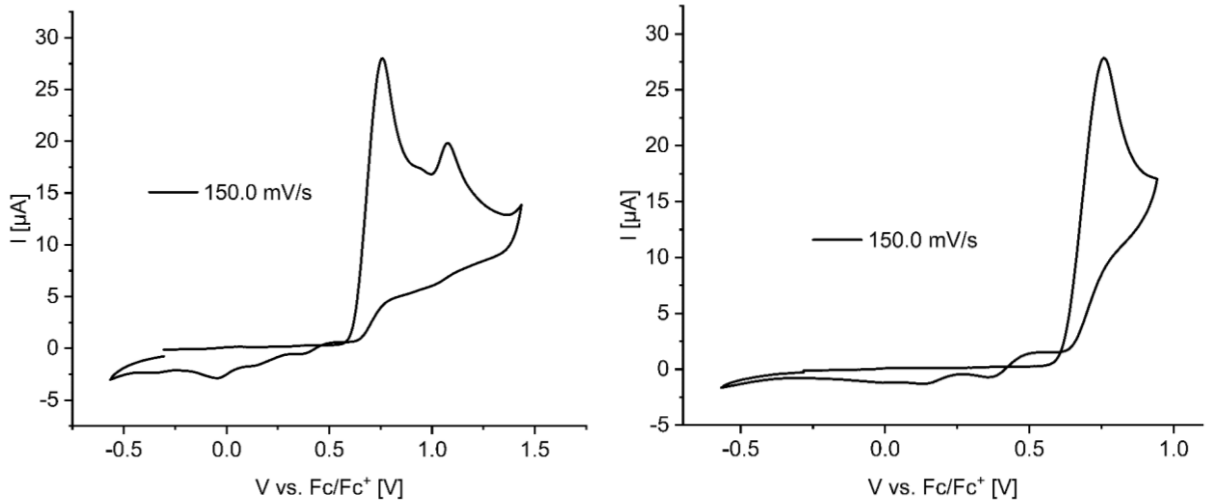

Figure S5.7.53. Cyclic voltammograms of the oxidation process (left) and the first oxidation event (right) of **6** in DCM (vs. $[Cp_2Fe]^{0/+}$, scan rate: 150 mV s^{-1}).

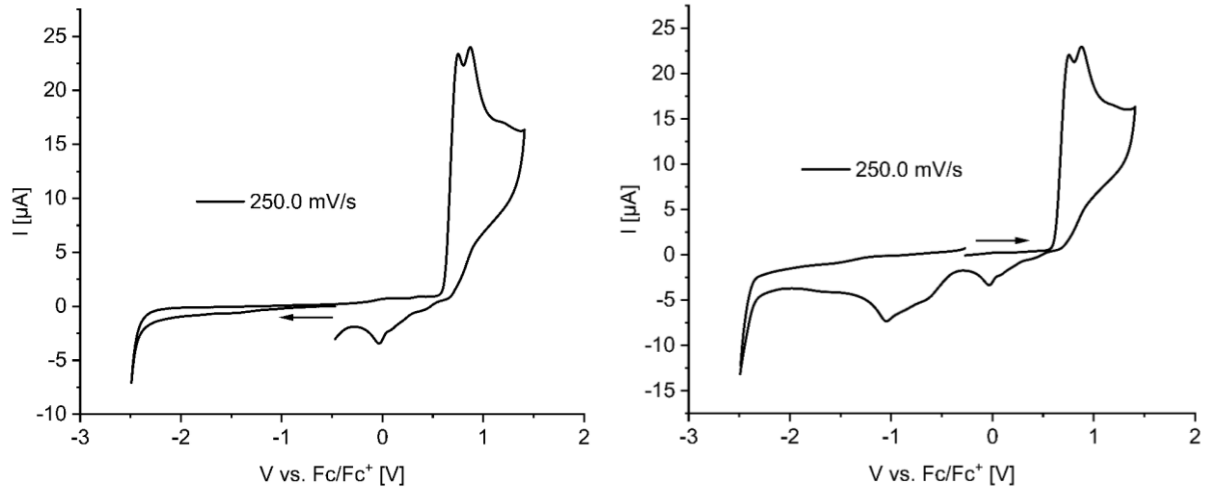

Figure S5.7.54. Cyclic voltammograms of **9** in DCM (vs. $[Cp_2Fe]^{0/+}$, scan rate: 250 mV s^{-1}).

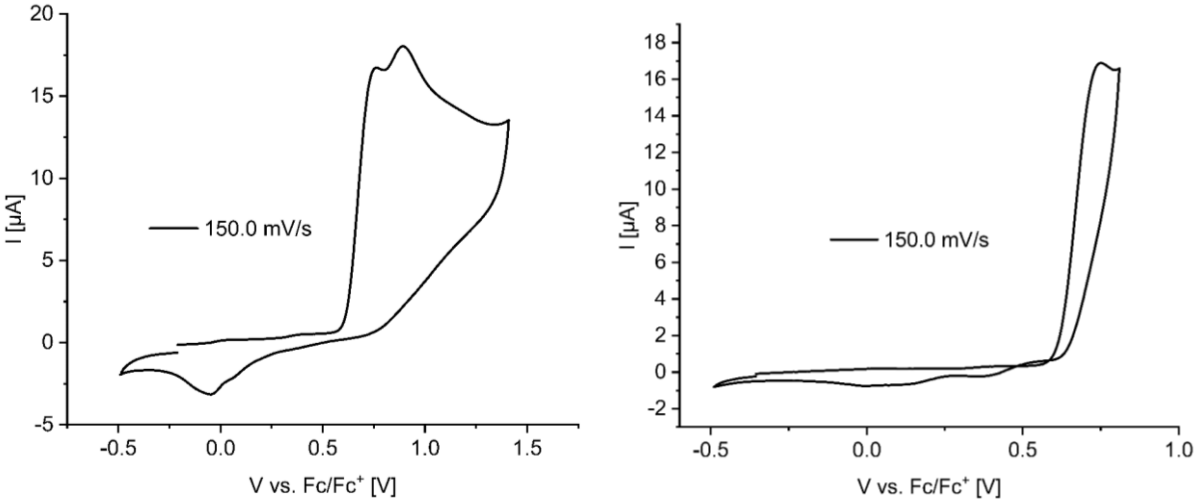

Figure S5.7.55. Cyclic voltammograms of the oxidation process (left) and the first oxidation event (right) of **9** in DCM (vs. $[Cp_2Fe]^{0/+}$, scan rate: 150 mV s^{-1}).

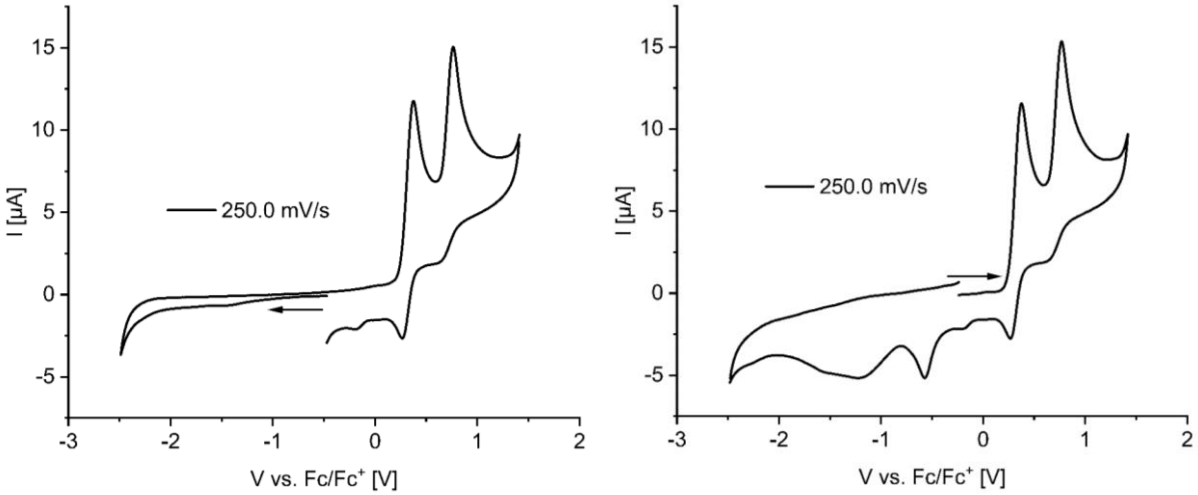

Figure S5.7.56. Cyclic voltammograms of **10** in DCM (vs. $[Cp_2Fe]^{0/+}$, scan rate: 250 mV s^{-1}).

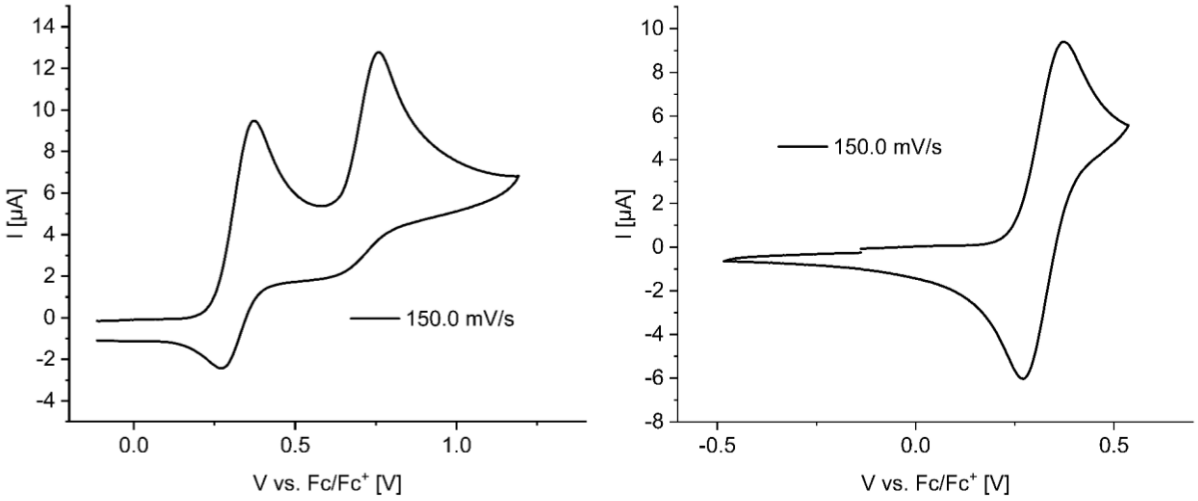

Figure S5.7.57. Cyclic voltammograms of the oxidation process (left) and the first oxidation event (right) of **10** in DCM (vs. $[Cp_2Fe]^{0/+}$, scan rate: 150 mV s^{-1}).

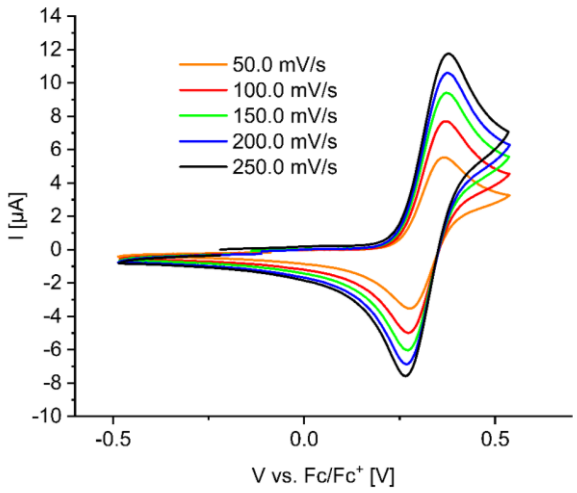

Figure S5.7.58. Cyclic voltammograms of the reversible first oxidation of **10** in DCM at different scan rates (vs. $[Cp_2Fe]^{0/+}$, scan rate: 50-250 mV s^{-1}).

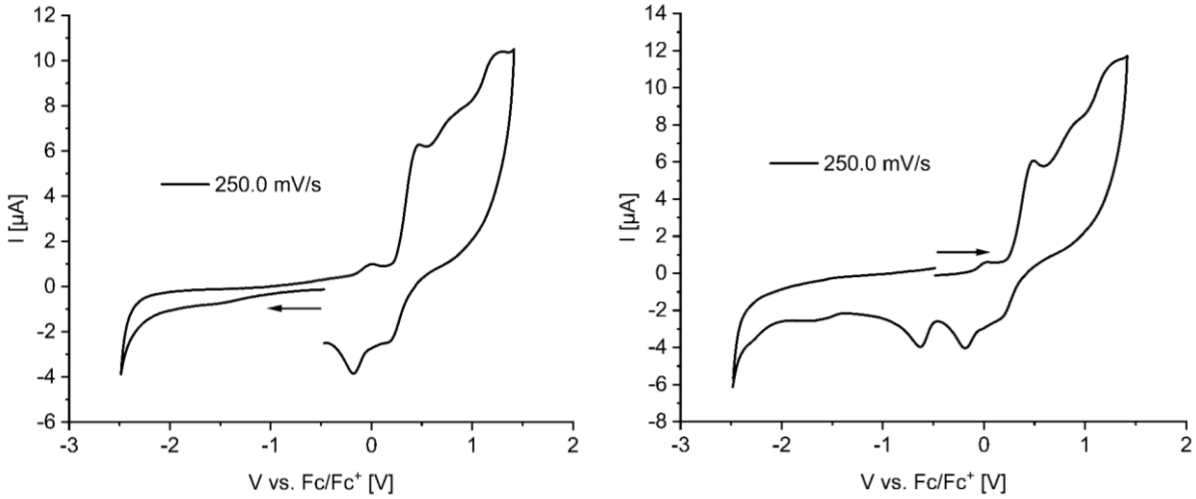

Figure S5.7.59. Cyclic voltammograms of **11** in DCM (vs. $[Cp_2Fe]^{0/+}$, scan rate: 250 mV s^{-1}).

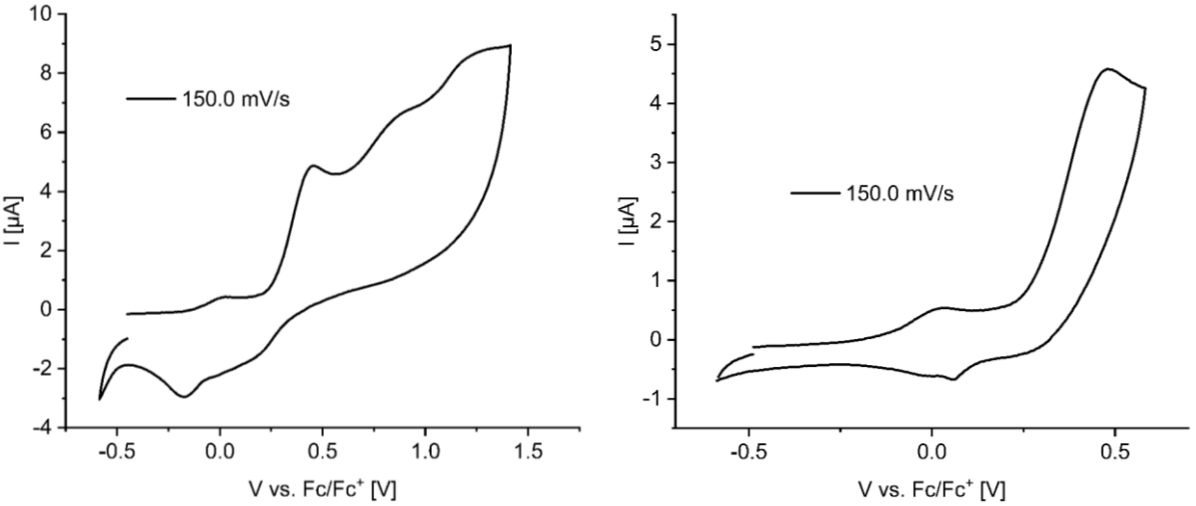

Figure S5.7.60. Cyclic voltammograms of the oxidation process (left) and the first oxidation event (right) of **11** in DCM (vs. $[Cp_2Fe]^{0/+}$, scan rate: 150 mV s^{-1}).

GPC traces

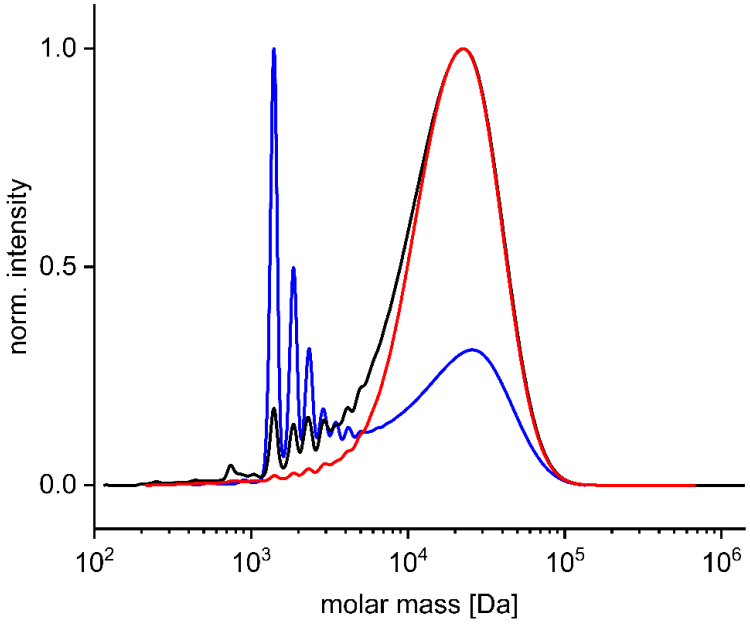

Figure S5.7.61. Normalized gel permeation chromatography (GPC) traces of **11** after termination with $TMSNMe_2$ (blue), after first (black) and second (red) precipitation in cold methanol detected by UV-vis detector at 254 nm.

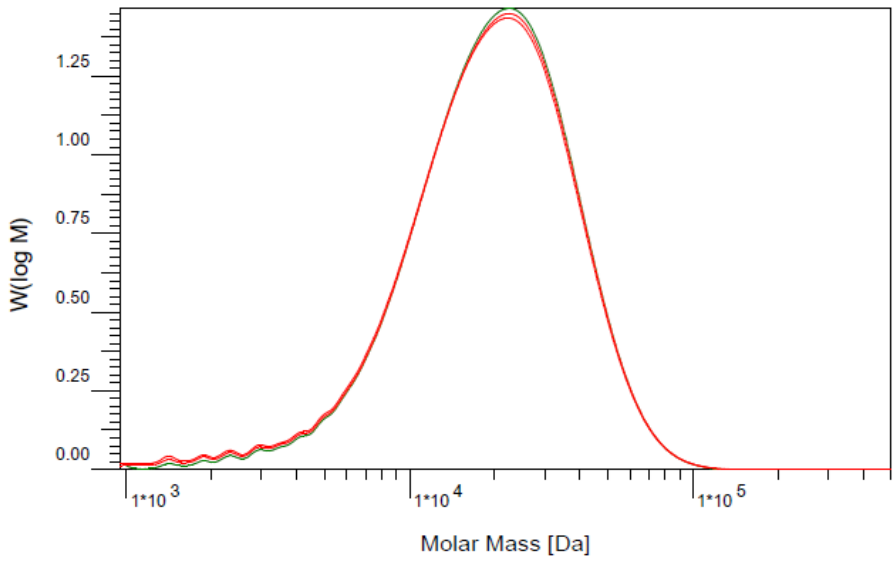

	I1: RID 1, RI Signal	Unsicherheit [%]	I1: VWD 1, Signal A	Unsicherheit [%]	I1: VWD 1, Signal B	Unsicherheit [%]	
Mn :	1.4875e4	3.85	1.4231e4	0.48	1.3743e4	0.37	g/mol
Mw :	2.3191e4	3.85	2.3040e4	0.46	2.2807e4	0.35	g/mol
Mz :	3.1963e4	3.85	3.2054e4	0.47	3.1936e4	0.37	g/mol
Mv :	0.000000	3.85	0.000000	0.48	0.000000	0.37	g/mol
D :	1.5591e0	5.44	1.6190e0	0.66	1.6596e0	0.50	
[n]:	0.000000	0.00	0.000000	0.00	0.000000	0.00	ml/g
Vp :	2.0982e1	3.85	2.0998e1	0.46	2.1015e1	0.35	ml
Mp :	2.4097e4	3.86	2.3928e4	0.49	2.3756e4	0.38	g/mol
FI :	1.7732e1	3.85	1.4202e3	0.46	1.6265e3	0.35	ml*V
< 948	0.00	3.85	0.00	0.46	0.00	0.35	
w% :	100.00	3.85	100.00	0.46	100.00	0.35	
> 501550	0.00	3.85	0.00	0.46	0.00	0.35	

Figure S5.7.62. Original GPC data of **11** (in THF, vs polystyrene standard).

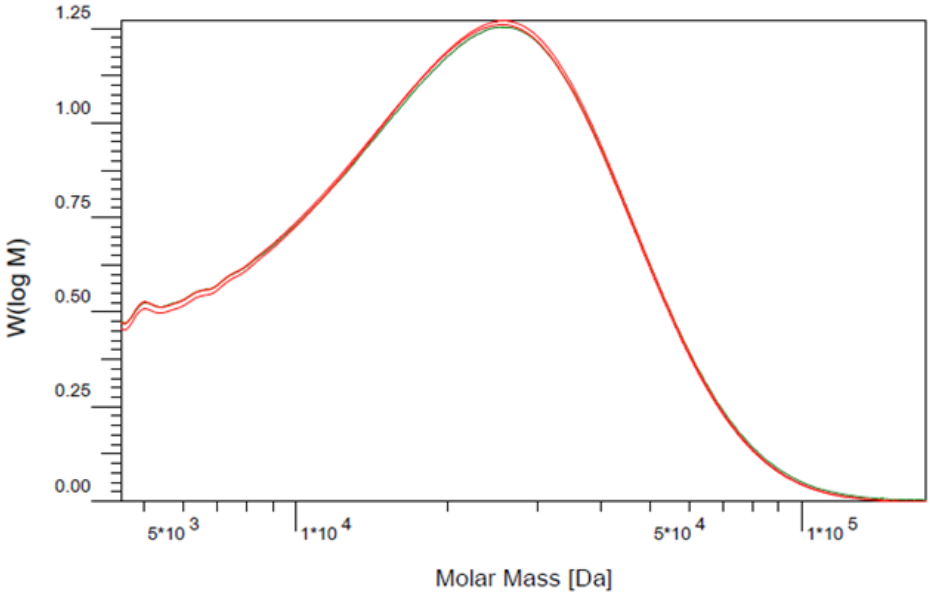

	I1: RID 1, RI Signal	Unsicherheit [%]	I1: VWD 1, Signal A	Unsicherheit [%]	I1: VWD 1, Signal B	Unsicherheit [%]	
Mn :	1.5231e4	3.35	1.5333e4	0.16	1.5170e4	0.20	g/mol
Mw :	2.4698e4	3.35	2.4597e4	0.09	2.4385e4	0.16	g/mol
Mz :	3.7090e4	3.35	3.6315e4	0.14	3.6114e4	0.19	g/mol
Mv :	0.000000	3.35	0.000000	0.16	0.000000	0.20	g/mol
D :	1.6215e0	4.73	1.6042e0	0.18	1.6074e0	0.25	
[n]:	0.000000	0.00	0.000000	0.00	0.000000	0.00	ml/g
Vp :	2.0663e1	3.35	2.0646e1	0.07	2.0663e1	0.14	ml
Mp :	2.7712e4	3.35	2.7922e4	0.18	2.7716e4	0.22	g/mol
FI :	7.8494e0	3.35	5.9836e2	0.07	6.8378e2	0.14	ml*V
< 4530	0.00	3.35	0.00	0.07	0.00	0.14	
w% :	100.00	3.35	100.00	0.07	100.00	0.14	
> 176036	0.00	3.35	0.00	0.07	0.00	0.14	

Figure S5.7.63. Detail of the original GPC data of the distribution around higher molecular weights of crude **11** (in THF, vs polystyrene standard).

Cartesian coordinates (Å) and total energies (a.u.) of optimized stationary points

Compound **6**:
Total energy (ωB97X-D/def2-SVP): -1769.33616638

C	-1.072693000	-4.874584000	-0.204109000
C	0.231945000	-4.492610000	-0.103518000
S	0.398877000	-2.773984000	-0.027841000
C	-1.324686000	-2.556914000	-0.133542000
C	-1.969933000	-3.765605000	-0.221718000
H	-1.393304000	-5.914720000	-0.264287000
H	1.119652000	-5.121408000	-0.068304000
H	-3.054743000	-3.853479000	-0.296823000
N	-1.945644000	-1.308920000	-0.128447000
H	-2.953123000	-1.410692000	-0.201711000
B	-1.422174000	0.004063000	-0.042079000
C	-2.044026000	2.551086000	0.017023000
C	-2.400914000	1.220530000	-0.065806000
S	-4.126177000	1.095356000	-0.203695000
C	-4.342694000	2.794719000	-0.149058000
C	-3.144951000	3.450011000	-0.029682000
H	-1.001671000	2.862108000	0.109395000
H	-3.057240000	4.535413000	0.022376000
C	0.124868000	0.294744000	0.078019000
C	0.728052000	0.402216000	1.343455000
C	0.898689000	0.494781000	-1.081609000
C	2.091066000	0.698381000	1.430505000
C	2.256431000	0.788988000	-0.957899000
C	2.873041000	0.891911000	0.291960000
H	2.564611000	0.780144000	2.413732000
H	2.854206000	0.940888000	-1.861587000
C	-0.090471000	0.207245000	2.612409000
H	-1.099912000	-0.118977000	2.308993000
C	0.480867000	-0.896912000	3.507301000
H	-0.181695000	-1.080219000	4.367382000
H	0.590323000	-1.838190000	2.948906000
H	1.470401000	-0.621548000	3.905234000
C	-0.255787000	1.526250000	3.373956000
H	-0.885392000	1.387421000	4.266708000
H	0.719580000	1.916183000	3.706468000
H	-0.727910000	2.290535000	2.738855000
C	0.263423000	0.401829000	-2.462340000
H	-0.773974000	0.051004000	-2.327553000
C	0.188118000	1.778492000	-3.130334000
H	-0.310737000	1.712794000	-4.109878000
H	-0.376120000	2.487695000	-2.506629000
H	1.195323000	2.195118000	-3.291679000

C	0.964604000	-0.625359000	-3.356486000
H	1.008704000	-1.608669000	-2.865594000
H	0.427409000	-0.739070000	-4.310831000
H	1.995577000	-0.317572000	-3.592721000
C	4.355670000	1.199474000	0.408143000
H	4.591897000	1.241154000	1.484823000
C	5.209004000	0.085499000	-0.207804000
H	6.281714000	0.285015000	-0.058747000
H	4.973617000	-0.889349000	0.244378000
H	5.031742000	0.002749000	-1.292009000
C	4.700946000	2.566257000	-0.192171000
H	5.765670000	2.802805000	-0.040397000
H	4.506885000	2.586060000	-1.276435000
H	4.102094000	3.365264000	0.269654000
H	-5.339821000	3.229136000	-0.207784000

Compound **9**:
Total energy (ωB97X-D/def2-SVP): -2985.96362470

C	7.425134000	-2.632411000	-1.257764000
C	7.477645000	-1.358969000	-0.774188000
S	5.912207000	-0.765920000	-0.344080000
C	5.165073000	-2.261324000	-0.823904000
C	6.097768000	-3.155248000	-1.287498000
H	8.303180000	-3.188208000	-1.587056000
H	8.349385000	-0.720175000	-0.645441000
H	5.837838000	-4.154665000	-1.639115000
N	3.794595000	-2.490406000	-0.725633000
H	3.555524000	-3.434041000	-1.010762000
B	2.736288000	-1.653860000	-0.307736000
C	0.736093000	-3.503068000	-0.345309000
C	1.279603000	-2.230572000	-0.262040000
S	0.018040000	-1.085548000	-0.035923000
C	-1.232266000	-2.265301000	-0.046955000
C	-0.675843000	-3.522906000	-0.220818000
H	1.334723000	-4.406844000	-0.482804000
H	-1.265684000	-4.441368000	-0.271395000
N	-3.748714000	-2.632571000	0.338714000
B	-2.696197000	-1.723217000	0.095522000
C	-6.050458000	-3.406012000	0.748012000
C	-5.122235000	-2.436423000	0.461699000
S	-5.879205000	-0.885588000	0.246302000
C	-7.443224000	-1.558239000	0.545608000
C	-7.382648000	-2.896825000	0.795999000
H	-5.784159000	-4.449889000	0.919512000
H	-8.319911000	-0.913706000	0.522725000
H	-8.258325000	-3.509281000	1.011390000
H	-3.502228000	-3.610557000	0.446825000
C	2.884214000	-0.142134000	0.140446000
C	3.072361000	0.159333000	1.504754000
C	2.587513000	0.896507000	-0.762301000
C	2.935999000	1.476992000	1.940086000
C	2.473010000	2.207459000	-0.291928000
C	2.619795000	2.515362000	1.059894000
H	3.055933000	1.709248000	3.003075000
H	2.239520000	3.004024000	-1.000922000
C	3.355529000	-0.949522000	2.510335000
H	3.582651000	-1.864983000	1.937615000
C	4.583983000	-0.658198000	3.376713000
H	4.812824000	-1.519679000	4.023026000
H	5.466207000	-0.452804000	2.753079000
H	4.419668000	0.210701000	4.033234000
C	2.119510000	-1.244749000	3.367656000
H	2.309666000	-2.085097000	4.053660000
H	1.844870000	-0.367191000	3.974517000
H	1.253011000	-1.500978000	2.740069000
C	2.382407000	0.607629000	-2.243591000
H	2.236470000	-0.481480000	-2.351206000
C	1.131201000	1.283276000	-2.812955000
H	0.933267000	0.924538000	-3.834848000
H	0.243423000	1.073898000	-2.197128000
H	1.251839000	2.376507000	-2.869458000
C	3.632528000	0.976691000	-3.050699000
H	4.520626000	0.449932000	-2.672357000
H	3.503291000	0.720447000	-4.113993000
H	3.830946000	2.058654000	-2.984212000
C	2.358467000	3.908491000	1.608127000
H	3.036936000	4.046165000	2.467771000
C	2.639664000	5.034421000	0.613267000
H	2.562936000	6.012431000	1.111980000
H	3.647159000	4.949241000	0.179390000
H	1.911763000	5.035738000	-0.213369000
C	0.919033000	3.992252000	2.136888000
H	0.714318000	4.982111000	2.574597000
H	0.198902000	3.819730000	1.321177000
H	0.732510000	3.228705000	2.906139000
C	-2.850005000	-0.155135000	-0.064792000
C	-2.566880000	0.695894000	1.020334000
C	-3.003288000	0.392467000	-1.354952000
C	-2.427631000	2.068078000	0.796977000
C	-2.840946000	1.764830000	-1.542788000
C	-2.535670000	2.618161000	-0.479195000
H	-2.194883000	2.730504000	1.635274000
H	-2.927643000	2.178850000	-2.551613000
C	-3.275127000	-0.511091000	-2.551130000
H	-3.510381000	-1.515669000	-2.159772000
C	-2.031962000	-0.647728000	-3.437236000
H	-2.216233000	-1.350545000	-4.264870000
H	-1.753352000	0.324413000	-3.874232000
H	-1.169927000	-1.013024000	-2.859415000
C	-4.494341000	-0.058629000	-3.359725000
H	-5.383566000	0.025513000	-2.718142000
H	-4.323009000	0.919623000	-3.835969000
H	-4.715518000	-0.780516000	-4.161118000
C	-2.397055000	0.135612000	2.426115000
H	-2.258578000	-0.955738000	2.331970000
C	-1.156295000	0.682390000	3.138608000
H	-0.981099000	0.135922000	4.078182000
H	-0.256991000	0.586382000	2.511756000
H	-1.276396000	1.746132000	3.397752000
C	-3.663920000	0.358397000	3.260347000
H	-3.559936000	-0.091806000	4.260076000
H	-3.856601000	1.435453000	3.391552000
H	-4.544965000	-0.082164000	2.771497000
C	-2.263822000	4.093736000	-0.710015000
H	-2.108887000	4.550238000	0.282409000
C	-0.969558000	4.283538000	-1.510314000
H	-0.710519000	5.350714000	-1.596253000
H	-0.129862000	3.758616000	-1.030136000
H	-1.071675000	3.877136000	-2.529325000
C	-3.444138000	4.811711000	-1.369876000
H	-3.241141000	5.889698000	-1.465983000
H	-3.636775000	4.419600000	-2.381098000
H	-4.364745000	4.686216000	-0.780883000

Compound **10**:
Total energy (ωB97X-D/def2-SVP): -2985.96183563

S	-0.729592000	0.294617000	-0.560431000
N	1.770587000	1.280435000	-0.898355000
H	1.308704000	2.174841000	-1.031276000
B	3.094546000	1.268633000	-0.395272000
N	-2.269319000	-1.982656000	-0.834593000
H	-2.212236000	-2.968124000	-1.072448000
B	-3.524885000	-1.473023000	-0.426845000
C	-1.029611000	-1.365714000	-0.997775000
C	0.100170000	-1.951928000	-1.502096000
H	0.128475000	-2.990171000	-1.835293000

C	1.221590000	-1.069383000	-1.561515000
H	2.208720000	-1.357564000	-1.917609000
C	0.931696000	0.177532000	-1.091762000
C	-3.747322000	0.053106000	-0.083929000
C	-4.142637000	0.942751000	-1.098418000
C	-4.369314000	2.285988000	-0.784913000
H	-4.669845000	2.981724000	-1.574598000
C	-4.216987000	2.770504000	0.513338000
C	-3.829943000	1.872242000	1.511883000
H	-3.706228000	2.236403000	2.535575000
C	-3.590652000	0.526826000	1.234108000
C	3.855701000	-0.081746000	-0.088064000
C	4.868066000	-0.519562000	-0.961871000
C	5.558701000	-1.702682000	-0.681164000
H	6.343885000	-2.044850000	-1.362793000
C	5.273582000	-2.466795000	0.449401000
C	4.262703000	-2.021458000	1.304465000
H	4.023079000	-2.609477000	2.195465000
C	3.547229000	-0.850183000	1.052176000
S	-4.669283000	-4.152282000	-0.600632000
C	-4.747851000	-2.439446000	-0.334103000
C	-6.048739000	-2.080643000	-0.045258000
H	-6.327582000	-1.045498000	0.161029000
C	-6.963103000	-3.169855000	-0.043472000
H	-8.029708000	-3.079012000	0.162979000
C	-6.348965000	-4.360883000	-0.330778000
H	-6.802126000	-5.349496000	-0.391727000
S	3.244239000	4.172032000	-0.641653000
C	3.818989000	2.623436000	-0.111750000
C	4.979074000	2.788550000	0.616214000
H	5.514609000	1.939725000	1.045742000
C	5.390205000	4.144020000	0.749040000
H	6.279767000	4.468087000	1.289690000
C	4.538457000	5.007543000	0.111417000
H	4.615416000	6.091710000	0.040038000
C	5.208334000	0.264376000	-2.223822000
H	4.520517000	1.124306000	-2.280849000
C	6.628496000	0.834727000	-2.170385000
H	6.756969000	1.483798000	-1.291833000
H	6.844584000	1.431897000	-3.069970000
H	7.379290000	0.030538000	-2.112012000
C	4.982598000	-0.566555000	-3.491420000
H	5.657747000	-1.435920000	-3.529766000
H	5.168774000	0.039251000	-4.391812000
H	3.949342000	-0.941503000	-3.544138000
C	2.454873000	-0.419946000	2.022406000
H	1.950098000	0.459981000	1.592332000
C	1.384318000	-1.501488000	2.198919000
H	0.946036000	-1.784621000	1.230197000
H	0.573553000	-1.140110000	2.848545000
H	1.799957000	-2.409938000	2.663216000
C	3.048241000	0.017064000	3.365935000
H	3.564514000	-0.819301000	3.864013000
H	2.258546000	0.377034000	4.043926000
H	3.777896000	0.829434000	3.228577000
C	6.033886000	-3.749313000	0.738247000
H	6.772465000	-3.874777000	-0.071527000
C	6.807808000	-3.663455000	2.057917000
H	7.488053000	-2.798870000	2.063141000
H	7.406141000	-4.573378000	2.221533000
H	6.123313000	-3.556118000	2.914451000
C	5.108432000	-4.970473000	0.710980000
H	4.351955000	-4.913555000	1.509880000
H	5.680380000	-5.900009000	0.858063000
H	4.575656000	-5.042376000	-0.248890000
C	-3.176378000	-0.421444000	2.351391000
H	-2.795410000	-1.342720000	1.877517000
C	-2.037603000	0.137837000	3.208808000
H	-1.189747000	0.451507000	2.582055000
H	-1.679988000	-0.624617000	3.918047000
H	-2.362897000	1.006732000	3.802158000
C	-4.382976000	-0.814644000	3.210897000
H	-4.090108000	-1.528495000	3.996671000
H	-5.168403000	-1.282615000	2.599649000
H	-4.816547000	0.071779000	3.701382000
C	-4.310846000	0.462566000	-2.533428000
H	-4.052906000	-0.609490000	-2.558601000
C	-3.344753000	1.173916000	-3.486559000
H	-3.569047000	2.250427000	-3.553961000
H	-3.419131000	0.754130000	-4.501759000
H	-2.305025000	1.066755000	-3.143590000
C	-5.763999000	0.581740000	-3.001916000
H	-6.096619000	1.631979000	-3.009192000
H	-6.438002000	0.017656000	-2.340113000
H	-5.879136000	0.186508000	-4.023198000
C	-4.450119000	4.237139000	0.830650000
H	-4.767102000	4.722607000	-0.107772000
C	-5.577131000	4.427472000	1.850893000
H	-5.314066000	3.983037000	2.823980000
H	-6.508230000	3.953090000	1.506919000
H	-5.777340000	5.497376000	2.017524000
C	-3.157557000	4.921137000	1.289485000
H	-3.319910000	5.997867000	1.453727000
H	-2.360123000	4.803480000	0.540766000
H	-2.793960000	4.489329000	2.235572000

Compound **Trimer**:

Total energy (ωB97X-D/def2-SVP): -4202.58750019

S	-3.749992000	-0.094899000	-0.858834000
N	-1.154762000	-0.088078000	-1.624280000
H	-1.360691000	0.823441000	-2.018710000
B	0.157728000	-0.337438000	-1.163352000
N	-5.870298000	-1.746360000	-0.224263000
H	-6.131634000	-2.723021000	-0.130284000
B	-6.841670000	-0.767758000	0.094406000
C	-4.551036000	-1.630275000	-0.659703000
C	-3.714188000	-2.664742000	-0.980904000
H	-4.018732000	-3.710590000	-0.923880000
C	-2.417400000	-2.238535000	-1.403392000
H	-1.609607000	-2.915949000	-1.672592000
C	-2.284297000	-0.881818000	-1.396183000
C	-6.563207000	0.780376000	-0.057371000
C	-6.889374000	1.426574000	-1.262750000
C	-6.672442000	2.802035000	-1.386581000
H	-6.918626000	3.305324000	-2.326832000
C	-6.142021000	3.555999000	-0.341069000
C	-5.828245000	2.900187000	0.852906000
H	-5.411463000	3.477931000	1.682439000
C	-6.026057000	1.528805000	1.009625000
C	0.609274000	-1.682595000	-0.459295000
C	1.465916000	-2.579997000	-1.127310000
C	2.043997000	-3.636133000	-0.418880000
H	2.715301000	-4.328468000	-0.934431000
C	1.824680000	-3.812088000	0.946403000
C	0.950204000	-2.933775000	1.588944000
H	0.762711000	-3.055075000	2.659796000
C	0.333337000	-1.882196000	0.908486000
S	-8.710503000	-2.872288000	0.866105000
C	-8.250971000	-1.222079000	0.589670000
C	-9.322122000	-0.396694000	0.865310000
H	-9.254387000	0.687913000	0.760977000
C	-10.491121000	-1.086873000	1.288950000
H	-11.432288000	-0.602657000	1.550155000
C	-10.302104000	-2.443498000	1.335502000
H	-11.019925000	-3.209250000	1.626650000
S	2.775595000	0.402651000	-0.563156000

C	1.245143000	0.788556000	-1.246208000
C	1.257068000	2.103290000	-1.684672000
H	0.402724000	2.586214000	-2.165147000
C	2.487183000	2.768497000	-1.446839000
H	2.674283000	3.804857000	-1.737679000
C	3.434919000	1.967489000	-0.830623000
C	1.778849000	-2.410519000	-2.608979000
H	1.498961000	-1.381274000	-2.891876000
C	3.270034000	-2.566851000	-2.921408000
H	3.885998000	-1.935985000	-2.262740000
H	3.475333000	-2.279460000	-3.964116000
H	3.603705000	-3.609261000	-2.798682000
C	0.930375000	-3.357796000	-3.465076000
H	1.133292000	-4.408734000	-3.203531000
H	1.152958000	-3.225264000	-4.535491000
H	-0.144555000	-3.174399000	-3.320689000
C	-0.583892000	-0.937797000	1.674986000
H	-0.990566000	-0.206116000	0.959341000
C	-1.783664000	-1.678443000	2.273928000
H	-2.354087000	-2.198505000	1.489820000
H	-2.461488000	-0.973889000	2.777999000
H	-1.465153000	-2.425827000	3.018089000
C	0.186673000	-0.141796000	2.733473000
H	0.610455000	-0.804221000	3.505177000
H	-0.476034000	0.579754000	3.236794000
H	1.019155000	0.414661000	2.276762000
C	2.588678000	-4.874028000	1.716494000
H	3.084195000	-5.517565000	0.969577000
C	3.689512000	-4.220947000	2.562946000
H	4.345372000	-3.592575000	1.941270000
H	4.308744000	-4.982239000	3.063331000
H	3.252641000	-3.573276000	3.340074000
C	1.681675000	-5.767070000	2.566307000
H	1.187635000	-5.194661000	3.367254000
H	2.264565000	-6.567916000	3.047132000
H	0.896093000	-6.234196000	1.953914000
C	-5.678180000	0.852438000	2.329101000
H	-5.646019000	-0.235130000	2.143260000
C	-4.296612000	1.251669000	2.855209000
H	-3.521559000	1.095488000	2.090095000
H	-4.034672000	0.650982000	3.739924000
H	-4.266086000	2.309036000	3.161468000
C	-6.769197000	1.105955000	3.375632000
H	-6.538525000	0.585432000	4.318280000
H	-7.748012000	0.751945000	3.020514000
H	-6.855618000	2.182628000	3.593897000
C	-7.457602000	0.642879000	-2.438007000
H	-7.515726000	-0.416275000	-2.135917000
C	-6.534569000	0.705450000	-3.659488000
H	-6.461748000	1.731493000	-4.054088000
H	-6.915348000	0.063653000	-4.469105000
H	-5.519074000	0.370245000	-3.401253000
C	-8.883127000	1.087503000	-2.777554000
H	-8.907841000	2.142148000	-3.095056000
H	-9.546386000	0.980335000	-1.906309000
H	-9.296890000	0.480611000	-3.597871000
C	-5.896788000	5.046162000	-0.500309000
H	-6.246377000	5.323639000	-1.509066000
C	-6.704614000	5.868189000	0.509115000
H	-6.387615000	5.655156000	1.542407000
H	-7.778812000	5.642609000	0.435281000
H	-6.566847000	6.946702000	0.334879000
C	-4.402162000	5.376864000	-0.423515000
H	-4.226973000	6.448723000	-0.605574000
H	-3.831571000	4.803143000	-1.169019000
H	-3.992379000	5.134517000	0.569990000
N	5.382533000	3.466403000	-0.049295000
H	4.730942000	4.239415000	-0.129833000
B	4.910113000	2.167680000	-0.341538000
C	6.630086000	3.812598000	0.474809000
S	6.744283000	5.077926000	1.663738000
C	7.850440000	3.232778000	0.249898000
H	7.995647000	2.409667000	-0.446542000
C	8.885716000	3.820338000	1.037348000
H	9.928113000	3.504019000	0.996374000
C	8.443511000	4.834783000	1.836450000
C	5.740444000	0.831944000	-0.158593000
C	5.698543000	0.131218000	1.059767000
C	6.200039000	-1.172362000	1.116764000
H	6.160092000	-1.724673000	2.059886000
C	6.719426000	-1.810093000	-0.008573000
C	6.783334000	-1.089587000	-1.204666000
H	7.190313000	-1.572207000	-2.098107000
C	6.309075000	0.219308000	-1.292905000
C	6.355147000	0.961790000	-2.623342000
H	6.077353000	2.011883000	-2.424055000
C	7.761495000	0.986403000	-3.230099000
H	8.500103000	1.393609000	-2.523329000
H	7.780848000	1.608282000	-4.138319000
H	8.095088000	-0.023636000	-3.515015000
C	5.332110000	0.402371000	-3.617473000
H	5.334117000	0.985814000	-4.551501000
H	4.315865000	0.426760000	-3.197584000
H	5.565341000	-0.643963000	-3.870581000
C	5.104695000	0.773544000	2.305633000
H	4.523721000	1.653058000	1.978183000
C	6.214204000	1.288648000	3.230780000
H	6.833318000	0.453112000	3.595675000
H	5.788305000	1.803458000	4.106250000
H	6.875063000	1.993570000	2.704706000
C	4.132633000	-0.150682000	3.045468000
H	4.655549000	-0.997700000	3.516924000
H	3.373390000	-0.561805000	2.362860000
H	3.614034000	0.398431000	3.846550000
C	7.137540000	-3.268178000	0.056128000
H	7.091973000	-3.567584000	1.117033000
C	6.140283000	-4.144985000	-0.711456000
H	6.153388000	-3.905631000	-1.786998000
H	5.113502000	-3.983021000	-0.350047000
H	6.384556000	-5.213145000	-0.599046000
C	8.572758000	-3.494485000	-0.426000000
H	8.865062000	-4.548387000	-0.298460000
H	9.283781000	-2.870372000	0.135467000
H	8.681599000	-3.249578000	-1.494495000
H	9.020789000	5.467063000	2.508169000

5.8 Poly(arylene iminoborane)s, Analogues of Poly(arylene vinylene) with a BN-Doped Backbone: A Comprehensive Study

NMR spectra

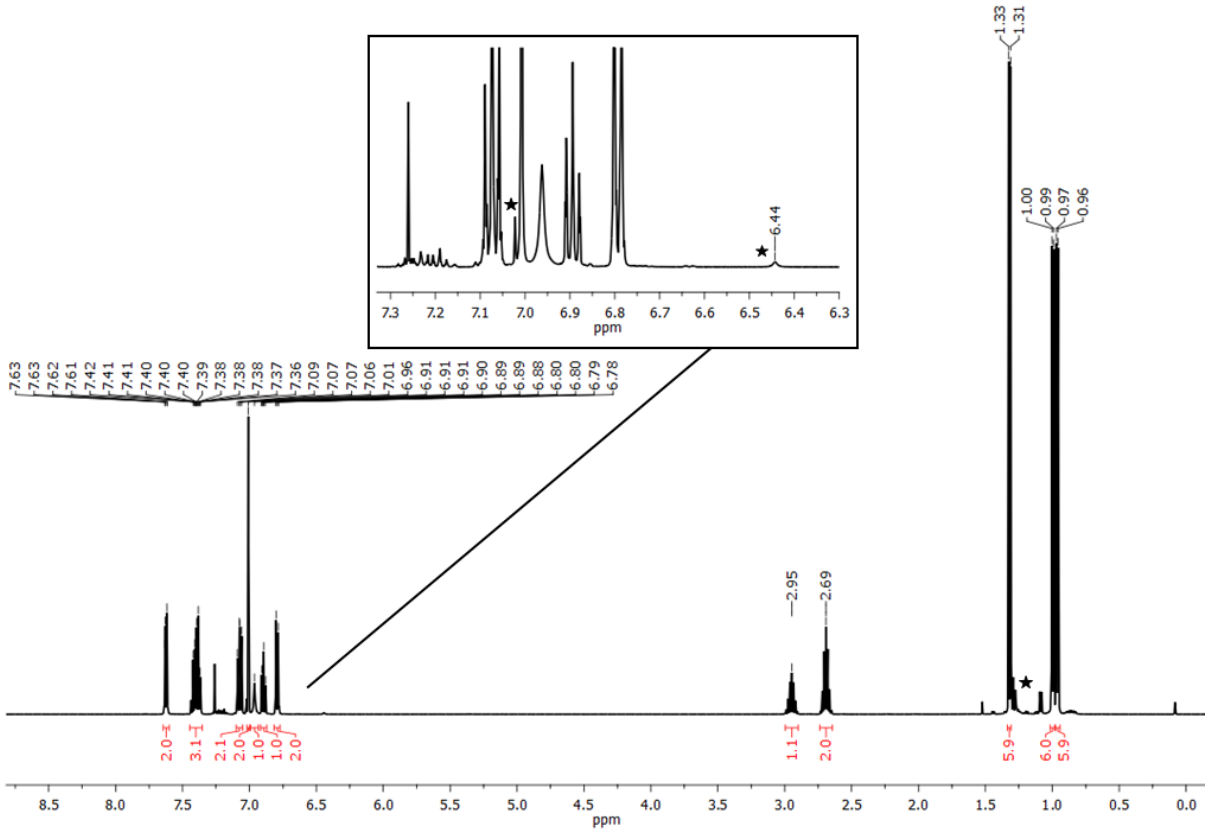

Figure S5.8.1. ^{1}H NMR spectrum (500 MHz) of **3** in $CDCl_3$. The signals marked with an asterisk belong to the minor isomer.

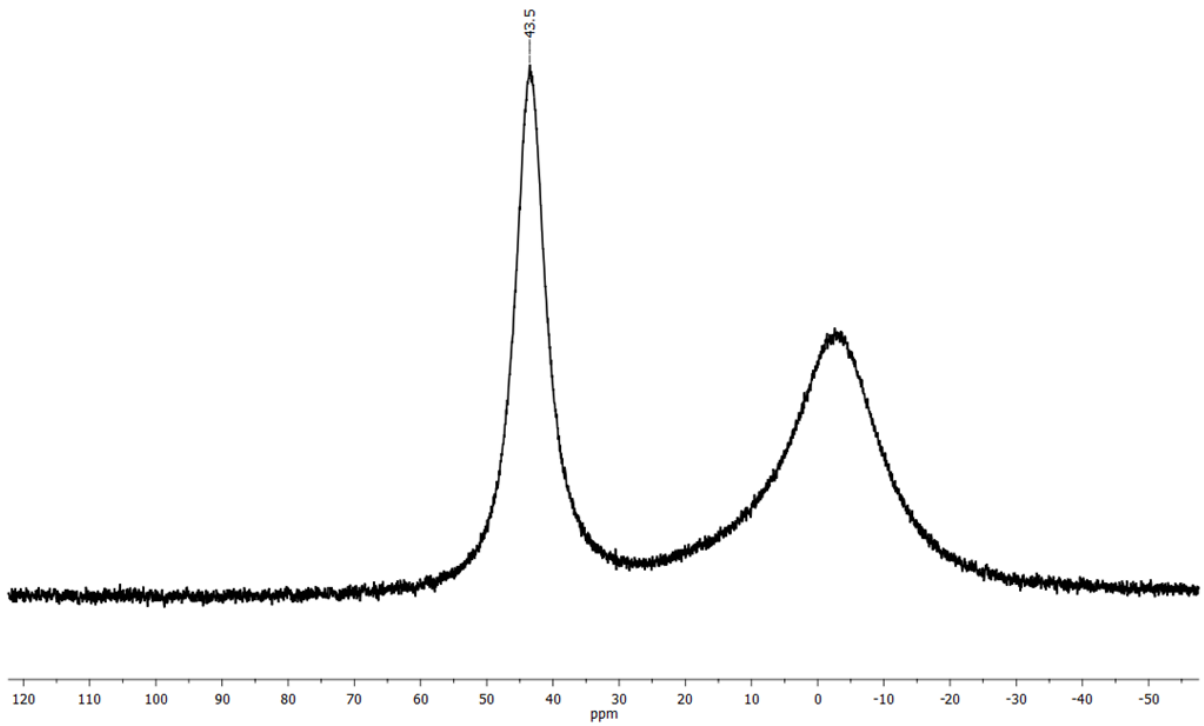

Figure S5.8.2. $^{11}B\{^{1}H\}$ NMR spectrum (160 MHz) of **3** in $CDCl_3$ with reduced glass background.

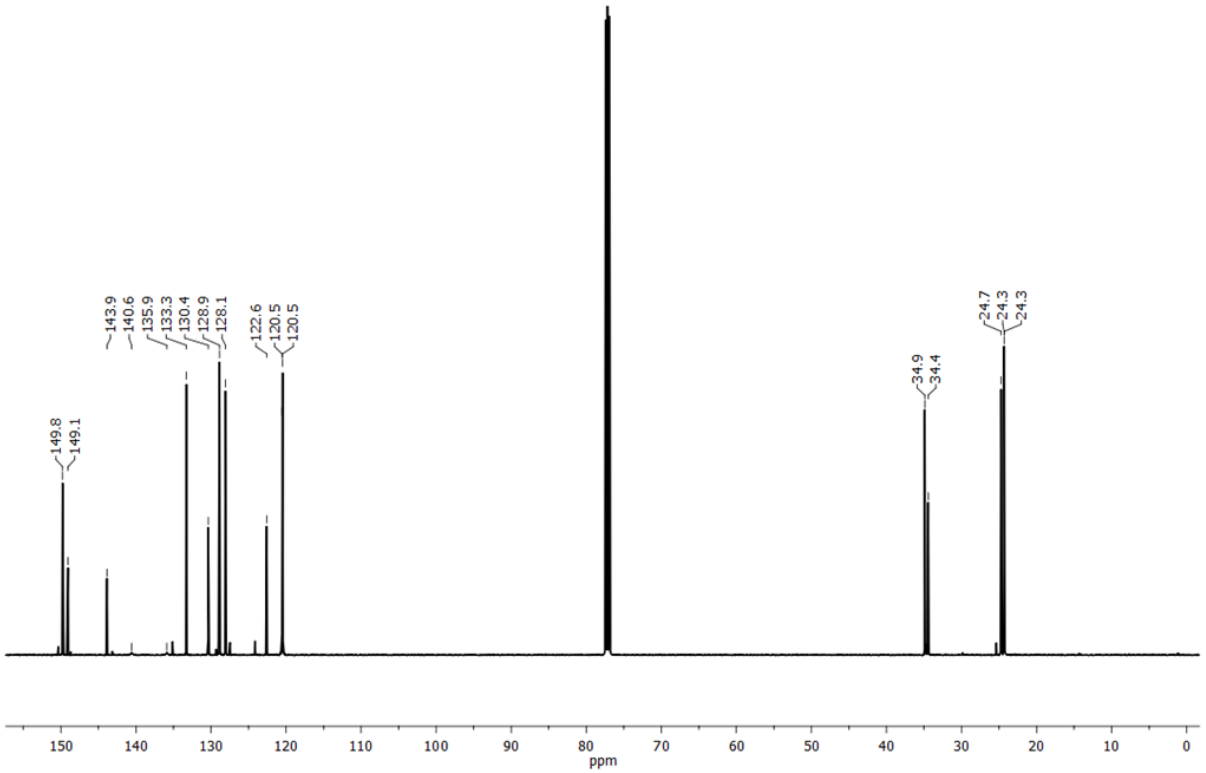

Figure S5.8.3. $^{13}C\{^{1}H\}$ NMR spectrum (126 MHz) of **3** in $CDCl_3$.

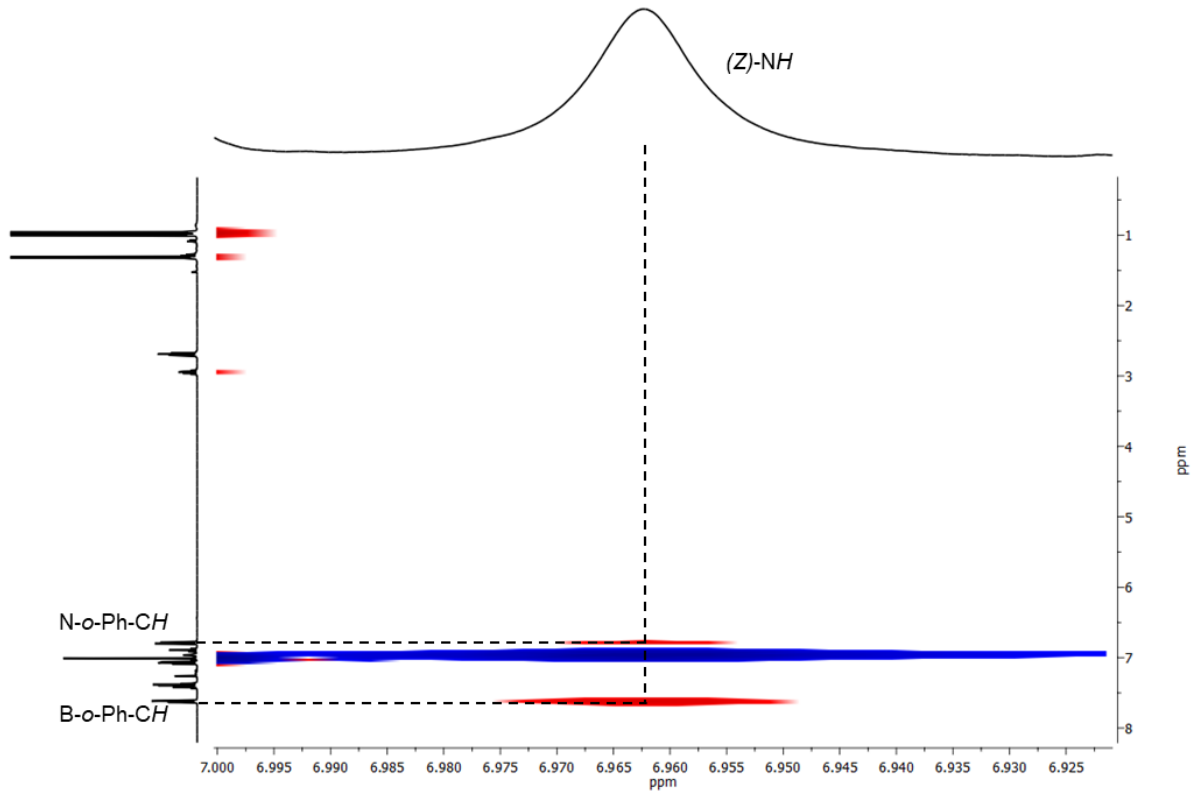

Figure S5.8.4. Detail of ^{1}H, ^{1}H NOESY spectrum of **3** ((*Z*)-Isomer) in $CDCl_3$.

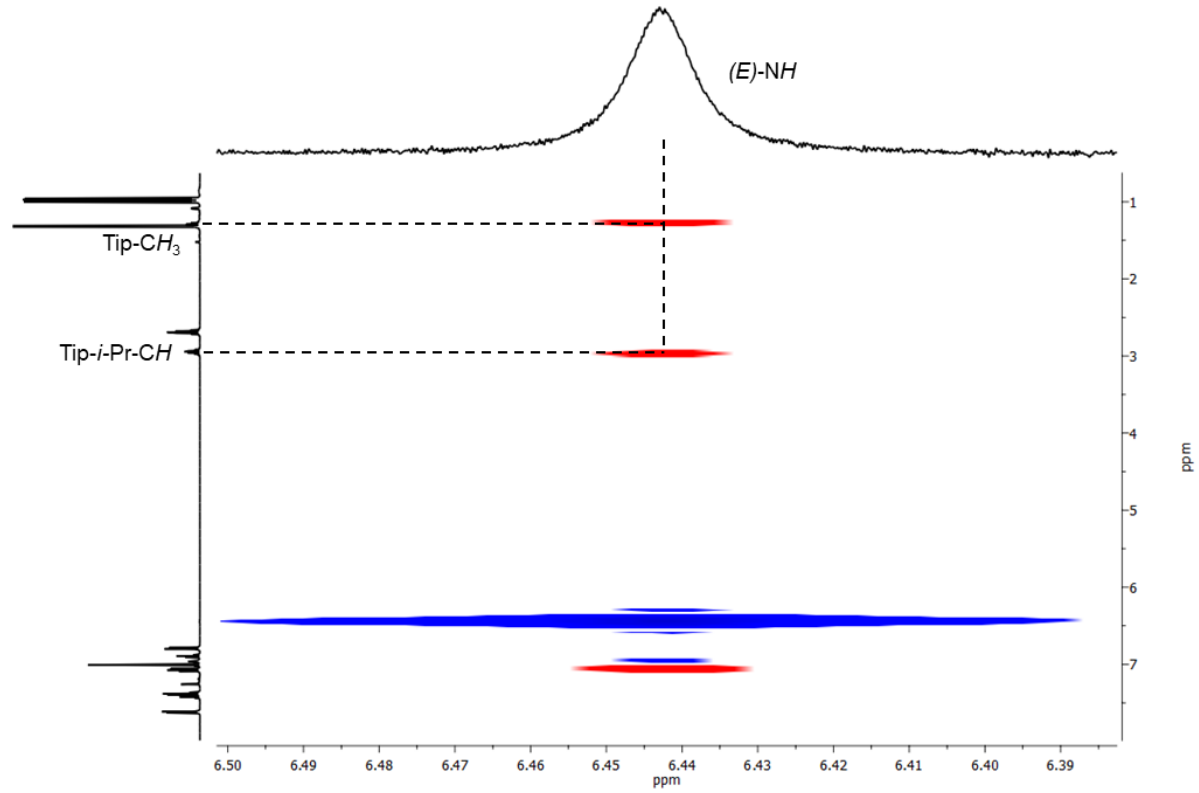

Figure S5.8.5. Detail of ^{1}H, ^{1}H NOESY spectrum of **3** ((*E*)-Isomer) in $CDCl_3$.

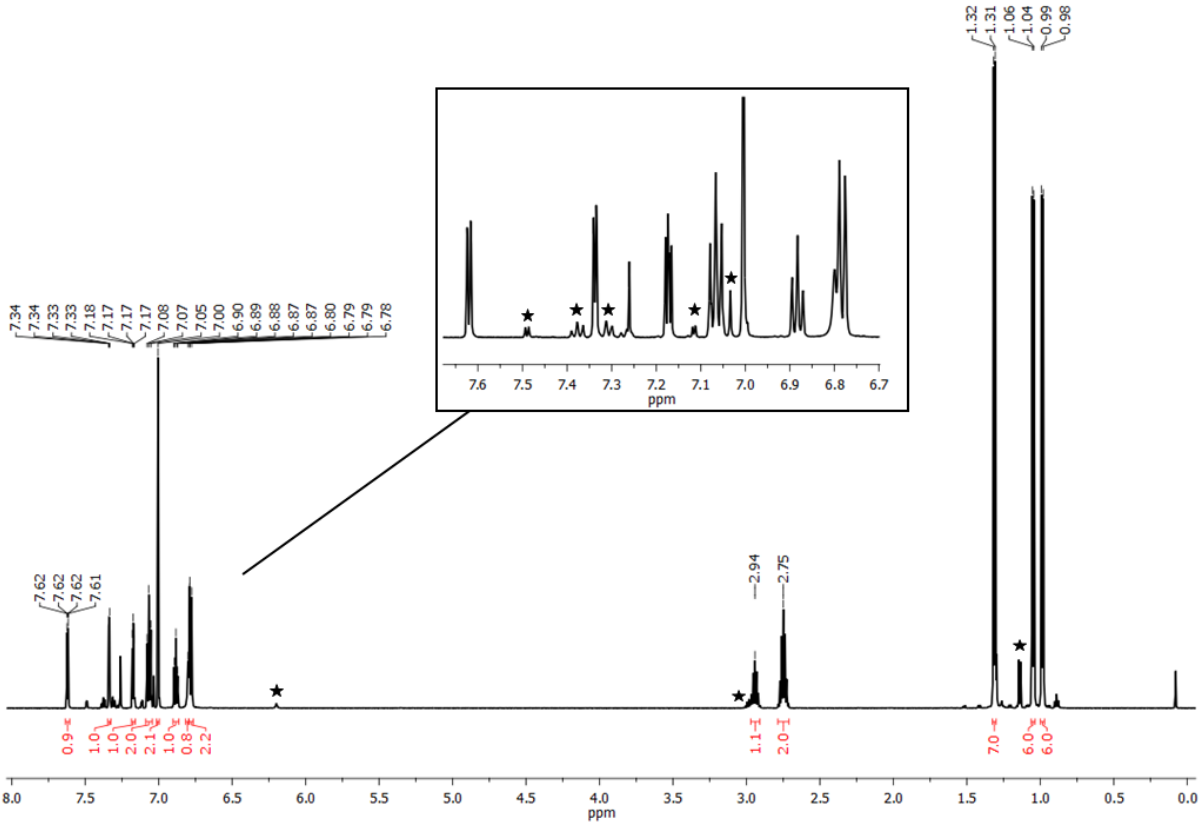

Figure S5.8.6. ^{1}H NMR spectrum (600 MHz) of **5** in $CDCl_3$. The signals marked with an asterisk belong to the minor isomer.

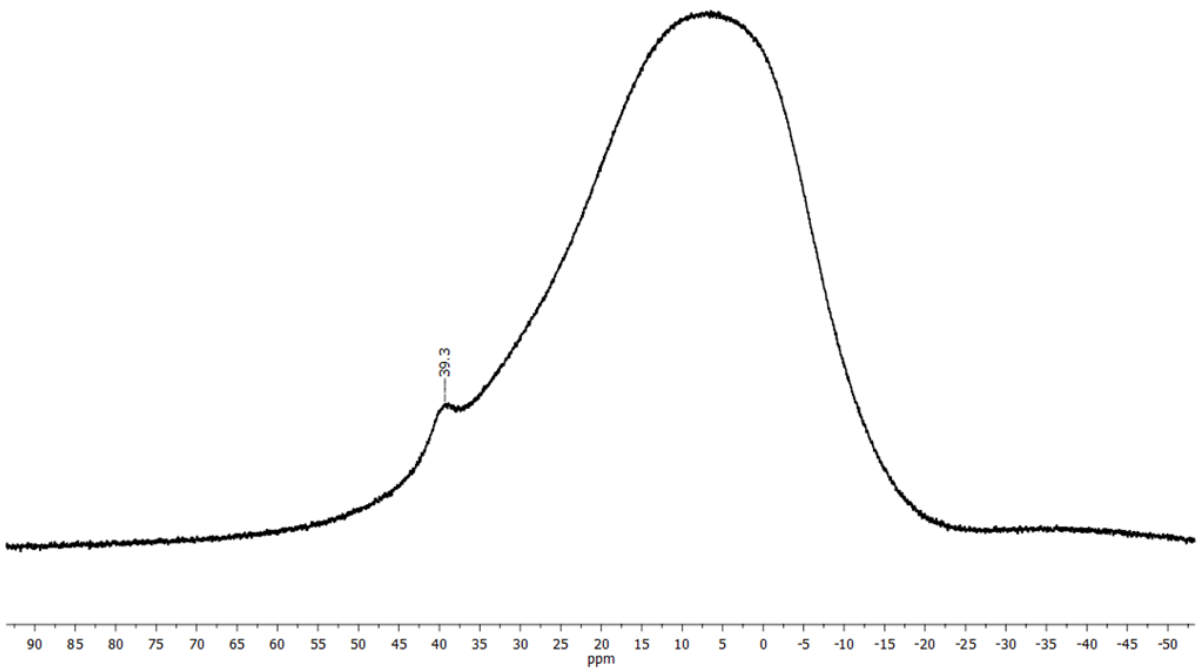

Figure S5.8.7. $^{11}B\{^{1}H\}$ NMR spectrum (193 MHz) of **5** in $CDCl_3$.

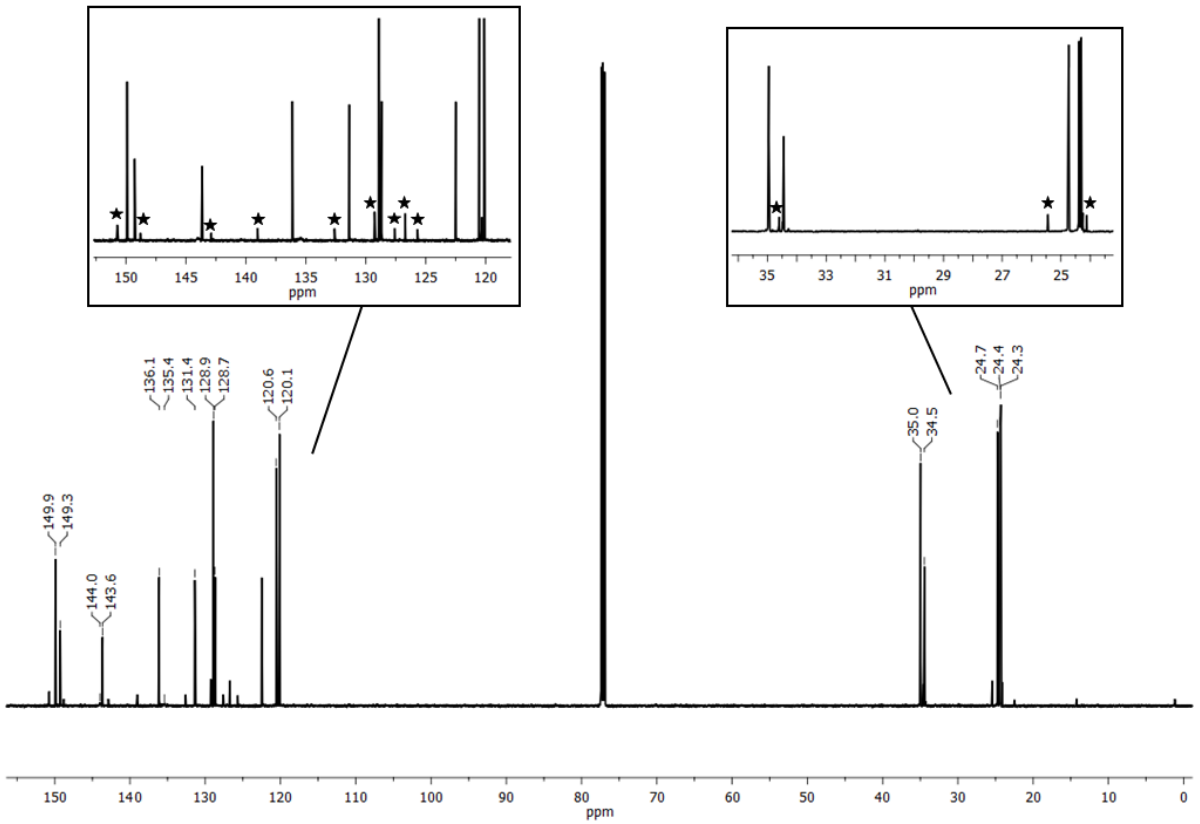

Figure S5.8.8. $^{13}C\{^{1}H\}$ NMR spectrum (151 MHz) of **5** in $CDCl_3$. The signals marked with an asterisk belong to the minor isomer.

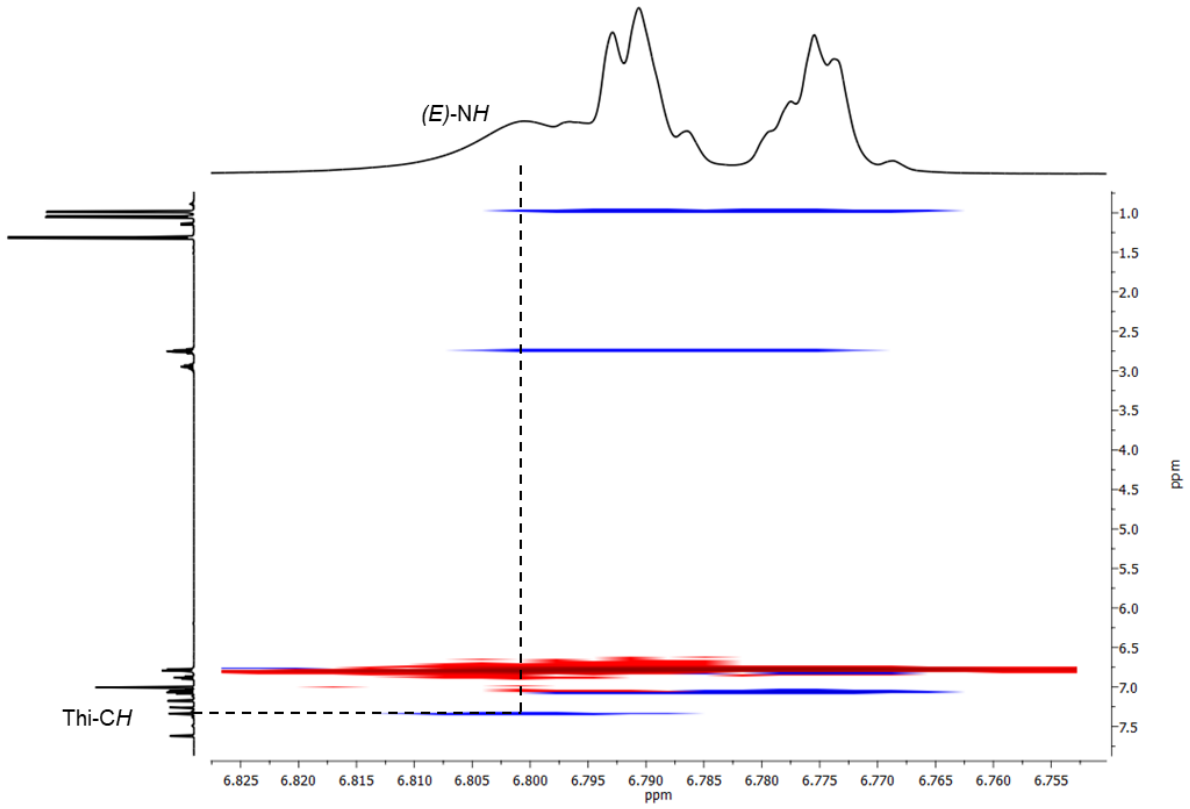

Figure S5.8.9. Detail of ^{1}H, ^{1}H NOESY spectrum of **5** ((*E*)-Isomer) in $CDCl_3$.

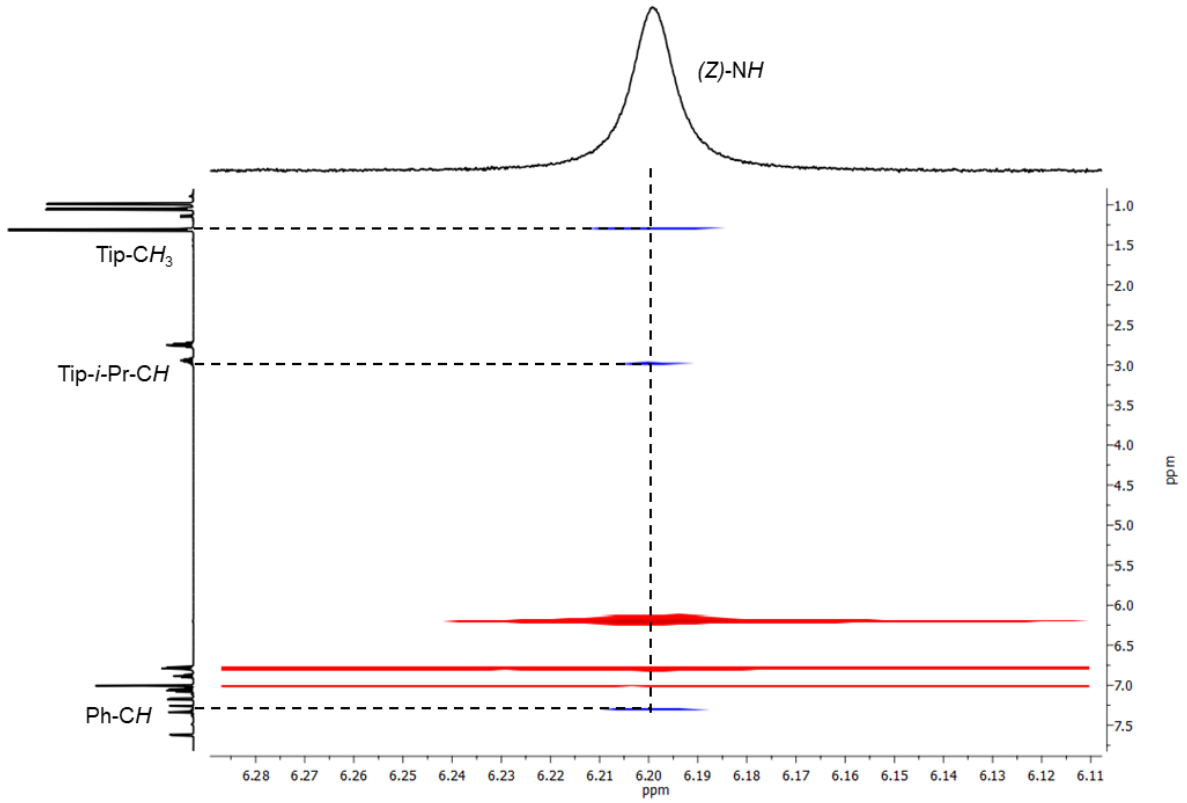

Figure S5.8.10. Detail of ^{1}H, ^{1}H NOESY spectrum of **5** ((*Z*)-Isomer) in $CDCl_3$.

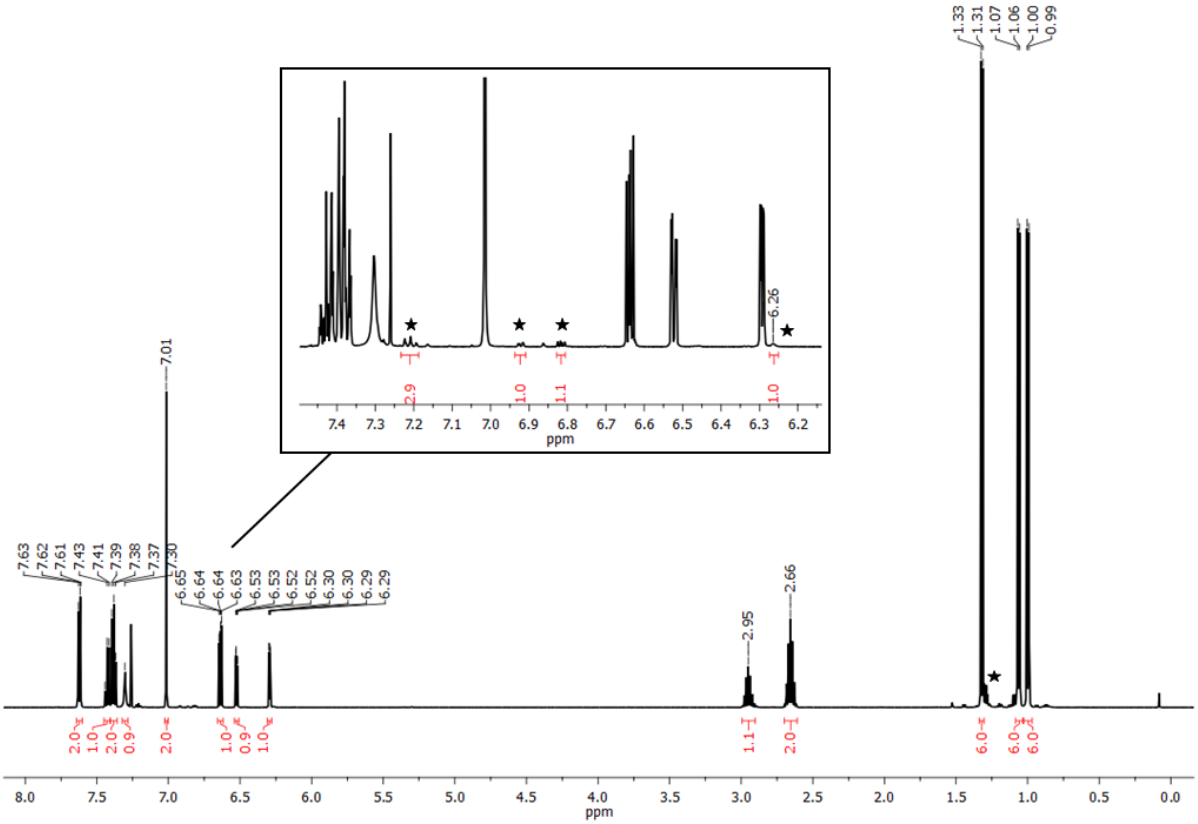

Figure S5.8.11. ^{1}H NMR spectrum (500 MHz) of **7** in $CDCl_3$. The signals marked with an asterisk belong to the minor isomer.

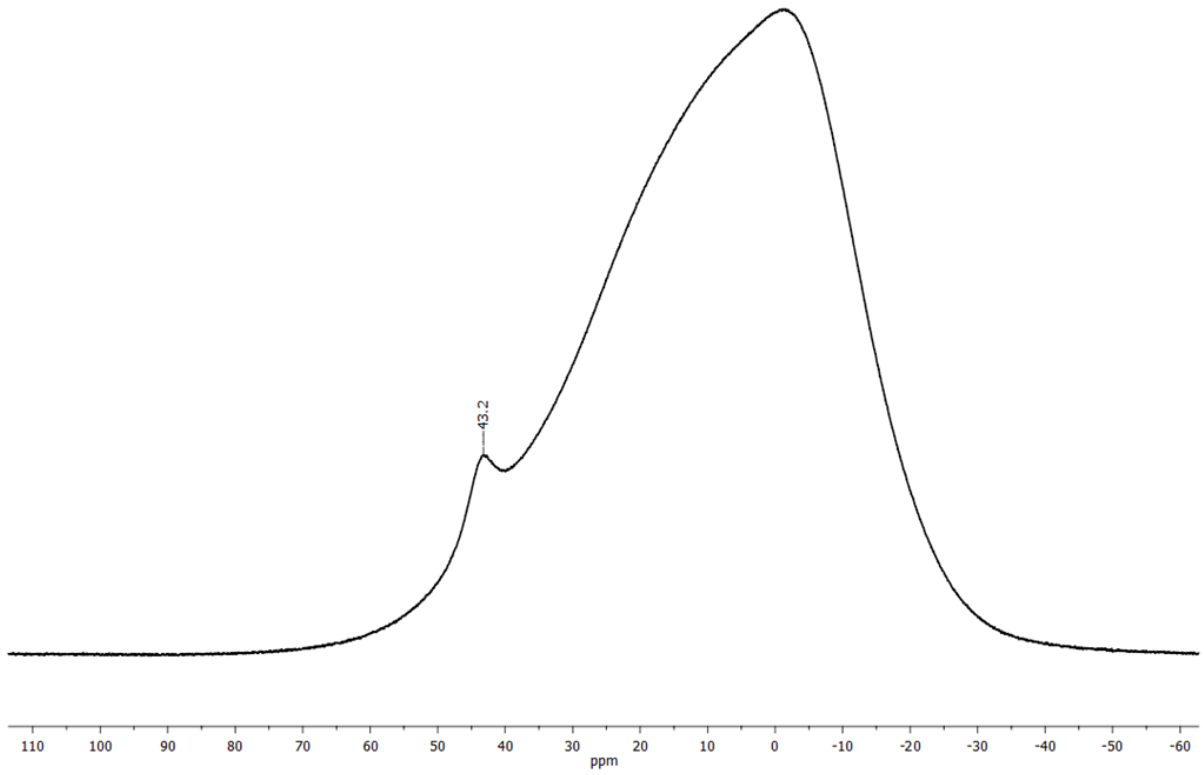

Figure S5.8.12. $^{11}B\{^{1}H\}$ NMR spectrum (160 MHz) of **7** in $CDCl_3$.

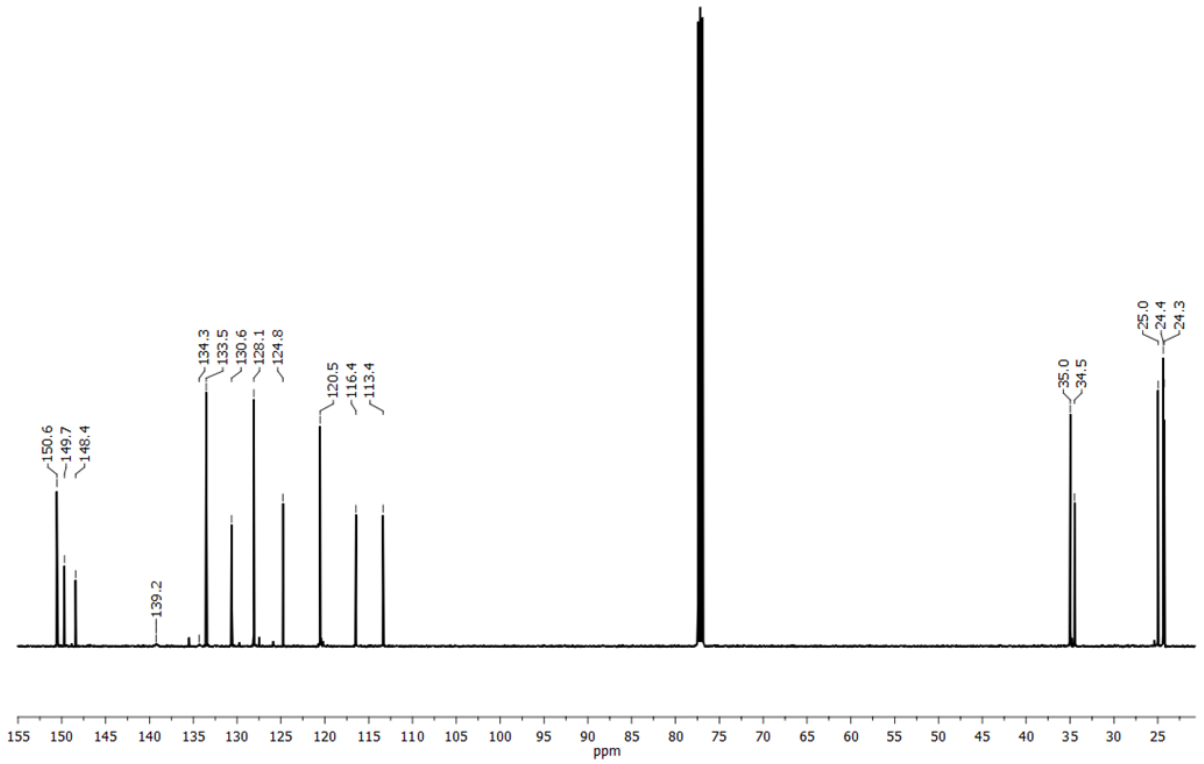

Figure S5.8.13. $^{13}C\{^{1}H\}$ NMR spectrum (126 MHz) of **7** in $CDCl_3$.

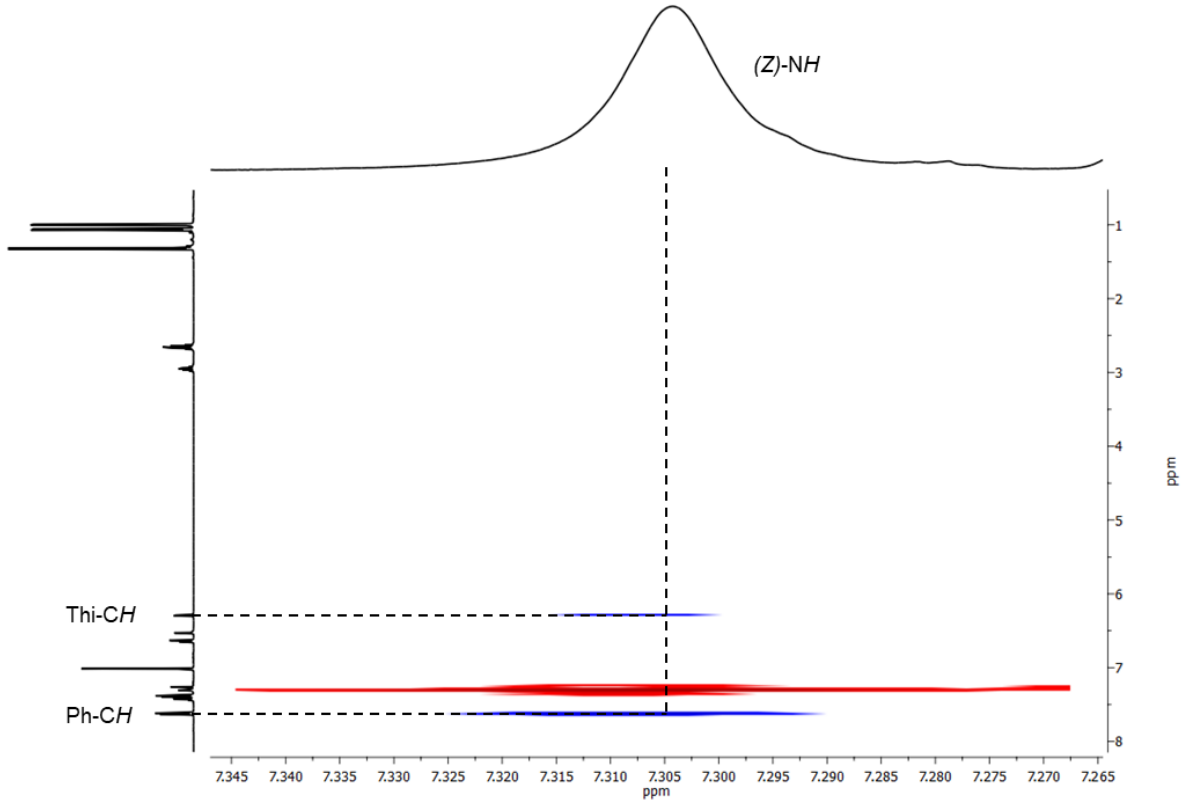

Figure S5.8.14. Detail of ^{1}H, ^{1}H NOESY spectrum of **7** ((*Z*)-Isomer) in $CDCl_3$.

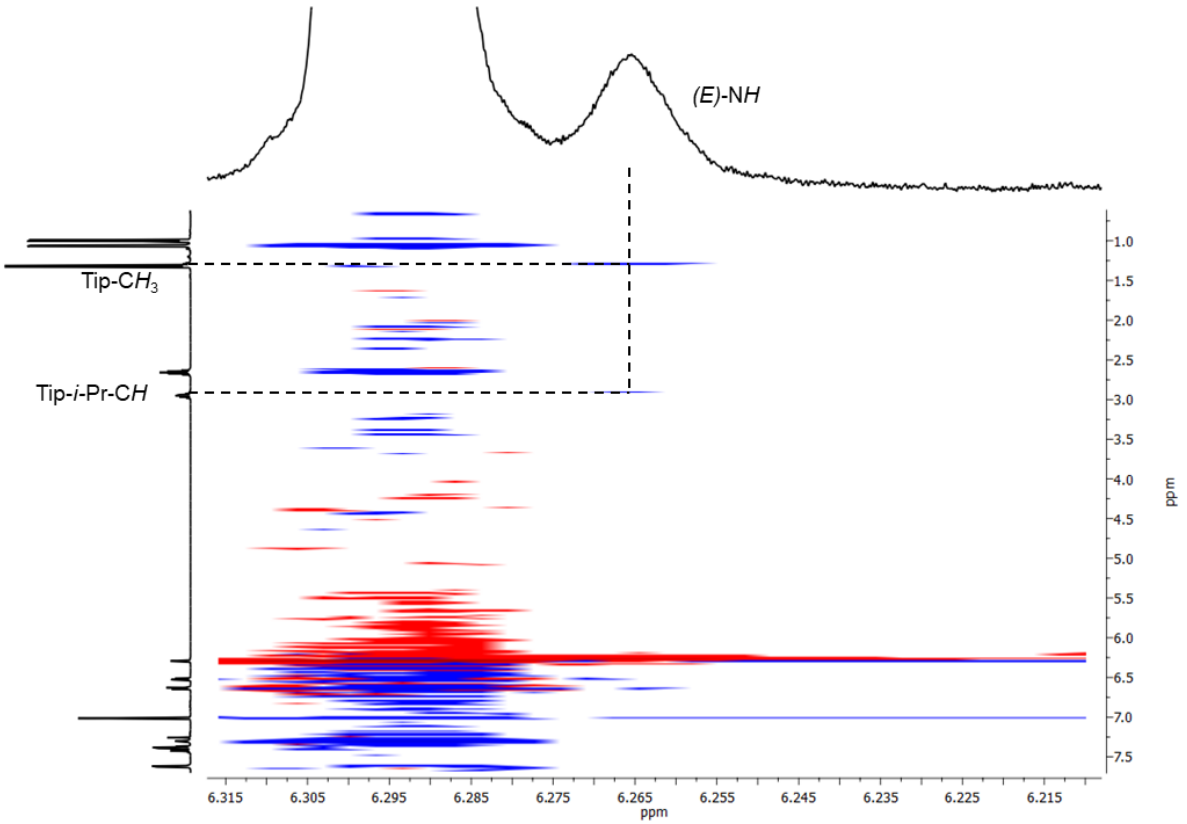

Figure S5.8.15. Detail of ^{1}H, ^{1}H NOESY spectrum of **7** ((*E*)-Isomer) in $CDCl_3$.

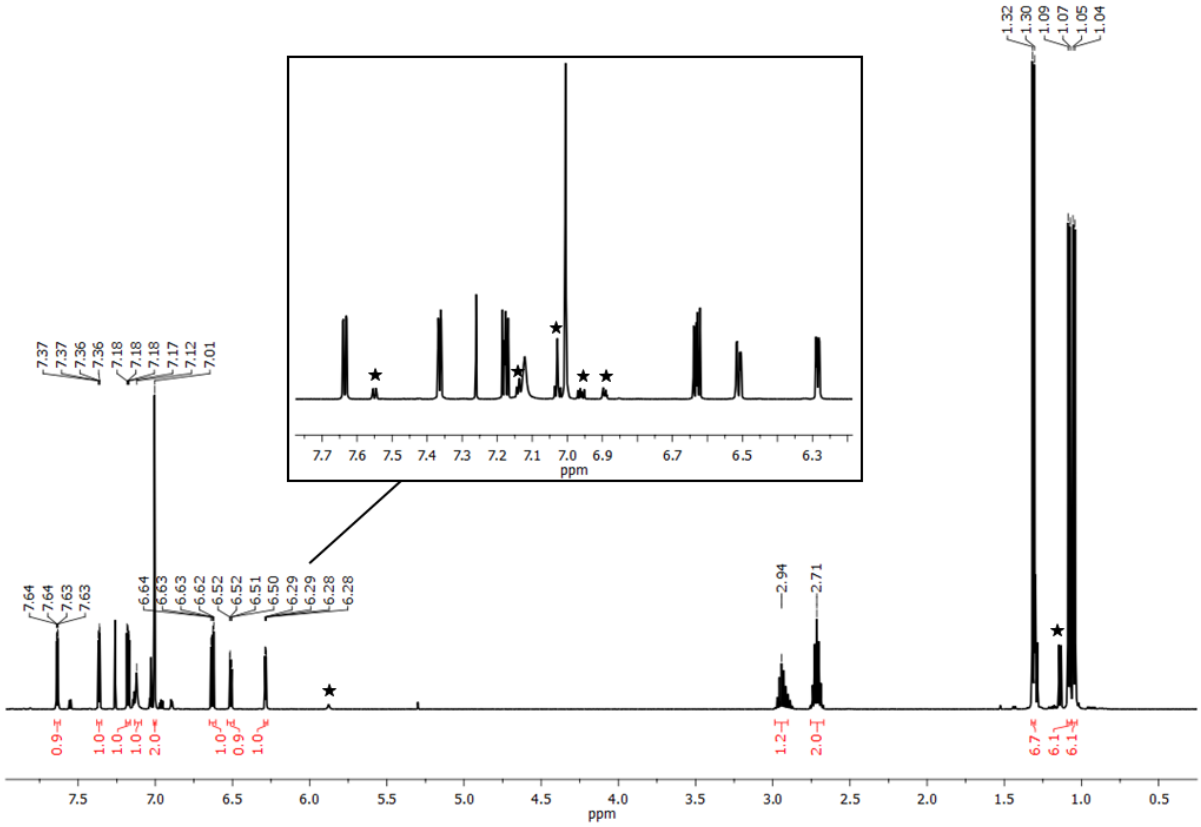

Figure S5.8.16. ^{1}H NMR spectrum (500 MHz) of **8** in $CDCl_3$. The signals marked with an asterisk belong to the minor isomer.

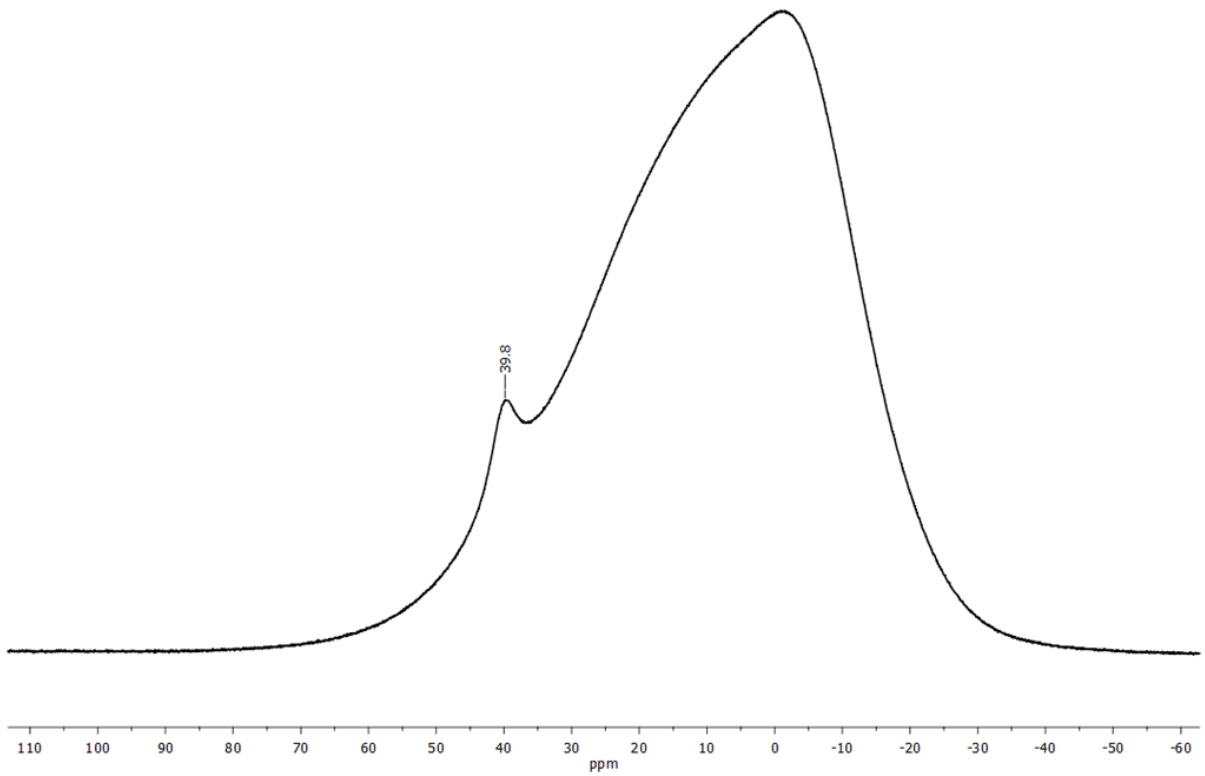

Figure S5.8.17. $^{11}B\{^{1}H\}$ NMR spectrum (160 MHz) of **8** in $CDCl_3$.

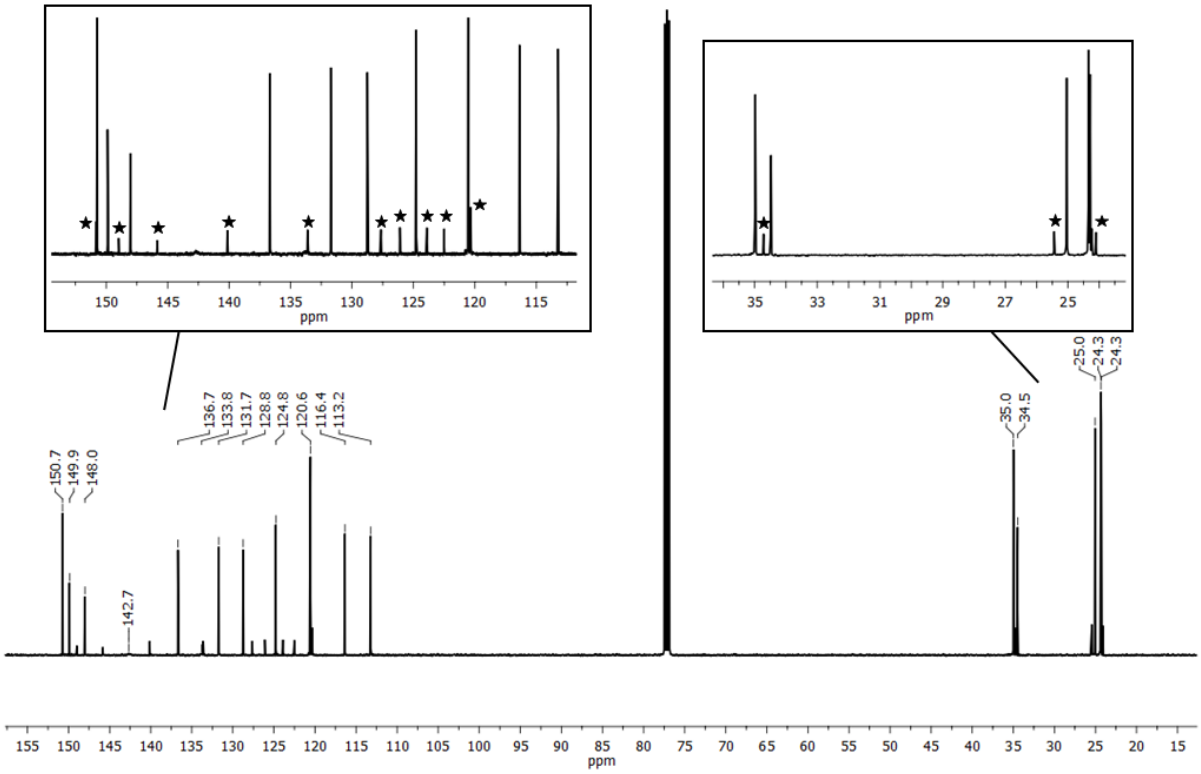

Figure S5.8.18. $^{13}C\{^{1}H\}$ NMR spectrum (126 MHz) of **8** in $CDCl_3$. The signals marked with an asterisk belong to the minor isomer.

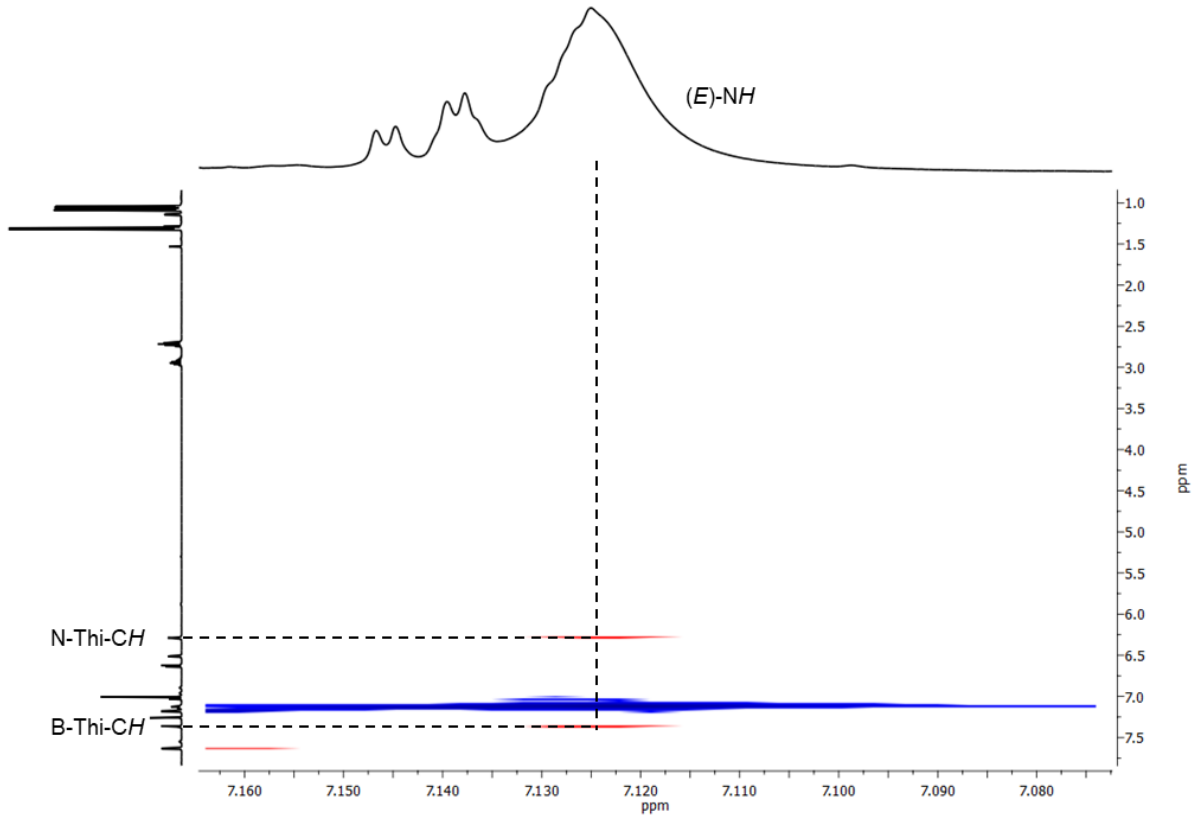

Figure S5.8.19. Detail of ^{1}H, ^{1}H NOESY spectrum of **8** ((*E*)-Isomer) in $CDCl_3$.

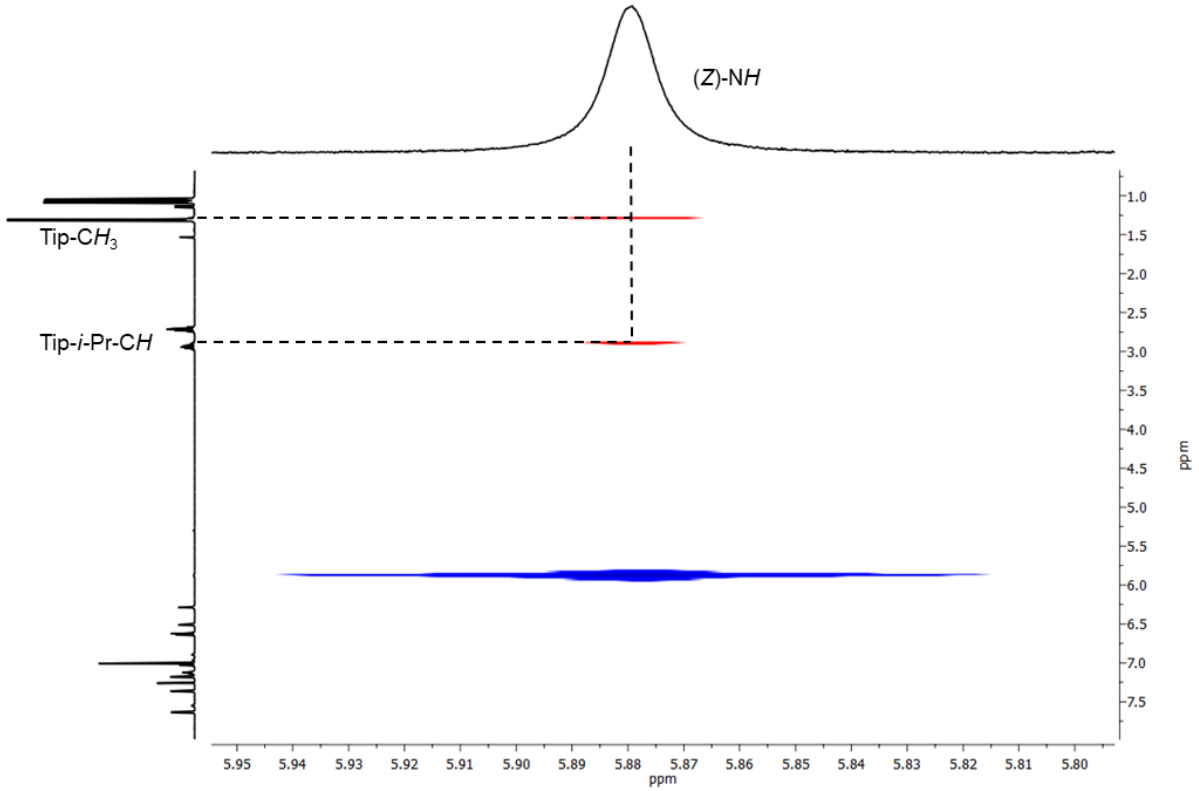

Figure S5.8.20. Detail of ^{1}H, ^{1}H NOESY spectrum of **8** ((*Z*)-Isomer) in $CDCl_3$.

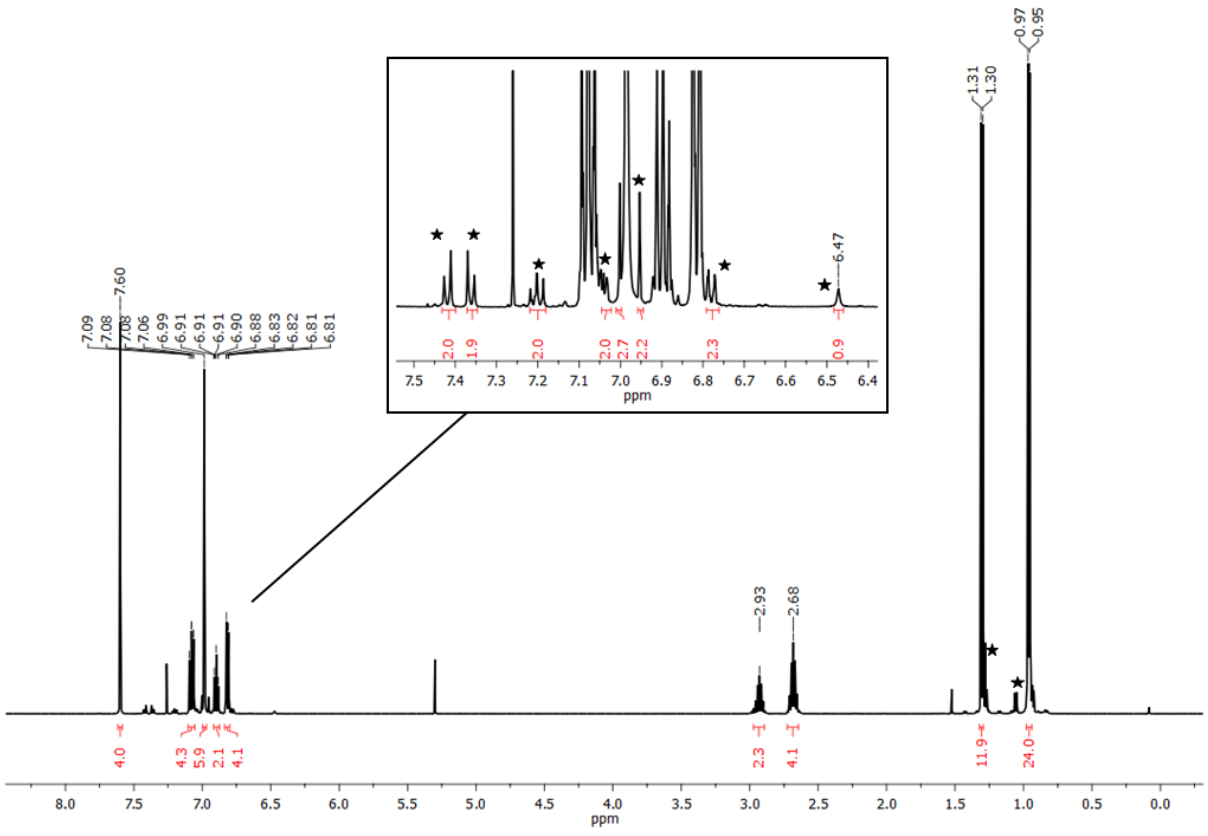

Figure S5.8.21. ^{1}H NMR spectrum (500 MHz) of **10** in $CDCl_3$. The signals marked with an asterisk belong to the minor isomer.

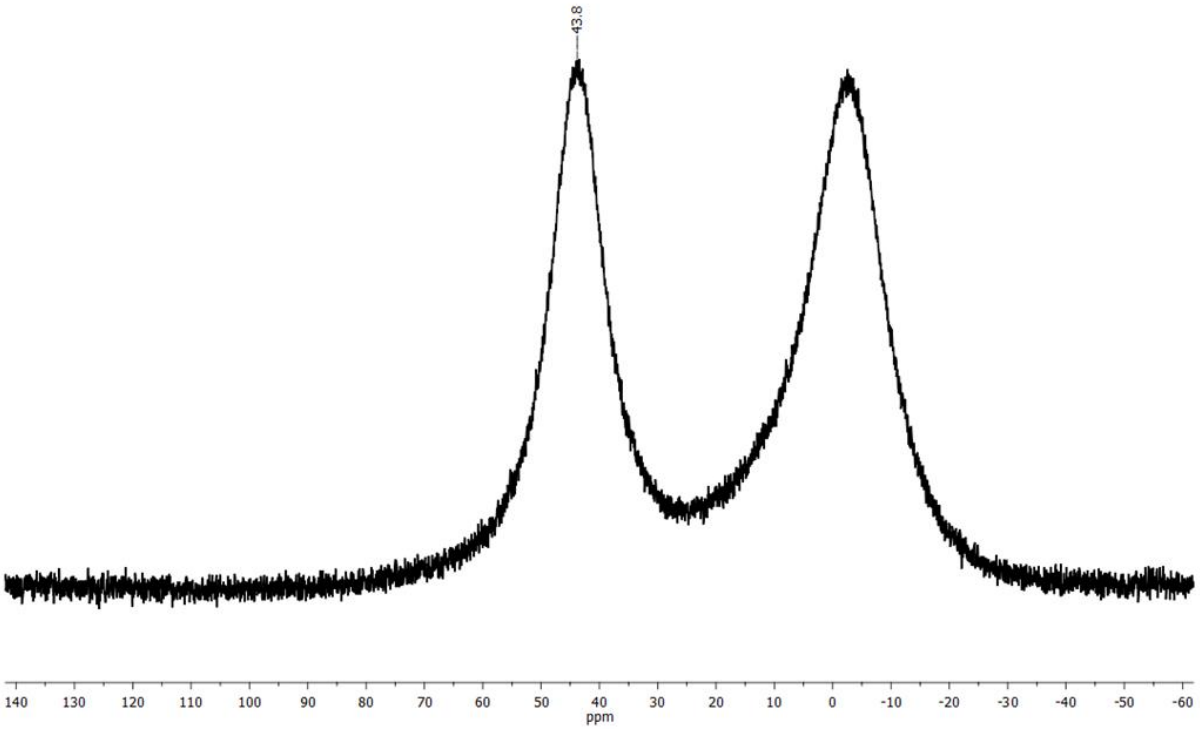

Figure S5.8.22. $^{11}B\{^{1}H\}$ NMR spectrum (160 MHz) of **10** in $CDCl_3$ with reduced glass background.

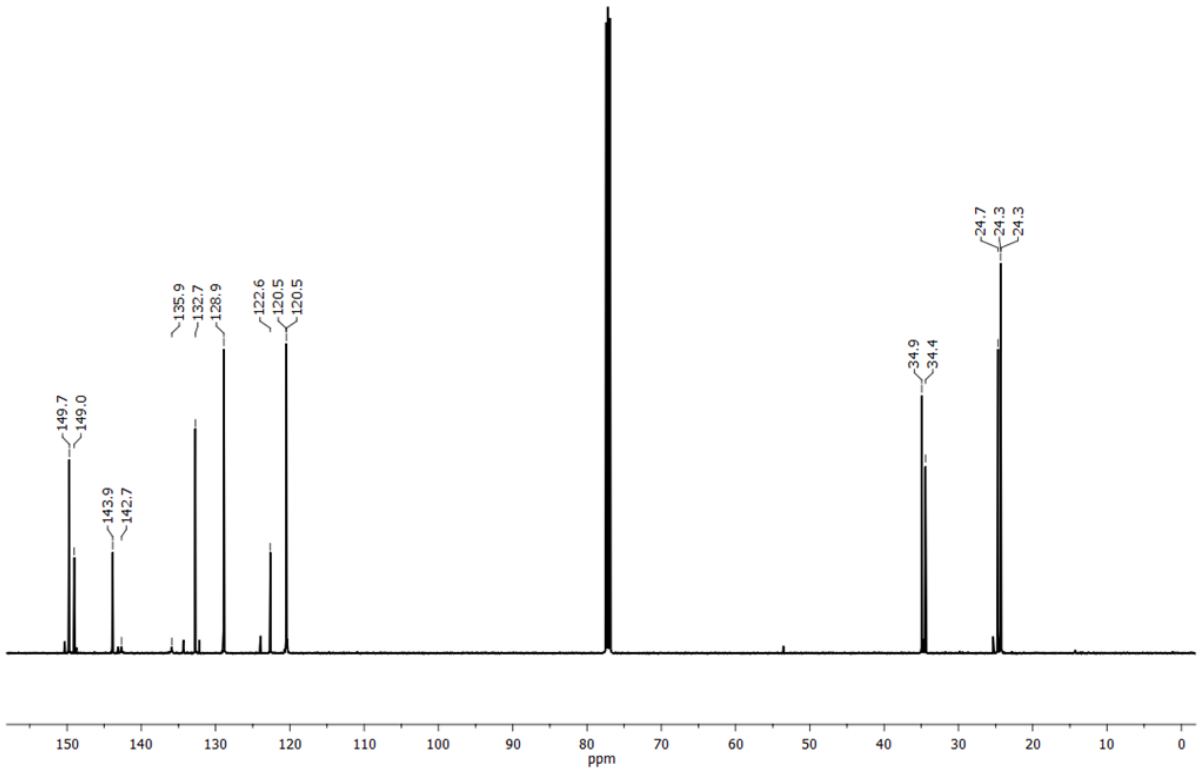

Figure S5.8.23. $^{13}C\{^{1}H\}$ NMR spectrum (126 MHz) of **10** in $CDCl_3$.

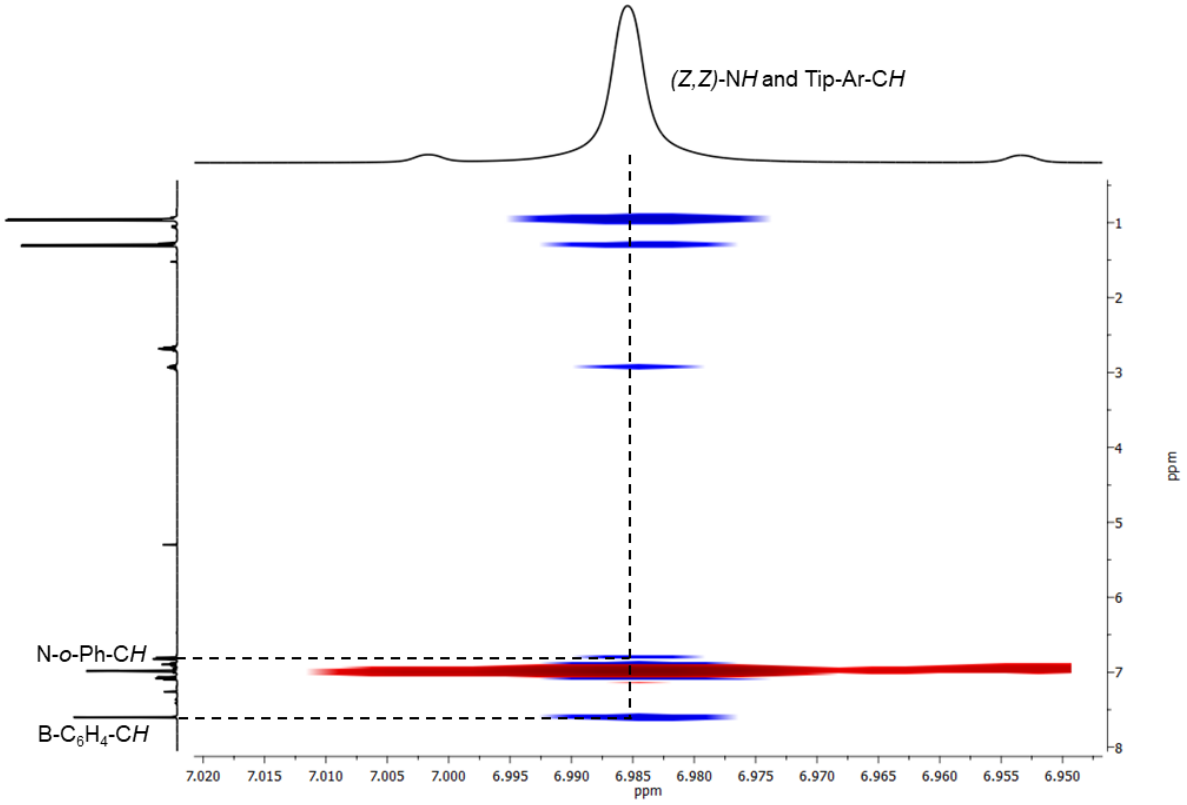

Figure S5.8.24. Detail of ^{1}H, ^{1}H NOESY spectrum of **10** ((*Z*,*Z*)-Isomer) in $CDCl_3$.

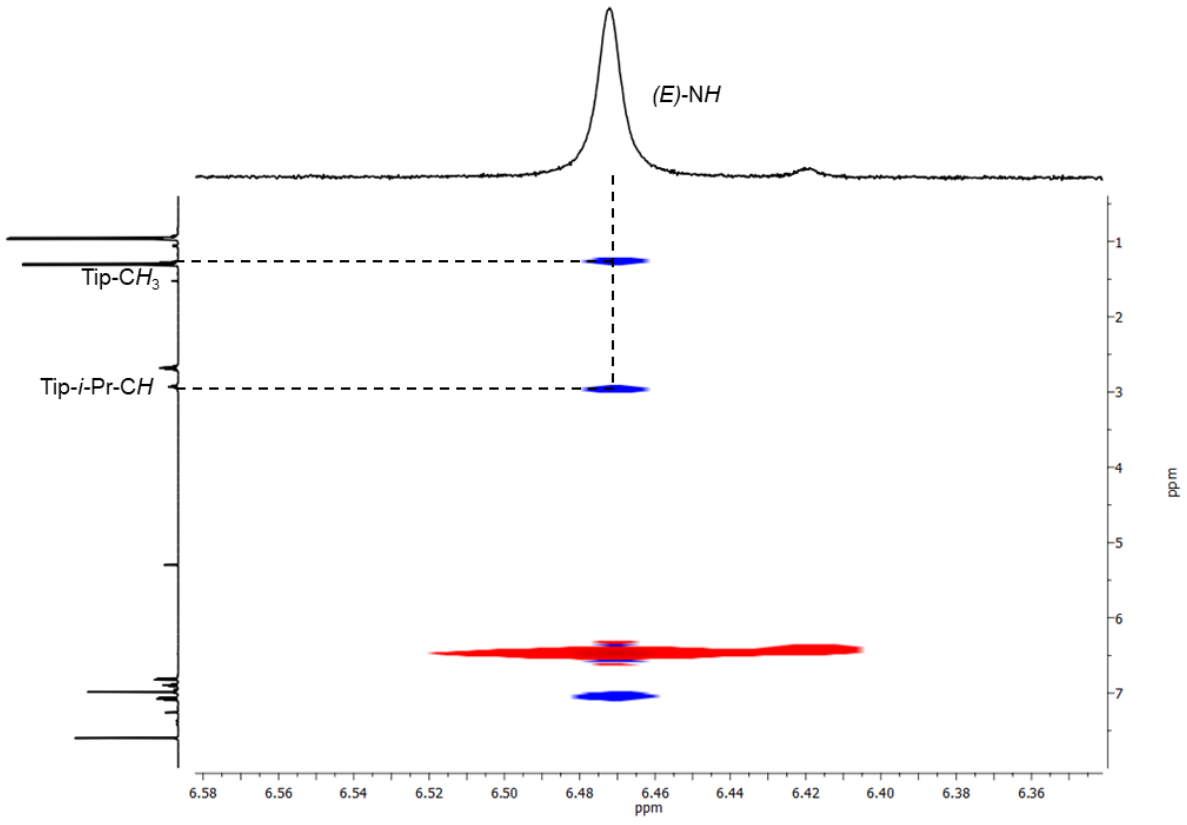

Figure S5.8.25. Detail of ^{1}H, ^{1}H NOESY spectrum of **10** ((*E*,*Z*)-Isomer) in $CDCl_3$. The N*H* signal of the *E*-configured double bond is shown.

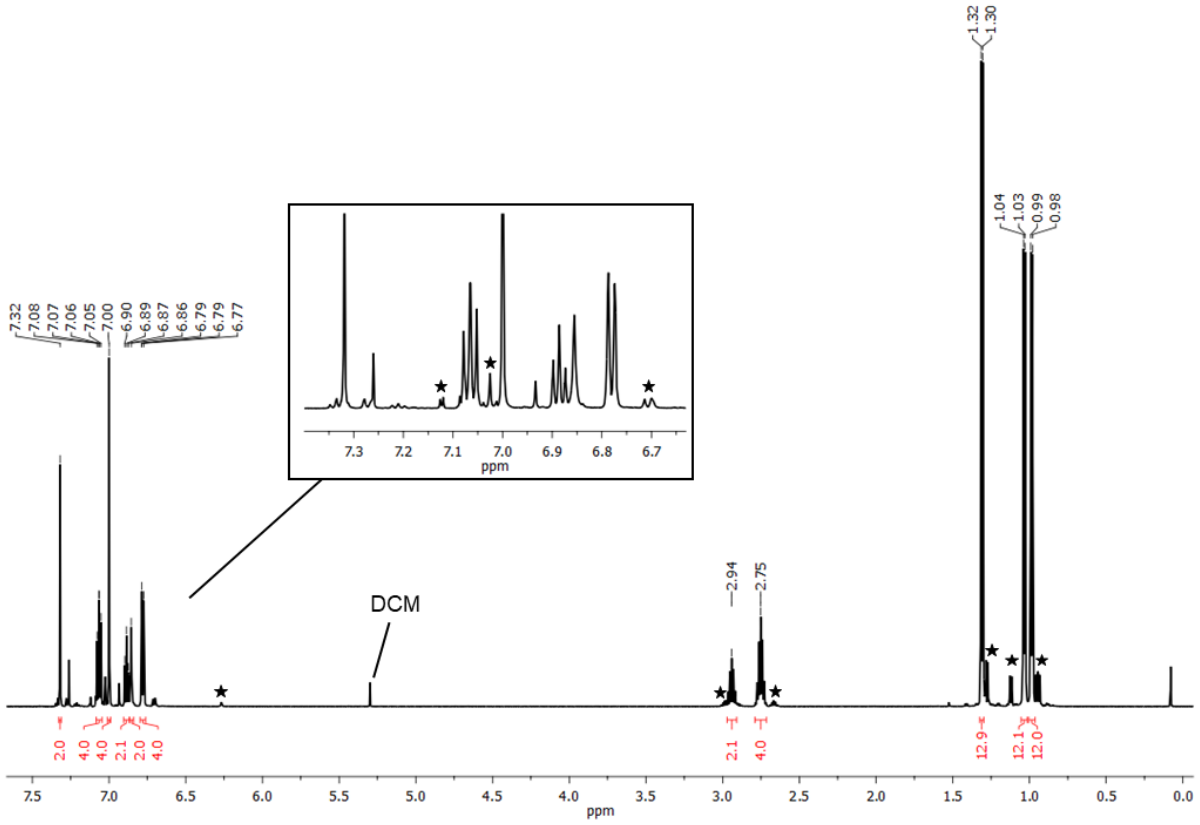

Figure S5.8.26. ^{1}H NMR spectrum (600 MHz) of **12** in $CDCl_3$. The signals marked with an asterisk belong to the minor isomer.

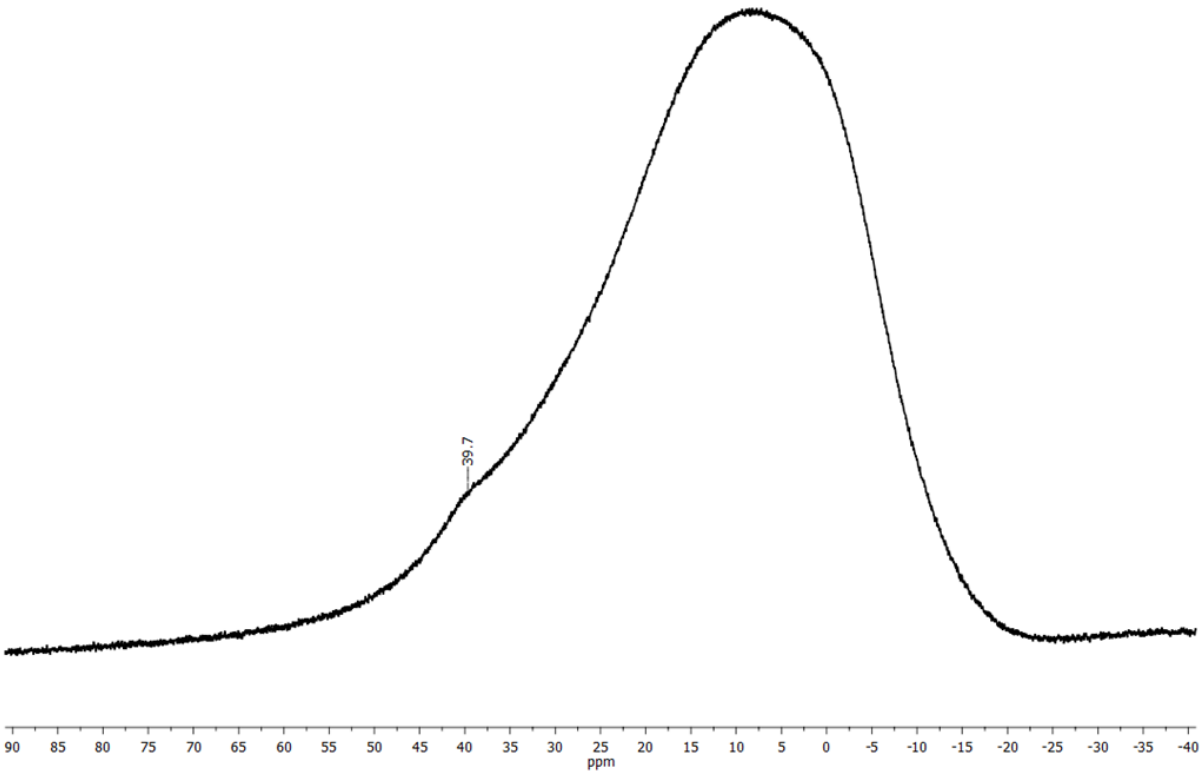

Figure S5.8.27. $^{11}B\{^{1}H\}$ NMR spectrum (193 MHz) of **12** in $CDCl_3$.

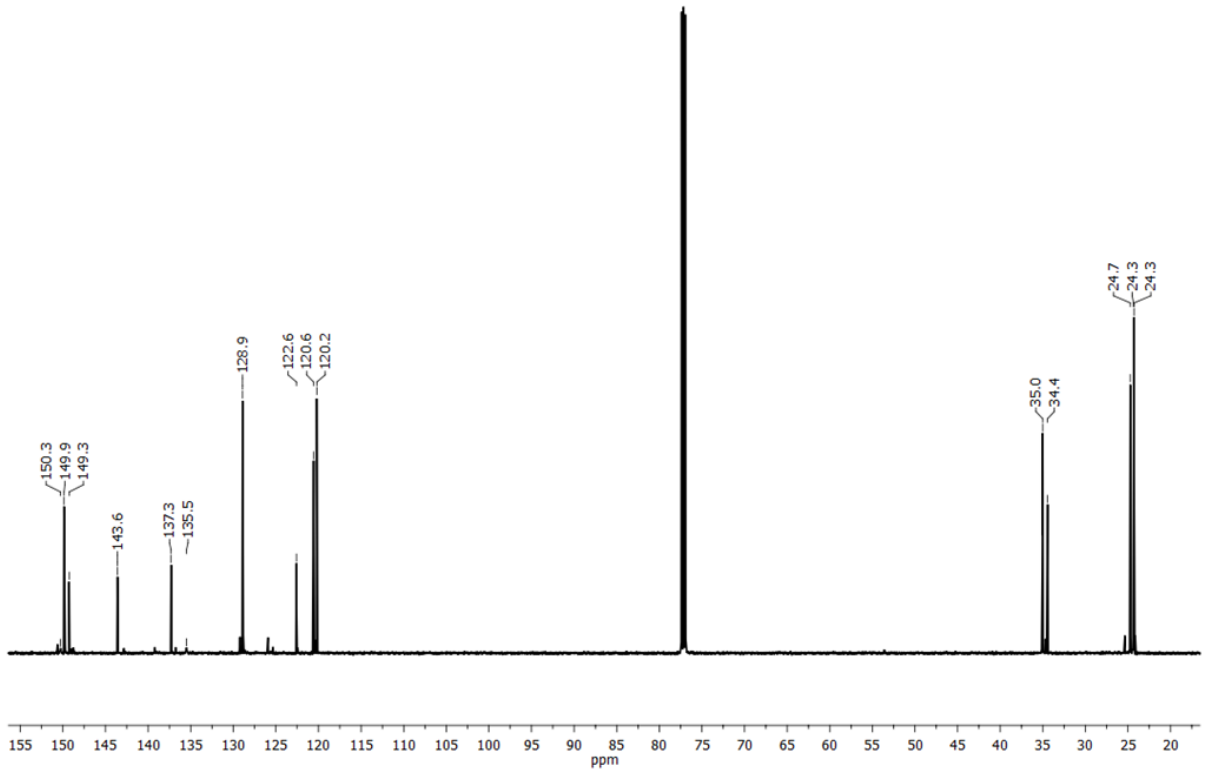

Figure S5.8.28. $^{13}C\{^{1}H\}$ NMR spectrum (151 MHz) of **12** in $CDCl_3$.

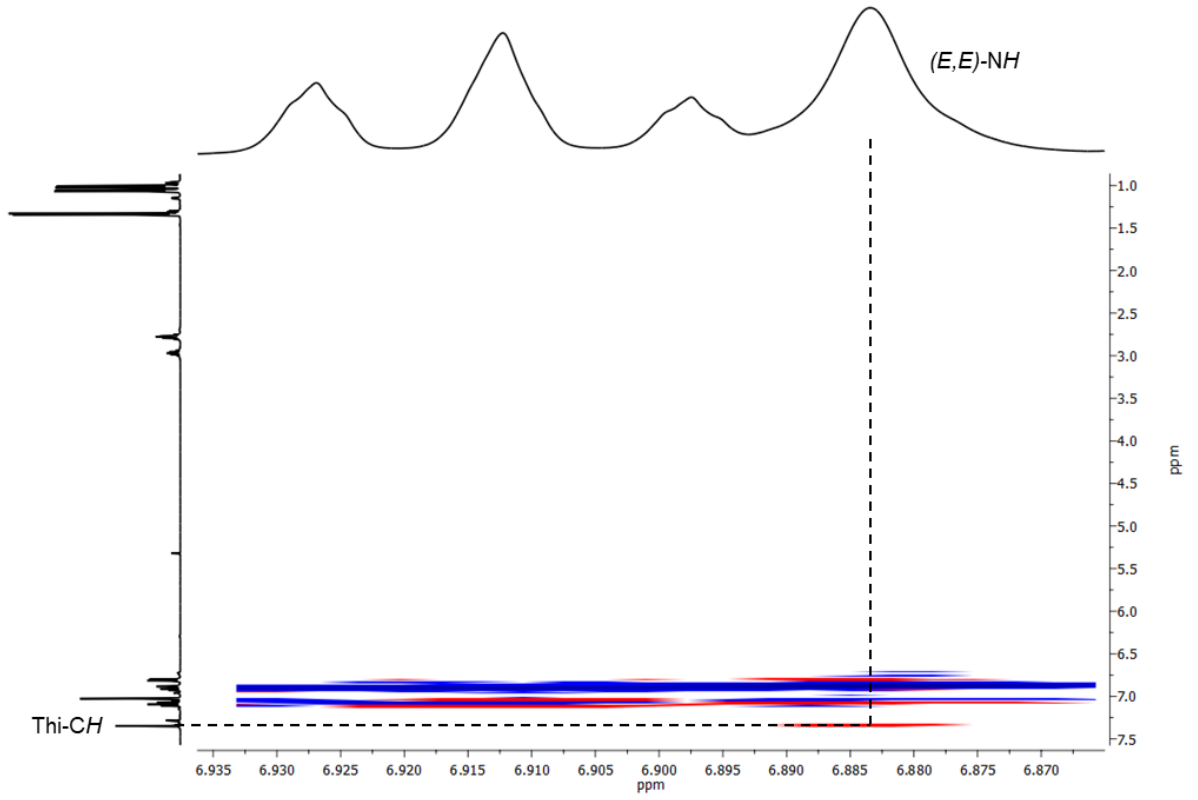

Figure S5.8.29. Detail of ^{1}H, ^{1}H NOESY spectrum of **12** ((*E*,*E*)-Isomer) in $CDCl_3$.

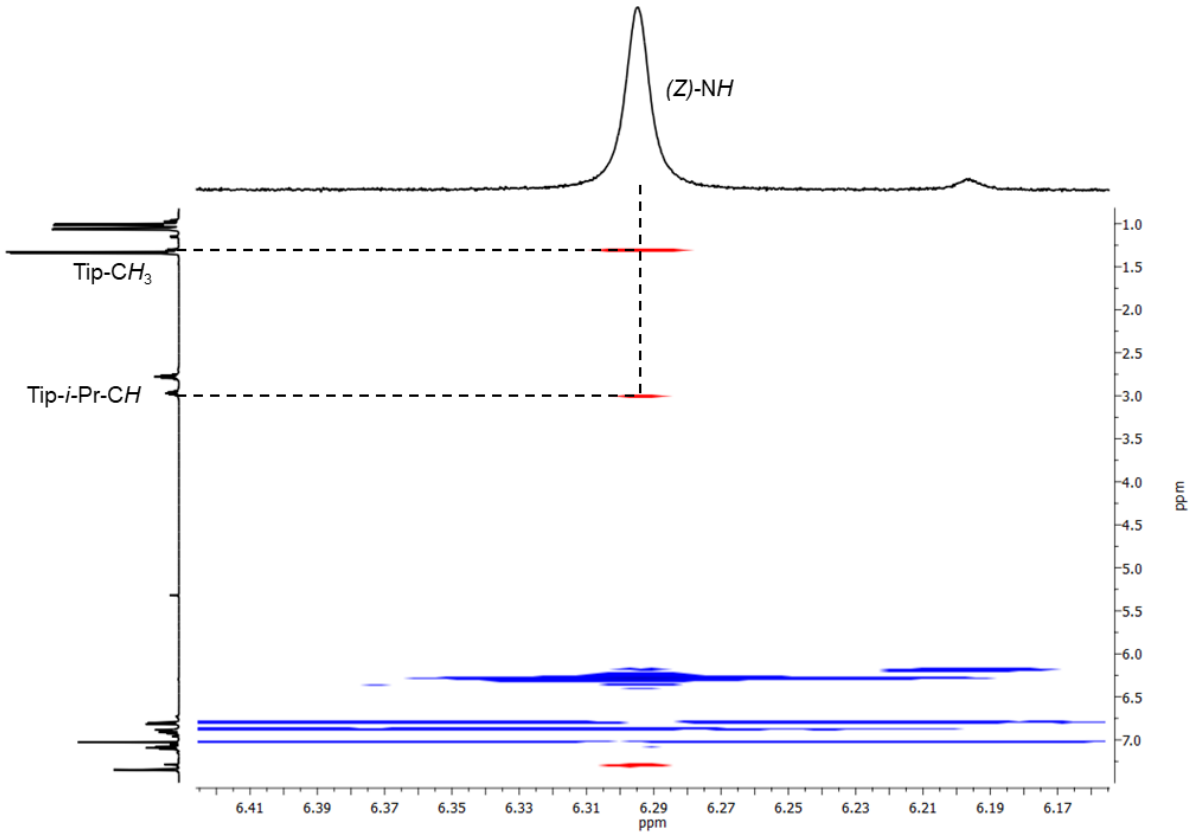

Figure S5.8.30. Detail of ^{1}H, ^{1}H NOESY spectrum of **12** ((*E*,*Z*)-Isomer) in $CDCl_3$. The N*H* signal of the *Z*-configured double bond is shown.

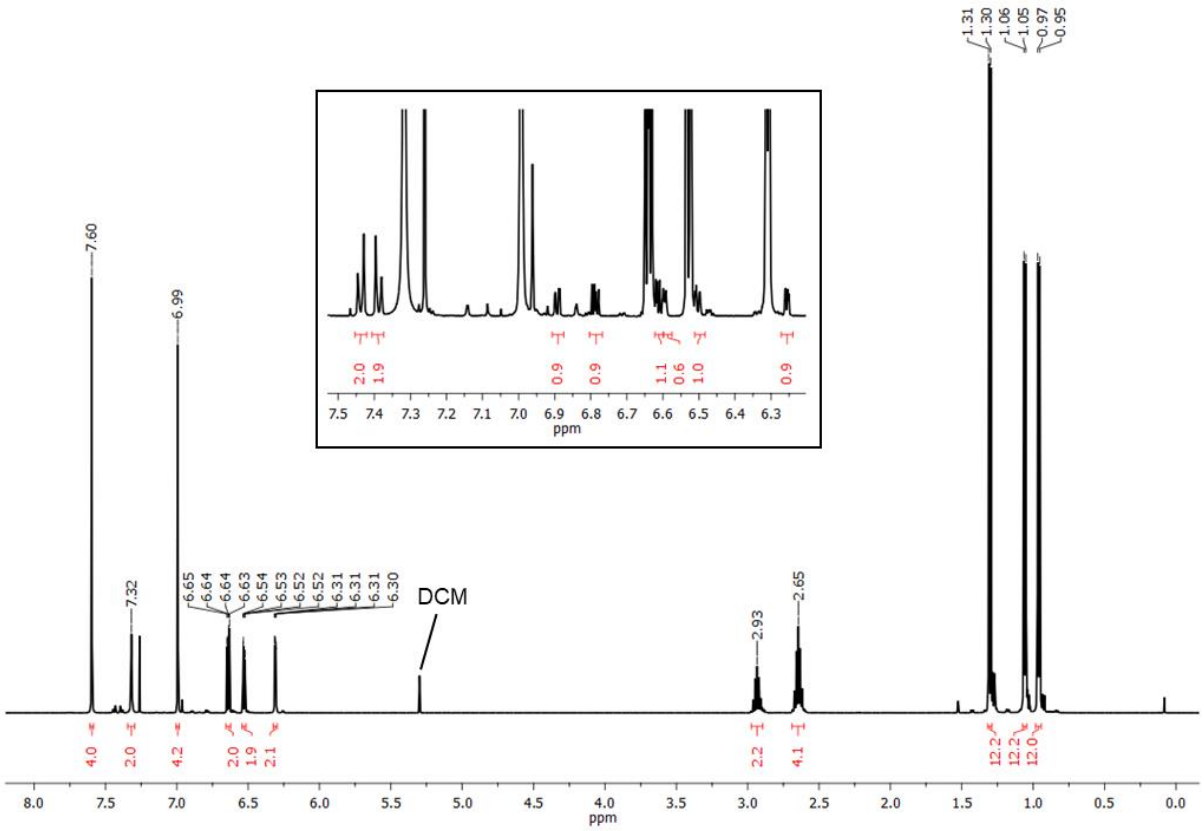

Figure S5.8.31. ^{1}H NMR spectrum (500 MHz) of **14** in $CDCl_3$. Inset: The signals marked with an integral belong to the minor isomer.

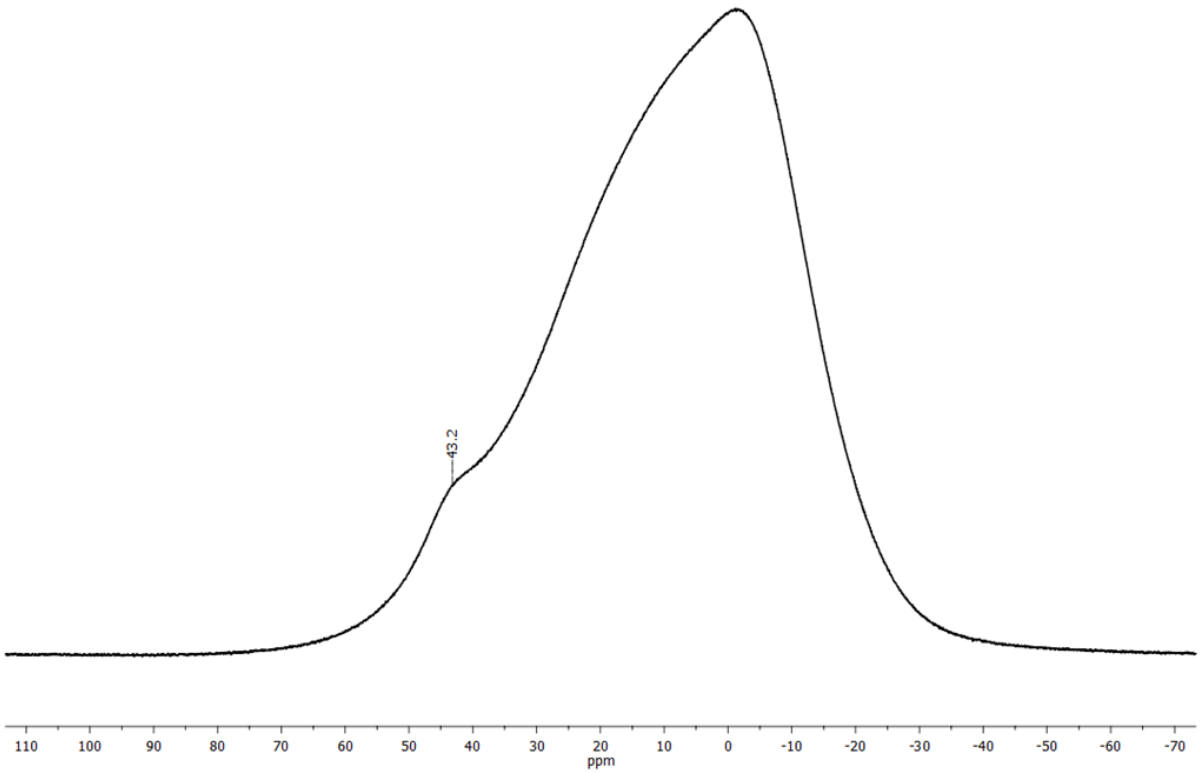

Figure S5.8.32. $^{11}B\{^{1}H\}$ NMR spectrum (160 MHz) of **14** in $CDCl_3$.

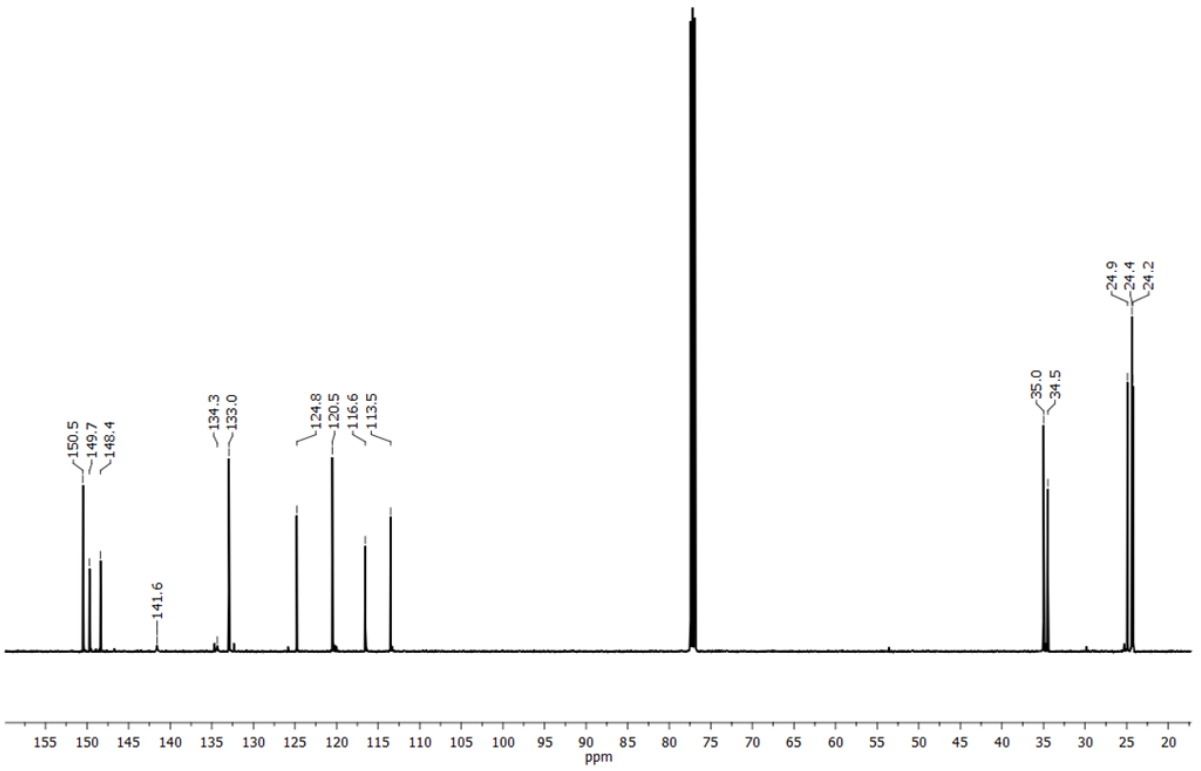

Figure S5.8.33. $^{13}C\{^{1}H\}$ NMR spectrum (126 MHz) of **14** in $CDCl_3$.

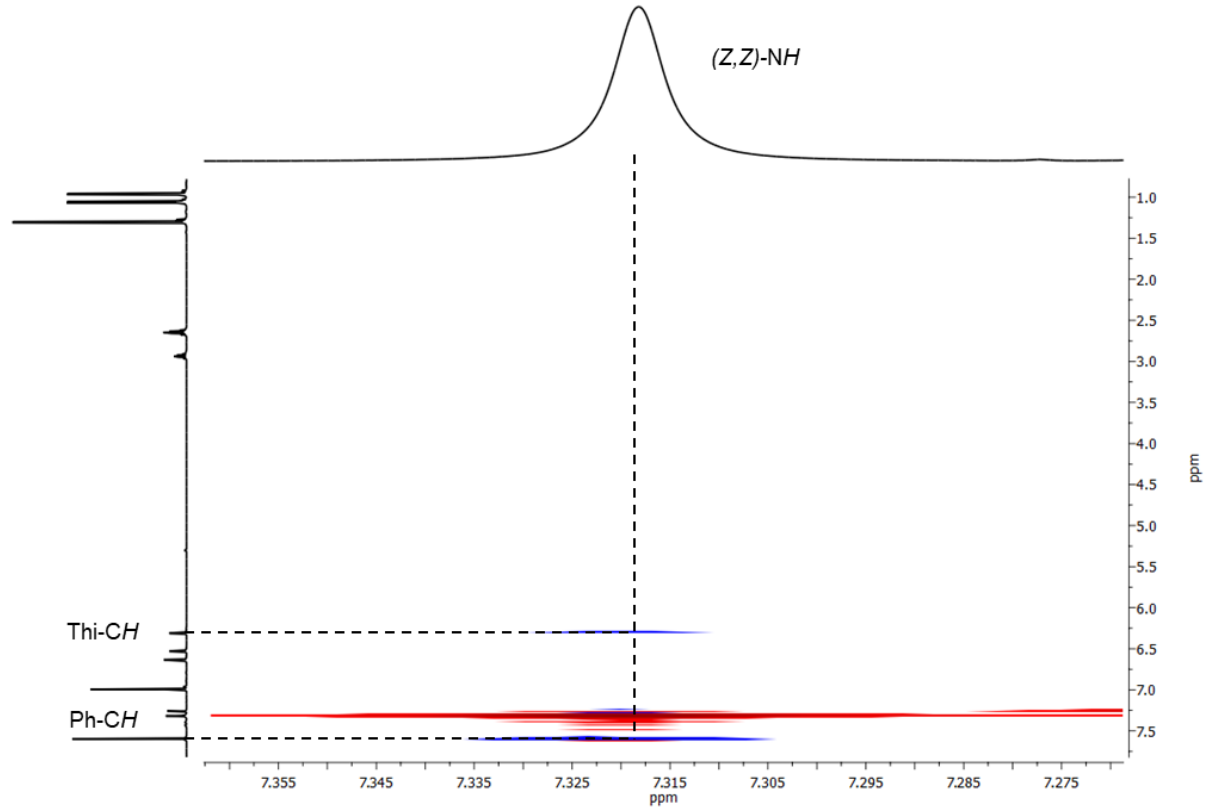

Figure S5.8.34. Detail of ^{1}H, ^{1}H NOESY spectrum of **14** ((*Z*,*Z*)-Isomer) in $CDCl_3$.

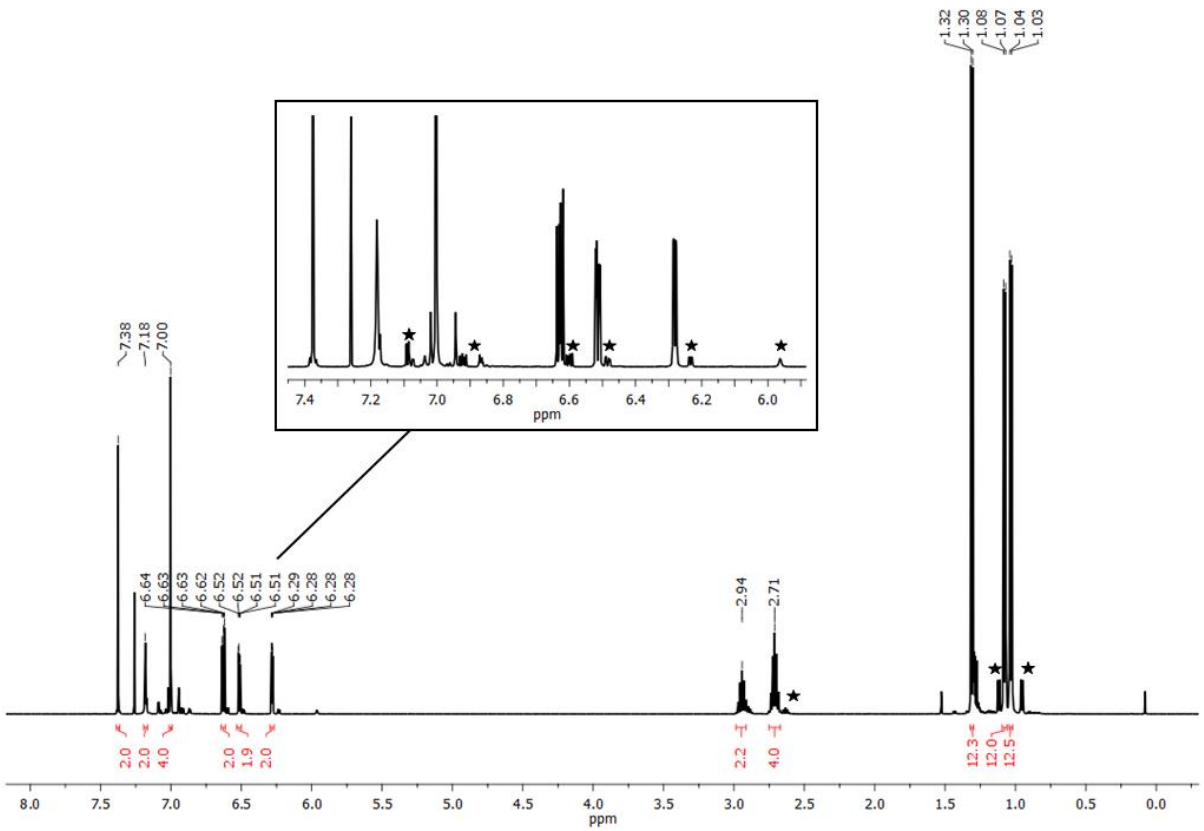

Figure S5.8.35. ^{1}H NMR spectrum (500 MHz) of **15** in $CDCl_3$. The signals marked with an asterisk belong to the minor isomer.

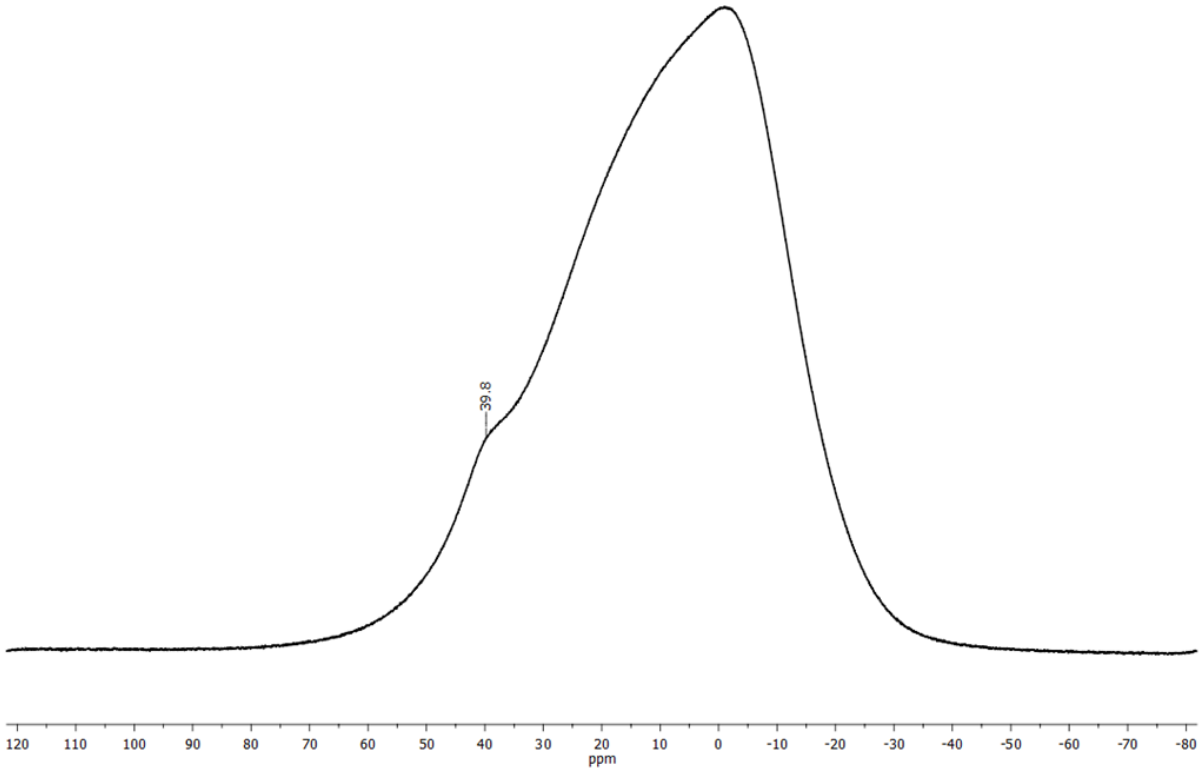

Figure S5.8.36. $^{11}B\{^{1}H\}$ NMR spectrum (160 MHz) of **15** in $CDCl_3$.

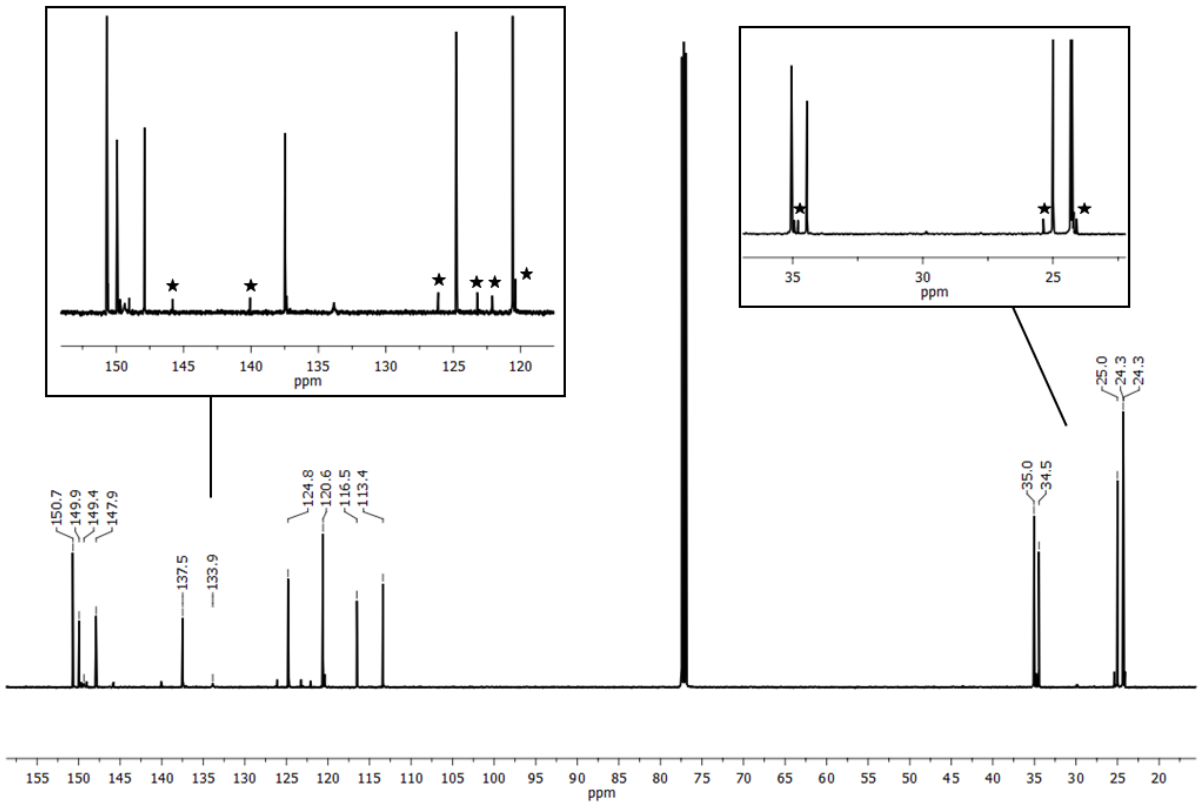

Figure S5.8.37. $^{13}C\{^{1}H\}$ NMR spectrum (126 MHz) of **15** in $CDCl_3$. The signals marked with an asterisk belong to the minor isomer.

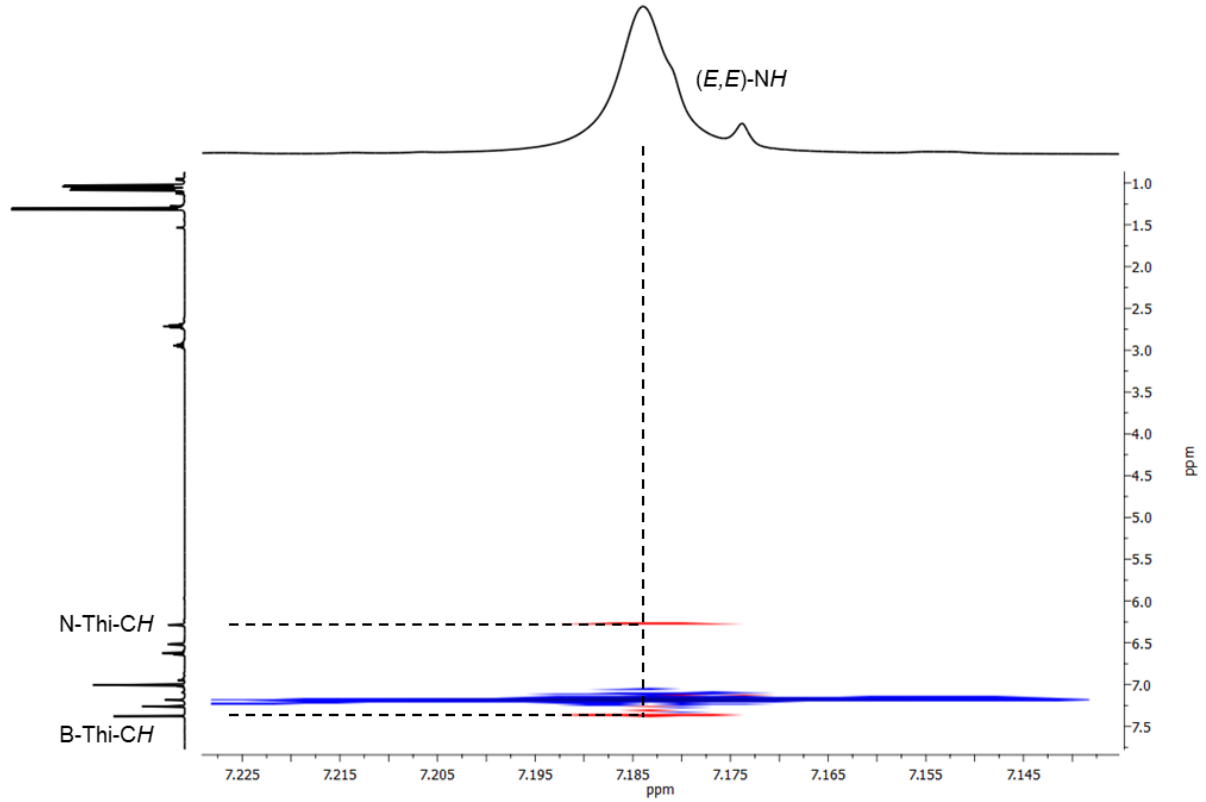

Figure S5.8.38. Detail of ^{1}H, ^{1}H NOESY spectrum of **15** ((*E*,*E*)-Isomer) in $CDCl_3$.

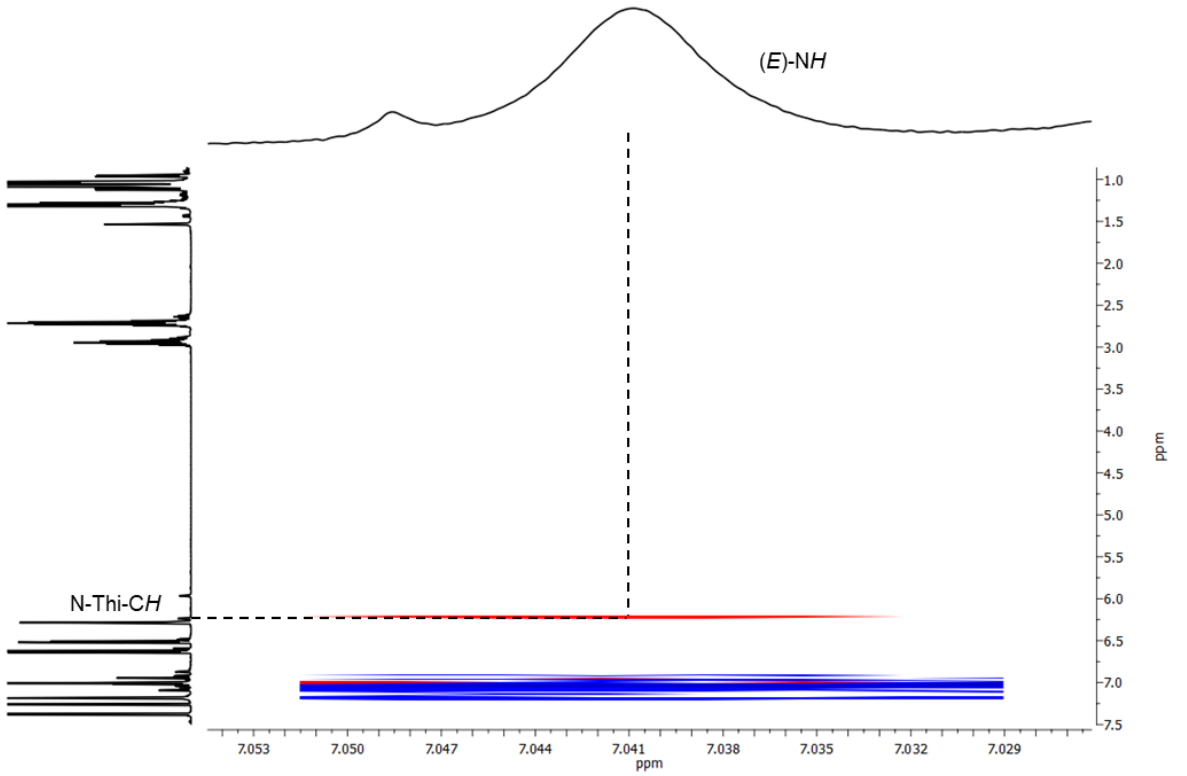

Figure S5.8.39. Detail of ^{1}H, ^{1}H NOESY spectrum of **15** ((*E*,*Z*)-Isomer) in $CDCl_3$. The N*H* signal of the *E*-configured double bond is shown.

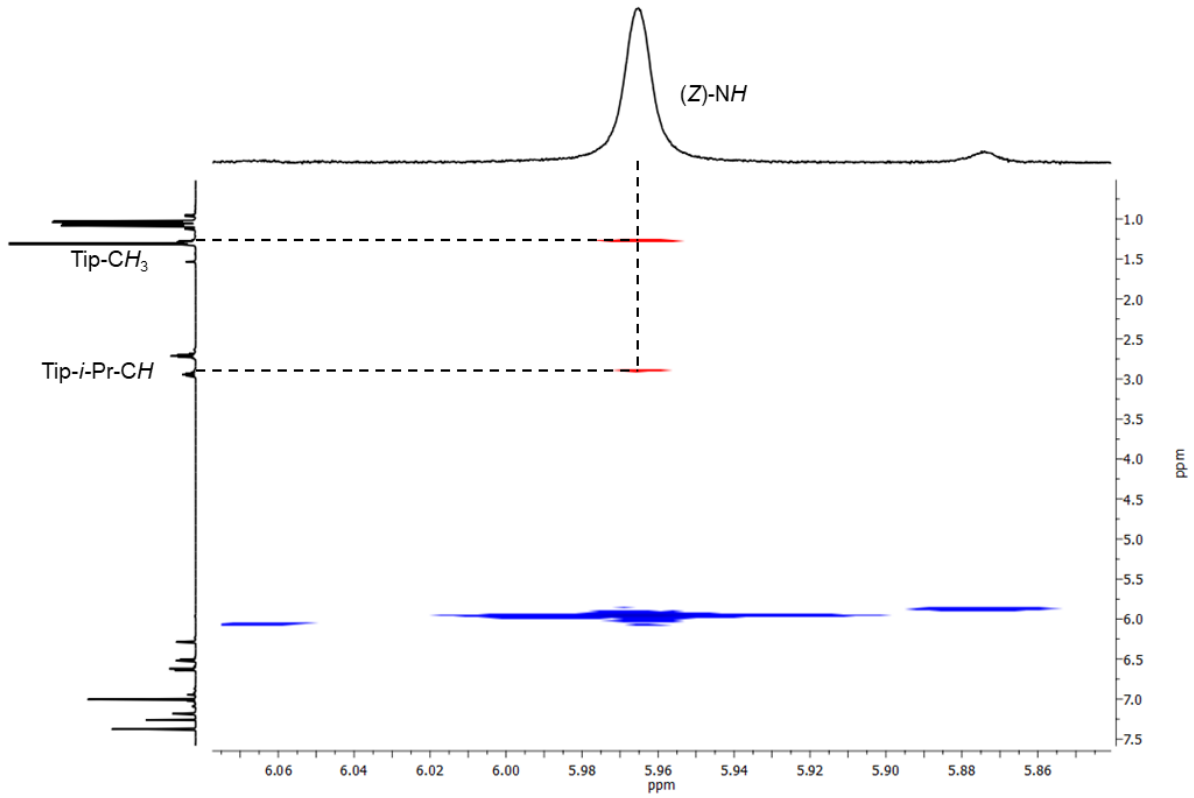

Figure S5.8.40. Detail of ^{1}H, ^{1}H NOESY spectrum of **15** ((*E*,*Z*)-Isomer) in $CDCl_3$. The N*H* signal of the *Z*-configured double bond is shown.

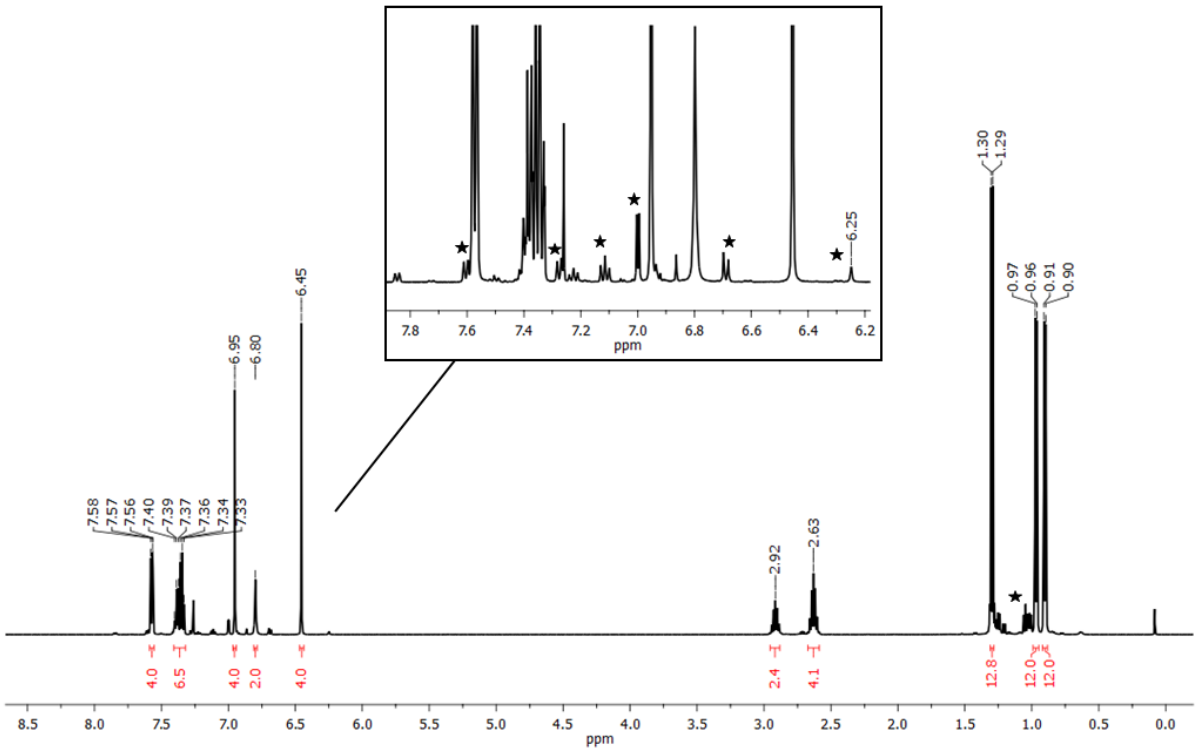

Figure S5.8.41. ^{1}H NMR spectrum (500 MHz) of **17** in $CDCl_3$. The signals marked with an asterisk belong to the minor isomer.

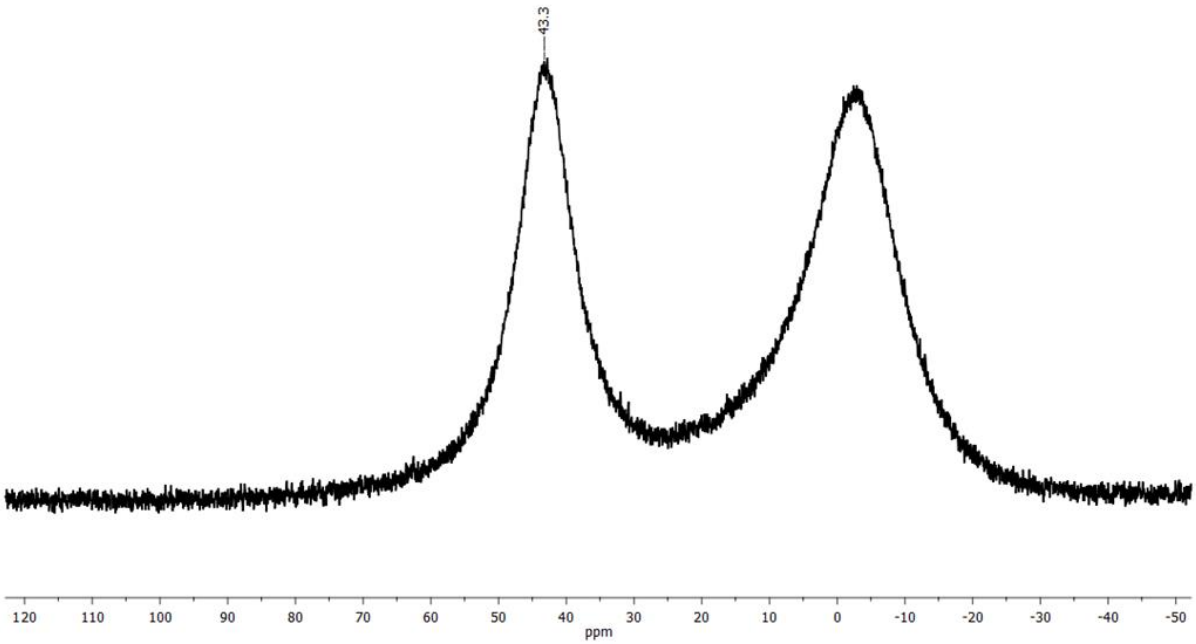

Figure S5.8.42. $^{11}B\{^{1}H\}$ NMR spectrum (160 MHz) of **17** in $CDCl_3$ with reduced glass background.

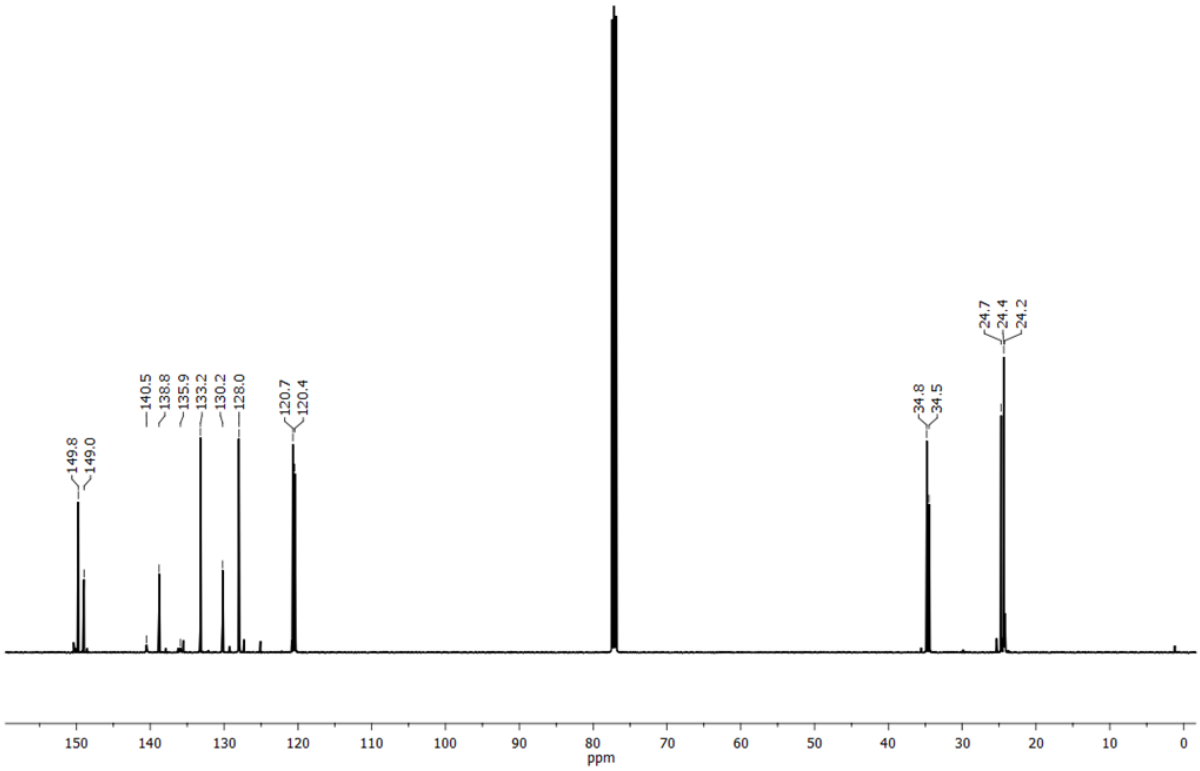

Figure S5.8.43. $^{13}C\{^{1}H\}$ NMR spectrum (126 MHz) of **17** in $CDCl_3$.

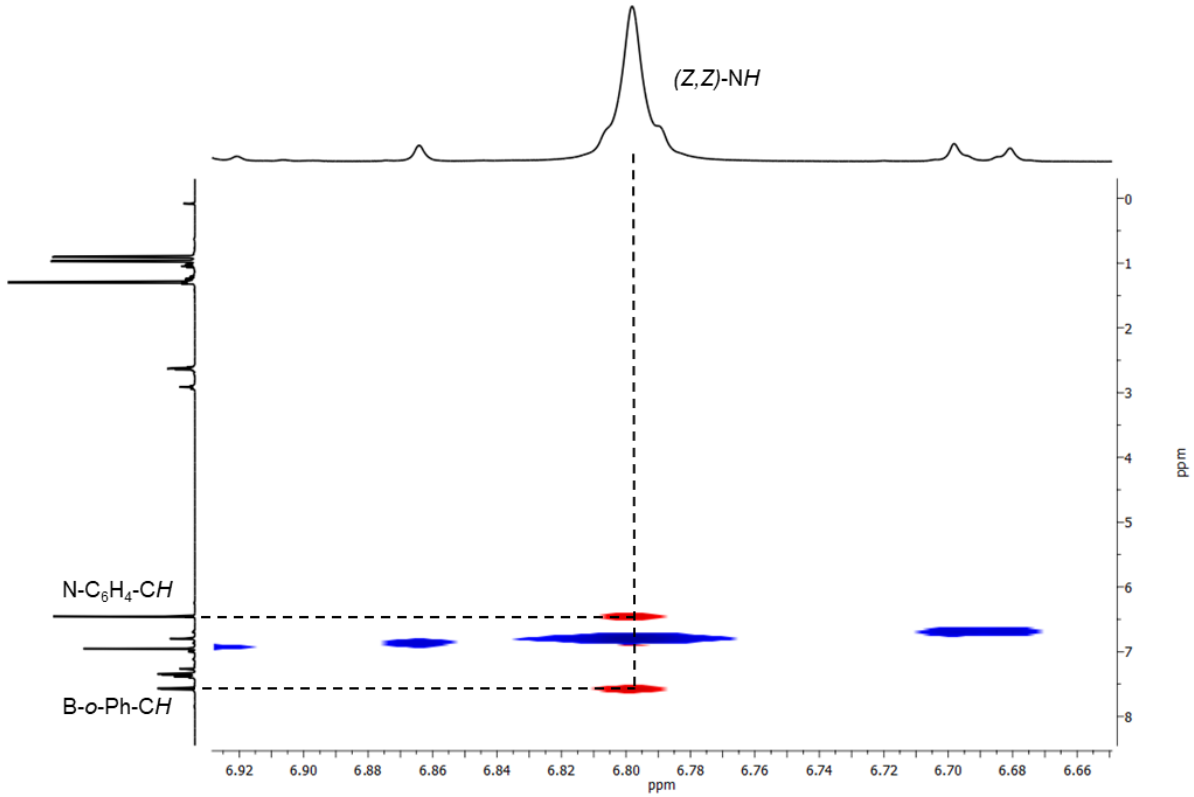

Figure S5.8.44. Detail of ^{1}H, ^{1}H NOESY spectrum of **17** ((*Z*,*Z*)-Isomer) in $CDCl_3$.

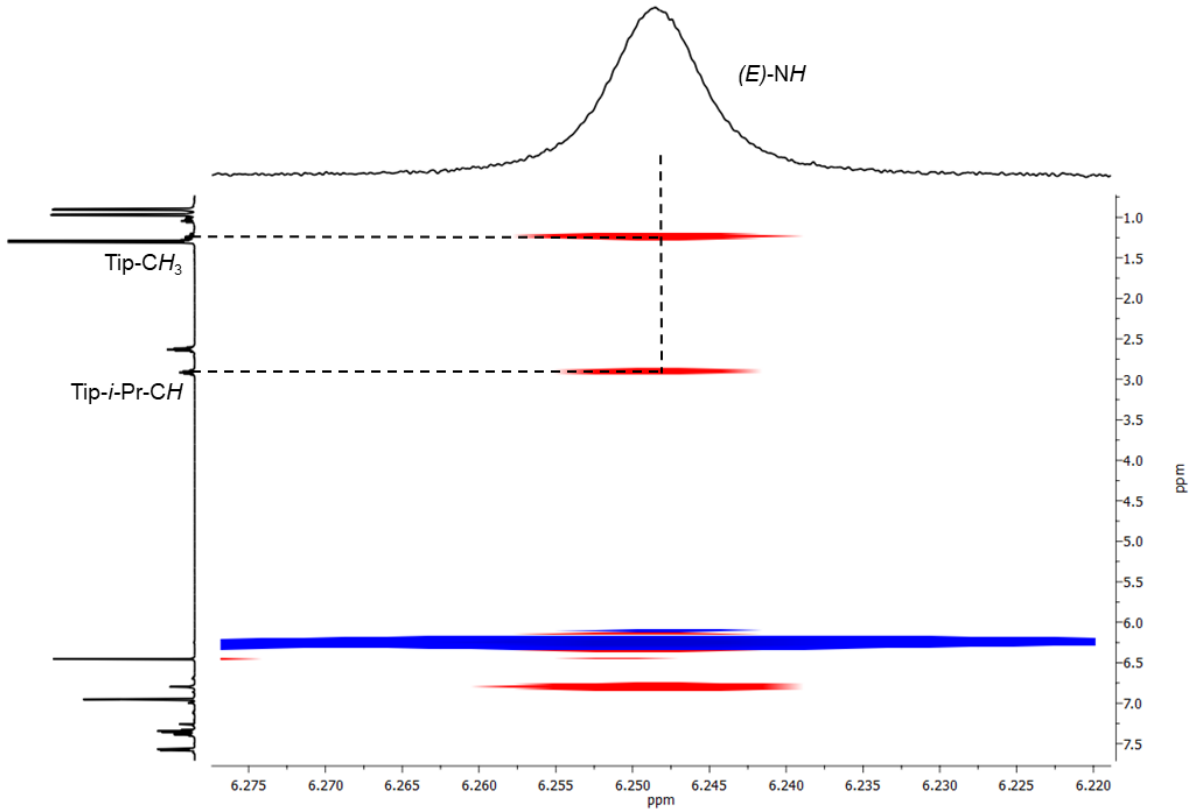

Figure S5.8.45. Detail of ^{1}H, ^{1}H NOESY spectrum of **17** ((*E*,*Z*)-Isomer) in $CDCl_3$. The N*H* signal of the *E*-configured double bond is shown.

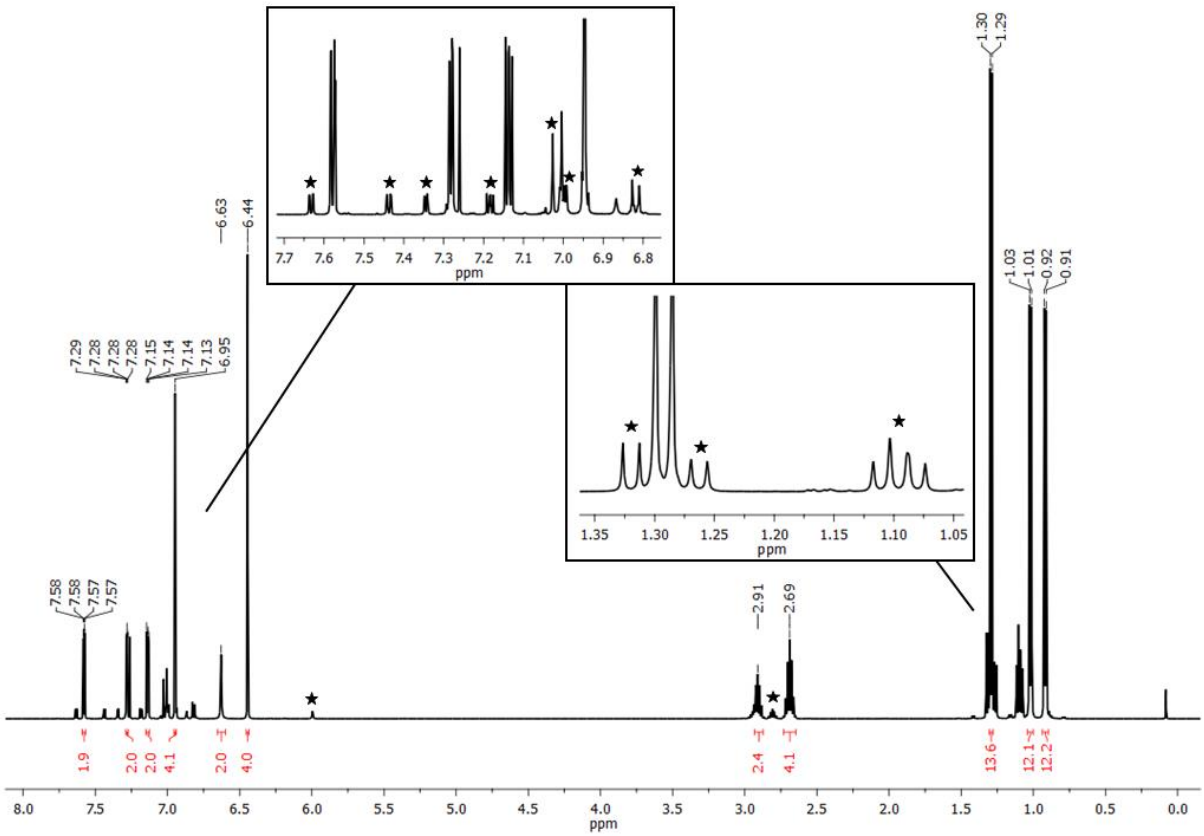

Figure S5.8.46. ^{1}H NMR spectrum (500 MHz) of **18** in $CDCl_3$. The signals marked with an asterisk belong to the minor isomer.

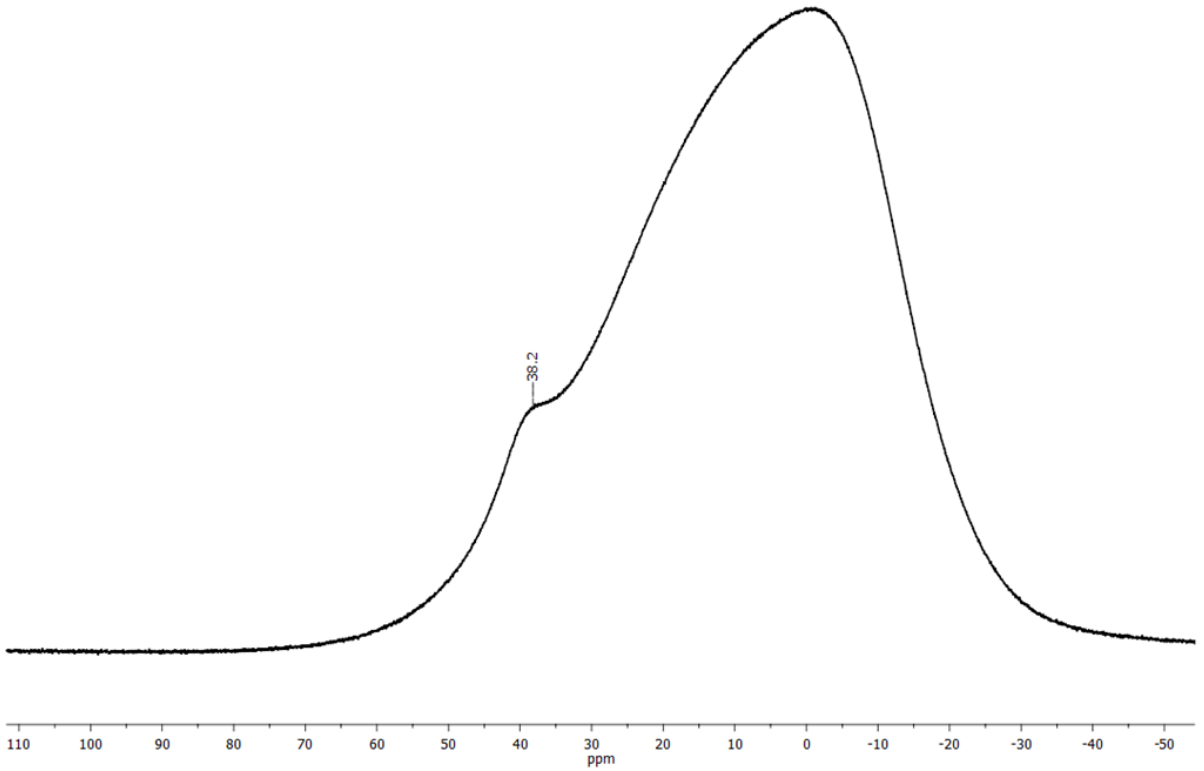

Figure S5.8.47. $^{11}B\{^{1}H\}$ NMR spectrum (160 MHz) of **18** in $CDCl_3$.

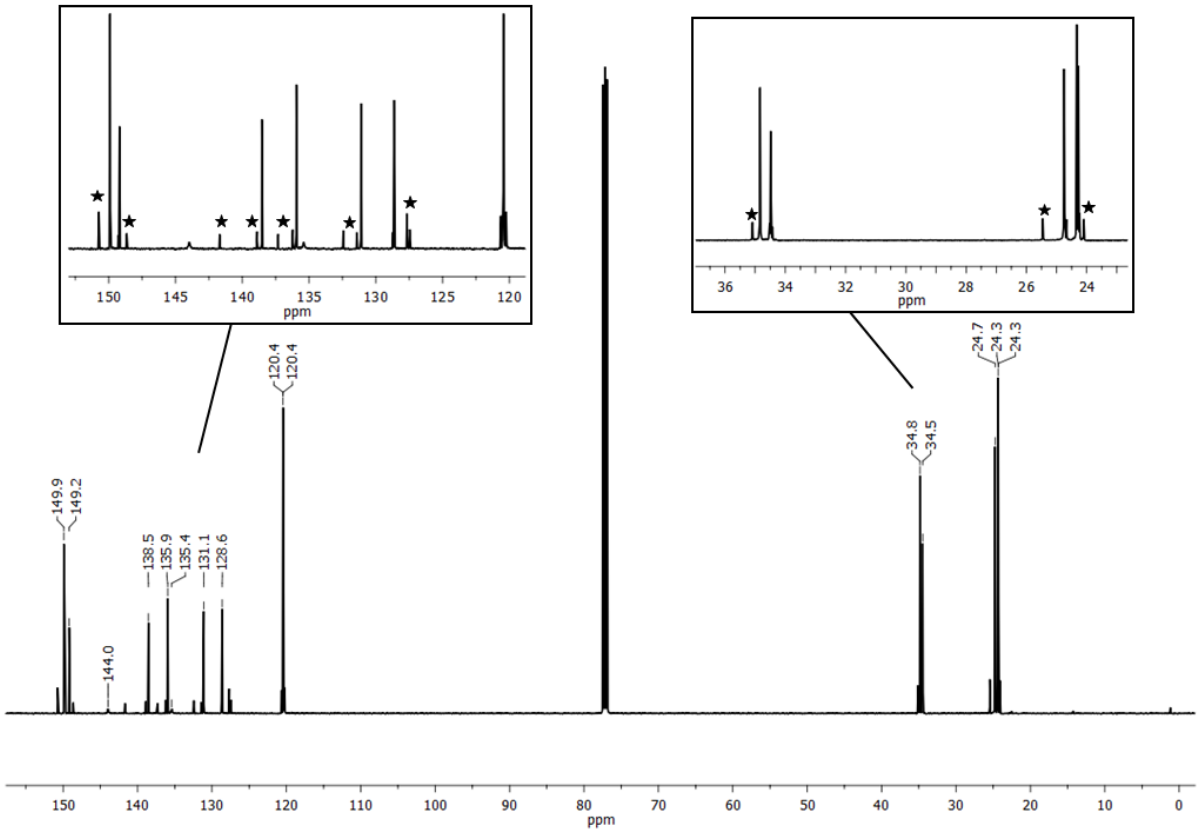

Figure S5.8.48. $^{13}C\{^{1}H\}$ NMR spectrum (126 MHz) of **18** in $CDCl_3$. The signals marked with an asterisk belong to the minor isomer.

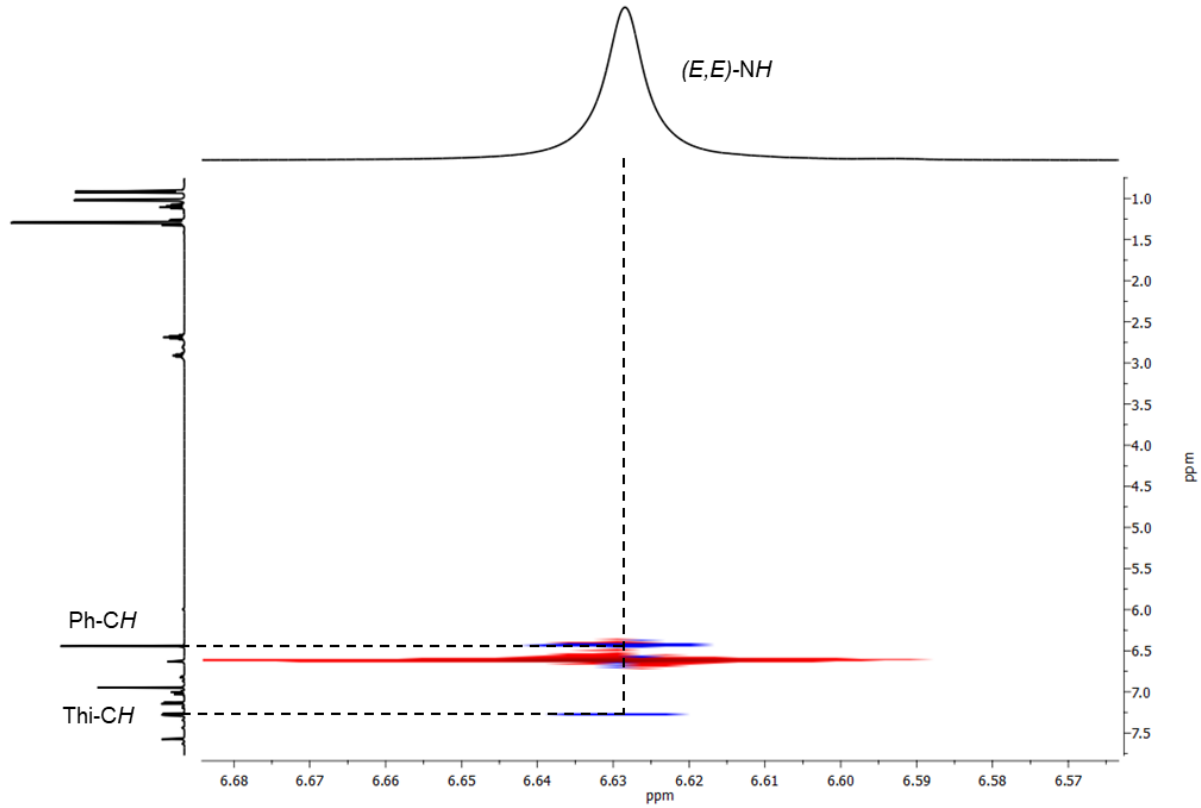

Figure S5.8.49. Detail of ^{1}H, ^{1}H NOESY spectrum of **18** ((*E*,*E*)-Isomer) in $CDCl_3$.

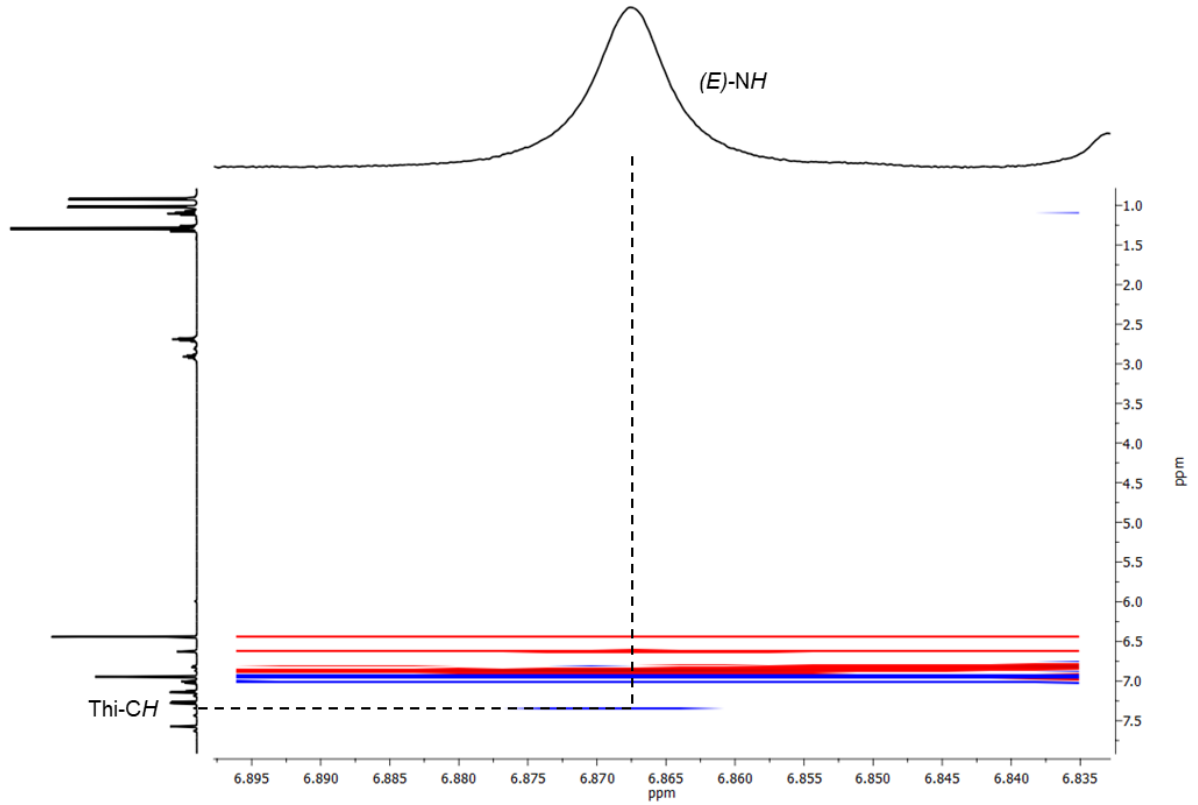

Figure S5.8.50. Detail of ^{1}H, ^{1}H NOESY spectrum of **18** ((*E*,*Z*)-Isomer) in $CDCl_3$. The N*H* signal of the *E*-configured double bond is shown.

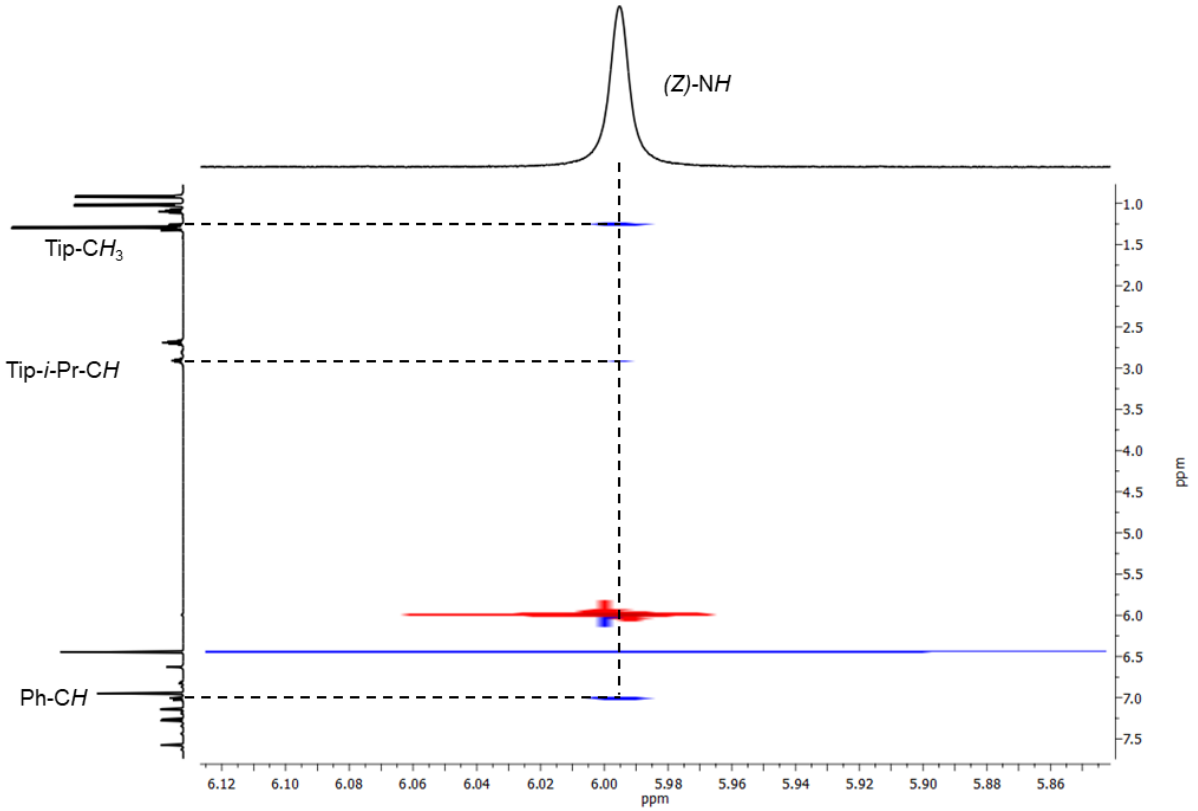

Figure S5.8.51. Detail of ^{1}H, ^{1}H NOESY spectrum of **18** ((*E*,*Z*)-Isomer) in $CDCl_3$. The N*H* signal of the *Z*-configured double bond is shown.

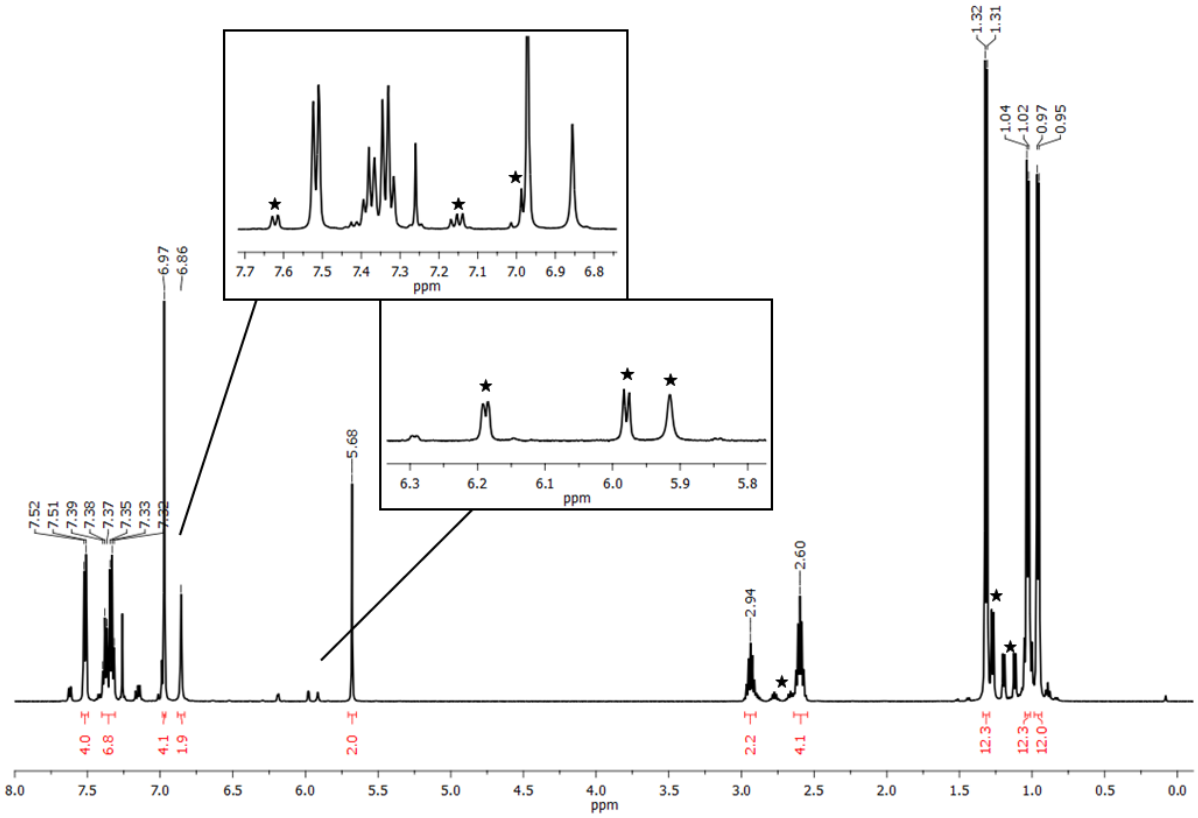

Figure S5.8.52. ^{1}H NMR spectrum (500 MHz) of **20** in $CDCl_3$. The signals marked with an asterisk belong to the minor isomer.

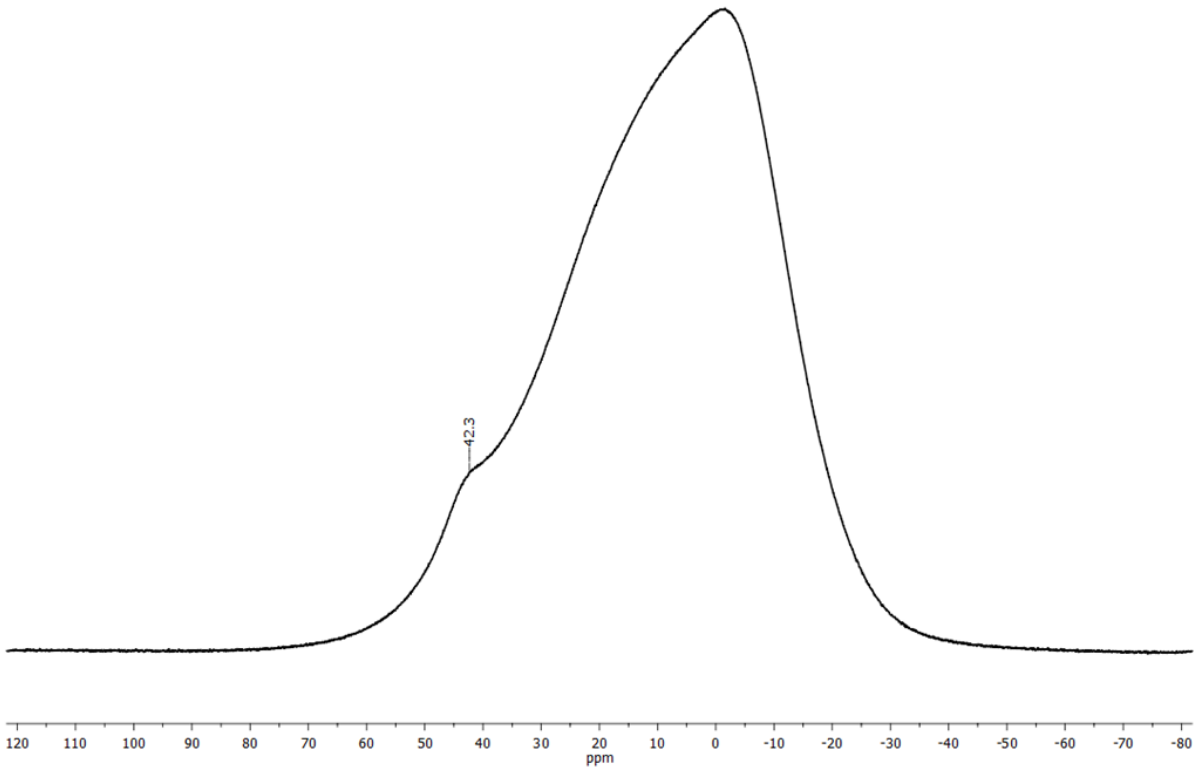

Figure S5.8.53. $^{11}B\{^{1}H\}$ NMR spectrum (160 MHz) of **20** in $CDCl_3$.

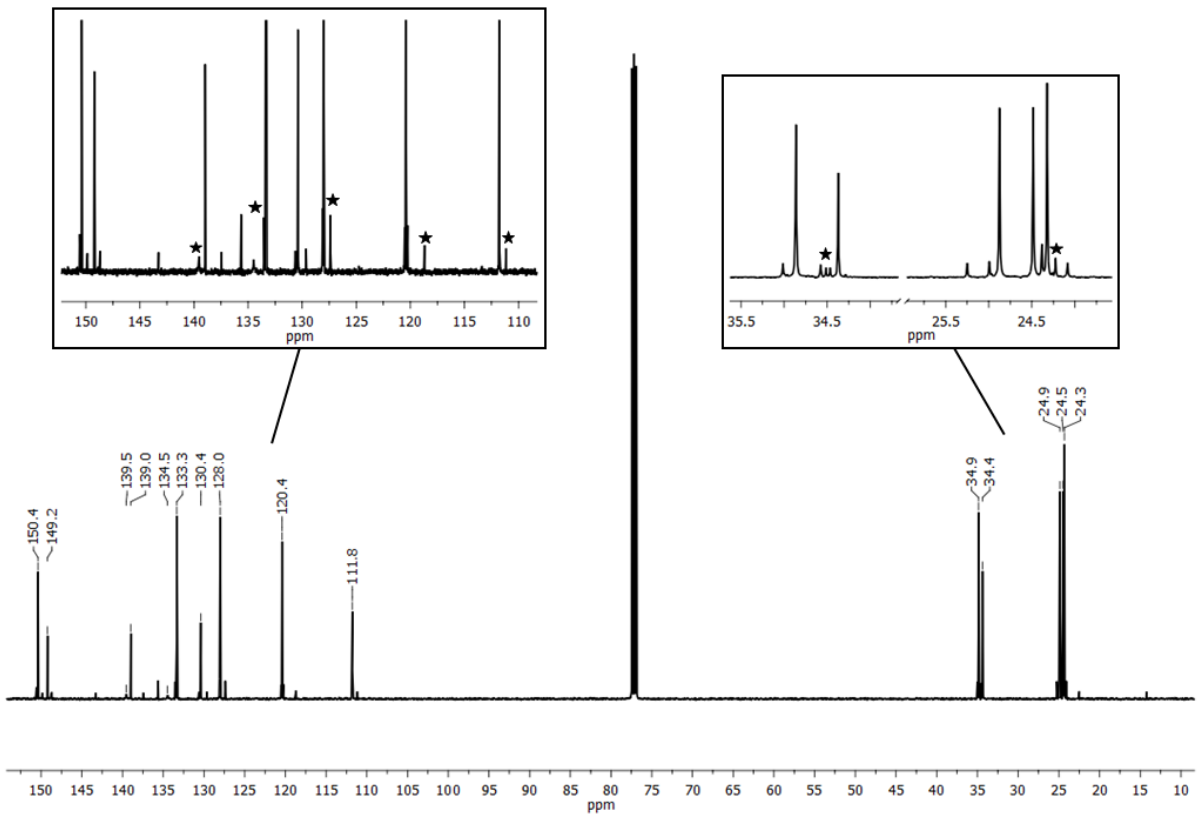

Figure S5.8.54. $^{13}C\{^{1}H\}$ NMR spectrum (126 MHz) of **20** in $CDCl_3$. The signals marked with an asterisk belong to the minor isomer.

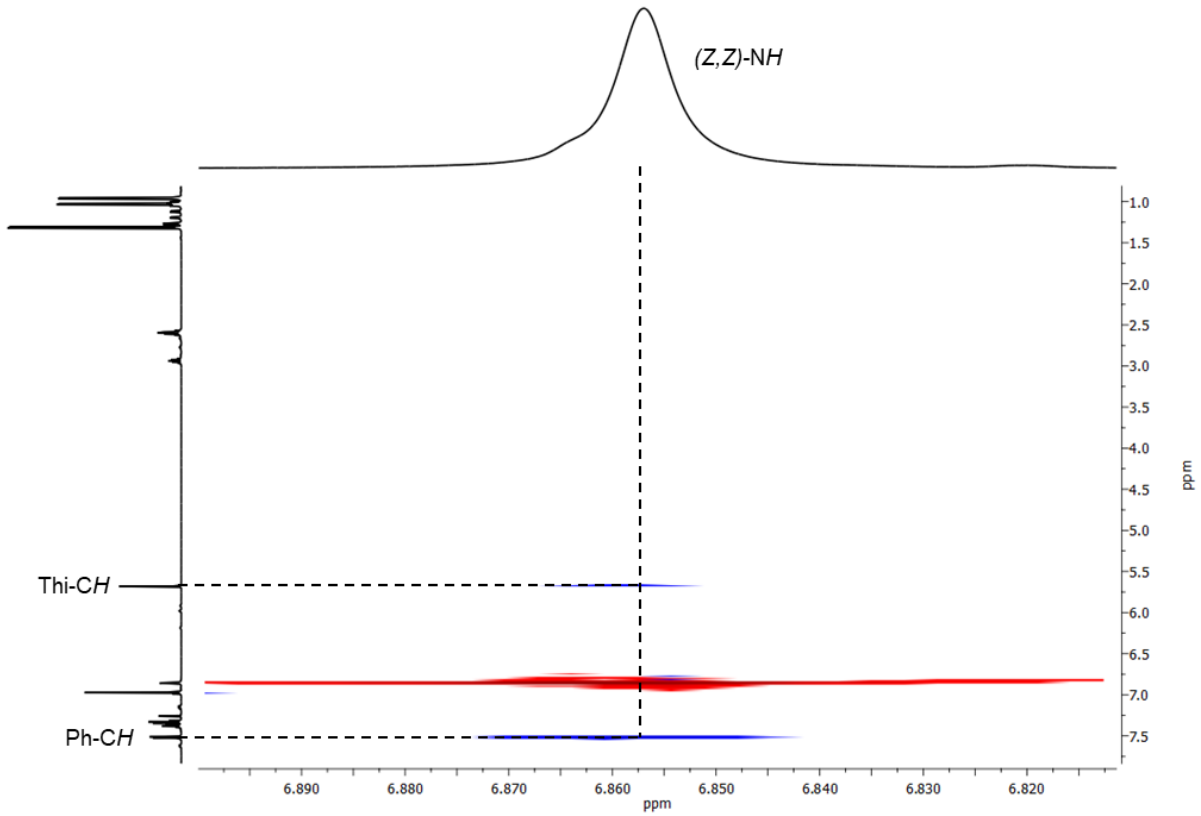

Figure S5.8.55. Detail of ^{1}H, ^{1}H NOESY spectrum of **20** ((*Z*,*Z*)-Isomer) in $CDCl_3$.

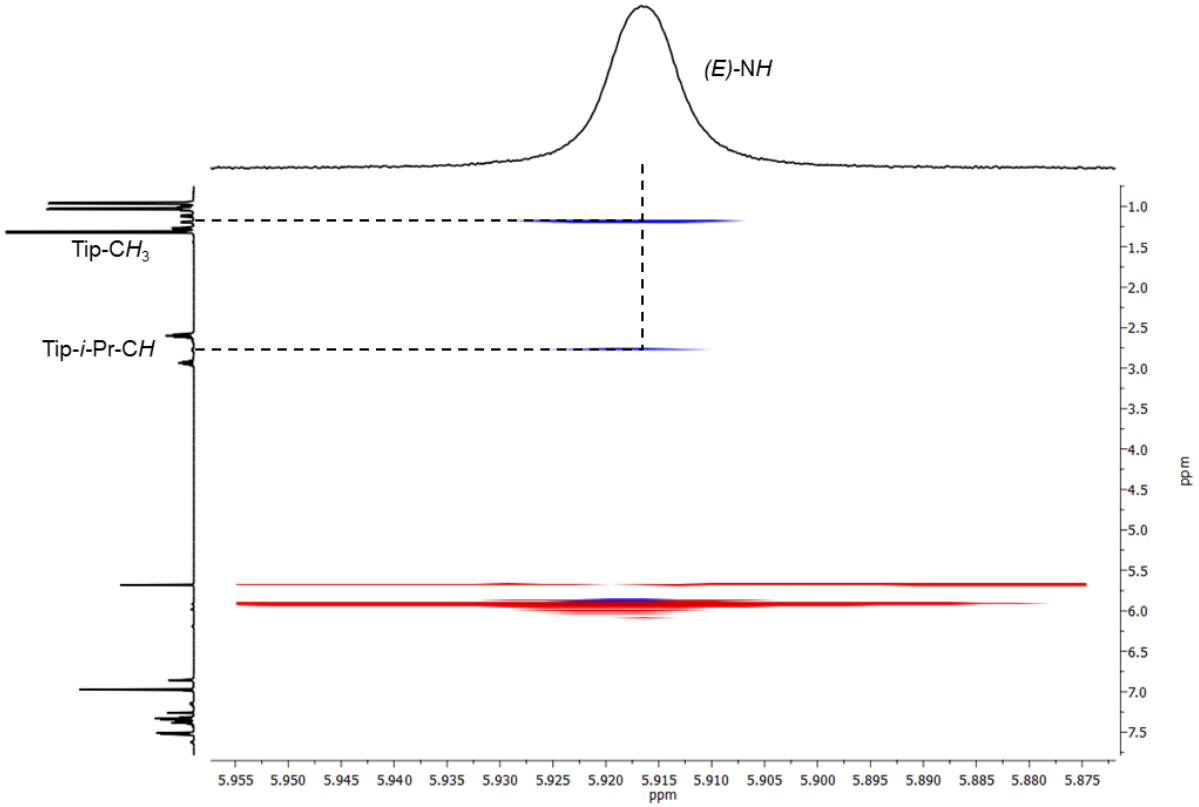

Figure S5.8.56. Detail of ^{1}H, ^{1}H NOESY spectrum of **20** ((*E*,*Z*)-Isomer) in $CDCl_3$. The N*H* signal of the *E*-configured double bond is shown.

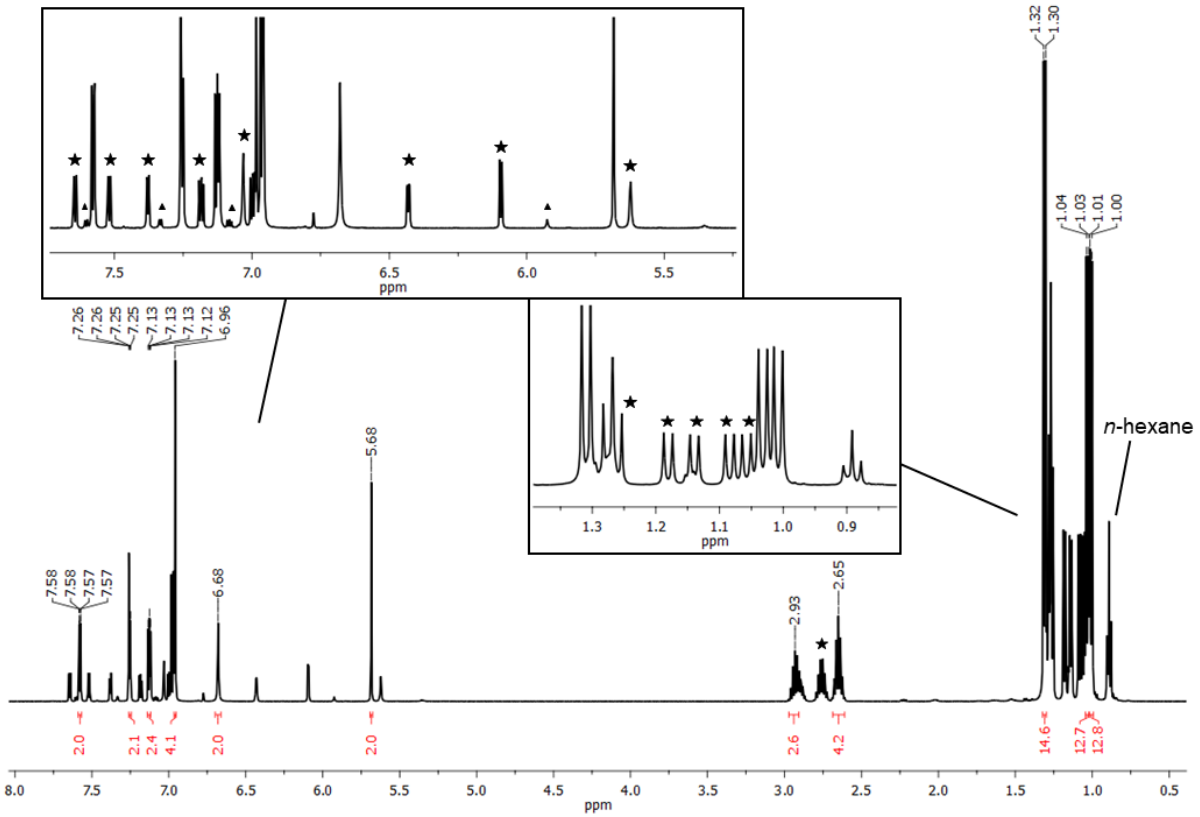

Figure S5.8.57. ^{1}H NMR spectrum (500 MHz) of **21** in $CDCl_3$. The signals marked with an asterisk and a triangle, respectively, belong to the minor isomers.

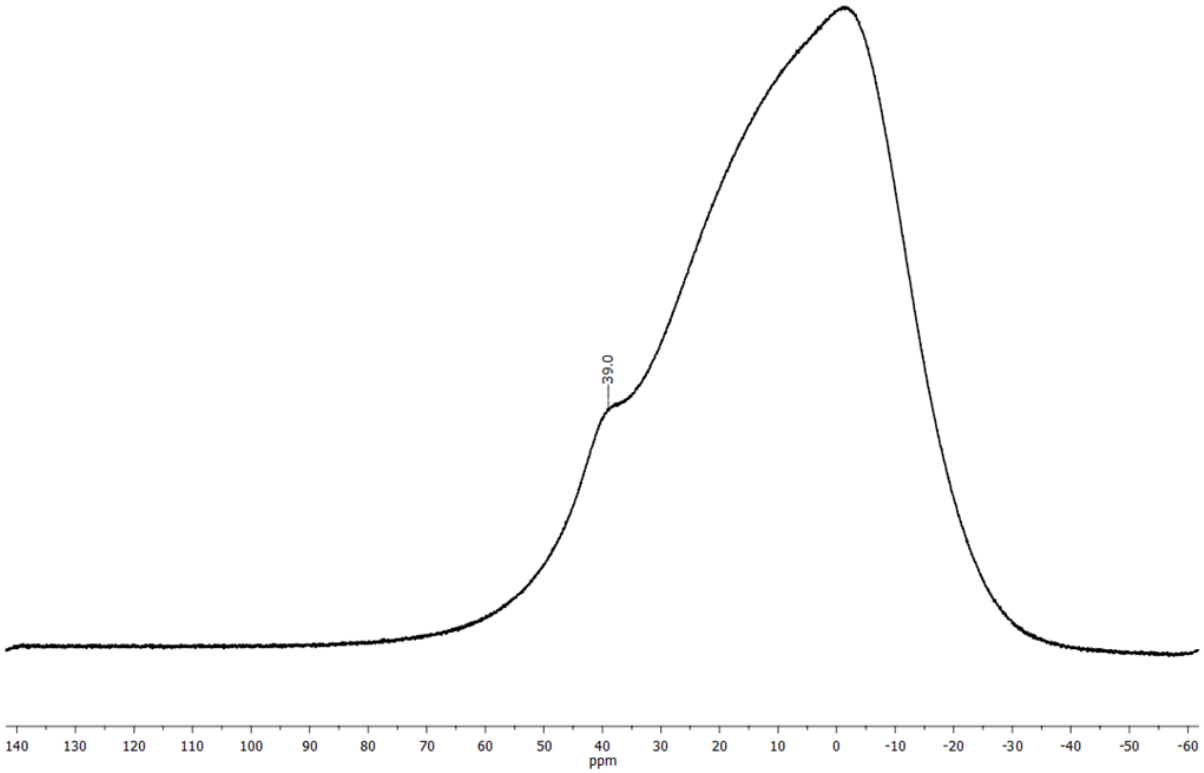

Figure S5.8.58. $^{11}B\{^{1}H\}$ NMR spectrum (160 MHz) of **21** in $CDCl_3$.

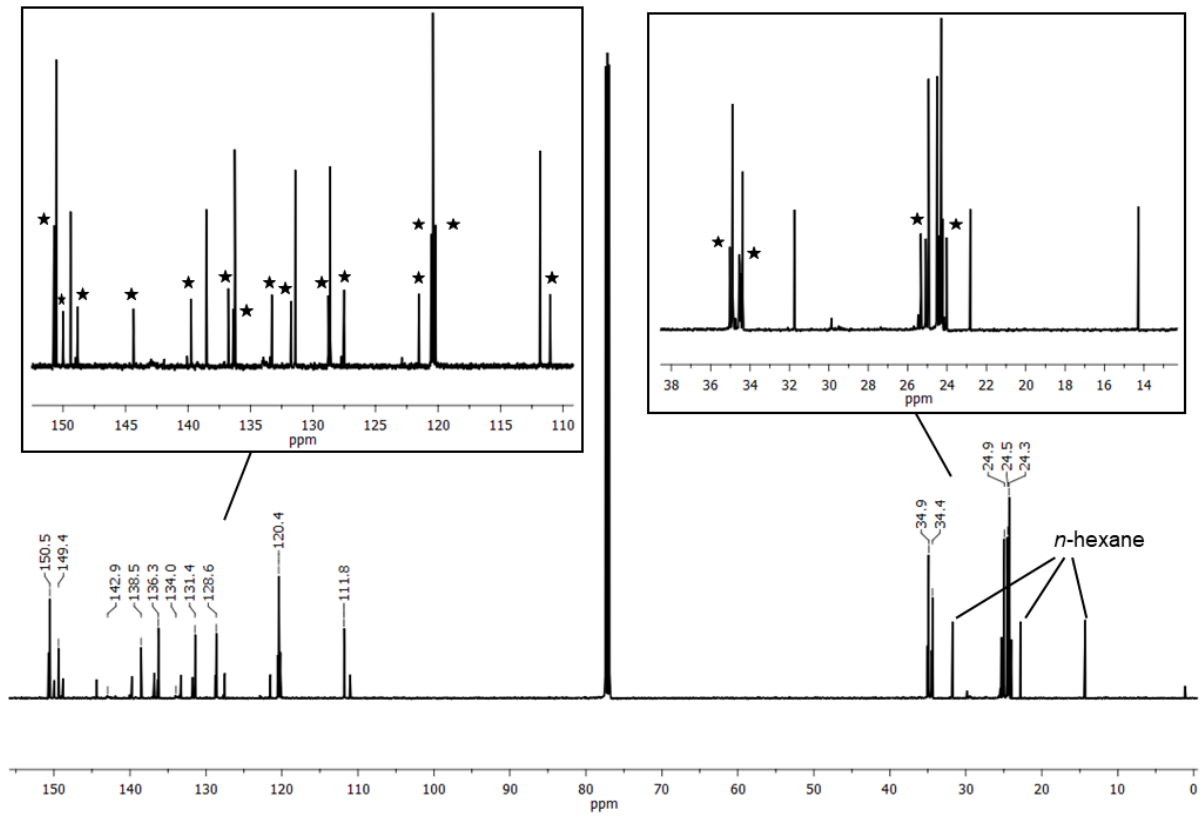

Figure S5.8.59. $^{13}C\{^{1}H\}$ NMR spectrum (126 MHz) of **21** in $CDCl_3$. The signals marked with an asterisk belong to the minor isomer.

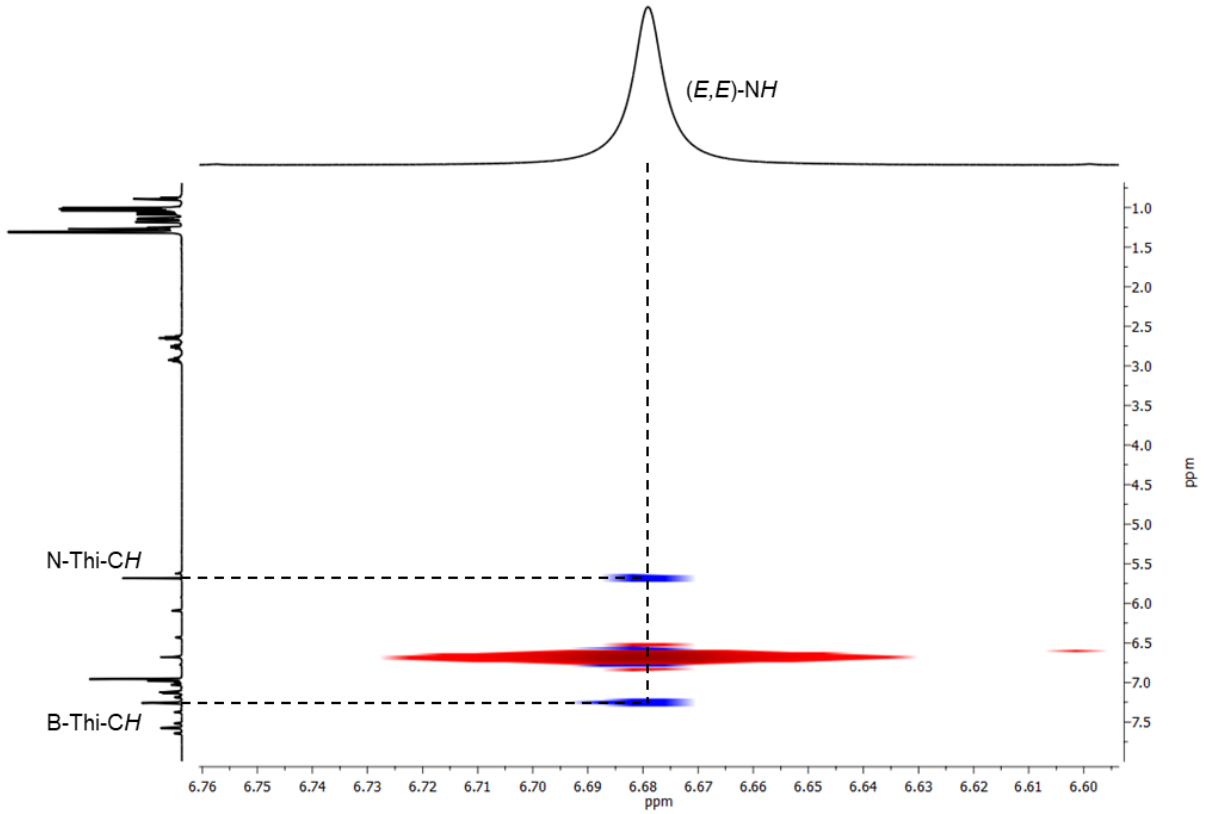

Figure S5.8.60. Detail of ^{1}H, ^{1}H ROESY spectrum of **21** ((*E*,*E*)-Isomer) in $CDCl_3$.

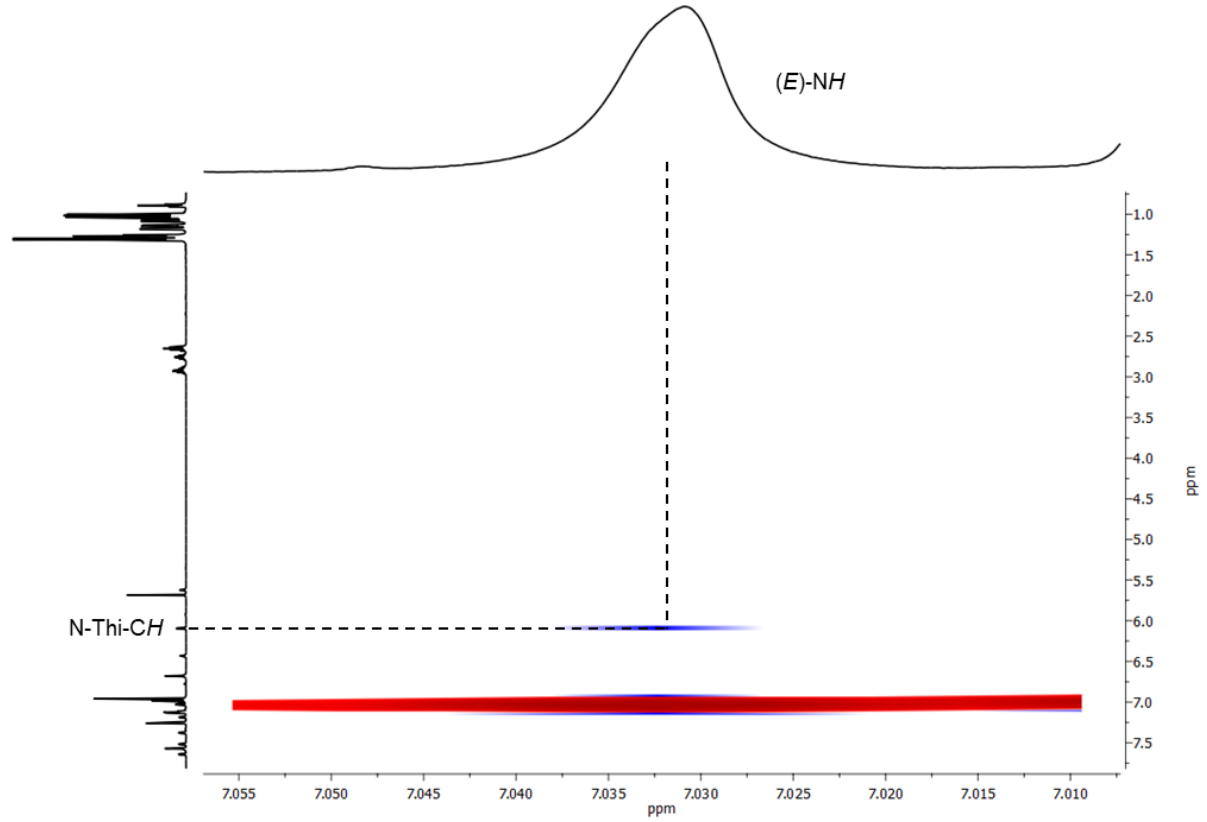

Figure S5.8.61. Detail of ^{1}H, ^{1}H ROESY spectrum of **21** ((*E*,*Z*)-Isomer) in $CDCl_3$. The N*H* signal of the *E*-configured double bond is shown.

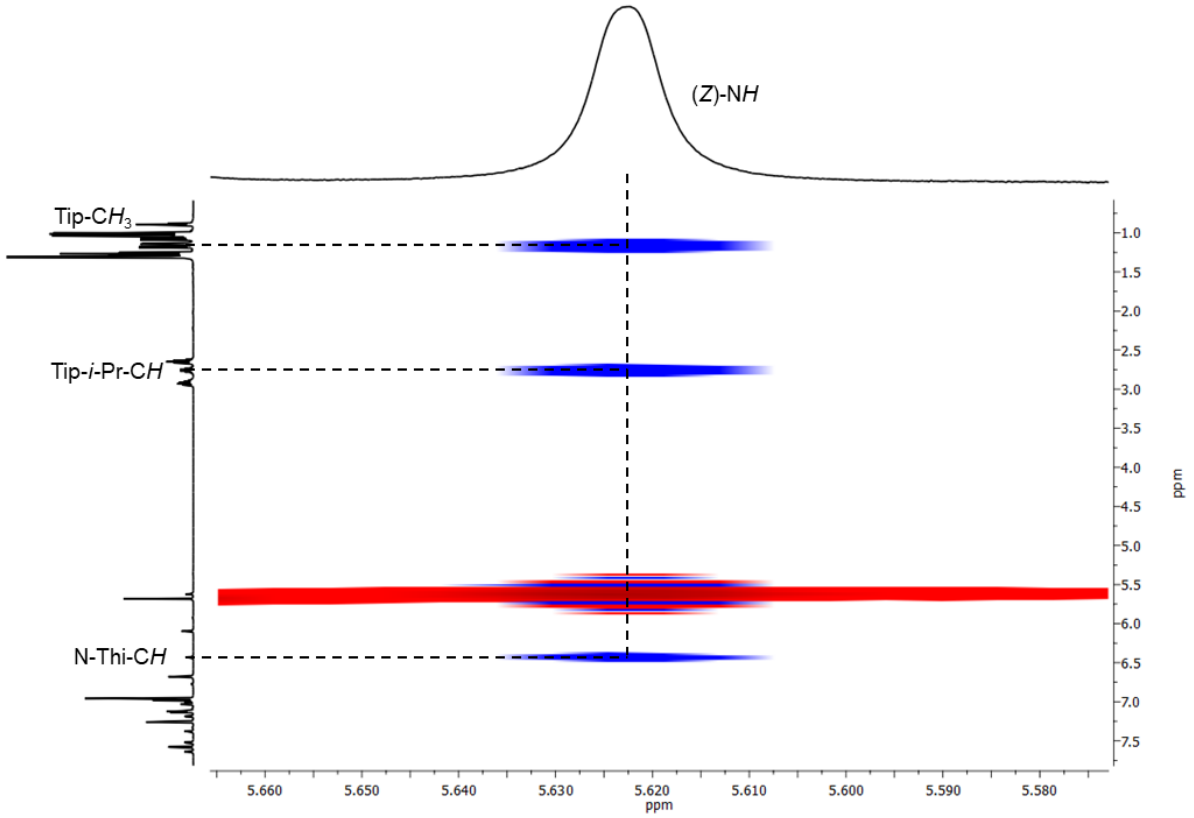

Figure S5.8.62. Detail of ^{1}H, ^{1}H ROESY spectrum of **21** ((*E*,*Z*)-Isomer) in $CDCl_3$. The N*H* signal of the *Z*-configured double bond is shown.

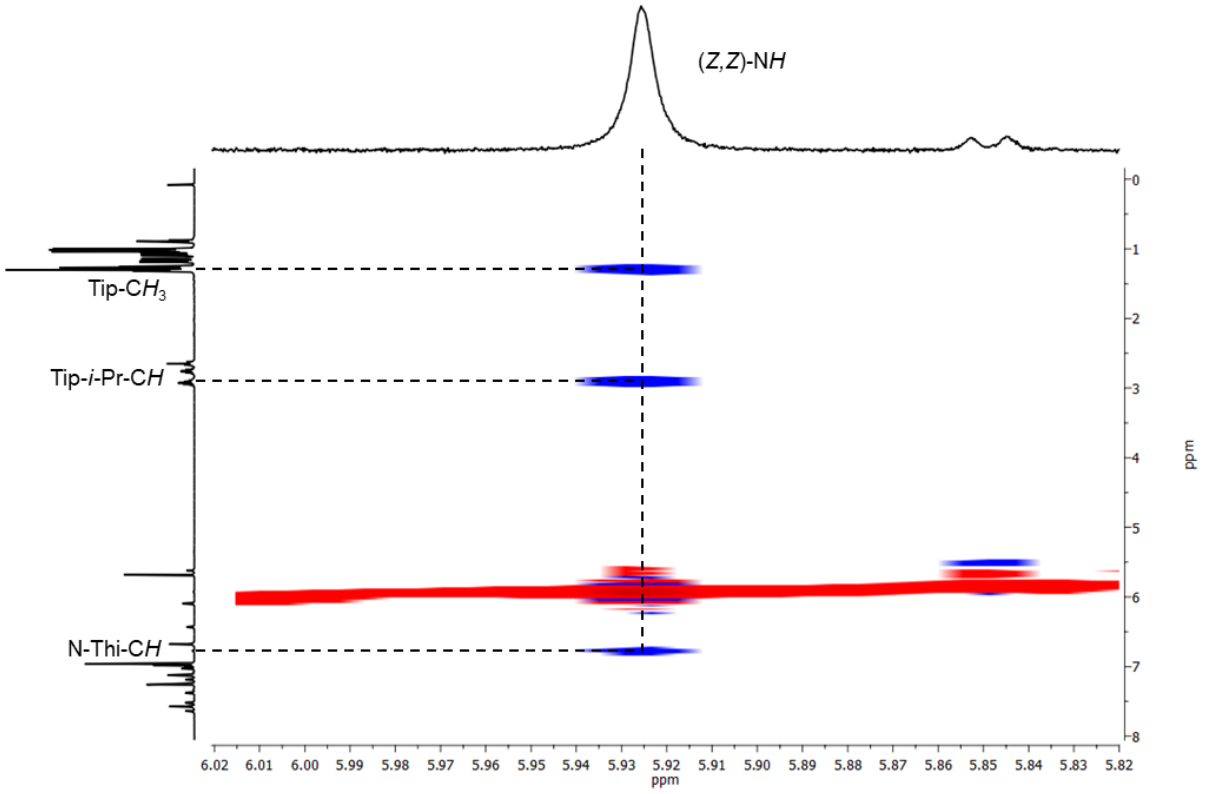

Figure S5.8.63. Detail of ^{1}H, ^{1}H ROESY spectrum of **21** ((*Z*,*Z*)-Isomer) in $CDCl_3$.

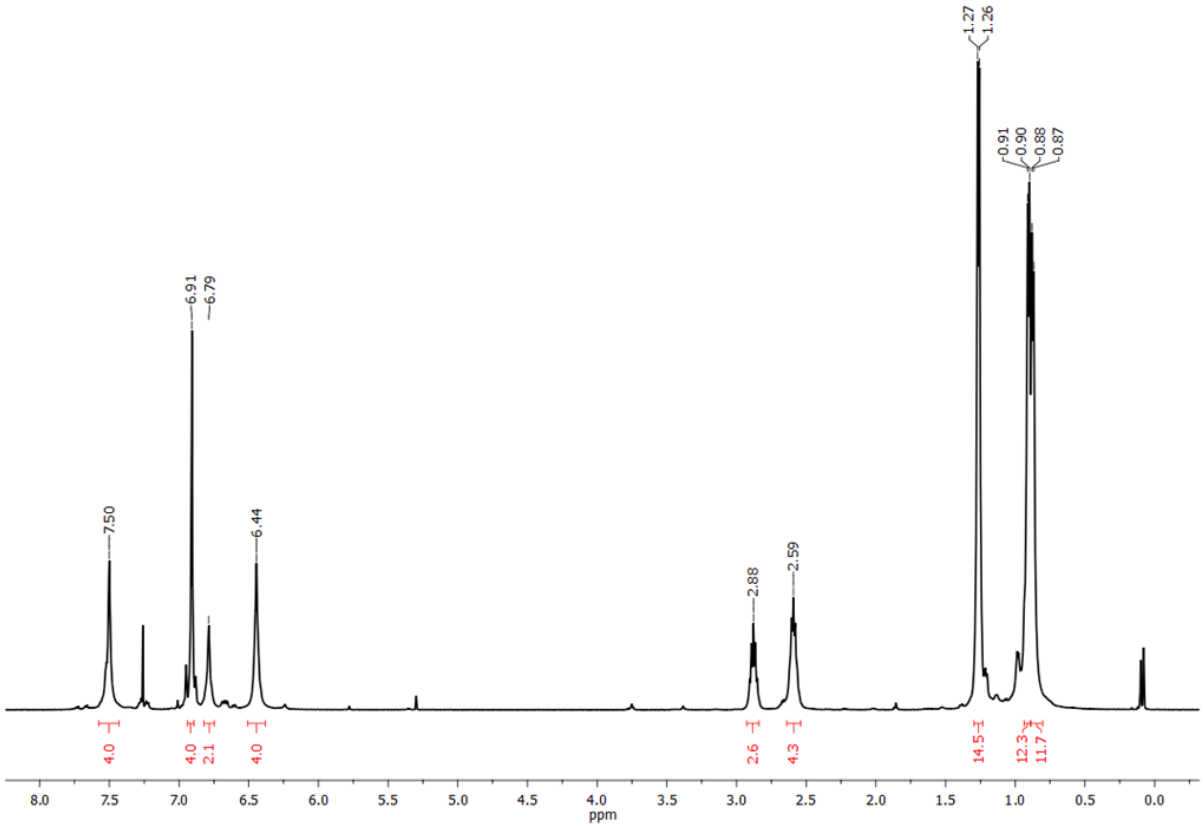

Figure S5.8.64. ^{1}H NMR spectrum (500 MHz) of **22** in $CDCl_3$.

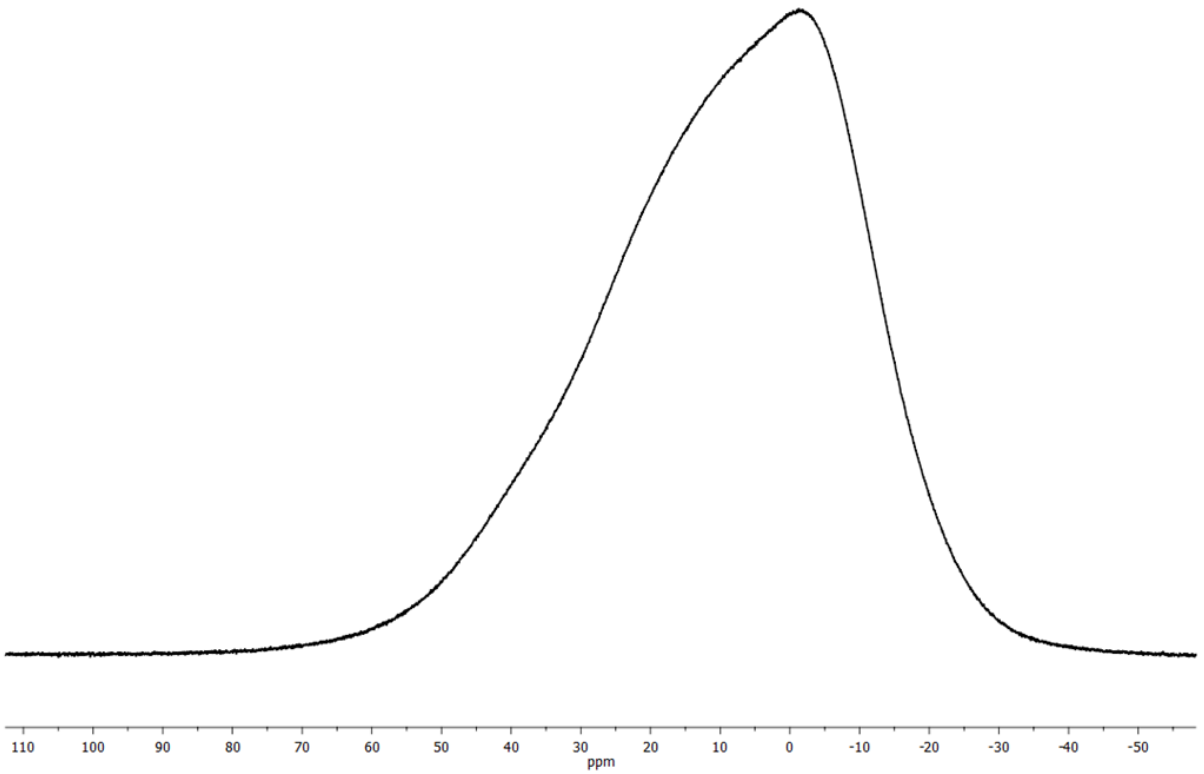

Figure S5.8.65. $^{11}B\{^{1}H\}$ NMR spectrum (160 MHz) of **22** in $CDCl_3$. No signal was observed.

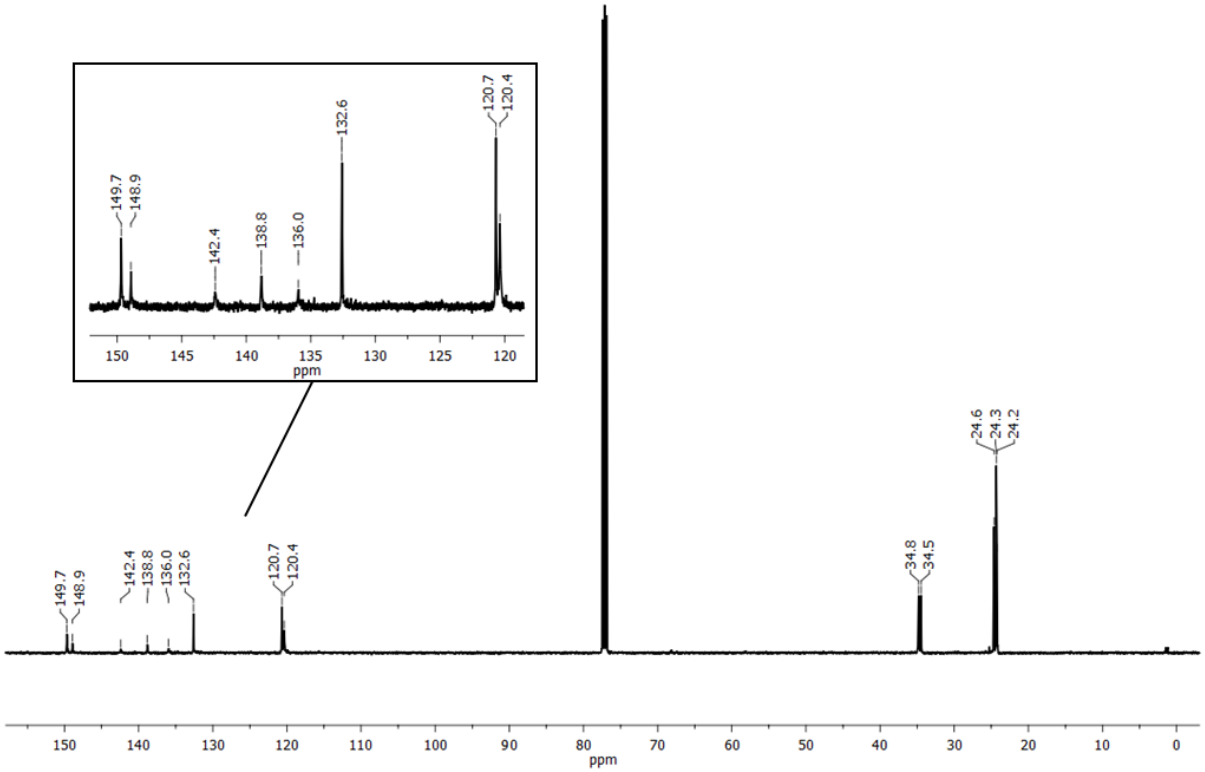

Figure S5.8.66. $^{13}C\{^{1}H\}$ NMR spectrum (126 MHz) of **22** in $CDCl_3$.

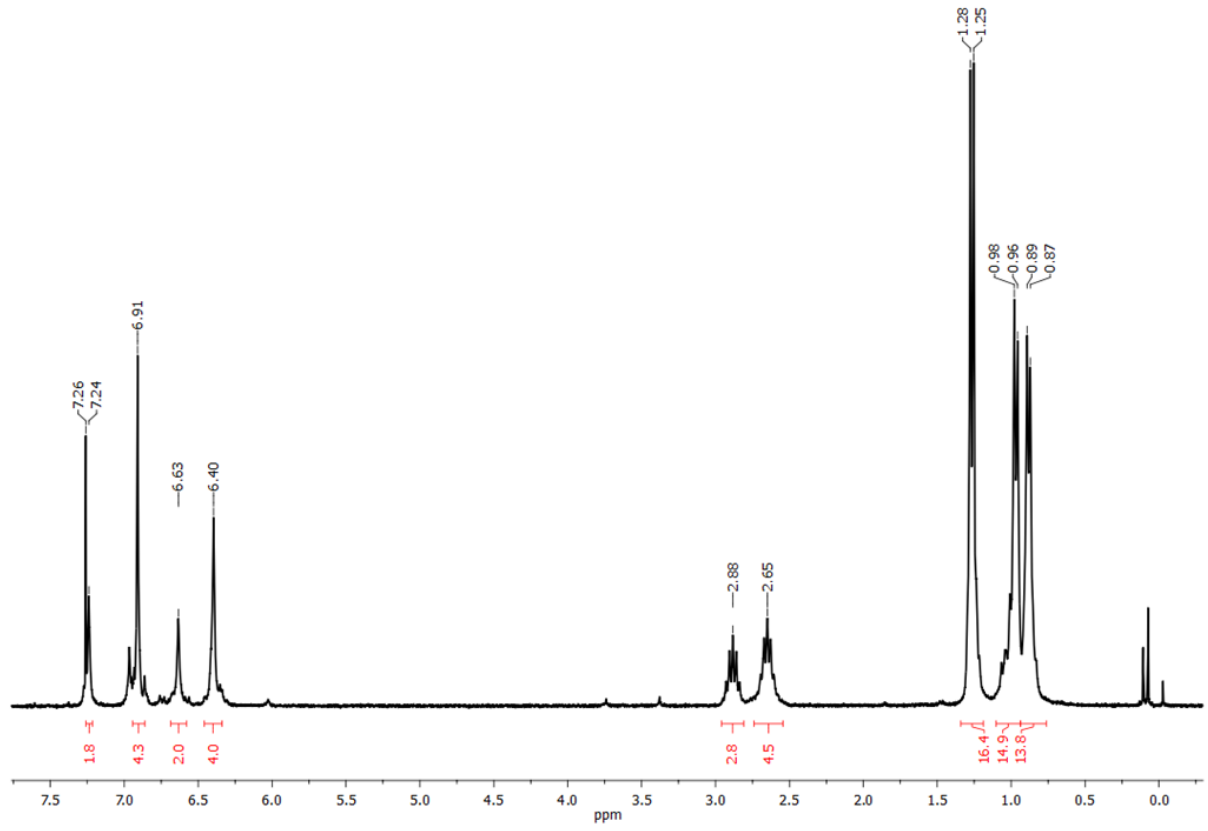

Figure S5.8.67. ^{1}H NMR spectrum (300 MHz) of **25** (by Si/B exchange) with integration of the main peaks in $CDCl_3$.

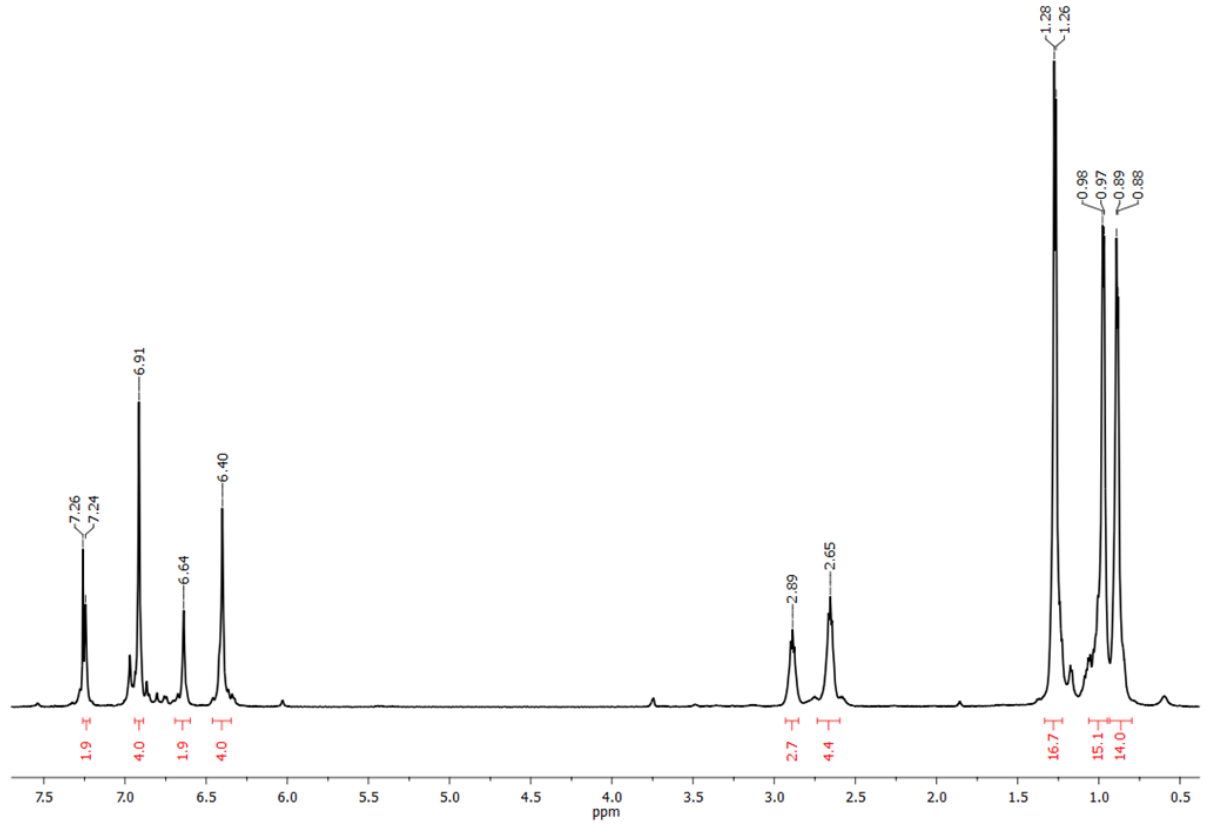

Figure S5.8.68. ^{1}H NMR spectrum (600 MHz) of **25** (by salt elimination) with integration of the main peaks in $CDCl_3$.

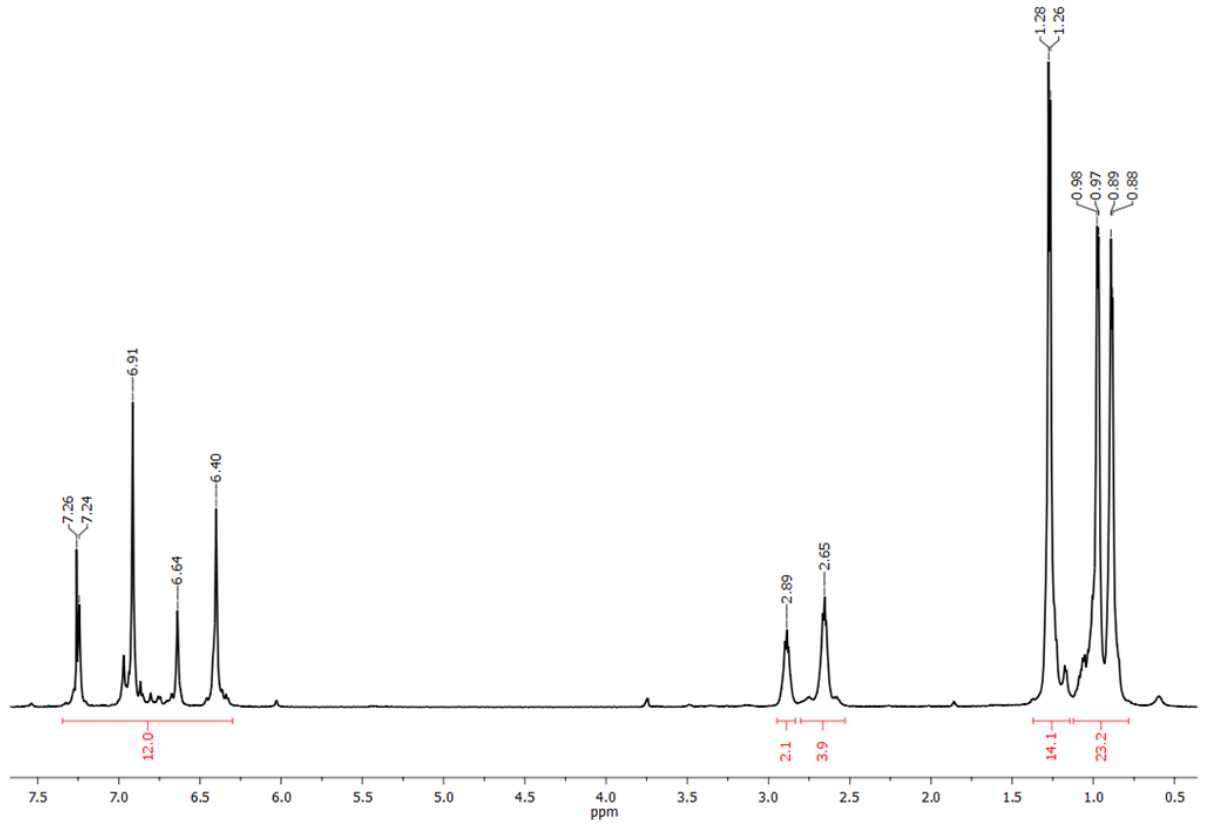

Figure S5.8.69. ^{1}H NMR spectrum (600 MHz) of **25** (by salt elimination) in $CDCl_3$.

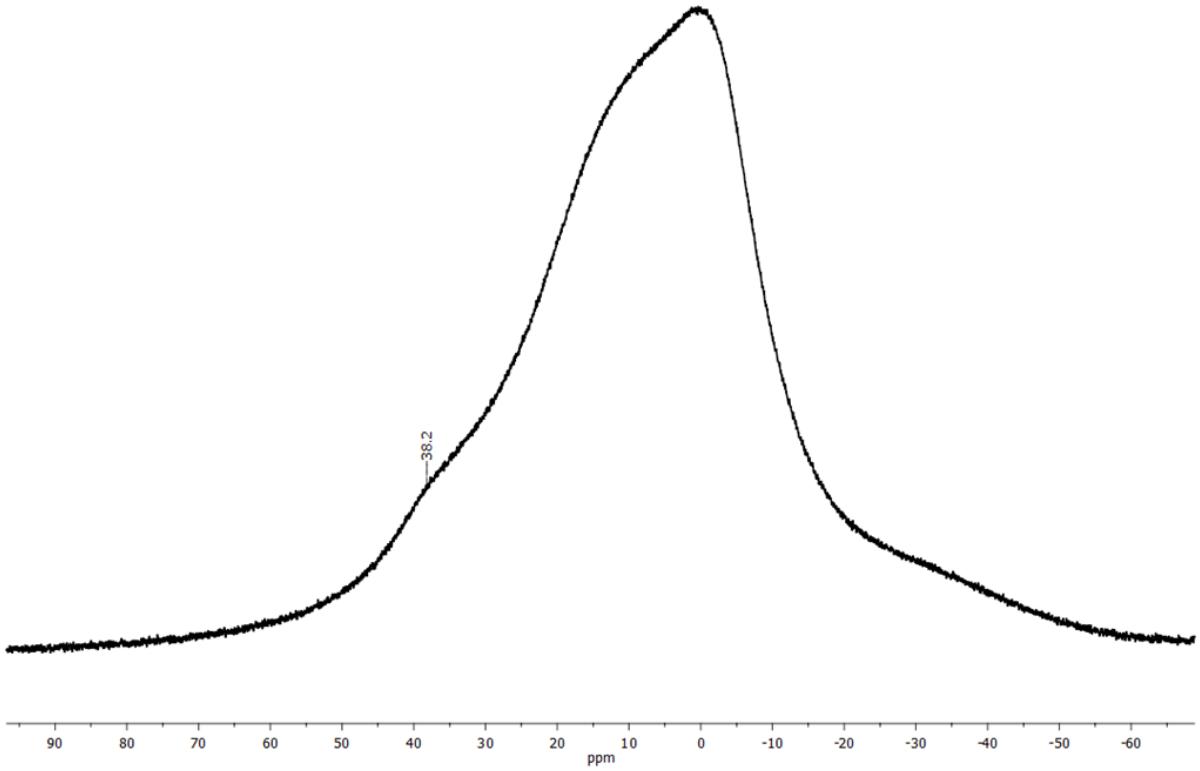

Figure S5.8.70. $^{11}B\{^{1}H\}$ NMR spectrum (193 MHz) of **25** (by salt elimination) in $CDCl_3$.

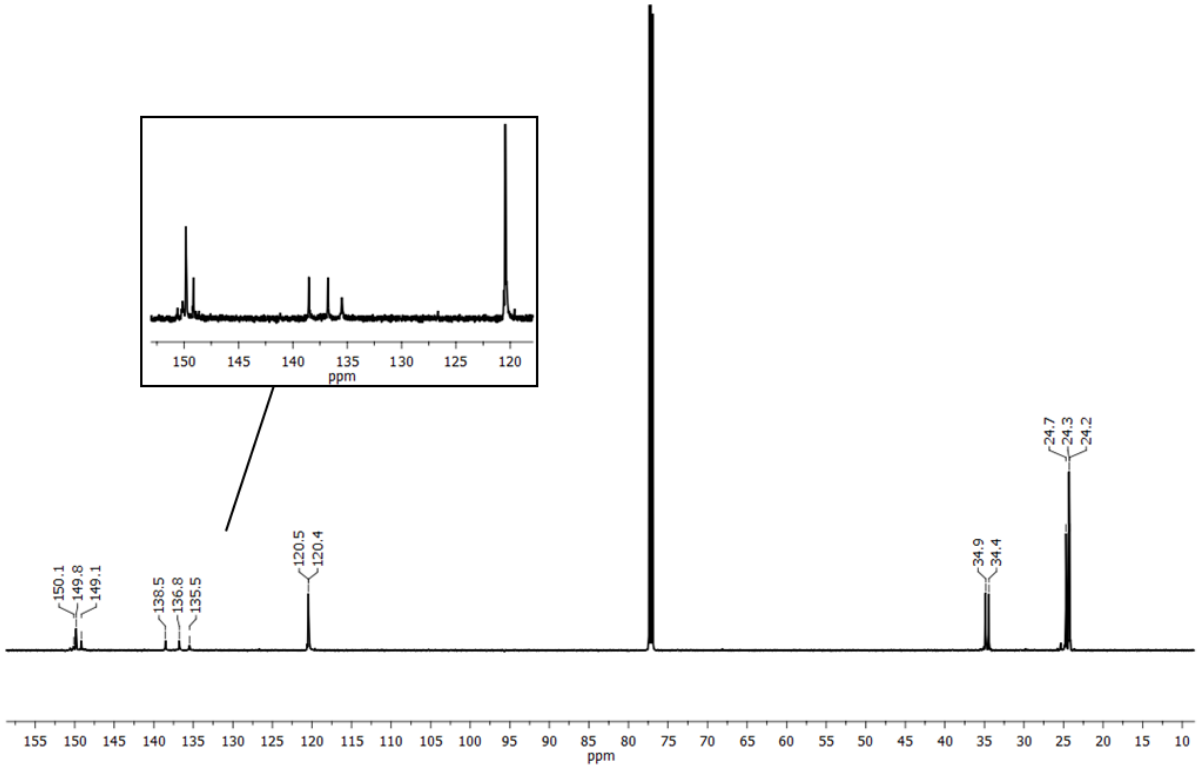

Figure S5.8.71. $^{13}C\{^{1}H\}$ NMR spectrum (151 MHz) of **25** (by salt elimination) in $CDCl_3$.

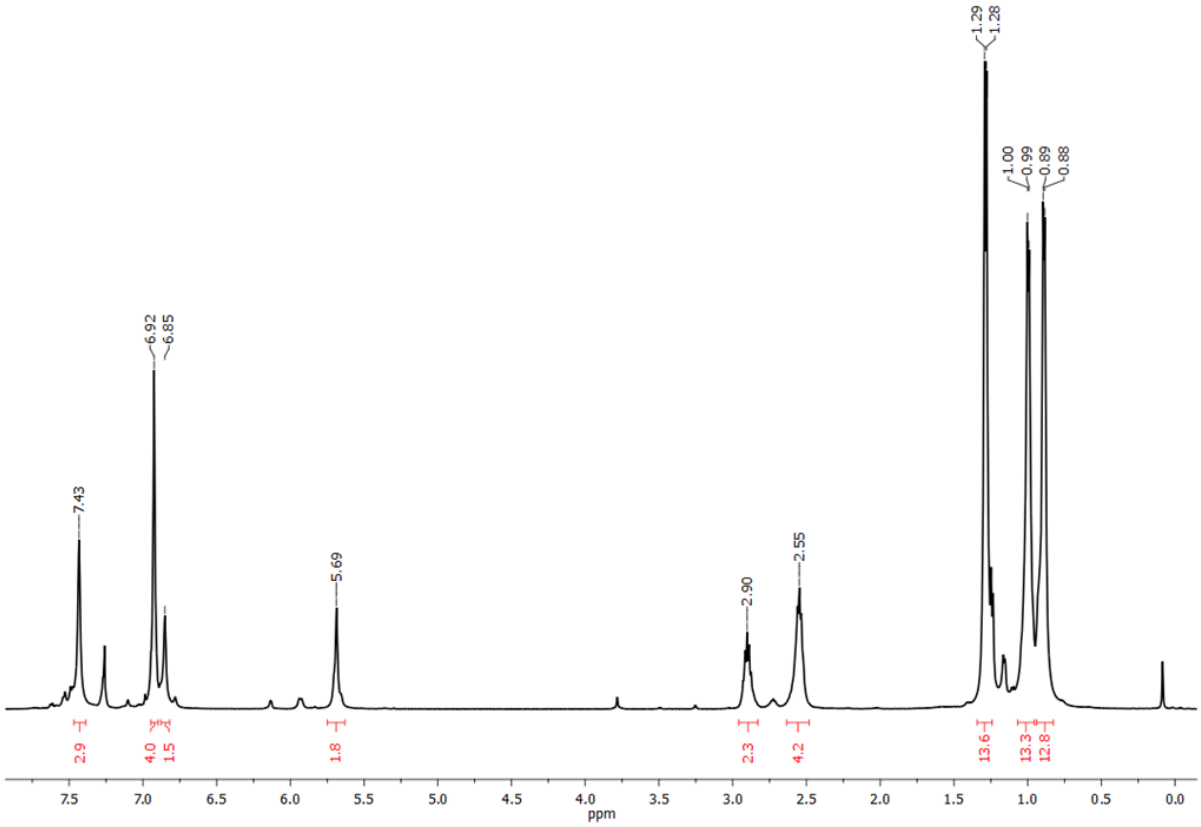

Figure S5.8.72. ^{1}H NMR spectrum (500 MHz) of **26** with integration of the main peaks in $CDCl_3$.

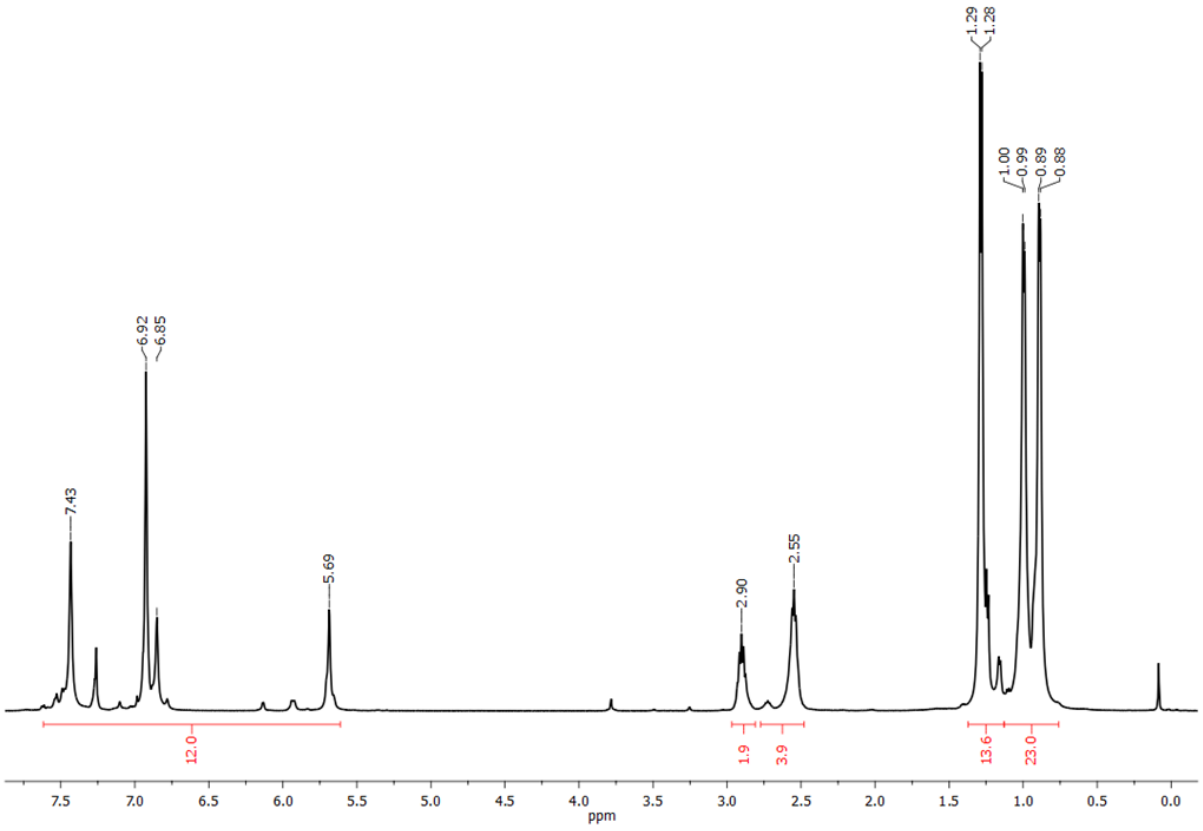

Figure S5.8.73. ^{1}H NMR spectrum (500 MHz) of **26** in $CDCl_3$.

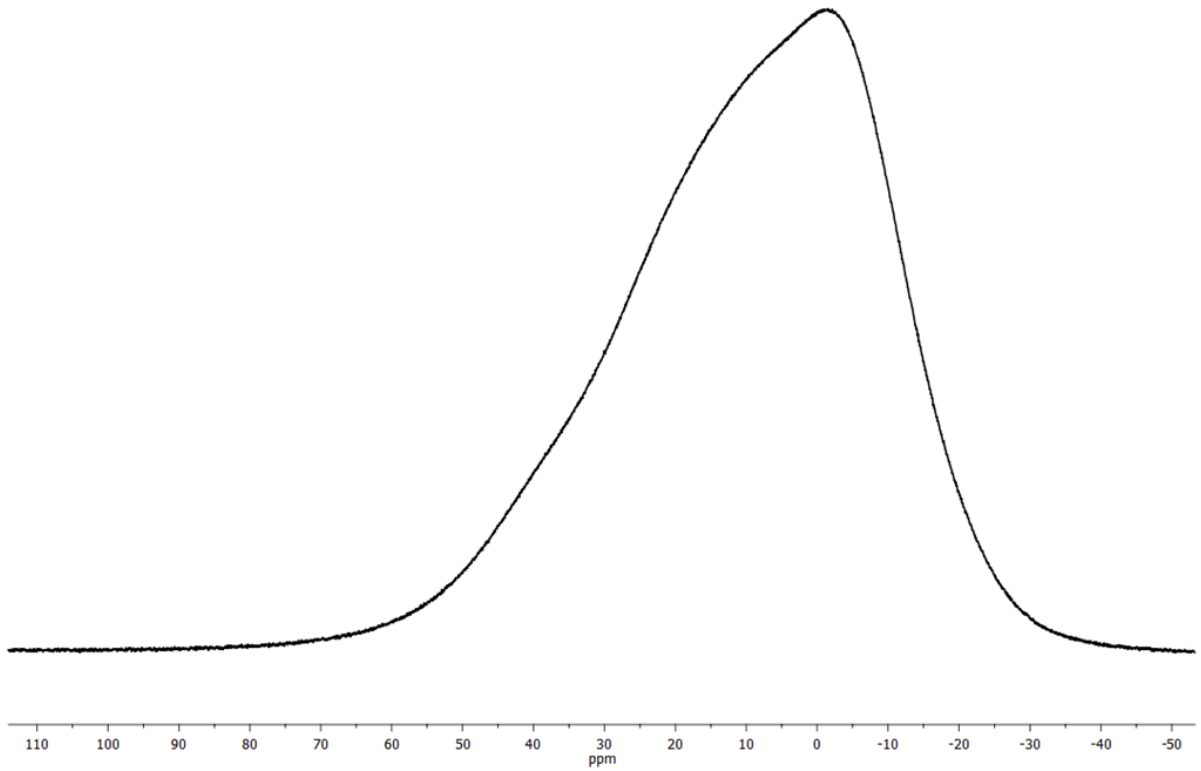

Figure S5.8.74. $^{11}B\{^{1}H\}$ NMR spectrum (160 MHz) of **26** in $CDCl_3$.

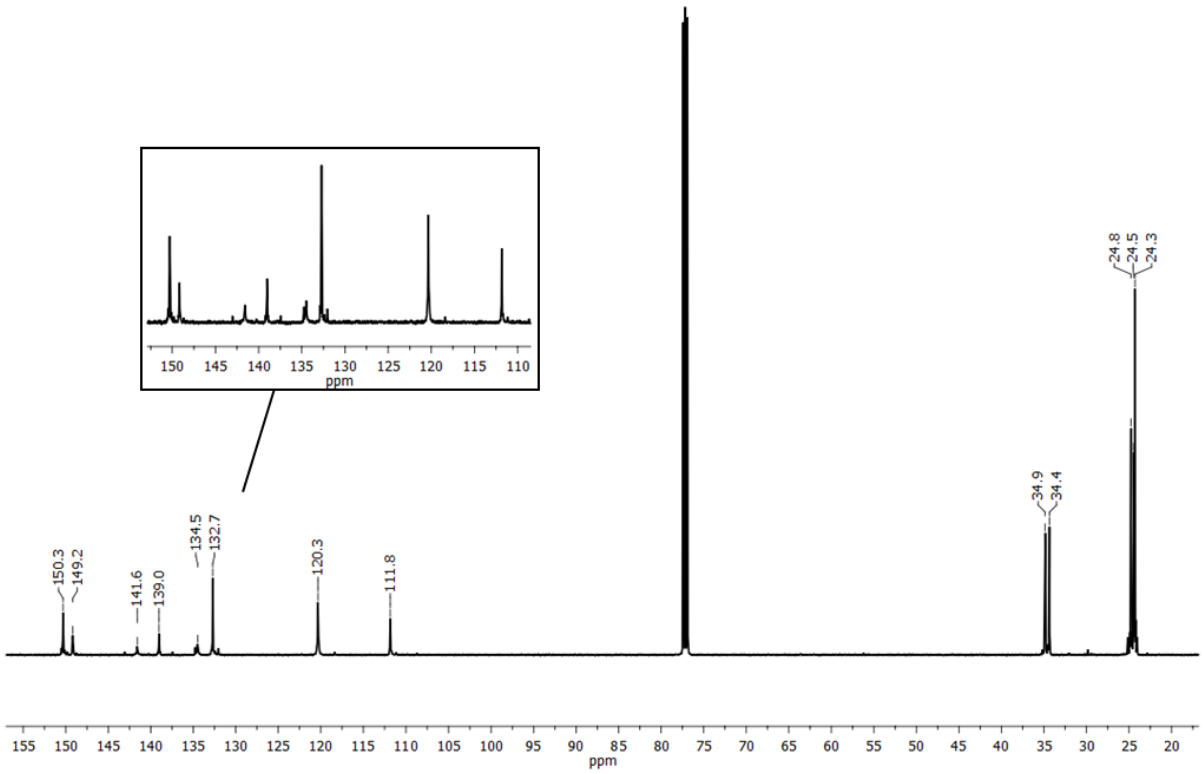

Figure S5.8.75. $^{13}C\{^{1}H\}$ NMR spectrum (126 MHz) of **26** in $CDCl_3$.

HRMS spectra

The mass spectra were processed using the Qual Browser of the XCalibur software. The figures show the total spectrum in the upper part, the product peak with isotope distribution in the middle and a corresponding simulation in the lower part.

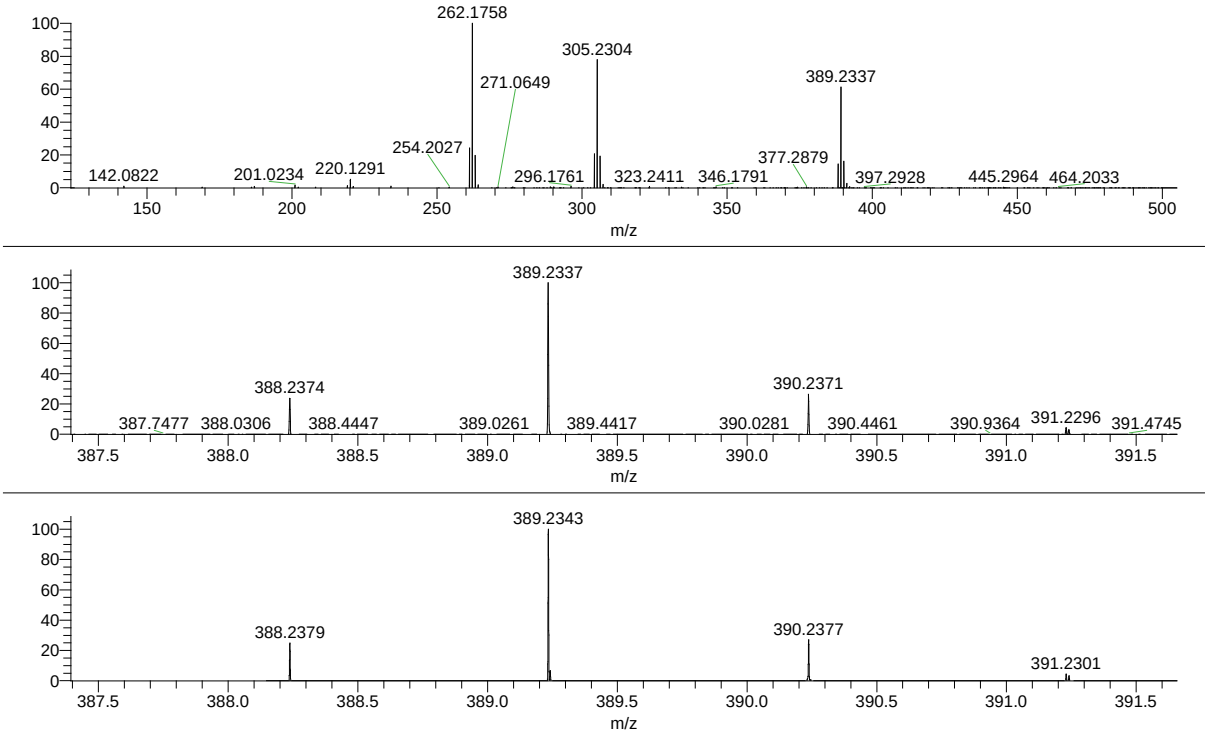

Figure S5.8.76. HRMS spectrum (LIFDI) of **5**.

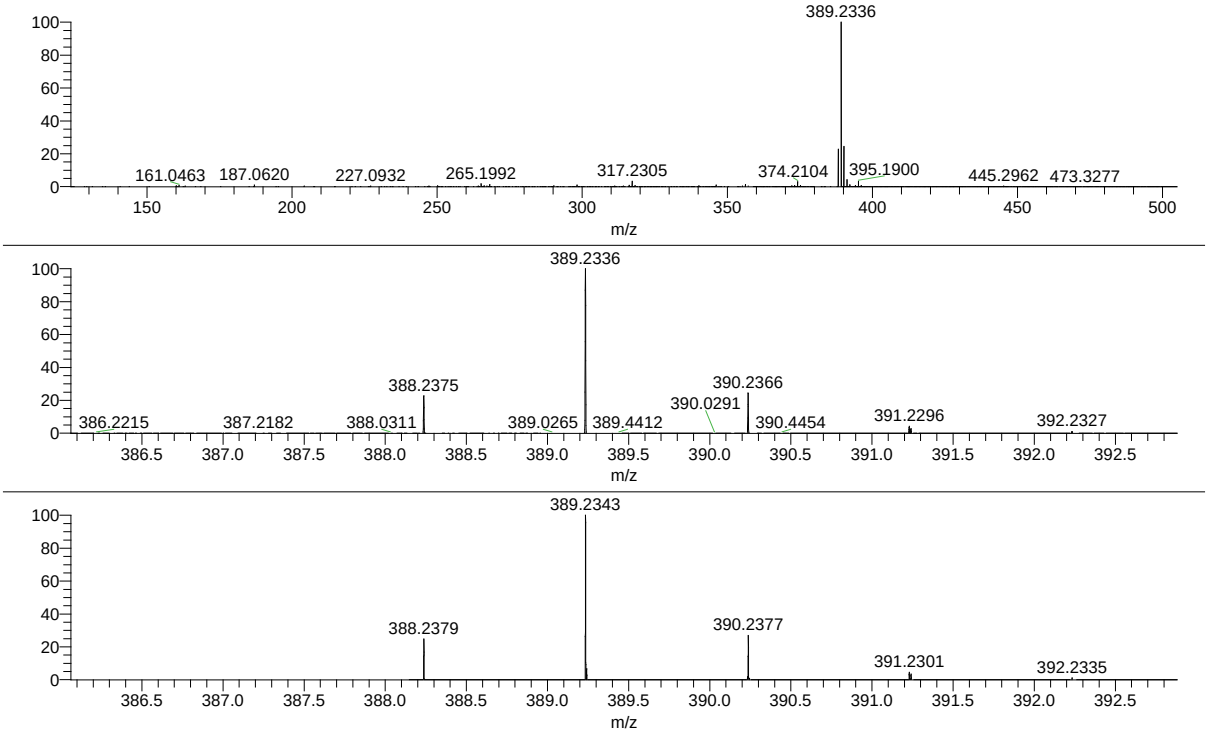

Figure S5.8.77. HRMS spectrum (LIFDI) of **7**.

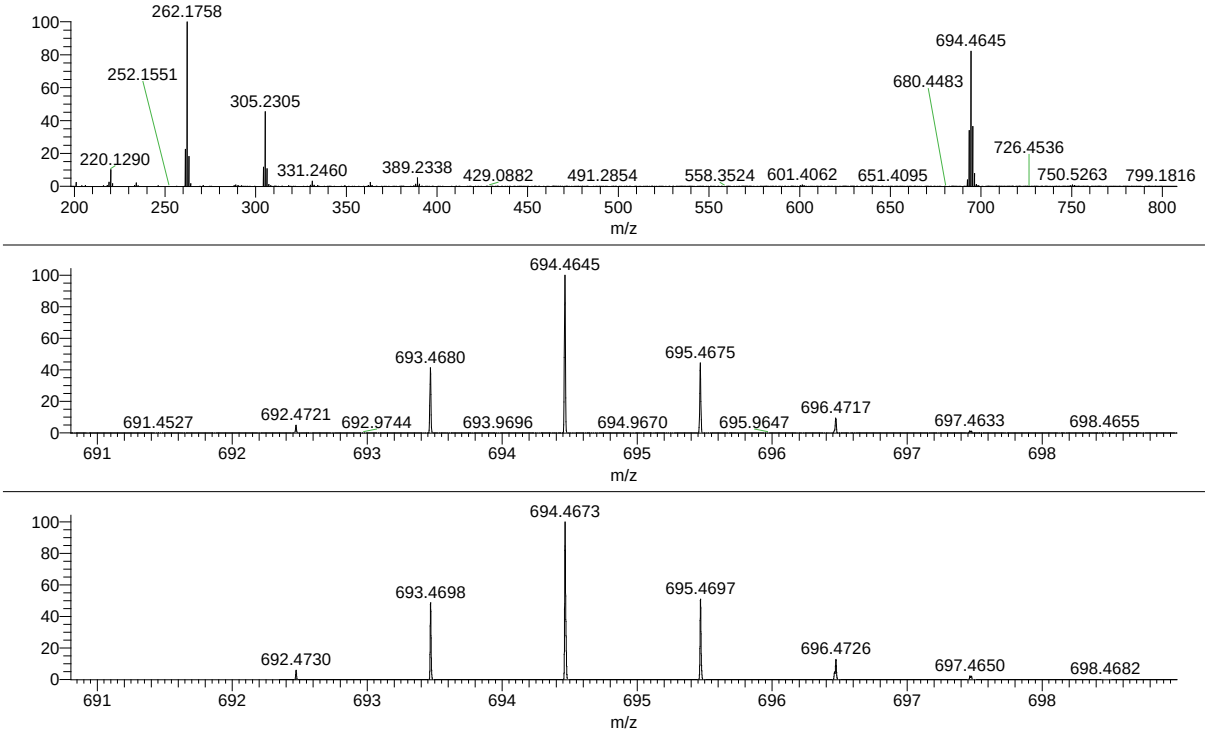

Figure S5.8.78. HRMS spectrum (LIFDI) of **12**.

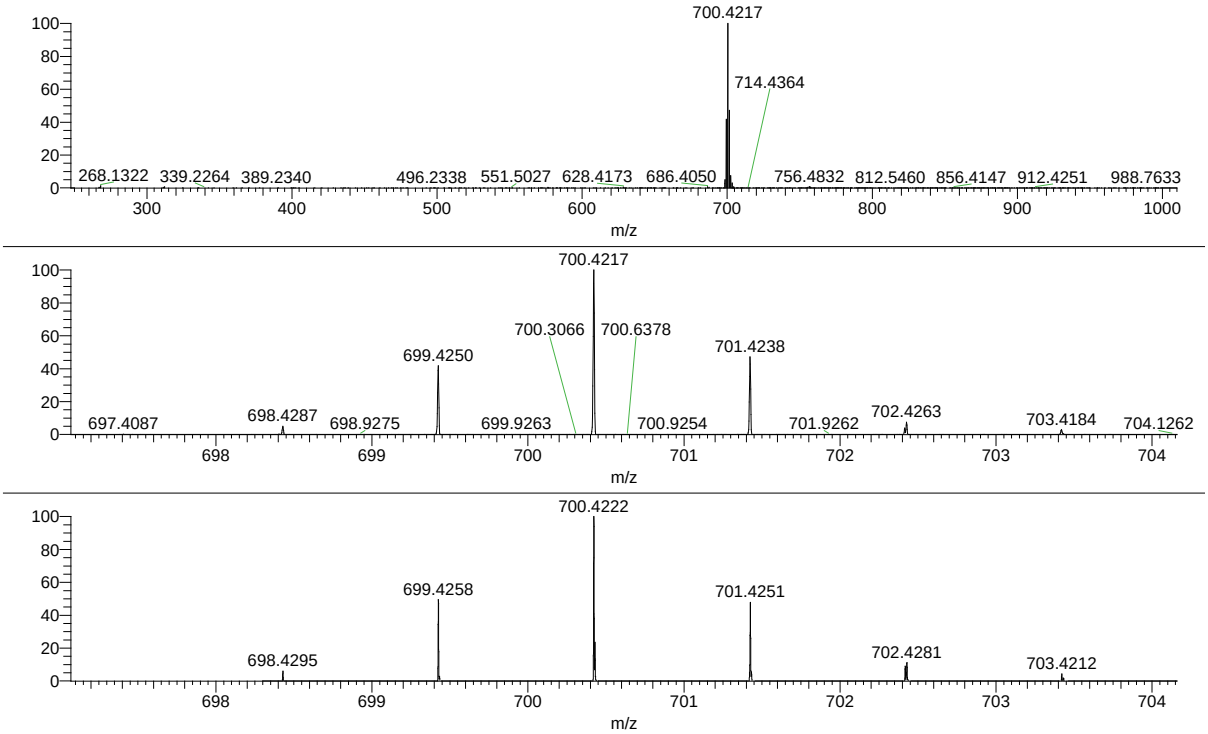

Figure S5.8.79. HRMS spectrum (LIFDI) of **14**.

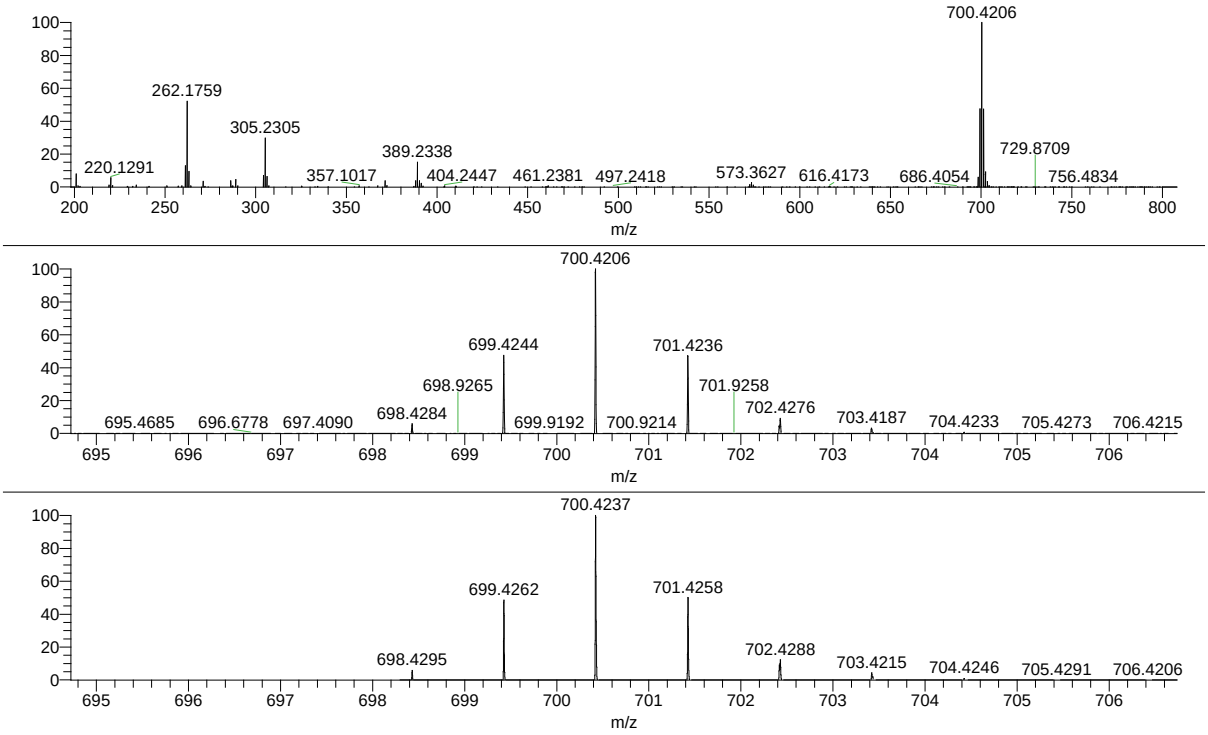

Figure S5.8.80. HRMS spectrum (LIFDI) of **18**.

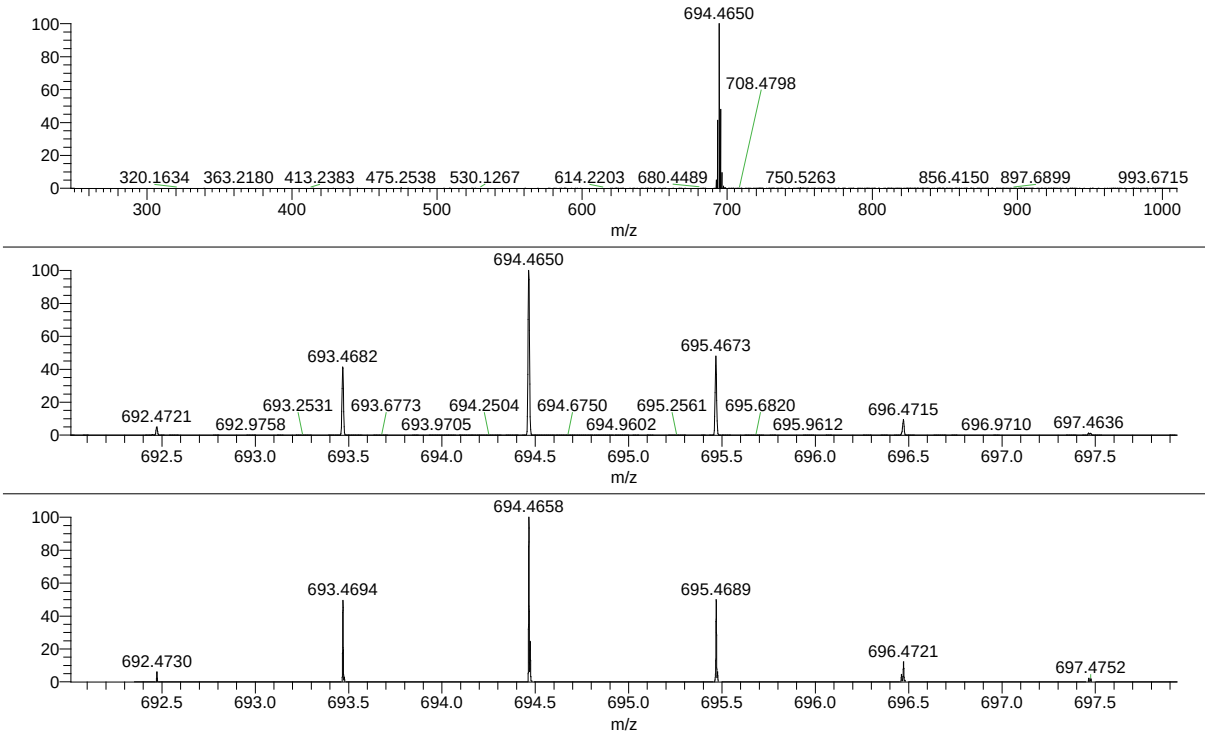

Figure S5.8.81. HRMS spectrum (LIFDI) of **20**.

UV-vis and emission spectra

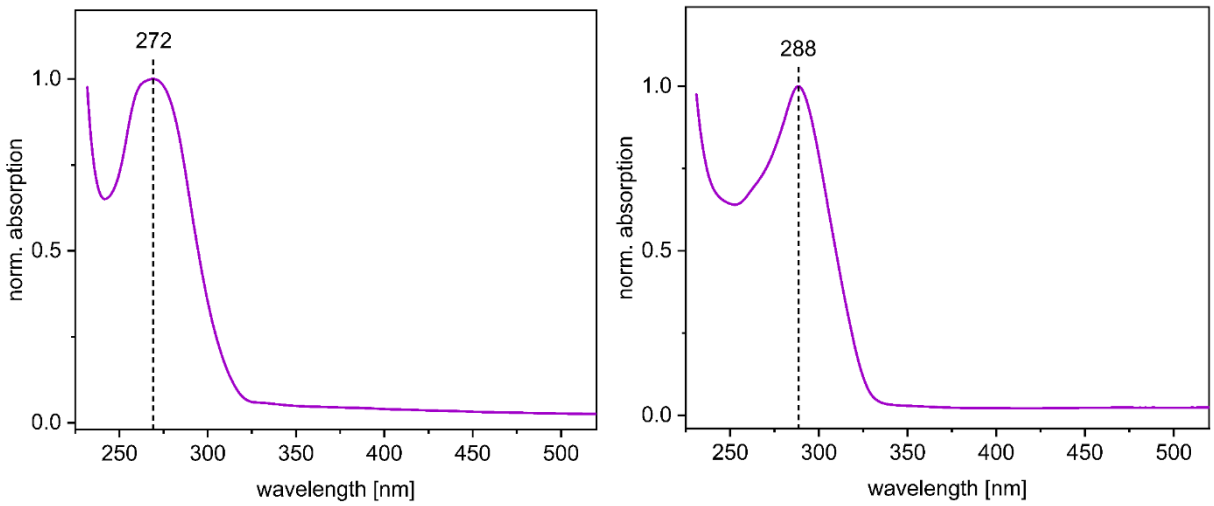

Figure S5.8.82. Normalized absorption spectra of **3** (left) and **5** (right) in THF.

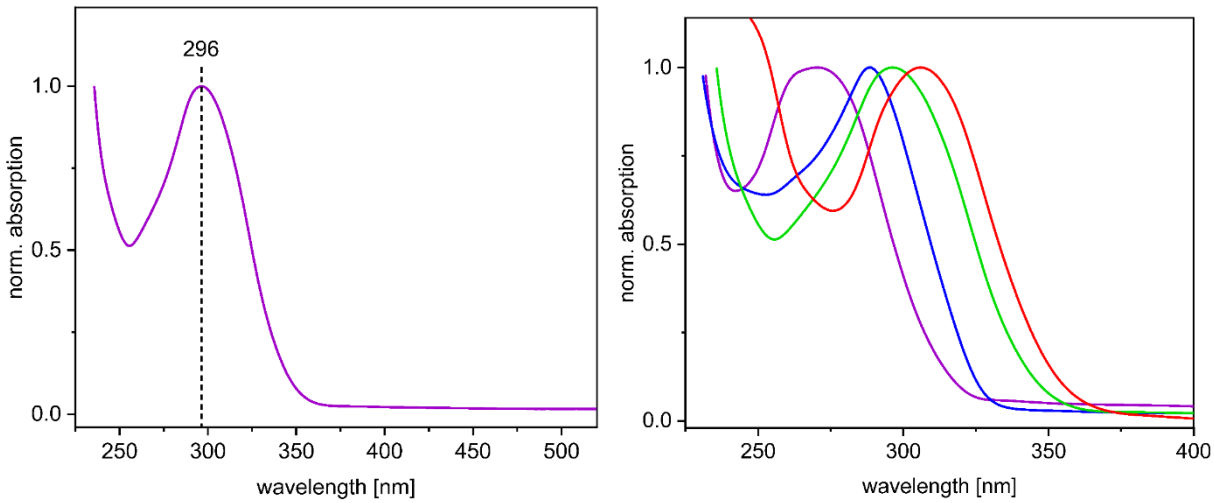

Figure S5.8.83. Normalized absorption spectrum of **7** (left) and comparison of the absorption spectra of **3** (purple), **5** (blue), **7** (green) and **8** (red) in THF (right).

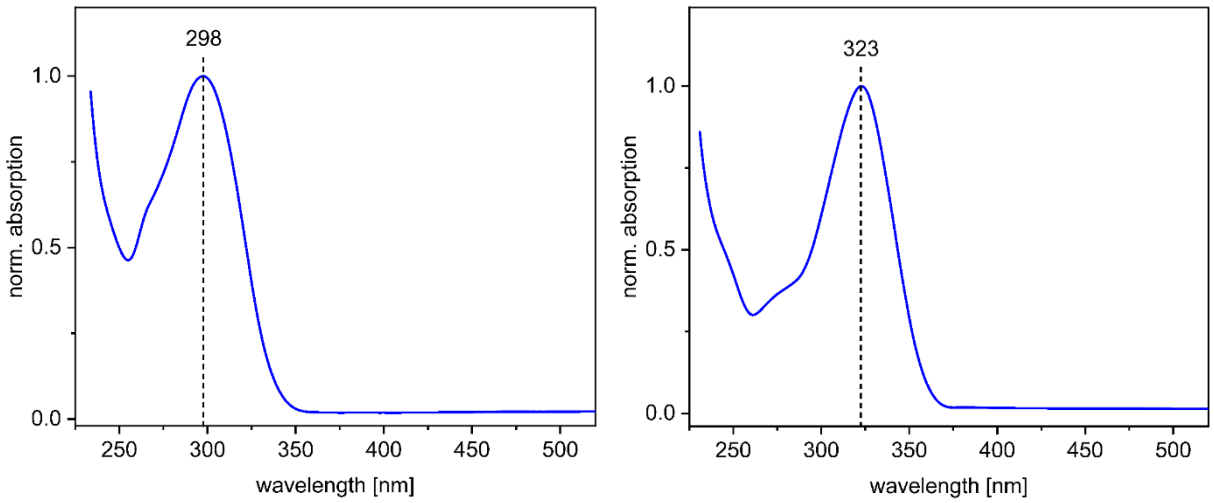

Figure S5.8.84. Normalized absorption spectra of **10** (left) and **12** (right) in THF.

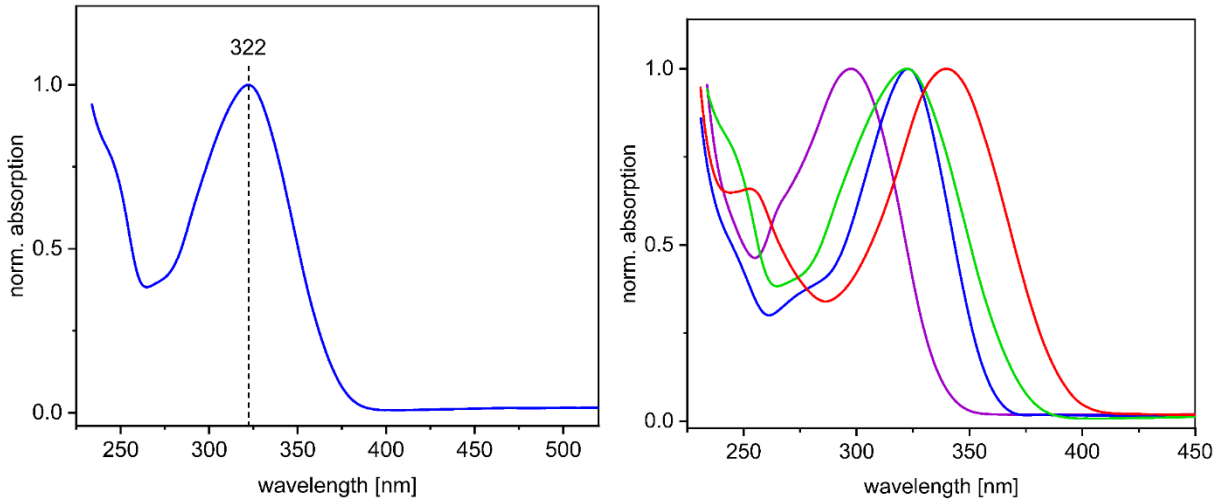

Figure S5.8.85. Normalized absorption spectrum of **14** (left) and comparison of the absorption spectra of **10** (purple), **12** (blue), **14** (green) and **15** (red) in THF (right).

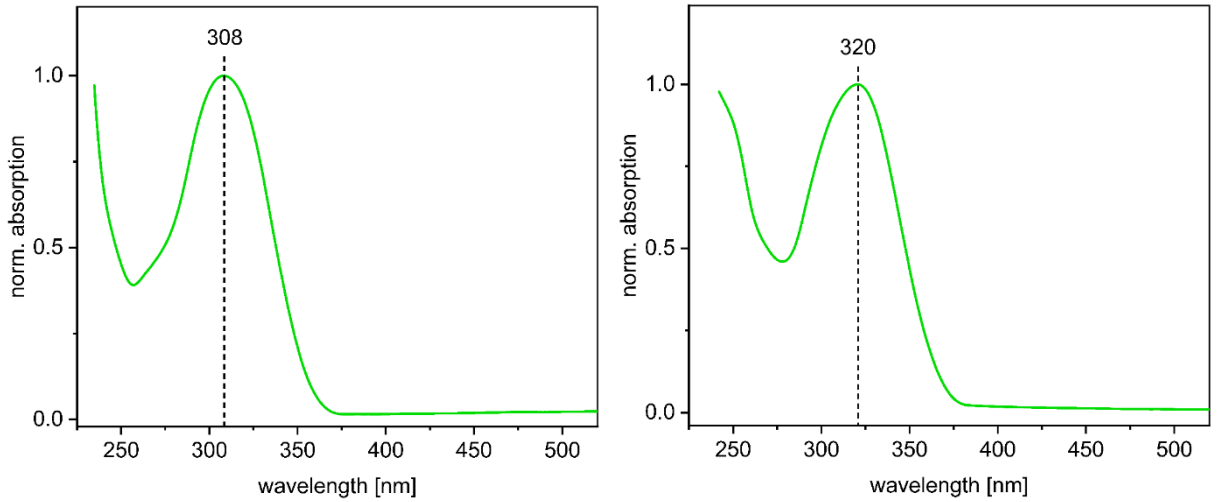

Figure S5.8.86. Normalized absorption spectra of **17** (left) and **18** (right) in THF.

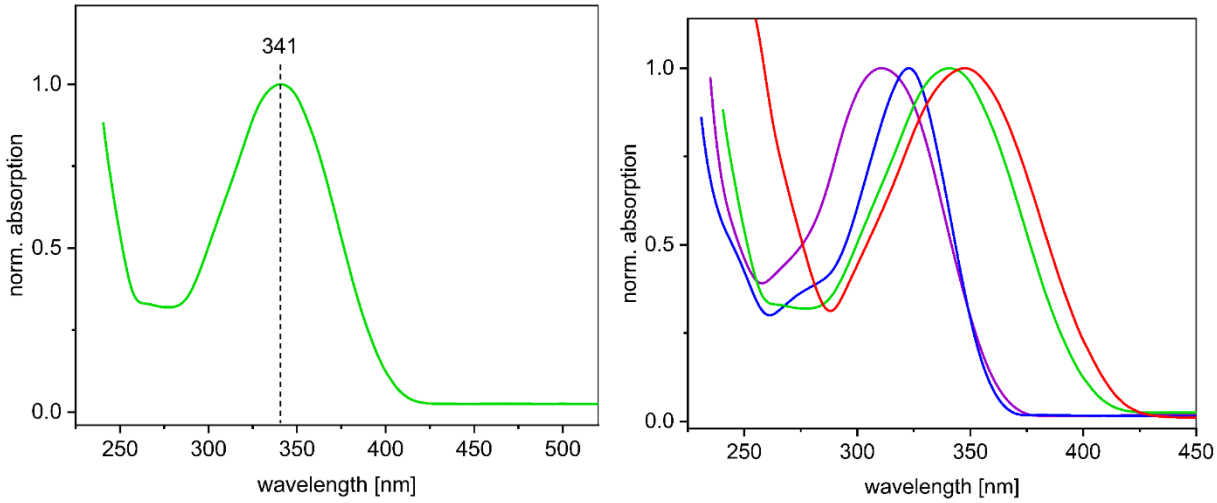

Figure S5.8.87. Normalized absorption spectrum of **20** (left) and comparison of the absorption spectra of **17** (purple), **18** (blue), **20** (green) and **21** (red) in THF (right).

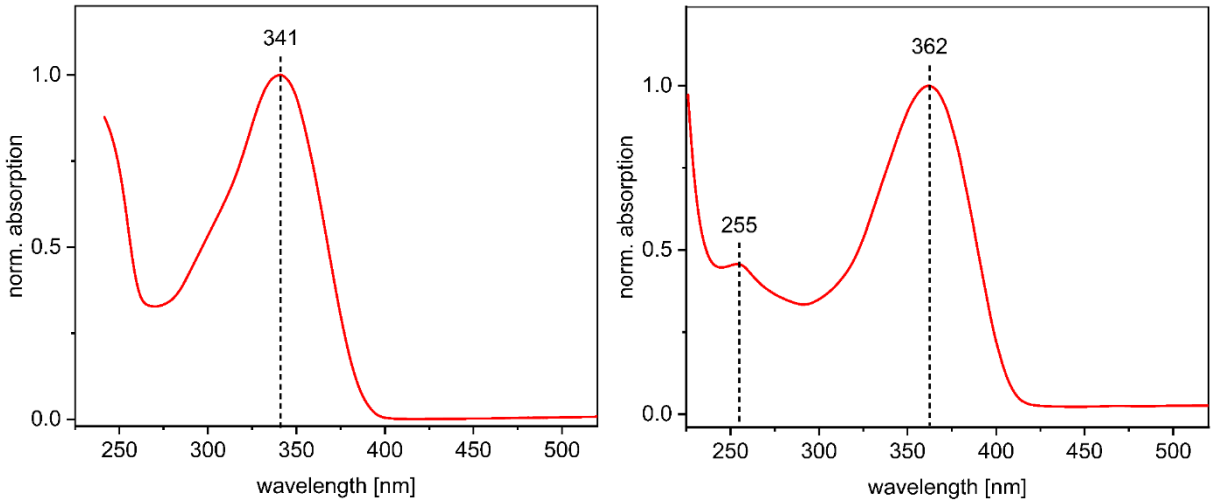

Figure S5.8.88. Normalized absorption spectra of **22** (left) and **25** (right) in THF.

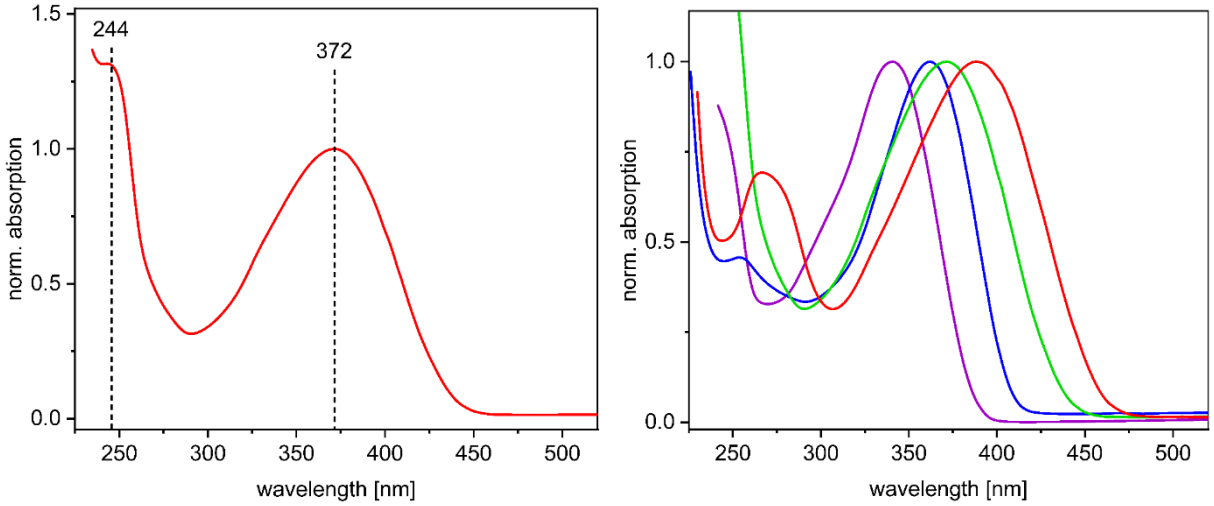

Figure S5.8.89. Normalized absorption spectrum of **26** (left) and comparison of the absorption spectra of **22** (purple), **25** (blue), **26** (green) and **23** (red) in THF (right).

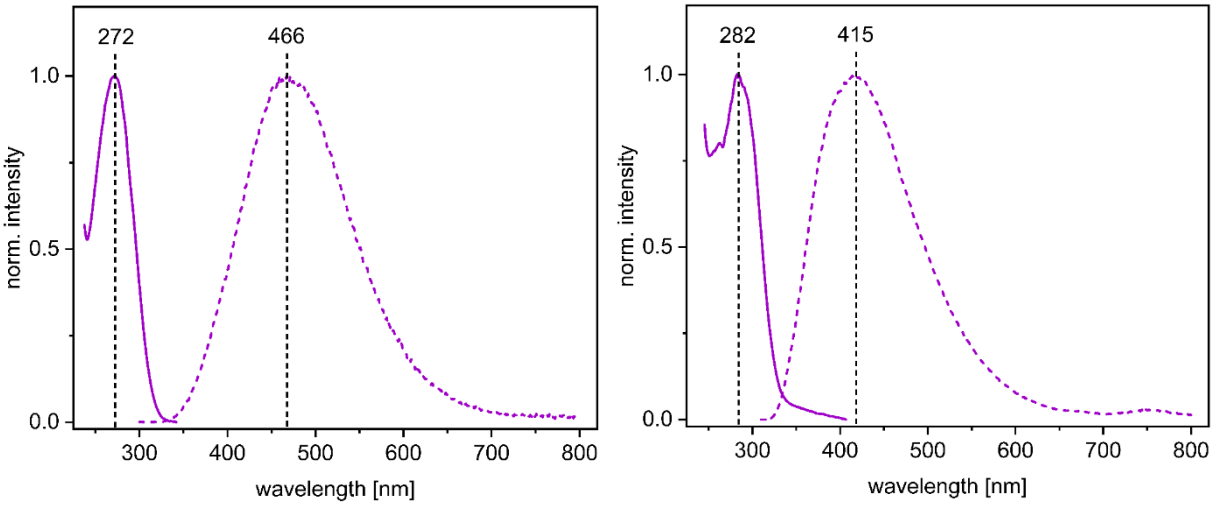

Figure S5.8.90. Normalized absorption and emission spectra of **3** (left) and **5** (right) as PMMA-film.

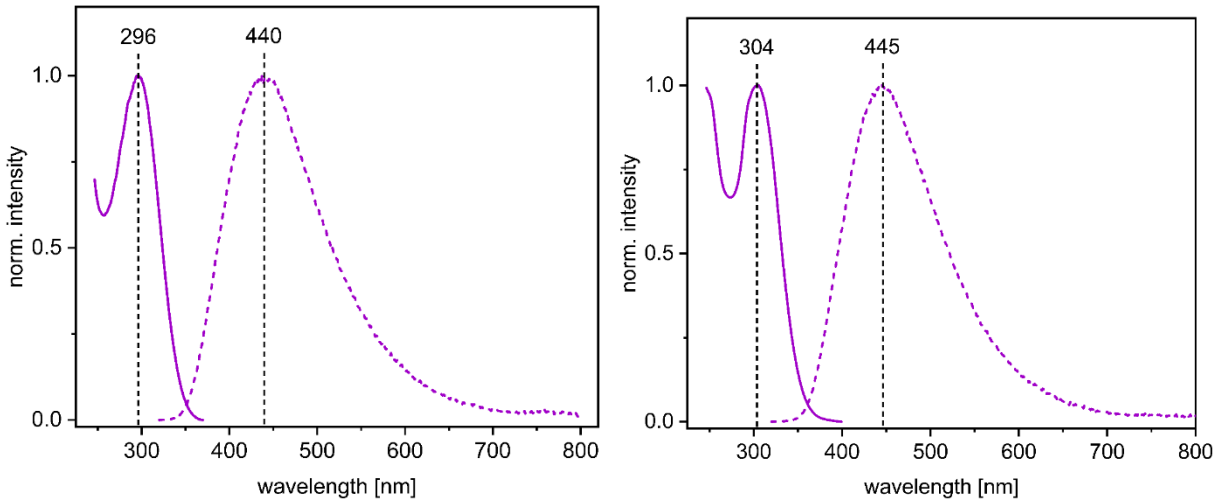

Figure S5.8.91. Normalized absorption and emission spectra of **7** (left) and **8** (right) as PMMA-film.

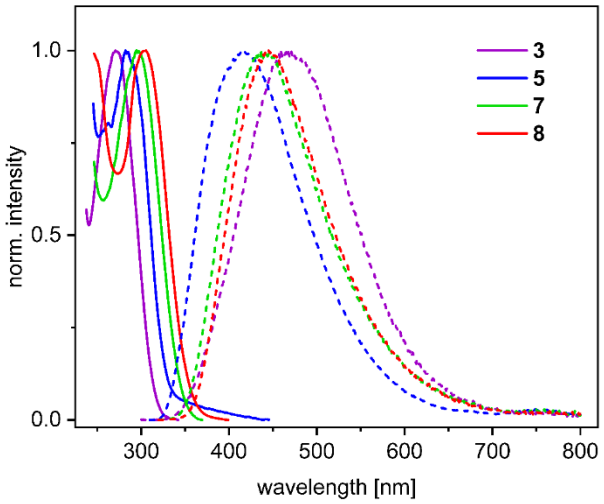

Figure S5.8.92. Normalized absorption and emission spectra of **3** (purple), **5** (blue), **7** (green) and **8** (red) as PMMA-film.

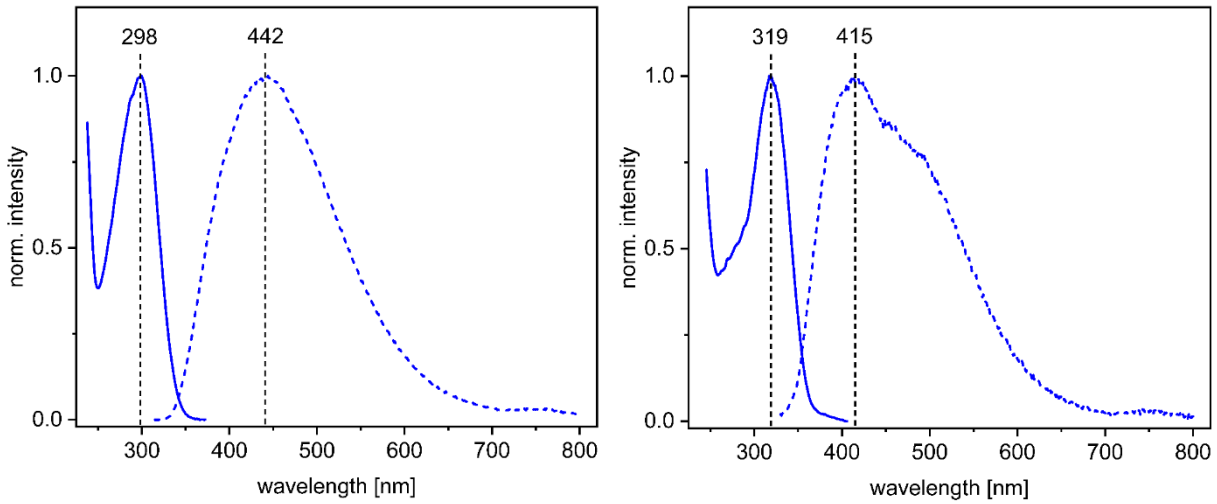

Figure S5.8.93. Normalized absorption and emission spectra of **10** (left) and **12** (right) as PMMA-film.

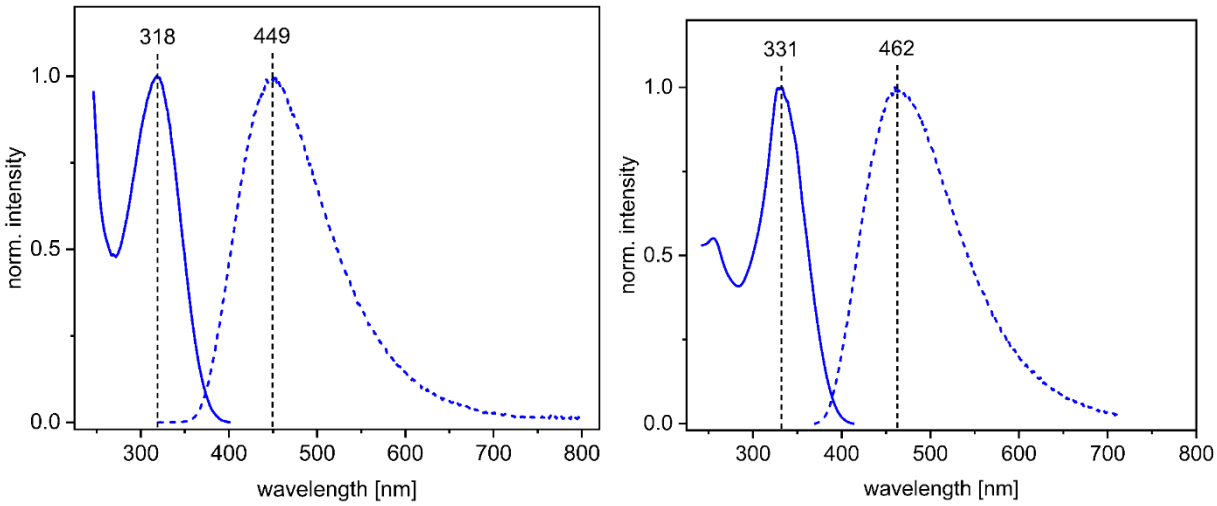

Figure S5.8.94. Normalized absorption and emission spectra of **14** (left) and **15** (right) as PMMA-film.

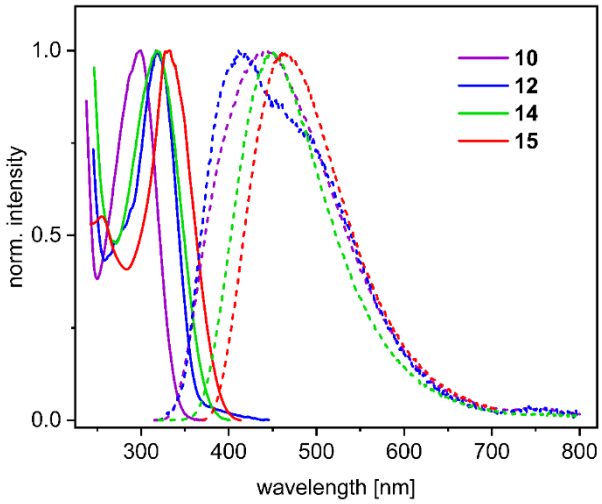

Figure S5.8.95. Normalized absorption and emission spectra of **10** (purple), **12** (blue), **14** (green) and **15** (red) as PMMA-film.

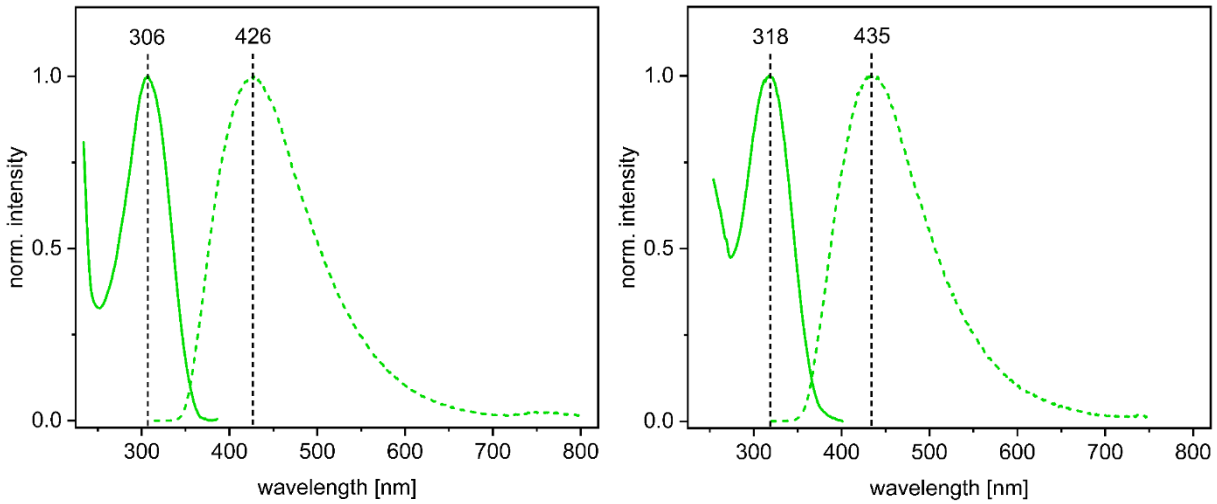

Figure S5.8.96. Normalized absorption and emission spectra of **17** (left) and **18** (right) as PMMA-film.

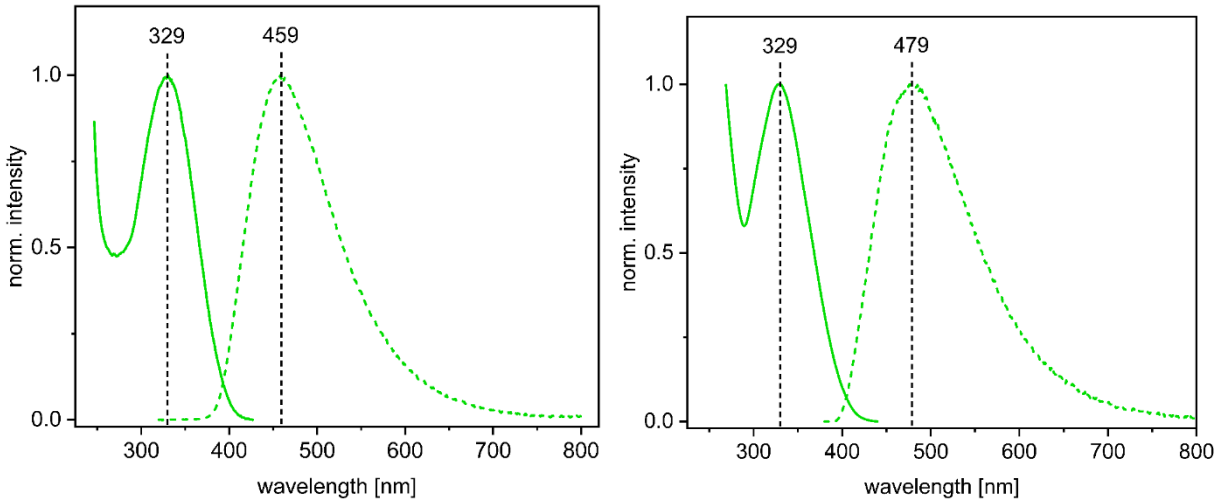

Figure S5.8.97. Normalized absorption and emission spectra of **20** (left) and **21** (right) as PMMA-film.

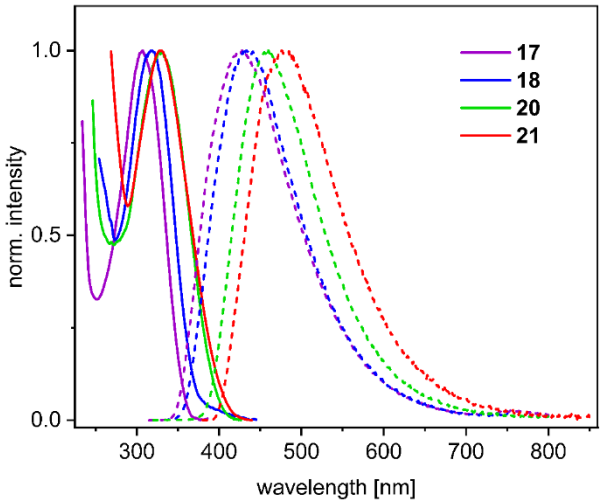

Figure S5.8.98. Normalized absorption and emission spectra of **17** (purple), **18** (blue), **20** (green) and **21** (red) as PMMA-film.

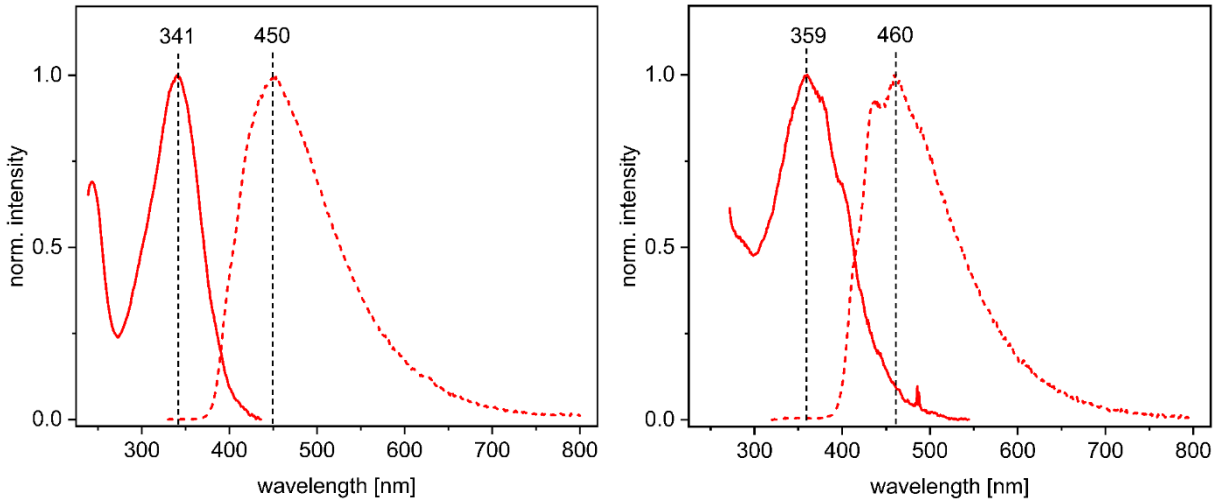

Figure S5.8.99. Normalized absorption and emission spectra of **22** (left) and **25** (right) as PMMA-film.

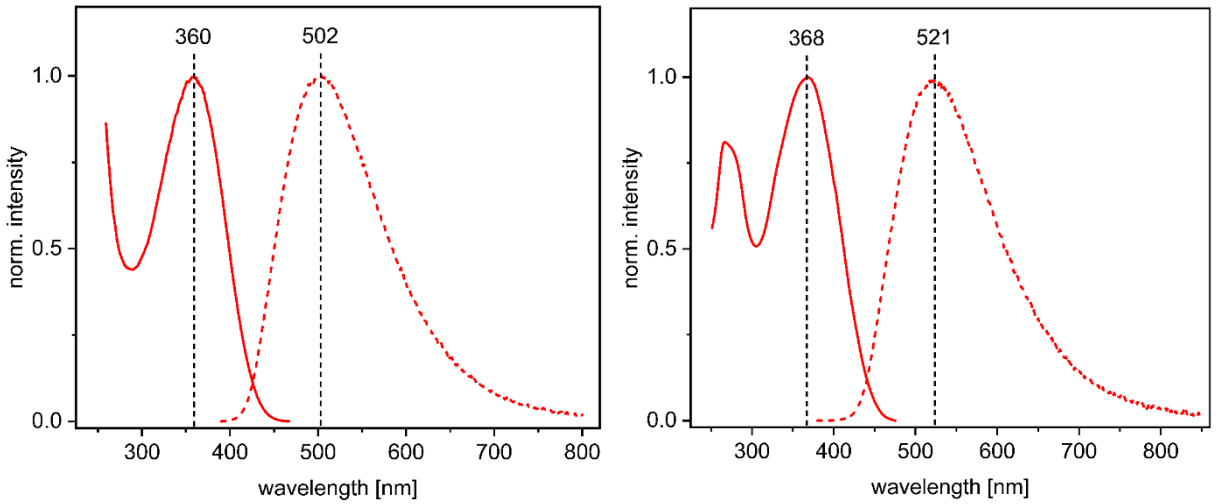

Figure S5.8.100. Normalized absorption and emission spectra of **26** (left) and **23** (right) as PMMA-film.

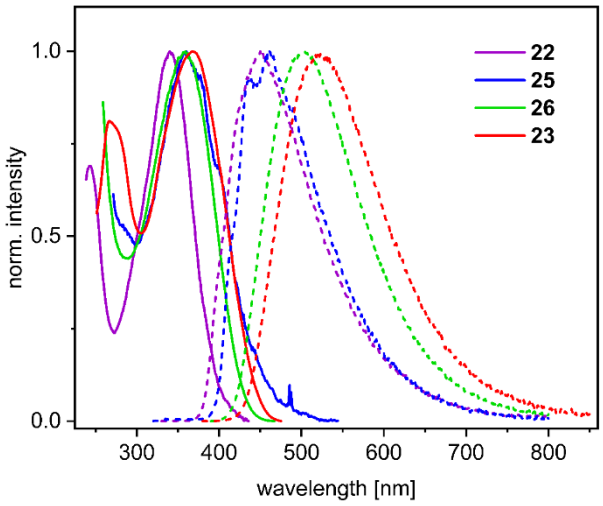

Figure S5.8.101. Normalized absorption and emission spectra of **22** (purple), **25** (blue), **26** (green) and **23** (red) as PMMA-film.

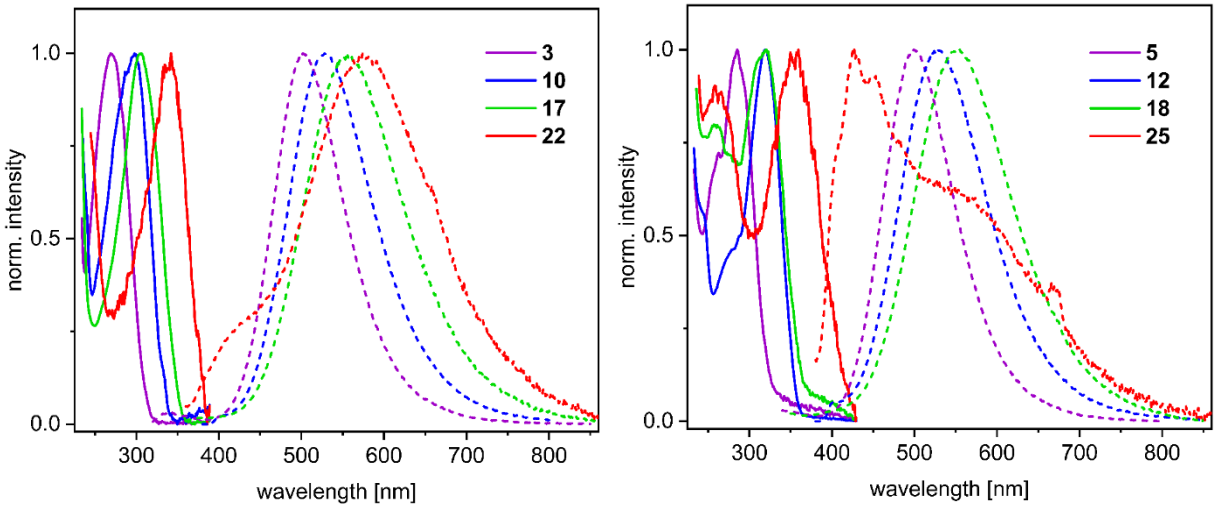

Figure S5.8.102. Normalized absorption and emission spectra of **3**, **10**, **17**, and **22** in *n*-hexane (left) and normalized absorption and emission spectra of **5**, **12**, **18**, and **25** in *n*-hexane (right).

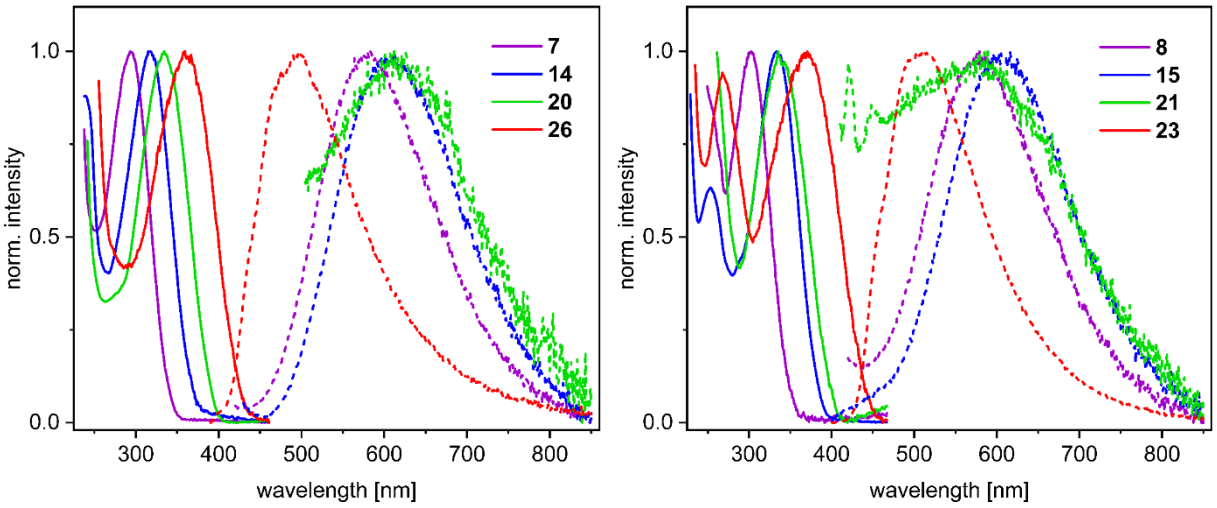

Figure S5.8.103. Normalized absorption and emission spectra of **7**, **14**, **20**, and **26** in *n*-hexane (left) and normalized absorption and emission spectra of **8**, **15**, **21**, and **23** in *n*-hexane (right).

Dynamic light scattering

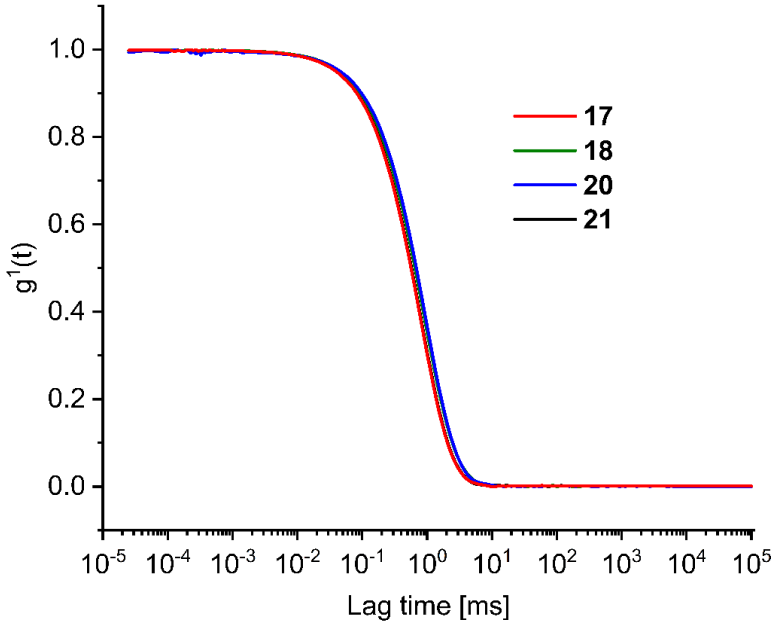

Figure S5.8.104. Autocorrelation functions $g^1(t)$ of aggregates of **17** (red), **18** (green), **20** (blue) and **21** (black) in an aqueous solution (THF/water: 10/90).

Cyclic voltammograms

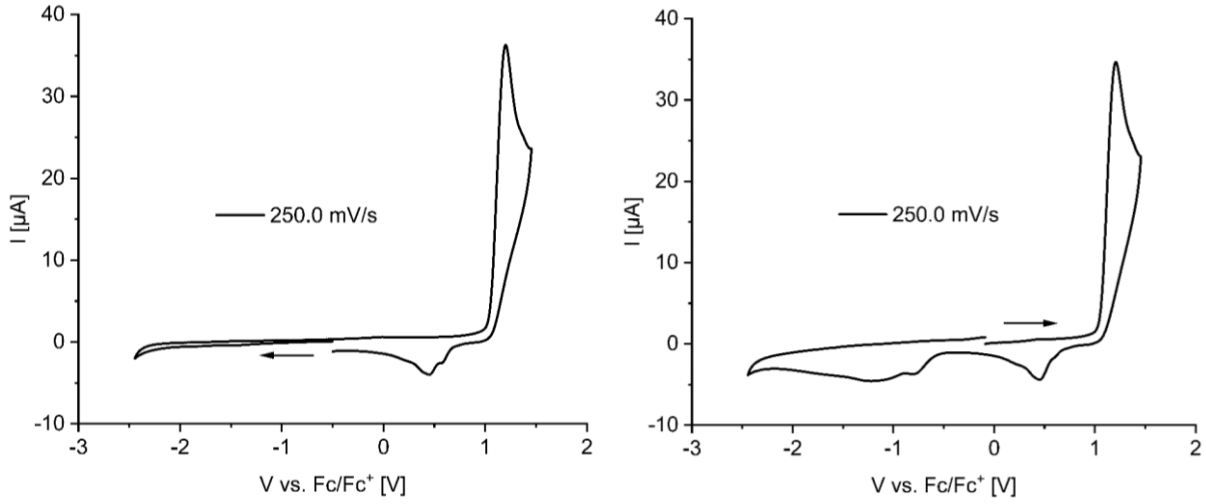

Figure S5.8.105. Cyclic voltammograms of **3** in DCM (vs. $[Cp_2Fe]^{0/+}$, scan rate: 250 mV s^{-1}).

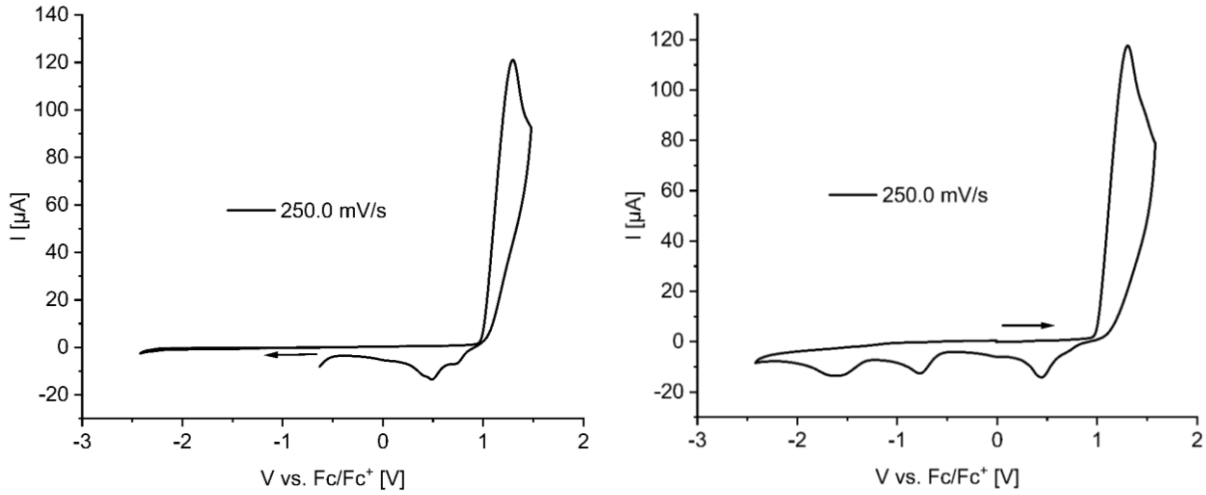

Figure S5.8.106. Cyclic voltammograms of **5** in DCM (vs. $[Cp_2Fe]^{0/+}$, scan rate: 250 mV s^{-1}).

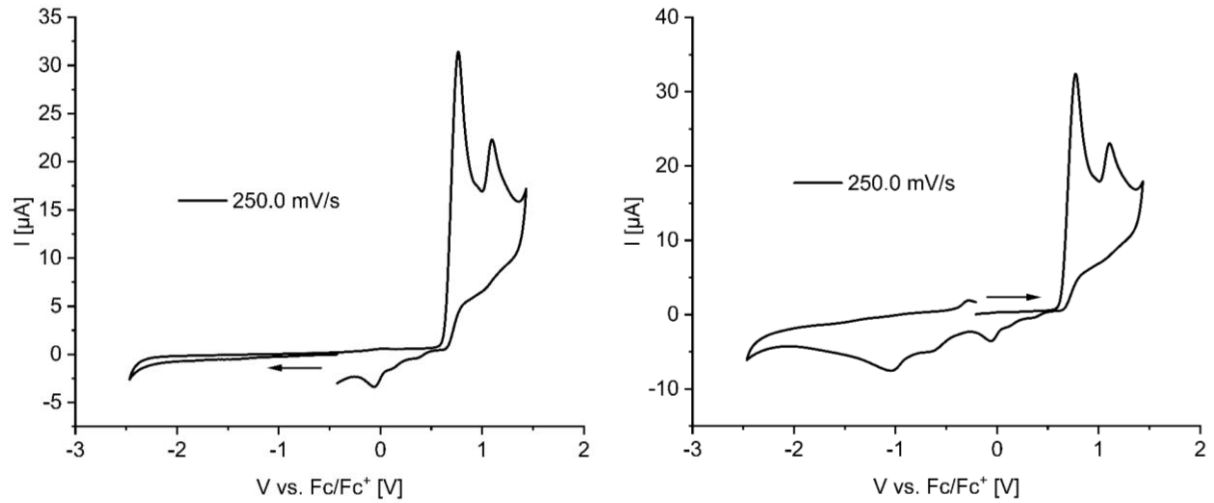

Figure S5.8.107. Cyclic voltammograms of **7** in DCM (vs. $[Cp_2Fe]^{0/+}$, scan rate: 250 mV s^{-1}).

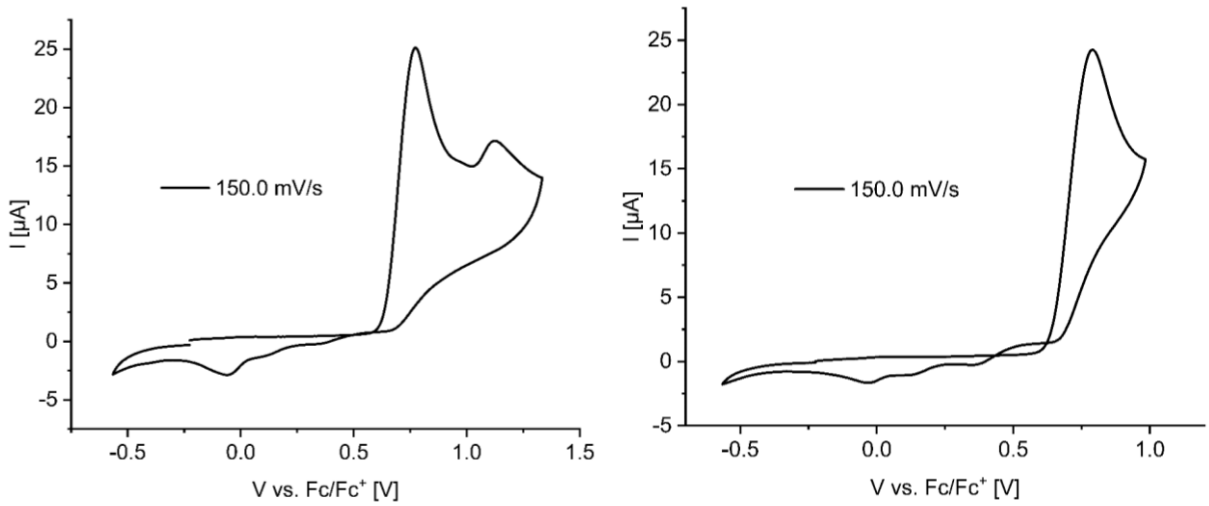

Figure S5.8.108. Cyclic voltammograms of the oxidation process (left) and the first oxidation event of **7** (right) in DCM (vs. $[Cp_2Fe]^{0/+}$, scan rate: 150 mV s^{-1}).

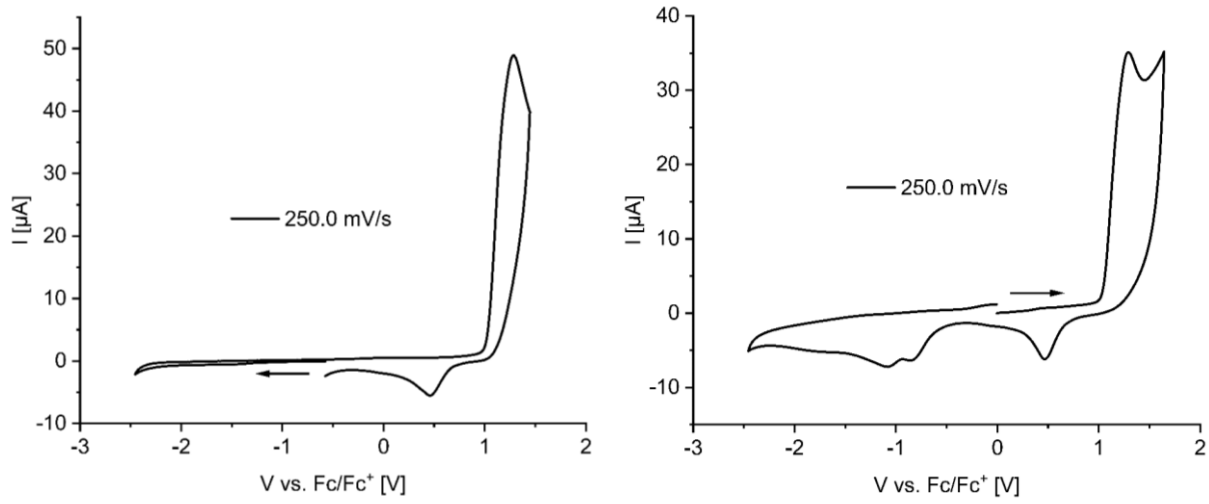

Figure S5.8.109. Cyclic voltammograms of **10** in DCM (vs. $[Cp_2Fe]^{0/+}$, scan rate: 250 mV s^{-1}).

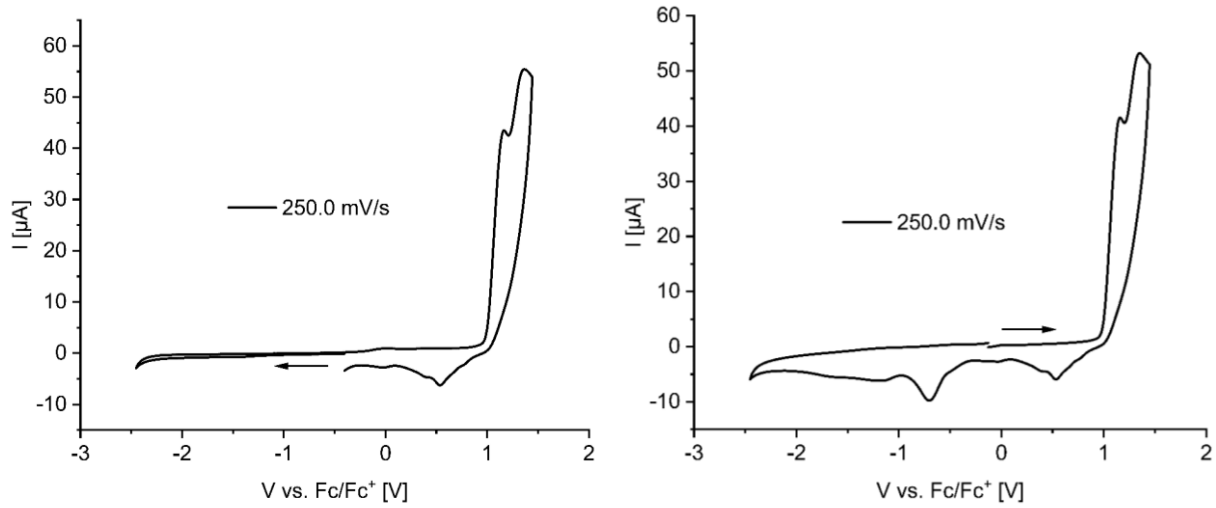

Figure S5.8.110. Cyclic voltammograms of **12** in DCM (vs. $[Cp_2Fe]^{0/+}$, scan rate: 250 mV s^{-1}).

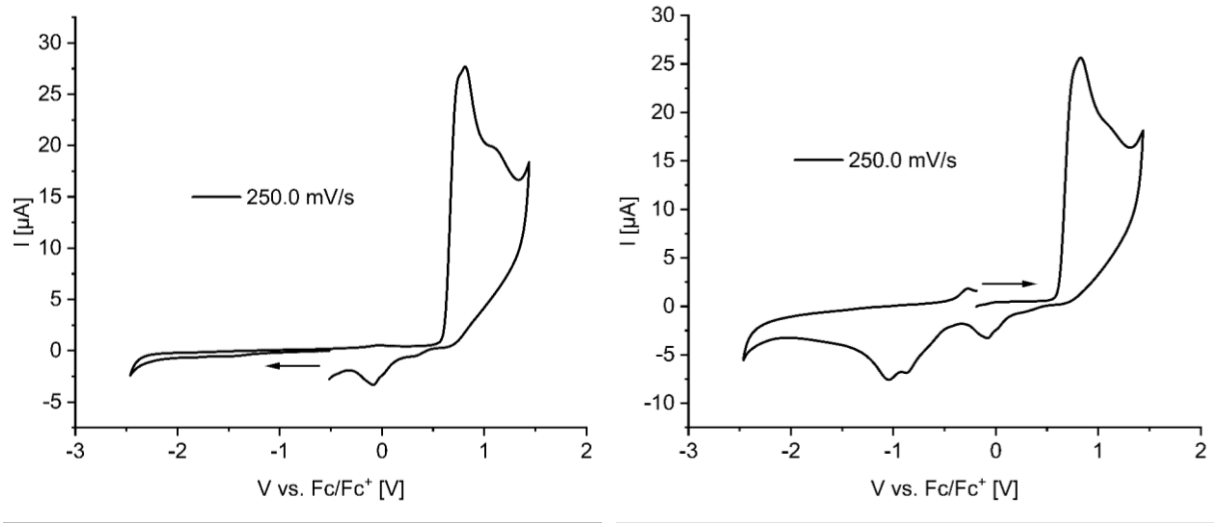

Figure S5.8.111. Cyclic voltammograms of **14** in DCM (vs. $[Cp_2Fe]^{0/+}$, scan rate: 250 mV s^{-1}).

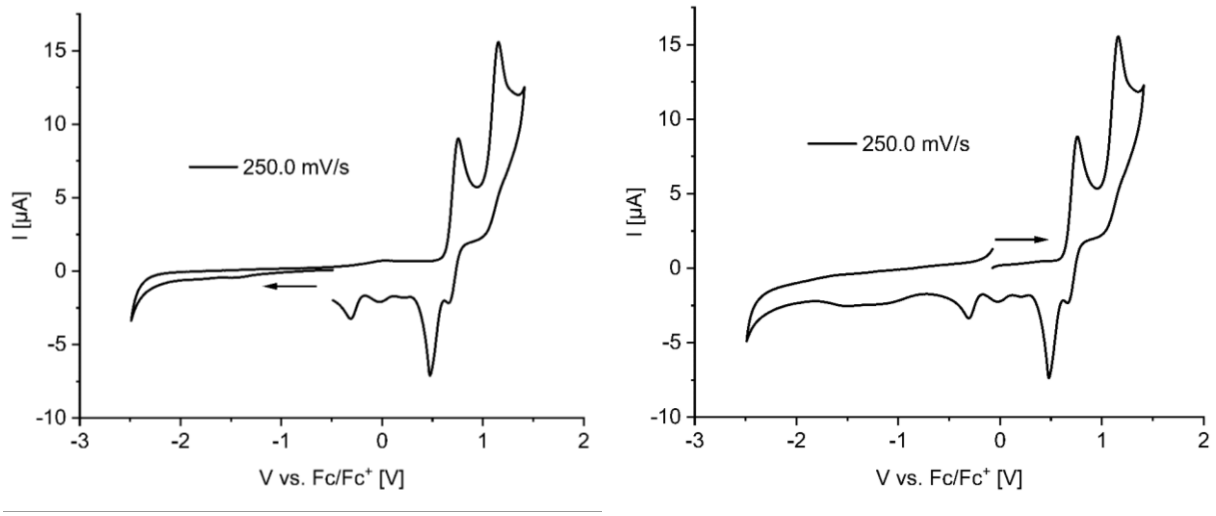

Figure S5.8.112. Cyclic voltammograms of **17** in DCM (vs. $[Cp_2Fe]^{0/+}$, scan rate: 250 mV s^{-1}).

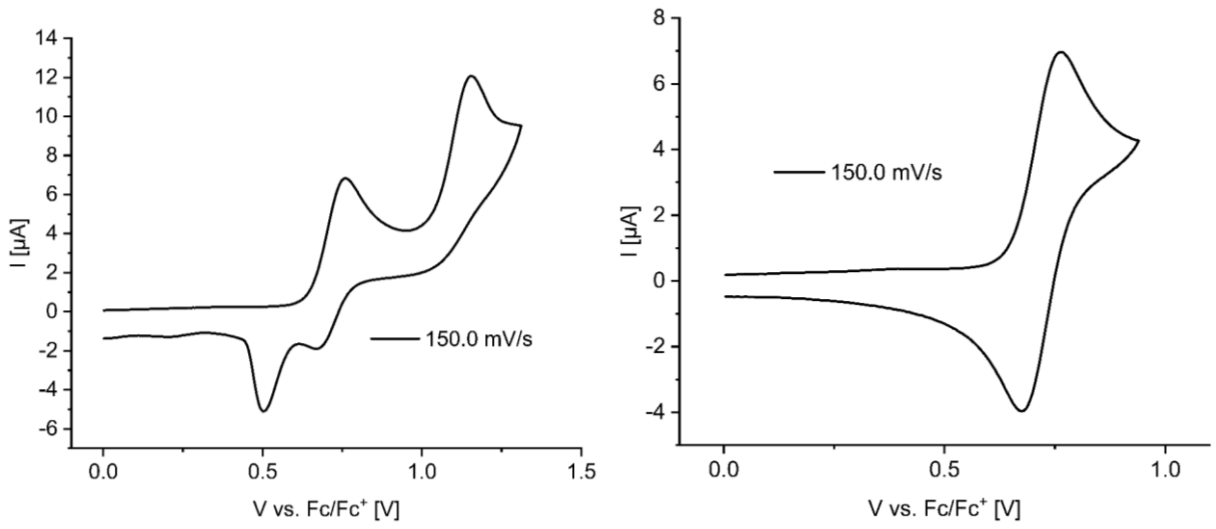

Figure S5.8.113. Cyclic voltammograms of the oxidation process (left) and the first oxidation event of **17** (right) in DCM (vs. $[Cp_2Fe]^{0/+}$, scan rate: 150 mV s^{-1}).

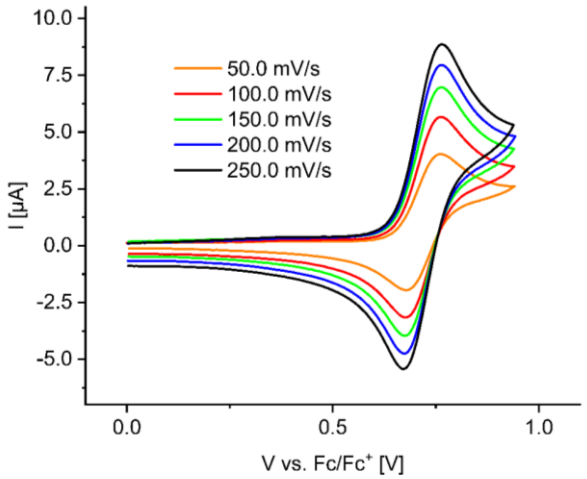

Figure S5.8.114. Cyclic voltammogram of the reversible first oxidation of **17** in DCM at different scan rates (vs. $[Cp_2Fe]^{0/+}$, scan rate: 50-250 mV s^{-1}).

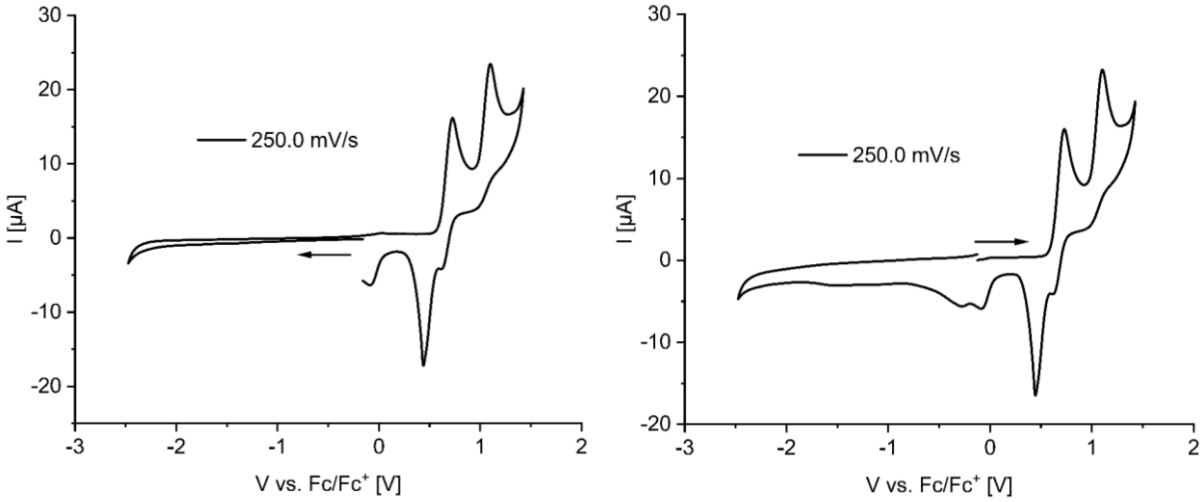

Figure S5.8.115. Cyclic voltammograms of **18** in DCM (vs. $[Cp_2Fe]^{0/+}$, scan rate: 250 mV s^{-1}).

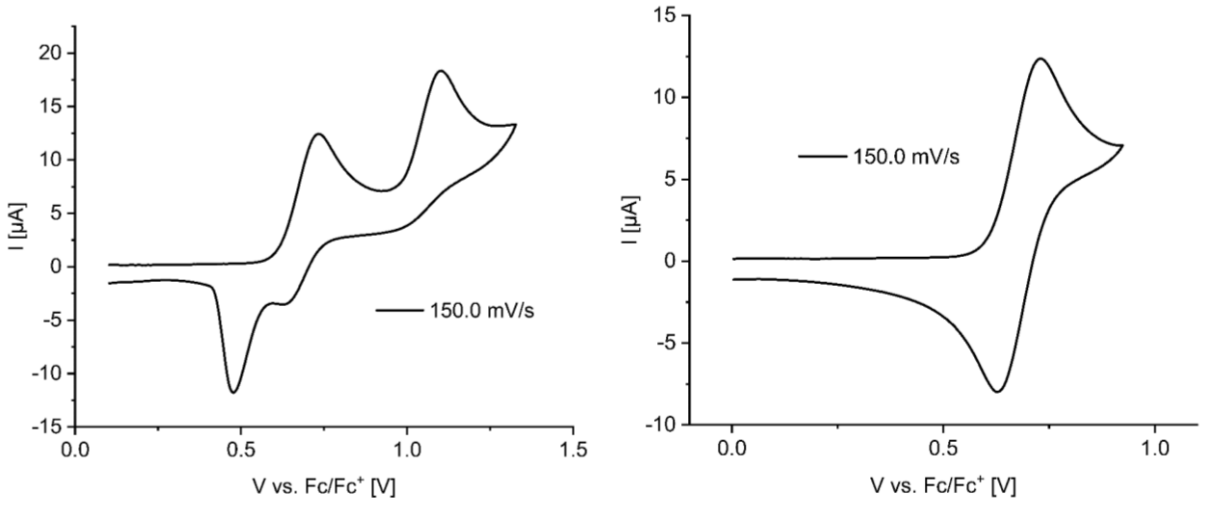

Figure S5.8.116. Cyclic voltammograms of the oxidation process (left) and the first oxidation event of **18** (right) in DCM (vs. $[Cp_2Fe]^{0/+}$, scan rate: 150 mV s^{-1}).

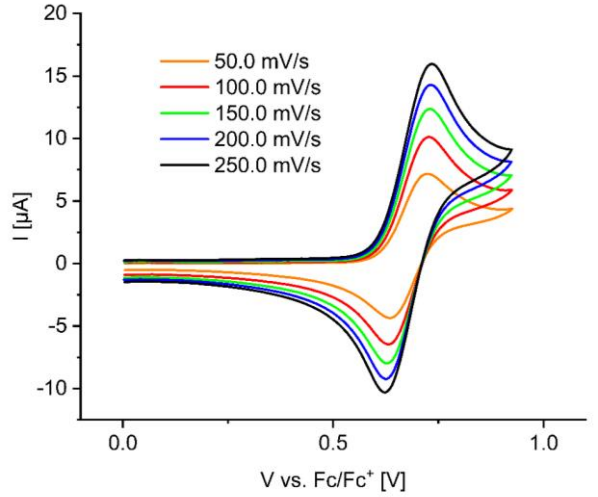

Figure S5.8.117. Cyclic voltammogram of the reversible first oxidation of **18** in DCM at different scan rates (vs. $[Cp_2Fe]^{0/+}$, scan rate: 50-250 mV s^{-1}).

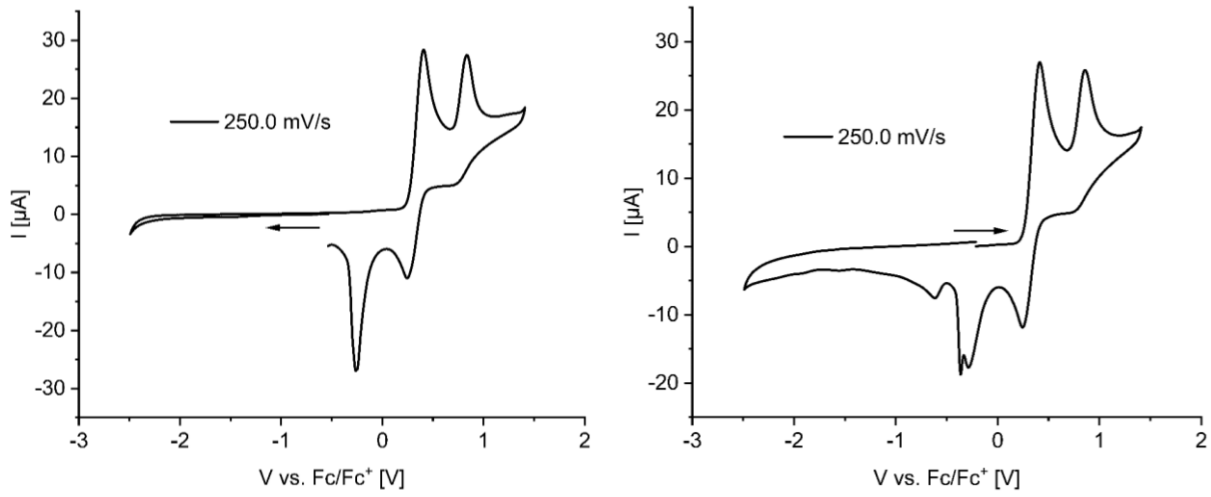

Figure S5.8.118. Cyclic voltammograms of **20** in DCM (vs. $[Cp_2Fe]^{0/+}$, scan rate: 250 mV s^{-1}).

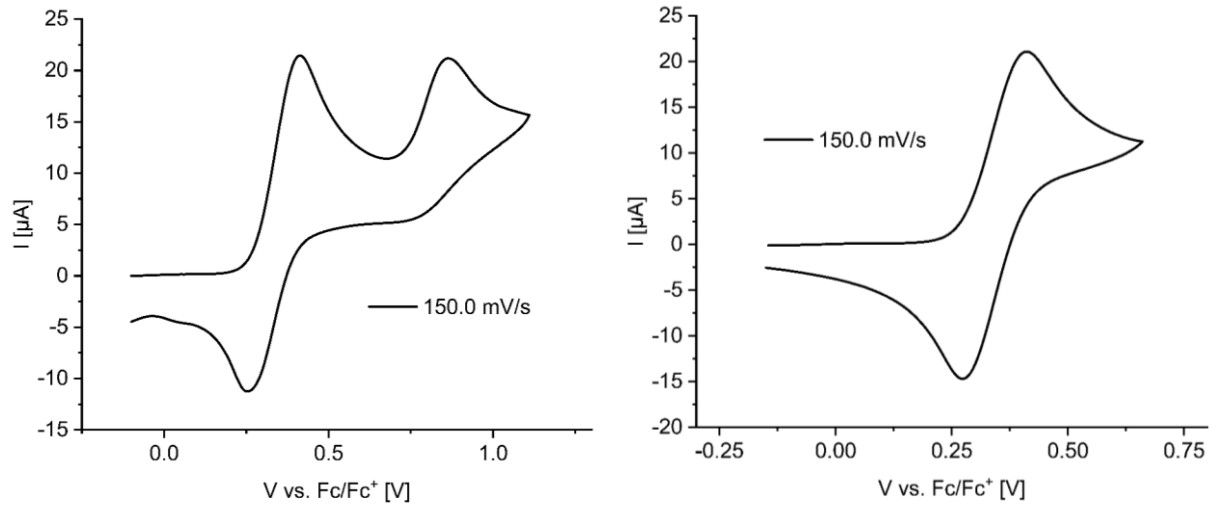

Figure S5.8.119. Cyclic voltammograms of the oxidation process (left) and the first oxidation event of **20** (right) in DCM (vs. $[Cp_2Fe]^{0/+}$, scan rate: 150 mV s^{-1}).

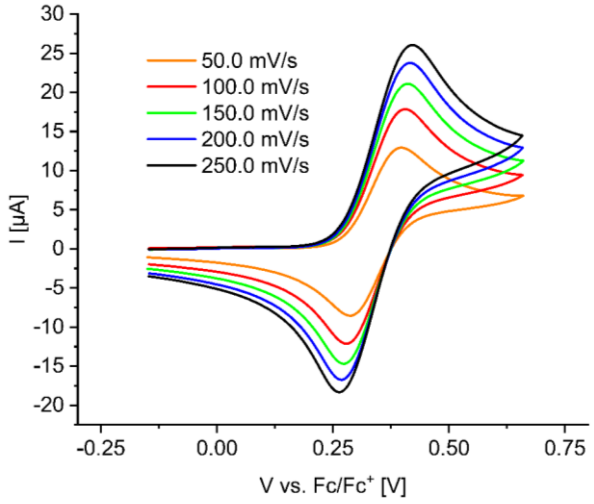

Figure S5.8.120. Cyclic voltammogram of the reversible first oxidation of **20** in DCM at different scan rates (vs. $[Cp_2Fe]^{0/+}$, scan rate: 50-250 mV s^{-1}).

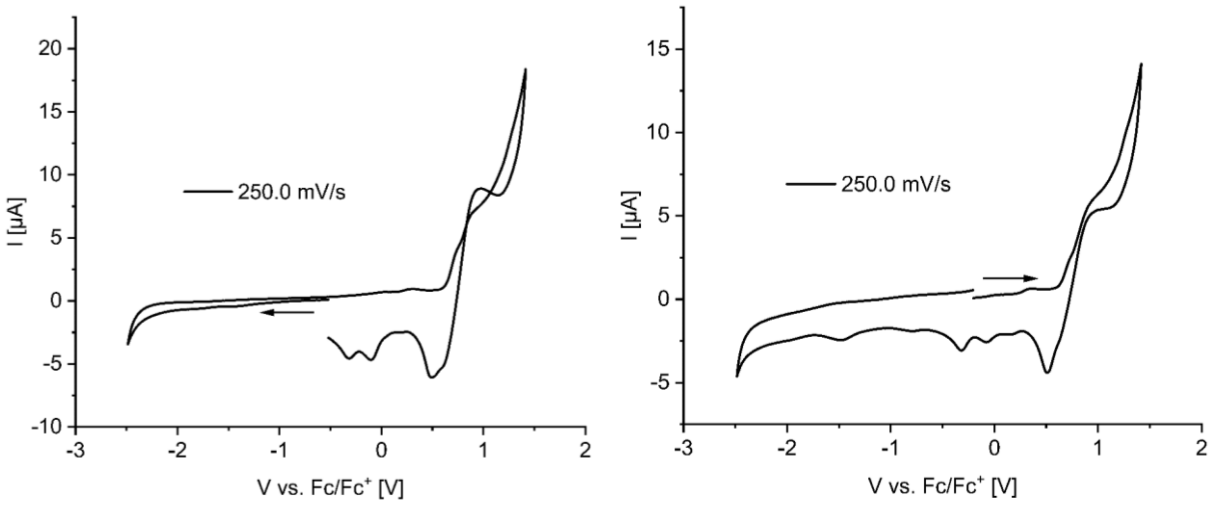

Figure S5.8.121. Cyclic voltammograms of **22** in DCM (vs. $[Cp_2Fe]^{0/+}$, scan rate: 250 mV s^{-1}).

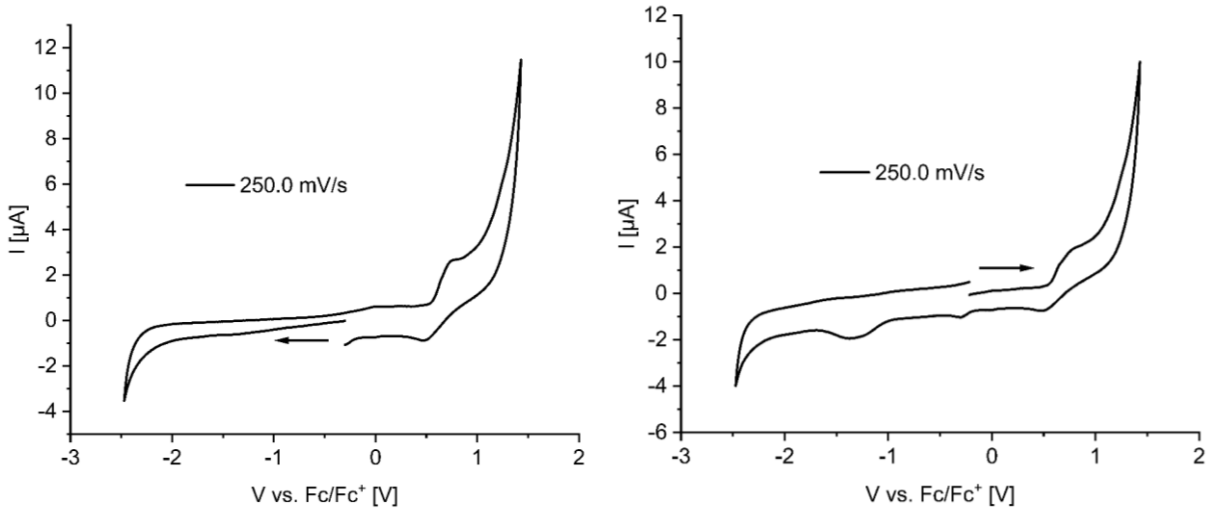

Figure S5.8.122. Cyclic voltammograms of **25** in DCM (vs. $[Cp_2Fe]^{0/+}$, scan rate: 250 mV s^{-1}).

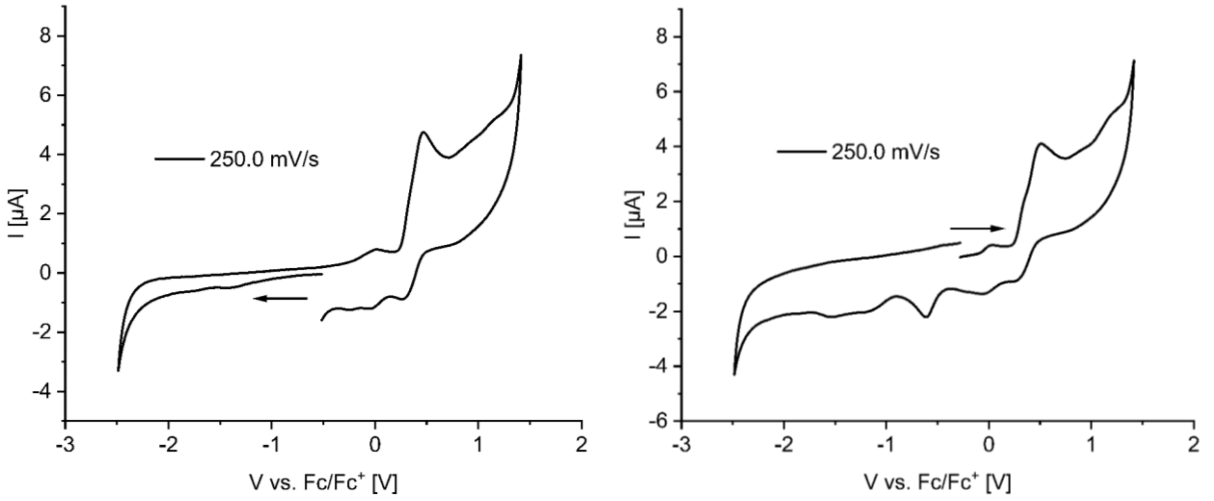

Figure S5.8.123. Cyclic voltammograms of **26** in DCM (vs. $[Cp_2Fe]^{0/+}$, scan rate: 250 mV s^{-1}).

GPC traces

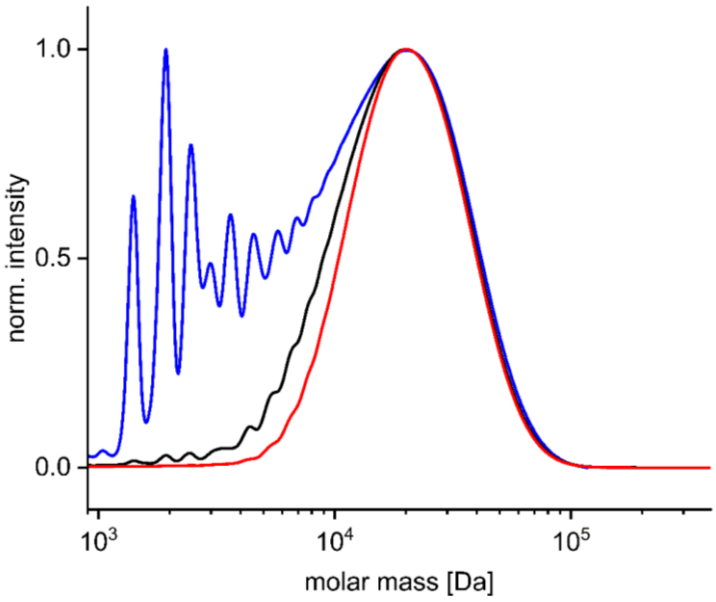

Figure S5.8.124. Normalized gel permeation chromatography (GPC) traces of **25** (by Si/B exchange) after termination with Me_3SiNMe_2 (blue), after first (black) and second (red) precipitation in cold methanol detected by UV-vis detector at 254 nm.

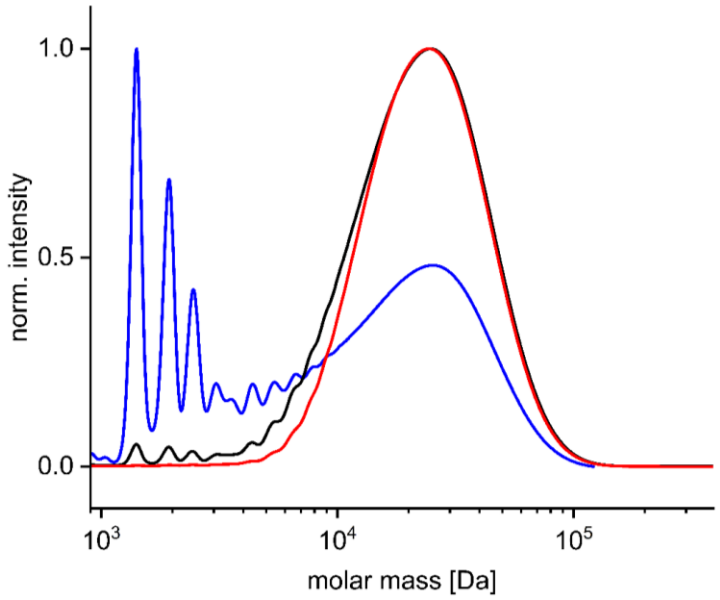

Figure S5.8.125. Normalized gel permeation chromatography (GPC) traces of **25** (by salt elimination) after termination with Me_3SiNMe_2 (blue), after first (black) and second (red) precipitation in cold methanol detected by UV-vis detector at 254 nm.

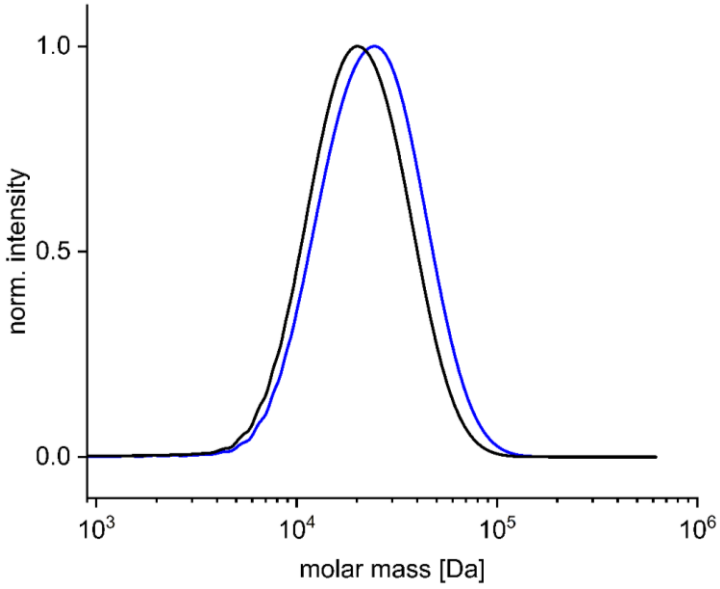

Figure S5.8.126. Normalized gel permeation chromatography (GPC) traces of **25** after termination with Me_3SiNMe_2, synthesized via salt elimination (blue) and Si/B exchange reaction (black) detected by UV-vis detector at 254 nm.

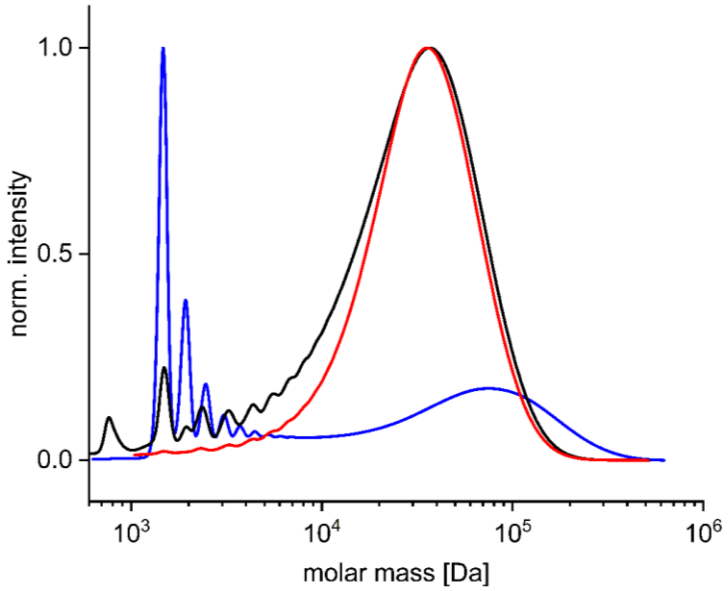

Figure S5.8.127. Normalized gel permeation chromatography (GPC) traces of **26** after termination with Me_3SiNMe_2 (blue), after first (black) and second (red) precipitation in cold methanol detected by UV-vis detector at 254 nm.

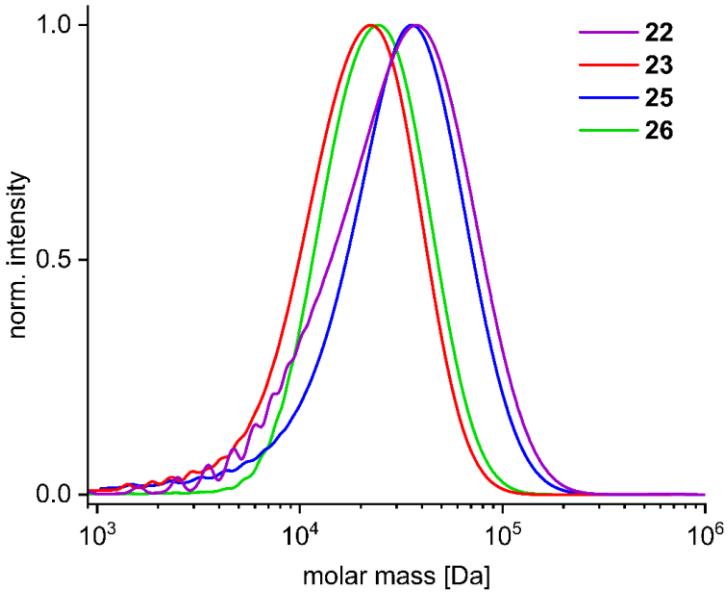

Figure S5.8.128. Normalized gel permeation chromatography (GPC) traces of **22** (green), **23** (red), **25** (by salt elimination – black) and **26** (blue) detected by UV-vis detector at 254 nm.

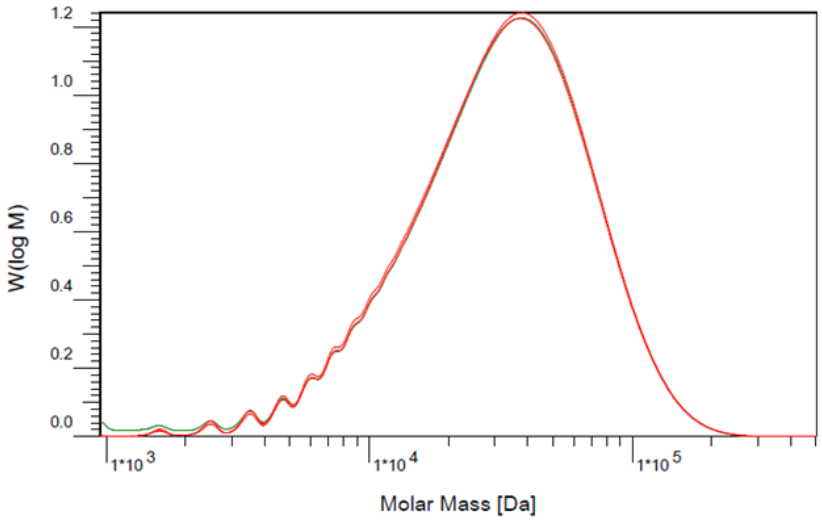

	I1: RID 1, RI Signal	Unsicherheit [%]	I1: VWD 1, Signal A	Unsicherheit [%]	I1: VWD 1, Signal B	Unsicherheit [%]	
Mn :	1.9479e4	1.66	2.1220e4	0.14	2.1839e4	0.14	g/mol
Mw :	3.9905e4	1.65	3.9885e4	0.06	4.0394e4	0.05	g/mol
Mz :	6.2240e4	1.66	6.2576e4	0.12	6.2888e4	0.12	g/mol
Mv :	0.000000	1.66	0.000000	0.14	0.000000	0.14	g/mol
D :	2.0486e0	2.34	1.8796e0	0.15	1.8496e0	0.14	
[n]:	0.000000	0.00	0.000000	0.00	0.000000	0.00	ml/g
Vp :	1.9684e1	1.65	1.9700e1	0.02	1.9684e1	0.00	ml
Mp :	4.3977e4	1.66	4.3615e4	0.16	4.3985e4	0.16	g/mol
FI :	2.3767e1	1.65	2.3319e3	0.02	1.7997e3	0.00	ml*V
< 948	0.00	1.65	0.00	0.02	0.00	0.00	
w% :	100.00	1.65	100.00	0.02	100.00	0.00	
> 501550	0.00	1.65	0.00	0.02	0.00	0.00	

Figure S5.8.129. Original GPC data of **22** (in THF, vs polystyrene standard).

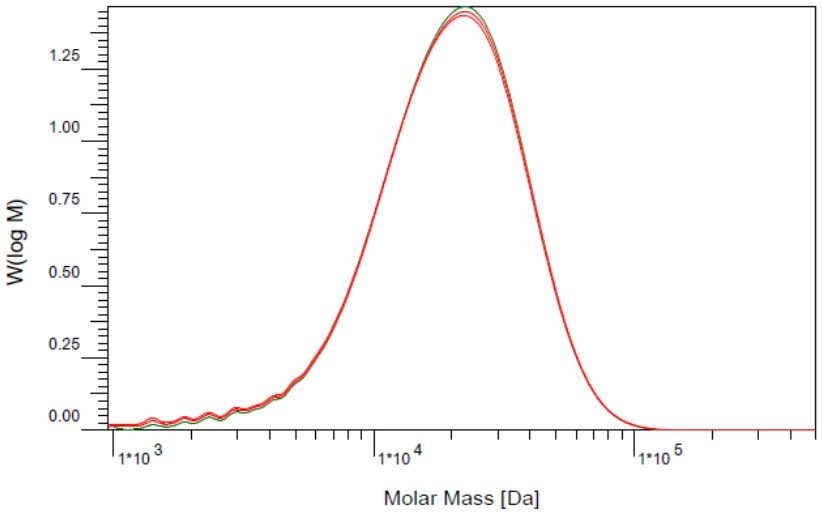

	I1: RID 1, RI Signal	Unsicherheit [%]	I1: VWD 1, Signal A	Unsicherheit [%]	I1: VWD 1, Signal B	Unsicherheit [%]	
Mn :	1.4875e4	3.85	1.4231e4	0.48	1.3743e4	0.37	g/mol
Mw :	2.3191e4	3.85	2.3040e4	0.46	2.2807e4	0.35	g/mol
Mz :	3.1963e4	3.85	3.2054e4	0.47	3.1936e4	0.37	g/mol
Mv :	0.000000	3.85	0.000000	0.48	0.000000	0.37	g/mol
D :	1.5591e0	5.44	1.6190e0	0.66	1.6596e0	0.50	
[n]:	0.000000	0.00	0.000000	0.00	0.000000	0.00	ml/g
Vp :	2.0982e1	3.85	2.0998e1	0.46	2.1015e1	0.35	ml
Mp :	2.4097e4	3.86	2.3928e4	0.49	2.3756e4	0.38	g/mol
FI :	1.7732e1	3.85	1.4202e3	0.46	1.6265e3	0.35	ml*V
< 948	0.00	3.85	0.00	0.46	0.00	0.35	
w% :	100.00	3.85	100.00	0.46	100.00	0.35	
> 501550	0.00	3.85	0.00	0.46	0.00	0.35	

Figure S5.8.130. Original GPC data of **23** (in THF, vs polystyrene standard).

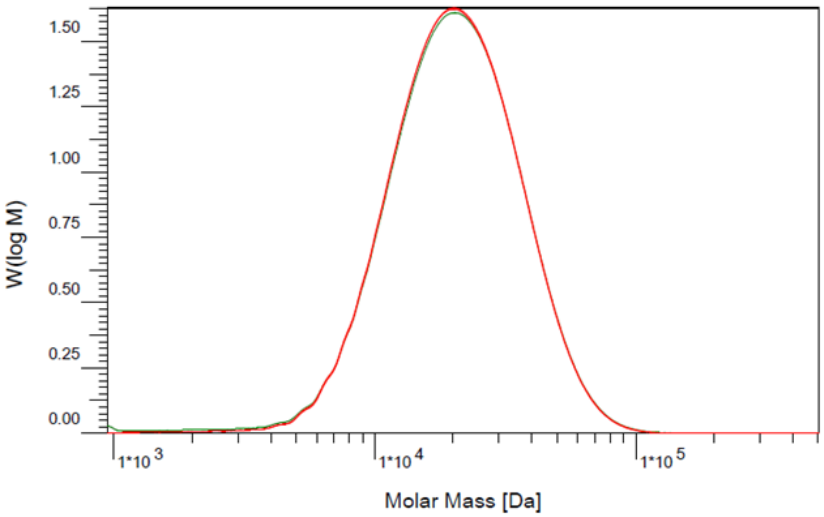

	I1: RID 1, RI Signal		I1: VWD 1, Signal A		I1: VWD 1, Signal B		
		Unsicherheit [%]		Unsicherheit [%]		Unsicherheit [%]	
Mn :	1.6253e4	4.41	1.6992e4	0.16	1.6846e4	0.14	g/mol
Mw :	2.3312e4	4.41	2.3293e4	0.09	2.3199e4	0.06	g/mol
Mz :	3.1397e4	4.41	3.0785e4	0.14	3.0710e4	0.12	g/mol
Mv :	0.000000	4.41	0.000000	0.16	0.000000	0.14	g/mol
D :	1.4344e0	6.23	1.3708e0	0.18	1.3772e0	0.15	
[n]:	0.000000	0.00	0.000000	0.00	0.000000	0.00	ml/g
Vp :	2.1254e1	4.41	2.1287e1	0.07	2.1287e1	0.01	ml
Mp :	2.1443e4	4.41	2.1144e4	0.18	2.1144e4	0.16	g/mol
FI :	2.8825e1	4.41	2.7789e3	0.07	2.0383e3	0.01	ml*V
< 948	0.00	4.41	0.00	0.07	0.00	0.01	
w% :	100.00	4.41	100.00	0.07	100.00	0.01	
> 501550	0.00	4.41	0.00	0.07	0.00	0.01	

Figure S5.8.131. Original GPC data of **25** synthesized by Si/B exchange (in THF, vs polystyrene standard).

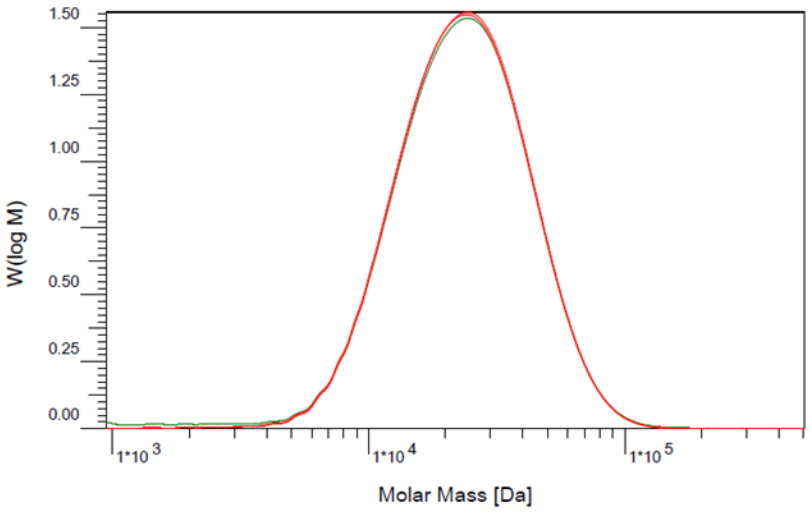

	I1: RID 1, RI Signal		I1: VWD 1, Signal A		I1: VWD 1, Signal B		
		Unsicherheit [%]		Unsicherheit [%]		Unsicherheit [%]	
Mn :	1.7858e4	1.80	1.9546e4	0.14	1.9210e4	0.14	g/mol
Mw :	2.7224e4	1.80	2.7169e4	0.06	2.6940e4	0.05	g/mol
Mz :	3.9381e4	1.80	3.6464e4	0.12	3.6269e4	0.12	g/mol
Mv :	0.000000	1.80	0.000000	0.14	0.000000	0.14	g/mol
D :	1.5245e0	2.54	1.3900e0	0.15	1.4024e0	0.14	
[n]:	0.000000	0.00	0.000000	0.00	0.000000	0.00	ml/g
Vp :	2.0772e1	1.80	2.0772e1	0.01	2.0789e1	0.00	ml
Mp :	2.6406e4	1.80	2.6410e4	0.16	2.6216e4	0.16	g/mol
FI :	2.5587e1	1.80	2.4204e3	0.01	1.8065e3	0.00	ml*V
< 948	0.00	1.80	0.00	0.01	0.00	0.00	
w% :	100.00	1.80	100.00	0.01	100.00	0.00	
> 501550	0.00	1.80	0.00	0.01	0.00	0.00	

Figure S5.8.132. Original GPC data of **25** synthesized by salt elimination (in THF, vs polystyrene standard).

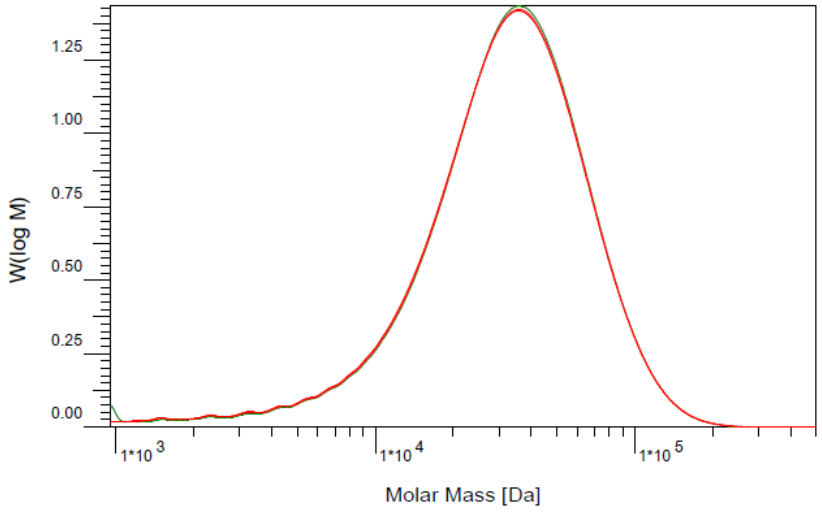

	I1: RID 1, RI Signal		I1: VWD 1, Signal A		I1: VWD 1, Signal B		
		Unsicherheit [%]		Unsicherheit [%]		Unsicherheit [%]	
Mn :	2.0574e4	0.98	2.0440e4	0.14	2.0446e4	0.14	g/mol
Mw :	3.9213e4	0.97	3.8934e4	0.07	3.9036e4	0.06	g/mol
Mz :	5.7209e4	0.98	5.7265e4	0.13	5.7324e4	0.12	g/mol
Mv :	0.000000	0.98	0.000000	0.14	0.000000	0.14	g/mol
D :	1.9059e0	1.37	1.9048e0	0.15	1.9092e0	0.15	
[n]:	0.000000	0.00	0.000000	0.00	0.000000	0.00	ml/g
Vp :	1.9868e1	0.97	1.9884e1	0.05	1.9867e1	0.01	ml
Mp :	4.0129e4	0.98	3.9809e4	0.17	4.0136e4	0.16	g/mol
FI :	1.9773e1	0.97	2.5435e3	0.05	9.9942e2	0.01	ml*V
< 935	0.00	0.97	0.00	0.05	0.00	0.01	
w% :	100.00	0.97	100.00	0.05	100.00	0.01	
> 501550	0.00	0.97	0.00	0.05	0.00	0.01	

Figure S5.8.133. Original GPC data of **26** (in THF, vs polystyrene standard).

Cartesian coordinates (Å) and total energies (a.u.) of optimized stationary points

Compound **17**:
Total energy (ωB97X-D/def2-SVP): -2023.81998695

N	-2.466613000	-1.846367000	-0.765555000
N	2.157288000	1.390834000	-1.007304000
C	-1.303039000	-1.054310000	-0.873908000
C	-0.085308000	-1.529730000	-0.378575000
H	-0.040651000	-2.524445000	0.072696000
C	1.041216000	0.535577000	-0.957098000
C	4.637781000	-1.062908000	-0.915100000
C	-1.327801000	0.223500000	-1.439655000
H	-2.256164000	0.619069000	-1.849248000
C	4.112658000	-0.088799000	-0.045323000
C	-4.867898000	-2.571071000	-0.207913000
C	3.960701000	3.832736000	-0.891772000
H	2.882132000	4.021849000	-0.889695000
C	1.070970000	-0.757949000	-0.418036000
H	1.993838000	-1.166142000	-0.012296000
C	5.166457000	-2.242032000	-0.387150000
H	5.562792000	-3.001193000	-1.068277000
C	4.449638000	2.522029000	-0.753579000
C	-4.925306000	0.789452000	-0.933963000
C	-4.111599000	0.058616000	-0.047564000
C	5.844818000	2.356825000	-0.719342000
H	6.257447000	1.352498000	-0.590127000
C	4.147845000	-0.307604000	1.342070000
C	-3.636334000	0.683469000	1.123595000
C	-0.177579000	1.001269000	-1.469934000
H	-0.228812000	2.001980000	-1.908137000
C	5.198758000	-2.479801000	0.989697000
C	4.600037000	-0.852920000	-2.423049000
H	4.255351000	0.179089000	-2.605187000
C	-4.828918000	-3.786459000	-0.912154000
H	-4.022464000	-3.976160000	-1.628051000
C	4.817362000	4.924705000	-1.007350000
H	4.408333000	5.932773000	-1.106981000
C	-5.448502000	0.152504000	-2.215928000
H	-4.976087000	-0.839382000	-2.313105000
C	6.711676000	3.441389000	-0.843618000
H	7.792204000	3.282179000	-0.820832000
B	-3.764370000	-1.452482000	-0.369829000
C	-5.249632000	2.117266000	-0.642291000
H	-5.880588000	2.684520000	-1.333704000
B	3.508075000	1.257123000	-0.613652000
C	6.198631000	4.729359000	-0.988670000
H	6.874151000	5.583132000	-1.079907000
C	-6.866281000	-4.533298000	0.144302000
H	-7.640148000	-5.292585000	0.279318000
C	4.689327000	-1.496807000	1.838637000
H	4.714728000	-1.669816000	2.919152000
C	-5.814568000	-4.756693000	-0.744797000
H	-5.766851000	-5.689135000	-1.312152000
C	-5.946376000	-2.363875000	0.668135000
H	-6.014076000	-1.417245000	1.211963000
C	-1.424073000	0.626159000	2.366486000
H	-0.877735000	0.770841000	1.422633000
H	-0.792873000	0.021858000	3.036150000
H	-1.554674000	1.613023000	2.838725000
C	-2.770310000	-0.066037000	2.128637000
H	-2.548239000	-1.058616000	1.706849000
C	-3.982409000	2.010882000	1.383580000

H	-3.611725000	2.487461000	2.296127000
C	3.589198000	0.735794000	2.299159000
H	3.157952000	1.547683000	1.689060000
C	-6.930009000	-3.334230000	0.853070000
H	-7.754155000	-3.151976000	1.546656000
C	5.985317000	-0.975917000	-3.063568000
H	6.701095000	-0.282481000	-2.597267000
H	5.937485000	-0.743975000	-4.138746000
H	6.389340000	-1.995678000	-2.963072000
C	-3.524346000	-0.296998000	3.443080000
H	-3.773640000	0.657966000	3.932776000
H	-2.914634000	-0.885852000	4.146163000
H	-4.465132000	-0.840919000	3.269570000
C	3.583958000	-1.788786000	-3.087319000
H	3.874246000	-2.843490000	-2.953927000
H	3.517250000	-1.592060000	-4.168776000
H	2.581906000	-1.657361000	-2.652727000
C	5.771182000	-3.771671000	1.546723000
H	5.690891000	-3.711358000	2.645226000
C	-4.787324000	2.747637000	0.512529000
C	-6.961323000	-0.078082000	-2.147996000
H	-7.222874000	-0.711324000	-1.287688000
H	-7.323781000	-0.575690000	-3.061083000
H	-7.501910000	0.876587000	-2.045484000
C	-5.056614000	0.949266000	-3.464568000
H	-5.531907000	1.942575000	-3.477788000
H	-5.372511000	0.419951000	-4.376839000
H	-3.967579000	1.099192000	-3.519750000
C	-5.142161000	4.194273000	0.808718000
H	-5.792515000	4.540483000	-0.012358000
C	-5.935778000	4.329158000	2.112396000
H	-6.840442000	3.703539000	2.092389000
H	-6.242990000	5.373632000	2.277994000
H	-5.332503000	4.017932000	2.980082000
C	-3.896544000	5.087076000	0.817312000
H	-3.208101000	4.800116000	1.628182000
H	-4.170663000	6.142827000	0.969296000
H	-3.346024000	5.007625000	-0.131950000
C	4.696727000	1.359918000	3.152923000
H	5.174520000	0.605316000	3.798102000
H	4.292186000	2.151075000	3.803278000
H	5.476711000	1.804337000	2.516529000
C	4.959169000	-4.989189000	1.092123000
H	3.899107000	-4.883616000	1.367082000
H	5.343916000	-5.912219000	1.553292000
H	5.010663000	-5.115724000	-0.001123000
C	2.447981000	0.176198000	3.154138000
H	1.653546000	-0.245791000	2.520618000
H	2.001757000	0.967859000	3.776008000
H	2.802665000	-0.618061000	3.830102000
C	7.255801000	-3.928819000	1.201710000
H	7.404838000	-4.015397000	0.113565000
H	7.672813000	-4.835002000	1.668172000
H	7.837837000	-3.063146000	1.551082000
H	1.908601000	2.287412000	-1.410655000
H	-2.274132000	-2.841453000	-0.807288000

Compound **18**:

Total energy (ωB97X-D/def2-SVP): -2665.25694953

N	2.405612000	-1.789388000	-0.995503000
H	2.189610000	-2.769621000	-1.139512000
C	1.255798000	-0.972297000	-1.019367000
B	3.716074000	-1.479187000	-0.566081000
N	-2.209229000	1.473589000	-0.945236000
H	-1.958836000	2.403689000	-1.264839000
C	0.013760000	-1.516224000	-0.676148000
H	-0.053461000	-2.573522000	-0.405958000
B	-3.555908000	1.293435000	-0.552452000
C	-1.142732000	-0.744138000	-0.650289000
H	-2.085460000	-1.211946000	-0.374956000
C	-1.089416000	0.621395000	-0.960669000
C	0.154521000	1.161003000	-1.315729000
H	0.226391000	2.221414000	-1.573437000
C	1.305086000	0.383976000	-1.356453000
H	2.250699000	0.842501000	-1.640314000
S	-4.135936000	4.052201000	-1.325804000
C	-4.546178000	2.499944000	-0.666573000
C	-5.865771000	2.509542000	-0.262975000
H	-6.337704000	1.631771000	0.182579000
C	-6.529418000	3.748771000	-0.479979000
H	-7.571307000	3.943100000	-0.224370000
C	-5.706776000	4.682471000	-1.053773000
H	-5.949418000	5.707227000	-1.332011000
S	6.193884000	-2.483323000	0.438289000
C	4.755909000	-2.649891000	-0.514137000
C	4.747580000	-3.889195000	-1.121658000
H	3.950788000	-4.216621000	-1.793388000
C	5.881625000	-4.690188000	-0.816073000
H	6.049734000	-5.694026000	-1.207312000
C	6.750649000	-4.050649000	0.030535000
H	7.689620000	-4.430659000	0.430988000
C	4.125338000	-0.024641000	-0.097005000
C	3.697373000	0.470053000	1.151818000
C	4.055143000	1.762387000	1.537774000
H	3.721008000	2.139042000	2.509219000
C	4.827147000	2.588596000	0.717976000
C	5.248519000	2.083363000	-0.511415000
H	5.855692000	2.721054000	-1.161656000
C	4.912568000	0.792508000	-0.929737000
C	2.868875000	-0.388607000	2.098642000
H	2.647815000	-1.337406000	1.584253000
C	5.195238000	3.996676000	1.151495000
H	5.804367000	4.433610000	0.342190000
C	5.383909000	0.300052000	-2.292695000
H	4.984761000	-0.717839000	-2.437204000
C	3.663465000	-0.740287000	3.361214000
H	4.606963000	-1.244982000	3.104205000
H	3.082451000	-1.409284000	4.015214000
H	3.911580000	0.163377000	3.940627000
C	1.520674000	0.254995000	2.438048000
H	1.651000000	1.195065000	2.997796000
H	0.917514000	-0.420477000	3.064096000
H	0.945684000	0.479836000	1.527187000
C	3.951678000	4.876504000	1.318604000
H	3.353778000	4.896977000	0.395265000
H	4.233517000	5.911115000	1.569390000
H	3.304852000	4.500987000	2.127506000
C	6.052352000	3.991968000	2.421608000
H	5.492652000	3.583123000	3.277920000
H	6.366673000	5.013726000	2.686043000
H	6.955064000	3.377561000	2.288379000
C	4.833564000	1.160091000	-3.435556000
H	3.734107000	1.202344000	-3.413239000
H	5.135608000	0.749353000	-4.411493000
H	5.210330000	2.193517000	-3.378349000
C	6.910591000	0.192799000	-2.356352000
H	7.384692000	1.180026000	-2.236154000
H	7.233336000	-0.218910000	-3.325336000
H	7.289396000	-0.464515000	-1.560100000
C	-4.140416000	-0.062055000	0.012483000
C	-4.098501000	-0.330994000	1.390730000
C	-4.639410000	-1.526402000	1.874393000
H	-4.601576000	-1.741174000	2.947019000
C	-5.226904000	-2.462602000	1.023589000
C	-5.269293000	-2.174698000	-0.343665000
H	-5.729304000	-2.895432000	-1.026716000

C	-4.737502000	-0.992091000	-0.859219000
C	-3.447132000	0.653220000	2.351699000
H	-3.122156000	1.526619000	1.761873000
C	-5.802360000	-3.758604000	1.567646000
H	-5.652748000	-3.742887000	2.660410000
C	-4.794817000	-0.720482000	-2.356133000
H	-4.279208000	0.237249000	-2.539698000
C	-4.436016000	1.169212000	3.400349000
H	-5.310313000	1.633993000	2.920335000
H	-3.960338000	1.922691000	4.047129000
H	-4.797900000	0.354718000	4.047806000
C	-2.189613000	0.057015000	2.992215000
H	-2.437390000	-0.807267000	3.629252000
H	-1.677809000	0.801966000	3.621374000
H	-1.480540000	-0.281441000	2.222568000
C	-7.309489000	-3.860689000	1.310746000
H	-7.842539000	-2.993749000	1.728475000
H	-7.724128000	-4.772661000	1.767914000
H	-7.527822000	-3.899996000	0.231608000
C	-5.057095000	-4.979860000	1.018605000
H	-5.440187000	-5.908734000	1.469269000
H	-3.979363000	-4.914354000	1.229946000
H	-5.180063000	-5.063138000	-0.073083000
C	-4.044741000	-1.787869000	-3.159478000
H	-4.519390000	-2.776619000	-3.055597000
H	-3.001314000	-1.875908000	-2.821282000
H	-4.035833000	-1.534297000	-4.230909000
C	-6.237787000	-0.549917000	-2.839786000
H	-6.819857000	-1.473619000	-2.691643000
H	-6.265269000	-0.303865000	-3.912713000
H	-6.741098000	0.259628000	-2.290341000

Compound **20**:
Total energy (ωB97X-D/def2-SVP): -2344.53470252

B	-3.311980000	-1.437656000	-0.331538000
N	2.564989000	-2.586976000	0.490724000
H	3.056300000	-3.385634000	0.878151000
C	0.666546000	-4.140026000	0.370576000
H	1.241027000	-5.027200000	0.640056000
N	-2.540095000	-2.601192000	-0.549942000
H	-3.011039000	-3.400200000	-0.961500000
C	1.227138000	-2.897325000	0.254763000
S	0.034074000	-1.696344000	-0.169577000
B	3.328753000	-1.423735000	0.245983000
C	-0.736771000	-4.144777000	0.116269000
H	-1.361911000	-5.037504000	0.153209000
C	-1.226527000	-2.906415000	-0.186854000
C	4.851764000	-1.433882000	0.673945000
C	5.726818000	-0.467767000	0.148155000
H	5.335372000	0.282373000	-0.544306000
C	7.077152000	-0.441268000	0.493366000
H	7.735364000	0.317454000	0.063888000
C	7.584420000	-1.377691000	1.392620000
H	8.640638000	-1.356630000	1.671027000
C	6.734483000	-2.337233000	1.943459000
H	7.122241000	-3.065517000	2.659469000
C	5.388961000	-2.360058000	1.584839000
H	4.744397000	-3.112297000	2.051666000
C	-4.804306000	-1.438375000	-0.851162000
C	-5.240774000	-2.244304000	-1.916463000
H	-4.529478000	-2.891547000	-2.440231000
C	-6.563341000	-2.221119000	-2.353526000
H	-6.874100000	-2.850033000	-3.191047000
C	-7.488495000	-1.387493000	-1.724761000
H	-8.526796000	-1.367082000	-2.064065000
C	-7.080241000	-0.574156000	-0.668392000
H	-7.799053000	0.085188000	-0.176446000
C	-5.751730000	-0.594897000	-0.246946000
H	-5.435070000	0.061099000	0.568770000
C	-2.765061000	-0.166627000	0.430647000
C	-2.669344000	-0.143993000	1.836321000
C	-2.348055000	1.051931000	2.478727000
H	-2.276349000	1.073862000	3.571083000
C	-2.100253000	2.230598000	1.771537000
C	-2.164155000	2.184181000	0.379107000
H	-1.959117000	3.086997000	-0.201075000
C	-2.499635000	1.007432000	-0.296767000
C	-2.909859000	-1.398995000	2.665211000
H	-3.184420000	-2.210574000	1.972523000
C	-1.631772000	-1.843718000	3.385727000
H	-0.812906000	-2.007449000	2.669472000
H	-1.799779000	-2.783620000	3.934367000
H	-1.298904000	-1.084497000	4.111675000
C	-4.079697000	-1.227076000	3.639069000
H	-3.868748000	-0.448995000	4.389669000
H	-4.277953000	-2.165574000	4.179963000
H	-4.998913000	-0.940147000	3.106251000
C	-1.825402000	3.512642000	2.540616000
H	-1.281352000	3.219576000	3.455500000
C	-3.147367000	4.158505000	2.977395000
H	-2.966371000	5.057591000	3.587389000
H	-3.756546000	3.458652000	3.568327000
H	-3.739294000	4.455498000	2.096826000
C	-0.951412000	4.516378000	1.790912000
H	-0.020739000	4.052683000	1.432865000
H	-0.684230000	5.358292000	2.447224000
H	-1.471804000	4.938337000	0.916727000
C	-2.577074000	1.002480000	-1.817437000
H	-2.822868000	-0.025528000	-2.134197000
C	-3.701391000	1.906222000	-2.330593000
H	-4.671425000	1.606826000	-1.906114000
H	-3.776055000	1.851684000	-3.427890000
H	-3.520332000	2.958595000	-2.058775000
C	-1.228683000	1.345803000	-2.453848000
H	-0.930308000	2.379819000	-2.223092000
H	-1.276832000	1.249773000	-3.550142000
H	-0.430997000	0.685963000	-2.084055000
C	2.742260000	-0.124817000	-0.436314000
C	2.433978000	0.986071000	0.367708000
C	2.071134000	2.197436000	-0.228729000
H	1.829767000	3.049474000	0.410631000
C	2.026562000	2.341062000	-1.614880000
C	2.319286000	1.222736000	-2.400189000
H	2.267518000	1.321388000	-3.489402000
C	2.665848000	-0.005654000	-1.838235000
C	2.497940000	0.875228000	1.884334000
H	2.798028000	-0.158094000	2.129508000
C	1.124621000	1.096887000	2.520854000
H	0.771309000	2.126244000	2.356492000
H	1.162498000	0.926093000	3.608473000
H	0.371485000	0.421697000	2.090366000
C	3.564588000	1.800034000	2.476709000
H	4.553249000	1.590157000	2.041237000
H	3.634939000	1.666098000	3.567423000
H	3.325379000	2.858289000	2.284553000
C	1.724374000	3.665393000	-2.297435000
H	1.153265000	3.424426000	-3.211094000
C	0.872291000	4.619081000	-1.462670000
H	-0.044985000	4.131261000	-1.102454000
H	0.582341000	5.496961000	-2.059446000
H	1.419973000	4.990702000	-0.582198000
C	3.030303000	4.342782000	-2.735128000
H	3.647688000	4.590199000	-1.856738000
H	2.827211000	5.275507000	-3.284551000
H	3.624149000	3.683545000	-3.385388000
C	2.977637000	-1.189758000	-2.743581000

H	3.142307000	-2.067465000	-2.096838000
C	4.268750000	-0.964046000	-3.537398000
H	4.173628000	-0.097770000	-4.211490000
H	4.509297000	-1.844532000	-4.153577000
H	5.119485000	-0.776638000	-2.865212000
C	1.800789000	-1.531360000	-3.663576000
H	0.884181000	-1.703485000	-3.080393000
H	2.014805000	-2.440796000	-4.246346000
H	1.599725000	-0.718183000	-4.379065000

Compound **21**:
Total energy (ωB97X-D/def2-SVP): -2985.96183563

S	-0.729592000	0.294617000	-0.560431000
N	1.770587000	1.280435000	-0.898355000
H	1.308704000	2.174841000	-1.031276000
B	3.094546000	1.268633000	-0.395272000
N	-2.269319000	-1.982656000	-0.834593000
H	-2.212236000	-2.968124000	-1.072448000
B	-3.524885000	-1.473023000	-0.426845000
C	-1.029611000	-1.365714000	-0.997775000
C	0.100170000	-1.951928000	-1.502096000
H	0.128475000	-2.990171000	-1.835293000
C	1.221590000	-1.069383000	-1.561515000
H	2.208720000	-1.357564000	-1.917609000
C	0.931696000	0.177532000	-1.091762000
C	-3.747322000	0.053106000	-0.083929000
C	-4.142637000	0.942751000	-1.098418000
C	-4.369314000	2.285988000	-0.784913000
H	-4.669845000	2.981724000	-1.574598000
C	-4.216987000	2.770504000	0.513338000
C	-3.829943000	1.872242000	1.511883000
H	-3.706228000	2.236403000	2.535575000
C	-3.590652000	0.526826000	1.234108000
C	3.855701000	-0.081746000	-0.088064000
C	4.868066000	-0.519562000	-0.961871000
C	5.558701000	-1.702682000	-0.681164000
H	6.343885000	-2.044850000	-1.362793000
C	5.273582000	-2.466795000	0.449401000
C	4.262703000	-2.021458000	1.304465000
H	4.023079000	-2.609477000	2.195465000
C	3.547229000	-0.850183000	1.052176000
S	-4.669283000	-4.152282000	-0.600632000
C	-4.747851000	-2.439446000	-0.334103000
C	-6.048739000	-2.080643000	-0.045258000
H	-6.327582000	-1.045498000	0.161029000
C	-6.963103000	-3.169855000	-0.043472000
H	-8.029708000	-3.079012000	0.162979000
C	-6.348965000	-4.360883000	-0.330778000
H	-6.802126000	-5.349496000	-0.391727000
S	3.244239000	4.172032000	-0.641653000
C	3.818989000	2.623436000	-0.111750000
C	4.979074000	2.788550000	0.616214000
H	5.514609000	1.939725000	1.045742000
C	5.390205000	4.144020000	0.749040000
H	6.279767000	4.468087000	1.289690000
C	4.538457000	5.007543000	0.111417000
H	4.615416000	6.091710000	0.040038000
C	5.208334000	0.264376000	-2.223822000
H	4.520517000	1.124306000	-2.280849000
C	6.628496000	0.834727000	-2.170385000
H	6.756969000	1.483798000	-1.291833000
H	6.844584000	1.431897000	-3.069970000
H	7.379290000	0.030538000	-2.112012000
C	4.982598000	-0.566555000	-3.491420000
H	5.657747000	-1.435920000	-3.529766000
H	5.168774000	0.039251000	-4.391812000
H	3.949342000	-0.941503000	-3.544138000
C	2.454873000	-0.419946000	2.022406000
H	1.950098000	0.459981000	1.592332000
C	1.384318000	-1.501488000	2.198919000
H	0.946036000	-1.784621000	1.230197000
H	0.573553000	-1.140110000	2.848545000
H	1.799957000	-2.409938000	2.663216000
C	3.048241000	0.017064000	3.365935000
H	3.564514000	-0.819301000	3.864013000
H	2.258546000	0.377034000	4.043926000
H	3.777896000	0.829434000	3.228577000
C	6.033886000	-3.749313000	0.738247000
H	6.772465000	-3.874777000	-0.071527000
C	6.807808000	-3.663455000	2.057917000
H	7.488053000	-2.798870000	2.063141000
H	7.406141000	-4.573378000	2.221533000
H	6.123313000	-3.556118000	2.914451000
C	5.108432000	-4.970473000	0.710980000
H	4.351955000	-4.913555000	1.509880000
H	5.680380000	-5.900009000	0.858063000
H	4.575656000	-5.042376000	-0.248890000
C	-3.176378000	-0.421444000	2.351391000
H	-2.795410000	-1.342720000	1.877517000
C	-2.037603000	0.137837000	3.208808000
H	-1.189747000	0.451507000	2.582055000
H	-1.679988000	-0.624617000	3.918047000
H	-2.362897000	1.006732000	3.802158000
C	-4.382976000	-0.814644000	3.210897000
H	-4.090108000	-1.528495000	3.996671000
H	-5.168403000	-1.282615000	2.599649000
H	-4.816547000	0.071779000	3.701382000
C	-4.310846000	0.462566000	-2.533428000
H	-4.052906000	-0.609490000	-2.558601000
C	-3.344753000	1.173916000	-3.486559000
H	-3.569047000	2.250427000	-3.553961000
H	-3.419131000	0.754130000	-4.501759000
H	-2.305025000	1.066755000	-3.143590000
C	-5.763999000	0.581740000	-3.001916000
H	-6.096619000	1.631979000	-3.009192000
H	-6.438002000	0.017656000	-2.340113000
H	-5.879136000	0.186508000	-4.023198000
C	-4.450119000	4.237139000	0.830650000
H	-4.767102000	4.722607000	-0.107772000
C	-5.577131000	4.427472000	1.850893000
H	-5.314066000	3.983037000	2.823980000
H	-6.508230000	3.953090000	1.506919000
H	-5.777340000	5.497376000	2.017524000
C	-3.157557000	4.921137000	1.289485000
H	-3.319910000	5.997867000	1.453727000
H	-2.360123000	4.803480000	0.540766000
H	-2.793960000	4.489329000	2.235572000

5.9 BN- and BO-Doped Inorganic–Organic Hybrid Polymers Based on Sulfur-Containing Building Blocks

NMR spectra

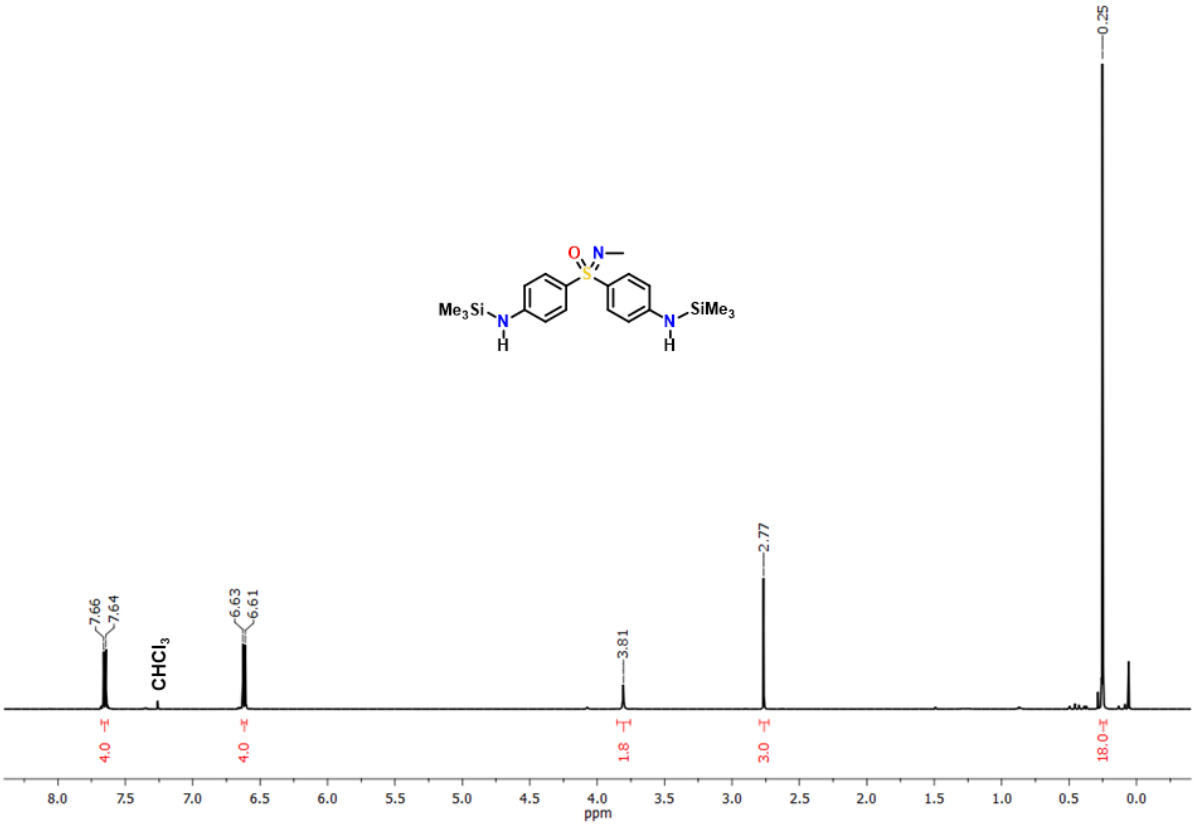

Figure S5.9.1. ^{1}H NMR spectrum (500 MHz) of **5** in $CDCl_3$.

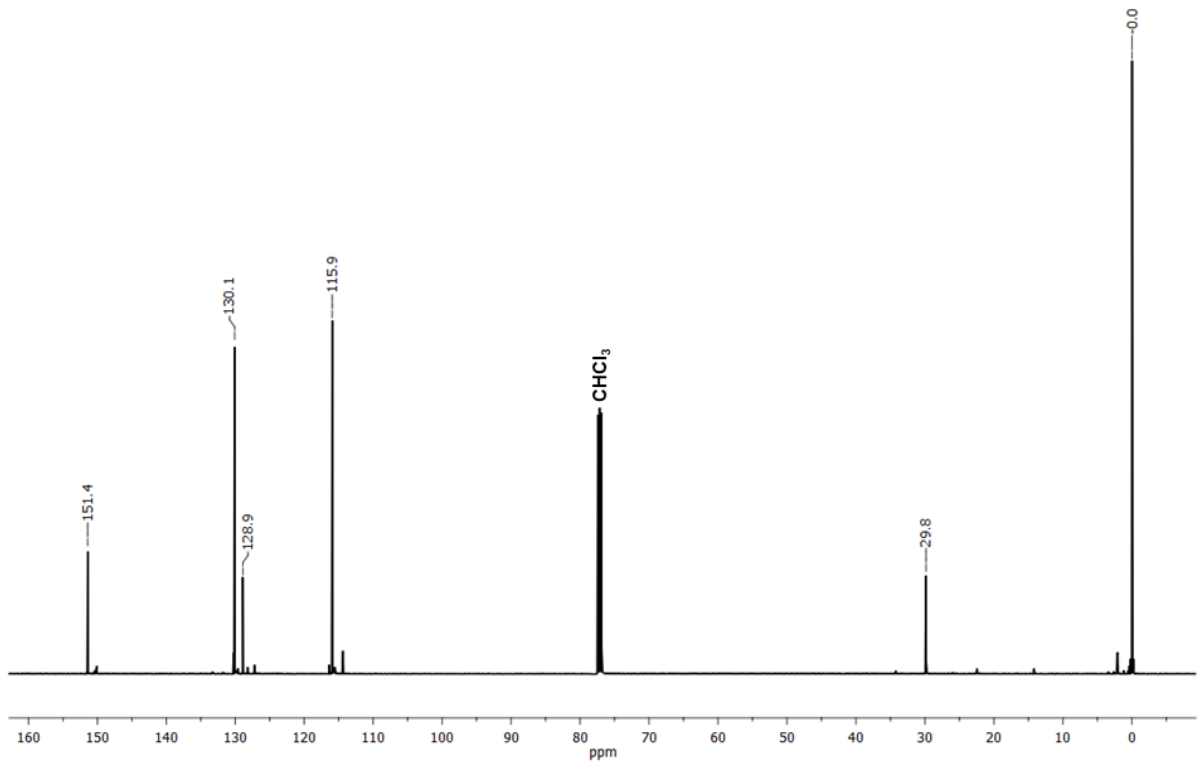

Figure S5.9.2. $^{13}C\{^{1}H\}$ NMR spectrum (125 MHz) of **5** in $CDCl_3$.

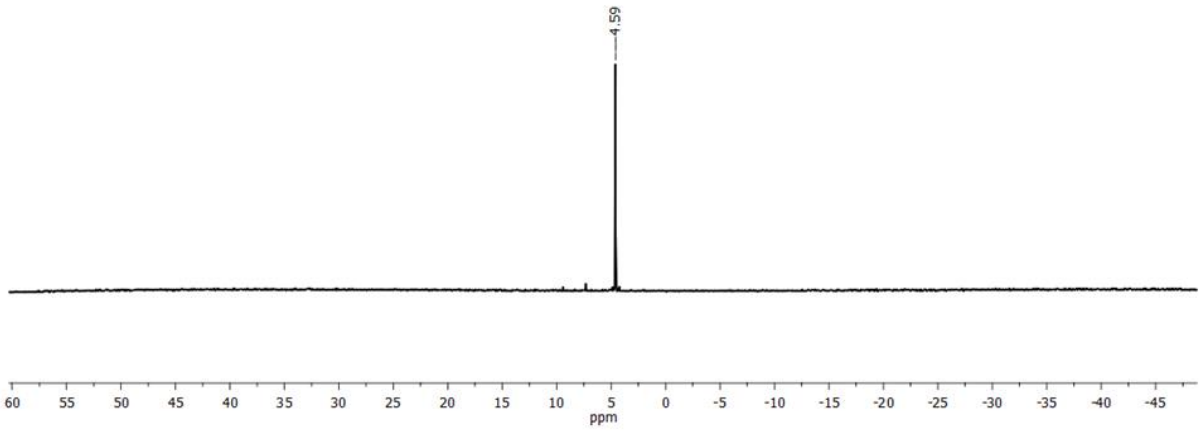

Figure S5.9.3. $^{29}Si\{^{1}H\}$ NMR spectrum (99.4 MHz) of **5** in $CDCl_3$.

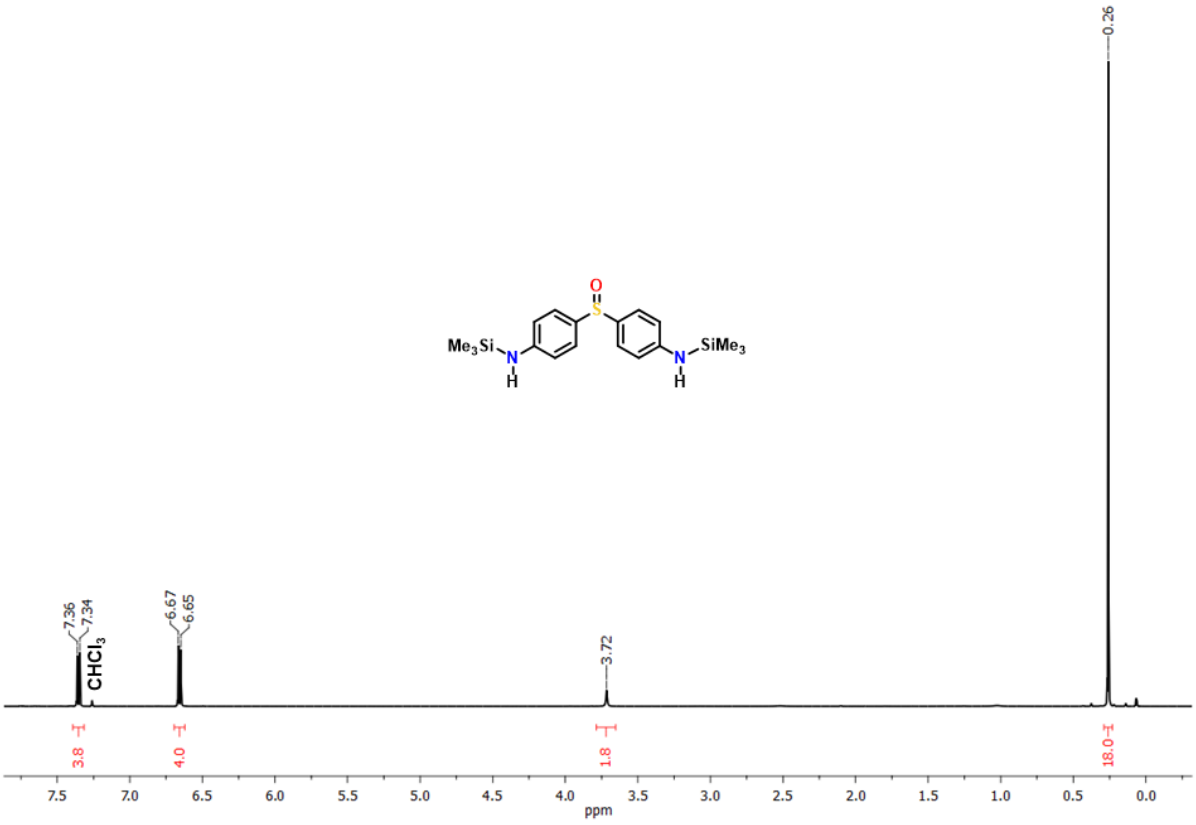

Figure S5.9.4. ^{1}H NMR spectrum (500 MHz) of **6** in $CDCl_3$.

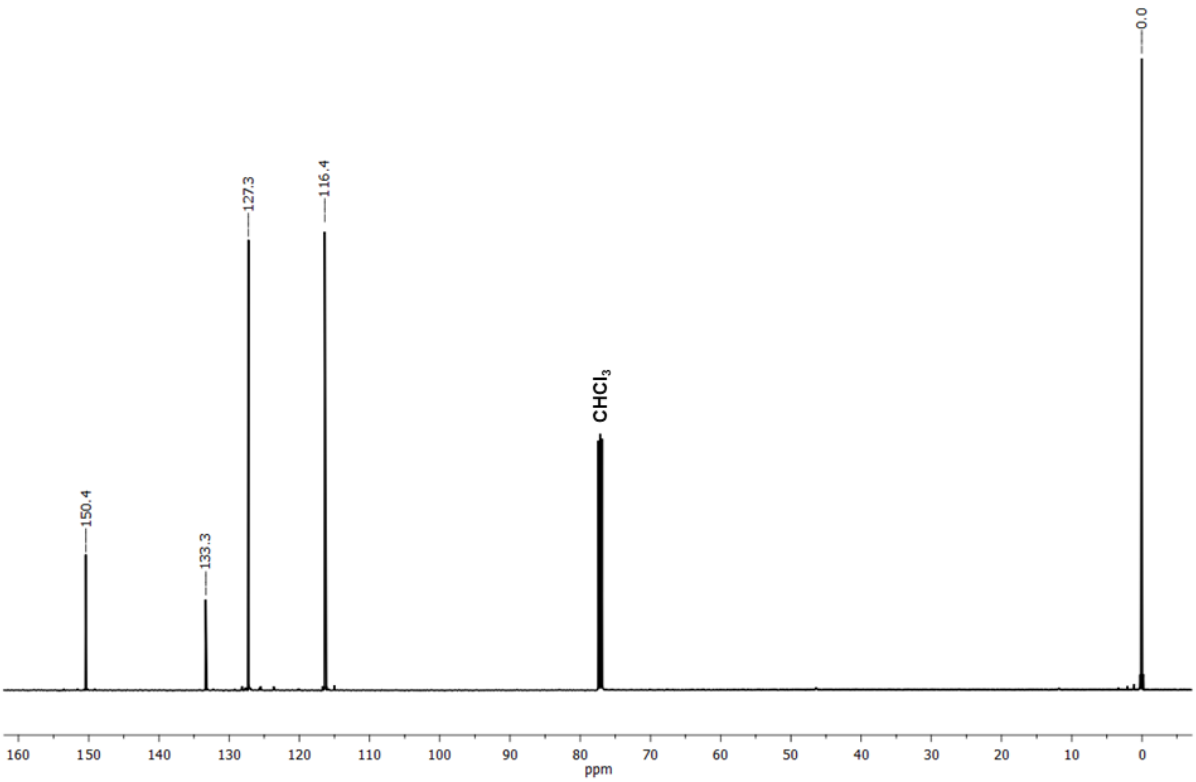

Figure S5.9.5. $^{13}C\{^{1}H\}$ NMR spectrum (125 MHz) of **6** in $CDCl_3$.

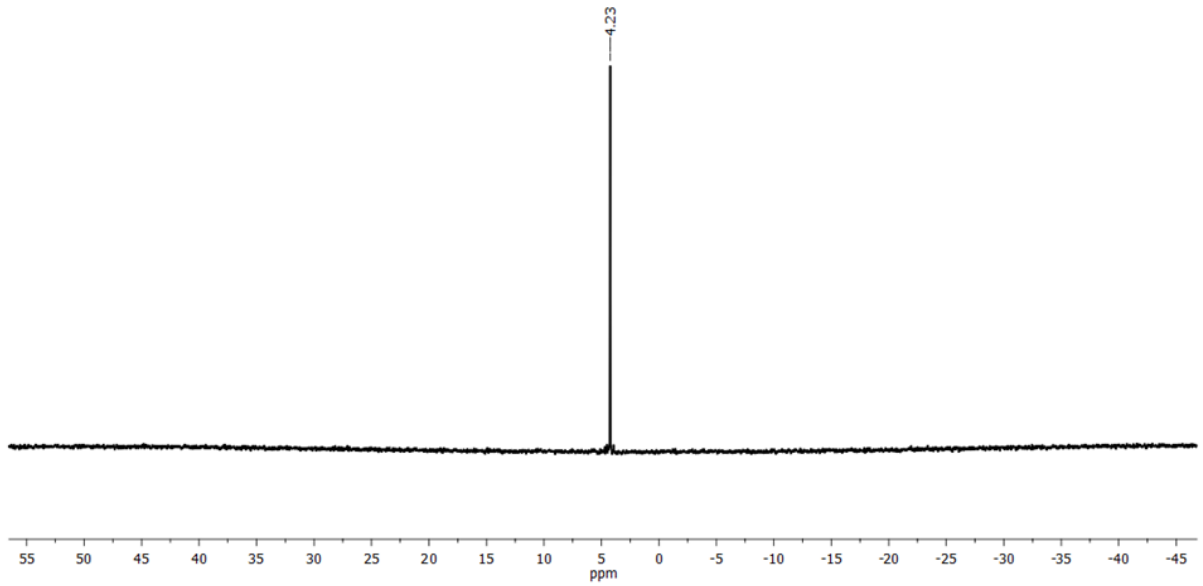

Figure S5.9.6. $^{29}Si\{^{1}H\}$ NMR spectrum (99.4 MHz) of **6** in $CDCl_3$.

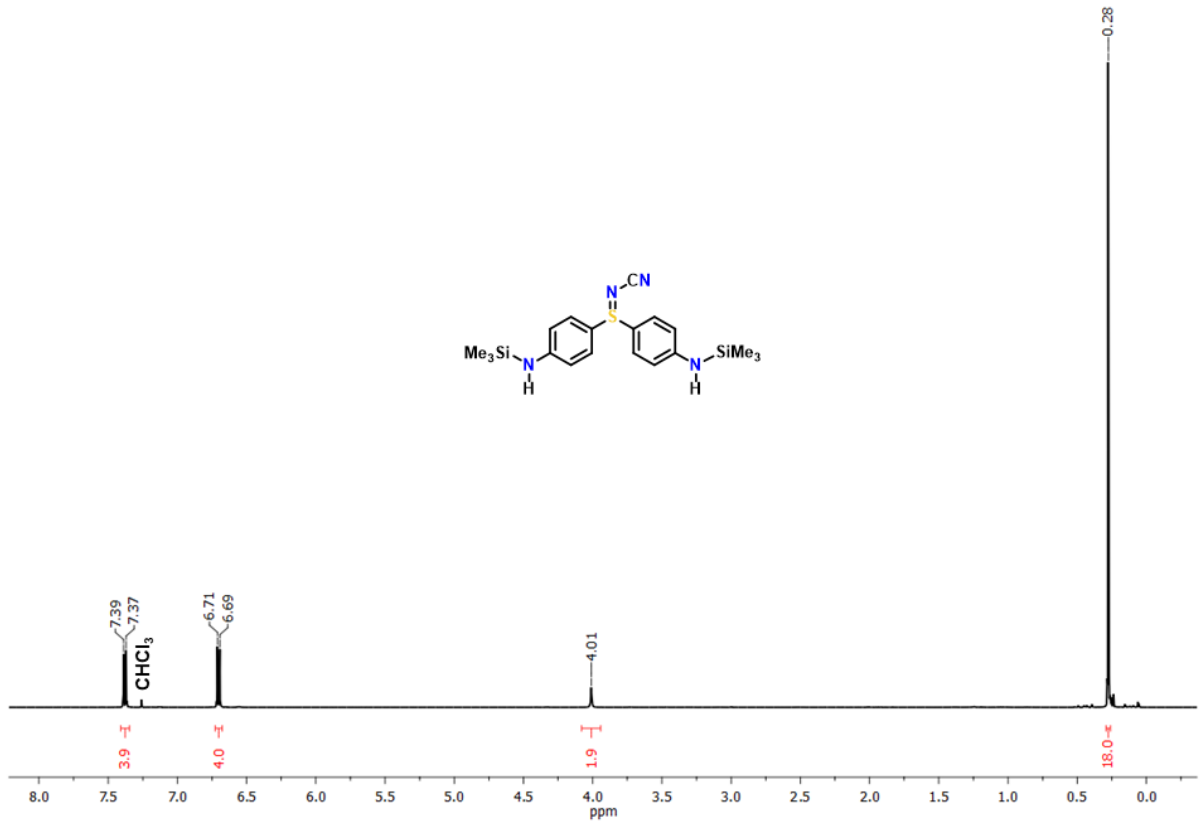

Figure S5.9.7. ^{1}H NMR spectrum (500 MHz) of **7** in $CDCl_3$.

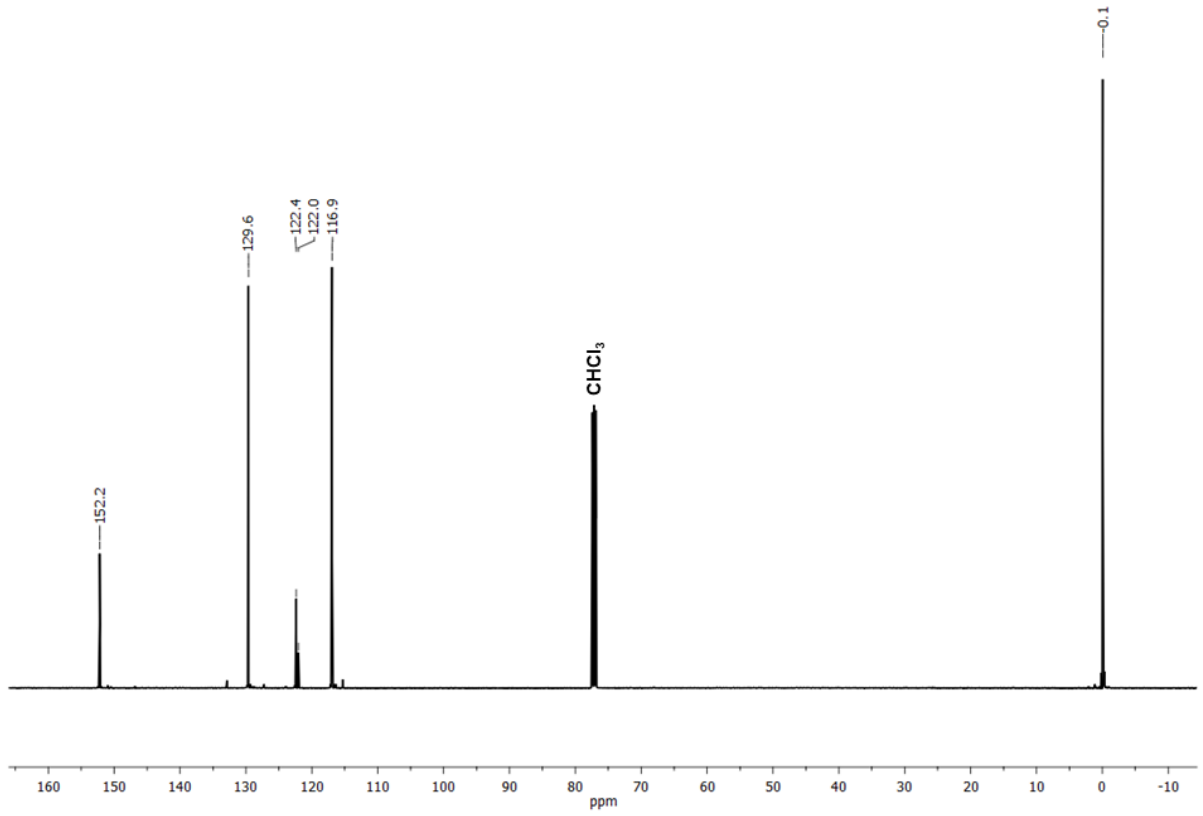

Figure S5.9.8. $^{13}C\{^{1}H\}$ NMR spectrum (125 MHz) of **7** in $CDCl_3$.

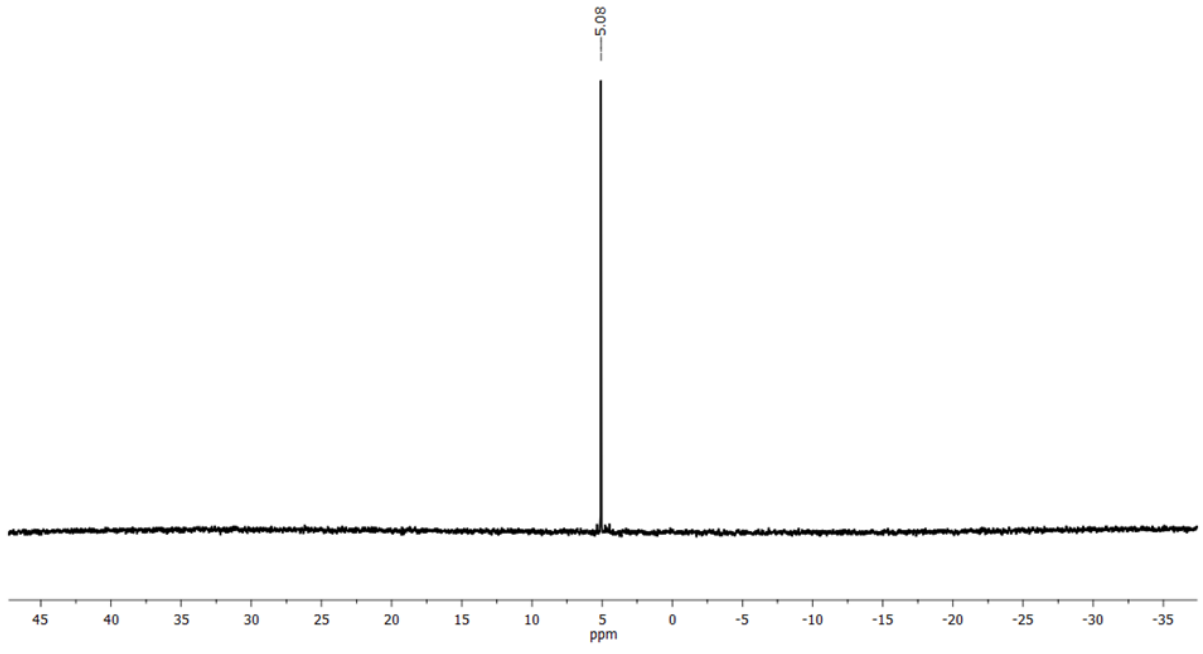

Figure S5.9.9. $^{29}Si\{^{1}H\}$ NMR spectrum (99.4 MHz) of **7** in $CDCl_3$.

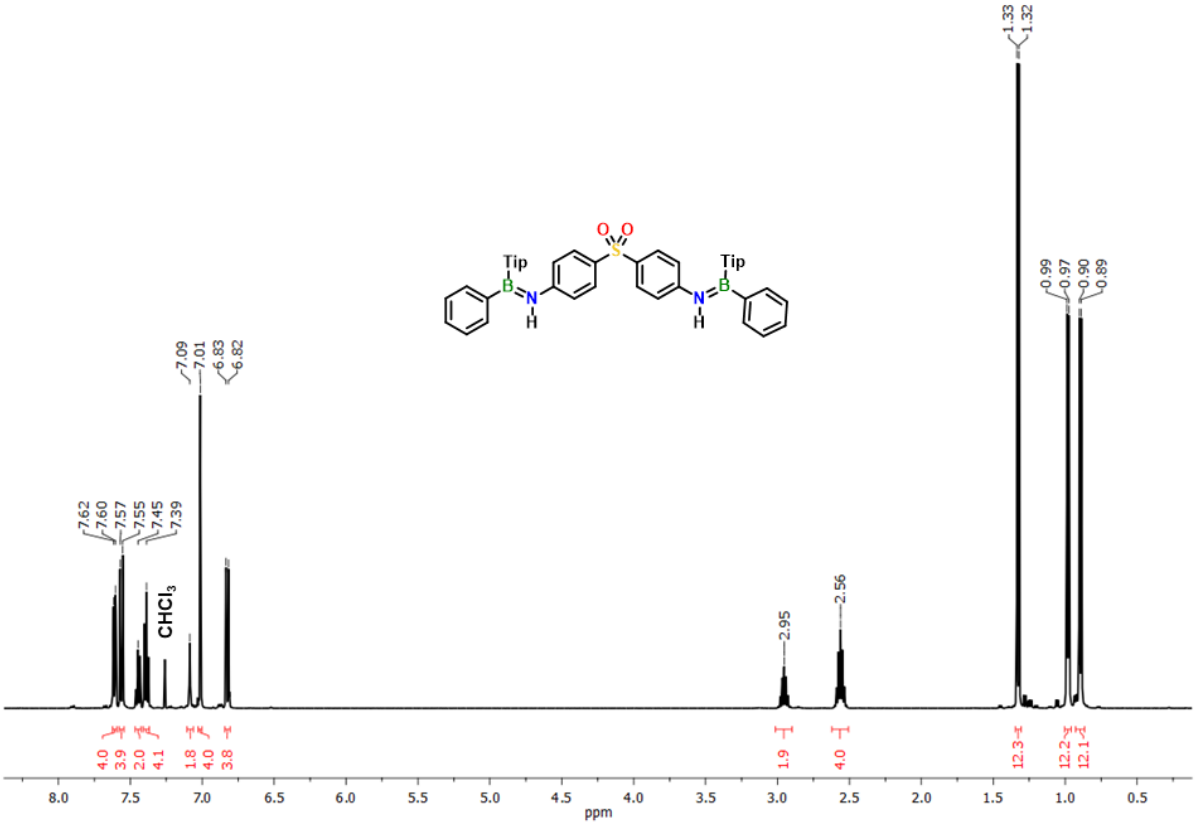

Figure S5.9.10. ^{1}H NMR spectrum (500 MHz) of **8** in $CDCl_3$.

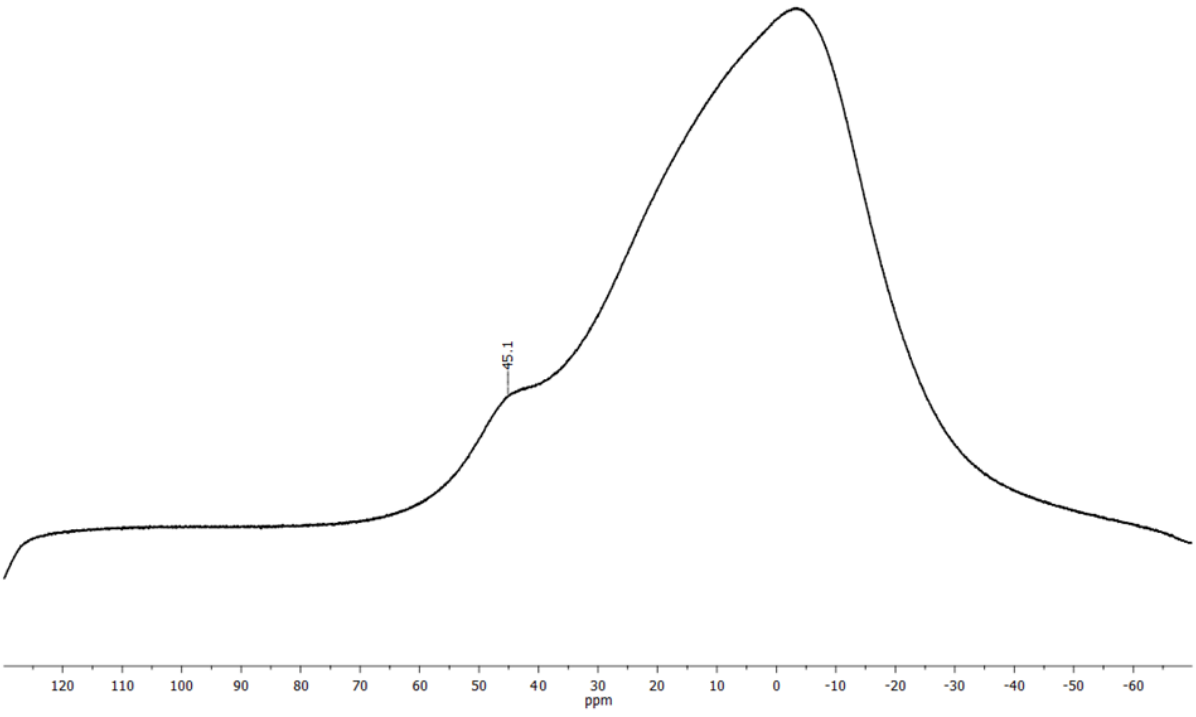

Figure S5.9.11. $^{11}B\{^{1}H\}$ NMR spectrum (160 MHz) of **8** in $CDCl_3$.

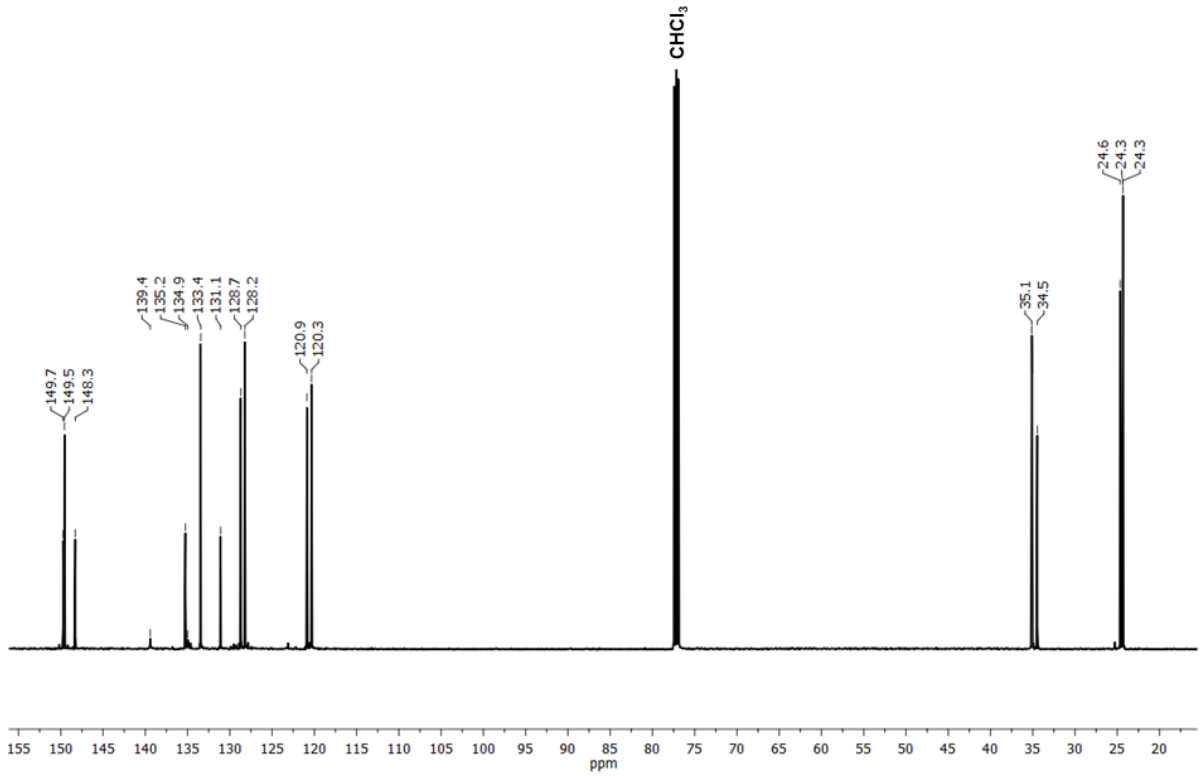

Figure S5.9.12. $^{13}C\{^{1}H\}$ NMR spectrum (125 MHz) of **8** in $CDCl_3$.

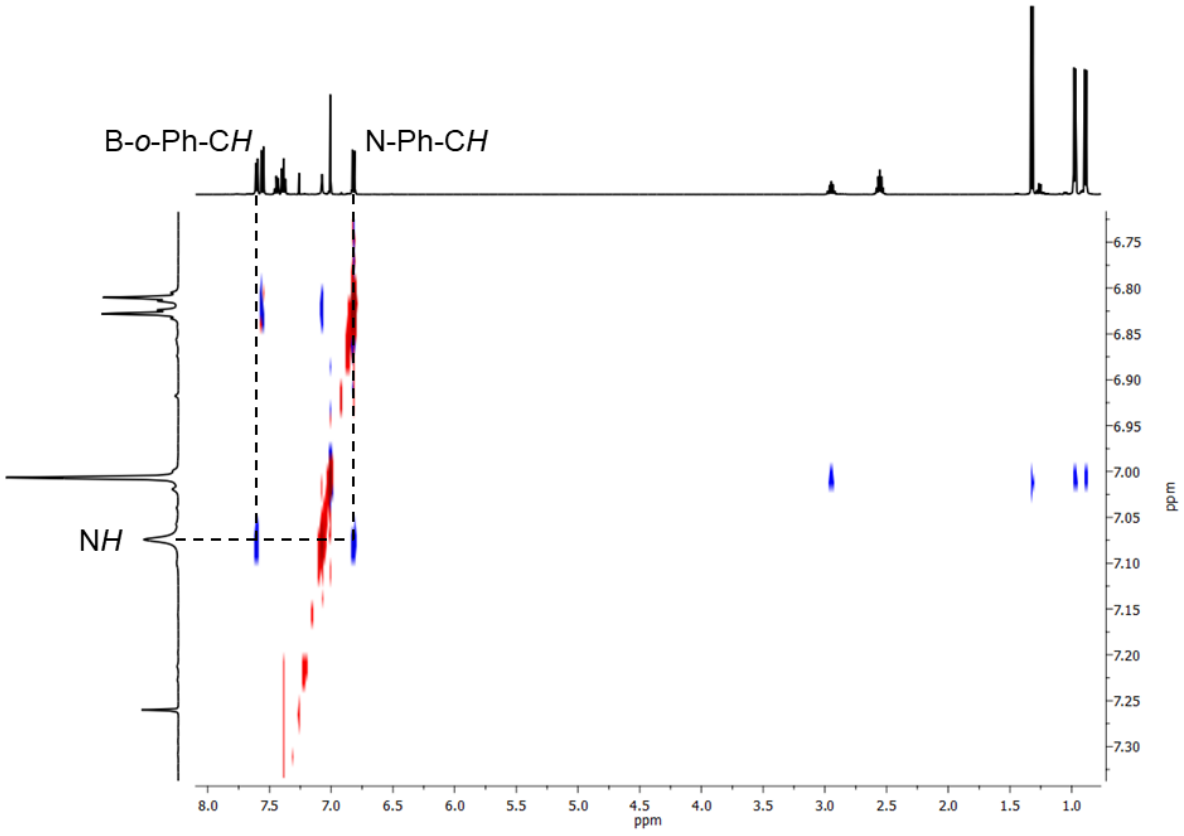

Figure S5.9.13. Detail of the ^{1}H, ^{1}H ROESY spectrum of **8** in $CDCl_3$.

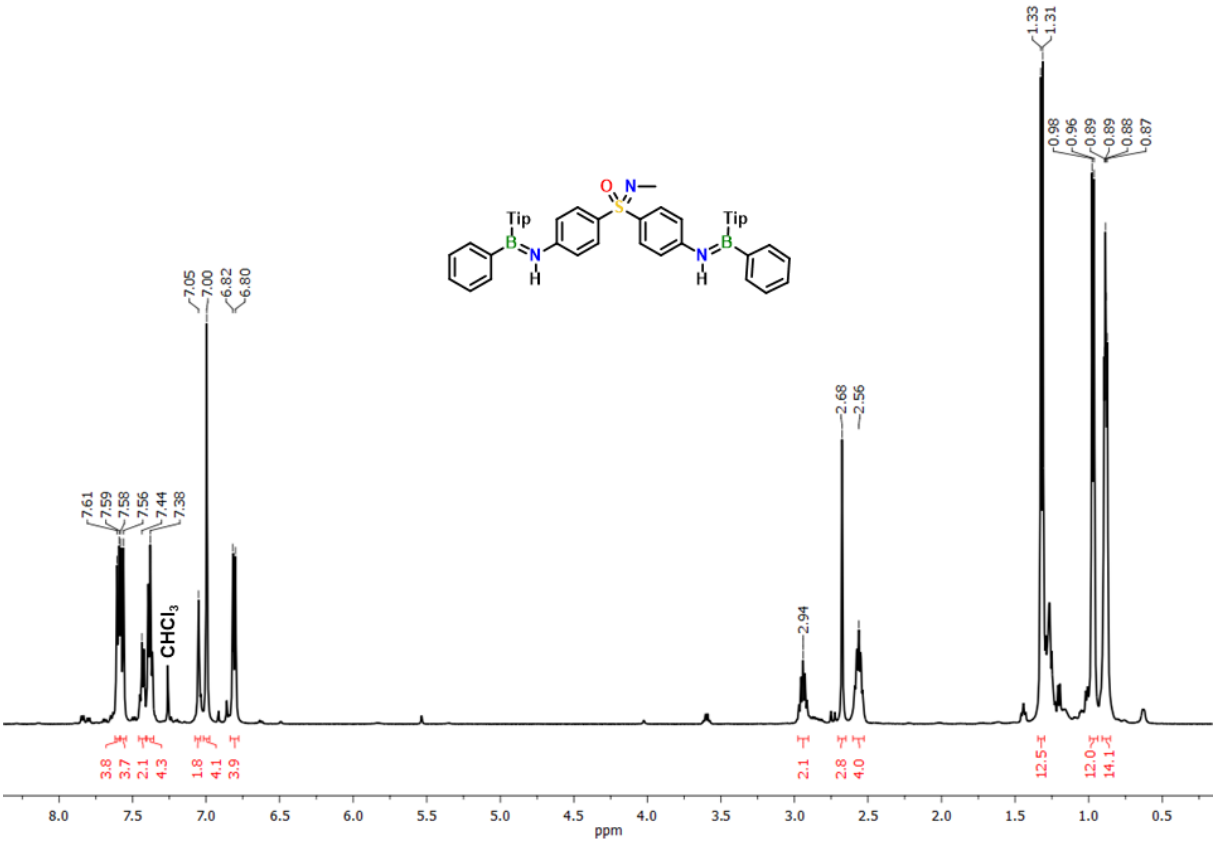

Figure S5.9.14. ^{1}H NMR spectrum (500 MHz) of **9a** in $CDCl_3$.

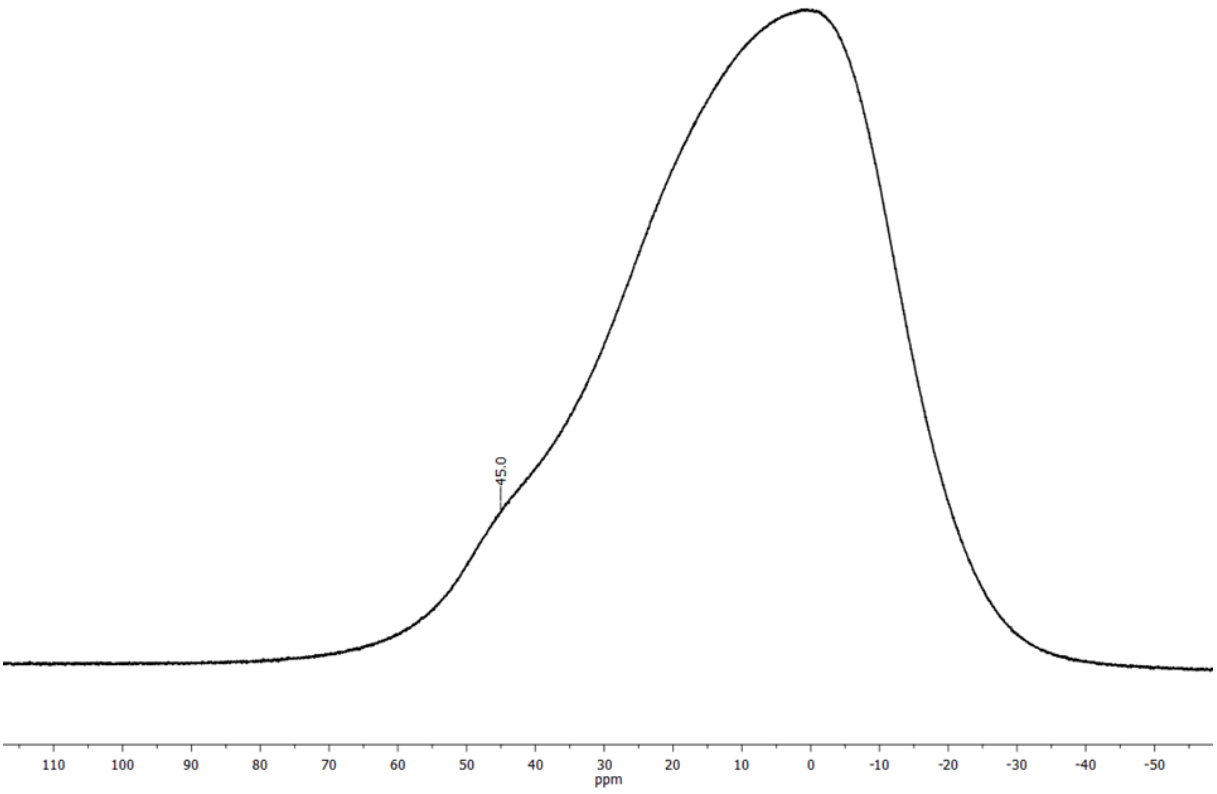

Figure S5.9.15. $^{11}B\{^{1}H\}$ NMR spectrum (160 MHz) of **9a** in $CDCl_3$.

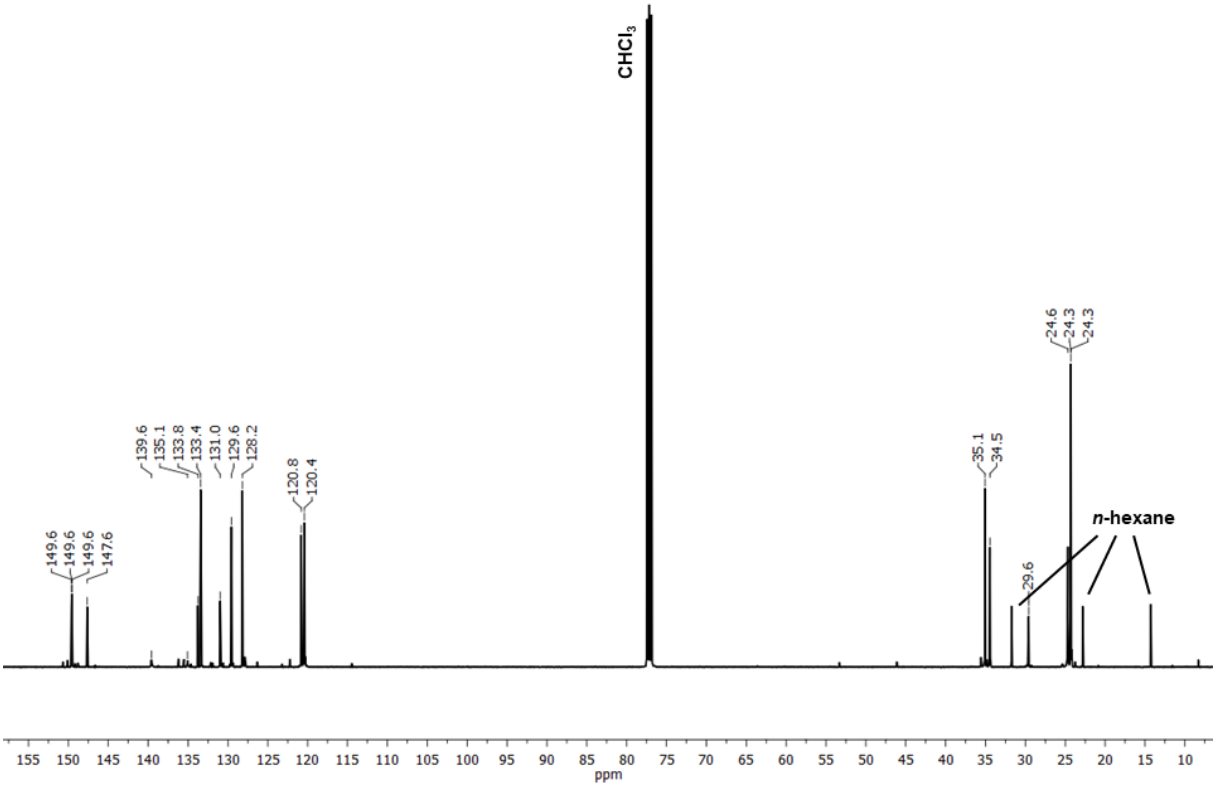

Figure S5.9.16. $^{13}C\{^{1}H\}$ NMR spectrum (125 MHz) of **9a** in $CDCl_3$.

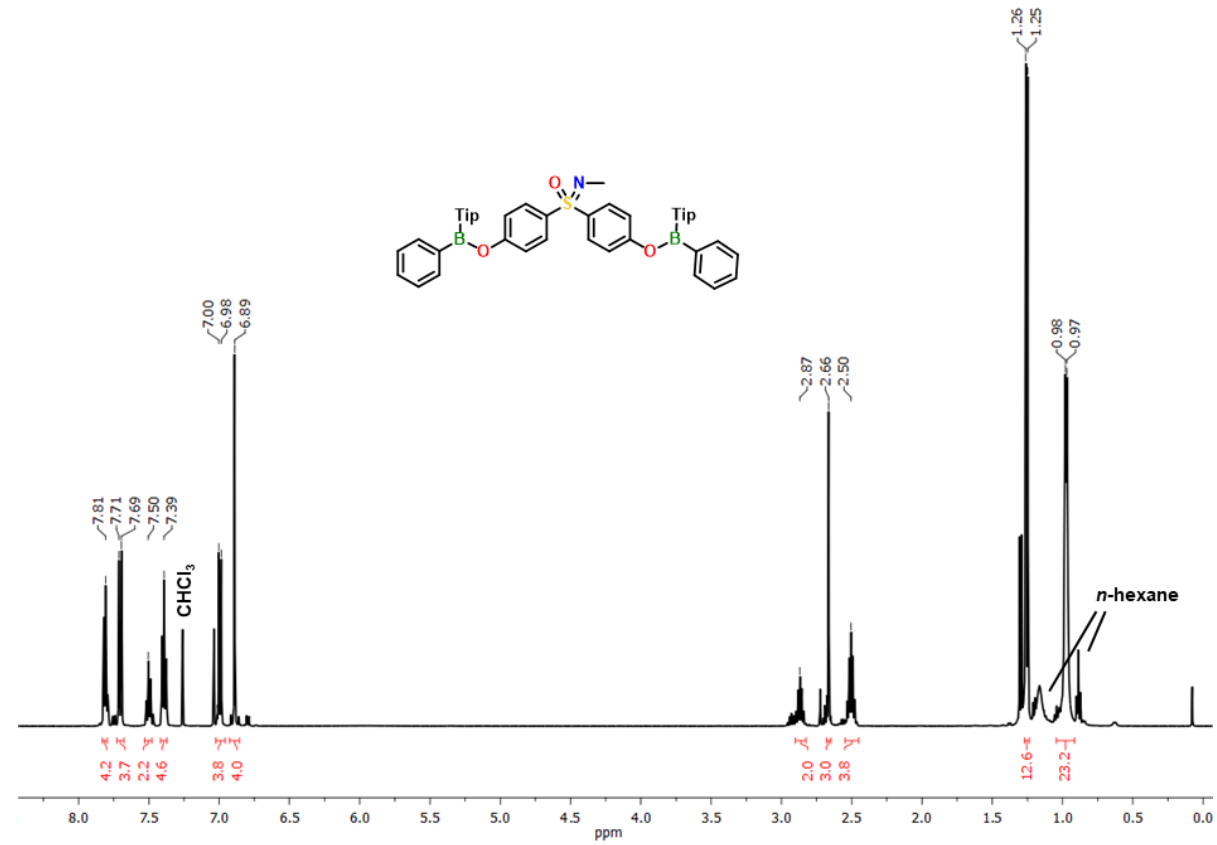

Figure S5.9.17. ^{1}H NMR spectrum (500 MHz) of **9b** in $CDCl_3$.

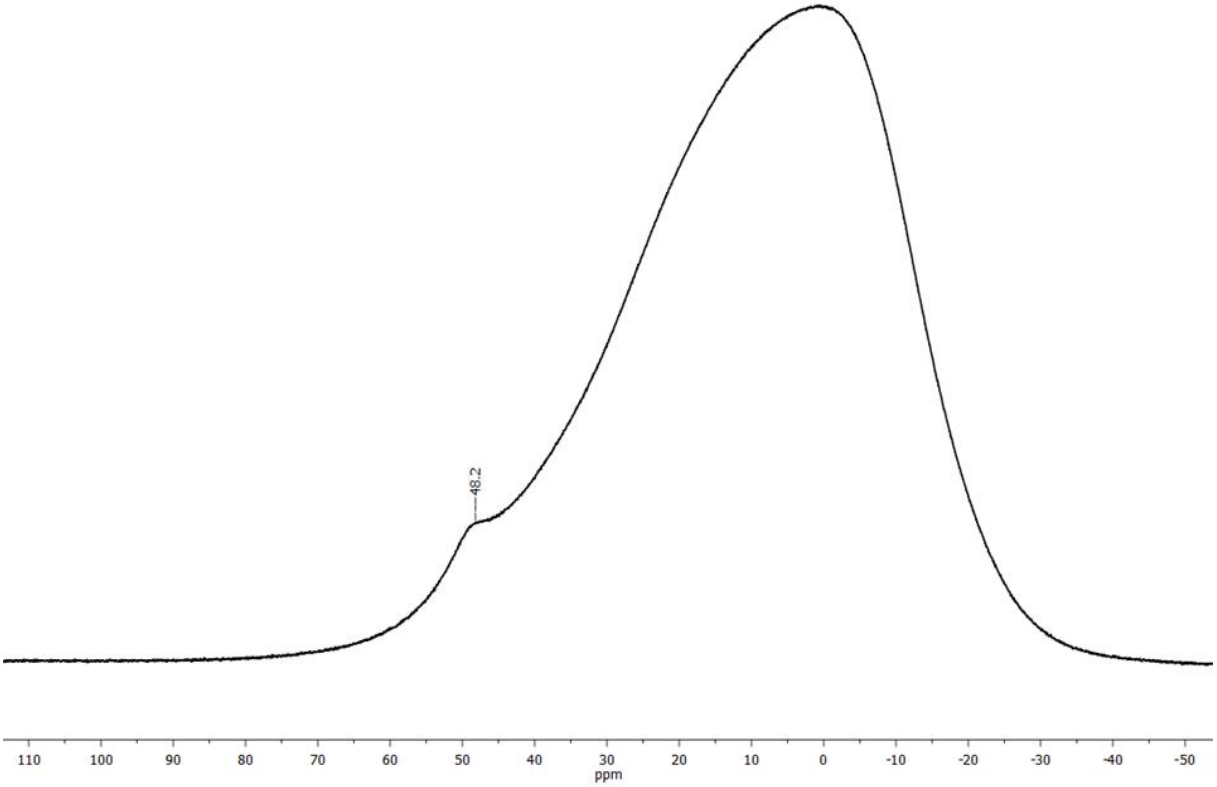

Figure S5.9.18. $^{11}B\{^{1}H\}$ NMR spectrum (160 MHz) of **9b** in $CDCl_3$.

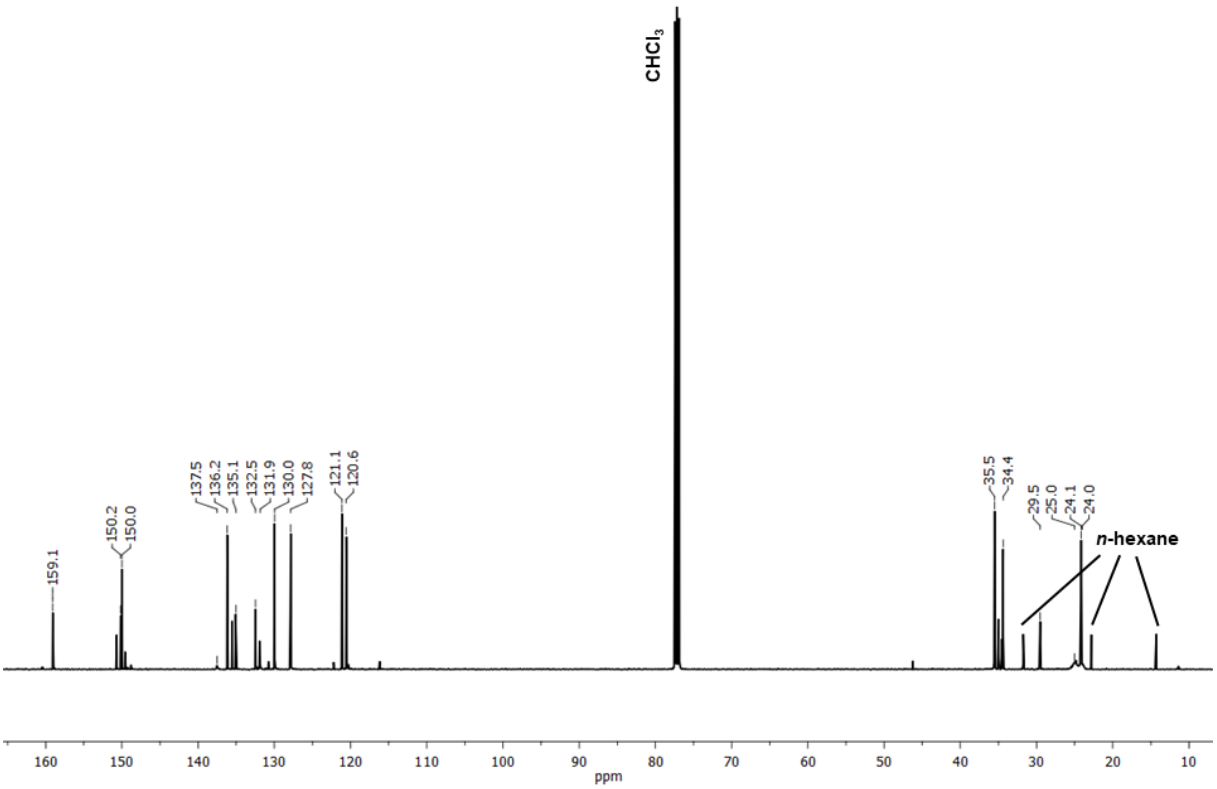

Figure S5.9.19. $^{13}C\{^{1}H\}$ NMR spectrum (125 MHz) of **9b** in $CDCl_3$.

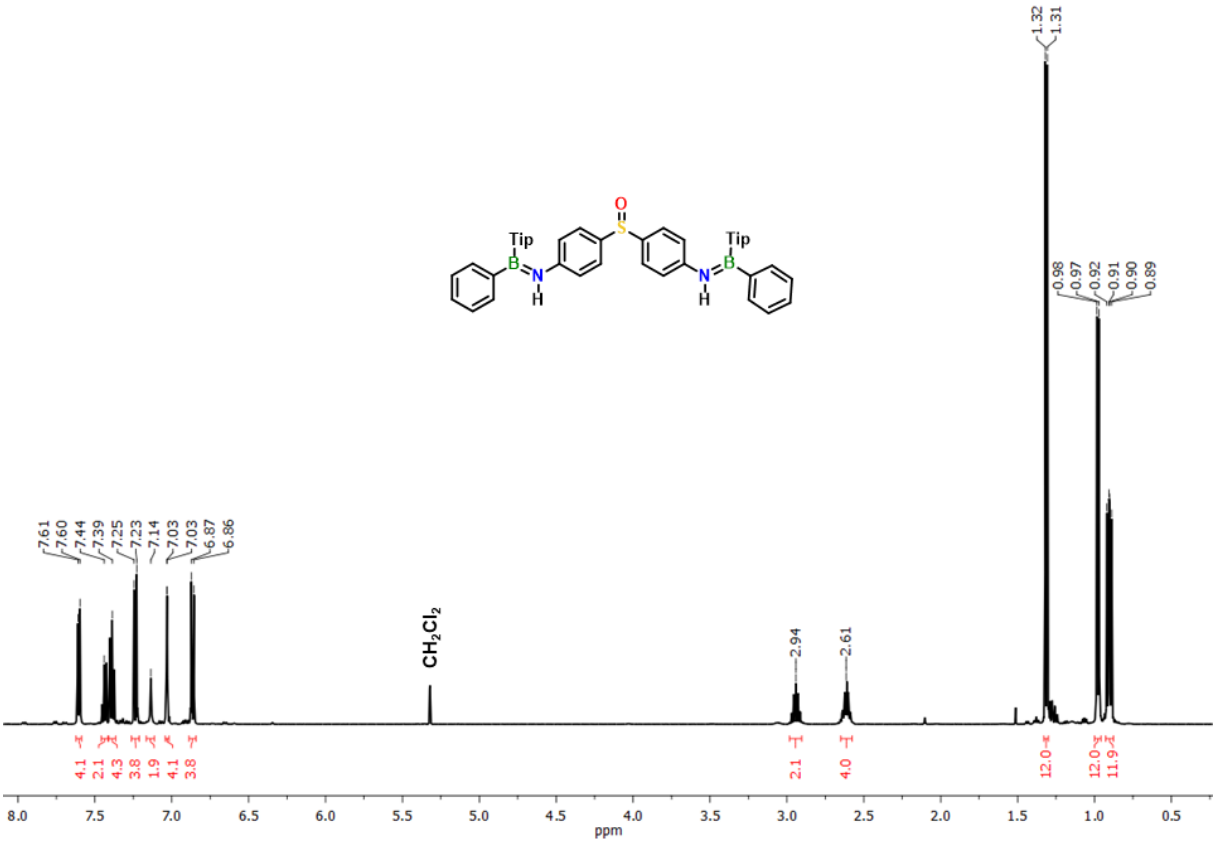

Figure S5.9.20. ^{1}H NMR spectrum (500 MHz) of **10a** in CD_2Cl_2.

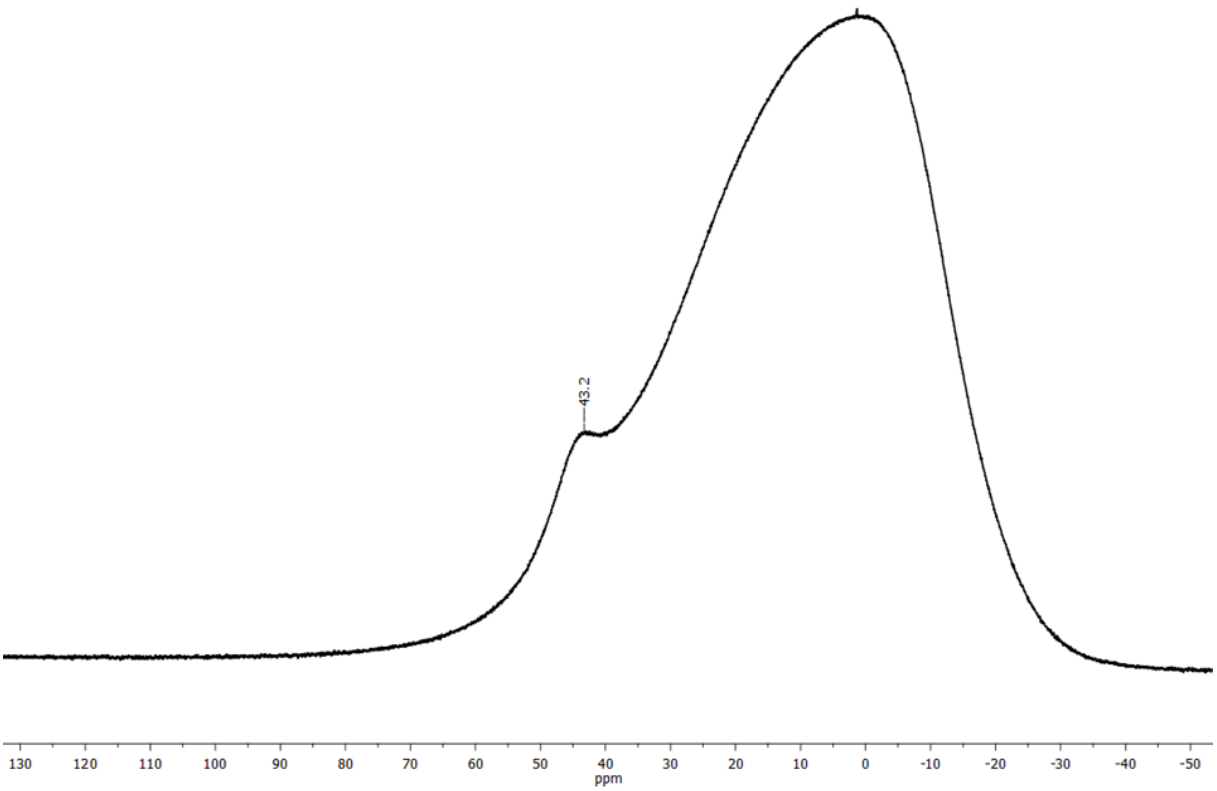

Figure S5.9.21. $^{11}B\{^{1}H\}$ NMR spectrum (160 MHz) of **10a** in CD_2Cl_2.

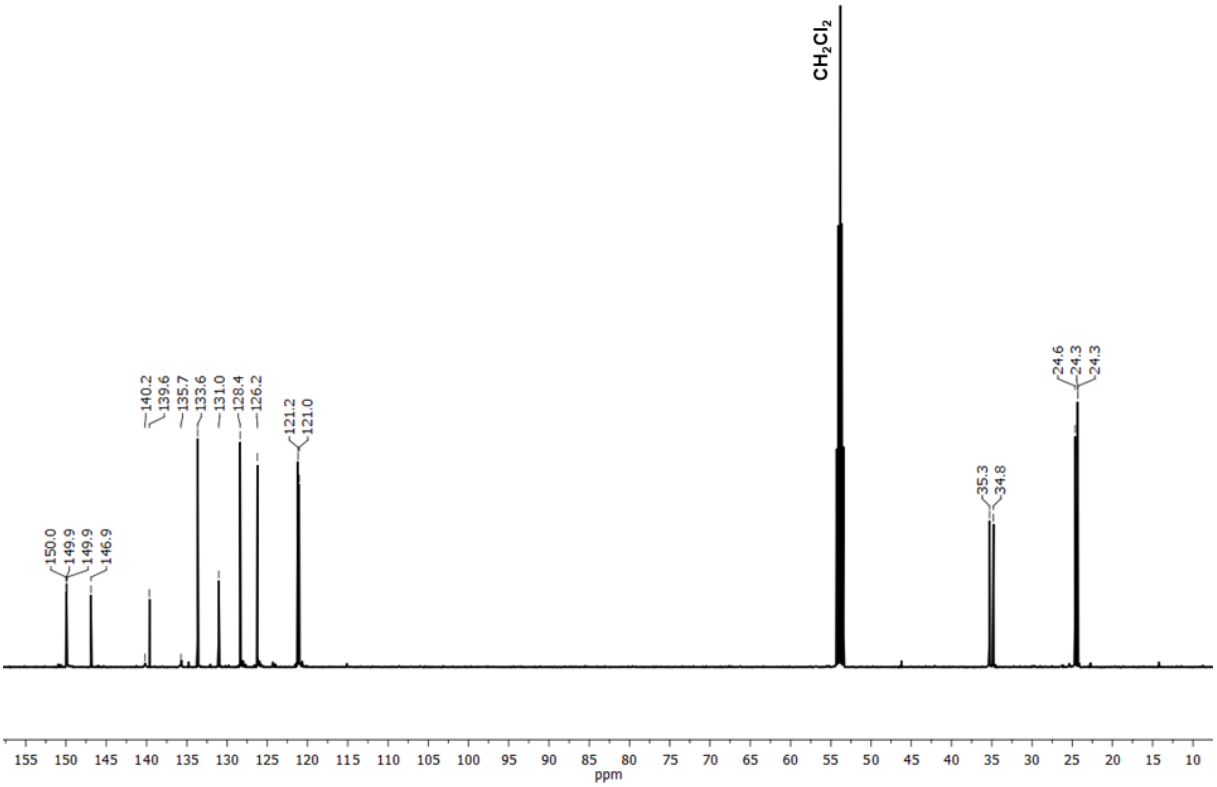

Figure S5.9.22. $^{13}C\{^{1}H\}$ NMR spectrum (125 MHz) of **10a** in CD_2Cl_2.

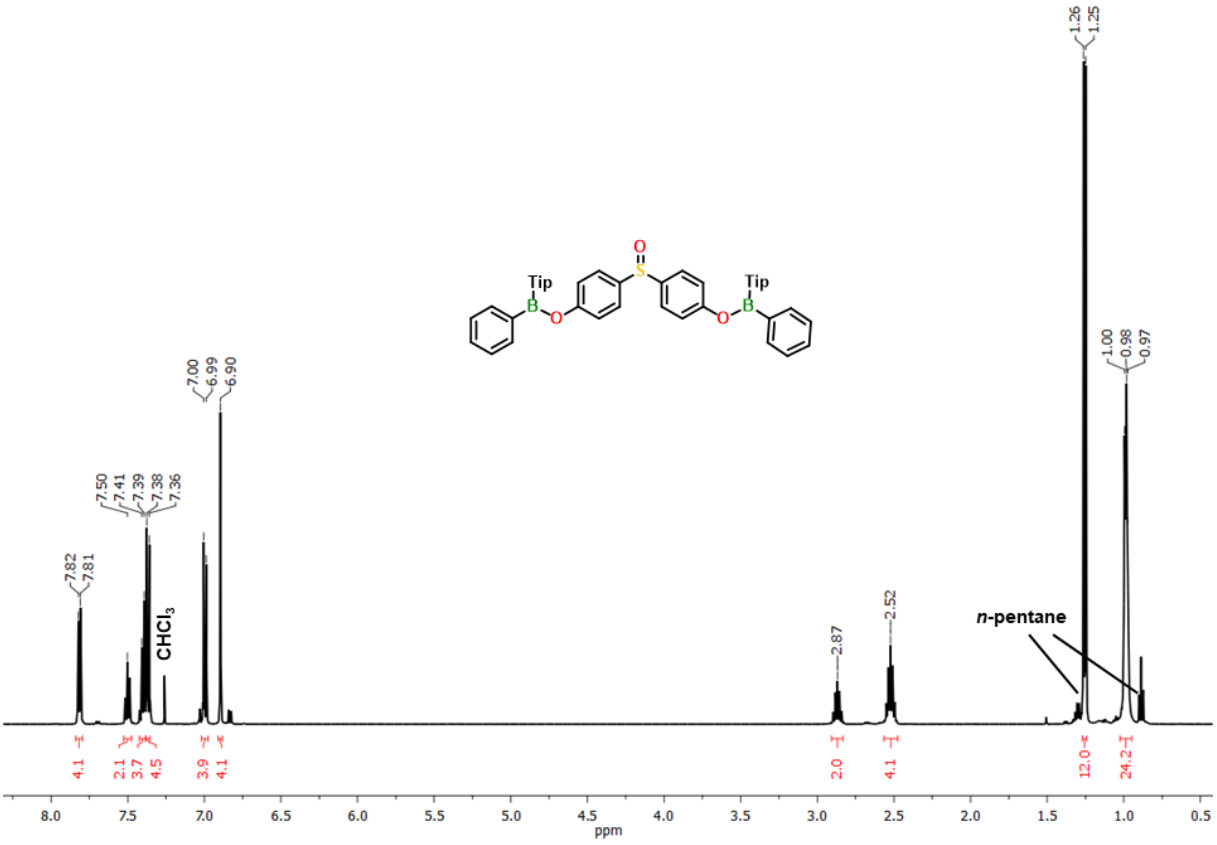

Figure S5.9.23. ^{1}H NMR spectrum (500 MHz) of **10b** in $CDCl_3$.

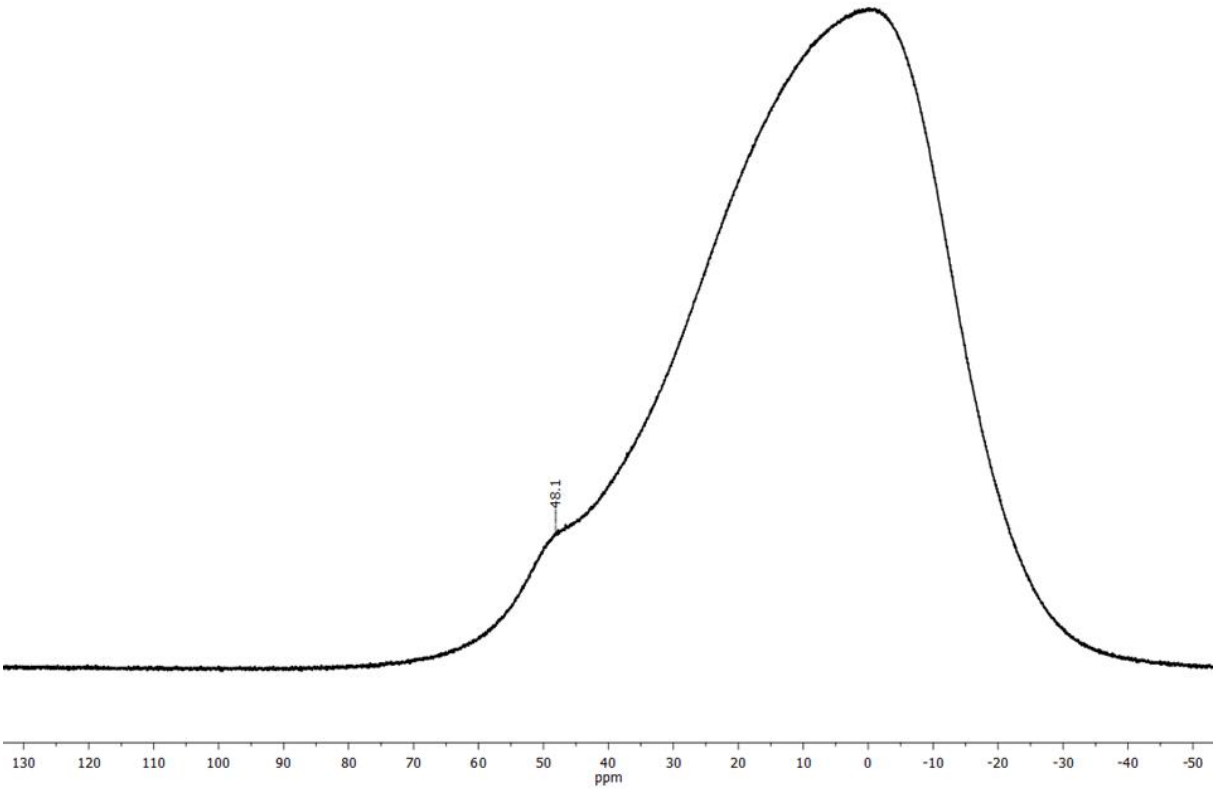

Figure S5.9.24. $^{11}B\{^{1}H\}$ NMR spectrum (160 MHz) of **10b** in $CDCl_3$.

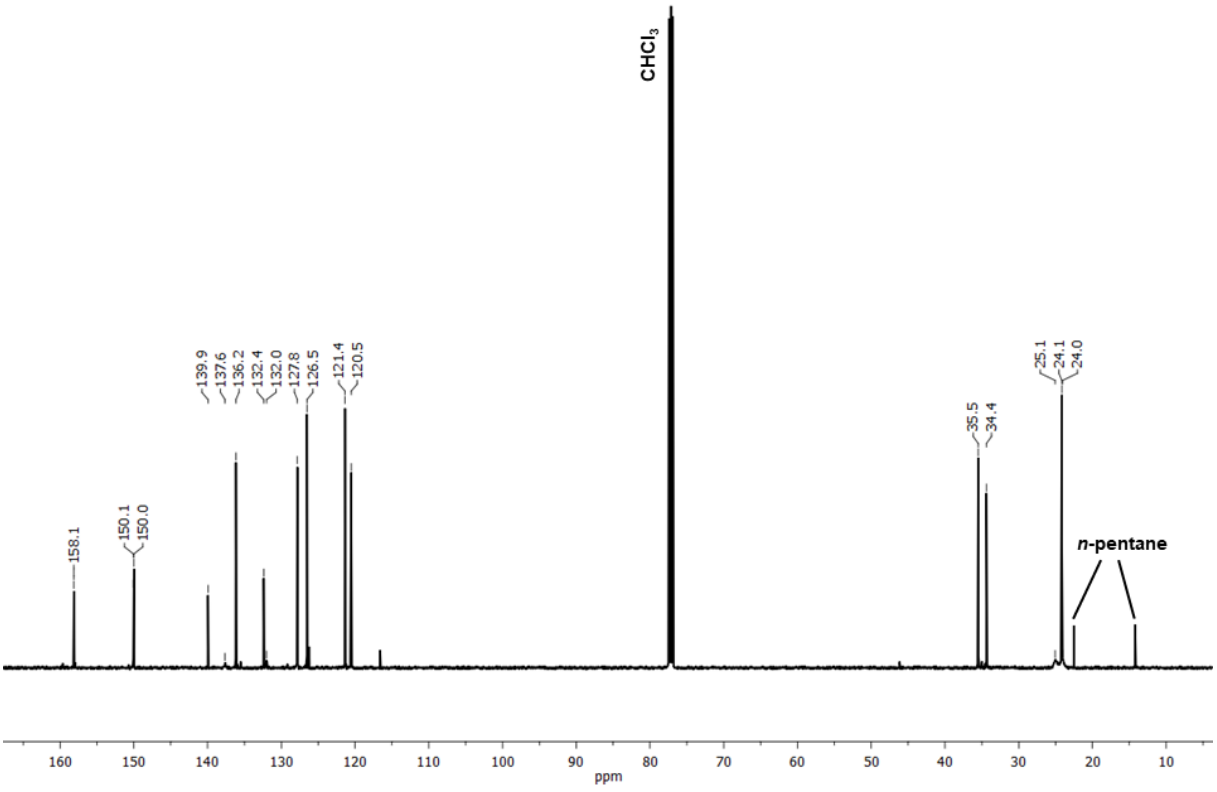

Figure S5.9.25. $^{13}C\{^{1}H\}$ NMR spectrum (125 MHz) of **10b** in $CDCl_3$.

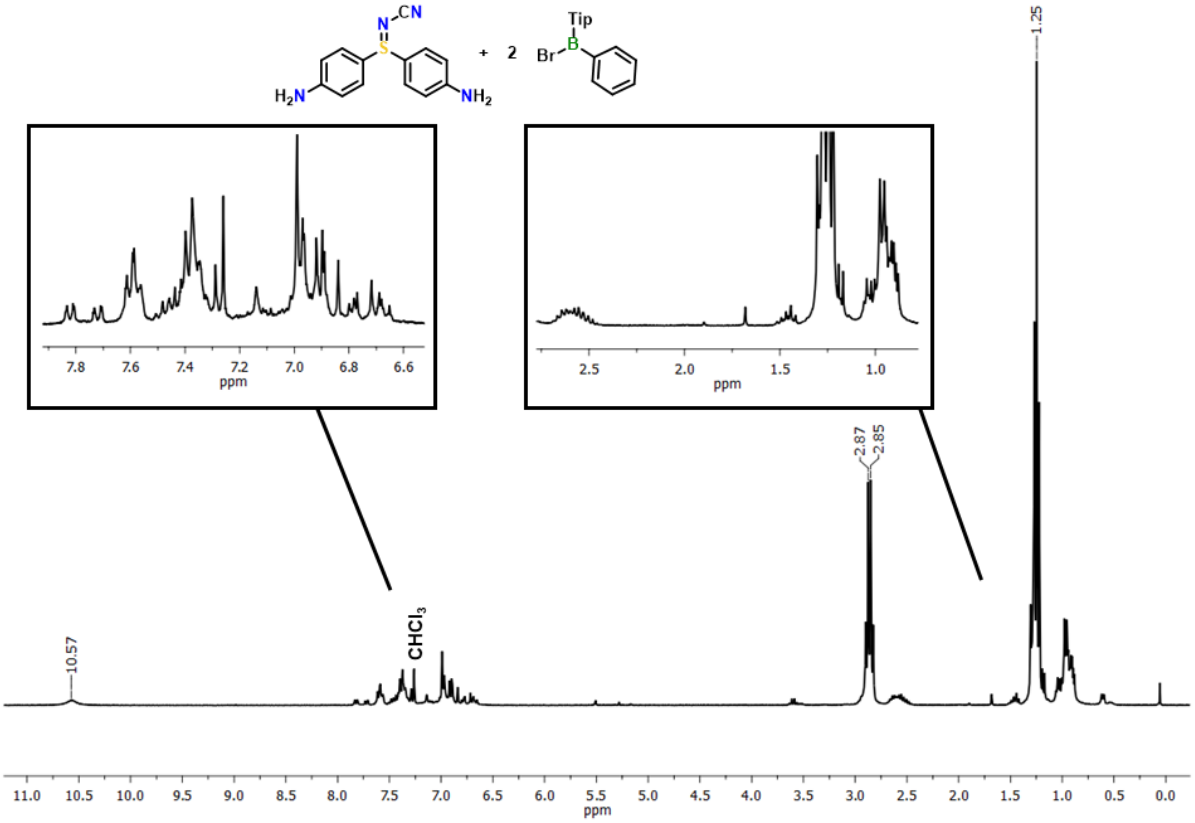

Figure S5.9.26. ^{1}H NMR spectrum (300 MHz) of the reaction of **3** with TipB(Ph)Br after 24 h in $CDCl_3$.

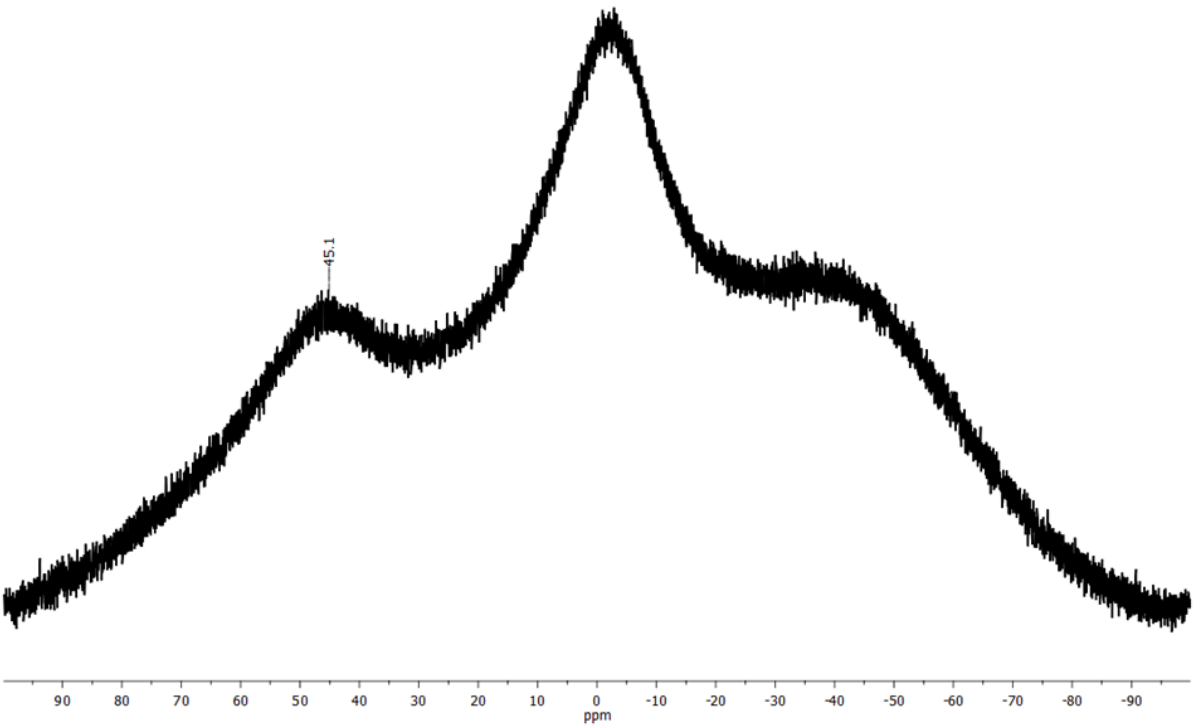

Figure S5.9.27. $^{11}B\{^{1}H\}$ NMR spectrum (96 MHz) of the reaction of **3** with TipB(Ph)Br after 24 h in $CDCl_3$.

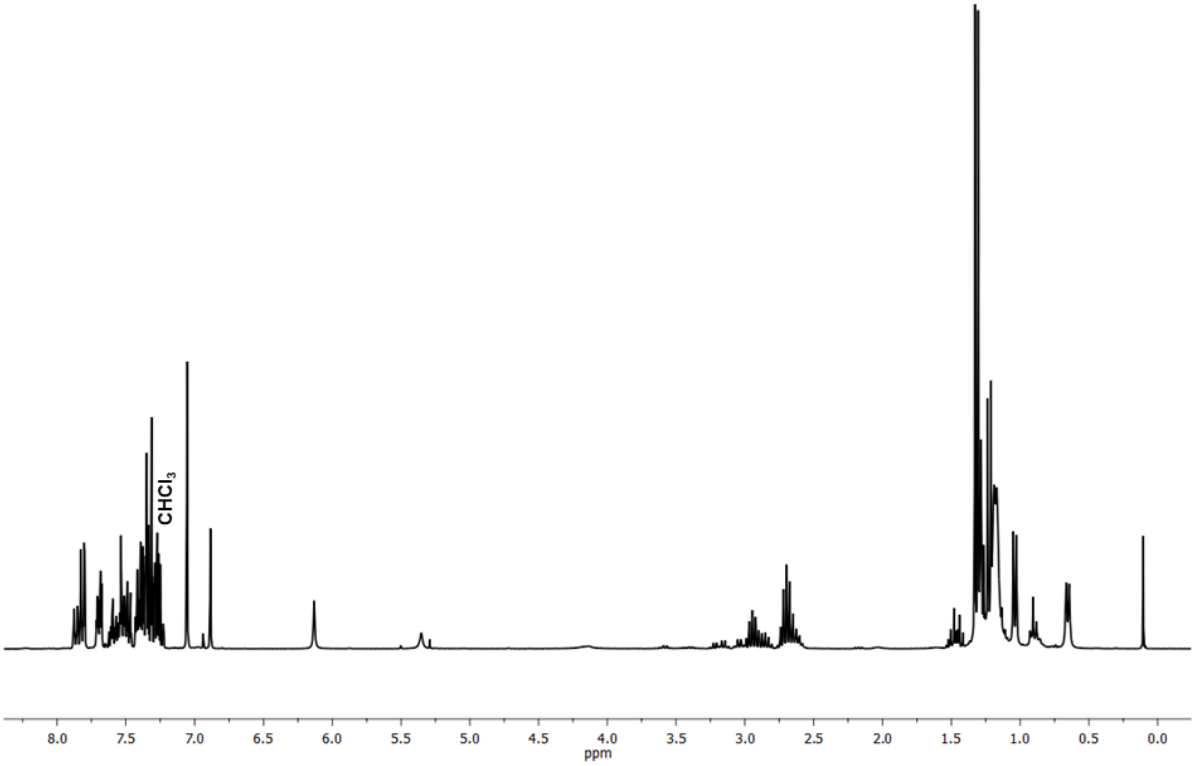

Figure S5.9.28. ^{1}H NMR spectrum (300 MHz) of the reaction of **12** with TipB(Ph)Br (*n*-hexane phase) in $CDCl_3$.

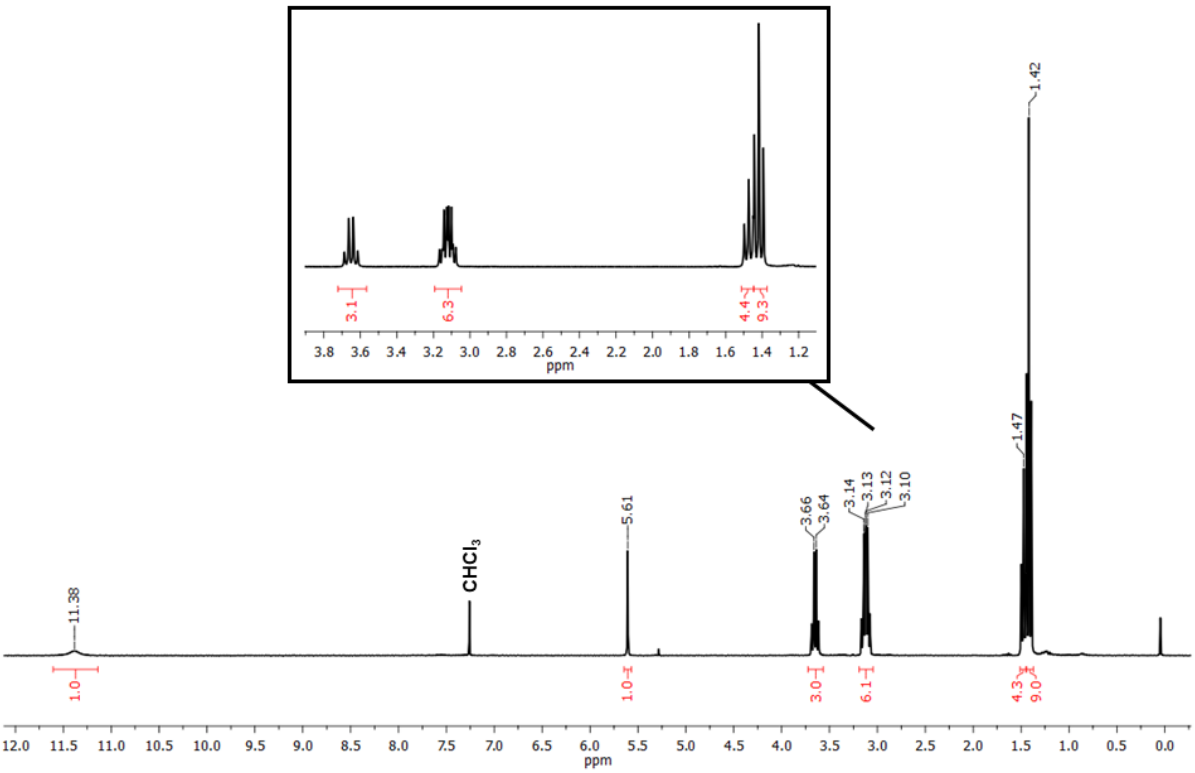

Figure S5.9.29. ^{1}H NMR spectrum (300 MHz) of the reaction of **12** with TipB(Ph)Br (residue) in $CDCl_3$.

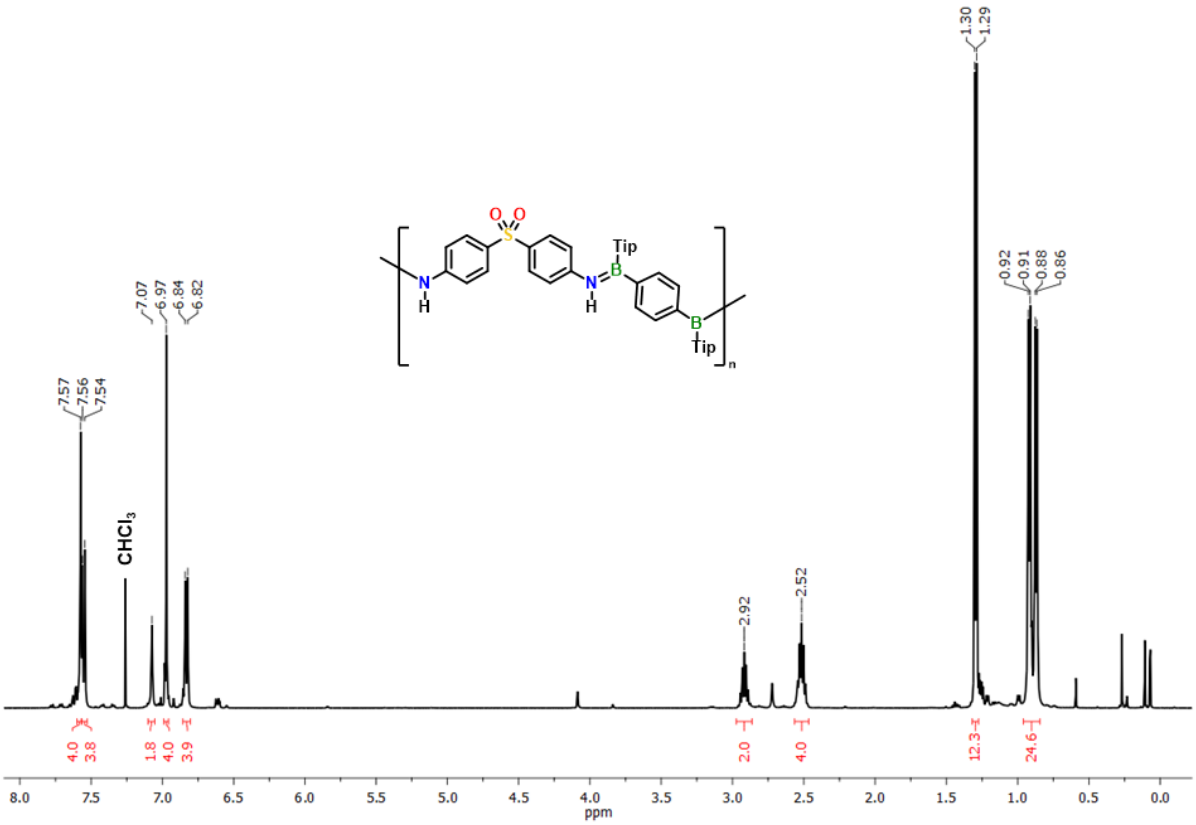

Figure S5.9.30. ^{1}H NMR spectrum (500 MHz) of **15** (Si/B exchange, CH_2Cl_2, r.t.) in $CDCl_3$.

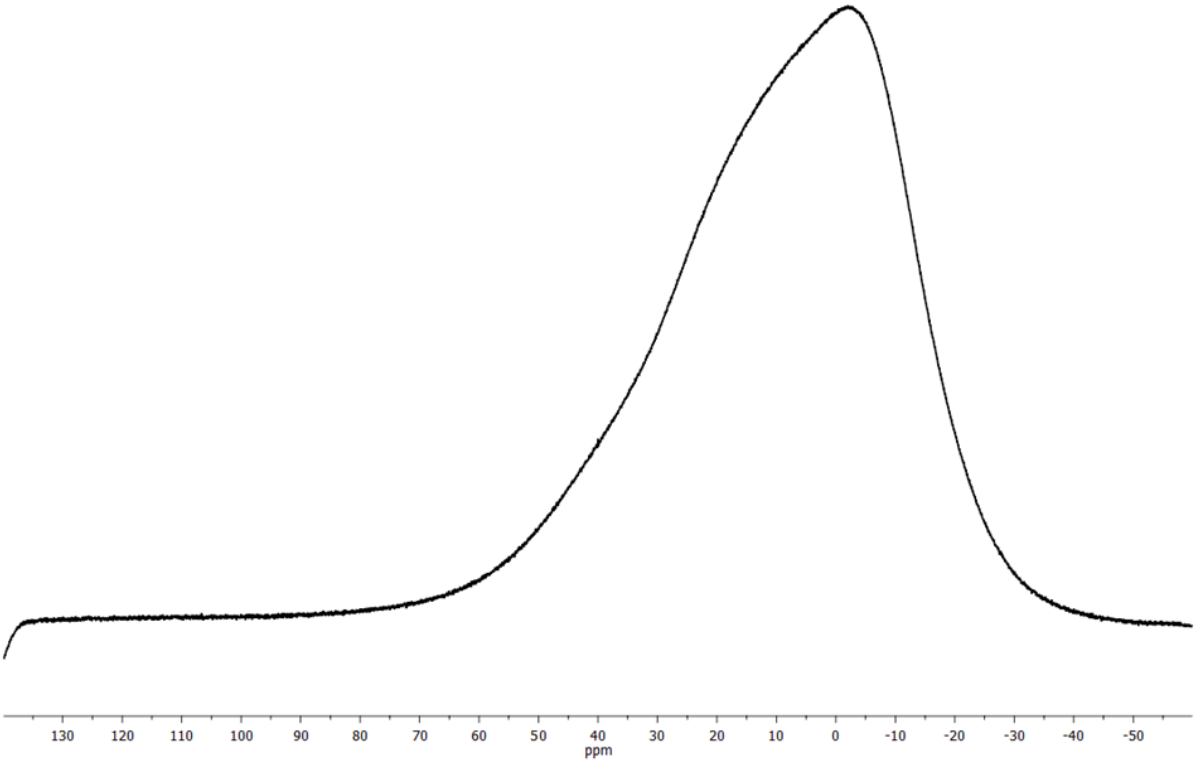

Figure S5.9.31. $^{11}B\{^{1}H\}$ NMR spectrum (160 MHz) of **15** (Si/B exchange, CH_2Cl_2, r.t.) in $CDCl_3$.

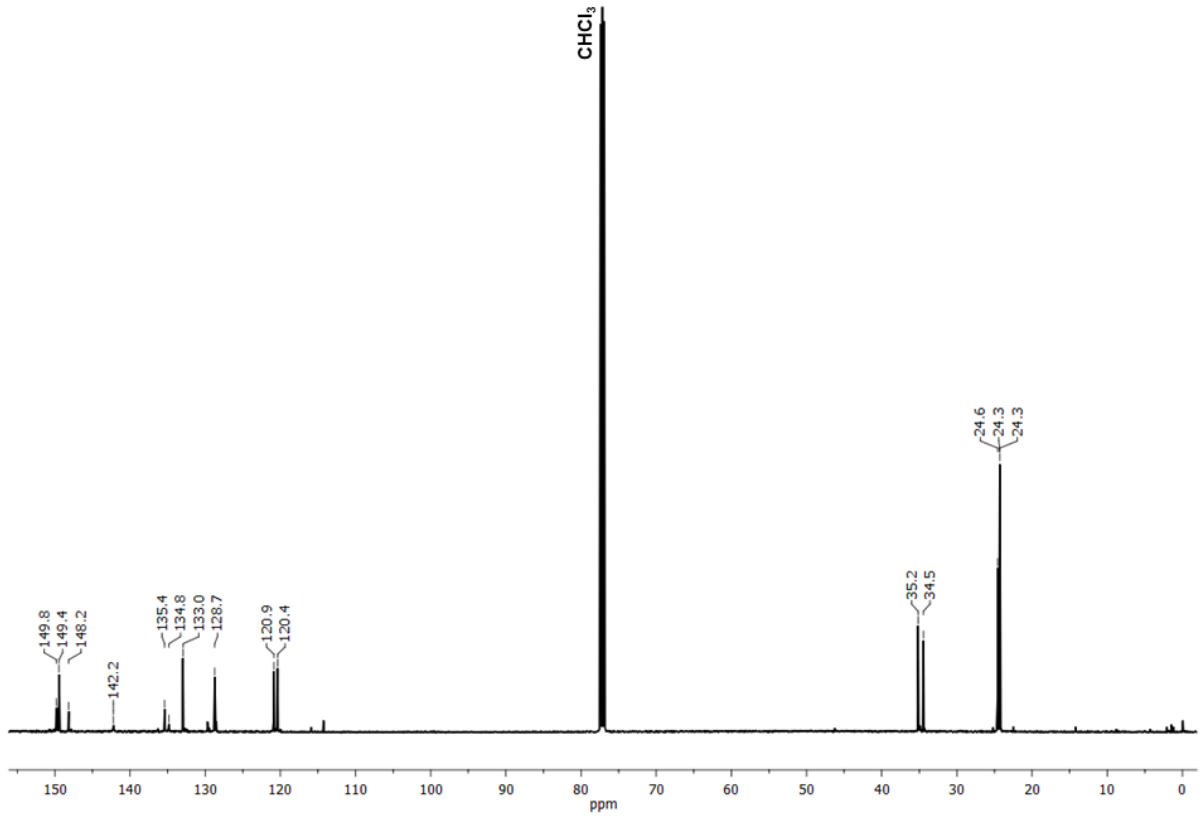

Figure S5.9.32. $^{13}C\{^{1}H\}$ NMR spectrum (125 MHz) of **15** (Si/B exchange, CH_2Cl_2, r.t.) in $CDCl_3$.

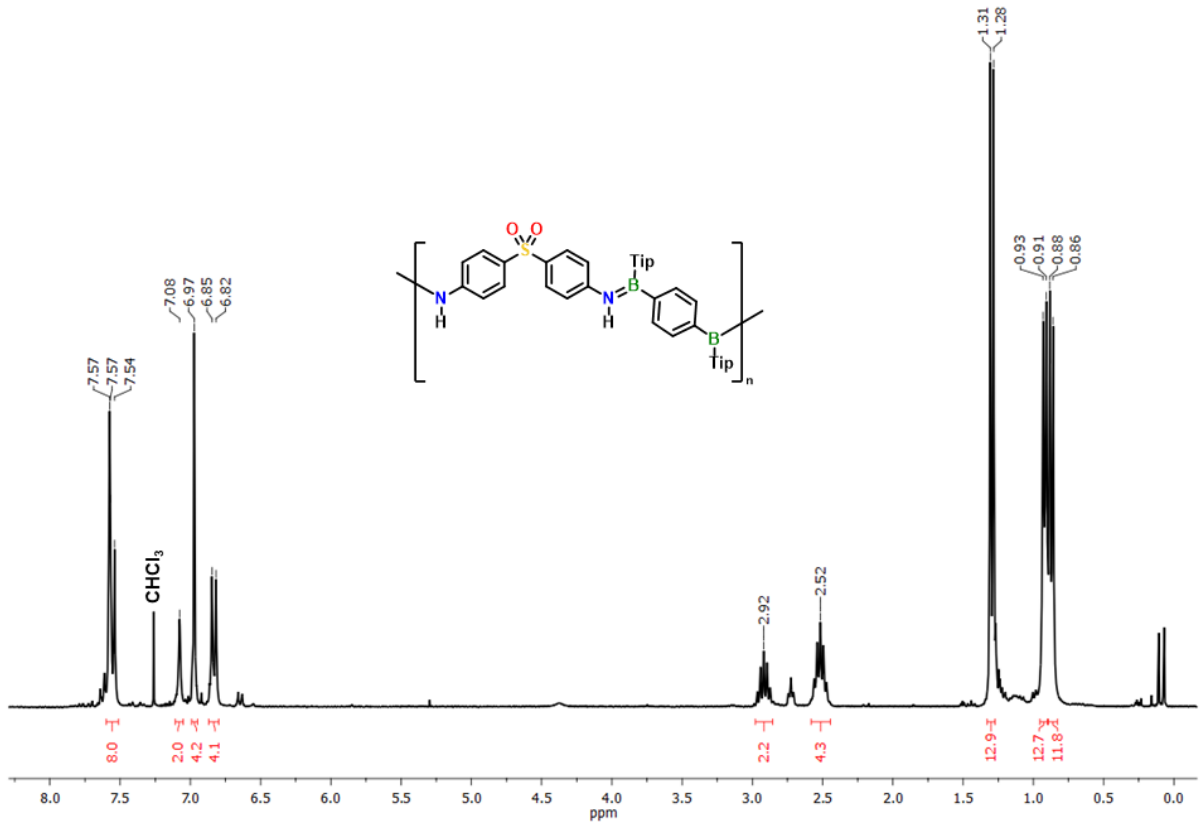

Figure S5.9.33. ^{1}H NMR spectrum (300 MHz) of **15** (Si/B exchange, *o*-DFB, 80 °C) in $CDCl_3$.

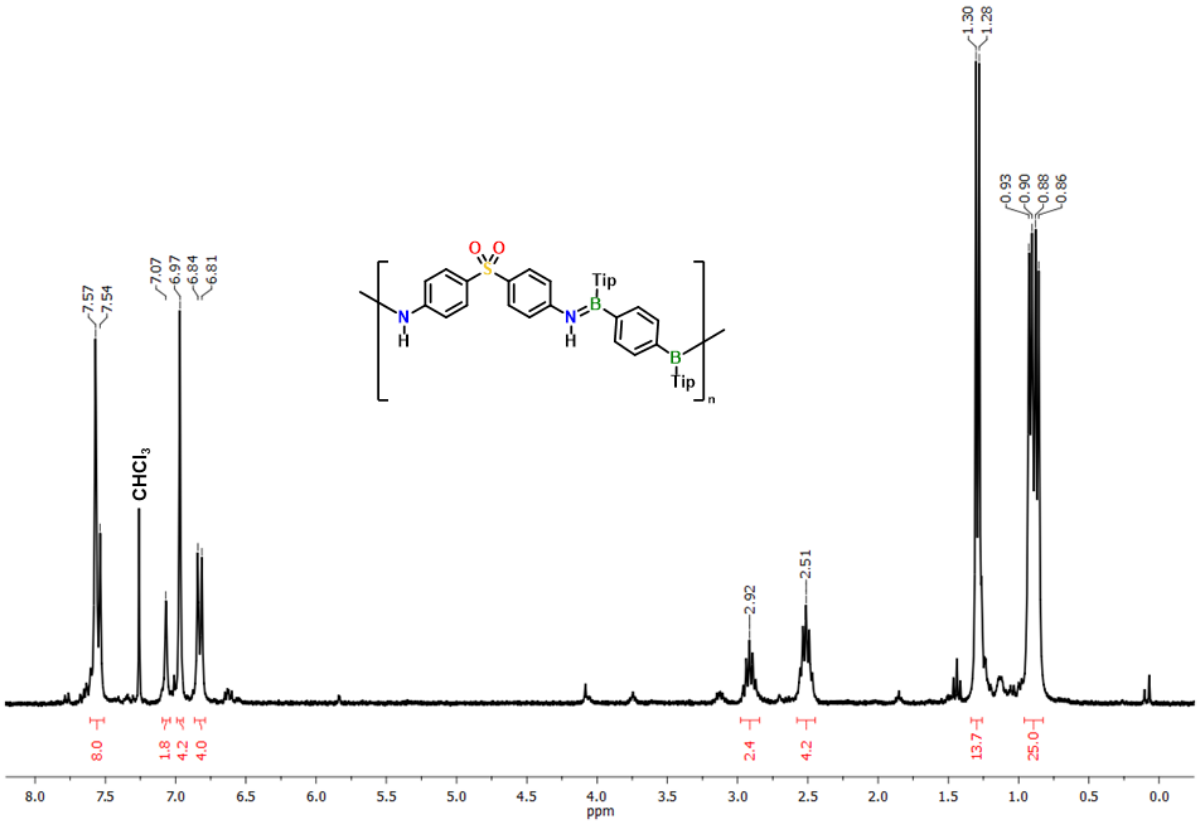

Figure S5.9.34. ^{1}H NMR spectrum (300 MHz) of **15** (salt elimination, CH_2Cl_2, r.t.) in $CDCl_3$.

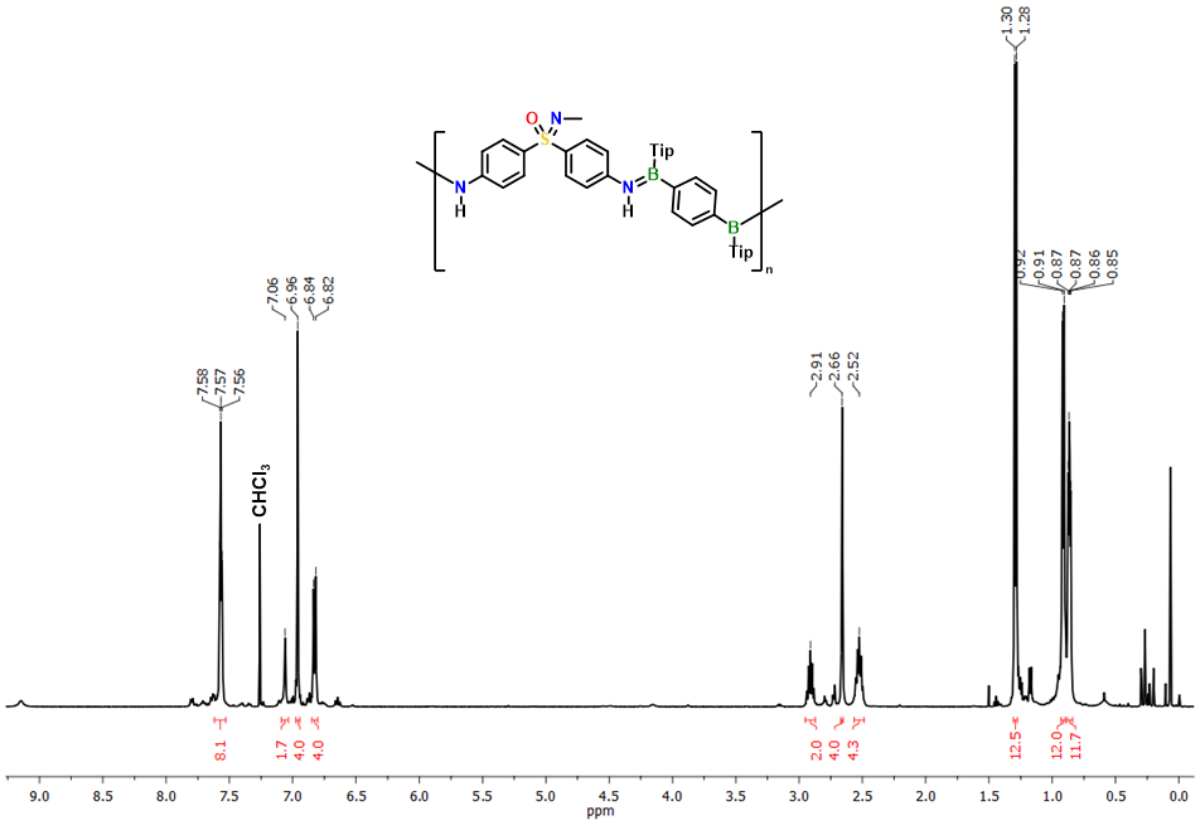

Figure S5.9.35. ^{1}H NMR spectrum (500 MHz) of **16** (Si/B exchange, CH_2Cl_2, r.t.) in $CDCl_3$.

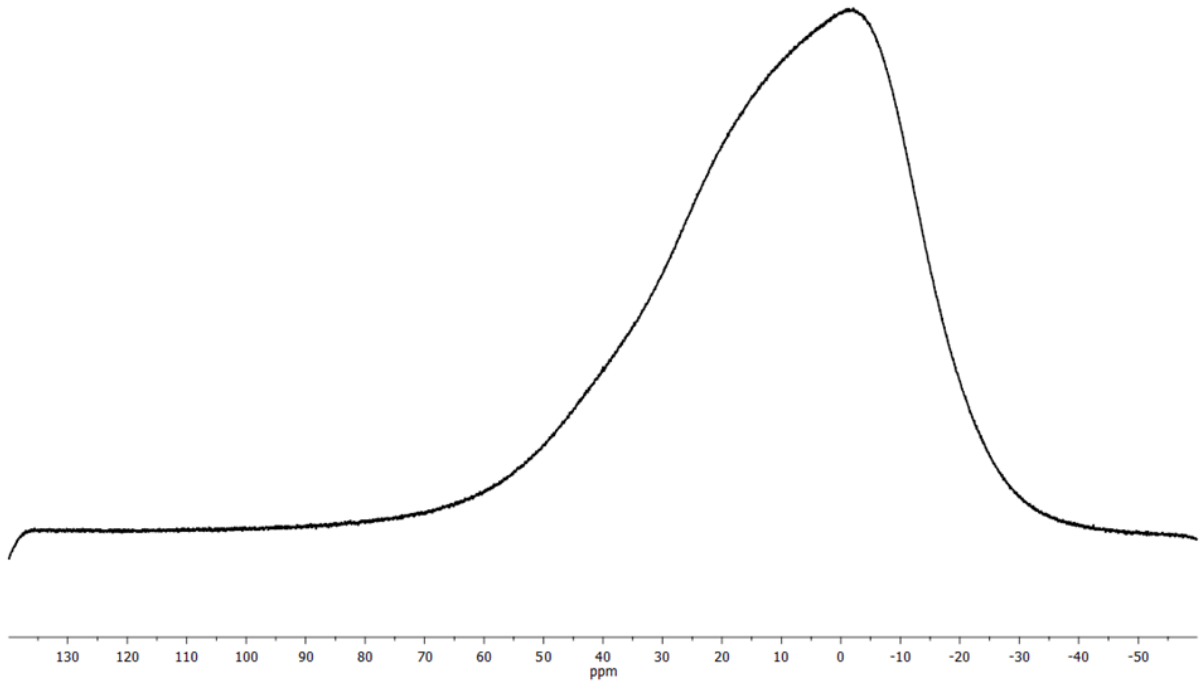

Figure S5.9.36. $^{11}B\{^{1}H\}$ NMR spectrum (160 MHz) of **16** (Si/B exchange, CH_2Cl_2, r.t.) in $CDCl_3$.

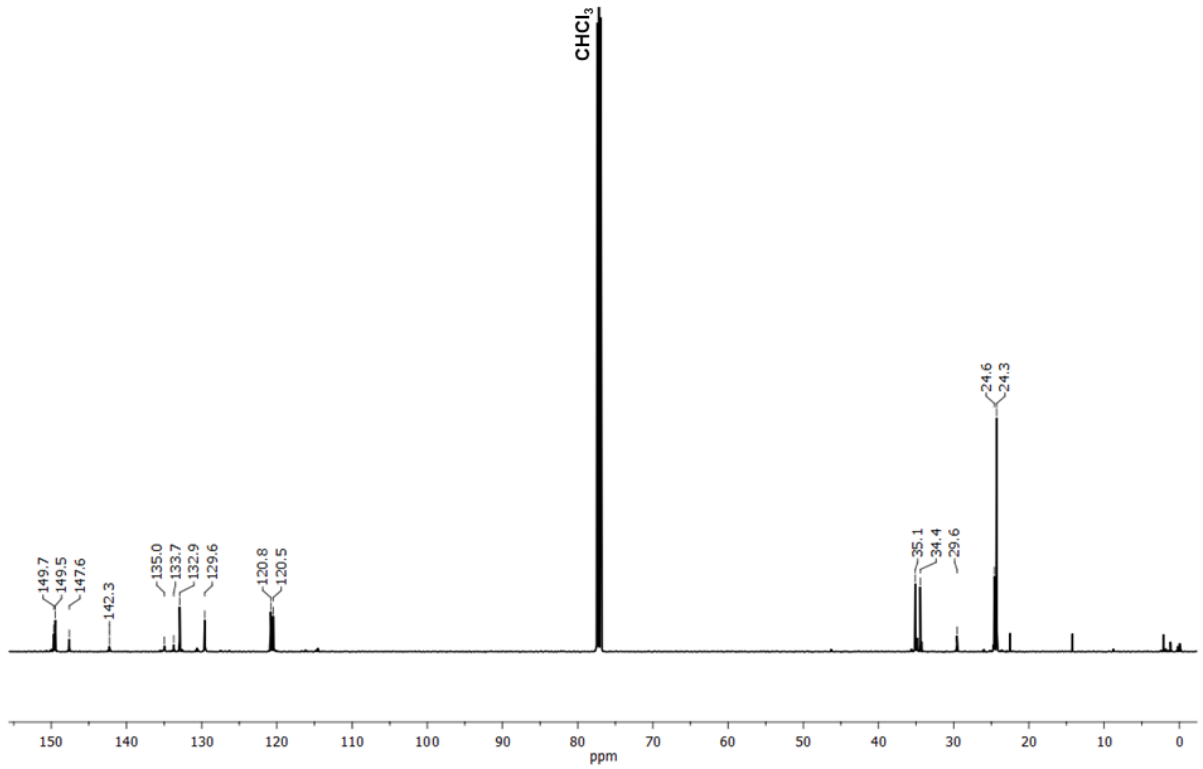

Figure S5.9.37. $^{13}C\{^{1}H\}$ NMR spectrum (125 MHz) of **16** (Si/B exchange, CH_2Cl_2, r.t.) in $CDCl_3$.

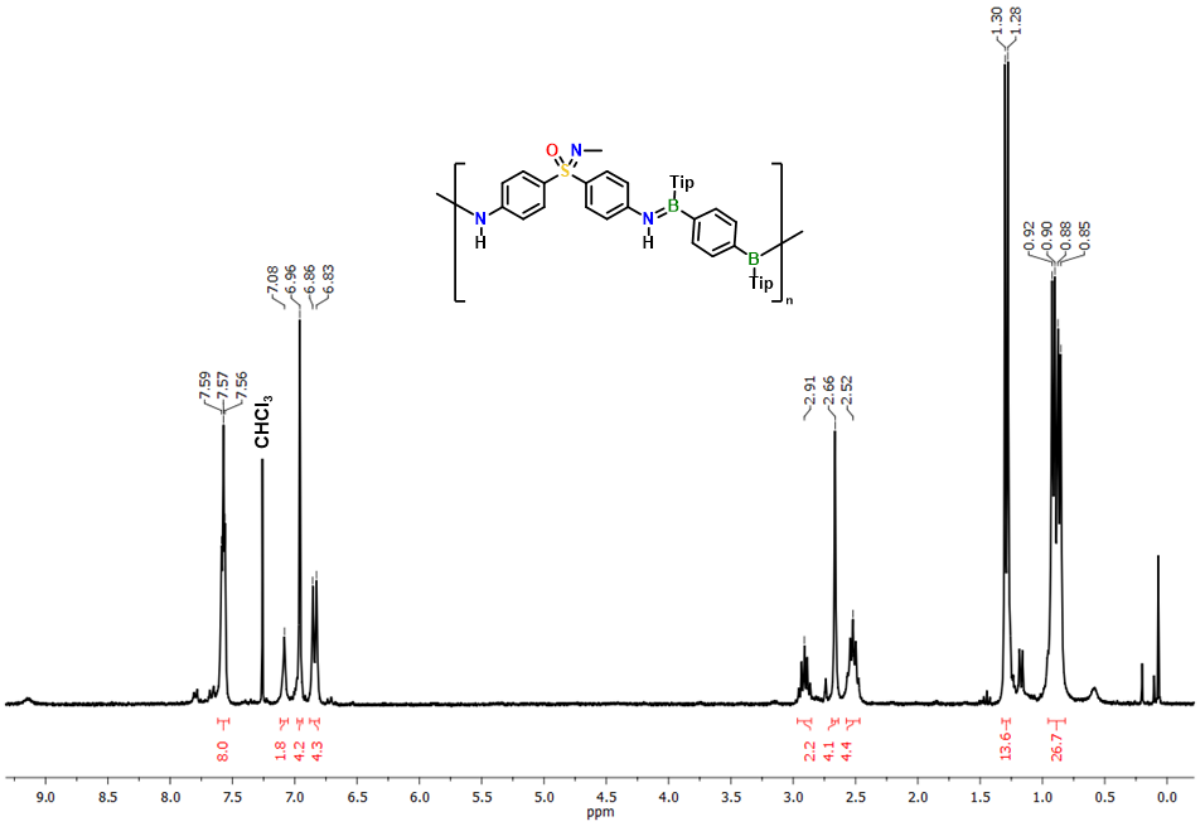

Figure S5.9.38. ^{1}H NMR spectrum (300 MHz) of **16** (Si/B exchange, *o*-DFB, 80 °C) in $CDCl_3$.

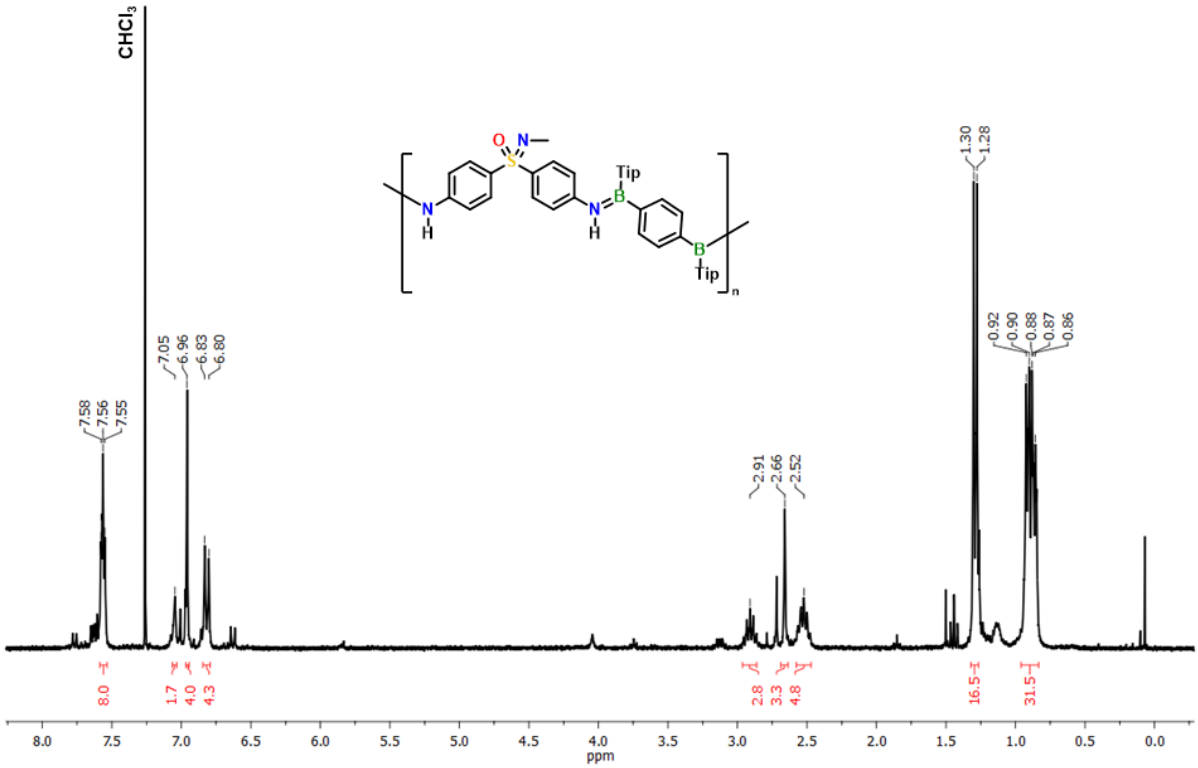

Figure S5.9.39. ^{1}H NMR spectrum (300 MHz) of **16** (salt elimination, CH_2Cl_2, r.t.) in $CDCl_3$.

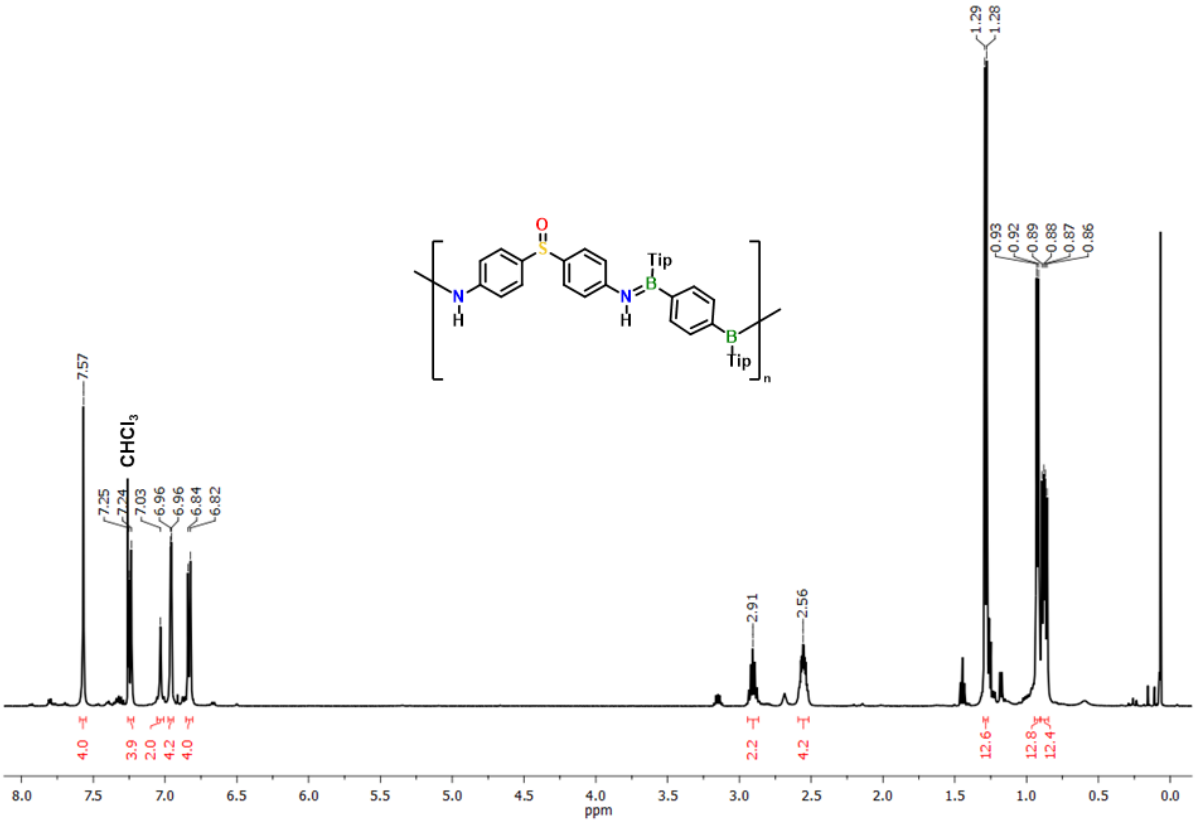

Figure S5.9.40. ^{1}H NMR spectrum (500 MHz) of **17** (Si/B exchange, CH_2Cl_2, r.t.) in $CDCl_3$.

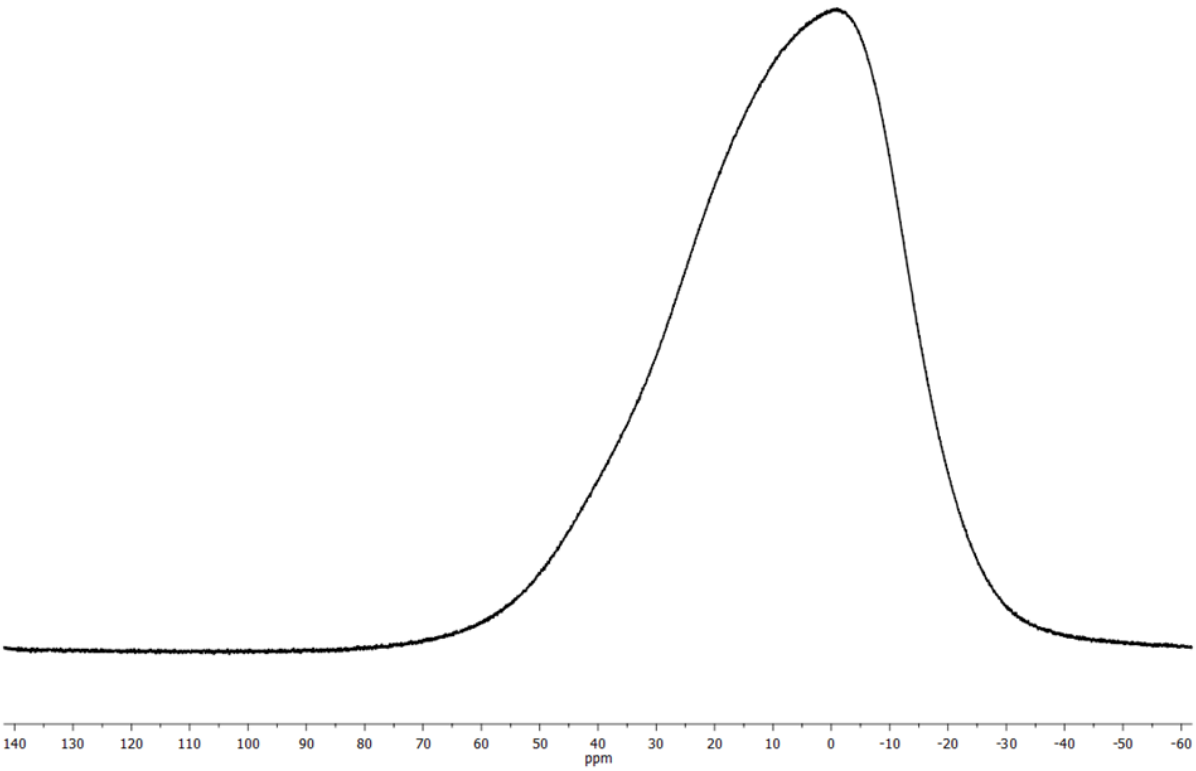

Figure S5.9.41. $^{11}B\{^{1}H\}$ NMR spectrum (160 MHz) of **17** (Si/B exchange, CH_2Cl_2, r.t.) in $CDCl_3$.

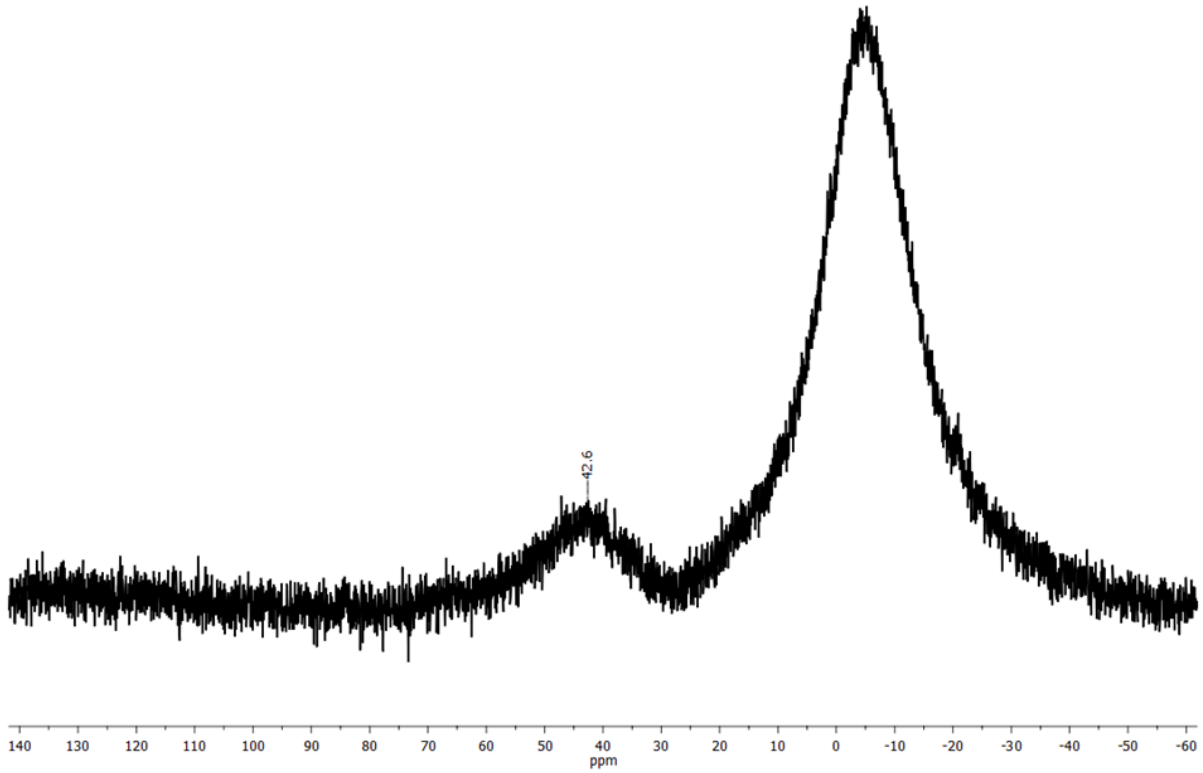

Figure S5.9.42. $^{11}B\{^{1}H\}$ NMR spectrum (160 MHz) of **17** (Si/B exchange, CH_2Cl_2, r.t.) with reduced glass background in $CDCl_3$.

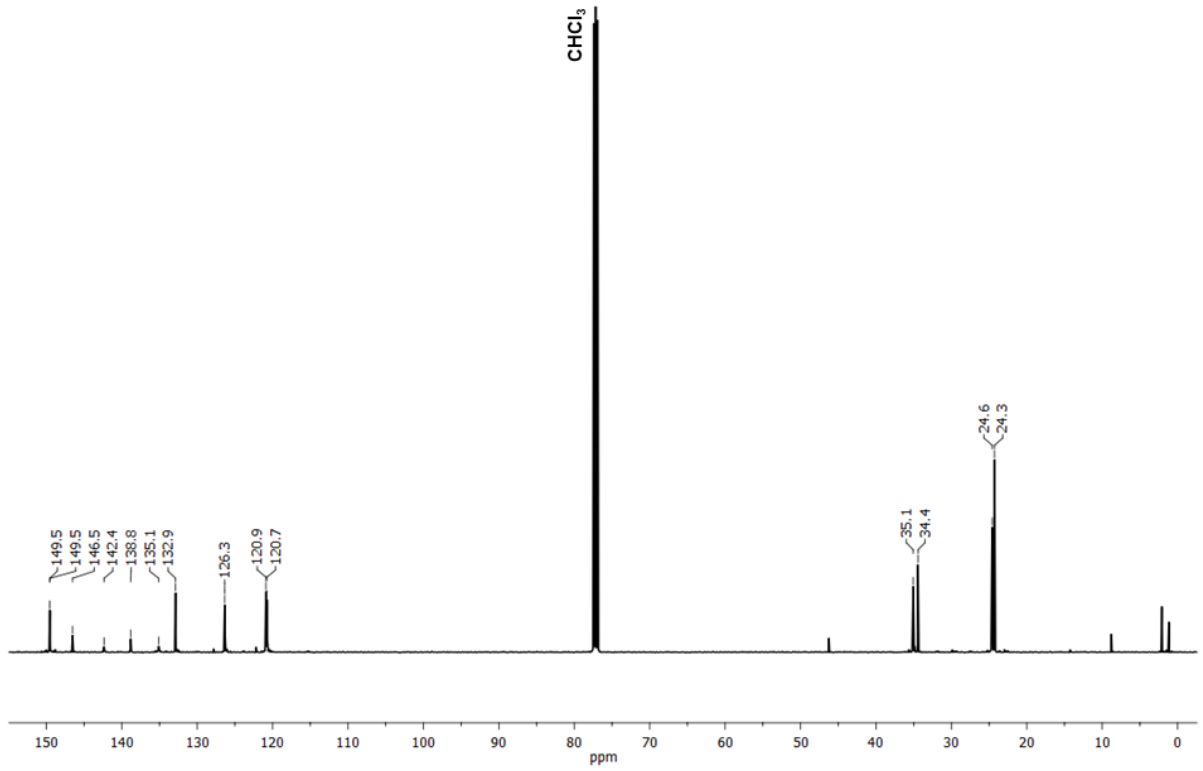

Figure S5.9.43. $^{13}C\{^{1}H\}$ NMR spectrum (125 MHz) of **17** (Si/B exchange, CH_2Cl_2, r.t.) in $CDCl_3$.

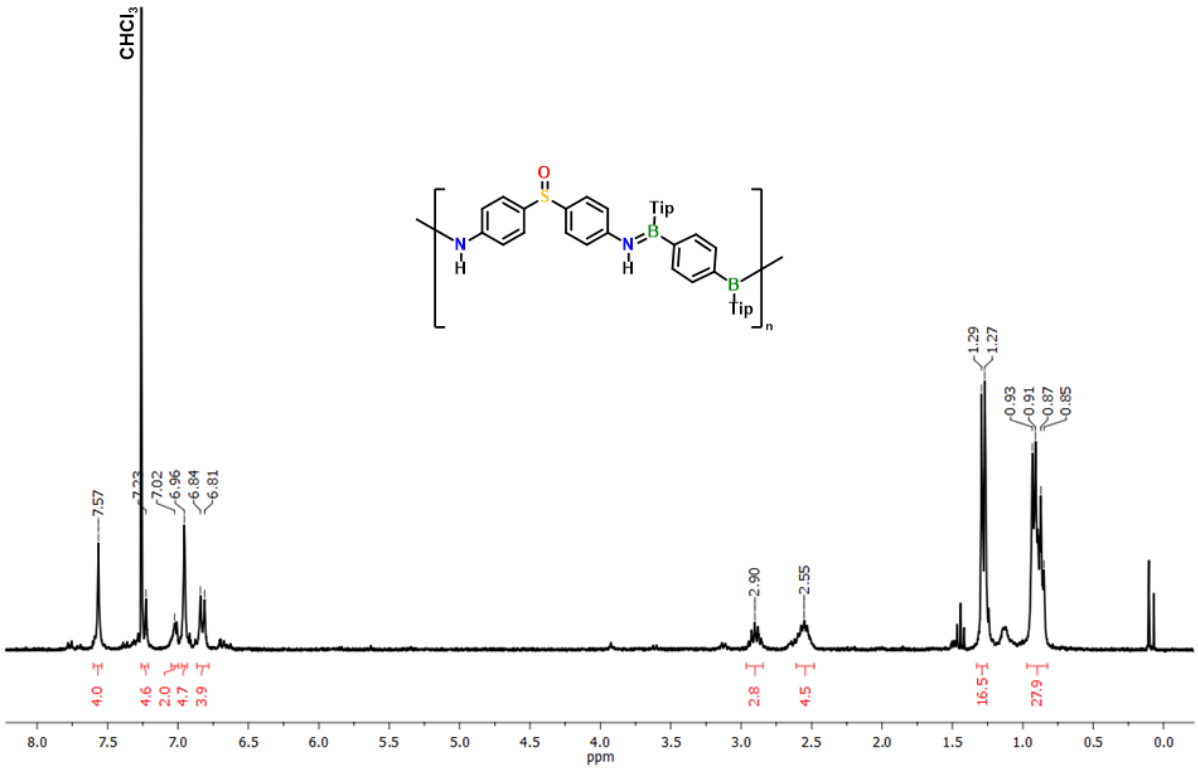

Figure S5.9.44. ^{1}H NMR spectrum (300 MHz) of **17** (salt elimination, CH_2Cl_2, r.t.) in $CDCl_3$.

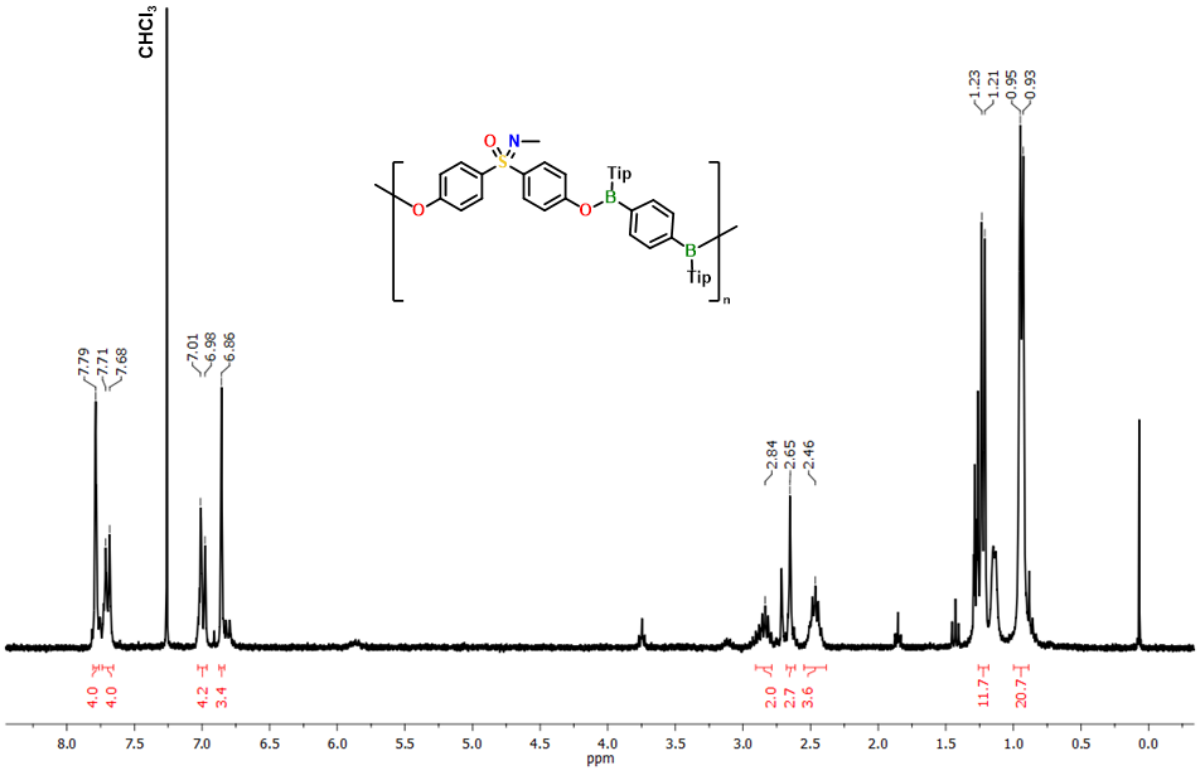

Figure S5.9.45. ^{1}H NMR spectrum (300 MHz) of **18** (salt elimination, CH_2Cl_2, r.t.) in $CDCl_3$.

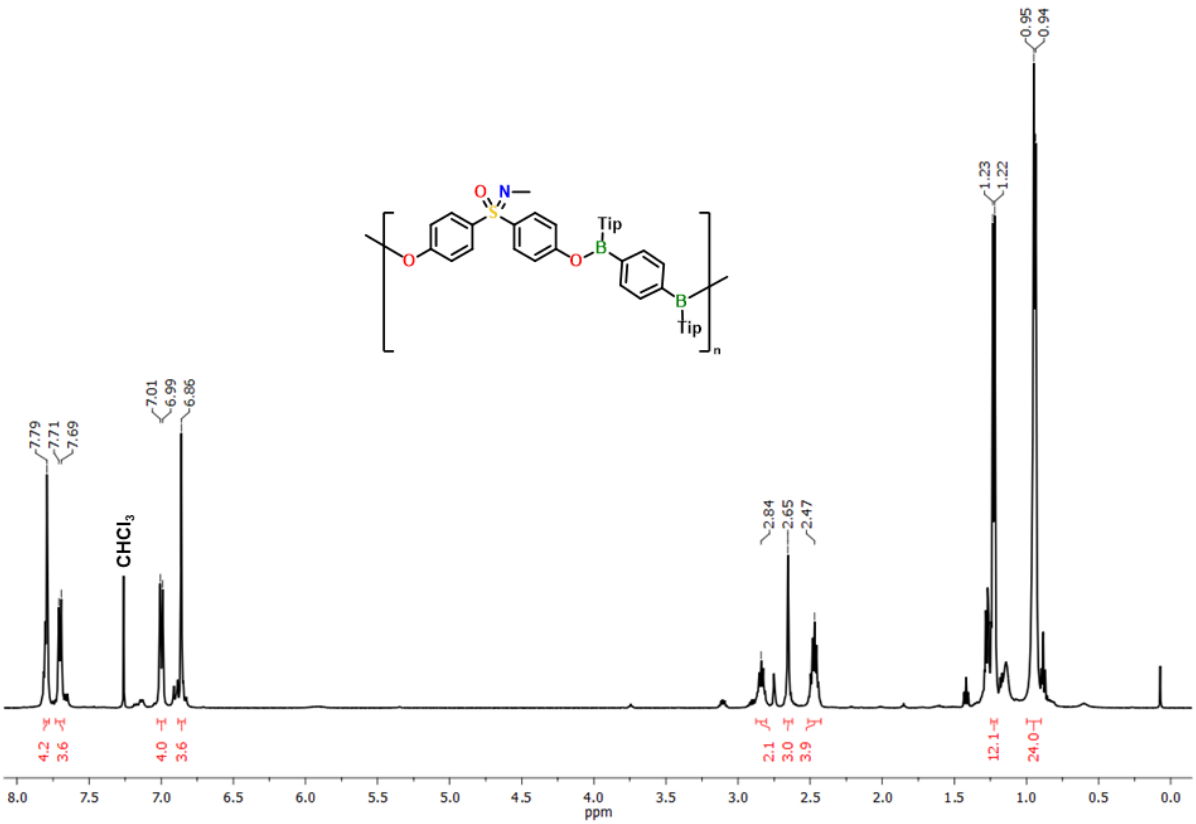

Figure S5.9.46. ^{1}H NMR spectrum (500 MHz) of **18** (salt elimination, *o*-DFB, 80 °C) in $CDCl_3$.

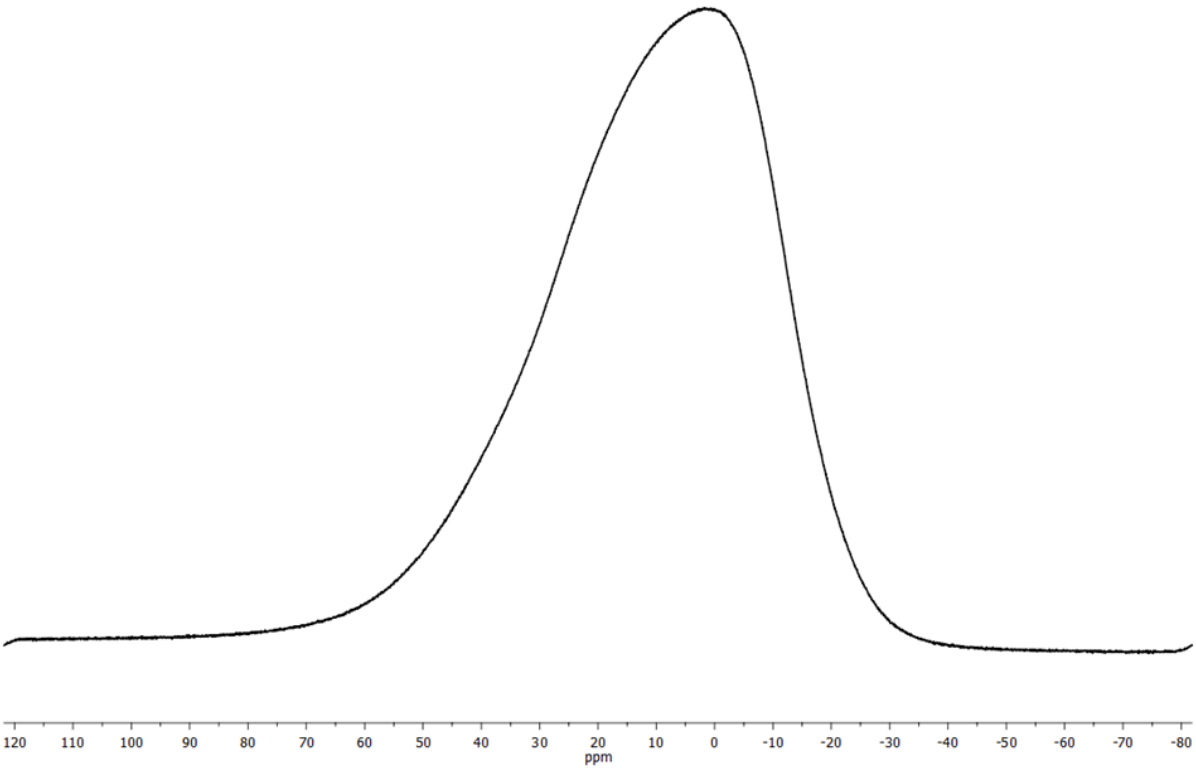

Figure S5.9.47. $^{11}B\{^{1}H\}$ NMR spectrum (160 MHz) of **18** (salt elimination, *o*-DFB, 80 °C) in $CDCl_3$.

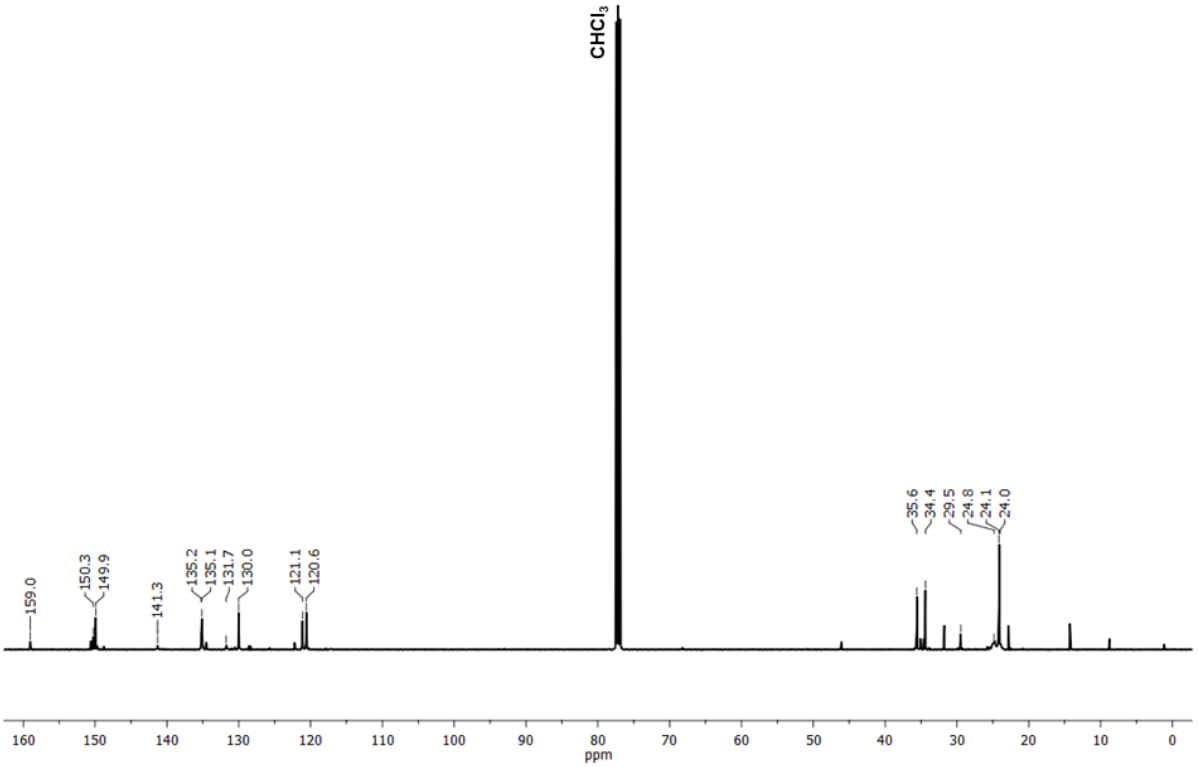

Figure S5.9.48. $^{13}C\{^{1}H\}$ NMR spectrum (125 MHz) of **18** (salt elimination, *o*-DFB, 80 °C) in $CDCl_3$.

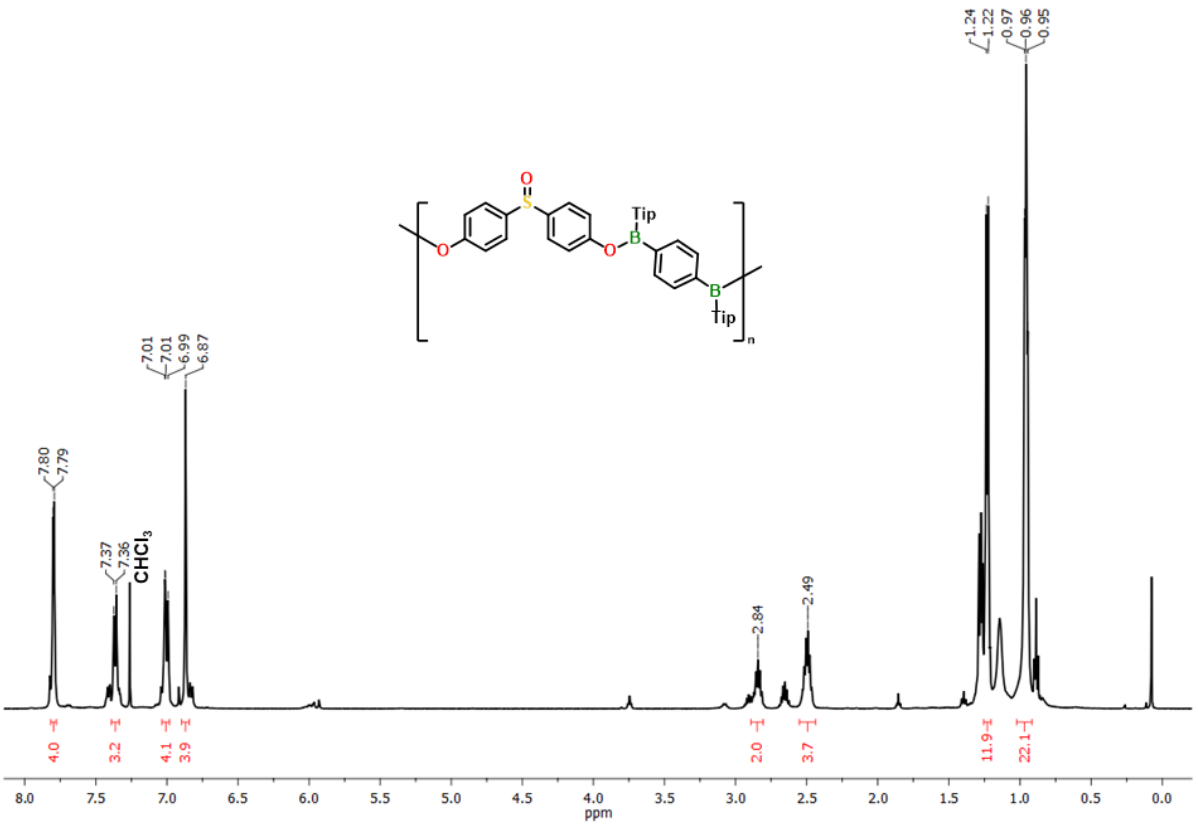

Figure S5.9.49. ^{1}H NMR spectrum (500 MHz) of **19** (salt elimination, CH_2Cl_2, r.t.) in $CDCl_3$.

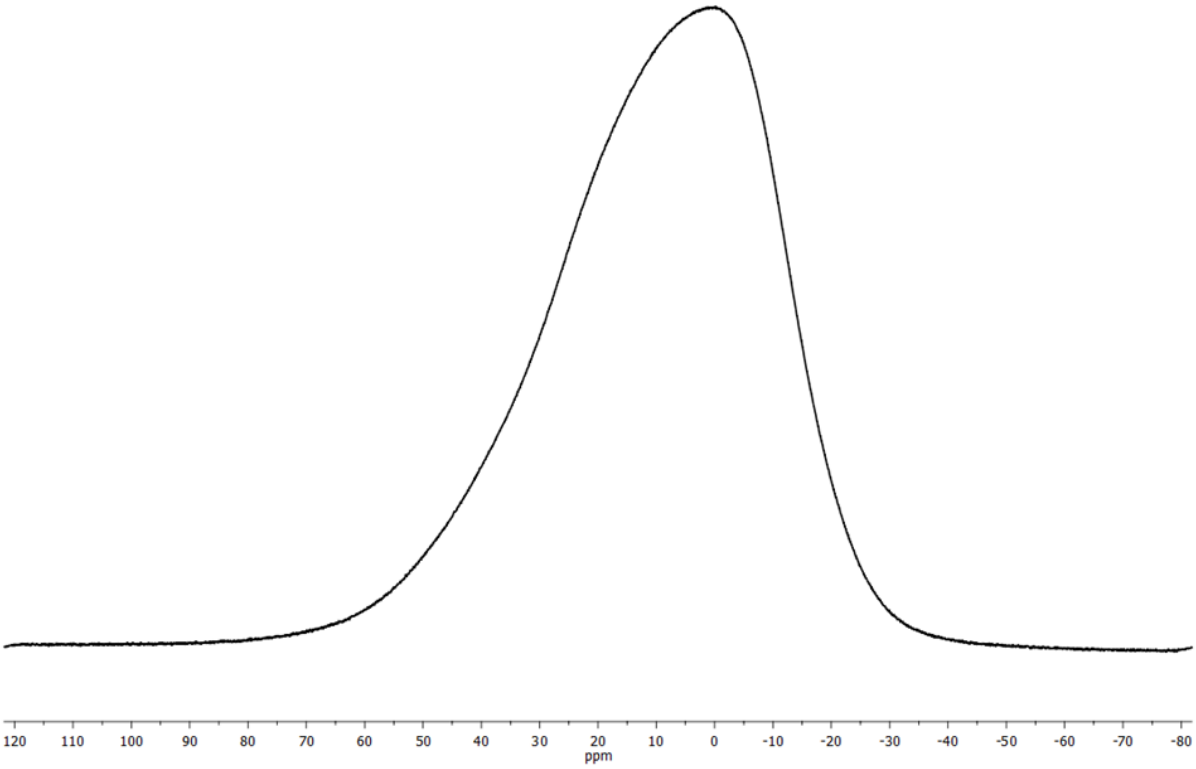

Figure S5.9.50. $^{11}B\{^{1}H\}$ NMR spectrum (160 MHz) of **19** (salt elimination, CH_2Cl_2, r.t.) in $CDCl_3$.

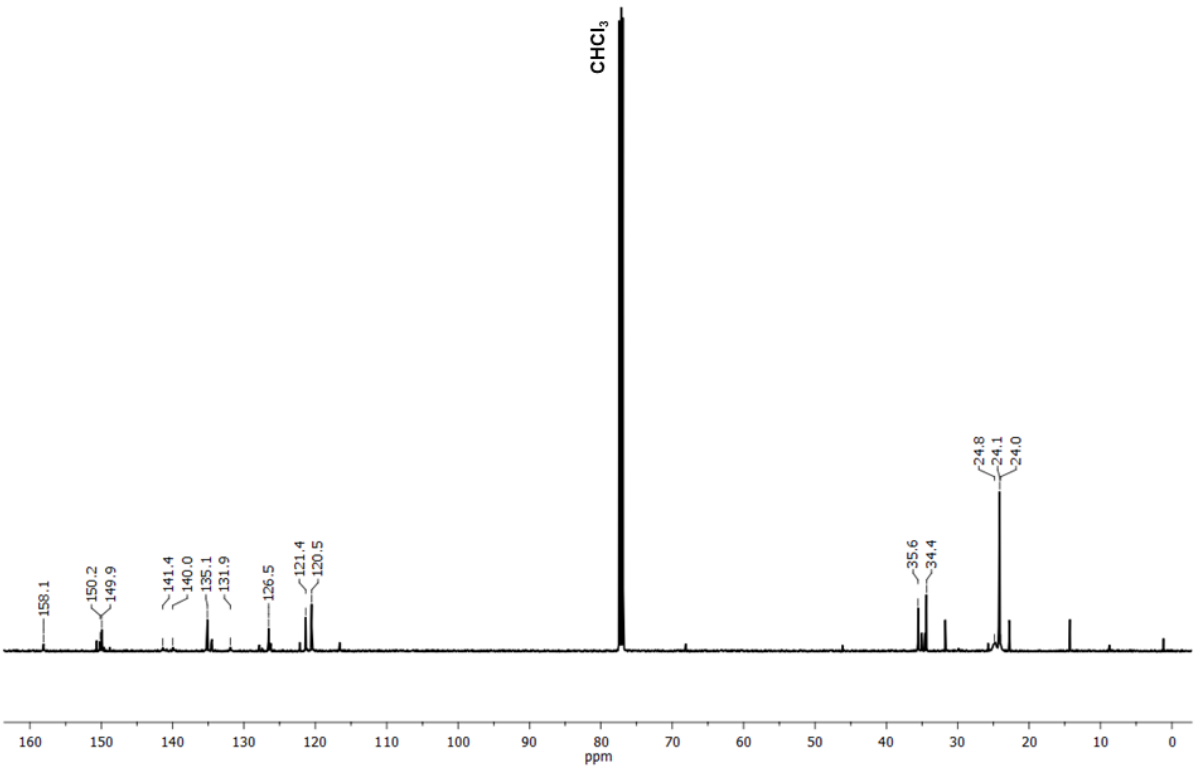

Figure S5.9.51. $^{13}C\{^{1}H\}$ NMR spectrum (125 MHz) of **19** (salt elimination, CH_2Cl_2, r.t.) in $CDCl_3$.

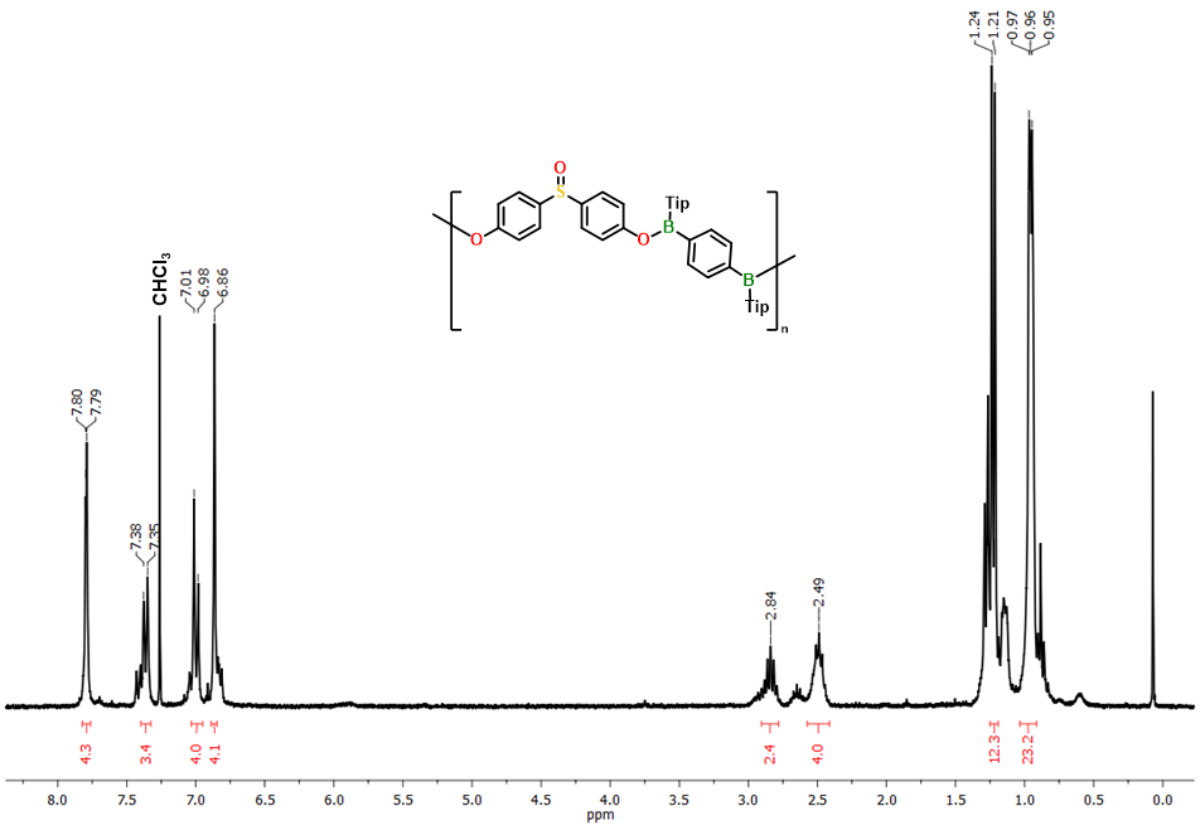

Figure S5.9.52. ^{1}H NMR spectrum (300 MHz) of **19** (salt elimination, *o*-DFB, 80 °C) in $CDCl_3$.

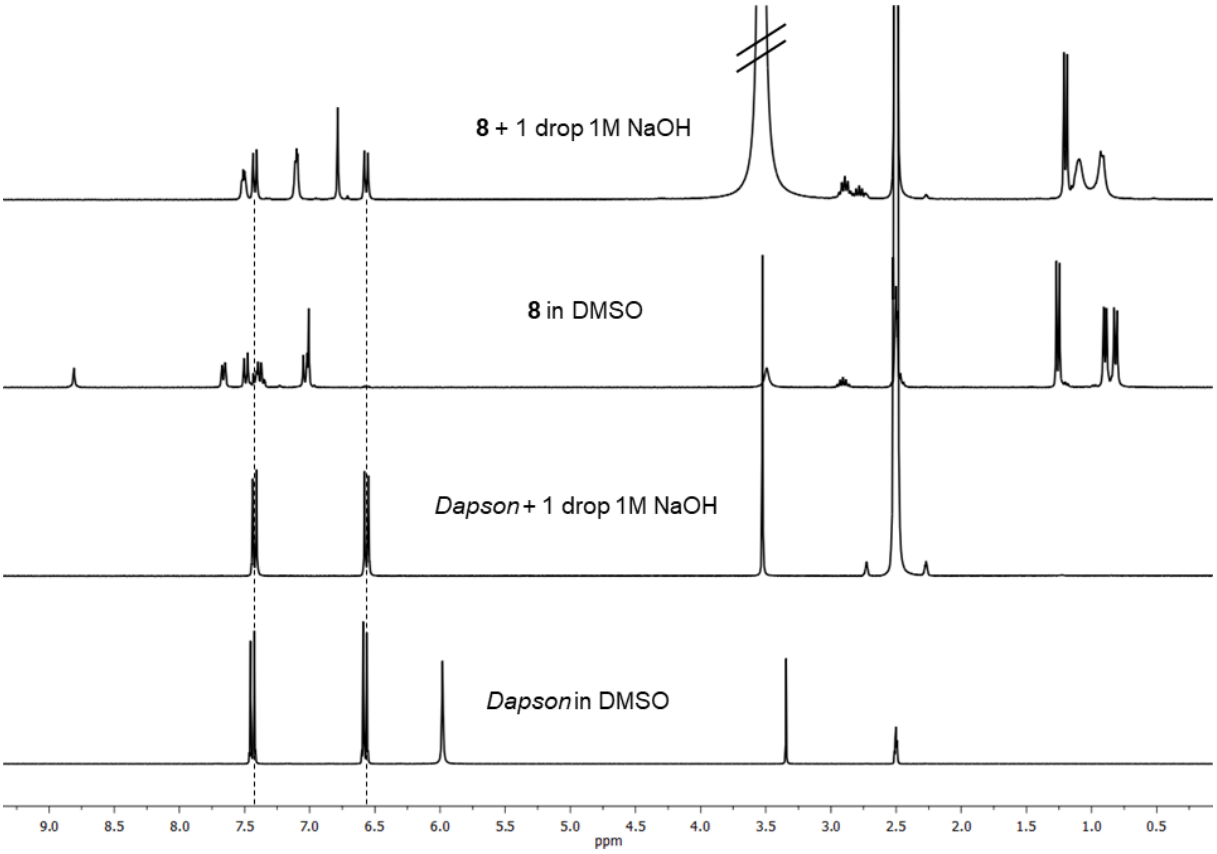

Figure S5.9.53. ^{1}H NMR spectra of the pH-triggered degradation (NaOH) of **8** with *Dapson* reference in DMSO-d_6.

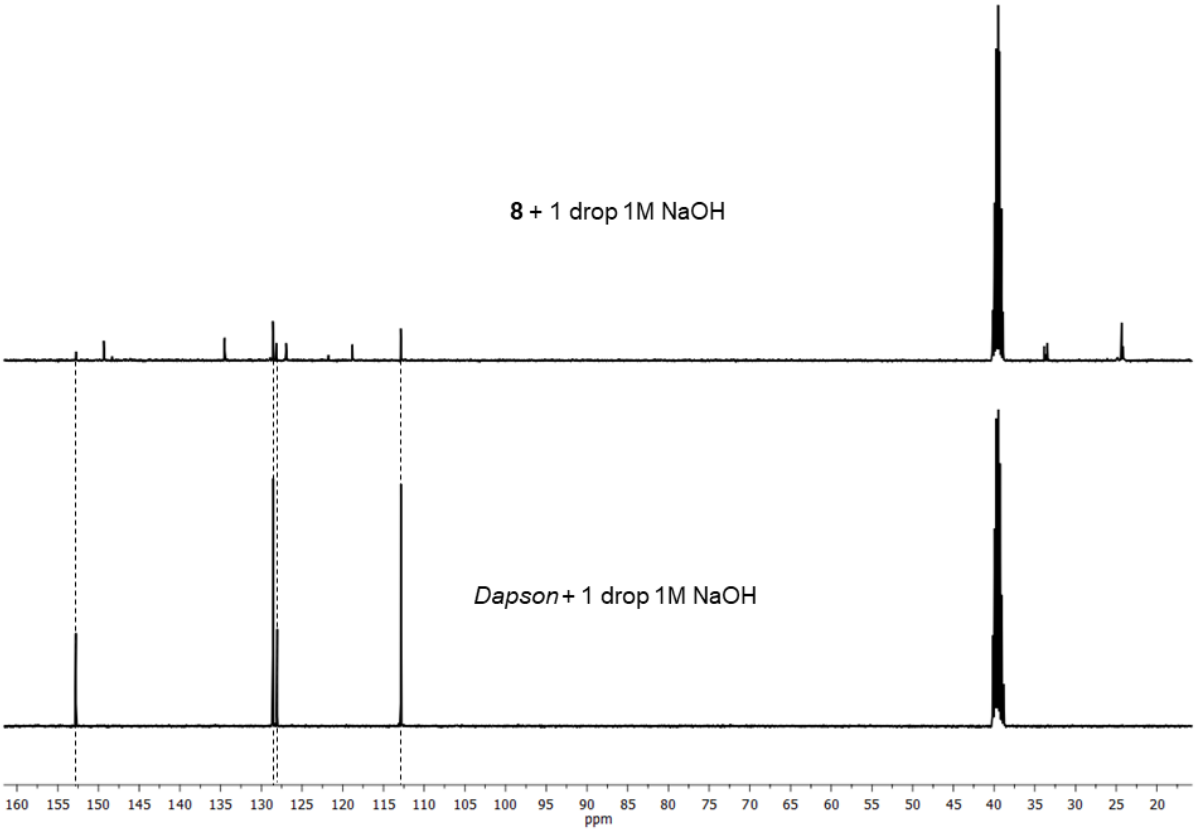

Figure S5.9.54. $^{13}C\{^{1}H\}$ NMR spectra of the pH-triggered degradation (NaOH) of **8** with *Dapson* reference in DMSO-d_6.

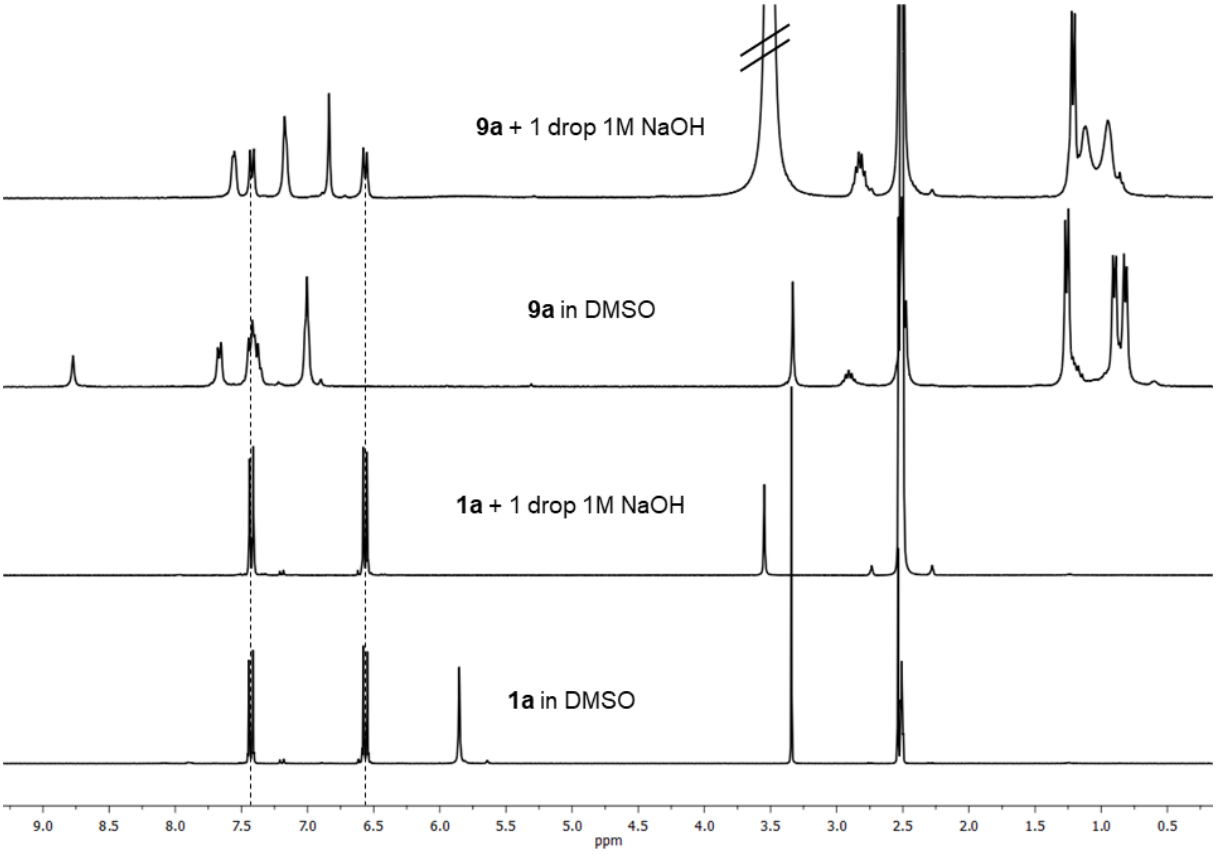

Figure S5.9.55. ^{1}H NMR spectra of the pH-triggered degradation (NaOH) of **9a** with **1a** reference in DMSO-d_6.

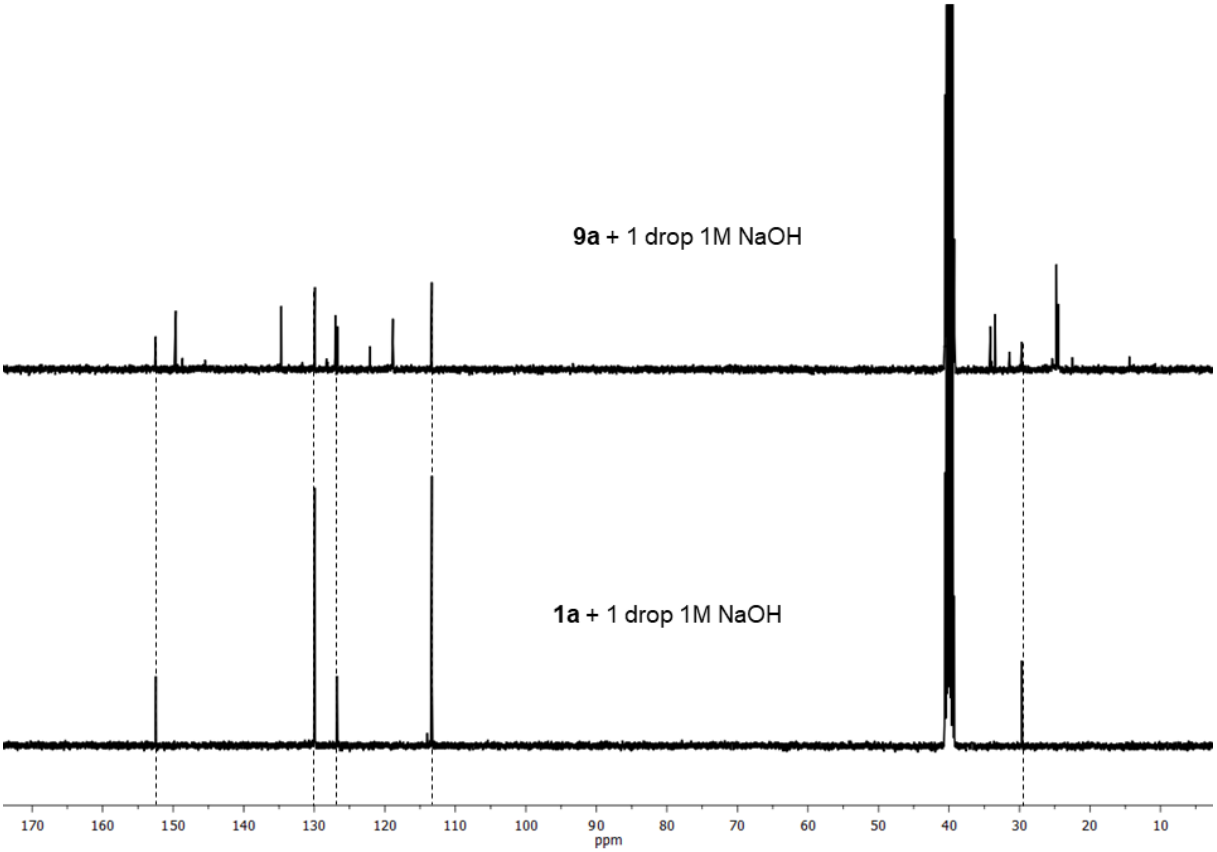

Figure S5.9.56. $^{13}C\{^{1}H\}$ NMR spectra of the pH-triggered degradation (NaOH) of **9a** with **1a** reference in DMSO-d_6.

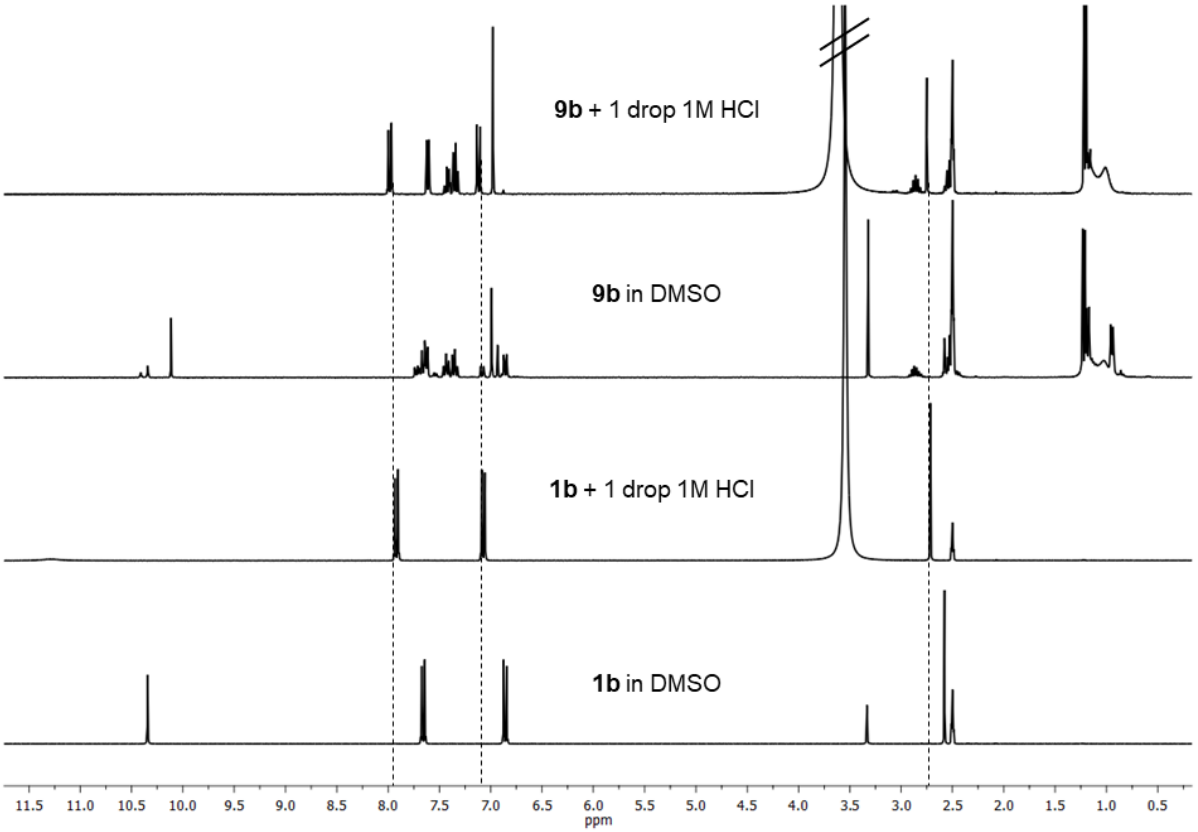

Figure S5.9.57. ^{1}H NMR spectra of the pH-triggered degradation (HCl) of **9b** with **1b** reference in DMSO-d_6.

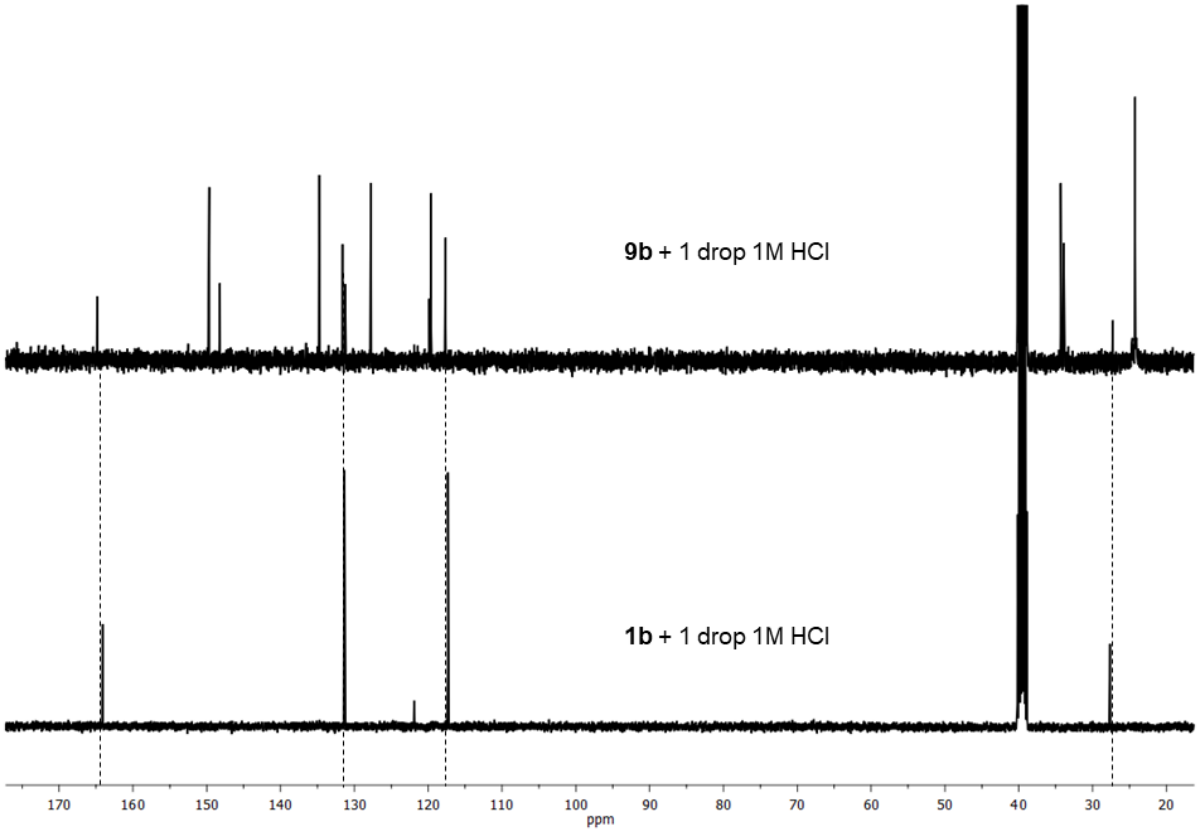

Figure S5.9.58. $^{13}C\{^{1}H\}$ NMR spectra of the pH-triggered degradation (HCl) of **9b** with **1b** reference in DMSO-d_6.

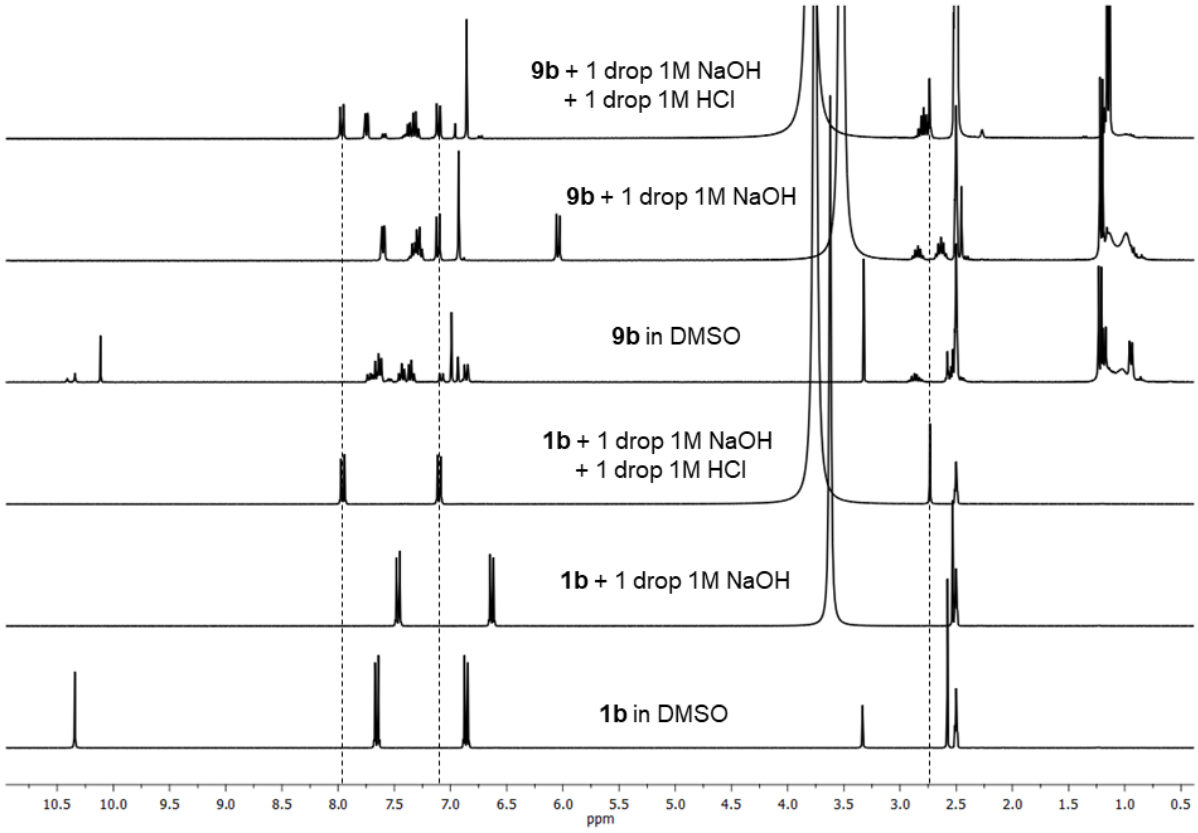

Figure S5.9.59. ^{1}H NMR spectra of the pH-triggered degradation (NaOH+HCl) of **9b** with **1b** reference in DMSO-d_6.

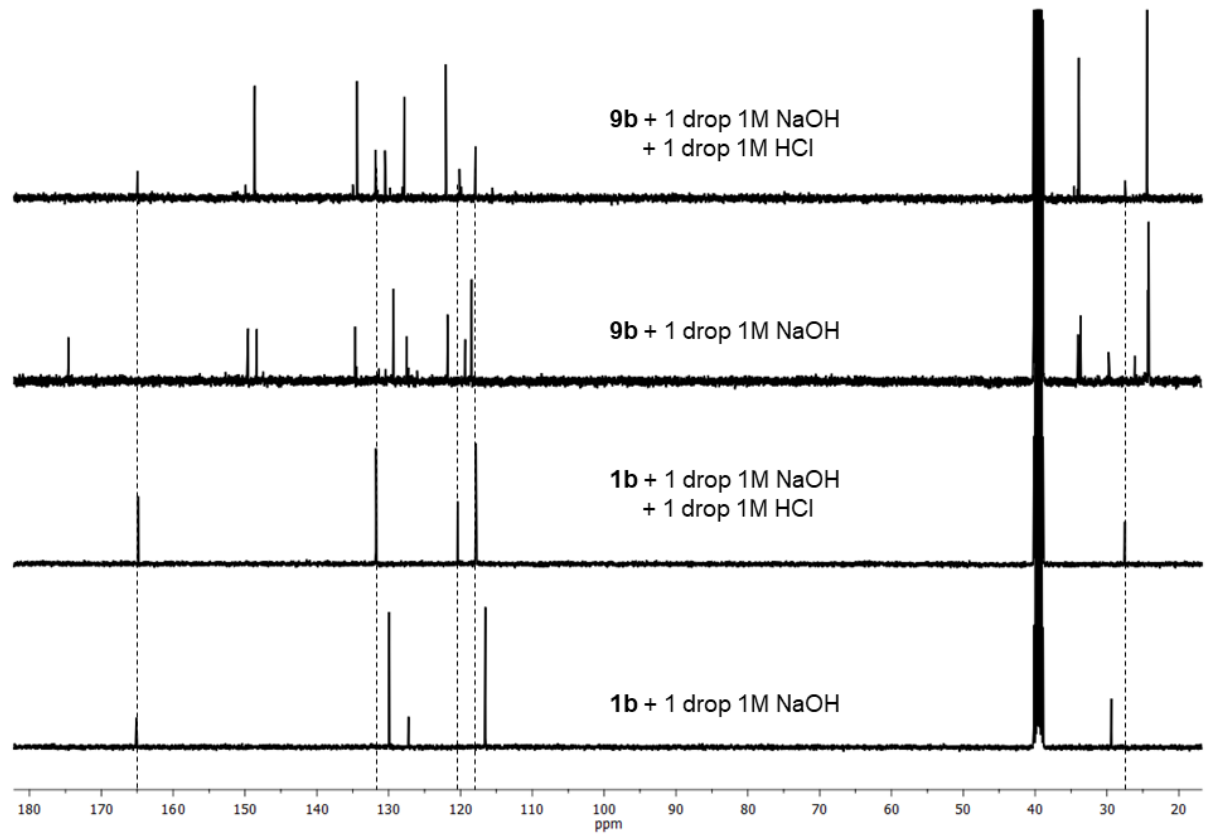

Figure S5.9.60. $^{13}C\{^{1}H\}$ NMR spectra of the pH-triggered degradation (NaOH+HCl) of **9b** with **1b** reference in DMSO-d_6.

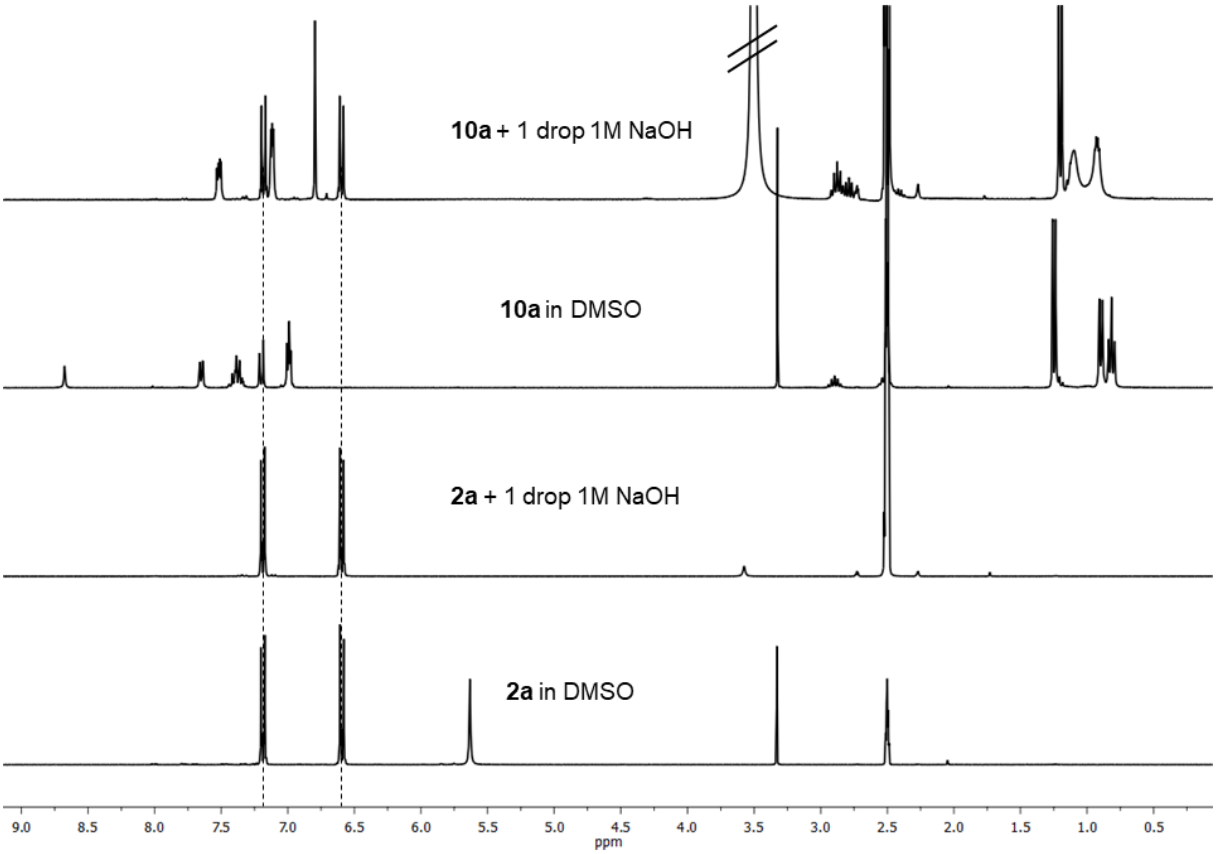

Figure S5.9.61. ^{1}H NMR spectra of the pH-triggered degradation (NaOH) of **10a** with **2a** reference in DMSO-d_6.

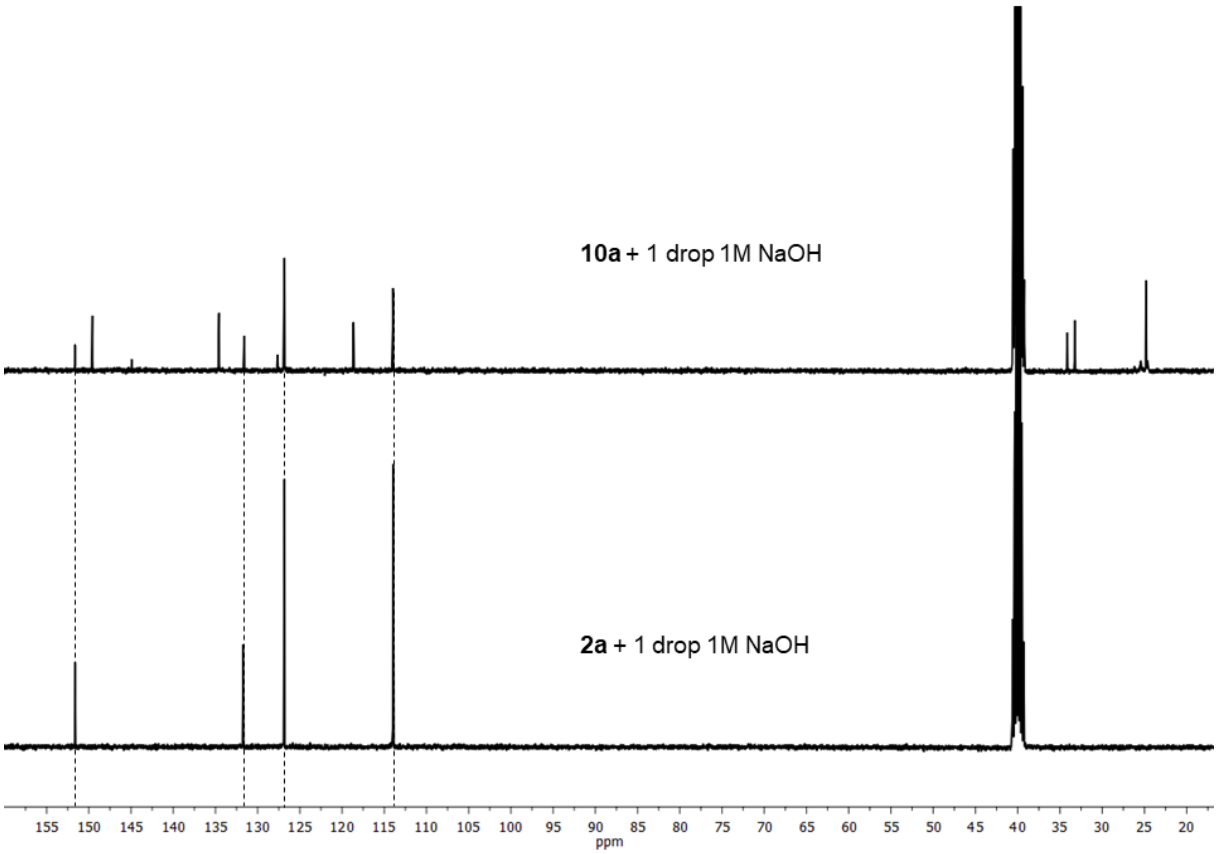

Figure S5.9.62. $^{13}C\{^{1}H\}$ NMR spectra of the pH-triggered degradation (NaOH) of **10a** with **2a** reference in DMSO-d_6.

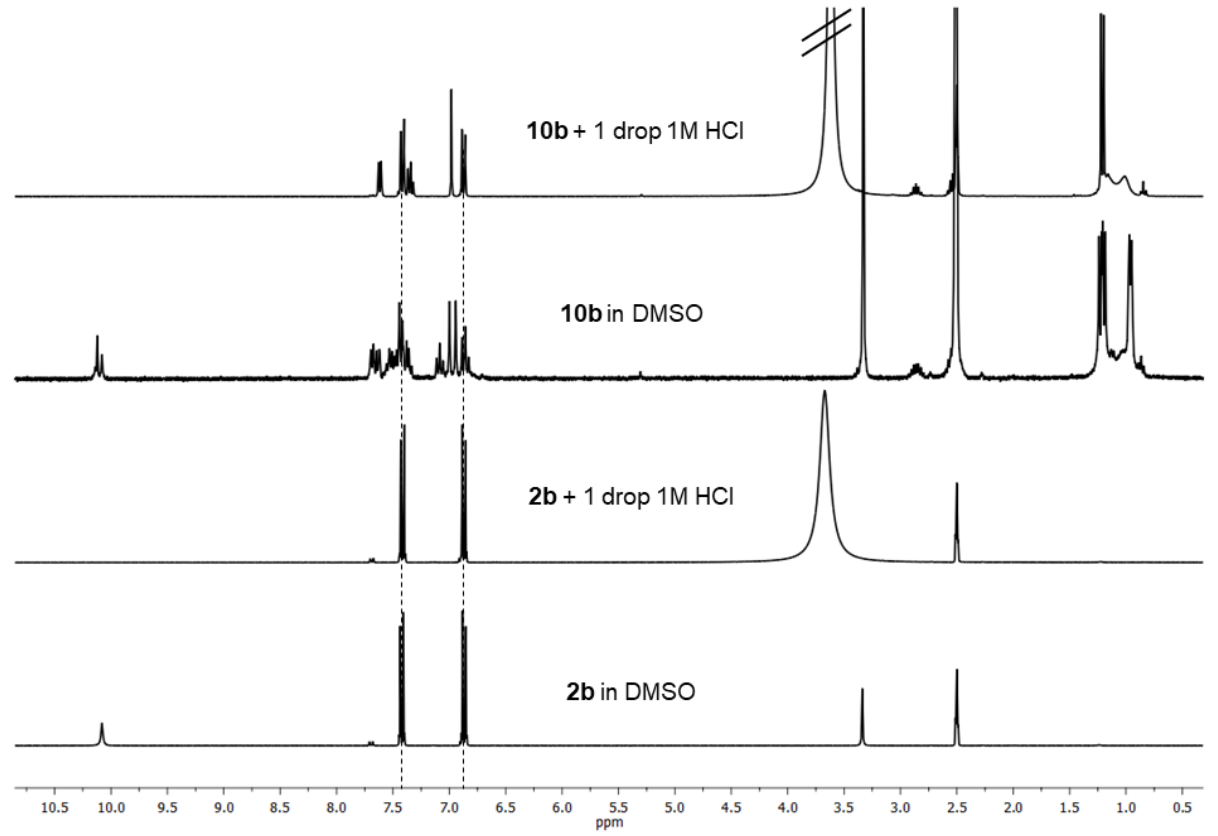

Figure S5.9.63. ^{1}H NMR spectra of the pH-triggered degradation (HCl) of **10b** with **2b** reference in DMSO-d_6.

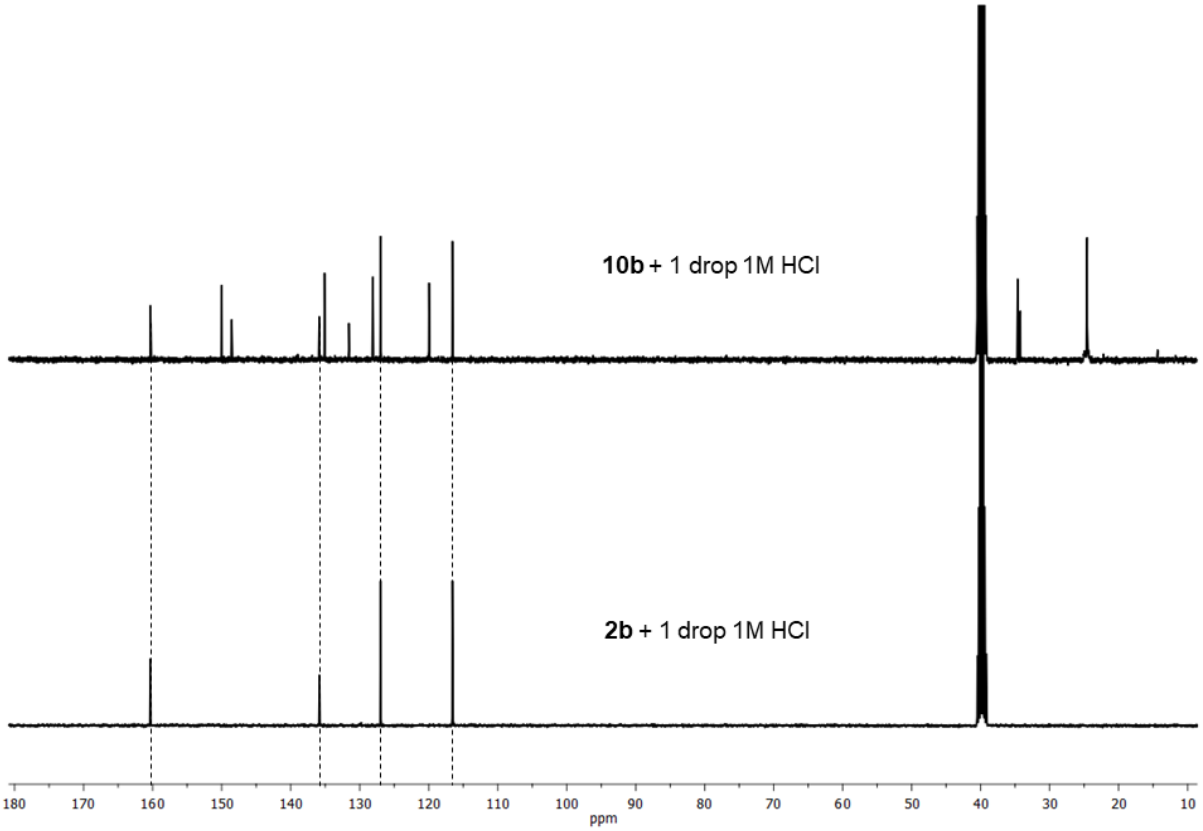

Figure S5.9.64. $^{13}C\{^{1}H\}$ NMR spectra of the pH-triggered degradation (HCl) of **10b** with **2b** reference in DMSO-d_6.

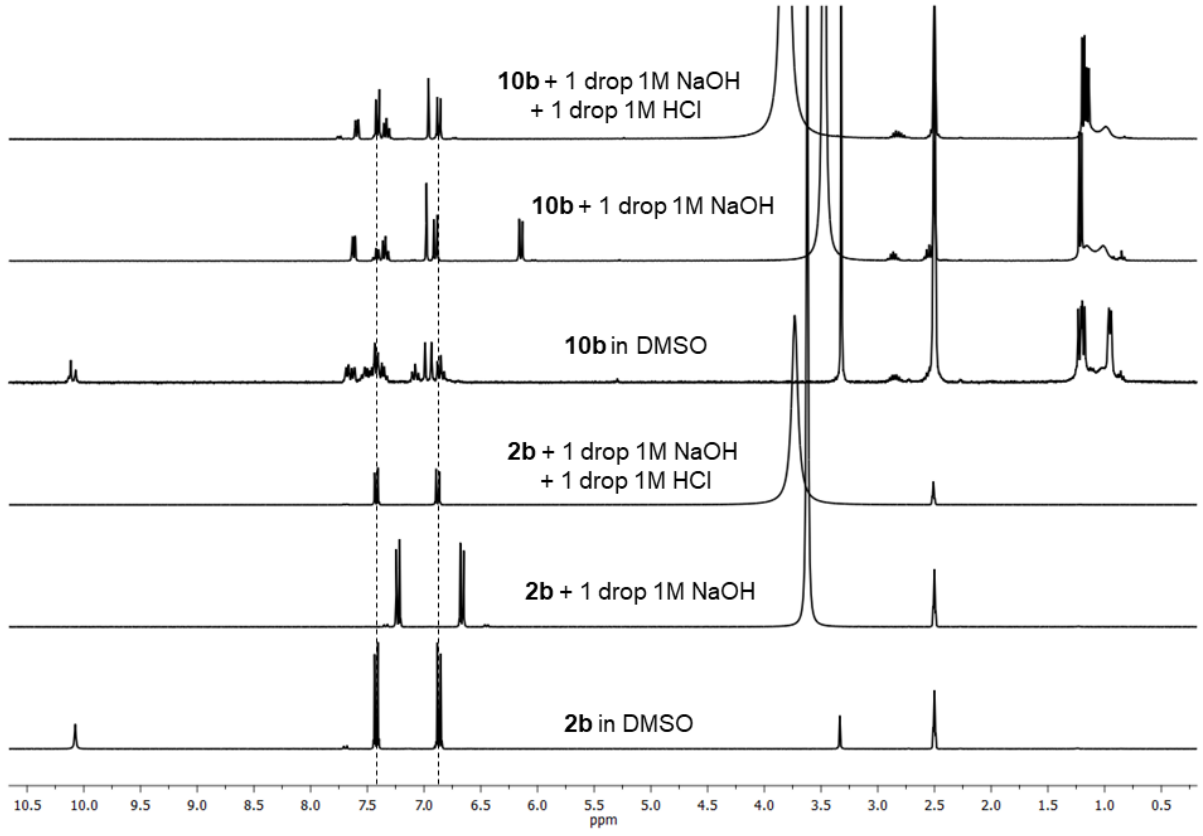

Figure S5.9.65. ^{1}H NMR spectra of the pH-triggered degradation (NaOH+HCl) of **10b** with **2b** reference in DMSO-d_6.

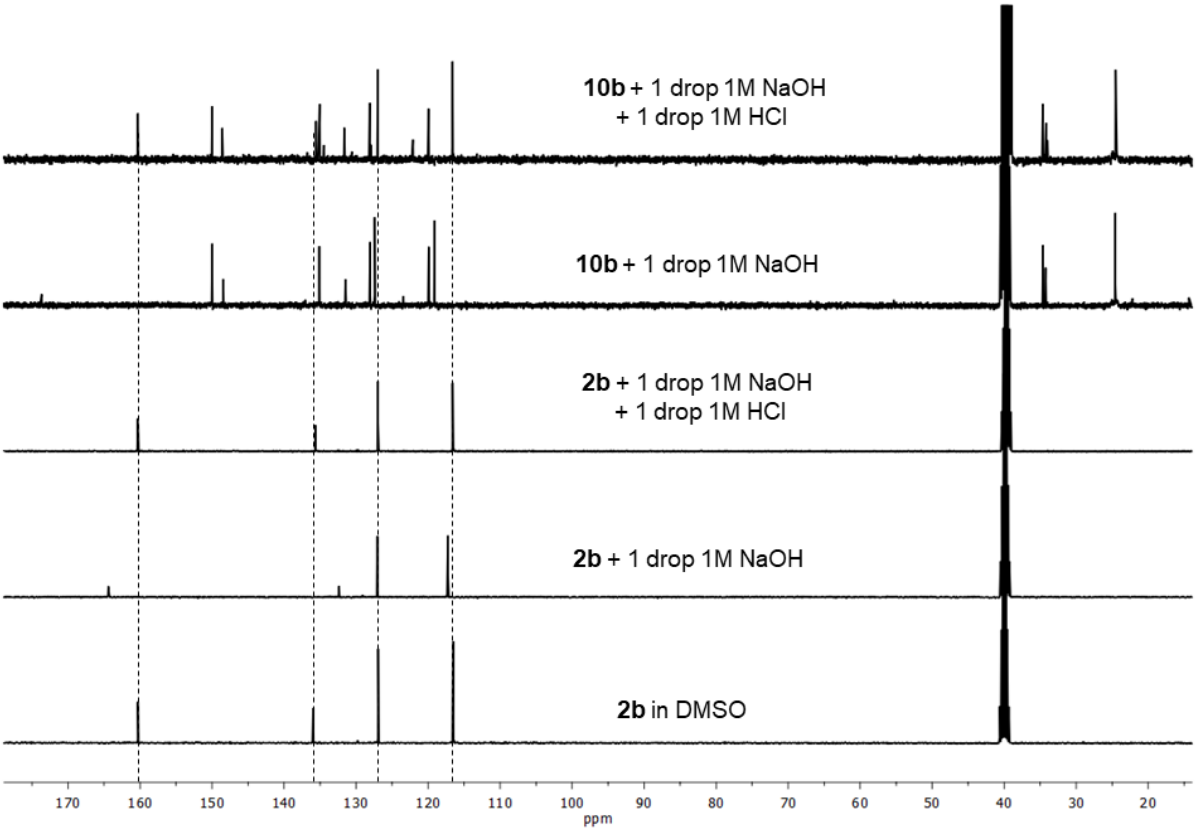

Figure S5.9.66. $^{13}C\{^{1}H\}$ NMR spectra of the pH-triggered degradation (NaOH+HCl) of **10b** with **2b** reference in DMSO-d_6.

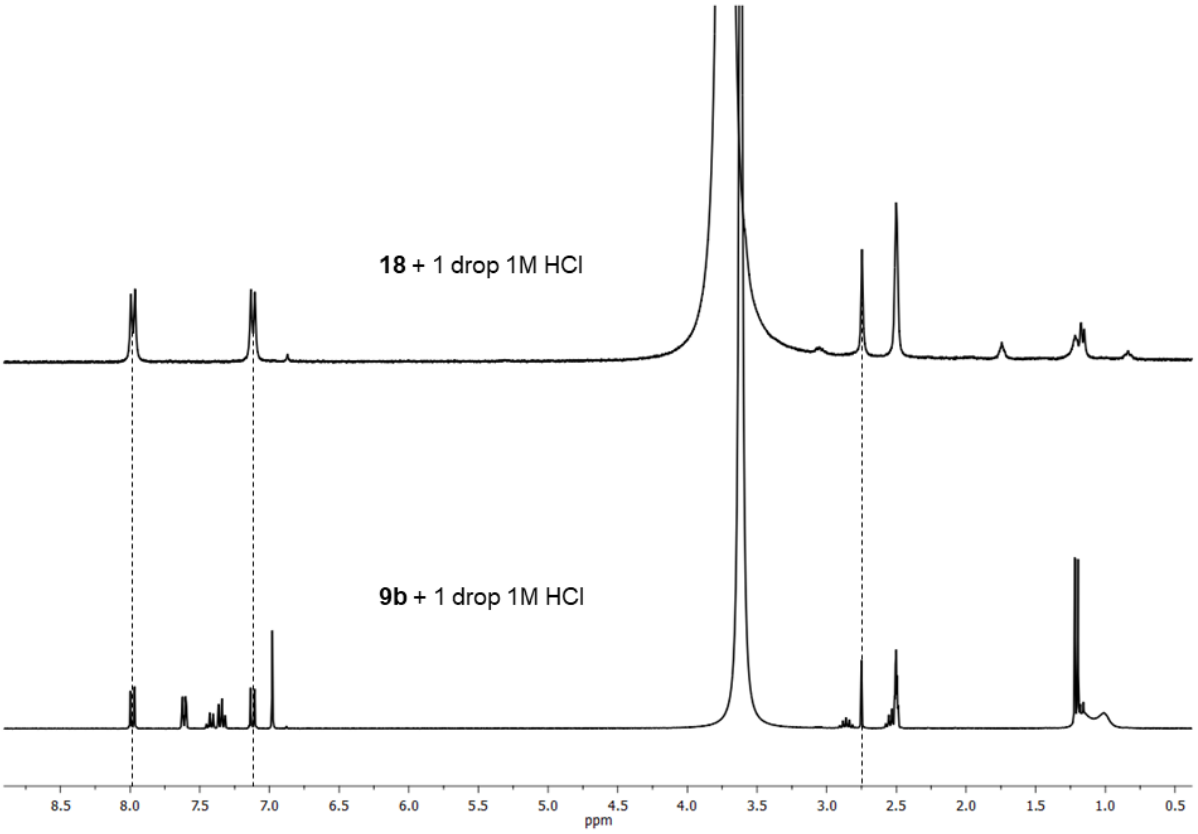

Figure S5.9.67. ^{1}H NMR spectra of the pH-triggered degradation (HCl) of **18** with **9b** reference in DMSO-d_6.

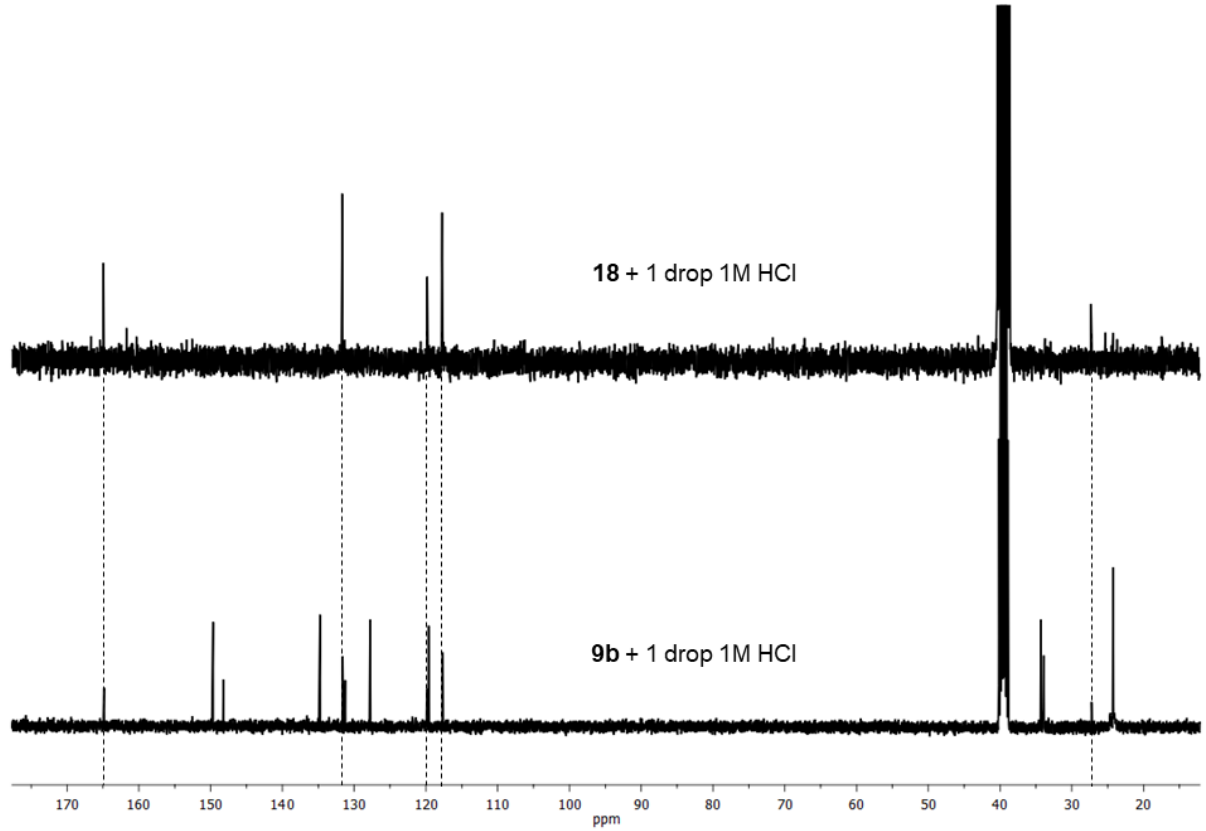

Figure S5.9.68. $^{13}C\{^{1}H\}$ NMR spectra of the pH-triggered degradation (HCl) of **18** with **9b** reference in DMSO-d_6.

HRMS spectra

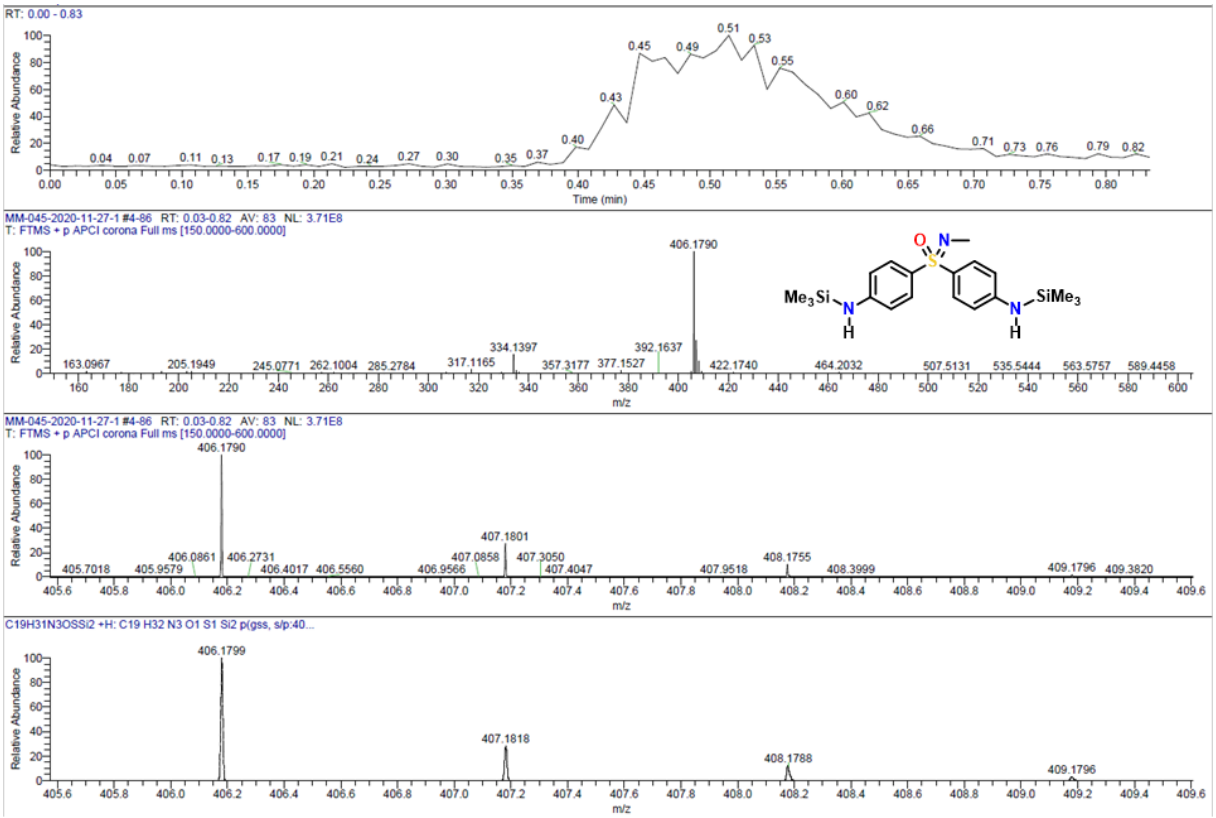

Figure S5.9.69. HRMS spectrum (ASAP pos) of **5**.

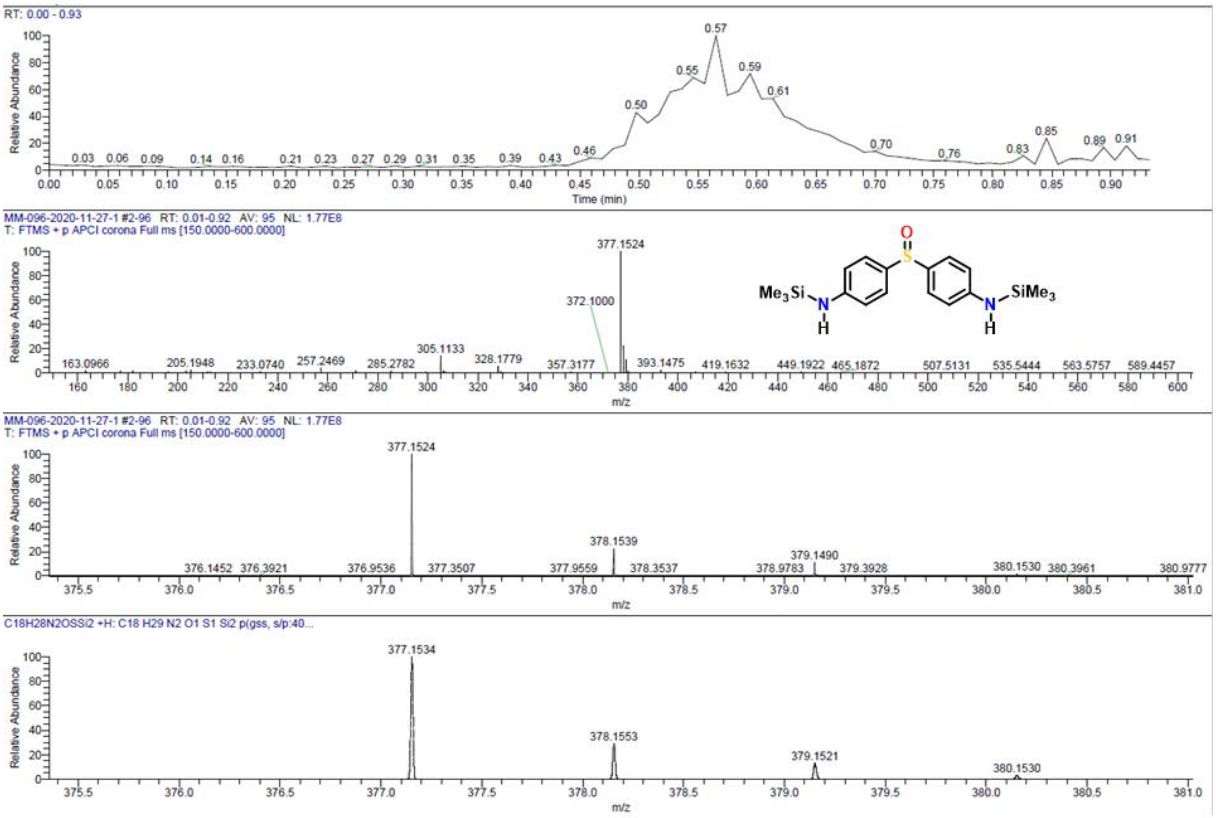

Figure S5.9.70. HRMS spectrum (ASAP pos) of **6**.

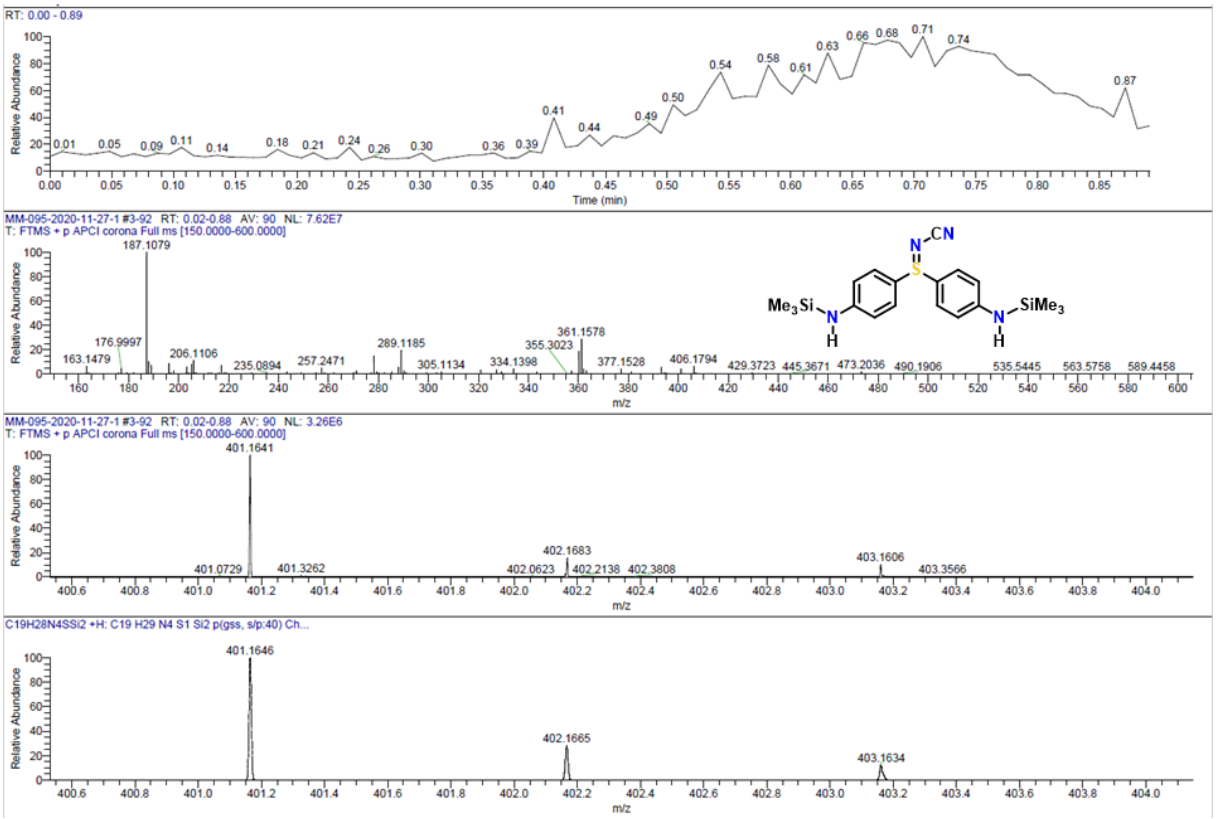

Figure S5.9.71. HRMS spectrum (ASAP pos) of **7**.

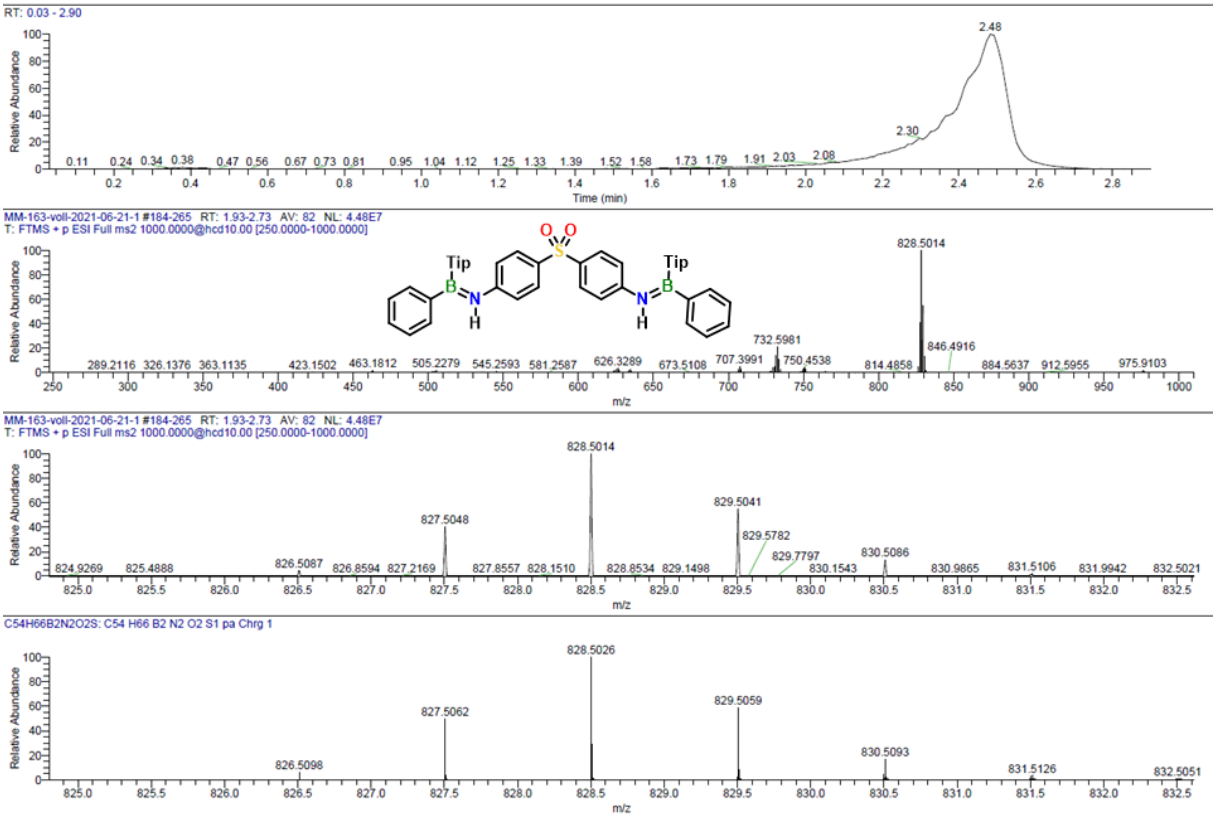

Figure S5.9.72. HRMS spectrum (LIFDI) of **8**.

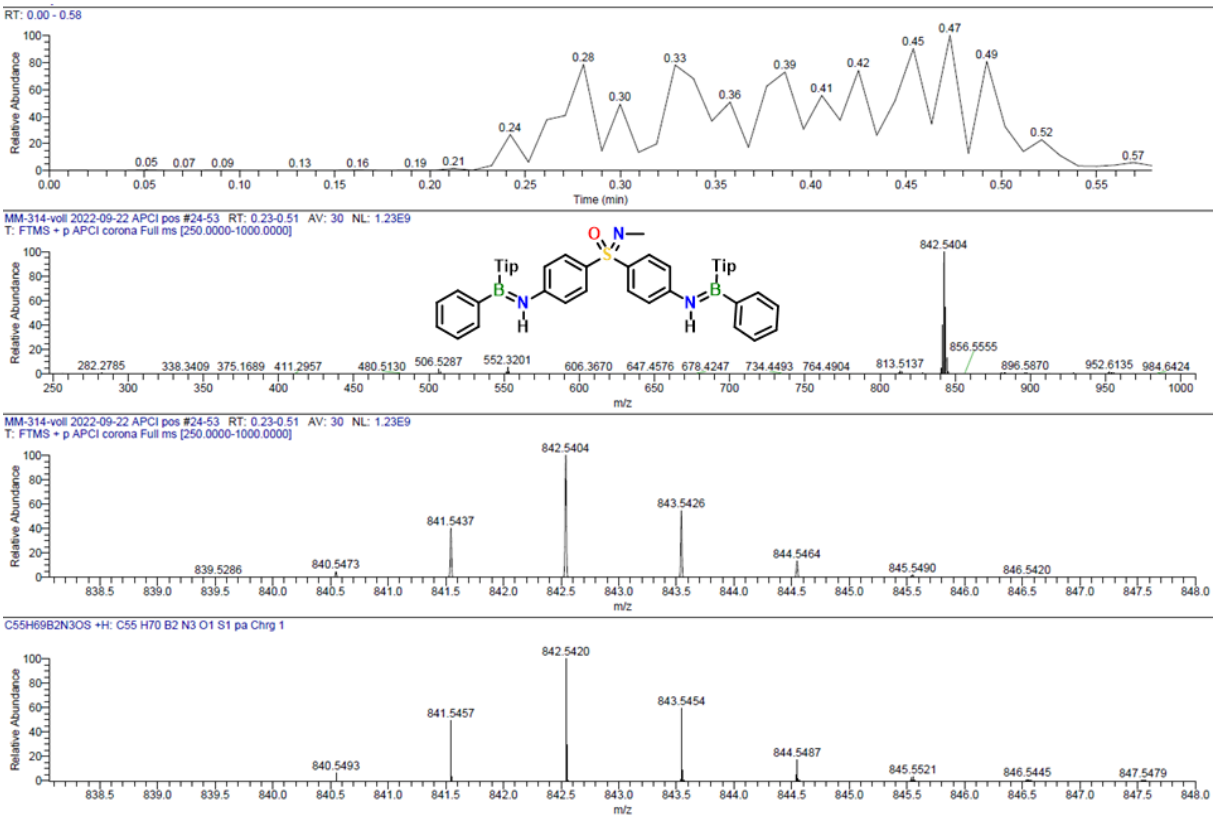

Figure S5.9.73. HRMS spectrum (LIFDI) of **9a**.

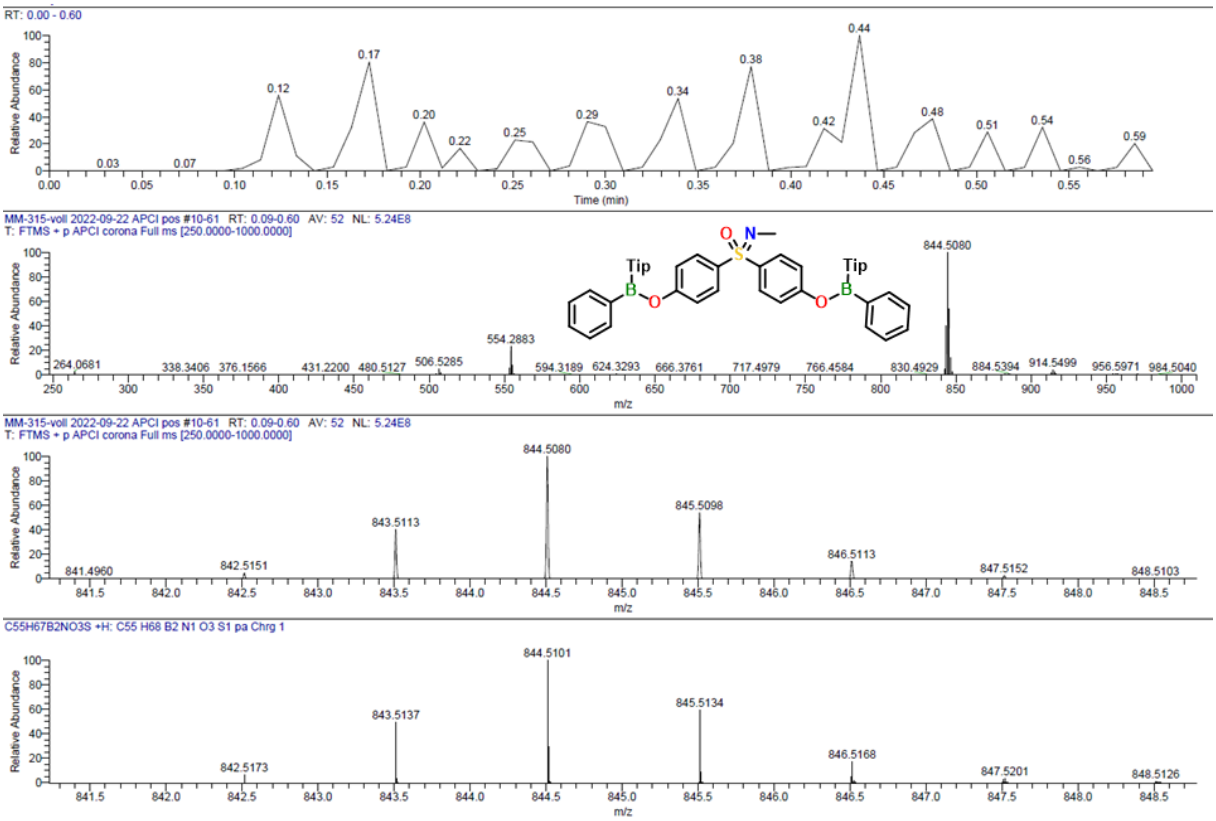

Figure S5.9.74. HRMS spectrum (APCI pos) of **9b**.

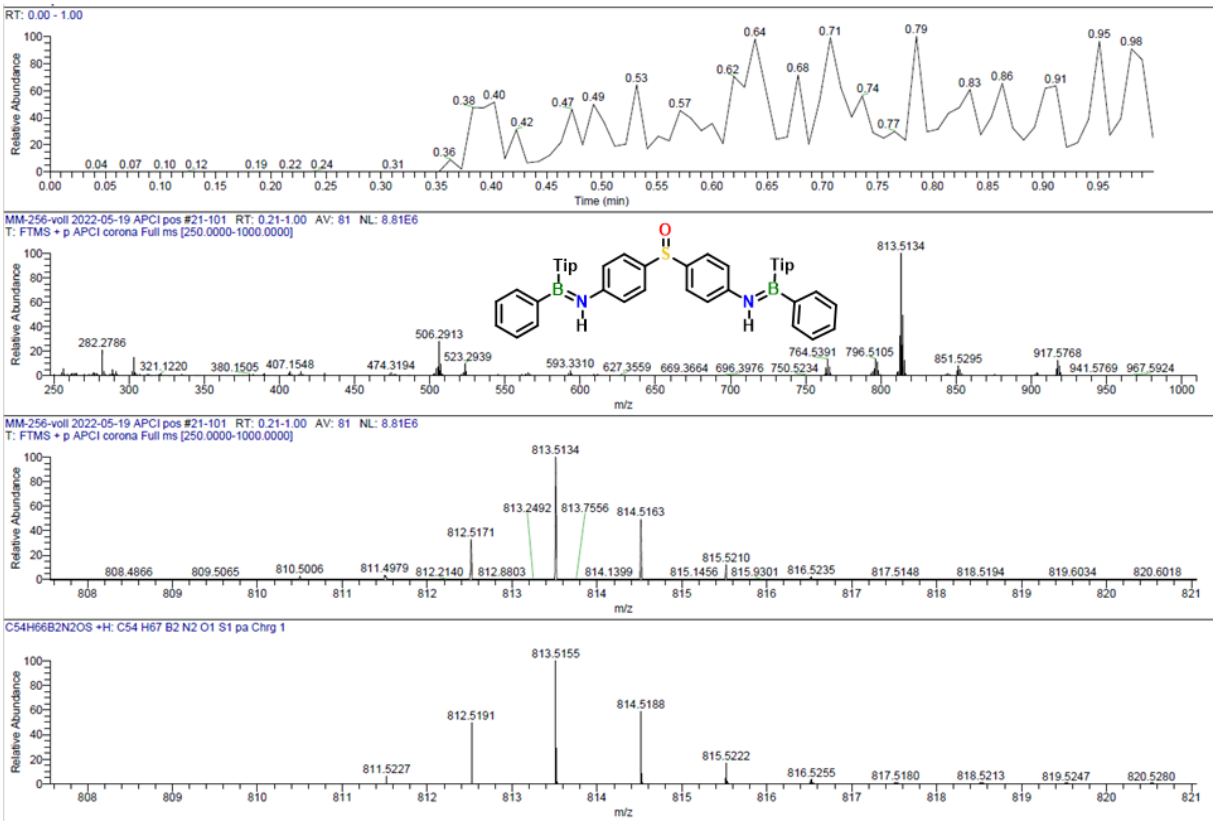

Figure S5.9.75. HRMS spectrum (APCI pos) of **10a**.

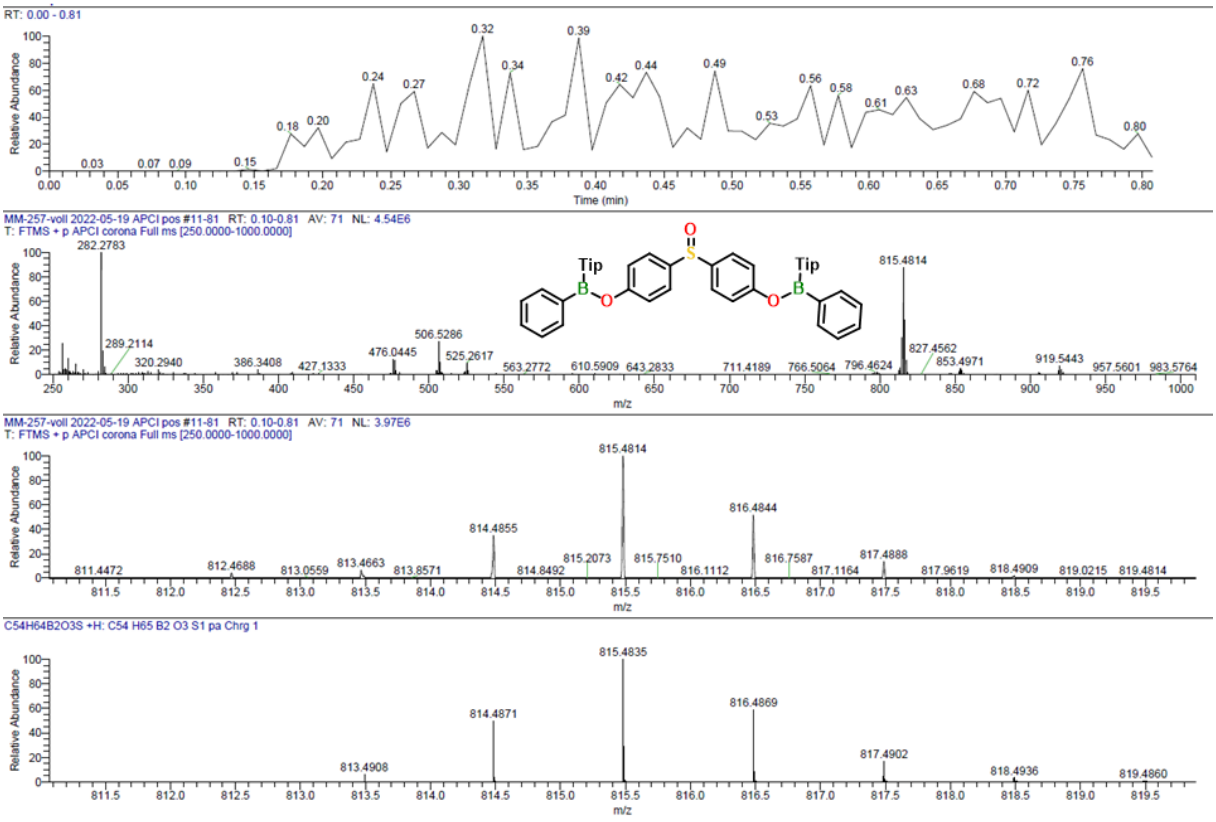

Figure S5.9.76. HRMS spectrum (APCI pos) of **10b**.

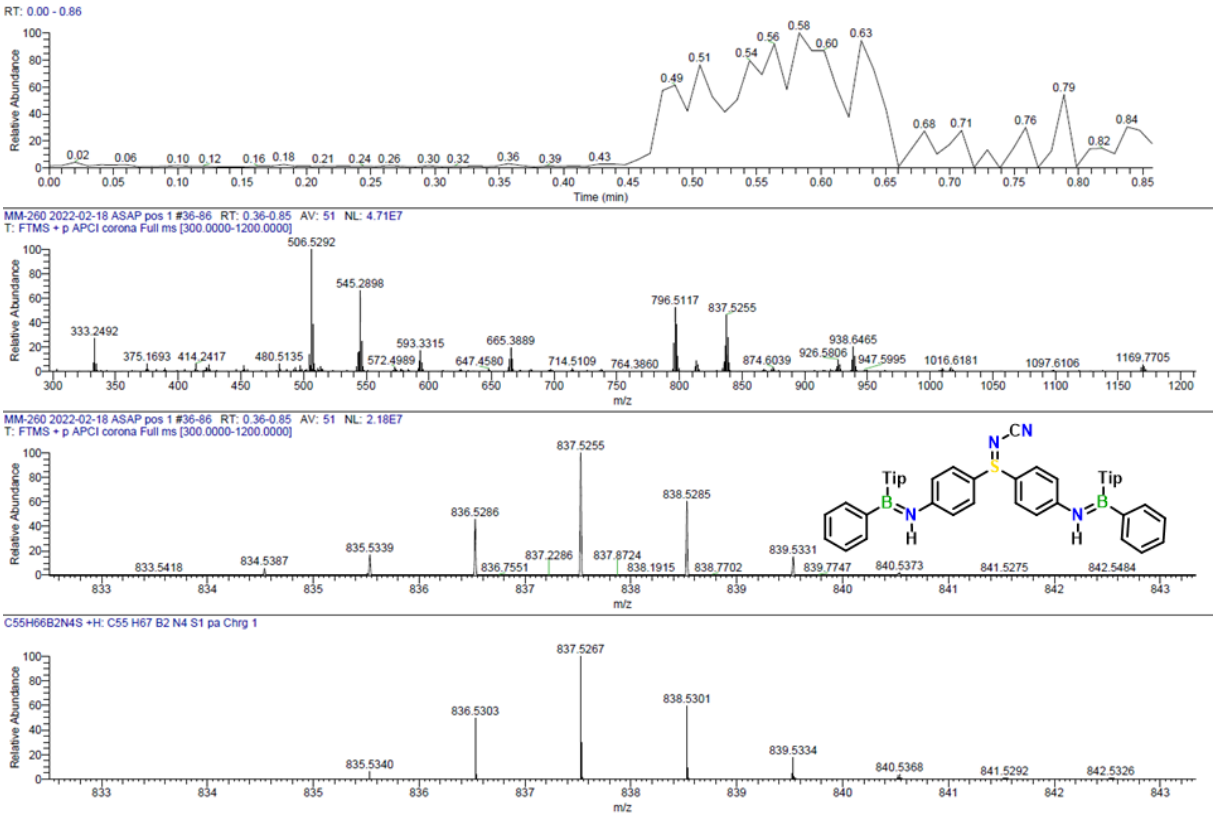

Figure S5.9.77. HRMS spectrum (APCI pos) after the reaction of **3** with TipB(Ph)Br.

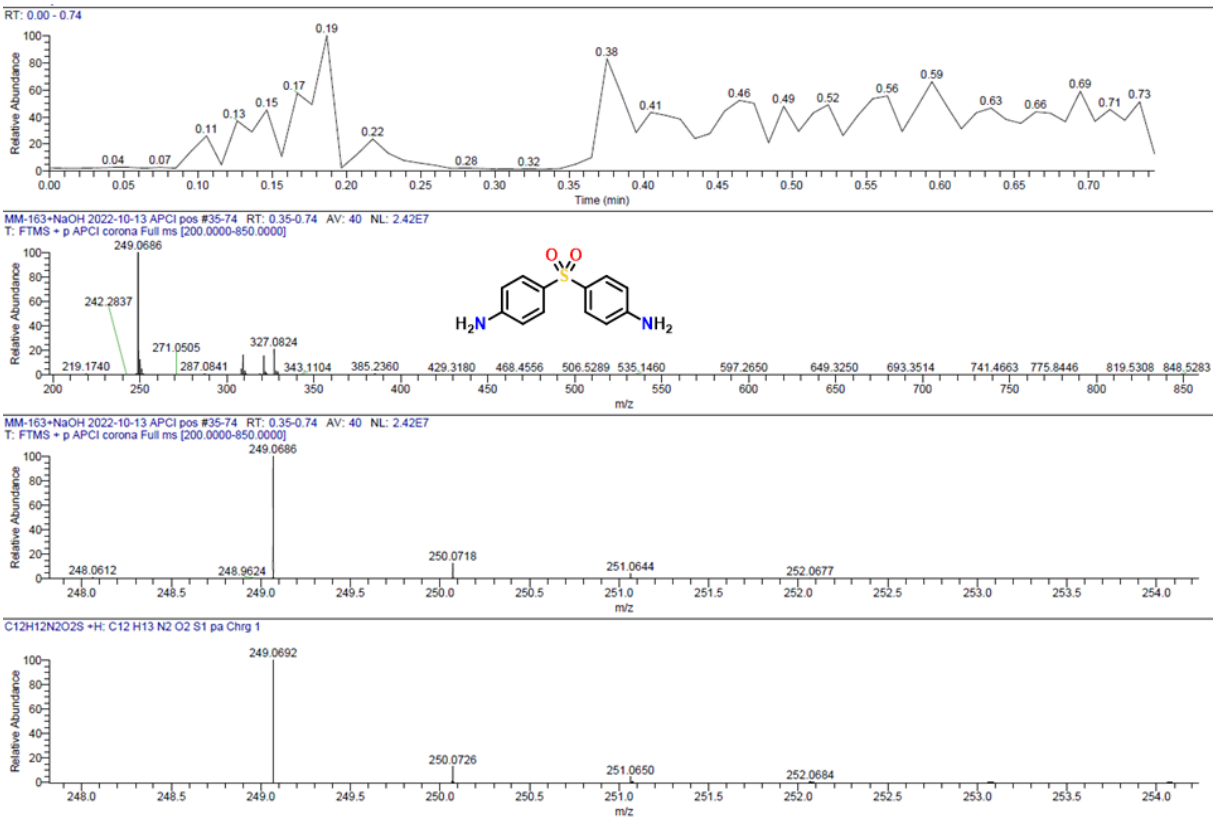

Figure S5.9.78. HRMS spectrum (APCI pos) of *Dapson* after the degradation of **8** with NaOH.

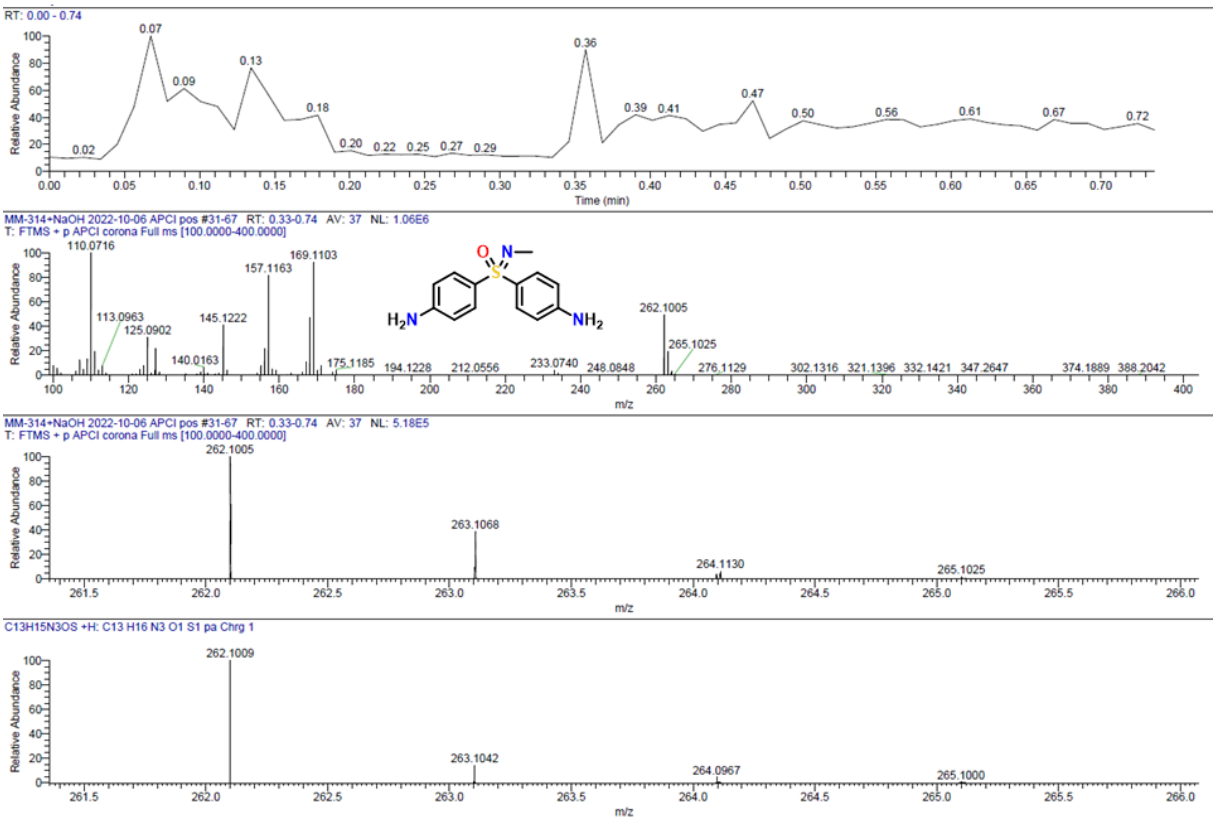

Figure S5.9.79. HRMS spectrum (APCI pos) of **1a** after the degradation of **9a** with NaOH.

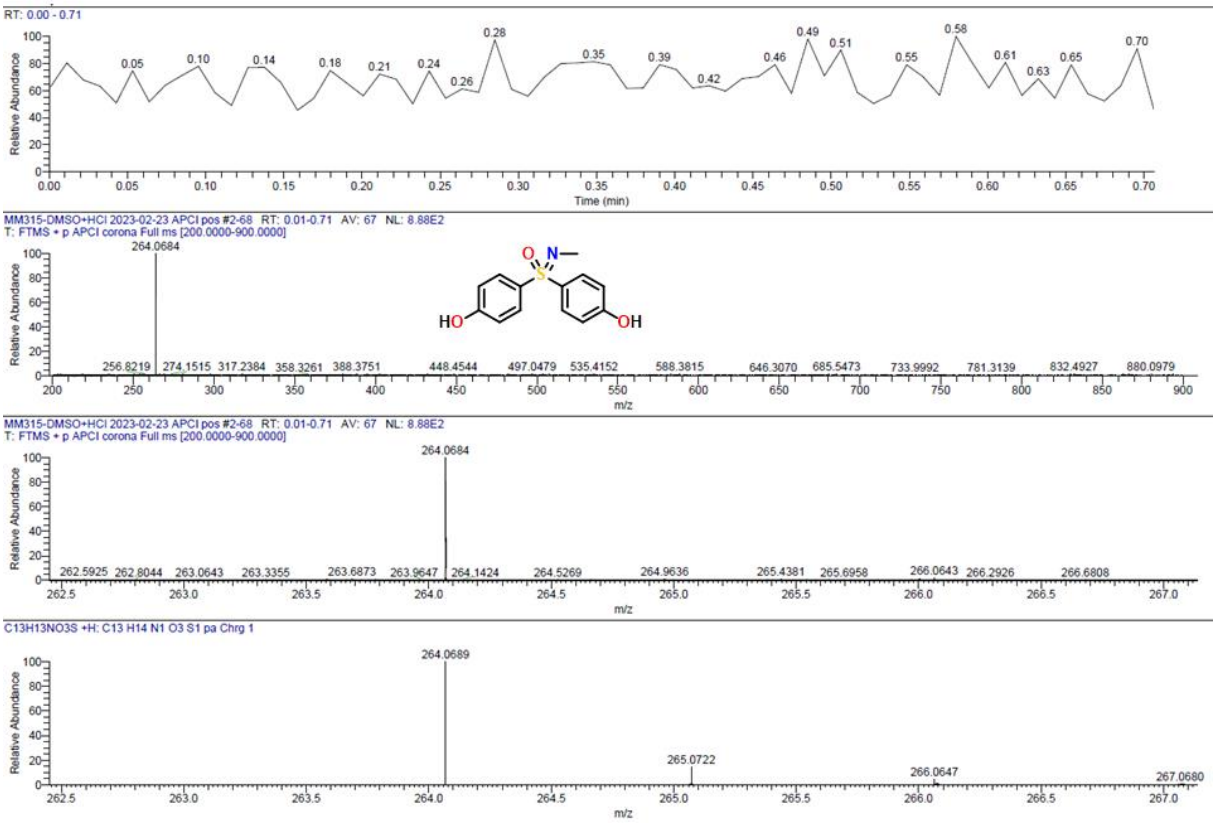

Figure S5.9.80. HRMS spectrum (APCI pos) of **1b** after the degradation of **9b** with HCl.

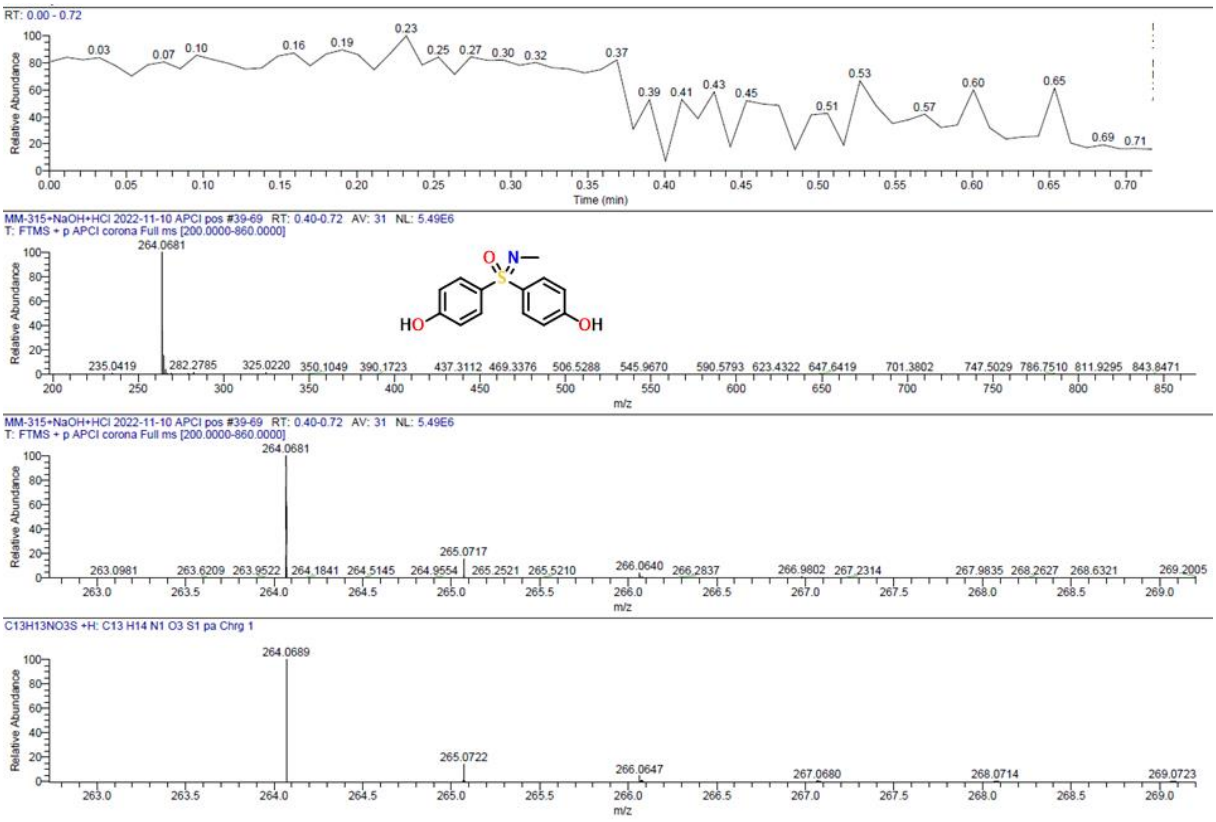

Figure S5.9.81. HRMS spectrum (APCI pos) of **1b** after the degradation of **9b** with NaOH followed by addition of HCl.

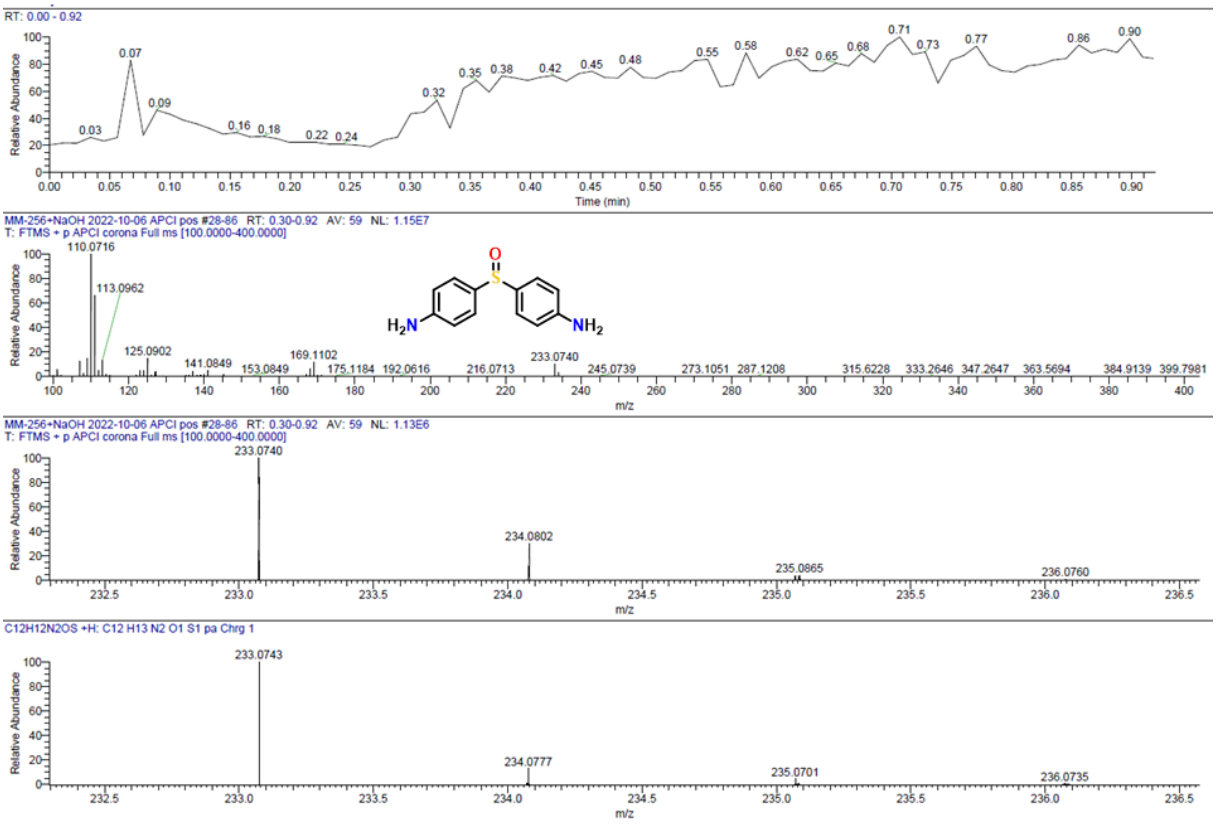

Figure S5.9.82. HRMS spectrum (APCI pos) of **2a** after the degradation of **10a** with NaOH.

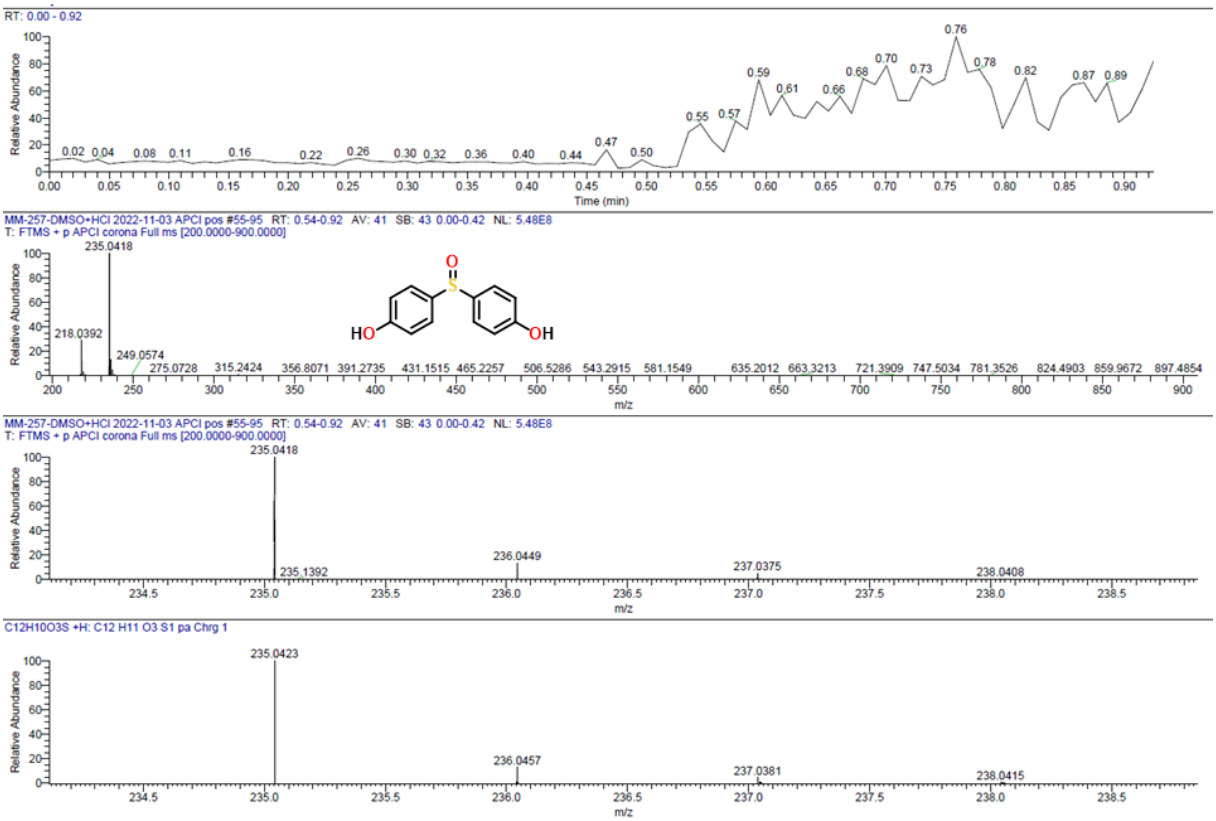

Figure S5.9.83. HRMS spectrum (APCI pos) of **2b** after the degradation of **10b** with HCl.

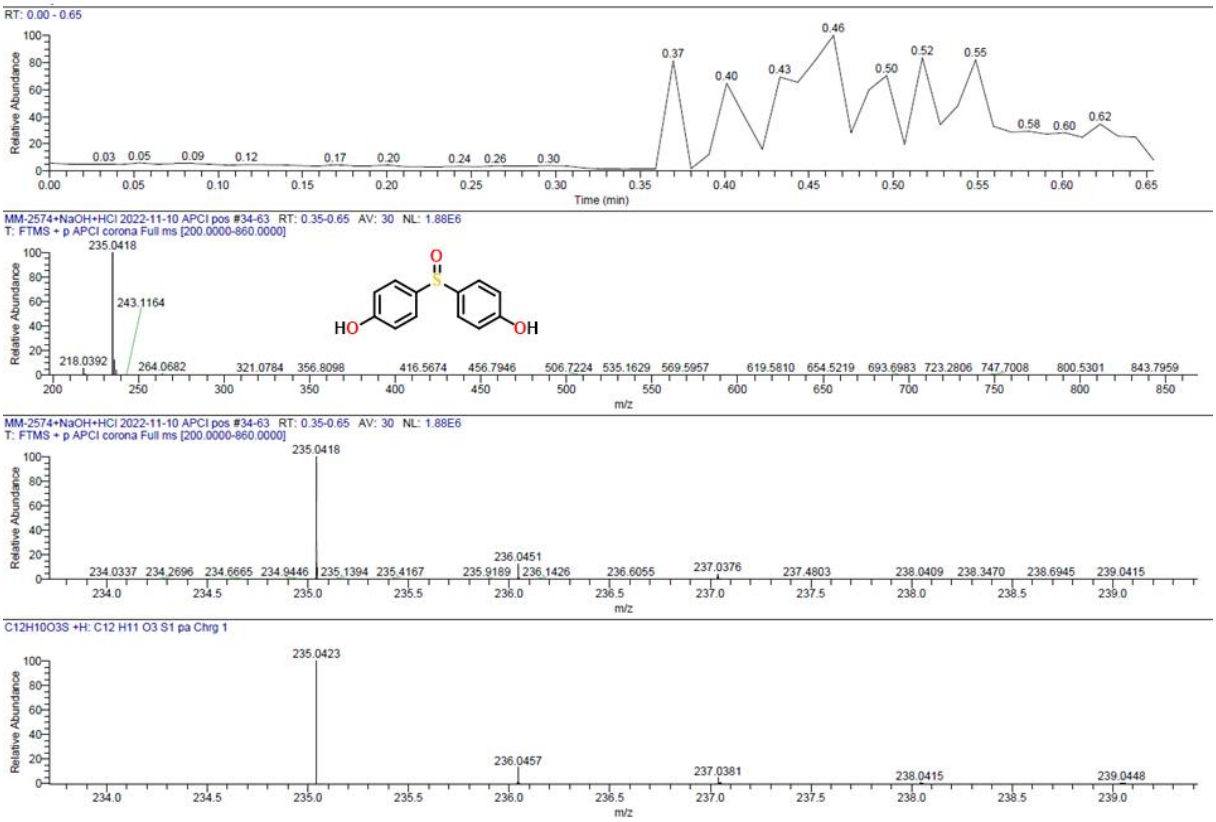

Figure S5.9.84. HRMS spectrum (APCI pos) of **2b** after the degradation of **10b** with NaOH followed by addition of HCl.

GPC traces

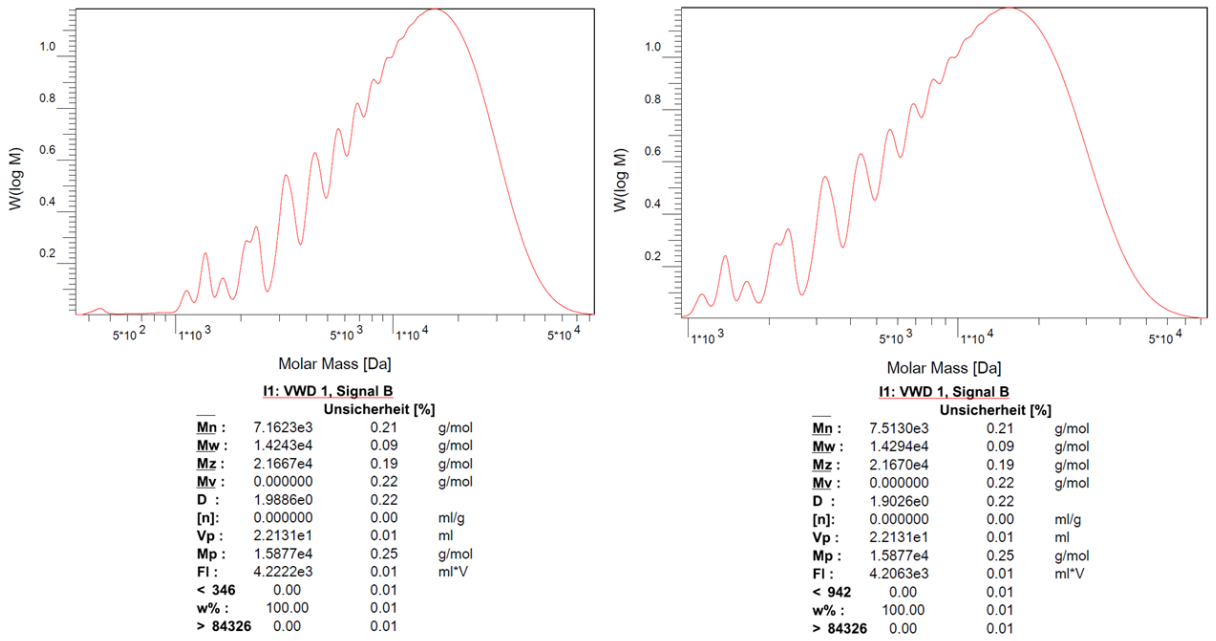

Figure S5.9.85. Normalized gel permeation chromatography (GPC) traces of **15** (Si/B exchange, CH_2Cl_2, r.t.; left: full spectrum, right: detail of higher molecular weights) detected by UV-vis detector at 280 nm.

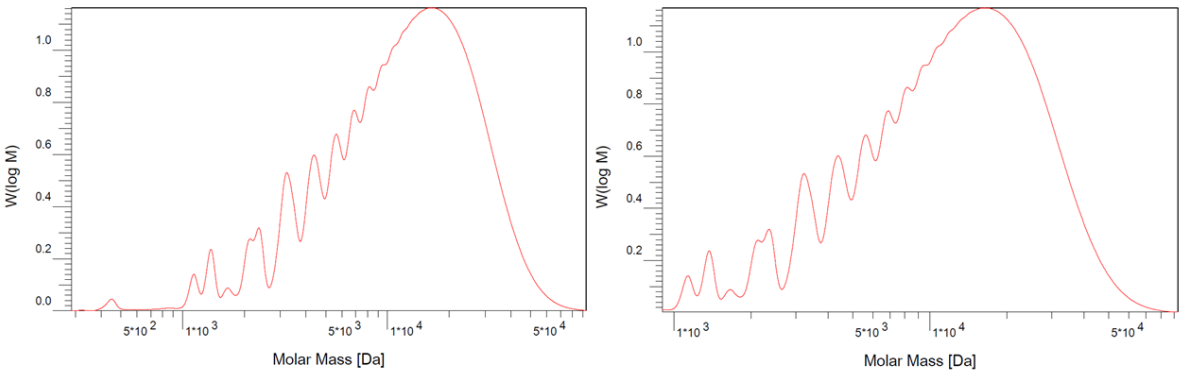

I1: VWD 1, Signal B

		Unsicherheit [%]	
Mn :	7.1823e3	0.22	g/mol
Mw :	1.5043e4	0.09	g/mol
Mz :	2.3218e4	0.19	g/mol
Mv :	0.000000	0.22	g/mol
D :	2.0945e0	0.23	
[n]:	0.000000	0.00	ml/g
Vp :	2.1934e1	0.01	ml
Mp :	1.7220e4	0.25	g/mol
FI :	3.5571e3	0.01	ml*V
< 286	0.00	0.01	
w% :	100.00	0.01	
> 93290	0.00	0.01	

I1: VWD 1, Signal B

		Unsicherheit [%]	
Mn :	7.6927e3	0.21	g/mol
Mw :	1.5115e4	0.09	g/mol
Mz :	2.3222e4	0.19	g/mol
Mv :	0.000000	0.21	g/mol
D :	1.9648e0	0.22	
[n]:	0.000000	0.00	ml/g
Vp :	2.1934e1	0.01	ml
Mp :	1.7220e4	0.25	g/mol
FI :	3.5396e3	0.01	ml*V
< 900	0.00	0.01	
w% :	100.00	0.01	
> 93290	0.00	0.01	

Figure S5.9.86. Normalized gel permeation chromatography (GPC) traces of **15** (Si/B exchange, *o*-DFB, 80 °C; left: full spectrum, right: detail of higher molecular weights) detected by UV-vis detector at 280 nm.

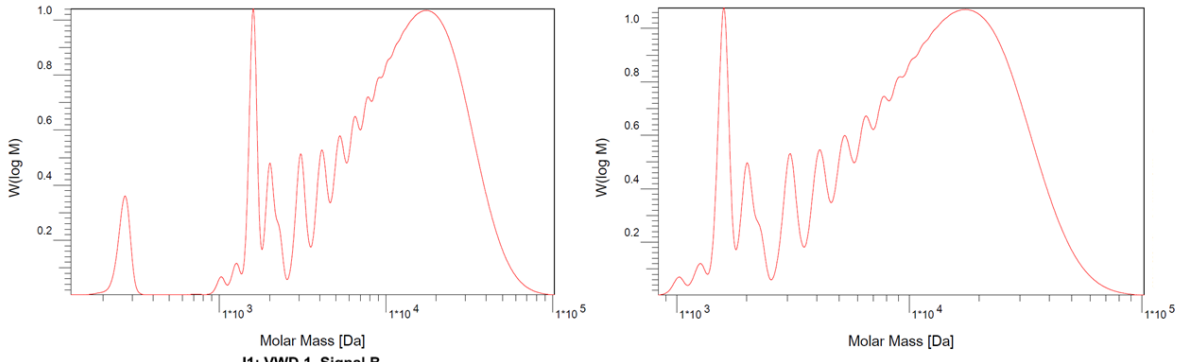

I1: VWD 1, Signal B

		Unsicherheit [%]	
Mn :	3.5496e3	1.66	g/mol
Mw :	1.4368e4	1.64	g/mol
Mz :	2.4424e4	1.65	g/mol
Mv :	0.000000	1.66	g/mol
D :	4.0478e0	2.33	
[n]:	0.000000	0.00	ml/g
Vp :	2.1676e1	0.05	ml
Mp :	1.8479e4	1.66	g/mol
FI :	2.6726e3	0.05	ml*V
< 127	0.00	0.05	
w% :	100.00	0.05	
> 102417	0.00	0.05	

I1: VWD 1, Signal B

		Unsicherheit [%]	
Mn :	6.2778e3	0.22	g/mol
Mw :	1.4862e4	0.10	g/mol
Mz :	2.4439e4	0.19	g/mol
Mv :	0.000000	0.22	g/mol
D :	2.3674e0	0.24	
[n]:	0.000000	0.00	ml/g
Vp :	2.1676e1	0.05	ml
Mp :	1.8479e4	0.26	g/mol
FI :	2.5822e3	0.05	ml*V
< 830	0.00	0.05	
w% :	100.00	0.05	
> 102417	0.00	0.05	

Figure S5.9.87. Normalized gel permeation chromatography (GPC) traces of **15** (salt elimination, CH_2Cl_2, r.t.; left: full spectrum, right: detail of higher molecular weights) detected by UV-vis detector at 280 nm.

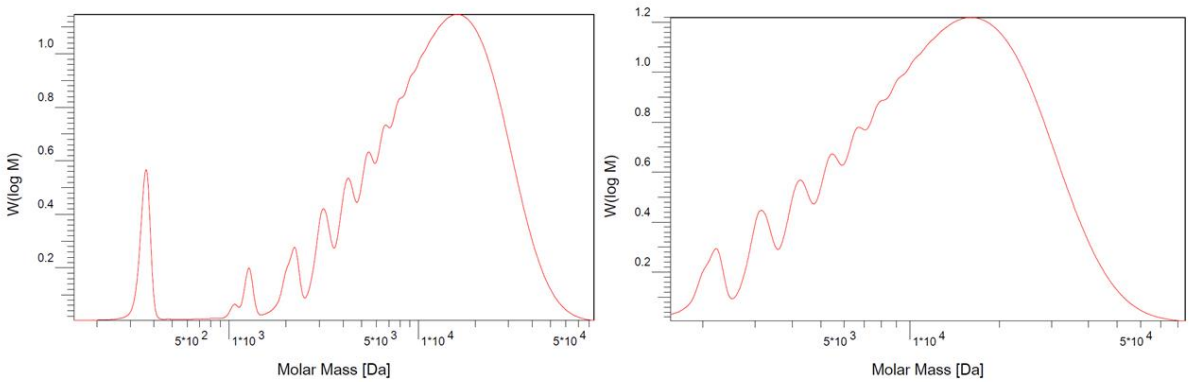

I1: VWD 1, Signal B

		Unsicherheit [%]	
Mn :	4.1794e3	1.18	g/mol
Mw :	1.4321e4	1.16	g/mol
Mz :	2.2507e4	1.17	g/mol
Mv :	0.000000	1.18	g/mol
D :	3.4266e0	1.65	
[n]:	0.000000	0.00	ml/g
Vp :	2.1998e1	0.00	ml
Mp :	1.6768e4	1.19	g/mol
FI :	2.9379e3	0.00	ml*V
< 150	0.00	0.00	
w% :	100.00	0.00	
> 84780	0.00	0.00	

I1: VWD 1, Signal B

		Unsicherheit [%]	
Mn :	8.7991e3	0.21	g/mol
Mw :	1.5181e4	0.09	g/mol
Mz :	2.2562e4	0.19	g/mol
Mv :	0.000000	0.21	g/mol
D :	1.7253e0	0.22	
[n]:	0.000000	0.00	ml/g
Vp :	2.1998e1	0.00	ml
Mp :	1.6768e4	0.25	g/mol
FI :	2.7645e3	0.00	ml*V
< 1554	0.00	0.00	
w% :	100.00	0.00	
> 84780	0.00	0.00	

Figure S5.9.88. Normalized gel permeation chromatography (GPC) traces of **16** (Si/B exchange, CH_2Cl_2, r.t.; left: full spectrum, right: detail of higher molecular weights) detected by UV-vis detector at 280 nm.

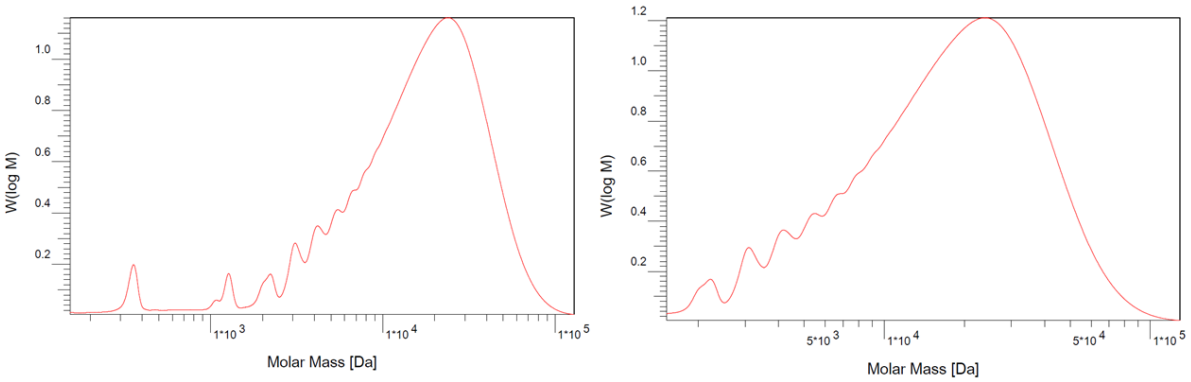

I1: VWD 1, Signal B

		Unsicherheit [%]	
Mn :	5.8634e3	0.72	g/mol
Mw :	2.0799e4	0.69	g/mol
Mz :	3.3256e4	0.71	g/mol
Mv :	0.000000	0.72	g/mol
D :	3.5472e0	0.99	
[n]:	0.000000	0.00	ml/g
Vp :	2.0989e1	0.04	ml
Mp :	2.5712e4	0.73	g/mol
FI :	2.9624e3	0.04	ml*V
< 152	0.00	0.04	
w% :	100.00	0.04	
> 129176	0.00	0.04	

I1: VWD 1, Signal B

		Unsicherheit [%]	
Mn :	1.1331e4	0.22	g/mol
Mw :	2.1672e4	0.10	g/mol
Mz :	3.3302e4	0.20	g/mol
Mv :	0.000000	0.22	g/mol
D :	1.9126e0	0.24	
[n]:	0.000000	0.00	ml/g
Vp :	2.0989e1	0.04	ml
Mp :	2.5712e4	0.26	g/mol
FI :	2.8389e3	0.04	ml*V
< 1517	0.00	0.04	
w% :	100.00	0.04	
> 129176	0.00	0.04	

Figure S5.9.89. Normalized gel permeation chromatography (GPC) traces of **16** (Si/B exchange, *o*-DFB, 80 °C; left: full spectrum, right: detail of higher molecular weights) detected by UV-vis detector at 280 nm.

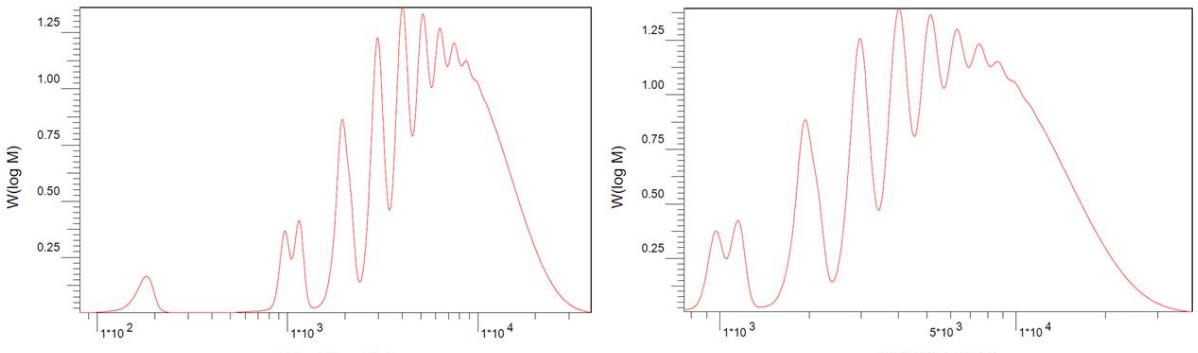

I1: VWD 1, Signal B

		Unsicherheit [%]	
Mn :	2.7134e3	1.12	g/mol
Mw :	7.0543e3	1.10	g/mol
Mz :	1.0903e4	1.12	g/mol
Mv :	0.000000	1.12	g/mol
D :	2.5998e0	1.56	
[n]:	0.000000	0.00	ml/g
Vp :	2.5401e1	0.13	ml
Mp :	4.0247e3	1.13	g/mol
FI :	3.7619e3	0.13	ml*V
< 80	0.00	0.13	
w% :	100.00	0.13	
> 39302	0.00	0.13	

I1: VWD 1, Signal B

		Unsicherheit [%]	
Mn :	4.1739e3	0.25	g/mol
Mw :	7.2245e3	0.16	g/mol
Mz :	1.0911e4	0.23	g/mol
Mv :	0.000000	0.25	g/mol
D :	1.7309e0	0.29	
[n]:	0.000000	0.00	ml/g
Vp :	2.5401e1	0.13	ml
Mp :	4.0247e3	0.28	g/mol
FI :	3.6707e3	0.13	ml*V
< 754	0.00	0.13	
w% :	100.00	0.13	
> 39302	0.00	0.13	

Figure S5.9.90. Normalized gel permeation chromatography (GPC) traces of **16** (salt elimination, CH_2Cl_2, r.t.; left: full spectrum, right: detail of higher molecular weights) detected by UV-vis detector at 280 nm.

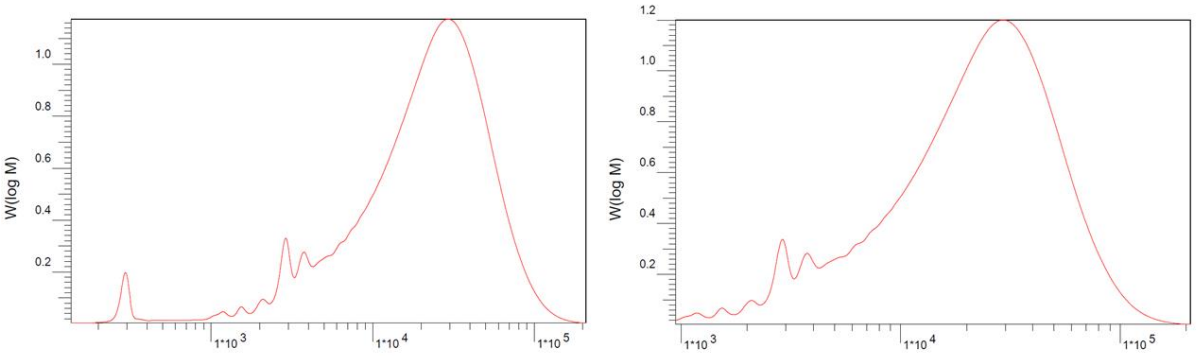

I1: VWD 1, Signal B

		Unsicherheit [%]	
Mn :	6.7741e3	0.81	g/mol
Mw :	2.7557e4	0.79	g/mol
Mz :	4.5600e4	0.81	g/mol
Mv :	0.000000	0.81	g/mol
D :	4.0681e0	1.13	
[n]:	0.000000	0.00	ml/g
Vp :	2.0473e1	0.04	ml
Mp :	3.2426e4	0.82	g/mol
FI :	2.9434e3	0.04	ml*V
< 135	0.00	0.04	
w% :	100.00	0.04	
> 209106	0.00	0.04	

I1: VWD 1, Signal B

		Unsicherheit [%]	
Mn :	1.2166e4	0.22	g/mol
Mw :	2.8164e4	0.10	g/mol
Mz :	4.5614e4	0.19	g/mol
Mv :	0.000000	0.22	g/mol
D :	2.3150e0	0.24	
[n]:	0.000000	0.00	ml/g
Vp :	2.0473e1	0.04	ml
Mp :	3.2426e4	0.26	g/mol
FI :	2.8792e3	0.04	ml*V
< 940	0.00	0.04	
w% :	100.00	0.04	
> 209106	0.00	0.04	

Figure S5.9.91. Normalized gel permeation chromatography (GPC) traces of **17** (Si/B exchange, CH_2Cl_2, r.t.; left: full spectrum, right: detail of higher molecular weights) detected by UV-vis detector at 280 nm.

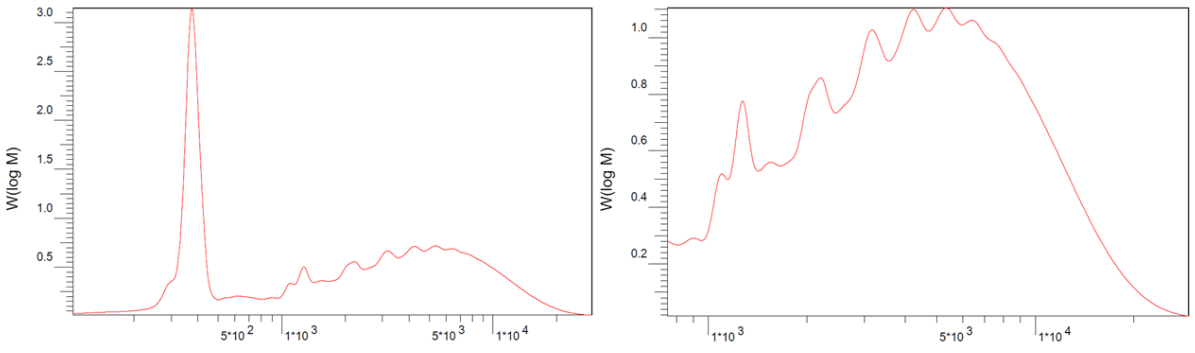

I1: VWD 1, Signal B

		Unsicherheit [%]	
Mn :	8.3965e2	6.49	g/mol
Mw :	3.6443e3	6.48	g/mol
Mz :	8.2899e3	6.49	g/mol
Mv :	0.000000	6.49	g/mol
D :	4.3403e0	9.17	
[n]:	0.000000	0.00	ml/g
Vp :	3.1938e1	0.11	ml
Mp :	3.7602e2	6.49	g/mol
FI :	1.3021e3	0.11	ml*V
< 102	0.00	0.11	
w% :	100.00	0.11	
> 29387	0.00	0.11	

I1: VWD 1, Signal B

		Unsicherheit [%]	
Mn :	3.0008e3	0.51	g/mol
Mw :	5.3993e3	0.47	g/mol
Mz :	8.5938e3	0.50	g/mol
Mv :	0.000000	0.51	g/mol
D :	1.7993e0	0.69	
[n]:	0.000000	0.00	ml/g
Vp :	2.4807e1	0.46	ml
Mp :	5.3453e3	0.52	g/mol
FI :	8.4616e2	0.46	ml*V
< 750	0.00	0.46	
w% :	100.00	0.46	
> 29387	0.00	0.46	

Figure S5.9.92. Normalized gel permeation chromatography (GPC) traces of **17** (Si/B exchange, *o*-DFB, 80 °C; left: full spectrum, right: detail of higher molecular weights) detected by UV-vis detector at 280 nm.

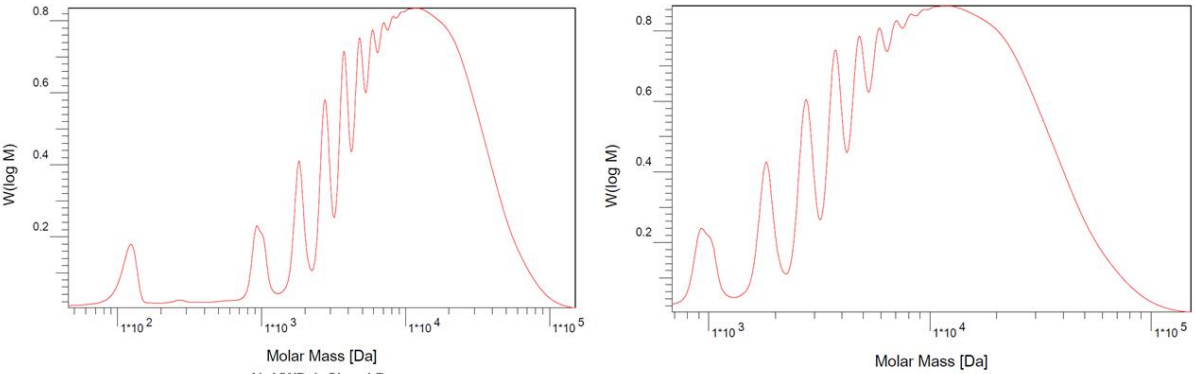

I1: VWD 1, Signal B

		Unsicherheit [%]	
Mn :	2.1334e3	1.76	g/mol
Mw :	1.4872e4	1.75	g/mol
Mz :	3.0833e4	1.76	g/mol
Mv :	0.000000	1.76	g/mol
D :	6.9709e0	2.48	
[n]:	0.000000	0.00	ml/g
Vp :	2.2741e1	0.15	ml
Mp :	1.1905e4	1.77	g/mol
FI :	3.2596e3	0.15	ml*V
< 45	0.00	0.15	
w% :	100.00	0.15	
> 150997	0.00	0.15	

I1: VWD 1, Signal B

		Unsicherheit [%]	
Mn :	5.9769e3	0.26	g/mol
Mw :	1.5494e4	0.18	g/mol
Mz :	3.0849e4	0.24	g/mol
Mv :	0.000000	0.26	g/mol
D :	2.5923e0	0.31	
[n]:	0.000000	0.00	ml/g
Vp :	2.2741e1	0.15	ml
Mp :	1.1905e4	0.29	g/mol
FI :	3.1272e3	0.15	ml*V
< 680	0.00	0.15	
w% :	100.00	0.15	
> 150997	0.00	0.15	

Figure S5.9.93. Normalized gel permeation chromatography (GPC) traces of **17** (salt elimination, CH_2Cl_2, r.t.; left: full spectrum, right: detail of higher molecular weights) detected by UV-vis detector at 280 nm.

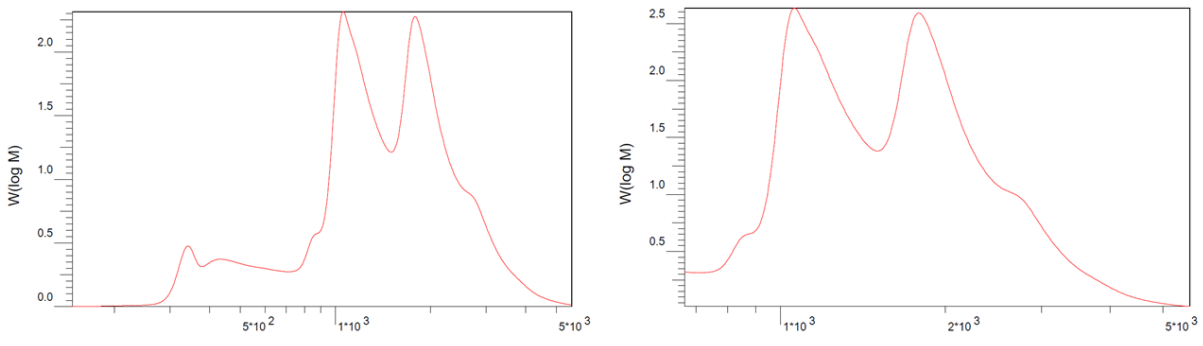

I1: VWD 1, Signal B

		Unsicherheit [%]	
Mn :	1.1295e3	1.69	g/mol
Mw :	1.5603e3	1.69	g/mol
Mz :	1.9653e3	1.69	g/mol
Mv :	0.000000	1.69	g/mol
D :	1.3815e0	2.39	
[n]:	0.000000	0.00	ml/g
Vp :	2.7290e1	0.14	ml
Mp :	1.7955e3	1.69	g/mol
FI :	2.5343e3	0.14	ml*V
< 147	0.00	0.14	
w% :	100.00	0.14	
> 5598	0.00	0.14	

I1: VWD 1, Signal B

		Unsicherheit [%]	
Mn :	1.4677e3	0.20	g/mol
Mw :	1.7133e3	0.16	g/mol
Mz :	2.0189e3	0.19	g/mol
Mv :	0.000000	0.20	g/mol
D :	1.1673e0	0.25	
[n]:	0.000000	0.00	ml/g
Vp :	2.7290e1	0.14	ml
Mp :	1.7955e3	0.22	g/mol
FI :	2.2280e3	0.14	ml*V
< 667	0.00	0.14	
w% :	100.00	0.14	
> 5598	0.00	0.14	

Figure S5.9.94. Normalized gel permeation chromatography (GPC) traces of **18** (salt elimination, CH_2Cl_2, r.t.; left: full spectrum, right: detail of higher molecular weights) detected by UV-vis detector at 280 nm.

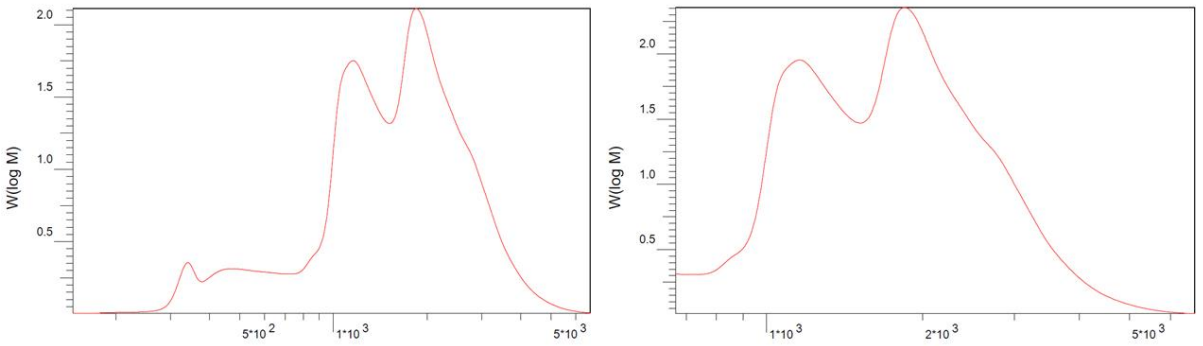

I1: VWD 1, Signal B

		Unsicherheit [%]	
Mn :	1.2375e3	1.36	g/mol
Mw :	1.7304e3	1.35	g/mol
Mz :	2.1798e3	1.36	g/mol
Mv :	0.000000	1.36	g/mol
D :	1.3982e0	1.91	
[n]:	0.000000	0.00	ml/g
Vp :	2.7209e1	0.01	ml
Mp :	1.8533e3	1.36	g/mol
FI :	2.5561e3	0.01	ml*V
< 145	0.00	0.01	
w% :	100.00	0.01	
> 6680	0.00	0.01	

I1: VWD 1, Signal B

		Unsicherheit [%]	
Mn :	1.5856e3	0.14	g/mol
Mw :	1.8768e3	0.06	g/mol
Mz :	2.2270e3	0.12	g/mol
Mv :	0.000000	0.14	g/mol
D :	1.1836e0	0.15	
[n]:	0.000000	0.00	ml/g
Vp :	2.7209e1	0.01	ml
Mp :	1.8533e3	0.16	g/mol
FI :	2.2929e3	0.01	ml*V
< 667	0.00	0.01	
w% :	100.00	0.01	
> 6680	0.00	0.01	

Figure S5.9.95. Normalized gel permeation chromatography (GPC) traces of **18** (salt elimination, *o*-DFB, 80 °C; left: full spectrum, right: detail of higher molecular weights) detected by UV-vis detector at 280 nm.

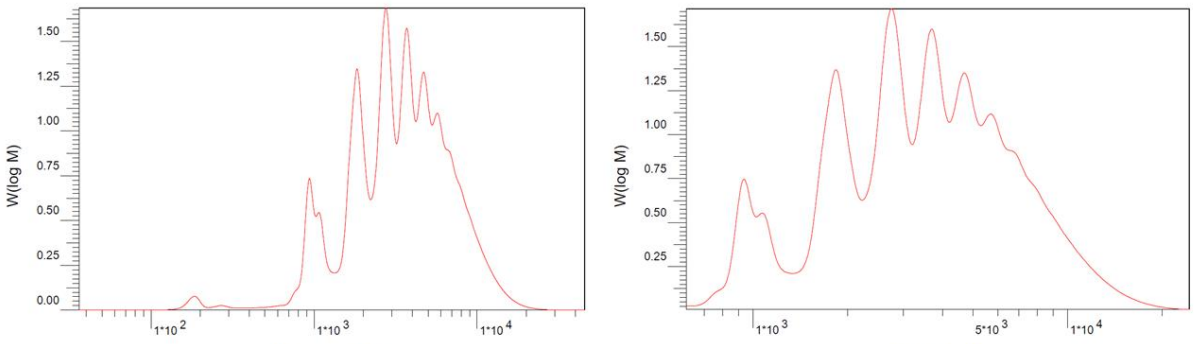

I1: VWD 1, Signal B

		Unsicherheit [%]	
Mn :	2.2746e3	0.66	g/mol
Mw :	4.1418e3	0.63	g/mol
Mz :	6.2477e3	0.66	g/mol
Mv :	0.000000	0.66	g/mol
D :	1.8209e0	0.91	
[n]:	0.000000	0.00	ml/g
Vp :	2.6329e1	0.07	ml
Mp :	2.7623e3	0.68	g/mol
Fl :	4.3967e3	0.07	ml*V
< 36	0.00	0.07	
w% :	100.00	0.07	
> 45685	0.00	0.07	

I1: VWD 1, Signal B

		Unsicherheit [%]	
Mn :	2.6916e3	0.23	g/mol
Mw :	4.1938e3	0.11	g/mol
Mz :	6.1743e3	0.20	g/mol
Mv :	0.000000	0.23	g/mol
D :	1.5581e0	0.25	
[n]:	0.000000	0.00	ml/g
Vp :	2.6329e1	0.07	ml
Mp :	2.7623e3	0.26	g/mol
Fl :	4.3229e3	0.07	ml*V
< 612	0.00	0.07	
w% :	100.00	0.07	
> 24367	0.00	0.07	

Figure S5.9.96. Normalized gel permeation chromatography (GPC) traces of **19** (salt elimination, CH_2Cl_2, r.t.; left: full spectrum, right: detail of higher molecular weights) detected by UV-vis detector at 280 nm.

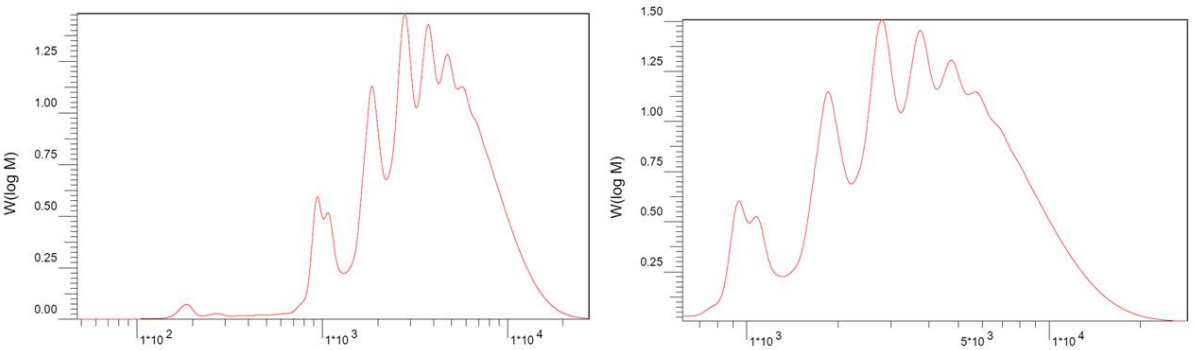

I1: VWD 1, Signal B

		Unsicherheit [%]	
Mn :	2.3869e3	0.67	g/mol
Mw :	4.4571e3	0.64	g/mol
Mz :	6.7064e3	0.67	g/mol
Mv :	0.000000	0.67	g/mol
D :	1.8673e0	0.92	
[n]:	0.000000	0.00	ml/g
Vp :	2.6296e1	0.04	ml
Mp :	2.7997e3	0.69	g/mol
Fl :	4.9010e3	0.04	ml*V
< 47	0.00	0.04	
w% :	100.00	0.04	
> 27580	0.00	0.04	

I1: VWD 1, Signal B

		Unsicherheit [%]	
Mn :	2.8682e3	0.22	g/mol
Mw :	4.5334e3	0.10	g/mol
Mz :	6.7223e3	0.19	g/mol
Mv :	0.000000	0.22	g/mol
D :	1.5806e0	0.24	
[n]:	0.000000	0.00	ml/g
Vp :	2.6296e1	0.04	ml
Mp :	2.7997e3	0.25	g/mol
Fl :	4.8151e3	0.04	ml*V
< 612	0.00	0.04	
w% :	100.00	0.04	
> 28582	0.00	0.04	

Figure S5.9.97. Normalized gel permeation chromatography (GPC) traces of **19** (salt elimination, *o*-DFB, 80 °C; left: full spectrum, right: detail of higher molecular weights) detected by UV-vis detector at 280 nm.

Julius-Maximilians-
UNIVERSITÄT
WÜRZBURG

Fakultät für
CHEMIE UND
PHARMAZIE

Erklärung zur Autorenschaft

Electrophilic activation of difunctional aminoboranes: B–N coupling versus intramolecular Cl/Me exchange,
M. Maier, J. Klopf, C. Glasmacher, F. Fantuzzi, J. Bachmann, O. Ayhan, A. Koner, B. Engels, H. Helten, *Chem. Commun.* **2022**, *58*, 4464–4467.

Detaillierte Darstellung der Anteile an der Veröffentlichung (in %)
Angabe Autoren/innen (ggf. Haupt- / Ko- / korrespondierende/r Autor/in) mit Vorname Nachname (Initialen)

Hauptautor: Matthias Maier (MM), Hauptautor: Jonas Klopf (JK), Clemens Glasmacher (CG), Felipe Fantuzzi (FF), Jonas Bachmann (JB), Ozan Ayhan (OA), Abhishek Koner (AK), korrespondierender Autor: Bernd Engels (BE), korrespondierender Autor: Holger Helten (HH)

Autor	MM	JK	CG	FF	JB	OA	AK	BE	HH			Σ in Prozent
Idee / Ideenentwicklung / Konzept	1%	1%				1%			10%			13%
Synthesen	19%		1%				1%					21%
Analysen	5%				1%							6%
Rechnungen		24%										24%
Verfassen der Veröffentlichung	3%	3%		2%				3%	6%			17%
Korrektur der Veröffentlichung	3%	3%		1%				2%	3%			12%
Koordination der Veröffentlichung								2%	5%			7%
Summe	31%	31%	1%	3%	1%	1%	1%	7%	24%			100%

Julius-Maximilians-
UNIVERSITÄT
WÜRZBURG

Fakultät für
CHEMIE UND
PHARMAZIE

Erklärung zur Autorenschaft

1,2,5-Azadiborolane as a Building Block for Inorganic–Organic Hybrid Polymers,
M. Maier, V. Zeh, N. Munker, J. Glock, K. Oberdorf, O. Ayhan, C. Lichtenberg, H. Helten, *Eur. J. Inorg. Chem.* **2024**, *27*, e202300490.

Detaillierte Darstellung der Anteile an der Veröffentlichung (in %)
Angabe Autoren/innen (ggf. Haupt- / Ko- / korrespondierende/r Autor/in) mit Vorname Nachname (Initialen)

Hauptautor: Matthias Maier (MM), Hauptautor: Vivien Zeh (VZ), Nadine Munker (NM), Julian Glock (JG), Kai Oberdorf (KO), Ozan Ayhan (OA), Crispin Lichtenberg (CL), korrespondierender Autor: Holger Helten (HH)

Autor	MM	VZ	NM	JG	KO	OA	CL	HH				∑ in Prozent
Idee / Ideenentwicklung / Konzept	1%	1%				1%		12%				15%
Synthesen	16%	16%	2%									34%
Analysen	7%	7%		1%	1%							16%
Verfassen der Veröffentlichung	5%	5%						10%				20%
Korrektur der Veröffentlichung	2%	2%					2%	4%				10%
Koordination der Veröffentlichung								5%				5%
Summe	31%	31%	2%	1%	1%	1%	2%	31%				100%

Julius-Maximilians-
UNIVERSITÄT
WÜRZBURG

Fakultät für
CHEMIE UND
PHARMAZIE

Erklärung zur Autorenschaft

Poly(thiophene iminoborane): A Poly(thiophene vinylene) (PTV) Analogue with a Fully B=N-Doped Backbone,
J. Chorbacher, M. Maier, J. Klopf, M. Fest, H. Helten, *Macromol. Rapid Commun.* **2023**, *44*, 2300278.

Detaillierte Darstellung der Anteile an der Veröffentlichung (in %)
Angabe Autoren/innen (ggf. Haupt- / Ko- / korrespondierende/r Autor/in) mit Vorname Nachname (Initialen)

Hauptautor: Johannes Chorbacher (JC), Hauptautor: Matthias Maier (MM), Jonas Klopf (JK), Maximilian Fest (MF), korrespondierender Autor: Holger Helten (HH)

Autor	JC	MM	JK	MF	HH							∑ in Prozent
Idee / Ideenentwicklung / Konzept	2%	2%			14%							18%
Synthesen	15%	15%										30%
Analysen	10%	10%		2%								22%
Rechnungen			2%									2%
Verfassen der Veröffentlichung	3%	3%			6%							12%
Korrektur der Veröffentlichung	3%	3%			6%							12%
Koordination der Veröffentlichung					4%							4%
Summe	33%	33%	2%	2%	30%							100%

Julius-Maximilians-
UNIVERSITÄT
WÜRZBURG

Fakultät für
CHEMIE UND
PHARMAZIE

Erklärung zur Autorenschaft

Poly(arylene iminoborane)s, Analogues of Poly(arylene vinylene) with a BN-Doped Backbone: A Comprehensive Study,
M. Maier, J. Chorbacher, A. Hellinger, J. Klopf, J. Günther, H. Helten, *Chem. Eur. J.* **2023**, *29*, e202302767.

Detaillierte Darstellung der Anteile an der Veröffentlichung (in %)
Angabe Autoren/innen (ggf. Haupt- / Ko- / korrespondierende/r Autor/in) mit Vorname Nachname (Initialen)

Hauptautor: Matthias Maier (MM), Hauptautor: Johannes Chorbacher (JC), Anna Hellinger (AH), Jonas Klopf (JK), Julian Günther (JG), korrespondierender Autor: Holger Helten (HH)

Autor	MM	JC	AH	JK	JG	HH						∑ in Prozent
Idee / Ideenentwicklung / Konzept	3%	3%				14%						20%
Synthesen	14%	14%	3%									31%
Analysen	8%	8%			2%							18%
Rechnungen				2%								2%
Verfassen der Veröffentlichung	3%	3%				6%						12%
Korrektur der Veröffentlichung	3%	3%				6%						12%
Koordination der Veröffentlichung						5%						5%
Summe	31%	31%	3%	2%	2%	31%						100%